PROCEEDINGS OF THE PHYSICAL SOCIETY

VOL 75, PART 1 1 January 1960 No. 481

EDITORIAL

The Editors wish to call the attention of authors to the importance of abstracts. The number of people who read the abstract of a paper is usually more than ten times those who read the paper itself. The abstract should be designed

(*a*) to help readers to decide whether the content of the paper is such that they desire to read it,

(*b*) to give readers for whom the paper is of " fringe interest " as much information as possible so as to make it unnecessary for them to read the whole paper.

The Editors wish authors to know that they are willing to publish abstracts of somewhat greater length than has in recent years been customary. For example, a half-page abstract of a paper which occupies 10 pages (or proportionately rather more in the case of a shorter paper) would not be regarded as excessive.

Specific reference to work of another author or to a figure in the paper may be given when appropriate.

The abstract should be designed to give precise and definite information, rather than vague indications. Consider the two following possible abstracts as an example of bad and good abstracting:

A. The absorption of cadmium has been measured in the range 1000 Å to 500 Å and results are not in agreement with theory.

B. Absorption measurements for cadmium vapour yield a smooth curve (fig. 3). Measured cross sections of 7, 9 and 12×10^{-18} cm^2 ($\pm 10\%$) at 500, 700 and 1000 Å are not in agreement with values of 20, 25 and 27×10^{-18} cm^2 calculated by Smith (1946) using a dipole velocity formula.

The second abstract is very much more useful and the extra length is justified.

Many authors find a special difficulty in abstracting their own papers. It is therefore suggested that authors should consult a colleague in regard to the adequacy of the abstract which they include with a manuscript submitted for publication. The Editors will be helped if Fellows of the Society who are communicating papers by junior workers will give special consideration to the abstract.

Abstract of

PRESIDENTIAL ADDRESS

Recent Trends in the Theory of the Ionosphere

BY J. A. RATCLIFFE

Delivered before the Society on 21*st May* 1959

Note. The full Presidential Address is published in the *Year Book of the Physical Society* for 1959

THE early theory of Chapman supposed that the layers were produced by ionizing radiation incident on a uniform atmosphere in equilibrium under gravity and the electrons disappeared by a process of recombination with a constant coefficient. Later theories due particularly to Bates and Massey suggested that electrons were lost by a double process of the type illustrated by the reactions

$$O^+ + O_2 \rightarrow O_2^+ + O$$

$$O_2^+ + e \rightarrow O' + O''.$$

In the E and F1 layers, where the concentration of O_2 is great, this double process simulates recombination of the type envisaged by Chapman; higher up, where the concentration of O_2 is less, it simulates attachment with a coefficient β which varies with height as though it had a scale height H_β determined by the scale height of the O_2.

It is supposed that the gas which is ionized in the F region is atomic oxygen, and that the peak rate of production of electrons is near the peak of the F1 layer, at a height of about 170 km. Above the F1 peak the loss process is effectively attachment (with coefficient β) having a scale height H_β. The magnitude of H_β is less than the scale height H_1 of the ionizable atomic oxygen, with the result that the electron concentration increases continuously upwards above the peak of F1, and if no other phenomenon intervened it would increase indefinitely up to heights so great that there was no air left to be ionized. It has, however, been shown by Yonezawa that a process of diffusion causes the electron concentration to reach a maximum at the peak of the F2 layer.

Recent results concerning (*a*) the density of the upper atmosphere, measured by satellites and rockets, and (*b*) the vertical distribution of electron concentration under quasi-equilibrium conditions, are considered in relation to this theory. It is concluded that the ratio H_1/H_β is of the order 1 to 1·2. If H_1 represented atomic oxygen, and H_β were determined by the distribution of molecular oxygen, this ratio would be 2. The fact that it appears to be smaller seems to require that the O and O_2 are fairly completely mixed up to the level of the F2 peak. The results are compatible with values of β given by

$$\beta = 10^{-4} \exp[(170 - h_{\text{km}})/50] \text{ sec}^{-1}$$

which also agree with observed decay of electron concentration at night.

It is pointed out that small changes in the ratio H_1/H_β, which could be produced by small changes in the amount of mixing, would profoundly alter the shape of the electron distribution. A small change of this kind could, for example, explain the striking anomalies in the critical frequency of f_0F2 known as the 'winter' and the 'December' anomaly.

Another consequence of the theory outlined here is that the equilibrium electron distribution above the F2 peak is controlled entirely by diffusion in such a way that the electron concentration decreases upwards with a scale height equal to twice the scale height of the ionized gas. Recent results of Bowles fit in with this explanation.

High Energy Photo-spallation leading to ^{18}F

By T. G. WALKER and W. T. MORTON
Natural Philosophy Department, University of Glasgow

MS. received 9th July 1959

Abstract. The cross sections for the production of ^{18}F from ^{19}F, ^{23}Na, ^{24}Mg, ^{27}Al, ^{28}Si, ^{31}P and ^{32}S by bremsstrahlung with a maximum energy of 240 Mev have been measured. The cross sections for the production of ^{18}F from ^{19}F, ^{23}Na and ^{27}Al have also been obtained for bremsstrahlung with maximum energies of 180 Mev and 120 Mev. The results are compared with other spallation work.

---

§ 1. Introduction

Many workers have investigated spallation reactions induced by high energy protons. Similar reactions induced by high energy γ-rays of peak energy greater than 100 Mev have been reported only for middle weight nuclei (Debs *et al.* 1955, Sugihara and Halpern 1956, Wolke and Bonner 1956). The present investigation extends these results to elements of lower atomic weights.

In general, spallation experiments have involved the measurement of the activities of the residual nuclei produced in reactions of the type (γ, xN), where x is an integer and N is a nucleon, for a particular target element. This method has a number of disadvantages. Comparisons of the activity of radioactive nuclei of different half lives are very sensitive to fluctuations in beam intensity, while the decay schemes of the various residual nuclei may be known with different degrees of accuracy. This method usually necessitates an accurate radiochemical separation. These difficulties have been overcome in the present work by inducing the spallation in a series of nuclei of increasing mass number, and measuring the residual activity of the same isotope in each case.

§ 2. Experimental Procedure

The targets consisted of sodium fluoride, sodium peroxide, red phosphorus, silicon and magnesium in powder form, aluminium in the form of thin sheets, and sulphur cast into thin blocks. The powders were packed uniformly into thin walled copper boxes. All the materials used were of high purity.

The elements being investigated, together with a piece of distrene (C_8H_8), were exposed in groups of three, all of the same surface area, one behind the other, to the uncollimated bremsstrahlung beam of the Glasgow synchrotron at a distance of one metre from the 0·02 in. diameter tungsten wire target. The attenuation of the γ-ray beam in passing through the sample was never greater than 8%.

After exposure the material was transferred to another copper box with walls thick enough to absorb the 0·65 Mev positrons from the decay of ^{18}F. The half life of this nucleus is 111 minutes (Ajzenberg-Selove and Lauritsen 1959). The activity was measured by placing the samples between two $1\frac{1}{2}$ in. diameter and

2 in. thick NaI(Tl) crystal scintillators mounted on E.M.I.6262 photomultipliers, and counting in coincidence the two 0·51 Mev quanta from the β^+ annihilation.

§ 3. RESULTS

The ratios of the cross sections for the formation of ^{18}F from ^{23}Na, ^{24}Mg, ^{27}Al, ^{28}Si, ^{31}P and ^{32}S to the cross section for the formation of ^{18}F from ^{19}F were obtained for bremsstrahlung with a maximum energy of 240 Mev. These results are shown in the figure plotted against the number of emitted nucleons. The natural isotopic abundance of the most abundant isotope for all the elements investigated here is greater than 95%, except magnesium for which it is 74%. Thus it has been assumed for simplicity that each element consists entirely of its most abundant isotope.

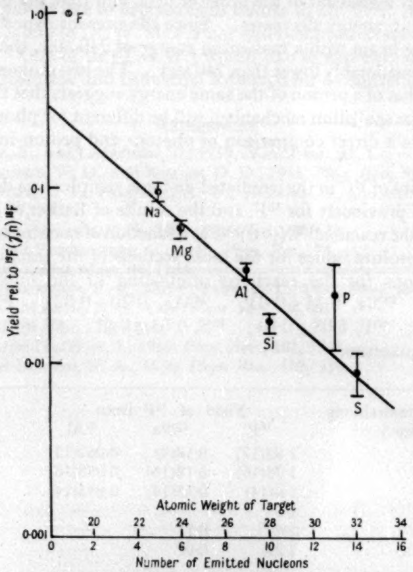

Yields relative to ^{19}F(γ, n)^{18}F at 240 Mev.

The figure indicates, as would be expected, that for a given bombarding energy the cross section for a reaction decreases as the number of emitted particles increases. For processes in which more than one nucleon is emitted, the logarithm of the yields relative to the ^{19}F (γ, n) ^{18}F reaction lie, within the present accuracy, on a straight line of gradient $0{\cdot}30 \pm 0{\cdot}04$ when plotted against the number of emitted nucleons. No attempt was made to draw this line through the point corresponding to the reaction ^{19}F(γ, n)^{18}F, since (γ, n) processes are in general produced by the low energy quanta of the bremsstrahlung beam (Barber, George and Reagan 1955) and so are not of the cascade type.

As is common to most spallation studies there exists a slight ambiguity as to the direct product nucleus of the spallation. The nucleus ^{18}F can arise as a direct result of spallation or by the emission of one or more β^+ particles from a nucleus with the same atomic mass number, but a larger charge than ^{18}F. A nucleus of this type would be expected to have a very short half life. It is shown in the work of Rudstam, Stevenson and Fowler (1952) that for proton-induced spallation the yield of nuclei of the same mass number decreases with the distance of the residual nucleus from the line of stable nuclei on the isotope chart. A photon-induced spallation might reasonably be expected to give a similar tendency.

Because of the spread of points in previous photo-spallation experiments it was not possible to compare the gradient of the logarithm of the yield against the number of emitted nucleons with the present results. Rudstam (1953) reports for the spallation of medium weight elements bombarded with protons with an energy of 187 Mev a gradient of the order of 0·32, and that the gradient increases as the bombarding energy decreases. Since the present experiments employed a bremsstrahlung beam with a maximum energy of 240 Mev, the effective photon energy will be considerably lower than 240 Mev. The low momentum of a photon compared with that of a proton of the same energy suggests that the Serber (1947) cascade part of the spallation mechanism will be different for photons and protons. This would make a direct comparison of photon- and proton-induced spallation difficult.

The β^+ activity of ^{11}C in the irradiated distrene samples was determined by the method outlined previously for ^{18}F, and the results of Barber *et al.* (1955) on the cross section for the reaction ^{12}C$(\gamma, n)^{11}$C as a function of maximum ray energy were used to obtain absolute values for the cross sections of the reactions studied here. The cross sections for the reactions originating in the nuclei studied were ^{19}F, 3·5 ± 0·3; ^{23}Na, 0·33 ± 0·03; ^{24}Mg, 0·20 ± 0·02; ^{27}Al, 0·12 ± 0·01; ^{28}Si, 0·06 ± 0·01; ^{31}P, 0·08 ± 0·04; ^{32}S, 0·03 ± 0·01; all in units of 10^{-27} cm^2 per equivalent quantum.

Maximum bremsstrahlung energy (Mev)	Yield of ^{18}F from			^{12}C$(\gamma, n)^{11}$C yield
	^{19}F	^{23}Na	^{27}Al	
240	1·83(17)	0·18(9)	0·062(13)	1·62
180	1·78(16)	0·18(16)	0·058(16)	1·50
120	1·6(14)	0·15(14)	0·045(14)	1·34
100	1·5	—	—	1·27
70	1·4	0·11	—	1·15
50	1·22	0·07	—	1·0

The table shows the variation of the cross section for the production of ^{18}F from ^{19}F, ^{23}Na and ^{27}Al at peak bremsstrahlung energies of 120, 180 and 240 Mev. The errors in these results are less than 8%. The numbers in brackets indicate the number of determinations which were made. Also shown in the table are the results of Perlman and Friedlander (1948) on the reaction ^{19}F$(\gamma, n)^{18}$F at maximum bremsstrahlung energies of 100 and 50 Mev, those of Holtzman and Sugarman (1952) on the production of ^{18}F from ^{23}Na at 50 Mev and those of Schupp and Martin (1954) on the production of ^{18}F from ^{19}F and ^{23}Na at an energy of 70 Mev. All these results have been normalized to the cross section for the reaction ^{12}C$(\gamma, n)^{11}$C of Barber *et al.* at a maximum bremsstrahlung energy of 50 Mev.

The table shows the expected increase in cross section for a given process with increase in maximum bremsstrahlung energy. No abrupt increase was observed as the maximum γ-ray energy increases above meson threshold.

§ 4. CONCLUSIONS

The present results show that photo-spallation reactions in the region of maximum bremsstrahlung energy of 120 to 240 MEV and light nuclei exhibit the expected trends of decrease in cross section with increasing number of emitted nucleons and with decreasing photon energy. The gradient of the logarithm of the yield against the number of emitted nucleons is similar to that obtained in proton-induced spallation work at 187 MEV.

ACKNOWLEDGMENTS

The authors would like to express their thanks to Dr. P. V. March for his help in all possible ways and to Dr. W. McFarlane and synchrotron staff for the operation of the machine. One of us (T.G.W.) would like to express his gratitude to the Department of Scientific and Industrial Research for a maintenance grant.

REFERENCES

AJZENBERG-SELOVE, F., and LAURITSEN, T., 1959, *Nucl. Phys.*, **11**, 1.
BARBER, W. C., GEORGE, W. D., and REAGAN, D. D., 1955, *Phys. Rev.*, **98**, 73.
DEBS, R. J., EISINGER, J. T., FAIRHALL, A. W., HALPERN, I., and RICHTER, H. G., 1955, *Phys. Rev.*, **97**, 1325.
HOLTZMAN, P. B., and SUGARMAN, N., 1952, *Phys. Rev.*, **87**, 633.
PERLMAN, M. L., and FRIEDLANDER, G., 1948, *Phys. Rev.*, **74**, 442.
RUDSTAM, S. G., 1953, *Phil. Mag.*, **44**, 1131.
RUDSTAM, S. G., STEVENSON, P. C., and FOWLER, R. L., 1952, *Phys. Rev.*, **74**, 442.
SCHUPP, F. D., and MARTIN, D. S., 1954, *Phys. Rev.*, **94**, 80.
SERBER, R., 1947, *Phys. Rev.*, **72**, 1114.
SUGIHARA, T. T., and HALPERN, I., 1956, *Phys. Rev.*, **101**, 1768.
WOLKE, R. L., and BONNER, N. A., 1956, *Phys. Rev.*, **102**, 530.

The Saturation Magnetostriction of Polycrystals

By R. R. BIRSS
Imperial College, London, S.W.7

MS. received 12*th May* 1959, *in revised form* 24*th June* 1959

Abstract. Relations between the single-crystal and polycrystalline saturation magnetostriction constants are derived for cubic materials of positive and negative anisotropies. Terms which are independent of the direction in which the magnetostrictive strain is measured are not neglected and the formulae obtained are thus directly applicable to the corresponding magnetoresistance constants. The method used is perfectly general and is extended to deal with materials of hexagonal (and cylindrical) symmetry for which the hexagonal axis is a direction of easy magnetization or for which the basal plane is a plane of easy magnetization. The relations obtained are compared with experimental data.

§ 1. Introduction

Since a polycrystalline substance is, ideally, an aggregate of a large number of individual crystallites orientated at random, it is possible, in principle, to relate the magnetostriction of a polycrystal to that of a single crystal specimen of the same material. In general, the mean magnetization in each crystal grain is influenced by that of its neighbours, but above the point of technical saturation a suitably shaped polycrystalline specimen may be uniformly magnetized by a uniform applied magnetic field. However, even at saturation the magnetostriction of a polycrystal may not necessarily be obtained by averaging, over all the relevant crystallographic directions, the magnetostrictive strain corresponding to a single crystal.

It has been pointed out by Vladimirsky (1943) that polycrystalline magnetostriction should depend not only on the magnetostrictive behaviour of single crystals but also on the elastic constants of the material, except in the limiting case in which the stress is uniform throughout the polycrystal. The situation has been reviewed recently by Lee (1955) who concluded that the assumption of uniform stress is, in fact, the best approximation. Moreover, this conclusion has been convincingly supported by more recent experimental work (Birss 1958) in which the polycrystalline magnetostriction constant of iron has been accurately determined and in which the relation between the single-crystal and polycrystalline saturation magnetostriction constants of nickel has been established experimentally over an extended range of temperatures. The latter measurements also show that this relation is substantially independent of temperature which suggests that the elastic constants of nickel are not involved and hence provides further evidence that the assumption of uniform stress is a valid one. It is therefore of some interest to calculate the relations which exist between the single-crystal and polycrystalline magnetostriction constants for the crystal classes to which the common ferromagnetic materials belong.

§ 2. Cubic Crystals

A relation between the single-crystal and polycrystalline saturation magnetostriction constants of cubic materials has been given by Becker and Döring (1939) for substances, such as nickel, for which the first anisotropy coefficient is negative, that is for materials in which the directions of easy magnetization are parallel to ternary crystallographic axes. For such materials it has been shown (Birss 1957) that the experimental data at present available are completely consistent with the assumption that the magnetostrictive strain which accompanies the magnetization of a single crystal to saturation is given by the well-known equation

$$\begin{aligned}\Lambda = {} & h_1(\alpha_1{}^2\beta_1{}^2+\alpha_2{}^2\beta_2{}^2+\alpha_3{}^2\beta_3{}^2-\tfrac{1}{3}) \\ & +2h_2(\alpha_1\alpha_2\beta_1\beta_2+\alpha_2\alpha_3\beta_2\beta_3+\alpha_3\alpha_1\beta_3\beta_1) \\ & +h_3(s-\tfrac{1}{3})+h_4(\alpha_1{}^4\beta_1{}^2+\alpha_2{}^4\beta_2{}^2+\alpha_3{}^4\beta_3{}^2+\tfrac{2}{3}s-\tfrac{1}{3}) \\ & +2h_5(\alpha_1\alpha_2\alpha_3{}^2\beta_1\beta_2+\alpha_2\alpha_3\alpha_1{}^2\beta_2\beta_3+\alpha_3\alpha_1\alpha_2{}^2\beta_3\beta_1) \qquad \ldots\ldots(1)\end{aligned}$$

with

$$s=\alpha_1{}^2\alpha_2{}^2+\alpha_2{}^2\alpha_3{}^2+\alpha_3{}^2\alpha_1{}^2$$

where α_1, α_2, α_3 and β_1, β_2, β_3 are the direction cosines, relative to the crystal axes, of the magnetization vector and the direction of observation respectively. Becker and Döring assumed that the coefficient h_3—which is associated with an isotropic change in volume—could be neglected, and by averaging Λ over all the relevant crystallographic directions they obtained, for the fractional change in length associated with magnetization, the expression

$$dl/l=Q\,(\cos^2\xi-\tfrac{1}{3}) \qquad \ldots\ldots(2)$$

where Q was determined as a function of the constants h_1, h_2, h_4, h_5 and where ξ is the angle between the polycrystalline magnetization vector and the direction in which the magnetostrictive strain is measured. It may be noted that equation (1) does not represent the spontaneous or intrinsic magnetostriction of a single crystal, but rather the strain accompanying magnetization to saturation referred to the ideal demagnetized state, in which the crystal is composed of many domains orientated so that there are equal numbers parallel to each of the crystallographically equivalent directions of easy magnetization.

Equation (2) is generally accepted as governing the saturation magnetostriction of polycrystalline materials, the saturation magnetostriction constant λ_s being defined as $\frac{2}{3}Q$. In fact, however, equation (2) is only obtained if the coefficient h_3 is neglected. Whilst it is true that this is a reasonable assumption for nickel and certain nickel-rich alloys (Bozorth and Hamming 1953), measurements on other single crystals (Bickford, Pappis and Stull 1955) have shown that h_3 may not be neglected for all cubic materials. There is considerably less evidence to show that the coefficient associated with an isotropic volume change may be neglected for crystals of lower symmetry. For cobalt, which is hexagonal at room temperature, this coefficient is found to be of the same order as the other experimentally determined magnetostriction coefficients (Bozorth and Sherwood 1954). Further, the magnetoresistive behaviour of single crystals must, from symmetry considerations, conform to equations of the same form as those governing the magnetostriction, and magnetoresistive measurements, even for nickel, lend no support to the view that the coefficient corresponding to h_3 may be neglected. For example, measurements of the saturation magnetoresistance of single crystals of nickel (Becker and Döring 1939) show that the coefficients corresponding to those of equation (1) are

$$k_1 = 63 \times 10^{-3},\ k_2 = 29 \times 10^{-3},\ k_3 = -36 \times 10^{-3},\ k_4 = -51 \times 10^{-3},\ k_5 = 14 \times 10^{-3}.$$

It therefore seems desirable to deduce the relationship between the single-crystal and polycrystalline saturation magnetostriction constants for cubic materials of both positive and negative anisotropy under the assumption that h_3 may not be neglected. No details have been published of Becker and Döring's calculations although the general method of procedure was indicated. A different treatment is adopted here which may be more readily extended to deal with non-cubic materials and which proceeds not by averaging Λ over various directions but rather by averaging the *spontaneous* magnetostriction λ both for saturated and for demagnetized states. The polycrystalline magnetostriction may thus be calculated as follows.

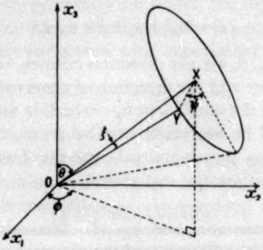

If the cubic axes of an individual crystallite are x_1, x_2, x_3 as shown in the figure, then the measuring direction OX may be defined by the polar and azimuthal angles θ and ϕ, whilst the position of the magnetization vector OY, which makes a constant angle ξ with the measuring direction, may be defined by the auxiliary angle ψ. The spontaneous magnetostriction, unlike Λ, may be expressed in the same form for all cubic crystals whatever the sign of the first anisotropy coefficient. In terms of the constants $h_1 \ldots h_5$ of equation (1)

$$\begin{aligned}\lambda = h_0 &+ h_1(\alpha_1^2\beta_1^2 + \alpha_2^2\beta_2^2 + \alpha_3^2\beta_3^2)\\ &+ 2h_2(\alpha_1\alpha_2\beta_1\beta_2 + \alpha_2\alpha_3\beta_2\beta_3 + \alpha_3\alpha_1\beta_3\beta_1)\\ &+ (h_3 + \tfrac{2}{3}h_4)(\alpha_1^2\alpha_2^2 + \alpha_2^2\alpha_3^2 + \alpha_3^2\alpha_1^2)\\ &+ h_4(\alpha_1^4\beta_1^2 + \alpha_2^4\beta_2^2 + \alpha_3^4\beta_3^2)\\ &+ 2h_5(\alpha_1\alpha_2\alpha_3^2\beta_1\beta_2 + \alpha_2\alpha_3\alpha_1^2\beta_2\beta_3 + \alpha_3\alpha_1\alpha_2^2\beta_3\beta_1) \qquad \ldots\ldots (3)\end{aligned}$$

where

$$\begin{aligned}\alpha_1 &= \cos\xi \sin\theta \cos\phi + \sin\xi\,(\cos\theta \cos\phi \cos\psi + \sin\phi \sin\psi)\\ \alpha_2 &= \cos\xi \sin\theta \sin\phi + \sin\xi\,(\cos\theta \sin\phi \cos\psi - \cos\phi \sin\psi)\\ \alpha_3 &= \cos\xi \cos\theta - \sin\xi \sin\theta \cos\psi \qquad \ldots\ldots (4)\end{aligned}$$

$$\beta_1 = \sin\theta \cos\phi, \qquad \beta_2 = \sin\theta \sin\phi, \qquad \beta_3 = \cos\theta. \qquad \ldots\ldots (5)$$

If the individual crystallites are orientated at random then, for any one crystallite, $(1/8\pi^2) \sin\theta\, d\theta\, d\phi\, d\psi$ is the probability of the measuring direction lying in the range from θ to $\theta + d\theta$ and ϕ to $\phi + d\phi$ whilst the angle defining the position of XY lies between ψ and $\psi + d\psi$. For the polycrystal the spontaneous magnetostriction in the direction OX is thus

$$\bar{\lambda} = \frac{1}{8\pi^2}\int_0^{\pi}\int_0^{2\pi}\int_0^{2\pi} \lambda \sin\theta \, d\theta \, d\phi \, d\psi. \qquad \ldots\ldots (6)$$

It is shown in the Appendix that if the values of $\alpha_1, \alpha_2, \alpha_3$ and $\beta_1, \beta_2, \beta_3$ given by equations (4) and (5) are inserted in equation (3) then, after integration, equation (6) may be written in the form

$$\bar{\lambda} = \left(h_0 + \frac{1}{5}h_1 - \frac{1}{5}h_2 + \frac{1}{5}h_3 + \frac{23}{105}h_4 - \frac{1}{35}h_5\right) + \left(\frac{2}{5}h_1 + \frac{3}{5}h_2 + \frac{12}{35}h_4 + \frac{3}{35}h_5\right)\cos^2\xi.$$

The corresponding spontaneous magnetostriction in the initial demagnetized state $\bar{\lambda}_i$ may be obtained by repeating the integration of equation (3) subject to the condition that the domains are magnetized parallel to directions of easy magnetization, the β's being again given by equations (5). When the easy directions are the quaternary axes, as in iron, the result is

$$\bar{\lambda}_i = h_0 + \tfrac{1}{3}h_1 + \tfrac{1}{3}h_4$$

whilst when the easy directions are the ternary axes, as in nickel,

$$\bar{\lambda}_i = h_0 + \tfrac{1}{3}h_1 + \tfrac{1}{3}h_3 + \tfrac{1}{3}h_4.$$

In neither case does the value of $\bar{\lambda}_i$ depend on assuming that the domains in each crystallite are initially divided *equally* between the various easy directions. Thus the fractional change in length of an ideal polycrystal between the demagnetized state and saturation is given by

$$dl/l = P + Q\cos^2\xi \qquad \ldots\ldots (7)$$

where

$$Q = \frac{2}{5}h_1 + \frac{3}{5}h_2 + \frac{12}{35}h_4 + \frac{3}{35}h_5 \qquad \ldots\ldots (8)$$

and where, for a material of positive anisotropy,

$$P = -\frac{2}{15}h_1 - \frac{1}{5}h_2 + \frac{1}{5}h_3 - \frac{4}{35}h_4 - \frac{1}{35}h_5$$

and, for a material of negative anisotropy,

$$P = -\frac{2}{15}h_1 - \frac{1}{5}h_2 - \frac{2}{15}h_3 - \frac{4}{35}h_4 - \frac{1}{35}h_5.$$

It may be observed that in neither case can equation (7) be put into the form of equation (2).

§ 3. HEXAGONAL CRYSTALS

The hexagonal case, which is applicable for example to cobalt and gadolinium, does not appear to have been considered previously. The axes x_1, x_2, x_3 may now be assumed to be the $[1\bar{2}{\cdot}0]$, $[10{\cdot}0]$ and $[00{\cdot}1]$ crystallographic axes respectively. In order to include a term which is characteristic of hexagonal symmetry, the expression for λ must, like equation (3), be of at least the fourth order in the α's. Such an expression was first derived by Mason (1954) and, when two additional terms which are independent of the αs are included (Birss 1958), Mason's expression becomes

$$\begin{aligned}\lambda = {} & A[2\alpha_1\alpha_2\beta_1 + (\alpha_1^2 - \alpha_2^2)\beta_2]^2 \\ & + B\alpha_3^2[(\alpha_1\beta_1 + \alpha_2\beta_2)^2 - (\alpha_1\beta_2 - \alpha_2\beta_1)^2] \\ & + C[(\alpha_1\beta_1 + \alpha_2\beta_2)^2 - (\alpha_1\beta_2 - \alpha_2\beta_1)^2] \\ & + D(1-\alpha_3^2)(1-\beta_3^2) + E\alpha_3^2\beta_3^2(1-\alpha_3^2) \\ & + F\alpha_3^2(1-\alpha_3^2) + G\beta_3^2(1-\alpha_3^2) \\ & + H\alpha_3\beta_3(\alpha_1\beta_1 + \alpha_2\beta_2) + I\alpha_3^3\beta_3(\alpha_1\beta_1 + \alpha_2\beta_2) \\ & + J + K\beta_3^2. \qquad \text{......(9)}\end{aligned}$$

If the substitutions given by equations (4) and (5) are made in equation (9) then, after integration, equation (6) may be written in the form

$$\begin{aligned}\bar{\lambda} = {} & \left(\frac{16}{105}A - \frac{4}{105}B - \frac{4}{15}C + \frac{2}{5}D + \frac{4}{105}E + \frac{2}{15}F + \frac{4}{15}G - \frac{1}{15}H - \frac{1}{35}I + J + \frac{1}{3}K\right) \\ & + \left(\frac{8}{105}A + \frac{4}{35}B + \frac{4}{5}C + \frac{2}{15}D + \frac{2}{105}E - \frac{2}{15}G + \frac{1}{5}H + \frac{3}{35}I\right)\cos^2\xi.\end{aligned}$$

The corresponding spontaneous magnetostriction in the demagnetized state $\bar{\lambda}_1$ may be found by a similar procedure to that outlined for cubic crystals in § 2. For hexagonal materials for which the easy directions are parallel to the hexagonal axis,

$$\bar{\lambda}_1 = J + \tfrac{1}{3}K$$

whilst if the basal plane is a plane of easy magnetization

$$\bar{\lambda}_1 = \tfrac{1}{3}A + \tfrac{2}{3}D + \tfrac{1}{3}G + J + \tfrac{1}{3}K.$$

It may thus be seen that in either case the fractional change in length of an ideal polycrystal between the demagnetized state and saturation is again given by equation (7) where the corresponding values of P are respectively

$$P = \frac{16}{105}A - \frac{4}{105}B - \frac{4}{15}C + \frac{2}{5}D + \frac{4}{105}E + \frac{2}{15}F + \frac{4}{15}G - \frac{1}{15}H - \frac{1}{35}I$$

and ......(10)

$$P = -\frac{19}{105}A - \frac{4}{105}B - \frac{4}{15}C - \frac{4}{15}D + \frac{4}{105}E + \frac{2}{15}F - \frac{1}{15}G - \frac{1}{15}H - \frac{1}{35}I$$

and where Q is, in both cases, given by

$$Q = \frac{8}{105}A + \frac{4}{35}B + \frac{4}{5}C + \frac{2}{15}D + \frac{2}{105}E - \frac{2}{15}G + \frac{1}{5}H + \frac{3}{35}I. \qquad \text{......(11)}$$

Again it may be observed that in neither case can equation (7) be put into the form of equation (2).

§ 4. Discussion

Even in an ideal polycrystal with a random distribution of crystallites, the domains need not necessarily be distributed uniformly over all directions in the demagnetized state. A preferred domain orientation may arise either from shape anisotropy or from residual stresses in the polycrystalline specimen. It is therefore generally of little value to attempt a comparison of the theoretical and experimental values of the coefficient P of equation (7) until accurate measurements have been made on well-annealed and spherical polycrystalline specimens containing crystallites of no preferred shape. Such comparisons are, however, of some value for materials, such as cobalt, which have very high values of magnetic anisotropy. The coefficient Q may, of course, always be unambiguously determined from measurements at saturation.

For nickel the generally accepted (Lee 1955) value of Q is -51×10^{-6} whilst the value obtained from equation (8) by the substitution of the values (Bozorth and Hamming 1953)

$$h_1 = (-68{\cdot}8 \pm 3{\cdot}8) \times 10^{-6}, \qquad h_2 = (-36{\cdot}5 \pm 1{\cdot}9) \times 10^{-6}$$

$$h_4 = (-7{\cdot}5 \pm 5{\cdot}2) \times 10^{-6}, \qquad h_5 = (7{\cdot}7 \pm 3{\cdot}1) \times 10^{-6}$$

is $-51{\cdot}3 \times 10^{-6}$ with a probable error of $2{\cdot}6 \times 10^{-6}$.

For iron it is known (Carr and Smoluchowski 1951) that

$$h_1 = 31{\cdot}1 \times 10^{-6}, \qquad h_2 = -31{\cdot}8 \times 10^{-6}$$

and that the constants h_3, h_4, h_5 are negligible. The figure obtained for Q by inserting these values in equation (8) is $-6{\cdot}6 \times 10^{-6}$ which is in reasonable agreement with the figure of $-5{\cdot}6 \times 10^{-6}$ obtained from measurements at saturation on polycrystalline iron (Birss 1958).

At present there is no hexagonal material for which the constants of equation (9) have been measured. It is possible, however, by assuming cylindrical rather than hexagonal symmetry, to caculate the coefficients P and Q of equation (7) for cobalt using an expression for the spontaneous magnetostriction of the form (Lee 1955)

$$\begin{aligned}\lambda = k_1\beta_3^2(\alpha_3^2 - 1) &+ k_2(\alpha_1^2\beta_1^2 + \alpha_2^2\beta_2^2) \\ &+ k_3(\alpha_1^2\beta_2^2 + \alpha_2^2\beta_1^2) + 2(k_2 - k_3)\alpha_1\alpha_2\beta_1\beta_2 \\ &+ 2k_4\alpha_3\beta_3(\alpha_1\beta_1 + \alpha_2\beta_2) + J + K\beta_3^2\end{aligned}$$

and the experimental values (Bozorth and Sherwood 1954)

$$k_1 = -110 \times 10^{-6}, \qquad k_2 = -45 \times 10^{-6}$$

$$k_3 = -95 \times 10^{-6}, \qquad 2k_4 = -465 \times 10^{-6}.$$

The theoretical expressions corresponding to equations (10) and (11) are then

$$P = -\frac{4}{15}k_1 + \frac{1}{15}k_2 + \frac{1}{3}k_3 - \frac{2}{15}k_4$$

$$Q = \frac{2}{15}k_1 + \frac{7}{15}k_2 - \frac{1}{3}k_3 + \frac{2}{5}k_4$$

and the figures obtained by inserting the experimental values of $k_1 \ldots k_4$ in these expressions are $P = 25{\cdot}7 \times 10^{-6}$ and $Q = -97{\cdot}0 \times 10^{-6}$. These figures appear to be in reasonable agreement with observations on polycrystalline cobalt but as yet no accurate values have been obtained because such large fields must be applied to saturate polycrystalline specimens. The work of Nishiyama (1929), for example, who measured the longitudinal and transverse magnetostriction of polycrystalline cobalt in magnetic fields of up to 7000 Oe, shows that $P > 13 \times 10^{-6}$, $Q < -53 \times 10^{-6}$ and that $P + Q \simeq -60 \times 10^{-6}$. It may be observed in conclusion that, if the value for P deduced from the single crystal measurements is compared with $-\frac{1}{3}Q = 32{\cdot}3 \times 10^{-6}$, it may be seen that the saturation magnetostriction of polycrystalline cobalt is unlikely to conform even approximately to equation (2).

REFERENCES

Becker, R., and Döring, W., 1939, *Ferromagnetismus* (Berlin: Springer) (Photo-lithoprint reproduction, 1943, Ann Arbor, Michigan: Edwards Brothers).
Bickford, L. R., Pappis, J., and Stull, J. L., 1955, *Phys. Rev.*, **99**, 1210.
Birss, R. R., 1957, *Proc. Phys. Soc.* B, **70**, 1093.
—— 1958, *Thesis*, University of Nottingham.
Bozorth, R. M., and Hamming, R. W., 1953, *Phys. Rev.*, **89**, 865.
Bozorth, R. M., and Sherwood, R. C., 1954, *Phys. Rev.*, **94**, 1439.
Carr, W. J., and Smoluchowski, R., 1951, *Phys. Rev.*, **83**, 1236.
Lee, E. W., 1955, *Rep. Progr. Phys.*, **18**, 184 (London: Physical Society).
Mason, W. P., 1954, *Phys. Rev.*, **96**, 302.
Nishiyama, Z., 1929, *Sci. Rep. Tôhoku Univ.*, **18**, 341.
Vladimirsky, K. V., 1943, *C.R.Acad. Sci. U.R.S.S.*, **41**, 10.

APPENDIX

To facilitate the calculation of $\bar{\lambda}$ for cubic crystals, λ may be expressed in the form

$$\lambda = \sum_{i=0}^{5} B_i S_i$$

where $S_0 \ldots S_5$ are the angular functions occurring in equation (3) associated respectively with the coefficients h_0, h_1, $2h_2$, $(h_3 + \frac{2}{3}h_4)$, h_4 and $2h_5$. The quantity $\bar{\lambda}$ may then be evaluated from equation (6) by separate integration of the functions S_i. If

$$I_i = \frac{1}{8\pi^2} \int_0^{\pi} \int_0^{2\pi} \int_0^{2\pi} S_i \sin\theta \, d\theta \, d\phi \, d\psi$$

it may be seen that $I_0 = 1$, and the evaluation of the remaining I_i is considerably simplified by the fact that many of the terms occurring in the S_i integrate to zero. Using equations (4) and (5), the quantities $I_1 \ldots I_5$ may be evaluated as follows.

$$\underline{B_1 S_1 = B_1(\alpha_1^2\beta_1^2 + \alpha_2^2\beta_2^2 + \alpha_3^2\beta_3^2)}$$

The terms in S_1 which do not integrate to zero are

$$\underline{\cos^2\xi}\,(1 - 2\sin^2\theta\cos^2\theta - 2\sin^4\theta\sin^2\phi\cos^2\phi) + \underline{\sin^2\xi}\,(\sin^2\theta\cos^2\theta\cos^4\phi\cos^2\psi$$
$$+ \sin^2\theta\cos^2\theta\sin^4\phi\cos^2\psi + \sin^2\theta\cos^2\theta\cos^2\psi + 2\sin^2\theta\sin^2\phi\cos^2\phi\sin^2\psi)$$

$$8I_1 = \cos^2\xi\left[8 - \frac{32}{15} - \frac{16}{15}\right] + \sin^2\xi\left[\frac{1}{5} + \frac{1}{5} + \frac{8}{15} + \frac{2}{3}\right],$$

$$I_1 = \frac{1}{5} + \frac{2}{5}\cos^2\xi.$$

$$\underline{B_2S_2 = B_2(\alpha_1\alpha_2\beta_1\beta_2 + \alpha_2\alpha_3\beta_2\beta_3 + \alpha_3\alpha_1\beta_3\beta_1)}$$

The terms in S_2 which do not integrate to zero are

$$\begin{aligned}&\cos^2\xi\,(\sin^2\theta\cos^2\theta + \sin^4\theta\sin^2\phi\cos^2\phi) + \sin^2\xi\,(\sin^2\theta\cos^2\theta\sin^2\phi\cos^2\phi\cos^2\psi\\ &\qquad - \sin^2\theta\sin^2\phi\cos^2\phi\sin^2\psi - \sin^2\theta\cos^2\theta\cos^2\psi)\end{aligned}$$

$$8I_2 = \cos^2\xi\left[\frac{16}{15} + \frac{8}{15}\right] + \sin^2\xi\left[\frac{1}{15} - \frac{1}{3} - \frac{8}{15}\right]$$

$$I_2 = -\frac{1}{10} + \frac{3}{10}\cos^2\xi.$$

$$\underline{B_3S_3 = B_3({\alpha_1}^2{\alpha_2}^2 + {\alpha_2}^2{\alpha_3}^2 + {\alpha_3}^2{\alpha_1}^2)}$$

The terms in S_3 which do not integrate to zero are

$$\begin{aligned}&\underline{\cos^4\xi}(\sin^4\theta\sin^2\phi\cos^2\phi + \sin^2\theta\cos^2\theta) + \underline{\sin^2\xi\cos^2\xi}\,(4\sin^2\theta\cos^2\theta\sin^2\phi\cos^2\phi\cos^2\psi\\
&\qquad + \sin^2\theta\sin^4\phi\sin^2\psi + \sin^2\theta\cos^4\phi\sin^2\psi\\
&\qquad - 2\sin^2\theta\sin^2\phi\cos^2\phi\sin^2\psi + \cos^4\theta\sin^2\phi\cos^2\psi\\
&\qquad + \cos^2\theta\cos^2\phi\sin^2\psi + \sin^4\theta\sin^2\phi\cos^2\psi\\
&\qquad - 2\sin^2\theta\cos^2\theta\sin^2\phi\cos^2\psi + \cos^4\theta\cos^2\phi\cos^2\psi\\
&\qquad + \cos^2\theta\sin^2\phi\sin^2\psi + \sin^4\theta\cos^2\phi\cos^2\psi\\
&\qquad - 2\sin^2\theta\cos^2\theta\cos^2\phi\cos^2\psi + 2\sin^2\theta\cos^2\theta\sin^2\phi\cos^2\phi\cos^2\psi\\
&\qquad - 2\sin^2\theta\sin^2\phi\cos^2\phi\sin^2\psi - 2\sin^2\theta\cos^2\theta\sin^2\phi\cos^2\psi\\
&\qquad - 2\sin^2\theta\cos^2\theta\cos^2\phi\cos^2\psi)\\
&\qquad + \underline{\sin^4\xi}(\cos^4\theta\sin^2\phi\cos^2\phi\cos^4\psi + \sin^2\phi\cos^2\phi\sin^4\psi\\
&\qquad + \cos^2\theta\cos^4\phi\sin^2\psi\cos^2\psi + \cos^2\theta\sin^4\phi\sin^2\psi\cos^2\psi\\
&\qquad - 4\cos^2\theta\sin^2\phi\cos^2\phi\sin^2\psi\cos^2\psi + \sin^2\theta\sin^2\psi\cos^2\psi\\
&\qquad\qquad + \sin^2\theta\cos^2\theta\cos^4\psi)\end{aligned}$$

$$\begin{aligned}8I_3 = {}&\cos^4\xi\left[\frac{8}{15} + \frac{16}{15}\right] + \sin^2\xi\cos^2\xi\left[\frac{3}{40} + \frac{3}{8} + \frac{1}{8} + \frac{1}{8} - \frac{1}{6} + \frac{2}{3} + \frac{2}{5}\right]\\
&+ \sin^4\xi\left[\frac{4}{15} + 1 + 1 - \frac{2}{3} + \frac{2}{5} + \frac{2}{3} + \frac{16}{15} - \frac{8}{15} + \frac{2}{5} + \frac{2}{3} + \frac{16}{15} - \frac{8}{15} + \frac{2}{15}\right.\\
&\qquad\left. - \frac{2}{3} - \frac{8}{15} - \frac{8}{15}\right]\end{aligned}$$

$$\begin{aligned}I_3 &= \frac{1}{5}(\cos^4\xi + 2\sin^2\xi\cos^2\xi + \sin^4\xi)\\ &= \frac{1}{5}.\end{aligned}$$

$$\underline{B_4S_4 = B_4({\alpha_1}^4{\beta_1}^2 + {\alpha_2}^4{\beta_2}^2 + {\alpha_3}^4{\beta_3}^2)}$$

The terms in S_4 which do not integrate to zero are

$$\begin{aligned}&\underline{\cos^4\xi}\,(\sin^6\theta\cos^6\phi + \sin^6\theta\sin^6\phi + \cos^6\theta) + \underline{\sin^2\xi\cos^2\xi}(6\sin^4\theta\cos^2\theta\cos^6\phi\cos^2\psi\\
&\qquad + 6\sin^4\theta\cos^2\theta\sin^6\phi\cos^2\psi + 6\sin^4\theta\cos^2\theta\cos^6\phi\cos^2\psi\\
&\qquad + 6\sin^2\theta\cos^4\theta\cos^2\psi) + \underline{\sin^4\xi}(\sin^2\theta\cos^4\theta\cos^6\phi\cos^4\psi\\
&\qquad + 6\sin^2\theta\cos^2\theta\sin^2\phi\cos^2\phi\sin^2\psi\cos^2\psi + \sin^2\theta\sin^2\phi\cos^2\phi\sin^4\psi\\
&\qquad\qquad + \sin^2\theta\cos^4\theta\sin^6\phi\cos^4\psi + \sin^4\theta\cos^2\theta\cos^4\psi)\end{aligned}$$

$$8I_4=\cos^4\xi\left[\frac{8}{7}+\frac{8}{7}+\frac{8}{7}\right]+\sin^2\xi\cos^2\xi\left[\frac{12}{21}+\frac{12}{21}+\frac{24}{15}+\frac{48}{35}\right]$$
$$+\sin^4\xi\left[\frac{3}{56}+\frac{1}{10}+\frac{1}{4}+\frac{3}{56}+\frac{8}{35}\right]$$
$$I_4=\frac{1}{35}(15\cos^4\xi+18\sin^2\xi\cos^2\xi+3\sin^4\xi)$$
$$=\frac{3}{35}(1+4\cos^2\xi).$$

$$\underline{B_5S_5=B_5(\alpha_1\alpha_2\alpha_3{}^2\beta_1\beta_2+\alpha_2\alpha_3\alpha_1{}^2\beta_2\beta_3+\alpha_3\alpha_1\alpha_2{}^2\beta_3\beta_1)}$$

The terms in S_5 which do not integrate to zero are

$$\underline{\cos^4\xi}(3\sin^4\theta\cos^2\theta\sin^2\phi\cos^2\phi)+\underline{\sin^2\xi\cos^2\xi}(\sin^2\theta\cos^2\theta\sin^4\phi\sin^2\psi$$
$$+\sin^2\theta\cos^2\theta\cos^4\phi\sin^2\psi-10\sin^4\theta\cos^2\theta\sin^2\phi\cos^2\phi\cos^2\psi$$
$$+7\sin^2\theta\cos^4\theta\sin^2\phi\cos^2\phi\cos^2\psi-5\sin^2\theta\cos^2\theta\sin^2\phi\cos^2\phi\sin^2\psi$$
$$+\sin^6\theta\sin^2\phi\cos^2\phi\cos^2\psi)+\underline{\sin^4\xi}(\sin^4\theta\cos^2\theta\sin^2\phi\cos^2\phi\cos^4\psi$$
$$-\sin^4\theta\sin^2\phi\cos^2\phi\sin^2\psi\cos^2\psi+4\sin^2\theta\cos^2\theta\sin^2\phi\cos^2\phi\sin^2\psi\cos^2\psi$$
$$-2\sin^2\theta\cos^4\theta\sin^2\phi\cos^2\phi\cos^4\psi-\sin^2\theta\cos^2\theta\sin^4\phi\sin^2\psi\cos^2\psi$$
$$-\sin^2\theta\cos^2\theta\cos^4\phi\sin^2\psi\cos^2\psi),$$

$$8I_5=\cos^4\xi\left[\frac{8}{35}\right]+\sin^2\xi\cos^2\xi\left[\frac{1}{5}+\frac{1}{5}-\frac{8}{21}+\frac{1}{5}-\frac{1}{3}+\frac{8}{35}\right]$$
$$+\sin^4\xi\left[\frac{1}{35}-\frac{1}{15}+\frac{1}{15}-\frac{3}{70}-\frac{1}{20}-\frac{1}{20}\right]$$
$$I_5=\frac{1}{70}(2\cos^4\xi+\sin^2\xi\cos^2\xi-\sin^4\xi)$$
$$=\frac{1}{70}(-1+3\cos^2\xi).$$

These values of the I_i permit $\bar{\lambda}$ to be expressed in terms of the coefficients B_i. Thus

$$\bar{\lambda}=\sum_{i=0}^{5}B_iS_i=\left(B_0+\frac{1}{5}B_1-\frac{1}{10}B_2+\frac{1}{5}B_3+\frac{3}{35}B_4-\frac{1}{70}B_5\right)$$
$$+\left(\frac{2}{5}B_1+\frac{3}{10}B_2+\frac{12}{35}B_4+\frac{3}{70}B_5\right)\cos^2\xi.$$

In terms of the coefficients $h_0\ldots h_5$ occurring in equation (3) $\bar{\lambda}$ is therefore given by

$$\bar{\lambda}=\left(h_0+\frac{1}{5}h_1-\frac{1}{5}h_2+\frac{1}{5}h_3+\frac{23}{105}h_4-\frac{1}{35}h_5\right)+\left(\frac{2}{5}h_1+\frac{3}{5}h_2+\frac{12}{35}h_4+\frac{3}{35}h_5\right)\cos^2\xi.$$

The Thermomagnetic Behaviour of Pure Nickel Ferrite

By L. F. BATES and H. CLOW
University of Nottingham

MS. received 6th July 1959

Abstract. The small heat changes accompanying the magnetization of pure nickel ferrite have been measured for a rod specimen at − 10° and 18°c. By making use of the correctness of current theory for thermal changes accompanying the magnetization of ferromagnetic substances in high fields, the results have been analysed, and some slight support found for the Lilley disperse field theory.

---

§ 1. Introduction

The thermal changes which accompany changes in the magnetization of a ferromagnetic material in low and moderate fields are usually discussed (cf. Bates and Sansom 1959) in terms of a theory by Stoner and Rhodes (1949), who showed that the reversible component of a recorded thermal change $\Delta Q'$ accompanying a field change from H_1 to H is given by

$$[\Delta Q'] = a\int_{H_1}^{H} d(HI) + b\int_{H_1}^{H} H\,dI \qquad \ldots\ldots(1)$$

where I is the intensity of magnetization and a and b are constants for the material. The first term on the right-hand side of equation (1) gives the thermal change due to the change in the intrinsic magnetization I_0 the constant a being equal to $-(T/I_0)(\partial I_0/\partial T)$. The second term gives the thermal change due to reversible rotation processes alone, and b is equal to $(T/K_1)(\partial K_1/\partial T)$ where K_1 is the appropriate anisotropy constant.

The constant a is usually positive, so that for a field decreasing from a high negative value the integral is negative, since by convention we always start with a field described as negative. Consequently, the first terms usually represent a cooling. As rotational processes are very small in high fields, the second term is very small or zero, if a and b are of reasonable magnitude. Hence, an initial cooling of the specimen is expected.

In low fields, rotational processes are usually important and the second term is no longer small. The sign of b depends on whether K_1 increases or decreases with rise in temperature. In low fields, especially around the coercive point H_c, irreversible processes occur, and equation (1) does not apply. Therefore, we subtract from the observed thermal changes those which are due to changes in intrinsic magnetization, and we write

$$Q'' = \sum dQ' - a\int d(HI) = \int b'' H\,dI. \qquad \ldots\ldots(2)$$

In equation (2), b'' corresponds to b in equation (1), but it is placed within the integral sign to allow for possible variation when calculated from experimental results.

Bates and Sherry (1955) endeavoured to make full advantage of the above theory by separating reversible and irreversible thermal changes by the method of small backward changes, writing

$$\begin{aligned} Q_{\text{tot}} \text{ (total change)} &= Q' \text{ (reversible)} + Q' \text{ (irreversible)} \\ &= Q_{\text{r}}' + Q_{\text{ir}}'. \qquad \ldots\ldots(3) \end{aligned}$$

We may further denote the energy changes due to rotations by Q_{r}''; these may be obtained by subtracting from Q_{r}' the effects due to changes in intrinsic magnetization. Hence, the Stoner and Rhodes theory may be tested by the consistency of the coefficient b'', defined as $\Delta Q_{\text{r}}'/\Delta(\int H\,dI_{\text{r}})$. We are greatly concerned in this work with the comparison of b and b''.

The effects of processes other than rotation against crystalline anisotropy on the value of b'' may be found by the procedure of Teale and Rowlands (1957) by writing

$$\left[\Delta Q_{\text{r}}'\right]_{H_1}^{H} = b\int_{H_1}^{H} H\,dI_{\text{r}} + a[HI - H_1 I_1]. \qquad \ldots\ldots(4)$$

The second term on the right in equation (4) now gives the contribution of the *magnetocaloric effect* to the thermal changes, both reversible and irreversible. The first term applies, as before, to reversible changes only and is determined by the kinds of magnetization processes which occur during the change from H_1 to H.

The anisotropy constant K_1 of nickel ferrite varies with temperature in such a way that it is worthwhile to study its thermomagnetic properties. Healey (1952) found that K_1 has a minimum, negative, value at -10°c. Consequently, at that temperature there should be no magnetothermal effects due to rotation of domain vectors against crystalline anisotropy and, therefore, any observed thermal changes due to wall movements should be clearly defined. It would be expected that b'' would vary with the field since, above the knee of the magnetization curve, rotations now unaccompanied by measurable heat changes account for very large changes in $\int H\,dI_{\text{r}}$.

Moreover, Christoffel (1957) found a 'dip' in the Q'' curve of a specimen of nickel ferrite, whose grain size was about 5 to 10 μ, at room temperature, and it is interesting to know whether a 'dip' is present at -10°c, when $(T/K_1)(\partial K_1/\partial T)$ is zero. Hence, thermal curves were taken at 18°c and at -10°c.

§ 2. EXPERIMENTAL DETAILS

A sample of pure nickel ferrite was available in the form of a rod some 0·38 cm in diameter and 19·3 cm long, supplied by the Philips Research Laboratories, Eindhoven. It had been prepared by milling Fe_2O_3 and $NiCO_3$, prefiring at 1000°c being followed by thorough milling. The rod was formed by extrusion and sintered for 2 hours at 1300°c. Chemical analysis showed it to contain 24·9 and 47·3% of Ni and Fe by weight, respectively, whereas the corresponding percentages for pure $NiFe_2O_4$ are 25·0 and 47·6. The grain size was approximately 5 μ. The d.c. resistivity of the specimen was 5×10^6 ohm cm. The overall density, 4·85 g cm^{-3}, corresponding to 90% packing, was low compared with 5·38 for pure nickel ferrite because of a few large cracks running down the middle of the rod rather than because of general porosity.

The length to diameter ratio of the rod was 50·4, and the corresponding demagnetization factor 0·015 (Bozorth and Chapin 1942). The (I, H) curves were moderately square, with a retentivity of $0{\cdot}65 I_s$ for the maximum fields used below. At 18°c, I_s was 205 gauss and the coercivity was 8·6 Oe, the hysteresis loss of 5650 erg cm^{-3} per cycle being rather large for a ferrite specimen.

The thermal Q_{tot}' and Q_r' curves taken by the direct method (cf. Bates and Sherry 1955) are given in figure 1, where the sensitivity of the apparatus was 43 erg cm^{-3} per mm scale deflection for high field measurements, and 10 erg cm^{-3} per mm for low field measurements. The measuring system could not be calibrated directly, and the above values were obtained by fitting the experimental results to the Stoner and Rhodes equation (1) at high fields, where it undoubtedly holds. The measured value of a was $+0{\cdot}23$, while from Healey's results $(T/K_1)(\partial K_1/\partial T)$ was $-0{\cdot}26$. Using these values in equation (1) exact agreement was obtained with the measured thermal changes over the range -950 to -300 Oe. A check value of $-0{\cdot}45$ for $(T/K_1)(\partial K_1/\partial T)$ for the specimen was obtained by measuring $\int H\,dI$ over the magnetization range $0{\cdot}86 I_s$ to saturation at the temperatures $-10°$, 18° and 38°c respectively. But good agreement between the two values of $(T/K_1)(\partial K_1/\partial T)$ was not expected as evidence of wall movement was found in high fields.

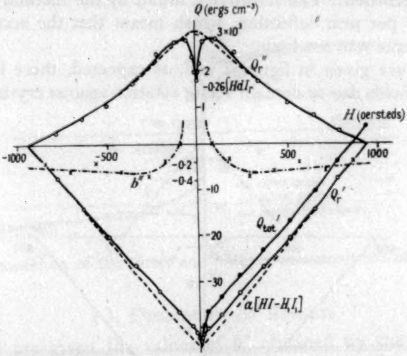

Figure 1. Curve of thermal changes at 18°c measured by the direct method; Q_{tot}' ' total ' measured changes; Q_r' reversible part of changes.

The shape of the Q_{tot}' curve is determined mainly by the magnetocaloric (intrinsic magnetization) effect. The observed cooling from high (negative) fields down to -300 Oe is, as already stated, in good agreement with the Stoner and Rhodes theory, and a large ' dip ' is apparent in fields below 100 Oe. The value of b'' changes gradually from the value of $(T/K_1)(\partial K_1/\partial T)$ in high fields to a slightly larger (negative) value in a field of 300 Oe. In lower fields b'' becomes positive, because of the presence of the ' dip ', and reaches a value of about $+2$ in fields smaller than 50 Oe.

For the thermal measurements at -10°c, the specimen and its thermocouple leads were placed inside a glass tube within a Dewar tube which lined the solenoid.

Between the surfaces of the glass tube and Dewar a mixture of frozen water and alcohol was packed. The thermal capacity of the cold portion of the system was increased by filling the glass tube with transformer oil, so that the temperature of the whole rose only by about 1°c per hour. The mean temperature of the specimen was measured by a copper–constantin thermocouple. The specimen was first cooled to about -12°c and readings commenced after about one hour, so that readings were taken at temperatures between -11° and -9°c. Temperature drift of the recording system was troublesome and could not be entirely prevented by feeding an opposing current into the recording system from a thermocouple on an electrically heated bar. In view of the experimental difficulties only the Q_r' curve was recorded. The sensitivity, found by the method described above, was 50 erg cm^{-3} per mm deflection, which meant that the accuracy of the low field measurements was not high.

The results are given in figure 2 and, as expected, there is no appreciable heating in high fields due to domain vector rotation against crystalline anisotropy.

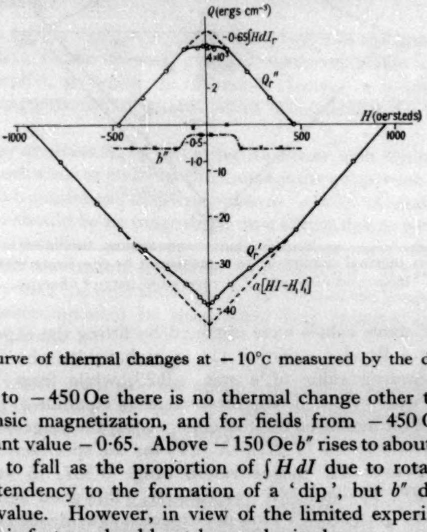

Figure 2. Curve of thermal changes at -10°c measured by the direct method.

From -950 Oe to -450 Oe there is no thermal change other than that due to change in intrinsic magnetization, and for fields from -450 Oe to -150 Oe, b'' has the constant value $-0{\cdot}65$. Above -150 Oe b'' rises to about $-0{\cdot}3$, although it was expected to fall as the proportion of $\int H\,dI$ due to rotations decreased. There is some tendency to the formation of a 'dip', but b'' does not actually take a positive value. However, in view of the limited experimental accuracy in this region, this feature should not be emphasized.

Measurements at 18°c were also made by an indirect method (see Tebble, Wood and Florentin 1957). The specimen was heated and cooled by a circulating liquid method. When the temperature of the specimen was changed in the course of about a minute by causing oil of appropriate temperature to replace oil already around the specimen, the corresponding change in magnetization was measured by a search coil connected to a sensitive electronic fluxmeter. This has undoubted limitations in the case of poorly conducting ferrites, where one cannot be sure that the specimen is uniformly heated throughout its volume. Consistent results were obtained, but the recorded magnetization changes were only half as great as were expected. Consequently, the results were again calibrated by application of the Stoner and Rhodes theory, when the sensitivity was found to be 0·0285 erg cm^{-3} Oe^{-1} per mm scale deflection. In figure 3 the results are compared with those expected for rotation processes only on the Stoner and Rhodes theory, and also with the measurements obtained by the direct method. There is agreement between the three curves from -950 down to about -400 Oe, but in lower field regions the indirect method gives smaller values of $\partial Q'/\partial H$ than does the Stoner and Rhodes theory, while here the direct method gives larger values, corresponding to the 'dip' phenomenon.

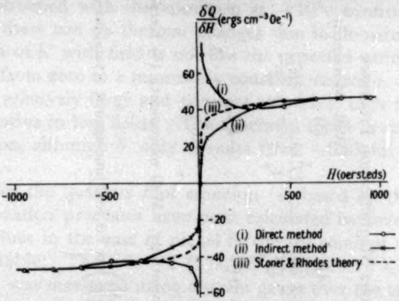

Figure 3. Comparison of the direct and indirect measurements of $\partial Q/\partial H$ at 18°c.

§ 3. DISCUSSION OF RESULTS

In figure 4 are given the values of b'' obtained by the two methods of measurement at 18°c. In fields from -950 to -300 Oe the values agree very closely. In the higher fields b'' is $-0{\cdot}26$, the value of $(T/K_1)(\partial K_1/\partial T)$, in exact agreement with the Stoner and Rhodes theory. There is at first a steady change in b'' which is probably due to wall movement, although the field region would appear *a priori* rather high for such movement to occur. However, there may be within the polycrystalline material certain grains exposed to peculiar demagnetizing fields, and these could account for the change. But, in the low field regions where wall movement predominates the values of b'' found by the two methods are greatly different, perhaps because the method of backward steps on which determinations of Q_r' depend is valid for small steps only, and it is virtually impossible to make the steps sufficiently small.

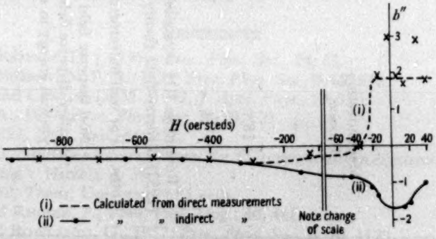

Figure 4. Values of b''.

Values of b for $NiFe_2O_4$ Specimen for various Magnetization Processes

Magnetization Process	Rotations (1)	Rotations (2)	Rotations (3)	Wall Movement (4)	Wall Movement (5)	Wall Movement (6)
—	$\frac{T}{K_1}\frac{\partial K_1}{\partial T}$	$\frac{T}{\lambda_s}\frac{\partial \lambda_s}{\partial T}$	$\frac{2T}{I_0}\frac{\partial I_0}{\partial T}$	$\frac{T}{\gamma}\frac{\partial \gamma}{\partial T}$	$\frac{2T}{\lambda_s}\frac{\partial \lambda_s}{\partial T}-\frac{T}{K}\frac{\partial K_1}{\partial T}$	$\frac{T}{2\lambda_s}\frac{\partial \lambda_s}{\partial T}+\frac{T}{I_0}\frac{\partial I_0}{\partial T}$
+18°c	−0·26	−0·7	−0·46	−0·07	−1·2	−0·58
−10°c	0	−0·45	−0·44	0	−0·9	−0·45

Rotations: (1) crystalline anisotropy; (2) strain anisotropy; (3) shape anisotropy. Wall movement: (4) Kersten (1943); (5) Lilley (1952) disperse-field theory; (6) strain theory.

Notes. For wall movement according to Néel disperse field theory $b=\frac{T}{K_1}\left(\frac{\partial K_1}{\partial T}\right)$ as for rotations against crystalline anisotropy.

Néel disperse field theory: non-magnetic inclusions.
Lilley disperse field theory: strain inclusions.
γ = wall energy in erg cm^{-2}.

However, as in high fields where the two methods give similar results, there is the same downward slope of the b'' values in figure 4, one feels inclined to trust the indirect method rather than the direct method in low fields where the former values continue to fall. Again, there is slightly less spread in the b'' values obtained by the indirect method. If this view is accepted, it would follow that the 'dip' phenomenon is due to the failure of the backward step method to separate reversible from irreversible changes, although one cannot see why this failure should give positive values of b''.

The results obtained with the specimen at -10°c confirm the theoretical expectation that there are no thermal changes due to domain vector rotation. But, the variation of b'' with field is not like the expected variation. Instead of falling gradually from zero to a reasonably constant, negative, value in low field regions, it has a relatively large and constant, negative, high field value which becomes less negative in low fields. The specimen tends therefore to show the 'dip' phenomenon, although b'' only changes from $-0{\cdot}65$ to $-0{\cdot}25$ and never becomes positive.

Expressions for the quantity b of equation (4) based on the assumption of specified magnetization processes have been calculated by several workers, and the numerical values in the case of nickel ferrite for some of these expressions are given in the table. The value of $(T/\lambda_s)(\partial\lambda_s/\partial T)$, where λ_s is the saturation magnetostriction, was measured using a strain gauge over the temperature range -70° to $+70$°c.

The Lilley disperse-field theory expression for b, namely $-1{\cdot}2$, gives the value nearest to b'' found by the indirect method of measurement, which lies between $-1{\cdot}5$ and $-2{\cdot}0$. As neither value is very accurate, the agreement is as good as can be expected. The measured value of b'' in high fields for the specimen at -10°c should be smaller than the appropriate calculated value of b as some contribution to the experimental value of $\int H\,dI_r$ is due to rotation processes. This value of b'' is $-0{\cdot}65$, and the only value in the table less than this is the value $-0{\cdot}9$ from the Lilley expression. We may therefore conclude from the above experiments there is some slight evidence in favour of the disperse field theory of magnetic coercivity.

ACKNOWLEDGMENTS

We are much indebted to Mr. Schulkes of the Philips Research Laboratories, Eindhoven, for the kind gift of the nickel ferrite rod. One of us (H. C.) thanks the Department of Scientific and Industrial Research for a maintenance allowance which enabled him to undertake the work.

REFERENCES

Bates, L. F., and Sansom, D. J., 1959, *Proc. Phys. Soc.*, **74,** 53.

Bates, L. F., and Sherry, N. P. R., 1955, *Proc. Phys. Soc.* B, **68,** 642.

Bozorth, R. M., and Chapin, D. M., 1942, *J. Appl. Phys.*, **13,** 320.

Christoffel, D. A., 1957, *Proc. Phys. Soc.* B, **70,** 623.

Healey, D. W., 1952, *Phys. Rev.*, **54,** 217.

Kersten, M., 1943, *Grundlagen einer Theorie der Ferromagnetischen Hysterese und Koerzitivkraft* (Leipzig : Hirzel), p. 36.

Lilley, B. A., 1952, *Thesis*, University of Leeds.

Stoner, E. C., and Rhodes, P., 1949, *Phil. Mag.*, **40,** 481.

Teale, R. W., and Rowlands, G., 1957, *Proc. Phys. Soc.* B, **70,** 1123.

Tebble, R. S., Wood, J. E., and Florentin, J. J., 1952, *Proc. Phys. Soc.* B, **65,** 858.

Momentum Distribution of Protons in Carbon

By J. D. DOWELL, W. R. FRISKEN, G. MARTELLI† AND
B. MUSGRAVE
Department of Physics, University of Birmingham

Communicated by P. B. Moon; MS. received 7th May 1959, *in final form* 15*th July* 1959

Abstract. Quasi-elastic interactions of 930 MeV protons with bound protons in carbon have been investigated, using a propane bubble chamber. A method has been devised to relate the measured scattering angles to the momenta of the bound nucleons. A Gaussian curve falling to 1/e at a momentum corresponding to a kinetic energy of 13 MeV has been fitted to the experimentally determined momentum distribution. The cross section for quasi-elastic reactions in carbon is found to be 46 ± 10 mbn, considerably higher than values which might be inferred from results of previous experiments.

§ 1. INTRODUCTION

THE aim of the work reported here is to investigate the internal momentum distribution of nucleons in carbon. Several workers have already described high energy scattering experiments yielding information about the structure of the nucleus in terms of this distribution. Such experiments can be divided into three main groups, according to the reaction involved: deuteron pick-up, meson production and quasi-elastic scattering. The interpretation of the results is usually based on the assumptions that an independent particle model for the nucleus is valid and that the interactions involve only the incident and struck particles, so that the presence of other nucleons has small or negligible effect. The evidence for the validity of these assumptions is quite strong in the case of quasi-elastic scattering, since the definite angle and energy relationships existing in the free nucleon–nucleon case are found experimentally to be replaced by distributions peaked about these values (Chamberlain and Segrè 1952). Gaussian momentum distributions have been found to give the best fit to most experimental values (Cladis, Hess and Moyer 1952, Wilcox and Moyer 1955), except perhaps in the region of high momentum components. A linear combination of two Gaussians has also been used to fit the experimental results (Selove 1955, 1956). However, since the tail of the distribution falls in the region where the above assumptions may not be valid and the corrections for background effects can be very large, most authors have been unable to give much reliable information about the high momentum values.

Chew–Goldberger distributions (Chew and Goldberger 1950) with parameters determined experimentally have also been used (Helmholz, McMillan and Sewell 1947), but they predict too many high momentum components. A Fermi gas model distribution (Block, Passman and Havens 1952, Henley and Huddlestone 1947) has been found to give too few.

---

† On leave of absence from the University of Pisa, Italy.

With the exception of that of Selove (1955, 1956), no experiment has been performed so far yielding the 1/e value (or its equivalent) of the distribution to better than about ± 3 MeV. The 1/e values obtained range between about 11 MeV and 20 MeV.

The disagreement amongst the results might perhaps be ascribed both to the inadequacies of the methods of deriving the distributions from the data and to the fact that the background is of a different kind in each case. This, combined with poor statistics, has prevented the reasons for the discrepancies from being isolated. Counters have been employed in each case, with the exception of the experiment of McEwen *et al.* (1957), where nuclear emulsions have been used.

The present research is concerned with the analysis of quasi-elastic interactions of 930 MeV protons with the protons bound in the carbon nuclei present in a propane bubble chamber. This method has proved particularly satisfactory, since accurate measurements of the directions of both scattered particles can be made, whilst contamination from other complex nuclei is not present.

§ 2. EXPERIMENTAL PROCEDURE

A propane bubble chamber having a useful volume 9 in. × 3 in. × $2\frac{1}{2}$ in. was placed in a beam of 950 MeV protons from the Birmingham proton synchrotron. Magnetic selection of the beam and the use of collimators ensured an energy spread not exceeding ± 20 MeV. The beam entered the central part of the chamber parallel to the main axis, through a thin window. The beam intensity was adjusted, within the limits set by amplitude fluctuations and time jitter, so that about ten protons per pulse traversed the chamber, since this number of tracks is convenient for scanning and measuring purposes. The cycling time of the chamber was of the order of 2 seconds, and since the synchrotron produces a pulse every 10 seconds, the remaining 8 seconds allowed the thermal equilibrium to be re-established.

A more detailed description of the bubble chamber and of the methods of scanning and measurement is given elsewhere (Musgrave 1958).

About 5000 stereo-photographs were taken, and 1200 events from protons moving parallel to the main beam direction, within 30′, were analysed. Scattering and azimuthal angles of each prong were measured. Ranges of particles stopping in the propane and, where possible, relative ionization density measurements have been used to provide auxiliary information.

§ 3. DYNAMICS OF THE QUASI-ELASTIC REACTIONS

3.1.

Before discussing the criteria which have been adopted to select the quasi-elastic events, we shall describe how the scattering angles of the quasi-elastic events have been used to calculate the momentum distribution of the protons in carbon.

In what follows, we have assumed the validity of the impulse approximation (Chew and Wick 1952), since the energy of the incident protons is high enough to justify this assumption.

We use the following notation (cf. figure 1): M is the mass of the proton (MeV), M_C the mass of the carbon nucleus, $\mathbf{p}$ the momentum of the incident proton, $\mathbf{q}$, $\mathbf{s}$ the momenta of the outgoing protons, $\mathbf{k}$ the momentum of the struck proton within the nucleus, before the collision; all quantities are referred to the laboratory system.

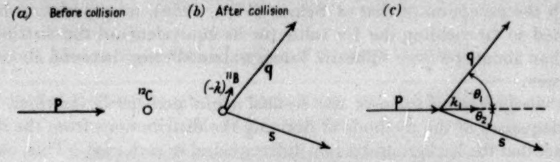

Figure 1. Dynamics of the quasi-elastic collision.

Under the above assumptions, the momentum acquired by the recoiling nucleus (^{11}B) will be just equal and opposite to $\mathbf{k}$. Therefore, we can write for conservation of momentum $\mathbf{p}=\mathbf{q}+\mathbf{s}+(-\mathbf{k})$ and for conservation of total energy $E_p+M_c=E_q+E_s+(M_c-M)+E_R$ where E_p, E_q, E_s are the total energies of protons having momenta $\mathbf{p}$, $\mathbf{q}$, $\mathbf{s}$ respectively and E_R is the energy given to the recoiling nucleus, as kinetic energy, binding energy, etc.

Hence

$$E_p+M-E_R=E_q+E_s \qquad \ldots\ldots(1)$$

and

$$\mathbf{p}+\mathbf{k}=\mathbf{q}+\mathbf{s}. \qquad \ldots\ldots(2)$$

Among the quantities which appear in these equations, $\mathbf{p}$ is known, the directions of $\mathbf{q}$ and $\mathbf{s}$ can be measured and a reasonable estimate of the value of E_R, which in any case is small compared with E_p+M, can be made. We are left with five unknowns (the magnitudes of $\mathbf{q}$ and $\mathbf{s}$ and the three components of $\mathbf{k}$) to be determined from four equations, so further approximation is required to solve the problem.

For this purpose we resolve $\mathbf{k}$ into three mutually perpendicular directions, with components k_1 and k_2 in the plane of $\mathbf{q}$ and $\mathbf{s}$, and with k_3 perpendicular to this plane. If k_1 is taken to be the component of $\mathbf{k}$ which is contained in the same plane as $\mathbf{p}$ and k_3, and if the effect of k_2 is ignored for the moment, equation (2) can be represented by the vector diagram given in figure 2.

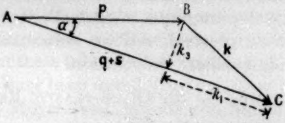

Figure 2. Non-coplanarity in quasi-elastic events.

Now k_3 is given by $k_3=p\sin\alpha$, where α is the angle of non-coplanarity (cf. figure 2). k_1 may be obtained from the equation

$$p\cos\alpha+k_1=|\mathbf{q}+\mathbf{s}|.$$

This describes an interaction where the bound proton, before the collision, is moving parallel to the incident one, which now has a momentum $p\cos\alpha$. Whichever of the suggested momentum distributions is chosen, the value of $\cos\alpha$ corresponding to the average value of k_3 comes to about 0·995. Therefore the above equation may be re-written as

$$p+k_1=\mathbf{q}+\mathbf{s}. \qquad \ldots\ldots(3)$$

Using relativistic mechanics, equation (1) may be re-written as

$$(p^2+M^2)^{1/2}+M-E_{\mathrm{R}}=(q^2+M^2)^{1/2}+(s^2+M^2)^{1/2}. \qquad \ldots\ldots(4)$$

From equation (3) we have (cf. figure 1)

$$p+k_1=q\cos\theta_1+s\cos\theta_2,$$
$$q\sin\theta_1=s\sin\theta_2=t, \quad \text{say,}$$

where t is the momentum transfer.

Therefore

$$q=t\operatorname{cosec}\theta_1; \quad s=t\operatorname{cosec}\theta_2$$

and

$$\begin{aligned} p+k_1&=t(\cot\theta_1+\cot\theta_2)\\ &=t(c_1+c_2) \quad \text{say.} \qquad \ldots\ldots(5)\end{aligned}$$

By putting the left-hand side of equation (4) equal to E, we obtain

$$t^4(c_1{}^2-c_2{}^2)^2-2E^2(c_1{}^2+c_2{}^2+2)t^2+E^2(E^2-4M^2)=0. \qquad \ldots\ldots(6)$$

This may be solved for t, which enables $p+k_1$ to be found from equations (5). For convenience, however, θ_1 is obtained in terms of θ_2. Equations (5) and (6) give:

$$c_1-c_2=\{A[B(c_1+c_2)^2+C]\}^{1/2} \qquad \ldots\ldots(7)$$

where

$$A=\frac{E^2}{(p+k_1)^2[(p+k_1)^2-E^2]}$$
$$B=(p+k_1)^2-(E^2-4M^2)$$

and

$$C=4(p+k_1)^2.$$

c_1-c_2 can be calculated in terms of c_1+c_2 for a series of values of k_1, and hence a family of curves relating θ_1 to θ_2 may be plotted. Some typical curves are given in figure 3. For each event a value of k_1 may be determined by interpolation between curves of this family. k_3 is obtained from the measured values of α. The resultant momentum $(k_1{}^2+k_3{}^2)^{1/2}$ can then be calculated in each case.

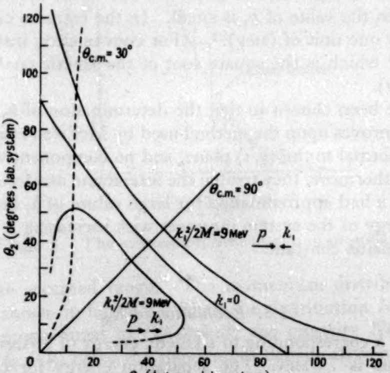

Figure 3. Relation between scattering and recoil angles, in quasi-elastic scattering.

3.2. *Effect of k_2*

Figure 4 shows the effect of the undetermined component k_2, which is to rotate the vector $\mathbf{q}+\mathbf{s}$ and to change the angles made by $\mathbf{q}$ and $\mathbf{s}$ with $\mathbf{p}$ by an amount β, where β has the same range of values as α. This increases one angle and decreases the other by the same amount, so that the effect is to move a point on the (θ_1, θ_2) plane along a line of slope -1 (cf. figure 3). Consequently, the recorded change in the value of k_1 is small. In the extreme case the effect of k_2 may change k_1 by one unit of (MeV)$^{1/2}$. (For convenience, instead of plotting k, we plot $k/(2M)^{1/2}$ which is the square root of the kinetic energy corresponding to a momentum k).

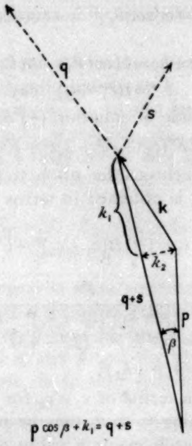

Figure 4. Effect of the momentum component k_2.

k_1 and k_3 have been chosen so that the determination of k_3 is not affected by k_1 or k_2. This improves upon the method used by McEwen *et al.* (1957) where k_3 was not defined normal to the (q, s) plane, and no component was independently determined. Furthermore, they treated the interaction as a free collision between protons, which is a bad approximation for large values of k, because this implies that the total energy of the system increases with increasing k, whereas the total energy in fact remains constant.

3.3. *Evaluation of E_R*

For a value of k corresponding to a kinetic energy of 80 MeV the recoil energy of the ^{11}B nucleus is 7·3 MeV. The separation energy for carbon is 8·5 MeV. Therefore, on the average, the value of E_R is of the order of 10 MeV, and may be neglected.

§ 4. SELECTION OF EVENTS

To select quasi-elastic events, the following limits have been imposed:

(*a*) The resultant momentum $(k_1^2 + k_3^2)^{1/2}$ must be less than that corresponding to a kinetic energy of 80 Mev. Other authors find this value to be well out on the tail of the distribution. This automatically imposes the condition $\alpha \leqslant 14°$.

(*b*) For the angles less than about 10° in the laboratory system (cf. figure 3), the determination of k_1 is likely to be rather inaccurate, because of both the large changes in slope and the uncertainties in the angular measurements. We must therefore impose an arbitrary angular limit for the acceptance of events, which is independent of k. An examination of p–p scattering data shows that the elastic and differential cross sections are relatively independent of k. Thus the limit may be chosen at a fixed angle in the centre of mass system which the two nucleons would have in the case of a free collision. We therefore reject all events to the left of the line $(\theta_{\text{c.m.}} = 30°)$ which is plotted on figure 3. The exact definition of this limit is not important, because only a few events are thus excluded.

It has not always been possible to use relative ionization density measurements as a reliable criterion for the identification of mesons; apart from 25 mesons which were identified in this way and 165 elastic hydrogen events,† all the remaining events were selected according to criteria (*a*) and (*b*) above. The correction for pions is considered in the next paragraph. 292 events were found to lie within the accepted range. The momentum distribution derived from these events is shown in figure 5. Since the distribution $N(k)$ of the resultant momentum is proportional to $P(k) 2\pi k\, dk$, the quantity $N(k)/2\pi k\, dk$ has been plotted against k, $P(k)$ being the momentum density distribution.

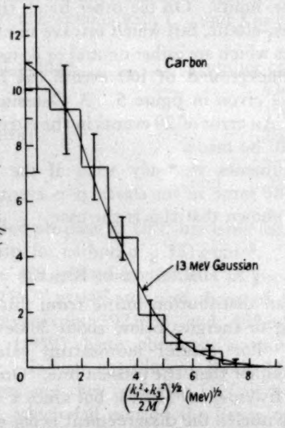

Figure 5. The momentum distribution of protons in carbon.

† An investigation of the p–p elastic events found during the same scanning, is reported in a separate paper (Dowell *et al.* 1959).

4.1. *Evaluation of Meson Background*

Meson production introduces an unavoidable contamination in the present experiment. In order to evaluate its magnitude, we have performed an analysis of 200 meson events from the experiment of Batson *et al.* (1959) on proton–proton scattering at 970 Mev. A representative sample of π^+ and π^0 events was studied and it was found that (*a*) 40% fell within the quasi-elastic selection limits, (*b*) the distribution of the apparent *k* for the events was flat within statistics.

The result (*a*) immediately enables a lower limit to be placed on the number of background meson events. From the values of the elastic and total p–p cross sections at this energy (Chen, Leavitt and Shapiro 1956), and from the number of elastic p–p events found (Dowell *et al.* 1959) during the same scanning, we estimate that about 190 meson-producing events occurred in free p–p collisions. Thus a minimum of 75 background events is obtained.

No figures are available for meson production for carbon at this energy, and at lower energies measurements have been made only at certain angles (Meshcheryakov *et al.* 1957). However, from considerations of the relative numbers of free hydrogen and carbon events, an additional background of 100 events has been estimated. This would bring the meson background to 175 events. This figure is an upper limit because we have assumed no reabsorption in the target nucleus.

The evaluation of background from carbon is necessarily crude. It is likely to be an overestimate because there are probably more quasi-elastic events which fall outside the selection limits. On the other hand, there may be some events which appear to be quasi-elastic, but which involve an evaporation of the nucleus into low energy particles which are either neutral or do not produce a visible track.

Therefore a total background of 160 events has been subtracted and the corrected distribution is given in figure 5. A Gaussian curve falling to 1/e at 13 Mev has been fitted. An error of 20 events in the estimation of the background will still allow this fit to be made.

The foregoing arguments are only valid if the scanning efficiency for background events is the same as for elastic p–p events; an azimuthal plot of background events has shown that this is the case.

§ 5. DISCUSSION OF RESULTS

The 13 Mev Gaussian distribution found from this experiment agrees, for momenta corresponding to energies below about 30 Mev, with that obtained by Selove (1955, 1956). For greater momentum values, however, Selove's distribution is slightly higher than the present one. Our distribution is broader than that found by McEwen *et al.* (1957), but since a high proportion of their events come from heavy nuclei, the disagreement is not surprising.

A Chew–Goldberger distribution gives poorer agreement with the present results than a Gaussian one. Although there is some uncertainty in the background correction, the former appears to predict too many high momentum components.

Brueckner, Eden and Francis (1955) have calculated momentum distributions for the shell model (independent particles in a potential well) using both a harmonic oscillator and a square well potential, and find that fewer high momentum values are predicted than experiments have shown. The high momenta can be accounted for by including strong two-body interactions in the nuclear ground state wave function, in addition to the potential well. In this way it is possible to derive momentum distributions agreeing with experiments, while still retaining the general features of the shell model.

If the high momenta are correctly accounted for by strong short range interactions between *pairs* of nucleons, then this sheds doubt on the assumption that quasi-elastic collisions result in only two prong events. This might suggest a systematic loss of high momentum components, both in the present experiment and in those of other authors.

In the present work no correction has been applied for the effects of the opacity of nuclear matter on the behaviour of the two secondary particles. To a first approximation this should not change the *shape* of the momentum distribution, since the effect of k on the elastic and differential cross sections may be neglected. A calculation of the magnitude of this effect is very difficult; calculations based on Monte Carlo methods for a uniform model (Metropolis *et al.* 1958) underestimate the probability of p–2p reaction in heavier nuclei by a factor of 3. A similar calculation performed by McEwen *et al.* (1957) for carbon gives an equally low value. Compared with the approximations already made, refraction effects are probably small at this energy.

§ 6. CROSS SECTIONS

To obtain the values of the total cross section for carbon and the cross section for quasi-elastic events (with $\theta_{\text{c.m.}} \geqslant 30°$), 311·15 metres of track have been rescanned. Taking into account the number of free p–p events, the following relative numbers of carbon interactions with 1, 2 and 3 or more prongs have been obtained:

Number of prongs	Number of events
1	530
2	390
3 or more	280
Total	1200

The density of expanded propane at 60°C has been taken to be 0·429 g cm^{-3}, which gives a partial density for carbon of 0·351 g cm^{-3}. The total cross section for carbon is found to be 420 ± 50 mbn, which is in good agreement with the results of Booth *et al.* (1957) at 895 MeV and those of Chen *et al.* (1955) at 860 MeV, who obtain respectively 392 mbn and 405 mbn. Recently, Law, Hutchinson and White (1959) have obtained a more accurate value of 362 ± 2·4 mbn at 910 MeV. In our experiment about 130 quasi-elastic events fall into the selected region, and they comprise 11% of the total carbon events. Another 20 to 30 events, which fall outside the limits of acceptance, increase to 13% the probability of a carbon interaction being a quasi-elastic proton–proton event. This figure, when normalized to the total cross section for carbon given by Law *et al.*, yields a cross section for quasi-elastic collisions in carbon of 46 ± 10 mbn. McEwen *et al.* estimated about 8% of the interactions in light nuclei at this energy to be quasi-elastic proton–proton events. Burcham *et al.* (1955) measured a cross section of 20 mbn for the reaction ^{12}C(p, pn)^{11}C at 950 MeV, although this value may be low by as much as 7 mbn (e.g. see Prokoshkin and Tiapkin 1956).

The present experiment gives a higher value for the cross section for p–2p reactions in carbon than that reported by other authors. The direct nature of the technique employed here and the small degree of ambiguity in the identification of these events suggest that this value may be more correct.

§ 7. Conclusions

The results of the present research indicate that the momentum distribution of the protons in carbon is represented, to a very good approximation, by a Gaussian distribution falling to 1/e at 13 Mev. The uncertainty in the background prevents very detailed information about the tail of the distribution from being obtained. Whilst the method is more direct than most others which have been used, additional means would be desirable in order to identify meson background events.

Acknowledgments

The authors are indebted to Professor P. B. Moon, for encouragement and support. They wish to acknowledge helpful discussions on this subject with Mr. L. Castillejo and Dr. G. Field, and to thank the members of the diffusion chamber and counter groups for making available their results prior to publication. Particular thanks are due to Dr. A. P. Batson for programming the data for electronic computation. The continued and valuable technical advice and assistance of Mr. G. Young and Mr. R. Joines is gratefully acknowledged.

W. R. F. is indebted to Queen's University, Canada, for an R. S. McLaughlin Travelling Fellowship and J. D. D. and B. M. to the Department of Scientific and Industrial Research for Research Studentships.

References

Batson, A. P., Culwick, B. B., Hill, J. G., and Riddiford, L., 1959, *Proc. Roy. Soc.* A, **251,** 218.
Block, M. M., Passman, S., and Havens, N. N., 1952, *Phys. Rev.*, **88,** 1239.
Booth, N. E., Ledley, B., Walker, D., and White, D. H., 1957, *Proc. Phys. Soc.* A, **70,** 209.
Brueckner, K. A., Eden, R. J., and Francis, N., 1955, *Phys. Rev.*, **98,** 1445.
Burcham, W. E., Symonds, J. L., and Young, J. D., 1955, *Proc. Phys. Soc.* A, **68,** 1001.
Chamberlain, O., and Segrè, E., 1952, *Phys. Rev.*, **87,** 425.
Chen, F. F., Leavitt, C. P., and Shapiro, A. M., 1955, *Phys. Rev.*, **99,** 857.
—— 1956, *Ibid.*, **103,** 211.
Chew, G. F., and Goldberger, M. L., 1950, *Phys. Rev.*, **77,** 470.
Chew, G. F., and Wick, G., 1952, *Phys. Rev.*, **85,** 636.
Cladis, J. B., Hess, W. N., and Moyer, B. J., 1952, *Phys. Rev.*, **87,** 425.
Dowell, J. D., Frisken, W. R., Martelli, G., and Musgrave, B., 1959, *Proc. Phys. Soc.*, **74,** 625.
Helmholz, A. C., McMillan, E. M., and Sewell, D. C., 1947, *Phys. Rev.*, **72,** 1003.
Henley, E. M., and Huddleston, R., 1947, *Phys. Rev.*, **82,** 754.
Law, M. E., Hutchinson, G. W., and White, D. H., 1958, *Nucl. Phys.*, **9,** 600.
McEwen, J. G., Gibson, W. M., and Duke, P. J., 1957, *Phil. Mag.*, **2,** 232.
Meshcheryakov, M. G., Vzorov, I. K., Zrelov, V. P., Neganov, B. S., Shabudin, A. F., 1957, *Soviet Physics J.E.T.P.*, **4,** 79.
Metropolis, N., Bivins, R., and Storm, M., 1958, *Phys. Rev.*, **110,** 185.
Musgrave, B., 1958, *Ph.D. Thesis*, University of Birmingham.
Prokoshkin, Iu. D., and Tiapkin, A. A., 1956, *Soviet Physics J.E.T.P.*, **32,** 177.
Selove, W., 1955, *Phys. Rev.*, **98,** 208.
—— 1956, *Ibid.*, **101,** 231.
Wilcox, J. M., and Moyer, B. J., 1955, *Phys. Rev.*, **99,** 875.

Internal Ferromagnetic Resonance in Small Cobalt Particles

By J. C. ANDERSON

Royal Holloway College, University of London, Englefield Green, Surrey

MS. received 1st *July* 1959

Abstract. Experiments are described in which small particles of cubic cobalt have been obtained by precipitation from a 2% Co–Cu alloy for the purpose of measuring the total internal magneto-crystalline anisotropy field as a function of particle radius. Two methods have been used, namely static torque measurements of the principal anisotropy constants and dynamic measurements based on spin resonance in the anisotropy field. The two methods yield fair agreement in the values calculated for the anisotropy field in a range of particle sizes.

The field is found to vary little with particle radius in a single crystal specimen and this is interpreted as evidence that internal resonance is independent of shape anisotropy.

§ 1. INTRODUCTION

In a recent paper (Anderson and Donovan 1959, to be referred to as I), it was reported that a resonance phenomenon, attributable to a spin resonance in the magneto-crystalline anisotropy field, had been observed in chemically prepared colloidal particles of nickel.

Reference was made in I to the difficulty of preparing a single crystal specimen suitable for the apparatus and type of measurement being made. The requirements are that the specimen should be a single magnetic domain and a single crystal of known orientation.

Becker (1957) produced single-crystal small particles of cobalt by controlled precipitation from an alloy containing 2% cobalt in copper and showed that the particles had the same crystallographic habit as the copper crystal in which they were precipitated. Since the particles can be grown small enough to be in the single domain range this alloy provides an ideal specimen for the internal resonance experiments.

The internal anisotropy field is calculated from the observed resonant frequency using the simple spin resonance theory. Static torque measurement of the anisotropy constants was undertaken to ascertain whether they would yield the same calculated values for anisotropy field as those obtained from the internal resonance measurements. The agreement obtained is reasonably good, and the values obtained for K_1, the principal anisotropy constant, for cubic cobalt are in fair agreement with those reported by Bean *et al.* (1958).

§ 2. EXPERIMENTAL DETAILS

2.1. *Polycrystalline Specimen*

To establish that internal resonance would be observable in precipitated cobalt in a copper matrix it was decided first to produce a polycrystalline alloy specimen. The alloy was melted in a graphite crucible under an atmosphere of dry nitrogen, maintained molten for 30 minutes and then quenched in iced brine. The resulting ingot was halved, one half being kept as a 'blank' specimen. This exhibited no ferromagnetic effect in a field of 15 000 oersteds. The other half was annealed *in vacuo* at 600°c following the pattern adopted by Bean *et al.* given in table 1. No attempt was made to measure the particle diameters, it being assumed that they would not differ radically from those reported by Bean *et al.*

Table 1

Total duration (min)	7	15	90	150	400	2400
Mean radius of particles (Å)	12	21	37	43	60	77

The resonance was observed using the apparatus described in I. A modified Foster–Seeley discriminator is used to measure complex permeability of the test specimen over the frequency range 140 to 250 Mc/s. Resonance is revealed by an increased absorption of power in the specimen, characterized by a peak in the curve for the imaginary part (μ_2) of permeability, and by a phase shift of the induced signal, characterized by a deviation in the curve for the real part (μ_1) of permeability, both being plotted against frequency.

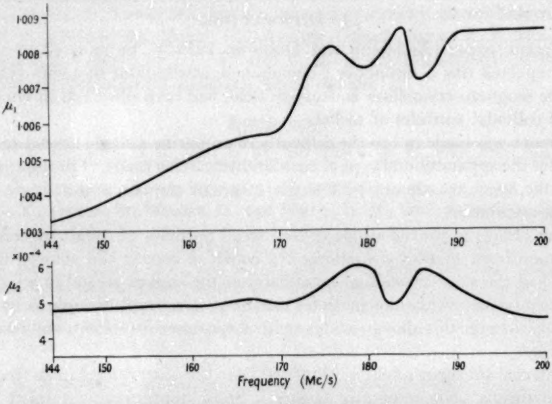

Figure 1. Real and imaginary parts of permeability as a function of frequency for cobalt particles of mean radius 12 Å in a copper matrix.

Results obtained for the 12 Å and 77 Å specimens are shown in figures 1 and 2. In the former a wide frequency range was covered, but only one pair of peaks was found. This was also true of the 21 Å particles, but at 37 Å a third peak began to emerge at a frequency above that of the first peak, and this increased in amplitude until the situation shown in figure 2 obtained for the 77 Å particles.

A graph showing the value of effective internal field, deduced from the frequency of the first resonant peak in each case, plotted against reciprocal radius is drawn in figure 3. A rather tentative extrapolation gives the value of approximately 110 Oe for infinite radius.

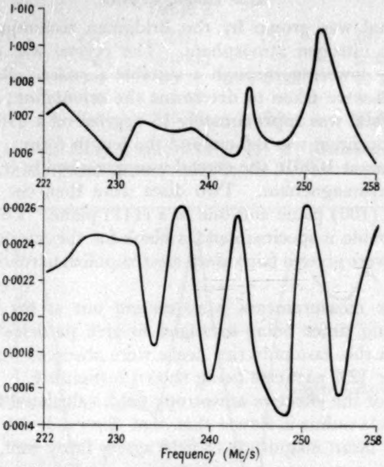

Figure 2. Real and imaginary parts of permeability as a function of frequency for cobalt particles of mean radius 77 Å in a copper matrix.

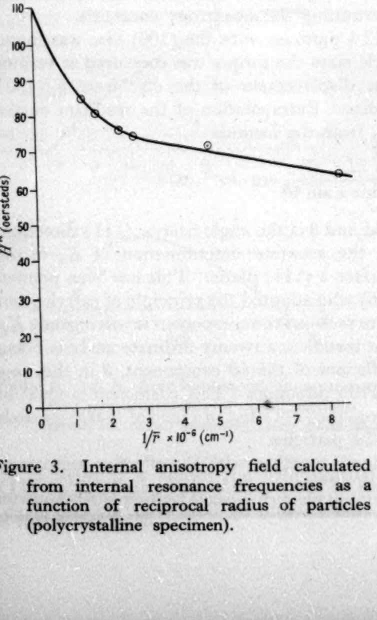

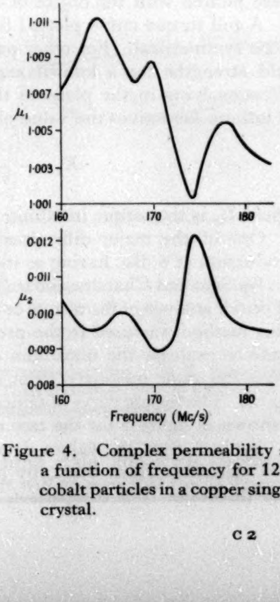

Figure 3. Internal anisotropy field calculated from internal resonance frequencies as a function of reciprocal radius of particles (polycrystalline specimen).

Figure 4. Complex permeability as a function of frequency for 12 Å cobalt particles in a copper single crystal.

2.2. *Single Crystal*

A single crystal was grown by the Bridgman technique using a graphite crucible in a dry nitrogen atmosphere. The crystal was grown at a rate of 1 cm per hour by lowering through a suitable furnace. Back-reflection Laue x-ray photographs were taken to determine the orientation, which showed that the axis of the crystal was approximately 15 degrees off a ⟨100⟩ direction. The diameter of the specimen was 0·6 cm and the length 6 cm. After annealing for 30 minutes *in vacuo* at 1000°c the crystal was quenched in iced brine and tested for absence of ferromagnetism. Two discs were then cut off, one having its faces parallel to a (100) plane and one to a (111) plane. The remaining crystal was halved to provide a specimen and a blank for the resonance measurements and all the pieces were given a fairly deep electro-polish to relieve strains produced by the cutting.

The resonance measurements were carried out as for the polycrystalline specimen, annealing times being arranged to give particles of 12, 21, 43 and 77 Å in radius. In this case only two peaks were observed for each particle size, a typical result for 12 Å particles being shown in figure 4.

The variation of the effective anisotropy field, calculated from the resonance results, with particle radius is slower than that observed with the polycrystalline specimen, but the mean magnitude of field agrees fairly well.

§ 3. STATIC MEASUREMENTS

The discs described in the previous section were annealed with the resonance specimen each time and then mounted in a torque magnetometer having a variable, uniform field of maximum strength 15 000 oersteds. Torque curves were plotted with the object of determining the anisotropy constants.

A full torque curve plotted for 12 Å particles with the (100) disc was found to be symmetrical. For other particle sizes the torque was measured at various field strengths for a known angular displacement of the disc from a ⟨100⟩ direction lying in the plane of the disc. Extrapolation of the resultant curves to infinite field gives the value of K_1 from the formula

$$K_1 = -\frac{2L_\infty}{\text{volume} \times \sin 4\theta} \text{ erg cm}^{-3}$$

where L_∞ is the torque in infinite field and θ is the angle from a ⟨111⟩ direction.

One of the major difficulties in the accurate determination of K_2 is the production of a disc having as its surface a (111) plane. This has been pointed out by Sato and Chandrasekhar (1956) who adopted the principle of carrying out a Fourier analysis of the torque curve to pick out the component involving only K_2. This method was used in the present instance, a twenty-ordinate analysis being made to evaluate the maximum coefficient of the 6θ component, θ in this case being the angle measured from a ⟨110⟩ direction. This coefficient is equal to $K_2/18$. The torque curve obtained from the (111) disc in a field of 15 000 oersteds is shown in figure 5 for the case of 12 Å particles.

Table 2 gives the values determined, together with the effective anisotropy field calculated from them, by means of the equation given in I for a ⟨111⟩ easy direction. For comparison the values found by Bean *et al.* are also given.

Table 2

(1)	(2)	(3)	(4)	(5)	(6)	(7)
12	−4·78	−6·62	+0·412	—	62·0	53·5
21	−5·12	−7·5	+1·78	+0·96	63·3	48·5
43	−5·74	−9·0	+1·67	—	66·2	47·5
77	−6·14	−9·5	−0·76	−8·3	67·8	56·8

(1) Mean radius (Å); (2) K_1 (erg $\mathrm{cm}^{-3} \times 10^5$); (3) K_1 (Bean) (erg $\mathrm{cm}^{-3} \times 10^5$); (4) K_2 (erg $\mathrm{cm}^{-3} \times 10^5$); (5) K_2 (Bean) (erg $\mathrm{cm}^{-3} \times 10^4$); (6) H^k resonance (Oe); (7) H^k static (Oe).

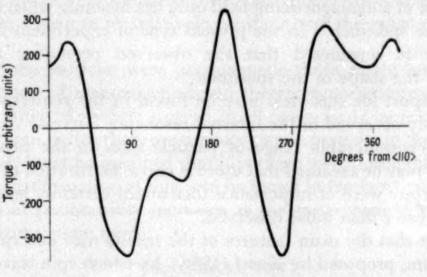

Figure 5. Torque curve for (111) disc of 12 Å cobalt particles in a copper single crystal. (*Note:* Abscissae should read 45, 90, 135, 180.)

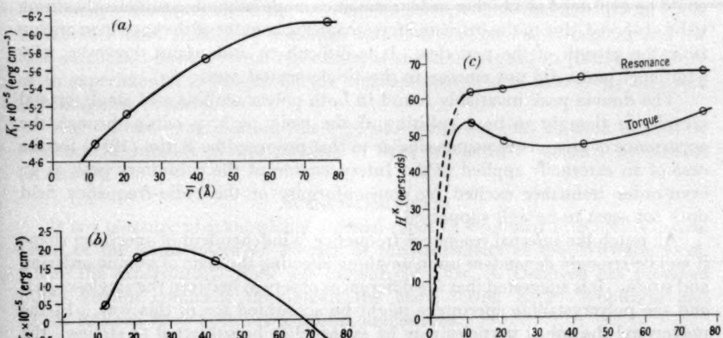

Figure 6. (*a*) K_1 from static torque measurements for cobalt particles. (*b*) K_2 from static torque measurements for cobalt particles. (*c*) Total anisotropy field as a function of radius for cobalt particles, from static and resonance measurements.

In figure 6 is shown the field calculated from static and from resonance measurements plotted against particle radius. It will be seen that the agreement is reasonably good.

§ 4. DISCUSSION

It has been shown by Bean *et al.* (1958) that in the early stages of precipitation the cobalt particles in 2% Co–Cu alloy are of spherical shape, but that as the size increases above about 25 Å they become ellipsoidal with increasing eccentricity and at a radius of 65 Å are markedly plate-like. With departure from sphericity the particles develop demagnetization coefficients with associated shape anisotropy. A relatively small departure from unity in the ratio of the principal axes will give rise to a quite large shape anisotropy field. The relative constancy of the total effective anisotropy field calculated from the internal resonance measurements is therefore surprising.

The concept of a demagnetizing field only has meaning when an external field is applied to the specimen. In the present type of experiment no external field is applied; it is considered that the observed resonance frequencies are independent of the shape of the specimen.

Further support for this view may be found in the remarkably narrow line widths invariably observed in the internal resonance curves. Becker has shown that there is a considerable range of particle sizes in the precipitated cobalt particles, and it may be assumed that there is also a distribution of particle shapes. If shape anisotropy were of importance this would certainly lead to line widths considerably greater than those observed.

It is thought that the main features of the results may be explicable in terms of the mechanism, proposed by Kittel (1958), by which spin waves are 'pinned' at the surface of the specimen because of the different anisotropy of the spins in the surface, brought about by their different environment.

The emergence of the third peak in the case of the polycrystalline specimen could be explained as a higher order resonance mode becoming sufficiently strong to be observed, due to the increased ferromagnetic content of the specimen arising from the growth of the particles. It is difficult to understand, however, why additional peaks did not emerge in the single-crystal case.

The double peak invariably found in both polycrystalline and single-crystal samples is thought to be a splitting of the main peak, possibly through the occurrence of an anti-resonance similar to that proposed by Kittel (1957) for the case of an externally applied field. Interpretation of the subsidiary peak as an even-order resonance excited by non-uniformity of the radio-frequency field does not seem to be well supported.

Although the internal resonance frequency is independent of specimen shape it will be strongly dependent upon anything affecting the state of atomic ordering and strain. It is suggested that the differences observed between the single-crystal and the polycrystalline specimens might be accounted for in this way. In the polycrystal the cobalt particles may be expected to be subjected to strains; the initial quench from melting temperature would give rise to very small crystallites and, if the precipitating anneal at 600°c does not allow much crystallite growth, the particles will be subject to increasing strain as they grow. This would account for the more rapid increase of resonant frequency with particle size observed in the polycrystalline sample.

Earlier experiments (Anderson and Donovan 1957) with nickel in the form of a strip led to a higher apparent anisotropy field than that obtained with the polycrystalline disc specimen described in I. Subsequent examination of the strip specimen showed a marked preferential domain orientation in the direction of rolling of the strip, suggesting a strain anisotropy field in this direction.

Bean and Livingston (1959) have pointed out that particles in the range of sizes used in these experiments are superparamagnetic. This implies that, although they are single domains, the direction of magnetization is subject to thermal fluctuations, so that the saturation magnetization is reduced. They also suggest that the value of K_1 is reduced by superparamagnetic effects. The present experiments do show a reduction of K_1 with particle size, as determined by static measurements, but K_2 actually increases as the particles become smaller. The most important point, however, is that the internal anisotropy field is dependent upon the ratio of the anisotropy constants to saturation magnetization and this has been shown to be relatively constant over the range of particle sizes studied.

Clearly if all the particles were paramagnetic there would be no such thing as an easy direction of magnetization and therefore no anisotropy field. It is known that the range of particle sizes is, in all cases, fairly large and even in the case of the 12 Å mean radius there are probably some particles in the ferromagnetic range present. It must be assumed that it is these which account for the results observed; some confirmation of this is to be found in the fact that the magnitude of the variation in permeability increases as the mean particle radius increases towards the ferromagnetic range.

§ 5. CONCLUSION

The total effective magneto-crystalline anisotropy field of cubic cobalt has been shown to be relatively independent of particle size when it is precipitated in a single crystal.

The agreement obtained between the anisotropy field calculated from static measurements of anisotropy constants and of saturation magnetization, and the field calculated from internal resonance, is sufficiently good to justify the latter as an experimental technique for the measurement of total anisotropy field in a ferromagnetic material.

With suitable modification this type of experiment may be used to provide evidence in support of the pinning of spin waves in a material by surface anisotropy.

ACKNOWLEDGMENTS

It is a pleasure to acknowledge the assistance of Professor F. R. N. Nabarro, Head of the Department of Physics of the University of the Witwatersrand, where the experimental work was carried out; Dr. B. Donovan has provided much helpful comment throughout the work. Drs. E. P. Wohlfarth and D. S. Rodbell have both made useful suggestions.

REFERENCES

ANDERSON, J. C., and DONOVAN, B., 1957, *Proc. Phys. Soc.* B, **70**, 186.
—— 1959, *Proc. Phys. Soc.*, **73**, 593.
BEAN, C. P., and LIVINGSTON, J. D., 1959, *J. Appl. Phys. Suppt*, **30**, 120S.
BEAN, C. P., LIVINGSTON, J. D., and RODBELL, D. S., 1958, *G.E.C. Res. Report* 58-RL-2004, June 1958.
BECKER, J. J., 1957, *Trans. Amer. Inst. Min. (Metall.) Engrs*, **209**, 59.
KITTEL, C., 1957, *Nuovo Cim., Suppt No.* 3, Vol. VI, Series X.
—— 1958, *Phys. Rev.*, **110**, 1295.
SATO, H., and CHANDRASEKHAR, B. S., 1956, *J. Phys. Chem. Solids*, **1**, 228.

Some Measurements of the Time Dependence of the Viscosity of Thixotropic Fluids

By E. W. BILLINGTON†
Admiralty Oil Laboratory, Brentford, Middlesex

MS. received 6th January 1959, in revised form 9th July 1959

Abstract. The time dependence of the viscosities of certain thixotropic fluids has been measured at constant rate of shear, using a Couette type viscometer. A time dependent yield value has been introduced which relates the instantaneous value of the observed viscosity, for a given rate of shear, to a time independent residual viscosity. The transient behaviour of the yield value has also been examined.

§ 1. INTRODUCTION

THIXOTROPY is defined as the reversible time dependent decrease of the resistance to flow accompanying the application of a shearing stress. The decrease in viscosity with shearing stress has been examined by Green and Weltmann (1943, 1946) using a rotational viscometer of the Couette type in which the rate of shear is continuously controlled. Green and Weltmann plot the rate of shear against shearing stress for continuously increasing and decreasing values of the rate of shear; if thixotropy exists two separate curves are obtained forming a hysteresis loop. The curve of decreasing rate of shear is the type indicated by Reiner and Riwlin when Bingham bodies are measured and the Reiner–Riwlin (1927) equation can be used for calculating a yield value. This method does not take account of the time dependence of the system, though Weltmann (1943) has attempted to develop the method to relate breakdown with time. An absolute method of measuring thixotropy using a Couette type viscometer has been developed by Goodeve and Whitfield (1938) by considering thixotropic breakdown as a form of chemical rate process. The concept of viscosity, and thixotropy in particular, as a rate process has also been developed by Ree and Eyring (1955) based on Eyring's (1936) general theory of absolute reaction rates.

It is desirable in any study of the flow properties of thixotropic fluids that the viscosity measurements be made under conditions of either constant applied shearing stress or constant rate of shear. The viscosity measurements on natural 'wax containing' residual oils to be described have been made at constant rate of shear, using a rotational viscometer of the Couette type. The thixotropic behaviour of wax containing oils is attributed to the individual wax crystallites which coalesce to form an internal structure of crystal aggregates (Ackroyd and Cawley 1953) when the system is maintained free of stress and in thermal equilibrium with the surroundings, thus showing increased resistance when sheared again. The crystal aggregates can be considered as deformable particles of time dependent particle size, which produce a time dependent increase in the resistance to flow. Viscosity experiments designed to examine the decay of flow resistance with time of shearing must be made on samples of the material which initially have the same uniform concentration of deformable particles.

---

†Now at Birkbeck College, University of London.

A method of making viscosity measurements on samples which are known to be uniform throughout, and which have not been disturbed by unnecessary shearing prior to the viscosity measurements, has been developed.

§ 2. THE YIELD VALUE

The thixotropic behaviour of the materials examined is attributed to a suspension of deformable particles of time-dependent particle size, in a Newtonian base liquid. Continuous shearing of the fluid causes breakdown of the deformable particles into 'individual particles' which are the smallest products of breakdown. Dispersed in the base liquid are the remaining fraction of individual particles which at any given instant are not contributing to the formation of the internal structure. The size of the individual particles is assumed to remain constant independent of the time of shearing. The size of the deformable particles increases with the time for which the system is maintained free of stress thus producing a time dependent internal structure which results in an increase in the resistance to flow; thus there will be a limiting value of the applied shearing stress below which flow does not occur. This limiting value of the applied shearing stress will be referred to as the yield stress or yield value p_Y. The use of the term yield value is confined to describing the change in resistance to flow produced by the internal structure. The yield value is defined as the maximum force per unit area that the deformable particles can sustain without flow occurring; that is, the yield value is a measure of the strength of the internal structure. It is assumed that the strength of the internal structure at any given instant is a characteristic property of the thixotropic fluid, dependent only on the concentration and size of the deformable particles and on the extent of consolidation in the structure. Thus at any time of shearing the force per unit area required to deform the internal structure to produce viscous flow, that is the yield value, should be independent of the rate of shear. The effect of an applied shearing stress greater than the yield value is to produce viscous flow accompanied by breakdown of the internal structure. After an infinite time of shearing the system has been transformed from the 'near solid state' to a liquid consisting of the individual particles dispersed in the Newtonian base liquid. At any time of shearing the system consisting of the remaining fraction of individual particles dispersed in the base liquid will be referred to as the residual liquid. The viscosity of the residual liquid, assumed to be Newtonian, is related to the rate of shear $\dot{S}$ by the equation

$$p_R = \eta_R \dot{S} \qquad \ldots\ldots (1)$$

where η_R is the residual viscosity and p_R is the shearing stress per unit area.

The instantaneous value of the viscosity η_t at a given time t of shearing is related to the rate of shear by the equation

$$p(t) = \eta_t \dot{S} \qquad \ldots\ldots (2)$$

where $p(t)$ is the observed shearing stress at time t. The difference between the observed shearing stress $p(t)$ and the shearing stress p_R associated with the viscous flow of the residual liquid is interpreted as a direct measure of the yield value at a time t of shearing; that is, from equations (1) and (2),

$$p(t) - p_R = (\eta_t - \eta_R)\dot{S} = p_y(t). \qquad \ldots\ldots(3)$$

From equation (3) the yield value at any given time of shearing is therefore the slope of the (viscosity, reciprocal rate of shear) curve. A relation similar to that given in (3) was proposed by Goodeve and Whitfield (1938) for the steady state condition in which an apparent equilibrium is maintained between the spontaneous growth of internal structure and its breakdown by an applied shearing stress. The steady state condition does not provide any information relating to the initial strength of the internal structure or the time dependence of the viscosity. In order to examine the decay of the yield stress and its dependence on the applied rate of shear and on the initial yield value, it is necessary to consider the transient behaviour of the viscosity.

Defining a new variable ψ by the relation

$$\psi(t) = \frac{(\eta_t - \eta_R)\dot{S}}{(\eta_0 - \eta_R)\dot{S}} = \frac{p_Y(t)}{p_Y(0)} \qquad (0 \leqslant \psi \leqslant 1) \qquad \ldots\ldots(4)$$

where $p_Y(t)$ and $p_Y(0)$ are the yield values at time t and at zero time of shearing respectively. Introducing the variable ψ into (3) we obtain the relation

$$\frac{(\eta_t - \eta_R)\dot{S}}{p_Y(0)} = \psi(t) \qquad \ldots\ldots(5)$$

where η_t is the instantaneous value of the viscosity at time t of shearing. The variable ψ is a dimensionless quantity which relates the viscosity for a given rate of shear to the two time independent quantities η_R and $p_Y(0)$. For the limiting condition $\psi = 1$ the size of the aggregates is assumed to be a maximum such that prolonged storage of the material in a condition such that it is free of stress and in thermal equilibrium with the surroundings will not produce any further increase in the size of the aggregates. After an infinite period of shearing ψ is zero which corresponds to the thixotropic fluid having been completely transformed into the liquid state. The variable ψ is an indication, at any given time of shearing, of the degree to which the internal structure has been reduced by continuous shearing.

The general case of a thixotropic fluid is that in which decay and growth of the internal structure occurs simultaneously. A distinction must be made between the rate of change of the viscosity and the rate of change of the yield stress. The property which is changing with time is the size of the deformable particles, that is the yield value; the viscosity changes with time only as a result of the change in resistance to flow. Further the viscosity is dependent on the rate of shear, whereas it has been assumed that the yield value is independent of the rate of shear. Thus the simplest assumption to make is that the change in the yield value in unit time is proportional to the strength of the remaining internal structure; that is

$$-dp_Y(t)/dt = Kp_Y(t)$$

where the factor K is related to a specific rate constant. Consider a steady state in which equilibrium exists between the spontaneous growth of the internal structure and its breakdown by an applied shearing stress. The specific rate constant associated with this steady state will be referred to as the absolute rate factor C and is defined as the number of times an individual particle passes between the internal structure and the residual liquid in unit time in the absence of stress.

Following Glasstone, Laidler and Eyring (1941) it is assumed that the factor K is related to the absolute rate factor C and the yield value by a relation of the form

$$K = 2C \sinh\left(\frac{v p_Y(t)}{2\boldsymbol{k}T}\right)$$

where v is a constant for a given temperature T. The rate of breakdown of internal structure is therefore given by the equation

$$-\frac{dp_Y(t)}{dt} = p_Y(t) 2C \sinh\{\tfrac{1}{2}\alpha p_Y(t)\} \qquad \ldots\ldots(6)$$

or introducing ψ we obtain

$$-\frac{d\ln\psi}{dt} = 2C\sinh(\tfrac{1}{2}b\psi) \qquad \ldots\ldots(7)$$

where

$$\alpha = \frac{b}{p_Y(0)} = \frac{v}{\boldsymbol{k}T}.$$

§ 3. EXPERIMENTAL

The change in viscosity with time of shearing for a given constant rate of shear was measured with a viscometer of the Couette coaxial type. The general design of the inner and outer cylinders is shown in figure 1; D_i and D_o are the diameters of the inner and outer cylinders respectively, and H is the height of the inner cylinder. The outer cylinder A is driven at constant speed by a high torque synchronous motor; the inner cylinder B is suspended in jewelled bearings and is free to rotate against a calibrated spring. Attached to the inner cylinder is a pointer which moves over a fixed scale to indicate the angular deflection of the inner cylinder. The cut-away parts of the inner cylinder reduces the 'end effects' to negligible values, thus ensuring that the whole of the sample is measured under uniform shear conditions. The fixed guard ring C confines the shear volume of the test sample to the cylindrical annulus between the cylinders. The tufnol tube D connecting the outer cylinder to the gear box acts as a thermal insulator to prevent transference of heat to or from the test sample by way of the main body of the instrument. A number of independent values of the rate of

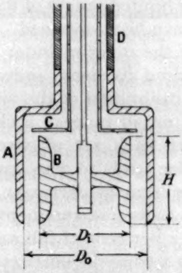

Figure 1. The viscometer cylinders.

shear are provided by the combined effect of a three-speed gear box and a set of nine interchangeable inner cylinders together with three outer cylinders. The values of the rate of shear and the maximum values of the shearing stress corresponding to full scale deflection, together with the main dimensions of the cylinders, are given in table 1.

Table 1. Dimensions of the Viscometer Cylinders

D_o (cm)	4·767			4·767			2·225		
Gearbox speed	Shear rate $\dot{S}$ (sec^{-1})			Shear rate $\dot{S}$ (sec^{-1})			Shear rate $\dot{S}$ (sec^{-1})		
1	3·20	1·10	0·69	1·63	0·84	0·58	0·79	0·43	0·31
2	13·3	4·58	2·85	6·75	3·50	2·42	3·28	1·78	1·29
3	36·9	12·7	7·91	18·8	9·71	6·71	9·05	4·93	3·59
D_i (cm)	3·971	4·285	4·605	3·813	4·129	4·445	1·270	1·590	1·905
Max. shear stress p_m (dyn cm^{-2})	142	159	189	217	253	297	2260	3420	5760
H (cm)	3·78			2·52			1·26		

It is evident from table 1 that the number of individual viscosity measurements which can be made at different rates of shear is limited by the maximum available shearing stress p_m for a given combination of inner and outer cylinders. From equation (3) the maximum available shearing stress must exceed the initial yield value by at least the shearing stress p_R associated with the residual liquid. In practice it is found that the viscosity measurements are in general confined to four rates of shear, though for limited ranges of the yield value viscosity measurements at five rates of shear have been obtained.

The degree of rotation of the inner cylinder is obtained from a linear scale which is divided into one hundred divisions; individual readings can be measured to ±0·1 of a division. The calibration of the viscometers is accurate to within ±1% of full scale deflection on all ranges; a check on the calibration of each instrument was made before each set of viscosity measurements. As the deflection of the inner cylinder tends to zero, corresponding to small restoring couples, the accuracy of measurement decreases due to such possible effects as friction at the bearings; viscosity measurements were therefore discontinued when the deflection fell to five per cent of full scale deflection.

The time interval between setting the outer cylinder in rotation and the inner cylinder attaining its equilibrium position, corresponding to the viscosity of the liquid under test, will be referred to as the 'delay time'. The dependence of the delay time on the rate of shear was examined for a Newtonian oil and a thixotropic fluid by attaching a mechanical pointer to the outer cylinder which in the stationary position could be aligned with the pointer attached to the inner cylinder. On rotating the outer cylinder the relative motion between the two cylinders could be directly observed. The same general dependence of the delay time on the rate of shear was observed for both the Newtonian oil and the thixotropic fluid. For rates of shear greater than 1·3 sec^{-1} the delay time did not exceed ten seconds, but for smaller rates of shear the delay time increased rapidly with decreasing rate of shear. For all values of the rate of shear it was observed that the relative motion between the cylinders produced only a small relative angular displacement; that is the inner cylinder follows the rotation of the outer cylinder very closely to the point at which the viscosity of the thixotropic fluid begins to decrease with continued shearing. During the delay time it is assumed that the velocity profile of the fluid is being developed across the annular gap between the cylinders. It is further assumed that viscous flow accompanied by breakdown of the internal structure of a thixotropic fluid does not occur until the velocity profile has been completely developed, that is from the instant at which the inner cylinder attains its maximum deflection. The time of shearing was therefore measured from the instant at which the inner cylinder attains its maximum deflection.

The viscosity measurements have been made on bulk samples maintained free of stress and in thermal equilibrium with the surroundings for a period of time sufficiently long to ensure that the build up of internal structure was complete; the normal period of storage was of the order of three weeks. The bulk sample was contained in a double walled bath having an exposed surface area sufficient to accommodate several sets of viscometer cylinders. The oil samples were introduced into the bath in the 'as received' condition, without any previous heat treatment. Three complete viscometers, each one with a different pair of cylinders, were mounted on a rigid framework which could be moved smoothly in the vertical and horizontal planes to enable the viscometer cylinders to be immersed in the oil without producing unnecessary shearing of the sample. The viscometer cylinders and the bulk oil sample were contained in a refrigerated vessel. A continuous record of the temperature at twelve points was obtained using thermocouples distributed over the surface of the bulk sample at varying depths of immersion. The temperature of the sample could be controlled to within ± 0·05°c. An estimate of the storage period necessary to produce maximum internal structure was obtained as follows. A sample of oil was set up under identical condtions to those of the test sample; a weighted glass tube, similar to a mercury in glass thermometer, was supported in a vertical position with the weighted end in contact with the surface of the oil. The tube was released and the time to penetrate a fixed distance at different points on the surface was measured. These measurements were repeated daily and when the penetration times for three consecutive days were in approximate agreement it was assumed that the internal structure was fully developed. The results from the control experiments showed a considerable scatter and could only be used to give a very approximate estimate of the degree to which the internal structure had developed in a given time of storage. To allow for the possibility that the internal structure was still being generated when the viscosity measurements were commenced, the three viscometers were set in operation with an interval of not more than two minutes between each. This procedure ensured that the initial condition of the bulk sample was the same for each of the three viscosity measurements. One or two of the viscometers were replaced in an unsheared portion of the oil sample, depending on the combination of inner and outer cylinders which would cover the viscosity range, and stored for a further twenty-four hours. At the end of the twenty-four hour period of storage the change in viscosity with time of shearing was measured. In this way viscosity measurements were obtained at four or five different rates of shear.

The temperature at which the thixotropic behaviour was measured for the samples examined is given in tables 2 and 3; the temperature at which the viscosity measurements were made lies in the range 0°c to 5°c. The thixotropic behaviour of sample B was measured at several temperatures in the range 1·7°c to 32°c. The temperature dependence of the residual viscosity in the temperature range from 82°c to the critical temperature at which thixotropic behaviour could just be detected, was obtained using capillary tube viscometers. The viscometers were mounted in a double walled bath the temperatures of which could be controlled to within ±0·01°c.

§ 4. RESULTS

Figure 2 shows how the viscosity depends on the time of shearing for sample A. The high initial yield value of this sample restricts the viscosity measurements to four different rates of shear. The graphs (η_t, $1/\dot{S}$) in figure 3 show how the viscosity depends on the reciprocal rate of shear, for samples A and D. For sample D viscosity measurements have been made at five different rates of shear but the time of shearing has been limited by the small initial deflection which decreased to five per cent of full scale deflection in about forty minutes. From equation (3) the intercept on the viscosity axis corresponds to the value of the residual viscosity η_R and the slope of the curve for zero time of shearing is the initial yield value $p_Y(0)$. The initial yield value and residual viscosity for four samples representative of the oils are given in table 2.

Table 2

Sample	T (°c)	η_R (poise)	$p_Y(0)$ (dyn cm^{-2})	$C \times 10^6$ (sec^{-1})	$\alpha \times 10^2$
A	5·0	22	1320	61·3	0·58
B1	5·0	25	535	12·3	1·72
B2	5·0	25	250	6·9	3·60
C	0·0	8	470	6·5	1·64
D	3·0	3	300	5·7	2·31

The viscosity data for samples B1 and B2 were obtained from two bulk samples of the same oil; both samples were stored under identical conditions with the exception that sample B1 was stored for three weeks and sample B2 for eight days. Sample B2 was examined at the same rates of shear as for B1 and the same value of the residual viscosity was obtained for both samples.

To obtain the yield value at a given time of shearing the residual viscosity is obtained from the intercept of the (viscosity, reciprocal rate of shear) curve as shown in figure 3. Using this value of the residual viscosity together with the experimentally determined values of the viscosity for a given rate of shear, corresponding yield values are calculated from equation (3). Several independent values of the yield stress for a given time of shearing are obtained, depending on the number of viscosity measurements at different rates of shear that are available. In this way sets of results similar to those shown in figure 2 compound into a single curve, showing the dependence of the yield value on the time of shearing, as shown in figure 4. For yield values greater than 140 dyn cm^{-2} the independent measurements of the yield value corresponding to the several rates of shear reduce to a mean yield value which can be measured with an accuracy to ±4%. For yield values less than 140 dyn cm^{-2} the accuracy of measurement decreases with decreasing yield value, the overall accuracy of measurement being to the order of ±7%. It is further important to note that the deviation of the individual values of the yield stress from the mean yield value is not a function of the rate of shear. That is the yield value at a given time of shearing does not decrease with increasing rate of shear. The initial yield value and residual viscosity for sample B, at several temperatures in the range 1·7°c to 32·0°c, are given in table 3. The initial yield value for sample B at a temperature of 32·0°c was obtained from viscosity measurements in which the initial deflection was less than five per cent of full scale deflection. The small initial deflection made it impossible to determine the time dependence of the viscosity at this temperature.

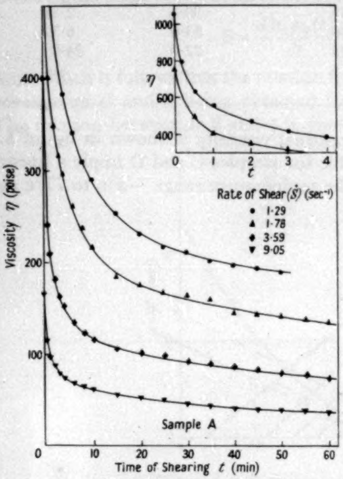

Figure 2. Variation of the viscosity with the time of shearing for various rates of shear.

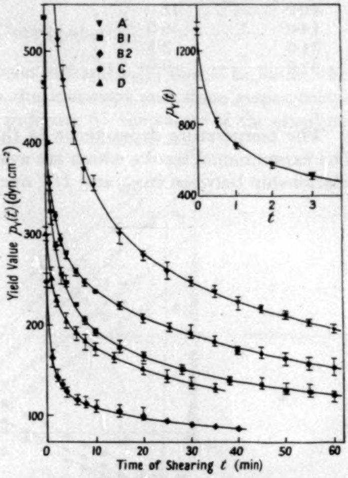

Figure 4. Variation of the yield value $p_y(t)$ with the time of shearing.

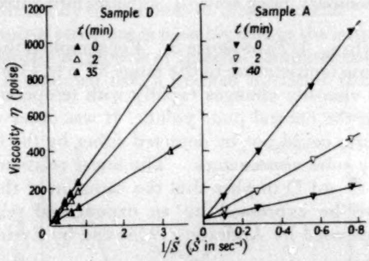

Figure 3. Dependence of the viscosity on the reciprocal rate of shear.

Table 3. Experimental Results for sample B1 at different Temperatures

T (°c)	η_R (poise)	p (0) (dyn cm^{-2})	$C \times 10^6$ (sec^{-1})	$\alpha \times 10^2$
1·7	50	1040	10·8	1·09
5·0	25	535	12·3	1·72
10·0	11	250	30·4	2·50
14·0	6·0	90	33·0	6·32
21·0	2·5	25	72·0	24·0
32·0	0·9	2	—	—

The temperature dependence of the residual viscosity is shown in figure 5. The experimental results which are available for samples C and D imply a linear relationship between $\ln \eta_R$ and $1/T$ over the temperature range -3°c to 77°c as shown by the graphs ($\ln \eta_R$, $1/T$) of figure 5. For sample B the graph ($\ln \eta_R$, $1/T$) is linear with decreasing temperature in the range 82°c to 43°c; in the range 43°c to 1·7°c the residual viscosity changes rapidly with temperature indicating that the oil is approaching the natural pour point. It was observed that above 43°c the thixotropic property could not be detected either by the Couette type viscometer or the capillary tube viscometers. The linear relationship between $\ln \eta_R$ and $1/T$ for samples C and D implies that the variation of the residual viscosity with temperature can be expressed by an exponential relation of the form $\eta_R = a \exp (c/T)$ as proposed by Andrade (1934) and by Eyring (1936).

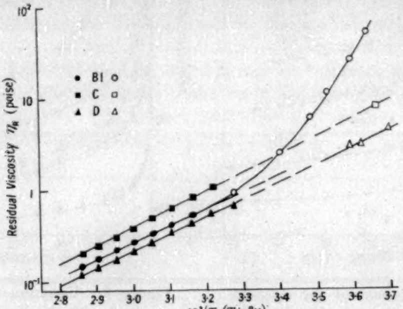

Figure 5. Temperature variation of the residual viscosity η_R. Open symbols: Couette type viscometer; black symbols: capillary tube viscometer.

§ 5. Discussion

From the viscosity measurements it is concluded for the materials examined that the yield value is independent of the rate of shear at any given time of shearing. Equation (3) has been applied over a range of yield values from 2 dyn cm^{-2} to 1320 dyn cm^{-2} showing that it is tenable for highly thixotropic materials as well as systems which exhibit only weak thixotropic behaviour. At no stage during any of the viscosity measurements was a steady state attained in which equilibrium existed between the spontaneous growth of internal structure and its breakdown by the applied shearing stress.

The conclusion that the yield value is independent of the rate of shear leads to the concept of an absolute rate of flow as introduced in § 2. Equation (6) can in the initial stage of the breakdown of the internal structure be approximated to

$$\beta = \frac{d \ln p_{Y}(t)}{dt} = C \exp\{\tfrac{1}{2}\alpha p_{Y}(t)\}$$

from which it follows that the relation between $\ln \beta$ and $p_Y(t)$ should be linear, the parameters C and α being obtained from the intercept and slope respectively. The relation between $\ln \beta$ and ψ is shown in figure 6; the values of the absolute rate factor C and the parameter α are given in table 2. The linear relation between $\ln \beta$ and the parameter ψ over the whole range for which experimental values of ψ are available implies that the growth of internal structure at any instant is such that it cannot be detected by the method of measurement. The failure to detect the growth of the internal structure is possibly due to the large shear volume of the sample, and the slow rate of growth of internal structure compared with the rate of breakdown. It is assumed that a marked deviation from the linear relation

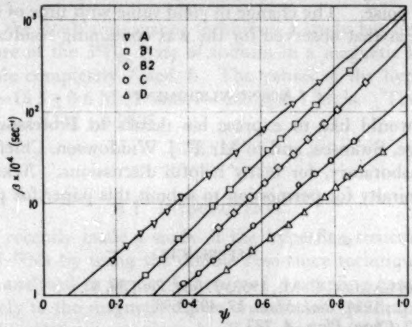

Figure 6. Variation of β $(= d \ln p_Y(t)/dt)$ with ψ.

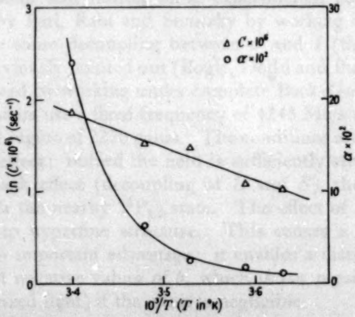

Figure 7. Temperature variation of the rate factor C and the parameter α.

between $\ln \beta$ and ψ would have been observed if a steady state, similar to that obtained by Goodeve and Whitfield, had been approached in any of the viscosity measurements which have been made. The initial yield values for sample B are given in table 3 together with the values of the parameters C and α.

The dependence of the parameter α on temperature is shown in figure 7, together with the absolute rate factor C. The change in α with decreasing temperature is relatively small as the near solid state is approached. This is in general agreement with α being independent of temperature in the solid–plastic region (Ree and Eyring 1958).

Viscosity measurements on a suspension of carbon black in mineral oil at a temperature of 21°C gave an initial yield value of 5000 dyn cm^{-2} and a residual viscosity of 1300 poise. The change in yield value with time of shearing follows the same pattern as that observed for the wax containing residual oils.

ACKNOWLEDGMENTS

The author would like to express his thanks to Professor E. S. Sellers, University College, Swansea, and to Mr. E. J. Widdowson, Chief Scientist of the Admiralty Oil Laboratory, for many helpful discussions. Acknowledgment is made to the Admiralty for permission to submit this paper for publication.

REFERENCES

ACKROYD, G. C., and CAWLEY, C. M., 1953, *J. Inst. Pet.*, **39**, 82.

ANDRADE, E. N. DA C., 1934, *Phil. Mag.*, **17**, 497, 698.

EYRING, H., 1936, *J. Chem. Phys.*, **4**, 283.

GLASSTONE, S., LAIDLER, K. J., and EYRING, H., 1941, *The Theory of Rate Processes* (New York, London: McGraw-Hill).

GOODEVE, C. F., and WHITFIELD, G. W., 1938, *Trans. Faraday Soc.*, **34**, 511.

GREEN, H., and WELTMANN, R. N., 1943, *Ind. Eng. Chem.*, **15**, 201.

—— 1946, *Ibid.*, **18**, 167.

REE, T., and EYRING, H., 1955, *J. Appl. Phys.*, **26**, 793, 800.

—— 1958, *Rheology*, Vol. II (Ed. F. R. Eirich) (New York : Academic Press).

REINER, M., and RIWLIN, R., 1927, *Kolloidzschr.*, **43**, 72.

WELTMANN, R. N., 1943, *J. Appl. Phys.*, **14**, 343.

The Hyperfine Structure of the $3^2P_{3/2}$ State of Sodium and the Quadrupole Moment of ^{23}Na

By J. N. DODD† and R. W. N. KINNEAR

Department of Physics, University of Otago, New Zealand

MS. received 28th April 1959, in revised form 4th August 1959

Abstract. Using the double resonance technique a study has been made of the hyperfine structure of the $3^2P_{3/2}$ state of sodium in a magnetic field sufficiently strong to decouple completely J and I. The values of the hyperfine coupling constants are $a = 18{\cdot}5 \pm 0{\cdot}6$ Mc/s and $b = 2{\cdot}25 \pm 0{\cdot}4$ Mc/s. The Landé factor for the state is $g_J = 1{\cdot}3341 \pm 0{\cdot}0003$.

§ 1. INTRODUCTION

We have recently made a study of the hyperfine structure of the $3^2P_{3/2}$ state of ^{23}Na by using the double resonance technique. The results can be analysed in terms of the a and b coupling constants which are related respectively to the magnetic dipole and electric quadrupole moments of the nucleus. The relations are given by Kopfermann (1958). The values of a and b for this state have previously been determined by Sagalyn (1954) using double resonance and by Perl, Rabi and Senitzky (1955) using an atomic beam. Both experiments were performed at zero magnetic field so that the transitions were observed between the various hyperfine states of the $P_{3/2}$ level characterized by $F = J + I$, the frequencies of the transitions being $3a + b$, $2a - b$, $a - b$. The fact that only two transitions were observed led to an indeterminacy in the results: $a = 19{\cdot}06 \pm 0{\cdot}36$ Mc/s, $b = +2{\cdot}58 \pm 0{\cdot}3$ or $-21{\cdot}64 \pm 0{\cdot}7$ Mc/s. The smaller positive value of b was preferred since it leads to a more likely value of the quadrupole moment and indeed some experimental confirmation of this value was obtained by Perl, Rabi and Senitzky by working in a stronger field, sufficient to produce some decoupling between J and I (the Back–Goudsmit effect). We have previously pointed out (Bogle, Dodd and Purser 1956) that the doubt could be resolved by working under complete Back–Goudsmit conditions. The present experiments use a fixed frequency of 4245 Mc/s (7 cm) and require a field intensity in the region of 2270 gauss. The conditions are therefore extreme for Back–Goudsmit effect; indeed the field is sufficiently strong to produce an incipient Paschen–Back effect (decoupling of L and S), thereby producing a slight admixture with the nearby $3^2P_{1/2}$ state. The effect of this is of the same order as those due to hyperfine structure. This causes a complexity in the analysis but it has an important advantage: it enables a distinction to be made between positive and negative values of b, which is not possible (in the case of excitation by π-polarized light) if the effect is negligible.

---

† 1959 at Clarendon Laboratory, Oxford.

§ 2. THE DOUBLE RESONANCE TECHNIQUE

This method of studying the structure of excited states has been described by various authors (Brossel and Kastler 1949, Brossel and Bitter 1952). The atoms are excited to the level to be studied by the absorption of suitably polarized radiation, thus producing differences of population between the various magnetic sub-states of the excited level. If, during the life of the excited level, transitions are caused by paramagnetic resonance between these sub-states, some characteristic (e.g. the polarization) of the resonance radiation will change; a measure of this change, called the double resonance signal, detects the occurrence of paramagnetic transitions.

Excitation may be accomplished by using either π, σ or circularly polarized light. In the case of π excitation only the $|\frac{3}{2}, \pm\frac{1}{2}\rangle$† sub-states become populated. In the case of σ excitation the $|\frac{3}{2}, \pm\frac{3}{2}\rangle$ sub-states become more strongly populated than $|\frac{3}{2}, \pm\frac{1}{2}\rangle$. In either case the paramagnetic transitions $m_J=\frac{3}{2}\rightarrow\frac{1}{2}$ and $m_J=-\frac{3}{2}\rightarrow-\frac{1}{2}$ will be detected by the change in the ratio of π to σ components of the resonance radiation.

Excitation by circularly (σ^+) polarized light results in a greater population in $|\frac{3}{2}, \frac{3}{2}\rangle$ than in $|\frac{3}{2}, \frac{1}{2}\rangle$, with zero population in the other sub-states. The population difference may also be enhanced by an optical pumping action tending to concentrate the ground level sub-state $m_J=+\frac{1}{2}$. Consequently, the paramagnetic transition $m_J=\frac{3}{2}\rightarrow\frac{1}{2}$ only is observed and not the corresponding negative one. If circular polarization in the resonance radiation were measured, transitions $m_J=+\frac{1}{2}\rightarrow-\frac{1}{2}$ would also be detected, but in the present experiments only the π and σ $(=\sigma^+ + \sigma^-)$ components were observed and for this case there is no difference in the observed polarization of resonance radiation from $m_J=+\frac{1}{2}$ and $m_J=-\frac{1}{2}$.

§ 3. APPARATUS

The apparatus is similar to that previously described (Bogle, Dodd and Purser 1956, Bogle, Dodd and McLean 1957); a schematic diagram of the essentials is shown in figure 1.

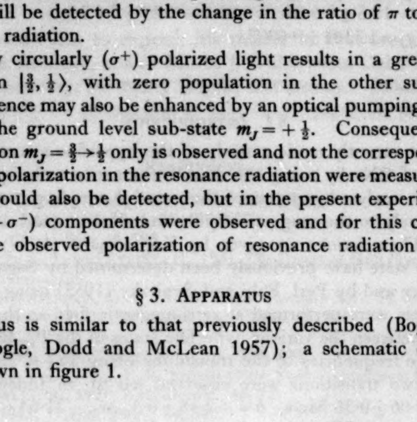

Figure 1. Schematic diagram of the essentials of the experimental apparatus.

The incident radiation is produced by a laboratory lamp operating either from a 50 c/s or a 1400 c/s supply, and the series resistance used to control the

† The notation is $|J, m_J\rangle$

intensity. After polarization, the radiation is focused into sodium vapour contained in a fused quartz cell situated at the centre of a microwave cavity. The resonance radiation is analysed by a polarizing prism of calcite with two fused quartz end pieces, and the π and σ components led to photomultipliers (RCA 6217) via fused quartz light pipes.

The microwave cavity, resonant for 7 cm waves, operates in the H_{210} mode producing an oscillating magnetic field at the centre. The cavity is excited by a CV 80 klystron which delivers power of the order of 100 w continuously, sufficient to produce an oscillating field of several gauss. In order to produce the appropriate sodium vapour pressure the cavity is heated by flat elements on the side walls and the coolest temperature of the cell is controlled by an oven into which the end of the cell extends.

The cavity is placed between the poles of a 4 in. electromagnet, the field of which has been adjusted by the use of ring shims to give maximum homogeneity at the position of the cell. The magnetizing current is produced by a d.c. generator and is stabilized electronically to nearly 1 part in 10^5. The current may be increased linearly with time by the use of a motor-driven Helipot in the reference circuit of the stabilizer. This enables the double resonance signal to be recorded while making a slow transit through the resonance region. The complete assembly of sodium lamp, polarizing equipment, microwave cavity and oven is mounted on a pivoted arm so that it may be moved out of the electromagnet to allow measurement of the field by a proton magnetometer.

The detection of the double resonance signal is accomplished by a method similar to that used by Brossel and Bitter. In order that the result can be displayed on a 2 mv recording potentiometer, one stage of current amplification is introduced using transistors. The balance resistors (R_1 and R_2) then do not need to exceed 100 ohm and the response time of the recorder is of the same order as the traverse time (4 sec). However, instead of adjusting the resistors to balance the photomultiplier currents (I_π and I_σ) it was found better to balance $\partial I_\pi/\partial V$ and $\partial I_\sigma/\partial V$, where V is the e.h.t. applied to the photomultipliers. The circuit is thereby stabilized against changes of e.h.t. The recorder is then brought to zero by introducing a small voltage in series with it.

Modification of this arrangement is required for excitation by circularly polarized light. A beam of circularly polarized light is directed perpendicular to the field direction along the outside of the cavity and reflected along the field direction by a metal mirror. The beam passes through a hole in the side of the cavity and hence into the resonance cell. The reflection changes the sense of polarization relative to the light direction. In order to preserve a reasonably high Q-value for the cavity, the hole, which is situated at a position of maximum microwave current density, is crossed by a number of metal louvres parallel to the current flow.

§ 4. THEORETICAL CONSIDERATIONS

The energies of the hyperfine sub-states of $^2P_{3/2}$ under conditions of complete Back–Goudsmit decoupling can be expressed as

$$W=\frac{g\beta B}{h}m_J+am_Jm_I+\frac{b}{4}\left(m_J{}^2-\frac{5}{4}\right)\left(m_I{}^2-\frac{5}{4}\right),$$

all terms being expressed in units of frequency. The first term expresses the Zeeman splitting, g being the Landé factor for the state. The second and third express the hyperfine splitting due to the magnetic dipole moment and electric quadrupole moment respectively of the nucleus. The energies of the states are shown in figure 2, which is drawn for positive a and b. The transitions detected in the experiment are indicated. The resonances are situated symmetrically about $B_0 = hf/g\beta$, where f is the frequency of the oscillating magnetic field. If b were zero four resonances only would be found separated by $\delta B = ha/g\beta$; with a finite value of b eight resonances occur, but they would not be resolved since δB is of the order of 10 gauss whereas the natural half-width at half-height of each resonance is about 6 gauss. However the shape of the overall resonance curve should enable a distinction to be made between small and large values of b. Since the effect of a change of sign of b is simply to interchange resonance positions of $m_J = \frac{1}{2} \rightarrow \frac{3}{2}$ and $m_J = -\frac{1}{2} \rightarrow -\frac{3}{2}$ transitions, an experiment performed under these conditions could not give the sign of b.

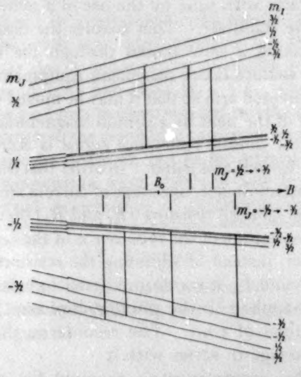

Figure 2. Zeeman effect on state $J = 3/2$, $I = 3/2$ including perturbation by quadrupole moment of the nucleus.

The field used in the present experiment causes a further perturbation to the $P_{3/2}$ state due to an incipient Paschen–Back effect which mixes a small amount of the $P_{1/2}$ sub-states with the $m_J = \pm\frac{1}{2}$ sub-states of $P_{3/2}$. The effect on the energies is to raise the levels of $m_J = \pm\frac{1}{2}$ by the addition of the term

$$\frac{3}{4}A\left[\left(1 \pm \frac{4}{9}x + \frac{4}{9}x^2\right)^{1/2} - 1 \mp \frac{2}{9}x\right],$$

where the upper sign is to be taken for $m_J = +\frac{1}{2}$. A is the fine structure coupling constant (for sodium $A = \frac{2}{3}\delta = 0{\cdot}344 \times 10^{12}$ c/s, δ being the doublet separation), and $x = \beta B/hA$. This perturbation has the effect of moving the $m_J = \frac{1}{2} \rightarrow \frac{3}{2}$ resonances to a slightly higher field, and those of $m_J = -\frac{1}{2} \rightarrow -\frac{3}{2}$ to a slightly lower (the shifts are equal to the third order in x). The effect enables one to distinguish a positive from a negative value of b in the experiments using π or σ excitation.

The field at which resonant transitions occur is given by the condition $W' - W'' = f$, where W' and W'' are the energies of the two sub-states between which the transitions occur. Solution of the equations lead to eight resonances:

$$B(m_I) = B_0\left[1 - m_I\frac{a}{f} - \frac{1}{2}\left(m_I{}^2 - \frac{5}{4}\right)\frac{b}{f} + \frac{1}{12}\frac{f}{A}\ldots\right], \quad \text{for } m_J = \tfrac{1}{2} \rightarrow \tfrac{3}{2},$$

$$B(m_I) = B_0\left[1 - m_I\frac{a}{f} + \frac{1}{2}\left(m_I{}^2 - \frac{5}{4}\right)\frac{b}{f} - \frac{1}{12}\frac{f}{A}\ldots\right], \quad \text{for } m_J = -\tfrac{1}{2} \rightarrow -\tfrac{3}{2},$$

where m_I takes the values $\frac{3}{2}$, $\frac{1}{2}$, $-\frac{1}{2}$, $-\frac{3}{2}$. The term in f/A is the lowest order Paschen–Back term, the one of next order (in f^2/A^2) having zero coefficient. Omitted from the expression are higher order terms in a^2/f^2, b^2/f^2, a/A, b/A, $f^3/A^3\ldots$ which are not significant in the present experiment, although they have been considered in the analysis.

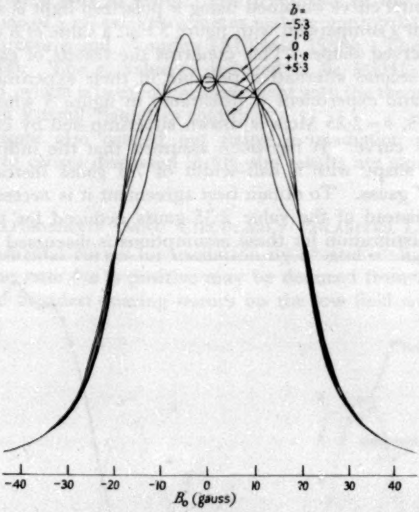

Figure 3. Theoretical overall resonance curves for π polarized excitation using various values of the quadrupole coupling constant b (in Mc/s).

The expected shapes for the overall resonance curves using various values of b, have been calculated using $a = 19{\cdot}0$ Mc/s and the individual resonances shifted by $\pm 2{\cdot}35$ gauss ($\pm B_0 f/hA$) as predicted for the incipient Paschen–Back effect in a field of 2270 gauss. The shapes of the overall resonances are shown in figure 3. The individual resonances are assumed to have a Lorentz shape and a half-width corresponding to a natural life of $1{\cdot}5 \times 10^{-8}$ sec.

A further perturbation due to the oscillating magnetic field of the microwaves is discussed in § 7; it causes an increase in the above figure for the shift of resonance due to incipient Paschen–Back effect.

If irradiation by circularly polarized light is used, only the first four resonances given above are observed with σ^+ light and the last four for σ^- light. The overall resonance would be asymmetrical since the four resonances are not equally spaced:

$$B(\tfrac{1}{2})-B(\tfrac{3}{2})=\frac{B_0}{f}(a+b),$$

$$B(-\tfrac{1}{2})-B(\tfrac{1}{2})=\frac{B_0}{f}a,$$

$$B(-\tfrac{3}{2})-B(-\tfrac{1}{2})=\frac{B_0}{f}(a-b).$$

The resonance curve for σ^- irradiation should be the mirror image of that for σ^+.

§ 5. EXPERIMENTS USING π POLARIZED LIGHT

An experimental curve obtained using π polarized light is shown in figure 4. It is obvious from a comparison with figure 3 that a value of b of about $+2$ Mc/s explains the observed shape. This confirms the results of earlier workers and disposes of the second alternative possible in their experiments. Agreement between theory and experiment is illustrated in figure 5 where the theoretical curve for $a=18{\cdot}5$, $b=2{\cdot}25$ Mc/s is drawn superimposed by crosses taken from the experimental curve. It has been assumed that the individual resonances have a Lorentz shape with a half-width of 7·3 gauss instead of the natural half-width of 5·7 gauss. To obtain best agreement it is necessary to use a shift of ±3·6 gauss instead of the value 2·35 gauss deduced for the Paschen–Back perturbation. Justification for these assumptions is discussed in § 7.

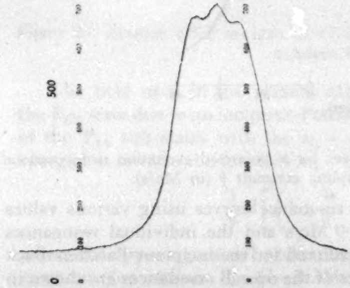

Figure 4. Experimental curve obtained using π polarized excitation.

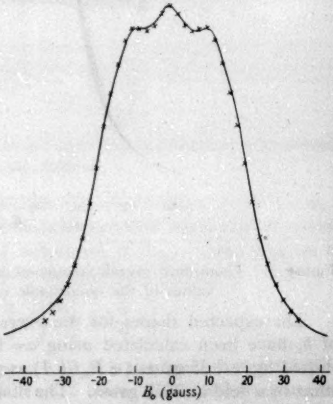

Figure 5. Theoretical overall resonance curve for π polarized excitation using $a=18{\cdot}5$, $b=2{\cdot}25$ Mc/s. The crosses represent experimental points taken from figure 4.

The centre of the overall resonance curve occurs at B_0 (the higher order terms neglected in the above expressions shift the resonance to a lower field by less than 0·1 gauss which is less than the experimental error); accurate measurement of this field and of the microwave frequency determine the g_J value of the $3^2P_{3/2}$ state of ^{23}Na. Many determinations were made using the following method. The field of the electromagnet was brought into a cyclic condition by raising and lowering the magnetizing current between two accurately determined values on each side of resonance. The field intensity was measured for various settings of the Helipot which controls the current. The cavity and associated equipment were then placed between the poles and the field taken through two cycles while recording four double resonance curves. Along the chart were marked readings from the Helipot, showing equal increments of the magnetizing current. Finally the field was again measured over several cycles. Throughout this procedure care was taken not to lose the cyclic condition. The experimental error in finding B_0 was estimated at 1 part in 4000. The frequency of the microwaves was measured by the use of a co-axial wavemeter making appropriate corrections for air temperature, pressure and humidity (Millman 1958). The estimated error was 1 part in 7000. The g_J value is deduced to be 1·3341 with a standard deviation of 0·0003, which is in excellent agreement with the theoretical prediction (1·33410) based on Russell–Saunders coupling.

Experiments were also carried out using σ irradiation and apart from asymmetries due to causes discussed in § 8, the results are similar to those for π irradiation.

§ 6. EXPERIMENTS USING CIRCULARLY POLARIZED LIGHT

Typical experimental curves for excitation by σ^+ and σ^- light are shown in figure 6. That the ratio b/a is positive may be deduced from the fact that, for σ^+ irradiation, the broadest spacing occurs on the low field side of resonance.

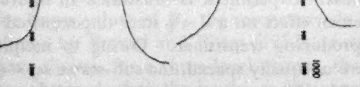

Figure 6.

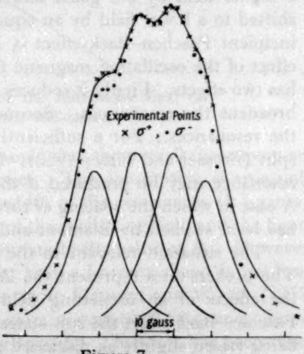

Figure 7.

Figure 6. Experimental curves obtained using circularly polarized excitation.

Figure 7. Theoretical overall resonance curve for circularly polarzeid excitation using $a = 18{\cdot}5$ Mc/s, $b = 2{\cdot}25$ Mc/s, with experimental points. The individual resonances shown have a half-width of 7·3 gauss and are weighted 0·9: 1·0: 1·0: 0·85 respectively.

The experimental curve has been fitted by four appropriately spaced Lorentz resonances. The agreement between theory and experiment is illustrated in figure 7 in which a curve drawn for $a = 18{\cdot}5$, $b = 2{\cdot}25$ Mc/s is superimposed by crosses marking points taken from the experimental curve. The half-widths of the separate resonances have been made 7·2 gauss instead of the natural half-width value of 5·7 gauss. A small increase was expected; for in order to accommodate the light input assembly for this experiment, the poles of the electromagnet had to be withdrawn further apart and the cavity placed near one pole-face. This resulted in the use of a less homogeneous field. Broadening is also expected due to the effect of the microwave field.

It has been necessary in fitting theory to experiment to weight separate resonances; the weighting used is indicated in figure 7. Justification for this procedure is discussed in § 8. The agreement in the position of the peaks of the curves is reasonable but it is not so good on the sides, especially in the case of the σ^- results. We believe that this is due to the less favourable experimental conditions in these experiments as compared with those achieved in the experiments using π polarized light. Theoretical curves for various values of a and b have been constructed in order to find the range of possible values which will fit the experimental results; the values of a and b used in figure 7 are those that give the best agreement.

The shift of $\pm 3{\cdot}6$ gauss needed to explain the π excitation results was confirmed by measurement of the fields at which the $\sigma^{\pm}$ resonances occur; these are in fact shifted by $\pm 3{\cdot}6 \pm 0{\cdot}2$ gauss respectively from the positions expected in neglect of the perturbations due to Paschen–Back and microwave field effects.

§ 7. PERTURBATION DUE TO THE MICROWAVE FIELD

Both the experiments using excitation by π polarized and circularly polarized light lead to the conclusion that the resonances $m_J = \frac{1}{2} \to \frac{3}{2}$ have been shifted to a higher field by 3·6 gauss and that the resonances $m_J = -\frac{1}{2} \to -\frac{3}{2}$ have been shifted to a lower field by an equal amount. The contribution to this effect by incipient Paschen–Back effect is 2·35 gauss; the rest can be explained by the effect of the oscillating magnetic field of the microwaves. The microwave field has two effects. Firstly it reduces the life of the sub-states involved, and thereby broadens the resonances. Secondly it can, under certain circumstances, shift the resonances. For a sufficiently strong oscillating field a resonance may be split (Brossel and Bitter 1952); but even for a weak oscillating field a shift of resonance may be produced if the sub-states involved are not equally spaced. A case in which the spacing of three Zeeman sub-states is altered by Stark effect has been studied by Blamont and Winter (1957).

The situation relevant to the present experiment is illustrated in figure 8. The broken lines represent the Zeeman effect on a $J = \frac{3}{2}$ state unperturbed by the effects of an oscillating field producing transitions. Owing to incipient Paschen–Back effect the sub-states are unequally spaced, the sub-states $m_J = \pm\frac{1}{2}$ being raised slightly as discussed in § 4. The resonant transitions which would be expected for a given frequency are indicated. The solid lines indicate the effect on the energy levels due to the microwave field (Pryce 1950). It can be seen how the presence of $m_J = -\frac{1}{2} \to +\frac{1}{2}$ transitions effect the resonant condition for $m_J = \frac{1}{2} \to \frac{3}{2}$ transitions. The $m_J = -\frac{1}{2} \to +\frac{1}{2}$ transitions, which are resonant at the field B_0, cause an increase of energy of the sub-state $m_J = \frac{1}{2}$ on the high field side, thereby producing a further shift to higher field for the $m_J = \frac{1}{2} \rightarrow \frac{3}{2}$ resonance.

Application of the methods described by Salwen (1955) leads to the conclusion that the extra shift is proportional to $B_1^2/\Delta B$ for small B_1 ($B_1 \leqslant \Delta B$) and proportional to B_1 for larger B_1, where $2B_1$ is the amplitude of the oscillating magnetic field and ΔB is the shift caused by the incipient Paschen–Back effect. A calculation of the magnitude of the oscillating field required to increase the shift from 2·35 to 3·6 gauss gives $2B_1 = 5{\cdot}3$ gauss. We had expected a value in the range two to ten gauss from an estimation based on approximate knowledge of the power consumption and the Q-value of the microwave cavity together with the frequency and the cavity dimensions. A similar argument applied to the $m_J = -\frac{1}{2} \rightarrow -\frac{3}{2}$ resonance gives an equal shift in the opposite direction.

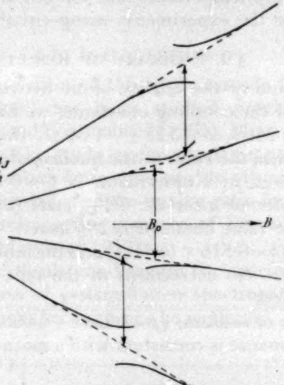

Figure 8. Illustrating the effect of the microwave field on unequally spaced Zeeman sub-states.

In the foregoing analysis it has been assumed that the overall resonances are obtained by a superposition of Lorentz curves. The assumption is true only if B_1 is much less than B', the natural half-width of the resonances (5·7 gauss). The resonances are broadened by the action of the oscillating field and the figure used for the half-widths (7·3 gauss) is appropriate to the value of B_1. However, for larger values of B_1, the resonances do not have a Lorentz shape as has been shown by Brossel and Bitter (1952); furthermore Blamont and Winter (1957) have shown, for a three-level system, that more complicated resonance shapes are obtained when the levels are not equally spaced. The view has been taken in the analysis of the present experiments that these multiple quantum effects simply broaden the resonances. In justification of this we point to the following. Deviation from pure Lorentz shape is due to terms involving $(B_1/B')^2$, which in these experiments is only of the order 1/4. Also by the use of Lorentz curves it has proved possible to match the experimental results not only in the position of the peaks but also, to a large extent, in contour. However, in view of the doubt, the quoted errors are rather larger than those expected from the analysis.

§ 8. EFFECT OF THE DISTRIBUTION OF INTENSITY FROM THE EXCITING LAMP ON THE SHAPE OF THE OVERALL RESONANCE

Because of the Zeeman effect, the optical frequencies in absorption between the sub-states of $3^2S_{1/2}$ and $3^2P_{3/2}$ are spread about the mean frequency. The magnitudes of the displacements are comparable with the breadth of the optical line from the exciting lamp, and consequently the hyperfine sub-states may be excited with different strengths. Estimations of the distribution of intensity obtained from measurements with a Fabry–Perot interferometer make it possible to explain the asymmetrical resonance curves obtained with π polarized excitation when the lamp temperature was too hot or too cold and to justify the weighting assumed for the experiments using circularly polarized light.

§ 9. SUMMARY OF RESULTS

From a consideration of the quality of fit between experiment and theory using various values of the coupling constants, we have arrived at the following results: $a = 18{\cdot}5 \pm 0{\cdot}6$ Mc/s, $b = 2{\cdot}25 \pm 0{\cdot}4$ Mc/s, the ratio b/a being positive.

Using this ratio of b/a, the value of the quadrupole moment of ^{23}Na calculated from the formulae given in Kopfermann is $Q = 0{\cdot}097 \pm 0{\cdot}013$ barn. If Q is calculated from the value of a for the $3^2P_{1/2}$ state ($a_{1/2} = 94{\cdot}45$ Mc/s, Perl, Rabi and Senitzky 1955) the value obtained is 2% lower. If Q is calculated from the fine structure splitting ($\delta = 0{\cdot}516 \times 10^{12}$ c/s) and the inner atomic number $Z_i = 7{\cdot}40$) the value is 7% lower. No corrections of the type discussed by Sternheimer (1954) have been applied.

For the $3^2P_{3/2}$ state of sodium, $g_J = 1{\cdot}3341 \pm 0{\cdot}0003$.

The breadth of resonance is consistent with a mean life of $(1{\cdot}5 \pm 0{\cdot}2) \times 10^{-8}$ sec for the $3^2P_{3/2}$ state.

ACKNOWLEDGMENTS

We wish to acknowledge the assistance and encouragement of Professor R. R. Nimmo and the helpful discussions with Dr. G. S. Bogle (Commonwealth Scientific and Industrial Research Organization, Sydney) and Dr. G. W. Series (Clarendon Laboratory, Oxford). It is a pleasure to record our indebtedness to Mr. A. E. Adam for his constructional and scientific ingenuity and for his invaluable technical assistance. The work has been supported by grants from the New Zealand Research Committee.

REFERENCES

BLAMONT, J.-E., and Winter, J.-M., 1957, *C.R. Acad. Sci., Paris*, **244**, 332.
BOGLE, G. S., DODD, J. N., and PURSER, K. H., 1956, *Phys. Rev.*, **101**, 246.
BOGLE, G. S., DODD, J. N., and MCLEAN, W. L., 1957, *Proc. Phys. Soc.* B, **70**, 796.
BROSSEL, J., and BITTER, F., 1952, *Phys. Rev.* **86**, 308.
BROSSEL, J., and KASTLER, A., 1949, *C.R. Acad. Sci., Paris*, **229**, 1213.
KOPFERMANN, H., 1958, *Nuclear Moments* (New York : Academic Press).
MILLMAN, G. H., 1958, *Proc. Inst. Radio Engrs, N.Y.*, **46**, 1492.
PERL, M. L., RABI, I. I., and SENITZKY, B., 1955, *Phys. Rev.*, **98**, 611.
PRYCE, M. H. L., 1950, *Phys. Rev.*, **77**, 136.
SAGALYN, P. L., 1954, *Phys. Rev.*, **94**, 885.
SALWEN, H., 1955, *Phys. Rev.*, **99**, 1274.
STERNHEIMER, R. M., 1954, *Phys. Rev.*, **95**, 736.

The Angular Correlation between some Coincident γ-rays of ^{192}Pt

By D. K. BUTT

Birkbeck College, Malet Street, London, W.C.1

MS. received 1st *June* 1959

Abstract. A re-investigation of the combined angular correlation existing between the 296, 308 and 316 kev γ-rays of ^{192}Pt has been found to be in agreement with spin 3 for the 4th excited state and M1/E2 mixtures of about 3% and 5% for the 308 and 296 kev transitions respectively.

§ 1. INTRODUCTION

THE total angular correlation of the triple cascade in the de-excitation of ^{192}Pt (308–296–316 kev) has been studied previously by Taylor and Pringle (1955), Kelly and Wiedenbeck (1956), Mráz (1957) and Kawamura, Hoki and Huyaski (1958). This study is of particular importance since not only is it at this nucleus that a transition from rotational to vibrational excitation occurs (Mottelson 1957), but a knowledge of the mixing ratio for the 296 kev transition provides a method for observing the presence of E0 radiation in this $2^+ \rightarrow 2^+$ transition (Lindqvist and Markland 1957).

The measurement is a difficult one because the spacing of the γ-rays is well within the energy resolution of γ-scintillation spectrometers and the effects of several interfering cascades can by no means be neglected.

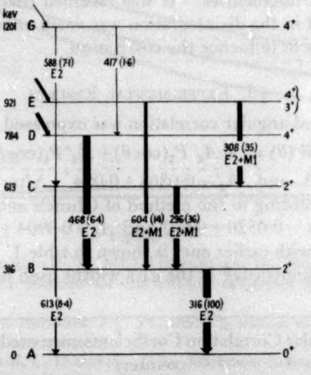

Figure 1. Principal modes of ^{192}Pt de-excitation according to Baggerly *et al.* (The terms in brackets denote the relative intensities of the γ-rays.)

The spins of the levels A, B, C and D of ^{192}Pt (figure 1) are known to be 0, 2, 2 and 4 respectively (Baggerly *et al.* 1955); hence an investigation of the angular correlation of the triple cascade gives information concerning the spin of level E and the mixing ratios of the 308 and 296 kev transitions.

Taylor and Pringle, Kelly and Wiedenbeck and Mráz showed that the correlation could be interpreted by assuming a spin 4 for level E and a small M1/E2 mixture for the 296 kev transition. Kelly and Wiedenbeck's results indicated that spin 3 was permissible also; however this work made no allowance for the interfering correlations. Mráz was unable to obtain agreement between the mixtures obtained for spin 3 and those from internal conversion studies. Recently, Kelman *et al.* (1957) have investigated the relative intensities of the L subshell internal conversion lines of ^{192}Pt with a high resolution spectrometer and it appears from this work that both the 308 and 604 kev transitions are mixed, requiring level E to have a spin 3. Kawamura *et al.* have shown that approximate agreement can be obtained between the angular correlation and the data of Kelman *et al.* on the assumption of spin 3 for level E.

The present work represents a re-investigation of this angular correlation and a more detailed comparison of it with internal conversion data. This has been made possible by the appearance of the tables of theoretical internal conversion coefficients of Rose (1958) and Sliv and Band (1958).

§ 2. EXPERIMENTAL METHOD

The correlation was measured with a conventional high speed coincidence circuit, similar to that of Bell *et al.* (1952) incorporating two 1 in. × 1½ in. NaI(T1) crystals and two slow channels with differential discriminators. The discriminator gates were set to span the 300 kev group photo-peaks. The resolving time of the fast circuit was $1{\cdot}2 \times 10^{-9}$ sec and the true coincidence to accidental counting ratio was about 30 : 1.

The source was a 3 mm diameter spot of natural iridium which had been sputtered on to a thin flake of quartz and irradiated in the Harwell BEPO pile. Its activity was about 10 microcuries. It was assumed that none of the transition probabilities involved in the disintegration was small enough to allow any extra-nuclear perturbations to influence the correlation.

§ 3. EXPERIMENTAL RESULTS

When the measured angular correlation was expressed in the form

$$W(\theta) = 1 + A_2' P_2(\cos\theta) + A_4' P_4(\cos\theta),$$

$A_2' = -0{\cdot}0512 \pm 0{\cdot}003$ and $A_4' = 0{\cdot}0863 \pm 0{\cdot}004$. After correction for finite counter apertures according to the method of Church and Kraushaar (1952) the coefficients were $A_2 = -0{\cdot}0520 \pm 0{\cdot}003$ and $A_4 = 0{\cdot}0904 \pm 0{\cdot}004$. A comparison of the present results with earlier ones is shown in table 1. An exact comparison, however, demands a knowledge of the gate widths used in each case.

Table 1. Total Angular Correlation Coefficients corrected for finite solid angles of counters

Authority	A_2	A_4
Taylor and Pringle	No comparison possible.	
Kelly and Wiedenbeck	$-0{\cdot}056 \pm 0{\cdot}004$	$0{\cdot}0929 \pm 0{\cdot}005$
Márz	$-0{\cdot}056 \pm 0{\cdot}0085$	$0{\cdot}104 \pm 0{\cdot}013$
Kawamura *et al.*	$-0{\cdot}055 \pm 0{\cdot}004$	$0{\cdot}102 \pm 0{\cdot}005$
Present author	$-0{\cdot}052 \pm 0{\cdot}003$	$0{\cdot}0904 \pm 0{\cdot}004$

§ 4. INTERPRETATION OF RESULTS

By measuring the slow channel pulse amplitude distribution for single γ-ray emitters whose energies corresponded approximately with those of the two higher energy γ-ray groups in ^{192}Pt (468 and 600 kev approximately)† an estimation was made of the amount of 468 and 600 kev radiation which passed through the gates spanning the 300 kev photo-peaks. The method used was similar to that

Table 2

(1)	(2)
296–316	1·00
308–296	0·80
308–316 (1st–3rd)	0·81
308–612	0·04
468–316	0·26
588–296	0·04
604–316	0·09
588–316 (1st–3rd)	0·04

(1) The cascades (kev); (2) the relative intensities of the participating angular correlations allowing for the discriminator gate settings.

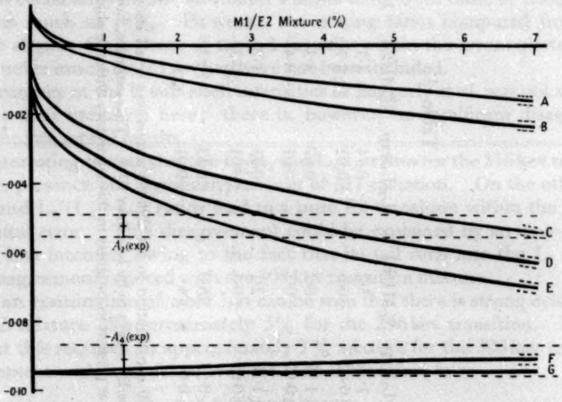

Figure 2.

A A_2 for the 308 kev transition 0–7% M1/E2 mixture and the 296 kev transition pure E2.

B A_2 for a 0–7% M1/E2 mixture for the 296 kev transition and a pure E2 308 kev transition.

C, D, E A_2 for the 308 kev transition 3%, 5%, and 7% mixed, respectively, and a 0–7% mixture for the 296 kev transition.

F A_4 belonging to curves B, C, D and E. (The differences between these cases were not great enough to warrant separate plots.)

G A_4 belonging to curve A.

Pairs of short dotted lines parallel with each curve show the errors due to the inaccuracy of the γ-ray intensities. Pairs of broken lines show the statistical error of the experimental coefficients.

---

† The isotopes used were ^{198}Au for the 468 kev γ-ray and ^{137}Cs for the 600 kev group. These isotopes emit γ-rays of 411 and 662 kev respectively.

Table 3

Transition Energy (kev)	(L_2/L_1)exp	%M1/E2	(L_3/L_1)exp	%M1/E2	$L_3/(L_1+L_2)$exp	%M1/E2	(K/L)exp	%M1/E2
296†	1·39	5·2	0·74	5·3	0·310	5·5	2·35	4·4
	±0·03	±0·6	±0·02	±0·7	±0·01	±2·3	±0·04	±0·6
308	1·18	8·2	0·67	5·3	0·307	2·0	2·38	3·2
	±0·02	±0·5	±0·01	±0·4	±0·007	±1·3	±0·02	±0·3
316	1·38	2·1	0·73	1·7	0·307	1	2·22	0
	±0·01	±0·3	±0·01	±0·3	±0·006	±1	±0·02	
604	0·33	26·0	0·13	16·3	0·098	14·1	4·7	12
	±0·01	±4	±0·01	±5	±0·008	±7	±0·1	±10

† It was assumed that the E0 contribution to the 296 kev ratios was small enough to be neglected. Lindqvist and Markland (1957) estimate the ratio E0 K electrons/E2 γ-rays to be less than 10^{-3}. This estimate, however, appears to be prone to a rather large error. An e–γ angular correlation study is at present in progress in this laboratory with the object of measuring this ratio more precisely.

employed by Mráz. These data, together with the relative γ-ray intensities† and internal conversion coefficients of Baggerly *et al.* (1955) allowed the relative intensities of the participating angular correlations to be calculated (table 2).

The total theoretical angular correlation coefficients were then calculated for the case of spin 3 for level E (Rose 1953, Biedenharn and Rose 1953). The work of Kelman *et al.* shows that the 604 kev transition is highly mixed. A 14% M1/E2 mixture (table 3) with a negative mixing ratio (Shiel, Wyly and Braden 1957) has been assumed for it for this calculation, although the overall correlation is not highly sensitive to this figure.

Figure 2 shows the angular correlation coefficients for a number of selected cases as a function of mixing ratio. Only negative values of the mixing ratios have been used, since positive ones give positive A_2's over the range of mixtures considered.

The theoretical conversion coefficients of Rose (1958) and Sliv and Band (1958) make possible a recalculation of the M1/E2 mixtures for the 296, 308, 316 and 604 kev γ-rays from the K and L shell ratios of Kelman *et al.* Dynamic nuclear structure effects are not expected to be present in these transitions (Nilsson and Rasmussen 1958).

The results for these in table 3 are based on Rose's tables. The internal conversion coefficients in Sliv and Band's tables differ from those of Rose in some cases by as much as 10%. However, the mixing ratios computed from them differ only slightly from those of table 3 (usually within the errors quoted in the table and never much more) so they have not been included.

The accuracy of the L sub-shell intensities of Baggerly *et al.* was not sufficient to warrant their inclusion here; there is, however, no significant disagreement between the two sets of results.

It is interesting to note that the L_2/L_1 and L_3/L_1 ratios for the 316 kev transition lead to the presence of a significant amount of M1 radiation. On the other hand the K/L and $L_3/(L_1+L_2)$ ratios lead to a pure E2 transition within the limits of experimental error. This disagreement could be explained by an over-estimate of the L_2 line intensity owing to the fact that its tail runs into the L_1 line. A similar disagreement is noted with the 308 kev transition mixture.

From an examination of table 3, it can be seen that there is strong evidence for an M1/E2 mixture of approximately 5% for the 296 kev transition. Figure 2 shows that this requires an approximately 3% mixture for the 308 kev transition. The agreement with internal conversion data is therefore fair.

§ 5. CONCLUSIONS

Satisfactory agreement can be obtained between internal conversion and γ–γ angular correlation data with the assumptions that level E has spin 3 and the 308 and 296 kev γ-rays have M1/E2 multipolarity mixing ratios of about 3% and 5% respectively.

ACKNOWLEDGMENTS

I am indebted to Professor J. D. Bernal for the laboratory facilities he placed at my disposal. The research was partially financed by a grant from the Department of Scientific and Industrial Research.

---

† Although Baggerly *et al.* claimed accuracy only to ±20% for their intensities their results agree, in fact, to within ±10% with those obtained by averaging the values of Bashilov *et al.* (1952), Johns and Nablo (1954), Baggerly *et al.* (1955) and Sumbaev (1957).

REFERENCES

BAGGERLY, L. L., MARMIER, P., BOEHM, F., and DUMOND, J. W. M., 1955, *Phys. Rev.*, **100**, 1364.

BASHILOV, A. A., ANTON'EVA, N. E., and DZHELEPOV, B. S., 1952, *Izv. Akad. Nauk, S.S.S.R., Ser. Fiz.*, **16**, 262.

BELL, R. E., GRAHAM, R. L., and PETCH, H. E., 1952, *Canad. J. Phys.*, **30**, No. 1, 35.

BIEDENHARN, L. C., and ROSE, M. E., 1953, *Rev. Mod. Phys.*, **25**, 729.

CHURCH, E. L., and KRAUSHAAR, J. J., 1952, *Phys. Rev.*, **88**, 419.

JOHNS, M. W., and NABLO, S. V., 1954, *Phys. Rev.*, **96**, 1599.

KAWAMURA, M., HOKI, A., and HUYASHI, T., 1958, *J. Phys. Soc., Japan*, **13**, 1071.

KELLY, W. H., and WIEDENBECK, M. L., 1956, *Phys. Rev.*, **102**, 1130.

KELMAN, V. M., METSKHVARISHVILI, R. YA., ROMANOV, V. A., TUCHKEVICH, V. V., 1957, *Nucl. Phys.*, **4**, 240.

LINDQVIST, T., and MARKLAND, I., 1957, *Nucl. Phys.*, **4**, 189.

MOTTELSON, B. R., 1957, *Rev. Mod. Phys.*, **29**, 186.

MRÁZ, J., 1957, *Nucl. Phys.*, **4**, 457.

NILSSON, S. G., and RASMUSSEN, J. O., 1958, *Nucl. Phys.*, **5**, 617.

ROSE, M. E., 1953, *O.R.N.L. Report*, 1555. Oak Ridge National Laboratory, U.S.A.

—— 1958, *Internal Conversion Coefficients* (Amsterdam: North-Holland).

SHIEL, V., WYLY, L. D., and BRADEN, C. H., 1957, *Phys. Rev.*, **105**, 1521.

SLIV, L. A., and BAND, I. M., 1956, 1958, *Coefficients of Internal Conversion of Gamma Radiation*, Part 1, K. Shell, 1956; Part 2, L Shell, 1958. Physico-Technical Institute, Academy of Sciences of the U.S.S.R.

SUMBAEV, O. I., 1957, *Soviet Physics, J.E.T.P.*, **5**, 170.

TAYLOR, H. W., and PRINGLE, R. W., 1955, *Phys. Rev.*, **99**, 1345.

Electron Detachment from the Negative Hydrogen Ion by Electron Impact

By S. GELTMAN
Atomic Physics Section, National Bureau of Standards, Washington, D.C., U.S.A.

MS. received 22*nd May* 1959, *in revised form* 20*th July* 1959

Abstract. The Born–Oppenheimer approximation has been used to evaluate the cross section for the detachment of electrons from H^- by electron impact over an energy range from threshold (0·75 ev) to 75 ev. An empirical correction was then applied to account approximately for the long range Coulomb repulsion between the incident electron and the negative ion. The resulting cross section has a broad maximum of $700\pi a_0^2$ centred at about 45 ev.

§ 1. Introduction

THE detachment of electrons from negative ions by the impact of free electrons is a process which has not yet been directly measured in the laboratory. The process is of general interest for the study of the properties of negative ions and how they compare with those of neutral atoms and positive ions. The H^- in the sun's photosphere has long been recognized as a primary source of continuous opacity for the visible spectrum. Consequently, it is of astrophysical interest to know to what extent the dissociation of H^- by electron impact influences photospheric processes (Pagel 1956). The rate of this process is also needed in the investigation of arc plasma properties (Boldt 1959).

§ 2. Formulation of Scattering Problem

The total cross section for the detachment of an electron by electron impact from H^- in its ground ${}^1S_0$ state is

$$\sigma = \int d\boldsymbol{\kappa} \iint \sin\theta \, d\theta \, d\phi \frac{k_{\mathrm{q}}}{k_{\mathrm{p}}} \{\tfrac{1}{4}|f_\kappa^{(1)} - g_\kappa^{(1)}|^2 + \tfrac{3}{4}|g_\kappa^{(3)}|^2\} \qquad \ldots\ldots(1)$$

where $\mathbf{k}_{\mathrm{p}}(k_{\mathrm{p}}, 0, 0)$, $\mathbf{k}_{\mathrm{q}}(k_{\mathrm{q}}, \theta, \phi)$, and $\boldsymbol{\kappa}$ are the incident, scattered, and ejected electron wave vectors, respectively, and in the Born–Oppenheimer approximation (Bates *et al.* 1950) the scattering amplitudes are

$$\{f_\kappa^{(1)}, g_\kappa^{(1)}\} = (2\pi)^{-1} \iiint d\tau_1 \, d\tau_2 \, d\tau_3 \exp(-i\mathbf{k}_{\mathrm{q}} \cdot \mathbf{r}_1)\psi_\kappa^{(1)*}(\mathbf{r}_2, \mathbf{r}_3)\left(\frac{1}{r_1} - \frac{1}{r_{12}} - \frac{1}{r_{13}}\right)$$
$$\times \{\exp(i\mathbf{k}_{\mathrm{p}} \cdot \mathbf{r}_1)\psi_0(\mathbf{r}_2, \mathbf{r}_3), \ \exp(i\mathbf{k}_{\mathrm{p}} \cdot \mathbf{r}_2)\psi_0(\mathbf{r}_1, \mathbf{r}_3)\}$$

(singlet–singlet transition)

$$g_\kappa^{(3)} = (2\pi)^{-1} \iiint d\tau_1 \, d\tau_2 \, d\tau_3 \exp(-i\mathbf{k}_{\mathrm{q}} \cdot \mathbf{r}_1)\psi_\kappa^{(3)*}(\mathbf{r}_2, \mathbf{r}_3)\left(\frac{1}{r_1} - \frac{1}{r_{12}} - \frac{1}{r_{13}}\right)$$
$$\times \exp(i\mathbf{k}_{\mathrm{p}} \cdot \mathbf{r}_3)\psi_0(\mathbf{r}_1, \mathbf{r}_2)$$

(singlet–triplet transition). $\ldots\ldots(2)$

In the above, ψ_0 is the ground state wave function while $\psi_\kappa^{(1)}$ and $\psi_\kappa^{(3)}$ are the final state singlet and triplet wave functions corresponding to one electron bound and the other electron free. The integration over $\boldsymbol{\kappa}$ in (1) is restricted to the volume in $\boldsymbol{\kappa}$-space where energy is conserved, i.e. where $k_p^2+2E_0=k_q^2+\kappa^2$ (E_0 = one electron binding energy in H^-). The atomic units used are length in units of a_0, energy in e^2/a_0, and wave number in units of $1/a_0$.

Bates *et al.* (1950) have tested the Born–Oppenheimer approximation for excitation to discrete states by electron impact and have found it to be very poor at low energies. It has until now not been applied to the case of ionization. The source of difficulty in the Born–Oppenheimer exchange amplitude is that the contribution of the electron–nucleus interaction term remains present even though the initial and final state atomic wave functions are orthogonal. We shall show that this term provides a negligible contribution to the angular integrations of both the direct and exchange amplitudes in the present calculation, except at the lowest energies. Thus we are relieved of the objectionable feature of the Born–Oppenheimer approximation encountered in excitation to discrete states.

An improvement in the approximation for this particular case of electron scattering by a negative ion would consist of replacing the incident plane wave in (2) by a repulsive Coulomb wave. The effect of this would be to reduce the cross section, as the wave function for the incident electron would be decreased in the region of greatest overlap. However, the use of a Coulomb function in (2) would make the integrals intractable, so we defer until later in the calculation an approximate correction for the initial Coulomb repulsion.

§ 3. Evaluation of Scattering Amplitudes

The simple product-type wave functions for H^-,

$$\psi_0=\phi_0(r_1)\phi_0(r_2)$$

$$\psi_\kappa^{(1)}=\phi_0(r_1)\phi_\kappa(r_2)+\phi_0(r_2)\phi_\kappa(r_1) \qquad \ldots\ldots(3)$$

have been found (Geltman 1956) to yield photodetachment cross sections in good agreement with more elaborate calculations and with experiment (Smith and Burch 1959) when one chooses ϕ_0 and ϕ_κ as the solutions of a one-electron Schrödinger equation with a short range attractive potential containing one bound 1s state at the known binding energy of 0·75 ev. For the present calculation we retain the above form for ψ_0 with the normalized orbital

$$\phi_0(r)=\begin{cases} 0{\cdot}757\pi^{-1/2}\exp(-1{\cdot}058r)\,{}_1F_1(0{\cdot}0548;\,2;\,2{\cdot}116r), & r<1{\cdot}88 \\ 0{\cdot}393\pi^{-1/2}r^{-1}\exp(-0{\cdot}234r), & r\geqslant 1{\cdot}88 \end{cases} \qquad \ldots\ldots(4)$$

while taking for the continuum state the simpler normalized form

$$\psi_\kappa=2^{-1/2}(2\pi)^{-3/2}[\phi_H(r_1)\exp(i\boldsymbol{\kappa}\cdot\mathbf{r}_2)\pm\phi_H(r_2)\exp(i\boldsymbol{\kappa}\cdot\mathbf{r}_1)] \qquad \ldots\ldots(5)$$

where ϕ_H is the ground state hydrogen function and the + and − signs go with the singlet and triplet states respectively.

Inserting these wave functions into the expressions for the amplitudes we obtain

$$\begin{aligned}
f_\kappa^{(1)} = 2^{-1/2}(2\pi)^{-5/2}\Big\{ & -2\int d\tau_3\phi_0(r_3)\phi_{\mathrm{H}}(r_3)\int d\tau_2\phi_0(r_2)\exp(-i\boldsymbol{\kappa}\,.\,\mathbf{r}_2) \\
& \times\int d\tau_1\frac{\exp[i(\mathbf{k}_{\mathrm{p}}-\mathbf{k}_{\mathrm{q}})\,.\,\mathbf{r}_1]}{r_{12}} \\
& +2\int d\tau_3\phi_0(r_3)\exp(-i\boldsymbol{\kappa}\,.\,\mathbf{r}_3)\int d\tau_1\exp[i(\mathbf{k}_{\mathrm{p}}-\mathbf{k}_{\mathrm{q}})\,.\,\mathbf{r}_1] \\
& \times\int d\tau_2\phi_0(r_2)\phi_{\mathrm{H}}(r_2)\left(\frac{1}{r_1}-\frac{1}{r_{12}}\right)\Big\}, \\
g_\kappa^{(1)} = 2^{-1/2}(2\pi)^{-5/2}\Big\{ & -\int d\tau_3\phi_0(r_3)\phi_{\mathrm{H}}(r_3)\int d\tau_2\phi_0(r_2)\exp(-i\mathbf{k}_{\mathrm{q}}\,.\,\mathbf{r}_2) \\
& \times\int d\tau_1\frac{\exp[i(\mathbf{k}_{\mathrm{p}}-\boldsymbol{\kappa})\,.\,\mathbf{r}_1]}{r_{12}} \\
& +\int d\tau_3\phi_{\mathrm{H}}(r_3)\exp(i\mathbf{k}_{\mathrm{p}}\,.\,\mathbf{r}_3)\int d\tau_2\phi_0(r_2)\exp(-i\boldsymbol{\kappa}\,.\,\mathbf{r}_2) \\
& \times\int d\tau_1\phi_0(r_1)\exp(-i\mathbf{k}_{\mathrm{q}}\,.\,\mathbf{r}_1)\left(\frac{1}{r_1}-\frac{1}{r_{12}}-\frac{1}{r_{13}}\right) \\
& +\int d\tau_3\exp[i(\mathbf{k}_{\mathrm{p}}-\boldsymbol{\kappa})\,.\,\mathbf{r}_3]\int d\tau_1\phi_0(r_1)\exp(-i\mathbf{k}_{\mathrm{q}}\,.\,\mathbf{r}_1) \\
& \times\int d\tau_2\phi_0(r_2)\phi_{\mathrm{H}}(r_2)\left(\frac{1}{r_1}-\frac{1}{r_{12}}\right)\Big\}, \\
g_\kappa^{(3)} = -g_\kappa^{(1)}. & \qquad\qquad\qquad\qquad\qquad\qquad\ldots\ldots(6)
\end{aligned}$$

The last term in $g_\kappa^{(1)}$ will vanish because of the plane wave integration

$$\int d\tau_3\exp[i(\mathbf{k}_{\mathrm{p}}-\boldsymbol{\kappa})\,.\,\mathbf{r}_3]=0$$

since energy conservation requires that $k_{\mathrm{p}}>\kappa$. Note that if we were presently dealing with excitation rather than detachment, $\exp(i\boldsymbol{\kappa}\,.\,\mathbf{r})$ in (6) would be replaced by a bound state function. Hence, instead of the last term in $g_\kappa^{(1)}$ vanishing identically, it would have its largest value at small k_{p} and thus contribute to the peak near threshold obtained by Bates *et al.* (1950). We neglect the second terms in $f_\kappa^{(1)}$, $g_\kappa^{(1)}$ and $g_\kappa^{(3)}$ and retain only the first terms. The justification for dropping these terms is discussed in the Appendix. This results in a considerable simplification in performing the space integrations, yielding

$$\left.\begin{aligned}
f_\kappa^{(1)} &= -4\pi^{-1/2}\Delta|\mathbf{k}_{\mathrm{p}}-\mathbf{k}_{\mathrm{q}}|^{-2}\frac{J(K)}{K} \\
g_\kappa^{(1)} &= -2\pi^{-1/2}\Delta|\mathbf{k}_{\mathrm{p}}-\boldsymbol{\kappa}|^{-2}\frac{J(K)}{K}
\end{aligned}\right\}\qquad\ldots\ldots(7)$$

where

$$\mathbf{K}=\mathbf{k}_{\mathrm{p}}-\mathbf{k}_{\mathrm{q}}-\boldsymbol{\kappa},\quad \Delta=\int d\tau\phi_0\phi_{\mathrm{H}}=0{\cdot}944,\quad\text{and}\quad J(K)=\int_0^\infty dr r\phi_0\sin Kr.$$

The function $J(K)/K$, which is $(4\pi)^{-1}$ times the Fourier transform of $\phi_0(r)$, is given in figure 1.

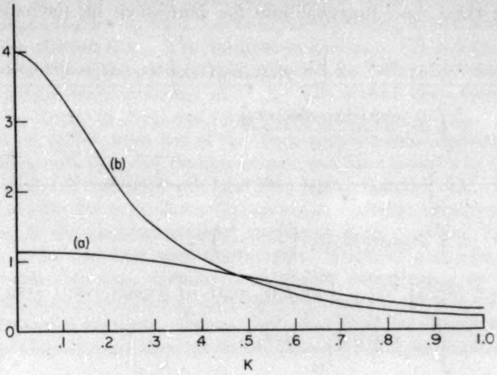

Figure 1. The quantity $(4\pi)^{-1}\int d\tau\phi\, e^{i\mathbf{K}\cdot\mathbf{r}}$ for (*a*) $\phi=\phi_{\mathrm{H}}$ and (*b*) $\phi=\phi_0$.

§ 4. TOTAL CROSS SECTION

To obtain the total cross section we must integrate over the angle of scattering (θ, ϕ), the angle of ejection (θ', ϕ'), and the accessible range of ejected electron wave number, $\kappa=0$ to $(k_{\mathrm{p}}^2+2E_0)^{1/2}$. The integrations over azimuthal angles may be done immediately by the proper choice of polar axes. These integrations can be conveniently described in terms of the dimensionless variables

$$\alpha=\cos\theta=\frac{\mathbf{k}_{\mathrm{p}}\,.\,\mathbf{k}_{\mathrm{q}}}{k_{\mathrm{p}}k_{\mathrm{q}}}, \qquad \beta=\frac{\boldsymbol{\kappa}\,.\,(\mathbf{k}_{\mathrm{p}}-\mathbf{k}_{\mathrm{q}})}{\kappa|\mathbf{k}_{\mathrm{p}}-\mathbf{k}_{\mathrm{q}}|},$$

$$q=k_{\mathrm{q}}/k_{\mathrm{p}}, \qquad s=\kappa/k_{\mathrm{p}}, \qquad t^2=2|E_0|/k_{\mathrm{p}}^2=1-s^2-q^2.$$

The total cross section in units of πa_0^2 is

$$\sigma=(8\Delta^2/k_{\mathrm{p}})\int_0^{1-t^2} ds^2 sq\int_{-1}^{1} d\alpha\int_{-1}^{1} d\beta[I_1(\alpha,\beta,q,s)+I_1(\alpha,\beta,s,q)-I_2(\alpha,\beta,q,s)] \qquad \ldots\ldots(8)$$

where

$$I_1(\alpha,\beta,q,s)=(1+q^2-2q\alpha)^{-2}(J/K)^2,$$

$$\begin{aligned}I_2(\alpha,\beta,q,s)=(1+q^2-2q\alpha)^{-1}(J/K)^2&\\ \times[(1-s^2)^2+4s^2\{\beta-s(1-q\alpha)(1+q^2-2q\alpha)^{-1/2}\}&\\ \times\{\beta-s^{-1}(1-q\alpha)(1+q^2-2q\alpha)^{-1/2}\}]^{-1/2},&\end{aligned}$$

and $K^2=2k_{\mathrm{p}}^2[1-t^2/2-q\alpha-s\beta(1+q^2-2q\alpha)^{1/2}]$.

Terms of the form $|f_\kappa^{(1)}|^2$, $|g_\kappa^{(1)}|^2$, or $|g_\kappa^{(3)}|^2$ lead to I_1, while the cross-term $f_\kappa^{(1)}g_\kappa^{(1)}$ leads to I_2. As s and q enter symmetrically,

$$\int_0^{1-t^2} ds^2 sqI_1(\alpha,\beta,s,q)=\int_0^{1-t^2} ds^2 sqI_1(\alpha,\beta,q,s).$$

The triple integrations have been done numerically on the IBM 704 computer and the result is given in figure 2. The contribution of the cross-term was small—less than 5% at all energies.

It is of interest to compare this result with that obtained from the Born approximation, i.e.

$$\sigma = \int d\kappa \int\int \sin\theta \, d\theta \, d\phi \frac{k_q}{k_p} |f_\kappa^{(1)}|^2. \qquad \ldots\ldots(9)$$

As the contribution of the cross-term was found to be small and that of $|f_\kappa^{(1)}|^2$ is four times that of $|g_\kappa^{(1)}|^2$ or $|g_\kappa^{(3)}|^2$, the cross section without exchange is reduced by about half with the inclusion of exchange. Unlike the case of excitation to a discrete bound state, the exchange amplitudes here do not become small compared with the direct amplitude in the high energy limit. Comparison of these results with a future experiment would give an indication of whether the Born or Born–Oppenheimer method is better for the case of ionization.

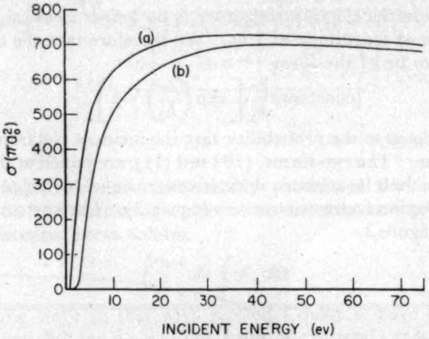

Figure 2. Total cross section for electron detachment: (*a*) Born–Oppenheimer approximation and (*b*) corrected for Coulomb repulsion.

§ 5. CORRECTION FOR INITIAL COULOMB REPULSION

The use of a plane wave to describe the initial state of an electron–negative ion collision is clearly a rough approximation. As mentioned previously, a much better one would be to use the repulsive Coulomb wave

$$\left(\frac{2\pi}{k_p}\right)^{1/2} \left[\exp\left(\frac{2\pi}{k_p}\right) - 1\right]^{-1/2} \exp(i\mathbf{k}_p \cdot \mathbf{r})\,{}_1F_1\left(\frac{i}{k_p}\,;\,1\,;\,i[k_p r - \mathbf{k}_p \cdot \mathbf{r}]\right).$$

The use of this function resulted in space integrals which could not be reduced analytically to a sufficient degree to make the entire calculation feasible. We were thus led to the necessity of attempting to correct the Born–Oppenheimer cross section for this effect. We consider the high and low energy regions separately.

5.1. *High Energies*

Our present result corresponds to the case of the long range repulsive field between electron and negative ion being switched off. As the effective radius for detachment b_0 (where $\sigma = \pi b_0^2$) is large compared with $1/k_p$ it is reasonable to think of the incident electron's trajectory classically. With the repulsion switched off the distance of closest approach is equal to the impact parameter.

When the repulsion is switched on, the distance of closest approach becomes larger than the impact parameter so that the apparent cross section is decreased by a factor equal to the ratio of the square of the impact parameter to the square of the distance of closest approach. Using the well-known relation between impact parameter and distance of closest approach for a Coulomb field (Goldstein 1950) the correction factor is

$$1-2/b_0k_p^2 \qquad \ldots\ldots(10)$$

where b_0 is equal to $\pi^{-1/2}$ times the square root of the Born–Oppenheimer cross section (in units of πa_0^2).

5.2. *Low Energies*

A difficulty with the above procedure is that below a particular incident energy, (10) will become negative. We also do not expect the above procedure to be valid because the electron trajectory is no longer classical, i.e. b_0 becomes of the same order of magnitude as $1/k_p$. We therefore take the correction factor at low energies to be of the form

$$(\text{constant})\frac{2\pi}{k_p}\left[\exp\left(\frac{2\pi}{k_p}\right)-1\right]^{-1} \qquad \ldots\ldots(11)$$

which is proportional to the probability that the incident electron is at the centre of the negative ion. The two forms, (10) and (11), are joined at the wave number $k_p = 0{\cdot}475$, where their logarithmic derivatives are equal. The constant is chosen to make the correction factor continuous (figure 3). The corrected cross section is also shown in figure 2.

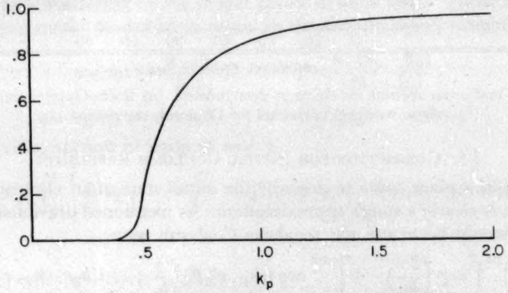

Figure 3. Correction factor for Coulomb repulsion.

§ 6. COMPARISON OF CROSS SECTIONS OF H^- WITH H

The resulting detachment cross section at its maximum is the order of 10^3 times larger than the H atom ionization cross section (Fite and Brackmann 1958). In what follows we shall try to understand the origins of this large difference factor by comparing the quantum mechanical calculations and by semi-classical arguments.

6.1. *Quantum Calculations*

The factor of 10^3 can be seen to arise from the following two sources:

(*a*) The electron cloud in the negative ion has a much larger extent than in the neutral atom because of the weaker binding. This can be seen by the comparison of the Fourier transform of ϕ_0 (divided by 4π) with that for ϕ_{H}. At $K=0$, where momentum is conserved and we have the greatest contribution to the differential cross section, $J(K)/K$ for ϕ_0 exceeds that for ϕ_{H} by a factor of 3·54 (see figure 1). The square of this then accounts for a factor of about 10.

(*b*) The remaining factor of 10^2 must then arise from the use of a plane wave to describe the final state ψ_κ rather than an attractive Coulomb wave. The differential cross section for the direct ionization of a hydrogen atom using a Coulomb wave for the ejected electron has been evaluated (Massey and Mohr 1933) and this may be compared with the easily obtainable analogous quantity using a properly normalized plane wave for the ejected electron. The resulting expressions for the differential cross section (after integration over all angles of ejection) are

$$\int \mathscr{I}_\kappa \, d\Omega' = \frac{2^{10} k_{\mathrm{q}} \kappa}{k_{\mathrm{p}} k^2 [1+(k+\kappa)^2]^3 [1+(k-\kappa)^2]^3}$$

$$\times \begin{cases} [k^2 + \frac{1}{3}(\kappa^2+1)] \dfrac{\exp\left[-\dfrac{2}{\kappa}\tan^{-1}\left(\dfrac{2\kappa}{1+k^2-\kappa^2}\right)\right]}{(1-\mathrm{e}^{-2\pi/\kappa})} \text{ (Coulomb)}, \\ \dfrac{\kappa}{2k^2}\left[1+k^4+\kappa^4+2(k^2+\kappa^2)+\dfrac{10}{3}k^2\kappa^2\right] \text{ (Plane)}, \end{cases}$$

where $k=|\mathbf{k}_{\mathrm{p}}-\mathbf{k}_{\mathrm{q}}|$. We have numerically performed the integrations over energy of ejection and scattering angle at an incident energy of 30 ev. The ratio for the differential cross section

$$\int_0^{\kappa_{\max}} d\kappa \int \mathscr{I}_\kappa \, d\Omega'$$

with ejected plane wave to that with ejected Coulomb wave is 870 for $\theta=0$, 6·8 for $\theta=\pi/2$, and 5·2 for $\theta=\pi$. The ratio of the total cross sections is 289. This is quite consistent with our results when we recall that a factor of 2 reduction in total cross section resulted from the inclusion of exchange and the factor of 10 from (*a*) is an upper limit (see figure 1).

6.2. *Semi-Classical Model*

Here we consider the photon flux corresponding to the Fourier transform of the electric field pulse at an H⁻ ion (or H atom) due to the straight line trajectory of an electron with velocity v and impact parameter b. Integrating this over the photodetachment (or photo-ionization) cross section, σ_{P}, gives the probability for electron detachment (in c.g.s. units),

$$P(b) = \frac{\pi e^2 c}{8hb^2 v^2} \int_{\nu_0}^{\infty} d\nu \sigma_{\mathrm{P}}(\nu) \frac{\exp(-4\pi\nu b/v)}{\nu} \qquad \text{......(12)}$$

from which the total cross section is obtained by integration over impact parameter,

$$\sigma(v) = \pi b_1^2 + 2\pi \int_{b_1}^{\infty} db \, bP(b); \; P(b_1)=1. \qquad \text{......(13)}$$

The difference between the detachment cross sections for H⁻ and for H is seen to depend on the threshold frequency ν_0 and σ_{P}. The maximum σ_{P} for H⁻ and H are $4{\cdot}0 \times 10^{-17}$ cm² and $0{\cdot}63 \times 10^{-17}$ cm², while their $h\nu_0$'s are 0·75 ev and 13·6 ev, respectively (although the shapes of σ_{P} near threshold differ). Both these sets of values work in the direction of a larger detachment cross section for H⁻ than for H. Estimating an upper bound to the integral in (12) we find $b_1(\mathrm{H}^-) < 8{\cdot}3a_0$ and $b_1(\mathrm{H}) < 1{\cdot}4a_0$ for a 50 ev electron. As the critical impact parameter for H is so small, the semi-classical model is inappropriate in that case but should be reasonable for H⁻. Similarly, taking an upper bound to (13) gives $\sigma(\mathrm{H}^-) < 208\pi a_0^2$ and the apparent overestimate of $\sigma(\mathrm{H}) < 6{\cdot}3\pi a_0^2$.

§ 7. CONCLUSIONS

As this is a three-electron problem involving excitation from bound to free states, various approximations had to be employed, not all of which can be given quantitative justification. We review these below with some remarks as to their expected validity:

(*a*) The Born–Oppenheimer method permits the separation of the incoming electron and bound electron parts of the total wave function. For analytical convenience we have represented the incoming electron beam by a plane wave even though it is in a repulsive Coulomb field at large distances. There are no analytical criteria available for the validity of this approximation for the present process. However, the work of Fite and Brackmann (1958) indicates that the Born approximation (ignoring exchange effects between incident and bound electrons) for the ionization of H atoms gives a result up to 50% too high below 75 ev.

(*b*) The wave function for H^- in the $^1\mathrm{S}$ state was taken to be of a simple form which proved satisfactory in describing the continuous absorption of radiation by H^- in the optical region. In the ultra-violet the continuous absorption coefficient obtained with this function becomes larger (by about 30%) than that obtained with more elaborate ground state wave functions. This would indicate, from the known relationship between the optical properties of an atom and its inelastic electron collision cross section, that our present cross section might be too large by a similar amount (Miller and Platzman 1957). The use of a many-parameter Hylleraas function in the present calculation would certainly improve the results but would also make the spatial integrals in (2) considerably more difficult to evaluate. The approximation used for the free state of H^- is probably quite good for all except the lowest energies of electron ejection.

(*c*) The retention of only the first term in the scattering amplitudes is discussed in the Appendix, with the conclusion that it results in an uncertainty of the total cross section on the order of 10% between 15 and 75 ev.

(*d*) The magnitude of the Coulomb correction at the higher energies is apparently less than the possible error from other sources. The method of joining the low and high energy corrections is somewhat arbitrary but based on the reasonable assumption that the correction factor be a monotonic function of energy. Most likely our low energy Coulomb correction (<3 ev) gives an extreme upper limit to the actual cross section and can be given no quantitative reliability with regard to magnitude, even though the shape is probably roughly correct. This is unfortunate for the application to solar physics where the electron temperatures correspond to energies close to threshold.

We conclude that the main features of the shape and magnitude of the cross section are properly described by our resulting curve, to within the above uncertainties.

The resulting detachment cross section at low energies (<10 ev) is similar to that obtained for O^- (Watanabe and Miida 1950) by means of a partial wave method. It is, however, very much larger than was obtained for Cl^- (Massey and Smith 1936), also on the basis of a partial wave method. A possible explanation for this disparity might lie in Massey and Smith's neglect of terms corresponding to p–p transitions, which terms Watanabe and Miida find to be exceptionally large.

ACKNOWLEDGMENTS

This research was supported in part by the Office of Naval Research. The author is indebted to Mrs. Sally Peavy for performing all the programming operations for the numerical integrals, and to Dr. E. C. Beaty for suggesting the semi-classical analysis in §6.2.

APPENDIX

TERMS NEGLECTED IN SCATTERING AMPLITUDES

For the purpose of testing the smallness of the neglected terms in (6), let us replace ϕ_0 by ϕ_H so that most of the space integrations may be performed analytically, giving

$$f_\kappa^{(1)} \simeq \frac{8}{\pi}\left[-\frac{1}{k^2(1+K^2)^2}+\frac{1+2/(4+k^2)}{(1+\kappa^2)^2(4+k^2)}\right].$$

In the integration over α,

$$\int_{-1}^{1} d\alpha |f_\kappa^{(1)}|^2 = 4qk_p^2 \int_{1-q}^{1+q} dk\, k |f_\kappa^{(1)}|^2,$$

and the greatest contribution will arise from forward scattering ($k \simeq 1-q$) for energies much greater than threshold. As the denominator of the first term in $f_\kappa^{(1)}$ gets very small while that of the second term does not, we neglect the second term. For the exchange amplitude,

$$g_\kappa^{(1)} \simeq \frac{4}{\pi}\left[-\frac{1}{k'^2(1+K^2)^2}+\frac{8}{(1+k_q^2)(1+\kappa^2)^2(1+k_p^2)^2}\right.$$
$$\left.-\frac{1}{4\pi}\iint d\tau_1\, d\tau_2 \frac{\exp(-i\mathbf{k}_q\cdot\mathbf{r}_1)\phi_H(r_1)\phi_H(r_2)}{r_{12}}\left\{\frac{\exp(i\mathbf{k}_p\cdot\mathbf{r}_2)}{(1+\kappa^2)^2}+\frac{\exp(-i\boldsymbol{\kappa}\cdot\mathbf{r}_2)}{(1+k_p^2)^2}\right\}\right]$$

where $k' = |\mathbf{k}_p - \boldsymbol{\kappa}|$. Similarly, in the angular integration of $|g_\kappa^{(1)}|^2$ or $|g_\kappa^{(3)}|^2$ the largest contribution will come from small angles of ejection with respect to direction of incidence, and hence we retain only the first term above. It is not possible to get a simple analytic reduction of the last term in $g_\kappa^{(1)}$ above, but it clearly will not contain any resonance denominator for forward electron ejection as is contained in the first term.

An estimate of the magnitude of the error involved in dropping all but the first term in $f_\kappa^{(1)}$ and $g_\kappa^{(1)}$ may be made by doing the angular and energy integrations with the above simple form for $f_\kappa^{(1)}$ and the additional simplifications: $K^2 \simeq \kappa^2$ in the first term and $k^2 \simeq 0$ in the second term. These simplifications are based on the fact that largest contributions to the integrals are for very small values of k. The resulting ratio of the contribution of the neglected term to that of the retained term in

$$\int ds^2 sq \int d\alpha \int d\beta\, |f_\kappa^{(1)}|^2$$

is 0·33 at 1·5 ev, 0·04 at 15 ev and decreases as k_p^{-2} for higher incident energies.

The relative effect on the cross term

$$\int ds^2 sq \int d\alpha \int d\beta f_\kappa^{(1)} g_\kappa^{(1)}$$

of neglecting all but the first terms in $f_\kappa^{(1)}$ and $g_\kappa^{(1)}$ is probably greater than in the case of the square terms because the neglected terms will contain a resonance denominator of the same order as the retained term. The net effect on the total cross section should not, however, exceed the order of 10% since in the present approximation (§§ 3, 4) the entire cross term contributes less than 5%.

REFERENCES

BATES, D. R., FUNDAMINSKY, A., and MASSEY, H. S. W., 1950, *Phil. Trans. Roy. Soc.*, **243**, 93.

BOLDT, G., 1959, *Z. Phys.*, **154**, 319, 330.

FITE, W. L., and BRACKMANN, R. T., 1958, *Phys. Rev.*, **112**, 1141.

GELTMAN, S., 1956, *Phys. Rev.*, **104**, 346.

GOLDSTEIN, H., 1950, *Classical Mechanics* (New York: Addison-Wesley, p. 83.

MASSEY, H. S. W., and MOHR, C. B. O., 1933, *Proc. Roy. Soc.* A, **140**, 613.

MASSEY, H. S. W., and SMITH, R. A., 1936, *Proc. Roy. Soc.* A, **155**, 472.

MILLER, W. F., and PLATZMAN, R. L., 1957, *Proc. Phys. Soc.* A, **70**, 229.

PAGEL, B. E. J., 1956, *Mon. Not. R. Astr. Soc.*, **116**, 608.

SMITH, S. J., and BURCH, D. S., 1959, *Phys. Rev. Lett.*, **2**, 165.

WATANABE, M., and MIIDA, J., 1950, *J. Phys. Soc., Japan*, **5**, 149.

Pair Distribution of Simple Non-spherical Liquids

By G. H. A. COLE

Physics Division, Clarke, Chapman and Co. Ltd., Gateshead, Co. Durham

Communicated by H. S. W. Massey; *MS. received 23rd June* 1959

Abstract. A procedure is discussed by which the spatial structure of classical simple non-spherical condensed systems (i.e. systems composed of non-spherical particles interacting in pairs) can be determined using the well established formulae of statistical mechanics without the need to appeal explicitly to vectorial integro-differential equations. In the mathematical method, the effects of particle asymmetry are introduced gradually starting from an appropriate symmetry already known from alternative calculations. The superposition approximation is invoked but its effect may be controlled if necessary. The case of slight molecular asymmetry is the one most conveniently treated although the procedure has a wider usefulness.

---

§ 1. INTRODUCTION

THE short-ranged molecular spatial ordering characteristic of a liquid is often expressed in terms of a pair distribution function describing the distribution of molecular pairs in the liquid, derived experimentally from x-ray, or neutron, diffraction data. The classical theory of the pair distribution is based on the principles of particle dynamics and statistical mechanics, augmented by a simplifying mathematical hypothesis, namely the superposition approximation, relating the many particle correlations to that between a representative pair (see for example de Boer 1949, Cole 1959 a). The use of the superposition approximation dictates the subsequent development of the theory. Because it largely disregards the particle interaction its *direct* introduction into the theory is unreliable (Yvon 1935) except in perturbation effects (Eisenschitz and Cole 1954, Cole 1958 a). The consequent rearrangement of the theory into a form which minimizes the role of the particle interaction has led to the development of non-linear integro-differential equations whose solution is the pair distribution. Equivalent first order vector equations have been proposed by Yvon (1935), Kirkwood and Boggs (1942), and Born and Green (1949); alternatively, Cole (1958 b) has proposed a second order tensor equation.

In addition to these special forms of the general theory, the effect of the superposition approximation can be gradually reduced, in principle almost indefinitely, by a procedure of variable interparticle coupling (Cole 1959 b).

Any calculations based on these several equations must be fraught with very severe computational difficulties even for the least complicated case of liquids composed of strictly spherical particles, where all the equations have scalar form. For this reason no full test of the theory is yet available; but the numerical solutions of the first order equations, involving electronic computer techniques

(Kirkwood, Lewinson and Alder 1952), and using data adapted, though rather crudely, to argon add confidence to the approach. Further solutions of the theory are in hand but not yet available.

The situation becomes complicated in the extreme when non-spherical liquids, whose constituent particles deviate from spherical symmetry, are considered. The equations now have full tensorial form, and the present electronic computer facilities are scarcely adequate to treat the problem in a reasonable way. There is, therefore, a great need to reconsider the determination of the spatial structure of simple non-spherical liquids with a view to simplification and this is the aim of the present paper. By accounting for the effects of particle asymmetry gradually, a procedure is developed which reduces the calculation for simple non-spherical liquids to a form of the same type as that for simple spherical liquids; emphasis is placed on the case in which particle asymmetry is slight. This study will allow a numerical study of the theory of the liquids to include also non-spherical liquids which are of great practical importance.

§ 2. THE PREMISES

The classical liquid is represented by N identical particles contained in a volume V, the average particle number density being denoted by n $(=N/V)$. The system is at temperature T, and k will denote the Boltzmann constant. Each particle is in interaction with its neighbours and $\Psi(\mathbf{r}_1, \mathbf{r}_2, \ldots \mathbf{r}_N)$ will denote the total interaction potential of the system, where $\mathbf{r}_i$ is the configuration vector for the centre of the ith particle. It is convenient to define also a reduced potential $\mathrm{X}(\mathbf{r}_1, \mathbf{r}_2, \ldots \mathbf{r}_N)$ according to the relation $kT\mathrm{X}=\Psi$.

The normalized probability for the instantaneous occurrence of h $(<N)$ arbitrarily chosen particles in the configuration $(\mathbf{r}_1, \mathbf{r}_2, \ldots \mathbf{r}_h)$ is written $n^{(h)}(\mathbf{r}_1, \mathbf{r}_2, \ldots \mathbf{r}_h)$ and according to statistical mechanics is defined by

$$n^h n^{(h)}(\mathbf{r}_1, \mathbf{r}_2, \ldots \mathbf{r}_h)=\frac{1}{(N-h)\,!}\frac{1}{Z_N}\int\ldots\int \exp\{-\mathrm{X}\}\,d\mathbf{r}_{h+1}\ldots d\mathbf{r}_N. \qquad \ldots\ldots(1)$$

Z_N is here the configurational partition function chosen to normalize the dimensionless distribution $n^{(h)}$ to unity

$$Z_N=\frac{1}{N\,!}\int\ldots\int \exp\{-\mathrm{X}\}\,d\mathbf{r}_1,\, d\mathbf{r}_2, \ldots d\mathbf{r}_N. \qquad \ldots\ldots(2)$$

When h is set equal to 2, these equations define the pair distribution $n^{(2)}(\mathbf{r}_1, \mathbf{r}_2)$.

A relation between distributions of consecutive order follows immediately from (1):

$$n^{(2)}(\mathbf{r}_1, \mathbf{r}_2)=\frac{1}{V}\int n^{(3)}(\mathbf{r}_1, \mathbf{r}_2, \mathbf{r}_3)\,d\mathbf{r}_3.$$

Alternatively, the superposition approximation asserts the validity of the sequence of relations the first two of which are:

$$n^{(3)}(\mathbf{r}_1, \mathbf{r}_2, \mathbf{r}_3)=n^{(2)}(\mathbf{r}_1, \mathbf{r}_2)n^{(2)}(\mathbf{r}_1, \mathbf{r}_3)n^{(2)}(\mathbf{r}_2, \mathbf{r}_3), \qquad \ldots\ldots(3\,a)$$

$$n^{(4)}(\mathbf{r}_1, \mathbf{r}_2, \mathbf{r}_3, \mathbf{r}_4)=n^{(3)}(\mathbf{r}_1, \mathbf{r}_2, \mathbf{r}_3)n^{(2)}(\mathbf{r}_1, \mathbf{r}_4)n^{(2)}(\mathbf{r}_2, \mathbf{r}_4)n^{(2)}(\mathbf{r}_3, \mathbf{r}_4). \qquad \ldots\ldots(3\,b)$$

For simple liquids, such as will be treated here, the total potential is to be equated to the sum of the separate pair potentials, each member being concerned with the mutual interaction between a single particle pair, whether or not the particles are spherically symmetric. If $\psi(\mathbf{r}_i, \mathbf{r}_j)$ is the mutual force potential for the particles i and j, and if we define a corresponding reduced potential function $\chi(\mathbf{r}_i, \mathbf{r}_j)$ according to the relation $kT\chi = \psi$, then

$$\mathrm{X}(\mathbf{r}_1, \mathbf{r}_2, \ldots \mathbf{r}_N) = \sum_{i=1}^{N} \sum_{j>i}^{N} \chi(\mathbf{r}_i, \mathbf{r}_j). \qquad \ldots\ldots(4)$$

For spherical particles χ is a function of the particle separation distance alone, but any departures from particle spherical symmetry demand also the inclusion of the relative particle orientation. In this more general case it will be assumed that each χ can be written as the sum of a term $\chi_0(r)$ that is angular independent and an angular dependent remainder $\chi_1(r, \vartheta, \varphi)$ where (r, ϑ, φ) are spherical polar coordinates with origin centred on the particle.

As a matter of nomenclature the insertion $\chi = \chi_0$ into (1) and (2) provides a definition of the pair distribution, written $n_0^{(2)}(r_{12})$ with $r_{12} = |\mathbf{r}_1 - \mathbf{r}_2|$, for a system of spherical particles, a function to be regarded as already known, e.g. from the equations mentioned in § 1.

§ 3. Variable Asymmetry

We are concerned now with the selection of the functions χ_0 and χ_1 appearing in (6). Clearly such a separation of the known function χ can be done in many ways: it is best to choose a form which lays most emphasis on the symmetric function χ_0 although this is not critical. For the present purpose we forget for the moment the actual particle under consideration and choose a function χ_0 for some different particle for which calculated data for the corresponding pair distribution $n_0^{(2)}$ are already independently and accurately known. This different particle can have a classical radius somewhere between the maximum and minimum radius of the actual particle. For definiteness the separate symmetric particle will be given a radius r_0 equal to the maximum radius of the actual asymmetric particle; the minimum actual particle radius will be written r_{m}.

The angular function, χ_1, can itself be split into two terms, namely ξ_1 referring to the spatial region $r > r_0$ and ξ_2 referring to the spatial region $r_{\mathrm{m}} \leqslant r \leqslant r_0$. While ξ_1 accounts for asymmetric attractive features, ξ_2 describes partly attractive features but mainly the repulsive effects due to particle shape. ξ_1 can be expected to have a form similar to that associated with a simple dipole, or perhaps multipole. This separation remains unchanged whatever the particular value r_0 chosen. If asymmetry is only slight, $\xi_1 \gg \xi_2$ almost everywhere.

The mathematical experiment of (hypothetically) varying the particle asymmetry from zero to its actual value in the real system can be effected by introducing a parameter of variable asymmetry α and so writing χ_1 as $\alpha\chi_1$. α is assumed continuous in the range 0 to 1. When $\alpha = 0$ each particle has complete spherical symmetry; when $\alpha = 1$ each particle has the asymmetry of the actual particles.

§ 4. Solution Procedure

It will now be explained how the pair distribution for a liquid composed of asymmetric particles can be related to the corresponding function for a liquid of symmetric particles by using the technique of variable asymmetry.

4.1. *Slight Asymmetry*

Apart from the case where the particles actually deviate only slightly from spherical form (when no parameter need necessarily be invoked since it is usually sufficient to put $\xi_2 = 0$) this situation can be mathematically simulated more generally by requiring that $\alpha \ll 1$. The exponential function in (1) and (2) then need be expanded only as far as the first term so that

$$\exp\{-\mathrm{X}\} = \exp\{-\mathrm{X}_0\}\left[1 - \alpha \sum_{i=1}^{N} \sum_{j>i}^{N} \chi_1(\mathbf{r}_i, \mathbf{r}_j) + \mathrm{O}(\alpha\chi_1)^2\right]$$

where X_0 refers to complete spherical symmetry. In this case the equations (1) and (2) can be rearranged into the following relationship between $n^{(2)}(\mathbf{r}_1, \mathbf{r}_2; \alpha)$ and $n_0^{(2)}(r_{12})$:

$$\begin{aligned}\mathscr{L} n^{(2)}(\mathbf{r}_1, \mathbf{r}_2 : \alpha) = {} & n_0^{(2)}(r_{12})[1 - \alpha\chi_1(r_1, \vartheta_1, \varphi_1, r_2, \vartheta_2, \varphi_2)] \\ & - 2\alpha n \int \chi_1(r_1, \vartheta_1, \varphi_1, r_3, \vartheta_3, \varphi_3) n_0^{(3)}(r_{13}, r_{23}, r_{12})\, d\mathbf{r}_3 \\ & - \alpha n^2 \int\int \chi_1(r_3, \vartheta_3, \varphi_3, r_4, \vartheta_4, \varphi_4) n_0^{(4)}(r_{12}, r_{13}, r_{23}, r_{24}, r_{34})\, d\mathbf{r}_3\, d\mathbf{r}_4\end{aligned} \qquad \ldots\ldots(7\,a)$$

$$\mathscr{L} = 1 - \frac{\alpha}{2} \int\int \chi_1(\mathbf{r}_1, \mathbf{r}_2) n_0^{(2)}(r_{12})\, d\mathbf{r}_1\, d\mathbf{r}_2 \qquad \ldots\ldots(7\,b)$$

the subscript 0 denoting angular independence. The triplet and quadruplet functions, referring to spherical particles and appearing on the right-hand side of (7 *a*), are defined from (1) and (2) by putting $\mathrm{X} = \mathrm{X}_0$ and setting h successively equal to 3 and 4. $n_0^{(3)}$ and $n_0^{(4)}$ can be expressed in terms of $n_0^{(2)}$ by invoking the relations (3): alternatively greater accuracy, but also greater complication, is obtained if these functions are obtained by the procedure of variable coupling explained elsewhere (Cole 1959 b).

If the particle asymmetry is actually very slight (i.e. $\chi_0 \gg \chi_1$; $\xi_2 \simeq 0$) the equations (7) are sufficient in themselves with $\alpha = 1$.

4.2. *Appreciable Asymmetry*

When the expansion of the exponential to only the first term in χ_1 is inadequate, (7) must be augmented. In this case, with $n^{(2)}$ known for some value α for which (7) does apply (and written $n^{(2)}(\alpha)$), the parameter can be continually increased by (if necessary unequal) increments $\Delta\alpha$ until the value $\alpha = 1$ is reached. At each stage the potential to be inserted into (1) and (2) is separated into the form:

$$\chi = (\chi_0 + \alpha\chi_1) + \Delta\alpha\chi_1 \qquad \ldots\ldots(8)$$

and $\Delta\alpha$ is chosen so that $(\chi_0 + \alpha\chi_1) \gg \chi_1\Delta\alpha$. For each successive form of (8), inserted into equations (1) and (2), an equation for $n^{(2)}(\alpha + \Delta\alpha)$ applies which has the same form as (7) but with $n_0^{(2)}$, $n_0^{(3)}$ and $n_0^{(4)}$ replaced respectively by $n^{(2)}(\alpha)$, $n^{(3)}(\alpha)$ and $n^{(4)}(\alpha)$, and α replaced by $\Delta\alpha$. All the distribution functions are now angular dependent. Again the distribution functions $n^{(3)}$ and $n^{(4)}$ can be expressed in terms of $n^{(2)}$ through the superposition approximation (3). Alternatively, variable coupling can be employed for this purpose; although the effect of the approximation can be reduced in this way it is still not completely eliminated.

In principle the pair distribution appropriate to any molecular shape can be accounted for although the procedure is clearly most simple if the asymmetry is only slight (ξ_2 almost everywhere zero).

§ 5. CONCLUSIONS

A procedure has been proposed by which the pair distribution for a simple classical liquid composed of asymmetric particles can be determined if the pair distribution for a corresponding liquid of spherical particles is already known. The method involves taking account of the asymmetry only gradually by using the mathematical procedure of introducing a coefficient of asymmetry which is continuous in the range 0 to 1. The simplest situation, and one of great practical interest, is that for which the particle asymmetry is only slight. If the asymmetry is small enough there is no need to use an asymmetry coefficient in order to employ the perturbation approach employed in the present arguments.

For only slight asymmetry no unacceptable error need be expected to result from the direct use of the superposition approximation with the triplet and quadruplet functions. This might not be true for stronger asymmetry and here, in principle at least, errors can be reduced by employing a process of variable interparticle coupling considered in a previous paper (Cole 1959 b).

The application of these arguments to actual liquids cannot avoid lengthy, though elementary, numerical operations even for the simplest case of slight asymmetry. However, the effort will be much less than that associated with any direct application of the most general formulae of statistical mechanics and should not prove impossible in practice. Indeed it is hoped to conduct numerical calculations along these lines for liquid particles that deviate only slightly from spherical symmetry.

REFEFENCES

DE BOER, J., 1949, *Rep. Progr. Phys.*, **12**, 305 (London : Physical Society).
BORN, M., and GREEN, H. S., 1949, *A General Kinetic Theory of Liquids* (Cambridge: University Press).
COLE, G. H. A., 1958 a, *Proc. Phys. Soc.*, **72**, 887.
—— 1958 b, *J. Chem. Phys.*, **28**, 912.
—— 1959 a, *Advanc. Phys.* (*Phil. Mag. Suppl.*), **8**, 225.
—— 1959 b, *Proc. Phys. Soc.*, **73**, 713.
EISENSCHITZ, R., and COLE, G. H. A., 1954, *Phil. Mag.*, **45**, 394.
KIRKWOOD, J. G., and BOGGS, E. M., 1942, *J. Chem. Phys.*, **10**, 394.
KIRKWOOD, J. G., LEWINSON, V. A., and ALDER, B., 1952, *J. Chem. Phys.*, **20**, 929.
YVON, J., 1935, *Actualités Scientifiques et Industrielles* (Paris: Hermann et Cie).

Ultrasonic Relaxation in Liquid Methylene Chloride

By J. H. ANDREAE, P. L. JOYCE and R. J. OLIVER

Imperial Chemical Industries Limited, Akers Research Laboratories, Welwyn, Herts.

MS. received 12th August 1959

Abstract. In order to answer the question left open by a previous publication ultrasonic measurements have been made in liquid methylene chloride at -22°c. These confirm that there is a relaxation of the vibrational specific heat less the contribution of the lowest frequency mode of vibration. The paper ends with a short discussion of some hypersonic measurements recently reported by Pesin and Fabelinskii.

---

§ 1. Introduction

The conversion of thermal energy from translational molecular motions to internal molecular vibrations gives rise to ultrasonic relaxational behaviour in many liquids (Andreae, Heasell and Lamb 1956, Andreae 1957, to be referred to as I, Bass and Lamb 1958). In the case of carbon disulphide it has been shown (Andreae, Heasell and Lamb 1956) that the relaxation of the whole of the vibrational specific heat occurs with a single relaxation time.

Measurements of the ultrasonic absorption in methylene chloride reported previously in I indicated that only part of the vibrational specific heat was responsible for the relaxation in this liquid in the region of 170 Mc/s at 25°c. Unfortunately, it was not possible to ascertain which part of the vibrational specific heat was responsible for the relaxation because three different divisions of the specific heat led to values compatible with the ultrasonic results.

In the first division it was assumed that the vibrational mode having the lowest frequency ($\nu = 283\,\mathrm{cm}^{-1}$) was associated with a relaxation at much higher frequencies, leaving the remaining modes, 2–9, to contribute an amount C_{29} to the relaxation observed below 200 Mc/s.

In the second division Fermi resonance was invoked to combine modes 1, 4, 5 and 7 to give a relaxing specific heat C_{1457}. A third division associated vibrations of the same species, nos. 1, 2, 7 and 8 in a possible specific heat C_{1278}.

At 25°c the quantities C_{29}, C_{1457} and C_{1278} are approximately equal and so the ultrasonic measurements at this temperature could not be used to determine the appropriate composition of the relaxing specific heat. It was pointed out in paper I that at lower temperatures the values of C_{29}, C_{1457} and C_{1278} would diverge and ultrasonic measurements could be used to identify the right one.

Measurements of the ultrasonic absorption in liquid CH_2Cl_2 at -22°c are presented below and these confirm that C_{29} is the relaxing part of the specific heat in the region of 170 Mc/s. In view of the discussion on energy transfer to vibrations given in I and because of the recent work carried out by Bass and Lamb (1958) on liquid sulphur dioxide, this result was to be expected.

Pesin and Fabelinskii (1958) have reported hypersonic velocity measurements on methylene chloride which indicate a surprisingly large velocity dispersion between the ultrasonic and hypersonic frequency ranges. This is discussed in § 4.

§ 2. RESULTS

The ultrasonic absorption, α, in methylene chloride at $-22°$c is shown in the figure as a graphical plot of the parameter α/f^2 against α (i.e. points for $B=0$). The five groups of points correspond to frequencies near 30, 70, 110, 170 and 230 Mc/s respectively. The scatter of the experimental points indicates that the experimental accuracy is not greater than $\pm 4\%$, but this is sufficient to demonstrate the nature of the ultrasonic relaxation. The measurements were made with a pulse technique described by Andreae, Bass, Heasell and Lamb (1958) as 'System B'.

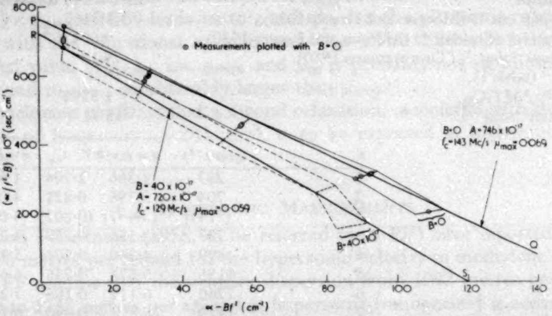

Methylene chloride at $-22°$c. Areas of $\pm 4\%$ error shown for $B=0$ and $B=40\times10^{-17}$.

Measurements of the ultrasonic velocity c_0 in methylene chloride at 2 Mc/s are presented in table 1, from which the velocity at $-22°$c is calculated by interpolation to be 1259 metres per second. These measurements were made with a simple ultrasonic interferometer using an X-cut quartz crystal and a movable reflector.

Table 1. Ultrasonic Velocity in CH_2Cl_2 at 2Mc/s

T (°c)	$-92{\cdot}9$	$-77{\cdot}2$	$-63{\cdot}8$	$-43{\cdot}1$	$-21{\cdot}4$	$-9{\cdot}5$
c_0 (m sec^{-1})	1546	1473	1422	1344	1255	1209

The well-known formula (recently discussed by Bass and Lamb 1958)

$$\alpha/f^2=\frac{A}{1+(f/f_c)^2}+B \qquad \ldots\ldots(1)$$

can be written

$$\alpha/f^2-B=-(\alpha-Bf^2)/f_c{}^2+A \qquad \ldots\ldots(2)$$

from which it follows that a plot of α/f^2-B against $\alpha-Bf^2$ should yield a straight line when the correct value of B is chosen. The intercepts of this line with the coordinate axes are then equal to A and $Af_c{}^2$.

The ultrasonic absorption measurements are analysed in the figure for $B=0$ and $B=40\times10^{-17}$ sec^2 cm^{-1}. It can be seen that $B=40\times10^{-17}$ is the maximum value of B which allows a straight line to pass through the area describing $\pm 4\%$ experimental scatter.

In order to determine limits for the maximum value of the absorption per wavelength, $\mu_{\max}=\frac{1}{2}Acf_c$, we note that the area under a straight line fitted to the experimental results in the figure is equal to $\frac{1}{2} \times A \times Af_c^2 = \frac{1}{2}A^2 f_c^2$, which is proportional to $(\mu_{\max})^2$.

The two lines, PQ and RS have been drawn in the figure to give the maximum and minimum values of $\mu_{\max}$ compatible with the experimental results. The small velocity dispersion which makes the velocity c, measured at the frequency f_c, larger than c_0 has been taken into account in calculating the limiting values of $\mu_{\max}$ given in the figure and table 2.

Table 2. Calculation of $\mu_{\max}$ for CH_2Cl_2

Temperature	25°C ≡ 298°K	−22°C ≡ 251°K
Density, ρ(g. cm^{-3}) (Morgan and Lowry 1930).	1·3167	1·4013
$\theta = -(1/\rho)(\partial\rho/\partial T)_p$(deg^{-1}) (Morgan and Lowry 1930).	0·001367	0·001285
C_{p_0} (cal mol^{-1} deg^{-1}) (Timmermans 1950).	24·18	23·29
c_0 m sec^{-1} (table 1).	1074	1259
$\gamma_0 = 1 + \theta^2 c_0^2 MT/C_{p_0}$.	1·5391	1·5725
C_{v_0} (cal mol^{-1} deg^{-1}).	15·71	14·81

i	ν_i(cm^{-1})	$x = h\nu/kT$	C_i	$x = h\nu/kT$	C_i
1	283	1·366	1·704	1·622	1·603
2	704	3·398	0·821	4·035	0·593
2	(714)†	(3·447)	(0·802)	(4·092)	(0·575)
3	737	3·558	0·759	4·224	0·535
4	899	4·340	0·501	5·152	0·309
5	1155	5·575	0·236	6·619	0·116
6	1266	6·111	0·165	7·255	0·074
7	1429	6·898	0·096	8·190	0·037
8	2984	14·40	0·000	17·10	0·000
9	3048	14·71	0·000	17·47	0·000

$C_{29} = C_2 + C_3 \ldots . C_9$	2·578 (2·559) cal mol^{-1} deg^{-1}	1·664 (1·645) cal mol^{-1} deg^{-1}
$C_{1457} = C_1 + C_4 + C_5 + C_7$	2·537 cal mol^{-1} deg^{-1}	2·065 cal mol^{-1} deg^{-1}
$C_{1278} = C_1 + C_2 + C_7 + C_8$	2·621 (2·602) cal mol^{-1} deg^{-1}	2·233 (2·215) cal mol^{-1} deg^{-1}
$C_{\text{tot}} = C_1 + C_2 \ldots . C_9$	4·282 (4·264) cal mol^{-1} deg^{-1}	3·267 (3·248) cal mol^{-1} deg^{-1}
μ_{29}	0·104 (0·104)	0·071 (0·070)
μ_{1457}	0·103	0·090
μ_{1278}	0·107 (0·106)	0·098 (0·098)
μ_{tot}	0·194 (0·193)	0·154 (0·153)
μ_{exp}	0·102	0·059–0·069

Equation (3) is used together with the Planck–Einstein formula

$$C_i = Rx^2 e^{-x} (1 - e^{-x})^{-2}$$

where $x = h\nu/kT$. Molecular weight, $M = 84{\cdot}94$.

† It appears from Herzberg (1945) that there is some doubt about the frequency ν_2 and so the calculations have been done for the alternative values 704 and 714 cm^{-1}. All bracketed figures correspond to the latter.

§ 3. CALCULATIONS

The calculation of the three specific heats C_{29}, C_{1457} and C_{1278} is carried out in table 2 in a manner similar to that used in I. The specific heats are then used for the computation of values of $\mu_{\max}$ from the formula

$$\mu_{\max} = \frac{\pi}{2} \frac{(C_{p_0} - C_{v_0}) C_{i_a}}{\{C_{p_0} C_{v_0} (C_{p_0} - C_{i_a})(C_{v_0} - C_{i_a})\}^{1/2}}, \qquad \ldots\ldots (3)$$

where C_{p_0} and C_{v_0} are the static specific heats of the liquid and C_{i_a} is the relaxing part of the vibrational specific heat. The formula is given in full in Andreae and Lamb (1956, eqn (35)), but the correction term involving the constant B has been omitted here because it contributes a negligible amount to $\mu_{\max}$ in the present case.

The ultrasonic velocity in methylene chloride was erroneously taken to be 1050 m sec^{-1} instead of 1074 m sec^{-1} in I. Values of $\mu_{\max}$ at +25°c have been recalculated with the correct velocity and are shown in table 2 together with those at −22°c.

A comparison of the values calculated for $\mu_{\max}$ in table 2 with the experimental limits $0{\cdot}059 < \mu_{\max} < 0{\cdot}069$ leads us to conclude that the ultrasonic relaxation is associated with the vibrational specific heat C_{29}. The difference between the experimental value of $\mu_{\max}$, i.e. $\mu_{\exp}$, and μ_{29} is probably not significant, while μ_{1457}, μ_{1278} and μ_{tot} are considerably larger than $\mu_{\exp}$.

This conclusion confirms that a second relaxation, associated with the vibrational mode of frequency $\nu = 283$ cm^{-1}, is to be expected at higher ultrasonic frequencies.

§ 4. HYPERSONIC MEASUREMENTS

Pesin and Fabelinskii (1958, to be referred to as PF) have reported a value of 1245 ± 36 metres per second for the hypersonic velocity in methylene chloride at 20°c. PF assume that the velocity dispersion from 1092 metres per second at 500 kc/s to 1245 metres per second at hypersonic frequencies† is accompanied by the disappearance of the parameter $\alpha'/f^2 (= \alpha/f^2 - \alpha_\eta/f^2)$, where α/f^2 is taken from ultrasonic absorption measurements below 10 Mc/s and α_η is the absorption due to shear viscosity. Using the approximate formula

$$\frac{\Delta c}{c} = \frac{\mu_{\max}}{\pi} = \frac{Acf_c}{2\pi} \qquad \ldots\ldots (4)$$

with $A = \alpha'/f^2$, they estimate f_c to be 480 Mc/s. Since it has been shown already in paper I that the major part of α'/f^2 takes part in a relaxation near 170 Mc/s, this procedure is not justified. PF's comment that the experimental results given in paper I do not fit a single relaxation time curve is difficult to understand: the agreement is within ±1%.

An interesting calculation results from considering the dispersion due to the relaxation of the whole of the vibrational specific heat of CH_2Cl_2 between 500 kc/s and hypersonic frequencies ($10^9 - 10^{10}$ c/s). The specific heats at frequencies above and below the relaxation of the vibrational specific heat can be obtained for 20°c in the same manner as that followed in table 2 for temperatures of 25°c and −22°c: they are $C_{\mathrm{p}_0} = 24{\cdot}12$; $\gamma = 1{\cdot}543$; $C_{\mathrm{v}_0} = 15{\cdot}63$; $C_{\mathrm{vib}} = 4{\cdot}17$; $C_{\mathrm{p}_\infty} = 19{\cdot}95$; $C_{\mathrm{v}_\infty} = 11{\cdot}46$ (cal mol^{-1} deg^{-1}). The subscripts 0 and ∞ signify that the parameters relate to frequencies below and above the region of relaxation, respectively.

The velocity dispersion may be calculated now from the elementary formula

$$(c_\infty/c_0)^2 = C_{\mathrm{v}_0} C_{\mathrm{p}_\infty} / C_{\mathrm{p}_0} C_{\mathrm{v}_\infty} \qquad \ldots\ldots (5)$$

which assumes, only, that the isothermal compressibility, β_T, is unchanged by a thermal relaxation, i.e. $c_0^2 = C_{\mathrm{p}_0}/(C_{\mathrm{v}_0}\beta_T\rho)$, $c_\infty^2 = C_{\mathrm{p}_\infty}/(C_{\mathrm{v}_\infty}\beta_T\rho)$. In the present instance the thermal relaxing specific heat is C_{vib} and so $C_{\mathrm{P}_0} = C_{\mathrm{P}_\infty} + C_{\mathrm{vib}}$ and $C_{\mathrm{V}_0} = C_{\mathrm{V}_\infty} + C_{\mathrm{vib}}$. From equation (5) and the values of the specific heat given above, we find $c_\infty/c_0 = 1{\cdot}062$, compared with the hypersonic–ultrasonic dispersion of $c_\infty/c_0 = 1245/1092 = 1{\cdot}14$.

---

†PF do not give the hypersonic frequency but 5000 Mc/s is deduced from their results.

If the hypersonic velocity is correct, we must look beyond the vibrational specific heat for the origin of the observed dispersion. Also it is clear that PF's procedure of assuming a single relaxation time for the ultrasonic–hypersonic dispersion is invalid: there are likely to be at least three relaxation times, two associated with the vibrational specific heat and one other. Presumably the latter will be due either (i) to the appearance of shear rigidity in the liquid by the 'freezing' of shear motions, or (ii) to some equilibrium between ordered and disordered configurations of the molecules in the, still, liquid state.

ACKNOWLEDGMENT

We should like to thank Dr. J. Lamb for bringing the hypersonic measurements to our notice.

REFERENCES

ANDREAE, J. H., 1957, *Proc. Phys. Soc.* B, **70**, 71.
ANDREAE, J. H., BASS, R., HEASELL, E. L., and LAMB, J., 1958, *Acustica*, **8**, 131.
ANDREAE, J. H., HEASELL, E. L., and LAMB, J., 1956, *Proc. Phys. Soc.* B, **69**, 625.
ANDREAE, J. H., and LAMB, J., 1956, *Proc. Phys. Soc.* B, **69**, 814.
BASS, R., and LAMB, J., 1958, *Proc. Roy. Soc.* A, **247**, 168.
HERZBERG, G., 1945, *Infra-red and Raman Spectra of Polyatomic Molecules* (New York : Van Nostrand).
MORGAN, S. O., and LOWRY, H. H., 1930, *J. Phys. Chem.*, **34**, 2385.
PESIN, M. S., and FABELINSKII, I. L., 1958, *Dokl. Akad. Nauk. SSSR*, **122** (4), 575.
TIMMERMANS, J., 1950, *Physico-chemical Constants of Pure Organi Compounds* (New York : Elsevier).

Ultra-violet Extensions of the Arc Spectra of the Alkaline Earths: The Absorption Spectrum of Barium Vapour

By W. R. S. GARTON AND K. CODLING
Physics Department, Imperial College, London

MS. received 15*th July* 1959

Abstract. The absorption spectra of the alkaline earth metal vapours have been photographed in the quartz ultra-violet and Schumann regions, by means of a 3 m vacuum spectrograph and large King furnace. Considerable extensions of the arc spectra of these elements have resulted, many of the new lines being two-electron transitions. Extreme cases of autoionization and many examples of series perturbations occur. The results are presented for the case of Ba, including assignments for 64 out of about 68 new lines. The presence of a doubly excited level practically coincident with the lowest ionization limit has striking effects on the photoionization cross section and on the intensities of the high members of the singlet principal series of Ba, which is extended to the $m=37$ member.

§ 1. INTRODUCTION

THE arc spectra of the alkaline earths, Ca, Sr, Ba, have been of central importance in the interpretation of line spectra, since it was in these that Russell and Saunders (1925) recognized for the first time multiplets due to simultaneous excitation of two electrons. The presence in these spectra of large numbers of lines superfluous to the simple series scheme of singlets and triplets was thus explained. The reason, of course, for the prominence of the lines which involve doubly excited states is that the ground-state of the atom has, in each case, an empty d-subshell of principal quantum number less than that of the s^2 valence electrons.

In addition to having this historical importance, the doubly excited energy-states of these atoms are of much interest in the study of the, still rather unexplored, phenomena of series perturbations and autoionization. Thus the spectra of Ca I, Sr I, Ba I receive emphasis in the most important contribution to date on series perturbations, that of Shenstone and Russell (1932), which is essentially an empirical quantitative description. Also, the occurrence of autoionization effects in these spectra has been illustrated by White (1931) in classifying a number of diffuse lines.

It is well recognized from the work of Beutler† that there are often better prospects of observing transitions which involve strongly autoionized upper states, when the spectrum of the element is obtained in absorption. In the elements mentioned we anticipate the combinations with the ground-state $s^2\,{}^1S_0 - dmp\ {}^1P_1^0$, ${}^3P_1^0$, ${}^3D_1^0$, to be strong. Lines of this sort are observed in emission for the lowest values of *m*; they fall amongst the lines of the *sml* series spectra, which are perturbed in consequence. For higher values of *m* the doubly excited dp levels lie above the ground-state of the ion, in each case, and do not produce observed emission lines, partly because of ready autoionization into the SE(p) continua of similar parity and J-value.

---

†A bibliography of Beutler's papers is given by Boyce (1941).

With these considerations in mind it was decided that the absorption spectra of Ca, Sr, Ba vapours be examined in the regions about, and the short-wavelength side of, the respective principal-series limits. Another consideration was the following. A number of new lines, some showing strong autoionization broadening, were obtained recently by us in absorption by Yb vapour, in the quartz ultra-violet and Schumann regions. In this case, the ground-state being $4f^{14}\,6s^{2}\,{}^1S_0$, the absorption spectrum will be expected more complicated than that of an alkaline earth, since in addition to single and double electron jumps of the s-electrons, we anticipate transitions of the type $4f^{14}\,6s^{2}\,{}^1S_0 - 4f^{13}\,6s^{2}\,md\,(g)\,{}^1P_1^0$ etc. It was hoped that comparison of the Yb absorption spectrum with that of the nearest alkaline earth, Ba, might assist analysis of the former.

The experiments have, in fact, yielded considerable extensions of the spectra Ca I, Sr I, Ba I. In each case many new lines of the singlet principal series ($s^{2}\,{}^1S_0 - smp\,{}^1P_1^0$) have been found, and new long series, due to double-electron jumps, and thus converging on excited states of the respective ions, have been observed. Extreme cases of autoionization and interesting examples of series perturbations occur in these spectra.

In the present paper the experimental technique is outlined, and the results and their analysis for Ba I are presented.

§ 2. THE BA I SPECTRUM

The most recent paper on Ba I, that of Russell and Moore (1955), summarized all data then available and listed 390 classified lines. The ground-state $6s^{2}\,{}^1S_0$ combines with $6smp\,{}^1P_1^0$ to give emission lines for $m=6$ to 12, and with $6smp\,{}^3P_1^0$ to give intercombination lines, $m=6$ and 7. Double-electron jumps to 6^1S_0, with $\Delta l_1 = 1$, $\Delta l_2 = 2$, listed by Russell and Moore are: $6^1S_0 - 5dmp\,{}^1P_1^0, {}^3P_1^0, {}^3D_1^0$, for $m=6$ and 7. Perturbations in the series level positions, occasioned by the $5dmp$ levels, have been discussed by Shenstone and Russell (1932).

The $Ba^{+}6\,{}^2S_{1/2}$ limit of the $6smp\,{}^1P_1^0$ series is given by Russell and Moore (1955) as 42032·4 cm^{-1}, corresponding to $\lambda_{vac} = 2379$ Å. The $5dmp$ levels converge on $Ba^{+}5\,{}^2D_{3/2,5/2}$, lying respectively 4873·85 and 5674·82 cm^{-1} above $6^2S_{1/2}$. A simple Rydberg extrapolation from the $m=6$ and 7, $5dmp$ ${}^1P_1^0$, ${}^3P_1^0$, ${}^3D_1^0$ levels shows that the next members ($m=8$) will lie close to the $6\,{}^2S_{1/2}$ limit, and the $m=9$ etc., levels will lie beyond it, and be thus in a position to autoionize. The region expected to be of greatest interest is thus $6\,{}^1S_0 - 6\,{}^2S_{1/2}$ to $6\,{}^1S_0 - 5\,{}^2D_{5/2}$, corresponding to $\lambda = 2379$ to 2096 Å.

§ 3. EXPERIMENTAL

The absorption spectra have been photographed with a recently erected 3 metre normal-incidence vacuum spectrograph provided with a Bausch and Lomb aluminized replica grating of 30 000 line/inch, blazed at 1500 Å in the first order. This instrument has excellent definition and speed. The mechanical arrangements permit recording of six or seven exposures on one plate (12 in. × 3 in.) by control from outside the vacuum housing, the wavelength range of one exposure being roughly 800 Å. Region and focus adjustments can also be made by external controls.

As absorption vessel, a large King-type carbon tube furnace has been used. This furnace can operate with a tube of graphite, or refractory carbide (e.g. TaC, ZrC), of up to 13 inches length and 3 inch bore. A stepdown transformer, with an inductive voltage regulator in its primary, can supply up to 40 kw. In experiments with the alkaline earth metals, graphite tubes 13 in. long, ½ in. to ¾ in. bore and ⅛ in. wall have been used. The central 8 in. length of graphite tube has been lined with a loosely fitting 16-gauge nickel tube, insulated from the graphite by thin mica. The alkaline-earth metal under study has been held inside this nickel liner by a few thin washers spaced at intervals within it. The purpose of the lining tube was, of course, to prevent rapid carbide formation by the Ba or other metal.

In operating the furnace, a fresh graphite–nickel assembly having been inserted, the temperature was raised to about 200° above that anticipated for the absorption spectrum, and the furnace tube outgassed for some minutes in an atmosphere of flowing helium at about 20–30 mm Hg pressure.

The furnace was then allowed to cool, and the pressure raised to atmospheric on the helium supply. The furnace was then opened and the metal under study introduced in small freshly cut pieces. The furnace was now connected to light-source and spectrograph slit and re-pumped. Before and during the exposures a current of helium was maintained within the furnace at 20–30 mm Hg pressure. It has been found that this sort of schedule—particularly the step of collapsing the furnace vacuum with clean helium, after outgassing a fresh furnace tube—is essential to the suppression of CO and H_2O absorption bands, which are common troubles when working in the Schumann ultra-violet. Moreover, when working with a strongly reactive metal, like Ba, it is important to avoid traces of oxygen and nitrogen in the furnace gases.

The background light-source used in the absorption experiments on Ca, Sr, Ba has been a 'Lyman continuum' flash tube, described previously (Garton 1953). Usually no window has separated this from the furnace, though it has been found advisable to place an insulating glass ring between the end of the flash tube and the earthed housing of the furnace. A window of lithium fluoride has been used to separate furnace and spectrograph slit, when working in the range above 1100 Å; in this way differential pumping between spectrograph and furnace has been avoided.

Using a slit width of 10 μ, set by the grain-size of the Ilford Q2 plates used, exposures of good density have required 100–500 flashes, spaced once per second. This seemingly large number of flashes is explained by the high dispersion, 2·7 Å mm^{-1}, and by the fact that the discharge tube has been used at about four feet from the slit with, so far, no intervening converging lens or mirror.

Measurements of the absorption lines have up to the present been made with respect to impurity lines arising either in the furnace in absorption, or in emission or absorption in the flash-tube spectrum. Care has to be taken in utilizing the flash-tube lines, since the extreme conditions existing in the discharge frequently produce shifts of the lines from their normal positions. As will appear, the measurement accuracy required on many of the new absorption lines is low, on account of large autoionization breadths. Some of the new lines are fairly sharp and will justify remeasurement against good wavelength standards. The measurements given in this paper are believed good to 0·01 Å.

§ 4. RESULTS AND INTERPRETATION

The absorption spectrum of barium vapour reproduced in the plate (*a*) was obtained at a furnace temperature of 1050°C. For accurate measurement of the sharper lines it was necessary to use other spectra obtained with less dense vapour in the light path. The few emisison lines present, and a few of the absorption lines, arise within the flash-tube light-source. Absorption lines of impurities occurring within the furnace are weak and are due mainly to Mg, Ca, Sr. Some of these impurity lines have been listed previously and hence have been used by us as wavelength standards; some of the Sr lines belong to an extension of the Sr I spectrum to be reported in another paper.

The classification into series of the new Ba I lines, which is indicated in the plate (*a*), and listed in tables 1 to 3, is based on the following considerations.

At the long wavelength end of the plate (*a*), the principal series $6s^2\,{}^1S_0 - 6smp\,{}^1P_1{}^0$, can be seen converging, with a peculiar course of intensity, to an apparent ionization continuum which extends a little way beyond the limit. This part of the spectrum is shown enlarged in the plate (*b*).

The apparently large photoionization cross section at and near the $6^2S_{1/2}$ limit is due to the presence of a strongly autoionizing level $5d8p\,{}^1P_1{}^0$, which is almost coincident with that limit. This provides explanation of the fact that the normal intensity decrement in the $6smp\,{}^1P_1{}^0$, series, from $m=15$ to $m=22$, is followed, after a gap, by a re-appearance in fair strength of the higher members, which can be measured as far as $m=37$. This type of intensity perturbation in the members of a series seems peculiar to barium, at least at the present date. Putting the explanation in alternative terms we can say that the higher $6s^2\,{}^1S_0 - 6smp\,{}^1P_1{}^0$ transitions acquire oscillator strength from the long wavelength wing of the extremely broad $5d8p\ {}^1P_1{}^0$ level, the centroid of which lies slightly to the short-wavelength side of the $6^2S_{1/2}$ limit.

The principal series is additionally perturbed, in both intensity and quantum defect, by the presence between the $m=13$ and $m=15$ levels of two other foreign levels, classified below as $5d8p\ {}^3P_1{}^0$, ${}^3D_1{}^0$.

The assignment of the diffuse absorption near the $6^2S_{1/2}$ limit to $6s^2\,{}^1S_0 - 5d8p\,{}^1P_1{}^0$ is easily justified, since the 5d6p and 5d7p ${}^1P_1{}^0$ members have been earlier listed (Russell and Moore 1955). A simple Rydberg extrapolation shows that the next member will lie near the $6^2S_{1/2}$ limit and the higher members then form the obvious series indicated in the plate (*a*), converging as expected on $Ba^+\ 5^2D_{5/2}$. The lines show the usual characteristic of autoionizing levels in becoming progressively less diffuse to higher *m* values.

It is reasonable to expect that the extended series mentioned could be used to improve the accepted value for the Ba I ionization potential (Russell and Moore 1955, Shenstone and Russell 1932); that value was obtained by making the best apparent adjustments in the formulae for the 6s*ml* series, all of which exhibit pronounced perturbations. Obviously, the new extension of the $6smp\ {}^1P_1{}^0$ series is not a great help without, at least, very accurate measurement of the tail of the series, which shows the curious enhancement of intensity. A casual inspection of the $5dmp\ {}^1P_1{}^0$ series, at any rate from $m=13$ onward, suggested that this might be perturbation free, and thus give an improved limit. If, following the technique of Shenstone and Russell (1932), we plot quantum defect against term value, use of the Russell and Moore (1955) value for $6^2S_{1/2}$ (which makes $5^2D_{5/2} = 47707{\cdot}2$), produces a rather rapid rise in the series tail. The appearance of the (n^*, n) plot can be improved by increasing the previous value for the limit by 0·8 cm^{-1}. Nevertheless the plot is still rather irregular, and before investigating the matter further the measurements on the high series members will have to be repeated against more reliable wavelength standards and with still larger dispersion. It is remarkable that the limit of Shenstone and Russell (1932) was judged so well, when we consider the irregular course of the series at their disposal.

Of the 5d*m*p series levels the $^1P_1^0$ thus give, as expected, the strongest combinations with the ground state; the other $J=1$ levels of 5d*m*p are $^3P_1^0$, $^3D_1^0$, and these have next to be located. Since 5d*m*p $^1P_1^0$ converges to Ba$^+$ $^2D_{5/2}$ the other two series must go to $^2D_{3/2}$ at 4873·85 cm^{-1} above $6^2S_{1/2}$. The first two members 5d6p, 5d7p $^3P_1^0$, $^3D_1^0$ have been found (Russell and Moore 1955) and a Rydberg extrapolation enables easy recognition of the next three members of each series. The $m=8$ members lie amongst the higher 6s*m*p $^1P_1^0$ levels, producing the perturbations already noted. The $^3P_1^0$, $m=9$ and 10 members give very diffuse lines beyond the $6^2S_{1/2}$ limit. The diffuseness is in conformity with the autoionization rules; the $m=9$ and 10, $^3D_1^0$ levels are correspondingly sharp. Identification of the $^3P_1^0$, $^3D_1^0$ series beyond $m=10$ is based entirely on the run of the quantum defect since the intensities behave peculiarly. Thus, there is certainly a very sharp intensity decrement, together with loss of line breadth, between 5d10p $^3P_1^0$ and 5d11p $^3P_1^0$. This may occasion less surprise, since other cases are known where a ^3P series exhibits a rapid intensity decrement. More surprisingly, the higher members of the 6^1S_0-5dmp $^3P_1^0$ combinations, if correctly identified in table 2, show an alternation of intensity, seemingly according to the following rule. A given 5d*m*p $^3P_1^0$ line lies, of course, between two members,

Table 1.† Ba I $6s^2\ {}^1S_0-6\,smp\ {}^1P_1^0$ Series Extension. Limit = 42033 cm^{-1}

λ_{vac} (Å)	*I*	ν (cm^{-1})	Identification	Rydberg denominator
2453·12	2	40764·4	$m=13$	9·301
2439·55	6	40991·2	14	10·263
2428·17	10	41183·3	15	11·364
2420 85	8	41307·8	16	12·301
2414·83	6	41410·8	17	13·280
2409·98	5	41494·1	18	14·270
2406·03	4	41562·2	19	15·268
2402·81	3	41617·9	20	16·259
2400·15	2	41664·1	21	17·247
2390·58	1	41830·8	27	23·296
2389·70	1	41846·3	28	24·243
2388·86	2	41861·0	29	25·259
2388·14	2	41873·6	30	26·238
2387·48	2	41885·2	31	27·248
2386·90	2	41895·3	32	28·230
2386·35	3	41905·0	33	29·280
2385·86	3	41913·6	34	30·316
2385·43	3	41921·2	35	31·330
2385·04	3	41928·0	36	32·328
2384·71	3	41933·8	37	33·260

† The intensity figures in the second column in tables 1–3 have only very rough significance, since the absorption lines are of such varying breadths. The symbols u, U, UU etc. indicate increasing breadth; s indicates asymmetrical shading to shorter wavelengths.

Table 2. $6s^2\,{}^1S_0-5dmp\,{}^1P_1^0,\,{}^3P_1^0,\,{}^3D_1^0$, Series

λ_{vac}(Å)	I	ν(cm^{-1})	Identification 5dmp $^1P_1^0$	Rydberg denominator Limit = 47708 cm^{-1}
2380·3	20UUUUs	42012	$m=8$	4·389
2277·3	20UUUs	43911	9	5·376
2221·77	20UU	45009·2	10	6·377
2188·74	20U	45688·4	11	7·371
2167·55	20u	46135·0	12	8·352
2152·68	15	46453·7	13	9·354
2142·14	15	46682·3	14	10·343
2134·25	14	46854·9	15	11·342
2128·25	12	46987·0	16	12·337
2123·57	12	47090·5	17	13·331
2119·83	12	47173·6	18	14·330
2116·81	10	47240·9	19	15·327
2114·33	10	47296·3	20	16·326
2112·27	10	47342·4	21	17·326
2110·53	8	47381·5	22	18·333
2109·08	8	47414·0	23	19·320
2107·83	6	47442·2	24	20·319
2106·76	6	47466·2	25	21·303
2105·81	6	47487·7	26	22·319
			5dmp $^3P_1^0$	Limit = 46907 cm^{-1}
2433·28	15	41096·8	$m=8$	4·346
2324·1	20UUUs	43027	9	5·318
2264·2	20UUs	44165	10	6·326
2229·43	12	44854·5	11	7·312
2207·15	18	45307·3	12	8·283
2191·70	2	45626·7	13	9·258
2180·40	13	45863·1	14	10·253
2172·12	5	46038·0	15	11·237
2165·78	13	46172·7	16	12·225
			5dmp $^3D_1^0$	Limit = 46907 cm^{-1}
2445·38	10	40893·4	$m=8$	4·272
2328·10	20	42953·5	9	5·269
2266·24	20	44125·9	10	6·282
2230·48	12	44833·4	11	7·275

5d($n-1$)p and 5dnp say, of the strong $^1P_1^0$ series. If the $^3P_1^0$ line lies closer to 5d($n-1$)p $^1P_1^0$ than to 5dnp $^1P_1^0$, i.e. closer to the $^1P_1^0$ line of longer wavelength, then it is relatively intensified. In the absence of a fuller understanding of the effects of series perturbation than currently exists, this conclusion has to remain empirical. It certainly seems impossible to make any better selection of the $6\,{}^1S_0-5dmp\,{}^3P_1^0$ series from amongst the absorption lines, than that suggested in table 2.

The above assignments, which apart from intensity peculiarities, are fairly straightforward, still leave unclassified some twenty-three lines, the pair λλ2311·38 and 2356·47 being quite strong, and asymmetrically shaded to shorter wavelengths. These lines cannot arise from 5dmp, if the ΔJ rule is to be met. The most obvious possibility is that some of the lines are $6s^2\,{}^1S_0-6pmd\,{}^1P_1^0,\,{}^3P_1^0$, i.e. form series converging on Ba$^+$ 6^2P, having first members in common with 5dmp. This

Table 3. $6s^2\ {}^1S_0 - 5dmf\ {}^1P_1{}^0,\ {}^3P_1{}^0$ (?) Series

λ_{vac}(Å)	I	ν(cm^{-1})	Identification Series A 5d*m*f $^1P_1{}^0$?	Rydberg denominator Limit = 47708 cm^{-1}
2454·81	2	40736·3	$m=4$	3·967
2311·38	20Us	43264·2	5	4·969
2240·27	15u	44637·5	6	5·978
2200·64	12	45441·3	7	6·957
2175·14	5	45974·0	8	7·955
			Series B 5d*m*f $^3P_1{}^0$?	Limit = 46907 cm^{-1}
—	—	39905†	$m=4$	3·959
2356·47	20Us	42436·4	5	4·954
—	—	—	6	—
2241·43	3	44614·4	7	6·918
2213·95	10	45168·1	8	7·944
2196·12	3	45534·8	9	8·943
2183·55	5	45797·0	10	9·943
2174·32	5	45991·4	11	10·946
2167·30	20	46140·4	12	11·961

† Level given by Russell and Moore (1955) as due 5d4f with $J=1$ or 2.

suggestion is discarded, since 6p6d etc., should lie above $^2D_{5/2}$ of Ba$^+$, and no absorption lines have been detected beyond the latter limit. Similarly, $6\,{}^1S_0 - 6p7s$ cannot account for the two diffuse lines mentioned, though possibly represented by weaker lines towards the ^2D limits. The only remaining possibility is $6^1S_0 - 5dmf$, which is a two-electron jump having $\Delta l_1 = 2$, $\Delta l_2 = 3$. The authors had the benefit of a conversation with Professor A. G. Shenstone, who recalled having identified such transitions in his analysis of Cu II. The suggested transitions will give two $J=1$ series converging on $^2D_{5/2}$ and one on $^2D_{3/2}$, since in (*jj*) notation

$$^2D_{5/2} + f_{5/2} \text{ gives } (5/2,\ 5/2)_1,$$
$$^2D_{5/2} + f_{7/2} \text{ gives } (5/2,\ 7/2)_1,$$
$$^2D_{3/2} + f_{5/2} \text{ gives } (3/2,\ 5/2)_1.$$

A study of all the possible ways of arranging the residue of absorption lines leads to the assignments listed in table 3. That the transitions indeed involve an f-electron is very probable since the quantum defects are seen to be nearly zero. Also a Rydberg extrapolation from the diffuse line at 2356·47 Å would place the first member of the series A at 39889 cm^{-1} which is close enough to the level 39905 cm^{-1} listed by Russell and Moore (1955) as due to 5d4f with $J=1$ or 2. The series B, if correct, shows the same peculiarity of intensity alternation discussed above for the case of the dp $^3P_1{}^0$ series. In particular the effect, if it is indeed real, accounts for the fact that the $m=12$ member of 5d*m*p $^1P_1{}^0$ has a close companion on its short wavelength side of practically the same intensity. It will be noticed that the $m=6$ member of series B is missing altogether. This, though awkward, is consistent with the intensity alternation since the predicted position of the line is slightly to the long wavelength side of the strong $m=9$ member of the 5d*m*p $^1P_1{}^0$ series. It must be admitted that series B of table 3 is very tentative.

It has been seen that the presence of 5d8p $^1P_1{}^0$ overlying the $6^2S_{1/2}$ limit has peculiar effects on the course of the 6sE(p) photoionization cross section and on the series lines converging to that limit. These effects presumably will have an important influence on the ionization balance in moderate and high ion-density discharges in barium vapour.

ACKNOWLEDGMENTS

The senior author is glad to express great appreciation of the help and encouragement of Dr. R. W. B. Pearse, Reader in Spectroscopy, who obtained several years ago the financial help necessary for construction of much of the apparatus used. Through Dr. Pearse, thanks are offered accordingly to the Royal Society for funds permitting purchase of a 3m concave grating and of auxiliary apparatus for construction of the spectrograph, and to the University of London Central Research Fund for funds covering erection of the King furnace and the necessary electrical gear. Considerable help on the details of the design of the spectrograph was provided by Mr. R. J. Webb, of the Atomic Energy Research Establishment Research Group, Woolwich.

The work has been in part performed under a supporting contract of the Atomic Energy Research Establishment, in the form of a Research Studentship awarded to the second author (K.C.).

REFERENCES

BOYCE, J. M., 1941, *Rev. Mod. Phys.*, **13**, 1.
GARTON, W. R. S., 1953, *J. Sci. Instrum.*, **30**, 119.
RUSSELL, H. N., and MOORE, C. E., 1955, *J. Res. Nat. Bur. Stand.*, **55**, 299.
RUSSELL, H. N., and SAUNDERS, F. A., 1925, *Astrophys. J.*, **61**, 38.
SHENSTONE, A. G., and RUSSELL, H. N., 1932, *Phys. Rev.*, **39**, 415.
WHITE, H. E., 1931, *Phys. Rev.*, **38**, 2016.

The $^{51}V(d, p)^{52}V$ Reaction

By A. W. DALTON, A. KIRK, G. PARRY and H. D. SCOTT
Nuclear Physics Research Laboratory, University of Liverpool

Communicated by H. W. B. Skinner; *MS. received* 16*th July* 1959, *in final form* 25*th August* 1959

Abstract. The energy spectra of the protons emitted from a vanadium target when bombarded by 8·9 MeV deuterons have been measured by magnetic analysis at angles of observation between 5° and 70°. The angular distributions of sixteen proton groups have been measured and compared with theoretical stripping curves to obtain information on parities, spins and reduced widths. Most of the transitions required an $l=1$ assignment. The results are compared with results on the $^{51}V(n, \gamma)^{52}V$ reaction.

---

§ 1. Introduction

The present paper is the first of a series reporting the results of d, p reactions in which deuterons of energy about 9 MeV have been used to bombard targets of medium heavy nuclei in the mass number region $51 \leqslant A \leqslant 65$. Measurements have been made on the energies of the proton groups and of the angular distributions of these groups.

The energies of some of the excited states of ^{52}V have been determined by Schwager and Cox (1953) from a study of the $^{51}V(d, p)^{52}V$ reaction. They were able to ascribe 23 proton groups to the above reaction, corresponding to transitions to states of ^{52}V up to an excitation of 3·30 MeV. Angular distribution measurements have been made on two proton groups from the same reaction by King and Parkinson (1953). One of their groups corresponded to the combined effect of the ground and first excited state at 0·131 MeV, for which they reported an $l=1+3$ combination. Their other group corresponded to an excitation of 0·8 MeV and gave an $l=1$ angular distribution. Recently El Bedewi and Tadros (1958) have reported angular distribution measurements of nine proton groups from the same reaction.

In the present investigation, the proton energy spectra resulting from the bombardment of ^{51}V with 9 MeV deuterons have been measured using the apparatus described by Green and Middleton (1956) and Dalton, Hinds and Parry (1957). Exposures were made for observations in the range 5° to 70°. From these spectra it has been possible to obtain angular distributions of many proton groups corresponding to transitions to the ground and excited states of ^{52}V. These distributions have been compared with theoretical curves deduced from stripping theories to obtain information on parities, spins and reduced widths. The results have been compared with the results of work on the $^{51}V(n, \gamma)^{52}V$ reaction (Bartholomew and Kinsey 1954, Groshev *et al.* 1957, Braid 1956).

§ 2. Experimental Procedure

Targets were prepared by the evaporation of powdered vanadium metal on to thin gold leaf. An alpha particle thickness gauge was used to select targets initially and a final selection was made after the yield and resolution had been checked by a trial bombardment. The thickness of the target was estimated as 0·25 mg cm^{-2} from data on the stopping power of materials for alpha particles.

The yield of protons was small and to get good statistical accuracy on the observations beam exposures of about 900 microcoulombs were necessary. Exposures of this magnitude would normally result in a background of scattered deuterons completely obscuring the proton spectra at most angles of observation. These deuterons were absorbed in a thin aluminium foil placed over the surface of the photographic emulsions used to record the protons. Over the length of the plate a varying thickness of absorber is needed. Fortunately the design of the spectrograph is such that the angle of incidence of particles on the emulsion decreases with decreasing energy. This makes it possible to use a strip of aluminium of uniform thickness with the variation of incidence angle providing sufficient variation in the effective thickness along the plate.

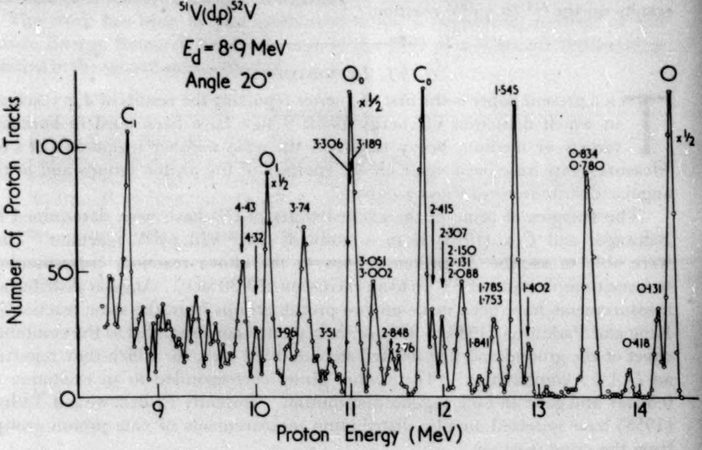

Figure 1. Proton spectrum observed at an angle of 20° from a target of ^{51}V bombarded by 8·9 MeV deuterons.

This technique permits the use of large exposures and is particularly important for observations at small angles where numerous disagreements between experimental and theoretical angular distributions have been reported for $l=1$ transitions.

§ 3. RESULTS

In figure 1 the proton energy spectrum obtained at 20° to the beam direction is illustrated. The energies of the proton groups were obtained from their positions on the plate using a calibration curve which had been experimentally determined from transitions with well-known Q-values. Where possible these groups have been identified with those reported by Schwager and Cox, who used an energy resolution considerably better than that of the present investigation. The groups which have been identified with transitions to excited states of ^{52}V have been labelled with their excitation energy in MeV. Proton groups arising from impurities of carbon and oxygen in the target were identified by their well established positions and shift with angles. These groups are labelled C_0, C_1, O_0 and O_1 the subscript signifying the level excited.

In the present investigation a number of proton groups additional to those of Schwager and Cox were observed and the corresponding levels in ^{52}V are 2·76, 3·51, 3·74, 3·96, 4·32 and 4·43 MeV. Some of these levels have also been reported by El Bedewi and Tadros. These authors also reported groups corresponding to excitations greater than 4·43 MeV and assigned energy values, but in our spectra these are shown to be composite groups due to closely spaced levels.

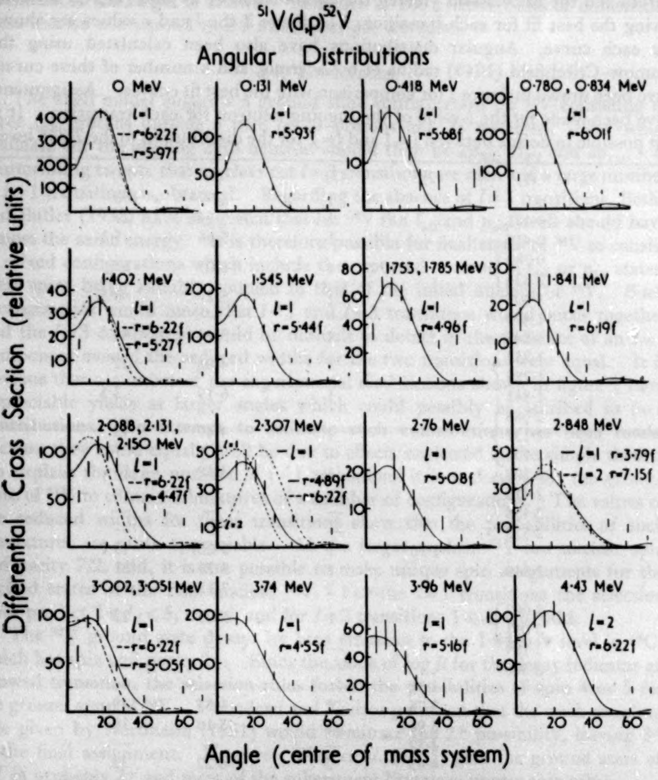

Figure 2. Angular distribution of proton groups from the ^{51}V(d, p)^{52}V reactions. The distributions are labelled by the excitation energy of the corresponding final state. 100 units of relative cross section are equivalent to 2·5 millibarns per steradian.

From the spectra it was possible to plot the angular distributions of many of the proton groups seen, corresponding to levels of ^{52}V. This was not possible for the groups corresponding to states at 2·415, 2·458, 2·525, 3·189, 3·306 and 4·32 MeV which were masked at several angles by impurity groups. The angular distributions are shown in figure 2. Each distribution has been fitted with Butler type stripping curves using the form suitable for numerical computation given by Enge and Graue (1955). These curves were fitted to the experimental data by means of weighted least squares fit calculations using the Manchester Mk. I computer. The use of a computer allowed a thorough search for the 'best-fit' curves and the calculations yielded the combination of l, r and $(2J_f+1)\gamma$ values giving the best fit for each transition. In figure 2 the l and r values are shown for each curve. Angular distributions have also been calculated using the Gamow–Critchfield (1949) radius of 6·22 fermis, and a number of these curves have been drawn in figure 2 for comparison with the best fit curves. Assignments have been made for the l-value of the ingoing neutron for each transition. It is not possible to decide between $l=1$ and $l=2$ for the distribution to the 2·848 level.

(1)	(2)	(3)	(4)	(5)
0		1	5·97	100
0·131		1	5·93	27
0·418		1	5·68	5·1
0·780 0·834		1	6·01	55
1·402		1	5·27	9·5
1·475		—	—	—
1·545		1	5·44	44
1·753 1·785		1	4·96	22
1·841		1	6·19	3·5
2·088 2·131 2·150		1	4·47	43
2·307		1	4·89	13
2·415		—	—	—
2·458		—	—	—
2·525		—	—	—
	2·76	1	5·08	5·1
2·848		1	3·79	21
	or	2	7·15	11
3·002 3·051		1	5·05	22
3·189		—	—	—
3·306		—	—	—
	3·51	—	—	—
	3·74	1	4·55	49
	3·96	1	5·16	10
	4·32	—	—	—
	4·43	2	6·22	32

(1) Levels of ^{52}V in MeV determined by Schwager and Cox; (2) additional levels from present investigation; (3) l-value of ingoing neutron; (4) radius r in fermis chosen for Butler stripping curves; (5) relative reduced width $(2J_f+1)\gamma$. γ is as defined by Blatt and Weisskopf (1952) and Evans (1955). It differs by $1/r$ from the more usually quoted reduced width having the symbol γ^2. 100 relative units correspond to 0·56 Mev.

For those angular distributions which appear to be best fitted by an $l=1$ assignment the radii used in the calculations are all less than the Gamow–Critchfield value of 6·22 fermis. For about half the $l=1$ transitions the experimental curve lies below the theoretical curve at small angles, and this effect is more marked if the Gamow–Critchfield radius is used in calculating the theoretical curves. The Q-values for the transitions showing these differences lie in the range 1·3 to 5 MeV. In the table are listed the excitation energies of the levels corresponding to observed proton groups together with the selected values of l and r for the transitions to these levels, and the calculated values of the relative reduced widths. Approximate values of the absolute cross sections can be calculated since the thickness of the target is known. In figure 2, 100 relative units of differential cross section correspond to 2·5 millibarns per steradian.

§ 4. DISCUSSION

The shell model suggests a ground state configuration for ^{51}V consisting of three $f_{7/2}$ protons outside a core of 20 protons and 28 neutrons. The orbits available for the ingoing 29th neutron should then be $2p_{3/2}$, $1f_{5/2}$ and $2p_{1/2}$. It is interesting to note that no clear cut $l=3$ transitions are seen and a large number of $l=1$ transitions is obtained. Regarding the absence of $l=3$ transitions, Bethe and Butler (1952) have suggested that for ^{52}V the $f_{5/2}$ and $p_{3/2}$ levels should have almost the same energy. It is therefore possible for final states of ^{52}V to consist of mixed configurations which include the captured neutron in $f_{5/2}$ or $p_{3/2}$ states, their spins being suitably coupled to that of the initial nucleus of ^{51}V. Such arrangements would mean that $l=1$ and $l=3$ transitions would occur together and the $l=3$ component would be difficult to detect in the presence of an $l=1$ component even if the reduced widths for the two transitions were equal. It is obvious that a number of the experimental distributions shown in figure 2 have appreciable yields at larger angles which could possibly be ascribed to $l=3$ contributions. No attempt to estimate such contributions has been made, because they could equally well be due to effects neglected in the simple theory. To explain the large number of $l=1$ transitions it is necessary for the ground state of ^{51}V to contain admixtures of a number of configurations. The values of the reduced widths for these transitions show that the probabilities of such admixtures are quite appreciable. As the target nucleus ^{51}V has nuclear spin and parity 7/2, odd, it is not possible to make unique spin assignments for the excited states of the final nucleus ^{52}V. For the $l=1$ transitions the selection rules predict $2 \leqslant J_f \leqslant 5$, even; and for $l=2$ transitions $1 \leqslant J_f \leqslant 6$, odd.

The ^{52}V ground state decays by beta emission to the 1·44 MeV level in ^{52}Cr which has spin and parity 2^+. Since the value of log ft for the decay indicates an allowed transition, the selection rules forbid the possibilities of spin 4 or 5 for the ground state of ^{52}V. El Bedewi and Tadros point out that the weak coupling rule given by Nordheim (1951) would eliminate the 2^+ possibility, leaving 3^+ as the final assignment. However, Way *et al.* (1955) give the ground state of ^{52}V as probably 2^+ and most of the subsequent literature quotes this value.

The results are also used to extend to vanadium the comparison made by Groshev *et al.* (1958) between the results of (n, γ) and (d, p) work on many elements. The basis of the comparison is the assumption that in the (n, γ) reactions the stronger gamma rays observed from the state capturing the thermal neutron are probably E1 radiation arising from transitions of the captured neutron, initially in an s state, to a p state of the final nucleus. On this single particle view of the (n, γ) process the transition is comparable with the $l=1$ transition to the same final level seen by a (d, p) process. If I is the intensity of the emitted gamma ray of energy E then I/E^3 should be compared with the reduced width for the (d, p) reaction to the same final level.

Groshev *et al.* list values of I/E^3 corresponding to 13 levels of ^{52}V. In our (d, p) work groups corresponding to all these levels are observed and angular distributions corresponding to eleven of them have been obtained. The assignment for ten of these angular distributions is $l=1$ showing that the corresponding states for the ingoing neutron are p states, thus confirming the general assumption about the E1 character of this gamma radiation in the (n, γ) reaction. It is not possible to compare values of I/E^3 and the reduced width γ, since the analysis of the stripping results yields $(2J_f+1)\gamma$ and J_f the spin of the final state is not known. Therefore I/E^3 is compared with $(2J_f+1)\gamma$ for the transitions to the levels of ^{52}V as shown in figure 3. Qualitative agreement is obtained, the main discrepancies occurring for the ground state and the level at 0·418 MEV.

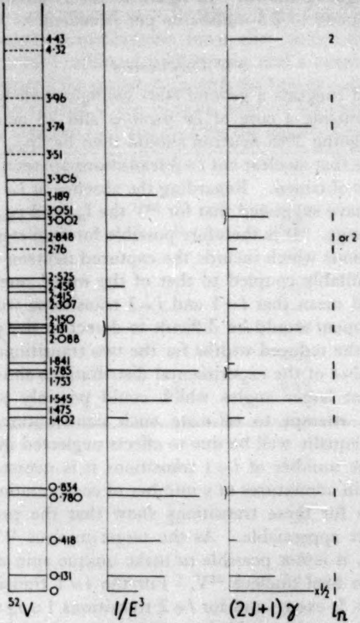

Figure 3. Comparison of the relative values of I/E^3 obtained from the $^{51}V(n, \gamma)^{52}V$ reaction with those of $(2J+1)\gamma$ obtained from the $^{51}V(d, p)^{52}V$ reaction.

REFERENCES

BARTHOLOMEW, G. A., and KINSEY, B. B., 1954, *Phys. Rev.*, **93**, 1434.

BETHE, H. A., and BUTLER, S. T., 1952, *Phys. Rev.*, **85**, 1045.

BLATT, J. M., and WEISSKOPF, V. F., 1952, *Theoretical Nuclear Physics* (New York: Wiley), p. 390.

Braid, T. H., 1956, *Phys. Rev.*, **102**, 1109.

Dalton, A. W., **Hinds**, S., and **Parry**, G., 1957, *Proc. Phys. Soc.* A, 70, 586.

El Bedewi, F. A., and **Tadros**, S., 1958, *Nucl. Phys.*, **8**, 71.

Enge, H. A., and **Graue**, A., 1955, *Univ. Bergen Årb. Naturv. R.*, No. 13.

Evans, R. D., *The Atomic Nucleus* (New York: McGraw-Hill), p. 401.

Gamow, G., and **Critchfield**, C. L., 1949, *Theory of the Atomic Nucleus* (Oxford: University Press) p.11.

Green, T. S., and **Middleton**, R., 1956, *Proc. Phys. Soc.* A. **69**, 16.

Groshev, L. V., **Demidov**, A. M., **Lutsenko**, V. N., and **Pelekhov**, V. I., 1957, *Atomnaya Energiya* **3**, 187.

—— 1958, *Second United Nations International Conference on the Peaceful Uses of Atomic Energy* A/Conf. 15/P/2029, U.S.S.R., 24 July 1958.

King, J. S., and **Parkinson**, W. C., 1953, *Phys. Rev.*, **89**, 1080.

Nordheim, L. W., 1951, *Rev. Mod. Phys.*, **23**, 322.

Schwager, J. E., and **Cox**, L. A., 1953, *Phys. Rev.*, **92**, 102.

Way, K., **King**, R. W., **McGinnis**, C. L., and **van Lieshout**, R., 1955, *Nuclear Level Schemes* (Washington D.C.: National Research Council).

Theory of Ultrasonic Vibration Potentials in Pure Liquids

By A. WEINMANN
Mathematics Department, University of Leicester

MS. received 11*th June* 1959, *in revised form* 25*th August* 1959

Abstract. Various possible mechanisms, which could produce potentials in a pure liquid through which an ultrasonic wave is propagating, are discussed. Alignment of molecular dipoles, due to density gradients, appears to be the most effective mechanism, and could account for the potentials observed in polar liquids. It is suggested that the non-polar heptane (and the similar paraffins of this series) really contain weak quasi-free dipoles, whose moment is of order $0{\cdot}2 \times 10^{-18}$ e.s.u. cm. This could account for the small potentials which have been observed in heptane by Rutgers and Rigole.

§ Introduction

Debye (1933) has suggested a method of measuring the effective masses of ions in solution, by measuring the electric potentials produced when ultrasonic waves are passed through an electrolyte. Recent experiments to detect this effect (Hunter 1958, Rutgers 1946, Rutgers and Vidts 1950, Rutgers and Rigole 1958, Yeager and Hovorka 1953, Yeager, Dietrick and Hovorka 1953, Yeager *et al.* 1949, Yeager, Booker and Hovorka 1959) show disagreement with Debye's formula, in that potentials are also observed in some pure liquids.

So far no satisfactory explanation of these effects has been given, though the results of Yeager, Booker and Hovorka (1959) seem to indicate that most of the anomalous effects are due to potentials produced at the liquid–glass–electrode surfaces. Their results are not however in complete agreement with those of Rutgers and Rigole (1958), who observed potentials in the non-polar heptane. Rutgers and Rigole also suggested various possible mechanisms for the production of potentials, but they found no satisfactory explanation.

It is the purpose of this note to investigate the possibility of potentials being produced in pure liquids by 'genuine causes'. Thus, for instance, varying contact potentials at the liquid–electrode boundaries, or various possible condenser-microphone effects are not considered. Such 'spurious effects' are perhaps best studied experimentally.

§ 2. Possible Mechanisms for Producing Potentials

When an ultrasonic wave is propagating through a liquid, density gradients are present. As a result the environment of any particular molecule is non-uniform, and its interactions with the other molecules not isotropic. This could lead to potentials being produced by, for instance, the alignment of molecular dipoles, or by induction. The effects of inertia, in displacing parts of a molecule relative to each other or the electrons relative to the nuclei, will be ignored except for a brief discussion in § 5. We will now discuss the above possibilities.

To clarify the situation, consider first the case of rigid polar molecules. Let coordinates specifying the orientation of a molecule be denoted by R. We note first that in general

(*a*) If the density is constant, then the probability that a certain molecule has orientation R is independent of R; and the potentials are zero by symmetry.

(*b*) For rigid molecules interacting as point dipoles (together with a central interaction), the probability of any configuration of the molecules is the same as that of the configuration in which the directions of the dipoles are reversed, provided there are no external fields, and the average electric potential at any point is therefore zero.

From (*b*) we conclude that potentials will only be produced if more complex interactions are present besides dipolar forces.

For ordinary polarizable polar molecules, the theory would clearly be very difficult. The polarizability is not an essential feature for the production of potentials by the mechanisms discussed here, and will be neglected for this case. The errors thereby introduced could clearly be quite large, as this approximation is known to be unreliable in evaluating dielectric constants.

An estimation shows that rigid molecules with no dipole moment, but only higher pole moments, could only produce potentials very much smaller than those with both dipole and higher moments. It is therefore important to investigate the effects of induced dipole moments, in the case of non-dipolar polarizable molecules. (In this connection it is important to note that the dipole moments are usually deduced from dielectric constant measurements. This is not very accurate for small dipole moments μ, as it measures essentially only μ^2. In some cases a molecule with a moment as large as $0{\cdot}2 \times 10^{-18}$ e.s.u. cm is classed as non-polar. As the potentials will be found to depend linearly on μ (and also on a combination of μ and the higher moments), a moment of this magnitude might not be negligible.) However, a very crude estimation shows that induced dipole moments, though possibly quite large for certain configurations of the molecules, tend to cancel out on averaging over all orientations, and give rise to very much smaller potentials than would result if permanent dipoles were present.

A more important case of deformable molecules 'without dipole moment' is that in which parts of a molecule are quasi-free to move relative to each other, for example, hindered rotation about a bond. If the parts each have a small dipole moment, then the average dipole moment may be zero or very small. The theory for such molecules would clearly be rather difficult, but it seems reasonable to suppose that potentials are possible, though perhaps smaller in than ordinary polar liquids.

In the following sections, estimates will be made of the potentials in the simple case of non-polarizable molecules with dipole and higher moments. In an earlier method of evaluation (unpublished), approximations more suitable to a description of the liquid state were made. Here we will employ a different method, which would be more appropriate to a dipolar crystal lattice. This shows more clearly the approximations made and gives similar results. The basic assumptions made are: (i) The molecules are located at the points of a crystal lattice, whose motion is independent of the orientations of the molecules. (ii) The vibrations of the crystal lattice due to the sound waves are slow compared with the period of rotational motion of the molecules. The orientations of the molecules can thus adjust themselves to an equilibrium distribution. (iii) When the system is in equilibrium (with no sound wave), all orientations of any single molecule are equally likely. (iv) Polarization effects may be neglected. (v) A 'liquid' approximation of averaging over all directions of the crystal is permissible. Assumption (v) is more a matter of computational convenience than an independent assumption (see the remarks before equation (13)).

§ 3. EVALUATION OF THE POTENTIALS

Let $\{R_1, R_2, \ldots, R_n\} = R$ denote the set of coordinates specifying the orientations of the n molecules, when at the displaced positions $\mathbf{p}_1, \mathbf{p}_2, \ldots, \mathbf{p}_n$. Let $\mathbf{r}_1, \mathbf{r}_2, \ldots, \mathbf{r}_n$ be the equilibrium positions of the molecules, so that, by assumption (i), when a small amplitude plane longitudinal sound wave is propagating through the crystal

$$\mathbf{p}_i = \mathbf{r}_i + \mathbf{u}(\mathbf{r}_i, t), \qquad \mathbf{u}(\mathbf{r}, t) = \mathbf{b}\exp\{i(\mathbf{k}\,.\,\mathbf{r} - \omega t)\}, \qquad \ldots\ldots (1)$$

with $\mathbf{b}$ parallel to $\mathbf{k}$. Let V_{ij} $(=V_{ji})$ be the interaction potential between molecules i and j, and let $V = \frac{1}{2}\Sigma V_{ij}$, the sum being over all i, j with $i \neq j$. By assumption (ii), the probability density $n(R) = n(R_1, R_2, \ldots, R_n)$ for the molecules to have orientation R, is given by

$$n(R) = Z^{-1}\exp(-V/\kappa T), \qquad Z = \int \exp(-V/\kappa T)\,dR, \qquad \ldots\ldots (2)$$

where κ is Boltzmann's constant, and T the temperature. If $\boldsymbol{\mu}_j$ is the dipole moment vector of the jth molecule then its average value $\langle\boldsymbol{\mu}_j\rangle$, in the strained lattice, is

$$\langle\boldsymbol{\mu}_j\rangle = \int n(R)\boldsymbol{\mu}_j\,dR. \qquad \ldots\ldots (3)$$

It is convenient to express this as an average over the equilibrium distribution $n^{(0)}(R)$, which is given by (2) when $\mathbf{u}(\mathbf{r}_i, t) = 0$. This is achieved by expanding

$$V = V^{(0)} + V^{(1)} \qquad \ldots\ldots (4)$$

where $V^{(0)}$ is the potential when $\mathbf{u}(\mathbf{r}_j, t) = 0$, and $V^{(1)} = V - V^{(0)}$ is the perturbation caused by the sound wave. Inserting (4) into (2), and expanding the exponential with the small term $V^{(1)}$ in it, as far as the linear term, and using the isotropy of the equilibrium distribution $n^{(0)}(R)$ implied by assumption (iii), gives the approximation

$$\begin{aligned}\langle\boldsymbol{\mu}_j\rangle &= -(\kappa T)^{-1}\langle\boldsymbol{\mu}_j V^{(1)}\rangle_0 \\ &= -(\kappa T)^{-1}[\textstyle\sum'\langle\boldsymbol{\mu}_j V^{(1)}{}_{js}\rangle_0 + \frac{1}{2}\sum''\langle\boldsymbol{\mu}_j V^{(1)}{}_{rs}\rangle_0], \qquad \ldots\ldots (5)\end{aligned}$$

where Σ' is a sum over s with $s \neq j$, and Σ'' is a sum ovre r, s with $r \neq s$, and both different from j; and $\langle\ \rangle_0$ denotes an average over the equilibrium distribution $n^{(0)}(R)$.

The main contribution to the sums in (5) come from the nearest neighbours of the jth molecule. We proceed to estimate the simpler first term of the last member of (5). The summand can be written

$$\langle\boldsymbol{\mu}_j V^{(1)}{}_{js}\rangle_0 = \int \boldsymbol{\mu}_j V^{(1)}{}_{js} n^{(0)}(R)\,dR = \int \boldsymbol{\mu}_j V^{(1)}{}_{js} n^{(0)}(R_j, R_s)\,dR_j\,dR_s, \qquad \ldots\ldots (6)$$

where $n^{(0)}(R_j, R_s)$ is the equilibrium probability density for molecules j and s to have orientations R_j, R_s respectively, when the rest of the molecules are not observed. If dipole and higher moments are allowed for in the evaluation of $n^{(0)}(R_j, R_s)$, then this will give different probabilities for molecules j and s to be parallel or antiparallel: the dipole–dipole interaction term in $V^{(1)}{}_{js}$ already gives a contribution to (6). Other contributions will be neglected. The dipole–dipole part of V_{js} is

$$V_{js}=(\boldsymbol{\mu}_j\,.\,\boldsymbol{\mu}_s)(p_{js})^{-3}-3(\boldsymbol{\mu}_j\,.\,\mathbf{p}_{js})(\boldsymbol{\mu}_s\,.\,\mathbf{p}_{js})(p_{js})^{-5}, \qquad \ldots\ldots(7)$$

where $\mathbf{p}_{js}=\mathbf{p}_s-\mathbf{p}_j$. The second term on the right-hand side of (7) will be omitted for brevity (see Appendix A); in the first term write

$$\mathbf{p}_{js}=\mathbf{r}_{js}+\mathbf{w}_{js}, \qquad \mathbf{w}_{js}=\mathbf{u}(\mathbf{r}_s,t)-\mathbf{u}(\mathbf{r}_j,t), \qquad \ldots\ldots(8)$$

where $\mathbf{r}_{js}=\mathbf{r}_s-\mathbf{r}_j$. It is found sufficient to expand the corresponding term in $V^{(1)}$ as far as the linear term in $\mathbf{w}_{js}$, so that

$$V^{(1)}{}_{js}=-3(\boldsymbol{\mu}_j\,.\,\boldsymbol{\mu}_s)(\mathbf{r}_{js}\,.\,\mathbf{w}_{js})(r_{js})^{-5}. \qquad \ldots\ldots(9)$$

Let the constant λ, which depends on r_{js} and T, be defined by

$$\int \boldsymbol{\mu}_j(\boldsymbol{\mu}_j\,.\,\boldsymbol{\mu}_s)n^{(0)}(R_j,R_s)\,dR_j\,dR_s=\lambda\mu^3\mathbf{r}_{js}/r_{js}. \qquad \ldots\ldots(10)$$

This gives a quantitative measure to the parallel–antiparallel asymmetry of $n^{(0)}(R_j,R_s)$. Inserting (9), (10) into (6) we obtain

$$\langle\boldsymbol{\mu}_j V^{(1)}{}_{js}\rangle_0=-3\lambda\mu^3(\mathbf{r}_{js}\,.\,\mathbf{w}_{js})\mathbf{r}_{js}(r_{js})^{-6}. \qquad \ldots\ldots(11)$$

This must be summed over s, the nearest neighbours giving the only significant contribution. As the wavelengths of ultrasonic waves are very long compared with the intermolecular distances r_{js}, $|\mathbf{k}\,.\,\mathbf{r}_{js}|\ll 1$; so $\mathbf{w}_{js}$ can be expanded:

$$\begin{aligned}\mathbf{w}_{js}&=\mathbf{u}(\mathbf{r}_j,t)[\exp(i\mathbf{k}\,.\,\mathbf{r}_{js})-1]\\&=\mathbf{u}(\mathbf{r}_j,t)[i\mathbf{k}\,.\,\mathbf{r}_{js}-\tfrac{1}{2}(\mathbf{k}\,.\,\mathbf{r}_{js})^2+\ldots].\end{aligned} \qquad \ldots\ldots(12)$$

The first term of (12) will give a zero contribution, when summed over s, for a sufficiently symmetric crystal. This is also zero, on average, in a liquid. The calculation can be simplified by use of assumption (v), which allows the sum over s to be calculated for the nearest neighbours by replacing r_{js} by ρ, the nearest neighbour distance, and replacing Σ' by

$$(4\pi)^{-1}N_1\int \sin\theta_{js}\,d\theta_{js}\,d\phi_{js},$$

N_1 being the number of nearest neighbours, and θ_{js}, ϕ_{js} the polar angles of $\mathbf{r}_{js}$. This procedure yields

$$\langle\boldsymbol{\mu}_j\rangle=-3\lambda\mu^3N_1k^2\mathbf{u}(\mathbf{r}_j,t)/(10\kappa T\rho^2), \qquad \ldots\ldots(13)$$

approximately. The electric polarization $\mathbf{P}$ in the liquid is then

$$\mathbf{P}=n_0\langle\boldsymbol{\mu}_j\rangle=-[3\lambda\mu^3N_1n_0k^2/(10\kappa T\rho^2)]\mathbf{b}\exp\{i(\mathbf{k}\,.\,\mathbf{r}_j-\omega t)\}, \qquad \ldots\ldots(14)$$

where n_0 is the equilibrium number density of molecules. Comparing this with the phenomenological expression $\mathbf{P}=(\epsilon-1)\mathbf{E}/(4\pi)+\alpha\nabla n$ (Weinmann 1959), we find the following approximation for the constant α:

$$\alpha=-3\lambda\mu^3N_1\epsilon/(10\kappa T\rho^2), \qquad \ldots\ldots(15)$$

where ϵ is the dielectric constant. The peak potential $\phi_{\max}$ follows from this, or more directly from (14),

$$\phi_{\max}=-\frac{12\pi\mu n_0\rho}{10}\left(\frac{\lambda\mu^2N_1}{\rho^3\kappa T}\right)\frac{a_0}{c}, \qquad \ldots\ldots(16)$$

where a_0 is the velocity amplitude of the sound wave, and c the speed of propagation (see also Appendix A).

§ 4. NUMERICAL MAGNITUDES

The constant λ, defined by equation (10), depends on the type of molecule. For *water* molecules we have tried to estimate it, by use of the model proposed by Lennard-Jones and Pople (1951), and Pople (1951). The result is very sensitive to the value of the H–O–H angle used, but a value for λ of *order* 0·02 seems reasonable, as explained in Appendix B. The combination $\lambda\mu^2 N_1/\rho^3\kappa T$, occurring in (16), would appear to depend more on the higher pole moments than on μ. The other constants for water are taken as

$$c=1{\cdot}4\times10^{5}\ \text{cm sec}^{-1},\qquad n_0=3{\cdot}3\times10^{22}\ \text{cm}^{-3},$$
$$\mu=1{\cdot}8\times10^{-18}\ \text{e.s.u. cm},\qquad \rho=2{\cdot}9\times10^{-8}\ \text{cm},$$
$$N_1=4,\qquad T=300^{\circ}\text{K}.$$

Inserting these into equation (16), and converting from e.s.u. to volts,

$$\phi_{\max}/a_0=3\times10^{-6}\ \text{volt}. \qquad \ldots\ldots(17)$$

The approximations on which this is based will be discussed further in the next section. Similar potentials would be expected in other polar liquids.

§ 5. DISCUSSION

The use of the approximations (i) to (v) stated in § 2, or some similar ones, is required because the statistical mechanical theory is at present insufficiently developed to allow a more systematic reduction (see, for example, Green 1952). The errors made are difficult to estimate. In the detailed calculations, the estimation of the asymmetry parameter λ appears to be the weakest point. The neglect of the higher powers of $V^{(1)}$ in equation (5), combined with the neglect of the polarizability of the molecules, is similar to neglecting 'local field corrections' in dielectric constant calculations (see, for example, Brown 1956). We have not found a systematic method of allowing for this.

The calculations show that potentials of the magnitude observed experimentally *could* occur in polar liquids. Similar potentials would be expected in crystals consisting of polar molecules, such as ice.

The only case where potentials have been reported in a non-polar liquid is in heptane (Rutgers and Rigole 1958). Yeager, Booker and Hovorka (1959) however find no potentials. The dipole moment of the 'non-polar' heptane has been measured by Dornte and Smyth (1930), using the temperature variation of dielectric constant method. They find that the 'polarization', instead of decreasing steadily with increasing temperature as expected in a polar substance, increases from a value of 34·09 cm³ at −90°C, to a maximum of 34·56 cm³ at 50°C, and then decreases to 34·44 cm³ at 90° C. They do not account for this small variation of 'polarization' with temperature, but conclude that the dipole moment of heptane is very small. It appears to us that this variation of the 'polarization' with temperature is of the type to be expected for molecules containing quasi-free dipoles (see, for example, Smyth 1955). We have tested the possibility of this by calculations using a very crude model of heptane, in which the dipoles are placed at the ends of the molecule, and the polarizability of the central portion is partially allowed for. This leads to a formula for the temperature dependence of the 'polarization' which can be fitted to the observed values with much greater accuracy (to within about 0·06 cm³), and suggests a moment of order $0{\cdot}2 \times 10^{-18}$ e.s.u. cm for the dipoles. Similar moments would be expected for the other paraffins of this series. If this view is correct, it might account for the potentials observed in heptane by Rutgers and Rigole (1958).

Rutgers and Rigole (1958, equation (4)) give an estimate for the potentials due to inertia, resulting from the displacement of parts of a molecule relative to to each other. The occurrence as a factor $1/D$ of the dielectric constant D in their formula appears to be incorrect. The factor depends on the details of the interactions of the molecules. If one uses the very crude 'Lorentz local field' (Brown 1956, § 22), then one finds a factor $(D+2)/(3D)$, instead of $1/D$. This would increase the potentials due to this cause only to a few tenths of a microvolt for unit velocity amplitude, for typical molecules. Inertia effects would also displace the electrons relative to the nuclei. An estimation shows that this effect is in general smaller than that due to the displacement of parts of a molecule relative to each other.

At present, it is not clear if the 'genuine' potentials discussed here have been observed in the experiments. As the estimate given in equation (17) may well be somewhat large, there may be some difficulty in detecting these potentials, due to the high noise level of existing detectors; even if the 'spurious effects' can be successfully eliminated, or allowed for. Hunter (1958) has proposed integrating his signals over many pulses. This would increase the signal/noise ratio by a factor $N^{1/2}$ approximately, where N is the number of pulses; and this gives some hope that the potentials may be detected.

ACKNOWLEDGMENTS

My thanks are due to Dr. A. N. Hunter for first interesting me in this work, and to Dr. K. V. Roberts and Dr. R. O. Gandy for helpful criticism of an earlier version of the theory.

APPENDIX A

It appears likely that the second omitted term in the dipole–dipole interaction (7) will not cancel out the first term treated in the text, and this is confirmed by the complete calculations, with the whole interaction (7). The result of this calculation is to replace λ, in (13) and all the following equations, by the factor

$$-\tfrac{1}{3}(4\lambda_1+4\lambda_2+6\lambda_3),$$

where the constants λ_1, λ_2, λ_3, λ_4 are defined by the equation (which follows from the symmetries of the left-hand side)

$$\int \mu_j{}^{\alpha}\mu_j{}^{\beta}\mu_s{}^{\gamma} n^{(0)}(R_j, R_s)\,dR_j\,dR_s = \mu^3[\lambda_1\delta^{\alpha\beta}\rho^{\gamma}\rho^{-1}+\lambda_2(\delta^{\alpha\gamma}\rho^{\beta}+\delta^{\beta\gamma}\rho^{\alpha})\rho^{-1}$$
$$+\lambda_3\rho^{\alpha}\rho^{\beta}\rho^{\gamma}\rho^{-3}+\lambda_4(\mathrm{e}^{\alpha\gamma\mu}\rho_{\mu}\rho^{\beta}+\mathrm{e}^{\beta\gamma\mu}\rho_{\mu}\rho^{\alpha})\rho^{-2}].$$

In this equation components of vectors and tensors are denoted by the appropriate subscripts or superscripts $\alpha, \beta, \gamma, \mu$; $\delta^{\alpha\beta}$, $\mathrm{e}^{\alpha\beta\gamma}$ are the usual δ and e tensors; and ρ^{α} is the vector $\mathbf{r}_{js}$.

APPENDIX B

EVALUATION OF λ

No attempt was made to evaluate the more correct combination

$$-\tfrac{1}{3}(4\lambda_1+4\lambda_2+6\lambda_3),$$

which replaces λ (Appendix A), as this refinement did not appear to be justified.

The estimation of λ proceeds as follows. According to Pople (1951)

$$n^{(0)}(R_j, R_s) = \text{const.} \exp\{g(\cos\chi_j + \cos\chi_s)/\kappa T\}, \qquad \text{......(B 1)}$$

where $\chi_j(\chi_s)$ is the angle between $\mathbf{r}_{js}$ and a 'bond-forming direction' of the water molecule $j(s)$; g is a force constant; and the constant is included to normalize $n^{(0)}$. Let $\Lambda(\vartheta_j, \vartheta_s)$ denote the value of λ, calculated by inserting (B 1) into equation (10), when the angle between $\boldsymbol{\mu}_j(\boldsymbol{\mu}_s)$ and one of the four 'bond-forming directions' in the $j(s)$ th molecule is $\vartheta_j(\vartheta_s)$. We find that

$$\Lambda(\vartheta_j, \vartheta_s) = -\tfrac{1}{2}\cos\vartheta_s[\coth\xi - \xi^{-1}] \times [\sin^2\vartheta_j + (3\cos^2\vartheta_j - 1)(1 - 2\xi^{-1}\coth\xi + 2\xi^{-2})], \qquad \text{......(B 2)}$$

where $\xi = g/\kappa T$. Now the expression (B 1) is incomplete, since there are four 'bond-forming directions' in each water molecule; therefore to get λ, the expression (B 2) must be averaged over all eight combinations giving hydrogen bonds between neighbouring molecules. Collecting equal terms, we obtain

$$\lambda = \tfrac{1}{2}[\Lambda(\vartheta, \vartheta') + \Lambda(\vartheta', \vartheta)], \qquad \text{......(B 3)}$$

where 2ϑ is the H–O–H angle and $2(\pi - \vartheta')$ the angle between the 'lone-pair directions'.

According to Pople (1951), $\xi = g/\kappa T = 10$ at 300°C. If one assumes an exactly tetrahedral structure for water, than $\cos\vartheta = -\cos\vartheta' = 3^{-1/2}$, and each Λ has magnitude 0·2, while $\lambda = 0$ due to exact cancellation in (B 3). However, the alternative assumption $2\vartheta = 105°$ (the experimental H–O–H angle quoted by Pople), with $\cos\vartheta' = -3^{-1/2}$ as before, gives $\lambda = 0{\cdot}002$.

The cancellation effects make the estimation of λ difficult. Also, the derivation of (B 2) assumed that each water molecule rotates about the oxygen nucleus, whereas it seems more correct to suppose that the rotation is about the centre of mass. The neglect of polarizability is also a cause of error. There is however no special symmetry which would make λ necessarily zero. Because of these various effects, it appears unlikely that λ is less than 0·002, while it seems probable that λ is less than 0·2. The order of magnitude estimate 0·02 used in the text, results from this in the absence of a better estimate.

REFERENCES

BROWN, W. F., JR., 1956, *Handb. d. Physik*, XVII (Berlin ; Göttingen ; Heidelberg : Springer).

DEBYE, P., 1933, *J. Chem. Phys.*, **1,** 13.

DORNTE, R. W., and SMYTH, C. P., 1930, *J. Amer. Chem. Soc.*, **52,** 3546.

GREEN, H. S., 1952, *The Molecular theory of Fluids* (Amsterdam: North-Holland).

HUNTER, A. N., 1958, *Proc. Phys. Soc.*, **71,** 847.

LENNARD-JONES, SIR JOHN, and POPLE, J. A., 1951, *Proc. Roy. Soc.* A, **205,** 155.

POPLE, J. A., 1951, *Proc. Roy. Soc.* A, **205,** 163.

RUTGERS, A. J., 1946, *Nature, Lond.*, **157,** 74.

RUTGERS, A. J., and RIGOLE, W., 1958, *Trans. Faraday Soc.*, **54,** 139.

RUTGERS, A. J., and VIDTS, J., 1950, *Nature, Lond.*, **165,** 109.

SMYTH, C. P., 1955, *Dielectric Behaviour and Structure* (New York; Toronto; London : McGraw-Hill).

WEINMANN, A., 1959, *Proc. Phys. Soc.*, **73,** 345.

YEAGER, E., BOOKER, J., and HOVORKA, F., 1959, *Proc. Phys. Soc.*, **73,** 690.

YEAGER, E., BUGOSH, J., HOVORKA, F., and MCCARTHY, J., 1949, *J. Chem. Phys.*, **17,** 411.

YEAGER, E., DIETRICK, H., and HOVORKA, F., 1953, *J. Acoust. Soc. Amer.*, **25,** 456.

YEAGER, E., and HOVORKA, F., 1953, *J. Acoust. Soc. Amer.*, **25,** 443.

Relations between the Friction Constant and the Force Correlation Integral in Brownian Movement Theory

A Comparison of the Microscopic and Macroscopic Theories

By A. SUDDABY and P. GRAY†

Sir John Cass College, Jewry Street, Aldgate, London, E.C.3

MS. received 27th May 1959, *in final form 30th July* 1959

Abstract. Kirkwood's expression for the friction constant is compared with the expression implicit in Brownian movement theory. Relations between the friction constant β and the fluctuating force $F(t)$ are obtained in the case of a white spectrum and of a general spectrum. The former relation resembles Kirkwood's expression and depends on the correlation function of $F(t)$ being sufficiently sharply peaked to permit the integral to reach a plateau value in a time τ_1 such that $\beta\tau_1 \ll 1$.

Since Kirkwood's expression involves the total force $X(t) = F(t) - \beta u$, the correlation integral of this force is calculated in the macroscopic theory of Brownian movement. The infinite integral

$$\int_0^\infty \langle X(t)X(t+\tau)\rangle_t \, d\tau$$

is found to be zero, but the incomplete integral

$$\int_0^{\tau_1} \langle X(t)X(t+\tau)\rangle_t \, d\tau$$

is found to be equal to the incomplete correlation integral of the fluctuating force

$$\int_0^{\tau_1} \langle F(t)F(t+\tau)\rangle_t \, d\tau$$

provided that the upper limit of integration τ_1 is large enough for the correlation function $\langle F(t)F(t+\tau)\rangle_t$ to have decayed to zero, but is sufficiently small to ensure that $\beta\tau_1 \ll 1$.

It follows that there is correspondence between the microscopic and macroscopic theories provided this condition holds.

---

§ 1. INTRODUCTION

THE molecular theory of transport processes in liquids developed by Kirkwood (1946) starts from the Liouville equation which determines the distribution function $f^{(N)}$ for the joint distribution of the N molecules of the system. A 'coarse graining' procedure is used to obtain partial differential equations for the joint distribution functions $f^{(n)}$ of n molecules ($n \ll N$) which have the property of irreversibility. These equations have the same form as the Fokker–Planck–Kramers equation of Brownian movement theory. A similar procedure enables the equation of motion of a single molecule to be obtained in a form similar to the Langevin equation.

---

† Formerly at E.M.I. (Electronics), and now at the Atomic Weapons Research Establishment, Aldermaston, Berks.

This reduction of the problem of irreversibility to equations of the Brownian movement type depends on the hypothesis that the integral of the auto-correlation function of the force reaches a plateau value. This hypothesis leads to an expression for the friction constant. Kirkwood's theory has been applied to the problem of the viscosity of liquids and has been found by Eisenschitz (1949) to give a temperature dependence of the right form. The theory of Eisenschitz has been used to calculate the anisotropy of flow in a pure liquid (Champion 1958) and the result has been confirmed experimentally. An application of Kirkwood's theory to liquid phase chemical reactions leads to the well-known transition state expression as a first approximation (Wood and Suddaby 1957).

The evaluation of the friction constant constitutes a major problem in the application of the Kirkwood theory to real physical systems. Kirkwood's assumption of a plateau value leads to a formal expression which relates the friction constant to the intermolecular forces. This expression has been regarded by some as the main contribution of Kirkwood's theory (Green 1952) and has been the basis of attempts to evaluate the friction constant (Suddaby 1954, Turner 1958).

In this paper we consider relations implicit in the ordinary Brownian movement theory which lead to an expression for the friction constant similar in general form to the expression of Kirkwood. This expression of macroscopic theory is compared with the expression of Kirkwood which arises from microscopic theory and the reasons for the difference are discussed. Conditions are found under which the expressions are compatible.

§ 2. KIRKWOOD'S EXPRESSION FOR THE FRICTION CONSTANT

The starting point of the theory of the Brownian movement is the Langevin equation,

$$\frac{du}{dt} + \beta u = F(t) \qquad \ldots\ldots(1)$$

which is based on the assumption that the force per unit mass on a Brownian particle may be divided into two parts, a frictional component $-\beta u$ which is proportional to the velocity and a random fluctuating component $F(t)$ which is characterized by a sharply peaked auto-correlation function.

In the paper on the statistical mechanical theory of transport processes Kirkwood (1946) has established that, under certain conditions, the Langevin equation is valid for a system of molecules n forming part of a large assembly N. This paper has formed the basis of the modern theory of non-uniform liquids (Eisenschitz 1951, 1952). In the following, Kirkwood's procedure, which is three-dimensional, is presented in a one-dimensional form.

In the classical equation of motion for a molecule,

$$\frac{du}{dt} = X(t)$$

where $X(t)$ is the total force on molecule 1 due to all the other molecules, Kirkwood makes the substitution $F(t) = X(t) - \langle (X(t))_\tau \rangle^{u_0}$ to give

$$\frac{du}{dt} - \langle (X(t))_\tau \rangle^{u_0} = F(t). \qquad \ldots\ldots(2)$$

$\langle (X(t))_\tau \rangle^{u_0}$ represents the average total force, the average being taken successively, over a short time interval τ, microscopically large but macroscopically small, and over an ensemble of the assemblies N in which the molecule considered (denoted by i) has the constant initial velocity u_0. He then establishes that

$$\langle (X(t))_\tau \rangle^{u_0} = -\zeta u$$

where

$$\zeta = \frac{m}{kt}\int_0^{\tau_1} \langle X(t)X(t+\tau)\rangle^{u_0}\,d\tau. \qquad \ldots\ldots (2\,a)$$

When the hypothesis is made that, for values of τ_1 still small compared with macroscopic times, the value of the integral reaches a plateau value independent of τ_1, ζ becomes a constant, independent of the time and (2) becomes formally identical with the Langevin equation (1), ζ taking the place of β. Thus (2 a) provides a relation between the friction constant and the total intermolecular force $X(t)$.

§ 3. THE EXPRESSION FOR THE FRICTION CONSTANT IN BROWNIAN MOVEMENT THEORY

There are two methods of developing Brownian movement theory from the Langevin equation. In the method of Uhlenbeck and Ornstein (1931) averages are taken over an ensemble of particles with constant initial velocity u_0, denoted by $\langle \ldots \rangle^{u_0}$, whilst in the spectral method (Ming Chen Wang and Uhlenbeck 1945) the averages are taken over the time, denoted by $\langle \ldots \rangle_t$ which as a consequence of the stationary property of the process, corresponds to averages over an ensemble in equilibrium.

3.1. *Ensemble Theory*

The Langevin equation (1) is integrated subject to the initial condition $u=u_0$ when $t=0$. On squaring and taking the average over the ensemble, this gives:

$$\langle u^2 \rangle^{u_0} = u_0^{\,2}\,e^{-2\beta t} + e^{-2\beta t}\int_0^t\int_0^t e^{\beta(\xi+\eta)}\,\langle F(\xi)F(\eta)\rangle^{u_0}\,d\xi d\eta. \qquad \ldots\ldots (3)$$

By taking $v=\xi+\eta$, $w=\xi-\eta$ as new variables, and using the fact that

$$\langle F(\xi)\,F(\eta)\rangle^{u_0} = \phi(\xi-\eta) = \phi(w)$$

where $\phi(w)$ has a very sharp maximum at $w=0$, the second term becomes

$$\frac{1}{2\beta}\int_{-\infty}^{\infty} \phi(w)\,dw.$$

If we now let $t \to \infty$ and replace the left-hand side by the equipartition value kT/m, we obtain the relation

$$\frac{2\beta kT}{m} = \int_{-\infty}^{\infty} \phi(w)\,dw.$$

Thus

$$\beta = \frac{m}{kT}\int_0^{\infty} \langle F(t)\,F(t+\tau)\rangle^{u_0}\,d\tau. \qquad \ldots\ldots (4)$$

3.2. *Spectral Theory*

The fluctuating force is a stationary random function of the time. Relations valid for functions of this kind are now applied. The fluctuating force $F(t)$ is specified by means of its spectral density $G_F(f)$, defined by

$$G_F(f)=\lim_{T\to\infty}\frac{2}{T}|A_F(f,T)|^2$$

where

$$A_F(f,T)=\int_{-T/2}^{+T/2}F(t)\,\mathrm{e}^{-2\pi ift}\,dt.$$

The correlation function is defined by

$$\langle F(t)F(t+\tau)\rangle_t=\lim_{T\to\infty}\frac{1}{T}\int_{-T/2}^{+T/2}F(t)F(t+\tau)\,dt$$

and is related to the spectral density by the Wiener–Khintchine relation:

$$\langle F(t)F(t+\tau)\rangle_t=\int_0^\infty G_F(f)\cos 2\pi f\tau\,df \qquad \ldots\ldots(5)$$

which is obtained by applying Parseval's theorem to the definition above.

In particular

$$\langle F(t)^2\rangle_t=\lim_{T\to\infty}\frac{1}{T}\int_{-T/2}^{+T/2}F(t)^2\,dt$$

$$=\int_0^\infty G_F(f)\,df. \qquad \ldots\ldots(6)$$

Integration of (5) over τ gives

$$\int_0^\infty \langle F(t)F(t+\tau)\rangle_t\,d\tau=\tfrac{1}{4}G_F(0+) \qquad \ldots\ldots(7)$$

where $G_F(0+)$ is the limiting value of $G_F(f)$ when $f\to 0$ from positive values.

If we take the Fourier transform of the Langevin equation, apply (6) to the velocity and substitute the equipartition value of $\langle u^2(t)\rangle_t$ we obtain

$$\langle u^2(t)\rangle_t=\frac{kT}{m}=\int_0^\infty\frac{G_F(f)}{\beta^2+(2\pi f)^2}\,df. \qquad \ldots\ldots(8)$$

Relations (7) and (8) are independent of any assumptions about the spectrum of $F(t)$. However, in Brownian movement theory it is usually assumed that $F(t)$ has a white spectral density:

$$G_F(f)=G_F(0+)=D,\ \text{a constant.}$$

Then, from (7) and (8) we obtain

$$\beta=\frac{m}{kT}\int_0^\infty\langle F(t)\,F(t+\tau)\rangle_t\,d\tau \qquad \ldots\ldots(9)$$

which is the expression in spectral theory corresponding to (4).

The relations (7), (8) and (9) appear to be well known to Brownian movement theory although they are not formulated explicitly in either of the references quoted.

§ 4. THE GENERAL EXPRESSION FOR β AS THE PLATEAU VALUE OF THE CORRELATION INTEGRAL

The chief interest in relations (4) and (9) lies in their resemblance to the expression (2) obtained by Kirkwood. The Kirkwood expression involves an ensemble average over the initial phase of molecules 2 to N to which the ensemble average in (4) is made to conform by the equipartition assumption. The spectral theory, on the other hand, involves an average over the time but the assumption that $u(t)$ may be taken as a stationary random process together with the equipartition assumption ensures some correspondence between the two expressions.

The expressions of Brownian movement theory, however, differ in important respects from Kirkwood's expression. In Kirkwood's expression, the integration is carried out over an interval τ_1 in which, according to Kirkwood's hypothesis, the value of the integral has reached a plateau value. In Brownian movement theory, on the other hand, the integrals extend formally over the infinite range but the assumption that the correlation function is sharply peaked means that the major contribution from the integrand is made in the region for which τ is still small. Both (4) and (9) were obtained by assuming an extreme but unspecified sharpness of the correlation function. The precise degree of sharpness required in order that relation (9) may hold may be determined by obtaining more general relations based on more realistic assumptions about the spectral density.

If it is assumed that $G_F(f) = D, f \leqslant f_1$; $G_F(f) = 0, f > f_1$, thus introducing a cut-off at $f = f_1$, the evaluation of (8) and substitution into (7) gives

$$\beta = \frac{m}{kT}\frac{2}{\pi} \arctan \frac{2\pi f_1}{\beta} \int_0^\infty \langle F(t)\,F(t+\tau)\rangle_t \, d\tau. \qquad \ldots\ldots(10)$$

When $f_1 \gg \beta$, $\arctan 2\pi f_1/\beta \simeq \pi/2$ and (10) approaches (9).

Taking the inverse relation of (5), namely,

$$G_F(f) = 4 \int_0^\infty \langle F(t)\,F(t+\tau)\rangle_t \cos 2\pi f\tau \, d\tau,$$

substituting into (8), and changing the order of integration we obtain a relation independent of any assumption about the spectrum:

$$\beta = \frac{m}{kT} \int_0^\infty \langle F(t)\,F(t+\tau)\rangle_t \, e^{-\beta\tau} \, d\tau. \qquad \ldots\ldots(11)$$

For this expression to assume the form (9), it is necessary that the main contribution to the integral must come from the range of τ for which $e^{-\beta\tau}$ does not differ significantly from unity, namely the range $\tau < \tau_1$ where $\beta\tau_1 \ll 1$. The time then corresponds to the time in which the integrals (9) and (11) reach a significant proportion of their asymptotic values.

Thus the relation between the fluctuating force and the friction constant in Brownian movement theory assumes the form (9) which resembles Kirkwood's expression provided that the correlation properties of the fluctuating force permit the integral to reach a plateau value in a time τ_1 such that $\beta\tau_1 \ll 1$. The infinite integral in the Brownian movement expression may thus be reconciled with a plateau value if the correlation time satisfies the stated condition.

There is another difference between (2*a*) and (9), however, which appears to be of a more profound character. The Brownian movement expression for β involves the fluctuating force $F(t)$, whereas Kirkwood's expression, on the other hand, involves the total force $X(t)$ or $F(t) - \beta u$. In order, therefore, to investigate further the correspondence between Kirkwood's theory and the conventional theory of Brownian movement, it is of interest to evaluate the correlation integral of the total force in Brownian movement theory and to discover whether a simple relation exists between this integral and the friction constant.

§ 5. EVALUATION OF THE CORRELATION INTEGRAL OF THE TOTAL FORCE

The total force per unit mass $X(t)$ is, by (1),

$$X(t)=\frac{du}{dt}=F(t)-\beta u(t)$$

and its correlation function is

$$\begin{aligned}\langle X(t)X(t+\tau)\rangle=\langle F(t)F(t+\tau)\rangle-\beta\langle F(t)u(t+\tau)\rangle-\beta\langle F(t+\tau)u(t)\rangle\\ +\beta^2\langle u(t)u(t+\tau)\rangle\end{aligned} \qquad \ldots\ldots(12)$$

where $\langle\ldots\rangle$ stands for either kind of average. We wish to evaluate

$$\int_0^\infty \langle X(t)X(t+\tau)\rangle\,d\tau.$$

5.1. *Ensemble Theory*

The terms on the right-hand side of (12) may be calculated by the method that was used to solve (3).
Thus we obtain

$$\begin{aligned}\langle F(t)u(t+\tau)\rangle^{u_0}&=e^{-\beta(t+\tau)}\int_0^{t+\tau} e^{\beta\xi}\,\langle F(t)F(\xi)\rangle^{u_0}\,d\xi\\ &=2\beta kT/m\end{aligned}$$

$$\langle F(t+\tau)u(t)\rangle^{u_0}=e^{-\beta t}\int_0^{t} e^{\beta\xi}\,\langle F(t+\tau)F(\xi)\rangle^{u_0}\,d\xi=0.$$

This last result is due to the fact that $t+\tau$ falls outside the range of integration of ξ and would be expected in any case because $F(t+\tau)$ and $u(t)$ are uncorrelated. Finally,

$$\begin{aligned}\langle u(t)u(t+\tau)\rangle^{u_0}&=u_0^2\,e^{-\beta(2t+\tau)}+e^{-\beta(2t+\tau)}\int_0^t\int_0^{t+\tau} e^{\beta(\xi+\eta)}\,\langle F(\xi)F(\eta)\rangle^{u_0}\,d\xi\,d\eta\\ &=e^{-\beta\tau}\left\{\frac{kT}{m}+e^{-2\beta t}\left(u_0^2-\frac{kT}{m}\right)\right\}\end{aligned}$$

and (12) becomes

$$\langle X(t)X(t+\tau)\rangle^{u_0}=\langle F(t)F(t+\tau)\rangle^{u_0}-\frac{\beta^2kT}{m}\,e^{-\beta\tau}+\beta^2\,e^{-\beta\tau}\left(u_0^2-\frac{kT}{m}\right)e^{-2\beta t}. \qquad \ldots\ldots(13)$$

Integration of (13) with respect to τ gives

$$\int_0^\infty \langle X(t)X(t+\tau)\rangle^{u_0}\,d\tau=\beta e^{-2\beta t}\left(u_0^2-\frac{kT}{m}\right).$$

The ensemble approaches an equilibrium distribution in the velocities as $t\to\infty$, when this expression reduces to

$$\int_0^\infty \langle X(t)X(t+\tau)\rangle^{u_0}\,d\tau=0. \qquad \ldots\ldots(14)$$

5.2. *Spectral Theory*

The terms on the right-hand side of (12) are calculated easily by an extension of the method of § 3.2. Together with (5) they are

$$\begin{aligned}\langle F(t)u(t+\tau)\rangle_t&=\lim_{T\to\infty}\frac{1}{T}\int_{-\infty}^{\infty} A_F(f,T)\,A_u^*(f,T)\,e^{-2\pi if\tau}\,df\\ &=\tfrac{1}{2}\int_{-\infty}^{\infty}\frac{G_F(f)}{\beta-2\pi if}\,e^{2\pi if\tau}\,df\end{aligned}$$

$$\langle F(t+\tau)\,u(t)\rangle_t = \tfrac{1}{2}\int_{-\infty}^{\infty} \frac{G_F(f)}{\beta - 2\pi i f}\, e^{-2\pi i f\tau}\, df$$

$$\langle u(t)\,u(t+\tau)\rangle_t = \tfrac{1}{2}\int_{-\infty}^{\infty} \frac{G_F(f)}{\beta^2 + (2\pi f)^2}\, e^{2\pi i f\tau}\, df$$

where the asterisk denotes the complex conjugate.

If we now insert the white spectrum value of $G_F(f) = 4\beta\, kT/m$, we find

$$\langle F(t)\,u(t+\tau)\rangle_t = \frac{2\beta kT}{m}\int_{-\infty}^{\infty} \frac{e^{2\pi i f\tau}}{\beta - 2\pi i f}\, df = \frac{2\beta kT}{m}\, e^{-\beta\tau}$$

$$\langle F(t+\tau)\,u(t)\rangle_t = \frac{2\beta kT}{m}\int_{-\infty}^{\infty} \frac{e^{-2\pi i f\tau}}{\beta - 2\pi i f}\, df = 0$$

where this result is due to the fact that $e^{-2\pi i f\tau}/(\beta - 2\pi i f)$ has no poles in the lower half-plane. Finally,

$$\langle u(t)\,u(t+\tau)\rangle_t = \frac{2\beta kT}{m}\int_{-\infty}^{\infty} \frac{e^{2\pi i f\tau}}{\beta^2 + (2\pi f)^2}\, df = \frac{kT}{m}\, e^{-\beta\tau}.$$

Substituting these results in (12) we obtain

$$\langle X(t)\,X(t+\tau)\rangle_t = \langle F(t)\,F(t+\tau)\rangle_t - \frac{\beta^2 kT}{m}\, e^{-\beta\tau} \qquad \ldots\ldots(15)$$

so that

$$\int_0^{\infty} \langle X(t)\,X(t+\tau)\rangle_t\, d\tau = 0. \qquad \ldots\ldots(16)$$

The relation (15) will be used in the discussion of the incomplete integral in § 6, and although (16) follows directly, this result is independent of any assumption about the spectrum. If we substitute the relations for a general spectrum into (12), we obtain

$$\langle X(t)\,X(t+\tau)\rangle_t = \tfrac{1}{2}\int_{-\infty}^{\infty} \frac{G_F(f)(2\pi f)^2}{\beta^2 + (2\pi f)^2} \cos 2\pi f\tau\, df.$$

Integrating this over τ first, we obtain

$$\int_0^{\infty} \langle X(t)\,X(t+\tau)\rangle_t\, d\tau = \tfrac{1}{2}\int_{-\infty}^{\infty} \frac{G_F(f)(2\pi f)^2}{\beta^2 + (2\pi f)^2}\, \delta(f)\, df$$

which clearly leads to the result (16).

§ 6. COMPARISON WITH KIRKWOOD'S EXPRESSION

Both the ensemble and spectral theories of Brownian movement lead, on the assumption of a sharp peak for $\langle F(t)\,F(t+\tau)\rangle$ at $\tau = 0$ or a white spectrum for $F(t)$, to the results

$$\int_0^{\infty} \langle F(t)\,F(t+\tau)\rangle\, d\tau = \frac{\beta kT}{m} \qquad \ldots\ldots(17\,a)$$

$$\int_0^{\infty} \langle X(t)\,X(t+\tau)\rangle\, d\tau = 0 \qquad \ldots\ldots(17\,b)$$

where $\langle \ldots \rangle$ indicates a partial ensemble average in the ensemble theory and a time average in the spectral theory.

On the other hand, Kirkwood obtains a result which may be expressed in the form

$$\int_0^{\tau_1} \langle X(t)\,X(t+\tau)\rangle^{u_0}\, d\tau = \frac{\beta kT}{m}$$

where the average has the same significance as in the ensemble form of Brownian movement theory, but the right-hand side of the expression is a plateau value which the integral is assumed to attain after a macroscopically short time τ_1. The relation (17 *b*) is derived from the ordinary assumptions of Brownian movement theory which are known to lead to results which agree with experiment. We should therefore expect Kirkwood's theory to lead to the same relation.

However, the Kirkwood expression is obtained only after the neglect of terms having the order of magnitude of τ_1. Our equation (15) gives the Brownian movement expression for $\langle X(t)X(t+\tau)\rangle$ in terms of τ. If this is integrated from $\tau=0$ to some arbitrary value τ_1, we have

$$\int_0^{\tau_1}\langle X(t)X(t+\tau)\rangle\,d\tau=\int_0^{\tau_1}\langle F(t)\,F(t+\tau)\rangle\,d\tau+\frac{\beta kT}{m}\,(e^{-\beta\tau_1}-1)$$

$$=\int^{\tau_1}\langle F(t)\,F(t+\tau)\rangle\,d\tau-\frac{\beta kT}{m}\,[\beta\tau_1+\text{higher powers of }\beta\tau_1].$$

The second term is negligible if τ_1 is small enough to ensure that $\beta\tau_1\ll 1$. Then if τ_1 is still large enough for the first integral to have reached its plateau value of $\beta kT/m$ we have

$$\int_0^{\tau_1}\langle X(t)X(t+\tau)\rangle\,d\tau=\int_0^{\tau_1}\langle F(t)\,F(t+\tau)\rangle\,dt=\frac{\beta kT}{m}\qquad\ldots\ldots(18)$$

which agrees with the Kirkwood expression.

Relation (18) depends on the assumption that the appropriate upper limit of integration can be both small enough to make the higher terms negligible yet large enough to ensure that the plateau value is reached.

In § 4 we have shown that the relation

$$\int_0^{\infty}\langle F(t)\,F(t+\tau)\rangle\,d\tau=\frac{\beta kT}{m}$$

in Brownian movement theory depends on the assumption that the function $\langle F(t)\,F(t+\tau)\rangle$ is so sharply peaked at $\tau=0$ that the integral reaches a value substantially equal to its asymptotic value in a time τ_1, sufficiently short to ensure that $\beta\tau_1\ll 1$. The condition for relation (18) to hold is thus implicit in the ordinary Brownian movement theory and to this extent Kirkwood's expression for the friction constant is consistent with the latter. Relation (18), however, does not in any way indicate that the integral

$$\int_0^{\tau}\langle X(t)X(t+\tau)\rangle\,d\tau=I(\tau)$$

reaches an asymptotic value of $\beta kT/m$. Indeed since Brownian movement theory attributes the asymptotic value $\beta kT/m$ to the other integral (17 *a*), the value of $I(\tau)$, after rising rapidly to the value $\beta kT/m$, would decrease at a slower rate until, for large τ, it again became zero. This situation is illustrated in figure 1. If the peak of $\langle F(t)\,F(t+\tau)\rangle$ is sufficiently sharp, the ordinate at the origin will have a value of the magnitude $\beta kT/m\tau_1$. The ordinate of the curve representing the remaining terms $e^{-\beta\tau}\,\beta^2 kT/m$ in $\langle X(t)X(t+\tau)\rangle$ is of the magnitude β^2kT/m at $\tau=0$. Thus, if $\beta\tau_1\ll 1$, only $\langle F(t)\,F(t+\tau)\rangle$ contributes appreciably to the integral $I(\tau)$ in the interval $0<\tau<\tau_1$. The value of both integrals at $\tau=\tau_1$ is substantially equal to the area A. On further increase of τ, there is no appreciable change in the value of the integral (11 *a*) but, in the case of $I(\tau)$, the area B ultimately cancels out the area A and the value of the integral tends to zero. Figure 2 shows the behaviour of the correlation integrals.

Thus, provided $\beta\tau \ll 1$, there is correspondence between Kirkwood's expression for the friction constants and the expression of Brownian theory. It has since been shown by one of us that the higher terms of Kirkwood's expression which are neglected in obtaining his expression, are in fact of the magnitude $\beta\tau_1$.

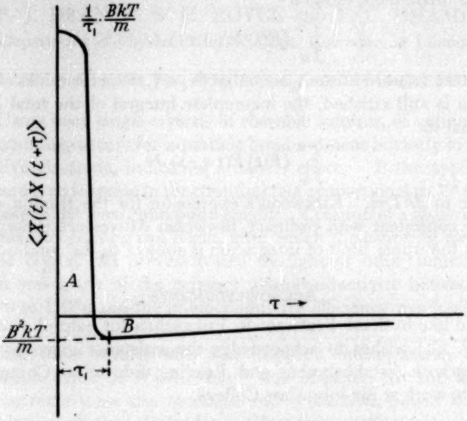

Figure 1. The correlation function of the total force as a function of τ.
Note. B should read β in expressions on curves.

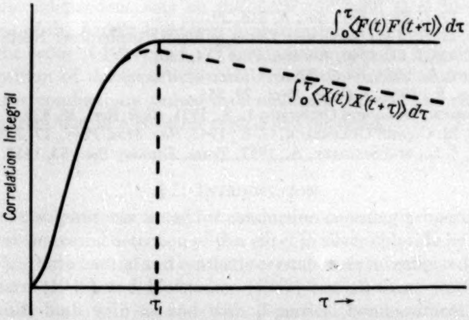

Figure 2. Correlation integrals of the fluctuating force $F(t)$ and the total force $X(t)$ as functions of the upper limit of integration.

It is from the outset unlikely that the conservative forces of molecular interaction should give rise strictly to the frictional force which is essential in the theory of Brownian movement. It is shown in the present paper that there is an approximate agreement which allows the microscopic equations of motion to be reconciled with the irreversible approach to equilibrium.

§ 7. CONCLUSIONS

(*a*) The complete correlation integral of the total force in the theory of the Brownian movement has the value zero, regardless of assumptions about the nature of the spectrum of the fluctuating force.

(*b*) If the incomplete integral

$$\int_0^{\tau_1} \langle F(t)\, F(t+\tau)\rangle\, d\tau$$

attains its plateau value in a time τ_1 such that $\beta\tau_1 \ll 1$, then, for values of τ_1 for which this condition is still satisfied, the incomplete integral of the total force is substantially equal to

$$\int_0^{\tau_1} \langle F(t)\, F(t+\tau)\rangle\, d\tau$$

and therefore to $\beta kT/m$. Kirkwood's expression for the friction constant can thus only be consistent with ordinary Brownian Movement theory in circumstances when the upper limit of integration is subject to the condition $\beta\tau_1 \ll 1$.

ACKNOWLEDGMENTS

We should like to thank Professor R. Eisenschitz for helpful discussions, and one of us (P. G.) wishes to acknowledge the assistance given by the Atomic Weapons Research Establishment and Reading Education Committee which enabled him to work at Sir John Cass College.

REFERENCES

CHAMPION, J. V., 1958, *Proc. Phys. Soc.*, **72,** 711.
EISENSCHITZ, R., 1949, *Proc. Phys. Soc.* A, **62,** 41.
—— 1951, *Nature, Lond.*, **167,** 216.
—— 1952, *Proc. Roy. Soc.* A, **215,** 29.
GREEN, H. S., 1952, *Molecular Theory of Fluids* (Amsterdam: North-Holland).
KIRKWOOD, J. G., 1946, *J. Chem. Phys.*, **14,** 180.
SUDDABY, A., 1954, *Ph.D. Thesis*, University of London.
TURNER, R., 1958, *J. Chem. Phys.*, **29,** 856.
UHLENBECK, G. E., and ORNSTEIN, L. S., 1931, *Phys. Rev.*, **36,** 823.
WANG, M. C., and UHLENBECK, G. E., 1945, *Rev. Mod. Phys.*, **17,** 323.
WOOD, J. L., and SUDDABY, A., 1957, *Trans. Faraday Soc.*, **53,** 1437.

Bombardment Conductivity and Photoconductivity in Rhombic Sulphur

By P. J. DEAN, B. S. H. ROYCE and F. C. CHAMPION
Department of Physics, King's College, University of London

MS. received 30*th June* 1959, *in final form* 13*th August* 1959

Abstract. Using pure single crystals of rhombic sulphur, of volume a few mm^3, conduction counting occurs for α-particle bombardment but only in a region close to the negative electrode, indicating a barrier effect. If the applied voltage is increased there is an increase in the counting rate proportional to V^n where $n=0{\cdot}7$, but no increase in the maximum pulse height. Creation of a space charge barrier is essential before counting can begin, after which the counting rate decays with time but the crystal can be reactivated by light or other ionizing radiations. Examination was made of the primary photoconductivity between 4400 Å and 9000 Å, down to 130°K and the photoconductive efficiency was found to be about $1{\cdot}5\ \mu\mathrm{AW}^{-1}$.

Comparing these results with von Hippel's interpretation for the alkali halides, a mean value of $N=10^{13}\,\mathrm{cm}^{-3}$ was obtained for the donor density. Secondary currents were also observed and breakdown pulses were attributed to field emission at the electrodes. The free path w per unit field was estimated as $\geqslant 5\times10^{-8}$ cm, and the lower limit of the mobility μ_e of the electrons, which were the charge carriers, as about $10^{-1}\,\mathrm{cm}^2\,\mathrm{v}^{-1}\,\mathrm{sec}^{-1}$. The energy per ion pair was found experimentally to be about 32 ev which agrees with the value deduced from independent data on the electronic band structure of sulphur. The thickness of the barrier layer was approximately 10^{-2} cm with barrier field strength of the order of $10^5\,\mathrm{v\,cm}^{-1}$. The conductivity pulse magnitude depends upon the position of the α-particle track inside the barrier and the excitation mechanism for conductivity pulses in a molecular crystal like sulphur differs considerably from that of a covalent crystal like diamond.

§ 1. INTRODUCTION

Rhombic sulphur was tested for conduction counting properties soon after the first successful detection of this effect in silver chloride by van Heerden (1945). Both natural and synthetic crystals were investigated by Jentschke (1948), Ahearn (1949) and Hofstadter (1949) but all these workers reported negative results both with α- and with β-particle bombardment. Georgesco (1949) reported positive results both for α- and β-particle bombardment, but later Saki and Lurçat (1952) using the same apparatus concluded that these results had been due to air breakdown.

Parsegian and Maininger (1949) used thin polycrystalline films of sulphur under very high field strengths ($\sim 10^5\,\mathrm{v\,cm}^{-1}$) and observed small conduction counting pulses with α-particle irradiation for some electrode configurations. There was a rapid decrease in the number and the height of the pulses with time of bombardment.

In view of these conflicting reports and because of an interest in extending work on the conduction pulse process in covalent crystals like diamond (Champion 1956) to molecular crystals, it was decided to re-examine the properties of single crystals of pure sulphur. An account of the preliminary experiments and the earlier results has already been given by Royce (1957) and therefore the present paper is concerned mainly with the confirmation and extension of Royce's work by Dean, enabling a degree of interpretation which could not be made from the earlier results alone.

§ 2. EXPERIMENTAL

2.1. *Preparation of Samples*

The crystals used in these investigations were grown from sulphur of very high purity supplied by Johnson Matthey. This material had been spectroscopically standardized and no impurity elements were found in a test capable of detecting 1 part in 10^4. The material showed a negative result in the test described by Bacon and Fanelli (1942) for the presence of organic oils which have a very disturbing effect on the viscosity and other properties of sulphur. It is claimed that this test is capable of detecting these oils if they are present to more than 1 part in 10^6. This material was dissolved in Analar carbon disulphide (total impurity content not greater than 1 part in 10^4) and the solution was allowed to evaporate slowly in a constant temperature enclosure held at 0°C. The resulting crystals were normally of a plate-like form similar to that described by Wiggins (1951) for these conditions of growth. The specimens selected were generally about 4 mm × 3 mm × 1 mm in size. The top surfaces, which had been in continuous contact with the solvent during growth, were usually smooth and regular but the opposite large surfaces were comparatively rough because of starvation of solute. The crystals were examined with a binocular microscope and only those with the best surfaces and no internal flaws were selected.

2.2. *Apparatus*

The crystals were mounted with various types of electrode configuration, some of which are shown in figure 1. This electrode system was mounted horizontally in a small metal chamber, with provision for irradiation of the crystal with α- and β-particles from radioactive sources contained in suitable holders inside the chamber. A lithium fluoride window was mounted in the wall of the chamber to enable electromagnetic radiation of a wide range of wavelengths to be focused on the crystal from sources external to the chamber. The light sources were a 250 watt mercury arc lamp, used in conjunction with a Wratten 18A filter to provide an intense source of radiation of wavelength 3650 Å and a tungsten strip filament lamp which was fed from a Variac and run at constant current. With the lens system employed the tungsten lamp provided an intensity of illumination of $3{\cdot}5 \times 10^4$ ft candles at the crystal surface with a filament colour temperature of 2900°K. Chance ON20 heat filters were used with both sources.

For the experiments on photoconductivity described in § 3.2 the electrode system was mounted vertically on a brass block soldered to the bottom of a thin-walled stainless steel Dewar flask. This Dewar flask fitted into the top of a larger chamber which was equipped with all the irradiation facilities mentioned in the previous paragraph. The temperature of the crystal could then be varied between 130°K and the melting point of sulphur. 130°K was the equilibrium temperature recorded on the electrodes by a thin-wire thermocouple when the Dewar flask contained liquid air. Another convenient fixed temperature was 210°K obtained by the use of solid carbon dioxide.

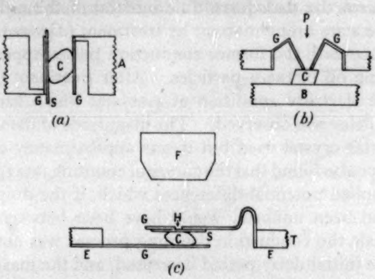

Figure 1. Electrode arrangements. A, to amplifier, B, P.T.F.E. base; C, crystal; E, brass electrode bars bolted to Perspex cylinders embedded in base of Dewar flask; F, camera shutter; G, gold electrodes; H, hole; P, α-particles; S, P.T.F.E. or glass sheets; T, to high tension.

Conventional pulse counting apparatus was used to detect the conduction pulses. The photocurrents were measured by a vibrating reed electrometer which was sometimes used with a pen recorder. Some measurements of the photocurrent were also made with a Tektronix type 545 oscilloscope equipped with a 53/54L preamplifier modified so that a current of 5×10^{-11} amp could be detected.

§ 3. Results and Discussion

3.1. *Conduction Counting in Rhombic Sulphur: Preliminary Survey*

Alpha particles of 5·3 MeV energy (from ^{210}Po) or β-particles of 2·2 MeV energy (from ^{90}Sr) were allowed to fall upon the surface of crystals grown as described in § 2.1. The electrode system of figure 1 (*a*) was employed, except that in these experiments the strip of insulating material was not used. Voltages of up to ± 4 kv were applied to the 'high tension' electrode. No effects were observed for any experimental arrangement when β-particles were used. With α-particles a small number of conduction pulses, of magnitude equivalent to the full separation of about 10^5 electron–hole pairs, were observed under some conditions. The number of pulses per unit time was always very much less than the flux of α-particles striking the surface of the crystal. With a crystal of typical size, having (111) faces of about 0·1 cm² area, about 5×10^5 α-particles per minute were absorbed in the crystal, yet with the arrangement of figure 1 (*a*) the observed counting rate never exceeded 10^4 counts min^{-1}. The effects were not very reproducible and appeared to depend critically upon the position of the electrodes on the crystal. The counting rate decreased smoothly and very rapidly with time and was usually negligible after about 5 minutes' irradiation for an initial counting rate of 10^4 counts min^{-1}.

These results are similar to those which had previously been obtained by Royce (1957) who also noticed that irradiation of the crystal with white light at zero external field was ineffective in returning the crystal to a state which would again exhibit appreciable conduction counting properties. Royce found that, at zero applied field, this condition could be restored (*a*) by irradiation of the crystal with α-particles for periods of the order of 1 hour or (*b*) by allowing the crystal to remain in the dark for a time interval of the order of 12 hours. It appeared that the state brought about by treatment (*a*) was not the same as with treatment (*b*) since with the former conduction pulses appeared simultaneously with the switching on of the α-particles. After treatment (*b*), which appeared to reproduce the electrical condition of a crystal which had had no deliberate pre-treatment, a delay was observed. The magnitude of the delay was dependent upon the particular crystal used but it was approximately constant for a given specimen. Royce also found that the curves of counting rate against field exhibited a threshold at applied potential differences which, if the drop in potential across the specimen had been uniform, would have been between 5 and 10 kv cm^{-1}. At lower potentials the conduction counting process was not observed. Above this threshold the initial delay period decreased, and the maximum counting rate increased, with increase of field.

Royce also found that conduction counting pulses were not observed using the electrode configuration of figure 1 (*b*) even for a crystal which gave positive results for the arrangement of figure 1 (*a*) when the same side of the crystal was irradiated. The present extension of these experiments resolved this discrepancy by showing that counting ability depended essentially upon bombardment of a sensitive layer very close to the negative electrode. In fact conduction counting was only observed when the α-particles were incident closer to this electrode than the thickness of the gold foil forming the electrode, that is, about 10^{-2} cm.

This result strongly suggests that the phenomenon of conduction counting in sulphur is a barrier effect as Royce suspected from the earlier results. He did not define the position of the barrier, or region of high internal field strength, but he came to the conclusion that the barrier or barriers were built up by charges released in the crystal by the α-particles. The present experiments show that the barrier is formed in the crystal immediately adjacent to the cathode.

3.2. *Reactivation*

By analogy with diamond counters, the rapid disappearance of the conduction counting property with time of irradiation was initially attributed to the trapping of electrical carriers in or near to the sensitive region of the crystal. Attempts were therefore made to reactivate the crystal by intense irradiation with electromagnetic radiation and with an externally applied field of the reverse polarity to that acting during the period of conduction counting. The arrangement of figure 1 (*a*) was used, the radiation was allowed to fall for a set interval on to the side of the crystal which had been irradiated by the α-particles and then the field was quickly returned to its original direction. Conduction counting was observed immediately the α-particles were allowed to fall on to the crystal and the initial counting rate was noted. The procedure was repeated and the new value of the counting rate found.

Figure 2 shows the variation of the equilibrium value of the counting rate with the time of previous irradiation at the reverse field. With the mercury arc lamp and the tungsten strip filament lamp the necessary pre-treatment times were about 2 minutes and 5 minutes respectively. Figure 2 also shows that a brief irradiation with light of wavelength greater than 4400 Å has very little reactivating effect upon the crystal and this, no doubt, accounts for Royce's initial failure to observe reactivation under this condition. A piece of P.T.F.E. (shown in figure 1) was used to prevent the appearance of pulses when the field was applied in the absence of α-particle irradiation. These pulses are shown, in § 3.7, to be due to secondary currents.

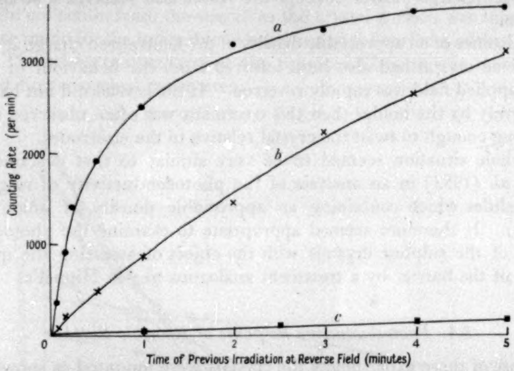

Figure 2. Counting rate plotted against time of previous irradiation at reverse field for crystal A1 at field strength 10 kv cm^{-1}. *a*, *b* and *c*, irradiation at 3650 Å, 3000–9000 Å and 4400–9000 Å respectively.

If the sensitive region of the surface is a rectangle of length that of the side of the crystal to which the electrode is applied, that is about 0·3 cm, and breadth about 10^{-2} cm then the number of α-particles striking the crystal which can give rise to conduction counting pulses is about $10^4\ \mathrm{min}^{-1}$. Initial counting rates of this order of magnitude were often observed with crystals of this size, so that it seems probable that initially every α-particle falling upon this region can give a detectable conduction pulse.

3.3. *Variation of Conduction Counting with Applied Field*

With the voltages available fields in the range of 0·5 kv cm^{-1} to 10 kv cm^{-1} could be applied to the crystal with the arrangement of figure 1 (*a*) on the assumption that the potential drop across the specimen was uniform. The magnitude of these 'apparent' fields was found to have no appreciable effect on the value of the maximum conduction pulse height which was about $1{\cdot}5 \times 10^5$ electron–hole pairs. On the other hand the counting rate was observed to increase roughly as $V_0{}^n$ where V_0 is the applied voltage; the average value of n for these large crystals was $0{\cdot}7 \pm 0{\cdot}2$.

The fact that the barrier, which must be due to an internal space charge layer, is formed close to the negative electrode indicates that only the negative charge carriers are free to move in sulphur (von Hippel 1948). However, according to Kommandeur and Schneider (1958) the dominant carriers in anthracene, which is also a molecular crystal, have been shown to be positively charged (holes) so generalizations on molecular crystals cannot yet be made. Evidence for the predominance of electron conduction in sulphur was also obtained from the earlier experiments of Royce using the electrode arrangement of figure 1 (*c*) without the glass spacer. Only when the electrode through which the crystal was bombarded was negative were conduction pulses observed. Royce suggested that this was because the distance of motion of the electrons was negligible compared to the crystal thickness when the top electrode was positive, since the penetration of the α-particles is only about 2×10^{-3} cm. In the terms of the present space charge barrier concept the result also receives a straightforward explanation.

The existence of an appreciable density of un-neutralized charge at the surface of a polarized crystal had also been inferred from the behaviour of the crystal when the applied field was rapidly reversed. If the crystal did not happen to be gripped firmly by the holder then this treatment was often observed to produce forces strong enough to twist the crystal relative to the electrodes.

The whole situation seemed to be very similar to that described by von Hippel *et al.* (1953) in an analysis of the photoconductivity of single crystals of alkali halides which containing an appreciable density of anion vacancies (F centres). It therefore seemed appropriate to examine the photoconductive properties of the sulphur crystals with the object of assessing the quantitative properties of the barrier by a treatment analogous to von Hippel's.

3.4. *Photoconductive Response of Rhombic Sulphur*

For most of these experiments the crystals were mounted as shown in figure 1 (*c*) and the electrode system was attached to the Dewar of the low temperature apparatus. The crystals were illuminated through the 1 mm diameter hole in the top electrode and the thin glass sheet; the wavelength range employed was between 4400 Å and 9000 Å at 130°K. These lower limits were imposed to ensure that the irradiation of the crystal was uniform as demanded by von Hippel's theory. As the glass sheet prevented the flow of continuous (secondary) photocurrents in the crystal the results must be interpreted in terms of a redistribution of charge in the crystals. The displacements of charge were measured from the transient currents caused to flow in the crystal.

It was only possible to record the photocurrent on the oscilloscope for the highest values of external field (30 kv cm^{-1}) because of the limited sensitivity of this technique. The use of the oscilloscope was therefore confined to checking the initial value of the photocurrent recorded by the electrometer and to an attempt to measure the rise and decay times of the photocurrent. It was found that this time was less than the time of opening of the Compur-Rapid camera shutter used to pulse the illumination of the crystals, both at 290°K and at 130°K. This time was found to be about 8×10^{-4} sec for the minimum time of opening of the shutter (about 3×10^{-3} sec).

Figure 3 shows a typical set of curves of ln (I_t) as a function of time where I_t is the photocurrent observed at a time t sec after switching the light on to the crystals for an applied field of 30 kv cm^{-1}. Similar results were obtained for both directions of applied field but the initial values I_0 were sometimes slightly different. These curves were obtained by direct calculation from traces recorded by the pen recorder. The results were also similar when the crystal was discharged, that is, when the polarized crystal was irradiated with light after the externally applied field had been reduced to zero. The experiments were repeated for a range of values of the incident light intensity.

The intensities quoted in figure 3 are in units of the number of quanta absorbed in the crystal per second. These quantities were obtained by two independent methods: (*a*) the intensity of illumination of the crystal surface was measured by replacing it by a Weston light meter which is calibrated directly in ft candles, (*b*) the incident energy was estimated from tabulated data on the thermal radiation from tungsten (Hughes and Dubridge 1932). The appropriate solid angle of light collection from the source to the crystal surface was measured and an allowance made for the losses due to reflection at the surfaces of the lenses, heat filter etc. The colour temperature of the tungsten filament was measured with a calibrated Foster optical pyrometer.

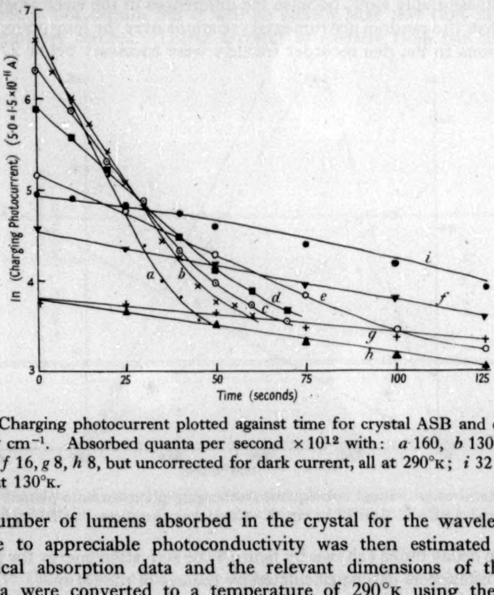

Figure 3. Charging photocurrent plotted against time for crystal ASB and external field 30 kv cm^{-1}. Absorbed quanta per second $\times 10^{12}$ with: *a* 160, *b* 130, *c* 100, *d* 64, *e* 32, *f* 16, *g* 8, *h* 8, but uncorrected for dark current, all at 290°K; *i* 32 uncorrected, but at 130°K.

The number of lumens absorbed in the crystal for the wavelength range giving rise to appreciable photoconductivity was then estimated (17%) by using optical absorption data and the relevant dimensions of the crystals. These data were converted to a temperature of 290°K using the coefficient $dE_g/dT = 11 \times 10^{-4}$ ev deg^{-1} for the range from 290°K to 390°K (this coefficient was obtained for these crystals by direct measurement), E_g being the energy calculated for the absorption limit. A correction was made for the energy lost by reflection at the crystal surface.

The results, for a colour temperature of 2850°K which was used throughout this work, were $7{\cdot}2 \times 10^{-5}$ watt and 5×10^{-5} watt (from methods (*a*) and (*b*)). A mean value of 6×10^{-5} watt was used to obtain the figures of figure 3 with a mean wavelength of 5200 Å. The lower values of figure 3 were obtained with the use of suitable neutral density filters. The curves of figure 3 have also been corrected for the contribution to the charging (and discharging) current of the carriers present in the crystal when no light was allowed to fall upon it. The importance of this effect was investigated by the measurement of the rate of discharge of the polarization of a crystal stored in the dark. The method of radiation discharge was used to avoid the necessity of measuring the small dark currents directly. The crystal was first polarized by irradiation with the maximum available light intensity at the same value of applied field strength as that used for figure 3. The charging current fell practically to zero in about 60 seconds, so that this time was used for the treatment. The external field was then removed and the initial value of the reverse photocurrent (obtained when the same intensity of light was allowed to fall upon the crystal) measured as a function of the time interval for which the crystal had been allowed to remain in the dark. The results are presented in figure 4 at two values of crystal temperature. For temperatures much below 270°K the rate of discharge had become unmeasurably slow, because the differences in the electrometer readings were less than the random instrumental variations over the long periods involved. No corrections to the pen recorder tracings were necessary below 270°K.

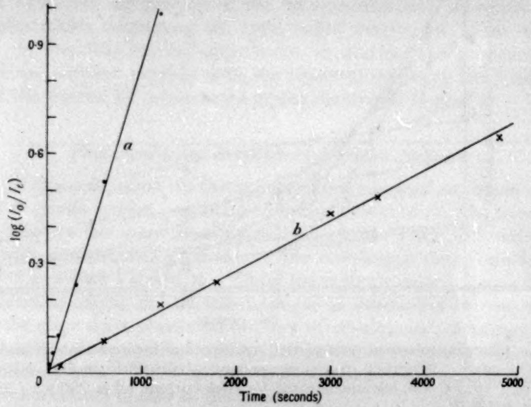

Figure 4. Ratio of initial and subsequent discharging photocurrents plotted against time for crystal ASB and field 30 kv cm^{-1}. Crystal temperatures: *a* 291°K, *b* 273°K.

With the decay times *t* shown by figure 4 the activation energy for the thermal production of carriers can be calculated by the use of the formula

$$t = s^{-1} \exp(E/kT) \qquad \ldots\ldots(1)$$

where s^{-1} is a constant for a given material and of the order of the fundamental frequency of vibration of the system to which the charge carriers are bound (Mott 1938). Assuming that these systems are individual sulphur molecules then the natural wave-number (stretching mode) is 500 cm^{-1} (Bernstein and Powling 1950). Substitution in (1) gives $E = 0{\cdot}92$ ev at 291°K and $E = 0{\cdot}91$ at 273°K. The activation energy of pure sulphur found by optical and thermal means is about 2·5 ev. The optical activation energies for the crystals used in these experiments were found to be 2·6 ev and 1·6 ev using the technique due to Lange (1938). Tartakowsky and Rekolova (1940) give curves of the spectral sensitivity of the photoresponse from which a value of 2·0 ev may be obtained as well as the main value at 2·6 ev.

The dark conductivity of the material used in the present experiments was about 10^{-14} ohm^{-1} cm^{-1} at an applied field of 30 kv cm^{-1}. Use of the formula

$$\sigma=\mu e(2N_{\mathrm{d}})^{1/2}\left(\frac{2\pi m^{*}kT}{h^{2}}\right)^{3/4}\exp\left(\frac{-\Delta E}{2kT}\right) \qquad \ldots\ldots(2)$$

where N_{d} is the density of donor centres which are assumed to be responsible for the conductivity, ΔE is the activation energy obtained above, m^{*} is the effective mass of the carriers (assumed equal to the electronic mass) and μ the mobility given by w/τ_{r} where the values of the free path per unit field, w, and the lifetime τ_{r} are given in § 3.6, gives a value of 10^{14} cm^{-3} for N_{d}. The nature of these donor centres is not certain but it will be shown later that they are probably defect or impurity centres. Direct transfer of carriers from the sulphur ring molecules to these centres may arise from the existence of vibrational ground states of high excitation energy for these molecules. The importance of these states in determining the photoconductive properties of this type of crystal has been emphasized by Gilleo (1951) and Bass (1953).

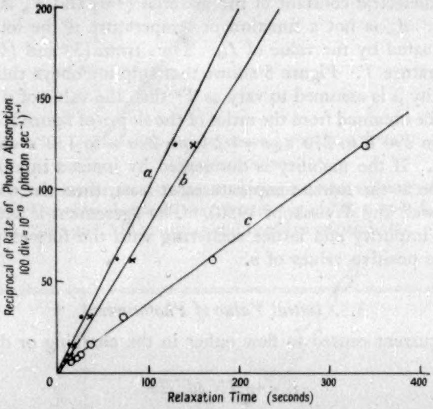

Figure 5. Reciprocal of rate of photon absorption plotted against relaxation time for ASB and field 30 kv cm^{-1}. Crystal temperatures *a* 290°K, *b* 210°K, *c* 130°K.

The measurements were repeated at 130°K and a typical curve so obtained is illustrated in figure 3 (*i*). Von Hippel has shown that the slopes of the curves of ln (I_t) against $t/2$ lead to the relaxation time τ of the space charge. The values of τ calculated from figure 3 are plotted in figure 5 against the reciprocal of the rate of absorption of photons in the crystal for three values of the crystal temperature. The relaxation times for the lowest temperature (130°K) were obtained from the part of the curve near $t=0$; it seemed reasonable to suppose that the slight curvature shown in curve 3 (*i*) was due to heating of the crystal by the light beam, because the effect was less marked at low intensities L_0 of illumination.

Theoretically,

$$\tau = d_\infty / 2\mu E_0 \qquad \ldots\ldots(3)$$

where d_∞ is the equilibrium width of the space-charge barrier and E_0 the applied field which is equal to the internal field only for an unpolarized crystal. Von Hippel suggests that the mobility $\mu \propto L_0$ for a crystal in which the value of w is very small, since if t_b is the time spent by a carrier in a localized trap, then it is reasonable to suppose that $t_b \propto L_0^{-1}$. Von Hippel assumes that only one type of trap is of importance, this being the F centre for the alkali halides. If the traps in sulphur are the defects of equation (2) then N_d corresponds to the N_0 of von Hippel. Hence

$$d_\infty = \left(\frac{2\epsilon V_0}{4\pi N_0 e}\right)^{1/2} \qquad \ldots\ldots(4)$$

where ϵ is the dielectric constant of the material (4·0) and V_0 is the externally applied voltage. d_∞ is not a function of temperature if the ionization of the centres is dominated by the value of L_0. Thus from (3) and (4) $\tau \propto L_0^{-1}$ at a constant temperature T. Figure 5 shows that sulphur obeys this relation.

If the mobility μ is assumed to vary as T^n then the value of n appropriate to this system can be obtained from the ratios of the slopes of figure 5. These results give $n = 0{\cdot}8$ from 290°K to 210°K, $n = 1{\cdot}2$ from 290°K to 130°K and $n = 1{\cdot}4$ from 210°K to 130°K. If the mobility is dominated by ionized impurity scattering, as it ought to be at the lower temperatures at least, then the theoretical value of $n = 1{\cdot}5$ (Conwell and Weisskopf 1950). The agreement is satisfactory for a combination of impurity and lattice scattering with the former predominating as shown by the positive values of n.

3.5. *Initial Value of Photocurrent*

The initial current caused to flow either in the charging or discharging can be shown to be

$$I_0 = 4\pi A N_0 e d_\infty / 2\tau \qquad \ldots\ldots(5)$$

where A is the effective area of the crystal. From equations (3) and (4) it can be shown that $I_0 \propto 1/t_b \propto L_0$ at constant applied field E_0.

The initial photocurrents, such as those shown in figure 3, exhibit this linear dependence on L_0. Equation (5) also predicts that $I_0 \propto E_0$ at a constant value of L_0. This prediction was also verified for several crystals, the results for three of these being shown in figure 6 for both polarities of applied field. It follows that, under these conditions, $N_0 e$ is not a function of either L_0 or E_0. The value of N_0 may be calculated from the total charge Q caused to flow during the polarization since

$$Q = 4\pi A N_0 e d_\infty . \qquad \ldots\ldots(6)$$

Q was determined experimentally from the area under the pen recorder traces. The mean value for the three crystals of figure 6 (independent of L_0) was $3{\cdot}2 \times 10^{-9}$ coulomb at $E_0 = 30$ kv cm^{-1}. The dependence of Q on V_0 was determined by plotting $\log Q$ against $\log V_0$ and the results for the typical crystal ASB are shown in figure 7. The average values of the index n in the relation $Q = V_0^n$ was 0·6, the predicted value being 0·5.

At $E_0 = 30$ kv cm^{-1} this average value of Q leads to a value of $N_0 = 7 \times 10^{13}$ cm^{-3} and $d_\infty = 1{\cdot}4 \times 10^{-2}$ cm^{-1}. At this value of applied voltage, the field in the barrier reaches the value of $4{\cdot}5 \times 10^5\,\mathrm{v\,cm^{-1}}$. The value of N_0 is in reasonable agreement with N_d calculated from equation (2) and d_∞ is not inconsistent with the value inferred from the conduction counting experiments of §§3.1 and 3.2.

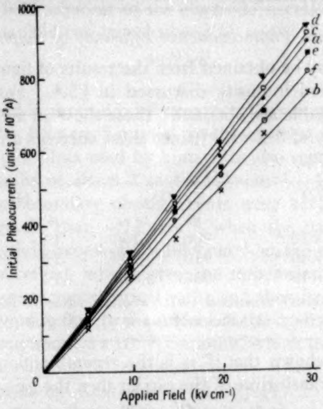

Figure 6. Initial photocurrent plotted against applied field for three crystals at 290°K and with 160×10^{12} quanta absorbed per second. *a* and *b*, *c* and *d*, *e* and *f* are for crystals ASA, ASB and ASC positive and negative respectively.

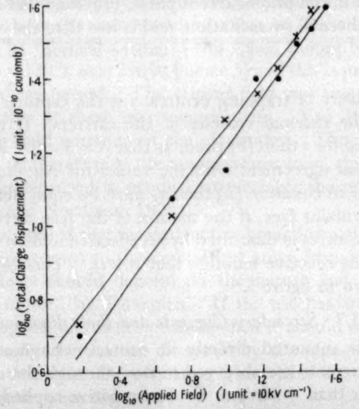

Figure 7. Polarization charge plotted against applied field for crystal ASB at 290°K. Crosses and circles, corresponding to negative and positive fields, show a wide scatter with a mean slope giving $n = 0{\cdot}60$.

The value of I_0 for a particular pair of values of E_0 and L_0 was dependent on temperature, a decrease of about 10% occurring between 290°K and 130°K as shown on figure 3. Over this range of temperature, the absorption curve shifts towards shorter wavelengths by about 250 Å and so the intensity of the light available for absorption in the crystal decreases. Tables given by Hughes and Dubridge show that the reduction will be about 12% so that the photosensitivity in terms of unit absorbed energy remains approximately constant over this range of temperature.

3.6. *Photoconductive Efficiency of Sulphur*

The efficiency may be obtained from the results of figure 6 and the measurements of the absorbed intensity discussed in § 3.4. For $E_0 = 30\,\mathrm{kv\,cm^{-1}}$, the values shown in the table are obtained; these show an average value of the gain or quantum efficiency of $3{\cdot}5 \times 10^{-6}$ since these currents are primary in the sense of van Heerden (1957).

(1)	(2)	(3)		(4)		(5)	
		+ve	−ve	+ve	−ve	+ve	−ve
ASA	6×10^{-5}	900	760	1·5	1·3	3·5	3·0
SAB	6×10^{-5}	910	940	1·5	1·6	3·5	3·5
ASC	5×10^{-5}	860	820	1·7	1·6	4·0	3·8

(1) Crystal; (2) intensity absorbed (w); average value of methods (*a*) and (*b*); (3) initial photocurrent (10^{-13}A); (4) efficiency (μA w^{-1}); (5) gain (units of 10^{-6}).

Rose (1956) has shown that if τ_r is the recombination lifetime for the free carrier and T is the transit time of the carrier then the gain G can be written

$$G = \tau_r / T. \qquad \ldots\ldots (7)$$

In this case $T = 2\tau$ where τ is given by (3) and the average value at 30 kv cm^{-1} is about 10 seconds. Hence $\tau_r = TG \simeq 3{\cdot}5 \times 10^{-5}$ sec. τ_r should be equal to the rise-time of the initial photocurrent pulse, provided that no shallow-trapping effects occur with thermal re-excitation, and is less than the minimum detectable experimental value quoted in § 3.4. τ_r can be written

$$\tau_r = 1/Nsv \qquad \ldots\ldots (8)$$

where N is the density of trapping centres, s is the capture cross section of the centres and v is the thermal velocity of the carriers. If the typical value of $10^{-15}\,\mathrm{cm^2}$ is assumed for s then (8) predicts that $N = 3 \times 10^{12}$ at room temperature which is again in fair agreement with the values for N_d and N_0. Since T has been replaced by 2τ in equation (7) then τ_r must be equivalent to t_f, the time for which the carrier remains free, if the motion of the free carriers and the retrapping by the defect centres is described by an effective mobility. It is assumed in the treatment of this effective mobility that $t_b \gg t_f$. This assumption is justified by the results shown in figure 5.

3.7. *Secondary Currents and Field Emission*

If the crystal is mounted directly in contact with metal electrodes, then continuous photocurrents are observed to flow through the crystal for values of applied field greater than +5 kv cm^{-1}. For negative applied fields, the required potential was somewhat larger. These results were erratic, probably because the barrier is only partly adjacent to the metal electrode in this case (figure 1 (*c*)) and Aquadag coating could not be used on this side of the crystal. The effect was noted as a sudden increase in the current flowing through the crystal after an initial delay period. The duration of this period decreased with increase in the value of the applied field E_0 and was repeatable at a given value of E_0 if the crystal was thoroughly depolarized between successive observations.

The value of the delay period was roughly equal to the transit time T which is characteristic of the formation of the space charge barrier for an applied voltage E_0 of about $+7\,\mathrm{kv\,cm^{-1}}$. If the value of the barrier field is set equal to the critical value of the field adjacent to the electrode necessary for the production of the effect, then this field can be calculated by use of the equation

$$E = \frac{4\pi N_0 e d_\infty}{\epsilon} \qquad \ldots\ldots (9)$$

and the value obtained is about $2 \times 10^5\,\mathrm{v\,cm^{-1}}$. This is in very good agreement with the figure of $1{\cdot}5 \times 10^5\,\mathrm{v\,cm^{-1}}$ quoted by Parsegian at which electrical breakdown set in for the thin films used by him. He also reports destructive breakdown for field strengths of about 2 to $4 \times 10^5\,\mathrm{v\,cm^{-1}}$. In the present work it was noticed that the secondary photocurrents were very 'noisy', particularly for applied fields greater than $+7\,\mathrm{kv\,cm^{-1}}$ when the barrier is attempting to produce a field strength in excess of $2 \times 10^5\,\mathrm{v\,cm^{-1}}$ at the electrode. Oscillatory effects were often observed, which gave the impression that the barrier was repeatedly building up to some critical value and then breaking down again.

The charge observed to flow to the surface of the crystal for the establishment of this critical field was about 5×10^{-10} coulomb, which implies a critical surface charge density of about $5 \times 10^{-9}\,\mathrm{coulomb\,cm^{-2}}$. This value is much higher than the early estimate by Kurrelmeyer (1927) ($4 \times 10^{-12}\,\mathrm{coulomb\,cm^{-2}}$) but it agrees better with values obtained for other insulating materials; for example, in zinc sulphide a critical charge density of $1 \times 10^{-8}\,\mathrm{coulomb\,cm^{-2}}$ is quoted by Gudden and Pohl (1923).

At 130°K the interval required before the secondary current was observed to flow was about twice the corresponding value at 290°K (for the same values of E_0 and L_0). The relaxation time of the space charge has also been shown to be twice as large at 130°K as at 290°K (figure 5) and this is presumably the reason for the increased delay period. The critical field was therefore found to have about the same value at these two temperatures. Von Hippel attributes the secondary effect to field emission at the electrodes. This process should not, in fact, depend on temperature at the temperatures used, these being very much less than the values required to produce appreciable thermionic emission from the metal (Fowler and Nordheim 1928).

It is therefore suggested that the destructive breakdown observed by Parsegian was not internal breakdown in the crystal but arose from strong field emission effects. These effects should depend on the nature and arrangement of the electrodes as was noticed by Parsegian. If the mechanism of internal crystal breakdown was responsible for the process, then it should occur whether or not the crystal was insulated from the electrode by the glass sheet. The present experiments show that when the insulating glass sheet was interposed no traces of these noisy currents were observed.

3.8. *Identification of the Parameter* N_0

The results of these experiments which have been described in this paper have shown that the photoconduction and dark conduction properties of rhombic sulphur can be explained in a quantitative manner by using the model established by von Hippel for a one carrier system. The interpretation of the parameter N_0 is not nearly so straightforward in sulphur as it is for the alkali halides where its magnitude can be varied at will. However, the ratio N_0/N where N is the number of atoms per cm^3 of the crystal is about the same as that found by Stratton (1957) for diamond, where N_0 was identified with defects. This number appears to be uniformly characteristic of the crystals which were prepared by the method outlined in § 2.1. Crystals which were prepared under less strict conditions of purity showed poorer counting properties (or none at all) and lower photoconductive gains.

3.9. *Mechanism for Production of Conduction Counting Pulses*

The conduction counting behaviour of sulphur is only superficially similar to diamond and it requires, in addition, a preactivation process. From the photoconductivity results, the equilibrium width of the space charge barrier (the formation of which constitutes the preactivation process) is compatible with the limiting value found from the conduction counting experiments. The variation of the conduction counting pulse rate with E_0 should follow the law $R \propto E_0^{1/2}$ because of equation (4); the experimental result quoted in § 3.3 was $R \propto E_0^{0 \cdot 7 \pm 0 \cdot 2}$.

The free path w per unit field can be shown, from § 3.3 to be $\geqslant 5 \times 10^{-8}$ cm. For $V_0 = 4$ kv, from equation (4) d_∞ is $1 \cdot 4 \times 10^{-12}$ cm. The barrier field is therefore about 3×10^5 v cm^{-1} giving a drift length of $1 \cdot 5 \times 10^{-2}$ cm. At $V_0 = 0 \cdot 2$ kv the average field in the barrier is still 6×10^4 v cm^{-1} with $d_\infty = 3 \times 10^{-3}$ cm so that even at this low voltage the drift length is still comparable with d_∞. Over the whole range of applied field, therefore, the electrons released by the α-particle in the barrier should be capable of being completely extracted from the barrier into the bulk of the crystal, as observed in § 3.3, if w is not less than 5×10^{-8} cm. These electrons make a contribution to the size of the observed conduction pulse the individual magnitude of which depends upon the fraction of the space-charge barrier through which they have travelled. This, in turn, depends only upon the position at which the incident α-particle enters the crystal. For α-particles which are absorbed in the region of the crystal immediately adjacent to the cathode, the observed maximum pulse should correspond to the full number of secondary electrons produced by the α-particle and it will be assumed in § 3.10 that this saturation condition was operative. Indeed, Parsegian found a saturation of the primary photocurrent at fields of the order of 1×10^5 v cm^{-1}.

The electrical conditions necessary for the observation of conduction counting pulses in the barrier region of a crystal have been discussed by McKay (1951); they are all fulfilled in these experiments with sulphur. The drift time of the carriers in the space charge region should determine the rise time of the conduction pulses (not equal to τ_r of § 3.6) and the upper limit to this time has been established at 5×10^{-7} sec. The minimum value of the mobility of the electrons is therefore 1×10^{-1} cm^2 v^{-1} cm^{-1} which is a very modest requirement.

The extremely low value of w is sufficient to explain why no conduction counting pulses are observed in a sulphur crystal unless it is irradiated by α-particles in the barrier layer. If $E_0 = 1 \times 10^4$ v cm^{-1} over the whole crystal the mean separation of the bound hole and free electron is only 5×10^{-4} cm so that the fractional charge induced at the electrodes is only about $Q_\alpha/1000$ if Q_α is the number of electrons liberated by each α-particle. It has been shown in § 3.5 that the charge displacement in the crystal necessary to build up the barrier is about 3×10^{-9} coulomb at a field of 3×10^{-4} v cm^{-1}. If the value of Q_α is about 10^5 (§3.10) then the number of α-particles which must be absorbed in the crystals to build up the barrier is about 2×10^5. With a flux of 5×10^5 min^{-1} the delay time for the observation of conduction pulses, starting with no barrier layer, should be about half a minute. Since much longer delay times were often observed, it is inferred that charge is being lost by some other process, such as columnar recombination, at these low field strengths. This direct recombination process is likely to be particularly important in a material where one of the carriers remains strongly coupled to the lattice (Rittner 1956).

The mechanism responsible for the rapid reduction of the counting rate with time is uncertain. The assumption that the reduction in efficiency is simply due to the build-up of a negative space charge region in the crystal, just outside the existing positively charged barrier, does not fully account for the difficulties experienced in restoring the crystals to the condition necessary for the observation of counting pulses. The results of §3.4 show that if this was the only cause, then light of wavelength greater than 4400 Å should be effective in restoring the crystal at zero field and that for an initial field of 30 kv cm^{-1} the necessary time of irradiation should not exceed 15 sec with the maximum available light intensity. It is possible that the combination of α-irradiation and the intense barrier field produce local disruptions of the S_8 ring molecules which can be reversed by the production of a higher density of ionization in this region. The effect of the absorption of even small radiant fluxes with wavelengths corresponding to high absorption coefficients may be to raise the local lattice temperature by an appreciable amount for a crystal of low thermal conductivity, thus promoting a reorganization of the crystal structure. The structure of a molecular crystal may be much more susceptible to this type of damage than that of homopolar crystals (McKay 1949).

3.10. *Magnitude of the Conduction Pulses*

The maximum initial pulse height has been found to be approximately independent of the applied field (§3.5) and reasons have been given for this in §3.9.

Assuming negligible loss of charge by recombination for these maximum pulses, the value of the average energy E_α necessary to produce one electron–hole pair by an α-particle in sulphur, can be estimated. Two crystals (ASB and ASC) which showed conduction counting properties of the order of the best which had been observed and also large and uniform primary photocurrents (figure 6) were selected for this measurement. The experimental arrangement was as in figure 1 (*a*) except that the side face of the crystal was bombarded so that a field strength of 3×10^4 v cm^{-1} could be employed, this giving a reasonably large value for the sensitive area of the crystal (d_∞). The maximum initial pulse height was measured using the recent photographic technique (Kennedy and Dean 1959) which is particularly suited to situations where the counting rate varies rapidly with time. The crystal was activated, the film was exposed for a 5-second period immediately after the instant when the α-particles were switched on and about 500 counts were recorded above the amplifier noise level. In order to minimize the grain produced on the film by the dot images of individual pulses, the effects of at least 10^4 pulses had to be recorded. Each density distribution on the film was therefore made up of 20 of these 5-second exposures and the crystal was reactivated between each exposure.

The film traces, when photodensitometered, showed a roughly linear decrease in the number of pulses with distance along the trace from the position of zero pulse height. The curves thus produced tailed off into the background of the film near the position of maximum recorded pulse height. The maximum pulse height was taken to be the value where the roughly linear portion of the curves, when extrapolated, intersected the pulse height axis. The experiment was repeated for a number of values of the energy of the incident α-particles obtained by the use of calibrated absorbing foils of aluminium and the maximum pulse height found in each case.

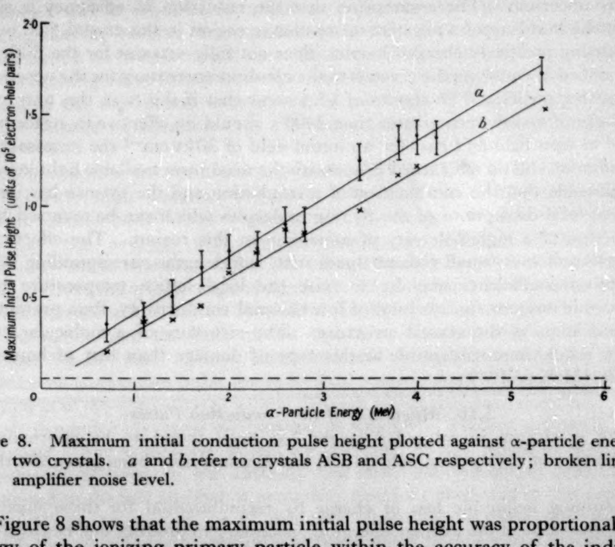

Figure 8. Maximum initial conduction pulse height plotted against α-particle energy for two crystals. *a* and *b* refer to crystals ASB and ASC respectively; broken line gives amplifier noise level.

Figure 8 shows that the maximum initial pulse height was proportional to the energy of the ionizing primary particle within the accuracy of the individual measurements (about ±10% maximum error on pulse height). The slopes of the lines drawn in figure 8 yield values of the parameter E_α assuming that all of the energy of the incident particle is lost in the ionization of electronic carriers (Seitz 1949) and that charge multiplication does not occur.

The values of E_α obtained from figure 8 are $31{\cdot}5 \pm 2{\cdot}5$ ev for crystal ASB and $34{\cdot}0 \pm 2{\cdot}0$ ev for crystal ASC. Use of an empirical relation given by McKay (1951)

$$E_\alpha = E_g + 2{\cdot}5\ \text{ev} \qquad \ldots\ldots (10)$$

where E_g is the width of the band of forbidden energies leads to $E_\alpha = 5{\cdot}0$ ev per electron–hole pair for rhombic sulphur. Thus (10) gives very poor agreement for sulphur as well as for diamond (Kennedy 1959) and cadmium sulphide (van Heerden 1957).

These disagreements led Kennedy and Dean to estimate E_α for any material, provided that E_g is known, using the form of the density of states distribution for the valence band.

The predicted value of E_α then becomes

$$E = E_v + E_g + E_k \qquad \ldots\ldots(11)$$

where E_v is the energy difference between the value corresponding to the peak of the density of states function and the value at the top of the valence band and E_k is an estimate of the average energy carried off by each secondary particle as kinetic energy. E_k will probably be less than 2·5 ev for sulphur; experiments on secondary electron emission show that the average energy of emission is usually of the order of a few ev (Rudberg 1930). Sulphur has been shown to be a very inefficient secondary emitter (Wilson 1950). E_v is about 26 ev from the soft x-ray emission data of Skinner (1940).

Equation (10) predicts a value of E_α equal to 30 ev per electron–hole pair so the agreement with the experimental value is satisfactory.

REFERENCES

Ahearn, A. J., 1949, *Phys. Rev.*, **75**, 1966.
Bacon, R. F., and Fanelli, R., 1942, *Industr. Engng Chem.*, **34**, 1043.
Bass, A. M., 1953, *J. Chem. Phys.*, **21**, 80.
Bernstein, H. J., and Powling, J., 1950, *J. Chem. Phys.*, **18**, 1018.
Champion, F. C., 1956, *Phil. Mag. Suppl.*, **5**, 383.
Conwell, E. M., and Weisskopf, V. F., 1950, *Phys. Rev.*, **77**, 388.
Fowler, R. H., and Nordheim, L., 1928, *Proc. Roy. Soc.* A, **119**, 173.
Georgesco, M., 1949, *C.R. Acad. Sci., Paris*, **228**, 383.
Gilleo, M. A., 1951, *J. Chem. Phys.*, **19**, 1291.
Gudden, B., and Pohl, R., 1923, *Z. Phys.*, **16**, 176;
—— 1926, *Ibid.*, **37**, 881.
van Heerden, P. J., 1945, *Ph.D. Thesis*, Utrecht.
—— 1957, *Phys. Rev.*, **106**, 468.
von Hippel, A., 1948, *J. Chem. Phys.*, **16**, 372.
von Hippel, A., Gross, E. P., Jelatis, J. G., and Geller, M., 1953, *Phys. Rev.*, **91**, 568.
Hofstadter, R., 1949, *Nucleonics*, **4**, 29.
Hughes, A. L., and DuBridge, L. A., 1932, *Photoelectric Phenomena* (London, New York: McGraw-Hill).
Jentschke, W., 1948, *Phys. Rev.*, **73**, 77.
Kennedy, P. J., 1959, *Proc. Roy. Soc.* A, **253**, 37.
Kennedy, P. J., and Dean, P. J., 1959, *J. Sci. Instrum.*, **36**, 126.
Kommandeur, J., and Schneider, W. G., 1958, *J. Chem. Phys.*, **16**, 372.
Kurrelmeyer, B., 1927, *Phys. Rev.*, **30**, 893.
Lange, B., 1938, *Photoelements* (New York : Reinhold).
McKay, M.G., 1949, *Phys. Rev.*, **76**, 1537.
—— 1951, *Ibid.*, **84**, 829.
Mott, N. F., 1938, *Proc. Roy. Soc.* A, **167**, 384.
Parsegian, V. L., and Maininger, —, 1949, *United States Atomic Energy Commission Rept.* A.E.C.D., 3049.
Rittner, E. S., 1956, *Photoconductivity Conference* (New York : Wiley).
Rose, A., 1956, *Photoconductivity Conference* (New York : Wiley).
Royce, B. S. H., 1957, *Ph.D. Thesis*, University of London.
Rudberg, E., 1930, *Proc. Roy. Soc.* A, **127**, 111.
Saki, M., and Lurçat, F., 1952, *C.R. Acad. Sci., Paris*, **234**, 2061.
Seitz, F., 1949, *Disc. Faraday Soc.*, **5**, 27.
Skinner, H. W. B., 1940, *Trans. Roy. Soc.* A, **239**, 95.
Stratton, K., 1947, *Ph.D. Thesis*, University of London.
Tartakowsky, P, and Rekolova, G., 1940, *J. Exp. Theor. Phys.*, **10**, 1025.
Wiggins, P. M., 1951, *Ph.D. Thesis*, University of London.
Wilson, C. W., 1950, *Brit. J. Radiol.*, **23**, 478.

RESEARCH NOTES

Paramagnetic Resonance Spectra of Impurities in Calcium Fluoride

By M. DVIR and W. LOW
Department of Physics, The Hebrew University, Jerusalem, Israel

MS. received 27th July 1959

§ 1. INTRODUCTION

IN a recent note Baker, Hayes and Jones (1959) have presented spin resonance data on paramagnetic impurities in single crystals of calcium fluoride.

During the past few years we have conducted a systematic research along similar lines; we have investigated in particular the spectra of various transition elements in calcium fluoride and in strontium chloride. Here we should like to report only a few of our results, which differ significantly from those reported by Baker *et al.*

The single crystals of calcium fluoride were grown by the Stockbarger process (Stockbarger 1949) in a similar manner as that reported by Baker *et al.* There are two main differences, however: the crystals were grown in a purified helium atmosphere at a dynamic pressure of slightly larger than one atmosphere and the rate of lowering of the graphite crucible through the induction furnace was about ½ to 1 inch per hour. The crystals were not annealed.

§ 2. THE SPECTRUM OF ERBIUM (Er^{3+}, $4f^{11}$, $^4I_{15/2}$)

A crystal containing thulium was investigated; no spectrum that could be explained as to arise from thulium was detected at 20°K and 3 cm wavelength. However, a strong spectrum was detected which is characteristic of erbium. It consists of (*a*) one isotropic main line with $g=6{\cdot}785\pm0{\cdot}002$ and a well resolved hyperfine structure with $I=7/2$ and $A=71{\cdot}2\pm1$ gauss due to the isotope ^{167}Er (22·94% abundance): this spectrum is interpreted to arise from erbium ions situated in the cubic field of the calcium fluoride lattice; (*b*) a spectrum of three lines with axial symmetry about the cubic axes, similar to those reported by Baker *et al.*

The main difference between our results and those reported by Baker *et al.* lies in the relative intensity of the two types of spectra. Whereas Baker *et al.* found that only 5% of the erbium ions are situated at a site of cubic symmetry our results seem to indicate that about 90% of the trivalent erbium ions are at such a site.

§ 3. THE SPECTRUM OF CERIUM (Ce^{3+}, $4f^1$, $^2F_{5/2}$)

Two different crystals were investigated. To one sample 0·01% of Ce was added to the melt; the crystal was clear and transparent. The resonance spectrum gave three strong lines and a number of weaker lines all of which were highly anisotropic at 4°K and 1·2 cm wavelength. Along the (1, 0, 0) direction a strong line was found, at $g=2{\cdot}00$ and a wider line at $g=3{\cdot}1\pm0{\cdot}1$ with the full widths at half power of about 100 gauss and 75 gauss respectively. An additional anisotropic line with a width of about 200–250 gauss was detected at

$g_{\parallel}=1{\cdot}297\pm0{\cdot}01$. The spectrum can be interpreted as cerium ions situated in the cubic field of calcium fluoride. The $S=5/2$ level of the free ion splits up by means of the cubic field of eight charges into a lower quartet (Γ_8) and a higher doublet (Γ_7). The two low field lines correspond to transition

$$\pm\sqrt{\tfrac{5}{6}}|\pm\tfrac{5}{2}\rangle\pm\sqrt{\tfrac{1}{6}}|\mp\tfrac{3}{2}\rangle\rightarrow\mp\tfrac{1}{2}\rangle$$

(theoretical $g=2{\cdot}00$) and to the transition

$$\sqrt{\tfrac{5}{6}}|+\tfrac{5}{2}\rangle+\sqrt{\tfrac{1}{6}}|-\tfrac{3}{2}\rangle\rightarrow-\sqrt{\tfrac{5}{6}}|-\tfrac{5}{2}\rangle-\sqrt{\tfrac{1}{6}}||+\tfrac{3}{2}\rangle$$

(theoretical $g=22/7$). Bleaney (1959) points out that the transitions within the Γ_8 quartet are expected to be highly anisotropic, and this is indeed confirmed by these results.

The high field transition is interpreted to arise from the doublet Γ_7 which has a theoretical g factor of 10/7. Apparently the crystal field is sufficiently weak so that this level is still populated at 4°K. The separation of this doublet from the quartet is however too large to be detected at 1 cm. The deviation of the experimental g values from the computed values are presumably caused by the admixture from the $J=7/2$ level. The angular variation deviates from that given by Bleaney (1959), whose calculations are based on the condition that

spin orbit coupling $\gg$ cubic splitting $\gg$ Zeeman energy.

Apparently the cubic splitting is not much larger than the Zeeman energy.

In the second sample 0·1% cerium was added to the melt; the crystal had a slightly grey tinge. The spectrum was investigated at 20°K and at 3 cm wavelength; the intensity of the cubic field spectrum was relatively weak. However, a new strong spectrum appeared which again could be interpreted to arise from three types of magnetic ions, each with axial symmetry. The measured values $g_{\parallel}=3{\cdot}04\pm0{\cdot}01$ and $g_{\perp}=1{\cdot}386\pm0{\cdot}003$ are in agreement with the values found by Baker *et al.*

In addition a number of weak anisotropic lines were found whose maximum and minimum g values lie along the cubic axes; these are still under investigation.

The optical spectrum of these crystals was investigated at room temperature. The spectrum shows a dominant absorption at 2280 cm^{-1}, and subsidiary peaks at 2000, 2200, 2400 and 2900 cm^{-1}, and a doubtful absorption at 2100 cm^{-1}; these absorptions arise presumably from two or three of the Kramers doublets of the ground state to the four doublets of $^2F_{7/2}$ excited states. The main peak at 2280 cm^{-1} is in approximate agreement with the separation of 2150 cm^{-1} as inferred from the spectrum of the free ion (Lang 1936).

§ 4. THE SPECTRUM OF COBALT (Co^{2+}, $3d^7$, $^4F_{9/2}$)

A sample to which 0·1% of CoF_2 had been added to the melt gave a strong spectrum at 20°K and at wavelength 3 cm. No spectrum was observed at liquid air temperature. The spectrum consisted of one sharp and slightly anisotropic line with maximum and minimum g values $g_{\max}=2{\cdot}010\pm0{\cdot}002$ and $g_{\min}=2{\cdot}0035\pm0{\cdot}002$. A barely resolved and slightly anisotropic hyperfine structure of eight lines was detected; this structure could not be accurately measured because of the superposition of a small effect of the hyperfine interaction produced by the surrounding nuclei. The total structure has a width extending about 15 gauss. In the same crystal Mn^{2+} was also present, whose fluorine structure at H parallel to a cube edge was extended about 50 gauss. It should be noted that a similar spectrum was observed in strontium chloride containing cobalt.

One would expect that the g factor of Co^{2+} in the field of CaF_2 would be $g=2-8\lambda/\Delta$. The optical spectrum of the same crystal had previously been investigated by Stahl-Brada and Low (1959). The optical absorption lines could be correlated to within $200\,cm^{-1}$ by assuming the cobalt ions to be situated in a cubic field and with the parameters $\lambda=-180\pm20\,cm^{-1}$ and $\Delta=3400\pm100\,cm^{-1}$. This would give a g factor of about 2·4. We have no explanation of this discrepancy with the experimental results. Similarly, in analogy with the chromium spectrum in an octahedral field, one would expect an extensive hyperfine structure in the case of cobalt in the field of CaF_2. The small hyperfine structure observed points to a small amount of configurational interaction in the symmetry of CaF_2.

§ 5. The Spectrum of Europium (Eu^{2+}, $4f^7$, $^8S_{7/2}$)

Our results are in agreement with those reported by Baker, Bleaney and Hayes (1958). We also observed a fluorine satellite structure which can be interpreted to arise through the simultaneous transitions of the electron spin and the spin of a neighbouring fluorine nucleus. In addition we observed a number of the so-called weak ' forbidden ' transitions (W. Low and J. T. Suss, to be published).

Acknowledgment

This research was supported in part by the U.S. Air Force, Office of Scientific Research (EOARDC), under contract No. AF 61(052)–59.

References

Baker, J. M., Bleaney, B., and Hayes, W., 1958, *Proc. Roy. Soc.* B, **247**, 141.
Baker, J. M., Hayes, W., and Jones, D. W., 1959, *Proc. Phys. Soc.*, **73**, 943.
Bleaney, B., 1959, *Proc. Phys. Soc.*, **73**, 937.
Lang, R. J., 1936, *Canad. J. Res.*, **14A**, 127.
Stahl-Brada, R., and Low, W., 1959, *Phys. Rev.*, **113**, 775.
Stockbarger, D. C., 1949, *J. Opt. Soc. Amer.*, **39**, 731.

Partial Variational Calculations on π-electron Systems: An Atomic Analogue

By E. THEAL STEWART
Chemistry Department, Queen's College, University of St. Andrews, Dundee, Scotland

MS. received 15*th June* 1959

ESSENTIALLY the same basic technique has been used in almost all ' non-empirical ' molecular-orbital calculations on the energy levels of conjugated and aromatic molecules carried out during the past two decades. It is that of Goeppert-Mayer and Sklar (1938), in which the wave functions for the ground state and the lower excited states of a σ–π system are taken to be functions of the coordinates of the π electrons only, and an incomplete Hamiltonian operator is defined accordingly; atoms other than those providing the π electrons are disregarded (Parr and Crawford 1948, Crawford and Parr 1949, Parr, Craig and Ross 1950).

There was no variational element in Goeppert-Mayer and Sklar's original work; but the great majority of subsequent calculations have depended on the variation principle for the determination of molecular-orbital expansion coefficients, configuration-interaction coefficients, atomic-orbital bases, or optimum values of scale parameters.

Variational studies on hydrocarbon molecules generally involve computations of considerable tedium and complexity, and it is thus surprising that scarcely any attention has been given to the fundamental problem of assessing the numerical significance of the results which they yield.

It is readily demonstrated that the use of a set of incomplete (π-electron) wave functions along with a Hamiltonian operator of the Goeppert-Mayer–Sklar type need not invalidate an otherwise unexceptionable variational calculation (McWeeny 1954, Lykos and Parr 1956). Our concern here, however, is to show, by means of a simple analogy, that even if a wave function for a σ–π system is written as a properly antisymmetrized function of the one-electron orbitals of *all* the electrons of the system, it is very doubtful whether the optimum forms of the π factors of the wave functions, and the corresponding energies, can be obtained by variation with respect to π parameters only; it may be essential that the σ orbitals should also be formulated with reasonable accuracy (a condition which can be fulfilled only fortuitously in a Goeppert-Mayer–Sklar calculation).

It seems impossible at present to settle the question by direct calculation: even if the least intractable examples were chosen (acetylene or ethylene), a numerical investigation sufficiently comprehensive to be unequivocal would require computations far more formidable than any hitherto carried out on molecular systems. There is no difficulty, however, in revealing the nature of the problem which arises in the interpretation of the results of partial variational calculations on unsaturated hydrocarbon molecules: it is a very familiar (though usually an unpublished) feature of wave-mechanical studies in which energies are minimized with respect to two or more parameters of comparable importance. To obtain the optimum value of any one parameter it is usually necessary to determine the optimum values of all.

This point may be illustrated by reference to calculations on any number of simple atomic systems, and of these we have selected the 2s2p configuration of the cation Li^+ (this rather artificial choice being determined mainly by the accessibility of the required integrals over atomic orbitals). The single 2s and 2p electrons of Li^+ may be regarded as analogues of the totalities of σ and π electrons in a hydrocarbon molecule. The analogy does not, of course, extend to spin coupling, and we have therefore considered both the ^1P and the ^3P states: a non-observable intermediate state in which the two electrons had independent spins would doubtless correspond most closely to a σ–π molecular state.

While representing the 2p electron by a conventional hydrogen-like wave function throughout, for the 2s electron we have used in turn a hydrogen-like wave function and a nodeless wave function, the latter to simulate a crude σ wave function. In non-normalized form the radial factors of these functions are as follows:

2p (H-like): $r \exp(-Z_{2p} r/2)$;
2s (H-like): $(r - 2/Z_{2s}) \exp(-Z_{2s} r/2)$;
2s (nodeless): $r \exp(-Z_{2s} r/2)$.

Calculated Total Electronic Energy and 2p Ionization Energy (Li^+ 2s2p)

	Singlet State (^1P)							
Z_{2s}	2·000	2·250	2·500	2·750	3·000	3·250	3·500	2·260†
H-like 2s orbital:								
Z_{2p} optimum ($\pm 0{\cdot}003$)	2·986	2·958	2·906	2·825	2·719	2·588	2·443	2·956
Electronic energy	−1·7234	−1·7303	−1·7249	−1·7085	−1·6825	−1·6476	−1·6040	−1·7304
2p ionization energy	0·7234	0·6757	0·6311	0·5913	0·5575	0·5305	0·5103	0·6738
Nodeless 2s orbital:								
Z_{2p} optimum ($\pm 0{\cdot}003$)	2·838	2·726	2·589	2·441	2·301	2·183	2·095	
Electronic energy	−1·9518	−2·0511	−2·1545	−2·2620	−2·3725	−2·4841	−2·5947	
2p ionization energy	0·6185	0·5745	0·5399	0·5146	0·4975	0·4867	0·4801	

	Triplet State (^3P)							
Z_{2s}	2·000	2·250	2·500	2·750	3·000	3·250	3·500	2·769†
H-like 2s orbital:								
Z_{2p} optimum ($\pm 0{\cdot}003$)	2·776	2·740	2·716	2·701	2·690	2·683	2·677	2·700
Electronic energy	−1·8021	−1·8382	−1·8610	−1·8694	−1·8631	−1·8416	−1·8048	−1·8695
2p ionization energy	0·8021	0·7835	0·7672	0·7522	0·7381	0·7244	0·7111	0·7511
Nodeless 2s orbital:								
Z_{2p} optimum ($\pm 0{\cdot}003$)	2·768	2·746	2·730	2·715	2·701	2·686	2·670	
Electronic energy	−2·1192	−2·2419	−2·3608	−2·4756	−2·5861	−2·6921	−2·7938	
2p ionization energy	0·7859	0·7653	0·7463	0·7282	0·7111	0·6947	0·6792	

†Optimum ($\pm 0{\cdot}003$) for hydrogen-like orbital.

Energies are in atomic units (A.U. = 27·210 ev).

For each value of Z_{2s}, the total electronic energy and the 2p ionization energy were calculated for $Z_{2p} = 2{\cdot}000(0{\cdot}250)3{\cdot}500$, and the energy minimum and the optimum value of Z_{2p} then located by four-point Lagrangian interpolation.

In the calculation of the 2p ionization energy the same arbitrary value of Z_{2s} was used for Li^{2+} (2s ^2S) as for Li^+ (2s2p $^{1,3}P$): this corresponds with the procedure used in π-electron calculations. If, instead, the exact value ($Z_{2s} = 3$) is used for the one-electron cation, there is, of course, a constant difference between the total electronic energy and the 2p ionization energy.

There is, of course, no tolerably simple technique for determining the optimum values of the scale parameters Z_σ and Z_π in a π-electron molecular system, and to reproduce the effects of this uncertainty we have carried out the present computations with $Z_{2s} = 2{\cdot}000(0{\cdot}250)3{\cdot}500$ for both types of 2s orbital. Corresponding to each arbitrary value of Z_{2s} we have calculated the optimum value of Z_{2p}, the total electronic energy, and the 2p ionization energy.

It is clear from the table that, in both the singlet state and (to a lesser extent) the triplet state, not only is the total electronic energy strongly dependent upon the form of the 2s wave function and upon the value of Z_{2s} (as would certainly be expected), but so also is the 2p ionization energy. Indeed, in the neighbourhood of the minima with respect to both scale parameters, variation of Z_{2s} affects the 2p ionization energy more than the total electronic energy, and (though this is not evident from the results summarized in the table) the 2p ionization energy depends more sensitively upon Z_{2s} than upon Z_{2p}. If the 2s electron is represented by a nodeless wave function, the minimum with respect to Z_{2s} is attained outside the range of the present calculations, because of ' sagging ' (Bethe and Salpeter 1957), and the corresponding values of Z_{2p} and of the 2p ionization energy are much too small.

The determination of an energy minimum with respect to Z_{2p} alone clearly has little significance unless the 2s wave function is roughly correct in form and in scale.

The possibility that these results may have a close parallel in molecular variational studies is disturbing. It may be observed, however, that, at least in π-electron systems, molecular calculations are usually concerned with the estimation of excitation energies rather than ionization energies. While the essential features of this work on Li^+ are quite general, the especially striking effects are attributable in large measure to the drastic change in 2s–2p repulsion energy produced by ionization: the analogous changes in σ–π repulsion energy brought about by excitation cannot be estimated satisfactorily by the techniques now available, but they must be relatively small.

The purpose of this note is thus not to suggest that conventional variational calculations on π-electron wave functions necessarily lack intrinsic numerical significance—a claim which could not possibly be justified on such slender evidence alone—but rather to emphasize the obvious danger that lengthy computations on an insecure basis may well involve an enormous waste of effort. The results of a more detailed appraisal of this hazard, embracing linear as well as exponential parameters, will be reported in later communications.

ACKNOWLEDGMENTS

This work was financed by the Carnegie Trust for the Universities of Scotland. The author is indebted to Professor C. A. Coulson for pointing out the need for a re-examination of the conventional variational procedures used in calculations on σ–π systems, to Dr V. W. Maslen for comments on a draft of this note, and to Mrs. T. E. Stewart for computational assistance.

REFERENCES

BETHE, H. A., and SALPETER, E. E., 1957, *Handbuch der Physik*, **35**, 204 (Berlin: Springer).
CRAWFORD, B. L., and PARR, R. G., 1949, *J. Chem. Phys.*, **17**, 726.
GOEPPERT-MAYER, M., and SKLAR, A. L., 1938, *J. Chem. Phys.*, **6**, 645.
LYKOS, P. G., and PARR, R. G., 1956, *J. Chem. Phys.*, **24**, 1166; **25**, 1301.
MCWEENY, R., 1954, *Proc. Roy. Soc.* A, **223**, 306.
PARR, R. G., CRAIG, D. P., and ROSS, I. G., 1950, *J. Chem. Phys.*, **18**, 1561.
PARR, R. G., and CRAWFORD, B. L., 1948, *J. Chem. Phys.*, **16**, 526, 1049.

Thermodynamics of an Isomeric Reaction from Ultrasonic Relaxation†

By G. S. VERMA
Department of Physics, University of Allahabad, Allahabad, India

MS. received 6th July 1959

In a relaxing medium, the propagation number k is given by

$$\frac{k^2}{\omega^2} = \rho\bar{K}_s\left\{1 - \sum_j \frac{ir_j\omega\tau_j}{1+i\omega\tau_j}\right\}$$

where $r_j = \delta_j K_s/\bar{K}_s$ is the jth relaxation strength, τ_j is the jth adiabatic–isobaric relaxation time, $\bar{K}_s$ is the equilibrium adiabatic compressibility of the fluid, ρ is the density and $\delta_j K_s$ is the jth incremental component of the compressibility. The amplitude absorption coefficient per unit distance α, is given by

$$\alpha/\omega(\rho\bar{K}_s)^{1/2} = \tfrac{1}{2}\sum_i \frac{r_i\omega\tau_i}{1+(\omega\tau_i)^2} + \tfrac{1}{4}\sum_i\sum_j \frac{r_i r_j(\omega\tau_i)^2\omega\tau_j}{[1+(\omega\tau_i)][1+(\omega\tau_j)^2]}.$$

Assuming $\omega\tau_j \ll 1$ for $j \gg 1$ and first relaxation at $i=1$, we have

$$\frac{\alpha\bar{C}}{\omega} = \frac{1}{2}\frac{r_1\omega\tau_1}{1+\omega^2[\tau_1(1-r_1)^{1/4}]^2} + \frac{1}{2}\sum_{j>1} r_j\omega\tau_j$$

where $\bar{C} = (\rho\bar{K}_s)^{-1/2}$.

In an isomeric reaction of the type $A_1 \rightleftharpoons A_2$, Davies and Lamb (1959) have shown that the relaxation strength r_1 is related to a function $F(p, T)$,

$$F(p,T) = \left[\frac{\bar{C}_p}{R}\frac{r_1}{\bar{\gamma}-1}\right]^{1/2}$$

where

$$F(p,T) = \left[\frac{\Delta H_0}{RT} - \frac{\bar{C}_p}{\bar{\alpha}RT}\frac{\Delta V_0}{RT}\right]\exp\left(\frac{\Delta G_0}{2RT}\right)\Big/\left[1+\exp\left(\frac{\Delta G_0}{RT}\right)\right]$$

ΔH_0, ΔV_0 and ΔG_0 are respectively, the enthalpy, volume and Gibbs free energy changes of the reaction, $\bar{C}_p$ is the equilibrium molar heat capacity of the fluid, $\bar{\gamma} = \bar{C}_p/\bar{C}_v$ and $\bar{\alpha}$ is the expansivity of the fluid.

It has been the established practice in the analysis of relaxation parameters to neglect the volume changes in an isomeric reaction. However, it has been shown recently by Davies and Lamb (1959) that what matters in an isomeric reaction is not $\Delta V/V$ but $\mathbf{V} \equiv (\bar{C}_p/\bar{\alpha}RT)(\Delta V/V)$ which can be comparable with $\mathbf{H} \equiv \Delta H_0/RT$.

In the present note the results of calculations are presented for two specific cases, methylcyclohexane and cyclohexene, the reaction parameters of which have been studied recently by Pedinoff (1959). In cyclohexene, $(\alpha\lambda)_{\max} = 5{\cdot}5 \times 10^{-3}$ at 25 °c where λ is wavelength and $(\alpha\lambda)_{\max} = \tfrac{1}{2}\pi[(\bar{\gamma}-1)/\bar{C}_p]\Delta C_p$, $\Delta C_p = 0{\cdot}13$ cal mol^{-1} where

$$\Delta C_p = R\left[\frac{\Delta H_0}{RT} - \frac{\bar{C}_p}{\bar{\alpha}RT}\frac{\Delta V}{V}\right]^2 \exp\left(-\frac{\Delta H_0}{RT}\right)\Big/\left[1+\exp\left(-\frac{\Delta H_0}{RT}\right)\right]^2$$

for $\Delta S = 0$, and $(\bar{C}_p/\bar{\alpha}RT) = 52$. With these values, ΔH_0 has been calculated for different values of $\Delta V/V$ and results are shown in figure 1. In methylcyclohexane $(\alpha\lambda)_{\max} = 15 \times 10^{-3}$ at 25°c. $\Delta C_p = 2{\cdot}54\,\mathrm{cal\,mol^{-1}}$ where

---

† This work was done at the Ultrasonics Research Laboratory, Western Reserve University, Cleveland, Ohio.

$$\Delta C_p = R\left[\frac{\Delta H_0}{RT} - \frac{\bar{C}_p}{\bar{\alpha}RT}\frac{\Delta V}{V}\right]^2 \exp\left(-\frac{\Delta H_0}{RT}\right) \times \exp\left(\frac{\Delta S}{R}\right)\Big/\left[1+\exp\left(-\frac{\Delta H_0}{RT}\right)\exp\left(\frac{\Delta S}{R}\right)\right]^2,$$

$\Delta S = 2{\cdot}22$ calories per mole degree, $\Delta H_0 = 1{\cdot}9\,\mathrm{kcal\,mol^{-1}}$ for $\Delta V/V = 0$ and $(\bar{C}_p/\bar{\alpha}RT) = 65$. Similar calculations have been done for this case too and results are shown in figure 2.

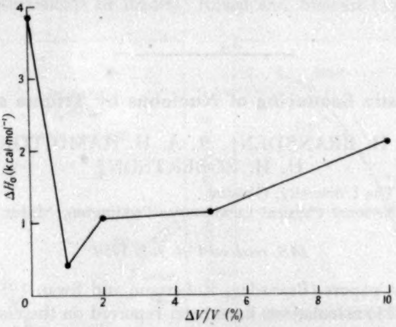

Figure 1. Enthalpy changes in cyclohexene at different changes in molecular volume.

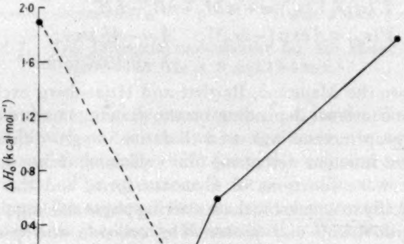

Figure 2. Enthalpy changes in methylcyclohexane at different changes in molecular volume.

The foregoing calculations show how serious are the errors involved in the determination of ΔH_0 by the neglect of volume changes howsoever small. The results are affected tremendously when $\Delta V/V$ is in the neighbourhood of 1%. 1% change in volume in cyclohexene drops ΔH_0 from $3{\cdot}85\,\mathrm{kcal\,mol^{-1}}$ to $0{\cdot}409\,\mathrm{kcal\,mol^{-1}}$. In methylcyclohexane, introduction of change in molar volume less than 4% leads to catastrophe, i.e. there does not exist any value of ΔH_0 which will give the observed value of ΔC_p. This shows that either ΔC_p, which is obtained from ultrasonic measurements, is too high or the theory is inadequate for such high values of absorption when volume changes are taken into account.

ACKNOWLEDGEMENT

The author wishes to thank Professor Ernest Yeager for his helpful comments.

REFERENCES

DAVIES, R. O., and LAMB, J., 1959, *Proc. Phys. Soc.*, **73**, 767.

PEDINOFF, M. E., 1959, *Tech. Rep.* No. XIV, Department of Physics, University of California Los Angeles.

The Elastic Scattering of Nucleons by Tritons and ^{3}He

BY B. H. BRANSDEN†, R. A. H. HAMILTON† AND
H. H. ROBERTSON‡

† The University, Glasgow
‡ National Physical Laboratory, Teddington, Middx.

MS. received 14*th July* 1959

IN two previous papers (Bransden, Robertson and Swan 1956, Bransden and Robertson 1958) calculations have been reported on the elastic scattering of neutrons and protons by tritons and ^{3}He for incident nucleon energies in the range 1 to 14 MEV. A central Gaussian potential was employed such that

$$\mathscr{V}(ij) = V(r_{ij})\{w + mM_{ij} + bB_{ij} + hH_{ij}\}$$
$$V(r_{ij}) = A\exp(-\lambda r_{ij}^2); \quad A = -45\text{ MeV}; \quad \lambda = 0{\cdot}2669\text{ fermi}^{-2}$$

where M, B, H are the Majorana, Bartlett and Heisenberg exchange operators and w, m, b, h are constants depending on the exchange nature of the potential. The resonating group method was used to derive integro-differential equations for the radial wave function describing the collisions, using internal triton or ^{3}He ground state wave functions of Gaussian form, and the equations were integrated numerically to determine the scattering phase and angular distributions.

For the neutron–triton and proton–^{3}He collision the predicted angular distributions, for the Serber exchange force, agree quite closely with the experimental results, except at the lower energy of 1 MEV. The agreement for the neutron–^{3}He and proton–triton collision is not so good, the calculated differential cross section, for the Serber potential, rising above the experimental results in the backward direction. It is probable that coupling to the charge-exchange channel accounts for this discrepancy. Nevertheless, the forward scattering, the position of the minimum and the neutron–^{3}He total elastic cross section are all well reproduced, except at the lowest energy.

Recently, measurements have been reported at higher energies (n–^{3}He at 17·5 MEV, Sayres, Jones and Wu 1958; p–^{3}He, p–T at 19·4 MEV, Vanetsian and Fedchenko 1957), and in this note new theoretical results are given for these energies.

Biel (1957) has shown that the correct binding energies of ^{8}Be and ^{12}C may be obtained from the potential (1), provided the exchange property is taken to be a 70% Serber 30% symmetrical mixture, and he has suggested that such a mixture may not provide scattering phases significantly different from those for the Serber potential, so that the Biel mixture may be consistent with both the scattering data and with the binding energies of ^{4}He, ^{8}Be and ^{12}C. The new calculations have been performed with both Serber and Biel potentials, and to test the Biel mixture at lower energies, the 8 MeV differential cross section for the p–^{3}He and n–^{3}He collision has been recalculated.

In figure 1, the p–^{3}He theoretical cross sections are compared with the 8 MeV experimental measurements of Brolley, Rosen and Stewart (1959). It is seen that the Serber results are slightly superior to those for the Biel potential; but that the difference is perhaps too small to be significant. In figure 2 the 20 MeV results (Vanetsian and Fedchenko 1957) for p–^{3}He collision are compared with the theoretical results. The agreement is not as good as at the lower energies, and of course it must be expected that an equivalent central force theory will begin to break down as the energy is increased. However, in this case the agreement may be better than appears at first sight, for Vanetsian and Fedchenko state that because of the resolution of their apparatus the minimum at 120° in centre of mass system may be deeper than appears from their measurements, also the cross section at small angles is subject to an error of from ± 15 to ± 25%.

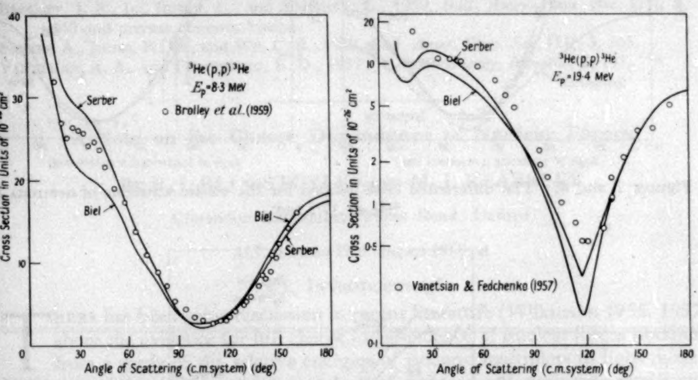

Figures 1 and 2. The differential cross section for the elastic scattering of protons by ^{3}He at 8 and 19·4 MeV.

The results for the n–^{3}He, p + T systems are shown in figures 3, 4 and 5. As expected from the results at lower energies, the Serber (and to a lesser extent the Biel) differential cross sections are in agreement with the experimental results at angles up to 120° for n–^{3}He at 8 and 17·5 MeV; the position of the minimum is given correctly and the calculated total cross section of 0·82 for the Serber potential agrees closely with the measured value of 0·8 barn (Sayres, Jones and Wu 1958). The 19·4 MeV results for p–T scattering conform to the same general picture.

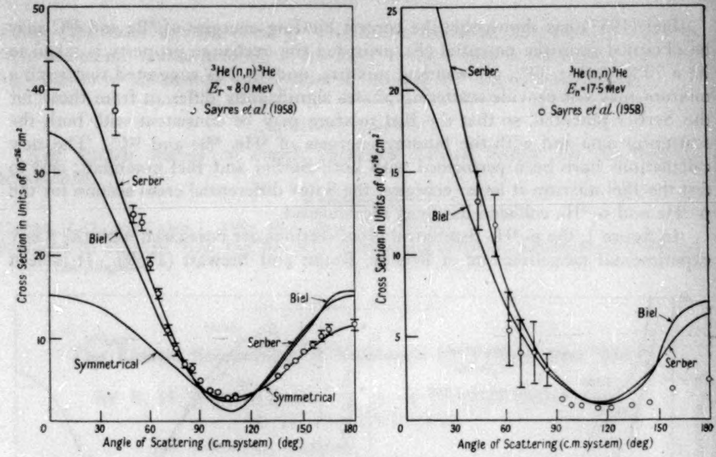

Figures 3 and 4. **The differential cross section for the elastic scattering of neutrons by ^{3}He at 17·5 MEV.**

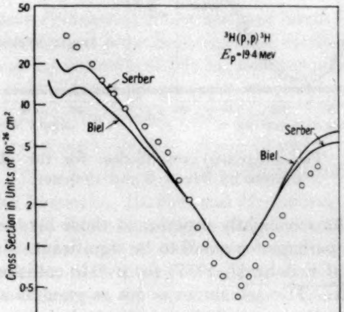

Figure 5. **The differential cross section for the elastic scattering of protons by tritons at 19·4 MEV.**

It may be concluded that for the p–^{3}He scattering the close agreement between the calculated results and experiment probably persists at energies up to 20 MEV (making due allowance for the uncertainties in the experimental results). For the n–^{3}He, p–T system the results again are similar to those at the lower energies. In general, the change from the Serber to Biel type potential either at the higher or at the lower energies produces quite small changes in the cross section, so

that a measure of consistency between the binding energies ^{4}He to ^{12}C and the four-body scattering data is achieved.

ACKNOWLEDGMENTS

We should like to thank Professor J. D. Seagrave and Dr. J. E. Brolley for informing us of the results on nucleon–T and nucleon–^{3}He scattering obtained at Los Alamos, prior to publication.

REFERENCES

BIEL, S. J., 1957, *Proc. Phys. Soc.* A, **70**, 866.

BRANSDEN, B. H., and ROBERTSON, H. H., 1958, *Proc. Phys. Soc.*, **72**, 770.

BRANSDEN, B. H., ROBERTSON, H. H., and SWAN, P., 1956, *Proc. Phys. Soc.* A, **69**, 877.

BROLLEY, J. E., Jr., ROSEN, L., and STEWART, L., 1959, *Bull. Amer. Phys. Soc.* [II], **4**, 140 and private communication.

SAYRES, A., JONES, K. W., and WU, C. S., 1958, *Bull. Amer. Phys. Soc.* [II], **3**, 365.

VANETSIAN, A. A., and FEDCHENKO, E. D., 1957, *J. Atom. Energy, Moscow*, **2**, 141.

A Note on the Charge Dependence of Nuclear Forces

BY R. J. BLIN-STOYLE† AND M. J. KEARSLEY

Clarendon Laboratory, Parks Road, Oxford

MS. received 27th August 1959

§ 1. INTRODUCTION

THERE has been some discussion in recent literature (Wilkinson 1956, 1957) about the evidence for full charge independence of nuclear forces obtained from a study of the relative energies of isobaric multiplets in light nuclei. Wilkinson (1956, 1957) makes an analysis of eighteen self-conjugate nuclei and comes to the conclusion that Δ, the average difference between the calculated and experimental values of the excitation energies of the first $T=1$ states, after allowing for Coulomb effects and the neutron–proton mass difference, is significantly positive but probably not greater than 50 kev. Explicitly

$$\Delta = E_{T=1}(\text{calc}) - E_{T=1}(\text{exp})$$

and for charge independent forces should be zero. Its deviation from zero can therefore be regarded as a measure of the departure of nuclear forces from charge independence. In the present note a theoretical evaluation of Δ is made for one of the nuclei considered by Wilkinson (1956, 1957), namely ^{6}Li, taking account of the charge dependence of nuclear forces resulting from the π^0, $\pi^\pm$ mass difference. Since the masses of the positive and negative pions are the same it follows that although the nuclear force is now no longer charge independent, it is still charge symmetrical, in agreement with the assumption made by Wilkinson in his analysis.

§ 2. CALCULATION OF Δ FOR ^{6}LI

In order to estimate Δ we need to calculate the energy difference between the $^1S_0$ levels of ^{6}He and ^{6}Li corresponding to the $T_z=1$, 0 members of the $T=1$ triplet.

---

† Present address: Dept. of Physics, Massachusetts Institute of Technology, Cambridge, Mass., U.S.A.

From symmetric pseudo-scalar meson theory with pseudo-scalar coupling, the second-order contribution to the internuclear potential is

$$V_2=\boldsymbol{\tau}_1\,.\,\boldsymbol{\tau}_2 f_2(\mu^{\pm})-\tau_1^z\,\tau_2^z\,[f_2(\mu^{\pm})-f_2(\mu^0)]$$

where $f_2(\mu^{\pm})$, $f_2(\mu^0)$ are the potentials due to charged and neutral meson exchange respectively. The matrix element of the tensor force for the $^1S_0$ states is zero and need not be considered here; further, at first we do not take repulsive core effects into account. The effective potential $f_2(\mu)$ is thus taken to have the form

$$f_2(\mu)=\frac{1}{3}\left(\frac{g}{2M}\right)^2\boldsymbol{\sigma}_1\,.\,\boldsymbol{\sigma}_2\,\mu^2\frac{e^{-\mu r}}{r}$$

so that

$$V_2(r)=\frac{1}{3}\left(\frac{g}{2M}\right)^2\boldsymbol{\sigma}_1\,.\,\boldsymbol{\sigma}_2\left\{\boldsymbol{\tau}_1\,.\,\boldsymbol{\tau}_2\,\mu^2\frac{e^{-\mu r}}{r}+\frac{\delta\mu}{\mu}\tau_1^z\,\tau_2^z\,\mu^2\left[\mu e^{-\mu r}-2\frac{e^{-\mu r}}{r}\right]\right\}$$

where

$$\frac{\delta\mu}{\mu}=\frac{\mu^{\pm}-\mu^0}{\mu^{\pm}}=0{\cdot}032.$$

It is a reasonable approximation to treat the charge dependent part of the nuclear force as a perturbation so that the differences in the diagonal matrix elements of this part of $V_2(r)$ for the $^1S_0$, $T=1$, $T_z=1$ and $T_z=0$ states then gives a measure of Δ. For ^{6}Li and ^{6}He the two nucleons outside the closed $(1s)^4$ core are in 1p states coupled to $L=0$, $S=0$. The 1p state wave functions are taken to be of harmonic oscillator form

$$\Phi_{01M}=\left[\frac{8\nu^{5/2}}{3\sqrt{\pi}}\right]^{\frac{1}{2}} r\exp\left(-\tfrac{1}{2}\nu r^2\right)Y_1^{\,M}(\theta\phi)$$

where the parameter ν can be estimated from either the Coulomb energy difference between ^{6}He and ^{6}Li or from their radii. In the former case $\sqrt{\nu}\simeq 0{\cdot}5\times 10^{13}\,\text{cm}^{-1}$, and in the latter, taking the r.m.s. radius to be $1{\cdot}2A^{1/3}\times 10^{-13}$ (Feingold 1956), $\sqrt{\nu}\simeq 0{\cdot}6\times 10^{13}\,\text{cm}^{-1}$. Since only a rough estimate of $\sqrt{\nu}$ can be made owing to the uncertainties in the Coulomb energy and effective radius of ^{6}Li, the matrix elements have been calculated for several values of $\sqrt{\nu}$.

The calculation is straightforward and the values obtained for Δ (using $(g\mu/2M)^2=0{\cdot}09$) are shown in the table

$\sqrt{\nu}\times 10^{-13}\,\text{cm}^{-1}$	0·4	0·5	0·6	0·7
Δ (kev)	56	106	166	238

§ 3. DISCUSSION

The values obtained for Δ are of the right sign but are significantly larger (for a reasonable value of $\sqrt{\nu}$) than the upper limit set by Wilkinson (1956, 1957). Of course this could result from the fact that we have only considered the second order potential with neglect of repulsive core effects. A rough estimate of the latter can be made by introducing a correlation function $\rho(|\mathbf{r}_{12}|)$ into the nuclear wave function, where

$$\begin{aligned}\rho(|\mathbf{r}_{12}|)&=0\quad\text{for}\quad |r_{12}|<0{\cdot}6\times 10^{-13}\,\text{cm}\\&=1\quad\text{for}\quad |r_{12}|>0{\cdot}6\times 10^{-13}\,\text{cm}.\end{aligned}$$

This reduces the results for Δ by approximately 30%. On the other hand it is to be expected that the fourth order potential will have an appreciable effect.

According to Sugie (1954) the central singlet charge dependent part of the fourth order potential is

$$V_4(r)=\tau_1^z\tau_2^z\left(\frac{g}{2M}\right)^4\mu^5\frac{8}{\pi}\left[\frac{K_0(2\mu r)}{\mu r}+\left(1+\frac{11}{4\mu^2r^2}\right)K_1(2\mu r)\right].$$

Outside the region of the repulsive core $V_4\simeq\frac{1}{2}V_2$ so that the V_4 contribution increases the magnitude of Δ by an amount which approximately compensates for the effect of the repulsive core. This means that the values for Δ in the table can still be taken as a reasonable estimate for the charge dependent effect of nuclear forces due to the mass difference between charged and neutral pions.

Accepting this estimate means that in order to account for the resulting discrepancy between theory and experiment, other charge dependent effects which can arise in nuclear forces must be considered. One such important effect is the difference between the coupling constants ($g_{\pi^+\mathrm{pn}}$, $g_{\pi^0\mathrm{pp}}$, $g_{\pi^0\mathrm{nn}}$) for charged and neutral pions which arises because of interaction of the pion and nucleon field with the photon field. These differences have been estimated by Riazuddin (1958) and are qualitatively such that they reduce the value of Δ by about $\Delta/4$. However, in these circumstances a breakdown in charge symmetry of the order of magnitude $\Delta/4$ is also to be expected since the electromagnetic renormalizing effects on $g_{\pi^+\mathrm{pn}}$, $g_{\pi^0\mathrm{pp}}$ and $g_{\pi^0\mathrm{nn}}$ are different in each case (Riazuddin 1958), which then removes one of the assumptions on which Wilkinson's (1956) analysis was based.

However, it seems difficult to escape the conclusion that the charge dependent pion mass effect alone leads to values of Δ larger than observed experimentally and that in order to reduce this value, electromagnetic renormalization of the pion–nucleon coupling constants must be appealed to, which then leads to an appreciable breakdown of charge symmetry.

REFERENCES

FEINGOLD, A. M., 1956, *Phys. Rev.*, **101**, 258.
RIAZUDDIN, 1958, *Nucl. Phys.*, **7**, 217, 223.
SUGIE, A., 1954, *Progr. Theor. Phys., Japan*, **11**, 333.
WILKINSON , D. H., 1956, *Phil. Mag.*, **1**, 1031.
—— 1957, *Proc. Rehovoth Conference on Nuclear Structure* p. 175.

Internal Ferromagnetic Resonance in Magnetite

BY J. C. ANDERSON† AND B. DONOVAN‡
† Department of Physics, Royal Holloway College, Englefield Green, Surrey
‡ Department of Physics, Bedford College, London

MS. received 10th August 1959, in final form 15th September 1959

PREVIOUS investigations of the complex permeability of iron–nickel alloys and of pure nickel (Anderson and Donovan 1957, 1959) have shown that the resonance phenomena observed may be attributed to the internal magnetic field, which arises from the anisotropy energy of the crystal. In the case of a dilute suspension of colloidal nickel particles, the temperature dependence of the resonant frequency was found to be reasonably consistent with the internal field, as derived from experimental values of the anisotropy constants.

Experiments on these lines have now been extended to other ferromagnetic substances and the purpose of the present note is to report some results obtained with a colloidal suspension of magnetite (Fe_3O_4), over the temperature range 30°–90°c. The particles were shown by electron micrographs to be roughly spherical in shape, and although the spread of diameters was appreciable (30–150 Å) it was still within the range of single domain behaviour. The experimental technique was exactly the same as that used in the previous work on colloidal nickel. In the present case, however, measurements were not made below 30°c, as, owing to the high dielectric constant of the suspension, it was not possible to obtain higher frequencies with the apparatus in its original form.

Figure 1 is typical of the results obtained and shows the real and imaginary parts of the complex permeability ($\mu = \mu_1 - i\mu_2$) at 70°c, plotted as functions of frequency. The curves are similar in form to those obtained for nickel, though in general the width of the resonance peak was found to be slightly greater. The temperature dependence of the resonant frequency is shown in figure 2 and again resembles nickel in that the internal field decreases with increasing temperature.

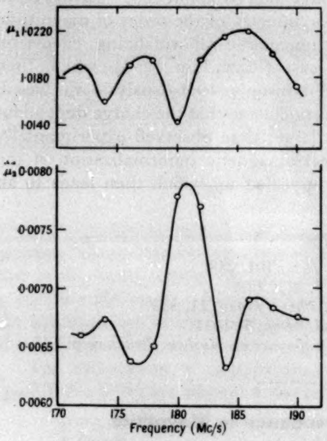

Figure 1. Variation of real and imaginary parts of complex permeability with frequency at 70°c.

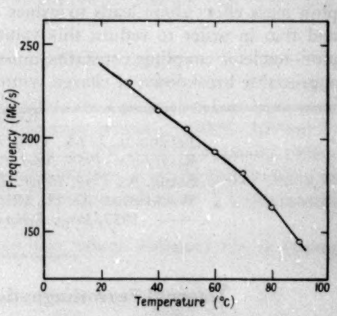

Figure 2. Variation of resonant frequency with temperature.

Magnetite is known to possess the inverse spinel structure, and to some extent it resembles nickel in its magnetic behaviour (cf. Domenicali 1950). It has a cubic lattice, with the easy direction of magnetization parallel to the (111) axis in the present range of temperature; hence, as in the case of nickel, the effect of the crystal anisotropy may be represented by an internal field H_1 given by

$$H_1 = \frac{4}{3I_s}\left(K_1 + \frac{K_2}{3}\right),$$

(cf. Anderson and Donovan 1959), where K_1 and K_2 are the first and second anisotropy constants and I_s is the saturation magnetization.

Very few experimental results are available with which to attempt any quantitative interpretation of figure 2. So far as the authors are aware, no measurements of K_1 have been carried out above room temperature and none at all of K_2. Using microwave resonance methods, Bickford (1949, 1950) found K_1 to be $-11{\cdot}1\times10^4\,\mathrm{erg\,cm^{-3}}$ at 20°c, and the value derived from the early work of Weiss lies between $-8{\cdot}5\times10^4$ and -10×10^4 (Bozorth 1952, chap. XII). If the internal field H_i is evaluated with these values for K_1, and $I_s=460$ c.g.s. units, the extrapolation of figure 2 indicates that, for agreement, K_2 would have to be positive and in the neighbourhood of $17\text{–}22\times10^4\,\mathrm{erg\,cm^{-3}}$. Such a high value seems rather unlikely (though not magnetically impossible, since the upper limit is $9|K_1|/4$).

A more plausible explanation is that in the case of small particles the anisotropy field may be different from that in the bulk material. In his connection it should be pointed out that sufficiently small particles can exhibit *superparamagnetism* (see, for example, Bean and Livingston 1959), which is characterized by thermal fluctuations of the direction of magnetization. The significance of this effect in the present work is that for particles in the superparamagnetic range the effective anisotropy may be appreciably reduced.† Thus in the present internal resonance experiments the effective field, and hence the resonant frequency, may be smaller than that anticipated on the basis of the experimental anisotropy constants. A further point concerning superparamagnetic particles has been discussed by Livingston and Bean (1959), namely that, at moderately high temperatures, the anisotropy measured by torque methods is less than that measured by microwave methods.

The effect of superparamagnetism in connection with internal resonance has also been investigated in small cobalt particles. In this case a more detailed examination is possible, in view of the experimental data on the anisotropy constants (Bean, Livingston and Rodbell 1959), and this will be dealt with in a separate paper.

REFERENCES

ANDERSON, J. C., and DONOVAN, B., 1957, *Proc. Phys. Soc.* B, **70,** 186.
—— 1959, *Ibid.*, **73,** 593.
BEAN, C. P., and LIVINGSTON, J. D., 1959, *J. Appl. Phys.* (Suppl.), **30,** 120S.
BEAN, C. P., LIVINGSTON, J. D., and RODBELL, D. S., 1959, *J. Phys. Radium,* **20,** 298.
BICKFORD, L. R., 1949, *Phys. Rev.*, **76,** 137.
—— 1950, *Ibid.*, **78,** 449.
BOZORTH, R. M., 1952, *Ferromagnetism* (New York: van Nostrand).
DOMENICALI, C. A., 1950, *Phys. Rev.*, **78,** 458.
LIVINGSTON, J. D., and BEAN, C. P., 1959, *J. Appl. Phys.* (Suppl.), **30,** 318S.

† The authors are indebted to Dr. D. S. Rodbell for helpful correspondence on this point.

The Absorption Spectrum of Calcium Vapour in the Vacuum Ultra-violet[†]

By T. R. KAISER
Department of Physics, The University, Sheffield

Communicated by R. W. Ditchburn; *MS. received* 19*th August* 1959

The absorption of light by calcium vapour has been investigated in the region 2000Å to 1500Å using a fluorite spectrograph. The absorption corresponding to the series limit of the 4s4s$^1S_0$–4snp$^1P_1^0$ series, previously observed by Jutsum (1954), was obtained and a number of intense autoionization lines were also recorded. Some of the lines were obviously broader than others and this was used to divide them into two series whose wavelengths are listed in table 1 ('broad' series) and table 2 ('narrow' series). The wavelengths of the first three members of the broad series are subject to a few ångströms error (due to their finite width on the photographic plate); the other wavelengths are accurate to within 1Å.

Consideration of the relevant spectroscopic data indicates that the absorption lines arise from transitions from the 4s4s$^1S_0$ level to the 3dnp$^1P_1^0$ and $^3P_1^0$ levels corresponding to $\Delta J=1$, $\Delta L=1$, and $\Delta S=0$, 1 respectively. The 3dnp series converge to the 3d^{2}D levels of the excited ion. The only other likely transitions with $\Delta J=1$ are to the 3dnp$^3D_1^0$ levels; however these require $\Delta L=2$, $\Delta S=1$

Table 1. Broad Series

n	λ(Å)	T_n(cm^{-1})	T_n(cm^{-1}) calc.	μ_n
5	1882·5	53121	52975	1·67
6	1768·0	56561	57207	1·88
7	1688·5	59224	59190	1·62
8	1658·3	60303	60296	1·64
9	1640·1	60972	60977	1·68
10	1627·9	61429	61431	1·68
11	1619·6	61744	61746	1·71
12	1613·6	61973	61975	1·74
13	1609·0	62150	62150	1·74
∞	—	—	63008	—

Table 2. Narrow Series

n	λ(Å)	T_n(cm^{-1})	T_n(cm^{-1}) calc.	μ_n
6	1772·0	56433	56818	1·90
7	1695·0	58997	58964	1·73
8	1662·8	60140	60139	1·76
9	1643·3	60853	60858	1·77
10	1630·4	61335	61333	1·77
11	1621·8	61660	61662	1·79
12	1615·4	61904	61900	1·78
13	1610·8	62081	62081	1·79
∞	—	—	62960	—

[†] This work was carried out while the author was in the Physics Department of the University of Reading.

and are hence more highly forbidden. In any case the $3d5p^3D_1^0$ level is known (Moore 1949) and no corresponding absorption line is observed. The 3d4p levels lie below the first series limit and are known (Moore 1949) but their order appears to be anomalous. However, if we re-order them to agree with Hund's rule before applying the criterion that with increasing n, terms with the same J values do not cross we find that the $3dnp^1P_1^0$ series converges to the $3d^2D_{5/2}$ level of the excited ion and the $3dnp^3P_1^0$ to the $3d^2D_{3/2}$ level, which agrees with the term scheme given by White (1934).

Using the above identification we may assign to the lines the values of n given in the tables. It may be noted that the narrow line corresponding to $n=5$ is not observed, probably due to obscuration by the corresponding broad line. The higher terms ($n \geqslant 8$) were fitted to the Rydberg–Ritz formula

$$\lambda^{-1} = T_n = T_\infty - \frac{R}{n^2} - \frac{10^3\alpha}{n^3} - \frac{10^6\beta}{n^6} \qquad \ldots\ldots (1)$$

giving for the narrow series

$$\alpha = 492{\cdot}4, \quad \beta = 38{\cdot}0, \quad T_\infty = 62960\,\mathrm{cm}^{-1}$$

and for the broad series

$$\alpha = 448{\cdot}5, \quad \beta = 32{\cdot}1, \quad T_\infty = 63008\,\mathrm{cm}^{-1}.$$

In view of the possible wavelength errors quoted the values for the series limits are in excellent agreement with those given by Moore (1949), namely $63016\,\mathrm{cm}^{-1}$ and $62955\,\mathrm{cm}^{-1}$ for the $3d^2D_{5/2}$ and $3d^2D_{3/2}$ levels of the excited ion respectively. Hence we conclude that the broad series corresponds to transitions from the $4s4s^1S_0$ ground state to $3dnp^1P_1^0$ levels and the narrow series to $3dnp^3P_1^0$ levels.

Term values calculated from (1) are given in the tables, together with the quantum defects μ_n determined from

$$T_n = T_\infty - \frac{R}{(n-\mu_n)^2} \qquad \ldots\ldots (2)$$

using Moore's values for T_∞ and the observed values of T_n.

ACKNOWLEDGMENTS

It is a pleasure to acknowledge the advice of Professor R. W. Ditchburn concerning the experimental techniques and of Dr. M. J. Seaton in connection with the interpretation of the spectrum.

REFERENCES

JUTSUM, P. J., 1954, *Proc. Phys. Soc.* A, **67**, 190.
MOORE, C. E., 1949, *Atomic Energy Levels* (Washington: National Bureau of Standards).
WHITE, H. E., 1934, *Introduction to Atomic Spectra* (New York: McGraw Hill).

The Energy Levels of ^{26}Al in the Region of 2 Mev

By E. E. BAART, L. L. GREEN AND J. C. WILLMOTT

Nuclear Physics Research Laboratory, University of Liverpool

MS. received 14*th September* 1959

The energies of the excited states of ^{26}Al have recently been determined with high accuracy by Hinds and Middleton (1959) by observing the charged particle groups from the reaction ^{27}Al(^{3}He, α)^{26}Al and ^{24}Mg(He^3, p)^{26}Al. Previous experiments on the γ-rays emitted in the reaction ^{25}Mg(p, γ)^{26}Al had suggested that the level at 2·06 Mev should be a doublet, although these levels could not be resolved by the sodium iodide crystal spectrometers used (Kavanagh, Mills and Sherr 1955, Green, Singh and Willmott 1956). Experiments on the ^{28}Si(d, α)^{26}Al reaction carried out by Browne (Browne 1954, 1956, 1959) gave some weight to this suggestion. In his first experiments Browne studied the α-particles emitted at 90° to the forward direction and found a single level at 2·06 Mev, which was strongly excited. He found all the other levels now known to exist below 2 Mev except for the first $T=1$ level at 0·229 Mev. In later experiments in the forward direction Browne found the yield of α-particles to the 0·229 Mev level varied with energy, but the yield was significantly lower than for the $T=0$ levels. This suggests that isotopic spin selection rules lead to some inhibition of α groups to $T=1$ levels and that the level observed by Browne at 2·06 Mev probably does not correspond to the second $T=1$ level which is expected at this energy.

The level observed by Hinds and Middleton at 2·06 Mev does not show complex structure in either of the two reactions observed and it is not possible in their reactions to invoke isotopic spin selection rules. We have consequently re-examined the resonances of the ^{25}Mg(p, γ)^{26}Al reaction whose decay schemes appeared to require a doublet at this excitation.

The previous experiments were carried out with 2 in. × 2 in. sodium iodide crystals. We have re-examined twelve resonances between 436 kev and 989 kev using 5 in. × 6 in. sodium iodide crystals as detectors singly, in coincidence, and in sum coincidence (Hoogenboom 1958). At all resonances except those at 811 kev and 956 kev a single level at 2·06 Mev was found sufficient to explain the γ-rays observed. This level is fed strongly at most resonances, but only at the three resonances at 726 kev, 776 kev and 940 kev were coincidence experiments possible. At these resonances γ-rays of energy 1·64 Mev, 1·02 Mev, 0·82 Mev and 0·42 Mev were observed in coincidence with a high energy γ-ray of correct energy to feed the 2·06 Mev level direct from the resonance. Earlier work with smaller crystals had suggested variations in the ratio of these two cascades from resonance to resonance and led to the suggestion that there were two levels at approximately 2·06 Mev decaying by one of these two cascades. The use of larger crystals has shown alternative sources of the 1·6 Mev γ-ray at certain of the resonances previously examined and this removes the variation of intensity of these two cascades except at the two resonances which are discussed in more detail below. It thus appears that the two cascades form alternative decay modes of a single level at 2·06 Mev through a state at 0·416 Mev to the ground state, and a state at 1·052 Mev to the 0·229 Mev state. The two cascades occur in the ratio of 1 to 3.

At the 811 kev and 956 kev resonances this simple decay scheme is not sufficient to account for the intensities of the γ-rays observed, and we discuss these resonances in more detail.

The 811 *kev resonance.*

The γ-rays observed at this resonance, with their relative intensities, are shown in table 1. The strength of the 1·02 Mev and 0·84 Mev γ-rays shows that not more than about four units of the intense 1·643 Mev γ-ray can be due to the normal decay of the 2·06 Mev level discussed above. Coincidence experiments showed the 1·643 Mev γ-ray to be in coincidence with the 5·24 Mev γ-ray, forming a cascade between the resonance level and the 0·229 Mev level. The 3·38 Mev γ-ray also appeared in the coincidence spectrum together with the 1·02 Mev and 0·84 Mev γ-rays, indicating the presence of the cascade, resonance →3·67 Mev→2·06 Mev→1·05 Mev→0·229 Mev, a cascade that has been observed at the 684 kev resonance.

Table 1. 811 kev Resonance

γ-ray energy (Mev)	Intensity	γ-ray energy (Mev)	Intensity
6·85 ± 0·04	11 ± 2	2·4	weak
5·24 ± 0·05	10 ± 4	2·17	weak
5·03 ± 0·03	45 ± 6	1·833 ± 0·007	47 ± 5
4·40	5	1·643 ± 0·007	28 ± 3
4·18	4	1·35 ± 0·03	5 ± 2
3·50 ± 0·04	5 ± 2	1·15 ± 0·03	5 ± 2
3·38 ± 0·03	12 ± 3	1·02 ± 0·03	10 ± 2
2·72 ± 0·03	5 ± 2	0·84 ± 0·03	13 ± 2
2·55 ± 0·03	7 ± 2	0·51 ± 0·02	65 ± 10
		0·43 ± 0·02	12 ± 3

These modes of decay between them account for the whole of the 1·643 Mev γ-rays, and, incidentally, of the normal decay of the 2·06 Mev level. We thus still have to account for the strong 5·03 Mev γ-ray.

Intensity considerations suggest this γ-ray is in coincidence with the 1·833 Mev γ-ray and coincidence and sum coincidence experiments verified that these γ-rays form a simple cascade leading to the 0·229 Mev level. Thus we must either have a level at 2·06 ± 0·017 Mev decaying solely to the 0·229 Mev level, or the 1·833 Mev γ-ray must be a feeder for a level at 5·27 ± 0·03 Mev; a level is observed by Hinds and Middleton at 5·238 ± 0·01 Mev.

The former case gives a slightly better overall agreement in the energies concerned, but leads to a doublet at 2·06 Mev.

The 956 *kev resonance.*

The γ-rays observed at this resonance, and their intensities, are shown in table 2. The intensities of the 5·15 Mev, 2·054 Mev and 1·644 Mev γ-rays indicate they are probably involved in a cascade through a level at 2·054 Mev, and a spectrum taken in coincidence with the 5·15 Mev γ-ray shows the 2·054, 1·644 Mev and the 0·43 Mev γ-rays very strongly. The 1·644 Mev and 2·054 Mev γ-rays could

Table 2. 956 kev Resonance

γ-ray energy (Mev)	Intensity	γ-ray energy (Mev)	Intensity
7·23 ± 0·03	3 ± 0·4	2·054 ± 0·015	31 ± 3
5·15 ± 0·02	100 ± 10	1·644 ± 0·005	69 ± 7
3·80 ± 0·03	6 ± 1	1·34 ± 0·02	6 ± 1
3·54 ± 0·02	11 ± 2	1·15 ± 0·02	6 ± 1
3·25 ± 0·02	7 ± 1	1·03 ± 0·02	8 ± 1
3·02 ± 0·02	6 ± 1	0·84 ± 0·02	6 ± 1
2·47 ± 0·02	2 ± 0·6	0·51 ± 0·02	11 ± 4
		0·43 ± 0·02	81 ± 15

thus represent alternative modes of decay of a single level at 2·054 Mev fed by the 5·15 Mev γ-ray. This level at 2·054 Mev has different decay properties from the level at 2·064 Mev encountered at the majority of the other resonances, and also from the level at 2·06 Mev required in one explanation of the decay properties of the 811 kev resonance. It is also, presumably, not the $T=1$ level expected at this energy, which should be a 2^+ level, and would therefore be unlikely to decay to the ground state which is known to be 5^+.

Alternative explanations of these γ-rays would be for one or both the low energy γ-rays to be primary γ-rays. The possible explanations are shown in the figure. There is some slight evidence that the 5·15 Mev γ-ray is complex as its shape is not quite consistent with that expected for a simple γ-ray of this energy. Neither of the two high energy levels required here corresponds to that required at the 811 kev resonance to avoid the occurrence of a doublet at 2·06 Mev.

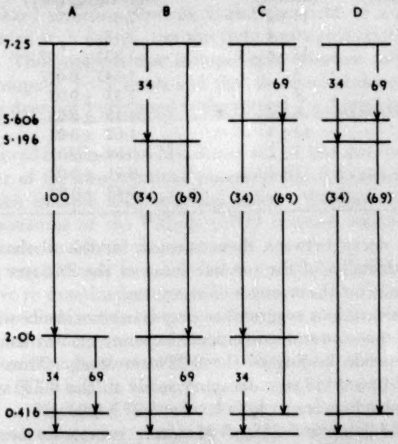

Alternative modes of decay at the 956 kev resonance.

We have attempted to detect differences in the energy of the 1·64 Mev γ-rays occurring at the 726 kev, 811 kev and 956 kev resonances, which should occur if some of the intensity of this γ-ray is due to a primary transition. No such shift was observed, the energy of this γ-ray remaining constant to within 10 kev.

It thus appears that most probably there is at least a doublet at 2·06 Mev, although one cannot rule out the alternative explanation of a singlet at this energy, with levels at 5·27 ± 0·03 Mev, 5·196 ± 0·025 Mev and 5·606 ± 0·25 Mev all fed strongly at either the 811 kev or 956 kev resonances. The existence of a doublet within 10 kev is consistent with the resolution of Hinds and Middleton.

REFERENCES

BROWNE, C. P., 1954, *Phys. Rev.*, **95**, 860.
—— 1956, *Massachusetts Institute of Technology Report*, February 1956.
—— 1959, *Phys. Rev.*, **114**, 807.
GREEN, L. L., SINGH, J. J., and WILLMOTT, J. C., 1956, *Proc. Phys. Soc.* A, **69**, 335.
HINDS, S., and MIDDLETON, R., 1959, *Proc. Phys. Soc.*, **73**, 501.
HOOGENBOOM, A. M., 1958, *Nucl. Inst.*, **3**, 57.
KAVANAGH, R. W., MILLS, W. R., and SHEER, R., 1955, *Phys. Rev.*, **97**, 248.

The Effect of an Electric Field on the Decay of Excess Carriers in Semiconductors

BY B. K. RIDLEY
Mullard Research Laboratory, Salfords, Surrey

MS. received 11*th August* 1959

§ 1. INTRODUCTION

IN order to measure the lifetime of excess carriers in semiconductors by the photoconductive decay method it is necessary to pass a current through the specimen and observe the change of voltage across the specimen with time when a short pulse of excess carriers is introduced into the material. The carriers decay by recombination not only in the bulk but also at the surfaces of the specimen and at the electrical contacts. These latter, if ohmic, may be regarded as surfaces having infinite recombination velocities and can therefore be important factors governing the decay rate. Their effect is enhanced by the presence of the electric field in the specimen which tends to sweep the carriers towards the contacts.

The theory of sweep-out effects under steady state conditions has been discussed fully by Rittner (1954), Grover and Harnik (1958) and F. Berz (to be published), but the problem under transient conditions has been comparatively neglected. Rittner (1954) has pointed out that the sweep-out effect in the transient case is qualitatively similar to that in the steady state case, i.e. it increases the decay rate. However, quantitative information is scant about a subject which can be important when the lifetimes of long-lifetime semiconducting crystals are being measured.

§ 2. THE GENERAL SOLUTION

For clarity we will limit the pertinent conditions to those of a rectangular parallelepiped semiconducting crystal of length $2L$ having ohmic contacts at $x = +L$ and $x = -L$ and zero surface recombination velocities at the surfaces. We shall assume a uniform distribution of excess carriers to be instantaneously injected at a time $t = 0$ so that we can limit ourselves to considering density variations solely in the x direction when $t > 0$, and we shall neglect trapping effects and assume recombination in the bulk to be characterized by a simple lifetime τ_0. Thus, for all times the density of excess holes is equal to the density of excess electrons, i.e. $\Delta n = \Delta p$, and we will limit ourselves to considering the excess hole distribution.

The continuity equation is (Rittner 1954),

$$D_0 \frac{\partial^2 \Delta p}{\partial x^2} + \mu_0 E \frac{\partial \Delta p}{\partial x} - \frac{\Delta p}{\tau_0} = \frac{\partial \Delta p}{\partial t} \qquad \ldots\ldots(1)$$

where

$$D_0 = D_n D_p \frac{n_0 + p_0}{D_n n_0 + D_p p_0}$$

and

$$\mu_0 = \mu_n \mu_p \frac{p_0 - n_0}{\mu_n n_0 + \mu_p p_0}$$

$$\Delta p \ll n_0 + p_0.$$

The boundary conditions are

$$\Delta p = 0 \Big|_{\substack{x=+L \\ x=-L \\ t>0}} \quad \text{and} \quad \Delta p = \Delta p_0 \Big|_{t=0}$$

Denoting the Laplace transform of the excess hole density by $\bar{p}$ and the Laplace parameter by σ we obtain

$$\bar{p} = \frac{\Delta p_0}{(1/\tau_0 + \sigma)\sinh(m_1 + m_2)L}$$
$$\times [\sinh(m_1 + m_2)L - \exp(m_1 x)\sinh m_2 L - \exp(-m_2 x)\sinh m_1 L] \qquad \ldots\ldots(2)$$

where

$$m_1 = -\frac{w_0}{2L_0^2} + \left[\frac{w_0^2}{4L_0^4} + \frac{1}{D}\left(\frac{1}{\tau_0} + \sigma\right)\right]^{1/2}$$

$$m_2 = \frac{w_0}{2L_0^2} + \left[\frac{w_0^2}{4L_0^4} + \frac{1}{D}\left(\frac{1}{\tau_0} + \sigma\right)\right]^{1/2}$$

and w_0, the drift length, is $\mu_0 E \tau_0$, and L_0, the diffusion length, is $(D_0 \tau_0)^{1/2}$. All the poles are simple and there is no branch point. Summing the residues of the poles gives us Δp, and averaging this over the length of the crystal we obtain

$$\overline{\Delta p} = \frac{\Delta p_0 \pi^2 L_0^4 \exp[-(1 + w_0^2/4L_0^2)t/\tau_0]}{4L^4}$$
$$\times \sum_{n=1}^{\infty} \frac{n^2(1 - \sec n\pi \cosh w_0 L/L_0^2)\exp[-(n^2\pi^2 L_0^2/4L^2)t/\tau_0]}{(w_0^2/4L_0^2 + n^2\pi^2 L_0^2/4L^2)^2}. \qquad \ldots\ldots(3)$$

This solution is not very informative as it stands and we must look to approximations to elucidate the effect of the electric field on the decay rate.

2.1. *Low Field Approximation*

If $w_0^2/4L_0^2 \lesssim \pi^2 L_0^2/4L^2$ we need retain only the first term of the series as a first approximation. The decay rate is then

$$\nu = \left(1 + \frac{w_0^2}{4L_0^2} + \frac{\pi^2 L_0^2}{4L^2}\right)\frac{1}{\tau_0}. \qquad \ldots\ldots(4)$$

Physically, this case corresponds to the situation in which normal end effects, governed by straightforward diffusion processes, predominate over sweep-out effects. Factors which are favourable to this approximation are (*a*) long diffusion length, (*b*) short specimen length, and (*c*) low sweep-out mobility.

2.2. *High Field Approximation*

At high fields ($w_0^2/4L_0^2 \gg \pi^2L_0^2/4L^2$) the series converges very slowly and equation (3) conveys little information beyond the fact that the decay is non-exponential unless t is great enough to make $\pi^2L_0^2t/4L^2\tau_0 > 1$. For such values of the time the decay is exponential with a decay rate given by equation (4).

For moderate fields the decay is approximately exponential and we can obtain an approximate value for the decay rate by assuming it to be the decay rate of the maximum term of the series. This approximation therefore takes in the low field case as well. Since the value of n giving the maximum term is a function of the time we must consider over what range of time we intend to take measurements. This range of time will be of the order of the field lifetime, therefore we find the maximum term when

$$t = \tau_0\left(1 + \frac{w_0^2}{4L_0^2} + \frac{\pi^2L_0^2}{4L^2}\right)^{-1} \qquad \ldots\ldots(5)$$

which is not far removed from the field lifetime.

We can write the decay rate for the maximum term as follows

$$\nu_{\mathrm{m}} = \left(1 + \frac{w_0^2}{4L_0^2} + \epsilon\right)\frac{1}{\tau_0}. \qquad \ldots\ldots(6)$$

The correction factor ϵ has been found for various values of the dimensionless parameters $w_0^2/4L_0^2$ and $\pi^2L_0^2/4L^2$, and the results are shown in figure 1. The following points may be noticed:

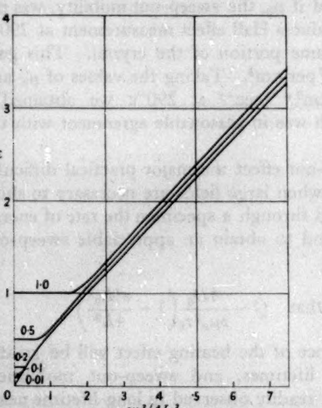

Figure 1. The sweep-out effect correction factor ϵ. Figures on the curves refer to values of $\pi^2L_0^2/4L^2$. The decay rate, $\nu = (1 + W_0^2/4L_0^2 + \epsilon)\ 1/\tau_0$.

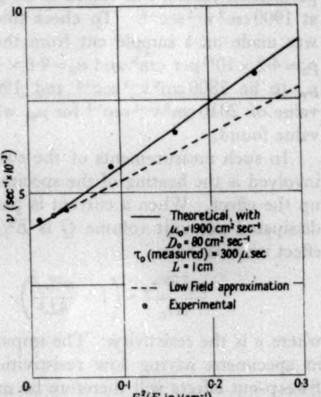

Figure 2. The sweep-out effect in a p-type sample of germanium ($\rho = 63\Omega$ cm at 290°K).

(*a*) When $w_0^2/4L_0^2 \gtrsim 2\,.\,\pi^2L_0^2/4L^2$, ϵ is very nearly independent of the value of $\pi^2L_0^2/4L^2$. The decay rate is governed solely by the normal recombination processes and the sweep-out effects, and the normal diffusion to the ohmic contacts has only a minor effect. Also we have the relationship, obtained from the slope of the linear region

$$\epsilon = \frac{4}{\pi^2}\frac{w_0^2}{4L_0^2}. \qquad \ldots\ldots(7)$$

(*b*) When $w_0^2/4L_0^2 \lesssim \pi^2 L_0^2/4L^2$, the low field approximation holds and the decay rate is affected by all three processes.

It must be emphasized that this approximation will hold good at high fields only over that part of the decay indicated by equation (5). If $\tau_{\mathrm{m}} = 1/\nu_{\mathrm{m}}$, then measurements should be made at that part of the decay where $t \sim 1{\cdot}4\tau_{\mathrm{m}}$ that is, towards the tail of the decay where it is more nearly exponential.

§ 3. EXPERIMENTAL

Figure 2 is a fit of equation (6) to experimental results, ϵ being found from figure 1. The sample was a p-type germanium bar of dimensions 20 × 10 × 3 mm, well-etched to keep surface effects to a minimum (the surface recombination velocity was about 200 cm sec^{-1}), and of resistivity 63 Ω cm at 290°K. The measurements were made using a spark in air as the source of transient illumination, and the light from this fell upon a 3 mm thick germanium filter before being incident on the sample. The decay curve was displayed on an oscillograph and photographed. The fit between the maximum term approximation and the experimental results was found to be good if μ_0, the sweep-out mobility, was put at 1900 cm^2 v^{-1} sec^{-1}. To check this value a Hall effect measurement at 290°K was made on a sample cut from the same portion of the crystal. This gave $p_0 = 4{\cdot}2 \times 10^{13}$ per cm^3 and $n_0 = 9{\cdot}6 \times 10^{12}$ per cm^3. Taking the values of μ_n and μ_p to be 3800 cm^2 v^{-1} sec^{-1} and 1900 cm^2 v^{-1} sec^{-1} at 290°K we obtained a value of 2010 cm^2 v^{-1} sec^{-1} for μ_0, which was in reasonable agreement with the value found.

In such measurements of the sweep-out effect the major practical difficulty involved is the heating of the specimen when large fields are necessary to show up the effect. When a current is passed through a specimen the rate of energy dissipated per unit volume Q is E^2/ρ and to obtain an appreciable sweep-out effect we must have

$$\frac{\mu_0^2 E^2 \tau_0}{4D_0} \sim \left(1 + \frac{\pi^2 L_0^2}{4L^2}\right), \quad \text{so that} \quad Q \sim \frac{4D_0}{\rho \mu_0^2 \tau_0}\left(1 + \frac{\pi^2 L_0^2}{4L^2}\right)$$

where ρ is the resistivity. The importance of the heating effect will be greater in specimens having low resistivities, lifetimes, and sweep-out mobilities. Sweep-out effects will therefore be most readily observed in long-lifetime near-intrinsic (but not absolutely intrinsic) material. For other materials means for cooling the specimen must be available. The use of pulsed electric fields is obviously very desirable.

§ 4. CONCLUSIONS

It has been shown that sweep-out effects increase the decay rate of excess carriers in semiconducting specimens and, if great enough, they can affect the form of the decay. Approximations have been found for the decay rate when the decay curve is not too far removed from an exponential, and compared favourably with experiment for one sample.

In conclusion, it should be pointed out that the measurement of the sweep-out effect will be a sensitive one for detecting small differences between the hole and electron densities in near-intrinsic material, since the sweep-out mobility depends upon this difference.

ACKNOWLEDGMENTS

The author would like to express his thanks to Mr. G. Osborne for his assistance in the measurements of lifetime, and to Mr. R. Pratt for measurements of Hall effect. Thanks are also due to Dr. K. Hoselitz, Dr. T. B. Watkins and the management of the Mullard Research Laboratories for their support of this work.

REFERENCES

GROVER, N. B., and HARNIK, E., 1958, *Proc. Phys. Soc.*, **72**, 267.

RITTNER, E. S., 1954, *Photoconductivity Conference, Atlantic City*, 1954 (London: Chapman and Hall), p. 215.

LETTERS TO THE EDITOR

Intensities in the Triplet System of CO Bands

Work recently carried out by Herman (shortly to be published) on discharges in mixtures of CO with rare gases, gives what appears to be evidence of energy transfer between metastable xenon atoms and CO molecules. For the better understanding of this phenomenon, it is desirable to know what the relative intensities of the CO triplet bands ($d^3\Pi \rightarrow a^3\Pi$) would be if there were no preferential excitement of particular levels.

The bands of interest correspond to $v' \ngtr 8$, and the 'distortion' method of obtaining wave functions from spectroscopic data (Pillow 1951) can be regarded as quite sufficiently accurate within these limits. A simple Franck–Condon treatment indicates that any preferential population of levels by direct electron excitation from the ground state would be to vibrational levels well above those considered here.

The intensities given in the table below are calculated from data given by Herzberg (1950) and on the assumption of equal population of all vibrational levels in the upper state. Because there has been some doubt about the numerical assignment of the levels, approximate mean wavelengths are quoted for the triplet groups.

Intensities of CO triplet bands (arbitrary units) for $T \rightarrow \infty$
(i.e. equal population of all vibrational levels in the upper state)

v'' v'	0	1	2	3	4	5
0	7500 1	8620 3	10080 5	12090 4	(very low)	
1	6900 5	7550 13	9050 11	10640 3		
2	6430 16	7210 24	8230 7	9524		
3	6010 35	6700 23	7545	8620 3		
4	5644 60	6250 20	6990 2	7900 10		
5	5325 90	5660 6	6500 11	7280 6		
6	5040 99	5520	6090 23	6760		
7	4800 120	5220 6	5730 14	6320 3		
8	4580 105	4960 49	5420 11	5940 15		

Northern Polytechnic,
London.
8th October 1959.

M. E. PILLOW.
A. L. ROWLATT.

HERZBERG, G., 1950, *Molecular Spectra and Molecular Structure* I, 2nd Edn (New York: Van Nostrand).

PILLOW, M. E., 1951, *Proc. Phys. Soc.* A, **64**, 772, 779.

Signal to Noise Ratio in Nuclear Magnetic Resonance

An expression derived by Bloembergen, Purcell and Pound (1948) from power considerations shows that the maximum available signal-to-noise voltage ratio in a nuclear magnetic resonance experiment is, *ceteris paribus*, directly proportional to $Q^{1/2}$ and inversely proportional to $F^{1/2}$, where Q and F are respectively the quality factor of the coil containing the sample and the noise figure of the amplifier. Now, the nuclear magnetic resonance signal (in the absence of radiation damping) is proportional to Q, the thermal noise generated in the resonant circuit is proportional to $Q^{1/2}$ and the amplifier noise is independent of Q. Hence the actual dependence of the signal-to-noise voltage ratio on Q varies from a proportionality to $Q^{1/2}$ when the amplifier generates no noise to Q when the thermal noise generated in the resonant circuit is negligible compared with the noise generated in the amplifier. This is not immediately obvious from the expression of Bloembergen, Purcell and Pound because F itself is a function of Q. It appears preferable to express the amplifier noise in terms of an equivalent input grid resistance rather than in terms of a noise figure.

Let us suppose that we are detecting the absorption mode and that we are using a modulated magnetic field, the modulation sweeping from just off resonance to the peak of the resonance. In the bridge method of detection, for example, the absorption signal will occur as a modulation of the amplitude unbalance voltage at the modulation frequency. Let us assume this modulation to be sinusoidal. On linear rectification, we obtain a sinusoidal signal at the modulation frequency whose r.m.s. value can be shown to be

$$V_{\mathrm{s}} = \frac{\pi^2 \nu_0^{3/2} Q^{1/2} V_{\mathrm{c}}^{1/2} f \chi_0 T_2^{1/2}}{\gamma T_1^{1/2}} R^{1/2} \qquad \ldots\ldots(1)$$

at the optimum strength of the radio-frequency field, assuming Bloch susceptibilities. Here ν_0 is the resonance frequency, χ_0 is the static nuclear susceptibility, γ is the gyromagnetic ratio of the nuclei, T_1 is the spin–lattice relaxation time, T_2 is the inverse line-width parameter, V_{c} is the effective volume of the sample coil, f is the filling factor for the sample and R is the effective shunt resistance of the tuned circuit at resonance. If a phase-sensitive detector of effective bandwidth B at the output is used, the true bandwidth for noise is $4B$. Therefore the r.m.s. noise voltage referred to the input grid is

$$V_{\mathrm{n}} = 4\{\boldsymbol{k}TB(R+R_{\mathrm{an}})\}^{1/2} \qquad \ldots\ldots(2)$$

where $\boldsymbol{k}$ is Boltzmann's constant, T is the temperature of R, and R_{an} is the equivalent input grid resistance representing the amplifier noise. The signal-to-noise voltage ratio obtained using equations (1) and (2) has to be multiplied by two factors—a factor $\mathscr{Y}$ to take into account the characteristics of the rectifier and the phase-sensitive detector and the fact that the nuclear resonance signal does not cause a sinusoidal modulation of the amplitude unbalance voltage, etc., and a hitherto neglected factor $\sqrt{2}$ representing the 3 dB improvement in signal-to-noise ratio due to the phase-sensitive detector (Tucker 1952). Hence the signal-to-noise voltage ratio is

$$\frac{A_{\mathrm{s}}}{A_{\mathrm{n}}} = \frac{\pi^2 \nu_0^{3/2} \chi_0 T_2^{1/2}}{2\sqrt{2}\gamma T_1^{1/2}} \frac{V_{\mathrm{c}}^{1/2} f \mathscr{Y}}{(\boldsymbol{k}TB)^{1/2}} \frac{Q}{\left(Q + \dfrac{R_{\mathrm{an}}}{2\pi\nu_0 L}\right)^{1/2}}, \qquad \ldots\ldots(3)$$

using the relation $R = 2\pi\nu_0 LQ$ where L is the inductance of the coil. When the dispersion signal is observed, the signal-to-noise ratio is twice this.

It is clear from the above expression that when the amplifier noise is small compared with the thermal noise generated in the resonant circuit, i.e. $R_{\mathrm{an}} \ll Q \,.\, 2\pi\nu_0 L = R$, $A_{\mathrm{s}}/A_{\mathrm{n}}$ is proportional to $Q^{1/2}$. When the reverse is the case, $A_{\mathrm{s}}/A_{\mathrm{n}}$ is proportional to Q. It may be noted that the discussion in the conclusion of the paper of Bloembergen, Purcell and Pound following the use of an empirical formula for Q is truly valid only when the detection system is noise-free.

The author is indebted to Professor R. S. Krishnan for his kind interest and encouragement and to Dr. G. Suryan for many helpful discussions. He is also grateful to the Department of Atomic Energy for a Research Fellowship.

Department of Physics,
Indian Institute of Science,
Bangalore-12, India.
R. CHIDAMBARAM.

17th June 1959, in final form 14th July 1959.

BLOEMBERGEN, N., PURCELL, E. M., and POUND, R. V., 1948, *Phys. Rev.*, **73**, 679.
TUCKER, D. G., 1952, *Wircless Engr*, **29**, 184.

Long Range Forces between Atoms

When the distance between two atoms is large, it is common practice to expand the interaction energy E in inverse powers of the internuclear separation R. Dalgarno and Lewis (1955) obtained a useful rule for evaluating the second order perturbation energy E_2:

$$E_2 = \sum{}' (0|\,V|\,m)^2/(E_0 - E_m) \qquad \ldots\ldots(1)$$

in the usual notation, where V is the interaction potential. Dalgarno and Lewis (1955 and 1956) made ingenious use of their sum rule to find an exact series expansion for the interaction energy between a proton and a hydrogen atom. Using this exact series as a standard, we have developed an improvement on the old Unsöld (1927) approximation for evaluating E_2. While all such approximation methods have only academic interest when applied to the hydrogen–proton problem, they may serve as models for better calculations when applied to complex atoms, where no exact methods are available.

Unsöld's method consisted of replacing $E_0 - E_m$ by a constant $-\epsilon$; this yields

$$E_2 = -\frac{1}{\epsilon}\{(0|\,V^2|\,0) - (0|\,V|\,0)^2\}. \qquad \ldots\ldots(2)$$

In many cases one or two terms in the series (1) contribute the major portion of E_2. Suppose $(0|\,V|\,1)^2/(E_0 - E_1)$ is such a term. We evaluate it exactly, and then use the Unsöld method to find the contribution of the remaining terms. This yields

$$E_2 = -\frac{1}{\epsilon'}\{(0|\,V^2|\,0)^2 - (0|\,V|\,0)^2\} + \left(\frac{1}{\epsilon'} + \frac{1}{E_0 - E_1}\right)(0|\,V|\,1)^2. \qquad \ldots\ldots(3)$$

Thus in the hydrogen–proton problem the term $(100|\,V|\,210)^2/(E_{100} - E_{210})$ was evaluated. This term contributes 44% of E_2 at $R = 4$ atomic units, and this contribution grows to 66% at large values of R. The Unsöld, improved, and exact series in Hartree atomic units are:

$$\text{Unsöld:}\quad E_2 = -\frac{1}{\epsilon}\left[\frac{4}{R^4} + \frac{18}{R^6} + \frac{180}{R^8} + \frac{3150}{R^{10}}\right] \quad \ldots\ldots(4)$$

$$\text{Improved:}\quad E_2 = -\frac{1}{\epsilon'}\left[\left(1{\cdot}7803 + \frac{8{\cdot}8789}{3\epsilon'}\right)\frac{1}{R^4} + \frac{18}{R^6} + \frac{180}{R^8} + \frac{3150}{R^{10}}\right] \ldots\ldots(5)$$

$$\text{Exact:}\quad E_2 = -\frac{9}{2R^4} - \frac{15}{R^6} - \frac{525}{R^8} - \frac{8505}{4R^{10}}. \quad \ldots\ldots(6)$$

One way of comparing the approximations with the exact expression is to equate the coefficients of R^{-l} in (4) and (5) with the corresponding coefficients in (6). For each term a different value of ϵ and ϵ' is thus obtained, and these values, ϵ_l and ϵ_l' are listed in table 1. The index l refers to the power to which R^{-1} is raised. The quality of the approximation is reflected in the constancy of the values of ϵ_l and ϵ_l' as functions of l.

Table 1. ϵ_l and ϵ_l'

l	4	5	8	10
ϵ_l (Unsöld)	0·889	1·200	1·371	1·481
ϵ_l' (Improved)	1·156	1·200	1·371	1·481

Since the R^{-4} term is dominant for all except small values of R, it is customary to choose ϵ so that the coefficient of this term will be exact. This choice, as table 1 shows, means that the coefficients of the higher powers of R^{-1} will be much more accurate in the improved series than in the Unsöld series. Table 2 lists the values of E_2 for intermediate values of R.

Table 2. $E_2 \times 10^{-4}$ (Ryd)

R	4	5	6	7	8	9	10
E_2 (Unsöld)	290	93·8	40·8	20·9	11·9	7·30	4·73
E_2 (Improved)	264	88·7	39·4	20·4	11·7	7·20	4·68
E_2 (Exact)	233	85·7	38·8	20·3	11·6	7·17	4·66

The problem of a helium atom perturbed by a proton was also investigated. Here $(100|V|210)^2/E_{100}-E_{210}$ contributes 20% of E_2 at $R=4$ A.U. and a maximum of 25% for large values of R. The exact calculation of this term had very little effect on the Unsöld series. This is essentially due to the stronger effective nuclear force field and to the larger energy gap between the ground and excited states.

Physics Department,
University of North Carolina,
Chapel Hill, North Carolina.
1st September 1959.

H. L. Kyle.†
E. Merzbacher.

Dalgarno, A., and Lewis, J. T., 1955, *Proc. Roy. Soc.* A, **233**, 70.
—— 1956, *Proc. Phys. Soc.* A, **69**, 57.
Unsöld, A., 1927, *Z. Phys.*, **43**, 563.

† Now with the National Aeronautics and Space Administration, Washington, D.C.

REVIEWS OF BOOKS

General Circuit Theory, by GORDON NEWSTEAD. Methuen Monographs. Pp. vii + 144. (London: Methuen, 1959.) 15*s*.

This book is concerned, essentially, with electric *circuit* theory and it starts directly with the concept of a two-terminal impedance Z. The origins of this concept, in Maxwell's field equations, is not considered, nor is the conversion of a field problem to a topological (circuit) problem investigated and justified. A further restriction is made, inasmuch as the steady-state impedance $Z(j\omega)$ is taken as the starting-point, and not the differential equations of electric fields or even of circuits.

These could well be points of criticism but, on second thoughts, they are perhaps justified here; for this is a short monograph and, presumably, intended as a brief and practical guide through the subject—which is, after all, *circuits*.

But the lack of a fundamental approach has led the author into a number of serious omissions and limitations. For example, dealing with electro-mechanical analogies, he lists only one set; namely ' voltage ' analogous to ' force ', ' current ' to ' velocity ', etc. The dual analogy is omitted. It is curious how this widely-held belief persists—that there is only one set of analogies (inductance–mass, for example, forgetting that the dual, capacity–mass, holds an equal claim). For electricity and mechanics are quite distinct ' worlds ' and in the Lagrangian function $(T-U)$ either the kinetic energy T *or* the potential energy U can be assumed to correspond to magnetic energy.

Even though we accept restriction to circuits here, surely the Principle of Duality deserves a most prominent place? But it is not listed in the Index.

A considerable part of this book concerns four-terminal circuit theory and contains the conventional, classical, theory of such circuits and their interactions when connected together.

The latter half of the text concerns circuits *not* in the steady state and, continuing with the steady-state impedance concept as fundamental, the approach is that of Fourier transforms, followed by Laplace transforms. It is true that circuit theory forms an admirable means of illustrating the theory of functions of a complex variable, and this the author does well. He refers also to the analogy with potential theory (leading to the electrolytic tank analogue computor), the origins of which go right back to Felix Klein in 1881.

The book ends with a chapter of 10 pages on the subject of non-linear circuits—and what can be said in such a short space? The author wisely restricts himself to sketching certain approximation methods. He also repeats that common saying: " No general theory of non-linear circuits has been developed." In one sense this is true: but there have been a number of general theorems produced relevant to non-linear circuits.

Remembering that this is a *monograph*, it will be of use mainly to those people already thoroughly grounded in electricity and magnetism, and in electromagnetic field theory. COLIN CHERRY.

Transistor Electronics, by A. W. LO, R. O. ENDRES, J. ZAWELS, F. D. WALDHAUER and C-C. CHENG. Pp. xii + 521. (London: Macmillan, 1958.) 45*s*.

The Macmillan edition of ' Lo *et al.*' is identical with the original version, first published in 1955. To workers in the fields of transistor circuits and device electronics it is a long-familiar friend; of the many books now available on transistors it is one that has stood the test of time remarkably well and is likely to be of value for some time to come. The reasons for the wide regard earned by the book are to be found in its broad yet basic coverage of most aspects of the transistor field. It still gives perhaps the best introduction both to transistor circuits and to the simpler aspects of device theory.

The book begins with a simple presentation of semiconductor properties, p–n junction theory and transistor action, including some indication of device construction. Of necessity, recent developments such as the drift transistor and four-layer structures are not included. A comprehensive treatment is then given of the d.c. characteristics, small signal parameters and low-frequency equivalent circuits of transistors, followed by a systematic analysis of transistor amplifier configurations in active four-pole terms, and some discussion of noise considerations. Practical amplifiers are treated in detail: after analysis of d.c. biasing requirements, low-frequency small- and large-signal amplifiers are examined at some length, with particular attention paid to methods of inter-stage coupling. A central feature in the book in the presentation of the high-frequency properties of transistors in terms of the ' physical ' equivalent circuit representation of the various frequency dependent mechanism. At the time of writing this material was a major contribution to transistor circuit theory and, although there have since been extensive further developments, it still stands as a basic work of reference and gives a good introduction to such aspects of the transistor. The three concluding chapters are on oscillators, modulation and demodulation, and pulse circuits. The last is now of little but historical interest, being concerned mainly with point-contact transistors; only a sketchy treatment of the transient switching properties of junction transistors is included.

The book can be recommended to the beginner as a good introduction to the more basic aspects of transistors and transistor circuits. It is also a useful reference on equivalent circuit representation of the device and on active four-pole analysis as applied to the transistor. Despite the number of contributing authors the presentation is uniformly good, systematic and readable, and it is well illustrated throughout. A. R. BOOTHROYD.

An Introduction to the Kinetic Theory of Gases, by SIR JAMES JEANS. Pp. vi + 311. (Cambridge: University Press, 1959.) 17*s*. 6*d*.

The volume under review is a paper-backed edition of the original, which was published in 1940. It contains a simplified version of the well-known Dynamical Theory of Gases, the emphasis being on the physical rather than the mathematical side. Apart from an account of experimental measurements of the Maxwellian distribution in gases, it does not depart in essence from the original treatise in being essentially classical in outlook—the word ' quantum ' does not appear in the index. It remains however, a valuable book, within its chosen terms of reference, and the appearance of a cheap edition will be widely welcomed. M. BLACKMAN.

Nuclear Reactor Physics, by R. L. MURRAY. Pp. xi + 317. (London: Macmillan, 1959.) 30*s*.

This book by Murray was first published in the United States two years ago and now appears at about half the American price as an edition printed in Europe. This considerable reduction is welcome and it will be interesting to see if the practice becomes more widespread. It may introduce a certain reluctance to buy new American books at their home price, but even this could be good if it produced a more rapid introduction of the European rate.

For people familiar with Murray it is sufficient to state that the new printing is identical with the old one in all detail except possibly the quality of the paper. For prospective new readers, a few words about the contents may not be out of place. It provides a useful introduction to those calculations in reactor design which are concerned with the production and loss of neutrons. The early chapters deal with the elements of neutron behaviour in moderators and in multiplying media. Neutron currents and fluxes are introduced, together with the elementary features of slowing down and diffusion; one-group diffusion theory is used to illustrate calculations of critical-mass and flux distributions. A chapter on the heterogeneous reactor is followed by one on two-group diffusion theory and there is also some discussion of the influence of temperature on neutron multiplication. It is, of course, very well known that the delayed neutrons from fission play an important part in settling the way a reactor behaves following a change in the amount of neutron absorption. Murray gives the differential equations for a few operational cases and mentions also the use of electrical circuits for the simulation of reactor behaviour. There is no doubt that simulators of electrical and other types are most valuable instructional tools for reactor engineers and physicists and any discussion of these instruments is to be encouraged. The book ends with a chapter on transport theory and one on multi-group methods of calculation. These chapters are, to some extent, away from the main theme but serve a useful purpose in indicating, and no more is required in an introductory book, the more complex methods of calculation which call for the use of electronic computers.

In this book, Professor Murray has presented an attractive introduction to neutron calculations. He does not claim more than this and readers wanting information on basic nuclear ideas or on the materials and thermodynamic aspects must look elsewhere. J. WALKER.

Cryogenic Engineering, by R. B. SCOTT. Pp. xi + 368. (Princeton, New Jersey, Toronto, London, New York: Van Nostrand, 1959.) 42*s*.

The author of this book is well known as the head of the U.S. Bureau of Standards Cryogenic Engineering Laboratory at Boulder, Colorado, where he has been concerned with the development of equipment for the liquefaction and storage of hydrogen on a gigantic scale. His book contains impressive sections on the Boulder liquefiers, capable of an output of 320 litres of liquid hydrogen an hour, and on transport vessels of 5000 litres capacity, but in the main his concern is with ordinary laboratory work. His outlook is thoroughly practical —the first paragraph in the section on 'Leak hunting and repairing' is headed 'Determining that a leak exists'—and there are many detailed drawings of such things as valves and vacuum seals for low temperatures. The final chapters on the properties of cryogenic fluids and of structural materials contain many useful tables and graphs.

The book suffers a little from the attempt to provide something for everybody. It is unlikely that many readers will need to be told how a rotary pump or a McLeod gauge works. Nevertheless, this is a very useful book, as much for readers in this country as in the United States. There is much to be learnt from modern American technique, with its emphasis on well-engineered apparatus which can be assembled and taken to pieces easily and quickly. A. H. COOKE.

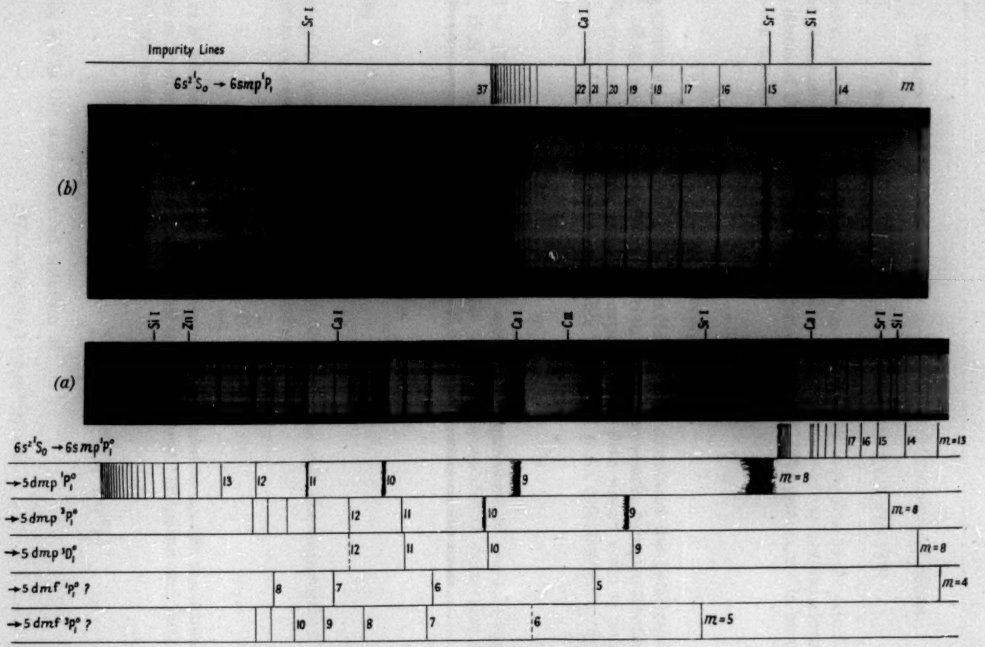

Barium vapour absorption spectrum.

(*a*) showing s*m*p $^1P_1$ and doubly-excited series. (*b*) showing intensity peculiarities in the region of the $Ba^+\,{}^2S_{1/2}$ limit.

Atomic Polarizabilities

By D. PARKINSON
Department of Applied Mathematics, The Queen's University of Belfast

Communicated by D. R. Bates; *MS. received* 13*th August* 1959

Abstract. An antisymmetrical Hartree approximation is applied to the calculation of the polarizabilities of lithium and beryllium and of various ions iso-electronic with atoms of the second row of the periodic table. The results are in harmony with the available experimental data.

---

§ 1. INTRODUCTION

RECENTLY Dalgarno and Parkinson (1959) have calculated the polarizabilities of the neutral atoms from boron to neon, their results being in satisfactory agreement with the available experimental data which refer to oxygen, nitrogen and neon. It seems desirable to extend their calculations to further systems.

§ 2. THEORY

The Hartree self-consistent field method is equivalent to the assumptions that, if H is the Hamiltonian operator and E_0 the associated eigenvalue of an N-electron system, the operator $(H-E_0)$ can be written in the form

$$(H-E_0)=\sum_{i=1}^{N}(H_i-\epsilon_0^{\,i}) \qquad \ldots\ldots(1)$$

where

$$H_i=-\tfrac{1}{2}\nabla_i^2+V_i(\mathbf{r}_i), \qquad \ldots\ldots(2)$$

$\mathbf{r}_i$ being the position vector of the ith electron, and that the unperturbed wave function ψ_0 can be written as the product

$$\psi_0=\prod_{i=1}^{N} u_i^{(0)}(a^i) \qquad \ldots\ldots(3)$$

where a^i denotes the set of quantum numbers required to specify the orbital $u_i^{(0)}$. Then according to the antisymmetrical approximation (Dalgarno and Parkinson 1959), the polarizability is given by

$$\alpha=2\sum_{i=1}^{N}\left\{(u_i^{(0)},h_iu_i^{(1)})-\sum_{i\neq j}(u_i^{(0)},h_iu_j^{(0)})(u_i^{(1)},u_j^{(0)})\right\} \qquad \ldots\ldots(4)$$

where $u_i^{(1)}$ is the well-behaved solution of

$$(H_i-\epsilon_0^{\,i})u_i^{(1)}(\mathbf{r}_i)+h_iu_i^{(0)}(\mathbf{r}_i)=0 \qquad \ldots\ldots(5)$$

and $h_i=r_i\cos\theta_i$. Writing the quantum numbers a^i more explicitly as (nlm) and putting $u_i^{(0)}$ and $u_i^{(1)}$ in the forms

$$u_i^{(0)}(nlm)=R_{nl}(r_i)\Theta_{l,m}(\boldsymbol{\theta}_i) \qquad \ldots\ldots(6)$$

$$u_i^{(1)}=2\left\{\frac{(l+1+m)(l+1-m)}{(2l+3)(2l+1)}\right\}^{1/2} R_{nl}^{+}(r_i)\Theta_{l+1,m}(\theta_i)$$
$$+2\left\{\frac{(l+m)(l-m)}{(2l+1)(2l-1)}\right\}^{1/2} R_{nl}^{-}(r_i)\Theta_{l-1,m}(\theta_i) \qquad \ldots\ldots(7)$$

where $\Theta_{l,m}$ are spherical harmonics as defined by Condon and Shortley (1935), equation (5) separates into a pair of uncoupled differential equations

$$\left\{\frac{d^2}{dr_i^2}+\frac{2}{r_i}\frac{d}{dr_i}+V_i(r_i)-\frac{(l+1)(l+2)}{r_i^2}-\epsilon_0^i\right\}R_{nl}^{+}(r_i)=r_iR_{nl}(r_i) \qquad \ldots\ldots(8)$$

$$\left\{\frac{d^2}{dr_i^2}+\frac{2}{r_i}\frac{d}{dr_i}+V_i(r_i)-\frac{l(l-1)}{r_i^2}-\epsilon_0^i\right\}R_{nl}^{-}(r_i)=r_iR_{nl}(r_i), \qquad \ldots\ldots(9)$$

V_i and ϵ_0^i being defined by the equation

$$\left\{\frac{d^2}{dr_i^2}+\frac{2}{r_i}\frac{d}{dr_i}+V_i(r_i)-\epsilon_0^i\right\}R_{nl}(r_i)=0. \qquad \ldots\ldots(10)$$

The equations may be solved by numerical integration (Sternheimer 1954).

§ 3. CALCULATIONS

Polarizabilities have been determined for all ions for which Hartree–Fock wave functions are available and which are iso-electronic with atoms of the second row of the periodic table. They comprise C^{2+} (Jucys 1939), N^-, Na^+ (Hartree and Hartree 1948), $O^{-,+,2+,3+}$ (Hartree, Hartree and Swirles 1940), Ne^{2+} (Garstang 1951), $Ne^{3+,4+}$ (Froese and Hartree 1957), Mg^{2+} (Yost 1940), F^-, Al^{3+} (Froese 1957), Si^{4+} (Hartree, Hartree and Manning 1941) and Ne^+ (obtained by Dr. M. J. Seaton by interpolation). In addition polarizabilities have been determined for Li and Be, adopting for Li the analytic wave function of Morse, Young and Haurwitz (1935) and for Be the Hartree–Fock wave functions of Hartree and Hartree (1935).

For the computation of V_i from (10) the Hartree–Fock orbitals R_{nl} were fitted by sums of products of polynomials and exponential functions using the technique of Appel and Löwdin (1956). The solutions $R_{nl}^{\pm}(r)$ of (8) and (9) which satisfy the boundary conditions

$$R_{nl}^{\pm}(0)=0, \qquad R_{nl}^{\pm}(\infty)\simeq\exp\{-(2|\epsilon_0^i|)^{1/2}r\} \qquad \ldots\ldots(11)$$

were then obtained by numerical integration using the Runge–Kutta method. The integration was started at a large radius r_0 according to

$$R_{nl}^{\pm}(r_0)=C\exp\{-(2|\epsilon_0^i|)^{1/2}r_0\} \qquad \ldots\ldots(12)$$

$$\left[\frac{d}{dr}R_{nl}^{\pm}(r)\right]_{r_0}=-(2|\epsilon_0^i|)^{1/2}C\exp\{-(2|\epsilon_0^i|)^{1/2}r_0\} \qquad \ldots\ldots(13)$$

and the constant C was determined by an interpolation method which ensures the correct behaviour of the solution at the origin and which makes use of a series of inward integrations. The procedure was tested for the cases of hydrogen, which may be solved analytically, and of helium, which may be solved variationally (Wikner and Das 1957, Dalgarno 1959). These tests showed that the solutions possessed a large degree of stability. All computations were performed with the DEUCE computer of Short Brothers and Harland, Belfast, using floating point methods.

The use of Hartree–Fock orbitals in the calculations of V_i introduces a difficulty as V_i may then be discontinuous at a node of R_{nl}. When this occurred

Table 1. Atomic Polarizabilities in units of $10^{-24}\,\text{cm}^3$†

	Nucleus									
Configuration	Boron	Carbon	Nitrogen	Oxygen	Fluorine	Neon	Sodium	Magnesium	Aluminium	Silicon
s^2p	5·1 5·9			*0·30* *0·29*						
s^2p^2		2·1 3·1		*0·34* *0·33*		*0·10* *0·068*				
s^2p^3			1·3 1·2	0·49 0·53		0·13 0·12				
s^2p^4			4·3 4·4	0·89 1·0		0·15 0·16				
s^2p^5				3·2 3·3		0·21 0·21				
s^2p^6					1·8 1·7	0·40 0·36	0·16 0·17‡	0·082 0·077	0·045 0·049	0·027 0·031

† The values in italics are uncertain.

‡ Sternheimer (1954) has computed a value of 0·145 from the non-exchange formula (4).

V_i was smoothed through the discontinuity. The error introduced by this procedure should not be significant except in the cases of highly stripped atoms where the 2s contribution is dominant. The values of O^{2+}, O^{3+} and Ne^{4+} are consequently rather uncertain. The difficulty can only be overcome by using a much more complicated complete Hartree–Fock treatment (Dalgarno 1959).

The results of the calculations are collected in table 1 in which are reproduced also the values for the neutral atoms calculated by Dalgarno and Parkinson. The upper value in each pair is that given by equation (4) and the lower value is that given by

$$\alpha = 2 \sum_{i=1}^{N} (u_i^{(0)}, h_i u_i^{(1)}) \qquad \ldots\ldots (14)$$

which follows from (4) if the exchange terms are ignored.

Formulae (4) and (14) are identical when the atom contains only s shells.

§ 4. Discussion

Examination of table 1 shows that there is little difference between the values obtained from equations (4) and (14) and so some cancellation of error must be occurring in the non-exchange case. A similar result was obtained by Dalgarno and Parkinson (1959). It appears probable therefore that the neglect by Sternheimer (1954) of the effect of exchange on the perturbed orbitals is not important. However, as Buckingham (1937) remarked, it is important to include the effect of exchange on the unperturbed orbitals, at least in the case of the neutral atoms and negative ions. Thus using unperturbed Hartree orbitals, Sternheimer (1954) obtains 3·20 Å^3 for F^- and 0·050 Å^3 for Al^{3+} compared with the values of 1·8 Å^3 and 0·045 Å^3 obtained here using unperturbed Hartree–Fock orbitals.

Table 2. The Polarizabilities of the Neon Iso-electronic Sequence in units of 10^{-24} cm^3

Atom	F^-	Ne	Na^+	Mg^{2+}	Al^{3+}	Si^{4+}
Measured	—	0·40†	0·17‡	0·10‡	0·053‡	—
Calculated	1·8	0·40	0·16	0·082	0·045	0·027

† Cuthbertson and Cuthbertson (1932).

‡ Mayer and Mayer (1933). (The value given by Mayer and Mayer for Al^{3+} is 0·53, which is clearly a misprint.)

Table 2 lists the experimental and theoretical values for the neon iso-electronic sequence. The agreement is very satisfactory. It is interesting to note that the crystal refractivities of Tessman, Kahn and Shockley (1953) are all smaller than those obtained for the free state (cf. Dick and Overhauser 1958), the difference being greater for the negative ion.

Table 3. The Polarizability of Lithium in units of 10^{-24} cm^3

Reference	α
Fues	27
Scheffers and Stark	12
Drechsler and Müller	16 ± 3
Sundbom	20
Dalgarno and Kingston	24·4
Parkinson	25·0

Experimental values for lithium have been derived by Scheffers and Stark (1934) using a molecular beam method, by Fues (1933) from measurements of the

Stark effect and by Drechsler and Müller (1952) from field emission electron microscope measurements. They are listed in table 3 which includes also the results of theoretical calculations by Sundbom (1958) and by Dalgarno and Kingston (1959). Since the antisymmetrizing procedure has no effect in the case of s-electrons, the method used by Sundbom is equivalent to that used in the present paper, the discrepancy arising from the different analytic representations employed for the unperturbed orbitals. The value given by Dalgarno and Kingston, which is based upon theoretical and experimental oscillator strengths and is probably the most reliable, is in excellent agreement with the value obtained here and suggests that the inherent accuracy of the method warrants considerable care in the choice of analytic representations.

There are no experimental data for beryllium but using his approximate formulae, Buckingham (1937) has computed a value of 9·3 Å^3 in harmony with the present value of 9·6 Å^3. However using a different formula, Knipp (1939) obtains a value of 4·1 Å^3. The magnitude of the discrepancy suggests that the polarizability of beryllium may be very sensitive to the effect of exchange.

ACKNOWLEDGMENTS

The author is grateful to Dr. A. Dalgarno for many stimulating discussions during the course of the work.

The research reported has been sponsored by the Air Force Cambridge Research Center, Geophysics Research Directorate, of the Air Research and Development Command, U.S. Air Force, through its European Office, under Contract No. AF 61(052)-131.

REFERENCES

APPEL, K., and LÖWDIN, P. O., 1956, *Phys. Rev.*, **103**, 1746.
BUCKINGHAM, R. A., 1937, *Proc. Roy. Soc.* A, **160**, 94.
CONDON, E. U., and SHORTLEY, G. H., 1935, *The Theory of Atomic Spectra* (Cambridge : University Press).
CUTHBERTSON, C., and CUTHBERTSON, M., 1932, *Proc. Roy. Soc.* A, **135**, 40.
DALGARNO, A., 1959, *Proc. Roy. Soc.* A , **251**, 282.
DALGARNO, A., and KINGSTON, A. E., 1959, *Proc. Phys. Soc.*, **73**, 455.
DALGARNO, A., and PARKINSON, D., 1959, *Proc. Roy. Soc.* A, **250**, 422.
DICK, D. G., and OVERHAUSER, A. W., 1958, *Phys. Rev.*, **112**, 90.
DRECHSLER, M., and MÜLLER, E. W., 1952, *Z. Phys.*, **132**, 195.
FROESE, C., 1957, *Proc. Camb. Phil. Soc.*, **53**, 206.
FROESE, C., and HARTREE, D. R., 1957, *Proc. Camb. Phil. Soc.*, **53**, 663.
FUES, E., 1933, *Z. Phys.*, **82**, 536.
GARSTANG, R. H., 1951, *Proc. Camb. Phil. Soc.*, **47**, 243.
HARTREE, D. R., and HARTREE, W., 1935, *Proc. Roy. Soc.* A, **150**, 9.
—— 1948, *Ibid.*, **193**, 299.
HARTREE, D. R., HARTREE, W., and MANNING, M. F., 1941, *Phys. Rev.*, **60**, 857.
HARTREE, D. R., HARTREE, W., and SWIRLES, B., 1940, *Phil. Trans. Roy. Soc.* A, **238**, 229.
JUCYS, C. A., 1939, *Proc. Roy. Soc.* A, **173**, 59.
KNIPP, J. K., 1939, *Phys. Rev.*, **55**, 1244.
MAYER, P. M., and MAYER, M. G., 1933, *Phys. Rev.*, **43**, 605.
MORSE, P. M., YOUNG, L. A., and HAURWITZ, E. S., 1935, *Phys. Rev.*, **48**, 948.
SCHEFFERS, H., and STARK, J., 1934, *Phys. Z.*, **35**, 625.
STERNHEIMER, R. M., 1954, *Phys. Rev.*, **96**, 951.
SUNDBOM, M., 1958, *Ark. Fys.*, **13**, 539.
TESSMAN, J. R., KAHN, A. H., and SHOCKLEY, W., 1953, *Phys. Rev.*, **92**, 890.
WIKNER, E. G., and DAS, T. P., 1957, *Phys. Rev.*, **107**, 497.
YOST, W. J., 1940, *Phys. Rev.*, **58**, 557.

The Anisotropy of the Conductivity of Hot Electrons and their Temperature in Germanium

By E. G. S. PAIGE
Royal Radar Establishment, St. Andrew's Road, Malvern, Worcs.

MS. received 23rd July 1959, *in revised form 14th September* 1959

Abstract. By making certain simplifying assumptions a method of analysing the anisotropy of the conductivity of electrons in germanium at high electric fields is presented. The method is applied to Koenig's data on a specimen having a free carrier concentration of $6\cdot5\times10^{14}\,\mathrm{cm}^{-3}$. The electron temperatures in each valley are obtained and the mobility and population of carriers within the valleys are calculated. These electron temperatures are compared with electron temperatures calculated from an energy balance equation applied to each valley as though it existed independently of the other valleys. The comparison shows that there is interaction between electrons in different valleys. Estimates are made of the rate of energy transfer between valleys.

---

§ 1. INTRODUCTION

In a recent note, Koenig (1959) has reported measurements on n-type germanium of the field dependence of the angle ϵ between the current density j and the electric field E for high electric fields. His observations extend those of Sasaki, Shibuya and Mizuguchi (1958) to lower resistivity samples. In particular it was shown that anisotropy occurs in a crystal at a lattice temperature of 77°K having a free carrier concentration of $6\cdot5\times10^{15}\,\mathrm{cm}^{-3}$. This implied that the mean energies of carriers in different valleys were not the same despite the effects of electron–electron collisions. As Koenig pointed out, this invalidated the interpretation of the experiment performed by the author (Paige 1958) to measure the electron temperature using the piezoresistance effect. In the interpretation it was necessary to assume that sufficient electron–electron scattering took place ($n=2\cdot5\times10^{15}\,\mathrm{cm}^{-3}$) to ensure that the free carriers had a single Maxwellian distribution.

The purpose of this paper is to demonstrate a method of analysis, using Koenig's anisotropy measurements, which enables the effective temperature of electrons in different valleys to be calculated. From this information the population and mobility of carriers in the individual valleys can be obtained. The results of the analysis applied to a specimen having a free carrier concentration of $6\cdot5\times10^{14}\,\mathrm{cm}^{-3}$ are presented. The variation of electron temperature with field obtained from the analysis is compared with that predicted by Stratton's (1958) theory applied to individual valleys. It is concluded that there is a significant interaction between electrons in different valleys. An estimate of the rate of energy transfer from electrons in one valley to electrons in another is obtained and compared with the theoretical estimate of Fröhlich and Paranjape (1956).

§ 2. THE ANISOTROPY OF THE CONDUCTIVITY OF HOT ELECTRONS

The origin of the anisotropic effects of hot electrons observed by Sasaki, Shibuya and Mizuguchi (1958) and Koenig (1959) is believed to be due to differences in the rate of power absorbed by electrons localized in different valleys. Sasaki *et al.* point out that as a result the mean energy of electrons within a valley is not the same for all valleys. This has two consequences: (i) the mobility relaxation times are no longer the same in all valleys, since the relaxation time is energy dependent, and (ii) the concentrations of electrons in the valleys are not equal because the probability of an intervalley transition is also energy dependent.

2.1. *The Effect of Electron–Electron Collisions*

We will consider the effect of electron–electron collisions on the anisotropy experiment for three ranges of electron concentration:

(1) High electron concentrations: Interelectronic collisions are sufficiently numerous for the energy distribution of the electrons to be Maxwellian and the same for all valleys.

(2) Low electron concentrations: The distribution function is not affected by interelectronic collisions. It departs from Maxwellian and in general differs from one valley to another.

(3) Electron concentrations intermediate between (1) and (2): The distribution within each valley is Maxwellian but the valleys are characterized by different electron temperatures.

For electron concentrations in range (1) no anisotropy would be observed, while for electron concentrations in ranges (2) and (3) anisotropy would appear.

Range (3) is thought to exist because the acceleration due to the electric field is the same for all electrons within one valley but differs between valleys. Furthermore, due to differences in the Bloch functions of electrons in different valleys, it is feasible that the interaction between electrons localized in different valleys may be less than the interaction between electrons localized in the same valley.

In the following analysis we shall assume that the distribution of electrons within each valley is Maxwellian, that is the electron concentration is in range (3).

While the actual distribution within a valley may depart from a Maxwellian distribution it is unlikely that these departures will be so significant as to render the results of the present analysis meaningless.

2.2. *The Temperatures of Electrons in Individual Valleys*

For n-type germanium, with the electric field in the ⟨100⟩ direction, the power absorbed from the field in each of the four valleys is equal, hence their electron temperatures will be the same. In the anisotropy experiment the field was applied at an angle θ to the [001] direction in the (110) plane. Sasaki, Shibuya and Mizuguchi (1958) found that the anisotropy was a maximum for $\theta = 30°$. For this direction of applied field and for low fields the ratios of power absorbed in the 111 valley to that in the $\bar{1}11$, $1\bar{1}1$ and $11\bar{1}$ valleys is 1:3·6, 3·6, 4·6 respectively. This estimate is based on an isotropic relaxation time and $m_{\parallel}/m_{\perp} = 20$, where $m_{\parallel}$ and $m_{\perp}$ are the effective masses parallel to and perpendicular to the symmetry axis of the ellipsoidal constant energy surface. For high fields, because the population of the 111 valley is increased relative to the other valleys and because the relaxation time within this valley is high compared with that in other valleys, **E** tends towards the 111 direction—a direction in which the power absorbed in the $\bar{1}11$, $1\bar{1}1$, $11\bar{1}$ valleys is identical. We see, therefore, that it is not unreasonable to assume that the power dissipation in the $\bar{1}11$, $1\bar{1}1$ and $11\bar{1}$ valleys is the same for all fields. This leads to a complete description of the electron distribution by two electron temperatures—the low temperature being associated with the distribution in the 111 valley, the high temperature being associated with the distribution in the other three valleys. It will be seen that the assumptions regarding the Maxwellian distribution of the electrons in valleys coupled with the assumption that three valleys are at the same temperature are basic to the simple method of analysis of the anisotropic experiment to be presented.

§ 3. THE ANALYSIS OF THE ANISOTROPY EXPERIMENT

In the anisotropy experiment two pieces of information are obtained on a specimen at a given field. They are the conductivity measured parallel to the filament σ_{p} and the anisotropy angle ϵ. In this section we shall relate σ_{p} and ϵ to $\sigma_{\perp\mathbf{l}}$ and $\sigma_{\perp\mathbf{h}}$, where $\sigma_{\perp}$ is the conductivity of a single valley for the electric field vector perpendicular to the symmetry axis of the ellipsoidal constant energy surface and **l** and **h** label low and high temperature valleys respectively. This notation for referring to the low and high temperature valleys will be used throughout this paper.

Referred to a 100, 010, 001 coordinate system the symmetrical mobility tensor, $\mu_{\alpha\beta}$, has the elements shown in table 1 for the four valleys. The current density due to electrons in the *i*th valley has components

$$j_{\alpha}{}^{i} = qn_i \sum_{\beta} \mu_{\alpha\beta}{}^{i} E_{\beta}$$

where q is the electronic charge and n_i is the concentration of free carriers in the *i*th valley.

Table 1

Valley	μ_{11}	μ_{22}	μ_{33}	μ_{12}	μ_{13}	μ_{23}
l 111	λ	λ	λ	γ	γ	γ
h $\bar{1}11$	λ	λ	λ	$-\gamma$	$-\gamma$	γ
h $1\bar{1}1$	λ	λ	λ	$-\gamma$	γ	$-\gamma$
h $11\bar{1}$	λ	λ	λ	γ	$-\gamma$	$-\gamma$

$$\lambda = \tfrac{1}{3}(\mu_{\parallel} + 2\mu_{\perp}), \quad \gamma = \tfrac{1}{3}(\mu_{\parallel} - \mu_{\perp})$$

The contribution of all four valleys to the current density is

$$J_{\alpha} = \sum_{i} j_{\alpha}{}^{i} = q \sum_{\beta} \sum_{i} n_i \mu_{\alpha\beta}{}^{i} E_{\beta}. \qquad \ldots\ldots(1)$$

Referring to the [100], [010] and [001] components as 1, 2, 3 and using the form of $\mu_{\alpha\beta}$ given in table 1, and taking the $\bar{1}11$, $1\bar{1}1$ and $11\bar{1}$ valleys to be at the same temperature we have from equation (1)

$$\begin{aligned} J_1 &= q\{(n_{\mathbf{l}}\lambda_{\mathbf{l}} + 3n_{\mathbf{h}}\lambda_{\mathbf{h}})E_1 + (n_{\mathbf{l}}\gamma_{\mathbf{l}} - n_{\mathbf{h}}\gamma_{\mathbf{h}})(E_2 + E_3)\}, \\ J_2 &= q\{(n_{\mathbf{l}}\lambda_{\mathbf{l}} + 3n_{\mathbf{h}}\lambda_{\mathbf{h}})E_2 + (n_{\mathbf{l}}\gamma_{\mathbf{l}} - n_{\mathbf{h}}\gamma_{\mathbf{h}})(E_1 + E_3)\}, \qquad \ldots\ldots(2) \\ J_3 &= q\{(n_{\mathbf{l}}\lambda_{\mathbf{l}} + 3n_{\mathbf{h}}\lambda_{\mathbf{h}})E_3 + (n_{\mathbf{l}}\gamma_{\mathbf{l}} - n_{\mathbf{h}}\gamma_{\mathbf{h}})(E_1 + E_2)\}. \end{aligned}$$

For the particular geometry that Sasaki, Shibuya and Mizuguchi (1958) used the components of current are

$$J_3 = J\cos\theta, \; J_1 = J_2 = J\sin\theta\cos 45^{\circ}, \qquad \ldots\ldots(3)$$

since the current is restricted to flow parallel to the filament; θ is the angle defined above and J is the total current density flowing in the filament. Since $J_1 = J_2$, it follows from equation (2) that $E_1 = E_2$. The components of the field are

$$E_3 = \cos(\theta+\epsilon)\frac{E_p}{\cos\epsilon}, \quad E_1 = E_2 = \sin(\theta+\epsilon)\frac{E_p}{\cos\epsilon}\cos 45°. \qquad \ldots\ldots (4)$$

Here E_p is the field measured parallel to the filament and is related to the total field in the specimen by $E_p = E\cos\epsilon$ and to the conductivity parallel to the filament by $\sigma_p = J/E_p$. We introduce the parameters x and y defined by

$$x = q[n_l\lambda_l + 3n_h\lambda_h]\left(\frac{\mu_\perp}{\lambda}\right) = \sigma_{\perp l} + 3\sigma_{\perp h},$$

$$\ldots\ldots (5)$$

and

$$y = q[n_l\gamma_l - n_h\gamma_h]\left(\frac{\mu_\perp}{\gamma}\right) = \sigma_{\perp l} - \sigma_{\perp h}.$$

Substituting x and y in equation (2) and for J and E using equations (3) and (4), and rearranging we have

$$y = \frac{c_2\sigma_p\cos\epsilon\cos 45°[\sin\theta - \cos\theta\tan(\theta+\epsilon)]}{\cos(\theta+\epsilon) + \sin(\theta+\epsilon)\{\cos 45° - \tan(\theta+\epsilon)\}} \qquad \ldots\ldots (6)$$

and

$$x = \frac{c_1}{c_2\cos(\theta+\epsilon)}[c_2\sigma_p\cos\theta\cos\epsilon - 2y\sin(\theta+\epsilon)\cos 45°], \qquad \ldots\ldots (7)$$

where

$$c_1 = \mu_\perp/\lambda, \text{ and } c_2 = \mu_\perp/\gamma. \qquad \ldots\ldots (8)$$

For an isotropic relaxation time

$$c_1 = 3(\mu_\parallel/\mu_\perp + 2)^{-1} = 1{\cdot}46 \text{ and } c_2 = 3(\mu_\parallel/\mu_\perp - 1)^{-1} = 3{\cdot}16,$$

c_1 and c_2 are independent of temperature except when two or more scattering processes are occurring, at least one of which has an anisotropic momentum relaxation time. An example in which this occurs is mentioned below; we shall treat c_1 and c_2 as independent of temperature.

From equations (5), (6), (7) and (8) $\sigma_{\perp l}$ and $\sigma_{\perp h}$ can be obtained in terms of the measured parameters σ_p and ϵ. We shall now obtain $\sigma_{\perp l}$ and $\sigma_{\perp h}$ in terms of the temperatures of electrons, T_l and T_h.

The free carrier concentrations in the low and high temperature valleys are given by

$$n_l = \tfrac{1}{3}N\langle 1/\tau_h\rangle[\langle 1/\tau_l\rangle + \tfrac{1}{3}\langle 1/\tau_h\rangle]^{-1}, \qquad \ldots\ldots (9)$$

$$n_h = \tfrac{1}{3}N\langle 1/\tau_l\rangle[\langle 1/\tau_l\rangle + \tfrac{1}{3}\langle 1/\tau_h\rangle]^{-1}, \qquad \ldots\ldots (10)$$

where N is the total concentration of free electrons, $\mathrm{n}_l + 3n_h$. τ is the relaxation time associated with an intervalley transition, and $\langle 1/\tau\rangle$ represents the probability of such a transition per unit time averaged over the electron distribution within the particular valley to which the subscript refers. In obtaining equations (9) and (10) use was made of the fact that τ is several orders of magnitude smaller than the duration of the experimental observation ($\sim 1\ \mu$sec), so we may assume that the populations in the valleys are determined by the steady state equation

$$n_l\langle 1/\tau_l\rangle = n_h\langle 1/\tau_h\rangle$$

since for conditions of interest the transition probability is independent of the occupancy of final states. The energy of the intervalley phonon operative at low temperature has been determined by Weinreich, Sanders and White (1959) to be 0·0273 ev. We evaluate $\langle 1/\tau \rangle$ for a given lattice temperature over a range of electron temperatures using the relation for $\langle 1/\tau \rangle$ given by Herring (1955) for a discrete phonon process. This is then fitted by a simple empirical relation between $\langle 1/\tau \rangle$ and the electron temperature T in certain temperature ranges. Having obtained n_l and n_h in terms of T_l and T_h it remains to write μ_{1l} and μ_{1h} in terms of these two temperatures. For acoustical mode scattering we have

$$\mu_A(T_L, T) = \mu_{0A}(T_L) \left(\frac{T_L}{T} \right)^{1/2} \qquad \ldots\ldots (11)$$

where μ_{0A} is the zero field mobility due to scattering by acoustical modes and T_L the lattice temperature. For ionized impurity scattering

$$\mu_I(T_L, T) = \mu_{0I}(T_L) \left(\frac{T}{T_L} \right)^{3/2} \qquad \ldots\ldots (12)$$

where $\mu_{0I}(T_L)$ is the zero field mobility due to ionized impurity scattering. The relationship for optical mode scattering, which is taken from Stratton (1958), is

$$\mu_o(T_L, T) = \mu_{0o}(T_L) N_o (2 + \gamma_o + \tfrac{1}{4}\gamma_o^2)(\gamma/\gamma_o)^{1/2} A^{-1}. \qquad \ldots\ldots. (13)$$

Here $\gamma_o = \theta_o / T_L$, $\gamma = \theta_o / T$, where θ_o is the optical mode temperature taken as 400°K. N_o, the equilibrium phonon density is $[\exp \gamma_o - 1]^{-1}$ and

$$A = (2 + \gamma + 0{\cdot}25\gamma^2)([N_o + 1]e^{-\gamma} + N_o) + 0{\cdot}25\gamma^2 \exp(\tfrac{1}{2}\gamma) K_1(\tfrac{1}{2}\gamma)([N_o + 1]e^{-\gamma} - N_o),$$

where K_1 is a Bessel function and $\mu_{0o}(T_L)$ is the zero field mobility due to optical phonons.

§ 4. ELECTRON TEMPERATURES DEDUCED FROM THE ANISOTROPY EXPERIMENT—ANALYSIS OF KOENIG'S DATA

In this section the method of deducing electron temperatures from the anisotropy experiment will be applied to Koenig's data on a sample at 77°K and 300°K which had a free carrier concentration of $6{\cdot}5 \times 10^{14}$ cm^{-3}.

4.1. *Lattice Temperature of* 77°K

It is found that at a lattice temperature of 77°K the relation between $\langle 1/\tau \rangle$ and T can be represented by

$$\langle 1/\tau \rangle = 2{\cdot}47 \times 10^8 (T - 90) \text{ sec}^{-1}$$

in the electron temperature range 140°K to 400°K within an error of less than 2%.† The approximation is made that the mobility is given by summing the reciprocals of the mobility for the individual scattering mechanisms.

The following values are used for the zero field mobilities:

$$\mu_{0A} = 3{\cdot}84 \times 10^4 \text{ cm}^2 \text{ v}^{-1} \text{ sec}^{-1}, \quad \mu_{0I} = 7{\cdot}00 \times 10^4 \text{ cm}^2 \text{ v}^{-1} \text{ sec}^{-1}$$
$$\text{and } \mu_{0o} = 6{\cdot}81 \times 10^5 \text{ cm}^2 \text{ v}^{-1} \text{ sec}^{-1}.$$

The zero field lattice mobilities are extrapolations using Stratton's (1958) equations. These incorporate a ratio R of the interaction constant of an optical phonon with an electron to that of an acoustical phonon with an electron of 0·14. The zero field impurity scattering mobility is then determined from $\mu_{0\mathrm{A}}$, $\mu_{0\mathrm{o}}$, and the observed low field mobility.

---

†The interaction constant between the electron and the intervalley phonon, ω_2, is taken as 10^{11} sec^{-1} from the work of Weinreich, Sanders and White (1959). The accuracy with which ω_2 has been determined is low, but since n_l and n_h are independent of the value of ω_2, it is unimportant in this instance.

The solid lines of figure 1 show the variation of valley temperature with the measured field deduced from the analysis. Below 140°K the curves are extrapolated to the lattice temperature at zero field. Figure 2 shows the ratio of the concentration of electrons at a given field to the concentration at zero field for the low temperature valley, n_l/n_0, and for one of the high temperature valleys, n_h/n_0. Also displayed is the ratio of mobility to zero field mobility, as a function of applied electric field, for both types of valley, μ_l/μ_0 and μ_h/μ_0. The curves shown in figure 2 are obtained using the electron temperatures shown in figure 1.

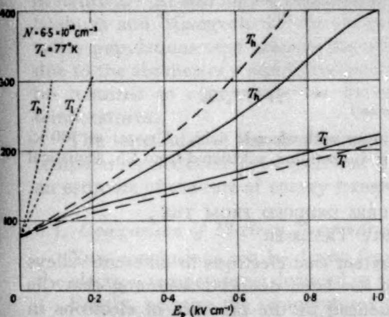

igure 1. The variation of electron temperature with electric field. Crystal at 77°K. Full line, calculated from Koenig's data; dotted line, calculated from § 5, acoustical mode scattering; broken line, calculated from § 5, acoustical plus optical mode scattering.

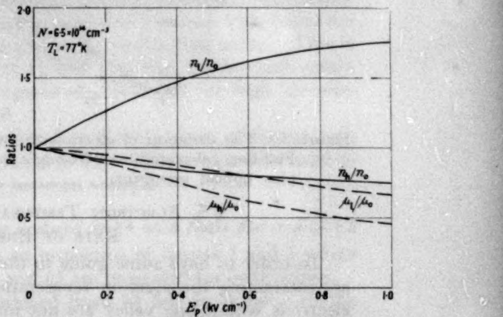

Figure 2. The ratios of the electron concentration and mobility in a valley as a function of field to their values at zero field. Crystal at 77°K.

The anisotropy of the relaxation time of ionized impurity scattering has not been taken into account in the analysis (Ham 1955, Laff and Fan 1958). The anisotropy is in such a direction that it reduces the anisotropy of the mobility arising from the anisotropic mass. The effect of this anisotropy of the relaxation times of ionized impurity scattering, combined with other scattering mechanisms, is to make c_1 and c_2 of equation (8) dependent on T. However, the temperature dependence of c_1 and c_2 is very slight at low T and absent at high T. Incorporation into the analysis only increases the separation of the T_l, T_h curves by a few per cent at low field and has no effect at high fields.

4.2. *Lattice Temperature of* 300°K

The empirical relation between $\langle 1/\tau \rangle$ and T obtained for a lattice temperature of 300°K is $\langle 1/\tau \rangle = 4{\cdot}2 \times 10^9 (T+90)$ sec^{-1}. It gives a fit to the calculated $\langle 1/\tau \rangle$ within an error of 4% in the temperature range of 320°K to 520°K. Using the same procedure as in the 77°K example the values used for the zero field mobilities are:

$$\mu_{0\mathrm{A}} = 4{\cdot}98 \times 10^3 \text{ cm}^2\,\text{v}^{-1}\,\text{sec}^{-1}, \quad \mu_{0\mathrm{o}} = 1{\cdot}97 \times 10^4 \text{ cm}^2\,\text{v}^{-1}\,\text{sec}^{-1}$$
$$\text{and } \mu_{0\mathrm{I}} = 5{\cdot}4 \times 10^5 \text{ cm}^2\,\text{v}^{-1}\,\text{sec}^{-1}.$$

Figure 3 shows the variation of valley temperatures with the measured field. The curves have been extrapolated from 320°K to the lattice temperature at zero field.

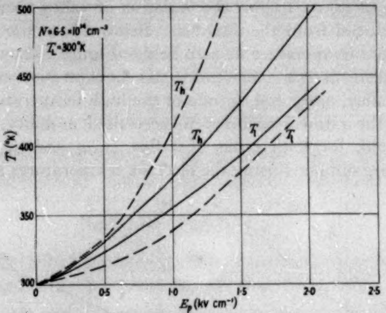

Figure 3. The variation of electron temperature with electric field. Crystal at 300°K. Full line, calculated from Koenig's data; broken line, calculated from § 5, acoustical plus optical scattering.

§ 5. Electron Temperatures deduced from the Rate of Energy Transfer

In order to have some guide to the extent that electrons in different valleys are interacting the electron temperature has been deduced assuming that the electrons within one valley are not influenced by the presence of electrons in other valleys. Stratton (1958) has given the following relation for the balance of rate of energy gain from the field to rate of loss to the acoustical and optical lattice vibrations:

$$\mu E^2 = \frac{3(\gamma_0/\gamma)^{1/2}[ms^2(\gamma_0/\gamma - 1) + \frac{1}{8}Rk\theta_0\gamma_0\gamma \exp(\frac{1}{2}\gamma)\mathrm{K}_1(\frac{1}{2}\gamma)\{(N_0+1)\mathrm{e}^{-\gamma} - N_0\}]}{m\mu_{0\mathrm{A}}} \qquad \ldots\ldots(14)$$

where s is the velocity of longitudinal sound waves, k is Boltzmann's constant, and m is the effective mass of the electron. From this equation a relationship between T and μE^2 can be obtained for a given lattice temperature. We proceed to find the value of μE^2, which is proportional to the rate of energy absorbed, for the individual valleys.

Writing $(\mu E^2)^i q \equiv P^i(E) = q\mathbf{E}\mu^i\mathbf{E}$, where μ^i is the tensor mobility for the ith valley, we have

$$P^i(E) = q[\tfrac{1}{3}(\mu_{\parallel} + 2\mu_{\perp})^i E^2 + 2\{E_1 E_2 \mu_{12}{}^i + E_2 E_3 \mu_{23}{}^i + E_3 E_1 \mu_{31}{}^i\}]. \qquad \ldots\ldots(15)$$

For the specimen orientation used by Koenig, anisotropy angle ϵ and field parallel to the filament E_{p}, equation (15) becomes

$$P^i(E) = E_{\mathrm{p}}{}^2 (\cos\epsilon)^{-2} q \times \{\tfrac{1}{3}(\mu_{\parallel} + 2\mu_{\perp})^i + \sin(\theta+\epsilon)[\sin(\theta+\epsilon)\mu_{12} + 2\sin(\theta+\epsilon)\cos 45°(\mu_{23} + \mu_{31})]\}. \qquad \ldots\ldots(16)$$

Now at a given field $P^i(\epsilon)$ can be calculated for the low temperature valley and one of the high temperature valleys $(1\bar{1}1)$ using equation (16), and the two corresponding temperatures found which satisfy equation (14). These have been plotted as broken lines in both figures 1 and 3. For comparison the valley temperatures deduced assuming that only acoustical mode scattering takes place ($R=0$ in equation (14)) are plotted in figure 1.

§ 6. DISCUSSION

It is apparent from figure 2, which shows the relative effects of valley population and of mobility, that changes in valley populations have an important effect on the overall mobility of a crystal, particularly at low fields. The rate of change of valley population with field decreases as the field increases; this can be seen in figure 2. At still higher fields the anisotropy decreases (Koenig 1959, Sasaki, Shibuya and Mizuguchi 1958). It is clear, then, that at these high fields the valley populations tend towards the normal thermal equilibrium value. This is due to the absence of a rapid divergence of T_h and T_l at high fields which would be required to compensate for the decrease of $d\langle 1/\tau\rangle/dT$ at high electron temperatures.

The remainder of the discussion is centred on a comparison of the electron temperature deduced in § 4 with that deduced in § 5. This comparison leads to an estimate of the rate of energy transfer between valleys.

6.1. *Comparison of Electron Temperatures deduced in* § 4 *with those deduced in* § 5

Two conclusions can be drawn from an inspection of figures 1 and 3 where the electron temperatures deduced in § 4 and § 5 are presented for comparison.

Firstly, because the temperatures deduced from § 4 fall on or between the temperatures deduced in § 5 we have a clear indication that the form of the energy loss process is correct. For example, if electron temperatures are calculated in § 5 taking into account acoustical mode scattering only, then the rate of increase of electron temperature with field is increased by an order of magnitude (see figure 1). Neglecting the effect of optical mode scattering in the analysis of Koenig's data affects the calculated temperatures by less than a factor of 2. This is due to the fact that in the calculation of § 5 it is the relative efficiency of the optical phonon in transferring energy which is important while in the calculation of § 4 it is the relative efficiency of the optical phonon as a scatterer of momentum which is important.

Secondly, we may conclude that interaction between electrons in one valley with electrons in another valley is significant. This is simply because the electron temperatures deduced in § 4 do not fall on but are between the temperatures deduced in § 5. An estimate of the rate of energy transfer between valleys is made below.

A noticeable feature of both figures 1 and 3 is that as the electron temperatures rise the temperatures of the hot valleys deduced by the two methods show an increasing divergence whereas a corresponding divergence is not seen between the low temperature curves. While it would be unwise to place too much emphasis on this, since it may be reflecting the inapplicability of some of the assumptions made in the analysis, it suggests that either (i) scattering mechanisms other than those included are important at high electron temperatures, or (ii) the electron interaction with optical modes is slightly stronger than that given by $R=0{\cdot}14$.

6.2. *The Rate of Transfer of Energy between Valleys*

From the information presented in figures 1 and 3 it is possible to make an order of magnitude estimate of the rate of energy transfer between valleys. Two possible mechanisms are:

(1) Energy transfer by a collision between two electrons in different valleys. The net rate of energy transferred by this process from a valley at a temperature T_h to a valley at temperature T_l is designated by $n_h P_{ee}(T_h, T_l)$.

(2) Energy exchange by intervalley transitions. The net rate of energy transferred by this process from a valley at temperature T_h to a valley at temperature T_l is $n_h P_{ex}(T_h, T_l)$.

Consider the situation with a field E_1 applied to a specimen. At this field the temperatures of the valleys are T_h or T_l and in the steady state

$$-P(T_h, E_1) + P_L(T_h) + P_{ee}(T_h, T_l) + P_{ex}(T_h, T_l) = 0, \quad \ldots\ldots (17)$$

and

$$-P(T_l, E_1) + P_L(T_l) + P_{ee}(T_l, T_h) + P_{ex}(T_l, T_h) = 0. \quad \ldots\ldots (18)$$

Here P_L is the mean rate of energy transfer from an electron to the lattice and $P(E)$ is the rate of absorption of energy by an electron from the electric field E (see equation (16)). These equations are coupled by the conservation of energy in transfer between the valleys, and since there are three valleys at T_h, the relations are

$$3n_h P_{ee}(T_h, T_l) = n_l P_{ee}(T_l, T_h) \text{ and } 3n_h P_{ex}(T_h, T_l) = n_l P_{ex}(T_l, T_h). \quad \ldots\ldots (19)$$

If there is no interaction between electrons in different valleys, then the temperatures T_h and T_l would be achieved by applied fields different from E_1. This is the situation considered in § 5 so that the field necessary to achieve a temperature T_h in the high temperature valley, E_1', and the field necessary to achieve a temperature T_l in the low temperature valley, E_1'', can be seen directly from the broken line curves of figures 1 and 3. Then

$$-P(T_h, E_1') + P_L(T_h) = 0, \quad \ldots\ldots (20)$$

and

$$-P(T_l, E_1'') + P_L(T_l) = 0. \quad \ldots\ldots (21)$$

Equations (17), (18), (20) and (21) give the total rate of energy transfer between the valleys in terms of known quantities,

$$P_{ee}(T_h, T_l) + P_{ex}(T_h, T_l) = P(T_h, E_1)\{(E_1'/E_1)^2 - 1\} \quad \ldots\ldots (22)$$

and

$$P_{ee}(T_l, T_h) + P_{ex}(T_l, T_h) = P(T_l, E_1)\{(E_1''/E_1)^2 - 1\}. \quad \ldots\ldots (23)$$

These equations are related to each other by equation (19). Calculations of $P_{ee} + P_{ex}$ show that in general equation (19) is not obeyed. This is another manifestation of the feature previously noted, that there is a divergence between the two methods of calculating T_h without a corresponding divergence in the calculation of T_l. We shall determine $P_{ee} + P_{ex}$ at a given field by adjusting the value of R used in the temperature calculation of § 5 so that equation (19) is obeyed.

The results of this procedure for a lattice temperature of 77°K are presented in table 2. The upper half of the table refers to energy transfer in a high temperature valley, the lower half to energy transfer in the low temperature valley. For the low field example, only a slight change in R was required to satisfy equation (19) whereas a significant alteration (17%) in R was necessary for the higher field. P_{ex} is calculated from a knowledge of the intervalley transition probability and the energy of the intervalley phonon (Weinreich, Sanders and White 1959). Essentially, to find, say, $P_{ex}(T_h, T_l)$, the rate of supply of energy to the high temperature valley by electrons arriving from the low temperature valley, by both absorption and emission of intervalley phonons, is subtracted from the rate of supply of energy to the low temperature valley by electrons making transitions from the high temperature valley. On the average energy is lost to the lattice by intervalley transitions and it might appear that another term should be added to equations (17) and (18) due to this process. However, this term is already incorporated in P_L since the value of R (equation (14)) is determined by accurately fitting to the observed temperature dependence of the zero field lattice mobility which is dependent upon both optical and intervalley phonon scattering.

Table 2

E_p(v cm^{-1})	T_h (°K)	T_l (°K)	$P_L(T_h)$	$P_{ex}(T_h, T_l)$	$P_{ee}(T_h, T_l)$	$P_{ee}(T_h)$
300	158	132	15	$\ll P_{ee}$	2·6	2
1000	400	223	88	5·6	14	1·6
			$P_L(T_l)$	$P_{ex}(T_l, T_h)$	$P_{ee}(T_l, T_h)$	
300	158	132	10	$\ll P_{ee}$	−6·4	
1000	400	223	34	−7·2	−18	

P's are in units of 10^8 ev sec^{-1}.

It is of interest to compare the effectiveness of electron–electron scattering in transferring energy with the estimate made from the usual formula for the rate of energy loss of an energetic electron, that is

$$P_{ee}(T_h) \simeq \frac{n_l 4\pi q^4}{\kappa^2(2mkT_h)^{1/2}}. \qquad \ldots\ldots (24)$$

Here κ is the dielectric constant and k Boltzmann's constant. The values of $P_{ee}(T_h)$ calculated from equation (24) are shown in table 2. The measure of agreement with $P_{ee}(T_h, T_l)$ for the lower temperatures is fortuitous, since equation (24) is no better than an order of magnitude estimate of the rate of energy loss. The changes which had to be made in R to obtain the high field estimate of $P_{ee}(T_h, T_l)$ imply that it is considerably less accurate than the low field value.

Equation (24) appears, therefore, to be a useful means of obtaining a crude estimate of the energy loss of an electron due to scattering by electrons in other valleys. This is important because equation (24) is used by Fröhlich and Paranjape (1956) in order to calculate the electron concentration at which the rate of transfer of energy between electrons was equal to the rate of transfer to the lattice. However, their calculation has to be modified to incorporate the rate of energy loss to the lattice by optical phonons.

§ 7. CONCLUSION

A method of analysing data obtained from the anisotropy of the high field conductivity has been presented. Further, it has been shown how the analysis of such data can lead to information on the effect of interelectronic collisions. It is clear that a series of observations of the anisotropy over a range of free carrier concentrations and lattice temperatures would be rewarding. As an example, the analysis has been applied to a sample of Koenig's (1959) containing

$6{\cdot}5 \times 10^{14}\,\mathrm{cm}^{-3}$ free electrons. This has led to the following conclusions for a sample having such a free carrier concentration.

(1) At a lattice temperature of 77°K the population of the low temperature valley may increase by as much as 75%. We anticipate, therefore, that when the electric field is parallel to a ⟨111⟩ direction the increase in population of the 111 valley may be $\simeq 100\%$, although no anisotropy would be observed due to the symmetry.

(2) Because of the magnitude of the change of valley population it is clear that for directions of E sufficiently inclined to a ⟨100⟩ direction a significant contribution to the deviation from Ohm's law is due to valley population changes.

(3) For a lattice temperature of 300°K, the changes in population are decreased by approximately tenfold.

(4) There is a large amount of interaction between electrons in different valleys. This interaction has been subdivided into two types—collisions between electrons in one valley with electrons in another and the exchange of electrons between valleys. At a lattice temperature of 77°K, for low fields the rate of energy transfer due to exchange is negligible compared with the transfer by electron collisions. At high fields energy transfer by both mechanisms is important.

(5) To within an order of magnitude the rate of energy transfer by electron–electron collisions agrees with the estimate of Fröhlich and Paranjape (1956).

(6) The estimate of the rate of energy transfer reveals inconsistencies between the electron temperatures deduced in § 4 and those deduced in § 5. These may be due to an underestimate of the efficiency with which electrons lose energy to the lattice or to the inapplicability of assumptions made in the analysis. The inconsistencies are small at low fields and high at large fields, although a change of 17% in R removes the inconsistency. This suggests that if the analysis of § 4 contains assumptions which cannot be made it is because either (i) the distribution of carriers within a valley is not Maxwellian, or (ii) the approximation to the mobility of summing the reciprocal mobilities is not sufficiently accurate, or (iii) Herring's 'single phonon' relation for the intervalley relaxation time becomes influenced by other phonon terms. It should be remembered that the inconsistency is revealed by a means which is a stringent test on both methods used in deducing the electron temperature. The inconsistency is sufficiently small to imply that the general conclusions reached are correct.

ACKNOWLEDGMENTS

The author would like to thank Dr. Koenig for sending a copy of his paper prior to publication. The author is indebted to Dr. A. F. Gibson for reading the manuscript and for helpful comments. This paper is published by permission of the Controller, H.M. Stationery Office.

REFERENCES

FRÖHLICH, H., and PARANJAPE, B. V., 1956, *Proc. Phys. Soc.*, B, **69**, 21.
HAM, F. S., 1955, *Phys. Rev.*, **100**, 1251.
HERRING, C., 1955, *Bell Syst. Tech. J.*, **34**, 237.
KOENIG, S. H., 1959, *Proc. Phys. Soc.*, **73**, 959.
LAFF, R. A., and FAN, H. Y., 1958, *Phys. Rev.*, **112**, 317.
PAIGE, E. G. S., 1958, *Proc. Phys. Soc.*, **72**, 921.
SASAKI, W., SHIBUYA, M., and MIZUGUCHI, K., 1958, *J. Phys. Soc., Japan*, **13**, 456.
STRATTON, R., 1957, *Proc. Roy. Soc.*, **242**, 355.
—— 1958, *J. Electronics and Control*, **5**, 157.
WEINREICH, G., SANDERS, T. M., and WHITE, H. G., 1959, *Phys. Rev.*, **114**, 33.

A Dielectric Approach to Impurity Conduction[†]

By D. G. H. FROOD[‡]

Department of Theoretical Physics, University of Liverpool

Communicated by H. Fröhlich; *MS. received* 28*th April* 1959, *in revised form* 10*th August* 1959

Abstract. Impurity conduction is formulated on a dielectric basis. It is assumed here that the condition for the transition from insulator to metal is provided by the dielectric catastrophe which occurs through the polarizability of the neutral particle. On the basis of the Onsager formula, the contribution to the permittivity arising from the hydrogenic donor atoms is calculated assuming all catastrophic excited states merge with the continuum. The upper temperature limit of the phase transition from N discrete levels to $N-1$ discrete levels can then be estimated and in this way the donor activation energy is found to be a stepwise decreasing function of both temperature and donor concentration.

The dielectric theory is next extended to include screening by the conduction electrons. With an appreciable number of carriers present the hydrogen model breaks down and there is no polar contribution to the dielectric constant. Furthermore, the donor activation energy decreases smoothly and more rapidly with increasing temperature and donor concentration than it would do had only the unscreened catastrophe been operative in producing the band model.

§ 1. Introduction

In the band model of a solid, a single electron is assumed to move in a potential having the lattice periodicity and which is formed by all the nuclei (assumed stationary) and all the other electrons. Although this picture takes into account the Coulomb interactions between charges, it does so in an obscure way. Furthermore, as pointed out by Mott (1956, 1957, 1958), the model must fail when we have to deal with conduction in an array of very widely spaced, single electron atoms since such a substance would be an insulator at the absolute zero of temperature. This failure in the band theory must occur through an incorrect formulation of the Coulomb interactions, and it is desirable to try to reformulate the problem in a way which includes these interactions more precisely. Such a possibility arises through the use of a dielectric constant since this quantity depends explicitly on the Coulomb interactions.

Here, the problem of impurity conduction in valence crystals is formulated on a dielectric basis. For this purpose the donors are considered to be hydrogenic atoms with an effective mass m^*, the same for all states. The ionization energy and Bohr radius of the isolated atom are then

$$I_0=\frac{m^*e^4}{2\epsilon_0{}^2\hbar^2}\simeq 0{\cdot}01\ \text{ev} \qquad \ldots\ldots(1.1)$$

$$a_0=\epsilon_0\left(\frac{\hbar^2}{m^*e^2}\right)\simeq 4\times 10^{-7}\ \text{cm} \qquad \ldots\ldots(1.2)$$

where ϵ_0 is the dielectric constant of the background valence crystal. In calculations for Ge, placing $\epsilon_0 = 16$, $m^* = 0{\cdot}2m$ leads to the numerical values on the right of (1.1) and (1.2). For simplicity, the continuum states of the electron are assumed to be plane waves, furthermore, self-energy effects and broadening due to the interaction between the electron and background crystal are neglected since this interaction is weak in valence crystals.

[†] Based on Electrical Research Association Report L/T. 387.

[‡] Now with Ministry of Supply, Royal Radar Establishment, Malvern, Worcs.

The connection used here between a dielectric and a conductor stems from a very old idea, namely, that of the 'dielectric catastrophe' which arises by use of the Lorentz local field in deriving the Clausius–Mossotti formula for the dielectric constant of a non-polar medium (see Fröhlich 1949). Thus, at $T=0$ all the donors are in the ground state and, as will be shown in § 2, the permittivity of the whole crystal plus donors is

$$\frac{\epsilon-\epsilon_0}{\epsilon+2\epsilon_0} = \frac{4\pi}{3\epsilon_0} D\alpha_1 \qquad \ldots\ldots(1.3)$$

where for hydrogen $\alpha_1 = 9a_0^3/2$ is the polarizability of the ground state and D is the number density of donor centres. From (1.3) it is seen that ϵ becomes very large when D approaches the value

$$D^{(c)} = \frac{3\epsilon_0}{4\pi\alpha_1} \simeq 10^{19}\ \mathrm{cm}^{-3} \qquad \ldots\ldots(1.4)$$

but for such densities the theory leading to (1.3) is usually considered inadequate since it has neglected short range Coulomb interactions between the atoms. It is a basic assumption of this paper, however, when $D = D^{(c)}$ i.e. $\epsilon \to \infty$, that the dielectric becomes a conductor. Donor concentrations higher than (1.4) would lead to negative values of ϵ in (1.3) and these are also associated with the metallic state.

When $T > 0$, however, the picture becomes much more complicated for, in addition to the ground state donors, it is necessary to take into account the contribution to the permittivity made by electrons in the discrete excited levels. This step will be taken formally in § 2 where the polarizations of all the levels of principal quantum number $n = 1, 2, 3 \ldots N$ will be added to give the total polarization of the dielectric. On this basis it is seen, for a finite donor concentration, that the total number N of discrete levels cannot be infinite (as for an isolated atom) since an infinite permittivity would result. One could then speak only of the metallic properties of the medium in contradistinction to the observation that most media behave both as conductors and dielectrics, simultaneously.

That N should be finite follows if the excited levels $n > N$ are considered to be catastrophic (in the sense indicated by the Clausius–Mossotti formula) and lead to infinite or negative dielectric polarizations. Such levels are to be associated with metallic conduction and cannot be included in the calculation of the dielectric constant. From what has been said, N is thus defined as the highest possible non-catastrophic principal quantum number compatible with the given temperature and donor concentration. In this way the permittivity of the donors is maintained finite and positive.

The catastrophe in level n will be shown to occur when

$$\frac{4\pi}{3\epsilon_0} A_n \alpha_n = 1 \qquad \ldots\ldots(1.5)$$

where $\alpha_n \simeq n^6 a_0^3$ is the polarizability of the level and

$$A_n = A(T)\frac{n^2 \exp(-E_n/kT)}{\sigma_N(T)} \qquad \ldots\ldots(1.6)$$

is its population density. In (1.6), $A(T)$ is the number density of un-ionized donors at the temperature T,

$$E_n = I_0\left(1 - \frac{1}{n^2}\right) \qquad \ldots\ldots(1.7)$$

is the energy of the level measured from the ground state, and

$$\sigma_N(T) = \sum_{n=1}^{N} n^2 \exp(-E_n/kT) \qquad \ldots\ldots(1.8)$$

is the electronic partition function of the bound donor electron corresponding to N discrete levels.

It is not immediately obvious that the catastrophe can occur more readily through an excited level than through the ground state because of the exponential factor determining A_n in (1.6). To show qualitatively that such is possible at the low temperatures (1°–20°K) where impurity conduction is observed, compare $A_n\alpha_n$ for an excited level to $A_1\alpha_1$ for the ground state. Thus from (1.6):

$$\frac{A_n\alpha_n}{A_1\alpha_1} \simeq n^8 \exp\left[-\frac{T_0}{T}\left(1 - \frac{1}{n^2}\right)\right] \qquad \ldots\ldots(1.9)$$

where $T_0 = I_0/k$. Hence for temperatures

$$T > \frac{T_0(1 - 1/n^2)}{8 \log n} \qquad \ldots\ldots(1.10)$$

the ratio (1.9) is greater than unity.

For $n=2$, for example, it is seen from (1.10) that the first excited level can become catastrophic before the ground state if $T > 16$°K. Similarly, $n=5$ can become catastrophic before the ground state if $T > 6{\cdot}8$°K.

The foregoing discussion for $T > 0$ has overlooked the Coulomb interactions between the donor atoms and the conduction electrons. In §4 it will be shown, however, that screening by the free carriers modifies the hydrogen model in such a way that catastrophes in the excited levels still occur, but at lower population densities than if screening were absent.

§ 2. DIELECTRIC CONSTANT OF THE DONOR ATOMS

When an electric field is applied to the hydrogen atom, the energy of the nth level is altered and the degeneracy is partially removed. Considering only the linear and quadratic Stark effects, the energy splits into a number of pairs of levels given by

$$E_{n,\lambda}^{(\pm)}(m) = E_n \pm \mu_{n,\lambda} f_{n,\lambda}(m) - \tfrac{1}{2}\alpha_{n,\lambda} f_{n,\lambda}^{2}(m) \qquad \ldots\ldots(2.1)$$

where n and m are the principal and magnetic quantum numbers and λ is a positive integer ($1 \leqslant \lambda \leqslant n$) which designates the pair of levels considered. The quantity $f_{n,\lambda}(m)$ is the local field acting on the electron in the state (n, λ, m). According to Condon and Shortley (1951) the dipole moment and polarizability of this state are

$$\mu_{n,\lambda} = \tfrac{3}{2}a_0 e n(n-\lambda), \qquad \ldots\ldots(2.2\,a)$$

$$\alpha_{n,\lambda}(m) = \tfrac{1}{8}a_0^3 n^4(14n^2 + 6n\lambda - 3\lambda^2 - 9m^2 + 19) \qquad \ldots\ldots(2.2\,b)$$

where in (2.2) m assumes a total of λ values

$$m = (\lambda-1), (\lambda-3), \ldots -(\lambda-3), -(\lambda-1). \qquad \ldots\ldots(2.3)$$

Each of the pair of levels (2.1) is thus λ-fold degenerate. From (2.2 *a*) and (2.3) it is seen that $\lambda=n$ leads to n non-polar states while the remaining values of λ lead to n^2-n polar states of the original level n.

While in principle the partition function of the donor atom in the presence of an electric field will alter from its value in zero field, for weak local fields such that

$$\mu_{n,\lambda} f_{n,\lambda} \ll kT \qquad \ldots\ldots(2.4)$$

this change can be neglected. From (2.1) the number density of electrons in the upper and lower dipolar states $(1 \leqslant \lambda \leqslant n-1)$ is thus

$$A_{n,\lambda}^{(\pm)}(m)=A_n\left(\frac{\lambda}{n^2}\right)\exp\left(\frac{\mp\mu_{n,\lambda} f_{n,\lambda}(m)}{kT}\right) \qquad \ldots\ldots(2.5)$$

while the number per unit volume in the non-polar states $(\lambda=n)$ is

$$A_{n,n}=\frac{n}{n^2}A_n \qquad \ldots\ldots(2.6)$$

where A_n is given by (1.6). To find the contribution of the donor atoms to the dielectric constant of the crystal, it is now required to find the local field acting on each of the particle types in the system. To do this, it is convenient to average the polarizability (2.2 *b*) over the allowed m values. This step will introduce little error into the formula for the permittivity.

The calculation of the dielectric constant on the basis of the Onsager formula (Fröhlich 1949) is then straightforward and will be given here in outline. The development differs from the usual one for the permittivity of a liquid composed of freely rotating dipoles in two regards: (i) because of the background valence crystal, the cavity field, reaction field, etc., must here correspond to a sphere filled with a continuous medium of dielectric constant ϵ_0; (ii) since the dipoles have only two equilibrium positions, the average permanent moment in the field direction must be suitably defined.

The moment per unit volume arising from the polar donors in the state (n, λ) is

$$\mathbf{P}_{n,\lambda}=\frac{(2\lambda/n^2)A_n}{1-\alpha_{n,\lambda}g_{n,\lambda}}\left\{\alpha_{n,\lambda}+\frac{\mu_{n,\lambda}^2}{(1-\alpha_{n,\lambda}g_{n,\lambda})kT}\right\}\mathbf{E}_c \qquad \ldots\ldots(2.7)$$

where

$$\mathbf{E}_c=\frac{3\epsilon_s}{2\epsilon_s+\epsilon_0}\mathbf{E} \qquad \ldots\ldots(2.8)$$

is the cavity field and $\mathbf{E}$ is the macroscopic field. The quantity

$$g_{n,\lambda}=\frac{2(\epsilon_s-\epsilon_0)}{\epsilon_0(2\epsilon_s+\epsilon_0)}\frac{1}{r_{n,\lambda}^3} \qquad \ldots\ldots(2.9)$$

is the reaction field factor. In (2.9), $r_{n,\lambda}$ is determined from the atomic volume of the donors in state (n, λ). From (2.5) the number density of particles in this state is

$$A_{n,\lambda}=A_{n,\lambda}^{(+)}+A_{n,\lambda}^{(-)}=\frac{2\lambda}{n^2}A_n \qquad \ldots\ldots(2.10)$$

for weak local fields, so that

$$\frac{1}{r_{n,\lambda}^3}=\frac{4\pi}{3}A_{n,\lambda}=\frac{8\pi\lambda}{3n^2}A_n. \qquad \ldots\ldots(2.11)$$

In a similar manner, the polarization of the non-polar particles in state (n, n) is

$$\mathbf{P}_{n,n} = \frac{(n/n^2)A_n}{1-\alpha_{n,n}g_{n,n}}\alpha_{n,n}\mathbf{E}_c \qquad \ldots\ldots(2.12)$$

where $g_{n,n}$ is defined similarly to (2.9) using (2.6). Adding (2.7) and (2.12), summing over all bound states of the donor atom and superposing the polarization of the background valence crystal leads in a straightforward manner to the weak field, static dielectric constant

$$\frac{(\epsilon_s-\epsilon_0)(2\epsilon_s+\epsilon_0)}{12\pi\epsilon_s} = \sum_{n=1}^{N}\frac{A_n(T)}{1-\alpha_n g_n}\left\{\alpha_n + \frac{\mu_n^2}{(1-\alpha_n g_n)kT}\right\} \qquad \ldots\ldots(2.13)$$

where

$$\alpha_n = \tfrac{3}{8}a_0^3 n^4(5n^2+7) \qquad \ldots\ldots(2.14)$$

and

$$\mu_n^2 = \tfrac{3}{8}a_0^2 e^2 n^2(n^2-1) \qquad \ldots\ldots(2.15)$$

are the average polarizability and (squared) dipole moment associated with the level n, and

$$g_n = \frac{4\pi}{3\epsilon_0}\left\{\frac{2(\epsilon_s-\epsilon_0)}{2\epsilon_s+\epsilon_0}\right\}A_n \qquad \ldots\ldots(2.16)$$

is the average reaction field factor for this level.

For (2.13) to represent a finite dielectric constant, N must be so chosen that the factors $1-\alpha_n g_n$ are positive for all $1 \leqslant n \leqslant N$ otherwise a catastrophe will occur in the dielectric constant. Hydrogenic levels having $n > N$ for which $1-\alpha_n g_n \leqslant 0$ are associated with infinite or negative polarizations and hence with the existence of conduction in these levels.

It is easily seen that the infinities in (2.13) are catastrophes in the same sense as implied by the Clausius–Mossotti formula (1.3). Suppose for $n \to N$ that $1-\alpha_n g_n \to 0$, then only the Nth term of the series (2.13) makes an appreciable contribution to ϵ. Since the catastrophe always occurs through the polarizability, the dipolar term in (2.13) may be omitted from the argument. The permittivity is then

$$\frac{(\epsilon-\epsilon_0)(2\epsilon+\epsilon_0)}{12\pi\epsilon} \simeq \frac{A_N\alpha_N}{1-\alpha_N g_N}. \qquad \ldots\ldots(2.17)$$

Employing (2.16), we may express (2.17) in the form (1.3) (see Fröhlich 1949, eqn (6.33)) with $D\alpha_1$ replaced by $A_N\alpha_N$.

It is of interest to compute the donor spacing associated with a catastrophe in level N. Use of (2.14) and (2.16) with $\alpha_N g_N = 1$ ($\epsilon_s \to \infty$) results in

$$\frac{r_N}{a_N} = \frac{1}{2}\left\{\frac{15}{\epsilon_0}\left(1+\frac{7}{5N^2}\right)\right\}^{1/3} \simeq \frac{1}{2} \qquad \ldots\ldots(2.18)$$

where r_N is the average distance between donor atoms in the level N and a_N is the Bohr radius of this level. When (2.18) applies, electrons in the levels N will overlap strongly and on the basis of the band model considerable electronic delocalization would be expected. On the other hand, the band model also predicts a certain amount of delocalization in *non*-catastrophic levels which the present theory maintains should be completely non-conducting.

§ 3. UPPER TEMPERATURE LIMIT OF THE PHASE TRANSITION

The problem remaining is to find for a given temperature and donor concentration, the maximum number of discrete levels N. To do this, the higher catastrophic levels $N+1, N+2, \ldots$ are assumed to form conducting states below and adjoining the ordinary conduction band. When N levels exist the activation energy is E_{N+1}, but if the temperature is raised the level N will become more and more populated until finally at a certain temperature T_N it becomes catastrophic and merges with the continuum. For $T = T_N - \delta T$ there are N discrete levels, but for $T = T_N + \delta T$ only $N-1$ discrete levels exist and the activation energy diminishes to E_N.

Strictly speaking, this change in the crystal at T_N should be regarded as a phase transition in which the free energy is continuous, but the model discussed here is too crude to warrant further investigation of this point. However, the upper temperature limit at which this transition can occur may readily be calculated by finding when the population of level N reaches catastrophic proportions.

With N discrete levels, the number density n_e of conduction electrons is given by the mass action law

$$n_e{}^2 = \left(\frac{2\pi m^* kT}{h^2}\right)^{3/2} \frac{A(T)}{\sigma_N} \exp\left(-\frac{E_{N+1}}{kT}\right). \qquad \ldots\ldots(3.1)$$

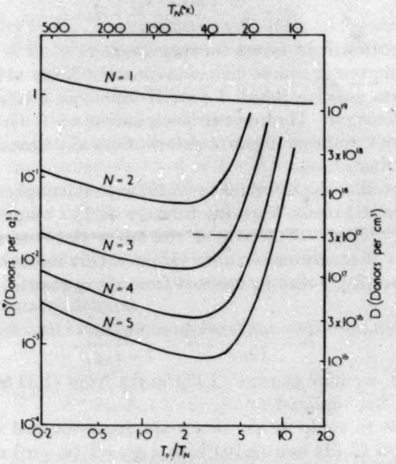

Eliminating A in favour of A_N in (3.1), using (1.6) and applying the restrictive condition $n_e + A = D$ we obtain a relationship between D, $A_N(T)$ and T. Now at $T = T_N$, A_N becomes catastrophic (see (1.5)) and for a given D there results a unique connection between N and T. For purposes of calculation, it is convenient to introduce dimensionless parameters:

$$\alpha_N{}^* = \alpha_N / a_0{}^3, \qquad x_N = T_0 / T_N$$

$$D^* = D a_0{}^3, \qquad A_N{}^* = 3\epsilon_0 / 4\pi\alpha_N{}^*$$

$$q_N = 1 - \frac{1}{N^2}, \qquad p_N = \frac{1}{2}\left(\frac{1}{N^2} - \frac{1}{(N+1)^2}\right)$$

so that the connection between N and T_N is

$$D^* = \frac{A_N{}^*}{N^2}\sigma_N \exp(q_N x_N) + \left(\frac{1}{4x_N}\right)^{3/4}\left(\frac{A_N{}^*}{N^2}\right)^{1/2} \exp(-p_N x_N). \quad \ldots\ldots(3.2)$$

Now the right-hand side of (3.2) exhibits a minimum and when this value is greater than D^* there is no solution for T_N and consequently no transition from N to $N-1$ discrete levels for that particular donor concentration. The right-hand side of (3.2) is illustrated in the figure and it is seen that as D^* is decreased the quantum numbers of levels that can become catastrophic are increased. For example, when $D=3\times10^{17}\,\text{cm}^{-3}$ there are four discrete levels between 14°K and 18°K and three discrete levels between 18°K and 29°K, but the level $N=2$ can never become catastrophic. It will be noticed from the figure that, in general, there are two solutions for T_N for a given donor concentration. In § 4 it will be seen, however, that the high temperature solution is without meaning when the model is extended to include screening by the conduction electrons.

On the basis of the hydrogen model, the present discussion shows that the activation energy is a stepwise decreasing function of both temperature and donor concentration. One may thus form a qualitative understanding of the results of Fritzsche and Lark-Horowitz (1954) and Fritzsche (1955, 1958) who found for germanium and silicon that the $(\log\rho,\, 1/T)$ curves exhibited various slopes in the temperature range 1°–20°K for $D\simeq10^{15}$–$10^{17}\,\text{cm}^{-3}$.

§ 4. SCREENING

The foregoing considerations have neglected Coulomb interactions between the conduction electrons and the donor atoms. This effect can be taken into account by considering that the free carriers (*a*) screen the long range dipolar forces between the neutral donor atoms and so reduce the reaction field, (*b*) screen the donor electron from its nucleus so that the energy (and hence the atomic polarizability) is increased.

The energy of the nth electronic level will then be split into n sub-levels ($l=0, 1, 2, \ldots, n-1$) and the dielectric constant ϵ, resulting from the occupation of all *non*-catastrophic sub-levels (n, l) will be a high frequency permittivity. This result follows since the degenerate states of (n, l) do not have the correct parity to exhibit a linear Stark effect and there can be no polar contribution to the dielectric constant in vanishingly weak electric fields (Frood 1958).

If $A_{n,l}$ is the number density of atoms in (n, l) each of polarizability $\hat{\alpha}_{n,l}$ (here $\wedge$ designates screening), the total polarization of the donor atoms is

$$\mathbf{P}_A=\left\{\sum_{n=1}^{N-1}\sum_{l=0}^{n-1}\frac{\hat{\alpha}_{n,l}A_{n,l}}{1-\hat{\alpha}_{n,l}\hat{g}_{n,l}}+\sum_{l=0}^{L}\frac{\alpha_{N,l}A_{N,l}}{1-\hat{\alpha}_{N,l}\hat{g}_{N,l}}\right\}\hat{\mathbf{E}}_c \qquad \ldots\ldots(4.1)$$

where N and L are the highest possible non-catastrophic principal and orbital quantum numbers. In (4.1) $\hat{\mathbf{E}}_c$ and $\hat{g}_{n,l}$ are the screened cavity field and reaction field factor of the level (n, l).

To obtain a knowledge of these latter quantities, consider in the usual way (Fröhlich 1949), a point dipole $\boldsymbol{\mu}$ at the centre of a sphere of radius a and dielectric constant ϵ_0. Surrounding this sphere is a medium of dielectric constant ϵ, the whole being in an electric field $\mathbf{E}$ which is uniform at infinity. Throughout the whole medium there is a certain number density of conduction electrons n_e, which gives rise to screening radii

$$a_s{}^0=\left(\frac{kT\epsilon_0}{4\pi n_e e^2}\right)^{1/2} \qquad \ldots\ldots(4.2\,a)$$

$$a_s=\left(\frac{kT\epsilon}{4\pi n_e e^2}\right)^{1/2} \qquad \ldots\ldots(4.2\,b)$$

inside and outside the spherical cavity, respectively. The potentials inside and outside the sphere are, respectively,

$$V_0 = \frac{\mu\cos\theta}{\epsilon_0 r^2}\left(1+\frac{r}{a_{\mathrm{s}}{}^0}\right)\exp\left(-\frac{r}{a_{\mathrm{s}}{}^0}\right) - Br\cos\theta \quad \ldots\ldots(4.3\,a)$$

$$V = \frac{C\cos\theta}{\epsilon r^2}\left(1+\frac{r}{a_{\mathrm{s}}}\right)\exp\left(-\frac{r}{a_{\mathrm{s}}}\right) - Er\cos\theta \quad \ldots\ldots(4.3\,b)$$

where (4.3) are appropriate solutions of Poisson's equation, including the boundary condition at infinity. The second term of (4.3 *a*) is a solution of Laplace's equation rather than a particular integral of Poisson's equation, since one requires the field inside when the dipole plus its polarizability (which depends on the inside space charge) is removed from the cavity.

The constants B and C are found by the conditions that the potential and radial component of the displacement vector should be continuous at $r=a$. With $\eta_0 = a/a_{\mathrm{s}}{}^0$, $\eta = a/a_{\mathrm{s}}$ there results from B the screened reaction field

$$\hat{\mathbf{R}} = \hat{g}\boldsymbol{\mu} \quad \ldots\ldots(4.4)$$

where

$$\hat{g} = g(1+\eta_0)\exp(-\eta_0)\left\{1+\frac{\epsilon}{2(\epsilon-\epsilon_0)}\left(\frac{\eta^2}{1+\eta}\right)-\frac{\epsilon_0}{2(\epsilon-\epsilon_0)}\left(\frac{\eta_0{}^2}{1+\eta_0}\right)\right\}\kappa \quad \ldots\ldots(4.5)$$

and the screened cavity field:

$$\hat{E}_{\mathrm{c}} = E_{\mathrm{c}}\left\{1+\frac{1}{3}\left(\frac{\eta^2}{1+\eta}\right)\right\}\kappa \quad \ldots\ldots(4.6)$$

where in (4.5) and (4.6) g and E_{c} are the unscreened reaction field factor and cavity field (see (2.9) and (2.8)), and

$$\kappa = \left\{1+\frac{\epsilon}{2\epsilon+\epsilon_0}\left(\frac{\eta^2}{1+\eta}\right)\right\}^{-1}. \quad \ldots\ldots(4.7)$$

From (4.6) $\hat{E}_{\mathrm{c}}$ is seen to be practically independent of η and to a good approximation the dielectric constant is obtained directly from (4.1) using (2.8). As before, a catastrophe in ϵ will occur when $\hat{\alpha}_{N,L}\hat{g}_{N,L}=1$. When $\epsilon\to\infty$ ($\eta\to 0$) in (4.5) and (4.7) this condition becomes

$$\frac{4\pi}{3\epsilon_0}A_{N,L}\hat{\alpha}_{N,L}(1+\eta_0)\exp(-\eta_0)=1 \quad \ldots\ldots(4.8)$$

but since the factor containing η_0 is always close to unity, (4.8) is practically the same condition for the transition from insulator to metal as in the unscreened case except that now the polarizability depends on the screening.

If $a_{N,L}$ is the Bohr radius of level (N, L), $\hat{\alpha}_{N,L}$ will become extremely large when

$$a_{\mathrm{s}}{}^0 \simeq a_{N,L}; \quad \ldots\ldots(4.9\,a)$$

furthermore, there can be found no bound state of the electron when

$$a_{\mathrm{s}}{}^0 < a_{N,L}. \quad \ldots\ldots(4.9\,b)$$

At low temperatures screening cannot much affect the levels of low principal quantum number and the hydrogen model holds as a good approximation. Screening will always be important, however, for discrete levels just below the bottom of the conduction band. Thus as T is lowered for a fixed donor concentration, more and more discrete levels condense out (see figure) but this process cannot continue indefinitely since it would result in an infinite number of discrete levels at $T=0$. Such an event cannot occur because the Bohr radius

$$a_N^4 \sim \exp(T_0/T_N) \qquad \ldots\ldots(4.10\,a)$$

increases more rapidly with decreasing temperature than the screening radius

$$(a_s^0)^4 \sim (T_N/T_0)^{1/2} \exp(T_0/T_N). \qquad \ldots\ldots(4.10\,b)$$

Hence for $N < N'$, $a_s^0 < a_N$ and no more bound states can exist.

Starting from $T = 0$ with all donors in the ground state, the excited levels $n < N'$ are populated to their equilibrium amounts as T is increased to $T_{N'}$. For $T > T_{N'}$, however, the uppermost levels become catastrophic through the screened polarizability and the activation energy decreases as the temperature is further increased. At temperatures where the carrier density is appreciable, the energies of the non-catastrophic levels increase considerably and sub-levels of high angular momentum move closer to the bottom of the conduction band. The hydrogen model then breaks down and states of low principal quantum number become catastrophic at lower densities and temperatures than was estimated neglecting screening.

From these qualitative considerations, it follows that the activation energy decreases smoothly and more rapidly with increasing temperature and donor concentration than it would do had only the unscreened catastrophe been operative in producing the band model.

ACKNOWLEDGMENTS

The author wishes to express his gratitude to Professor H. Fröhlich for advice and encouragement at all stages of this work, to the Electrical Research Association for financial assistance and to the National Research Council of Canada for a Special Scholarship.

REFERENCES

CONDON, E., and SHORTLEY, G., 1951, *The Theory of Atomic Spectra* (Cambridge: University Press).
FRITZSCHE, H., 1955, *Phys. Rev.*, **99**, 406.
—— 1958, *J. Phys. Chem. Solids*, **6**, 69.
FRITZSCHE, H., and LARK-HOROWITZ, K., 1954, *Physica*, **20**, 834.
FRÖHLICH, H., 1949, *Theory of Dielectrics* (Oxford: Clarendon Press).
FROOD, D. G. H., 1959, *Electrical Research Association Report*, L/T. 383.
MOTT, N. F., 1956, *Canad. J. Phys.*, **34**, 1356.
—— 1957, *Phil. Mag.*, **2**, 1364.
—— 1958, *Suppl. Nuovo Cim.*, **12**, 312.

Electron Capture by Protons passing through Hydrogen

By N. C. SIL

Department of Theoretical Physics, Indian Association for the Cultivation of Science, Calcutta

MS. received 6th April 1959, in revised form 6th July 1959

Abstract. A variational method is applied to the problem of electron capture by protons from the ground state of hydrogen atoms. The problem is treated as a simplified one-body problem, viz. that of an electron in the Coulomb field of two protons, the proton–proton interaction being neglected. The numerical results of our theoretical calculations at low incident proton energies are in good agreement with the recent experimental findings of Fite, Brackmann and Snow. At low incident proton energies our theoretical results agree closely with those of Dalgarno and Yadav, though the methods of approach are different. Further, our results may, with suitable approximations, be easily reduced to those of Brinkman and Kramers or of Bates and Dalgarno and Jackson and Schiff.

---

§ 1. INTRODUCTION

THE importance of the problem of capture of electrons by an ion passing through gaseous matter has of late increased in view of its application to the explanation of spectral lines of aurora and of solar corona. The theoretical calculations on electron capture in fast collisions are essentially based on the Born approximation method of Brinkman and Kramers (1930) which have been extended by Saha and Basu (1945), Bates and Dalgarno (1952, 1953), Jackson and Schiff (1953) and Sil (1954). Bates and Dalgarno and Jackson and Schiff in their calculations have included the ion–nucleus interaction and they find that in the case of electron capture by protons in hydrogen atoms this interaction reduces to about one-fifth of the value of cross section of capture in the ground state at 100 kev incident proton energy. It is not quite clear why the ion–nucleus interaction should have such marked influence on the capture probability; Wick (cf. Jackson and Schiff 1953) has pointed out that the ion–nucleus interaction can be removed by canonical transformation. Moreover, it should be borne in mind that the initial and final wave functions are not orthogonal to each other; this lack of orthogonality gives rise to ambiguity in the capture cross section (Takayanagi 1955, Bates 1958) as will be apparent from the fact that even a constant potential term will give finite values of the cross section even though the relevant force is zero.

The calculations for the capture cross section for slow protons in hydrogen atoms have been made by Dalgarno and Yadav (1953) based on the perturbed stationary states method of Bates, Massey and Stewart (1953). The treatment of the capture problem by these authors as well as that by Gurnee and Magee (1957) are restricted to low velocities of relative motion of the colliding systems. This paper derives the expression for the capture cross section of electrons by protons passing through hydrogen atoms by a new variational method which is valid for both moderately high and low velocities of the incident proton, and also seeks to illuminate the capture problem and explain the results obtained in various other calculations which have been made. The numerical values of the theoretical calculations for low incident proton energies are in good agreement with the recent experimental results of Fite, Brackmann and Snow (1958).

§ 2. THEORY

We consider the capture of an electron e by the proton B from the ground state of the hydrogen atom A+e. Because of the heavy mass of a proton compared with that of an electron the collision process is treated as a simplified one-body problem, viz. that of an electron in the Coulomb fields of two protons. The calculation is made in the coordinate system in which C, the centre of mass of the two protons, is at rest while the protons A and B move in straight lines with uniform velocities $-\frac{1}{2}\mathbf{v}$ and $+\frac{1}{2}\mathbf{v}$ respectively; the effect of proton–proton interaction is completely neglected. Let $\mathbf{R}$ be the position vector of B relative to Aand let $\mathbf{r}_1$, $\mathbf{r}_2$ and $\mathbf{r}$ be the position vectors of e from A, B and C respectively. We choose the time $t=0$ when the two protons are nearest to each other.

Initially at $t=-\infty$ we have the electron attached to the proton A in its ground state. The time rate of change of the electron state wave function ψ is given by the time-dependent Schrödinger equation

$$H\psi = i\hbar\frac{\partial\psi}{\partial t} \qquad \ldots\ldots(1)$$

where H is the Hamiltonian corresponding to the motion of the electron in the Coulomb fields of the two nuclei:

$$H = -\left(\frac{\hbar^2}{2m}\nabla^2 + \frac{e^2}{r_1} + \frac{e^2}{r_2}\right),$$

$\hbar$ is Planck's constant divided by 2π, e the charge and m the mass of an electron. We neglect the proton–proton interaction.

The value of the ψ function at $t=\infty$ is determined by the equation (1) together with the above-mentioned initial condition.

The Schrödinger equation (1) may be obtained by making stationary the following variation integral I:

$$I = \int\left(-\tfrac{1}{2}\bar{\psi}H\psi - \tfrac{1}{2}\psi H\bar{\psi} + \tfrac{1}{2}i\hbar\bar{\psi}\frac{\partial\psi}{\partial t} - \tfrac{1}{2}i\hbar\frac{\partial\bar{\psi}}{\partial t}\psi\right)dV\,dt, \qquad \ldots\ldots(2)$$

with respect to small arbitrary variations of ψ and $\bar{\psi}$ ($\bar{\psi}$ is the complex conjugate of ψ). The integration extends over the whole of space and time.

For a suitable approximation to ψ we choose a trial wave function ψ_{T} which is a linear combination of the two ground state wave functions around the two protons, the coefficients being left free as functions of time. Thus we write

$$\psi_{\mathrm{T}} = A(t)\psi_1 + B(t)\psi_2, \qquad \ldots\ldots(3)$$

where

$$\left.\begin{aligned}\psi_1 &= \psi_{1\mathrm{orb}}\psi_{1\mathrm{tr}} = (\pi a_0^3)^{-1/2}\exp\left(-\frac{r_1}{a_0} + \frac{i}{\hbar}\epsilon t\right)\exp\left[-\frac{im}{\hbar}\left(\tfrac{1}{2}\mathbf{v}\cdot\mathbf{r} + \tfrac{1}{8}v^2 t\right)\right]\\ &\text{and}\\ \psi_2 &= \psi_{2\mathrm{orb}}\psi_{2\mathrm{tr}} = (\pi a_0^3)^{-1/2}\exp\left(-\frac{r_2}{a_0} + \frac{i}{\hbar}\epsilon t\right)\exp\left[\frac{im}{\hbar}\left(\tfrac{1}{2}\mathbf{v}\cdot\mathbf{r} - \tfrac{1}{8}v^2 t\right)\right]\end{aligned}\right\};\ldots(4)$$

a_0 is the radius of the first Bohr orbit of the hydrogen atom, and ϵ is the binding energy of the electron in that orbit. ψ_1 is the normalized ground state electron wave function around the proton A and consists of two parts: (1) $\psi_{1\mathrm{orb}}$ due to the orbital motion of the electron around the proton A and (2) $\psi_{1\mathrm{tr}}$ due to the translatory motion of the electron, i.e. the motion which the electron shares because of its being attached to the moving proton. Similarly ψ_2, the normalized electron ground state wave function around the proton B, consists of two parts $\psi_{2\mathrm{orb}}$ and $\psi_{2\mathrm{tr}}$.

Here we consider only the two main possibilities for the electron state: (i) the electron may remain attached to the proton A or (ii) it may be captured by the proton B in ground state.

Besides the above two there are other possibilities, e.g. the electron may be left in the original atom in an excited state, it may be captured by the proton B in any of its excited orbits, or it may be knocked off the original atom without being captured by the proton B (ionization without capture). The probabilities of these latter processes are assumed to be small.

In the variation integral (2) we substitute for ψ its trial value ψ_{T} the space part of which is specified already and we have the freedom of arbitrary variations of $A(t)$, $\overline{A(t)}$, $B(t)$ and $\overline{B(t)}$ only. We may now write

$$I = \int L\,dt,$$

where

$$L = (\bar{A}A + \bar{B}B)f_1 + (\bar{A}B + A\bar{B})f_2 + \frac{i\hbar}{2}\left(\bar{A}\frac{dA}{dt} + \bar{B}\frac{dB}{dt} - \frac{d\bar{A}}{dt}A - \frac{d\bar{B}}{dt}B\right) + \frac{i\hbar}{2}\left(\bar{A}\frac{dB}{dt} + \frac{dA}{dt}\bar{B} - \frac{d\bar{A}}{dt}B - A\frac{d\bar{B}}{dt}\right)f_3,$$

$$f_1 = \int \frac{e^2}{r_2}\bar{\psi}_1\psi_1\,dV = \int \frac{e^2}{r_1}\bar{\psi}_2\psi_2\,dV = e^2\left[\frac{1}{R} - \frac{1}{a_0}\exp\left(-\frac{2R}{a_0}\right) - \frac{1}{R}\exp\left(-\frac{2R}{a_0}\right)\right], \quad \ldots\ldots(5\,a)$$

$$f_2 = \frac{e^2}{2}\int\left(\frac{1}{r_1} + \frac{1}{r_2}\right)\bar{\psi}_1\psi_2\,dV, \quad \ldots\ldots(5\,b)$$

$$f_3 = \int \bar{\psi}_1\psi_2\,dV; \quad \ldots\ldots(5\,c)$$

f_1, f_2 and f_3 are all real.

Making the integral $\int L\,dt$ stationary with respect to small arbitrary variations of $\bar{A}$ and $\bar{B}$ we obtain the following differential equations:

$$f_1 A + \left(f_2 + \frac{i\hbar}{2}\frac{df_3}{dt}\right)B + i\hbar\frac{dA}{dt} + i\hbar f_3\frac{dB}{dt} = 0, \quad \ldots\ldots(6)$$

$$\left(f_2 + \frac{i\hbar}{2}\frac{df_3}{dt}\right)A + f_1 B + i\hbar f_3\frac{dA}{dt} + i\hbar\frac{dB}{dt} = 0. \quad \ldots\ldots(7)$$

If we make the integral stationary with respect to small arbitrary variations of A and B we would get the complex conjugate equations.

From equations (6) and (7) we get

$$\left(f_1 + f_2 + \frac{i\hbar}{2}\frac{df_3}{dt}\right)(A+B) + i\hbar(1+f_3)\frac{d}{dt}(A+B) = 0 \quad \ldots\ldots(8)$$

and

$$\left(f_1-f_2-\frac{i\hbar}{2}\frac{df_3}{dt}\right)(A-B)+i\hbar(1-f_3)\frac{d}{dt}(A-B)=0. \qquad \ldots\ldots(9)$$

Using the initial conditions $|A(t=-\infty)|^2=1$ and $|B(t=-\infty)|^2=0$ and the fact that $f_3=0$ at $t=\pm\infty$ we obtain from equations (8) and (9)

$$|B(t=\infty)|^2=\sin^2\left[\frac{1}{\hbar}\int_{-\infty}^{\infty} f\,dt\right], \qquad \ldots\ldots(10)$$

where

$$f=(f_2-f_1f_3)/(1-f_3^2). \qquad \ldots\ldots(11)$$

The capture cross section Q is given by

$$Q=2\pi\int_0^{\infty}|B(t=\infty)|^2 p\,dp, \qquad \ldots\ldots(12)$$

p being the impact parameter on which $B(t=\infty)$ depends.

An expression of similar form has already been derived by the present author (1957) for the capture cross section Q in which the translatory motion of the protons has been neglected and as such is only valid for low incident energy.

Bates, Massey and Stewart (1953) and Gurnee and Magee (1957) have approximately solved the differential equation (1) under certain assumptions and their results are only valid for low velocity; the former authors have used a linear combination of the two lowest hydrogen *molecular* ion states with the two protons moving very slowly relative to each other while Gurnee and Magee have taken a linear combination of *atomic* wave functions around the two nuclei like ours, but have neglected the translatory motion of the protons (cf. equations (3) and (4)).

At fairly high energies our present expression is superior to theirs because it has taken into account the translatory motion of the protons. At low energies, however, the expression of Bates, Massey and Stewart is more exact than ours because of its use of the exact hydrogen molecular ion states.

§ 3. CAPTURE CROSS SECTION AT LOW ENERGIES OF THE INCIDENT PROTON

For the special case of very low velocity of relative motion of the incident proton with respect to the hydrogen atom we may evaluate the integrals for f_2 and f_3 approximately without much error by putting the translatory parts of the electron wave functions $\psi_{1\mathrm{tr}}$, $\psi_{2\mathrm{tr}}$ equal to unity. Thus we get

$$f_2=\frac{e^2}{a_0}\left(1+\frac{R}{a_0}\right)\exp\left(-\frac{R}{a_0}\right), \qquad \ldots\ldots(5\,b')$$

$$f_3=\left(1+\frac{R}{a_0}+\frac{1}{3}\frac{R^2}{a_0^2}\right)\exp\left(-\frac{R}{a_0}\right). \qquad \ldots\ldots(5\,c')$$

The value of the function in (11) which occurs as the integrand in (10) may now be easily calculated with the help of (5 *a*), (5 *b*′), and (5 *c*′). The value of the capture probability $|B(t=\infty)|^2$ which we obtain from equation (10) after evaluation of the integral

$$\int_{-\infty}^{\infty} f\,dt,$$

is next substituted in equation (12) and a further integration with respect to the impact parameter gives the capture cross section Q.

The numerical results of our theoretical calculations over the energy range 1 to 10 kev of the incident proton, shown as the continuous curve in the figure, are in fairly good agreement with the recent experimental findings of Fite, Brackmann and Snow (1958) whose mean values are shown by the broken line in the figure. The agreement may be better than appears because the authors think that their curve is on the high side and real values may be lower by about 15%.

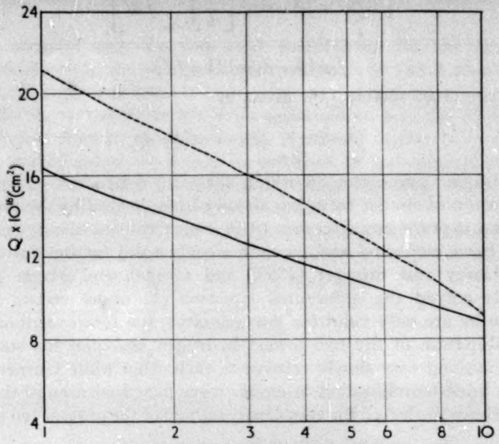

Electron-capture cross section Q per atom for protons in hydrogen atoms as a function of incident proton energy. The continuous curve is the theoretical result and the broken curve the experimental mean value of Fite, Brackmann and Snow (1958).

The results of our theoretical calculations at low incident proton energies agree closely with those of Dalgarno and Yadav (1953), who used the perturbed stationary states method discussed in detail by Bates, Massey and Stewart (1953). The capture cross sections for incident proton energies 1 and 10 kev as calculated by these authors and ourselves are given below for comparison:

Incident proton energy (kev)	1	10
Q (Dalgarno and Yadav) (10^{-16} cm^2)	16·54	8·62
Q (present work) (10^{-16} cm^2)	16·37	8·89

§ 4. RELATION OF THE APPROXIMATION OF BRINKMAN AND KRAMERS TO THAT OF BATES AND DALGARNO AND JACKSON AND SCHIFF

Our approximation gives the same result as that of Brinkman and Kramers (1930) if we make the following two alterations: (i) we replace the sine function on the right-hand side of equation (10) by its argument; this is justified when the argument is small, e.g. at high incident proton energies; (ii) we put $f_3 = 0$ in equation (11) which gives the value of the function f occurring as the integrand in equation (10). Now $f_3 = \int \bar{\psi}_1 \psi_2 \, dV$ is a measure of the lack of orthogonality of the initial and final state wave functions ψ_1 and ψ_2. Hence putting $f_3 = 0$ is equivalent to assuming orthogonality of the initial and final state wave functions.

If, however, we assume that f_3 is not zero but small compared with 1, so that $f_3^2 \ll 1$, we may write (cf. eqn (11)) $f = f_2 - f_1 f_3$. The term $-f_1 f_3$ which appears here in addition to f_2 occurring already in the calculation of Brinkman and Kramers may be written from (5 *a*) and (5 *b*) as follows:

$$-f_1 f_3 = -\int \bar{\psi}_1 e^2 \left[\frac{1}{R} - \frac{1}{a_0} \exp\left(-\frac{2R}{a_0} \right) - \frac{1}{R} \exp\left(-\frac{2R}{a_0} \right) \right] \psi_2 \, dV.$$

The first term

$$-\int \bar{\psi}_1 \left(\frac{e^2}{R} \right) \psi_2 \, dV$$

which is the most important one is just the additional term considered by Bates and Dalgarno and Jackson and Schiff in their perturbation calculation. They however, attributed this term to the proton–proton interaction whereas the same term appears naturally in our calculations without introducing *ad hoc* the proton–proton interaction and the value of this term is non-zero on account of the non-orthogonality of ψ_1 and ψ_2. In view of the same nature of matrix elements the results of our theoretical calculation for the capture cross section at high incident proton energies are close to those of Bates and Dalgarno and Jackson and Schiff. The numerical results of these authors at high incident proton energies are in agreement with the experimental findings of Ribe (1951) (the data refer to capture by a proton passing a hydrogen molecule which may be regarded as equivalent to two atoms, a procedure reasonably justified at high energies). The results of Dalgarno and Yadav (1953) are, however, much higher than the experimental results at such high energies because of their neglect of the translatory motion of the protons as will be evident from the following figures at 100 kev incident proton energy:

Ground state capture cross section	
as calculated by Jackson and Schiff	$0{\cdot}65 \times 10^{-17}\,\text{cm}^2$
as calculated by Dalgarno and Yadav	$18{\cdot}5 \times 10^{-17}\,\text{cm}^2$
Experimental capture cross section	
due to Ribe	$1 \times 10^{-17}\,\text{cm}^2$

The nuclear–nuclear interaction and non-orthogonality of the initial and final state wave functions have been discussed by earlier workers (Takayanagi 1955, Bates 1958).

The sine function in our equation (10) guarantees that the capture probability $|B(t=\infty)|^2$ is always less than unity. In the calculations of Brinkman and Kramers, Bates and Dalgarno and Jackson Schiff the capture probability would sometimes be larger than unity which is inadmissible.

ACKNOWLEDGMENT

The author wishes to thank Professor D. Basu for his kind interest in the problem and for valuable discussions.

REFERENCES

BATES, D. R., 1958, *Proc. Roy. Soc.* A, **247**, 294.
BATES, D. R., and DALGARNO, A., 1952, *Proc. Phys. Soc.* A, **65**, 919.
—— 1953, *Ibid.*, **66**, 972.
BATES, D. R., MASSEY, H. S. W., and STEWART, A. L., 1953, *Proc. Roy. Soc.* A, **216**, 437.
BRINKMAN, H. C., and KRAMERS, H..A., 1930, *Proc. Acad. Sci. Amsterdam*, **33**, 973.
DALGARNO, A., and YADAV, H. N., 1953, *Proc. Phys. Soc.* A, **66**, 173.

Fite, W. L., Brackmann, T., and Snow, W. R., 1958, *Phys. Rev.*, **112,** 1161.
Gurnee, E. F., and Magee, J. L., 1957, *J. Chem. Phys.*, **26,** 1237.
Jackson, J. D., and Schiff, H., 1953, *Phys. Rev.*, **89,** 359.
Ribe, F., 1951, *Phys. Rev.*, **83,** 1217.
Saha, M. N., and Basu, D., 1945, *Indian J. Phys.*, **19,** 121.
Sil, N. C., 1954, *Indian J. Phys.*, **28,** 232.
—— 1957, *Ph.D. Thesis*, submitted at the Trinity College, Dublin.
Takayanagi, K., 1955, *Sci. Rep. Saitama Univ.* A, **2,** 33.

The Elastic and Inelastic Scattering of Protons by ^{58}Ni

BY G. W. GREENLEES AND P. M. ROLPH
Physics Department, University of Birmingham

MS. received 6th August 1959

Abstract. Absolute differential cross sections are given for the elastic scattering by ^{58}Ni of 9·53 MeV, 9·12 MeV, 8·80 MeV, 8·34 MeV and 7·83 MeV protons for an angular range of 15° – 156° (centre-of-mass coordinates). The angular distributions show characteristic maxima and minima, the patterns varying slowly with energy as might be expected on the basis of the optical model. The results are in good agreement with earlier measurements on natural Ni except at backward angles, where higher cross sections are obtained with ^{58}Ni. This is attributed to differing compound elastic contributions from the various Ni isotopes. Absolute differential cross sections are also given for the inelastic scattering of protons at these five energies from the 1·45 MeV level of ^{58}Ni. All the inelastic angular distributions show a forward peaking characteristic of a direct interaction mechanism. It is probable that a distorted wave treatment will be necessary to fit these results.

---

§ 1. INTRODUCTION

EARLIER papers (Greenlees *et al.* 1957 a, 1957 b, 1958) presented results on the elastic and inelastic scattering of protons by magnesium, aluminium and silicon at five energies between 7·8 and 9·6 MeV. The angular distributions for elastic scattering by magnesium showed marked energy variations not readily explained by an optical model type of analysis, whereas with aluminium and silicon only small variations with incident energy were observed.

The magnesium and silicon inelastic angular distributions also varied rapidly with incident energy and were asymmetric about 90° with a forward peaking in some cases. The forward peaking could not be explained by a direct interaction mechanism since such a mechanism would not be expected to show a rapid energy variation. The asymmetry about 90° is unexpected on a compound nucleus picture if a large number of compound levels are concerned in the reaction. The excitations of the compound nuclei concerned are about 12 MeV and it is not certain that many levels are available at this energy with nuclei of mass numbers 24–30. Thus the marked energy dependence observed in both elastic and inelastic scattering may be due to the effects of a limited number of compound nucleus levels being concerned in the reaction.

The present experiments with ^{58}Ni were undertaken to see if the rapid energy variations still persisted in a heavier nucleus in which a higher level density of the compound nucleus would be expected.

§ 2. APPARATUS AND PROCEDURE

The 9·62 MeV proton beam from the Nuffield 60 in. cyclotron passed through a self-supporting ^{58}Ni target at the centre of a scattering chamber and was collected in a Faraday cup and integrated. The scattered beam was detected by a CsI(Tl) crystal and photomultiplier and the spectra were displayed on a 100-channel pulse height analyser. Laboratory angles between 15° and 165° were available with an angular definition to ± 1°. A more detailed description of the apparatus and experimental procedure is given elsewhere (Greenlees *et al.* 1957 a).

Figure 1 shows two typical spectra taken at 62° and 147° (c.m.) for a known charge collected in the Faraday cup. The two well-resolved groups are due to elastic scattering ($Q=0$) and to inelastic scattering ($Q=-1{\cdot}45$ MEV) from ^{58}Ni. Similar spectra were obtained at other angles and angular distributions for the elastic and inelastic groups were plotted. Absolute differential cross sections were obtained from the observed spectra together with a knowledge of the charge collected, the target thickness ($4{\cdot}95\,\mathrm{mg\,cm^{-2}}$), and the solid angle subtended by the detector.

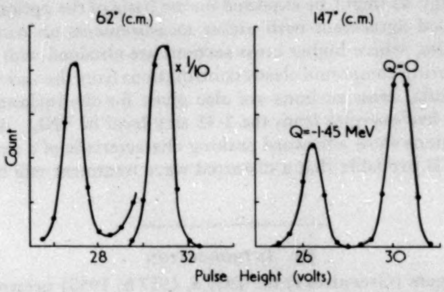

Figure 1. Pulse height spectra for the scattering of 9·12 MEV protons from ^{58}Ni at 62° and 147° (c.m.)

The maximum beam energy was found by measurement of the range of protons elastically scattered from a thin aluminium foil into a photographic emulsion. The energy of protons entering the emulsion was reduced by means of aluminium absorbers so that only elastically scattered particles were recorded.

Reduced incident energies were obtained by placing aluminium absorbers in front of the collimator used to define the incident beam. Angular distributions were obtained at energies (at the centre of the target foil) of 9·53 MEV, 9·12 MEV, 8·80 MEV, 8·34 MEV and 7·83 MEV, all ± 0·07 MEV.

§ 3. RESULTS

Figure 2 shows the elastic differential cross sections at these five energies plotted as the ratio of the observed cross section to the corresponding cross section calculated on the basis of Rutherford scattering from a point charge. The errors in the absolute cross sections are ± 3% in general and the errors in the angles ± 30′. Figure 3 shows the inelastic differential cross sections at the five incident energies, the errors are also estimated at ± 3%.

§ 4. DISCUSSION

The ^{58}Ni elastic scattering curves of figure 2 show small systematic variations with energy at angles forward of 110°. It is expected that these can be well represented by an optical model with a suitable choice of parameters. At angles greater than 110° no systematic variation with energy is apparent. Figure 2 also shows some earlier results obtained using 9·37 Mev protons and a natural nickel target. These points agree well with the present results except at large angles, where ^{58}Ni gives higher cross sections. Similar data have been obtained by Hintz (1957) using 9·87 Mev protons and a natural nickel target. Glassgold *et al.* (1957) have fitted Hintz's data using a Saxon potential. Glassgold (private communication) also finds a fit with the 9·37 Mev natural nickel points using the same parameters as used for the 9·87 Mev data. For both sets of natural nickel results the fits are excellent at angles forward of 110° but at backward angles the observed cross sections are greater than those predicted by the model. The discrepancy at backward angles will obviously be greater for the present ^{58}Ni results.

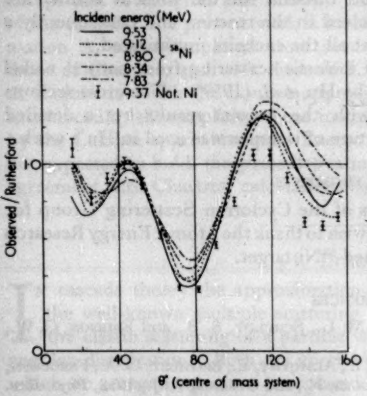

Figure 2. Ratio of observed to Rutherford elastic scattering cross sections of protons of various energies by ^{58}Ni and natural nickel.

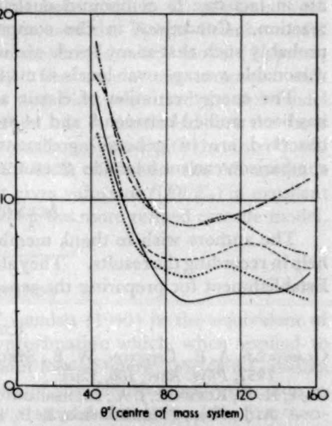

Figure 3. Differential cross sections for inelastic scattering ($Q = -1{\cdot}45$ Mev) of protons of various energies by ^{58}Ni. (For key see figure 2.)

The difference between natural nickel and ^{58}Ni can be explained on the basis of differing compound elastic contributions. At forward angles the large shape elastic contribution masks any compound elastic effects. Natural nickel comprises 68% ^{58}Ni, 26·2% ^{60}Ni and 5·8% ^{61,62,64}Ni; thus the essential difference between natural nickel and ^{58}Ni is the addition of 26·2% ^{60}Ni. In the decay of the compound nucleus various processes will compete with the emission of a full energy proton; the main competing process will be neutron emission. The (p, n) thresholds for ^{58}Ni and ^{60}Ni are 9·459 Mev and 7·028 Mev respectively (Gove *et al.* 1958). Thus in the range of energies used in the present experiments (7·83 – 9·53 Mev) (p, n) reactions can occur with ^{60}Ni but not with ^{58}Ni. Hence one expects more compound nucleus elastic scattering from ^{58}Ni than ^{60}Ni and hence larger cross sections at backward angles from ^{58}Ni than from natural nickel (26% ^{60}Ni) as is in fact observed. The fact that the ^{58}Ni cross sections are always greater than those of natural nickel suggests an incoherent compound elastic contribution. Effects at backward angles attributed to compound elastic scattering have also been observed by Preskitt and Alford (1958) using 4–7 MeV protons and by Waldorf and Wall (1957) using 7·5 MeV protons.

The inelastic scattering angular distributions of figure 3 all show a forward peaking. This is indicative of a direct interaction mechanism. On the basis of plane wave direct interaction calculation, these angular distributions would follow a $j_2^2(QR)$ variation. To obtain such a fit requires unreasonably large values for the interaction radius R, and it seems that a distorted wave treatment will be necessary to fit the present results.

Neither the elastic nor the inelastic angular distributions for ^{58}Ni show the marked energy dependence reported previously for magnesium and silicon. It seems probable, therefore, that the magnesium and silicon energy variations are in fact due to compound nucleus effects with few levels concerned in the reaction. Conditions in the compound nucleus for the present results are probably such that many levels are involved in the reaction and consequently a reasonable average over levels is made at all the energies investigated.

The energy variation of elastic and inelastic scattering from natural nickel has been studied between 8 and 14 MeV by Hu *et al.* (1959). The cross sections observed are in general agreement with the present results but a detailed comparison cannot be made since a mixture of isotopes was used in Hu's work.

ACKNOWLEDGMENTS

The authors wish to thank members of the Cyclotron Scattering Group for help in recording the results. They also wish to thank the Atomic Energy Research Establishment for preparing the separated ^{58}Ni target.

REFERENCES

GLASSGOLD, A. E., CHESTON, W. B., STEIN, M. L., SCHULDT, S. B., and ERIKSON, G. W., 1957, *Phys. Rev.*, **106**, 1207.

GOVE, H. E., KUEHNER, J. A., LITHERLAND, A. E., ALMQVIST, E., BROMLEY, D. A., FERGUSON, A. J., ROSE, P. H., BASTIDE, R. P., BROOKS, N., and CONNOR, R. J., 1958, *Phys. Rev. Letters*, **1**, 251.

GREENLEES, G. W., HAYWOOD, B. C., KUO, L. G., and PETRAVIC, M., 1957 a, *Proc. Phys. Soc.* A, **70**, 331.

GREENLEES, G. W., KUO, L. G., and PETRAVIC, M., 1957 b, *Proc. Roy. Soc.* A, **243**, 206.

GREENLEES, G. W., KUO, L. G., LOWE, J., and PETRAVIC, M., 1958, *Proc. Phys. Soc.*, **71**, 347.

HINTZ, N., 1957, *Phys. Rev.*, **106**, 1201.

HU, C., KIKUCHI, K., KOBOYASKI, S., MATSUDA, K., NAGAHARA, Y., ODA, Y., TAKANO, N., TAKEDA, M., and YAMAZAKI, I., 1959, *J. Phys. Soc. Japan*, **14**, 861.

PRESKITT, C. A., JR., and ALFORD, W. P., 1958, *Report No.* NYO-2172, University of Rochester.

WALDORF, W. F., and WALL, N. S., 1957, *Phys. Rev.*, **107**, 1602.

Cascade Theories and the Landau Approximation

By J. W. GARDNER

Atomic Power Division, English Electric Co., Ltd., Whetstone, Leicester

MS. received 15*th April* 1959, *in final form* 7*th August* 1959

Abstract. The track-length angular structure function $f(E\theta/E_s)$ of high energy ($>5\times10^8$ ev) electrons in air showers is calculated without the use of the Landau multiple scattering approximation, which has been used in all previous work except that of Chartres and Messel. Chartres used the Tamm–Belenky model of the cascade; the present work is based on the simpler 'AS' model (Approximation A, super-simplified cross sections). Our results are compared with those of Chartres, and with those of Kalos and Blatt who used the AS model in conjunction with the Landau approximation. It is concluded that the error introduced by the simplicity of our model is small compared with that introduced by the Landau approximation. Except near $E\theta/E_s=0$, where the AS model is not expected to hold, the present treatment gives values of $f(E\theta/E_s)$ in excellent agreement with Chartres' calculations based on the more refined cascade model.

§ 1. Introduction

In cascade theory the approximation of Landau (1940) is the equivalent of the well-known multiple scattering approximation which, when applied to the elastic scattering of a particle without loss of energy, yields a Gaussian angular distribution. Both are special cases of the diffusion approximation in which an integral operator is replaced by a second derivative (the first non-vanishing term in a Taylor expansion). Calculations by Snyder *et al.* (1949) and by Molière (1948) have emphasized the limitations of the approximation in multiple scattering theory; more recently Chartres and Messel (1955, 1956) have criticized its use in cascade theory. These authors calculated the track-length angular distribution using the model of Tamm and Belenky (1939) both with, and without, the Landau approximation and they found that the approximation introduces large inaccuracies at both small and large distances from the shower axis.

The Tamm–Belenky model of the cascade was introduced originally for the purpose of yielding an analytical solution for the track-length average numbers when the ionization loss is included, although in some later work by Belenky (1944) as well as that of Chartres the ionization term is omitted. It is of interest to examine the sensitivity to the Landau approximation of calculations based on other models of the electron–photon cascade, and to compare this with Tamm–Belenky type calculations. A model very widely used for interpreting experimental measurements on the lateral spread of the cascade is that described as 'Approximation A' by Rossi and Greisen (1941) combined with the 'super-simplified' cross sections of Friedman (1949). The present paper investigates the effect of the Landau approximation in calculations of the track-length angular distribution in air using this model, which we shall refer to briefly as the AS model.

§ 2. ASSUMPTIONS AND DEFINITIONS

In this section are collected for convenient reference the various assumptions and definitions associated with the AS model. 'Approximation A' postulates that ionization loss, Compton collisions and knock-on collisions are ignored, and that the cross sections for pair production and bremsstrahlung are replaced by their extreme relativistic values. This set of approximations is reasonable for electrons of energy much higher than the critical energy (much higher than 100 MEV in air).

The 'super-simplified' cross sections of Friedman are:

$$\sigma_{\mathrm{pair}}(E, E') = 7/(9E), \quad \sigma_{\mathrm{brems}}(E, E') = (E - E')^{-1}. \quad \ldots\ldots (1)$$

Here E is the energy of the initial particle or photon and E' is the energy of a secondary electron; in the case of bremsstrahlung the secondary photon has energy $E - E'$, in the case of pair creation the second member of the pair has this energy. We shall use expressions (1) rather than the full expressions for the extreme relativistic cross sections: the resulting errors are less than 10% in the energy region of interest here, and the mathematics is made much more tractable.

As far as the angular spread of the cascade is concerned, all spreading processes other than Coulomb scattering of electrons by the nuclei of the air will be ignored. The most important processes neglected are the angular deviations in bremsstrahlung and pair creation, and the angular deviation due to the action of the Earth's magnetic field. The neglect of these spreading processes is standard in the AS model and, so far as the author is aware, in all other cascade models. Kalos and Blatt (1954) discuss the effect of this approximation: the error is probably comparable with that resulting from the expressions (1).

The following definitions are used in the paper:

E_s ($= 21$ MEV) is the 'characteristic' multiple Coulomb scattering energy.

σ_0 ($= 7/9$ in the AS model) is the total pair production cross section.

$\phi_\pi(E_0, E, t, \theta)\, dE\, d\theta$ is the average number of electrons in the energy interval $E, E + dE$ at depth t making a projected angle with the shower axis (direction of initial electron's velocity) in the range $\theta, \theta + d\theta$; the initial electron is assumed to have energy E_0 at $t = 0$.

$\phi_\gamma(E_0, E, t, \theta)$ is the corresponding distribution function for the photons.

$v(E_0, E, \theta)$ is the track length defined by

$$v(E_0, E, \theta) = \int_0^\infty \phi_\pi(E_0, E, t, \theta)\, dt. \quad \ldots\ldots (2)$$

$z_\pi(E_0, E)$ is the longitudinal track length defined by

$$z_\pi(E_0, E) = \int_{-\infty}^\infty v(E_0, E, \theta)\, d\theta. \quad \ldots\ldots (2a)$$

Other terms will be defined in the text as they arise.

§ 3. BASIC EQUATION

It will be convenient to introduce integral operators A, B and C as follows: let $f(E)$ be an arbitrary function of E, other variables being suppressed for the moment; then

$$Af=\lim_{\epsilon\to 0}\left[-\int_{E+\epsilon}^{\infty} f(E')\sigma_{\mathrm{brems}}(E',E)\,dE' + f(E)\int_{0}^{E-\epsilon}\sigma_{\mathrm{brems}}(E,E')\,dE'\right] \qquad \ldots\ldots(3)$$

$$Bf=2\int_{E}^{\infty} f(E')\sigma_{\mathrm{pair}}(E',E)\,dE' \qquad \ldots\ldots(4)$$

$$Cf=\int_{E}^{\infty} f(E')\sigma_{\mathrm{brems}}(E',E'-E)\,dE'. \qquad \ldots\ldots(5)$$

The limiting process is necessary because the bremsstrahlung cross section contains the infra-red catastrophe. The signs are chosen in such a way that the quantities $A(s)$, $B(s)$ and $C(s)$ of Rossi and Greisen (1941) are the Mellin transform images of the operators A, B and C respectively.

In what follows all angles are projected angles, i.e. the whole shower is projected onto a plane containing the shower axis. This corresponds experimentally to taking measurements of angles in a cloud chamber without stereoscopic photographs. Furthermore, consonant with the assumption $E \gg E_s$ of the present model, all angles are taken to be much less than one radian.

The diffusion equations for the distribution functions ϕ_π, ϕ_γ are well known [see for example Rossi and Greisen (1941)]. Most work on the Landau approximation has however been presented in terms of the track length v, defined above: this quantity has the advantage of combining mathematical tractability with an accurate simulation of the overall spread of the shower. The diffusion equation for v, obtained by integrating that for ϕ_π over t from zero to infinity is

$$Fv-\left(\frac{\partial v}{\partial t}\right)_{\mathrm{scatt}}=\delta(\theta)\delta(E_0-E) \qquad \ldots\ldots(6)$$

where the operator F is defined by

$$F=A-\frac{BC}{\sigma_0}. \qquad \ldots\ldots(7)$$

The term $(\partial v/\partial t)_{\mathrm{scatt}}$ would in the Landau approximation be replaced by

$$\left(\frac{E_s}{2E'}\right)^2\frac{\partial^2 v}{\partial \theta'^2}$$

where E', θ' are integration variables for the energy and angle integrations respectively. In the present work we retain the 'exact' expression

$$\left(\frac{\partial v}{\partial t}\right)_{\mathrm{scatt}}=\int_{-\infty}^{\infty}[v(\theta'+\alpha)-v(\theta')]\xi(\alpha)\,d\alpha \qquad \ldots\ldots(8)$$

where $\xi(\alpha)$ is given by the well-known Snyder–Scott projected-angle scattering formula, which reads in standard notation (see for example Rossi 1952):

$$\xi(\alpha)=\frac{2\pi NZ^2}{A}\left(r_e\frac{mc}{p\beta}\right)^2\left[\alpha^2+\left(\frac{Z^{1/3}}{137}\,\frac{mc}{p}\right)^2\right]^{-3/2}, \text{ for } |\alpha|\leqslant\alpha_c \qquad \ldots\ldots(9a)$$

$$\xi(\alpha)=0, \quad \text{for} \quad |\alpha|>\alpha_c. \qquad \ldots\ldots(9b)$$

In view of (9*b*) the infinite limits of integration in (8) can be replaced by the finite limits $\pm\alpha_c$.

§ 4. ITERATION SOLUTION

An integro-differential equation such as (6) may be solved by the variation-iteration technique formulated by Friedman (1949) and published in modified form by Kalos and Blatt (1954). Any iteration procedure requires of course some reasonably good trial function as a basis: in the present instance there is a considerable choice of rough solutions available from models of the cascade which use the Landau approximation.

Let us assume that we have a trial solution $v_0(E_0, E, \theta)$ to equation (6), and let η denote the difference between v_0 and the exact solution v. Then if v_1 is the first iterate obtained by the Friedman scheme it may be shown that the normalizations of v_0 and v_1 are independent; moreover, since it has been obtained by a variation method, $v_1 = v + \mathrm{O}(\eta^2)$. The relation between v_0 and v_1 is given by

$$v_1(E_0, E, \theta) = \frac{[v_0(E_0, E, \theta)]^2}{\int_E^{E_0} dE' \int_{-\infty}^{\infty} d\theta' \left[F v_0(E_0, E', \theta') - \left(\frac{\partial v_0}{\partial t}\right)_{\mathrm{scatt}} \right] v_0(E', E, \theta - \theta')} . \qquad \ldots\ldots(10)$$

It is readily seen from (6) that the choice $v_0 = v$ leads to $v_1 = v$ also.

Kalos and Blatt (1954) have evaluated (10) in the Landau approximation, i.e. with

$$\left(\frac{\partial v}{\partial t}\right)_{\mathrm{scatt}} \quad \text{replaced by} \quad \left(\frac{E_s}{2E'}\right)^2 \frac{\partial^2 v_0}{\partial \theta'^2} ;$$

we shall evaluate it using the full expression (8) for $(\partial v/\partial t)_{\mathrm{scatt}}$ and compare our results with Kalos' and other calculations. We shall use the following trial function:

$$v_0(E_0, E, x) = \frac{E_0}{E}\left[\exp(-|x|) - \frac{1}{\sqrt{2}} \exp(-\sqrt{2}|x|)\right] \qquad \ldots\ldots(11)$$

with

$$x = 2\mu E\theta/E_s \qquad \ldots\ldots(12)$$

where μ is a numerical constant associated with the AS model and has the value 1·46 (see Friedman 1949 or Kalos and Blatt 1954). Our trial function differs from that used by Kalos only in the omission of a term in $\delta(E_0 - E)$ which stems from the Landau approximation itself rather than the physics of the cascade. In the present work we may therefore use Kalos' results for the integration of the term involving F in (10), after subtracting any terms arising from the integration of the delta function.

It then remains to evaluate the integrals involving the $(\partial v_0/\partial t)_{\mathrm{scatt}}$ term (briefly referred to as the 'scattering integrals') and substitute back into the iteration formula. This programme occupies the next four sections of this paper.

§ 5. FIRST SCATTERING INTEGRAL

From (8) and (10) it is seen that integration over three variables occurs in the scattering term, which we will denote by Σ. Thus:

$$\begin{aligned}\Sigma &= \int_E^{E_0} dE' \int_{-\infty}^{\infty} d\theta' \left(\frac{\partial v_0}{\partial t}\right)_{\mathrm{scatt}} v_0(E', E, \theta - \theta') \\ &= \int_E^{E_0} dE' \int_{-\infty}^{\infty} d\theta' \int_{-\infty}^{\infty} d\alpha [v_0(\theta' + \alpha) - v_0(\theta')] \xi(\alpha) v_0(E', E, \theta - \theta').\end{aligned} \qquad \ldots\ldots(13)$$

The integration over α may be transformed by using (9) with β equated to unity (valid at the high energies we are considering) to give

$$\left(\frac{\partial v}{\partial t}\right)_{\text{scatt}} = \frac{E_s}{E}\int_{-\infty}^{\infty} d\alpha S\left(\frac{E\alpha}{E_s}\right)\frac{\partial^2 v(\alpha+\theta)}{\partial\theta^2} \qquad \ldots\ldots(14)$$

where

$$S(r) = \frac{1}{\gamma^2}\left[(\gamma^2+r^2)^{1/2} - r\right] \qquad \ldots\ldots(15)$$

and

$$\gamma = \frac{Z^{1/3}}{137}\frac{mc^2}{E_s}. \qquad \ldots\ldots(16)$$

Substitution of (11) and (14) into (13) and use of the geometrical representation of a double integral to change the order of integration transforms (13) to

$$\Sigma = \frac{4E_0E_s}{E}\int_0^{\infty} dz\, S\left(\frac{z}{2\mu}\right) T(x,z) \qquad \ldots\ldots(17)$$

with

$$T(x,z) = \int_0^{\infty} dx' \int_1^{y_0} dy\left[K(z,yx') - \sqrt{2}K(\sqrt{2}z, \sqrt{2}yx')\right] \times \left[K(x,x') - \frac{1}{\sqrt{2}}K(\sqrt{2}x, \sqrt{2}x')\right] \qquad \ldots\ldots(18)$$

and

$$y_0 = E_0/E. \qquad \ldots\ldots(19)$$

The function $K(x_1, x_2)$ is defined by

$$K(x_1, x_2) = \cosh x_2 \exp(-x_1), \quad x_1 > x_2 \qquad \ldots\ldots(20a)$$

$$K(x_1, x_2) = \cosh x_1 \exp(-x_2), \quad x_2 > x_1. \qquad \ldots\ldots(20b)$$

The integration over x' in (18) may be accomplished by using the following general result:

$$\int_0^{\infty} dx' K(rx, rx')K(sz, syx') = G_{rs}(x,y,z) \qquad \ldots\ldots(21)$$

with

$$G_{rs}(x,y,z) = \frac{1}{r^2-(sy)^2}\left\{rK(sz, syx) - sy\,K\left(rx, \frac{rz}{y}\right)\right\}. \qquad \ldots\ldots(22)$$

Here r and s denote numerical coefficients which in the application to (18) assume the values unity or $\sqrt{2}$. The proof of (21) follows readily, if somewhat tediously, from repeated application of standard elementary integrals; the cases of $x > z/y$ and $x < z/y$ must be taken separately, and in each case the integration range $0 < x' < \infty$ must be subdivided into the three regions:

$$0 < x' < \frac{z}{y}\ (\text{or } x)$$

$$\frac{z}{y}\ (\text{or } x) < x' < x\left(\text{or } \frac{z}{y}\right)$$

$$x\left(\text{or } \frac{z}{y}\right) < x' < \infty.$$

Substitution of (21) in (18) yields

$$T(x,z) = \int_1^{y_0} dy\left[G_{rr}(x,y,z) + G_{ss}(x,y,z) - \frac{1}{s}G_{sr}(x,y,z) - sG_{rs}(x,y,z)\right] \qquad \ldots\ldots(23)$$

where r, s now have the particular values $r = 1$, $s = \sqrt{2}$.

§ 6. SECOND SCATTERING INTEGRAL

Although the integration limits in (23) appear finite the ratio E_0/E may in fact be extremely large, and so it is necessary to investigate what happens as $y_0 \to \infty$. Now in view of the definitions (20) and (22) of the K and G functions (23) must, as $y_0 \to \infty$, be expressible entirely in terms of elementary functions (log, cosh, etc.) combined with the exponential integrals Ei, for which tables exist. As a number of slightly different notations are in currency for these integrals we postulate here the following definitions:

$$\mathrm{Ei}(w) = \int_{-\infty}^{w} \frac{\mathrm{e}^u}{u}\,du \quad (24a); \qquad \mathrm{Ei}(-w) = -\int_{w}^{\infty} \frac{\mathrm{e}^{-u}}{u}\,du. \quad (24b)$$

It is of course also necessary to verify that the right-hand side of (23) remains finite as $y_0 \to \infty$. This may be done by writing out the full expressions for the G's and noting that, although each G must on integration give rise to a term which diverges logarithmically as $y_0 \to \infty$, the signs of these terms alternate so that all divergencies cancel.

As in the previous section we shall omit the details of the term by term integrations and the tedious algebraic 'tidying-up'; it is however necessary to define a few ancillary functions before we can write in a reasonably amenable form the final expression for $T(x, z)$, in the limit $y_0 \to \infty$ (which is always implied henceforth).

We define

$$\mathrm{Che}(a, b;\ c) = \mathrm{e}^a \mathrm{Ei}\{-(a+b)+c\} + \mathrm{e}^{-a}\mathrm{Ei}\{a+b+c\} \qquad \ldots\ldots (24)$$

$$\mathrm{She}(a, b;\ c) = \mathrm{e}^a \mathrm{Ei}\{-(a+b)+c\} - \mathrm{e}^{-a}\mathrm{Ei}\{a+b+c\} \qquad \ldots\ldots (25)$$

$$M_{rs}(x, z) = \frac{\mathrm{e}^{-rx}}{2r}\left[\mathrm{Che}(zr, 0;\ 0) - \mathrm{Che}(zs, 0;\ 0)\right] + \frac{\mathrm{e}^{-sz}}{4r}\,\mathrm{She}(rx, 0;\ -sx) \qquad \ldots\ldots (26)$$

$$N_{rs}(x, z) = \frac{1}{4r}\left[\mathrm{Ei}\{\lambda z(s-r)\} - \mathrm{Ei}\{\lambda x(s-r)\}\right]\mathrm{e}^{-\lambda(sz-rx)} \qquad \ldots\ldots (27)$$

with

$$\lambda = \overline{z-x}/|z-x|$$

$$\begin{aligned} P_{rs}(x, z) = {} & \frac{\cosh(rx_<)}{2r}\left[\mathrm{e}^{-rx_>}\ln(x/z) - \mathrm{e}^{rx_>}\,\mathrm{Ei}(-2rx_>)\right] \\ & - \frac{\mathrm{e}^{-rx_>}}{4r}\,\mathrm{Che}(rx_<, rx_<;\ 0) + \frac{\mathrm{e}^{-rx}}{4r}\,\mathrm{Che}(sz, 0;\ -rx_<) \\ & + \frac{1}{4r}\left[\mathrm{e}^{(sz+rx)}\,\mathrm{Ei}\{-(r+s)x_>\} + \mathrm{e}^{-(sz+rx)}\,\mathrm{Ei}\{(r+s)x_<\}\right] \end{aligned} \qquad \ldots\ldots (28)$$

where $x_>$, $x_<$ denote respectively the greater and lesser of x, z.

It is also convenient to define a single function to represent the sum of the three functions defined by (26), (27) and (28), thus:

$$\Phi_{rs}(x, y) = M_{rs}(x, y) + N_{rs}(x, y) + P_{rs}(x, y). \qquad \ldots\ldots (29)$$

In terms of the Φ functions the final expression for $T(x, z)$ then reads

$$T(x, z) = \Phi_{rs}(x, z) + \Phi_{sr}(x, z). \qquad \ldots\ldots (30)$$

Here, as in (23), $r = 1$ and $s = \sqrt{2}$.

§ 7. THIRD SCATTERING INTEGRAL

To complete the evaluation of the scattering term Σ it remains to perform the integration over z in (17). Since closed expressions do not exist for the exponential integrals occurring in $T(x, z)$ it is not to be expected that the integral in (17) can be evaluated in closed form. It will be shown, rather, to be expressible as a rapidly convergent series, suitable for computation to any desired practical accuracy.

Let us first consider the series expansion of $T(x, z)$ or rather of $\Phi_{rs}(x, z)$, since the expansion of $\Phi_{sr}(x, z)$ and hence $T(x, z)$ will then follow automatically from symmetry. As would be expected from the form of $P_{rs}(x, z)$ and $N_{rs}(x, z)$ the expansion of $\Phi_{rs}(x, y)$ has alternative forms according as to whether z is greater or less than x. In either case the expansion may be obtained by substituting into (24)–(30) the familiar series for the Ei functions (see for example Jahnke and Emde 1945). After considerable algebraic manipulation of the resulting expressions, with appropriate checks on convergency at each stage, the expansions may be written as follows:

$$\Phi_{rs}(x \geqslant z) = a_0 + a_2 z^2 + a_4 z^4 + \ldots.. \qquad \ldots\ldots(31)$$

$$\Phi_{rs}(x < z) = \omega(z) + b_0 + b_1 z + b_2 z^2 + b_3 z^3 + \ldots.. \qquad \ldots\ldots(32)$$

where the coefficients a_i, b_i are functions of x given explicitly in the Appendix, and $\omega(z)$ stands for terms logarithmic in z, also given explicitly in the Appendix. The expansions for $T(x, z)$ may now be written

$$T(x \geqslant z) = A_0 + A_2 z^2 + A_4 z^4 + \ldots.. \qquad \ldots\ldots(33)$$

$$T(x < z) = \Omega(z) + B_0 + B_1 z + B_2 z^2 + B_3 z^3 + \ldots.. \qquad \ldots\ldots(34)$$

with

$$A_i = a_i + \tilde{a}_i \qquad \ldots\ldots(35)$$

$$B_i = b_i + \tilde{b}_i \qquad \ldots\ldots(36)$$

$$\Omega = \omega + \tilde{\omega} \qquad \ldots\ldots(37)$$

and where $\tilde{a}_i$, $\tilde{b}_i$, $\tilde{\omega}$ are the quantities in the expansion of Φ_{sr} adjoint to a_i, b_i, ω in the expansion of Φ_{rs}; that is to say $\tilde{a}_i$ is obtained from a_i by interchanging r and s in the appropriate formula in the Appendix, and similarly for $\tilde{b}_i$ and $\tilde{\omega}$.

If in the integrand of (17) we now substitute formula (15) for $S(z/2\mu)$ and formula (34) for $T(x, z)$ we obtain terms of two general types:

$$(a) \qquad z^i[\{1 + (\zeta z)^2\}^{1/2} - \zeta z] \quad \text{with} \quad \zeta = 1/2\mu\gamma$$

and

$$(b) \qquad e^{mz} \ln(nx)[\{1 + (\zeta z)^2\}^{1/2} - \zeta z]$$

where m and n are very simple multipliers—usually just unity or $\sqrt{2}$.

Had we used formula (33) for $T(x, z)$ we would have obtained terms of type (*a*) only, and with even values of i only.

Now a term by term integration of the right side of (17) can be justified, so it remains to integrate functions such as (*a*) and (*b*) with respect to z between the lower limit $z = 0$ and the upper limit $z = \infty$, or effectively some value z_c determined the cut-off angle α_c in (9), and then sum the results. (For practical purposes as we shall see, the summation of only the first few terms is required.) The integration of terms of type (*a*) can be achieved in closed form by elementary methods; integration of type (*b*) terms may be accomplished by using expansions of both e^{mz} and $[\{1+(\zeta z)^2\}^{1/2}-\zeta z]$ in powers of z to transform to integrals of the general type $\int z^{\nu} \ln z \, dz$ which can be evaluated by elementary methods. (Again only the first few such integrals are significant numerically.)

To decide how many terms to take in evaluating the integral on the right side of (17) it is necessary to consider the accuracy of the scattering formula (9). For scattering in air of high energy electrons ($E>12mc^2$) the α_c of the Snyder–Scott formula has the value $280mc^2/A^{1/3}E$, corresponding to a value of z_c of about 0·85. However Olbert (1952) has given arguments for taking $\alpha_c=328mc^2/A^{1/3}E$, corresponding to $z_c \simeq 1{\cdot}0$ The discrepancy between the Snyder–Scott formula and the Olbert formula seems to be the measure of the present uncertainty in α_c, corresponding to a 15% to 20% uncertainty in z_c.

If we denote by $I(x,z)$ the indefinite integral:

$$\int dz \, S\left(\frac{z}{2\mu}\right) T(x,z)$$

then (17) becomes

$$\Sigma=\frac{4E_0E_s}{E}[I(x,z_c)-I(x,0)]. \qquad \ldots\ldots(38)$$

Let us further denote by $\Delta I(x,z_c)$ the error in $I(x,z_c)$, and hence in the definite integral $I(x,z_c)-I(x,0)$, associated with the uncertainty in z_c; and let $E_j(x,z)$ be the error in $I(x,z)$ resulting from cutting off its series expansion, derived from the term by term integration, at the term of power j in z. Then we require that $E_j(x,z_c) \ngtr \Delta I(x,z_c)$. This gives a value of j between 2 and 3, so the evaluation of $I(x,z)$ should be taken as far as the z^3 term if formula (34) is used and as far as the z^2 term if (33) is used. The numerical computation of $[I(x,z_c)-I(x,0)]$ was in fact done for the following values of x: 0, 1, 2, 4, 6, 8. For all except the first of these values $x \geqslant z_c$ and formula (33) applies; for $x=0$ formula (34) applies but in this case the logarithmic terms in z vanish and (34) then assumes a simple, readily computable, form. Thus, except for $x=0$, it was necessary to consider only terms of type (*a*) above, with $i=0$ and 2, for the term by term evaluation of $I(x,z)$, and this led to the following formula for practical computation of the definite integral

$$I(x,z_c)-I(x,0)=\nu\left[\tfrac{1}{2}(\tfrac{1}{2}+\ln 2-\mathrm{1n}\,\nu)A_0(x)+\tfrac{1}{3}(\tfrac{3}{2}-\nu)A_1(x)+\tfrac{1}{4}(1+\frac{\nu^2}{2}\ln\nu)A_2(x)\right] \qquad \ldots\ldots(39)$$

with $\nu=\zeta^{-1}$.

§ 8. CALCULATION OF STRUCTURE FUNCTION

It is usual, and convenient, to express results for the track-length angular distribution in terms of the angular structure function $f(E\theta/E_s)$ defined by, $f=(E_s/E)(v/z_\pi)$. As is well known, the longitudinal track length for the AS model is given by

$$z_\pi(E_0,E)=\frac{[E_0/E^2+\delta(E_0-E)]}{\mu^2}. \qquad \ldots\ldots(40)$$

To find f, then, it remains to combine (40) with v_1 as calculated by (10)†. In the preceding sections we have described the calculation of those terms in v_1, namely the scattering integrals, which arise from the removal of the Landau approximation; the remaining terms have been computed by Kalos, whose results we have used. The final formula for the structure function then reads:

---

† Any apparent accuracy gained by proceeding to iterates higher than v_1 would be spurious due to the approximate nature of the AS model; in this context therefore it is justified to equate v and v_1.

$$f(x)=\frac{\mu^3\{\exp(-|x|)-2^{-1/2}\exp(-2^{1/2}|x|)\}^2}{H_1(x)+H_2(x)+4\mu^2\{I(x,z_c)-I(x,0)\}} \qquad \ldots\ldots(41)$$

where, as will be recalled from (12), $x=2\mu E\theta/E_s=2{\cdot}93E\theta/E_s$. The last term in the denominator may be computed from (39) (or a similar but simpler formula when $x=0$); the first two terms represent integrals which have been computed by Kalos, whose definitions we reproduce here for completeness:

$$H_1(x)=\int_0^\infty dx'\,[\tfrac{1}{2}\bar{g}(x')+\bar{g}_1(x')]K(x,x'), \qquad \ldots\ldots(42)$$

$$H_2(x)=-2^{-1/2}\int_0^\infty dx'\,\bar{g}_1(x')K(2^{1/2}x,2^{1/2}x'), \qquad \ldots\ldots(43)$$

where

$$\bar{g}(x)=\Gamma(x)-2^{-1/2}\Gamma(2^{1/2}x) \qquad \ldots\ldots(44)$$

$$\bar{g}_1(x)=\Gamma_1(x)-2^{-1/2}\Gamma_1(2^{1/2}x) \qquad \ldots\ldots(45)$$

with

$$\Gamma(x)=\{\ln(\gamma'|x|)+2\}\exp(-|x|)+(1+2|x|)\mathrm{Ei}(-|x|) \qquad \ldots\ldots(46)$$

$$\Gamma_1(x)=\{|x|^{-1}\ln(\gamma'|x|)-1\}\exp(-|x|)-(|x|+1+|x|^{-1})\mathrm{Ei}(-|x|) \qquad \ldots\ldots(47)$$

and where γ' has been written for the Euler constant 1·7811 (see for example Jahnke and Emde 1945).

Values of $f(x)$ were computed for $x=0, 1, 2, 4, 6, 8$; the results are displayed graphically in the figure.

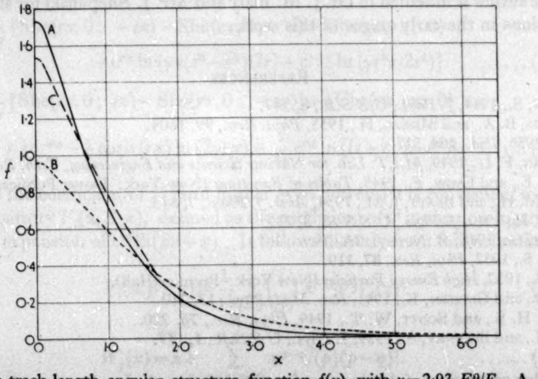

Results for track-length angular structure function $f(x)$, with $x=2{\cdot}93\ E\theta/E_s$. A, present calculation on AS model without Landau approximation; B, Kalos' calculation on AS model with Landau approximation; C, Chartres' calculation on Tamm–Belenky model without Landau approximation.

§ 9. DISCUSSION AND CONCLUSION

In this paper we have described the calculation of the structure function $f(x)$ for the track-length angular distribution of the high energy electron–photon cascade in air. The calculation has been based on the AS model and no use has been made of the Landau approximation. It is interesting to compare our results with; (*a*) results obtained from the same model, plus the use of the Landau approximation; and (*b*) results from a different model without the use of the Landau approximation. This comparison is made in the figure where, in addition, to our $f(x)$, are presented that calculated by Kalos and Blatt (1954) for case (*a*) and that of Chartres and Messel (1956) for case (*b*). It will be seen that our results agree much better with Chartres' than with Kalos', indicating that the difference between these authors' results is attributable mainly to the use by Kalos of the Landau approximation, rather than to Chartres' use of the more sophisticated (Tamm–Belenky) model†.

From the above comparisons it may reasonably be concluded that, provided the scattering integrals are retained and not replaced by the Landau approximation, the simple AS model gives almost as good a picture of the angular structure function at high energies as other more elaborate models of the cascade. The limitation to high energies cannot of course be removed without replacing the supersimplified cross sections of the AS model by more realistic ones; it is the use of these supersimplified cross sections which leads our calculation to overestimate $f(x)$ near $x=0$. The *under*estimation of $f(x)$ over a much wider range of x by Kalos is due to the large negative error introduced by the Landau approximation in this range; indeed this error is larger than would appear from a straight comparison of his results with Chartres' since it is partially cancelled by the positive error arising from the AS model near $x=0$.

ACKNOWLEDGMENTS

The author is indebted to Dr. J. M. Blatt and Mr. J. Shepanski for stimulating discussions in the early stages of this work.

REFERENCES

BELENKY, S., 1944, *J. Phys., U.S.S.R.*, **8**, 347.
CHARTRES, B. A., and MESSEL, H., 1955, *Phys. Rev.*, **99**, 1604.
—— 1956, *Ibid.*, **104**, 517.
FRIEDMAN, F. L., 1949, *M.I.T. Lab. for Nuclear Science and Engineering, Tech. Rep.* No. 31.
JAHNKE, E., and EMDE, F., 1945, *Tables of Functions* (New York: Dover Publications).
KALOS, M. H., and BLATT, J. M., 1954, *Aust. J. Phys.*, **7**, 543.
LANDAU, L., 1940, *J. Phys., U.S.S.R.*, **3**, 237.
MOLIÈRE, G., 1948, *Z. Naturf.*, **3A**, 78.
OLBERT, S., 1952, *Phys. Rev.*, **87**, 319.
ROSSI, B., 1952, *High Energy Particles* (New York: Prentice Hall).
ROSSI, B., and GREISEN, K., 1941, *Rev. Mod. Phys.*, **13**, 240.
SNYDER, H. S., and SCOTT, W. T., 1949, *Phys. Rev.*, **76**, 220.
TAMM, I., and BELENKY, S., 1939, *J. Phys., U.S.S.R.*, **1**, 177.

---

† Other calculations of the structure function based on the Landau approximation have been discussed by Chartres and Messel (1956). They conclude, as we do, that it depends much more sensitively on the use, or non-use, of the Landau approximation, than it does on the detailed model assumed for the cascade.

APPENDIX

EXPANSIONS FOR $\Phi_{rs}(x, z)$

In what follows, the Euler constant 1·7811 is denoted by the standard symbol γ rather than by γ', since the other quantity γ defined by equation (16) of the text does not occur at all.

Case (*a*) $z \leqslant x$.

$$\Phi_{rs}(x, z) = \sum_{i=0}^{\infty} a_i(x) z^i \qquad \ldots\ldots \text{(A1)}$$

with

$$a_0(x) = \frac{1}{2r}\left[\text{She}\,(rx, 0;\ -sx) - e^{rx}\text{Ei}(-2rx) + e^{-rx}\ln\{\gamma rx(s^2 - r^2)/2s^2\}\right] \qquad \ldots\ldots \text{(A2)}$$

$$\begin{aligned} a_2(x) = {} & \frac{s^2}{4r}\,\text{She}(rx, 0;\ -sx) - \frac{re^{rx}}{4}\,\text{Ei}(-2rx) \\ & + \frac{s}{2}e^{-rx} + \frac{e^{-rx}}{4r}\left[r^2\ln(\gamma rx/2) + s^2\ln\{(s^2 - r^2)/s^2\}\right] \end{aligned} \qquad \ldots\ldots \text{(A3)}$$

$a_1(x) = a_3(x) = a_{2n+1}(x) = 0$, for all positive integral n.

Case (*b*) $z > x$.

$$\Phi_{rs}(x < z) = \omega(x, z) + \sum_{i=0}^{\infty} b_i(x) z^i \qquad \ldots\ldots \text{(A4)}$$

with

$$\begin{aligned} \omega(x, z) = {} & \frac{e^{-rx}}{4r}\left[e^{sz}\ln|sz + rx| + e^{-sz}\ln|sz - rx|\right] \\ & + \frac{\ln(z)}{r}\left[\sinh(rx)\{\cosh(sz) - \cosh(rz)\} - \frac{e^{-rx}}{2}\cosh sz\right] \end{aligned} \qquad \ldots\ldots \text{(A5)}$$

$$\begin{aligned} b_0(x) = {} & \frac{1}{4r}\left[\text{She}(rx, 0;\ -sx) - \text{She}(rx, 0;\ r'x) - \text{Che}(rx, rx;\ 0)\right. \\ & \left. + e^{rx}\ln\{\gamma x(s^2 - r^2)/2r\} + e^{-rx}\ln(\gamma r^3 x/2s^4)\right] \end{aligned} \qquad \ldots\ldots \text{(A6)}$$

$$\begin{aligned} b_1(x) = {} & \frac{s}{4r}\left[\text{She}(rx, 0;\ sx) - \text{She}(rx, 0;\ -sx)\right] + \tfrac{1}{4}\text{Che}(rx, rx;\ 0) \\ & + \tfrac{1}{2}e^{-rx} - \tfrac{1}{2}\cosh(rx)\ln(2\gamma rx) + \frac{s}{4r}e^{rx}\ln\{(s + r)/(s - r)\}. \end{aligned} \qquad \ldots\ldots \text{(A7)}$$

To express the coefficient of z^2 (and higher even powers) it is convenient to introduce the quantity $V_i(\alpha, \beta; x)$, defined as the coefficient of z^i in the non-logarithmic part of the expansion of $e^{\alpha z}\text{Ei}(\beta z + x)$. It follows directly from this definition that

$$V_i(\alpha, \beta;\ x) = \frac{1}{i!}\sum_{j=0}^{i}\binom{i}{j}\alpha^{i-j}\beta^j W_j(x) \qquad \ldots\ldots \text{(A8)}$$

with

$$W_q(x) = x + \sum_{p=q,\, q\neq 0}^{\infty} x^{p-q}/(p)(p-q)!. \qquad \ldots\ldots \text{(A9)}$$

Due to mutual cancellation the V_i do not appear in the coefficients of odd powers of z.

In terms of the V_2, then we have

$$\begin{aligned} b_2(x) = {} & \frac{s^2}{8r}[\mathrm{She}(rx,0;\; -sx) - \mathrm{She}(rx,0;\; sx)] - \frac{r}{8}\mathrm{Che}(rx,rx;\; 0) \\ & + \frac{\mathrm{e}^{rx}}{8r}[3(r^2-s^2) + s^2 \ln\{\gamma^2(s^2-r^2)\}] + \frac{r}{4}\cosh(rx)\ln(x/2\gamma r) \\ & + \frac{\mathrm{e}^{-rx}}{4r}[3s^2 - 2r^2 + 2\{r^2\ln(\gamma r) - s^2\ln(s\gamma^{1/2})\} + V_2(s,-s;\; -rx) \\ & + V_2(-s,s;\; -rx)] \qquad \text{......(A10)} \end{aligned}$$

and finally

$$\begin{aligned} b_3(x) = {} & \frac{s^3}{24r}[\mathrm{She}(rx,0;\; sx) - \mathrm{She}(rx,0;\; -sx)] + \frac{r^2}{24}\mathrm{Che}(rx,rx;\; 0) \\ & + \frac{\mathrm{e}^{rx}}{24}\left[2(r^2-s^2) - r^2\ln(2\gamma rx) + \frac{s^3}{r}\ln\left|\frac{s+r}{s-r}\right| + \frac{r^2\mathrm{e}^{-rx}}{72}[8 - 3\ln(2\gamma rx)]\right]. \\ & \qquad \text{......(A11)} \end{aligned}$$

Effect of Strange Particles on Nucleon Magnetic Moment

By S. K. KUNDU†

Department of Theoretical Physics, Indian Association for the
Cultivation of Science, Calcutta

MS. received 20*th July* 1959

Abstract. The contribution from hyperons and K-mesons to nucleon magnetic moment is calculated in the non-relativistic limit to the second order in the coupling constant. The Hamiltonian chosen corresponds to the derivative coupling of the pseudo-scalar K-meson with a fixed extended source. To fit with the existing experimental results for neutron magnetic moment a lower limit to the N–π coupling is suggested. Also the N–K–$\frac{\Lambda}{\Sigma}$ coupling is found here to be much smaller than the N–π coupling.

§ 1. INTRODUCTION

In view of the recent experimental trend that K-mesons are pseudo-scalar in nature and that hyperons are treated on the same footing as nucleons, it is interesting to investigate the effect of strange particles to neutron and proton magnetic moment in Chew–Low theory. One must further mention that parities of Λ and Σ particles are taken to be even relative to the nucleon, relative Λ and Σ parity is also even and the spins of K and (Λ, Σ) particles are 0 and $\frac{1}{2}$ respectively. In so far as strange particles are concerned Chew's theory neglects the mass difference of nucleon and hyperon which is too large and so a correction term is to be added to the energy of K-meson due to this fact. Considering the above, the effect of K-meson and hyperon contribution to nucleon magnetic moment is calculated similarly to that obtained by Friedman (1955) and Kundu (1958 a) in calculating the π-meson and nucleon current contribution respectively. It is found that this contribution improves the previous theoretical calculations where only the effect of π-meson and nucleon current has been taken into account. Of course, the effect of nucleon recoil should be of importance with the emission of the K-meson. In order to obtain quantitative agreement with experiment so far as neutron magnetic moment is concerned, this method suggests that the N–π coupling (f_π^2) should have a value greater than 0·079 and the N–K–$\frac{\Lambda}{\Sigma}$ coupling (f_K^2) is much smaller than the N–π coupling. Also the values of the coupling constants used here give the ratio $f_K^2/f_\pi^2 = 0{\cdot}082$, which agrees well with that obtained by Kumar and Biswas (1958) in calculating the relativistic contribution to nucleon magnetic moment from strange particles assuming K-mesons to be pseudo-scalar.

§ 2. THEORETICAL PROCEDURE

The conservation of strangeness at each vertex leads to the following Feynman diagrams to the second order

---

†Now at School of Physics, The University of Sydney

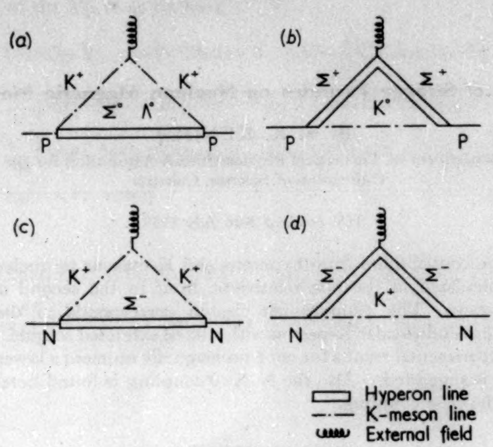

The matrix element corresponding to the diagram (*a*) is given by (Friedman 1955)

$$M_a = \left(\frac{e}{2M_N}\right)(\sigma\,.\,\mathbf{H})\ \frac{8}{3\pi} f_K{}^2 \left(2\,\frac{M_N}{M_K}\right)\frac{1}{M_K}\int_0^\infty \frac{v^2(K)\,K^4\,dK}{\Omega_K{}^4} \qquad \ldots\ldots(1)$$

where $\Omega_K = (K^2 + M_K{}^2)^{1/2} + |\,M_\gamma - M_N\,|$ and $|M_\gamma - M_N\,|$ is the absolute value of the nucleon–hyperon mass difference, K is the momentum of K-meson; M_N, M_γ and M_K are the masses of nucleon, hyperon and K-meson respectively.

On simplification (1) reduces to

$$\begin{aligned} M_a &= \left(\frac{e}{2M_N}\right)(\sigma\,.\,\mathbf{H})\,(f_K{}^2)\,(7{\cdot}449) \\ &= \left(\frac{e}{2M_N}\right)(\sigma\,.\,\mathbf{H})\,\mu_{PK^+} \qquad \ldots\ldots(2) \end{aligned}$$

where for the cut-off momentum $K_{\max}$ we use the relation $v^2(K) = 1$ between $K = 0$ and $K = K_{\max}$ and $v^2(K) = 0$ elsewhere, with $K_{\max} = 6\,M_K$, $M_K = 966\,m_e$ and $M_N = 1840\,m_e$.

Again the matrix element corresponding to the diagram (*b*) is (Kundu 1958 a)

$$M_b = \left(\frac{e}{2M_N}\right)(\sigma\,.\,\mathbf{H})\,\frac{1}{3\pi}\,\frac{M_N}{M_{\Sigma^+}}\,\frac{1}{M_K{}^2}\int_0^\infty \frac{v^2(K)\,K^4\,dK}{\Omega_K{}^3} \qquad \ldots\ldots(3)$$

which after simplification gives

$$\begin{aligned} M_b &= \left(\frac{e}{2M_N}\right)(\sigma\,.\,\mathbf{H})\,(f_K{}^2)\,(0{\cdot}8997) \\ &= \left(\frac{e}{2M_N}\right)(\sigma\,.\,\mathbf{H})\,\mu_{P\gamma^+} \qquad \ldots\ldots(4) \end{aligned}$$

with $M_{\Sigma^+} = 2340\,m_e$.

Similarly, from diagrams (*c*) and (*d*) we find

$$M_c = \tfrac{1}{2} M_a \quad \text{and} \quad M_d = -M_b$$

which gives

$$\mu_{\mathrm{NK}^+} = \tfrac{1}{2}\mu_{\mathrm{PK}^+} \quad \text{and} \quad \mu_{\mathrm{N}\gamma^-} = -\mu_{\mathrm{P}\gamma^+}. \qquad \ldots\ldots (5)$$

Thus the total contribution to neutron and proton magnetic moment including Dirac moment, π-meson, nucleon, K-meson and hyperon will be (in nuclear magnetons)

$$\mu_{\mathrm{N}} = 0 + \mu_{\mathrm{N}\pi^-} + \mu_{\mathrm{NP}} + \mu_{\mathrm{NK}^+} + \mu_{\mathrm{N}\gamma^-} \qquad \ldots\ldots (6)$$

and

$$\mu_{\mathrm{P}} = 1 + \mu_{\mathrm{P}\pi^+} + \mu_{\mathrm{PN}} + \mu_{\mathrm{PK}^+} + \mu_{\mathrm{P}\gamma^+} \qquad \ldots\ldots (7)$$

where

$$\mu_{\mathrm{N}\pi^-} = -\mu_{\mathrm{P}\pi^+} = -22{\cdot}5 f_\pi^2, \quad \mu_{\mathrm{NP}} = -1{\cdot}644 f_\pi^2 \quad \text{and} \quad \mu_{\mathrm{PN}} = 0.$$

For the π-meson current contribution ($\mu_{\mathrm{N}\pi^-}$ or $\mu_{\mathrm{P}\pi^+}$) and nucleon current contribution (μ_{NP} or μ_{PN}) the cut-off limit to the π-meson momentum is taken as $k_{\max} = 6\mu$, where k is the momentum of the π-meson and μ is its mass.

Now, to fit with the experimental results for neutron magnetic moment (i.e. $\mu_{\mathrm{N}} = -1{\cdot}913$) it is found from (6) that f_π^2 should be greater than 0·079 and for agreement with nucleon magnetic moments, the values for the coupling constant must be taken as $f_\pi^2 = 0{\cdot}08$ and $f_{\mathrm{K}}^2 = 0{\cdot}0066$ respectively. The ratio f_{K}^2/f_π^2 will thus be 0·082 against the relativistically calculated value 0·06.

§ 3. DISCUSSION

The effect of strange particles on nucleon magnetic moment is calculated here to the second order only and gives a lower limit to N–π coupling which is in good agreement with that used in connection with dispersion relations for the meson–nucleon problem (Salam 1956). Further the N–π coupling is found to be very large compared with N–K–$\frac{\Lambda}{\Sigma}$ coupling. It is worth mentioning that while the higher order corrections were considered by Friedman and Kundu using the renormalization effect of Chew, which is an approximate procedure (Chew 1954), the total second order effect from nucleon, π-meson and strange particles gives quite signficant results for nucleon magnetic moment if one assumes for f_π^2 and f_{K}^2 the values 0·08 and 0·066 respectively. Also the ratio f_{K}^2/f_π^2 which is in good agreement with that obtained from relativistic calculation indicates the possibility of treating the strange particles in non-relativistic limit. Of course, the effect of nucleon recoil could be taken into account with the space–time extension of the source (Kundu 1958 b).

ACKNOWLEDGMENT

The author is grateful to Professor D. Basu for helpful discussions. Thanks are also due to Professor G. C. Wick for useful criticism.

REFERENCES

CHEW, G. F., 1954, *Phys. Rev.*, **94**, 1755.
FRIEDMAN, M. H., 1955, *Phys. Rev.*, **97**, 1123.
KUMAR, K., and BISWAS, S. N., 1958, *Nucl. Phys.*, **9**, 446.
KUNDU, S. K., 1958 a, *Proc. Phys. Soc.*, **72**, 49.
—— 1958 b, *Nuovo Cim.*, **8**, 888.
SALAM, A., 1956, *Cern Symposium on High Energy Accelerators and Pion Physics*, p. 176.

The Scale Parameters in Non-empirical Molecular-orbital Calculations on σ–π Systems

BY E. THEAL STEWART
Chemistry Department, Queen's College, University of St. Andrews, Dundee, Scotland

MS. received 8*th July* 1959

Abstract. Parr and Crawford's (1948) calculations on the ethylene molecule have been extended so as to constitute a systematic study of the dependence of calculated π-electron excitation energies on the exponential scale parameter Z. An examination of the results and their wave-mechanical basis leads to the following conclusions: (i) In the neighbourhood of $Z_\sigma = Z_\pi = 3{\cdot}18$ both state energies and excitation energies are so sensitive to small changes in Z that they can have little quantitative meaning. (ii) Joint variation of Z_σ and Z_π between different π-electron states is inadmissible, and, provided its consequences are not masked by the use of the W_{2p} approximation, it can easily give transition energies incorrect even in sign. (iii) If Z_σ is kept constant, the independent variation of Z_π yields results which, though they have the partial validity characteristic of a partial-variation calculation, are not necessarily numerically significant: the 'optimum' values of Z_π for the various π-electron states and the corresponding 'minimum' energies almost certainly vary considerably with the form of the σ wave function and with the value of Z_σ. (iv) The establishment of a sound parametric basis for computations on systems described by π-electron wave functions is unlikely to result from anything less comprehensive than a 6-centre–16-electron variational study on ethylene. Until this can be achieved, non-empirical calculations on unsaturated hydrocarbon molecules seem bound to be ineffectual.

§ 1. INTRODUCTION

OF the many difficulties which have beset all 'non-empirical' calculations on the energy levels of unsaturated hydrocarbon molecules the most formidable has been the lack of any manifestly well-founded procedure for determining the optimum values of the adjustable parameters in the π-electron wave functions. The most important of these—if calculations on much simpler molecules may serve as a guide—is the scale parameter Z, which appears in the form $\exp(-Zr/n)$ in the molecular wave functions and the atomic wave functions from which they are constructed† (Löwdin 1959).

The best analytical wave functions for the carbon atom ($1s^2 2s^2 2p^2\ {}^3P$) available when Goeppert-Mayer and Sklar (1938) carried out their pioneer antisymmetrized molecular-orbital calculations on the π-electron energy levels of benzene were those of Zener (1930). Goeppert-Mayer and Sklar accepted Zener's value of the atomic scale factor for the L shell ($Z = 3{\cdot}18$), though, oddly enough, they used not Zener orbitals but unmodified hydrogen-like orbitals (Kauzmann 1957) in their calculations.

---

† In a variational calculation an adjustable scale parameter has, of course, no place in the true Hamiltonian operator. Nevertheless, Z is commonly known as the 'effective nuclear charge' of the atom to which it relates, and the difference between Z and the atomic number as the 'screening constant'. These pre-wave-mechanical terms are apt to suggest an illusory physical interpretation, which can lead to confusion even in the simplest systems (Altmann and Cohan 1954). In current American quantum-chemical usage the non-committal term 'orbital exponent' is applied to Z and also to Z/n.

They recognized the limitations imposed on their molecular calculation by the adoption of a scale factor appropriate to the ground state of an isolated carbon atom, and undoubtedly intended their value of Z to be modified as experience dictated. But in fact it has survived to the present day, unchanged and too often unchallenged. Inevitably the question arises whether non-empirical calculations in which an all-important parameter has to be chosen so arbitrarily can have any quantitative meaning; and we have endeavoured to answer the question in this paper by examining the Z-dependence of the spacing of the calculated energy levels of ethylene (the simplest π-electron system). It is only too well known that molecular-orbital calculations without a substantial empirical element are almost always markedly at variance with spectroscopic measurements (see, for example, Parr, Craig and Ross 1950, Moffitt and Scanlan 1953), and it is of considerable interest to determine to what extent this may be the consequence of an unlucky choice of Z.

To have any numerical significance, energies calculated by the method of Goeppert-Mayer and Sklar clearly need to be shown to be insensitive to reasonably small changes in Z (up to 10%, say) in the neighbourhood of $Z = 3{\cdot}18$ (or whatever other value may be selected). This same criterion may, we believe, be used to decide whether a useful purpose is served by attempts to refine linear variational parameters in wave functions which are almost certainly incorrect in scale, i.e. whether the greatly increased computational complexity arising from the introduction of configuration interaction and orbital self-consistency into the original Goeppert-Mayer–Sklar procedure can be expected to lead to results of enhanced significance. We hope to consider this problem in some detail in a later communication.

§ 2. THE Z-DEPENDENCE OF THE CALCULATED EXCITATION ENERGIES OF PLANAR ETHYLENE

The choice of the π-electron system of ethylene for an investigation of Z-dependence is an obvious one. The molecular-orbital expansion coefficients are determined by symmetry alone (the problem of orbital self-consistency thus being settled automatically); $2p\pi$ configuration interaction may be dealt with easily and completely; and, as no three- or four-centre integrals are involved, the results are free from an element of uncertainty (important at low values of Z) not fundamental to the Hückel π-electron approximation (Altmann 1951) or to the Goeppert-Mayer–Sklar procedure. Moreover, the absorption spectrum of ethylene has been examined with unusual rigour (Wilkinson and Mulliken 1955, Hammond and Price 1955), and there seems to be little doubt about the location or the form of the band corresponding to the allowed transition ${}^1A_g - {}^1B_{1u}$.

Preliminary studies of the Z-dependence of the calculated π-electron energies of hydrocarbon molecules have already been reported by Parr and Crawford (1948), by Shull and Ellison (1951) and by Murai (1952), but for the present purpose the first two are invalidated by the use of what we call the W_{2p} approximation (Goeppert-Mayer and Sklar 1938, Ross 1952, Stewart 1959). They lead indeed to the surprising conclusion that, in the range of Z concerned, calculated excitation energies tend to decrease as Z increases. Murai's calculations are considered in § 3.

Parr and Crawford (1948) have provided a comprehensive account of the application of the Goeppert-Mayer–Sklar technique to ethylene, and we recount here only sufficient to define our notation and to emphasize variants in the present procedure.

Four orthonormal spatial wave functions may be constructed from the appropriate 2p wave functions, π_a and π_b, of the carbon atoms $C_{(a)}$ and $C_{(b)}$. In the simplest molecular-orbital approximation they are, in order of decreasing energy (as in the figure),

$$\begin{aligned}
\Psi({}^1A_g^*) &= \tfrac{1}{2}(1-S)^{-1}[\pi_a\pi_b+\pi_b\pi_a-\pi_a\pi_a-\pi_b\pi_b];\\
\Psi({}^1B_{1u}) &= 2^{-1/2}(1-S^2)^{-1/2}[\pi_a\pi_a-\pi_b\pi_b];\\
\Psi({}^3B_{1u}) &= 2^{-1/2}(1-S^2)^{-1/2}[\pi_a\pi_b-\pi_b\pi_a];\\
\Psi({}^1A_g) &= \tfrac{1}{2}(1+S)^{-1}[\pi_a\pi_b+\pi_b\pi_a+\pi_a\pi_a+\pi_b\pi_b].
\end{aligned}$$

In the bracketed expressions the first factor of each term relates to the first electron, and the second factor to the second electron. S is the overlap integral $(\pi_a|\pi_b)$. The four wave functions correspond with Parr and Crawford's ψ_2, ψ_V, ψ_T, ψ_1. In principle, the first and the last of these functions may be improved by the formation of suitable orthonormal linear combinations; but, where there is no indication to the contrary, the results quoted in this paper have been obtained from calculations in which 'interaction' between $\Psi({}^1A_g)$ and $\Psi({}^1A_g^*)$ has not been taken into account. $\Psi({}^1B_{1u})$ and $\Psi({}^3B_{1u})$ may be regarded as either molecular-orbital or valency-bond wave functions.

The π-electron Hamiltonian operator may be written

$$H=-\tfrac{1}{2}\nabla_1^2-\tfrac{1}{2}\nabla_2^2+V_{a1}+V_{a2}+V_{b1}+V_{b2}+1/r_{12},$$

no attempt being made to allow for the energy of repulsion between the two cationic 'cores' (C $1s^2 2s 2p^2$, trigonally hybridized *ad libitum*).

Goeppert-Mayer and Sklar's core-potential function, V, may be defined as follows, the nucleus and the $1s^2$ electrons of each carbon atom being taken together as a point charge of $4e$, and the presence of the hydrogen atoms ignored:

$$(\pi_\alpha|V_a|\pi_\beta)=\left(s_a s_a\left|\frac{1}{r_{s\pi}}\right|\pi_\alpha\pi_\beta\right)+\left(y_a y_a\left|\frac{1}{r_{y\pi}}\right|\pi_\alpha\pi_\beta\right)+\left(z_a z_a\left|\frac{1}{r_{z\pi}}\right|\pi_\alpha\pi_\beta\right)$$
$$-\left(\pi_\alpha\left|\frac{4}{r_a}\right|\pi_\beta\right).$$

$$[\alpha=\text{a or b};\ \beta=\text{a or b}]$$

The function s_a is the 2s wave function of $C_{(a)}$; y_a and z_a are the 2p wave functions orthogonal to π_a. The symbols for wave functions relating to the same electron are juxtaposed in the electron-repulsion integrals. For example,

$$\left(s_a s_a\left|\frac{1}{r_{s\pi}}\right|\pi_a\pi_b\right)=\int s_a(i)s_a(i)\,\frac{1}{r_{ij}}\,\pi_a(j)\pi_b(j)\,d\tau_i\,d\tau_j,$$

where i is a number representing the coordinates of the σ electron, and $j=1$ or 2. For economy in notation we refer to s, y and z collectively as σ wave functions (though indeed we do not consider σ bonding explicitly), and we use the terms σ and π with reference to atomic orbitals as well as molecular orbitals.

It seems pointless to complicate the simple Goeppert-Mayer–Sklar core-potential function unnecessarily, so we have made no attempt to allow for the energy of 'exchange' between the π electrons and the electrons of the cores (Ross 1952, Niira 1953): this cannot be estimated with much accuracy in a calculation implying a very crudely formulated σ wave function. Transformation of the atomic orbitals s, y and z into a trigonally hybridized set is accordingly without effect on the calculated energies.

We have not, of course, adopted Goeppert-Mayer and Sklar's W_{2p} approximation, that is

$$(\pi_a|-\tfrac{1}{2}\nabla^2+V_a|\pi_a)\simeq W_{2p},$$

and, correspondingly,

$$(\pi_b|-\tfrac{1}{2}\nabla^2+V_a|\pi_a)\simeq SW_{2p},$$

where W_{2p} is an ill-defined quasi-atomic parameter. If valid at all, this device for avoiding the evaluation of kinetic energies† can clearly be valid only for a single (optimum) value of Z appropriate not to a molecular, but to an atomic environment.

Because Goeppert-Mayer and Sklar's technique provides no means of allowing for changes in nuclear configuration, we have calculated only 'vertical' excitation energies, and have ignored the probable non-planarity of the excited states of ethylene (Walsh 1953, Wilkinson and Mulliken 1955). We are in any case concerned primarily not with the comparison of theoretical and experimental excitation energies, but with the intrinsic validity of the former.

Using the tables compiled by Kopineck (Preuss 1956) and by Roothaan (1951, 1955 b) as a source of integrals over atomic orbitals, we have evaluated the energy integrals $(\Psi|H|\Psi)$ for

$$Z=Z_\pi=Z_s=Z_y=Z_z=0{\cdot}79040(0{\cdot}39520)4{\cdot}34718,$$

that is for

$$ZR/2=1{\cdot}0(0{\cdot}5)5{\cdot}5,$$

where $R=1{\cdot}339/0{\cdot}52917$ is the equilibrium C–C distance in Bohr radii (Costain and Stoicheff 1959). There is no justification for supposing that $Z_\sigma=Z_\pi$, but this is one of the over-simplifications invariably employed in the non-empirical calculations whose numerical significance we are examining.

We have evaded the problem of deciding how best to adjust the radial-node parameter in a Zener 2s wave function as Z is varied by using a hydrogen-like 2s wave function in obtaining all the results quoted in § 3. As a precaution, however, we have determined the effect of replacing the hydrogen-like orbital by a nodeless orbital. It is evident (table 1) that the analytical form of the 2s wave function has little effect on calculated excitation energies over a wide range of Z. A 2s wave function of optimum form would doubtless give results lying between those obtained with a hydrogen-like wave function and those obtained with a nodeless wave function. [We have verified this for a Zener 2s function with $Z=3{\cdot}18$.]

§ 3. RESULTS AND DISCUSSION

The calculated π-electron energies of ethylene, $(\Psi|H|\Psi)$, are shown as functions of Z in the figure. As would be expected, our results are altogether different from those which Parr and Crawford obtained (for four values of Z within our range) with the use of the W_{2p} approximation.

---

† It has been stated, with reference to 2p orbitals and not merely to nodeless (non-orthogonalized) s orbitals, that Slater (1930) wave functions cannot be used satisfactorily in the calculation of kinetic energies (Moser 1953, cf. Ross 1952). In so far as it relates to molecular calculations based on linear combinations of 2pπ atomic orbitals, there seems to be no evidence to support this view; and calculations on atomic systems suggest quite the contrary (Duncanson and Coulson 1949, Roothaan 1955 a). Slater, Zener, and hydrogen-like 2p orbitals are, of course, identical in form.

It is obvious from the form of the Goeppert-Mayer–Sklar core-potential function that the minima of the curves in the figure have no significance in relation to the variation principle: the wave functions are functions of the two π electrons only, whereas the corresponding energies include substantial σ–π contributions. Any doubt on this score is readily resolved by considering an analogous calculation on the $[1s^2]2s2p^3$ configuration of the carbon atom. If, in the manner of Goeppert-Mayer and Sklar, we evaluate the energy of one of the p electrons (which we arbitrarily label π_a) in the field provided by the rest of the atom (i.e. by the core) we obtain

$$(\pi_a| -\tfrac{1}{2}\nabla^2 + V_a|\pi_a) = \tfrac{1}{8}Z^2 - 0{\cdot}48867Z.$$

This artificially defined energy is minimized when Z has the absurdly low value of 1·955 (cf. figure). For the trigonal valency state the optimum value of Z is in fact 3·065.

Table 1. Calculated Energies (ev) of ^1A_g and the $^1B_{1u}$ Configurations of Ethylene

	Hydrogen-like 2s Wave Function					
Z	1·5	2·0	2·5	3·0	3·5	4·0
$^1B_{1u}$	−35·464	−34·251	−29·154	−20·857	− 9·540	4·949
^1A_g	−40·698	−41·332	−38·141	−31·789	−22·256	−9·236
^1A_g–$^1B_{1u}$	5·234	7·081	8·987	10·932	12·716	14·185
	Nodeless 2s Wave Function					
$^1B_{1u}$	−32·940	−31·285	−25·845	−17·218	− 5·531	9·366
^1A_g	−38·174	−38·419	−34·965	−28·357	−18·503	−5·077
^1A_g–$^1B_{1u}$	5·234	7·134	9·120	11·139	12·972	14·443

The energies have been obtained by four-point Lagrangian interpolation from values calculated directly from Kopineck's tables (Preuss 1956) and from Roothaan's formulae and tables (Roothaan 1951, 1955 b). A.U. = 27·210 ev.

Attention must this be focused on the region around $Z = 3{\cdot}2$, and it is at once obvious from the steepness of the curves that calculated configuration energies can have little meaning if the scale parameter cannot be specified with precision (table 2). It is interesting to note that a trifling decrease (about 0·06) in the value of Z appears to depress the energy of the lower ^1A_g configuration to the same extent as 'interaction' with the upper configuration of the same symmetry.

Excitation energies are much less sensitive to variation in Z than configuration energies, but they also cannot be calculated with any degree of reliability, even on the assumption that the scale factor is independent of the state of excitation.

Careful work on simpler molecules would lead one to expect, however, that the scale factor for the lowest configuration (Z_{gd}) should be higher than that for a free carbon atom (Z_{atom}), and the scale factors for the excited configurations (Z_{exc}) progressively lower (Altmann and Cohan 1954, cf. Davies 1958). An adjustment of this kind might seem at first sight to provide a means of reducing the exaggerated spacing of energy levels characteristic of Goeppert-Mayer–Sklar calculations; but it would in fact be both hazardous and improper.

An increase in Z_{gd} of only 2·6% (or 3·7% if configuration interaction is taken into account), with a corresponding decrease in Z_{exc}, is sufficient to invert the order of the ^1A_g and the $^3B_{1u}$ states. Likewise, with Craig's (1950 a) scale parameters ($Z_{gd} = 1{\cdot}1 \times 3{\cdot}12$; $Z_{exc} = 0{\cdot}9 \times 3{\cdot}12$), the calculated energy of even

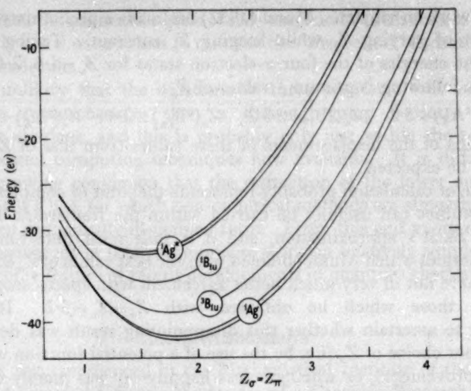

Calculated energies $(\Psi \mid H \mid \Psi)$ of the π-electron states of ethylene. The outermost curves represent calculations in which configuration interaction has been estimated in the conventional way.

Table 2. Calculated Energies (ev) of the π-Electron States of Ethylene

Z	2·6	2·8	3·0	3·2	3·4	3·6
$^1A_g^*$ (c.i.†)	−23·276	−19·922	−16·137	−11·914	− 7·262	− 2·165
$^1A_g^*$	−23·954	−20·715	−17·058	−12·981	− 8·495	− 3·585
$^1B_{1u}$	−27·738	−24·534	−20·857	−16·696	−12·050	− 6·901
$^3B_{1u}$	−33·868	−31·377	−28·451	−25·075	−21·249	−16·951
^1A_g	−37·117	−34·695	−31·789	−28·372	−24·430	−19·938
^1A_g (c.i.†)	−37·796	−35·488	−32·710	−29·438	−25·663	−21·359

See footnote to table 1.

† The second and the seventh rows of the table give the results of calculations in which configuration interaction has been taken into account (Parr and Crawford 1948, Craig 1950 b).

---

the $^1B_{1u}$ configuration lies 0·8 ev below that of the ^1A_g configuration, a catastrophe which is only just averted by allowance for ^1A_g–$^1A_g^*$ interaction.

These arithmetical quirks have, of course, no physical interpretation, and it is easily seen that the adjustments in *Z* which give rise to them are doubly fallacious. With wave functions built up solely from π orbitals there can be no justification for the joint variation of Z_σ and Z_π between different states: this gives a quite spurious σ-electron contribution to the calculated excitation energies (σ–π repulsion terms without other counterbalancing σ terms). Moreover, whereas $Z_{\sigma \mathrm{gd}}$ may well be higher than Z_{atom}, there is no reason to suppose that $Z_{\sigma \mathrm{exc}}$ is appreciably different from $Z_{\sigma \mathrm{gd}}$. The Goeppert-Mayer–Sklar formalism neither requires nor permits anything but a constant value of Z_σ for all π-electron states.

There is no objection in principle to applying the minimum-energy criterion to Goeppert-Mayer–Sklar calculations in which variation is confined to π-electron parameters (linear or exponential) and, in an interesting extension of Parr and

Crawford's work on ethylene, Murai (1952) has made a preliminary examination of the effect of varying Z_π while keeping Z_σ constant. Taking $Z_\sigma = 3{\cdot}2$, he calculated the energies of the four π-electron states for $Z_\pi = 1{\cdot}6$, $2{\cdot}4$, $3{\cdot}2$, and so obtained the following 'optimum' values of Z_π:

$$Z_\pi(^1\mathrm{A_g}) > 3{\cdot}2;\quad Z_\pi(^3\mathrm{B_{1u}}) \simeq 3{\cdot}2;\quad Z_\pi(^1\mathrm{B_{1u}}) \simeq 2{\cdot}4;\quad Z_\pi(^1\mathrm{A_g^*}) < 2{\cdot}4.$$

The directions of the displacements of these values from that of Z_{atom} are just what would be expected.

This type of calculation probably represents the limit of complexity to which variational studies can usefully be carried within the framework of Goeppert-Mayer and Sklar's approximation, and it is thus most unfortunate that the excitation energies which Murai obtained with the best values of Z_π corresponding to $Z_\sigma = 3{\cdot}2$ were not in very much better agreement with spectroscopic measurements than those which he obtained with $Z_\pi = Z_\sigma = 3{\cdot}2$. It would be enlightening to ascertain whether this disappointing result was determined by a possibly poor choice of Z_σ (i.e. by the use of a potential function which admits of ready improvement), or whether—less happily—it was merely one of many instances of the ineffectiveness of conventional variational techniques when applied to the estimation of the energies of excited states.

There being obviously no recourse to the variation principle, however, it is not clear how the most suitable value of Z_σ could be determined. One might calculate the energies of the π-electron states for various values of Z_σ, but, unless the corresponding transition energies proved unexpectedly 'stable', the results would be of little use. We have not attempted this tedious and probably unrewarding investigation, but instead we have extended the ingenuous calculation described in the second paragraph of this section by relaxing the condition $Z_\pi = Z_\sigma$; i.e. we have determined to what degree the scale parameter of an atomic 'π' orbital depends on the arbitrary scaling of the core orbitals. Table 3 provides a dismal augury of the discomfiting results that might be expected in a molecular calculation (see also Stewart 1960). The energies listed have, of course, no variational significance as functions of Z_σ: we quote them merely to emphasize this.

Table 3. Calculated Energy (ev) of an Atomic 'π' Electron subject to the Goeppert-Mayer–Sklar Core Potential

Z_σ (arbitrary)	2·50	2·75	3·00	3·25	3·50	3·75
Z_π (optimum)	3·46	3·30	3·11	2·86	2·56	2·19
$(\pi_\mathrm{a}\lvert -\frac{1}{2}\nabla^2 + V_\mathrm{a}\rvert\pi_\mathrm{a})$	−13·958	−11·446	−9·299	−7·537	−6·180	−5·234

See footnote to table 1.

§ 4. CONCLUSION

We are evidently very far from being able to establish criteria for the reliable calculation of excitation energies within the limitations of the Hückel approximation; indeed, we have at hand no means of justifying the approximation itself. We still do not know whether the gross disparities which almost invariably exist between the results of wave-mechanical calculations and those of spectroscopic observations are due essentially to the inadequacies of π-electron wave functions or to the crudity of the core-potential functions used in the evaluation of their energies. In fact, the parametric basis of non-empirical calculations is so insecure that we scarcely know what values to claim as the 'theoretical' excitation energies of any given molecule.

It seems unlikely that the solutions to these problems will emerge from anything less comprehensive than a thorough-going 6-centre–16-electron calculation on ethylene, and this is probably only just within the scope of the most sophisticated computing techniques now available. It is difficult not to endorse the growing conviction that the estimation of the lower energy levels of σ–π systems is a task for which non-empirical methods are altogether unsuited in their present numerically ill-defined form. From this and many other points of view the resurgence of interest in precise work on relatively simple molecules is a most welcome feature of recent developments in quantum chemistry.

ACKNOWLEDGMENTS

This work was commenced in the Mathematical Institute of the University of Oxford and completed during the tenure of a Carnegie Research Fellowship in the University of St. Andrews. The author is greatly indebted to Professor C. A. Coulson for much valuable discussion and correspondence.

REFERENCES

ALTMANN, S. L., 1951, *Proc. Roy. Soc.* A, **210**, 327, 343.
ALTMANN, S. L., and COHAN, N. V., 1954, *Trans. Faraday Soc.*, **50**, 1151.
COSTAIN, C. C., and STOICHEFF, B. P., 1959, *J. Chem. Phys.*, **36**, 777.
CRAIG, D. P., 1950 a, *Proc. Roy. Soc.* A, **200**, 272.
—— 1950 b, *Ibid.*, **200**, 474.
DAVIES, D. W., 1958, *Trans. Faraday Soc.*, **54**, 1429.
DUNCANSON, W. E., and COULSON, C. A., 1949, *Nature, Lond.*, **164**, 1003.
GOEPPERT-MAYER, M., and SKLAR, A. L., 1938, *J. Chem. Phys.*, **6**, 645.
HAMMOND, V. J., and PRICE, W. C., 1955, *Trans. Faraday Soc.*, **51**, 605.
KAUZMANN, W., 1957, *Quantum Chemistry*, App. III (New York: Academic Press Inc.).
LÖWDIN, P.-O., 1959, *J. Mol. Spectroscopy*, **3**, 46.
MOFFITT, W., and SCANLAN, J., 1953, *Proc. Roy. Soc.* A, **218**, 464; **220**, 530.
MOSER, C. M., 1953, *J. Chem. Phys.*, **21**, 2098.
MURAI, T., 1952, *Progr. Theor. Phys. Japan*, **7**, 345.
NIIRA, K., 1953, *J. Phys. Soc. Japan*, **8**, 630.
PARR, R. G., CRAIG, D. P., and ROSS, I. G., 1950, *J. Chem. Phys.*, **18**, 1561.
PARR, R. G., and CRAWFORD, B. L., 1948, *J. Chem. Phys.*, **16**, 526.
PREUSS, H., 1956, *Integraltafeln zur Quantenchemie* (Berlin: Springer).
ROOTHAAN, C. C. J., 1951, *J. Chem. Phys.*, **19**, 1445.
—— 1955 a, Laboratory of Molecular Structure and Spectra, University of Chicago, Technical Report, 24.
—— 1955 b, *Ibid.*, Table of Two-Center Coulomb Integrals (Special Technical Report).
ROSS, I. G., 1952, *Trans. Faraday Soc.*, **48**, 973.
SHULL, H., and ELLISON, F. O., 1951, *J. Chem. Phys.*, **19**, 1215.
SLATER, J. C., 1930, *Phys. Rev.*, **36**, 57.
STEWART, E. T., 1959, *J. Chem. Soc.*, 70.
—— 1960, *Proc. Phys. Soc.*, **75**, 138.
WALSH, A. D., 1953, *J. Chem. Soc.*, 2325.
WILKINSON, P. G., and MULLIKEN, R. S., 1955, *J. Chem. Phys.*, **23**, 1895.
ZENER, C., 1930, *Phys. Rev.*, **36**, 51.

Large Scale Irregularities in High Altitude Winds

By J. S. GREENHOW and E. L. NEUFELD

Jodrell Bank Experimental Station, University of Manchester

Communicated by A. C. B. Lovell; MS. received 15th June 1959, in final form 30 July 1959

Abstract. Large scale irregularities in the wind at heights of 80 to 100 km are discussed. Measurements of the wind at different heights using radio echoes from meteor trails show the presence of irregularities with a depth of about 10 km and a horizontal extent of over 100 km. These are identified with the large eddies detected using a two-station wind measuring system described in an earlier paper. The lifetimes of these large irregularities given by auto-correlation curves derived from the time variation of the turbulent wind component, is found to be about 1·5 hours. Slow variations in the prevailing wind with periods of several days, produced by pressure systems similar in dimensions to the pressure systems at the earth's surface, are also observed in this region.

§ 1. INTRODUCTION

In a previous paper (Greenhow and Neufeld 1959) some measurements of turbulence at heights of 80 to 100 km are described. A spaced station radio echo technique was used in order to determine the wind velocity at the same time at two points along a meteor trail. In this way the wind shear could be measured and by varying the distance apart of the points of reflection velocity correlations could be investigated as a function of separation in space. The vertical scale of the large eddies was found to be approximately 7 km, although the horizontal scale appeared to be of the order of 150 km. The mean turbulent wind shear was $10\,\mathrm{m\,sec^{-1}\,km^{-1}}$, values as high as $100\,\mathrm{m\,sec^{-1}\,km^{-1}}$ being observed, while the r.m.s. turbulent velocity was $25\,\mathrm{m\,sec^{-1}}$. Similar values have been found using photographic meteor techniques (Liller and Whipple 1954).

This paper describes some single station measurements of upper atmospheric turbulence. Direct evidence is presented showing the existence of irregularities in the wind with a horizontal scale greater than 100 km and a vertical depth of only a few kilometres. These irregularities are identified with the large scale turbulence discussed in the previous paper.

§ 2. TECHNIQUE

The coherent-pulse method for the measurement of wind velocities from the drifts of meteor trails has been described previously (Greenhow 1954). Briefly, a beamed aerial system is pointed in two directions at right angles for alternate periods of ten minutes. Radial components of the drifts of 50 to 500 meteor trails are determined each hour, and by combining the means of the individual measurements in both directions, the resultant wind vector can be obtained. For simplicity of analysis and presentation the components of the mean wind, in the two directions, are plotted separately at hourly intervals throughout the day.

As an example of the results obtained the North–South and East–West components of the wind for 22nd–23rd September 1954 are shown in figure 1 (*a*). A harmonic analysis is carried out using the 24-hourly wind measurements in order to resolve the various uniform wind components. On most days the wind is well represented by a semi-diurnal tidal component with an amplitude of 10 to 30 m sec^{-1}, together with a prevailing wind of 10 to 20 m sec^{-1} which has a constant velocity throughout the day. Small 8-hour and 24-hour components are also observed. The broken curves in figure 1 (*a*) show the sums of the first three terms of the Fourier series, representing the prevailing, 12-hour and 24-hour wind components. The agreement with the experimental points is good, although there are some deviations from the fitted curves.

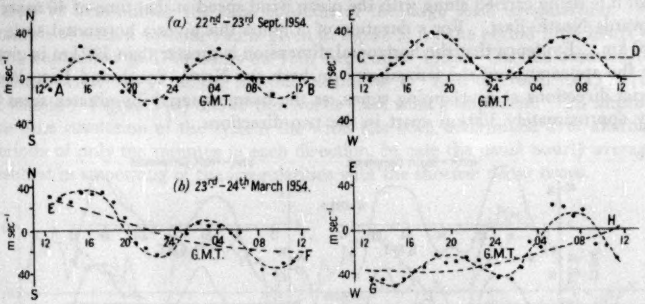

Figure 1. North–South and East–West wind components for two 24-hour periods: (*a*, shows the 12-hour periodic wind superimposed on a steady prevailing wind (AB) CD); (*b*) the periodic wind is superimposed on a rapidly varying ' prevailing ' wind (EF, GH).

Each point in figure 1 (*a*) is the mean of a large number of separate meteor drift measurements, and inspection of the distribution of individual values shows that there is a very large spread due to turbulence. Thus the r.m.s. turbulent wind speed is usually of the order of 25 m sec^{-1}, even at times when the mean wind speed is zero (Greenhow and Neufeld 1959).

§ 3. Results

3.1. *Irregularities in the Dirunal Wind Variations*

Although theoretical curves may be fitted to the hour by hour wind measurements, there are frequently deviations from these curves showing the presence of irregularities in the wind which may last for several hours. These irregularities are largely smoothed out when echoes at all heights and ranges are grouped together in order to give the mean wind at a height of 90 to 95 km. To emphasize these large scale deviations from the regular wind components, echoes have therefore been divided into four height groups centred about 85, 90, 95 and 100 km (Greenhow and Neufeld 1956). These height groups are only 5 km apart, which is less than the vertical extent of a single large eddy deduced from two station wind measurements.

North–South and East–West components of the wind for a day in January 1954 are shown in figure 2; here harmonic analysis to derive the first three terms of the Fourier series has not been carried out, and instead smooth curves have been drawn through the individual hourly wind measurements. The large 12-hour periodic wind is still clearly resolvable at all heights (with an amplitude increasing with height), but the wind variations are by no means purely sinusoidal. For example, between 0500 and 0800 hours in the East–West direction at a height of 90 km there is a large irregularity in the wind lasting for three hours. This disturbance is also present in the North–South direction from about 0400 to 0700 hours. In both directions the amplitude of the irregularity falls off rapidly at greater and lesser heights, and its vertical depth is only of the order ±5 km. The horizontal extent of the irregularity can be determined on the assumption that it is being carried along with the mean wind speed at that time of 40 m sec^{-1} towards North–East. For a duration of 3 hours this gives a horizontal scale of 400 km. Evidence that the horizontal dimension is greater than 300 km is given by the appearance of the irregularity on both the North–South and East–West aerial directions at overlapping times, as the beamed aerial illuminates areas of sky approximately 300 km apart in the two directions.

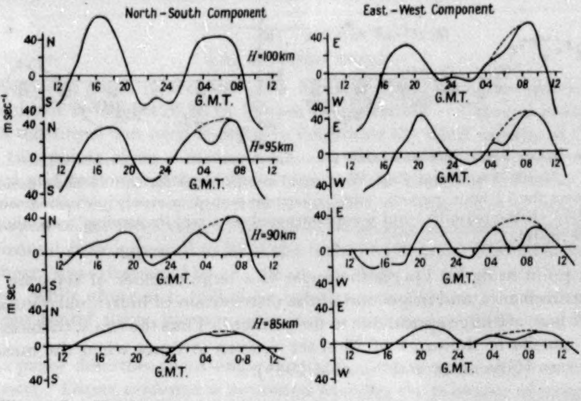

Figure 2. Height variation of the wind, showing large scale irregularities.

While large irregularities of this type are observed almost continuously, it is possible that, because of the method of averaging measurements in hourly intervals, those with decay times of less than one hour are smoothed out. This difficulty has been overcome by plotting the wind at intervals of only 20 minutes, when it is shown that the time constant of these large irregularities is approximately 1·5 hours.

3.2. *Time Scale derived from the Auto-correlation Coefficient*

In the spaced station turbulence measurements the scale of the large eddies was determined by observing the fall off in correlation of the wind velocity at two points, as their separation was increased. Similarly, the time scale of the eddies can be obtained by investigating the variation of wind velocity with time at a single point.

Thus an auto-correlation function $g(\tau)$ may be defined, which correlates the turbulent wind velocity u_s at time s, with the velocity $u_{s+\tau}$ at a time τ later.

$g(\tau)$ is given by the expression

$$g(\tau)=\frac{\Sigma u_s u_{s+\tau}}{[\Sigma u_s{}^2\,\Sigma u_{s+\tau}{}^2]^{1/2}}.$$

The value of τ at which the auto-correlation function falls to zero can be used to define the decay time of the large eddies.

A number of continuous 24- and 48-hour wind measurements, obtained during systematic wind observations over a period of five years, have been analysed with a view to determining the time constant of the large scale irregularities. An example of such a 48-hour run is given in figure 3, for the period 1700 hours on 16th September to 1700 hours on 18th September 1953. On this occasion the beamed aerial was switching between azimuths 45° East of North to 45° West of North. Figure 3 (*a*) shows the North–East wind component. To improve the time resolution of the system the wind has been determined over alternate periods of only ten minutes in each direction, in case the usual hourly averages resulted in smoothing of the irregularities with the shortest decay times.

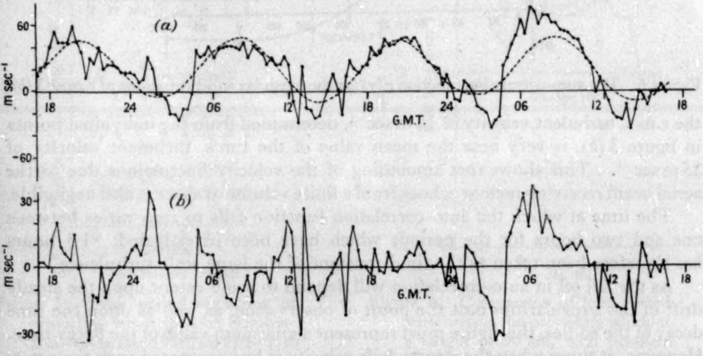

Figure 3. (*a*) Measurements of wind speed at 20 minute intervals for a two-day period. The broken line is the sum of the first three terms of the harmonic analysis representing the regular prevailing, diurnal and semi-diurnal wind components. (*b*) The irregular departures of the measured wind from the smooth curve of (*a*).

It is, of course, necessary to subtract the steady wind components from the observed wind in order to determine the turbulent velocities. This has been done by harmonic analysis of the 48-hour results for prevailing, semi-diurnal and diurnal components. The sum of these first three terms of the Fourier series is shown by the broken line in figure 3 (*a*). The 12-hour component is the largest with a magnitude of 30 m sec^{-1}, next is the prevailing wind with an amplitude of 10 m sec^{-1}, while the 24-hour component is hardly significant with a magnitude of only 3 m sec^{-1}.

The deviations of the individual points from the smooth curve in figure 3(*a*) than give the magnitude of the turbulent wind, and these deviations are plotted in figure 3 (*b*). The turbulent wind component is seen to be of large amplitude, and visual inspection of the figure shows the presence of irregularities with periods of about half an hour up to several hours. The auto-correlation function has been determined for all pairs of points separated by integral numbers of 20 minutes and the resulting auto-correlation curve is plotted in figure 4. $g(\tau)$ falls to zero in approximately two hours, giving the mean lifetime of the large scale irregularities for this two-day period.

From the slow fall off in the value of $g(\tau)$ with τ, it is clear that any reduction in $g(\tau)$ due to taking a finite time interval of 20 minutes is negligible. Similarly, the r.m.s. turbulent velocity of 18 m sec^{-1}, determined from the individual points in figure 3 (*b*), is very near the mean value of the r.m.s. turbulent velocity of 25 m sec^{-1}. This shows that smoothing of the velocity fluctuations due to the aerial beam receiving meteor echoes from a finite volume of space is also negligible.

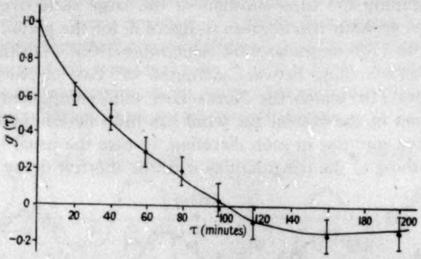

Figure 4. The auto-correlation function $g(\tau)$ for the irregular wind variations of figure 3 (*b*).

The time at which the auto-correlation function falls to zero varies between one and two hours for the periods which have been investigated. 1·5 hours has therefore been taken as the time constant of the large scale turbulence.

As the fall off in auto-correlation will depend to some extent upon the steady drift of the irregularities past the point of observation, as well as upon the time decay of the eddies, this figure must represent a minimum value of the decay time. However, at times when the steady drift velocity is low compared with the r.m.s. turbulent velocity, the fluctuations in wind speed are similar to those in figure 3. Thus the effect of steady drift on the auto-correlation curve is small compared with the effect of the irregular wind variations.

3.3. *Horizontal Dimensions of the Large Scale Turbulence*

The horizontal dimensions of the large eddies may be deduced assuming that a relationship of the type $L = Vt$ holds for eddies of all sizes (Batchelor 1953), where L is the length parameter of the turbulence, V the r.m.s. velocity and t the decay time. In the height region 90 to 100 km, $V = 25$ m sec^{-1} and $t = 6 \times 10^3$ sec, giving $L = 150$ km. This figure is in good agreement with the horizontal scale determined from the velocity correlations described in the previous paper, for eddies with a vertical scale of only 7 km. Direct evidence that the horizontal dimensions are of this order is given by the absence of smoothing of the velocity fluctuations described in § 3.2. Because of the finite beam width of the aerial, meteors are collected over a region at least 50 km in diameter. If the eddies are only of the same order of size or smaller, the velocity fluctuations will be largely smoothed out. In this case r.m.s. velocities determined from the velocity fluctuations would be much less than the true r.m.s. velocities measured using the spaced station technique. This sets a lower limit of 50 km for L, which is consistent with the value of 150 km deduced from turbulence theory.

3.4. *Long Period Variations in the Mean Wind*

In the previous paragraphs it has been assumed that the prevailing wind, represented by the constant term in the harmonic analysis of 24-hour wind observations, does not vary throughout the day. This assumption is apparently confirmed by the closeness of the fit of the theoretical curves, such as those in figure 1 (*a*), to the experimental points. Also the seasonal variations in prevailing wind have repeated themselves quite closely in five successive years, showing that we are concerned with a regular wind structure rather than random variations.

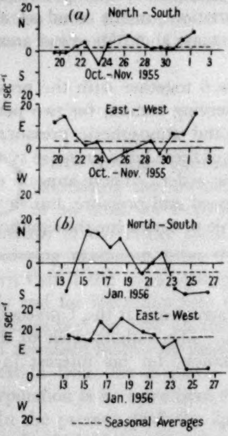

Figure 5. Long period variations of prevailing wind: (*a*) 19th October–2nd November 1955; (*b*) 13th–27th January 1956.

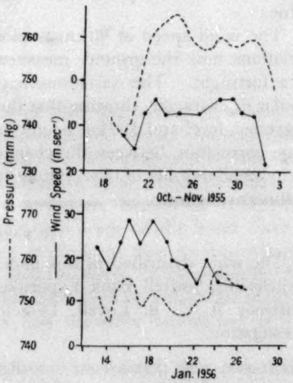

Figure 6. Comparison of long period variations in the prevailing winds at a height of 90 km, with pressure changes at the earth's surface.

In figure 1 (*a*) North–South and East–West components of the wind are plotted for a day in September 1954. Prevailing wind components of 1 m sec^{-1} towards South and 10 m sec^{-1} towards East are observed, together with a regular 12-hour oscillation superimposed on this constant wind vector. On the other hand during the period 23rd–24th March (figure 1 (*b*)), the two maxima of the semi-diurnal oscillation have very different values, and harmonic analysis taking 24 hours as the fundamental period gives a very large diurnal wind. However, at the end of the period F the wind has not returned to its initial value at E, and it is clear that this is not a true 24-hour periodic wind but rather a steady change in the mean wind throughout the day. This is shown by the curves EF and GH. Slow variations of this sort have been resolved in greater detail by a number of continuous weekly and fortnightly wind measurements. Two series of measurements lasting 14 days are shown in figure 5, where the mean value of the wind has been determined over successive periods of 24 hours. Between 13th and 27th January 1956, for example, the North–South component of prevailing wind swings from 13 m sec^{-1} towards South to 13 m sec^{-1} towards North, and then again to 18 m sec^{-1} towards South. Similarly, the East–West component varies over a range of 25 m sec^{-1} about the mean seasonal value of 16 m sec^{-1}. These variations in prevailing wind have periods ranging from a few days up to a fortnight, and for a mean drift velocity of 10 m sec^{-1} the horizontal scale of the pressure system giving rise to the winds would be of the order of several thousand kilometres. Thus, there exist in the region 80 to 100 km above the earth pressure systems similar in scale and duration to the weather systems present at the surface of the earth. These give rise to slow variations in the wind of about ± 10 m sec^{-1}, causing the prevailing wind to fluctuate about its mean seasonal value.

The wind speed at 90 km is plotted in figure 6 together with the pressure variations near the ground, measured at the observing station, for two periods of a fortnight. The variations in wind speed and atmospheric pressure are similar in character, showing that the dimensions of these large pressure systems at ground level and 100 km height are of the same order. There appears to be some correlation between the changes in wind speed and pressure, but in view of the small number of observations it is not possible to determine the significance of this correlation.

ACKNOWLEDGMENTS

The work described in this paper has been carried out at the University of Manchester, Jodrell Bank Experimental Station. The authors wish to thank Professor A. C. B. Lovell, Director of the Station, for his interest in the investigation.

REFERENCES

BATCHELOR, G. K., 1953, *Homogeneous Turbulence* (Cambridge: University Press).
GREENHOW, J. S., 1954, *Phil. Mag.*, **45**, 471.
GREENHOW, J. S., and NEUFELD, E. L., 1956, *Phil. Mag.*, **1**, 1157.
—— 1959, *Proc. Phys. Soc.*, **74**, 1.
LILLER, W., and WHIPPLE, F. L., 1954, *J. Atmos. Terr. Phys. Special Suppl.*, **1**, 112.

Electron Excitation of Atomic Hydrogen in the 2p Level

By D. McCREA and T. V. M. McKIRGAN
Department of Applied Mathematics, The Queen's University of Belfast

Communicated by D. R. Bates; *MS. received* 29*th June* 1959, *in final form* 17*th August* 1959

Abstract. Using an interpolation procedure the Born approximation to the cross sections for the excitation of atomic hydrogen from the 2p level to the eighth and higher levels has been obtained from computed cross sections for transitions to the lower discrete levels and to the continuum. The total ionization cross sections have also been obtained. An incident energy range of from 5 ev to 120 ev is covered.

---

§ 1. INTRODUCTION

Owing to the algebraic complexity of the expressions involved in calculating the excitation cross sections of the higher discrete levels of an atom by Born's approximation, it is advantageous to adopt an alternative to the direct method of computation of these cross sections. In considering excitation from the 1s state of hydrogen, McCarroll (1957) has shown that if the cross sections for excitation into a few of the lower discrete levels and for ionization into the continuum are known, then an interpolation procedure may be used for the intervening discrete levels. This procedure has been discussed further by Boyd (1958) and has been used by him in the study of excitation from the 2s state. It is judged that the error introduced by the interpolation is no more than 0·2%.

In the present work the 2p ($m=0, \pm 1$) states are treated, thus completing the task of obtaining Born's approximation to the cross sections for excitation from the lower states. The report given will be brief since the analysis, though more complicated, is not essentially different from that described by McCarroll and Boyd.

§ 2. THEORY

It is convenient to consider excitation from the $2p_0$ and $2p_{\pm 1}$ states independently, and so the total cross section for the excitation of the nth group of levels from the 2p level is given by

$$Q^{e}(2p, n) = \tfrac{1}{3}Q^{e}(2p_0, n) + \tfrac{2}{3}Q^{e}(2p_{\pm 1}, n) \qquad \ldots\ldots (1)$$

where $Q^{e}(2p_m, n)$, ($m=0, \pm 1$) is the corresponding cross section from the state indicated. The interpolation method depends on the continuity of $\frac{1}{2}n^3Q^{e}(2p_m, n)$ regarded as a function of the energy E_n, with $Q^{i}(2p_m, \epsilon)$ regarded as a function of ϵ, $Q^{i}(2p_m, \epsilon)$ being the cross section for the ejection of the atomic electron into the continuum with energy between ϵ and $\epsilon + d\epsilon$. According to Born's approximation

Table 1. The Coefficients c_0 and a_{r0} appearing in equation (6) of the text

n	c_0	a_{00}	a_{10}	a_{20}	a_{30}	a_{40}	a_{50}	a_{60}
3	$\frac{2^5}{3^4.5^2}$	179	−490	675	—			
4	$\frac{1}{2.3^4}$	17	315	−765	729	—		
5	$\frac{2^5}{5^4.7^5}$	4923	104076	314818	−871220	756315	—	
6	$\frac{1}{2^4.3^4.7}$	35	770	4053	2156	−12880	12096	—
7	$\frac{2^5}{3^{10}.7^3}$	17171875	388361250	2560981725	5262840540	−2178376659	−8638042014	10460353203

Table 2. The Coefficients c_1 and a_{r1} appearing in equation (6) of the text

n	c_1	a_{01}	a_{11}	a_{21}	a_{31}	a_{41}
3	$\frac{2^{10}}{3^6}$	1	—			
4	$\frac{1}{2^6.3}$	8	120	—		
5	$\frac{2^{10}}{3.5^6.7^3}$	81	1386	5145	—	
6	$\frac{7}{2^{13}.3^6}$	1024	18432	98304	163840	—
7	$\frac{2^{11}}{7^5.3^{14}}$	15625	292500	1858950	4960116	4782969

the total cross section for the excitation of all discrete levels with principal quantum number n from the $2\mathrm{p}_m$ state is

$$Q^{\mathrm{e}}(2\mathrm{p}_m, n) = \frac{2}{(ka_0)^2}\int_{K_{\min}}^{K_{\max}} I(2\mathrm{p}_m, n, K)K\,dK(\pi a_0^2) \qquad \ldots\ldots(2)$$

where

$$I(2\mathrm{p}_m, n, K) = \frac{4}{K}\sum_{l=0}^{n-1} |\epsilon(2\mathrm{p}_m, n, l, K)|^2 \qquad \ldots\ldots(3)$$

$$\epsilon(2\mathrm{p}_m, n, l, K) = \int_0^\infty \mathrm{e}^{i\mathbf{K}.\mathbf{r}}\psi^*_{2\mathrm{p}_m}(\mathbf{r})\psi_{nl}(\mathbf{r})\,d\mathbf{r} \qquad \ldots\ldots(4)$$

$$K_{\substack{\max\\ \min}} = ka_0 \pm [(ka_0)^2 - \tfrac{1}{4}]^{1/2} \qquad \ldots\ldots(5)$$

and $\mathbf{K} = \mathbf{k}_\mathrm{i} - \mathbf{k}_\mathrm{f}$ where $\mathbf{k}_\mathrm{i}$ and $\mathbf{k}_\mathrm{f}$ are the initial and final propagation vectors of the incident electron. We choose the polar axis of the coordinate system in the direction of $\mathbf{k}_\mathrm{i}$. Then the substitution $x = K^2$ and the simplification of equation (4) give a general expression for $I(2\mathrm{p}_m, n, x)$ which may be written in the form

$$I(2\mathrm{p}_m, n, x) = \frac{c_{|m|}}{x(\gamma^2 + x)^{(n-|m|+5)}}\sum_{r=0}^{n-2|m|-1} a_{r,|m|}x^r\gamma^{2(n-2|m|-r-1)} \qquad \ldots\ldots(6)$$

where

$$\gamma = \frac{n+2}{2n} \qquad \ldots\ldots(7)$$

and the external factor $c_{|m|}$ and the coefficients $a_{r,|m|}$ are given in tables 1 and 2. By integrating over x, expressions for $Q^{\mathrm{e}}(2\mathrm{p}_m, n)$ may be found without difficulty.

The formulae for $Q^{\mathrm{i}}(2\mathrm{p}_m, \epsilon)$ are derived by a method analogous to that used by Massey and Mohr (1933) for excitation from the ground state. Since the formulae for $Q^{\mathrm{i}}(2\mathrm{p}_m, \epsilon)$ have already been given by Burhop (1940), Mandl (1952) and Swan (1955), it is only necessary to remark that the expression obtained for $Q^{\mathrm{i}}(2\mathrm{p}_0, \epsilon)$ is equivalent to those given by Burhop and Mandl and for $Q^{\mathrm{i}}(2\mathrm{p}_{\pm1}, \epsilon)$ to those given by Swan and Mandl.

The value of the cross section at the spectral head is of special importance since it gives the limiting value of the excitation cross sections of the discrete levels. Defining $\mathbf{k}$ to be $2\pi m\mathbf{v}/h$ where $\mathbf{v}$ is the velocity of the incident electron, m is its mass and h is Planck's constant, and performing the integration over the change of momentum analytically, it is found that

$$Q^{\mathrm{i}}(2\mathrm{p}_0, 0) = \frac{2^6}{15(ka_0)^2}\Big[23 \times 2^{10} \times \mathrm{e}^{-8} \times \mathrm{Ei}(2t) + \{t^8 - 6t^7 + 3t^6 - 5t^5 - t^4 + 44t^3 + 250t^2 + 986t + 3437\}\mathrm{e}^{-2t}\Big]_{t_1}^{t_2}(\pi a_0^2) \qquad \ldots\ldots(8)$$

$$Q^{\mathrm{i}}(2\mathrm{p}_{\pm1}, 0) = \frac{2^8}{15(ka_0)^2}\Big[2^{12} \times \mathrm{e}^{-8} \times \mathrm{Ei}(2t) + \left\{-\frac{t^6}{2} - t^5 - \frac{t^4}{2} + 7t^3 + \frac{85t^2}{2} + \frac{341t}{2} + \frac{2389}{4}\right\}\mathrm{e}^{-2t}\Big]_{t_1}^{t_2}(\pi a_0^2) \qquad \ldots\ldots(9)$$

in which

$$\mathrm{Ei}(x) = \int_{-\infty}^{x} \frac{\exp(p)}{p}\,dp \qquad \ldots\ldots(10)$$

$$t_1 = (x_{\max} + \tfrac{1}{4})^{-1} \quad ; \quad t_2 = (x_{\min} + \tfrac{1}{4})^{-1} \qquad \ldots\ldots(11)$$

$$x_{\substack{\max\\ \min}} = \{ka_0 \pm [(ka_0)^2 - \tfrac{1}{4}]^{1/2}\}^2 \qquad \ldots\ldots(12)$$

and a_0 is the atomic unit of length.

For values of ϵ near the threshold $Q^{\mathrm{i}}(2\mathrm{p}_m, \epsilon)$ has been evaluated by numerical integration.

The total cross section for ionization into the continuum from the $2\mathrm{p}_m$ state is given by

$$Q^{\mathrm{I}}(2\mathrm{p}_m) = \int_0^{\epsilon_{\max}} Q^{\mathrm{i}}(2\mathrm{p}_m, \epsilon)\, d\epsilon \qquad \ldots\ldots (13)$$

where

$$\epsilon_{\max} = k^2 - \frac{2mE_1}{\hbar^2} \qquad \ldots\ldots (14)$$

and E_1 is the threshold energy of the process. To supplement the values of $Q^{\mathrm{i}}(2\mathrm{p}_m, \epsilon)$ obtained in connection with the interpolation of the excitation cross sections, further values completing the coverage of the ejection energy range from 0 to $\epsilon_{\max}$ were calculated. Owing to the length of the work involved DEUCE was used to calculate these supplementary values. The evaluation of equation (13) presented no further difficulty.

§ 3. CALCULATIONS AND RESULTS

Cross sections for the excitation of the third, fourth, fifth, sixth and seventh groups of levels of atomic hydrogen from the $2\mathrm{p}_0$ and $2\mathrm{p}_{\pm 1}$ states were computed for values of the incident electron energy ranging from 0·36 to 9 rydbergs.

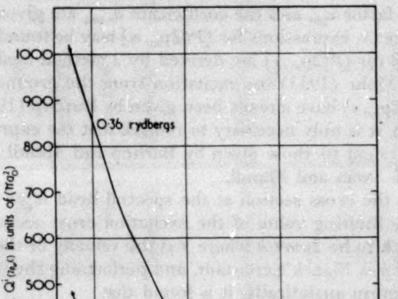

Figure 1. Illustration of the continuity of $\frac{1}{2}n^3Q^e(2\mathrm{p}_0, n)$ (as a function of E_n) with $Q^{\mathrm{i}}(2\mathrm{p}_0, \epsilon)$ (as a function of ϵ). The numbers on the graphs refer to the energy of impact of the incident electron in rydbergs. Positive energies of the excited electron correspond to the ejection of the electron into the continuum and negative energies to the excitation of a discrete level. The interpolated sections of the curves for which $-1/49 < E_n < 0$ yield information on the cross sections for the excitation of the eighth and higher levels.

Writing $\varkappa = 2\pi m\mathbf{v}/h$ where $\mathbf{v}$ is the velocity of ejection into the continuum, $Q^{i}(2p_0, \epsilon)$ and $Q^{i}(2p_{\pm 1}, \epsilon)$ were determined for values of κ near the ionization threshold ($\kappa = 0{\cdot}10, 0{\cdot}15, 0{\cdot}20$), the integrations over K (the change in momentum of the incident electron) being performed numerically. Graphs of the functions $\frac{1}{2}n^3 Q^{e}(2p_m, n)$ and $Q^{i}(2p_m, \epsilon)$ were then plotted for the given range of incident energies. A representative selection of these is given in figures 1 and 2, for the $m = 0$ and $m = \pm 1$ cases respectively. The values of the computed cross sections for $n = 3$, 4, 5, 6, 7, and of the interpolated cross sections for $n = 8$, 9, 10 are displayed in tables 3 and 4. Where $n > 10$ linear interpolation is adequate. In this case the relationship between the cross sections for the excitation of the discrete levels and the cross sections at the spectral head is given by

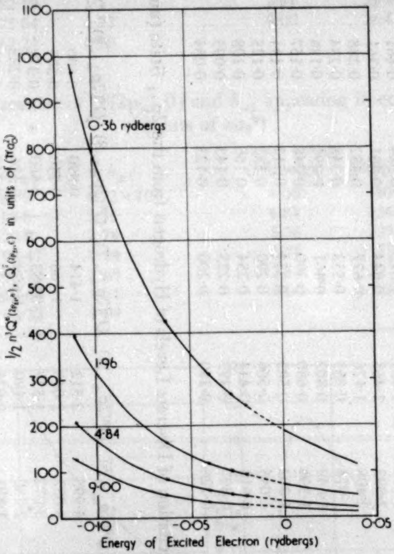

Figure 2. Illustration of the continuity of $\frac{1}{2}n^3 Q^{e}(2p_{\pm 1}, n)$ with $Q^{i}(2p_{\pm 1}, \epsilon)$.

$$\tfrac{1}{2}n^3\, Q^{e}(2p_m, n) = Q^{i}(2p_m, 0) + b_m n^{-2}. \qquad \ldots\ldots(15)$$

Tables 5 and 6 give the values of $Q^{i}(2p_m, 0)$ and b_m for $m = 0$ and $m = \pm 1$ respectively, over the given range of incident energies.

As one would expect the values obtained for the cross sections for excitation from the $2p_{0,\pm 1}$ states are much larger than the corresponding cross sections obtained for excitation from the 1s state. Swan (1955) calculated the ionization cross sections from each of the 2s, $2p_{0,\pm 1}$ states. Our values of $Q^{i}(2p_0, \epsilon)$ differ from Swan's values, being about half as great. However, our $Q^{e}(2p_0, 3)$ and $Q^{e}(2p_0, 4)$ are in satisfactory accord with results calculated using Bethe's formula at high energies of incidence. This accord coupled with the continuity displayed in the graphs should eliminate the possibility that we have made a

Table 3. Total Cross Sections for the Excitation of Discrete Levels of Hydrogen from the $2p_0$ State (units of πa_0^2)

Impact Energy (rydbergs)	$Q^e(2p_0, 3)$	$Q^e(2p_0, 4)$	$Q^e(2p_0, 5)$	$Q^e(2p_0, 6)$	$Q^e(2p_0, 7)$	$Q^e(2p_0, 8)$	$Q^e(2p_0, 9)$	$Q^e(2p_0, 10)$
0·36	74·837	14·426	5·259	2·499	1·409	0·892	0·601	0·424
0·64	64·529	12·323	4·749	2·347	1·348	0·861	0·586	0·417
1·00	52·482	9·826	3·790	1·859	1·072	0·684	0·461	0·328
1·44	42·803	7·833	2·993	1·465	0·844	0·531	0·361	0·255
1·96	35·403	6·352	2·408	1·176	0·677	0·432	0·288	0·207
2·56	29·727	5·246	1·974	0·963	0·553	0·348	0·234	0·165
3·24	25·324	4·406	1·649	0·802	0·461	0·291	0·196	0·138
4·00	21·836	3·755	1·399	0·680	0·390	0·248	0·167	0·119
4·84	19·038	3·241	1·202	0·583	0·334	0·211	0·141	0·100
5·76	16·759	2·828	1·045	0·506	0·290	0·182	0·125	0·087
6·76	$14·876_5$	2·491	0·918	0·444	0·254	0·160	0·108	0·077
7·84	13·304	2·213	0·807	0·393	0·225	0·143	0·095	0·066
9·00	11·976	1·988	0·726	0·350	0·200	0·125	0·084	0·059

Table 4. Total Cross Sections for the Excitation of Discrete Levels of Hydrogen from the $2p_{\pm 1}$ State (units of πa_0^2)

Impact energy (rydbergs)	$Q^e(2p_{\pm 1}, 3)$	$Q^e(2p_{\pm 1}, 4)$	$Q^e(2p_{\pm 1}, 5)$	$Q^e(2p_{\pm 1}, 6)$	$Q^e(2p_{\pm 1}, 7)$	$Q^e(2p_{\pm 1}, 8)$	$Q^e(2p_{\pm 1}, 9)$	$Q^e(2p_{\pm 1}, 10)$
0·36	76·515	13·346	4·995	2·512	1·414	0·890	0·600	0·424
0·64	57·44	10·692	4·052	2·040	1·166	0·740	0·505	0·358
1·00	45·051	8·181	3·077	1·537	0·883	0·560	0·378	0·270
1·44	35·937	6·381	2·380	1·190	0·679	0·426	0·288	0·202
1·96	29·278	5·102	1·891	0·935	0·537	0·342	0·229	0·160
2·56	24·313	4·173	1·538	0·758	0·435	0·268	0·180	0·128
3·24	20·535	3·480	1·276	0·625	0·359	0·224	0·151	0·108
4·00	17·587	2·949	1·077	0·528	0·302	0·190	0·129	0·091
4·84	15·248	2·533	0·922	0·451	0·258	0·164	0·110	0·078
5·76	13·360	2·202	0·799	0·391	0·223	0·140	0·094	0·067
6·76	$11·812_5$	1·934	0·700	0·341	0·195	0·123	0·082	0·058
7·84	10·527	1·713	0·618	0·301	0·172	0·108	0·072	0·052
9·00	$9·447_5$	1·534	0·551	0·272	0·153	0·096	0·064	0·046

Table 5. Parameters $Q^{\mathrm{I}}(2\mathrm{p}_0, 0)$ and b_0 appearing in eqn (15) in text (units of πa_0^2)

Impact energy (rydbergs)	$Q^{\mathrm{I}}(2\mathrm{p}_0, 0)$	b_0	Impact energy (rydbergs)	$Q^{\mathrm{I}}(2\mathrm{p}_0, 0)$	b_0
0·36	184·3	$2{\cdot}8 \times 10^3$	4·00	52·48	$5{\cdot}4 \times 10^2$
0·64	184·7	2·3	4·84	44·86	4·96
1·00	147·6	1·6	5·76	38·84	4·48
1·44	115·6	1·2	6·76	33·96	4·24
1·96	92·19	1·1	7·84	29·97	3·63
2·56	75·04	0·73	9·00	26·66	2·30
3·24	62·24	0·60			

Table 6. Parameters $Q^{\mathrm{I}}(2\mathrm{p}_{\pm1}, 0)$ and $b_{\pm1}$ appearing in eqn (15) of text (units of πa_0^2)

Impact energy (rydbergs)	$Q^{\mathrm{I}}(2\mathrm{p}_{\pm1}, 0)$	$b_{\pm1}$	Impact energy (rydbergs)	$Q^{\mathrm{I}}(2\mathrm{p}_{\pm1}, 0)$	$b_{\pm1}$
0·36	188·7	$4{\cdot}72 \times 10^3$	4·00	40·54	$9{\cdot}7 \times 10^2$
0·64	159·8	3·75	4·84	34·51	8·5
1·00	120·9	2·78	5·76	29·78	7·3
1·44	92·47	1·94	6·76	25·97	6·0
1·96	72·72	1·69	7·84	22·86	4·8
2·56	58·64	1·21	9·00	20·29	3·6
3·24	48·32	1·09			

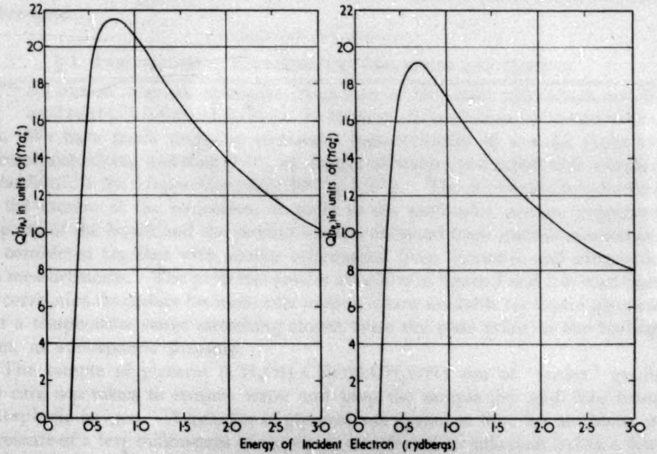

Figure 3. Total ionization cross sections.

serious error. Figure 3 gives the cross sections $Q^{\mathrm{I}}(2\mathrm{p}_{0,\pm1})$ describing ionization from the $2\mathrm{p}_{0,\pm1}$ states. The values of $Q^{\mathrm{I}}(2\mathrm{p}_0)$ are about half those given by Swan in conformity with what was said in the preceding paragraph. In the case of $Q^{\mathrm{I}}(2\mathrm{p}_{\pm1})$ there is good agreement with the results obtained both by Swan and by Mandl. Born's approximation to the cross sections describing ionization from all the lower states has now been published. $Q^{\mathrm{I}}(1s)$ have been given by Fite (1958) and $Q^{1}(2s)$ by Yavorsky (1945) and Swan (1955)†.

ACKNOWLEDGMENTS

This work was carried out under contract for the United Kingdom Atomic Energy Authority, to whom thanks are due for permission to publish. The authors are also indebted to Professor D. R. Bates, for many helpful suggestions and much encouragement during the course of the work.

REFERENCES

BETHE, H. A., 1930, *Ann. Phys., Lpz.*, **5**, 325.
BOYD, T. J. M., 1958, *Proc. Phys. Soc.*, **72**, 523.
BURHOP, E. H. S., 1940, *Proc. Camb. Phil. Soc.*, **36**, 43.
FITE, W. L., and BLACKMANN, R. T., 1958, *Phys. Rev.*, **112**, 1141.
MCCARROLL, R., 1957, *Proc. Phys. Soc.* A, **70**, 460.
MANDL, F., 1952, *A.E.R.E. Report* T/R 1006 (London: H.M.S.O.).
MASSEY, H. S. W., and MOHR, C. B. O., 1933, *Proc. Roy. Soc.* A, **140**, 613.
MOTT, N. F., and MASSEY, H. S. W., 1949, *Theory of Atomic Collisions* (Oxford: Clarendon Press).
SWAN, P., 1955, *Proc. Phys. Soc.* A, **68**, 1157.
SOMMERFELD, A., 1931, *Ann. Phys., Lpz.*, **9**, 257.
YAVORSKY, B., 1945, *C.R. Acad. Sci. U.R.S.S.*, **49**, 250.

---

† The two sets of results on $Q^{1}(2s)$ differ considerably. Work by Boyd strongly suggests that those of Yavorsky are correct.

Molecular Motion in Liquid Glycerol by Proton Magnetic Relaxation

By K. LUSZCZYNSKI, J. A. E. KAIL and J. G. POWLES
Physics Department, Queen Mary College, London, E.1

MS. received 1st *July* 1959, *in revised form* 26th *August* 1959

Abstract. Proton magnetic resonance relaxation times for liquid and supercooled glycerol of low water content have been measured in the temperature range 200°K to 435°K. The spin–lattice relaxation times differ substantially from the earlier measurements.

The results are used to deduce correlation frequencies for motion of the glycerol molecules and these are compared with correlation frequencies deduced from dielectric and ultrasonic measurements. Values are now available in the range 10^{-1} to 2×10^{10} c/s which is almost the complete temperature range, glass point to boiling point. Some indication is found that translational molecular motion may be faster than rotational motion in liquid glycerol and possibly dipolar reorientation is faster than that of the whole molecule. Several difficulties in the interpretation are encountered which are no doubt connected with the hydrogen bonding in liquid glycerol. A distribution of correlation frequencies of an extent depending on the temperature is required. The dielectric internal field correction is discussed.

§ 1. Introduction, Experimental Procedure and Results

The proton magnetic resonance properties of molecular substances can be used to obtain information about the motions of the protons in the substance. We have made magnetic resonance measurements of various types on glycerol (containing less than 0·2% by weight of water) as a liquid and a supercooled liquid in the temperature range 200° to 435°K. The correlation frequencies for the motion of the molecules, or parts of the molecules, are an important property of the liquid and the present results, obtained from nuclear resonance, are considered together with similar information from dielectric and ultrasonic loss measurements. The principal results are given in figure 3 and it is seen that the correlation frequency for molecular motion is now available for liquid glycerol over a temperature range stretching almost from the glass point to the boiling point, at atmospheric pressure.

The sample of glycerol ($CH_2OH.CHOH.CH_2OH$) was of 'analar' grade and care was taken to remove water and keep the sample dry and free from atmospheric oxygen. A quantity of glycerol was heated at 80°c for ten hours at a pressure of a few millimetres of mercury, transferred to spherical bulbs a few millimetres in diameter and sealed under vacuum. The Fischer test showed less than 0·2% water by weight. These precautions are necessary because of the well known hygroscopic nature of glycerol and because of the important effect of a small proportion of water on many of its properties. Because we shall have to consider some published results on 'wet' glycerol, we give the effect of water on a typical property, the shear viscosity η_S, in the table. Glycerol from the 'bottle' may contain about 1·3% of water.

% water by weight in glycerol	0	0·2	0·8	1·3	2	5
η_s (poise at 20°c) (Sheely 1932)	14·99	14·39	12·57	11·29	9·74	5·45
η_s for pure glycerol/η_s for solution	1·0	1·04	1·19	1·33	1·54	2·75

The glass transition temperature of glycerol is 185°K (Simon 1922); the melting point of crystalline glycerol is approximately 290°K. Glycerol is induced to crystallize only with difficulty (see for example Schulz 1954) and we are confident that negligible crystallization occurred in our specimens. The boiling point of glycerol is 563°K at one atmosphere.

In the temperature range 200°K to 250°K we have measured the steady state absorption ξ at a frequency of $15{\cdot}3 \times 10^6$ c/s using a marginal oscillator method (Gutowsky, Mayer and McClure 1953) which has been described elsewhere (Powles 1956). The results are obtained as a plot of $d\xi/dH$ against H. None of these derivative curves showed structure and so we report in figure 1 only the values of the line width δH, the distance between extrema of $d\xi/dH$, and the second moment values ΔH_2^2 which are the mean square width of the absorption curve $\xi(H)$.

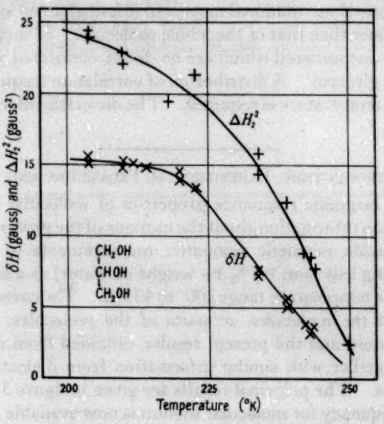

Figure 1. Line width δH in gauss and second moment ΔH_2^2 in gauss^2 as functions of temperature for supercooled glycerol.

In the temperature range 240°K to 435°K we have measured the proton magnetic resonance relaxation times by observing nuclear signals after various trains of intense radio frequency pulses (Hahn 1950, Carr and Purcell 1954). The resonant frequency in this case was 21·5 Mc/s. The apparatus has been described elsewhere (Luszczynski and Powles 1959 a). The decay of longitudinal and transverse magnetization with time was exponential in all cases and so we give only the spin–lattice and spin–spin relaxation times T_1 and T_2 in figure 2. Also on figure 2 we have plotted values of T_2 derived from δH and denoted by $T_2(\delta H)$ using the formula

$$T_2 = \alpha/\gamma\delta H \qquad \text{......(1)}$$

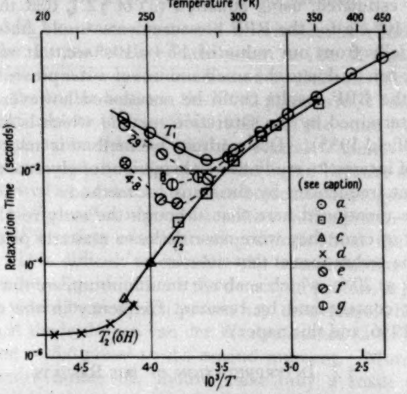

Figure 2. Values of spin–lattice and spin–spin relaxation times T_1 and T_2 at $21{\cdot}5 \times 10^6$ c/s for the protons in glycerol as functions of temperature. Values are plotted on a logarithmic scale against $10^3/T$ for convenience. Also shown are values of T_2 derived from δH of figure 1 using equation (1) and denoted by T_2 (δH).
a, T_1 by 180°, 90° pulse sequence; *b*, T_2 by 90°, 180°, 180° . . . pulse sequence; *c*, T_2 by Bloch decay; *d*, T_2 derived from δH; *e*, T_1 at 29×10^6 c/s by saturation (BPP 1948); *f*, T_1 at $4{\cdot}8 \times 10^6$ c/s by saturation (BPP 1948); *g*, T_1 at 8×10^6 c/s by adiabatic fast passage (Drain 1949).

where γ is the proton gyromagnetic ratio and α is a constant of order unity. We have assumed without much error that the inner part of the line is Lorentzian, in which case $\alpha = 2/\sqrt{3}$. Thus $T_2(\delta H)$ is a number which indicates the general behaviour of the transverse magnetization. More precise information about the transverse relaxation is obtainable from figure 1. In the region of overlap of the two methods ($\simeq 240$°K) the line is fairly well narrowed and the values of T_2 by the two methods should agree. Part of the discrepancy may be due to experimental error since both pieces of apparatus are at their limit in this region. At temperatures above about 320°K self-diffusion effects rendered the measurement of T_2 rather difficult even using the Carr and Purcell (1954) 90°, 180°, 180° . . . pulse sequence; nevertheless, we are confident that T_2 does not differ from T_1 by more than a factor 2 in this region. Apart from these two regions the accuracy is estimated as follows, $T_1 \pm 5\%$, $T_2 \pm 5\%$, $\delta H \pm 5\%$ and $\Delta H_2^2 \pm 10\%$.

The importance of measurements of the proton magnetic resonance properties of glycerol is increased by the fact that it is often quoted in textbooks (Andrew 1955, Pake 1956, Lösche 1957, etc.) as showing typical nuclear magnetic resonance behaviour. It is of interest therefore that our results differ substantially from the original ones of Bloembergen, Purcell and Pound (1947 and 1948, to be referred to as BPP) but still show the 'typical' behaviour. The BPP results for T_1 for resonant frequencies of 29×10^6 c/s and $4{\cdot}8 \times 10^6$ c/s and some by Drain (1949) at 8×10^6 c/s are shown in figure 2. There is some uncertainty in the position of these curves on the temperature scale because the water content of the glycerol is not accurately known. Since a viscosity figure of 10 poise at 20°c is used by BPP we assume their glycerol contained about 2% water.

It is readily estimated, using equation (3) of § 2.1, that the minimum value of T_1 at $21{\cdot}5\times10^6$ c/s for the BPP measurements would be 4×10^{-3} sec which differs substantially from our value of $17{\cdot}4\times10^{-3}$ sec. It seems unlikely that this discrepancy can be due to the small amount of water present. A considerable uncertainty in the BPP results could be occasioned however by the T_1 values having been determined by the saturation method which is known to be rather inaccurate (Redfield 1955). Drain admits his method is inaccurate for short T_2. It is evidently of interest to study the T_1 behaviour of glycerol near the minimum at other resonant frequencies by the transient method.

It should be mentioned here that although the early results of BPP appear to be somewhat in error they were nevertheless a masterly piece of work in view of the state of the techniques at that time.

Values of T_1 at 20°C, which is above the minimum, are not much affected by moderate water content and by resonant frequency in the usual range (BPP 1948, Giulotto 1956, and this paper).

§ 2. INTERPRETATION OF THE RESULTS

2.1. *Introduction*

The proton magnetic resonance results will be used principally to deduce the nature and rate of motion of the glycerol molecules as a function of temperature. In this connection it will be of interest to compare the present measurements with those of dielectric constant and loss and of ultrasonic absorption as has been initiated for glycerol by Litovitz (1957) and this is done in § 2.6.

We base our interpretation on the BPP theory (1948) in which T_1 and T_2 are given essentially by

$$\frac{1}{T_2{}^2}=\left(\frac{1}{T_{2\mathrm{r}}{}^2}\right)\frac{2}{\pi}\tan^{-1}(\alpha K/2\pi\nu_\mathrm{c}T_2) \qquad \ldots\ldots(2)$$

$$\frac{1}{T_1}=\left(\frac{1}{T_{2\mathrm{r}}{}^2}\right)\frac{\alpha K}{3\pi^2\nu_\mathrm{r}}\left[\frac{\nu_\mathrm{r}/\nu_\mathrm{c}}{1+(\nu_\mathrm{r}/\nu_\mathrm{c})^2}+\frac{\beta(2\nu_\mathrm{r}/\nu_\mathrm{c})}{1+(2\nu_\mathrm{r}/\nu_\mathrm{c})^2}\right] \qquad \ldots\ldots(3)$$

where $\beta=1$ and K is a constant of order unity which covers an uncertainty in the theory. α is defined in § 1; $T_{2\mathrm{r}}$ is the effective rigid lattice transverse relaxation time, ν_c is the correlation frequency for the motion. We shall use correlation frequencies ν_c rather than correlation times τ_c, where $2\pi\nu_\mathrm{c}\tau_\mathrm{c}=1$, for convenience. ν_r is the resonant frequency ($21{\cdot}5\times10^6$ c/s in this paper).

More recent modifications of the theory (Kubo and Tomita 1954) change these equations to some extent, e.g. $\beta=2$, but not so as to affect our interpretation substantially. We shall find it necessary to generalize the BPP theory for distributions of correlation frequencies.

For the broad line region (figure 1) we also use Van Vleck's (1948) theory of the second moment which, applied to the present case, where the protons are the only magnetic nuclei, is expressed by

$$\Delta H_{2\mathrm{r}}{}^2=720\frac{1}{N}\sum_{i>j}R_{ij}{}^{-6}\ \mathrm{gauss}^2 \qquad \ldots\ldots(4)$$

where N is the number of protons interacting and the R_{ij} are their separations in ångströms. When the absorption lines are motionally narrowed a useful but approximate form of equation (2) is

$$\Delta H_2{}^2=\Delta H_{2\mathrm{r}}{}^2(2/\pi)\tan^{-1}(\gamma\Delta H_2/\pi\nu_\mathrm{c}). \qquad \ldots\ldots(5)$$

2.2. *The Rigid Lattice Second Moment*

The value of ΔH_{2r}^2 contains intra- and intermolecular contributions. We have calculated the intramolecular contribution to be 10·7 gauss^2 using the structure of the molecule in the gas as determined by electron diffraction (Bastiansen 1949) in which the angles between the CCO planes are 71° and the O in each $H_2(OH)C$– is almost *trans* to C′ in –CH(OH)C′ and the outer hydroxyl protons form hydrogen bonds symmetrically with the central O atom. The molecular structure, or structures, may be different in the liquid because of the formation of intermolecular as well as, or instead of, intramolecular hydrogen bonds. However, the figure of 10·7 gauss^2 is not very sensitive to the precise arrangement of the molecule even if a variety of rotational positions about the C–C and C–O bonds is allowed. It is difficult to calculate the intermolecular contribution to the second moment for a liquid. Since the density of protons is high in glycerol, a reasonable guess would be that each proton has, on average, about three extramolecular protons at the hydrogen van der Waals distance (2·4 Å) from it. This gives a contribution of 5·6 gauss^2 to the second moment. More distant neighbours, although more numerous, should make only a small contribution to ΔH_{2r}^2 and this may be about 1·5 gauss^2. Therefore the expected rigid lattice second moment for glycerol is 17·8 gauss^2. The experimental value is 24 gauss^2. The discrepancy of 6·2 gauss^2 suggests an unusually close approach of some extramolecular protons and this could be brought about by intermolecular hydrogen bonding. The present measurements may be indirect evidence of this. Nevertheless, this seems hardly likely to explain all of the discrepancy. Further evidence of an unexpectedly large intermolecular contribution to the rigid lattice second moment is found below.

Another value of rigid lattice second moment, but not necessarily quite the same quantity, may be deduced from the value of T_1 at its minimum since according to equation (3)

$$T_{1\,\mathrm{min}} = (9\sqrt{3}/4\sqrt{2})\pi^2\nu_r T_{2r}^2 = 27\cdot1\,\nu_r T_{2r}^2. \qquad \ldots\ldots(6)$$

Assuming $T_{2r} = 1/(\sqrt{3}\gamma\Delta H_{2r})$ and from experiment $T_{1\,\mathrm{min}} = 17\cdot4 \times 10^{-3}$ sec we find $\Delta H_{2r}^2 = 16\cdot0$ gauss^2. It will be shown in §2.3 that because of a distribution of correlation frequencies this value should be increased by the factor 1·2 to 19·2 gauss^2. This value therefore lies between the expected and the observed value of rigid lattice second moment. A possible explanation of this will be given in §2.6. The $T_{1\,\mathrm{min}}$ values observed by BPP (1947, 1948) correspond on the same basis, to a rigid lattice second moment of about 80 gauss^2 even without the distribution. This is far greater than the experimental rigid lattice second moment and is indeed incomprehensible.

2.3. *Correlation Frequencies from Nuclear Resonance*

From the variation of the second moment with temperature shown in figure 1 and using equation (5) we can deduce the correlation frequency ν_c as a function of temperature over a limited range. We call this $\nu_c(\Delta H_2)$ and it is given in figure 3.

Using the minimum of T_1 and equation (6) to determine a value of $T_{2r}(=5\cdot45 \times 10^{-6}\,\mathrm{sec})$ and then using the experimental values of T_1 in equation (3) we deduce a correlation frequency which we call $\nu_c(T_1)$ which is plotted in figure 3.

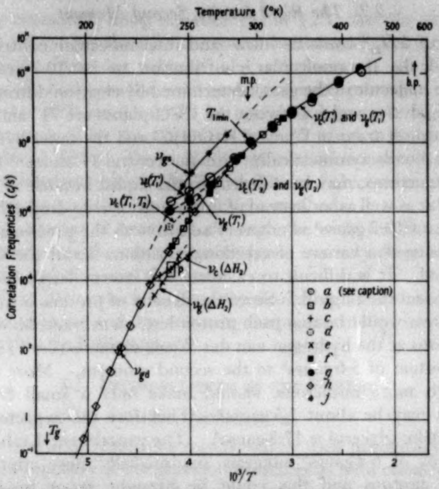

Figure 3. Correlation frequencies as a function of temperature, deduced from nuclear resonance, dielectric and ultrasonic measurements with various assumptions.

a, $\nu_c(T_1)$ deduced from T_1 using the minimum of T_1 to determine $T_{2r}(=5{\cdot}45\times10^{-6}$ sec) and using equation (3).

b, $\nu_c(T_2)$ deduced from T_2 only, with $T_{2r}(=5{\cdot}45\times10^{-6}$ sec) using equation (2).

c, $\nu_c(\Delta H_2)$ deduced from ΔH_2 only, using $\Delta H_{2r}{}^2=24$ gauss^2 and equation (5).

d, $\nu_c(T_1, T_2)$ deduced from T_1 *and* T_2 using equations (2) and (3) together.

e, $\nu_g(\Delta H_2)$ deduced from ΔH_2 with a distribution having $b_{\mathrm{NMR}}=10$.

f, $\nu_g(T_2)$ deduced from T_2 with a distribution having $b_{\mathrm{NMR}}=4$.

g, $\nu_g(T_1)$ deduced from T_1 with a distribution having $b_{\mathrm{NMR}}=4$.

h, ν_{gD} deduced from dielectric measurements, ν for maximum of $\epsilon''(\nu)$ (Morgan 1934, Davidson and Cole 1951, Schulz 1954).

j, ν_{gs} deduced from ultrasonic measurements (Piccirelli and Litovitz 1957), curve extrapolated using shear viscosity values.

The special point P is discussed in the text.

Since the observed values of T_1 and T_2 are about equal at temperatures sufficiently above that for the minimum of T_1 we use the same value of T_{2r} in equation (2) and deduce a correlation frequency $\nu_c(T_2)$ which, apart from this choice of T_{2r}, is obtained entirely from T_2 and it is shown in figure 3.

An alternative procedure is to use the values of both T_1 and T_2, where they are different, in equations (2) and (3). This determines two unknowns, a correlation frequency which we call $\nu_c(T_1, T_2)$ and the parameter T_{2r} which is now a function of temperature and which we call $T_{2r}(T)$. The values of $\nu_c(T_1, T_2)$ are shown on figure 3. Values of $T_{2r}(T)$ are for example $3{\cdot}2\times10^{-6}$ sec at 250°K and $1{\cdot}84\times10^{-6}$ sec at 238°K. This rapid fall in T_{2r} with falling temperature is suspicious since it would be expected that T_{2r} would be substantially independent of temperature in this small temperature range. Also $T_{2r}=1{\cdot}84\times10^{-6}$ sec corresponds to $\Delta H_{2r}{}^2=140$ gauss^2!

It has been found necessary in several cases to generalize the BPP theory for a distribution of correlation frequencies which may be continuous or discrete

(Gutowsky *et al.* 1957, Miyake 1958, Powles and Luszczynski 1959, Luszczynski and Powles 1959 b, McCall *et al.* 1959). A similar situation is encountered in dielectric and ultrasonic measurements and in particular for glycerol (Morgan 1934, Davidson and Cole 1951, Schulz 1954, Piccirelli and Litovitz 1957).

One indication of the presence of a distribution of correlation frequencies is the value of the ratio T_1/T_2 at the minimum of T_1 which we call $(T_1/T_2)_{\min T_1}$. According to the BPP (1948) theory (equations (2) and (3)), $(T_1/T_2)_{\min T_1} = 2{\cdot}25$. For the theory of Kubo and Tomita (1954) it is 1·60. For *iso*-butyl bromide, where there are independent reasons for believing the distribution is small, the observed value of $(T_1/T_2)_{\min T_1}$ is 2·2 (Luszczynski and Powles 1959 b) whereas in polyisobutylene, where there is reason to suppose a very substantial distribution exists, the observed values is 100 (Powles and Luszczynski 1959). The observed value of $(T_1/T_2)_{\min T_1}$ in glycerol is 3·8. If we assume a continuous 'rectangular' distribution of correlation frequencies $I(\ln \nu_c)$ on a logarithmic scale given by

$$\begin{aligned} I(\ln \nu_c) &= 1/(2 \ln b) \quad \text{for} \quad \nu_g/b < \nu_c < b\nu_g \\ &= 0 \quad \text{for} \quad \nu_g/b > \nu_c \quad \text{and} \quad \nu_c > b\nu_g \quad \ldots\ldots (7) \end{aligned}$$

the distribution width is characterized by the parameter b and the geometric mean value of ν_c is ν_g. The effect on T_1 and T_2 is discussed by Luszczynski and Powles (1959 b, figure 4) and the effect on T_1 and T_2 and their ratio at the minimum of T_1, in particular, is shown in figure 4. $(T_1/T_2)_{\min T_1} = 3{\cdot}8$ corresponds to $b_{\mathrm{NMR}} = 4$. The dielectric loss measurements in this temperature region (Morgan 1934) show almost no distribution, although the accuracy is rather poor owing to the incompleteness of the data. Ultrasonic shear absorption measurements (Piccirelli and Litovitz 1957) on the other hand suggest a distribution $b_S \simeq 3$. Piccirelli and Litovitz (1957), afterwards called PL, assume a Gaussian distribution function in place of equation (7) and the quoted value of b_S is the equivalent for our distribution function.

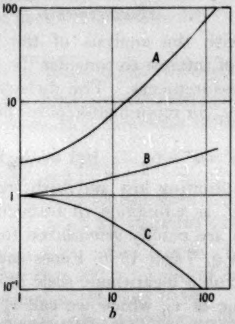

Figure 4. The effect of a distribution of correlation frequencies (equation (7)) on the nuclear resonance parameters at the minimum of T_1; b is the 'width' of the distribution.

A, T_1/T_2 at the minimum of T_1; B, value of T_1 at its minimum relative to value for $b=1$; C, (T_2 at minimum of T_1 for $b>1$)/(T_2 at minimum of T_1 for $b=1$).

Note that T_2 is more affected by the distribution than is T_1 and it is reduced whereas T_1 is increased.

We have already used in §2.1 the result that for a distribution with $b_{\mathrm{NMR}}=4$ the value of $\Delta H_{2r}{}^2$ deduced from the minimum value of T_1 is larger by the factor 1·2.

It can be shown that the inconsistency of $\nu_c(T_1)$ and $\nu_c\ (T_2)$, or alternatively the apparent temperature variation $T_{2r}(T)$ at temperatures well below the minimum of T_1, cannot be explained by a continuous distribution of any extent. An explanation is given in §2.6; a similar situation was encountered in *iso*-butyl bromide (Luszczynski and Powles 1959b).

A distribution of correlation frequencies also affects the values of ν_c deduced from ΔH_2 and this is particularly important since b generally increases with falling temperature. The dielectric measurements (Morgan 1934, Davidson and Cole 1951, Schulz 1954) at temperatures in the region of 230°K correspond to $b_D \simeq 3$ and the value of b_{NMR} in this temperature region may be even larger. It has been shown (Powles and Luszczynski 1959) that the effect of assuming a distribution of ν_c on the apparent values of ν_c deduced from ΔH_2 is to increase the slope of the curve corresponding to $\nu_c(\Delta H_2)$ in figure 3 by rotating it about the invariant point P. Since $\nu_c(\Delta H_2)$ and $\nu_c(T_2)$ should be a continuous curve, or at least have the same slope, we have introduced a distribution to accomplish the latter. This requires $b_{\mathrm{NMR}}=10$, which is rather larger than the value $b_{\mathrm{NMR}}=4$ at 280°K as expected. The new values which we call $\nu_g(\Delta H_2)$ are plotted in figure 3. The subscript g is now used since these are geometric mean values over the assumed symmetric distribution. Similarly the values of $\nu_c(T_1)$ and $\nu_c(T_2)$ should be corrected and if we use the value $b_{\mathrm{NMR}}=4$ deduced from the nuclear resonance measurements at the minimum of T_1 the effect is small (see figure 4). The new values $\nu_g(T_1)$ and $\nu_g(T_2)$ are not sufficiently different to warrant separate curves in figure 3.

We emphasize that so far we have used nuclear magnetic resonance measurements only.

2.4. *Correlation Frequencies deduced from Dielectric and Ultrasonic Absorption Measurements*

Before proceeding with the analysis of the proton magnetic resonance measurements it will be of interest to consider the closely related dielectric and ultrasonic absorption measurements. The dielectric measurements determine the correlation frequency ν_D for reorientation of the dipole moment of the molecule through the relation

$$\epsilon' - i\epsilon'' = (\epsilon_0 - \epsilon_\infty)/(1 + i\nu/\nu_D) + \epsilon_\infty \qquad \ldots\ldots (8)$$

where ϵ_0 and ϵ_∞ are the limiting low and high frequency dielectric constants. Thus the dielectric loss ϵ'' as a function of frequency ν has a maximum when $\nu = \nu_D$. These equations are readily generalized for a distribution of dielectric correlation frequencies (e.g. Yager 1936, Fuoss and Kirkwood 1941) but if the distribution is symmetric on a logarithmic scale of ν_D the maximum of ϵ'' gives the geometric mean value of ν_D which we call ν_{gD}. Actually in glycerol the distribution is slightly asymmetric (Davidson and Cole 1951). In figure 3 we show the values of ν_{gD} deduced from the observed maxima of $\epsilon''\ (\nu)$ at various constant temperatures.

The complex shear modulus for a viscous fluid with a shear strain relaxation process is given by (Litovitz *et al.* 1954)

$$G' + iG'' = iG_\infty/(1 - i\nu_S/\nu) \qquad \ldots\ldots (9)$$

where G_∞ is the limiting high-frequency shear modulus and ν_S is the shear stress relaxation correlation frequency. The 'static' shear viscosity η_S is given by Maxwell's relation

$$\eta_S = G_\infty / 2\pi\nu_S. \qquad \ldots\ldots (10)$$

Equation (9) may be readily generalized to a distribution of shear stress relaxation correlation frequencies (PL 1957). If the distribution is symmetric, the peak of $G''(\nu)$ or the value of ν at which $G' = G_\infty/2$ for a particular temperature gives the geometric mean value of ν_S, which we call ν_{gS}.

We have calculated the values of ν_{gS} from the ultrasonic measurements of PL made in the range $\nu = 14{\cdot}7 \times 10^6$ c/s to $84{\cdot}5 \times 10^6$ c/s and these are shown in figure 3. The effect of a distribution of ν_S on equation (10) is to multiply the right-hand side by a numerical factor which, for a limited temperature range near 260°K and for glycerol, is 4·1 (PL 1957). Thus we can extrapolate the values of ν_{gS} by using the measured values of η_S and sufficiently accurate values of G_∞ which only, in any case, varies by a factor of about two over the temperature range in question. Similar results are found for the compressibility modulus K and the corresponding correlation frequency; the two correlation frequencies are similar in magnitude.

2.5. *Internal Field and other Corrections*

Both these results, ν_{gD} and ν_{gS}, are subject to a correction factor since they are the macroscopic values determined by studying a macroscopic quantity, whereas what is required is the microscopic parameter.

For dielectrics this correction is almost equivalent to the internal field problem. According to Debye (1929) the relation between the two frequencies is

$$\nu'_D/\nu_D = (\epsilon_0 + 2)/(\epsilon_\infty + 2) \qquad \ldots\ldots (11)$$

where the microscopic correlation frequency is primed.

This factor is an important one for glycerol amounting to about 10. However, it is probable that the difference between ν_D and ν'_D is not as great as given by equation (11) (O'Dwyer and Sack 1952, Powles 1953). An approximate formula (Powles 1953) is

$$\nu'_D/\nu_D = 3\epsilon_0/(2\epsilon_0 + \epsilon_\infty) \simeq 3/2 \text{ for glycerol.} \qquad \ldots\ldots (12)$$

The values of ν_c and ν_D also differ, even for the same motion, by a small factor since they depend on the correlation functions of different angular functions. In the BPP theory (1948),

$$\nu_c/\nu'_D = 3. \qquad \ldots\ldots (13)$$

Thus for glycerol $\quad \nu_c/\nu_D \simeq 30$ for equation (11)

$\simeq 4{\cdot}5$ for equation (12).

In figure 3 we see that in fact $\nu_c/\nu_D \simeq 1$ or less in glycerol. Hence our results favour the relation (12) rather than (11). A recent comparison of ν_c and ν_D for water reaches the same conclusion (Hennel 1959).

The ultrasonic measurements suffer a rather similar correction (Litovitz and Sette 1953) given by

$$\nu'_S/\nu_S = [K_\infty + (4/3)G_\infty]/K_0 \qquad \ldots\ldots (14)$$

where K_0 and K_∞ are the static and the limiting high-frequency bulk moduli respectively. For glycerol this factor is about 2 and is such as to *increase* the difference between ν_{gS} and $\nu_g(T_2)$ or ν_{gD} in figure 3.

2.6. *Comparison of Correlation Frequencies*

We now compare (in figure 3) the values of ν_{gD} and ν_{gS} with ν_g deduced from proton magnetic resonance measurements.

We note the almost exact agreement between the correlation frequency $\nu_g(T_2)$ derived from the nuclear resonance measurements and the ν_{gD} derived from dielectric loss measurements although they should differ by a factor about 3 (equation (13)). The correlation frequencies $\nu_g(\Delta H_2)$ deduced from ΔH_2 values with the correction for the distribution $b_{NMR}=10$ fall below the ν_{gD} values by a factor of about 3. The discrepancy with theory (equation (13)) by a factor of about 9 in the lower temperature region and by about 3 in the higher temperature region suggests a real difference between the nuclear resonance and the dielectric correlation frequencies, the dielectric reorientation being faster. This is reasonably explained when we note that the main contribution to the dipole moment is that of OH (1·51 debye) rather than C–O (0·74 debye). Thus reorientation of the OH bond has the major effect in determining dielectric relaxation and this involves breaking of hydrogen bonds, as does translational motion which is shown below to be fast. On the other hand five of the eight protons are attached to the skeletal carbon atoms and will reorient with the C–O bonds. Thus, in general, since OH probably reorients faster than CO it is reasonable to find nuclear resonance correlation frequencies below those for dielectric relaxation.

The trend of ν_{gS} from ultrasonic measurements with temperature is similar to that of ν_g and ν_{gD} but the numerical value of ν_{gS} is greater by a factor of about twenty. (From an analysis of his own results Schulz (1954) concludes that the ultrasonic correlation frequency is greater by a factor about 3·5 at 243°K.) A similar situation is found in other hydrogen bonded liquids, e.g., $\nu_S/\nu_D=4$ in propanediol 1,2 (Litovitz 1958) and 19 in *n*-propyl alcohol (Lyon and Litovitz 1956). These differences seem too large to be accounted for by uncertainties in the theories which have been used to deduce the correlation frequencies from the experimental results and in correction factors such as those discussed in § 2.5. We therefore think that the molecular process controlling shear stress relaxation may be some ten or more times faster than that controlling dielectric relaxation and that in turn is faster than the processes controlling nuclear relaxation. In other words translational motion of the glycerol molecules is faster than rotational or possibly internal motion. However, since the temperature variation of ν_{gS}, ν_{gD} and ν_g are similar the processes are not unrelated. Possibly reorientation of the glycerol molecules occurs when allowed by the translational motion but on the average several translational jumps are required to permit appreciable molecular reorientation.†

If translational motion is faster than the rotational then at the observed minimum of T_1 the intermolecular proton interactions will not contribute appreciably to T_1 and the T_1 minimum should reflect a smaller interaction ($\Delta H_{2r}{}^2$ from $T_{1\min}$) than is found from the observed rigid lattice absorption at low temperatures. We recall that the actual values are 19·2 gauss^2 and 24 gauss^2 respectively.

One remaining difficulty is that even the assumption of a reasonable continuous distribution (and indeed for any continuous distribution) $\nu_g(T_1)$ and $\nu_g(T_2)$

---

† *Note added in proof.* Another interpretation has been given recently (Herzfeld and Litovitz 1959).

differ in the temperature range below 260°K. A similar situation in *iso*-butyl bromide (Luszczynski and Powles 1959 b) was explained by the assumption that some of the nuclear interactions were subject to faster motional effects than the main interactions. Consider two motions having correlation frequencies comparable with, but rather below, the resonant frequency, the faster motion being associated with the smaller nuclear interaction. Then in the region below the principal minimum of T_1 this has little effect on T_2 but diminishes T_1 to an important extent. Consequently, if one calculates correlation frequencies ignoring the minor faster motion the deduced values of $\nu_c(T_2)$ are hardly affected but those of $\nu_c(T_1)$ are too high. Above the principal minimum of T_1, T_1 also is primarily sensitive to the slower motion and so $\nu_c(T_1)$ becomes similar to $\nu_c(T_2)$. Then the effect of the faster motion is only observed indirectly in a larger effective T_{2r} value. The general effect is illustrated in figure 5, where we have taken $\Delta H_{2r_2} = \frac{1}{3}\Delta H_{2r_1}{}^2$ and $\nu_{c_2} = 10\nu_{c_1}$. In *iso*-butyl bromide the faster

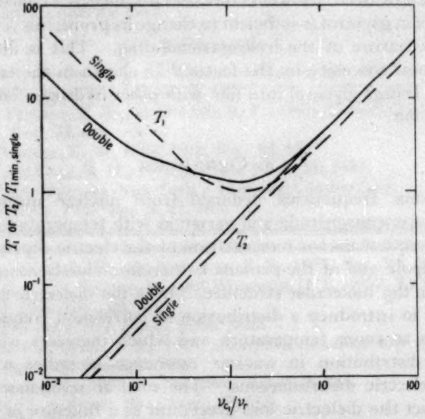

Figure 5. Calculated variation of T_1 and T_2 for two motions (marked ' double ') ν_{c_1} and ν_{c_2} where $\nu_{c_2}/\nu_{c_1} = 10$ and the nuclear interactions associated with each are given by $\Delta H_{2r_2}{}^2/\Delta H_{2r_1}{}^2 = 1/3$ compared with the values for a single motion (marked ' single ') and the same total interaction. Note that T_1 is more affected than T_2 below the minimum of T_1 and in such a way as to explain the observed T_1 in glycerol (figure 2).

motion was an internal molecular motion of a methyl group. In glycerol the internal hydrogen bonds would tend to prevent internal rotation, however as stated earlier, in the liquid one expects to find a proportion of intermolecular hydrogen bonds. During molecular translation and/or reorientation these bonds will be broken and so some internal molecular motion is possible. However this internal motion would affect both the proton resonance *and* the dielectric relaxation, so that this effect, if any, is already included in the curves of ν_{gD} and $\nu_g(T_2)$. It is tempting therefore to associate the faster motion sought with the translational molecular motion determining the ultrasonic relaxation. As indicated in figure 3, this motion is faster by a factor of ten or more and as shown in figure 5, with plausible parameters a second minimum of T_1 will not be resolved. Thus T_1 in this temperature region could be determined mainly by the intermolecular interactions of the protons rather than by their intramolecular interactions.†

It is interesting to note that the distribution function for the dielectric measurements is slightly asymmetric (Davidson and Cole 1951) with a contribution at the high-frequency end. This may well be connected with the faster translational motion postulated here which has some influence on the dielectric relaxation.

The conclusions of an earlier comparison of nuclear resonance T_1 values and ultrasonic absorption for glycerol (Litovitz 1957) must be modified in view of the new T_1 measurements presented in this paper which we believe to be more accurate than the old ones.

We must also consider a comparison of the ultrasonic and dielectric measurements on glycerol $+5\%$ water (Litovitz and Sette 1953). In this paper the values of ν_S and ν_D were found to agree, in contradistinction to our conclusions for glycerol $+0{\cdot}2\%$ water. However this does not affect our conclusions adversely since 5% of water in glycerol is sufficient to change its properties very considerably, in particular the nature of the hydrogen bonding. This is illustrated by the change in the shear viscosity by the factor 2·75 shown in the table (§ 1). The present analysis brings glycerol into line with other hydrogen bonded liquids as already pointed out.

§ 3. CONCLUSION

The correlation frequencies deduced from nuclear magnetic resonance measurements have a magnitude and variation with temperature very similar to the correlation frequencies for reorientation of the electric dipole. The motion of the electric dipole and of the protons is therefore closely connected as would be expected from the molecular structure. As in the dielectric case, it has been found necessary to introduce a distribution of correlation frequencies which is appreciable even at room temperature and which increases with falling temperature. The distribution in nuclear resonance is rather wider than that found in the dielectric measurements. The nuclear resonance measurements allow us to predict the dielectric loss maximum as a function of temperature in the range 10^8 c/s to 2×10^{10} c/s (the curve in figure 3) with some confidence. This is valuable since this is a difficult frequency region for dielectric measurements. The motional frequency for nuclear resonance is rather higher than for dipolar reorientation and this can also be explained by the structure of the molecule.

We find from a consideration of ultrasonic measurements that the correlation frequency for translational motion of the glycerol molecules may be rather faster than the rotational motion at least in the room temperature region. If this is so, it partially explains some anomalies in the nuclear magnetic resonance measurements such as (i) that the nuclear interaction deduced from the minimum of T_1 is smaller than that for the observed rigid lattice second moment and (ii) that the T_1 values at temperatures below the minimum of T_1 are unexpectedly short.

---

† *Note added in proof.* A recent theory (Skrotskii and Kokin 1959) suggests that the T_1 minimum may be asymmetric in the way described here.

The comparison between nuclear resonance and dielectric measurements suggests that the Debye internal field correction for the dielectric relaxation time is too large.

The measurements confirm and extend the (correlation frequency, temperature) curve for glycerol and in particular show the fall in rate of rise with temperature at high temperatures which is commonly found in liquids. This fall off occurs at a higher temperature than in non-hydrogen bonded liquids but is in a similar position relative to the melting point. The precise interpretation of this curve is a problem in itself and will not be discussed here.

ACKNOWLEDGMENTS

We thank Dr. J. Haslam of Imperial Chemical Industries (Plastics Division) Analytical Department, for analysing the samples of glycerol for water.

Part of the apparatus was provided by the Central Research Fund of the University of London and part by Imperial Chemical Industries Ltd.

One of us (J. A. E. K.) was supported during this work by a grant from Imperial Chemical Industries Ltd.

REFERENCES

ANDREW, E. R., 1955, *Nuclear Magnetic Resonance* (Cambridge: University Press), p. 125.
BASTIANSEN, O., 1949, *Acta Chem. Scand.*, **3**, 415.
BLOEMBERGEN, N., PURCELL, E. M., and POUND, R. V., 1947, *Nature, Lond.*, **160**, 475.
—— 1948, *Phys. Rev.*, **73**, 679.
CARR, H. Y., and PURCELL, E. M., 1954, *Phys. Rev.*, **94**, 630.
DAVIDSON, D. W., and COLE, R. H., 1951, *J. Chem. Phys.*, **19**, 1484.
DEBYE, P., 1929, *Polar Molecules* (New York: Chemical Catalog Co.).
DRAIN, L. E., 1949, *Proc. Phys. Soc.* A, **62**, 301.
FUOSS, P. M., and KIRKWOOD, J. G., 1941, *J. Amer. Chem. Soc.*, **63**, 385.
GIULOTTO, L., 1956, *Arch. Sci., Genève* (5th Colloque Ampère), **9**, 212.
GUTOWSKY, H. S., MAYER, L. H., and MCCLURE, R. E., 1953, *Rev. Sci. Instrum.*, **24**, 644.
GUTOWSKY, H. S., SAIKA, A., TAKEDA, M., and WOESSNER, D. E., 1957, *J. Chem. Phys.*, **27**, 534.
HAHN, E. L., 1950, *Phys. Rev.*, **80**, 580.
HENNEL, J. W., 1959, *Acta Phys. Polon.*, in the press.
HERZFELD, K. F., and LITOVITZ, T. A., 1959, *Absorption and Dispersion of Ultrasonic Waves* (New York: Academic Press), p. 502.
KUBO, R., and TOMITA, K., 1954, *J. Phys. Soc., Japan*, **9**, 888.
LITOVITZ, T. A., 1957, *J. Acoust. Soc. Amer.*, **29**, 648.
—— 1958, *Ibid.*, **30**, 383.
LITOVITZ, T. A., LYON, T., and PESELNICK, L., 1954, *J. Acoust. Soc. Amer.*, **26**, 566.
LITOVITZ, T. A., and SETTE, D., 1953, *J. Chem. Phys.*, **21**, 17.
LÖSCHE, A., 1957, *Kerninduction* (Berlin: Veb. Deutscher Ver. d. Wiss.), p. 331.
LUSZCZYNSKI, K., and POWLES, J. G., 1959 a, *J. Sci. Instrum.*, **36**, 57.
—— 1959 b, *Proc. Phys. Soc.*, **74**, 408.
LYON, T., and LITOVITZ, T. A., 1956, *J. Appl. Phys.*, **27**, 179.
MCCALL, D. W., DOUGLASS, D. C., and ANDERSON, E. W., 1959, *J. Chem. Phys.*, **30**, 1272.
MIYAKE, A., 1958, *J. Polymer Sci.*, **28**, 476.
MORGAN, S. O., 1934, *Trans. Amer. Electrochem. Soc.*, **65**, 109.
O'DWYER, J. J., and SACK, R. A., 1952, *Aust. J. Sci. Res.*, **5a**, 647.
PAKE, G. E., 1956, *Solid State Physics*, Vol. 2 (New York: Academic Press), p. 72.
PICCIRELLI, R., and LITOVITZ, T. A., 1957, *J. Acoust. Soc. Amer.*, **29**, 1009.
POWLES, J. G., 1953, *J. Chem. Phys.*, **21**, 633.
—— 1956, *Proc. Phys. Soc.* B, **69**, 281.
POWLES, J. G., and LUSZCZYNSKI, K., 1959, *Physica*, **25**, 455.
REDFIELD, A. G., 1955, *Phys. Rev.*, **98**, 1787.
SCHULZ, A. K., 1954, *Z. Naturf.*, **9a**, 944.

Sheely, M. L., 1932, *Industr. Engng Chem.*, **24**, 1060.
Simon, F., 1922, *Ann. Phys., Lpz.*, **68**, 278.
Simpson, J. H., and Carr, H. Y., 1958, *Phys. Rev.*, **111**, 1201.
Skrotskii, G. V., and Kokin, A. A., 1959, *J. Exp. Theor. Phys. U.S.S.R.*, **36**, 481 (Soviet Physics JETP, **36**, 335).
Van Vleck, J. H., 1948, *Phys. Rev.*, **74**, 1168.
Yager, W. A., 1936, *Physics*, **7**, 434.

γ-rays from 2^+ States in ^{16}O

By R. E. MEADS and J. E. G. McILDOWIE
Clarendon Laboratory, Oxford

MS. received 21st September 1959

Abstract. The 9·84 Mev and 11·51 Mev levels in ^{16}O have been excited by the $^{12}C(\alpha,\gamma)^{16}O$ reaction. The ground state radiation widths of these levels have been measured as $0{\cdot}02 \pm 0{\cdot}01$ ev and $0{\cdot}9 \pm 0{\cdot}2$ ev respectively. These values are discussed in terms of the extreme single particle and collective models.

---

§ 1. INTRODUCTION

CALCULATIONS have been made by Barton (1959) and Barton *et al.* (1959, private communication) on the enhancement of electric quadrupole effects in the mirror nuclei ^{17}O and ^{17}F, using Rayleigh–Schrödinger, and later Brillouin–Wigner perturbation theory, on the basis of the coupling of the motion of an odd nucleon with that of a distorted ^{16}O core. The existence of core distortion is shown by the fact that ^{17}O has a measurable electric quadrupole moment (Kamper *et al.* 1957). In order to explain the magnitude of the quadrupole moment, the calculation requires the existence of parent core states similar to those of the ^{16}O nucleus, having spin 2^+, and ground state radiation widths considerably greater than the extreme single-particle Weisskopf values. No such states are known in the energy range 13–20 Mev, and of the 2^+ states below this, the value of Γ_γ has previously been obtained only for the 6·91 Mev level (Swann and Metzger 1957). This was found to be of the order of one Weisskopf unit. It was therefore of interest to measure Γ_γ for the ground state transitions from the other 2^+ levels at 9·84 and 11·51 Mev.

In the present work, these levels were excited by the $^{12}C(\alpha,\gamma)^{16}O$ reaction. The 1^- level at 9·58 Mev has already been studied in this way by Bloom *et al.* (1957).

§ 2. EXPERIMENTS

An enriched ^{12}C target supplied by the Electromagnetic Separator Group at the Atomic Energy Research Establishment, Harwell, was bombarded by α-particles from the 6 Mv Van de Graaff generator at the Atomic Weapons Research Establishment, Aldermaston, and the γ-radiation detected using a 4 in. × 4 in. cylindrical NaI(Tl) crystal supplied by the Harshaw Chemical Company, mounted on an E.M.I. type 6099 A photomultiplier. The principal difficulty of the experiment lay in the presence of an intense neutron background from the $^{13}C(\alpha,n)^{16}O$ reaction due to residual ^{13}C in the target. The relative sensitivity of the detector to neutrons could have been reduced by the use of a three-crystal pair spectrometer, but the consequent reduction of γ-ray sensitivity made this impracticable, as the yield of γ-rays was small. An attempt was made to reduce the rate of deposition of natural carbon on the target due to cracking of vapour during beam bombardment, by heating the target to about 100°C and placing a liquid nitrogen trap immediately in front of it. Rubber vacuum gaskets near the target were avoided by the use of indium wire seals. Although no detailed measurements were made on the effectiveness of these precautions, no significant increase in the neutron background was noticed during the course of the experiment.

With the discriminator bias on the counter set to accept γ-radiation of energy greater than 4 Mev, an excitation function was obtained for α-particle bombarding energies from 2·0 to 6·2 Mev. Resonances were observed at 3·32, 3·68, 4·37, 4·57, 5·29, 5·50, 5·83 and 6·14 Mev. By the use of a BF_3 'long' counter and also examination of the spectra from the NaI(Tl) crystal it was shown that these resonances were probably all due to the $^{13}C(\alpha, n)^{16}O$ reaction. The spectra showed a continuum of pulses due to neutrons, rising rapidly towards low energies, and for high bombarding energies superposed peaks due to γ-radiation from the 6·14 Mev level in ^{16}O. This level can be excited in the $^{13}C(\alpha, n)^{16}O$ reaction for α energies above 5·05 Mev (Bonner *et al.* 1956).

Spectra taken at about 5·9 Mev α energy showed a peak at a γ-ray energy of about 11 Mev, thought to be due to the excitation of the 11·51 Mev level in ^{16}O by the $^{12}C(\alpha, \gamma)^{16}O$ reaction. The yield of this radiation, relative to the total counting rate above the bias level was insufficient for it to show up in the original excitation function.

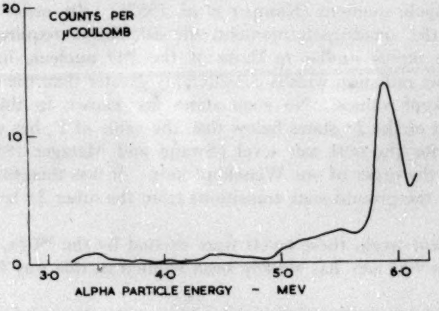

Figure 1. Excitation function for α-particle bombardment of the ^{12}C target, obtained by counting radiation in the energy range 8·3–13·5 Mev.

Another excitation function, covering the range from 3·2 to 6·2 Mev, was obtained by counting radiation in the range from 8·3 to 13·5 Mev selected by a single channel analyser. The result is shown in figure 1. The main feature is a resonance approximately 200 kev in width centred on a bombarding energy of 5·91 Mev. This was certainly due to the ground state transition from the 11·51 Mev level. If the total width of the level is assumed to be 80 kev (Ajzenberg-Selove and Lauritsen 1959) the above value of 200 kev for the measured width gives a value of about 185 kev for the target thickness. No resonance was noticed at about 3·6 Mev α energy, corresponding to the excitation of the 9·84 Mev level in ^{16}O, but a series of γ-ray spectra taken over a range of

α energies from 3·5 to 3·8 MeV showed a weak peak due to radiation of about 10 MeV. This was not strong enough to appear in the excitation function.

Spectra of the 11·5 MeV γ-ray were taken at angles of 0°, 45° and 90° to the beam direction, with the counter 3 inches from the target, in order to confirm that the angular distribution corresponded to that expected for a $2^+ \rightarrow 0^+$, E2 transition. The theoretical distribution is $W(\theta) = \cos^2\theta(1-\cos^2\theta)$. To get the true counting rate for the 11·5 MeV γ-ray it was necessary to subtract the high energy tail of the neutron background. The need for this is illustrated by figure 2 which shows the spectrum taken at 45°. To fix the level of the background to be subtracted it was assumed that the distribution of counts in the γ-ray spectrum was the same as that for a 12·15 MeV γ-ray obtained from the ^{11}B(p, γ)^{12}C reaction at the resonance at 0·68 MeV (Huus and Day 1953). This γ-ray was used as a calibration standard.

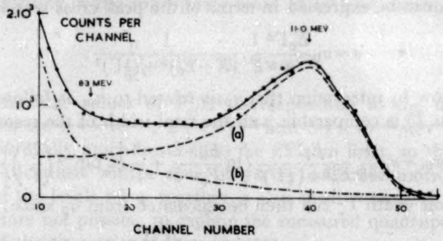

Figure 2. Spectrum of the 11·5 MeV γ-ray taken at 45° to the beam direction. The broken lines indicate the number of counts attributed (*a*) to the γ-ray itself and (*b*) to the background.

An estimate of the counting rate which would be expected at each of the three chosen angles, for the geometry used, was obtained by dividing the crystal into a number of elements and adding together the contributions of each element, taking into account its counting efficiency and angular position relative to the beam. The calculated values (normalized to the rate at 45°) are compared with the experimental results in the table. The results show the expected strong maximum at 45°. The rather large discrepancy at 0° can probably be accounted for by crudities in the calculation.

Comparison between calculated relative count rates at 0°, 45° and 90° to the beam direction, for a $2^+ \rightarrow 0^+$, E2 transition, and experimental values for the 11·5 MeV γ-ray.

Angle (deg)	0	45	90
Calculated count rate	0·46	1·00	0·23
Measured count rate	0·37	1·00	0·20

The absolute yield of the γ-rays was calculated using the crystal efficiency data of Wolicki *et al.* (1956). A correction was made for absorption of the radiation in the target mounting at each angle.

A more accurate value for the target thickness was obtained by measuring the apparent width of the ^{12}C(p, γ)^{13}N resonance at 0·459 MeV proton energy (Hunt and Jones 1953). Corrected for differences in stopping power, the result for 6 Mev α-particles was 171 kev. This value was taken in the subsequent calculations.

In measurement of beam currents, a sufficient positive potential was applied to the target to ensure suppression of secondary electrons.

§ 3. RESULTS

The experimental results were expressed as a mean cross section σ_{m} for production of the γ-ray at the middle of the measured resonance, integrated over all angles and over the thickness of the target.

Assuming the single level Breit–Wigner formula, applicable in this case:

$$\sigma=(2l+1)\pi\lambdabar^2\frac{\Gamma_\alpha\Gamma_\gamma}{(E-E_0)^2+(\frac{1}{2}\Gamma)^2}$$

where $l=2$. σ can be expressed in terms of the peak cross section σ_{p}:

$$\sigma=\sigma_{\mathrm{p}}\frac{E_0\Gamma^2}{4}\frac{1}{E}\cdot\frac{1}{(E-E_0)^2+(\frac{1}{2}\Gamma)^2}.$$

One can show by integration that σ_{p} is related to σ_{m} as follows, for a target whose thickness 2δ is comparable with the total width of the resonance Γ

$$\sigma_{\mathrm{m}}=\sigma_{\mathrm{p}}\frac{1}{8\delta}\,\frac{E_0\Gamma^2}{E_0^2+(\frac{1}{2}\Gamma)^2}\left\{\ln\frac{E_0+\delta}{E_0-\delta}+\frac{4}{\Gamma}E_0\tan^{-1}\left(\frac{2\delta}{\Gamma}\right)\right\}.$$

The radiation width Γ_γ can then be calculated from σ_{p} since:

$$\sigma_{\mathrm{p}}=4(2l+1)\pi\lambdabar_0^2\frac{\Gamma_\alpha\Gamma_\gamma}{\Gamma^2}$$

$\lambdabar_0$ is the centre-of-mass wavelength for α-particles at the resonance maximum. In the calculation, since $\Gamma_\alpha \gg \Gamma_\gamma$ one may take $\Gamma_\alpha=\Gamma=80$ kev.

An estimate of the radiation width for the ground state transition from the 9·84 Mev level was obtained from a γ-ray spectrum taken at 45° to the beam direction at an α-particle energy of 3·65 Mev, using a value of $\Gamma=0{\cdot}8$ kev (Ajzenberg-Selove and Lauritsen 1959). Since in this case Γ is much smaller than the target thickness, the relation between σ_{m} and σ_{p} reduces to $\sigma_{\mathrm{m}}=\sigma_{\mathrm{p}}\pi\Gamma/4\delta$.

The final results were as follows: for the ground state transition from the 11·51 Mev level: $\Gamma_\gamma=0{\cdot}9\pm0{\cdot}2$ ev; for the ground state transition from the 9·84 Mev level: $\Gamma_\gamma=0{\cdot}02\pm0{\cdot}01$ ev.

§ 4. DISCUSSION

The work of Ehrenberg *et al.* (1959) on high energy electron scattering yields a value for $\langle r^2\rangle^{1/2}$, the r.m.s. radius of the charge distribution in the ^{16}O nucleus, equal to $2{\cdot}70\times10^{-13}$ cm. Assuming uniform charge density, the nuclear radius R is related to $\langle r^2\rangle$ by $\langle r^2\rangle=3R^2/5=3r_0^2A^{2/3}/5$ where r_0 is the nuclear radius constant. From this, we obtain the value $r_0=1{\cdot}38$ fermis.

Using this value, the Weisskopf single particle values for the radiation widths for E2 transitions are given by the formula (Weisskopf 1951, Wilkinson 1958)

$$\Gamma_{\gamma\mathrm{W}}=8{\cdot}6\times10^{-8}A^{4/3}E_\gamma^{\,5}\ \mathrm{ev}$$

where E_γ is in Mev.

For transitions of 9·84 and 11·51 Mev in ^{16}O these widths are 0·32 and 0·70 ev respectively, compared with the measured values of 0·02 and 0·9 ev. Swann and Metzger (1957) obtain a value of $1 \cdot 2 \pm 0 \cdot 3 \times 10^{-14}$ sec for the mean γ-lifetime of the 6·91 Mev level. This corresponds to a value of $\Gamma_\gamma = 0 \cdot 05$ ev which almost exactly equals the Weisskopf value calculated as above.

If one of these states could be expressed entirely as a single phonon excitation of the surface oscillations of a liquid drop, then we should expect the value of Γ_γ for the ground state transition to reach the maximum allowed by the E2 sum rule (Gell-Mann and Telegdi 1953, Wilkinson 1955)

$$\frac{\Gamma_\gamma}{E^4} \leqslant \frac{1}{60} \frac{e^2}{\hbar c} \frac{A}{\hbar^2 c^2} \frac{\langle r^2 \rangle}{Mc^2}$$

where M is the mass of one nucleon. This is appropriate to the case of a transition of energy E between such a 2^+ state and the 0^+ ground state of a nucleus with $T_z = 0$. Putting in the appropriate value of $\langle r^2 \rangle$ we obtain, in the case of ^{16}O,

$$\frac{\Gamma_\gamma}{E^4} \leqslant 3 \cdot 9 \times 10^{-10} \,\text{Mev}^{-3}.$$

The experimental values of Γ_γ / E^4 corresponding to the 6·91, 9·84 and 11·51 Mev levels are $2 \cdot 4 \times 10^{-11}$, $2 \cdot 1 \times 10^{-12}$ and $5 \cdot 1 \times 10^{-11}$ Mev^{-3} respectively. These are individually much lower than the E2 sum limit, so that none of the levels can be identified with a state of purely collective motion. The total contribution of the levels taken together is also small compared with the limit, and it is therefore not possible to explain the measured quadrupole moment of ^{17}O in terms of the properties of these states.

ACKNOWLEDGMENTS

We would like to thank the Director of the Atomic Weapons Research Establishment, Aldermaston, and Dr. K. W. Allen, for the use of the 6 MV Van de Graaff generator. We are most grateful to Professor D. H. Wilkinson, who suggested the experiment, for helpful discussions. One of us (J. E. G. McI.) is indebted to the Ministry of Education for Northern Ireland for a Research Studentship.

REFERENCES

AJZENBERG-SELOVE, F., and LAURITSEN, T., 1959, *Nucl. Phys.*, **11**, 1.
BARTON, G., 1959, *Nucl. Phys.*, **11**, 466.
BLOOM, S. D., TOPPEL, B. J., and WILKINSON, D. H., 1957, *Phil. Mag.*, **2**, 57.
BONNER, T. W., KRAUS, A. A., MARION, J. B., and SCHIFFER, J. P., 1956, *Phys. Rev.*, **102**, 1348.
EHRENBERG, H. F., HOFSTADTER, R., MEYER-BERKHOUT, U., RAVENHALL, D. G., and SOBOTTKA, S. E., 1959, *Phys. Rev.*, **113**, 666.
GELL-MANN, M., and TELEGDI, V. L., 1953, *Phys. Rev.*, **91**, 169.
HUNT, S. E., and JONES, W. M., 1953, *Phys. Rev.*, **89**, 1283.
HUUS, T., and DAY, R. B., 1953, *Phys. Rev.*, **91**, 599.
KAMPER, R. A., LEA, K. R., and LUSTIG, C. D., 1957, *Proc. Phys. Soc.* B, **70**, 897.
SWANN, C. P., and METZGER, F. R., 1957, *Phys. Rev.*, **108**, 982.
WEISSKOPF, V. F., 1951, *Phys. Rev.*, **83**, 1073.
WILKINSON, D. H., 1955, *Phys. Rev.*, **99**, 1347.
—— 1958, *A.E.R.E. Report* T/R 2492, Harwell.
WOLICKI, E. A., JASTROW, R., and BROOKS, F., 1956, *Naval Research Laboratory Report* NRL 4833, Washington.

A Lattice Model of a Classical Hard Sphere Gas

By D. M. BURLEY

Mathematics Department, University of Glasgow

Communicated by C. Domb; *MS. received* 26*th June* 1959, *in revised form* 18*th September* 1959

Abstract. From an examination of the proposed lattice model of a hard sphere gas, several interesting features are observed. It is found that for loose packed lattices it is necessary to consider two regions, one ordered and one disordered, so that the whole pressure–density curve may be described. The disordered region, for these lattices, produces virial coefficients which oscillate in sign every three or four terms, and above a certain density the phase becomes unstable. Treatment of the ordered region is not altogether satisfactory but it appears that the phase disappears below a certain density. Consequently, there is a strong indication that a transition occurs for loose packed lattices, but the nature and position of the transition is still in doubt. For the close packed lattices however, it is found that the gas has virial coefficients which are all positive and so seems to be able to condense into an ordered phase without any transition.

§ 1. INTRODUCTION

THERE has been considerable interest recently in systems with hard sphere interactions. A great deal of work has been produced, notably by Lee, Huang and Yang (1957) and Brueckner and Sawada (1957), on hard sphere systems using quantum statistics. On the other hand, much work has been undertaken in calculating the equations of state of hard sphere systems using Boltzmann statistics by Monte Carlo methods, the work being performed by Metropolis *et al.* (1953), Alder and Wainwright (1957) and Wood and Jacobson (1957). Since a large number of gases show no quantum effects except at very low temperatures, attention will be paid only to gases for which classical mechanics provides an adequate description of the assembly.

The statistical mechanical calculation of the equation of state of a classical hard sphere gas has been surrounded by many difficulties. Even on the Mayer cluster theory (Mayer and Mayer 1940) it has been possible to evaluate only three virial coefficients directly, although the Monte Carlo calculations have extended the number to four. It is observed that these coefficients are temperature independent since they are calculated from a Mayer interaction function

$$f_{ij}=\begin{cases} 0 & |\mathbf{r}_i-\mathbf{r}_j|>b \\ -1 & |\mathbf{r}_i-\mathbf{r}_j|<b \end{cases} \qquad \ldots\ldots(1)$$

and since any more realistic interaction function must include the temperature explicitly, there is a corresponding increase in the difficulty of the calculations. However, the first two virial coefficients, B_2 and B_3, have been calculated for the most common intermolecular potentials and the results and methods are well reported by Hirschfelder, Curtis and Bird (1954).

An interesting modification of the hard sphere potential was put forward by Zwanzig (1956). He replaced the usual f_{ij} of (1) by

$$f_{ij} = -f(x_i - x_j) f(y_i - y_j) f(z_i - z_j)$$
$$f(x) = \begin{cases} 1 & |x| < b \\ 0 & |x| > b. \end{cases} \qquad \ldots\ldots(2)$$

This modification led him to a model of hard cubes (or squares in the two-dimensional case) in which the sides of the cube are restricted to remain parallel to the coordinate axes. The merit of this method is that the cluster integrals all reduce to the one-dimensional integrals, which have been evaluated up to B_5 by Riddell and Uhlenbeck (1953); Zwanzig was thus able to calculate up to B_5 for his model. He then makes an interesting comparison in which he suggests that his model will produce negative virial coefficients for B_7 or B_8. This behaviour was shown to occur for four or five dimensional gases in a note by Temperley (1957) and again it was inferred that negative coefficients would occur in three dimensions.

The question of whether an assembly of hard spheres would show a transition has been answered by the Monte Carlo calculations, since Alder and Wainwright (1957) have been able to predict that a first order phase transition should occur at a volume $V/V_0 = 1{\cdot}5$, where V_0 is the close packing volume, and their photographs of the tracks of particles at different volumes, displayed on a cathode-ray tube screen, are most convincing. These calculations have therefore given a considerable stimulus to try to reproduce this first order phase transition by direct calculation. This paper is an attempt to make such calculation for a simple model and to relate the results to a real hard sphere gas and to the study of virial coefficients in general.

§ 2. THE MODEL USED

A natural extension of Zwanzig's work is not only to restrict the particles to remain parallel to the coordinate axes, but also to restrict them to remain on lattice points so that they can move only from one lattice point to another. Although this may be a severe restriction, the resulting model shows excluded volume effects and the mathematics of the model can be derived from those of the Ising model of an antiferromagnetic in a magnetic field. Yang and Lee (1952) used a similar model with great success for the liquid-vapour problem, by considering a transformation of the ferromagnetic Ising model. The antiferromagnetic corresponds to a hard sphere gas with purely repulsive interactions and it is hoped that the model can provide similar information about any critical phenomena.

The model used here was briefly explained in a preliminary report of this work, given in a review paper by Domb (1958). In order to describe the model in more detail, it is necessary to consider a magnetic Ising lattice, which consists of N spins, with a magnetic moment per spin of m, where each spin may be either parallel or antiparallel to a magnetic field H. When two neighbouring spins change from being parallel to each other to antiparallel, it is assumed that the energy change is a constant ϵ. If $\epsilon < 0$, neighbours with opposite spins are more stable, so that, at low temperatures, opposite spins will tend to arrange themselves on alternate lattice sites and hence antiferromagnetic behaviour will appear. The partition function per spin of such an assembly can be written in terms of the two variables

$$z = \exp(-\epsilon/kT) \text{ and } \mu = \exp(-2mH/kT)$$

and in the case of a simple quadratic lattice at low temperatures, Brooks and Domb (1951) write it as

$$\Lambda^{(\alpha)} = 1 + \tfrac{1}{2}(\mu z^4)^{-1} - \tfrac{1}{8}(\mu z^4)^{-2} + \quad \ldots$$
$$+ z^{-2}[2(\mu z^4)^{-2} - 3(\mu z^4)^{-3} + \ldots] + \ldots \quad . \qquad \ldots\ldots(3)$$

The magnetization of this assembly is derived from the free energy $F = -NkT \ln \Lambda^{(\alpha)}$ by the equation $I = \partial F/\partial H$. This quantity, however, is just the equilibrium value of the net number of spins parallel to the magnetic field, so that if the proportion of spins antiparallel to the field is α, then $I/Nm = 1 - 2\alpha$ or using the above formulae

$$\partial(\ln \Lambda^{(\alpha)})/\partial(\ln \mu) = \alpha - \tfrac{1}{2}. \qquad \ldots\ldots(4)$$

Suppose now that each spin antiparallel to the field is replaced by a molecule of a gas and the site of each parallel spin left vacant. The resulting assembly represents a configuration of a lattice gas. Since this assembly must be studied at a constant concentration α of molecules, the partition function of the magnetic problem (3) must be always restricted by the equation (4). It was assumed in the magnetic case that ϵ was the change in energy resulting from a pair of neighbours changing from being parallel to antiparallel to each other. Since the corresponding lattice gas contains a fixed number of molecules, the change in energy of a pair of molecules changing from being neighbours to non-neighbours is 2ϵ. Thus the interaction energy between two neighbouring molecules is 2ϵ, so that the Mayer interaction function is $f = -1 + z^{-2}$ if two molecules are neighbours and zero otherwise. To treat this problem generally is still difficult, so a simplification was considered which leads to a lattice model of rigid squares (in the simple quadratic case). This simplification is to neglect all terms of order z^{-2} so that $f = -1$. This corresponds in the magnetic case to considering only terms of the type μz^4, since restricting the partition function (3) by the equation (4) implies that as $z^{-1} \to 0$, μz^4 must tend to a finite non-zero constant depending on the fixed number α. The only magnetic configurations which can now occur are those where every spin antiparallel to the magnetic field is surrounded by four spins

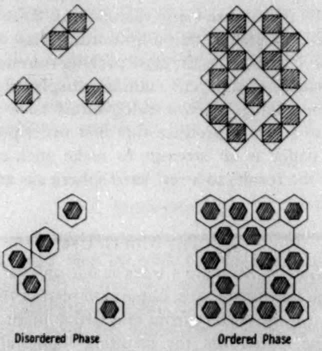

Figure 1. Typical configurations for the model of hard spheres.

parallel to the field. In figure 1 this situation is depicted by shading each molecule of the gas (antiparallel spins) and joining the lattice points of the four neighbouring vacant sites (parallel spins) to form a square around the shaded parts. These larger squares may now be considered to represent the non-overlapping molecules of the gas. The transformations applied above may be applied to any lattice and figure 1 shows the results for the triangular and simple quadratic lattices.

Temperley (1959) treats the same problem from a more general point of view and his results and those of this paper are in general agreement.

§ 3. THE DISORDERED REGION

3.1. *From the Exact Series Expansion*

It was shown in §2 that to study the lattice gas problem, it is necessary to consider the partition function of the antiferromagnetic problem for the appropriate lattice and in the appropriate region. For the disordered region it is necessary to consider the high temperature partition function, which is equivalent to considering series expansions of the type

$$\Lambda(\mu, z) = \sum_{r=0}^{\infty} \mu^r f_r(z) \qquad \ldots\ldots(5)$$

where $f_r(z)$ are finite polynomials in z and extensive lists of them are given by Domb and Sykes (1956). Considering for the moment only the simple quadratic lattice and taking into consideration only terms of the type $\omega = \mu z^4$ gives for the partition function

$$\Lambda(\omega) = 1 + \omega - 2\omega^2 + 8\omega^3 - 40\omega^4 + 225\omega^5 - 1362\omega^6 + 8670\omega^7 - 57\,253\omega^8 + 388\,802\omega^9 - 2\,699\,202\omega^{10} + \ldots \quad . \qquad \ldots\ldots(6)$$

(The last two terms of this series were kindly made available by Dr. M. F. Sykes (unpublished work).) The restrictive condition on the partition function (5), corresponding to (4) described in the previous section, is now given by

$$x = \partial(\ln \Lambda)/\partial(\ln \omega) \qquad \ldots\ldots(7)$$

where x is the number of particles per unit volume (and called the number density). To calculate the virial series for the pressure of the gas, an expansion in this variable x is required; so firstly the free energy of the assembly is calculated from the equation

$$-F/NkT = -x \ln \omega + \ln \Lambda(\omega). \qquad \ldots\ldots(8)$$

It can now be seen that ω and $\Lambda(\omega)$ are required as series expansions in x, so that it is necessary to invert the series obtained by substituting (6) into (7), giving

$$\omega = x + 5x^2 + 19x^3 + 59x^4 + 152x^5 + 316x^6 + 470x^7 + 198x^8 - 1675x^9 - 7583x^{10} - \ldots \quad . \qquad \ldots\ldots(9)$$

This series itself proves to be quite interesting since it shows a small number effect similar to that described by Temperley (1958), for the smooth series (6) has been transformed by a division and an inversion into the series (9) with terms which firstly appear to be increasing steadily and then, quite suddenly, become large and negative. A partial explanation can be given in this case since the series (6) takes into account all configurations of the given type, whilst the series (9) takes into account only the irreducible ones, so that the transformation has eliminated a large number of the contributions. Consequently, it can be seen that the effect of one particular configuration on the series (6) would be small, but on the series (9) it could be large or even dominant.

The free energy of the assembly can now easily be calculated from equations (8) and (9) giving

$$-F/NkT = -\ln x + x - 2{\cdot}5x^2 - 2{\cdot}167x^3 - 1{\cdot}417x^4 + 0{\cdot}95x^5 + 5{\cdot}833x^6 + 11{\cdot}976x^7 + 12{\cdot}411x^8 - 5{\cdot}180x^9 - 35{\cdot}389x^{10} - \dots \qquad \dots\dots (10)$$

and the pressure of the assembly is given by

$$P/kT = x + 2\tfrac{1}{2}x^2 + 4\tfrac{1}{3}x^3 + 4\tfrac{1}{4}x^4 - 3\tfrac{4}{5}x^5 - 29\tfrac{1}{6}x^6 - 71\tfrac{6}{7}x^7 - 86\tfrac{7}{8}x^8 + 41\tfrac{4}{9}x^9 + 318\tfrac{1}{2}x^{10} + \dots \qquad \dots\dots (11)$$

(In connection with the order–disorder problem Brooks and Domb (1951) calculated the series (10) and despite the fact that they produce the inverted series (9) correctly, they made errors in the series (10) in the terms x^5, x^6 and x^8.) The expansion (11) is now just the virial series for the pressure, valid at low number densities, for this model of hard squares on a simple quadratic lattice. The method was also followed for other lattices and the virial coefficients obtained for the simple cubic (S.C.), body centred cubic (B.C.C.), face centred cubic (F.C.C.) and triangular (Tri.) lattices are listed in table 1.

Table 1

Lattice	B_2	B_3	B_4	B_5	B_6	B_7	B_8
S.C.	$3\frac{1}{2}$	$6\frac{1}{3}$	$1\frac{3}{4}$	$-29\frac{4}{5}$	$-138\frac{5}{6}$	$-509\frac{6}{7}$	$-1819\frac{7}{8}$
B.C.C.	$4\frac{1}{2}$	$8\frac{1}{3}$	$-21\frac{3}{4}$	$-215\frac{4}{5}$	$-653\frac{1}{2}$	—	—
Tri.	$3\frac{1}{2}$	$10\frac{1}{3}$	$28\frac{3}{4}$	$78\frac{1}{5}$	$206\frac{1}{2}$	—	—
F.C.C.	$6\frac{1}{2}$	$28\frac{1}{3}$	$96\frac{1}{4}$	$252\frac{1}{5}$	—	—	—

Comparing these coefficients with those obtained by Zwanzig and by the Monte Carlo methods, it can be seen that, whilst the trend of the coefficients is reproduced quite well, at least for the loose packed lattices, the more idealized the model the more violently do the coefficients behave. The set of coefficients obtained for the loose packed lattices seem to oscillate in sign every three or four terms, supporting the suggestion that the 'parallel square and cube' models will produce negative virial coefficients, and further suggesting that the possibility of negative coefficients for the hard sphere problem cannot be ruled out.

It may be noticed from table 1 that distinct behaviour occurs between loose and close packed lattices, for whilst the former have virial coefficients which oscillate in sign, the latter have coefficients which are all positive and increasing steadily. In all the cases, it is seen that the first few virial coefficients show the usual deviation from the perfect gas law $P/kT = x$, but when the effect of the higher coefficients becomes noticeable, differences occur. For the close packed lattices, the deviation increases steadily since all the coefficients are positive, so that it appears that the model of the gas can enter into an ordered state (see figure 1) without any phase transition. For the loose packed lattices, however, the negative terms will reduce the deviation and possibly produce a maximum in the (P, x) curve, indicating that some sort of phase transition into the ordered region is necessary. Figures 2, 3 and 4 show the (P, x) curves obtained for the triangular, simple quadratic and simple cubic lattices.

3.2. *From the Method of Rushbrooke and Scoins*

Although the results of table 1 indicate that the loose packed lattices may show a maximum, it is possible that if the whole series were known, the resulting (P, x) curve would be monotonically increasing. An estimation of the asymptotic behaviour of these series is therefore of considerable importance in determining this question, and the approximate method described by Rushbrooke and Scoins (1955) proves to be helpful. This method was introduced originally by Fuchs (1942) and is a lattice analogue of the Mayer imperfect gas theory and is consequently in a very convenient form for the present work. In general, cofficients, $\beta_k(f)$, are obtained corresponding to irreducible cluster sums, dependent on the Mayer interaction function $f = z^{-2} - 1$. Again neglecting terms of order z^{-2} we obtain the coefficients as $\beta_k(-1)$.

The first approximation derived by Rushbrooke and Scoins is exactly the Bethe approximation and calculating the pressure for a lattice with coordination number q gives

$$P/kT = (q-1)\ln(1-x) - \tfrac{1}{2}q\ln(1-2x)$$

and hence the virial coefficients as

$$B_k = \{1 + q(2^{k-1} - 1)\}/k.$$

This approximation neglects all effects produced by closed configurations on the lattice, so that all aggregations must consist of chains of molecules. One would intuitively expect from this that any sudden transition to an ordered state is unlikely. This proves to be true, and figures 2, 3 and 4 show the behaviour obtained.

The second approximation, or the 'ring approximation' as it will be called here, is more illuminating since it considers the contribution to the virial coefficients from the first closed configuration on the lattice, i.e. a triangle for close packed and square for loose packed lattices. Thus the difference between the two types of lattice is now taken into account and if ordered aggregations of molecules occur, this approximation should be sufficiently accurate to detect the occurrence and any associated transition. By a little manipulation of the results of Rushbrooke and Scoins it is possible to calculate explicitly the pressure for the various lattices when terms of order z^{-2} are neglected. The results are as follows:

Close packed.

$$P/kT = -a\ln(1-x) + b\ln(1-2x) - c\ln(1-3x) \qquad \ldots\ldots(12)$$

for the triangular lattice $a = 1$, $b = 3$, $c = 2$, and for the face-centred cubic lattice $a = 13$, $b = 18$, $c = 8$.

Loose packed.

$$P/kT = -A\ln(1-x) + B\ln(1-2x) + C\ln\{2x + (1 - 4x + 8x^2)^{1/2}\} \qquad \ldots\ldots(13)$$

where $A = 1$, $B = 0$, $C = 1$ for the simple quadratic lattice, $A = 7$, $B = 3$, $C = 3$ for the simple cubic lattice and $A = 41$, $B = 20$, $C = 12$ for the body-centred cubic lattice. The virial coefficients obtained from these expansions are given in table 2.

Comparing these values with those from the exact expansions in table 1, we see that remarkable agreement is obtained up to B_7 for the simple quadratic, B_5 for the triangular and simple cubic lattices etc.

Table 2

Lattice	B_2	B_3	B_4	B_5	B_6	B_7	B_8	B_9	B_{10}
S.Q.	$2\frac{1}{2}$	$4\frac{1}{3}$	$4\frac{1}{4}$	$-3\frac{4}{5}$	$-29\frac{1}{6}$	$-71\frac{6}{7}$	$-79\frac{7}{8}$	$129\frac{4}{9}$	$894\frac{1}{5}$
S.C.	$3\frac{1}{2}$	$6\frac{1}{3}$	$1\frac{3}{4}$	$-29\frac{4}{5}$	$-118\frac{5}{6}$	$-269\frac{4}{7}$	$-359\frac{1}{8}$	—	—
B.C.C.	$4\frac{1}{2}$	$8\frac{1}{3}$	$-21\frac{3}{4}$	$-167\frac{4}{5}$	$-558\frac{1}{2}$	—	—	—	—
Tri.	$3\frac{1}{2}$	$10\frac{1}{3}$	$28\frac{3}{4}$	$78\frac{1}{5}$	$211\frac{1}{6}$	—	—	—	—
F.C.C.	$6\frac{1}{2}$	$28\frac{1}{3}$	$93\frac{1}{4}$	$276\frac{1}{5}$	—	—	—	—	—

For the close packed lattices, it is noticed that the ring approximation produces virial coefficients which are all positive and have a (P, x) curve which diverges at $x = \frac{1}{3}$. Figure 2 shows the curves obtained for the triangular lattice by the various methods. For this lattice $x = \frac{1}{3}$ is exactly the close packing volume and since the ring approximation increases steadily to infinity at this point, it suggests that the ordered region is reached without any phase transition. From figure 2 and from consideration of the radii of convergence of the series expansion, it appears that one of two things can happen. Firstly, the model of the gas for the triangular lattice may behave essentially as the ring approximation and condense without any phase transition, all the virial coefficients remaining positive, or secondly, some of the higher coefficients may become negative and produce a maximum value consistent with a phase transition. It seems difficult to decide which of these possibilities is the correct one, since very few other data have been obtained for close packed lattices; the last possibility seems unlikely however. For the face-centred cubic lattice, it appears that this approximation is inadequate since the close packing volume for this lattice occurs at $x = \frac{1}{4}$.

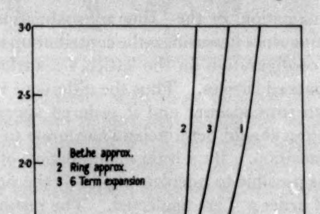

Figure 2. Triangular lattice, pressure plotted against number density.

For the loose packed lattices, interest is centred around whether the approximate method produces the maximum suggested by the series expansions. The term in equation (13) which determines the oscillatory sign of the coefficients is the third, which can be expanded as

$$\ln\{2x+(1-4x+8x^2)^{1/2}\}=\sum_{N=2}^{\infty}\frac{2^N x^N}{N}\left\{\sum_{r=1}^{N-1}2^{r/2}P_r(\cos\tfrac{1}{4}\pi)\right\}$$

where $P_r(\cos\theta)$ is the rth Legendre polynomial. An asymptotic expansion made for large N shows that the coefficient of x^N has magnitude $(2^N/N)^{3/2}$ and oscillates in sign every four terms. The interesting feature of this function, however, is that, despite the changes of sign, in the whole of the interesting region the function is slowly increasing as x increases. Consequently it can be seen that in the case of the simple quadratic lattice when $B=0$ in equation (13) the pressure is just slowly increasing and shows no maximum. In the other two cases, however, when $B\neq 0$, since the function $\ln(1-2x)$ has a negative singularity at $x=\frac{1}{2}$, a maximum is produced in similar manner to that predicted by the exact expansions.

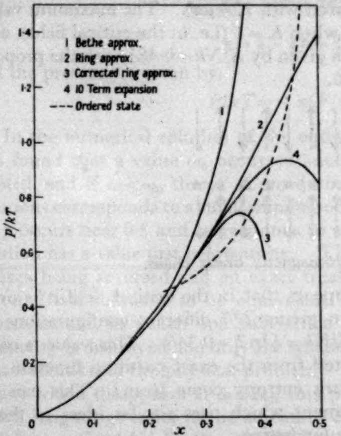

Figure 3. Simple quadratic lattice, pressure plotted against number density.

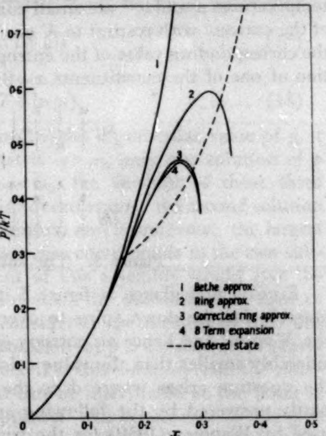

Figure 4. Simple cubic lattice, pressure plotted against number density.

Although the ring approximation is sufficiently accurate to decide whether a maximum is produced (except for the simple quadratic lattice), a better approximation is necessary to determine the more detailed behaviour in the transition region and to gain more accuracy in this region the 'corrected ring approximation' is used. This follows by adding the contribution from the next configuration which affects the lattice; in the case of the simple quadratic lattice this is an octagon, and for the simple cubic lattice a hexagon. The addition of the different configurations can be performed since it may be noticed that the contributions to the pressure are additive. The calculation was performed for the simple quadratic and simple cubic lattices and the results for this approximation and from the other methods are shown in figures 3 and 4.

From figures 3 and 4 and from the above discussion it seems certain that a maximum is produced in the pressure–density curve for the loose packed lattices, although the exact position of this maximum seems to be difficult to locate. This maximum indicates that above a certain density the disordered phase becomes unstable, so it is now necessary to consider the ordered region to decide whether any phase transition occurs.

§ 4. THE ORDERED REGION

Since very few data are available for the appropriate partition function for the loose packed lattices for the ordered state, a new method was employed, which was suggested by a study of the entropy of the antiferromagnetic linear chain at absolute zero. The partition function per spin of this assembly is given by

$$\Lambda(\mu, z) = \tfrac{1}{2}[1+\mu+\{(1-\mu)^2+4\mu z^2\}^{1/2}]$$

where $z \geqslant 1$ for the antiferromagnetic case. The entropy can be calculated from the free energy $F = -kT \ln \Lambda$ by the equation $S = -(\partial F/\partial T)$. At low temperatures μ and z^{-1} are small compared with $K = \mu z^2$. The maximum value of the entropy with respect to K occurs when $K = 1$ (i.e. in the critical field), and the corresponding value of the entropy is given by $S/Nk = 0{\cdot}481$ with the proportion of one of the constituents $x = 0{\cdot}276$.

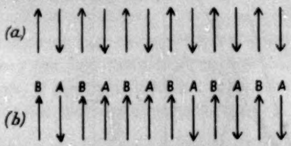

Figure 5. The antiferromagnetic linear chain.

From a first glance at figure 5 it appears that in the critical field it is only possible for the down spins to overturn giving $2^{N/2}$ different configurations of the N spins, and hence an entropy of $S/Nk = \tfrac{1}{2} \ln 2 = 0{\cdot}346$. This value is considerably smaller than the value calculated from the exact partition function, so the question arises where does the extra entropy come from? This can be partly answered by the following argument which uses similar ideas to those used by Wannier (1950) for the triangular lattice.

Consider the situation depicted in figure 5 (*b*) when two neighbouring down spins (A's) have overturned, then since the field is the critical one the up spin (B) between them can now overturn without change in energy and hence gives an entropy contribution of 2. Now suppose that r of the down spins have overturned then the probability that one particular down spin has overturned is r/m $(m = N/2)$. Thus the mean number of pairs of neighbouring down spins to have overturned is r^2/m, and the total entropy can be written

$$S = k \ln \sum_{r=0}^{m} {}^{m}C_{r} 2^{r^2/m}.$$

Since only the logarithm of this sum is required, the sum can be replaced by its maximum term. Using Stirling's approximation on the factorials, the maximization gives $S/Nk = 0{\cdot}476$ and $x = 0{\cdot}268$, which is in excellent agreement with the exact values. As a consequence of these calculations, it was assumed that this sort of mean field approximation may prove useful for the calculation of the free energy of a general loose packed lattice.

Consider such a lattice with coordination number q and for which the energy contribution of overturning a down spin is ω. Using a similar probability argument to that used above, the partition function can be written

$$(\text{P.F.}) = \sum_{r=0}^{m} {}^{m}C_r \omega^r (1+\omega^{-1})^{r^q/m^{q-1}} \qquad \ldots\ldots(14)$$

and again since only ln (P.F.) is required to determine the free energy this sum can be replaced by its maximum term. Putting $p = r/m$ and if x is the number density then introducing the zero point energy terms gives

$$-F/mkT = \frac{1}{2x}\{(2x-1)\ln\omega - \ln(1-p) - p^q \ln(1+\omega^{-1})\} \qquad \ldots\ldots(15)$$

where

$$\ln(p^{-1}-1) + \ln\omega + qp^{q-1}\ln(1+\omega^{-1}) = 0 \qquad \ldots\ldots(16)$$

and

$$x = \tfrac{1}{2} - \tfrac{1}{2}p + \tfrac{1}{2}p^q/(1+\omega) \qquad \ldots\ldots(17)$$

and the pressure is given by

$$P/kT = -x(F/mkT + \ln\omega). \qquad \ldots\ldots(18)$$

In the numerical solution of the equation (16) for a particular value of q, it was found that a value ω_0 occurred such that if $\omega > \omega_0$ only one solution of p existed and if $\omega < \omega_0$ three. Considering $\omega < \omega_0$, the smallest of these three solutions corresponds to a small number of spins overturning; the second solution for p occurs near 0·5 and corresponds to a minimum and is spurious; the largest solution has a value just below unity. The last case corresponds to the two sub-lattices being reversed and an exact treatment of this assembly would give the first and last solutions to be equivalent. However, the above method uses an approximation in which one sub-lattice is considered specifically, so that this symmetry is destroyed and only the smallest solution for p is considered to represent a solution to the physical problem. Since it is this solution (and the minimum) which disappears at $\omega = \omega_0$, this point can be interpreted as the point at which long range order in the assembly disappears. An occurrence of this type was first noticed by Easthope (1937) when he used the Bethe approximation for a binary alloy with unequal constituents. Brooks and Domb (1951) also considered the problem in connection with order–disorder phenomenon for the simple quadratic lattice. The values of the proportion of one of the constituents x that were obtained, are compared in table 3 with the values calculated from (16) and (17).

Table 3

Lattice	Easthope	Brooks and Domb	Present estimate
S.Q.	0·250	0·226	0·229
S.C.	0·167	—	0·160
B.C.C.	0·125	—	0·122

The pressure curves for this phase calculated from (18) for the simple quadratic and simple cubic lattices are shown in figures 3 and 4.

§ 5. DISCUSSION

The results of the previous sections for the model of the gas are firstly summarized. For loose packed lattices, there is sufficient evidence to show that a phase transition occurs between the ordered and disordered regions. The transition regions for the various lattices are simple quadratic, $0{\cdot}30 < x < 0{\cdot}40$, simple cubic, $0{\cdot}24 < x < 0{\cdot}30$, and body centred cubic $0{\cdot}17 < x < 0{\cdot}24$, and the curves obtained from the disordered phase are accurate to about 10% in these regions. For the close packed lattices however there is no evidence of any instability and the transition appears to be perfectly smooth. These results lead to three main questions (*a*) why do the results for the loose and close packed lattices differ ?, (*b*) what is the exact position and nature of the transition for the loose packed lattices ?, (*c*) from the results obtained can any inference be made about the hard sphere problem described in § 1 or about any other physical assembly ?

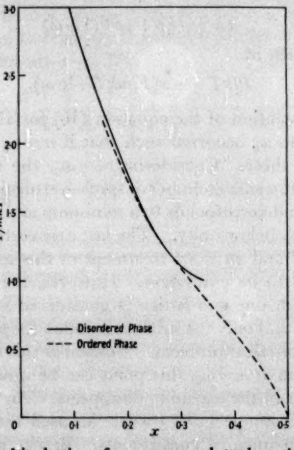

Figure 6. Simple cubic lattice, free energy plotted against number density.

To the first question it seems difficult to find any convincing answer. The differences must certainly be connected with the differences in behaviour between an antiferromagnetic in zero field for a close packed lattice and a loose packed lattice. The former shows no long range order at any temperature and hence no transition, while for the latter, long range order exists at low temperatures and a co-operative transition is observed. The detailed connection still remains obscure, however, since for the case considered here both types of lattices show long range order at a high enough pressure. A further study of the antiferromagnetic problem, particularly for the close packed lattices, in a general field, seems essential before any definite conclusions can be reached.

In answer to (*b*) the crucial test is derived from a study of the free energies of the phases, since the position and nature of the intersection of these curves indicate the position and nature of the transition, if one occurs. For the ordered state the free energy was calculated from (15) and (16) and for the disordered state from integration of the pressure series. All the loose packed lattices show similar behaviour and figure 6 shows the results obtained for the simple cubic lattice.

It can be seen that the situation is not altogether satisfactory since although the curves touch, the free energy of the ordered state is always less than that for the disordered state. It seems, therefore, that it would be very difficult for the gas to get out of its ordered state as the density is decreased, since the ordered state is always the more stable. It is considered, however, that the approximation used in this region is not satisfactory and needs considerable improvement before any quantitative results can be given. The fact that long range order disappears below a certain value of x strongly indicates, however, that the ordered phase is entering a metastable region and with a further reduction of the pressure it seems certain to link up with the disordered phase.

The third question asked above concerned possible inferences from the results obtained about more general problems. The virial coefficients for the loose packed lattices were seen to compare reasonably with those derived from Zwanzig's work and with those for the hard sphere problem described in §1. Hence the assumption that Zwanzig's model will produce negative coefficients is again strongly supported and the possibility for the hard sphere gas cannot be ruled out. It was shown that the function which generated the major negative contributions to the virial coefficients was a slowly increasing function in the whole of the interesting region. Thus even if the hard sphere gas does have negative coefficients, this is not necessarily indicative of an unstable region and hence of a phase transition.

A physical problem to which this analysis may be helpful is in the theory of supercooling. Greenwood and Martin (1952) studied the supercooling of certain organic liquids and found that discontinuities occurred in the viscosity and dielectric constant at the melting point but that otherwise the liquid remained the same. They attributed these phenomena to small aggregates of the particles. This type of aggregation for the lattice gas leads to a metastable region where, although further compression of the gas leads to a continuation of the (P, x) curve, there is a strong indication that a condensation is possible. A similarity between the two problems is thus observed, although extending the analogy much further would not be particularly useful.

ACKNOWLEDGMENTS

The author wishes to thank Professor C. Domb of King's College, University of London, for suggesting this work and for many helpful discussions. He also wishes to thank the Department of Scientific and Industrial Research for a maintenance grant for the period during which this work was completed.

REFERENCES

ALDER, B. J., and WAINWRIGHT, T. E., 1957, *J. Chem. Phys.*, **27**, 1208.
BROOKS, J. E., and DOMB, C., 1951, *Proc. Roy. Soc.* A, **207**, 343.
BRUECKNER, K. A., and SAWADA, K., 1957, *Phys. Rev.*, **106**, 1117.
DOMB, C., 1958, *Nuovo Cim. Suppl.*, Series X, **9**, 26.
DOMB, C., and SYKES, M. F., 1956, *Proc. Roy. Soc.* A, **235**, 247.
EASTHOPE, C. E., 1937, *Proc. Camb. Phil. Soc.*, **33**, 502.
FUCHS, K., 1942, *Proc. Roy. Soc.* A, **179**, 340.
GREENWOOD, N. N., and MARTIN, R. L., 1952, *Proc. Roy. Soc.* A, **215**, 46.

HIRSCHFELDER, J. O., CURTIS, C. F., and BIRD, R. E., 1954, *Molecular Theory of Gases and Liquids* (New York : Wiley).
LEE, T. D., HUANG, K., and YANG, C. N., 1957, *Phys. Rev.*, **106**, 1135.
MAYER, J. E., and MAYER, M. G., 1940, *Statistical Mechanics* (New York : Wiley).
METROPOLIS, N., ROSENBLUTH, A. W., ROSENBLUTH, M. N., TELLER, A. H., and TELLER E., 1953, *J. Chem. Phys.*, **21**, 1087.
RIDDELL, R. J., and UHLENBECK, G. E., 1953, *J. Chem. Phys.*, **21**, 2056.
RUSHBROOKE, G. S., and SCOINS, H. I., 1955, *Proc. Roy. Soc.* A, **230**, 74.
TEMPERLEY, H. N. V., 1957, *Proc. Phys. Soc.* B, **70**, 537.
—— 1958, *Ibid.*, **71**, 238.
—— 1959, *Ibid.*, **74**, 432, 444,
WANNIER, G. H., 1950, *Phys. Rev.*, **79**, 357.
WOOD, W. W., and JACOBSON, T. D., 1957, *J. Chem. Phys.*, **27**, 1207.
YANG, C. N., and LEE, T. D., 1952, *Phys. Rev.*, **87**, 404.
ZWANZIG, R. W., 1956, *J. Chem. Phys.*, **24**, 855.

The Band Spectra of NiCl and NiBr in the Visible

By S. PADDI REDDY and P. TIRUVENGANNA RAO
Department of Physics, Andhra University, Waltair

Communicated by T. E. Nevin; MS. received 22nd June 1959, *in revised form* 14*th September* 1959

Abstract. The emission spectra of NiCl and NiBr in the region λ3900–4800 Å have been photographed under high dispersion. The spectrum of NiCl consists of nine separate brief systems of bands while the NiBr spectrum consists of six systems of bands. The observed bromine isotope effect in three of the band systems of the NiBr molecule confirms the vibrational analyses. Tables of vibrational constants of the different band systems of each molecule are presented.

---

§ 1. INTRODUCTION

THE emission spectra of NiCl and NiBr were investigated earlier by Mesnage (1935, 1939), More (1938) and Krishnamurty (1952 a, b). According to the recent work of Krishnamurty, the bands of NiCl in the region λ3900–4800 Å were classified into five systems, designated as A, B, C, D and E. The NiBr bands in the region λ3900–5000 Å were assigned into four systems designated as α, β, γ and δ. Each of the systems A and B of NiCl and α and β of NiBr were interpreted on the basis of a $^4\Pi_{a,b}$–$^4\Sigma$ transition and the E system of NiCl on the basis of a $^2\Pi$–$^4\Sigma$ transition. The analyses of the different band systems of NiCl and NiBr were based on plates taken under low dispersion (20–30 Å mm^{-1}).

On the basis of the high dispersion spectrograms obtained in the present work, new vibrational analyses of the different electronic band systems of NiCl and NiBr are proposed and presented below.

§ 2. EXPERIMENTAL

The spectra were excited using anhydrous B.D.H. samples of $NiCl_2$ or $NiBr_2$ in a conventional heavy current discharge tube with hollow internal nickel electrodes. The source employed was a 2000 volt d.c. generator. Currents of 0·2 to 0·25 ampere were found favourable for the excitation of the different band systems in both cases. Spectra were photographed both on a Hilger three prism glass Littrow instrument (dispersion 7–15 Å mm^{-1}) and in the second order of a 21 ft concave grating spectrograph (dispersion 1·25 Å mm^{-1}) using Ilford S.R. plates. Exposures of 3 to 5 minutes on the Littrow instrument and 1 to 2 hours on the grating spectrograph were found necessary.

§ 3. RESULTS

3.1. *The Spectrum of NiCl*

According to our analyses based on high dispersion spectrograms, the bands of NiCl in the region λ3800–4800 Å can be classified as belonging to nine separate brief systems. The A system in Krishnamurty's analysis is shown to consist of A_1, A_2 and A_3 systems, the B system of B_1 and B_2 and the E system of E_1 and E_2. Of these nine band systems A_1, A_2, C, D and E_2 systems consist of double-headed bands interpreted as R and Q heads while the remaining four systems consist of only single-headed bands. Each of these systems is characterized by a strong

Table 1. Band Heads of NiCl in the Region λ3995–4715Å

k_{vac}	I	Classification v', v''
System A_1		
25007·8†	2	1, 0 Q
24991·6†	2	2, 1 Q
24615·4	10	0, 0 R
613·4	10	0, 0 Q
609·0	6	
597·5	5	1, 1 R
595·7	3	1, 1 Q
581·3	1	2, 2 Q
201·9	3	0, 1 R
199·7	4	0, 1 Q
System A_2		
24417·9	7	0, 0 R
411·6	6	0, 0 Q
388·1	4	1, 1 R
383·2	5	1, 1 Q
359·5	3	2, 2 R
355·0	4	2, 2 Q
332·5	5	3, 3 R
328·8	2	3, 3 Q
305·5	2	4, 4, R
System A_3		
24495·2	4	2, 1
478·0	3	3, 2
129·8	4	0, 0
112·7	6	1, 1
23732·6	3	0, 1
713·8	3	1, 2
System B_1		
23333·6	2	0, 0
307·2	2	1, 1
279·5	1	2, 2
251·8	1	3, 3
22904·4	1	1, 2
848·8	4	3, 4
System B_2		
23597·0†	2	2, 1
568·3†	2	3, 2
223·0	10	0, 0
200·9	9	1, 1
177·8	7	2, 2
153·0	4	3, 3
126·6	2	4, 4
System B_2 (*Contd*)		
23099·6	1	5, 5
22782·8	1	1, 2
763·4	2	2, 3
System C		
22745·4	2	0, 0 R
738·8	7	0, 0 Q
725·2	8	1, 1 R
718·5	6	1, 1 Q
705·3	6	2, 2 R
697·9	3	2, 2 Q
684·4	4	3, 3 R
676·7	2	3, 3 Q
663·8	2	4, 4 R
656·2	2	4, 4 Q
303·1	1	1, 2 Q
283·4	3	2, 3 Q
245·1	1	4, 5 Q
System D		
21910·4	15	0, 0 R
905·2	10	0, 0 Q
891·0	10	1, 1 R
493·3	4	0, 1 R
488·0	4	0, 1 Q
System E_1		
21747·3	10	0, 0
718·3	6	1, 1
690·4	4	2, 2
315·7	3	0, 1
209·4	3	1, 2
System E_2		
21639·4	4	0, 0 Q
627·3	9	1, 1 R
621·4	3	1, 1 Q
613·1	10	2, 2 R
607·3	6	2, 2 Q
592·0	6	3, 3 R
586·2	3	3, 3 Q
246·1	5	0, 1 R
237·7	3	0, 1 Q
230·2	7	1, 2 R
223·0	3	1, 2 Q
218·3	1	2, 3 R

k_{vac} = vacuum wave number. † Measured on prism plates.

$\Delta v = 0$ sequence with weaker $\Delta v = \pm 1$ sequences as is typical of a band system with values of ω_e' and ω_e'' close to each other. The data and classifications of the bands are given in table 1. Grating spectrograms of the prominent bands of the different systems are shown in figure 1 (Plate I). In the bands of the weaker $\Delta v = \pm 1$ sequences, only the band heads of $Ni^{35}Cl$ species could be identified. The heads of $Ni^{37}Cl$ species are too weak to be observed. Table 2 summarizes the vibrational constants of the different band systems of NiCl.

Table 2. Vibrational Constants of Band Systems of NiCl

System	$\nu_{(0,0)}$	ω_e'	$x_e'\omega_e'$	ω_e''	$x_e''\omega_e''$
A_1	24613·4(Q)	394·5	0·35	415·5	1·3
A_2	24411·6(Q)				
A_3	24129·8	380		397	
B_1	23333·6	375		402	
B_2	23223·0	406·6	2·75	426·3	1·9
C	22738·8(Q)	397·8	0·75	418·2	0·70
D	21905·2(Q)	398		417	
E_1	21747·3	405·2	1·3	435·3	1·85
E_2	21639·4(Q)	383·1		404·0	1·65

The proximity of the two systems C and D and the near equality of their vibrational constants suggest that they may belong to a doublet–doublet transition of the type Π–Σ or Π–Δ.

3.2. *The Spectrum of NiBr*

Our analysis of the bands of NiBr in the region λ4050–4700 Å shows the existence of six separate brief systems. Figure 2 (Plate II) gives the grating spectrograms of the prominent bands of the different systems of NiBr. The α system in Krishnamurty's analysis is shown to consist of three systems α_1, α_2 and α_3 and the β system of two systems β_1 and β_2. Of these six systems of bands, systems α_1, β_2 and γ consist of double-headed bands while α_2, α_3 and β_1 consist of only single-headed bands. The band heads of the former systems are interpreted as R and Q heads and accordingly each of these could arise from a transition of the type Π–Σ or Π–Δ. The single-headed band systems could arise from transitions of the type Σ–Σ or Δ–Δ.

As in NiCl, each of the band systems in NiBr consists of a strong $\Delta v = 0$ sequence and weak $\Delta v = \pm 1$ sequences. The data and classifications of the bands of the different systems are given in table 3. The isotope effect associated with ^{79}Br and ^{81}Br is readily observed in systems α_1, β_1 and γ and it confirms the vibrational analyses of these systems. The vibrational constants of the different band systems are summarized in table 4. The isotopic shift $\Delta\nu$ is calculated from the usual formula (Jevons 1932). The heads of the two species of $Ni^{79}Br$ and $Ni^{81}Br$ are observed to be of equal intensity as expected. The observed and calculated shifts are given in tables 5 and 6 and the agreement between them may be regarded as satisfactory.

ACKNOWLEDGMENTS

In conclusion, the authors would like to express their grateful thanks to Professor T. E. Nevin for his interest in this work and to Professor K. R. Rao for his encouragement in the course of this investigation.

Table 3. Band Heads of NiBr in the Region λ4060–4670Å

k_{vac}	I	Classification v', v''
System α_1		
24609·7†	2	1, 0 R
584·2†	2	2, 1 R
558·9†	2	3, 2 R
527·2†	2	4, 3 R
318·5	7	0, 0 R
311·9	3	0, 0 Q
300·6	4	1, 1 R
294·3	3	1, 1 Q
270·8	3	2, 2 Q
232·2	2	
012·5	2	0, 1 R^i
011·2	2	0, 1 R
23997·3	3	1, 2 R^i
995·8	3	1, 2 R
977·3	3	2, 3 R^i
975·7	3	2, 3 R
953·8	3	3, 4 R^i
952·2	3	3, 4 R
System α_2		
23904·7	3	0, 0
873·0	2	1, 1
611·6	2	0, 1
580·0	1	1, 2
550·3†	2	2, 3
513·4†	2	3, 4
System α_3		
23786·4	4	0, 0
777·4	2	1, 1
769·6	3	2, 2
472·4	2	0, 1
465·0	2	1, 2
457·6†	1	2, 3
446·6†	2	3, 4
437·5†	2	4, 5
428·7†	2	5, 6
420·7†	2	6, 7
System β_1		
23249·5	2	1, 0
248·2	2	1, 0 i
213·0	2	2, 1
211·8	2	2, 1 i
173·1	2	3, 2
System β_1 (*Contd*)		
23172·0	2	3, 2 i
129·2	2	4, 3
128·3	2	4, 3 i
22960·6	10	0, 0
928·6	6	1, 1
894·2	3	2, 2
641·6	2	0, 1 i
639·9	2	0, 1
611·9	2	1, 2 i
610·1	2	1, 2
579·5	2	2, 3 i
577·4	2	2, 3
544·1	2	3, 4 i
542·0	2	3, 4
System β_2		
22688·5†	2	1, 0 R
683·5†	3	1, 0 Q
434·2	7	0, 0 R
427·4	5	0, 0 Q
415·3	2	1, 1 R
409·7	2	1, 1 Q
396·6	3	2, 2 R
375·6	3	3, 3 R
370·2	2	3, 3 Q
System γ		
22085·2	2	1, 0 R
083·6	2	1, 0 R^i
075·3	2	1, 0 Q
073·8	2	1, 0 Q^i
055·2	2	2, 1 R
053·7	2	2, 1 R^i
047·7	2	2, 1 Q
046·4	2	2, 1 Q^i
21789·7	4	0, 0 R
779·8	9	0, 0 Q
754·6	4	1, 1 Q
741·0	6	2, 2 R
460·9	2	0, 1 Q^i
459·4	2	0, 1 Q
438·2	2	1, 2 Q
436·4	2	1, 2 Q
414·8	2	2, 3 Q^i
412·9	2	2, 3 Q

† Measured on prism plates. The heads of $Ni^{61}Br$ are marked with ‘ i ’.

Table 4. Vibrational Constants of Band Systems of NiBr

System	ν_e	ω_e'	$x_e'\omega_e'$	ω_e''	$x_e''\omega_e''$
α_1	24326·2(R)	297·0	3·35	311·6	1·7
α_2	~23920·3	~262		293·2	
α_3	23791·1	305·4	0·2	315·0	0·5
β_1	22975·5	293·8	2·5	322·8	1·0
β_2	~22435	257		274	
γ	21792·6(Q)	292·5	1·1	323·0	1·2

Table 5. Isotope Effect in Systems of α_1 and β_1 NiBr

v', v''	System α_1 $\Delta\nu_{calc}$	$\Delta\nu_{obs}$	v', v''	System β_1 $\Delta\nu_{calc}$	$\Delta\nu_{obs}$
0, 1	+1·7	+1·3	1, 0	−1·4	−1·3
1, 2	+1·7	+1·5	2, 1	−1·2	−1·2
2, 3	+1·8	+1·6	3, 2	−0·9	−1·1
3, 4	+1·8	+1·6	4, 3	−0·6	−0·9
			0, 1	+1·8	+1·7
			1, 2	+1·9	+1·8
			2, 3	+2·1	+2·1
			3, 4	+2·4	+2·1

Table 6. Isotope Effect in System γ of NiBr

v', v''	$\Delta\nu_{calc}$	$\Delta\nu_{obs}$(Q)	$\Delta\nu_{obs}$(R)
1, 0	−1·5	−1·5	−1·6
2, 1	−1·3	−1·3	−1·5
0, 1	+1·8	+1·6	—
1, 2	+1·9	+1·8	—
2, 3	+2·0	+1·9	—

REFERENCES

JEVONS, W., 1932, *Report on Band Spectra of Diatomic Molecules* (London: Physical Society), p. 213.

KRISHNAMURTY, V. G., 1952 a, *Ind. J. Phys.*, **26**, 207.

—— 1952 b, *Ibid.*, **26**, 429.

MESNAGE, P., 1935, *C.R. Acad. Sci., Paris*, **200**, 2072.

—— 1939, *Ann. Phys., Paris*, **12**, 5.

MORE, K. R., 1938, *Phys. Rev.*, **54**, 122.

Magnetoresistance in Gallium Arsenide†

By R. K. WILLARDSON‡ and J. J. DUGA
Battelle Memorial Institute, Columbus, Ohio

MS. received 15*th June* 1959

Abstract. The transverse magnetoresistance in n-type gallium arsenide has been studied as a function of impurity concentration and density of defects introduced by fast-neutron irradiation. The data are consistent with theoretical predictions based on mixed scattering and a spherical-energy-surface model. The change in the magnetoresistance with fast-neutron bombardment suggests the introduction of levels other than the deep-lying ones revealed by changes in the carrier concentration and that some of these levels may be multiply ionized.

§ 1. Introduction

The transverse magnetoresistance in a classical semiconductor is strongly affected by a small amount of ionized-impurity scattering. By a classical semiconductor is meant one with a non-degenerate spherical energy band and a carrier concentration small enough that Maxwell–Boltzmann statistics can be used. Unfortunately, the better known semiconductors such as germanium and silicon have anisotropic conduction bands and warped degenerate valence bands. The effect of anisotropy, warping, or multiple bands is to increase the transverse magnetoresistance by a factor of 10 to 100 and also drastically to reduce the effect of ionized-impurity scattering. For low carrier concentrations, the conduction bands in indium antimonide, indium phosphide and gallium arsenide are nearly spherical, and one would expect nominal amounts of impurity scattering to reduce the magnetoresistance by a factor of fifty. This effect of impurity scattering on the magnetoresistance in InSb has recently been discussed (Bate, Willardson and Beer 1959). Values of magnetoresistance described as anomalously low have been reported in InP (Glicksman 1959) and in GaAs (Glicksman 1959, Edmond, Broom and Cunnell 1957, Emelyanenko and Nasledov 1958). Orientation studies (Glicksman 1959, Edmond, Broom and Cunnell 1957) indicate that the magnetoresistance in GaAs is not strongly dependent on crystallographic orientation and that the longitudinal magnetoresistance is extremely small. This is in agreement with the conception of a spherical conduction band and the calculations and speculations of Callaway (1957) and Herman (1955).

The observations of a negative transverse magnetoresistance in GaAs at low temperatures by Edmond, Broom and Cunnell (1957), and by Emelyanenko and Nasledov (1958) are similar to those on InSb by Fritzsche and Lark-Horovitz (1955) and by Broom (1958). In these cases the semiconductor is completely degenerate and impurity-band conduction must be considered. Quantization and oscillatory transport effects become important, and there is even evidence that dislocations are effective in the conduction processes (Broom 1958).

---

† This research was supported by the Aeronautical Research Laboratory, Wright Air Development Center.

‡ Now at Consolidated Electrodynamics Corporation, Pasadena, California.

In this report, the primary concern is with the weak-field limit of the magnetoresistance in relatively high-purity samples of GaAs with low carrier concentrations in temperature regions where the semiconductor is not more than slightly degenerate. The magnitude of the impurity scattering in the samples to be considered is of the same order as that in the InSb samples described by Bate, Willardson and Beer (1959). It should be noted that, since high-purity InSb is intrinsic at temperatures above 80°K, studies of magnetoresistance in n-type InSb must be made at temperatures lower than this in order to avoid the contributions of the positive carriers. In the case of GaAs investigation of the region of primary interest (where the magnetoresistance changes very rapidly with small increases in the amount of impurity scattering) can be made at room temperature with samples at least two orders of magnitude less pure.

§ 2. EXPERIMENTAL TECHNIQUE

The purification and preparation of GaAs has been described by Edmond, Broom and Cunnell (1957) and by Folberth and Weiss (1955). The growth of single crystals of GaAs by a modified Czochralski technique has been discussed by Gremmelmaier (1956), while Whelan and Wheatley (1958) use a floating-zone method.

The specimens used in this investigation were single crystals of GaAs from which 'bridge' samples were cut with an ultrasonic tool. The samples were 1·6 cm long and 0·04 cm^2 in cross section with spacing of 0·90 cm between the resistivity potential arms. The specimens were etched using a 1 : 1 mixture of nitric–hydrochloric acids and rinsed with distilled water. Current and potential leads and thermocouples were soldered with indium using an ultrasonic soldering iron to promote better adhesion to the sample. The sample was then baked at 250°C for approximately one hour. This baking procedure is necessary to obtain good electrical contacts. The samples were then sealed in Pyrex tubes in a helium atmosphere. All voltage measurements were made with an L & N type K-2 potentiometer.

Measurements of the Hall coefficient and magnetoresistance were made at fixed temperatures for magnetic fields in the range 1000 to 20 000 gauss. The constant-temperature baths and the associated temperatures were dry ice and acetone, 196°K; liquid nitrogen, 77°K; pumping of vapour from liquid nitrogen containing oxygen, approximately 56°K. In taking the measurements, the sample current and magnetic field were reversed independently and the readings averaged to eliminate thermomagnetic and thermoelectric voltages.

The fast-neutron bombardments were made in the Battelle pool-type research reactor operating at 1 megawatt and a fast-neutron flux of 6×10^{12} cm^{-2} sec^{-1}. Fast neutrons are defined as those with energies greater than 0·5 MeV, the density of which was determined by the ^{32}S(n, p)^{32}P reaction. The exposure time for the GaAs samples was 170 seconds. Control samples of n-type germanium with a carrier concentration of $8 \cdot 1 \times 10^{15}$ cm^{-3} were used. The carrier concentration in the germanium decreased by about $3 \cdot 8 \times 10^{15}$ cm^{-3}, corresponding to a carrier-removal rate of 3·8 carriers per fast neutron cm. A 0·05 cm thickness of cadmium foil was used to reduce the thermal-neutron flux from 6×10^{12} cm^{-2} sec^{-1} to about 2×10^{10} cm^{-2} sec^{-1}.

§ 3. Development of Equations

The relationships between current densities j_x and j_y and corresponding longitudinal and transverse electric fields E_x and E_y in the presence of a magnetic field H_z and in the absence of temperature gradients can be written in the form

$$j_x = AE_x - BE_y \qquad \ldots\ldots (1)$$

$$j_y = BE_x + AE_y. \qquad \ldots\ldots (2)$$

When both lattice scattering (mean free path independent of energy ϵ) and ionized-impurity scattering (mean free path proportional to ϵ^2) are present, the coefficients A and B can be expressed in terms of a magnetic-field parameter γ, the carrier density n, and the zero-magnetic-field-lattice and ionized-impurity-scattering mobilities $\mu_L{}^0$ and $\mu_I{}^0$ (Johnson and Whitesell 1953) (superscript zero refers to absence of magnetic field):

$$A = ne\mu_L{}^0 \int_0^\infty \frac{x^3 e^{-x}(x^2+\beta)dx}{(x^2+\beta)^2+\gamma x^3} = ne\mu_L{}^0 K(\beta, \gamma) \qquad \ldots\ldots (3)$$

$$B = ne\mu_L{}^0 \gamma^{1/2} \int_0^\infty \frac{x^{9/2} e^{-x}\, dx}{(x^2+\beta)^2+\gamma x^3} = \tfrac{1}{2}\pi^{1/2} ne\mu_L{}^0 \gamma^{1/2} L(\beta, \gamma). \qquad \ldots\ldots (4)$$

The integrals $K(\beta,\gamma)$ and $L(\beta,\gamma)$ have been tabulated by Beer, Armstrong and Greenberg (1957). Classical statistics and spherical-energy surfaces have been assumed, and β and γ are defined by

$$\beta \equiv 6\mu_L{}^0/\mu_I{}^0, \qquad \gamma \equiv (9\pi/16)(\mu_L{}^0)^2 H^2.$$

By expanding the quantities $K(\beta,\gamma)$ and $L(\beta\ \gamma)$ in a series and neglecting terms of higher order than H^2 (weak-magnetic-field approximation), the following expression for the magnetoresistance coefficient is obtained (Appel 1954):

$$\frac{\Delta\rho}{\rho H^2} = \frac{9\pi}{16}(\mu_L{}^0)^2 \left[-\frac{K'(\beta,0)}{K(\beta,0)} - \frac{\pi}{4}\frac{L^2(\beta,0)}{K^2(\beta,0)} \right] \qquad \ldots\ldots (5)$$

where

$$K'(\beta,0) = \left(\frac{\partial K(\beta,\gamma)}{\partial\gamma}\right)_{\gamma=0}.$$

For $\beta = 1$ the ionized-impurity scattering has reduced the magnetoresistance to about 1/50 of the value that would be obtained if only lattice scattering were present. For $\beta = 0$ (lattice scattering only), equation (5) reduces to the familiar weak-field approximation for magnetoresistance:

$$\frac{\Delta\rho}{\rho\gamma} = \left(1 - \frac{\pi}{4}\right). \qquad \ldots\ldots (6)$$

It is of interest to define a magnetoresistance parameter $G(\beta, 0)$, which reduces to 1·0 in the case of lattice scattering only and can be used to compare values of magnetoresistance calculated from equation (5) with experimental values measured on different materials and at various temperatures.

$$G(\beta,0) \equiv \frac{1}{(1-\frac{1}{4}\pi)}\frac{\Delta\rho}{\rho\gamma}, \text{ experimental}, \qquad \ldots\ldots (7)$$

$$G(\beta,0) \equiv \left(\frac{-K'/K - \pi L^2/4K^2}{1-\frac{1}{4}\pi}\right), \text{ theoretical}. \qquad \ldots\ldots (8)$$

The Hall coefficient at weak magnetic fields is given by

$$R=\frac{3\pi}{8ne}\frac{L(\beta,0)}{K^2(\beta,0)}. \qquad \ldots\ldots(9)$$

From equation (3) it is seen that the actual mobility of the carriers μ^0 is related to the lattice mobility by $\mu^0=K(\beta,0)\mu_L{}^0$. Thus if the Hall coefficient, the resistivity, and the lattice mobility are known, a value for the impurity scattering parameter β can be determined from equations (3) and (9). Theoretical curves for $K(\beta,0)$ and $G(\beta,0)$ are shown in figure 1. It should be noted that the magnetoresistance parameter $G(\beta,0)$ initially decreases much more rapidly than the mobility parameter $K(\beta,0)$. Thus, for a semiconductor with a single spherical energy band the magnetoresistance is much more sensitive to small amounts of ionized-impurity scattering than is the carrier mobility. It is well known that the effect of an anisotropic conduction band and warped or degenerate valence bands is to increase greatly the weak-field transverse magnetoresistance and to reduce the effects of impurity scattering.

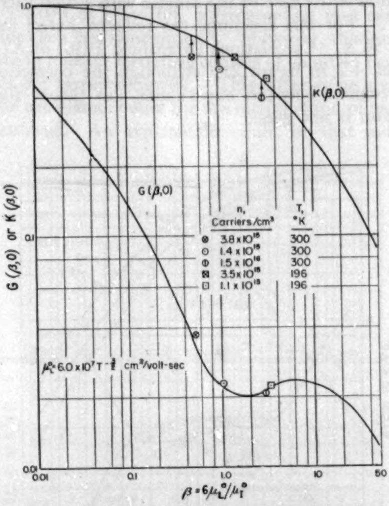

Figure 1. Magnetoresistance in non-degenerate GaAs.

§ 4. WEAK-FIELD MAGNETORESISTANCE

Figure 1 shows experimental magnetoresistance data for three samples of GaAs at coordinates determined by the mobility and the $K(\beta,0)$ curve as indicated by the arrows. The ordinate of the experimental points is dependent on the square of the value chosen for the lattice mobility. A value of 11 500 cm² v^{-1} sec^{-1} was used for the lattice mobility of the electrons at 300°K (Reid and Willardson 1958). It will be noted that at 300°K excellent agreement between theory and experiment is obtained. The data taken at 196°K are indicated by the square symbols. The temperature variation of β was calculated by using a $T^{-3/2}$ dependence for the lattice mobility and calculating the temperature variation of the impurity scattering mobility from the Brooks–Herring relationship, taking into account the effect of temperature and carrier concentration in the logarithmic term. These calculations had to be done independently for each sample because of the different carrier concentrations.

By using this procedure of determining β by the electron mobility at 300°K and calculating its temperature dependence, excellent agreement with the theoretical $K(\beta, 0)$ curve is found for the experimental mobility data at 77° and 56°K. An exception is the case of the sample with a high carrier concentration, i.e. $1{\cdot}5 \times 10^{16}/\mathrm{cm}^3$. For this specimen the reduced Fermi level η was $-1{\cdot}5$ at 77°K and $-1{\cdot}0$ at 56°K. Calculations (Mansfield 1956) of $K(\beta, 0, \eta)$ are shown for $\eta = -\infty, 0$ and $+2$ in figure 2. Although the correction is in the right direction the agreement between experiment and theory for this degenerate carrier concentration is not good.

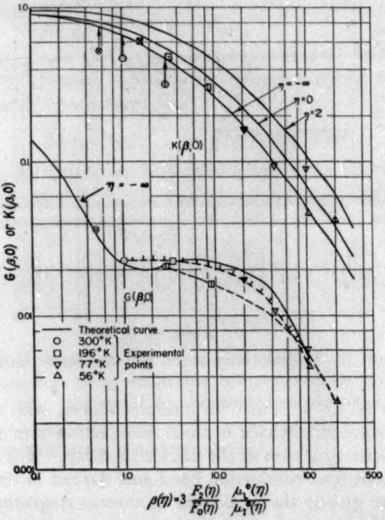

Figure 2. Magnetoresistance in GaAs as a function of impurity scattering.

The experimental magnetoresistance curves in figure 2 have the same general shape and values as the theoretical one. The experimental points are within 25 per cent of the theoretical curve and since impurity scattering has lowered the magnetoresistance by a factor of 50 to 300, the 25% appears almost insignificant.

As can be seen from the experimental data in figure 2 the effect of a small amount of carrier degeneracy on the magnetoresistance for large amounts of impurity scattering ($\beta > 100$) is apparently to increase the magnetoresistance.

The effect, if any, of small amounts of degeneracy when lattice scattering predominates could not be determined from these experiments, since the sample with $1{\cdot}5 \times 10^{16}$ electrons/cm³ had an η of $-3{\cdot}2$ at 300°K.

The question then arises as to what would be the effect of defects introduced by bombardment. Because adequate gamma sources which could produce a homogeneous distribution of simple vacancies and interstitials are not available, one of these samples was irradiated with 1×10^{15} fast neutrons/cm². The results are shown in figure 3. To give the most satisfactory fit of the post-irradiation points to the experimental curve it was assumed that β was increased by a factor of 1·5. During the irradiation, the carrier concentration at room temperature decreased from $1{\cdot}5 \times 10^{16}$ to $1{\cdot}2 \times 10^{16}$, corresponding to a carrier-removal rate of 3 carriers/cm³ for each fast neutron/cm². However, the increase in β corresponds to an increase in ionized scattering centres of about 45 per fast neutron/cm² or about 15 centres per carrier removed. This latter value gives the same order of magnitude as the calculated values for the introduction of vacancies and interstitials by fast neutrons. An explanation could be that most of the defects introduced are in levels near the band edge so they are always ionized, and only a few of the deeper lying defect levels that produce changes in carrier concentration are created. This would be similar to the explanation of experiments (Longo and Lark-Horovitz 1957) on deuteron irradiation of heavily doped silicon, which suggest donor levels 0·025 ev from the conduction band and acceptor levels at 0·055 ev from the valence band. Multiple ionization could greatly increase the effectiveness of the bombardment-induced levels to scatter the carriers and could give rise to both the shallow and deep lying defect levels.

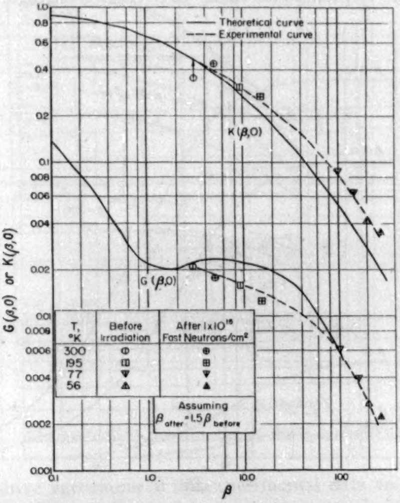

Figure 3. Effects of fast neutrons on magnetoresistance in GaAs.

§ 5. MAGNETIC-FIELD DEPENDENCE OF THE HALL COEFFICIENT AND MAGNETORESISTANCE

The Hall coefficient and magnetoresistance as a function of magnetic field can be calculated from

$$R = \frac{3\pi}{8|e|}\frac{L(\beta,\gamma)}{K^2(\beta,\gamma)+\frac{1}{4}\pi\gamma L^2(\beta,\gamma)} \qquad \ldots\ldots(10)$$

$$\frac{\Delta\rho}{\rho_0} = \frac{K(\beta,0)}{K(\beta,\gamma)+\frac{1}{4}\pi\gamma L^2(\beta,\gamma)/K(\beta,\gamma)} - 1. \qquad \ldots\ldots(11)$$

Equations (10) and (11) are obtained from the definition of the Hall coefficient and magnetoresistance and equations (1), (2), (3) and (4).

Figure 4 shows the variation of the Hall coefficient with magnetic-field parameter $\gamma^{1/2}$ for several values of the impurity-scattering parameter β. Experimental data for the sample of GaAs having a carrier concentration of $1{\cdot}5 \times 10^{16}$ at 300°K is also shown. The ordinate chosen for the experimental points at each temperature was arbitrary, while lattice mobilities of 11 500, 88 500, and 142 500 cm^2 v^{-1} sec^{-1} were used to determine the appropriate $\gamma^{1/2}$ value at 300°, 77° and 56°K, respectively. Experimental values of β taken from figure 2 are shown for this sample at the different temperatures. The Hall coefficient is seen to be dependent on magnetic field and qualitatively in agreement with the theoretical curves. The experimental value of magnetic field or $\gamma^{1/2}$ for which the Hall coefficient begins to depart rapidly from the weak field value at 77° and 56°K is somewhat higher than the theory would predict. This could be related to the carrier degeneracy as was previously discussed in relation to this sample.

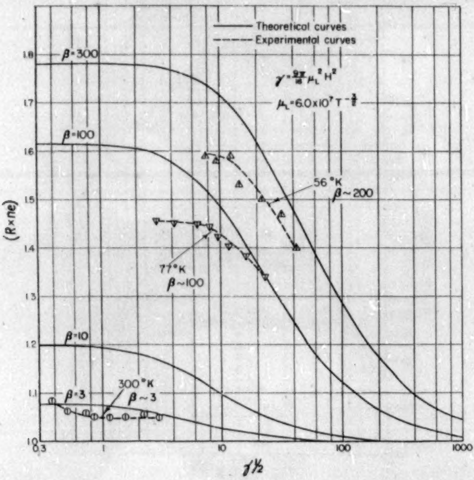

Figure 4. Magnetic-field dependence of the Hall coefficient in GaAs.

Calculations of the magnetoresistance coefficient as a function of magnetic field for several values of the impurity-scattering parameter β and lattice electron mobilities of 11 500, 21 700, 88 500, and 142 500 cm^2 v^{-1} sec^{-1} are shown in figure 5. The experimental data points are connected by dashed lines and labelled with the appropriate β values taken from figure 3. An examination of the theoretical curves shows that the effect of additional impurity scattering is to lower the weak-field value for magnetoresistance and to increase the strong-field value. Hence, the dependence of the magnetoresistance on magnetic field can be greatly decreased by additional impurity scattering. The experimental data give good qualitative agreement with the theoretical predictions. The fast-neutron irradiation decreases the weak-field magnetoresistance and increases the strong-field values at 300° and 195°K. Both the weak and strong field values are decreased at 77° and 56°K, but as expected there is a much greater change in the former. The magnetoresistance data at 56°K after irradiation are not plotted since they were almost identical with the pre-irradiation values at 77°K.

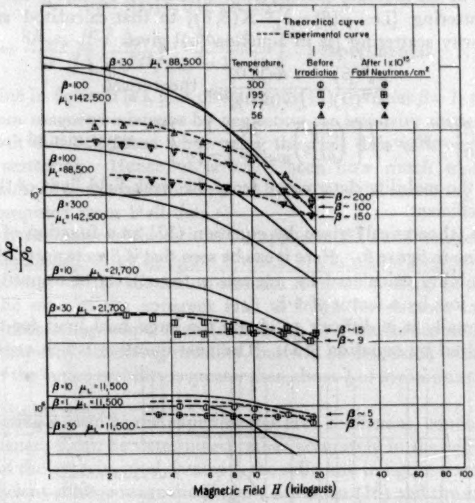

Figure 5. Magnetic-field dependence of the magnetoresistance in GaAs.

The quantitative agreement of the experimental data and theory at 300°K is good, and at 196°K the experimental data at weak magnetic fields are low by about 25%. At 77°K it appears that a value of 100 for β for the unirradiated data is 10 to 20% too large. In general, the decrease of the magnetoresistance coefficient with increasing magnetic field does not appear to be quite as rapid as predicted by the theory, especially at weak magnetic fields. Part of the difficulty may be due to experimental error in determining the small differences in resistivity at the weak magnetic fields. However, since the statistics are partially degenerate for these carrier concentrations at low temperatures, it might be expected that the weak-field values would be somewhat lower than predicted by using classical statistics.

§ 6. DISCUSSION

The determination of β by using a lattice electron mobility of 11 500 $\mathrm{cm^2\,v^{-1}\,sec^{-1}}$ at 300°K and the $\mu = \mu_L K(\beta, 0)$ relationship, as discussed in the section on weak-field magnetoresistance, may appear somewhat arbitrary. In particular, one might be concerned about the value of 11 500 $\mathrm{cm^2\,v^{-1}\,sec^{-1}}$ that was originally calculated (Reid and Willardson 1958) on the basis of a single mobility value from a relatively impure sample of GaAs. However, the positioning of the experimental magnetoresistance data in figures 1 and 2 depends on the square of the value chosen for the lattice mobility and seems to verify the value for the electron mobility. Furthermore, the magnetic-field dependence of the Hall coefficient and magnetoresistance indicates that 11 500 $\mathrm{cm^2\,v^{-1}\,sec^{-1}}$ is approximately correct. On the other hand, it is instructive to compare the values already obtained for β with those determined by a somewhat different approach.

The ratio of the mobility that would be calculated by taking into account the impurity scattering [i.e. $\mu(\beta) = \mu_L{}^0\, K(\beta, 0)$] to that calculated assuming no ionized impurity scattering [as in equation (6)] gives

$$\frac{\mu_\rho{}^0(\beta)}{\mu\,{}^0(0)} = \frac{K(\beta,0)}{[G(\beta,0)]^{1/2}}, \text{ theoretical,} \qquad \ldots\ldots(12)$$

$$\frac{\mu_\rho{}^0(\beta)}{\mu_\rho{}^0(0)} = R_\infty\sigma_0 \Bigg/ \left[\left(\frac{\Delta\rho}{\rho H^2}\right)_{H\to 0} \frac{16}{9\pi}\frac{1}{1-\frac{1}{4}\pi}\right]^{1/2}, \text{ experimental} \qquad \ldots\ldots(13)$$

where $\mu_\rho{}^0$ is the mobility determined from the weak-field limit of the magnetoresistance coefficient.

The ratio (theoretical) given by equation (12) as a function of β is shown by the solid line in figure 6. Here it can be seen that if β were unity, the magnetoresistance mobility calculated by neglecting the effects of impurity scattering would be too low by a factor of 4·5.

Experimentally it is difficult to obtain the large field limit for the Hall coefficient required by equation (13). The next question which arises is that of

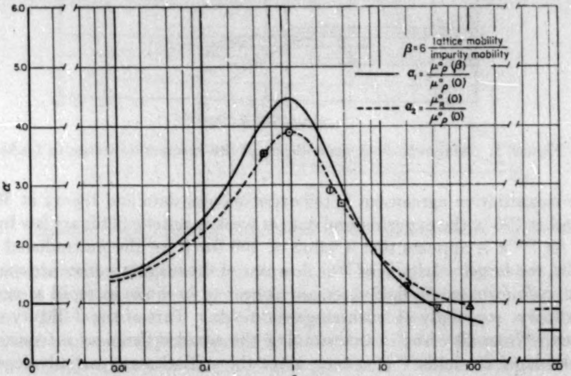

Figure 6. Ratios of Hall and magnetoresistance mobilities as a function of ratios of lattice and impurity-scattering mobilities.

the ratio of the apparent mobilities as calculated from magnetoresistance and from the Hall effect ($8R\sigma/3\pi$), assuming a weak-field approximation is valid with neglect of the effects of impurity scattering.

Since spherical energy surfaces have been assumed, the mobilities as calculated by use of the Hall effect μ_{R} and magnetoresistance μ_{ρ} should differ only because of the scattering mechanism. Accounting for the scatterings by the use of the parameter β, it follows that

$$\mu_{\rho}{}^{0}(\beta)=\mu_{\mathrm{R}}{}^{0}(\beta)=\mu_{\mathrm{R}}{}^{0}(0)\,\frac{K^{2}(\beta)}{L(\beta)}. \qquad \ldots\ldots(14)$$

The last equality follows from the expression of the Hall coefficient in the weak-magnetic-field limit. Thus, the ratio of the Hall and magnetoresistance mobilities as calculated neglecting impurity scattering are given as a function of β by

$$\frac{\mu_{\mathrm{R}}{}^{0}(0)}{\mu_{\rho}{}^{0}(0)}=\frac{1}{[G(\beta,0)]^{1/2}}\,\frac{L(\beta,0)}{K(\beta,0)},\ \text{theoretical}, \qquad \ldots\ldots(15)$$

$$\frac{\mu_{\mathrm{R}}{}^{0}(0)}{\mu\ {}^{0}(0)}=\frac{8R_{0}\sigma_{0}}{3\pi}\Big/\left[\left(\frac{\Delta\rho}{\rho_{0}H^{2}}\right)_{H\to 0}\frac{16}{9\pi}\,\frac{1}{1-\frac{1}{4}\pi}\right]^{1/2},\ \text{experimental}. \qquad \ldots\ldots\ldots(16)$$

The dashed line in figure 6 is a plot of equation (15). When $\beta=1$, the mobility calculated from magnetoresistance by neglecting the impurity scattering will be only one-fourth that calculated when using the Hall data with similar neglect of impurity scattering. Hence, it is easily seen how much more sensitive mobilities calculated from magnetoresistance data are to the scattering mechanism than those computed from Hall data.

One important feature of the ratio of the apparent Hall and magnetoresistance mobilities—the dashed curve in figure 6 which is calculated neglecting ionized-impurity scattering—is the maximum and the reversal in slope at $\beta\simeq 1$. This means that the ratio of the apparent Hall to magnetoresistance mobility will increase with decreasing temperature (increasing β) if the lattice mobility is less than $\frac{1}{6}$ of the impurity-scattering mobility, but will be decreased with decreasing temperature if the lattice mobility is greater than about $\frac{1}{6}$ of the impurity-scattering mobility.

Thus by using a ratio of the experimental Hall coefficient, conductivity, and magnetoresistance, β can be determined rather accurately in the region of $\beta=1$. Comparison of the experimental data with the solid line in figure 6 would require the Hall coefficient at large magnetic fields. Equation (16) and the experimental data from figure 2 are used to obtain the experimental points to be compared with the dashed line in figure 6. These data then indicate, by a somewhat different representation, that the initial choice for a value for β and the calculation of the temperature dependence of β are, at least, consistent with theory under the assumptions required. The existence of a maximum for the experimental data shown in figure 6 is characteristic of a nearly spherical conduction band. Similar data for germanium, silicon and p-type InSb and AlSb give a minimum and values less than unity for this ratio in the low β region and values approaching unity for large amounts of impurity scattering.

The following can be concluded: (i) The magnetoresistance values observed between 56° and 300°K in relatively pure GaAs are consistent with what one would expect for a spherical conduction band and for mixed acoustical mode and ionized-impurity scattering. (ii) The data are consistent with a $T^{-3/2}$ dependence of the lattice mobility. (iii) Magnetoresistance in GaAs can give important information on the number and type of defects introduced by fast neutrons.

Also, it should be possible to examine the region where the magnetoresistance is extremely sensitive to small amounts of impurity scattering by using higher purity GaAs. This does not appear feasible with InSb, since material of at least a hundred times higher purity must be used because of the low temperatures required to get into the extrinsic range.

ACKNOWLEDGMENTS

The authors wish to express their appreciation to Dr. A. C. Beer and Dr. L. W. Aukerman for valuable discussions and to Mr. F. J. Reid and Mr. J. W. Moody for their contributions to the experimental work. The samples of GaAs were supplied through the courtesy of the Sponsors of the Compound Semiconductor Research Group at Battelle.

REFERENCES

APPEL, J., 1954, *Z. Naturf.*, **9a**, 167.
BATE, R. T., WILLARDSON, R. K., and BEER, A. C., 1959, *J. Phys. Chem. Solids*, **9**, 119.
BEER, A. C., ARMSTRONG, J. A., and GREENBERG, I. N., 1957, *Phys. Rev.*, **107**, 1506.
BROOM, R. F., 1958, *Proc. Phys. Soc.*, **71**, 470.
CALLAWAY, J., 1957, *J. Electronics*, **2**, 330.
EDMOND, J. T., BROOM, R. F., and CUNNELL, F. A., 1957, *Report of Meeting on Semiconductors, Rugby* (London : Physical Society), p. 109.
EMELYANENKO, O. V., and NASLEDOV, D. N., 1958, *J. Tech. Phys.*, **28**, 1177.
FOLBERTH, O. G., and WEISS, H., 1955, *Z. Naturf.*, **10a**, 615.
FRITZSCHE, H., and LARK-HOROVITZ, K., 1955, *Phys. Rev.*, **99**, 400.
GLICKSMAN, M., 1959, *J. Phys. Chem. Solids*, **8**, 511.
GREMMELMAIER, R., 1956, *Z. Naturf.*, **11a**, 511.
HERMAN, F., 1955, *J. Electronics*, **1**, 103.
JOHNSON, V. A., and WHITESELL, W. J., 1953, *Phys. Rev.*, **89**, 941.
LONGO, T. A., and LARK-HOROVITZ, K., 1957, *Bull. Amer. Phys. Soc.*, Ser. II, **2**, 157.
MANSFIELD, R., 1956, *Proc. Phys. Soc.* B, **69**, 76.
REID, F. J., and WILLARDSON, R. K., 1958, *J. Electron. Control*, **5**, 54.
WHELAN, J. M., and WHEATLEY, G. H., 1958, *J. Phys. Chem. Solids*, **6**, 169.

An Investigation of some (^{3}He, d) Reactions in Light Nuclei at 5·2 Mev

By P. D. FORSYTH, F. de S. BARROS†, A. A. JAFFE,
I. J. TAYLOR and S. RAMAVATARAM

The Physical Laboratories, University of Manchester

MS. received 10*th August* 1959

Abstract. A broad range magnetic spectrograph has been used to analyse the deuterons emitted from targets of ^{10}B, ^{11}B, ^{14}N and ^{27}Al bombarded with 5·2 Mev singly ionized ^{3}He particles. The angular distributions of a number of the deuteron groups have been measured and an attempt has been made to fit them with the predictions of stripping theory. The absolute differential cross sections have been compared with those of the corresponding (d, n) reactions and the published differential cross sections for some (d, t) and (p, d) reactions have been similarly compared.

§ 1. Introduction

It has been suggested that (^{3}He, d) reactions at sufficiently high bombarding energies should proceed by a stripping mechanism similar to that which has been well established for (d, p) and (d, n) reactions (Newns 1952, Butler and Salpeter 1952). Since there was little available experimental evidence on these reactions, it was considered worth-while to measure angular distributions and absolute cross sections for a number of (^{3}He, d) reactions where the corresponding (d, n) reactions had already been investigated and where the properties of most of the initial and final states were known.

The following reactions: ^{10}B(^{3}He, d)^{11}C, ^{11}B(^{3}He, d)^{12}C, ^{14}N(^{3}He, d)^{15}O and ^{27}Al(^{3}He, d)^{28}Si were therefore studied at 5·2 Mev bombarding energy using the Manchester University Van de Graaff accelerator and a broad range magnetic spectrograph (Barros *et al.* 1959). An attempt has been made to interpret the results in terms of the stripping theories of Bhatia (Bhatia *et al.* 1952) and Butler (1951) modified for application to (^{3}He, d) or (t, d) reactions (Newns 1952, Butler and Salpeter 1952, Butler and Hittmair 1957) and comparisons have been made with the published results for the corresponding deuteron stripping reactions.

§ 2. Experimental Details

After analysis by a 90° deflecting magnet, beams of approximately 0·4 μA singly ionized ^{3}He particles were used to bombard a target spot (0·020 in. × 0·040 in.) on a target at a distance of 24 feet. The ^{3}He gas used in the ion source was mixed with ^{4}He at approximately 30% concentration. The mixture was purified by charcoal at liquid air temperature and was used at a rate of about 3 cm^3 at N.P.T. per hour. Subsequent recovery with at least 95% efficiency was achieved. The triton contamination in the beam was found to be very small and certainly less than 0·01%.

---

† On leave of absence from the Centre for Physical Research, Rio de Janeiro.

Targets of natural boron and of adenine which had been prepared on VYNS foils, in some cases reinforced with a thin layer of evaporated gold, proved unable to withstand reasonable bombardment. Consequently, targets of natural boron and of adenine on aluminium foil were used. Although the attainable energy resolution was thus greatly reduced it was still sufficiently good for our main purpose of studying angular distributions of reactions leading to well established nuclear levels.

The target thicknesses were measured with an alpha-particle thickness gauge (Ramavataram and Porat 1959). The natural boron target was found to be 30 $\mu g\, cm^{-2}$ thick and the adenine target which contained 52% nitrogen had an effective thickness of 25 $\mu g\, cm^{-2}$ of ^{14}N. The aluminium backing was about 170 $\mu g\, cm^{-2}$ in each case.

The target plane lay along the $-45° + 135°$ direction with respect to the beam with the backing facing the beam. The total beam bombardment was measured by current integration from a Faraday cup and, in addition, protons from the target were counted with a monitor at $-135°$.

The deuteron groups present on the photographic plates were identified by the variation of their energy with angle with respect to the ^3He beam. This identification was greatly facilitated by plotting a graph of the energies of the groups against the angle of observation and drawing loci connecting the points corresponding to particular groups. The shape of these loci gave an immediate indication of the probable target nuclei responsible, because the slopes of the curves depended mainly on the mass of the target nucleus, and a comparison could then be made between the loci and the theoretical curves for the various probable target masses and Q-values.

In the case of the boron target the beam energy could be estimated from the energy of a group of singly ionized elastically scattered ^3He which was present on the plates. A comparison between the energies of the corresponding groups from ^{27}Al showed that the beam energy for the adenine target was 20 ± 10 kev higher than for the boron target.

The solid angle of the spectrograph was calculated from the geometry of the instrument and has been checked previously by observation of Rutherford scattering.

§ 3. RESULTS

Typical spectra from each of the targets are shown in figures 1 and 2.

The ^{28}Si (d_2) group on the spectrum from the boron target contains a small contribution from the contaminant group ^{15}O (d_0) which is observed at other angles but which overlaps with this group at 40°.

The observed levels for which the angular distributions were measured are presented in the table, and a number of the angular distributions are shown in figures 3, 4 and 5.

The levels of ^{11}C, ^{12}C and ^{15}O correspond well with known states of these nuclei, though these have not been previously studied in (^3He, d) reactions. The Q-value for the reaction $^{14}N(^3He, d_0)^{15}O$ agrees well with the value calculated

(1)	(2)	(3)	(4)	(5)	(6)	(7)	(8)	(9)	(10)
^{10}B(^{3}He, d_0)^{11}C	3·174 ± 0·015	3·206[a]	0	0	1	6·5[f]	4·3[h], 5·8[j]	2·9 (19°)	3·3
^{10}B(^{3}He, d_1)^{11}C	—	—	1·990 ± 0·005	1·99 ± 0·02	1	6·2[f]	4·3[h], 5·8[j]	0·4 (19°)	—
^{11}B(^{3}He, d_2)^{12}C	2·780 ± 0·015	2·808[a]	—	7·656 ± 0·007[c]	1	4·5[f]	4·4[h]	0·1 (29°)	—
^{11}B(^{3}He, d_3)^{12}C	—	—	9·629 ± 0·010[m]	9·63 ± 0·014	2	6·0[f]	4·4[h]	0·5 (29°)	0·7
^{14}N(^{3}He, d_0)^{15}O	1·802 ± 0·015	1·806[a]	0	0	1	5·0[f]	4·7[k]	2·5 (18°)	2·4
^{27}Al(^{3}He, d_2)^{28}Si	1·432 ± 0·015	1·478[b]	—	4·617 ± 0·010[d]	—	—	—	0·15 (33°)	—
^{27}Al(^{3}He, d_3)^{28}Si	—	—	4·979 ± 0·015[m]	5·0	—	—	—	0·02 (44°)	—
^{27}Al(^{3}He, d_4)^{28}Si	—	—	6·272 ± 0·015[m]	6·2	0	4·5[g]	6·4[l]	0·7 (9°)	1·4
^{27}Al(^{3}He, d_5)^{28}Si	—	—	6·880 ± 0·015[m]	6·9	3	4·5[g]	—	0·2 (66°)	—
^{27}Al(^{3}He, d_6)^{28}Si	—	—	7·392 ± 0·015[m]	7·3	—	—	—	0·05 (67°)	—
^{27}Al(^{3}He, d_7)^{28}Si	—	—	7·807 ± 0·015[m]		3	4·5[g]	—	0·13 (67°)	—
^{27}Al(^{3}He, d_8)^{28}Si	—	—	7·948 ± 0·015[m]		—	—	—	—	—

(1) Reaction, (2) measured *Q*-value (MEV), (3) previous *Q*-value (MEV), (4) measured excitation (MEV), (5) previous excitation[e] (MEV), (6) *l*-value, (7) radius (10^{-13} cm), (8) radius used in (d, n) analyses (10^{-13} cm), (9) differential cross section at the centre-of-mass angle shown (mbn sterad^{-1}), (10) $|A_0|^2 N_i^2$ (10^{12} cm^{-1}).

---

[a] Calculated from mass excesses and excitations listed by Ajzenberg-Selove and Lauritsen (1959)

[b] Calculated from mass excesses given by Endt and Braams (1957) and excitation given by Endt and Paris (1957)

[c] The value given by Ajzenberg-Selove and Lauritsen (1959)

[d] The value found by Endt and Paris (1957)

[e] Ajzenberg-Selove and Lauritsen (1959) and Endt and Braams (1957)

[f] Using Butler theory

[g] Using the Born approximation theory

[h] Maslin *et al.* (1956)

[j] Cerineo (1956)

[k] Evans *et al.* (1953)

[l] Calvert *et al.* (1955)

[m] Calculated from the measured *Q*-value difference from the lowest observed state and the excitation of this state given in (5).

from the masses *using the recently revised mass of* ^{15}O (Ajzenberg-Selove and Lauritsen 1959) but the *Q*-value for the ^{10}B (^{3}He, d_0)^{11}C reaction is somewhat lower than the calculated value.

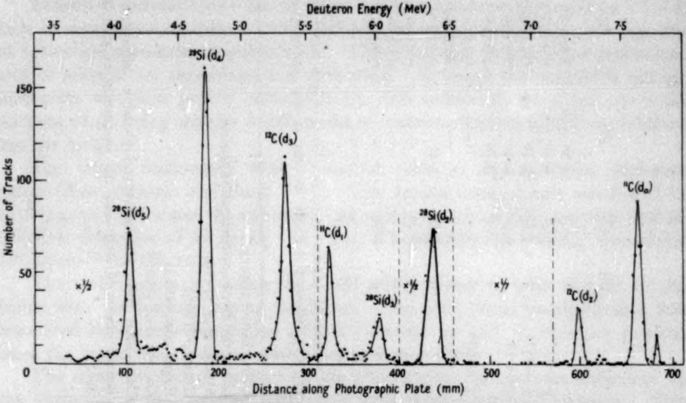

Figure 1. The 40° deuteron spectrum from the boron target bombarded with 5·22 Mev ^{3}He. The small groups of slightly higher energy than some of the larger groups are assumed to arise from the presence of a small quantity of boron on the beam side of the aluminium backing.

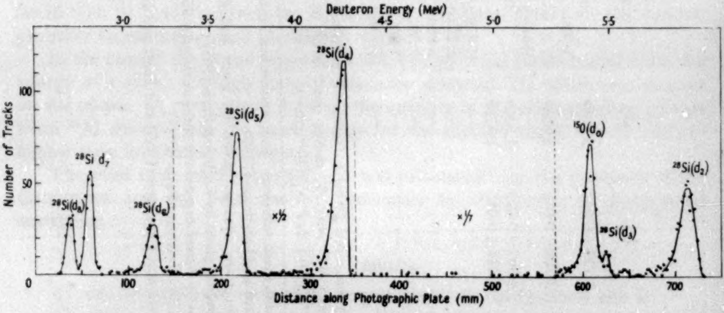

Figure 2. The 80° deuteron spectrum from the adenine target bombarded with 5·24 Mev ^{3}He.

The energies of some of the levels of ^{28}Si, particularly those of higher excitation, differ from earlier data, but this is not surprising since, in this region of excitation, the only alternative reaction which has been used to produce these states is ^{27}Al(d, n)^{28}Si which gives poor resolution.

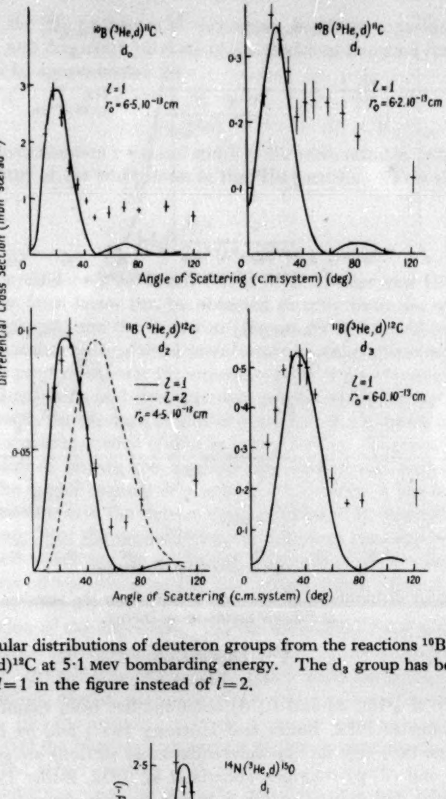

Figure 3. Angular distributions of deuteron groups from the reactions ^{10}B(^{3}He, d)^{11}C and ^{11}B(^{3}He, d)^{12}C at 5·1 MeV bombarding energy. The d_3 group has been erroneously labelled $l=1$ in the figure instead of $l=2$.

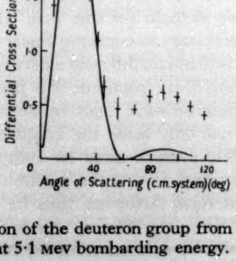

Figure 4. Angular distribution of the deuteron group from the reaction ^{14}N(^{3}He, d_0)^{15}O at 5·1 MeV bombarding energy.

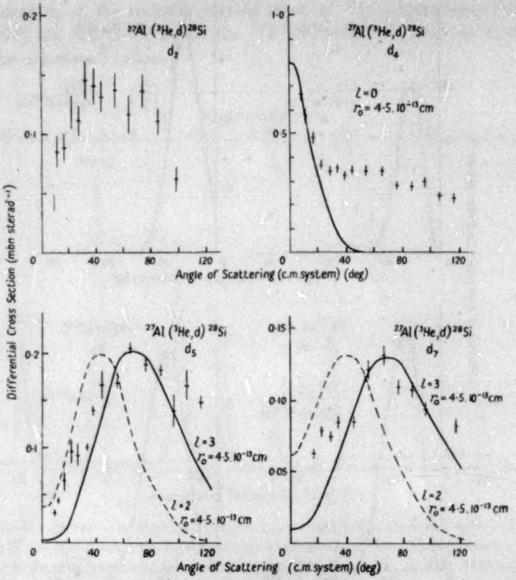

Figure 5. Angular distributions of deuteron groups from the reaction ^{27}Al(^{3}He, d)^{28}Si at 5·2 MEV bombarding energy.

§ 4. DISCUSSION

4.1. *Theory*

The theory of (^{3}He, d) and (t, d) reactions has been examined by Butler (Butler and Salpeter 1952, Butler and Hittmair 1957) and by Newns (1952). The expressions they give for the differential cross sections are similar to those for the (d, n) and (d, p) reactions (Bhatia *et al.* 1952, Butler 1951). In both cases the angular distribution of the outgoing particle depends on the orbital angular momentum transferred to the nucleus by the captured nucleon and on the effective radius at which the capture takes place. The angular distribution is modified by the presence of a form factor which is the probability of the captured nucleon in the bombarding particle (in this case ^{3}He) having the appropriate internal momentum ($\hbar\mathbf{K}$) necessary to conserve linear momentum in the reaction. The variation of this factor is the main difference between the two types of stripping process. For the (d, n) and (d, p) reactions, it is just the square of the Fourier transform of the internal deuteron wave function, normalized to unity. However, for the (^{3}He, d) reaction not only must the captured proton have the correct momentum but also the ^{3}He particle must be comprised of a deuteron in its ground state plus an odd proton, so that the reaction can take place by a simple stripping mechanism. The form factor can thus be written $|A_0|^2\{\phi(\mathbf{K})\}^2$ where $|A_0|^2$ is the probability of finding the ^{3}He nucleus in the required state and $\phi(\mathbf{K})$ is the Fourier transform of the wave function for the odd proton (again normalized to unity) when the ^{3}He nucleus is in this state. For large separations r between the odd proton and the centre of mass of the deuteron the wave function for the odd proton can be approximated by

$$\frac{N_1}{\sqrt{(4\pi)}}\frac{e^{-\lambda r}}{r},$$

where N_1 is a normalization constant and λ is the wave number corresponding to the binding energy of the odd proton in the ^{3}He particle. This leads to a form factor

$$|A_0|^2\frac{N_1^2}{2\pi^2}\frac{1}{(\lambda^2+K^2)^2}$$

which would be valid only for small values of K (Butler and Hittmair 1957). Alternatively the form factor can be obtained directly from the wave functions for the mass-3 particle and the deuteron (Newns 1952, French and Fujii 1957) and will depend on the choice of these wave functions, although not very sensitively.

The nuclear properties enter the expressions for the differential cross section for both mass-3 stripping and deuteron stripping primarily through the presence of a reduced width (in the case of Butler's theory) or a capture probability (in the Born approximation theory of Bhatia *et al.* (1952)). These are proportional to the probability of finding the captured nucleon at the surface of the final nucleus with the orbital angular momentum with which it has been captured, when the final nucleus is in the state of target nucleus in its ground state plus the captured nucleon. For the various stripping reactions between the same initial and final nuclear states one would expect these factors to be almost the same, differing because of variations in the interaction radius (Butler and Salpeter 1952, Butler and Hittmair 1957).

The derivation of the expressions for the differential cross sections involves a number of major assumptions. These are that (i) the stripping occurs at a definite radius; (ii) the outgoing particle comes from the bombarding particle and not the nucleus, that is, exchange effects and compound nucleus formation are neglected; (iii) the outgoing particle does not interact with the initial or final nucleus; (iv) the bombarding particle does not undergo elastic or inelastic scattering by the target nucleus and (v) Coulomb effects can be neglected. Generally for deuteron stripping at moderately high energies these assumptions are reasonable, because the deuteron is loosely bound. However, for the (^{3}He, d) reaction, for example, they are questionable because the ^{3}He nucleus is more strongly bound than the deuteron and because its double charge makes Coulomb effects more serious. This will be especially true at the energies used in the present experiment.

Only in those cases where the (^{3}He, d) and (d, n) reactions between the same nuclear states proceed predominantly by a stripping mechanism can one expect the cross sections to be related, and then the relationship will only be straightforward if in both cases the above assumptions are justified. The angular distributions of the outgoing particles should indicate whether stripping is important and if so the ratio of the absolute cross sections will give a measure of the extent to which the above assumptions are valid. In view of the high excitation of the compound system in the reactions we have studied (between 20 and 26 MeV), it is unlikely that such angular distributions could result from a small number of overlapping levels in a compound nucleus. Also, if a compound nucleus is formed by absorption of the incident ^{3}He particle it is relatively improbable that it will decay by deuteron emission since several more favourable channels are always open.

4.2. *Angular Distributions*

A number of the angular distributions strongly indicate a stripping mechanism. In such cases they could apparently be equally well fitted by the Born approximation theory or the Butler theory and with a variety of form factors providing the interaction radius parameter was suitably adjusted.

Reasonably good fits were obtained, for example, with the angular distributions of the ^{10}B(^{3}He, d$_0$)^{11}C, ^{11}B(^{3}He, d$_2$)^{12}C, ^{11}B(^{3}He, d$_3$)^{12}C and ^{14}N(^{3}He, d$_0$)^{15}O groups. Those from ^{27}Al(^{3}He, d)^{28}Si could not be fitted quite as well, probably because the angular distributions were distorted by the Coulomb potential. This is borne out by the fact that the best fitting radius is small compared with that of the corresponding (d, n) reaction, as might be expected if large Coulomb effects were present. The theoretical curves shown in figures 3, 4 and 5 were calculated using the form factor given above, i.e.

$$|A_0|^2 \frac{N_1^2}{2\pi^2} \frac{1}{(\lambda^2+K^2)^2}$$

and the choice between Born approximation and Butler theories was governed by corresponding (d, n) work and is indicated in the table.

Specific points concerning some of the angular distributions are dealt with below.

^{10}B(^{3}He, d$_0$)^{11}C.

A good fit was obtained using the *l*-value which had been used to explain the ^{10}B(d, n$_0$)^{11}C angular distributions at 9 Mev (Maslin *et al.* 1956) and at 7·5 Mev (Cerineo 1956).

^{10}B(^{3}He, d$_1$)^{11}C.

The situation here is not simple. Previously, good $l=1$ stripping distributions have been reported from the (d, n) reaction leading to this state of ^{11}C (Maslin *et al.* 1956, Cerineo 1956). However, since the spin and parity of the ^{10}B ground state is 3$^+$ and the first excited state of ^{11}C should have spin and parity of $\frac{1}{2}^-$, as does the corresponding level in the mirror nucleus ^{11}B (Ajzenberg-Selove and Lauritsen 1959), the usual stripping selection rules for angular momentum conservation cannot hold if $l=1$. The deuteron stripping results have been explained on the grounds that the outgoing particle suffers a spin reversal brought about either by a spin-flip mechanism (Wilkinson 1957) or by a nucleon exchange process (Evans and French 1958). It is not surprising, then, that the simple stripping theory cannot be well applied to the reaction ^{10}B(^{3}He, d$_1$)^{11}C. It is relevant that the (d, p) reaction leading to the mirror of this level in ^{11}B also appears to have only a small component in its angular distribution which is amenable to an $l=1$ fit (Zeidman and Fowler 1958, Evans and Parkinson 1954).

^{11}B(^{3}He, d$_2$)^{12}C.

The angular distribution of the corresponding (d, n) reaction has not been observed at bombarding energies where stripping might predominate. This is probably because of the low intensity of the group and the poor neutron energy resolution (Maslin *et al.* 1956). The peak cross section in our work is about one fifth of that of the d$_3$ group. An $l=1$ fit gives quite good agreement with the observed angular distribution. This is the value to be expected from the spin and parity assignment of 0^+ for this astrophysically significant level (Cook *et al.* 1957, Salpeter 1957). It is perhaps of interest that this result rules out the possibility of a spin and parity of 4^+.

^{11}B(^{3}He, d_3)^{12}C.

Quite good agreement is achieved with an $l=2$ fit, and this l-value agrees with the value used for the corresponding (d, n) angular distribution (Maslin *et al.* 1956).

^{14}N(^{3}He, d_0)^{15}O.

A good fit is obtained using an $l=1$, agreeing with the value used for the ^{14}N(d, n_0)^{15}O angular distribution at 7·7 Mev (Evans *et al.* 1953).

^{27}Al(^{3}He, d_4)^{28}Si.

The value $l=0$ may be considered well established from the (d, n) reaction at 9 Mev (Calvert *et al.* 1955) and 6 Mev (Rubin 1957). This is the only group from ^{27}Al(^{3}He, d)^{28}Si for which we have observed a peak in the 0° direction. Only partial agreement with the theoretical curve is obtained, however, but the Coulomb effect is almost certainly a distorting factor.

^{27}Al(^{3}He, d_5 and d_7)^{28}Si.

Again the fits are not good but $l=3$ is best in both cases, suggesting that both these states have negative parity.

4.3. *Absolute Cross Sections*

The peak values of the absolute cross sections are given in the table and these may well be in error by ± 25% mainly because of the uncertainty in target thickness.

The (^{3}He, d) cross sections have been compared with the coresponding (d, n) cross sections in four instances: ^{10}B(^{3}He, d_0)^{11}C, ^{11}B(^{3}He, d_3)^{12}C, ^{14}N(^{3}He, d_0)^{15}O and ^{27}Al(^{3}He, d_4)^{28}Si. This was done by fitting the (^{3}He, d) angular distributions with the same theory, Butler or Born approximation, as had been used for the (d, n) work with the form factor

$$|A_0|^2\frac{N_1^2}{2\pi^2}\frac{1}{(\lambda^2+K^2)^2}$$

mentioned above. The only unknown quantities in the expressions are $|A_0|^2N_1^2$ and the reduced width or proton capture probability, depending on which theory had been used. Assuming that these latter factors are the same as for the corresponding (d, n) reactions, the factor $|A_0|^2N_1^2$ could be estimated in each case at the peak of the angular distribution after a theoretical fit had been found. Reduced widths have been reported for the ^{10}B(d, n_0)^{11}C and ^{11}B(d, n_3)^{12}C reactions (Maslin *et al.* 1956) and also the proton capture probability for ^{27}Al(d, n_4)^{28}Si (Calvert *et al.* 1955). Although no reduced width was available for ^{14}N(d, n_0)^{15}O, it could be estimated because a reduced width has been reported for ^{14}N(d, p_0)^{15}N (Warburton and McGruer 1957) and the ratio of reduced widths for these two reactions has been determined (Calvert *et al.* 1956). It was necessary that the reduced widths or capture probabilities should all have been calculated using the same deuteron form factor so that the values of $|A_0|^2N_1^2$ could be compared correctly. This necessitated an adjustment in the published values of the reduced widths or capture probabilities obtained from the ^{27}Al, ^{10}B and ^{11}B(d, n) reactions because in these cases a different form factor from that given by Butler (1951) had been used.

The values of $|A_0|^2 N_l^2$ obtained are shown in the table.

The variations in this factor, which indicate variations in the validity of the stripping assumptions, are larger than the probable errors which arise from uncertainty in the reduced widths (possibly ± 50%). The smallness of this factor for ^{27}Al(^{3}He, d_4)^{28}Si is not surprising since a large Coulomb effect would be expected to reduce the observed cross section in this case. The value of $|A_0|^2 N_l^2$ in the case of ^{11}B(^{3}He, d_3)^{12}C is only one-fifth of that for ^{10}B(^{3}He, d_0)^{11}C where one might have expected similar values. It is possible that the ^{11}B(d, n_3)^{12}C reaction may not proceed by a simple stripping mechanism. This is supported by the fact that the angular distributions of the n_0 and n_1 groups from this reaction at 10 Mev bombarding energy have been explained by a mixture of simple stripping and heavy particle stripping (Zeidman and Fowler 1958). However, it is unlikely that a factor of five can be explained in this way.

It is of interest to compare those values of $|A_0|^2 N_l^2$ with values obtained from other experiments. At present, there are no (^{3}He, d) results available, although a number of reactions of the type (d, ^{3}He) and (d, t) have been studied. The (d, t) experiments are particularly suitable because the Coulomb effects will generally be smaller than in the ^{3}He experiments and because they can be compared with the corresponding (p, d) or (d, p) reactions between the same nuclear levels. The values of $|A_0|^2 N_l^2$ obtained from such comparisons will, of course, refer to the triton but will not be expected to differ greatly from the ^{3}He particle because the internal wave functions for the triton and ^{3}He are similar.

Comparisons have been made for the following (d, t) reactions:

^{7}Li(d, t)^{6}Li.

This reaction has been studied at 14·4 Mev (Levine *et al.* 1955) and angular distributions of triton groups leaving ^{6}Li in its ground state and first excited state have been reported. The corresponding (p, d) reactions have been studied at 17·5 Mev (Reynolds and Standing 1956) and reduced widths have been determined using Butler theory.

We have fitted the angular distributions of tritons with Butler theory and the form factor

$$|A_0|^2 \frac{N_l^2}{2\pi^2} \frac{1}{(\lambda^2 + K^2)^2}$$

where λ^2 is related to the binding energy of the odd neutron in the triton. Good fits have been obtained using $l = 1$ and radii of $6{\cdot}0 \times 10^{-13}$ cm and $6{\cdot}5 \times 10^{-13}$ cm for the t_0 and t_1 group angular distributions respectively. Insertion of the appropriate reduced widths gives values of $16{\cdot}7 \times 10^{12}$ cm^{-1}† and $16{\cdot}4 \times 10^{12}$ cm^{-1} for $|A_0|^2 N_l^2$ for the reactions leading to the ground state and first excited state of ^{6}Li respectively, these being evaluated for the peaks of the angular distributions.

---

† These results differ from those of Werner (1956) and El Nadi and Abou Hadid (1958) who obtain values of $|A_0|^2 C_T^2$ of 1·8, 1·08, and 0·27 for the reactions ^{13}C(d, t)^{12}C, ^{7}Li (d, t)^{6}Li ground state and ^{19}F(d, t)^{18}F respectively. The quantity C_T^2 is apparently intended to be the same as Butler's N_l^2 used above but no units are given in either of these papers and the results are presumably intended to be expressed in units of 10^{13} cm^{-1}. Although they use the same experimental results as we do their method of calculation differs only slightly from ours and we have been unable to explain the discrepancy between their results for the ^{13}C(d, t)^{12}C and ^{7}Li(d, t)^{6}Li reactions and our own.

^{13}C(d, t)^{12}C.

The angular distribution of the ground state triton group has been studied at 3·3 Mev and 2·2 Mev by Holmgren *et al.* (1954) and the (d, p) reaction between the same nuclear states has been investigated at 8 Mev (Rotblat 1951). We have fitted the angular distribution for the (d, p) reaction with Butler theory (Butler and Hittmair 1957) using $l=1$, $r_0=5{\cdot}3\times10^{-13}$ cm and have obtained a value of about $1{\cdot}0\times10^{-19}$ erg cm for the reduced width of the captured neutron.

We have fitted the triton angular distribution at 3·3 Mev quite well with Butler theory and using the same form factor as in the ^{7}Li(d, t)^{6}Li calculation with $l=1$, $r_0=5{\cdot}8\times10^{-13}$ cm but we can only achieve a poor fit with the angular distribution at 2·2 Mev. Inserting the reduced width, the factor $|A_0|^2N_1^2$ was evaluated for the peaks of the angular distributions and was found to be about $8{\cdot}8\times10^{12}$ cm^{-1} at 3·3 Mev† and $5{\cdot}8\times10^{12}$ cm^{-1} at 2·2 Mev, the latter value being relatively more uncertain because of the poor fit with theory at this energy.

^{19}F(d, t)^{18}F.

El Bedewi and Hussein (1957) have obtained the ground state triton angular distribution at 8·9 Mev and we have obtained a good fit with this using Butler theory and the usual form factor with $l=0$, $r_0=6{\cdot}0\times10^{-13}$ cm. The reduced width for the corresponding (p, d) reaction has been found at 18·9 Mev by Reynolds and Standing (1956) and using this we obtain a value of $3{\cdot}2\times10^{12}$ cm^{-1} for $|A_0|^2N_1^2$ evaluated at 10°†.

Since in all the (^{3}He, d) and (d, t) reactions studied, with the exception of the ^{13}C(d, t)^{12}C reactions, the deuteron energy is farther above the Coulomb barrier than the mass-3 particle energy, it seemed of interest to investigate the effect of the Coulomb interaction between the nucleus and the mass-3 particle on $|A_0|^2N_1^2$. This is shown in figure 6 where the values of $|A_0|^2N_1^2$ are plotted against the ratio of the energy of the mass-3 particle in the centre-of-mass system to the approximate Coulomb barrier height. The inclusion of points corresponding to the ^{13}C(d, t)^{12}C reaction is questionable because in this case the Coulomb potential probably has a greater effect on the deuteron than on the triton. However, the general trend of the points suggests that the Coulomb effect on the mass-3 particle is an important factor in determining the magnitudes of stripping cross sections using mass-3 particles, even at energies well above the Coulomb barrier.

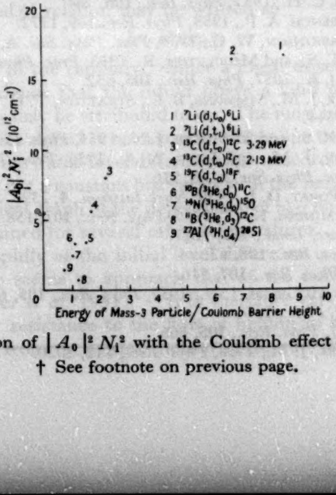

Figure 6. The variation of $|A_0|^2N_1^2$ with the Coulomb effect on the mass-3 particle.

† See footnote on previous page.

§ 5. CONCLUSIONS

The angular distributions of the (^{3}He, d) we have studied could be explained by an extension of the simple deuteron stripping theory provided the bombarding energy was above the Coulomb barrier and the corresponding deuteron reaction showed good stripping. The absolute cross sections appear to be reduced below the value expected from simple theory, the reduction being largely due to the Coulomb effect on the mass-3 particle.

Thus the (^{3}He, d) reaction which can be studied at high resolution, may be used to derive useful information about nuclear levels in cases where the level structure is too complex to allow for investigation by the (d, n) reaction.

ACKNOWLEDGMENTS

The authors wish to thank Professor S. Devons for helpful discussions. One of us (I.J.T.) acknowledges the receipt of a Nuffield Science Teaching Fellowship, and another (P.D.F.) a research fellowship from the Department of Scientific and Industrial Research.

REFERENCES

AJZENBERG-SELOVE, F., and LAURITSEN, T., 1959, *Nucl. Phys.*, **11**, 1.
BARROS, F. DE S., FORSYTH, P. D., JAFFE, A. A., and TAYLOR, I. J., 1959, *Proc. Phys. Soc.*, **73**, 793.
BHATIA, A. B., HUANG, K., HUBY, R., and NEWNS, H. C., 1952, *Phil. Mag.*, **43**, 485.
BUTLER, S. T., 1951, *Proc. Roy. Soc.* A, **208**, 559.
BUTLER, S. T., and HITTMAIR, O. H., 1957, *Nuclear Stripping Reactions* (London: Pitman).
BUTLER, S. T., and SALPETER, E. E., 1952, *Phys. Rev.*, **88**, 133.
CALVERT, J. M., JAFFE, A. A., LITHERLAND, A. E., and MASLIN, E. E., 1955, *Proc. Phys. Soc.* A, **68**, 1008.
CALVERT, J. M., JAFFE, A. A., and MASLIN, E. E., 1956, *Phys. Rev.*, **101**, 501.
CERINEO, M., 1956, *Nucl. Phys.*, **2**, 113.
COOK, C. W., FOWLER, W. A., LAURITSEN, C. C., and LAURITSEN, T., 1957, *Phys. Rev.*, **107**, 508.
EL BEDEWI, F. A., and HUSSEIN, I., 1957, *Proc. Phys. Soc.* A, **70**, 233.
EL NADI, M., and ABOU HADID, L., 1958, *Nucl. Phys.*, **8**, 51.
ENDT, P. M., and BRAAMS, C. M., 1957, *Rev. Mod. Phys.*, **29**, 683.
ENDT, P. M., and PARIS, C. H., 1957, *Phys. Rev.*, **106**, 764.
EVANS, N. T. S., and FRENCH, A. P., 1958, *Phys. Rev* **109**, 1272.
EVANS, N. T. S., and PARKINSON, W. C., 1954, *Proc. Phys. Soc.* A, **67**, 684.
EVANS, W. H., GREEN, T. S., and MIDDLETON, R., 1953, *Proc. Phys. Soc.* A, **66**, 108.
FRENCH, J. B., and FUJII, A., 1957, *Phys. Rev.*, **105**, 652.
HOLMGREN, H. D., BLAIR, J. M., SIMMONS, B. E., STRATTON, T. F., and STUART, R. V., 1954, *Phys. Rev.*, **95**, 1544.
LEVINE, S. H., BENDER, R. S., and MCGRUER, J. N., 1955, *Phys. Rev.*, **97**, 1249.
MASLIN, E. E., CALVERT, J. M., and JAFFE, A. A., 1956, *Proc. Phys. Soc.* A, **69**, 754.
NEWNS, H. C., 1952, *Proc. Phys. Soc.* A, **65**, 916.
RAMAVATARAM, K., and PORAT, D. I., 1959, *Nucl. Instrum.*, **4**, 239.
REYNOLDS, J. B., and STANDING, K. G., 1956, *Phys. Rev.*, **101**, 158.
ROTBLAT, J., 1951, *Nature, Lond.*, **167**, 1027.
RUBIN, A. G., 1957, *Phys. Rev.*, **108**, 62.
SALPETER, E. E., 1957, *Phys. Rev.*, **107**, 516.
WARBURTON, E. K., and MCGRUER, J. N., 1957, *Phys. Rev.*, **105**, 639.
WERNER, A., 1956, *Nucl. Phys.*, **1**, 9.
WILKINSON, D. H., 1957, *Phys. Rev.*, **105**, 666.
ZEIDMAN, B., and FOWLER, J. M., 1958, *Phys. Rev.*, **112**, 2020.

‘Eddy’ Viscosity in Liquid Helium II

By S. M. BHAGAT
Clarendon Laboratory, Oxford

Communicated by K. Mendelssohn; *MS. received 27th October* 1959

Abstract. Isothermal flow of liquid helium II through a wide capillary has been studied. The flow of the liquid is found to be complex and to obey a modified form of Poiseuille’s law. Further, the effective viscosity thus deduced varies fairly strongly with the initial pressure difference. A possible explanation, introducing an ‘eddy’ viscosity in the superfluid, is suggested.

About a year ago we reported some experiments on the isothermal flow of liquid helium II through a system consisting of a porous glass filter in series with a capillary (Bhagat and Mendelssohn 1958). The observed behaviour was unusual as well as very complex, suggesting a dependence of the flow mechanism not only on the pressure head but also on the history of the experiment. A possible explanation of these results is the presence of vorticity in the superfluid. In order to investigate this phenomenon further, flow observations have now been carried out with the capillary alone. The present paper describes some of the characteristic features of the flow phenomena observed with a 142·3 cm long capillary with an internal diameter of 0·068 cm. The experiments were made at several temperatures varying between 1·3 and 2·1°K.

It is found that log $(h+c)$, where h is the level difference and c is a parameter determined for each flow experiment separately, is a linear function of time. Hence, one may write for the average velocity of liquid helium in the capillary

$$\bar{v} = v_0 + k\,\mathrm{grad}\,p \qquad \ldots\ldots(1)$$

where v_0 is again a parameter, closely related to the c mentioned above. The slope k in the $(\bar{v}, \mathrm{grad}\,p)$ relation may be written as

$$k = a^2/8\eta_{\mathrm{eff}} \qquad \ldots\ldots(2)$$

where a is the radius of the capillary. Since a linear dependence of $\bar{v}$ on grad p may be taken as evidence that the liquid obeys a kind of Poiseuille’s law, an effective viscosity η_{eff} may be attributed to it. The most important feature of the flow seems to be that the slope k is not a constant from one flow curve to another but depends strongly on the initial level difference h_1. Accordingly, the effective viscosity of the liquid is not a constant but varies with the *initial* pressure difference. Figure 1 shows a typical graph of the dependence of η_{eff} on h_1, at 1·72°K. Similar plots have been obtained for several other temperatures. The effective viscosity of the liquid falls rapidly as the initial level difference is reduced and for small enough h_1 the value seems to approach that of the total viscosity η of liquid helium II (de Troyer *et al.* 1951). It is therefore very tempting to attribute the additional linear resistance to the flow of helium to an ‘eddy’ viscosity—a contribution arising from the vortex motion in the superfluid component. The existence of turbulence in the superfluid was first suggested by Bowers, Chandrasekhar and Mendelssohn (1950, see also Chandrasekhar and Mendelssohn 1952) from their detailed observations of the passage of helium II through tubes filled with fine powder. More recently Vinen (1958) and Hall (1958) have obtained rather direct evidence for the presence of vorticity in the superfluid. Vinen (1957) also suggested that there may be a fairly large eddy viscosity associated with the superfluid once the possibility of vortex motions was included. Consequently, using the two-fluid equations of motion one may write for the pressure dependent part of the velocity in equation (1) the expression

$$v_{\mathrm{p}}=\frac{a^2}{8}\left[\left(\frac{\rho_{\mathrm{n}}}{\rho}\right)^2\frac{1}{\eta_{\mathrm{n}}}+\left(\frac{\rho_{\mathrm{s}}}{\rho}\right)^2\frac{1}{\eta_{\mathrm{s}}}\right] \qquad \ldots\ldots(3)$$

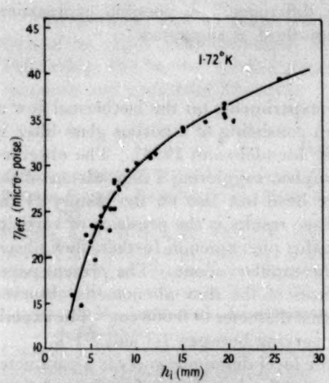

Figure 1. Variation of effective viscosity η_{eff} as a function of the initial level difference h_{l} at 1·72°K. The circles show the observed points and the full curve is the smoothed curve drawn through them.

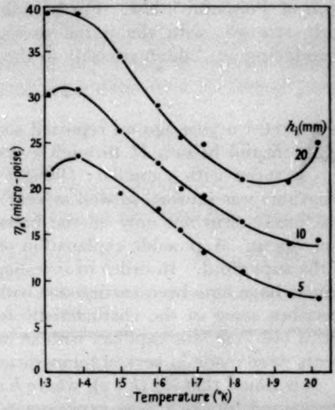

Figure 2. Variation of the eddy viscosity η_{s} as a function of temperature for various values of the initial level difference h_{l}.

where η_{n} and η_{s} are the viscosities, respectively, for the normal component (Brewer and Edwards 1959) and the eddies, and the other symbols have their usual meanings. In figure 2 we have shown the variation of η_{s}, as calculated from our results using (3), as a function of temperature for various values of the initial level difference. It is too early to suggest a detailed explanation for the rather complex dependence of η_{s} on temperature. However, one may state that the eddy viscosity should be expected to decrease with increasing temperature as the density of the superfluid supporting the vorticity is falling. On the other hand, large densities of vorticity should be more probable at higher temperatures and hence may lead to an increase in the eddy viscosity. This should be of importance only for rather large values of h_{l} since then, presumably, large densities of vorticity would be involved. Hence, one may expect η_{s} to vary in a rather complicated manner with temperature and pressure head.

The physical meaning of the term v_0 in equation (1) which represents the limiting velocity of the liquid for vanishingly small pressure gradients is evidently identical with that of the so-called critical velocity. It should be pointed out that the observed value of v_0 ($\sim 2\,\mathrm{cm\,sec^{-1}}$ at $1{\cdot}7^\circ\mathrm{K}$) rises somewhat with h_1. This may be a consequence of hysteresis effects involved in the decay of the vorticity in the liquid (cf. Brewer, Edwards and Mendelssohn 1956, Mendelssohn and Steele 1959). On the other hand there may be a sizeable contribution to v_0 due to slipping of the superfluid at the walls of the capillary. Only more detailed investigation of isothermal flow through capillaries of various diameters will throw further light on the nature of v_0.

The present observations indicate that there exists a fairly large contribution due to vorticity towards a linear flow resistance in liquid helium II. In the present paper we have written this as a lumped parameter, that is, as an eddy viscosity. However, the details of the processes involved can hardly be stressed at this stage and must await further observations. Experiments with this end in view are being carried out.

ACKNOWLEDGMENTS

My thanks are due to Dr. K. Mendelssohn for suggesting this research, to Mr. G. Lampel for help with the observations, and to the Government of India for financial assistance.

REFERENCES

BHAGAT, S. M., and MENDELSSOHN, K., 1958, *Physica*, **24**, *Proceedings of the Kamerlingh Onnes Conferences on Low Temperature Physics*, S147.

BOWERS, R., CHANDRASEKHAR, B. S., and MENDELSSOHN, K., 1950, *Phys. Rev.*, **80**, 856.

BREWER, D. F., and EDWARDS, D. O., 1959, *Proc. Roy. Soc.* A, **251**, 247.

BREWER, D. F., EDWARDS, D. O., and MENDELSSOHN, K., 1956, *Phil. Mag.*, **1**, [8], 1130.

CHANDRASEKHAR, B. S., and MENDELSSOHN, K., 1952, *Proc. Roy. Soc.* A, **218**, 18.

HALL, H. E., 1958, *Physica*, **24**, *Proceedings of the Kamerlingh Onnes Conference on Low Temperature Physics*, S141.

MENDELSSOHN, K., and STEELE, W. A., 1959, *Proc. Phys. Soc.*, **73**, 144.

DE TROYER, A., VAN ITTERBEEK, A., and VAN DEN BERG, G. J., 1951, *Physica*, **17**, 50.

VINEN, W. F., 1957, *Proc. Roy. Soc.* A, **243**, 400.

—— 1958, *Physica*, **24**, *Proceedings of the Kamerlingh Onnes Conference on Low Temperature Physics*, S 13.

RESEARCH NOTES

On the Dielectric Constant of Germanium at Microwave Frequencies

By A. C. BAYNHAM, A. F. GIBSON AND J. W. GRANVILLE
Royal Radar Establishment, Malvern, Worcs.

MS. received 15th October 1959

§ 1. Introduction

It is generally believed that the dielectric constant of intrinsic germanium at room temperature is about 16·0 and independent of frequency throughout the long wavelength infra-red, microwave and radio frequency spectrum. During measurements on certain electrical properties of germanium at 34·75 kMc/s(Gc/s) it was desirable to check the dielectric constant and we were surprised to obtain a value of 14·94. Further detailed examination around this frequency showed up a small but significant dispersion region and it is the purpose of this note to describe the results obtained.

§ 2. Experimental Results

Measurements were made of the attenuation and phase shift resulting from the insertion of a sample which completely filled the rectangular waveguide of a conventional microwave bridge (see, for example, Montgomery 1947). The sample thickness in the propagation direction was then reduced by grinding and remeasured, so that curves of phase shift and attenuation against thickness could be obtained. A typical curve of phase shift against thickness is shown in figure 1.

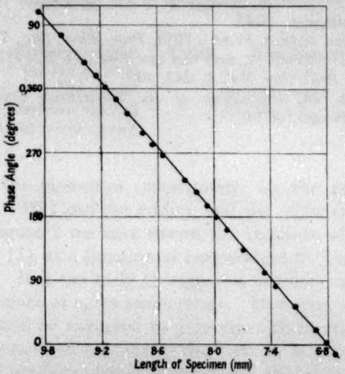

Figure 1. Measured phase shift as a function of sample thickness at 34·75 Gc/s. Points corrected for multiple reflections in the sample.

The microwave bridge, which was isolated from the Klystron oscillator by a ferrite isolator, contained the specimen in a section of electroformed guide in one arm with attenuators on both sides of the specimen section and a phase shifter and Elliott rotary vane attenuator in the other arm. Except at 30·4 Gc/s, no component had a standing wave ratio greater than 1·02. The phase shifter was calibrated at each wavelength used against an adjustable reflecting plunger and the whole system was checked by noting the phase shift when short, accurate sections of extra guide were inserted.

In spite of the use of electroformed guide and attenuators around the specimen the observed phase shift on inserting the sample was not entirely independent of sample position. This source of error was reduced to negligible proportions by making measurements at six positions in the guide (covering one guide wavelength) and the four possible sample orientations. Hence each point on figure 1 is the average of 24 readings. The results were then corrected for multiple reflections in the sample but this correction never exceeded ±4° in phase.

The experimental points in figure 1 allow the position of the line to be fixed with an accuracy to at least 1°. As the total phase shift in the sample is around 1200°, the wavelength in the medium λ_{m} can be determined to within 1 part in 1000. Compared with this experimental accuracy, other effects are important, namely the phase shift on transmission at the sample surfaces and the conductivity contribution to the phase shift. For 50 Ω cm samples these effects contribute about 4° per 1000° but are of opposite sign and have been neglected.

Finally the dielectric constant is computed from the equations

$$\lambda_{\mathrm{m}} = \frac{\lambda_0}{[k' - (\lambda_0/2a)^2]^{1/2}} \quad \text{and} \quad \kappa = \frac{b}{d}(\kappa' - 1) + 1$$

where λ_0 is the free space wavelength, a and b are the long and short dimensions of the rectangular guide, respectively, and d is the sample thickness in the b direction (Montgomery 1947). κ was typically 1% greater than κ'.

The samples were cut from two single crystals of germanium, namely 50 Ω cm N type and 60 Ω cm P type. There was no detectable difference in the dielectric constants so the results are believed to be characteristic of 'pure' germanium.

The results obtained are summarized below.

Frequency (Gc/s)	36·62	34·75	32·78	30·40
Dielectric Constant	15·35 ± 0·10	14·94 ± 0·05	14·90 ± 0·10	17·4 ± 0·5

The very large uncertainty at 30·4 Gc/s arose because the Elliott attenuator had a significant and variable phase shift at this frequency, though a correction was made for this effect.

Other published data on the dielectric constant of germanium, which is of assistance in constructing a dispersion curve, include the following: (i) The results of Salzberg and Villa (1957) have been analysed by Moss (1959) and indicate $\kappa = 15{\cdot}98 \pm 0{\cdot}01$ at long infra-red wavelengths, (ii) Goldey and Brown (1955) give two values of κ at 24·15 Gc/s, namely 16·4 ± 0·2 and 16·6 ± 0·3, (iii) Dunlap and Watters (1953) have measured the dielectric constant of gold doped germanium at 1 Mc/s, at a temperature of 77°K, and obtained a value of 15·8 ± 0·2. This value must be corrected to room temperature, using the known temperature coefficient of the dielectic constant (Cardona, Paul and Brooks 1958) and is equivalent to 16·27 ± 0·2 at 290°K.

§ 3. Discussion of Results

All the above results are plotted in figure 2. The curve shown is a theoretical dispersion curve, given by

$$\epsilon(\omega) = \epsilon_\infty + \frac{C(f_0^2 - f^2)}{(f_0^2 - f^2)^2 + f^2 g^2}$$

where $\epsilon_\infty = 15{\cdot}98$, f_0 = the resonance frequency = 32·20 Gc/s, $C = 203{\cdot}0\,(\mathrm{Gc/s})^2$, $g^2 = 3{\cdot}16\,(\mathrm{Gc/s})^2$.

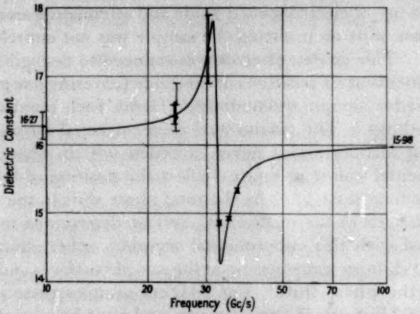

Figure 2. Theoretical dispersion curve (see text) and experimental values of dielectric constant of germanium.

As there are four adjustable parameters in a dispersion formula, four points are required to fix the curve. The values at 32·78, 34·75, 36·62 Gc/s and the infra-red value were used. The agreement with the remaining (less accurate) data is satisfactory. Though the experimental data are of insufficient accuracy to specify the dispersion curve uniquely it is believed to be adequate to show that a dispersion region does indeed exist. However, the fit between theory and experiment is particularly insensitive to the value of g^2 and a value of g^2 an order of magnitude larger than that chosen will give almost as good a fit to the available data.

The additional absorption associated with the dispersion can be calculated from the above data and is found to be small (~ 3 dB cm^{-1} at 34·75 Gc/s). This absorption is in addition to the free carrier absorption which gives a wavelength independent background of about 8 dB cm^{-1}. However the latter absorption is strongly temperature dependent in intrinsic material and increases by about 0·5 dB cm^{-1} deg^{-1} around room temperature. Furthermore no reliance could be placed on attenuation measurements at 30·4 Gc/s, as explained above, and indeed at all frequencies other than 34·75 Gc/s the Elliott attenuator was operating on the limits of its specified bandwidth. In view of these features, no attempt was made to obtain quantitative data from the absorption measurements.

References

Cardona, M., Paul, W., and Brooks, H., 1958, *Brussels Solid State Conference* (New York: Academic Press); see also *J. Phys. Chem. Solids*, **8**, 204, 1959.

Dunlap, W. C., and Watters, R. L., 1953, *Phys. Rev.*, **92**, 1396.

Goldey, J. M., and Brown, S. C., 1955, *Phys. Rev.*, **98**, 1761.

Montgomery, E. G., 1947, *Technique of Microwave Measurement* (New York : McGraw-Hill).
Moss, T. S., 1959, *Optical Properties of Semiconductors* (London : Butterworths Scientific Publications).
Salzberg, C. D., and Villa, J. J., 1957, *J. Opt. Soc. Amer.*, **47**, 244.

A Note on the Viscosity and Resistivity of Liquid Gallium

By N. CUSACK and P. KENDALL
Department of Physics, Birkbeck College, London

MS. received 13*th July* 1959

According to the formula proposed by Batschinski in 1913, the viscosity η and specific volume v of liquids are connected by

$$v = a + c/\eta \qquad \ldots\ldots(1)$$

where a and c are constants for a given substance. This is normally tested by plotting v against $1/\eta$, or d/η, against d, where d is the density. Straight lines which may be called Batschinski plots are found for a wide variety of substances over considerable ranges of temperature. Greenwood and Martin (1952) discussed extensively the application of Batschinski plots to polar compounds containing boron. One interesting feature of their experiments was that the viscosity was measured in the normal and supercooled states and the plots showed a change of slope at the melting point. This was interpreted as indicating the onset of some form of aggregation which changed the size of the flow units; c in equation (1) is related theoretically, if rather loosely, to this size. Analogous phenomena were shown by several properties other than viscosity. The effect was later discovered to occur also in non-polar liquids (Greenwood 1957).

Gorjaga and Morgunova (1958) have recently measured the viscosity of gallium in the normal and supercooled states. The Batschinski plot showed a marked change of slope near 350°c, but not at the melting point (figure 1). If $\ln \eta$ is plotted against $1/T$ the graph is not straight and shows a point of inflection near 350°c, the activation energy being higher on the low temperature side. The viscosity of gallium had previously been measured by Spells (1936) who found much higher values of the kinematic viscosity. Gorjaga and Morgunova suggest some sources of error in Spells' experiment but do not point out that, despite the different values, Spells' results show an equally definite discontinuity in the slope of the Batschinski plot, though nearer 430° than 350°c.

Greenwood and Martin remark that the discontinuities they found may well be related to the fact that, at the melting point, the liquid becomes metastable with respect to the solid. While a discontinuity at the melting point might reasonably be associated with the unique nature of that particular temperature, it is not clear why a discontinuity should occur about 300°c above the melting point in gallium. It is possible that the change in slope in the Batschinski plot is connected with the fact that gallium contracts on melting, the change occurring at or near the temperature at which liquid gallium regains the specific volume it had as a solid just before melting. From the densities given in the *Liquid Metals Handbook* (1952) and the volume contraction on melting (Frost 1954), this temperature is of the order of 315°c. Between this temperature and the melting point, the liquid has a volume compatible with solid structure at the prevailing pressure; above 315°c, both temperature and volume are too high for the ordered structure. It is conceivable that this circumstance influences the size of the viscous flow unit by affecting the stability of temporary bonds between adjacent atoms. If there is any validity in this suggestion, similar discontinuities of slope might be found for other metals which contract on melting but not for those that expand. Unfortunately there are few data with which to check this point. It was formerly believed that antimony contracted on melting but this appears not to be so (Klemm 1958). Bismuth contracts and the liquid regains the density of the solid at about 530°c, but there seem to be insufficient viscosity data to draw a Batschinski plot in this temperature region. Nothing like figure 1 can be found for metals which expand on melting; their plots are either straight lines (In, Sb) or smooth curves (Cd, Hg, Na, Pb, Zn).

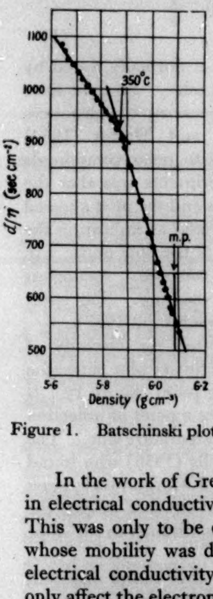

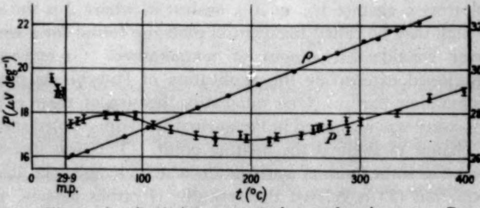

Figure 2. Resistivity ρ and thermoelectric power P (against alumel) of liquid gallium.

Figure 1. Batschinski plot of the viscosity of liquid gallium (after Gorjaga and Morgunova).

In the work of Greenwood and Martin previously referred to, discontinuities in electrical conductivity corresponding to those in viscosity were also detected. This was only to be expected because the units of charge transport were ions whose mobility was determined by the viscosity. In gallium no peculiarity in electrical conductivity need be expected because any aggregation effects could only affect the electron relaxation time very indirectly. Nevertheless a change in slope of the conductivity versus temperature curve was said to occur near 275°c by Gorjaga and Belozerova (1958) who connected it with the same structure change that they supposed would account for the unusual behaviour of the Batschinski plot. As it is unusual for metals at the lower end of their liquid range to show effects of structure on electrical properties, experiments were performed to see whether the thermoelectric power showed any peculiarity near 275°c; the resistivity was also measured. Spectroscopically pure gallium supplied by Johnson, Matthey was used.

The gallium was contained in a Pyrex tube sealed off under vacuum and fitted with tungsten electrodes. Resistivity measurements were made by conventional techniques on two independent lengths of metal. No abnormality in the resistivity curve could be detected and the results fall on the line (see figure 2)

$$\rho = 0{\cdot}0195T + 19{\cdot}9 \qquad \ldots\ldots(2)$$

where ρ is in $\mu\Omega$ cm and T in degrees Kelvin. The average deviation of the experimental points from this line was one part per thousand. The measurements of Powell (1951) up to 40°C, and those of Bridgman (1921) at 65° and 100°C, agree well with equation (2).

The thermoelectric power of liquid gallium relative to chromel and alumel was measured on another sample in an alumina tube, under an argon atmosphere. One set of values, which have an error of about 1·5%, is shown in figure 2. The results agree with the resistivity measurements in failing to detect any feature that could be connected with the effect proposed by Gorjaga and Belozerova. The absolute thermoelectric power of chromel and alumel are about 23 and $-18\,\mu\text{v deg}^{-1}$ respectively in this temperature range, consequently it is not possible to decide with certainty the sign of the rather small absolute thermoelectric power of the gallium. The latter quantity decreases by approximately $1\mu\text{v deg}^{-1}$ when gallium melts, but the experiment was not designed to measure this change accurately. The shape of the thermoelectric power curve was repeatable with ascending and descending temperatures and on different occasions, and the maxima and minima below 200°C may represent changes in the sign of the Thomson coefficient of liquid gallium. However, this requires further investigation with, *inter alia*, other materials as counter electrodes. This will be discussed more thoroughly in a later paper.

We conclude that the electrical measurements made so far do not lend any support to an explanation of figure 1 in terms of structure change or aggregation.

REFERENCES

BATSCHINSKI, A. J., 1913, *Z. Phys. Chem.*, **84**, 643.

BRIDGMAN, P., 1921, *Proc. Amer. Acad. Arts Sci.*, **56**, 104.

FROST, B. T. R., 1954, *Progr. Met. Phys.*, **5**, 96.

GORJAGA, G. I., and BELOZEROVA, P., 1958, *Vest. Mosk. Univ.*, **1**, 133.

GORJAGA, G. I., and MORGUNOVA, M. V., 1958, *Nauchnyje Doklady Vysshej Shkoly (Fiz.-Mat. Nauki)*, **1**, **180**.

GREENWOOD, N. N., 1957, *J. Nucl. Inorg. Chem.*, **3**, 349.

GREENWOOD, N. N., and MARTIN, R. L., 1952, *Proc. Roy. Soc.*, A **215**, 46.

KLEMM, W., 1958, *Proc. Chem. Soc.*, 331.

Liquid Metals Handbook, 1952, Ed. R. N. Lyon, 2nd edn (Washington: Atomic Energy Commission).

POWELL, R. W., 1951, *Proc. Roy. Soc.* A, **209**, 525.

SPELLS, K., 1936, *Proc. Phys. Soc.*, **48**, 209.

LETTERS TO THE EDITOR

Wall Velocity in Ferroelectrics

Reversal of polarization P_r in ferroelectric crystals (switching) occurs under applied field E by the advance of the reversed phase behind '180° walls'. The geometry of the progress of the walls partly controls the switching characteristics. Since about 1954 until last year, it was thought that the advance in barium titanate was always in the form of a great many domain spikes growing along the ferroelectric axis, from one face of the crystal to the other, after nucleation at the faces. Miller and Savage (1958) showed that with liquid electrodes and very low E, the geometry is quite different, consisting of only one or two domains which expand radially sideways to cover the whole electroded crystal. The velocity of these walls is constant throughout the switching, at constant E, and has the dependence

$$v \sim \exp(-\delta/E) \qquad \ldots\ldots(1)$$

over an E range of 3 : 1 at least. In this laboratory we find (*a*) that the small number is characteristic, not of the low E, but of the absence (G. W. Taylor, to be published) of solid electrodes on the surface (equation (1) also holds, though the shape of the domain cross section may be different at the higher E values) and (*b*) that limited radial expansion probably occurs also in the *multi*domain situations under solid electrodes (Peacock 1959, Burfoot and Peacock 1959).

$$\frac{i}{g} \sim (gt)^n \exp\{-C(gt)^{n+1}\}$$

	$n=2$ t small	$n=1$ t large	
where $g=$		$E\,R$	Pulvari and Kuebler (1958) (empirical)
	$E^{2/3}\,R^{4/3}$	$E\,R^{3/2}$	Chynoweth (1958) (model)
	$E^{2/3}\,R^{1/3}$	E	Peacock (1959) (model)
Also	$i \sim \exp -Ct$		Landauer, Young and Drougard (1956)

It appears that single domain work with liquid electrodes will soon give plenty of clear experimental evidence for study of the *physics* of the growth process. But for *applications* it will still be necessary to elucidate the complicated multidomain processes of nucleation and growth if the well-known difficulties are to be overcome; the switching behaviour will not be amenable to adjustment until its relation to the domain behaviour is fully understood. It is the purpose of this note to examine some of the existing evidence on this point, particularly at 'normal' E rather than low E, and to discuss the implications for v. Normal E means upwards of 1 kv cm^{-1}.

Experimental facts about the *multi*domain geometries are not clear for the following reasons. (i) Direct observation is difficult. The domain thicknesses are of the order of microns only; the fast switching required in applications implies exceedingly high domain velocities; and the opposite phases are optically indistinguishable unless cross fields are applied, which may alter the process. Partial switching and etch techniques cannot follow individual domains in growth. (ii) There may be differences in specimens and electrodes used in different laboratories. (iii) Evidence such as switching current variations $i(E, t)$, where t is the time, and Barkhausen pulses becomes very indirect when there are many domains, and needs elaborate interpretation. In particular it is difficult to distinguish nucleation from subsequent growth, and from the later effects of coalescences of domains. It is not even easy to say whether an observed $i(t)$ or $i(E)$ is well fitted by a particular empirical function or model. Many versions exist which have been thought satisfactory; e.g. see the table, which refers to solid electrodes and normal E. The expressions have been rewritten in comparable terms. The initial rate R of nucleation was taken to be of the Merz form

$$R \sim \exp(-\beta/E). \qquad \ldots\ldots(2)$$

This can be predicted by any activation model in which all the non-bulk effects for one nucleus (volume s) are represented by a free-energy term proportional to $\sqrt{s}$, as in the expanding cylinder models. For the maximum of $F = -aEs + 2b\sqrt{s}$ is $\hat{F} = b^2/aE$. Here $a \equiv 2P_r$, for it can be shown that higher degree terms in E are negligible at any reasonable E. Measurements at varying temperature would confirm or deny a thermal activation, but such measurements have not often been made. Doubtless the confusion expressed in the table will soon be resolved. Meanwhile the following comments may be made about v.

(i) The models assumed v to reach a constant value in a negligibly short time. But the following simple treatment with radically different assumptions is also plausible for the first (rising) part of $i(t)$. If R were to remain constant and coalescence is negligible, the models may readily be seen to give (*a*) $i \propto t^2 R$ for constant acceleration, or (*b*) $i \propto tR$ for constant v. So if instead R is taken to fall off as $2P_r - P$, as the available nucleation surface decreases, then $i \propto t^2(2P_r - P)$ for (*a*) or $i \propto t(2P_r - P)$ for (*b*). Now the net polarization P at any instant is $-P_r + \int i\,dt$, so that the $i(t)$ expressions in the table may be rewritten in the simpler form $i \propto t^n(2P_r - P)$. We see that, with this form for R, assumption (*a*) or (*b*) reproduces the same form as in the table, for the early or late part of $i(t)$, respectively. Contrast the assumption that (*b*) holds at all times. Notice that now the factor t^n represents both nucleation and growth, while the exponential is due largely to the decreasing nucleation surface.

The treatment is not quite exact. For t large, coalescence will invalidate this approach, and the previous models are better. For t small, the new assumptions are not necessarily better, but they show that fitting $i(t)$ does not give an adequate test of the model. v may not be a constant.

(ii) When v is constant, equation (1) suggests an activation mechanism with activation energy $H \sim 1/E$:

$$\log v = m(D - H) \qquad \ldots\ldots(3)$$

m and D are constants. Perhaps such a mechanism should be identified with nucleation at existing walls. But it is possible to explain the results by quite a different mechanism, in which parts of the existing wall are moved past 'barriers', and in which the fluctuations allow an appreciable reverse process.

The form of $H(E)$ is quite different, as shown below. The conclusion again is that it is difficult to postulate a unique mechanism.

If a jump affects a volume δs on average, the corresponding change in free energy due to the applied field is $2P_r E\delta s$, so $H = 2B - 2P_r E\delta s$, where $2B$ is the value of H at zero E. More realistically, E probably displaces the position of the barrier maximum. The form of $H(E)$ will then differ. For a simple sinusoidal barrier, the free-energy is $F=-2EP_r s+B\sin Ks$, in which π/K replaces δs, and one finds

$$H=2B(\sin\theta-\theta\cos\theta) \qquad \ldots\ldots(4)$$

where $\cos\theta\equiv 2EP_r/BK$.

The nucleation postulate describes equation (1) as a consequence of an equation like (2); new wall is being created, so that H becomes infinite at zero E, i.e. the creation restrains v. With the alternative mechanism just suggested, H is finite ($=2B$, on average) at zero E, and it is the reverse process which restrains v when E is not too large. The behaviour is statistical, because it is supposed that the fundamental 'jumps' are reasonably independent, though there must in fact be some coherence or the wall would disintegrate. From equation (4), even with no reverse process, log v plotted against sec θ or $-1/E$ now gives a plausible straight line, over an E range of 3:1 below its maximum value, compare equation (3). Strictly, sec θ involves BK, so if lower barriers are narrower in proportion, the result is not altered. At smaller E values, v is too large, but the reverse process reduces it. The reverse barrier height is $H+4\pi EP_r/K$, so v is multiplied by

$$1-\exp(-m4\pi EP_r/K);$$

the constant m depends on the detailed assumptions, but the correcting effect is of the right order if Bm is of order 1.

Queen Mary College,
London.
J. C. Burfoot.

30th July 1959, in revised form 13th October 1959.

Burfoot, J. C., and Peacock, R. V., 1959, *Proc. Phys. Soc.*, **73**, 973.
Chynoweth, A. G., 1958, *Phys. Rev.*, **110**, 1316.
Landauer, R., Young, D. R., and Drougard, M. E., 1956, *J. Appl. Phys.*, **27**, 752.
Miller, R. C., and Savage, A., 1958, *Phys. Rev.*, **112**, 755.
Peacock, R. V., 1959, *Ph.D. Thesis*: University of London.
Pulvari, C. F., and Kuebler, W., 1958, *J. Appl. Phys.*, **29**, 1315.

A Comparison of Static and Microwave Measurements of Magnetocrystalline Anisotropy in Cobalt Manganese Ferrite

During an investigation of the magnetocrystalline anisotropy of cobalt substituted manganese ferrite crystals by microwave resonance and torque curve measurements, a difference has been found in some instances between the values of the anisotropy constants obtained by these methods. The crystals were cut from single crystal boules grown by the flame-fusion method (by Mr. J. Page of these laboratories) and shaped into spheres of diameter 0·3 mm to 1·5 mm. Measurements were made on samples cut from adjacent places in the same single crystal boule, or, in the case where a difference in K_1 was first noticed,

($Co_{0\cdot25}Mn_{0\cdot75}Fe_2O_4$), on the same sample. The results obtained and the chemical analyses of the crystal are shown in the following table.

Magnetic Anisotropy Constants of $Co_xMn_{1-x}Fe_2O_4$ (erg cm^{-3})

At room temperature

x	K_1 Torque	K_1 Resonance	Temperature (°K)
0	-37900 ± 1500	-36000 ± 1500	298
0·25	$+164000 \pm 3000$	$+116000 \pm 10000$	291

At $T = 82$°K

	Torque			Resonance		
x	K_1	K_2	K_3	K_1	K_2	K_3
0	-221000 ± 3000	—	—	-229000 ± 20000	-47000 ± 30000	
0·01	$+198000$	$-1\cdot04 \times 10^6$	-67000	$+258000$	$-1\cdot23 \times 10^6$	-126000

x	Nominal composition	Chemical analysis
0	$MnFe_2O_4$	$Mn_{0\cdot98}Fe_{1\cdot99}O_4$
0·01	$Co_{0\cdot01}Mn_{0\cdot99}Fe_2O_4$	$Co_{0\cdot009}Mn_{0\cdot99}Fe_{1\cdot98}O_4$
0·25	$Co_{0\cdot25}Mn_{0\cdot75}Fe_2O_4$	$Co_{0\cdot245}Mn_{0\cdot747}Fe_{1\cdot99}O_4$

Values of saturation magnetization required in deducing the anisotropy constants from the microwave experiments were measured by F. W. Harrison of these laboratories.

The measurements at room temperature and 82°K show that the values of K_1 obtained by the two methods for $x = 0$, i.e. $MnFe_2O_4$, are not significantly different if we take into account the experimental errors indicated. However, for the sample $Co_{0.25}Mn_{0.75}Fe_2O_4$, the difference, $48\,000 \pm 13\,000$ erg cm^{-3}, is definitely larger than the experimental error. A difference is also present in the sample of composition $Co_{0.01}Mn_{0.99}Fe_2O_4$ at 82°K, where the effect of the cobalt content on the anisotropy is much greater, though here higher order terms were required to describe the anisotropy energy and, therefore, the difference should be treated with caution. The expression for the magnetocrystalline free energy of the crystal was assumed to be of the form

$$E_1 = K_1(\alpha_1^2\alpha_2^2 + \alpha_2^2\alpha_3^2 + \alpha_3^2\alpha_1^2) + K_2(\alpha_1^2\alpha_2^2\alpha_3^2) + K_3(\alpha_1^2\alpha_2^2 + \alpha_2^2\alpha_3^2 + \alpha_3^2\alpha_1^2)^2.$$

A possible explanation of the discrepancy in the values of K_1 deduced from microwave and static measurements was recently put forward by Anderson and Donovan (1959) who suggested that the two methods measure the anisotropy at constant strain and constant stress respectively. Kittel (1949) has shown that this difference ΔK_1 is given by

$$\Delta K_1 = \tfrac{9}{4}(c_{11} - c_{12})\,\lambda_{100}^2 - 2c_{44}\,\lambda_{111}^2$$

where c_{11}, c_{12}, c_{44} are the usual elastic constants of a cubic crystal and λ_{100}, λ_{111} are magnetostriction coefficients. Values for ΔK_1 have been derived by Baltzer (1957) for some ferrites.

For the crystal $Co_{0\cdot25}Mn_{0\cdot75}Fe_2O_4$ we estimate $c_{11} - c_{12} = c_{44} = 10^{12}$ erg cm^{-3} and use the measured values of the magnetostriction $\lambda_{100} = -111 \pm 6 \times 10^{-6}$,

$\lambda_{111} = +19 \pm 1 \times 10^{-6}$ at 290°K. We obtain $\Delta K_1 = 28000 \pm 3000$ erg cm^{-3}. The mechanism thus seems able to account for the major part, and possibly all, of the discrepancy in the observed values if uncertainties in the elastic constants are taken into account. Bozorth *et al.* (1955) reported a difference in the values of K_1, measured by static and microwave resonance methods, for a crystal of nickel ferrous ferrite. In this case the difference was not related to the elastic response of the sample but to electronic relaxations associated with the ferrous ions present in the crystal.

Mullard Research Laboratories,
Cross Oak Lane,
Salfords, Nr. Redhill, Surrey.
5th October 1959.

R. F. Pearson.
R. W. Teale.

Anderson, J. C., and Donovan, B., 1959, *Proc. Phys. Soc.*, **73**, 593.
Baltzer, P. K., 1957, *Phys. Rev.*, **108**, 580.
Bozorth, R. M., Cetlin, B. B., Galt, J. K., Merritt, F. R., and Yager, W. A., 1955, *Phys. Rev.*, **99**, 1898.
Kittel, C., 1949, *Rev. Mod. Phys.*, **21**, 541.

Ionization by Ion Impact in a Collapsing Current Sheet

A theory of the trapping of gas inside a collapsing current sheet in a gas discharge is described by Phillips (1959), in which the mechanism by which neutral gas is trapped is supposed to be ionization by electron impact.

Russian work recently reported in the *Journal of Nuclear Energy*, shows that the electron temperature in the current sheet in a typical fast pinch discharge is only a few (2–4) electron volts. Borzunov, Orlinsky and Osovets (1959) describe experimental work and Kogan (1959) and Borzunov, Kogan and Orlinsky (1959) describe theoretical calculations which substantiate the above claims. The result of such a low electron temperature will be a marked reduction in the rate of ionization of the incoming neutral particles by electron impact compared with the rate at the electron temperature of 50 ev assumed in the previous paper.

The conclusion drawn by the Russians is that the charge exchange process whereby an incoming neutral particle strikes an ion in the sheet, becomes charged and is subsequently held, dominates other processes.

It is important to note that the neutral particle which results from the charge-exchange process is left with the thermal velocity of the ion and may move out of the sheet at a speed much less than the speed of the sheet. Thus charge exchange is not necessarily as clean as electron impact ionization in sweeping up the gas.

The charged reaction product will either spin around the magnetic lines of force or suffer collisions with other particles. If the cylotron radius of the charged product is much greater than the appropriate collision mean free path then the ionized gas particles will move freely in the magnetic field and a pressure wave will travel inwards because of the matter which piles into the current sheet. In this way, a hydrodynamic shock wave can build up. The trapping parameter Π is easily shown to be the ratio of the mean cyclotron radius of ions in the current sheet to the mean free path of an ion in a background of the neutral gas. When the trapping is good it would appear that the conditions may also be right to produce a shock wave. It is hoped to give a detailed discussion of this point in the future.

For moderate electric fields (100 v cm^{-1}) and particle densities of the order of 10^{16} cm^{-3} which represent the conditions envisaged in the earlier paper, ionization by electron impact should be at least as important as the charge-exchange process. However it is of interest to draw attention to the effect of charge-exchange processes in modifying the efficiency of trapping.

Evidently, for very fast pinch work involving large electric fields, the trapping theory must be built around the term $\langle \sigma_{1a} g_{1a} \rangle$ for reactions between positive ions and neutral particles, with g_{1a} taken to be $\dot{r}$ the speed of the sheet and σ_{1a} the appropriate charge-exchange cross section.

New experimental results on charge-exchange cross sections in hydrogen for the reactions $p + H \rightarrow H + p$ and $p + H_2 \rightarrow H + H_2^+$ have been reported by Fite (1960). For a 100 ev collision the cross section for the former is about 4×10^{-15} cm^2 and for the latter is of the order of 10^{-16} cm^2, a difference which arises because the former is an energy-resonant process. The $p + H$ cross section is so large that it easily explains the observed efficiencies of trapping. However, if the discharge takes place in molecular hydrogen, then by some means or other, the H_2 must first be dissociated before charge-exchange collisions are effective. It is most probable that the electrons play an important part in the dissociation process and that the actual sequence of events which follows the entry of the neutral particle into the current sheet is a little more complex than that assumed in the present theory.

Atomic Weapons Research Establishment, N. J. Phillips.
Aldermaston, Berks.

7th September 1959, in final form 29th October 1959.

Borzunov, N. A., Kogan, V. I., and Orlinsky, D. V., 1959, *J. Nucl. Energy*, **9**, 143.
Borzunov, N. A., Orlinsky, D. V., and Osovets, S. M., 1959, *J. Nucl. Energy*, **9**, 135.
Fite, W. L., 1960, *Proceedings of the Uppsala Conference on Ionization Phenomena in Gases*, 1959, in the press.
Kogan, V. I., 1959, *J. Nucl. Energy*, **9**, 140.
Phillips, N. J., 1959, *Proc. Phys. Soc.*, **74**, 700.

On the Measurement of Deuteron Polarization

When unpolarized deuterons are scattered from spin 0 nuclei, their resulting polarization involves four parameters. Double scattering gives three functions of these parameters, which are therefore not fully determined by one experiment.

This note shows that for a light nucleus which can itself be used as a projectile, a suitable set of double-scattering measurements determines the polarization. For a heavy nucleus, on the other hand, some indeterminacy persists however many double scatterings† are made, unless a previously calibrated polarizer or analyser is available.

The polarization of a deuteron beam can be specified by the statistical expectation values $\langle S_i \rangle \equiv P_i$ and $\langle \frac{1}{2}(S_i S_j + S_j S_i) - \frac{2}{3}\delta_{ij} \rangle \equiv T_{ij}$, where $S_i (i = 1, 2, 3)$ is the spin 1 operator. P_i and T_{ij} are called the vector and tensor polarizations

---

† Excluding the use of magnetic fields for spin precession, suggested by Lakin (1955).

(we follow the notation of Stapp (1955, 1957) who derives many of the formulae used below).

An unpolarized beam scattering from a spin 0 target develops polarization of the form†

$$\left.\begin{aligned} P_i &= \beta N_i, \\ T_{ij} &= \eta(N_iN_j - \tfrac{1}{3}\delta_{ij}) + \kappa(D_iD_j - E_iE_j) + \tau(D_iE_j + E_iD_j) \end{aligned}\right\} \quad \ldots\ldots (1)$$

E, **D** and **N** are unit vectors in the directions $\mathbf{k}_f - \mathbf{k}_1$, $\mathbf{k}_f + \mathbf{k}_1$ and $\mathbf{k}_1 \times \mathbf{k}_f$ respectively, where $\mathbf{k}_1$ and $\mathbf{k}_f$ are initial and final relative momenta. β, η, κ and τ are independent parameters, functions of energy and scattering angle, which completely describe the polarization (incidentally, this is not the most general polarization deuterons can have). The analysing power of a scattering is given by the vector and tensor coefficients $\hat{P}_i$ and $\hat{T}_{ij}$.

$$\left.\begin{aligned} \hat{P}_i &= P_i \\ \hat{T}_{ij} &= T_{ij} - 2\tau(D_iE_j + E_iD_j) \end{aligned}\right\} \quad \ldots\ldots (2)$$

such that the differential cross section for a second scattering is

$$I = I_0(1 + \tfrac{3}{2}P_i\hat{P}_i' + 3T_{ij}\hat{T}_{ij}'). \quad \ldots\ldots (3)$$

I_0 is the unpolarized cross section and the primes distinguish the second scattering.

For the experimenter equation (3) proves to have the form

$$I = I_0(1 + A + B\cos\phi + C\cos 2\phi), \quad \ldots\ldots (4)$$

where ϕ is the angle between **N** and **N′**. A, B and C are functions of energy and angle at the two scatterings, and are the quantities measured. A is manifested as a change in the azimuthally averaged cross section, B as a left–right asymmetry and C as an up–sideways asymmetry.

When the target nucleus is relatively light, its recoil is not negligible and the change in deuteron energy between successive scatterings is serious. However, the centre-of-mass energies can be made equal if the light nucleus is itself the projectile at the first scattering‡; we then find

$$\left.\begin{aligned} A &= \tfrac{1}{2}(\eta + 3\kappa)(\eta' - 3\kappa'\cos\theta' - 3\tau'\sin\theta') \\ B &= \tfrac{3}{2}\beta\beta' - 6\tau(\kappa'\sin\theta' - \tau'\cos\theta') \\ C &= \tfrac{3}{2}(\eta - \kappa)(\eta' + \kappa'\cos\theta' + \tau'\sin\theta') \end{aligned}\right\} \quad \ldots\ldots (5)$$

where θ is the centre-of-mass scattering angle, and primes refer to the second scattering. Let us now select two different processes (same centre-of-mass energy but different angles or targets), labelled 1 and 2 say. Then it can be seen that the three double-scattering experiments (1, 1), (2, 2) and (1, 2)—in an obvious notation—determine the polarization parameters of both processes. The measurements of A and C determine all the η, κ and τ to within a number of discrete solutions§, for the Jacobian of the equations does not vanish in general.

† This notation is related to the angular momentum representation (e.g. Hamilton 1959) as follows $\langle\Omega_{11}\rangle = -i\tfrac{1}{2}\sqrt{3}\beta$, $\langle\Omega_{20}\rangle = (3/\sqrt{2})(\kappa\cos\theta + \tau\sin\theta - \tfrac{1}{3}\eta)$, $\langle\Omega_{21}\rangle = \sqrt{3}\ (\kappa\sin\theta - \tau\cos\theta)$, $\langle\Omega_{22}\rangle = -\tfrac{1}{2}\sqrt{3}(\kappa\cos\theta + \tau\sin\theta + \eta)$, where the y and z axes are along **N** and $\mathbf{k}_f$, and θ is the centre-of-mass scattering angle.

‡ This arrangement is being used by several groups working on d–α scattering. A range of angles is possible at the first scattering if the intermediate beam can be slowed. (Private communications from Dr. M. J. Scott and Dr. J. B. Reynolds.)

§ Only real solutions need be retained. The numerical solution of the equations probably needs an automatic computer.

Two measurements of B then give the parameters β. The third measurement of B over-determines the problem and reduces the number of solutions: we expect the solution to be unique apart from an overall sign for the parameters β and another for the η, κ and τ. Since there is always some experimental uncertainty in practice, it would be better also to perform the double scattering (2, 1) and to make a 'best fit' of the eight parameters to the twelve data. The ambiguities in sign can be settled if the scattering phase shifts are approximately known, as for instance in low-energy *d*–α scattering (Galonsky and McEllistrem 1955, Goldfarb and Rook 1959, Pondrom 1959, Phillips 1959).

For double scattering from heavy targets, on the other hand, we find

$$A=\tfrac{1}{2}tt', \quad B=\tfrac{2}{3}(uu'-vv'), \quad C=\tfrac{1}{6}ww' \qquad \ldots\ldots(6)$$

where

$$\left.\begin{aligned} &t=3\kappa\cos\theta+3\tau\sin\theta-\eta, \quad u=\tfrac{3}{2}\beta \\ &v=3(\kappa\sin\theta-\tau\cos\theta), \quad w=-3(\kappa\cos\theta+\tau\sin\theta+\eta). \end{aligned}\right\} \ldots\ldots(7)$$

The centre-of-mass angle θ is now also the laboratory angle; t, u, v and w are linearly independent combinations of β, η, κ and τ. If we have the same target and angle at both scatterings, t and w may be found to within a sign, but u and v cannot be separated. At first sight it seems we might determine them by taking three different processes (same energy but different angles or targets) and using the six possible combinations of first and second scatterings to find the six u and v. However, the bilinear form $u_iu_j-v_iv_j$ is unchanged by the simultaneous transformation

$$\left.\begin{aligned} u&\to u\sec\alpha+v\tan\alpha \\ v&\to u\tan\alpha+v\sec\alpha \end{aligned}\right\} \qquad \ldots\ldots(8)$$

for each pair, u, v (α being any angle). As long as we are restricted to simple double scattering, and none of the u or v are known in advance, there must remain an indeterminacy like this.

When a previously calibrated polarizer or analyser (labelled 2) is available, however, a given scattering process (labelled 1) can be determined directly without ambiguities of sign. The experiments (1, 1) and (1, 2) or (2, 1) are enough, whether the target nucleus in '1' is light or heavy. Calibrated nuclear reactions (Galonsky, Willard and Welton 1959, Goldfarb 1959) can also be helpful for measuring deuteron polarization.

R. J. N. Phillips.

Atomic Energy Research Establishment,
Harwell,
Didcot, Berks.

16th November 1959.

Galonsky, A., and McEllistrem, M. T., 1955, *Phys. Rev.*, **98**, 590.
Galonsky, A., Willard, H. B., and Welton, T. A., 1959, *Phys. Rev. Letters*, **2**, 349.
Goldfarb, L. J. B., 1959, *Nucl. Phys.*, **12**, 657.
Goldfarb, L. J. B., and Rook, J. R., 1959, *Nucl. Phys.*, **12**, 494.
Hamilton, J., 1959, *The Theory of Elementary Particles* (Oxford: Clarendon Press).
Lakin, W., 1955, *Phys. Rev.*, **98**, 139.
Phillips, R. J. N., 1959, *Phys. Rev. Letters*, **3**, 101.
Pondrom, L. G., 1959, *Phys. Rev. Letters*, **2**, 346.
Stapp, H. P., 1955, *Thesis*, University of California, UCRL-3098.
—— 1957, *Phys. Rev.*, **107**, 607.

REVIEWS OF BOOKS

Finite Difference Equations, by H. LEVY and F. LESSMAN. Pp. viii + 275. (London: Sir Isaac Pitman and Sons, 1959.) 37*s.* 6*d.*

The book starts with an elementary account of the properties of the finite difference operators E, Δ defined by the equations

$$Ef(x)=f(x+1)$$
$$\Delta f(x)=f(x+1)-f(x)$$

and of their applications in problems of the summation of series, interpolation, curve fitting by polynomials and numerical differentiation and integration. It continues with chapters on the origins, in the mathematical sense, of finite difference equations and on methods of solution of certain classes; there is one short chapter on applications in pure and applied mathematics including one example from the theory of sequential sampling.

The real purpose of much of the first part is not very clear, for whilst more is given than is needed to lay the foundations of the second part, there is not enough, nor is the tone right, to provide a satisfactory treatment of numerical techniques. The detail of the numerical work is certainly not that of the best modern practice; for example, central difference operators are never mentioned, nothing is said about the 'vanishing differences' in a table by means of which the accuracy of the entries can be judged, and in every table printed the differences are given not in the convenient form of integers in units of the last decimal, but with decimal points and all leading zeros. There is, in fact, a distinct academic air about all this. Thus while a good deal of attention is given to the summation of series which all look very much like examination questions, the important Euler transformation appears only as an example (on page 27) and even then is not mentioned by name. The notation is often confusing, thus expressions like

$$\sum_{1}^{n-1} y_n$$

appear throughout the book; this may not matter very much in single summations, but in multiple summations can cause great confusion, so that, as far as one can understand what is meant, the relations given in Example 2, page 20, seem to be wrong. There seems to be a serious mistake in the interpretation of the Euler–Maclaurin summation formula which expresses the definite integral as a discrete sum together with a series of 'correction terms' involving the derivatives of the integrand; this series terminates if the integrand is a polynomial, but otherwise is not in general convergent but has asymptotic qualities. By ignoring this fact the authors have invited the reader in Examples 3 to 6, page 62, to prove some relations which do not hold; a very simple calculation with six-figure tables will show that

$$\sum_{1}^{\infty} e^{-r^2}$$

is not in fact $\frac{1}{2}(\sqrt{\pi}-1)$.

The chapters on finite difference equations contain a lot of interesting material not readily accessible elsewhere; indeed, the authors say that much of this has never been published previously. Equations are considered in four classes: there is a first division into discrete and continuous independent variables and then into linear and non-linear forms. Thus typical linear first order equations with constant coefficients are

$$ay_{n+1}+by_n+c=0$$

for the discrete variable and

$$ay(x+1)+by(x)+c=0$$

with x a continuous variable. As would be expected, reasonably general results can be obtained for linear equations with constant coefficients, less so when the coefficients are not constant and still less for non-linear equations. There is an interesting semi-graphical treatment of the general first order equation and a treatment of linear equations by definite integrals. A large part of the text is taken up with special cases and the present reviewer found the arrangement rather confusing. General methods and important techniques do not stand out clearly from the mass of detail; the argument could often be shortened without loss of clarity and many of the examples are exceedingly trivial. The real importance of difference equations lies in practical uses of mathematics where often the numerical aspect dominates; in this book the flavour is much more academic, and the numerical properties of the recurrence relations are never discussed.

To sum up, the book provides a useful and interesting collection of information on a fairly elementary level, but would have benefited from a closer contact with practical numerical work. J. HOWLETT.

Optical Properties of Semi-conductors, by T. S. Moss. Pp. x+279. (London: Butterworths Scientific Publications, 1959.) 50*s*.

Dr. Moss' book is one of a new series of monographs on semiconductors. It is several years since he published *Photoconductivity in the Elements* which had a similar structure and so the appearance of the present volume is most welcome in view of the many recent advances in this field. As before, he presents his subject matter in two parts. In the first there is an extensive review of theoretical ideas on a wide range of optical and electrical phenomena in solids. Perhaps the two important chapters are that concerned with photo effects, e.g. photoconductivity, photovoltaic effect, Dember effect and photoelectromagnetic effect, and that dealing with emission of radiation from semiconductors. This part of the text is valuable because it provides an idea of current perspective and of the co-ordinating features of modern semiconduction research.

In the second section of the book, attention is concentrated on specific semiconductors, including elemental solids and the most important photoconducting compounds, such as those of the III–V and II–VI elements and the sulphide, selenide and telluride of lead. It is rather a pity that considerable condensation of material has been forced upon the author because of a restricted length of text, for it is necessary to follow up the references provided to obtain a complete picture of the state of knowledge in each case. This is particularly true of the chapter on the zinc sulphide group of photoconductors. However, references are up-to-date, a very commendable feature.

One very important aspect of the field is missing from the book and it might well provide the basis of a separate volume, if possible from the same author's pen. It is a detailed and critical account of the many and varied techniques involved in experimental investigations. Otherwise the book will be a welcome addition to the shelves of solid state and other scientists. G. F. J. GARLICK.

Semiconductors, edited by N. B. HANNAY. Pp. xxiii + 767. (New York: Reinhold.) £6.

This symposium of papers is subtitled 'a definitive new work on principles, phenomena and materials'. A book of this kind should meet two principal objectives, that of informing the newcomer of the present state of the subject and that of aiding the extension of our knowledge to substances and phenomena which are not yet familiar. The first objective is satisfied in high measure, the second extremely well.

The editor contributes an introductory chapter on semiconductor principles which maintains a very high didactic standard. With one or two reservations (e.g. concerning the spin correction of the carrier concentration at impurity levels and the treatment of the carrier injection concept), it should serve the average reader for whom the book is intended very well. The same applies to the second introductory chapter by J. J. Lander which is concerned with a survey of semiconductor chemistry and with the formation of crystal imperfections. This is followed by two superb chapters on the growth of single crystals (by M. Tannenbaum) and on impurity control by freezing methods (by C. D. Thurmond) including, of course, zone melting, rate growing, and remelt procedures. These treatments include extensive descriptions of methods which are not generally known, with informative emphasis on the fundamental processes involved. C. S. Fuller contributes a chapter on defect interaction in which he considers, amongst other things, the analogies between impurity semiconductors and aqueous solutions containing a weak electrolyte. Germanium and silicon are, of course, stock examples since these materials have been produced in the purest and most perfect form and have received the most detailed study. T. H. Geballe gives an extensive high-level survey of their electronic properties and J. N. Hobstetter deals with theoretical and experimental aspects of dislocations, including the effects of bombardment, deformation and quenching. H. Reiss and C. S. Fuller discuss diffusion problems on which so much of present device fabrication depends. Certain Group II–IV compound semiconductors are dealt with by D. G. Thomas, with special reference to the work carried out in Holland, and by A. R. Hutson who includes accounts of polaron behaviour and of the idiosyncracies of non-single-crystal samples. Alas, zinc sulphide is not included; as principal electroluminescent material it would have been very interesting. J. M. Whelan gives a short but informative account of Group III–IV compounds and various other mainly covalent materials.

Infra-red absorption has long been used as an important investigational tool, and H. J. Hrostowski contributes a chapter on this topic in which he also deals with free charge carrier absorption and infra-red cyclotron resonance. Problems and results concerning recombination and trapping are briefly surveyed by R. G. Shulman and there is also a chapter by F. J. Morin on the interesting properties of the oxides formed by 3d transition metals. C. G. B. Garrett's account of organic semiconductors is believed to be the only systematic summary now available. It serves to illustrate the complexities of the subject and to foreshadow some of its potentialities. The general importance of surface properties has been increasingly recognized during the last few years and J. T. Law gives a selective survey. There is also a chapter on semiconductor electrodes by J. F. Dewald, interesting for its relevance to etching processes.

It has obviously been necessary to limit the subject matter, and such topics as contact rectification, junction breakdown, parametric amplification and electrical noise are not dealt with. The amount of overlap between chapters has been kept low. The book can be widely recommended, the only major regret being its price. H. K. HENISCH.

Principles and Applications of Random Noise Theory, by J. S. BENDAT. Pp. xxi +481. (New York: John Wiley and Sons, 1958.) 88*s*.

The term 'random noise' was originally introduced by the electrical communication engineers to describe the random component of the time variation of electric current or voltage, superimposed over a regular 'signal' and thus more or less impeding communication by means of electric signals. In a wider sense it is nowadays frequently applied to all kinds of random or 'stochastic' processes in physics, engineering, meteorology and even economics.

In the present book the author in the first place sets himself the task to develop the theory of stochastic time series in such a way that it can be applied to all such phenomena and to present it in a language familiar to engineers. Only a modest mathematical knowledge is required and the reader is not supposed to have any previous experience in probability theory and the technique of Fourier and Laplace transforms. The author further develops the mathematical methods for the statistical analysis of random processes and the design of 'filters' for obtaining the least distortion of the signals by noise, and he also describes certain analogue computer devices for solving the mathematical problems involved.

Special items of particular interest are dealt with in some detail, in particular, random noise with 'exponential cosine autocorrelation functions', the statistical properties of the 'envelope' of noise which has passed through a narrow filter and the so-called 'zero-crossing problem', the derivation of formulae for estimating the statistical errors in the evaluation of the statistical parameters of random time series, problems to the solution of which the author has himself made important contributions.

The book is well written and the readers will have no difficulty in following the mathematical arguments which are presented in considerable detail and, in general, with sufficient rigour. There are a number of points on which one can take issue with the author, for example on the use he makes of the central limit theorem in cases where its application is not justified and in fact the noise is known to be non-Gaussian in character, and further on, the way in which derivatives of stochastic functions are treated as if they were derivatives of ordinary functions in the strict mathematical sense. It is also regrettable that almost exclusively American publications are quoted and no publications at all in other than the English language, making it appear as if this subject had been developed entirely in the U.S.A.

Nevertheless, the book can be highly recommended to all practical workers in fields where 'noise' is involved, and also to students who wish to acquire knowledge in this important field. R. FÜRTH.

Exploring the Structure of Matter, by JEAN-JACQUES TRILLAT. Pp. 214. (London: George Allen and Unwin, 1959.) 30*s*.

This book, which is addressed to the layman or non-specialist physicist, is a translation of the author's *Découverte de la Matière* published in 1956. It is concerned with the methods used for studying the fine structure of matter. The first part describes X-ray and electron microradiographic techniques based on a × 600 optical enlargement of a contact radiograph. Subsequent parts of the book deal with electron microscopy, electron diffraction and neutron diffraction. Each part starts with an account of the principles involved and a description of the apparatus and concludes with examples, profusely illustrated with plates, of the technique. The subject matter is competently handled, but the translation is not above reproach. In a few places, the meaning is definitely obscure. Technical terms are often mis-translated (e.g. *weak* instead of *soft* X-rays; *node* instead of *lattice point*). References to figures do not appear to have been properly checked. Thus, Plate XXIII B referred to on p. 188 as a neutron, and on p. 208 as an X-ray diffraction pattern; and the legend of figure 5 does not precisely agree with the figure. In spite of these blemishes, the book gives in a small compass a good indication of the aims of an important branch of physics. T. B. RYMER.

Handbuch der Physik, Vol. LIII, *Astrophysik* IV, *Sternsysteme*, edited by S. FLÜGGE. Pp. viii + 565. (Berlin : Springer, 1959.) DM 142.

Though astronomy in both the technique and the interpretation of its observations is completely dependent on physics, only infrequently, other than as a background, does it make any significant contribution to the body of physical knowledge. So substantial, however, has been the growth of astronomy in the last fifty years that we may well be entering a period when a detailed study of the subject will repay the physicist. Presumably with this in mind the new edition of the *Handbuch der Physik* will contain several volumes devoted to astronomical topics.

The volume under review is concerned with systems of stars, and is apparently intended to be both an introduction for physicists and an account of the most recent advances for astronomers. It may be said at once that it succeeds better in the latter than the former respect. What is lacking for the physicist is an introductory article which sets out concisely present knowledge of the structure, kinematics and dynamics of our own galactic system and gives some account of the methods by which this knowledge has been gained, as well as briefly reviewing our much sketchier information about external galaxies with their differences in stellar population and their multiplicity of forms. Without such a guide, confused indeed will be the ordinarily intelligent reader who strives to master the whole of this volume.

Several articles in the volume, however, can be recommended without reservation to astronomers and physicists alike. Thus McVittie's account of Distance and Time in Cosmology provides a badly needed critical assessment of photometric methods of distance determination, an assessment which brings out the large uncertainty inherent in all distances beyond the trigonometric range. Likewise Hanbury Brown on Discrete Radio Sources provides a balanced and informative account of a problem bristling with difficulties but full of promise as providing a means of exploration beyond the optical range. On the other hand there are some articles which are mere bibliographies and which obscure for the reader the great classics of astronomical discovery. At best the remaining articles, with one or two exceptions (for example Heckmann and Schücking on Newtonian and Einsteinian Cosmology), have much more the character of contributions to a symposium, surely the most ephemeral of scientific literature, rather than of those permanent contributions of knowledge such as Rayleigh's encyclopaedia articles and many of the articles in the first edition of the *Handbuch*. H. H. PLASKETT.

Group Theory and its Application to the Quantum Mechanics of Atomic Spectra, by E. P. WIGNER. Pp. xi + 372. (New York: Academic Press Inc., 1959.) $8.80.

The German original of this book was first published in 1931. Since then the author must surely have been inundated with requests for a translation, and there is probably no other work for the understanding of which more young English-speaking quantum theorists have struggled through courses of scientific German ! It is of course a classic and even to-day the translation will be extremely welcome.

As an exposition of the principles of group theory in the form needed in physics the book has not dated at all and the fact that, as the title indicates, the applications are confined to the quantum mechanics of atomic spectra only slightly diminishes its usefulness to those interested primarily in other fields, e.g. nuclear theory.

It may astonish to see such modern ideas on the role of symmetries in quantum theory emerging in a text which at the same time shows some amusing traces of its antiquity : few present-day students will recognize ' Schrödinger's equation ' in the original form given here ! In the main, however, the text of the original needed no emendation, except in so far as the abandonment of the left-handed coordinate system has happily brought all sign conventions into line with current usage. Three new chapters have been added; one on Racah coefficients and the like, bringing formal development up to date, a second, most notably, which expounds the author's important, more recent, work on the time inversion operation and a third final chapter on the physical interpretation of various group theoretically defined quantities, which well deserves careful study. Undoubtedly this new ' Wigner ' will carry on the reputation of its predecessor. N. KEMMER.

Causality, by MARIO BUNGE. Pp. xx + 380. (Cambridge, Mass.: Harvard University Press; London : Oxford University Press, 1959.) 60*s*.

" An essay on determinism, with special emphasis on causal determinism—or causality, for short." The author analyses causality as it is actually used in various sciences, particularly physics. He concludes that " the causal principle is neither a panacea nor a superstition ", but " a philosophical hypothesis employed in science " of " an approximate validity . . . in competition with other principles of determination ". But his conclusion is far less interesting for the working scientist than the path leading to it. A short review can give no idea of the richness of these closely packed pages. The first part of the book clarifies the meaning to be given to causality, determinism and related words, and surveys the formulation of the causal principle. Part 2 explains what causality is not contrary to the assertions of various empiricists it does not by itself involve contiguity or antecedence, it is not merely identical with invariable succession in time and it is not just what is mirrored by differential equations. Contrary to the romantic views it is not merely interdependence, does not imply the 'block universe' of complete interconnection, and need not be fatalistic, nor mechanistic.

Part 3 explains what causality does assert; it involves linearity (i.e. 'multiple causation' is rejected as not strictly causal), an artificial isolation, either a first cause or an infinite regress, and continuity. It neglects the response of the system, involves superposition of causes and renders genuine novelty impossible. The last part (over 100 pages) examines in detail the status of causality in modern science; a summary is impossible. (The discussion of quantum mechanics accepts Bohm's presentation a little uncritically.)

Such a book must contain much to disagree with; its success is measured by how much one feels the trouble of disagreement is made worth while by the rest of the book. One reads with the continual desire to re-write, though altering little, but with a complete lack of the author's wide learning. C. W. KILMISTER.

Handbuch der Physik, Vol. LII. *Astrophysik* III, *Das Sonnen-system*, edited by S. FLÜGGE. Pp. vii + 601. (Berlin : Springer, 1959). DM. 148.

Although this is the only volume of the Encyclopedia concerned with the solar system, most of it is taken up with a series of articles on solar physics, excluding the interior of the sun. Apart from a chapter by F. J. Kerr, optimistically entitled 'Radar reflections from sun, moon, and planets'—reflections have been obtained only from the moon so far—the remainder of the text is divided between articles on planetary atmospheres and interiors by H. C. Urey and S. C. de Marcus, and comets and meteors by K. Wurm and F. L. Whipple.

Most of the text is taken up with surveys of recent advances rather than the basic groundwork so that this *Handbuch* has very little in common with its predecessor of a quarter of a century ago. Solar physics in particular has advanced rapidly in the intervening years, quite apart from the increased knowledge resulting from the application of rockets and satellites. The masterly survey of solar physics, chiefly by C. de Jager, who has himself contributed so much to the subject, is therefore especially welcome. Inevitably, there are some mistakes. It is particularly unfortunate that von Klüber, in his pioneering interferometric work on the width of the coronal emission lines is credited with a resolving power of only 2600 instead of 26 000. This article is well illustrated with the remarkable photographs taken by R. B. Dunn at the Sacramento Peak Observatory, and other workers. A comprehensive account of the solar photosphere by L. Goldberg and A. K. Pierce completes the section on solar physics.

It is a disturbing, although understandable, feature of the book that it is concerned almost entirely with the work of Western astronomers. The important contribution of the Russian astronomers to coronal studies for example, is clear from Shklovskii's book on the solar corona published in 1951, and it is a pity that so much of this work has to be overlooked in an authoritative work of this kind. Some authors virtually ignore the Russian contributions to their subjects.

All of the articles are in English with the exception of that by K. Wurm on comets, which is in German; the standard of English of one article is rather low. There are two full subject indexes, one in English and one in German, but no author index. D. E. BLACKWELL.

Statistical Physics. Vol. 5. *Course of Theoretical Physics*, by L. D. LANDAU and E. M. LIFSHITZ. Translated by E. PEIERLS and R. E. PEIERLS. Pp. x + 484. (London, New York, Paris, Los Angeles: Pergamon Press, 1958.) 80*s*.

This book, the second volume to appear in English translation of the authors' comprehensive Course of Theoretical Physics, effectively replaces their earlier work with the same title (Clarendon Press, 1938), while adding greatly to its scope and usefulness.

The earlier book became well known as an almost unique source, at that time and at textbook level, for a thorough discussion of thermodynamic stability, critical phenomena, and the Einstein–Smoluchowski theory of statistical fluctuations. With very few exceptions (sections on convection, Bernoulli's equation, and a rather full treatment of Liouville's theorem have been omitted), everything in that book is to be found in this one: seldom seriously changed, though with a new recognition of the uncertain validity of thermodynamic expansion methods near critical lines and points.

But whereas previously the statistical theory was confined to the Boltzmann distribution, indeed to classical mechanics, in the present work quantum mechanics is taken as basic. Thus the specific heats of diatomic gases, electronic specific heats, and black-body radiation, excluded from the earlier work, are now discussed in some detail: so also are less familiar topics, as superfluidity, negative temperatures, and the properties of matter at very great temperatures and pressures. Electric and magnetic properties are omitted, to be dealt with in another volume of the series.

The result is a stimulating book and, in conjunction with the other volumes of this series, undoubtedly a useful one. Taken by itself, it is neither an introductory nor a comprehensive course in statistical thermodynamics. It is not particularly easy reading, more references would have been welcome, and there are some oddities of thermodynamic notation (not present in the earlier edition). More seriously, perhaps, a rather strange feature is the virtually complete absence of comparison between theory and experimental measurements. Possibly an equally thorough knowledge of experimental physics is presupposed: but the usefulness of statistical theory as a working tool (as in the comparison of spectroscopic and calorimetric entropies) is never illustrated. Nevertheless, there is a grandeur of outlook and wealth of incidental wisdom which compensate for many lesser things: and no student, of reasonable ability, will waste his time in reading it. Indeed, one is tempted to add, every postgraduate theoretical physicist ought to be reading the complete Course, as it appears. G. S. R.

Liquids and Liquid Mixtures, by J. R. ROWLINSON. Pp. ix + 360. (London: Butterworths Scientific Publications, 1959.) 75*s*.

This book deals with the equilibrium properties, particularly the (p, V, T) relationships and heat capacities, of non-electrolytic solutions and the corresponding pure liquids. It does not deal with transport coefficients, nor with such liquids as molten metals. Polymers are also deliberately excluded. But within this useful, if restricted, field it is a mine of reliable information, critically examined, and of indispensable references, carefully compiled. Written with chemical engineers in mind, as well as physicists and chemists, it is likely to prove popular, at both textbook and reference levels, with a wide audience.

The author has divided the work into three, roughly equal, sections, each of three chapters: the first two parts concern pure liquids and liquid mixtures, respectively, and contain almost no theory other than thermodynamics. They are largely concerned with a critical appraisal of experimental results. The last section, which is more mathematical, introduces intermolecular forces and statistical mechanics. But after this brief indication of the scope of the book, it is convenient to discuss the three parts separately.

In view of the achievements of the present decade, in predicting the properties of mixtures from those of their pure components through a somewhat sophisticated theory of corresponding states, demanding accurate knowledge of the thermodynamic properties of suitable reference substances, it is natural that the author should first survey the properties of pure liquids, paying particular attention to the reliability, and mutual consistency, of experimental measurements. The result is an invaluable and comprehensive compendium of our present calorimetric knowledge of pure liquids and, to a lesser extent, dense gases. The complicated specific heat anomalies in the neighbourhood of the critical point, not yet perhaps fully explored, are very carefully discussed, together with their bearing on ultrasonic absorption.

The second part of the book, on liquid mixtures, is equally lucid and well balanced. Paying particular attention to excess functions, the author considers mixtures of increasing complexity, from condensed non-polar gases to hydrogen-bonded structures, first at low pressures and then at high pressures, in which connection there is a very thorough and detailed survey of azeotropy. As it proceeds, this middle part of the book becomes increasingly technical and condensed, but it remains much more than a mere guide to the relevant literature. The reviewer's only adverse criticism concerns the absence of any indication of the extent to which the survey of calorimetric measurements of the highest accuracy has been selective: it is certainly not complete, the much studied benzene–diphenyl system for example receives no mention. And the author's concern, expressed in the preface, to keep to a minimum material that can readily be found elsewhere, is hardly an adequate guide.

Finally, we have three more theoretical chapters, on inter-molecular forces, pure liquids, and liquid mixtures, respectively. They are all highly condensed, but become increasingly so, to the point of unintelligibility. They remain, of course, a very good guide to the literature, and the chapter on pure liquids is balanced and by no means unreadable. It is the last chapter, on mixtures, that the reviewer found disappointing. He is aware that this is subjective and perhaps not entirely fair criticism, but this chapter is so highly condensed and erudite that it is singularly hard to see the wood for the trees: the Appendix hardly helps. That it should deal entirely with modern extensions of conformal solution theory is entirely proper and in keeping with the plan of the book as a whole: but to attempt this in three dozen pages was an impossible task. Anyone who has not read Prigogine's *Molecular Theory of Solutions* should first do so, and proceed to the papers by Scott and W. B. Brown. The present account avowedly owes much to Brown's work, and incorporates the author's own recent applications of the theory. If it whets the appetite it will serve a most useful purpose: but in itself it is too indigestible to be entirely satisfying.

The production of the book is excellent, and there are few printing errors.

G. S. R.

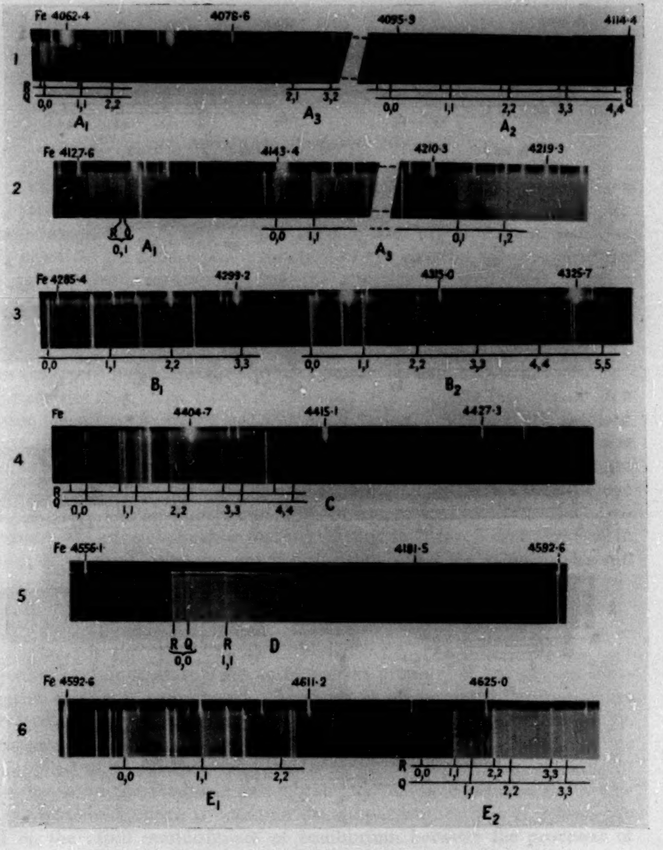
1
Fe 4062·4
4078·6
4095·9
4114·4
R
Q
0,0
1,1
2,2
A1
2,1
3,2
A3
0,0
1,1
2,2
3,3
4,4
R
Q
A2
2
Fe 4127·6
4143·4
4210·3
4219·3
R Q
0,1
A1
0,0
1,1
A3
0,1
1,2
3
Fe 4285·4
4299·2
4315·0
4325·7
0,0
1,1
2,2
3,3
B1
0,0
1,1
2,2
3,3
4,4
5,5
B2
4
Fe
4404·7
4415·1
4427·3
R
Q
0,0
1,1
2,2
3,3
4,4
C
5
Fe 4556·1
4181·5
4592·6
R Q
0,0
R
1,1
D
6
Fe 4592·6
4611·2
4625·0
0,0
1,1
2,2
E1
R
Q
0,0
1,1
2,2
3,3
1,1
2,2
3,3
E2

Figure 1. The spectrum of NiCl; 21 ft grating spectrograms.
Strips 1 and 2; systems A_1, A_2 and A_3.
Strip 3, $\Delta v = 0$ sequences of systems B_1 and B_2.
Strip 4, $\Delta v = 0$ sequence of system C.
Strip 5, $\Delta v = 0$ sequence of system D.
Strip 6, $\Delta v = 0$ sequences of systems E_1 and E_2.

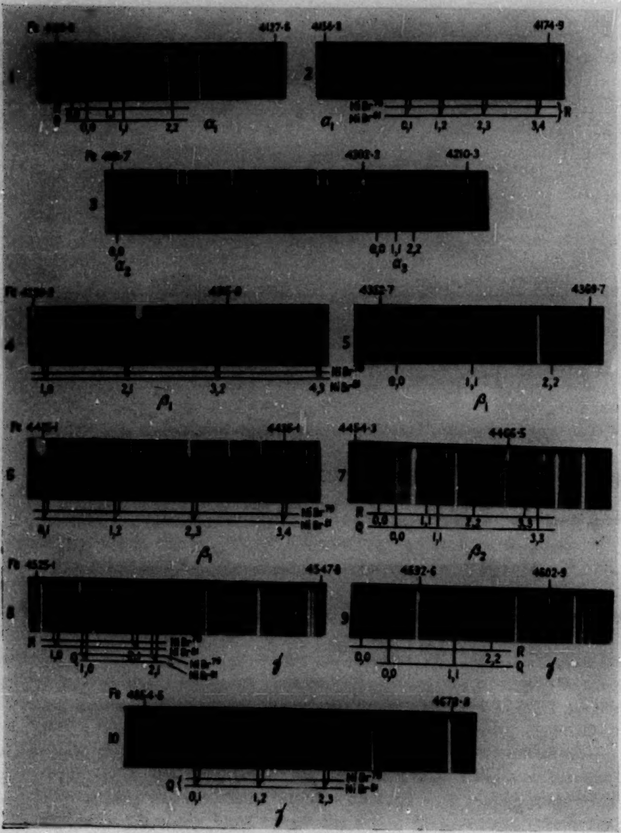
4127·6
4156·8
4174·9
4202·2
4210·3
4362·7
4369·7
4454·3
4466·5
4436·1
4602·9
NiBr^{79}
NiBr^{81}
R
Q
α_1
α_2
α_3
β_1
β_2
γ

Figure 2. The spectrum of NiBr; 21 ft grating spectrograms.
Strips 1 and 2, system α_1.
Strip 3, $\Delta v=0$ sequences of systems α_2 and α_3.
Strips 4, 5 and 6, system β_1.
Strip 7, $\Delta v=0$ sequence of system β_2.
Strips 8, 9 and 10, system γ.

The Measurement of Electron Temperature in High Temperature Plasmas

By R. V. WILLIAMS and S. KAUFMAN†

Research Laboratory, Associated Electrical Industries Limited,
Aldermaston Court, Aldermaston, Berks.

MS. received 14*th September* 1959

Abstract. The method is based on the simplifying features of helium-like ions and on the rapid establishment of equilibrium between the processes of populating and de-populating the 2^3P_2 level. The specific intensity of the emission line 2^3S_1–2^3P_2 can then be deduced as a function of the electron temperature. In order to test the basic assumption that the electron velocity distribution is Maxwellian for the very fast electrons which produce the atomic excitation, more than one member of the iso-electronic sequence must be studied. Also, an expression containing the relative emission from two members of the sequence eliminates the electron concentration which can only be estimated at present.

The intensities of C V and B IV lines from SCEPTRE IIIA were measured with a combination of a monochromator and a photomultiplier. A carbon arc was used to calibrate the intensities absolutely, and the spatial intensity distribution was determined by means of the Abel integral equation. For typical discharge conditions, the maximum electron temperature attained was in the range $(2–3) \times 10^5$ deg K. The electron temperature was unaltered by the introduction of the methane. The results suggest that any existing departure from a Maxwellian distribution of electron velocities did not seriously affect the value of electron temperature derived by this method.

§ 1. INTRODUCTION

THE electron temperature T_e is an important property of any plasma irrespective of how it is produced. Methods of measuring or estimating the electron temperature include the use of microwave probes, spectroscopy, bremsstrahlung, Langmuir probes and the electrical conductivity. Spectroscopic methods applied to an optically thin plasma as existing in ZETA and SCEPTRE III cannot be based on the establishment of thermodynamic equilibrium. A new spectroscopic method, which is based on the simplifying features of helium-like ions and on the rapid establishment of equilibrium between the processes of filling and emptying the 2^3P_2 level of this ion, has been reported in a preliminary account (Kaufman and Williams 1958).

The deduction by this method of an electron temperature of about $2{\cdot}5 \times 10^5$ deg K in SCEPTRE III assumes that the distribution of electron velocities is Maxwellian, even at energies exceeding the high excitation potential of C V, namely, 304 ev. The very existence of a plasma current implies a perturbation of the velocity distribution function which, in this case, may have been serious because X-rays produced by energetic electrons have been detected. Thus, the principal aim of the present investigation was to test the character of the distribution function by studying another member of the He I iso-electronic sequence for which the appropriate excitation potential is less than that of C V. Also, it would be possible to determine the electron temperature without the need to estimate the electron concentration, as was previously necessary.

---

† Now at Department of Physics, Hebrew University, Jerusalem, Israel.

Three comparative values of electron temperature have been evaluated from the measured intensities of C V and B IV lines emitted from SCEPTRE IIIA (Ware 1959) under typical operating conditions, and they are in agreement within the range (2–3) × 10^5 deg K. The results suggest that any existing departure from a Maxwellian distribution of electron velocities has not seriously affected the value of electron temperature derived by this method.

The assumption that the addition of methane to the deuterium does not alter the electron temperature has been verified experimentally. It is also assumed that the presence of the spectroscopic viewing window has not disturbed the plasma. In the main, repetition of the earlier paper is avoided but some aspects which were briefly reported before are now elaborated.

§ 2. THEORY

We suppose that the 2^3P_2 level of a helium-like ion is filled entirely by electronic excitation from the ground-level 1^1S_0 (population N_1) at a rate q, and that de-excitation from this level takes place solely by the radiative transition 2^3S_1–2^3P_2. The spontaneous transition probability for this emission line is at least 10^7 sec^{-1} depending on the helium-like ion selected. Hence, after about 10^{-7} sec an equilibrium between these two processes is established. The rapid attainment of equilibrium is important in high-current discharges like SCEPTRE where the duration of the complete current pulse is only about 1 msec.

The rate

$$q = N_1 Q_{12} \int_{v_{12}}^{\infty} v f(v)\, dv,$$

where $f(v)$ is the electron velocity distribution function and v_{12} the electron velocity corresponding to the threshold energy E_{12}. The cross section Q_{12} for excitation of the 2^3P_2 level from the ground level by electron impact is finite at the threshold energy (Seaton 1958) and is regarded as invariant with energy above threshold. The specific intensity I of the emission line is $q\boldsymbol{h}\nu$ where $\boldsymbol{h}$ is Planck's constant and ν the frequency of the line. On the supposition that the velocity-distribution function is Maxwellian,

$$I = 2\left(\frac{2\boldsymbol{k}T_e}{\pi \boldsymbol{m}}\right)^{1/2} N_1 n Q_{12} \boldsymbol{h}\nu \left(1 + \frac{E_{12}}{\boldsymbol{k}T_e}\right) \exp\left(-\frac{E_{12}}{\boldsymbol{k}T_e}\right) \qquad \ldots\ldots(1)$$

where $\boldsymbol{m}$ is the electron mass, $\boldsymbol{k}$ Boltzmann's constant and n the electron concentration.

If we consider a second helium-like ion (with primed symbols) then,

$$\frac{I'}{I} = \frac{N_1' Q_{12}' \nu'}{N_1 Q_{12} \nu} \frac{1 + (E_{12}'/\boldsymbol{k}T_e)}{1 + (E_{12}/\boldsymbol{k}T_e)} \exp\left(\frac{E_{12} - E_{12}'}{\boldsymbol{k}T_e}\right) \qquad \ldots\ldots(2)$$

and the electron concentration is eliminated. Through the use of two helium-like ions, three comparative values of electron temperature can be derived from equations (1) (two values) and (2). Only the ratio of intensities need be known when applying equation (2).

§ 3. EXPERIMENTAL ARRANGEMENT

The two helium-like ions selected were C v and B iv. As previously reported, methane proved to be a satisfactory carrier for the carbon. The boron was introduced into the torus of SCEPTRE IIIA in the form of diborane. This gas requires very careful handling; it is very toxic and must be excluded from contact with air (Schechter, Jackson and Adams 1954). Earlier attempts to introduce the boron in the form of boron trifluoride were spoilt by the interference of the relevant B iv spectral line with a F iv line. The ionization-gauge sensitivity factors for methane and diborane relative to nitrogen are 0·71 (the same as argon) and 3·5 respectively.

The C v and B iv lines corresponding to the transition 2^3S_1–2^3P_2 are at 2270·91 Å and 2821·68 Å (Edlén 1934) respectively. The specific intensity of each line was conveniently measured with a Hilger quartz monochromator (focal ratio f/7) to which was attached a photomultiplier. The photomultiplier signal was displayed on a twelve-channel oscillograph concurrently with the electrical parameters of the discharge, so as to provide the necessary temporal resolution. The C v and B iv emissions were not confined to one region of the plasma and so it was necessary to determine the spatial intensity distribution of each line. This was obtained by scanning the length of the vertical viewing window on SCEPTRE (Allen *et al.* 1958) with an aperture of height 1·2 cm, and the resultant intensity distribution was converted to a radial distribution by use of the Abel integral equation (Meek and Craggs 1953).

Table 1. Variation of Cv Intensity with Methane Content

Measurement Sequence	3	1	6	4	2	7	5
p'	3·5	4·8	5·5	7·1	7·9	9·5	12
I (arbitrary units)	2·9	4·0	7·0	4·6	6·9	6·9	9·9
α	0·97	0·97	1·5	0·75	1·0	0·86	0·95

p', partial pressure of methane expressed as a percentage of the deuterium pressure. α, I/p' expressed as a fraction of the mean I/p' of the seven readings.

The monochromator–photomultiplier combination was calibrated for absolute intensity measurement with the aid of a carbon arc run under standard conditions (MacPherson 1940). The values accepted for the emissivity and temperature of the positive crater were respectively 0·98 and 3804 °K (Null and Lozier 1958), and a correction factor of 2 was applied to the intensity of the C v line to account for the apparent departure from grey-body radiation at this wavelength (Johnson 1956).

§ 4. RESULTS

The specific intensities of the C v and B iv lines were measured on consecutive days under as nearly as possible the same discharge conditions, namely, deuterium at a pressure of 1·8 millitorr, the capacitor bank charged to 25 kv, turns ratio 16 : 1, initial toroidal magnetic field of 500 oersteds and a peak gas current of $7{\cdot}5 \times 10^4$ amp. The intensities quoted in table 1 were measured at a time 0·35 msec after the initiation of the discharge and for a volume 1·6 cm^3 of cross section $(2{\cdot}5 \times 2{\cdot}5)$ cm^2 about the torus axis. This time was close to peak excitation of the C v, B iv and also O V lines. Because the oscillograms of light intensity showed high-frequency fluctuations superimposed on the main waveform, the oscillograms for ten discharges were superimposed on a single plate (see figure 1). In this way it was possible to obtain a mean value for the intensity independent of the fluctuations.

The spatial intensity distribution of the B IV emission is shown in figure 2; the C V emission shows a similar distribution. The electron concentration was estimated to be 7×10^{14} cm^{-3} in the following way. The deuterium was considered fully ionized with a particle concentration corresponding to the initial gas pressure. Allowance was made for plasma compression by determining the enhancement of the toroidal field from magnetic probe measurements, and for contamination of the plasma by 10% impurity of mean ionic charge 5. The best estimate (M. J. Seaton, private communication) of the magnitude of the cross section Q_{12} for both C V and B IV, namely $0{\cdot}2\,\pi a_0^2$, has been accepted until a more reliable value will be forthcoming from wave-mechanical calculations. The estimates of N_1 and N_1' were obtained by making assumptions of complete ionization and compression similar to those for the estimate of the electron concentration. In addition, it was supposed that all the carbon and boron atoms at the torus axis were in the respective ground levels of C V and B IV. The spatial intensity distributions of B III (ionization potential 37·9 ev) and B IV as shown in figure 2 are a convincing demonstration of the validity of this assumption for B IV. It was not possible to obtain the C IV intensity distribution because of interfering lines, but from an examination of the O III (2984 Å), O IV (3381 Å) and O V (2781 Å) spatial distributions it was inferred that most of the carbon atoms were raised to the ground level of C V.

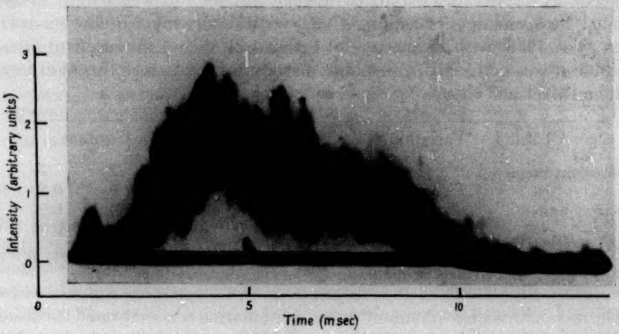

Figure 1. Oscillographic record of C V (2271 Å) intensity. Ten discharges superimposed. Duration of first half-cycle of current: 0·9 msec.

The possibility that the introduction of the methane could have affected the electron temperature (for example, by increasing the energy loss from the plasma by means of spectral line radiation) was checked by observing the C V emission for various partial pressures of methane up to 12% of the deuterium pressure. The results (table 1) give no indication of the electron temperature having been altered by the introduction of the methane. This test also proves that interference from

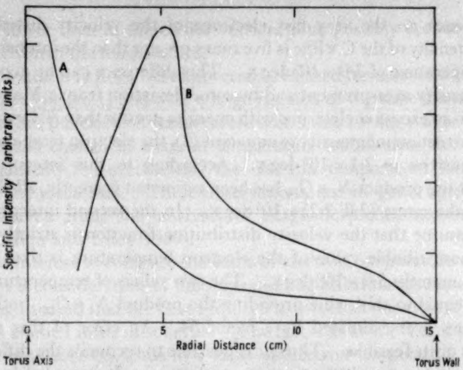

Figure 2. Spatial intensity distribution of B IV and B III lines.
A: B IV, 2822 Å; B: B III, 2066 Å.

the neighbouring Cu III line 2271·69 Å which was observed on some spectrograms was not serious. A similar check has not yet been performed with the diborane.

The close agreement between the two values of electron temperature (table 2) from the independent intensity measurements of the B IV and C V lines suggests that, in the respective excitation of these lines, the number of electrons with energies greater than 203 eV and 304 eV is approximately that given by a Maxwellian distribution of velocities. At first sight the value of electron temperature derived

Table 2. Values of Electron Temperature

Ion	E_{12}(eV)	p (torr)	N_1(cm^{-3})	I(erg cm^{-3} sec^{-1})	T_e(°K)
C V	304	$1{\cdot}1\times10^{-4}$	1×10^{13}	9×10^{2}	$2{\cdot}2\times10^{5}$
B IV	203	$2{\cdot}1\times10^{-4}$	6×10^{13}	1×10^{5}	$2{\cdot}0\times10^{5}$
B IV/C V (relative intensities)					$3{\cdot}0\times10^{5}$

p, partial pressure of impurity (methane or diborane).

from equation (2) might be regarded as the most acceptable of the three from the following considerations. The electron concentration need not be known. The error is reduced by employing the relative magnitudes of Q_{12} and Q_{12}' rather than their absolute values which are only estimates. There is likewise less error in using the relative magnitudes of N_1 and N_1': the possible factors which may lead to errors by expressing N_1/N_1' as the ratio of the initial partial pressures of carbon to boron, are the differences in ionization potential between C IV and B III, and in dissociation rates of methane and diborane by electron impact. However, it should be borne in mind that the exponential factor in equation (2) is much less sensitive to changes in the electron temperature compared with that in equation (1). Hence, some departure from a Maxwellian velocity distribution can be expected to influence markedly the value of the electron temperature derived from equation (2). This is demonstrated by the first of two interpretations of the results which follow.

There is a greater likelihood that the electron temperature derived from the B IV emission is nearer to the truth than that from the C V emission, because there is less dependence on the very fast electrons of the velocity distribution. The measured intensity of the C V line is five times greater than the intensity given by an electron temperature of $2{\cdot}0 \times 10^5$ deg K. This difference can be accounted for by errors in intensity measurement and by some deviation from a Maxwellian distribution due to an excess of electrons with energies greater than 304 eV. Thus, if we apply this correction in intensity to equation (2), the electron temperature from the relative intensities is $2{\cdot}1 \times 10^5$ deg K. According to this interpretation which assumes that the product $N_1 n Q_{12}$ has been estimated correctly, all three temperatures are in the range $(2{\cdot}0\text{–}2{\cdot}2) \times 10^5$ deg K. In the second interpretation of the results we assume that the velocity distribution function is strictly Maxwellian. Then the most reliable value of the electron temperature is that derived from equation (2), namely $3{\cdot}0 \times 10^5$ deg K. The two values of temperature from equation (1) are equal to this value providing the product $N_1 n Q_{12}$, both for C V and B IV, has been over-estimated by a factor 54. An error of this magnitude in estimation is quite feasible. Thus, it is possible to reconcile the differences in the results by two extreme alternative interpretations. It is probable that the discrepancy can be accounted for by a combination of these two factors, that is, a smaller departure from a Maxwellian distribution and a smaller error in the estimation of the product $N_1 n Q_{12}$. At this stage it is impossible to be more precise and we conclude that the maximum electron temperature attained in SCEPTRE IIIA most probably lies in the range $(2\text{–}3) \times 10^5$ deg K.

§ 5. DISCUSSION

The discussion in the earlier paper of the competing processes which fill and empty the 2^3P_2 level of C V can be extended to the case of B IV. If we suppose that excitation from the 2^3S_1 level by electron impact is the principal means of filling the 2^3P_2 level, then the electron temperature from the B IV emission is little altered. Just as for C V, super-elastic collisions from the 2^3P_2 level are unimportant. We also neglect absorption of the line $2^3S_1\text{–}2^3P_2$ in the plasma for both C V and B IV. Excitation by ions is also neglected for, in general, very much greater ion energies relative to the electron energy would be needed to be of any significance. Even if we accept the Doppler broadening of spectral lines to be due entirely to temperatures of several million degrees Kelvin (Hughes and Kaufman 1959), the relative difference in ion and electron energies is not important.

An inherent weakness of the present method is the reliance on the very few fast electrons of the velocity distribution to characterize the mean energy. In this connection it is to be noted that X-rays emanating from SCEPTRE IIIA have been detected. Some preliminary experiments (Payne and Kaufman 1959) suggest that they are produced by electrons with energies greater than about 1 keV striking the walls, but no information is available on electrons with lesser energy. A large number of runaway electrons may perturb the Maxwellian velocity distribution sufficiently so as to falsify the spectral excitation of helium-like ions in the deduction of the electron temperature. The results suggest that this is not so.

The present value of electron temperature from the C V emission is slightly less than the preliminary value given in the earlier paper. Comparison of the data shows that there is a genuine reduction in the intensity of the C V emission from SCEPTRE IIIA compared with the earlier version, SCEPTRE III. Although the conditions were apparently otherwise the same†, the gas current in the IIIA version was distinctly lower than in the earlier version, thus possibly accounting for the apparent reduction in the temperature.

---

† The deuterium pressure in the earlier paper should be corrected to 1·8 millitorr.

Both the C V and B IV lines were appreciably excited for most of the duration of the current pulse (figure 1) and over a large fraction of the tube diameter. This would suggest that the electron temperature was about 10^5 deg K over wide limits, since only a small change in electron temperature would alter the intensity of these lines markedly. Nevertheless, the electron temperature had a distinct maximum on the torus axis. These observations are in good agreement with the results derived from the analysis of magnetic-probe measurements on SCEPTRE IIIA (Allen and Liley 1959).

It is also of interest to compare the value of electron temperature derived here with that from a consideration of the ionization equilibrium discussed by Knorr (1958), bearing in mind that the time required to establish this type of equilibrium for O V ions is about 1 msec in SCEPTRE. The fact that O V, F V and F VI lines are strongly excited in SCEPTRE leads to a value of electron temperature in the range $(2\text{–}3) \times 10^5$ deg K from Knorr's results (Knorr 1958, figures 5 and 6).

§ 6. CONCLUSION

The method presented here of estimating the electron temperature from the spectral emission of helium-like ions is now more firmly established. Under typical conditions of SCEPTRE IIIA, the maximum electron temperature achieved is in the range $(2\text{–}3) \times 10^5$ deg K, so confirming a preliminary estimate previously reported. The results also indicate that spectral excitation, even of the highly ionized C V atom, is not seriously influenced by the possible presence of runaway electrons.

The method can be considered a proper measurement rather than a good estimate after a number of points have been further investigated. For example, it would be valuable to study the Be III emission so that in the excitation there would be still less dependence on the very fast electrons of the velocity distribution. In the case of lithium, since the Li III spectrum would be predominantly excited on the torus axis, it would be difficult to estimate N_1. There is also an urgent need for more reliable data on the cross section Q_{12} and on the cross section for excitation from the 2^3S_1 metastable level to the 2^3P_2 level by electron impact. In addition, independent measurement of N_1 and n would be valuable.

It should now be possible to examine variations in electron temperature for different plasma conditions which may entail alterations in the magnitude of the electron concentration. In these circumstances, the ratio of the C V and B IV intensities should be a reasonably reliable guide to changes in the electron temperature.

The method may be applicable to other forms of high-temperature plasma and for even higher temperatures than attained hitherto, providing contamination of the plasma caused by the helium-like impurity can be tolerated. However, when attempting to measure an electron temperature of several million degrees Kelvin difficulties can already be foreseen, including the questions of absolute intensity measurement in the vacuum ultra-violet region and the identification of the 2^3S_1–2^3P_2 line in the higher helium-like spectra.

ACKNOWLEDGMENTS

We are grateful to a number of colleagues for their assistance, in particular, to Mr. B. A. Irving and Dr. A. A. Woolf who supplied the diborane and advised us on the method of handling it, and to Mr. R. N. Bloomer and his colleagues (Research Laboratory, Siemens Edison Swan Limited, Harlow) who measured the ionization-gauge factor for this gas. We also acknowledge discussions with our colleagues at the Atomic Energy Research Establishment, Harwell. This work was supported in part by the Atomic Energy Research Establishment and is published with the permission of Dr. T. E. Allibone, Director of the Laboratory.

REFERENCES

ALLEN, N. L., *et al.*, 1958, *Nature, Lond.*, **181,** 384.
ALLEN, N. L., and LILEY, B. S., 1959, *Proc. 4th Int. Conf. on Ionization Phenomena in Gases, Uppsala* (Amsterdam: North-Holland).
EDLÉN, B., 1934, *Nova Acta Soc. Sci. Uppsal.*, **9,** No. 6, 32.
HUGHES, T. P., and KAUFMAN, S., 1959, *Nature, Lond.*, **183,** 7.
JOHNSON, F. S., 1956, *J. Opt. Soc. Amer.*, **46,** 101.
KAUFMAN, S., and WILLIAMS, R. V., 1958, *Nature, Lond.*, **182,** 557.
KNORR, G., 1958, *Z. Naturf.*, **13a,** 941.
MACPHERSON, H. G., 1940, *J. Opt. Soc. Amer.*, **30,** 189.
MEEK, J. M., and CRAGGS, J. D., 1953, *Electrical Breakdown of Gases* (Oxford: Clarendon Press), p. 400.
NULL, M. R., and LOZIER, W. W., 1958, *J. Appl. Phys.*, **29,** 1605.
PAYNE, R. M., and KAUFMAN, S., 1959, *Proc. Instn Elect. Engrs*, **106** A, Convention on Thermonuclear Processes.
SCHECHTER, W. H., JACKSON, C. B., and ADAMS, R. M., 1954, *Boron Hydrides and Related Compounds*, 2nd edn, Chapters 1 and 6 (Callery, Pa.: Callery Chemical Co.).
SEATON, M. J., 1958, *Rev. Mod. Phys.*, **30,** 980.
WARE, A. A., 1959, *Proc. Instn Elect. Engrs*, **106** A, Convention on Thermonuclear Processes.

The Correction of Spectral Line Shapes for Instrumental and Other Broadening

BY C. P. FLYNN AND E. F. W. SEYMOUR
Physics Department, University of Leeds

MS. received 16*th July* 1959, *in final form* 6*th October* 1959

Abstract. A simple and rapid procedure is described for the correction of line shapes observed in any branch of spectroscopy, for distortions governed by the equation

$$f(x_0)=\int_{-\infty}^{\infty} g(x)h(x_0-x)dx,$$

where $f(x)$ is the observed line shape, $g(x)$ the true line shape and $h(x)$ an instrumental or intrinsic broadening function, provided that the moments of $h(x)$ are finite. As an illustration the method is applied to the case of the distortion, inherent in the modulation technique, of magnetic resonance spectra. Formulae for the correction of moments of lines are also given.

§ 1. INTRODUCTION

IN all forms of spectroscopy, the fact that the spectrograph has a finite resolving power causes the output reading of the instrument to be to some extent a distortion of the true or input reading, which could only be observed by using an instrument of infinite resolving power. The distortion may be expressed in terms of the output line shape $h(x)$ observed for an input line of infinitesimal width: the output line shape $f(x)$ is related to the input shape $g(x)$ and the ' folding function ' $h(x)$ by

$$f(x_0)=\int_{-\infty}^{\infty} g(x)h(x_0-x)dx=\int_{-\infty}^{\infty} g(x_0-x)h(x)dx. \qquad \ldots\ldots(1)$$

This equation describes the resultant shape whenever each element of a function $g(x)$ is spread in some way to the shape $h(x)$; this occurs in several cases of interest other than that of limited instrumental resolving power. For instance, the *true* line shape may be the result of two broadening influences $g(x)$ and $h(x)$ occurring together; in nuclear magnetic resonance spectra of solids such influences might be spin–spin and spin–lattice relaxation. Again magnetic resonance spectra are often observed by superimposing a sinusoidal modulation on the steady magnetic field and measuring the component of the output signal at the modulation frequency. In the limit of infinitesimal modulation amplitude the output is a measure of the field derivative of the line shape; at finite amplitudes the output differs from the derivative by an amount which can be expressed in terms of an appropriate folding function (Spry 1957).

The present paper describes a simple procedure for determining the true line shape $g(x)$ from the observed shape $f(x)$.

§ 2. Requirements of a Practical Correction Scheme

Two methods which rely on essentially the same principle have been proposed for the manipulation of equation (1) to give $g(x)$ in terms of the observed $h(x)$ and $f(x)$; a brief discussion of them will help to emphasize the requirements of a practical correction scheme. A function $G(x)$ is chosen which has the property

$$\int_{-\infty}^{\infty} G(\alpha x)G\{\beta(x_0 - x)\}dx = G(\gamma x_0)$$

where γ is a function of α and β. By analysing both $f(x)$ and $h(x)$ into series in $G(x)$ and substituting in equation (1), it may be possible to obtain a similar series representing $g(x)$. In general, however, unless the functions $G(x)$ form an orthogonal set, the coefficients α of the expansion of $g(x)$ are overdetermined by the β and γ occurring in $h(x)$ and $f(x)$ whenever it is required to represent both of these functions by more than one term each in $G(x)$.

In practice, therefore, when using non-orthogonal functions, it is necessary to represent either $f(x)$ or $h(x)$ by a single term. This restriction applies to an analysis in terms of the error function (Shull 1946) for which $\gamma = \alpha\beta(\alpha^2 + \beta^2)^{-1/2}$, and would also apply in the case of the Lorentzian function $G(x) = a/\pi(a^2 + x^2)$, for which $\gamma = \alpha\beta(\alpha + \beta)^{-1}$. In any event, Shull uses the method of least squares in his analysis and this is too lengthy for the system to be of general utility. The system does, however, have the advantage that the observed curves are represented by functions of shape similar to their own and therefore a short series can give a reasonable representation of the data.

This advantage is lost in the second method which has been proposed by Stokes (1948) and Spry (1957), who analyse $f(x)$ and $h(x)$ into orthogonal sets of harmonic functions, thus permitting the use of more than one term in the representation of both functions. Moreover the number of terms needed in the expansions increases as the width of $h(x)$ relative to that of $f(x)$ decreases, since the analysis of the two functions must extend over the same interval. This results in a low efficiency when making relatively small corrections. Also one is inevitably left with spurious oscillations in the wings of the corrected curves, as may be seen in the papers of Stokes and Spry, where the amplitude of the oscillations amounts to about $2\frac{1}{2}\%$ of the peak height of $g(x)$.

Since it is not usual for an apparatus to be used for investigations in which its resolving power is grossly inadequate, it follows that the normal use of a correction scheme will be in making small significant corrections to observed data, and therefore that the technique adopted must be particularly efficient in this limit. This suggests that the most efficient unfolding technique would represent the corrected shape as the observed shape with the addition of a correction term, or possibly a rapidly convergent series of terms, rather than as a completely re-synthesized curve. Further it is often the case that many different functions $f(x)$, possibly of widely differing widths, are observed without altering an apparatus, in which case $h(x)$ remains unchanged throughout the analysis of these curves. It is clear that in the interests of rapid correction, the method adopted should not demand the re-analysis of $h(x)$ for each observed curve. It is with such a general technique for the correction of all distortions of the type governed by equation (1) that this paper is concerned.

§ 3. General Expression for the Correction

In some cases the folding function $h(x)$ is a bell-shaped curve, and in the limit when $h(x)$ is very narrow compared with $g(x)$ it is possible to replace $h(x)$ by a delta function $\delta(x)$, so that equation (1) reduces to $f(x_0)=g(x_0)$. However in general the limit of $h(x)$ cannot be represented by a delta function, and the undistorted shape $f(x_0)$ is not the same as $g(x_0)$. It is useful to consider the more general case where, in the absence of distortion, $f(x_0)=\xi g(x_0)$, where ξ is a linear operator acting on functions of x_0. In the case of magnetic resonance spectra observed by the modulation technique, for instance, ξ is the differential operator D. It is readily shown from equation (1) that

$$\phi_n(x_0)=\int_{-\infty}^{\infty}\chi_m(x_0-x)\psi_{n-m}(x)dx \qquad \ldots\ldots(2)$$

where $\phi_r(x_0)=\xi^r f(x_0)$, $\chi_r(x_0)=\xi^r g(x_0)$, $\psi_r(x_0)=\xi^r h(x_0)$, and r is a positive or negative integer. It follows as a special case of equation (2) that

$$\phi_0(x_0)=f(x_0)=\int_{-\infty}^{\infty}\chi_1(x_0-x)\psi_{-1}(x)dx. \qquad \ldots\ldots(3)$$

The significance of equation (3) is that $f(x_0)$ may be considered as the fold of the undistorted output curve $\chi_1(x_0)=\xi g(x_0)$ and the generalized folding function $\xi^{-1}h(x_0)$, which must reduce to a delta function in the limit.

By performing a Taylor expansion of $\chi_1(x_0-x)$ in x around x_0, equation (3) becomes

$$f(x_0)=\sum_{n=0}^{\infty}\left\{\frac{(-1)^n}{n\,!}\int_{-\infty}^{\infty}x^n\psi(x)dx\,.\,D^n\right\}\chi(x_0) \qquad \ldots\ldots(4)$$

where the suffixes on ψ and χ have been dropped. Introducing the normalized moments of the folding function, defined by

$$M_n(\psi)=\int_{-\infty}^{\infty}x^n\psi(x)dx\Big/\int_{-\infty}^{\infty}\psi(x)dx,$$

equation (4) reduces to

$$\chi(x_0)=\left\{\sum_{n=0}^{\infty}\frac{(-1)^n}{n\,!}M_n(\psi)D^n\right\}^{-1}f(x_0) \qquad \ldots\ldots(5)$$

provided that we choose $\int_{-\infty}^{\infty}\psi(x)dx=1$. Expanding equation (5) and placing $M_1(\psi)=0$, the required correction series is obtained:

$$\chi(x_0)=f(x_0)-\frac{M_2(\psi)}{2\,!}f^{\mathrm{II}}(x_0)+\frac{M_3(\psi)}{3\,!}f^{\mathrm{III}}(x_0)$$
$$-\left\{\frac{M_4(\psi)}{4\,!}-\left[\frac{M_2(\psi)}{2\,!}\right]^2\right\}f^{\mathrm{IV}}(x_0)+\ldots \qquad \ldots\ldots(6)$$

The choice $M_1(\psi)=0$ corresponds to choosing the origin of x at the centre of gravity of the folding function, and is convenient since a number of correction terms are thus eliminated; any other choice of origin of x would merely have the effect of shifting the corrected curve $\chi(x_0)$ along the x_0 axis without changing its shape. It may be noted that equation (6) embraces the simple case when the undistorted form of $f(x_0)$ is the same as that of $g(x_0)$, in this case $\chi(x_0)$ being identical with $g(x_0)$ and $\psi(x)$ with $h(x)$. An analogous correction for this case, restricted to the terms in M_2 and M_3 only, has been given by Tournarie (1957) for the folding of histograms.

§ 4. COMPUTATION OF CORRECTED LINE SHAPES

In applications where the moments of $h(x)$ are to be determined from experimental data, they may be computed by the standard methods of numerical integration. The derivatives of the observed curve $f(x)$ are also required and the following method has been found convenient for their evaluation. The calculus of finite differences supplies formulae for the derivatives of a curve in terms of its differences at intervals along the curve; of these formulae, those in terms of horizontal differences are the most convenient for the present purpose for reasons of rapid convergence. Equations for the first four derivatives are given below to the fourth order of differences, in terms of the interval w in x, and the operations δ of horizontal differencing and μ of averaging two successive entries in a column of differences (Whittaker and Robinson 1944),

$$wf^{\mathrm{I}}(x)=\mu\delta^1 f(x)-\tfrac{1}{6}\mu\delta^3 f(x)+\dots$$
$$w^2 f^{\mathrm{II}}(x)=\delta^2 f(x)-\tfrac{1}{12}\delta^4 f(x)+\dots$$
$$w^3 f^{\mathrm{III}}(x)=\mu\delta^3 f(x)-\dots$$
$$w^4 f^{\mathrm{IV}}(x)=\delta^4 f(x)-\dots$$

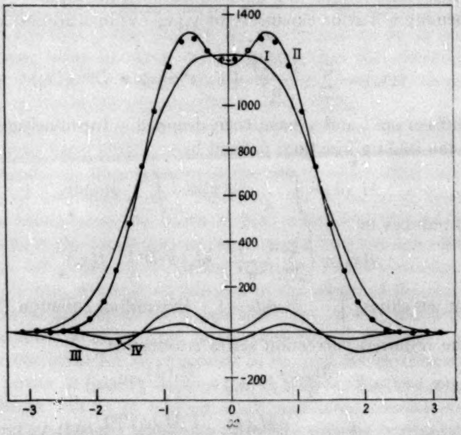

The points represent values of $\chi(x)$ calculated from the observed line shape $f(x)$ (curve I) using the correction procedure detailed in the table. Curve II shows the true shape $\chi(x)$. Curves III and IV show the correction terms in $\delta^2 f(x)$ and $\delta^4 f(x)$, respectively.

In terms of these differences, equation (6) becomes

$$\chi(x_0)=f(x_0)-\frac{M_2(\psi)}{2w^2}\delta^2 f(x_0)+\frac{M_3(\psi)}{6w^3}\mu\delta^3 f(x_0)$$
$$-\frac{1}{24w^4}\left\{M_4(\psi)-6M_2^2(\psi)-w^2 M_2(\psi)\right\}\delta^4 f(x_0)+\dots \quad \dots\dots(7)$$

An example of the application of equation (7) is shown in the figure and the accompanying table. Curve I represents the observed shape $f(x)$ and actually consists of two Gaussian curves $10^3 \times \exp\{-(5x/4)^2\}$ separated by 1·4 units along the x-axis, the whole being folded with a Gaussian function

$$\psi(x) = (5/3\sqrt{\pi}) \exp\{-(5x/3)^2\}.$$

Table

Since $f(x)$ is symmetrical about $x = 0$, differences are given only for positive values of x. $w = 0{\cdot}2$, $\psi(x) = (5/3\sqrt{\pi})\exp\{-(5x/3)^2\}$, $M_2(\psi) = 9/50$, $M_4(\psi) = 243/2500$.

Column 7 is calculated from

$\chi(x) = f(x) - 2{\cdot}25\,\delta^2 f(x) + 2{\cdot}72\,\delta^4 f(x)$ (see equation (7)).

x	$f(x)$	$\delta^1 f(x)$	$\delta^2 f(x)$	$\delta^3 f(x)$	$\delta^4 f(x)$	$\chi(x)$
−0·1	1225		−5		−12	1204
		0		0		
0·1	1225		−5		−12	1204
		−5		−12		
0·3	1220		−17		−6	1242
		−22		−18		
0·5	1198		−35		7	1296
		−57		−11		
0·7	1141		−46		13	1280
		−103		2		
0·9	1038		−44		14	1175
		−147		16		
1·1	891		−28		6	970
		−175		22		
1·3	716		−6		1	732
		−181		23		
1·5	535		17		−9	472
		−164		14		
1·7	371		31		−9	277
		−133		5		
1·9	238		36		−8	135
		−97		−3		
2·1	141		33		−4	56
		−64		−7		
2·3	77		26		−2	13
		−38		−9		
2·5	39		17		3	9
		−21		−6		
2·7	18		11		0	−7
		−10		−6		
2·9	8		5		4	7
		−5		−2		
3·1	3		3		0	−4
		−2		−2		
3·3	1		1			
		−1				
3·5	0					

This broadening is so severe that the two component peaks of the broadened curve are not resolved. Curve II shows the sum of the two Gaussian curves with no broadening and thus represents $\chi(x)$. The points lying near curve II are calculated from curve I using equation (7) including terms up to that in $\delta^4 f(x)$, as shown in the table; the two correction terms in $\delta^2 f(x)$ and $\delta^4 f(x)$ are shown in curves III and IV respectively; that in $\delta^3 f(x)$ is zero since the folding function is even. The r.m.s. error in the corrected points is about 1% of the peak height.

With decreasing width of the folding function the contribution from the δ^4 term decreases rapidly. For a single Gaussian curve, folded with a Gaussian function of width one-third of its own, for example, the greatest values of the δ^2 and δ^4 terms are about 5% and 0·5%, respectively, of the peak height of the observed curve. In many applications, therefore, the correction procedure may be terminated at the δ^2 term. (It may be noted that the δ^4 term is abnormally large compared with the δ^2 term in the example given in the figure because of the flat-topped nature of the curve $f(x)$.)

In practice the output from an apparatus is subject to some degree of random fluctuation. It is usual to allow for such errors by drawing the 'best' smooth curve through the data. It will be evident that it is necessary to draw this curve, and to read off ordinates from it, with some care, since the operation of differencing tends to produce larger percentage errors in the differences than exist in the original data. It may also be advisable to smooth the differences obtained, although this has not been done in the example given.

§ 5. THE FOLDING FUNCTION FOR SINUSOIDAL MODULATION

As an illustration of the method, the effect of a finite modulation amplitude on a magnetic resonance line shape, observed with an apparatus which detects only the Fourier component of the signal at the modulation frequency, is investigated. Since in the limit of infinitesimal modulation amplitude the output signal is proportional to the derivative of the true line shape, ξ is the operator d/dx_0 and thus the effective folding function $\psi(x_0)$ is the integral (i.e. ξ^{-1}) of the shape of the output signal for a very narrow true line shape. This latter output signal shape has been obtained empirically by Spry; it can also be derived analytically as follows, so as to obtain exact values of its moments.

Let the modulation displacement be given by $x=a\sin\omega t$, and the input signal by a rectangular curve of unit area and width $\epsilon \ll a$ centred at $x=x_0$. The input signal will eventually be considered to collapse to the delta function $\delta(x_0)$. The input signal is then non-zero only near $t=t_0$, say, and $t=\pi/\omega-t_0$, and the time spent in traversing the input signal is $\tau=|\epsilon/a\omega\cos\omega t_0|$. The Fourier component of the output signal at frequency ω is then

$$h(t_0)=\frac{\omega}{\pi}\int_0^{2\pi/\omega}\left\{\delta(t_0)+\delta\left(\frac{\pi}{\omega}-t_0\right)\right\}\sin\omega t\,dt$$

$$=\frac{2}{\pi a}\tan\omega t_0,$$

$$\text{or}\quad h(x_0)=\frac{2}{\pi a}\frac{x_0}{(a^2-x_0{}^2)^{1/2}},\quad -a\leqslant x_0\leqslant a.$$

The folding function is obtained by integration of $h(x_0)$ followed by normalization:

$$\psi(x_0)=\frac{2(a^2-x_0{}^2)^{1/2}}{\pi a^2}.$$

The normalized moments of this function are

$$M_{2q}(\psi)=\frac{a^{2q}}{2^q}\prod_{p=0}^{q-1}\left\{\frac{2p+1}{p+2}\right\},$$

$$M_{2q+1}(\psi)=0.$$

On substituting these moments into equation (6), we obtain finally

$$\chi(x_0)=f(x_0)-\frac{a^2}{8}f^{\mathrm{II}}(x_0)+\frac{a^4}{96}f^{\mathrm{IV}}(x_0)-\dots \qquad \dots\dots(8)$$

or, in terms of finite differences

$$\chi(x_0)=f(x_0)-\frac{a^2}{8w^2}\,\delta^2 f(x_0)+\frac{a^4}{96w^4}\left(1+\frac{w^2}{a^2}\right)\delta^4 f(x_0)-\dots \qquad \dots\dots(9)$$

Equation (8) may also be obtained by inverting equation (3) of a paper by Andrew (1953) in which he calculates the correction to be applied to the second and higher moments of magnetic resonance lines for a finite amplitude of modulation. It may sometimes be convenient, when observing weak lines, to increase the signal-to-noise ratio by using a rather large amplitude of modulation even though this may tend to smear out any structure of the line, and to recover the true shape and structure by the use of equation (9).

§ 6. MOMENT CORRECTION

In some fields of spectroscopy the even moments of a line are of importance. It is advisable in their determination to make a direct correction to the observed moment since a shape correction followed by a moment evaluation introduces extra errors and extra labour.

The unnormalized qth moment of the fold of $\chi(x)$ and $\psi(x)$ may be written

$$M_q'(f)=\int_{x=-\infty}^{\infty}\int_{y=-\infty}^{\infty}(x+y)^q\chi(x)\psi(y)\,dx\,dy$$

$$=\sum_{p=0}^{q}\frac{q\,!}{p\,!(q-p)\,!}\int_{-\infty}^{\infty}y^p\psi(y)\,dy\int_{-\infty}^{\infty}x^{q-p}\chi(x)\,dx$$

where $y=x_0-x$. This equation may be written in terms of the normalized moments M_p by dividing both sides of the equation by $M_0'(f)=M_0'(\chi)M_0'(\psi)$:

$$M_q(f)=\sum_{p=0}^{q}\frac{q\,!}{p\,!(q-p)\,!}M_p(\psi)M_{q-p}(\chi). \qquad \dots\dots(10)$$

An analogous equation has previously been given for the folding of histograms (Tournarie 1957).

The required quantity $M_q(\chi)$ may be expressed in terms of the sets of known quantities $M_p(f)$ and $M_p(\psi)$ by successive elimination of lower-order moments of χ. Writing, as before, $M_1(\psi)=0$,

$$\left.\begin{aligned}
M_1(\chi)&=M_1(f)\\
M_2(\chi)&=M_2(f)-M_2(\psi)\\
M_3(\chi)&=M_3(f)-3M_1(f)M_2(\psi)-M_3(\psi)\\
M_4(\chi)&=M_4(f)-6\{M_2(f)-M_2(\psi)\}M_2(\psi)\\
&\quad-4M_1(f)M_3(\psi)-M_4(\psi),
\end{aligned}\right\} \qquad \dots\dots(11)$$

and so on. The second and fourth of equations (11) reduce to the expressions given by Andrew for the particular case of broadening by a sinusoidal modulation; for broadening due to a square-wave modulation the second of the equations reduces to that given by Perlman and Bloom (1952). More generally these equations can be used to correct any moment of an observed curve for any broadening influence conforming to equations (1) or (3), provided that the moments of the folding function are finite.

ACKNOWLEDGMENTS

One of us (C.P.F.) is grateful to the Department of Scientific and Industrial Research for the award of a maintenance allowance.

REFERENCES

ANDREW, E. R., 1953, *Phys. Rev.*, **91**, 425.
PERLMAN, M. M., and BLOOM, M., 1952, *Phys. Rev.*, **88**, 1290.
SHULL, C. G., 1946, *Phys. Rev.*, **70**, 679.
SPRY, W. J., 1957, *J. Appl. Phys.*, **28**, 660.
STOKES, A. R., 1948, *Proc. Phys. Soc.*, **61**, 382.
TOURNARIE, M., 1957, *C.R. Acad. Sci., Paris*, **245**, 1301.
WHITTAKER, E., and ROBINSON, G., 1944, *The Calculus of Observations*, 4th edn (London: Blackie).

The Polarization in Neutron–Proton Scattering at 77 Mev

By C. WHITEHEAD, S. TORNABENE† and G. H. STAFFORD†
Atomic Energy Research Establishment, Harwell, Berkshire

Communicated by B. Rose; *MS. received* 12*th August* 1959, *in final form* 1*st October* 1959

Abstract. A measurement is described of the polarization in neutron–proton scattering at an effective neutron energy of 77 Mev. The beam of polarized neutrons was produced by proton irradiation of a beryllium target. The neutrons emerging at a production angle of 55° were 23·7 ± 1·8% polarized, the beam polarization being measured by using the calculable polarization dependence of small angle scattering from uranium. In the neutron–proton experiment, an angular range from 20·6° to 159·2° was covered detecting either scattered neutrons or recoil protons. The polarization effects are large and there is a marked difference between the present results and those obtained previously at 95 Mev. A broad neutron spectrum was used extending from 50 Mev to 130 Mev but arguments are advanced to establish that the spectrum does not seriously vitiate the validity of the results.

§ 1. Introduction

This experiment was performed as part of a general programme to investigate nucleon–nucleon scattering in the energy range from 50 to 150 Mev using the Harwell 110 inch synchrocyclotron. Two previous measurements of polarization in neutron–proton scattering at 95 Mev have been reported by us (Hillman and Stafford 1956, Stafford, Whitehead and Hillman 1957). In the present experiment a reduced neutron energy of 77 Mev was obtained by using the neutrons produced in a beryllium target at 55° to the direction of the 165 Mev incident proton beam. The polarization of 23·7 ± 1·8% obtained at this scattering angle (Stafford, Tornabene and Whitehead 1957) was appreciably larger than was available for the experiments at 95 Mev although the neutron flux was a factor five smaller. In order to make a more precise measurement of the polarization in neutron–proton scattering, without using a large amount of machine time, a multiple-detector system was employed and the angular resolution of the detectors broadened. Scattered neutrons were detected in the centre-of-mass angular region from 20° to 90° at four angles concurrently, using large liquid scintillation counters. In the angular region from 70° to 160° recoil protons were detected using coincidence telescopes; ten telescopes were used at the same time.

The polarization of the incident neutron beam was measured by small angle scattering of uranium where interference between nuclear scattering and the Coulomb scattering of the neutron magnetic moment gives large and calculable asymmetries (Schwinger 1948). Asymmetry measurements were made, as in the previous experiment, by using a fixed detector and precessing the polarization vector of the beam.

---

† Now at the National Institute for Research in Nuclear Science, Harwell, Berkshire.

§ 2. Method

The asymmetry produced by scattering a polarized neutron beam through an angle θ is given by

$$e=\frac{I(\theta,0)-I(\theta,\pi)}{I(\theta,0)+I(\theta,\pi)}.$$

$I(\theta\phi)$ is the intensity of protons at polar angle θ and azimuthal angle ϕ, measured with respect to the plane perpendicular to the direction of polarization of the incident neutron beam. In conventional asymmetry measurements with a vertically polarized beam $I(\theta,0)$ and $I(\theta,\pi)$ are determined by counting first with the detector on the left [$I(\theta,0)$, say] of the incident beam and, after rotation of the detector system through π about the incident beam, counting with the detector on the right [$I(\theta,\pi)$]. In our experiment systematic errors are reduced and detecting apparatus simplified by placing a stationary detector above (or below) the beam and first, with the plane of polarization of the neutron beam precessed clockwise through $\pi/2$, counting $I(\theta,0)$ say and then, with the polarization precessed anti-clockwise through $\pi/2$, counting $I(\theta,\pi)$. The neutrons are precessed by means of a longitudinal magnetic field, produced in a solenoid. The technique has been described in detail previously (Hillman, Stafford and Whitehead 1956).

The measured asymmetry is simply related to the beam polarization P_1 and the polarization in scattering P_2 by the relation $e=P_1P_2$.

In our beam polarization measurement P_2 (uranium) is calculable, so P_1 the polarization of the neutron beam is deduced from the observed asymmetry. In the neutron–proton scattering measurement, we use the same neutron beam so P_1 is known and from the observed asymmetries we deduce P_2 (hydrogen) the polarization in neutron–proton scattering.

§ 3. Apparatus

The experiment was carried out in two halves which are described separately below. At forward scattering angles where the scattered neutron energy is large, neutrons were detected. At large scattering angles recoil protons were detected.

3.1. *Detection of the Scattered Neutrons*

The neutron beam was collimated for this experiment to 8 cm × 8 cm and was scattered in an 18 cm long liquid hydrogen target. This target is similar to the one used previously (Stafford, Whitehead and Hillman 1957) but has double the active volume. Four large liquid scintillation counters were used to detect the neutrons (see figure 1). They were fixed in a frame at angles of 10° and 30° above the beam and 25° and 45° below the beam, rotation of the whole frame through 5° vertically brought the counters to 15°, 35°, 20° and 40° respectively.

The dimensions of the liquid scintillator volumes were 7·5 cm × 28 cm × 50 cm for one and 7·5 cm × 40 cm × 50 cm for the other three. The containers were made of welded aluminium and one large face on each was made of 1·5 mm glass cemented to the aluminium. The liquid scintillator was viewed through the glass by four photomultipliers (EMI type 6097B) connected in parallel and set with their photocathodes 10 cm from the glass at the bottom of a rectangular truncated pyramid which was painted white to improve the light collection. The gains of the photomultipliers were individually adjusted by means of potentiometers in their dynode chains so that the total current collected was independent of the position of a ^{90}Sr electron source immersed in the liquid scintillator. It was found necessary to inhibit the light collection in the immediate vicinity of each photomultiplier to obtain the best uniformity of sensitivity throughout the detecting volume and this was done empirically by painting small black spots on the glass face immediately under each photomultiplier. With this system the response from the ^{90}Sr source was uniform over the volume of the liquid scintillator to within ± 5% and only fell off appreciably within 2 cm of the edges.

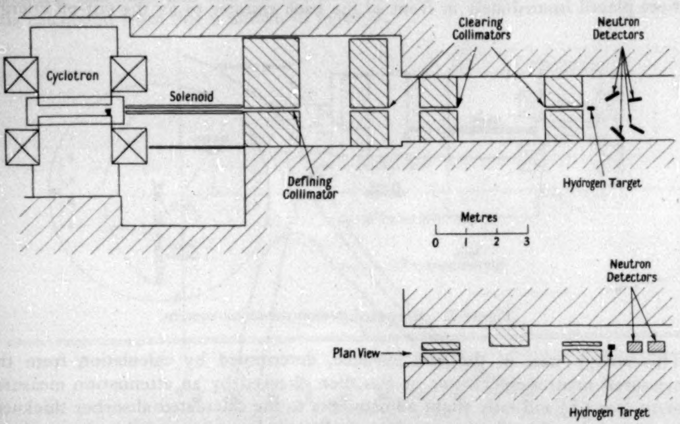

Figure 1. Scattered neutron detection system.

The e.h.t. on each counter was adjusted for the same overall gain and then the threshold bias voltage was adjusted to give similar effective energies at the various scattering angles used in the experiment. The procedure has been described in detail elsewhere (Thresher, Voss and Wilson 1955). The relative counting rates in the four counters, each at a different angle, were consistent with the differential cross section (Bowen, Scanlon, Stafford and Thresher 1960).

To reduce the cosmic ray background the output from each discriminator was gated by a pulse obtained from the cyclotron when the dee voltage reached a frequency corresponding to the production of the 300 microsecond long neutron burst. The length of the gating pulse was 750 microseconds.

A boron trifluoride slow neutron detector was used as a beam monitor. Previous measurements had shown that, under the stable conditions of cyclotron operation that were used in the experiment, it was a reliable monitor.

3.2. *Detection of the Recoil Protons*

For this part of the experiment the neutrons were collimated to give a beam 3 cm high and 5 cm wide at the target of liquid hydrogen which was contained in a thin walled (0·0025 cm) nickel cylinder, 2·5 cm in diameter. The axis of the nickel cylinder was horizontal and normal to the incident neutrons. The height of the beam used was therefore defined by the target, the width by the collimator.

Ten two-unit coincidence scintillation telescopes were used, symmetrically positioned above and below the liquid hydrogen target (see figure 2) first at angles ± 10°, ± 20°, ± 30°, ± 40°, ± 50° and then, after a 5° shift of each bank, at ± 15°, ± 25°, ± 35° and ± 45°. Measurements could not be made at 55° because of the low energy of the recoil protons. Only two front detectors were used to make five telescopes, four separate outputs from one large detector being used in coincidence separately with four back detectors. Aluminium absorbers were placed immediately in front of the back counter to fix the cut-off energy. This energy was, in the first instance, determined by calculation from the measured neutron spectrum; it was then checked by an attenuation measurement (see § 5) and only slight adjustments to the calculated absorber thickness made to bring the effective energies of all ten telescopes to within 4 Mev of one another.

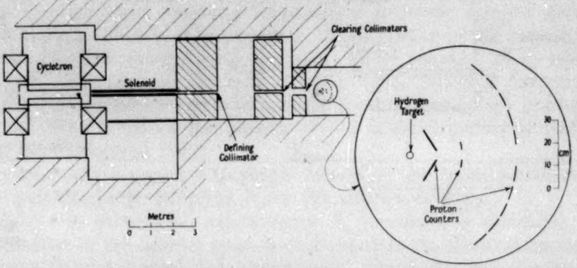

Figure 2. Scattered proton detection system.

The telescopes had a triangular resolution function 10° wide at the base. Simple ten nanosecond coincidence units were used and no gating was necessary.

Due to the symmetrical arrangement, the telescopes formed self-monitoring pairs and this also enabled the reliability of the boron trifluoride monitor used in the neutron detection experiment (§ 3.1) to be checked.

§ 4. EXPERIMENTAL PROCEDURE

After the counter arrays had been adjusted to give similar effective energies, cycles of runs were made with the direction of the neutron polarization precessed either through 90° in one direction or in the opposite direction.

This was done, of course, by reversing the direction of the current (and hence the field) in the solenoid. For convenience we refer to the current settings as 'normal' and 'reverse' and cycles of runs were taken with the following settings, 'normal', 'reverse', 'reverse', 'normal' each run being of 10 to 15 minutes duration.

The numbers obtained were then analysed statistically using the χ^2 test. In most cases the results agreed within the statistical distribution expected and the asymmetry was calculated from the total counts. In the neutron detection experiment the counting rate was very dependent on the stability of the electronics. Some variations in counting rate greater than those expected statistically were observed. However these drifts were slow by comparison with the cycling time and when ratios of adjacent 'reverse' to 'normal' runs were taken, the subsequent χ^2 test indicated a normal statistical distribution.

§ 5. THE NEUTRON ENERGY SPECTRUM AND EFFECTIVE ENERGY

The energy spectrum of the polarized neutron beam was determined in a separate experiment using a liquid hydrogen target and counter telescope at 15° (lab.) to the neutron direction. The counting rate as a function of absorber thickness was measured and the neutron spectrum in the incident beam which was calculated from this is shown in figure 3.

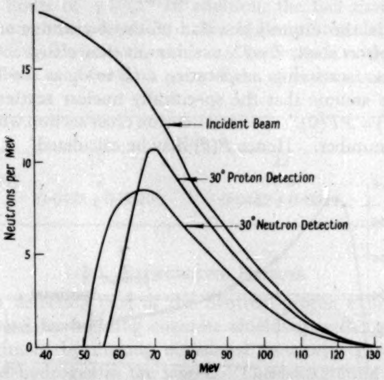

Figure 3. Neutron spectra.

The neutron spectrum used in the polarization experiments depended upon the incident spectrum and the threshold sensitivity of the detector. The threshold was adjusted according to the technique described by Thresher, Voss and Wilson (1955) to obtain, as closely as possible, the same effective energy. The measured values were in all cases within 6 Mev of one another; the standard deviation on individual measurements being ± 3 Mev. Effective energy of a neutron spectrum is defined here as being equal to the energy which is derived from a measurement of the total cross section (measured with a 40 cm long piece of polythene). With an effective energy of 77 Mev the calculated neutron spectrum extended from 50 to 130 Mev. The calculated shape of the spectrum was not quite the same in the neutron detection half of the experiment as in the proton detection half. In figure 3 is illustrated our estimate of these effective neutron spectra.

Independent effective energy measurements were made at four angles in the scattered neutron experiment and at five angles in the recoil proton experiment, the polythene attenuator being inserted into the incident beam before the hydrogen scatterer.

§ 6. POLARIZATION OF THE NEUTRON BEAM

The beam polarization was measured using small angle scattering from uranium. This method of producing polarized neutrons was first suggested by Schwinger (1948) on the assumption of a point nucleus. The polarization of an initially unpolarized neutron beam after scattering from uranium at a small angle θ is given by

$$P(\theta)=\frac{-2\lambda\mathscr{I}F(\theta)\cot\theta/2}{\sigma(\theta)},$$

where $\sigma(\theta)$ is the differential scattering cross section (nuclear plus electrodynamic scattering) which we measure (see Appendix),

$$\lambda=\tfrac{1}{2}|\mu_n|\frac{Ze^2}{\hbar c}\frac{\hbar}{Mc},$$

$\mu_n=1{\cdot}91$ (which is the numerical value of the neutron moment in units of $e\hbar/2Mc$), M = neutron mass, $Z=92$, uranium nuclear charge, $\mathscr{I}F(\theta)$ = imaginary part of the nuclear scattering amplitude, $=(k/4\pi)\sigma_t$ at $\theta=0°$. In the small angular region we assume that the specifically nuclear scattering is insensitive to angle and $\mathscr{I}F(\theta)=\mathscr{I}F(0)$. σ_t = total neutron cross section which we measured, k = neutron wave number. Hence $P(\theta)$ may be calculated.

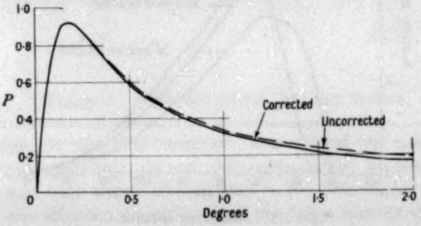

Figure 4. Polarization in neutron scattering from uranium at 77 MeV.

This method of measuring the polarization of neutrons has been used previously by Voss and Wilson (1956) and by Stafford, Whitehead and Hillman (1957). Voss and Wilson point out that corrections should be made to allow for the finite size of the nucleus. This reduces $P(\theta)$ and is proportional to θ^2 for $\theta<5°$. Our calculated correction for uranium at 75 MeV is 2% at 1·5°.

It is also necessary to correct for the nuclear polarization assumed to be zero in our expression for $P(\theta)$. This has been done using the results of Harding (1958) and Dickson, Rose and Salter (1955). The magnitude of the polarization in purely nuclear scattering of 75 MeV neutrons from uranium for $\theta<5°$ has been estimated to have a linear dependence on θ with $P=1\%$ per degree; this is the opposite sign to $P(\theta)$ the Schwinger polarization. We have made a correction by a simple subtraction of P (elastic) from P (Schwinger).

The calculated variation of polarization in small angle scattering from uranium is illustrated in figure 4, both uncorrected and corrected for these two effects.

The scattering geometry chosen for this measurement optimized the product P^2N where P = efficiency of the polarization analyser and N = counting rate.

The mean scattering angle used was 1·4°. The neutron detector had an area 120 cm^2 and was placed 5 metres from the uranium scatterer. The neutron beam was collimated to a size 5 cm × 4 cm at the uranium.

Measurements by Carpenter and Wilson (1959) have shown that the neutron beam polarization may be sensitive to the effective energy selected by the counter bias. We have simultaneously measured the asymmetry in small angle scattering from uranium at three different bias levels (and, with reduced statistical accuracy, using a pulse amplitude analyser). Our results given in table 1 show that near the bias setting used, the variation in polarization with bias is not large. On the average it is approximately 2% per volt. As the four counters were adjusted in the direct neutron beam for the same overall gain it is believed that the relative settings of the threshold bias voltage were adjusted to appreciably better than one volt, so that uncertainty in the beam polarization should fall safely within the limits of ±1%. In addition, the fact that the two overlap points between the neutron detection half and the proton detection half of the experiment agree to well within the statistical accuracy is evidence that a similar beam polarization was used for both parts of the experiment.

Table 1

Bias (V)	18	22	27
Effective energy (MeV)	72	76·5	81
Asymmetry	0·0478 ± 0·0020	0·0482 ± 0·0024	0·0573 ± 0·0032

§ 7. BACKGROUND EFFECTS

In the proton detection part of the neutron–proton experiment the background was reduced by building concrete shielding walls, and was measured during the experiment by making occasional runs with gaseous hydrogen in place of the liquid hydrogen in the target. The background was less than 6% of the real effect at all angles. The general layout of shielding is shown in figure 2.

In the neutron detection part of the experiment the background, in the worst case, was equal to the effect. Consequently it was necessary to investigate carefully the origin of the background in order to make a correct allowance for it. A measurement was first made with the liquid hydrogen in the target replaced by hydrogen gas. This gave the contribution to the background from cosmic radiation, radiation coming through the shielding wall and through the collimation. Neutrons scattered by the hydrogen could have been detected after a secondary scattering by the surrounding walls. This effect was estimated by measuring the liquid hydrogen 'in–out' difference with a large block of steel 70 cm long placed between the hydrogen target and the detector. By suitably combining the counting rates with the cyclotron off and the collimation channel blocked it was possible to separate the contribution from the collimation, cosmic radiation and radiation penetrating the shielding wall. The contribution to the background from the various sources is broken down into components in table 2.

In the uranium experiment since the neutron detector at 1·4° was close (4 cm) to the unscattered neutron beam, this beam was carried through a section

Table 2. Sources of Background in the Gated Neutron Detectors in the n-p Experiment

θ_{lab} (deg)	**10**	**25**	**30**	**45**
Type				
Real hydrogen effect	1200	840	2360	1400
Cosmic radiation	170	50	240	280
Through collimation	45	160	300	430
Through shielding wall	890	270	440	320
Double scattered	10		20	

Counts per 10 min

of evacuated pipe, in the neighbourhood of the counter, to prevent background from air scattering. In addition, a clearing collimator was used to screen the detector from the beam defining collimator.

§ 8. ERRORS AND CORRECTIONS

Some corrections in the uranium experiment to $P(\theta)$ have been described in § 6. The correction for multiple scattering of neutrons in the uranium target (19%) occurs in both the differential cross section measurement and the asymmetry measurement and cancels.

The energy spread in the neutron beam causes the neutrons to precess in the longitudinal field of the solenoid through a range of angles, depending on energy, from 70° to 110°. This angular spread is folded with the ϕ resolution of the neutron counter ($\pm 10°$ at half height) and a correction to the observed asymmetry calculated assuming:

$$I(\theta, \phi) = I(\theta, 0)(1 + P_1 P_2 \cos\phi).$$

The correction for the uranium experiment was 5%.

The value of the correction in the neutron–proton polarization measurement varied with angle and lay in the range 1% to 6% depending on the angle.

The estimated errors are listed in table 3.

Table 3. Errors

Uranium experiment	%
Statistical on total cross section	1·6
Statistical on asymmetry	5·0
Statistical on differential cross section	2·8
Systematic on differential cross section	2·8
Systematic on the ϕ correction	0·5
Systematic on polarization formula	3·0
Systematic on background	2·0
Total	7·6
Neutron–proton experiment	
Statistical on asymmetry	see table 4
Systematic on ϕ correction	0·5

§ 9. WIDTH OF NEUTRON SPECTRUM

As it was necessary for various reasons, in our experiment to use a broad neutron spectrum it is important to get some idea how the measured results would compare with a measurement using a more nearly monokinetic beam of neutrons. We have attempted to do this by subtracting from our angular distribution the 95 MeV polarization results of Stafford, Whitehead and Hillman

(1957). The approximation made was that the neutron energy spectrum in the 95 MeV experiment was the same as the high energy tail of the neutron spectrum used in the present 77 MeV experiment. The resulting polarization angular distribution does not differ very much from our unmodified 77 MeV results.

In the calculation, the 77 MeV neutron spectrum was considered as the sum of two component spectra, a low energy component A and a high energy component B identical in energy distribution with the 95 MeV spectrum of Stafford *et al.* The results for polarization in neutron–proton scattering of components A and B were separated using the relationship:

$$P_{\mathrm{A}} = P + \frac{f}{k}(P - P_{\mathrm{B}})$$

$$\text{where } f = \frac{\text{polarization of the B component of the 77 MeV neutron spectrum}}{\text{polarization of the A component of the 77 MeV neutron spectrum}}$$

$$\text{and } k = \frac{\text{total intensity A}}{\text{total intensity B}},$$

P_{A}, P_{B} = neutron–proton polarization of A, B, P = neutron–proton polarization of the combined spectra; P_{B} was obtained from results of Stafford *et al.*, P was our present result. $f = 1{\cdot}2$, obtained from our measurement of the variation of beam polarization with bias, $k = 3$ (estimated). The 'improved' neutron spectrum had an effective energy of 68 MeV and an estimated width at half height, shown in figure 5, of 30 MeV.

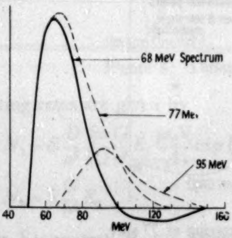

Figure 5. The 68 MeV spectrum.

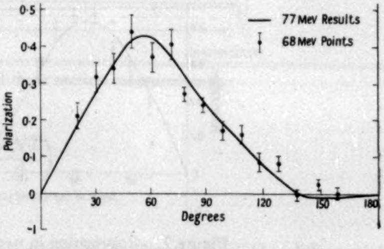

Figure 6. Polarization in n–p scattering.

The calculated values for P_{A} are shown in figure 6 together with a solid curve representing the 77 MeV results for comparison.

It is interesting to note that although we have drastically affected the high energy component in the neutron spectrum the values of the polarizations are not seriously modified. We therefore conclude that our results can be taken as being a satisfactory measurement of the polarization in neutron–proton scattering at 77 MeV.

§ 10. RESULTS AND DISCUSSION

The results are presented in table 4. In the second column the measured asymmetries are given; in the last column are listed the calculated polarizations and the corrections discussed in § 8. The assigned error does not include the uncertainty in the value of the beam polarization as this can only influence the absolute and not the relative value of the polarization.

Table 4. Polarization in Neutron–Proton Scattering

	Asymmetry	77 MEV c.m. angle (deg)	Polarization
Neutrons detected	0·042 ± 0·006	20·6	0·185 ± 0·025
	0·063 ± 0·005	30·4	0·275 ± 0·025
	0·077 ± 0·005	40·6	0·335 ± 0·025
	0·098 ± 0·007	50·4	0·430 ± 0·030
	0·097 ± 0·004	61·4	0·425 ± 0·020
	0·088 ± 0·005	71·4	0·390 ± 0·025
	0·064 ± 0·007	80·8	0·280 ± 0·030
	0·057 ± 0·005	90·6	0·245 ± 0·025
Protons detected	0·071 ± 0·003	78·8	0·303 ± 0·012
	0·058 ± 0·002	88·8	0·250 ± 0·009
	0·045 ± 0·002	98·8	0·197 ± 0·009
	0·031 ± 0·002	108·6	0·134 ± 0·009
	0·017 ± 0·002	118·6	0·073 ± 0·008
	0·010 ± 0·002	128·4	0·042 ± 0·008
	−0·002 ± 0·0015	138·2	−0·008 ± 0·007
	−0·001 ± 0·002	149·4	−0·003 ± 0·009
	−0·002 ± 0·002	159·2	−0·009 ± 0·009

Beam polarization 23·7 ± 1·8%

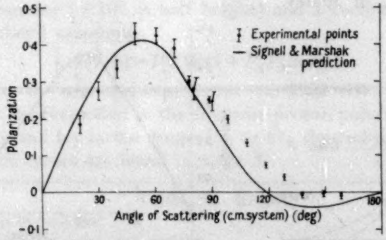

Figure 7. Polarization in n–p scattering at 77 MEV.

It was pointed out in § 1 that this experiment was one of a set aimed at providing information for a detailed study of the nucleon–nucleon interaction. For this reason, a discussion of the significance of the results can profitably await completion at a similar energy of the measurement of the differential cross section and, one trusts in time, of the triple scattering parameters. It is interesting, however, to compare our measured values for the polarization with those predicted by the Signell and Marshak potential (see figure 7). Within the limits of the experimental accuracy there is satisfactory agreement at the smaller scattering angles but at large angles the agreement is less satisfactory. This discrepancy cannot be explained away by the high energy tail of the neutron spectrum as at higher neutron energies the point at which the polarization changes sign moves to smaller scattering angles. The high energy tail would, if anything, tend to increase the magnitude of the negative polarization.

ACKNOWLEDGMENTS

Our grateful thanks are extended to Professor Marshak and his collaborators of the University of Rochester for making the theoretical computations of the neutron–proton polarization for us. Mr. F. Uridge was a tower of strength to us in all things and the cyclotron crew were most willing and co-operative helpers.

APPENDIX

MEASUREMENTS OF THE URANIUM DIFFERENTIAL CROSS SECTION

A technique for measuring differential cross sections for neutrons has been described previously by Thresher, Voss and Wilson (1955). We have used a modified and simpler technique which is of interest.

In principle, two measurements are required. The experimental arrangements for these measurements are illustrated schematically in figure 8. The

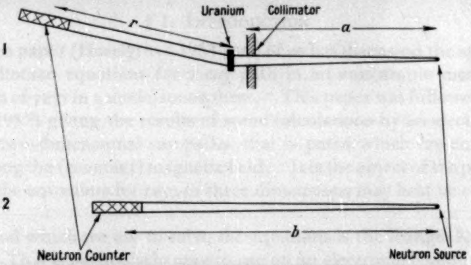

Figure 8. Differential cross section measurements.

counting rates are given by

1. $N_1 = S\dfrac{D}{a^2}\dfrac{\partial\sigma}{\partial\Omega}\dfrac{G}{r^2}E_1\dfrac{\rho t N}{A}\exp\left(-\dfrac{\rho t N T}{A}\right)$

2. $N_2 = S\dfrac{G}{b^2}E_2$

where S = neutron source strength, D = area of collimator, $\partial\sigma/\partial\Omega$ = differential cross section, G = geometric area of counter,

$$E_1 = \text{counter efficiency} = \frac{\text{neutrons detected}}{\text{neutrons incident}},$$

T = uranium total cross section, ρ, t, A = constants for uranium, N = Avogadro's number, so that

$$\frac{\partial\sigma}{\partial\Omega} = \frac{A\exp(\rho NTt/A)}{\rho t N}\frac{r^2a^2}{b^2D}\frac{N_1}{N_2}\frac{E_2}{E_1}.$$

It was assumed that $E_1 = E_2$ since the neutron spectra detected in the two measurements are similar, neutron collimation conditions are similar and the detector efficiency is uniform over its volume.

In practice the counting rate in measurement 2 was too great to measure directly and so an absorber was placed in the beam, and a further simple experiment was performed to measure its attenuation.

REFERENCES

BOWEN, P., SCANLON, J. P., STAFFORD, G. H., and THRESHER, J. J., 1960, *The International Conference on the Nucleon–Nucleon Interaction and the Few Nucleon Problem* (London: Pergamon Press), in the press.

CARPENTER, S. G., and WILSON, R., 1959, *Phys. Rev.*, **113,** 650.

DICKSON, J. M., ROSE, B., and SALTER, D. C., 1955, *Proc. Phys. Soc.* A, **68,** 361, and private communication.

HARDING, R. S., 1958, *Thesis*, University of Rochester, or United States Atomic Energy Commission Report, NYO, 8056.

HILLMAN, P., and STAFFORD, G. H., 1956, *Nuovo Cim.*, **3,** 633.

HILLMAN, P., STAFFORD, G. H., and WHITEHEAD, C., 1956, *Nuovo Cim.*, **4,** 67.

SCHWINGER, J., 1948, *Phys. Rev.*, **73,** 407.

STAFFORD, G. H., TORNABENE, S., and WHITEHEAD, C., 1957, *Phys. Rev.*, **106,** 831.

STAFFORD, G. H., WHITEHEAD, C., and HILLMAN, P., 1957, *Nuovo Cim.*, **5,** 1589.

THRESHER, J. J., VOSS, R. G. P., and WILSON, R., 1955, *Proc. Roy. Soc.* A, **229,** 492.

VOSS, R. G. P., and WILSON, R., 1956, *Phil. Mag.*, **8** [1], 175.

Twisted Ray Paths in the Ionosphere

By C. B. HASELGROVE and JENIFER HASELGROVE
The University, Manchester

Communicated by K. G. Budden; *MS. received* 14*th August* 1959

Abstract. It is shown how the Hamiltonian equations for a ray in an anisotropic medium can be used on an electronic computer to calculate ray paths in three dimensions in a model ionosphere. A programme has been written for a digital computer and some ray paths have been calculated.

§ 1. Introduction

In a previous paper (Haselgrove 1954) one of us has discussed the application of the Hamiltonian equations for a ray path in an anisotropic medium to the calculation of rays in a model ionosphere. This paper was followed by another (Haselgrove 1957) giving the results of some calculations by an electronic digital computer of two-dimensional ray paths, that is paths which lay entirely in the plane containing the (constant) magnetic field. It is the object of the present paper to show how the equations for rays in three dimensions may best be expressed for computing.

The method which we use to solve the equations is the Runge–Kutta method (Gill 1951). This is particularly easy to use on an electronic computer for equations such as the Hamiltonian ones. We show how the calculations are carried out and how they may be checked continually.

Most of the paper is written in terms of Cartesian coordinates. Calculations done so far have been for a horizontally stratified ionospheric layer over a flat earth, and for these Cartesian coordinates were used. For calculations taking into account a spherical earth it might be better to use spherical polar coordinates and so we give the equations in this form also. However, they are more complicated and it may be found easier to express the curvature of the earth in Cartesian coordinates and use the simpler equations.

In the next section the Hamiltonian equations for the ray path are quoted and in the following two sections the algebraic forms of the formula for the refractive index and its derivatives are discussed. § 5 is concerned with the practical aspects of the use of the equations in a digital computer programme.

§ 2. Hamiltonian Equations

2.1. *Cartesian Coordinates*

In the Hamiltonian equations a point on a ray path in three dimensions has three position coordinates x_1, x_2, x_3, and three direction coordinates u_1, u_2, u_3. The u_i are such that the direction of the vector $\mathbf{u}$ is the direction of the wave normal at the point (x_1, x_2, x_3) and the length $u = (u_1^2 + u_2^2 + u_3^2)^{1/2}$ of $\mathbf{u}$ is equal to the refractive index μ at that point and for that direction of wave normal.

The equations are expressed in terms of partial derivatives of a scalar quantity G. G is written as u/μ; its value is therefore always unity but its partial derivatives with respect to the x_i and u_i are not zero, since $u=(u_1^2+u_2^2+u_3^2)^{1/2}$ and μ is a function of the x_i and u_i whose form we shall discuss in a later section. μ is homogeneous of degree zero in the u_i.

The independent variable t in the equations is some function of the distance along the ray path and it need not be further defined.

With these definitions, the Hamiltonian equations for a ray path take the familiar form

$$\frac{dx_i}{dt}=\frac{\partial G}{\partial u_i}, \qquad \text{......(1)}$$

$$\frac{du_i}{dt}=-\frac{\partial G}{\partial x_i}. \qquad \text{......(2)}$$

2.2. *General Curvilinear Coordinates*

In the first paper (Haselgrove 1954) the derivation of the Hamiltonian equations was given for general curvilinear coordinates. The method used there was a difficult one but the same results can be reached by the ordinary methods of tensor calculus, and we quote them here without proof. We are indebted to Dr. Julius J. Brandstatter for an independent verification of them.

We define the general curvilinear coordinates by the metric in which the line element ds is given by $ds^2=g_{ij}\,dx^i\,dx^j$, where the g_{ij} are functions of the x_i and we use the repeated suffix summation convention. We write the tensor contravariant to g_{ij} as g^{ij}. The vector **u** is a contravariant vector with elements u^i, and we have

$$u^2=g_{ij}u^iu^j.$$

In these coordinates the Hamiltonian equations become

$$\frac{dx_j}{dt}=g^{ij}\frac{\partial G}{\partial u^i}, \qquad \text{......(3)}$$

$$\frac{du^j}{dt}=-g^{ij}\frac{\partial G}{\partial x_i}-g^{ij}g^{km}u^l\frac{\partial G}{\partial u^m}\left(\frac{\partial g_{li}}{\partial x_k}-\frac{\partial g_{kl}}{\partial x_i}\right). \qquad \text{......(4)}$$

2.3. *Polar Coordinates*

We first specialize (3) and (4) to the case of orthogonal coordinates where $g_{ij}=0$ if $i\neq j$. We shall not use the summation convention in this section so that for the orthogonal case we may write

$$g_{ii}=1/g^{ii}=h_i^2.$$

Instead of the vector **u** we use **v**, where $v_i=h_iu^i$, so that

$$u^2=v^2=(\Sigma v_i^2)^{1/2}$$

and the ratios v_i/v represent direction cosines of the wave normal direction with respect to local rectilinear axes.

The Hamiltonian equations now take the form

$$\frac{dx_i}{dt}=\frac{1}{h_i}\frac{\partial G}{\partial v_i}, \qquad \text{......(5)}$$

$$\frac{dv_i}{dt}=-\frac{1}{h_i}\frac{\partial G}{\partial x_i}-\frac{1}{h_i}\sum_k\frac{1}{h_k}\frac{\partial G}{\partial v_k}\left(v_i\frac{\partial h_i}{\partial x_k}-v_k\frac{\partial h_k}{\partial x_i}\right). \qquad \text{......(6)}$$

In spherical polar coordinates r, θ, ϕ we have $h_1 = 1$, $h_2 = r$ and $h_3 = r \sin\theta$. Then the six equations become

$$\frac{dr}{dt} = \frac{\partial G}{\partial v_r}, \quad \frac{d\theta}{dt} = \frac{1}{r}\frac{\partial G}{\partial v_\theta}, \quad \frac{d\phi}{dt} = \frac{1}{r\sin\theta}\frac{\partial G}{\partial v_\phi},$$

$$\frac{dv_r}{dt} = -\frac{\partial G}{\partial r} + \frac{1}{r}v_\theta\frac{\partial G}{\partial v_\theta} + \frac{1}{r}v_\phi\frac{\partial G}{\partial v_\phi},$$

$$\frac{dv_\theta}{dt} = \frac{1}{r}\left(-\frac{\partial G}{\partial \theta} - v_\theta\frac{\partial G}{\partial v_r} + \cot\theta\, v_\phi\frac{\partial G}{\partial v_\phi}\right),$$

$$\frac{dv_\phi}{dt} = \frac{1}{r\sin\theta}\left(-\frac{\partial G}{\partial \phi} - \sin\theta\, v_\phi\frac{\partial G}{\partial v_r} - \cos\theta\, v_\phi\frac{\partial G}{\partial v_\theta}\right).$$

We have stated this form of the equations for completeness. For the remainder of this paper we shall be concerned with Cartesian coordinates, and we shall see how their symmetry is an advantage. The polar form can, however, be used in a way exactly analogous to that which we shall describe.

§ 3. THE REFRACTIVE INDEX

The refractive index μ is to be regarded as a function of the scalar quantity $X = Ne^2/\pi\epsilon_0 mf^2 = f_0{}^2/f^2$ (with the usual notation) and of the vector $\mathbf{Y}$ which is parallel to the earth's magnetic field $\mathbf{H}$ and whose length is $Y = \mu_0 He/2\pi mf = f_H/f$. X and $\mathbf{Y}$ are given functions of the position coordinates x_i.

The refractive index satisfies a biquadratic equation. This is a form of the Appleton–Hartree equation, but we shall express it in a vector form which is more convenient than the usual one.

In the absence of absorption we have

$$A\mu^4 + 2B\mu^2 + C = 0, \qquad \ldots\ldots(7)$$

where

$$\left.\begin{aligned} A &= 1 - X - Y^2 + X(\mathbf{Y}\,.\,\mathbf{u})^2/u^2, \\ 2B &= -2(1-X)(1-X-Y^2) + XY^2 - X(\mathbf{Y}\,.\,\mathbf{u})^2/u^2, \\ C &= (1-X)[(1-X)^2 - Y^2]. \end{aligned}\right\} \qquad \ldots\ldots(8)$$

Hence $G = u/\mu$ satisfies the biquadratic equation

$$aG^4 + 2bG^2 + c = 0 \qquad \ldots\ldots(9)$$

with

$$\left.\begin{aligned} a &= C = (1-X)[(1-X)^2 - Y^2], \\ 2b &= 2Bu^2 = -2(1-X)(1-X-Y^2)u^2 + XY^2u^2 - X(\mathbf{Y}\,.\,\mathbf{u})^2, \\ c &= Au^4 = (1-X-Y^2)u^4 + X(\mathbf{Y}\,.\,\mathbf{u})^2u^2. \end{aligned}\right\} \qquad \ldots\ldots(10)$$

We consider the partial derivatives of G required for the differential equations (1) and (2). First we differentiate (9) with respect to a general variable y, obtaining

$$\frac{\partial a}{\partial y}G^4 + 4aG^3\frac{\partial G}{\partial y} + 2\frac{\partial b}{\partial y}G^2 + 4bG\frac{\partial G}{\partial y} + \frac{\partial c}{\partial y} = 0.$$

Thus

$$\frac{\partial G}{\partial y} = -\left(\frac{\partial a}{\partial y}G^4 + 2\frac{\partial b}{\partial y}G^2 + \frac{\partial c}{\partial y}\right)\Big/\, 4G(aG^2 + b).$$

But $G = 1$, so that

$$\frac{\partial G}{\partial y} = -\left\{\frac{\partial}{\partial y}(a + 2b + c)\right\}\Big/\, 4(a + b).$$

The factor $1/4(a+b)$ will appear in all the differential equations, so we may ignore it. This is equivalent to a change of independent variable, from t to t^*, say. Then if we write

$$Q = a + 2b + c \qquad \ldots\ldots(11)$$

the equations become

$$\frac{dx_i}{dt^*} = -\frac{\partial Q}{\partial u_i}, \qquad \ldots\ldots(12)$$

$$\frac{du_i}{dt^*} = \frac{\partial Q}{dx_i}. \qquad \ldots\ldots(13)$$

It should be noted that Q is equal to the left-hand side of (9) and is therefore always zero, but its partial derivatives must be found from the formulae for a, b and c and do not in general vanish.

However, equations (12) and (13) are not directly suitable for computation since when $X=0$, for instance at the bottom of the ionosphere where a ray path calculation commences, we have also $u=\mu=1$ and all the partial derivatives of Q vanish. We therefore extract a factor X from the derivatives and use the equations in the form

$$\frac{dx_i}{dt^{**}} = -\frac{1}{X}\frac{\partial Q}{\partial u_i}, \qquad \ldots\ldots(14)$$

$$\frac{du_i}{dt^{**}} = \frac{1}{X}\frac{\partial Q}{\partial x_i}. \qquad \ldots\ldots(15)$$

§ 4. THE PARTIAL DERIVATIVES

We have

$$\begin{aligned} Q &= a+2b+c \\ &= (1-X-Y^2)(u^2-1)^2 + X\{(\mathbf{Y}\,.\,\mathbf{u})^2 + 2(1-X) - Y^2\}(u^2-1) + X^2(1-X). \end{aligned}$$

When $X=0$, $u^2=1$ but the quantity $(u^2-1)/X$, which we call q, is finite and not zero. We therefore write

$$Q/X^2 = (1-X-Y^2)q^2 + \{(\mathbf{Y}\,.\,\mathbf{u})^2 + 2(1-X) - Y^2\}q + (1-X) \qquad \ldots\ldots(16)$$

and we shall also express the partial derivatives in terms of q.

If we differentiate Q with respect to the ith component of $\mathbf{u}$ we obtain

$$\begin{aligned} \frac{\partial Q}{\partial u_i} &= 2[2(1-X-Y^2)(u^2-1) + X\{(\mathbf{Y}\,.\,\mathbf{u})^2 + 2(1-X) - Y^2\}]u_i \\ &\quad + 2X(u^2-1)(\mathbf{Y}\,.\,\mathbf{u})Y_i. \end{aligned}$$

Hence

$$\frac{1}{X}\frac{\partial Q}{\partial u_i} = 2\{2(1-X-Y^2)q + (\mathbf{Y}\,.\,\mathbf{u})^2 + 2(1-X) - Y^2\}u_i + 2(u^2-1)(\mathbf{Y}\,.\,\mathbf{u})Y_i.$$

Q varies with the x_i through its dependence on X and on $\mathbf{Y}$. We consider these two separately.

For the X variation we have

$$\frac{\partial Q}{\partial X} = -(u^2-1)^2 + \{(\mathbf{Y}\,.\,\mathbf{u})^2 + 2(1-2X) - Y^2\}(u^2-1) + 2X(1-X) - X^2$$

and

$$\frac{1}{X}\frac{\partial Q}{\partial X} = \{-(u^2-1) + (\mathbf{Y}\,.\,\mathbf{u})^2 + 2(1-2X) - Y^2\}q + 2 - 3X.$$

For the $\mathbf{Y}$ variation we have two types of term, namely Y^2 and $\mathbf{Y}.\mathbf{u}$. These give, differentiating with respect to x_i,

$$\frac{\partial}{\partial x_i}(Y^2)=2\sum_j Y_j\frac{\partial Y_j}{\partial x_i}, \qquad \frac{\partial}{\partial x_i}(\mathbf{Y}.\mathbf{u})=\sum_j u_j\frac{\partial Y_j}{\partial x_i}.$$

Thus

$$\frac{\partial Q}{\partial x_i}=\frac{\partial Q}{\partial X}\frac{\partial X}{\partial x_i}+\sum_j\{-2[(u^2-1)^2+X(u^2-1)]Y_j+2X(\mathbf{Y}.\mathbf{u})(u^2-1)u_j\}\frac{\partial Y_j}{\partial x_i}$$

and

$$\frac{1}{X}\frac{\partial Q}{\partial x_i}=\frac{1}{X}\frac{\partial Q}{\partial X}\frac{\partial X}{\partial x_i}+\sum_j\{-2(u^2-1)(q+1)Y_j+2(\mathbf{Y}.\mathbf{u})(u^2-1)u_j\}\frac{\partial Y_j}{\partial x_i}.$$

We gather up these results and express the differential equations in the form

$$\frac{dx_i}{dt^{**}}=Ju_i-KY_i, \qquad \ldots\ldots(17)$$

$$\frac{du_i}{dt^{**}}=L\frac{\partial X}{\partial x_i}+\sum_j(Ku_j+MY_j)\frac{\partial Y_j}{\partial x_i}, \qquad \ldots\ldots(18)$$

where

$$J=-2\{2(1-X-Y^2)(q+1)+(\mathbf{Y}.\mathbf{u})^2+Y^2\}, \qquad \ldots\ldots(19)$$

$$K=2(u^2-1)(\mathbf{Y}.\mathbf{u}), \qquad \ldots\ldots(20)$$

$$L=\{-(u^2-1)+(\mathbf{Y}.\mathbf{u})^2+2(1-2X)-Y^2\}q+2-3X, \qquad \ldots\ldots(21)$$

$$M=-2(u^2-1)(q+1). \qquad \ldots\ldots(22)$$

§ 5. THE USE OF THE EQUATIONS

5.1. *Integration*

In the Runge–Kutta process (Gill 1951) the six derivatives forming the right-hand sides of (17) and (18) are calculated as functions of the six variables, four times in each integration step. The equations as set out above can be seen to be particularly suitable for this calculation. Because we have retained symmetry throughout, most of the coefficients need calculating only once for three variables. This makes the equations even easier to use than those used for the calculations in two dimensions described by Haselgrove (1957).

The simplest way of using the Runge–Kutta process gives integration steps of equal length in the independent variable. It is clearly most efficient, however, for the step in terms of actual path length to be large where the ray is nearly straight and small where the curvature of the ray is liable to introduce truncation errors. A suitable way of achieving this is to multiply the right-hand sides of (17) and (18) by a further scaling function

$$\left(1-X\right)^{1/2}\bigg/\left\{\left(\frac{dx_1}{dt^{**}}\right)^2+\left(\frac{dx_2}{dt^{**}}\right)^2+\left(\frac{dx_3}{dt^{**}}\right)^2\right\}^{1/2}.$$

The denominator alone would have the effect of making the path length into the independent variable, and the numerator reduces the step length near the region where $X=1$ and the rays are most curved.

5.2. *A Single Ray Path*

The computation proceeds step by step from a given set of initial values of the variables. For a flat earth it is convenient to set the x-coordinates at zero initially. The direction coordinates u_i may be expressed in terms of two angles, the angle of

incidence *i* and the angle ζ between the two vertical planes containing respectively the initial direction of the ray and the 'north–south' direction. (Initially, when $X=0$, the ray path direction and $\mathbf{u}$ coincide and $u=\mu=1$.) Then if the x_1 axis is vertical and the x_2 axis points to the north the initial values of the u_i are

$$u_1=\cos i, \quad u_2=\sin i\cos\zeta, \quad u_3=\sin i\sin\zeta.$$

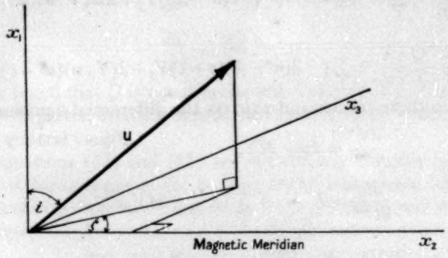

Initial direction of ray. When $X=0$, $u=1$.

For a reflected ray it is required to find the exact point at which the path returns to the level of the bottom of the ionosphere, that is where x_1 again becomes zero. This is done by continuing the calculation until x_1 becomes negative, and then performing one step of integration in the opposite direction. In order to make the length of this one step exact we divide all the derivatives by the derivative of x_1 and multiply them by a 'step length' h, where $-h$ is the negative value reached by x_1. This changes the independent variable to x_1 for this one step (Wheeler 1959). A similar technique could be used to find the point at which a penetrating ray reached the top of an ionospheric layer.

For a curved earth, the origin of the x-coordinates should be taken at the centre of the earth and a horizontally stratified layer then takes the form of a function of $x_1^2+x_2^2+x_3^2$. A reflected ray returns to the bottom of the ionosphere when $x_1^2+x_2^2+x_3^2$ again reaches its initial value.

5.3. *The Computation of q*

The calculation of the derivatives as functions of the variables is straightforward except perhaps for the value of q. Equation (16) gives a quadratic formula for q. This is equal to zero since, as may be verified from the Appleton–Hartree equation, $Q/X^2=0$ even when $X=0$. Thus we have

$$\alpha q^2+2\beta q+\gamma=0 \qquad \text{......(23)}$$

with

$$\left.\begin{aligned}\alpha&=1-X-Y^2,\\ 2\beta&=2(1-X)-Y^2+(\mathbf{Y}.\mathbf{u})^2,\\ \gamma&=1-X.\end{aligned}\right\} \qquad \text{......(24)}$$

Then

$$q=\frac{-\beta\pm(\beta^2-\alpha\gamma)^{1/2}}{\alpha}=\frac{\gamma}{-\beta\mp(\beta^2-\alpha\gamma)^{1/2}}.$$

The upper sign refers to the ordinary ray and the lower to the extraordinary. Since we may have $\alpha = 0$ or, for the extraordinary ray, $\gamma = 0$, we choose that formula for q, at any point in the calculation, that has the larger numerical values in the numerator and denominator.

5.4. *Checking*

We have used three direction coordinates as variables where two angles would have been sufficient to define the wave normal direction. This gives a method of continual checking of the calculations. We have defined $q = (u^2 - 1)/X$, but this formula is not used anywhere in the calculation. At every step, therefore, we may calculate $u^2 - 1$ and Xq from the x_i and u_i and compare them. This check may be used to show whether it is necessary to use a smaller integration step, besides testing for machine errors and programme blunders.

§ 6. CONCLUSION

A programme has been written for the Ferranti Mercury computer at Manchester University to compute ray paths using the Hamiltonian equations as set out above. Calculations have so far been confined to the case of Ordinary rays with a flat earth, a horizontally stratified 'parabolic' layer and a constant magnetic field, but these limitations were only imposed by a desire to reduce the number of variable parameters and to give results directly comparable with those of the earlier paper (Haselgrove 1957). It is hoped to publish these comparable results shortly.

ACKNOWLEDGMENTS

We acknowledge the facilities provided by the computing and engineering staff at the Manchester University Computing Machine Laboratory.

REFERENCES

GILL, S., 1951, *Proc. Camb. Phil. Soc.*, **50**, 604.

HASELGROVE, J., 1954, *Report of Conference on the Physics of the Ionosphere* (London: Physical Society), p. 355.

—— 1957, *Proc. Phys. Soc.* B, **70**, 653.

WHEELER, D. J., 1959, *The Computer Journal*, **2**, 23.

An Electron Diffraction Study of the Effects of Heat Treatment on α-Fe_2O_3 (Haematite) Single Crystals

By M. BLACKMAN and G. KAYE

Physics Department, Imperial College, London

MS. received 6th October 1959

Abstract. Electron diffraction patterns have been taken from a large variety of natural single crystals of α-Fe_2O_3 (haematite) which had previously been heated to 500°c. Some of these showed additional patterns similar to those observed by Finch and Sinha in 1957. Measurements of the basic plane spacings associated with the extra patterns showed that these differed considerably from the corresponding basic plane spacings of α-Fe_2O_3. This result is in contradiction to the findings of Finch and Sinha who claimed that the basic plane spacings associated with the extra patterns approximated closely to those of α-Fe_2O_3. There is therefore no justification for assuming that a new form of Fe_2O_3 (β-Fe_2O_3) exists.

Experiments were also carried out on crystals of α-Fe_2O_3 which had been heated to temperatures between 700° and 1000°c. In some cases oriented layers of Fe_3O_4 (magnetite) were observed but no evidence was found for the presence of γ-Fe_2O_3 (maghemite) in contrast to the results of Finch and Sinha. These investigators claimed that γ-Fe_2O_3 was formed when α-Fe_2O_3 crystals were heated in air to temperatures above 700°c.

---

§ 1. INTRODUCTION

The present paper is concerned with examining the changes produced at the surface of α-Fe_2O_3 (haematite) crystals on heating in air. The investigations were prompted by the work of Finch and Sinha (1957) who provided evidence for the existence of a new phase of Fe_2O_3 (termed β-Fe_2O_3). This phase was found in studying the diffraction of electrons from the basal (00.1) plane of crystals heated in air to 500°c and then cooled. A diffraction pattern different from that due to haematite, although of similar trigonal symmetry, was observed. In this pattern reflections were found such as (00.2), (10.0) which are normally forbidden by the space group of haematite. Certain plane spacings associated with this new pattern were however found to approximate closely to those of haematite and it is because of this that the diffraction patterns were attributed to a new form of Fe_2O_3.

In addition Finch and Sinha found that on heating to 700°c in air another diffraction pattern was obtained, which was consistent with a cubic structure. Their analysis gave diffraction spots with mixed indices and it was decided on this evidence that the overgrowths found were composed of γ-Fe_2O_3 crystallites and not Fe_3O_4 (magnetite)—both of which have similar lattice dimensions. It was concluded that γ-Fe_2O_3 was the stable form of Fe_2O_3 at high temperatures, which differs from the widely held opinion that the γ form is unstable on heating.

Finch and Sinha are of the opinion that the β-phase is associated with the migration of cations in the haematite lattice to sites with four-fold coordination in the oxygen frame of haematite and reasons are given for believing that this

β-phase would be ferrimagnetic. This would be a possible cause of the parisitic ferromagnetism of haematite, the existence of which has been the subject of much speculation and argument.

Because of the interest in the existence of a hitherto unknown and probably highly magnetic phase of Fe_2O_3 a large number of haematite single crystals from different sources have been examined in the course of the present work. While layers which gave diffraction patterns similar to those observed by Finch and Sinha were obtained by heating α-Fe_2O_3 to 500°c in air, the plane spacings found differed considerably from those of haematite; the existence of a new phase could not therefore be confirmed.

Heating these crystals to 700°c produced evidence of oriented Fe_3O_4 on the surface, but in no case did the patterns show the mixed indices to be expected of γ-Fe_2O_3.

§ 2. EXPERIMENTAL DETAILS

2.1. *Heating in Air*

In the majority of cases haematite single crystals having smooth natural (00.1) faces were chosen in order that reasonably good electron diffraction patterns would be obtained. After cleaning or etching in hydrochloric acid, diffraction patterns were taken from the surfaces of these specimens. These showed no diffraction spots other than those of haematite. They were then placed in a nickel container and heated in a wire-wound resistance furnace for a given time and cooled either relatively quickly (over a period of about one half hour) or more slowly (for about three hours).

A number of experiments was devised to investigate the possibility of deposition on to the crystal from the furnace walls; for example lithium fluoride crystals (whose cleaved (100) faces had been initially examined) were heated with haematite crystals in the furnace. No layers were observed. On the other hand layers, similar to those obtained from crystals heated in air, have been observed on haematite crystals heated in sealed Pyrex tubes in the furnace.

Crystals from various sources were used and those from a particular source were subjected to various degrees of etching before heat treatment. The time of heating was varied from one to five hours in the temperature ranges 500–550°c and 700–1000° c.

2.2. *Heating under Reduced Pressure*

These experiments were designed to investigate the layers, if any, formed on single crystals of haematite which had been heated under reduced pressures of either 10^{-2} or 10^{-4} mm Hg. In the former case the specimens were placed in a silica tube, which could be evacuated to a pressure of about 10^{-2} mm Hg by means of a rotary pump, and then heated in the furnace. The temperature of the specimens was measured by an iron–constantan thermocouple. The time of heating was varied between one and four hours in the temperature ranges 500–550°c and 700–800°c. Experiments at lower pressures of the order of 10^{-4} mm Hg were carried out in the diffraction camera. In these cases the specimens were heated in a furnace constructed for use inside the specimen chamber of the diffraction camera at temperatures up to 800°c. A chromel–alumel thermocouple, with the hot junction placed immediately behind the specimen, was used to measure temperature. The diffraction patterns were photographed during the heating process.

§ 3. Results

3.1. *Heating in Air*

3.1.1. *Heating in air* 500–550°c.

The factors which govern the appearance of the layers giving diffraction patterns different from that of haematite could not be precisely determined although the time and temperature of heating were varied as well as the time of cooling. Epitaxial layers have been detected on about one-third of the specimens examined after heating to 500–550°c, the majority of these being crystals which had unetched surfaces. Further in any batch of specimens heated together these layers could again only be observed on a proportion of the specimens examined. Figures 1 (*a*) and (*b*) (Plate) show the diffraction patterns from the natural unetched basal (00.1) plane of a haematite single crystal heated in the furnace for one and a half hours at 550°c. Figure 1 (*a*) shows the pattern produced by continuous variation of the glancing angle of incidence during the exposure, the electron beam being directed along the [10.0] direction. The diffraction pattern at higher glancing angles is due to the haematite substrate. This streaked pattern indicates a good single crystal. As the glancing angle is reduced the arced diffraction pattern from the epitaxial layers becomes visible. This pattern is characteristic of layers almost perfectly oriented with respect to the haematite. Figure 1 (*b*) is similar to figure 1 (*a*) except that the beam is directed along the [1$\bar{1}$.0] direction in this case. It is evident from these patterns (figures 1 (*a*) and (*b*)) that plane spacings from the oriented layers do not approximate closely to those of haematite. The diffraction patterns from these layers have a symmetry similar to the haematite (00.1) plane and their intensity varied according to the portion of the surface of the crystal being examined. Measurements of plane spacings have been made of the layers formed on haematite from various sources. The method of measurement was to compare directly, on the same photographic plate, the diffraction patterns from the layers and the haematite substrate. This was done by changing the glancing angle of incidence in a continuous manner during the exposure of the photographic plate. The cell dimensions of the haematite have been assumed

Plane Spacing Measurements of Layers formed on Haematites from Various Sources

Sample No.	Origin	Main Impurities	d_2(Å)	d_1(Å)	d_3(Å)
S–H (Orig)	Unknown	1·5% Ti	4·81	7·31	2·78
S–H(S–S)	St. Gotthard Switzerland	5·0% Ti 0·5% V 0·15% Al 0·15% Cr	4·82	7·05	2·78
A–H	Arizona, U.S.A.	0·3% Ti 0·1% Al	4·84	7·32	2·80
S–H(RSM)	Unknown	0·35% Ti 0·4% Ba	4·86	7·30	2·81
—	Finch and Sinha (1957)		4·47	6·86	2·57

Here d_1 is the plane spacing obtained from the distance between diffraction spots, measured perpendicular to the shadow edge. d_2 is the plane spacing obtained from the diffraction pattern of figure 1 (*a*), the appropriate distance being measured between spots in a direction parallel to the shadow edge. d_3 is the plane spacing obtained in a manner similar to d_2 but from the diffraction pattern of figure 1 (*b*). The corresponding spacings for pure haematite are 4·36, 13·72, 2·57Å.

and used as the standard. The results of these spacing measurements are shown in the table.

3.1.2. *Heating in air* 700–1000°c.

The results for these experiments varied from specimen to specimen and could be classified under three headings: (*a*) specimens whose surfaces gave diffraction patterns which showed only haematite reflections; (*b*) specimens whose surfaces had become covered with epitaxial layers; diffraction patterns from these layers gave plane spacings similar to those obtained for the layers described in §3.1.1; (*c*) specimens whose surfaces had become covered with a very thin oriented layer of another material. The diffraction patterns from these new layers were consistent with a cubic structure with $a = 8{\cdot}4$ Å and their analyses showed reflections whose indices were either all odd or all even. This indicated Fe_3O_4 rather than γ-Fe_2O_3 since in the latter case reflections having mixed indices would also be expected to be present. The magnetite was oriented in the following way:

(111) Magnetite parallel to the (00.1) Haematite

$[1\bar{1}0]$ or $[\bar{1}10]$ Magnetite parallel to the $[1\bar{1}.0]$ Haematite.

3.2. *Heating under Reduced Pressure*

The diffraction patterns from haematite crystals, heated to 500–550°c under pressures of the order of 10^{-2} mm Hg using the apparatus described in §2.2, showed in the majority of cases an epitaxial layer of magnetite. This was oriented as described above. In some cases, however, only haematite reflections were present in the diffraction patterns after heat treatment.

Haematite crystals were heated in the diffraction camera under a pressure of the order of 10^{-4} mm Hg. The diffraction patterns from the (00.1) faces were observed during heating. As the temperature of these specimens was raised to about 400°c, diffraction spots due to an oriented layer of magnetite began to appear. The intensity of the pattern due to this magnetite layer increased as the temperature was further raised to 700°c until after a certain time the thickness of the layer was sufficient to mask the diffraction pattern from the haematite substrate. The magnetite was again oriented as described in §3.1.2.

§ 4. Discussion

Layers differing from haematite have been observed on haematite crystals heated in air in the temperature range 500–550°c. The diffraction patterns from these layers show a geometrical similarity to those obtained by Finch and Sinha but measurements of plane spacings (cf. table) do not agree with those given by Finch and Sinha. The evidence for the existence of the 'β' phase of Fe_2O_3 is the approximate equality of certain measured plane spacings of the extra layers with those of haematite. The results presented here are not consistent with this requirement for a new phase of Fe_2O_3.

The diffraction patterns (figures 1 (*a*) and (*b*)) from these extra layers show trigonal symmetry. The reciprocal lattice appears to be a primitive hexagon but this information is not sufficient to determine the structure. Prolonged heating of specimens in this temperature range did not increase the thickness of the extra layers. Further, specimens on whose surfaces layers had previously been observed, were reheated and this also failed to increase the intensity of the diffraction pattern, i.e. the thickness of these layers. In some cases the previously formed layers were removed with dilute hydrochloric acid and the crystal reheated. On subsequent examination only traces of the extra layers were observed in the diffraction patterns. In addition, the extra layers were found to be soluble in water. These experiments suggest as a possible mechanism for the origin of these layers, the diffusion of some substance from the interior of the crystal towards the surface.

The diffraction patterns obtained from haematite crystals heated in air in the temperature range 700–1000°c differed also from those found by Finch and Sinha. These authors state that oriented layers of γ-Fe_2O_3 are formed on the haematite substrate at these temperatures. While the presence of γ-Fe_2O_3 has not been confirmed the present work has shown that in some cases a thin oriented layer of Fe_3O_4 was formed.

ACKNOWLEDGMENT

One of us (G. K.) wishes to thank the Department of Scientific and Industrial Research for a maintenance grant.

REFERENCE

FINCH, G. I., and SINHA, K. P., 1957, *Proc. Roy. Soc.* A, **241,** 1.

The Stability of a Dielectric Liquid Jet in the Presence of a Longitudinal Electric Field

By N. K. NAYYAR and G. S. MURTY †
Department of Physics, University of Delhi, India

Communicated by F. C. Auluck; *MS. received 10th August* 1959

Abstract. The stability of a cylindrical jet of incompressible inviscid liquid in the presence of a longitudinal electric field is investigated. It is shown that the electric field increases the stability of the jet. For given values of electric field, the wavelength of the disturbance at which the instability sets in and the wavelength which has maximum rate of instability are calculated.

§ 1. INTRODUCTION

RAYLEIGH had shown that the critical length λ_c of a cylindrical liquid jet is $2\pi R$, where R is the radius of the jet. Recently Glonti (1958) has shown that the critical length of the jet increases in the presence of a longitudinal electric field. His analysis is based on the hydrodynamical equation satisfied by the perturbed stream function with proper boundary conditions on the surface of the jet. We shall re-investigate the problem by applying the Rayleigh energy principle and calculate for a given electric field the modes of critical stability. Also we shall calculate the wavelength for which the instability will develop at a maximum rate.

§ 2. FORMULATION OF THE PROBLEM

Let us consider an infinitely long cylindrical jet of radius R_0 of an incompressible, inviscid dielectric liquid, placed in a uniform electric field E directed along the axis of the cylindrical jet. Since the field is assumed to be uniform we have by virtue of the boundary conditions

$$\phi^i = -EZ, \quad \phi^o = -EZ, \qquad \ldots\ldots(1)$$

where ϕ^i and ϕ^o are the electric potentials inside and outside the cylinder.

In order to study the stability, we imagine that the surface of the jet is deformed by an axisymmetric perturbation and the resulting surface is given by

$$r = R + a\cos kz. \qquad \ldots\ldots(2)$$

Since the liquid is assumed to be incompressible the mass per unit length must be the same before and after the deformation. This requires that

$$R_0^2 = R^2 + \tfrac{1}{2}a^2. \qquad \ldots\ldots(3)$$

The investigation of the stability of the jet consists of two parts. First we calculate the change in surface tension energy $\Delta\sigma$ and the electric energy ΔW per unit length resulting from the perturbation. Then depending upon whether

---

† Now at the Tata Institute of Fundamental Research, Bombay.

$\Delta\sigma+\Delta W$ is positive or negative the jet is stable or unstable. This is essentially the Rayleigh principle of investigating the stability of a system by the energy method.

§ 3. THE CHANGE IN ELECTRIC ENERGY PER UNIT LENGTH CAUSED BY THE DEFORMATION

In order to calculate the change in electric energy we need the changes in the electric field due to the deformation which can be determined from the boundary conditions, namely (i) the normal component of the electric displacement and (ii) the tangential component of the electric field are continuous at the deformed surface.

The change in the electric field distribution can be derived from an electrostatic potential $\delta\phi$ satisfying the Laplace equation

$$\nabla^2\delta\phi=0. \qquad \ldots\ldots(4)$$

For the problem on hand we can represent $\delta\phi$ as a series in powers of a of the form

$$\delta\phi^{\mathrm{i}}=\sum\frac{a^nA_n}{nk}\,\mathrm{I}_0(nkr)\sin nkz$$

$$\delta\phi^{\mathrm{o}}=\sum\frac{a^nB_n}{nk}\,\mathrm{K}_0(nkr)\sin nkz, \qquad \ldots\ldots(5)$$

where $\delta\phi^{\mathrm{i}}$ and $\delta\phi^{\mathrm{o}}$ are potentials inside and outside the jet respectively; A_n and B_n are constants to be determined and I_n and K_n are Bessel functions of order n for purely imaginary argument, which have no singularity at the origin and at infinity respectively.

The constants A_n and B_n in equation (5) are to be determined by the condition that $\delta\phi^{\mathrm{i}}$ and $\delta\phi^{\mathrm{o}}$ and $\epsilon_1(\partial\phi^{\mathrm{i}}/\partial n)$ and $\epsilon_2(\partial\phi^{\mathrm{o}}/\partial n)$ must be continuous on the boundary given by equation (2), where ϵ_1 and ϵ_2 are the dielectric constants of the fluid and the surrounding medium respectively and $\partial/\partial n$ indicates the normal derivative across the boundary. Carrying out the calculation up to second order in a we find that the boundary conditions at the deformed boundary give

$$\begin{gathered}A_1\mathrm{I}_0(kR)=B_1\mathrm{K}_0(kR)\\ A_2\mathrm{I}_0(2kR)=B_2\mathrm{K}_0(2kR). \qquad \ldots\ldots(6)\\ \epsilon_1A_1\mathrm{I}_0'(kR)-\epsilon_1Ek=\epsilon_2B_1\mathrm{K}_0'(kR)-\epsilon_2Ek\\ k\epsilon_1A_1\mathrm{I}_0(kR)+2\epsilon_1A_2\mathrm{I}_0'(2kR)=\epsilon_2B_1\mathrm{K}_0(kR)+2\epsilon_2B_2\mathrm{K}_0'(2kR),\end{gathered}$$

where the prime denotes differentiation with respect to the argument. Solving equation (6) one gets the coefficients A_1, A_2, B_1 and B_2 and hence the potential distribution from equation (5). We can now evaluate the change in electrical energy ΔW per unit length as follows.

Let us suppose that an electrostatic field $\mathbf{E}$ has been established in a dielectric medium of dielectric constant ϵ_2. A dielectric body whose dielectric constant is ϵ_1 is now introduced into the field while the sources of $\mathbf{E}$ are maintained constant. Then one can show that the electric energy of the dielectric body in the electric field is given by (Stratton 1941)

$$W'=\frac{1}{8\pi}(\epsilon_2-\epsilon_1)\int_v \mathbf{E}\,.\,\mathbf{E}'dv, \qquad \ldots\ldots(7)$$

where $\mathbf{E}'$ is the modified field distribution when the dielectric body is introduced into the medium. If we suppose that the body is deformed and the electric field distribution now becomes, say $\mathbf{E}''$, the electric energy of the deformed body is given by

$$W''=\frac{\epsilon_2-\epsilon_1}{8\pi}\int_{v'}\mathbf{E}\,.\,\mathbf{E}''dv. \qquad \ldots\ldots(8)$$

Therefore, the change in electrical energy due to deformation is given by

$$\Delta W=W''-W'. \qquad \ldots\ldots(9)$$

We shall calculate the value of W' and W'' per unit length of cylinder. We have from equations (1) and (7)

$$W'=\frac{E^2}{8\pi}(\epsilon_2-\epsilon_1)R_0{}^2. \qquad \ldots\ldots(10)$$

Similarly the energy per unit length of the deformed cylinder is, from equations (1), (5) and (8), given by

$$\begin{aligned}W''&=\tfrac{1}{4}(\epsilon_2-\epsilon_1)\left\{\int_0^{R+a\cos kz}\left(E^2-EaA_1\mathrm{I}_0(kr)\cos kz-Ea^2A_2\mathrm{I}_0(2kr)\cos 2kz\right)rdr\right\}_{\text{av}}\\&=\frac{E^2}{8\pi}(\epsilon_2-\epsilon_1)R_0{}^2-\frac{a^2}{8}(\epsilon_2-\epsilon_1)A_1ER\mathrm{I}_0(kR),\end{aligned} \qquad \ldots\ldots(11)$$

where we have retained terms up to order a^2 only. Therefore the change in electric energy per unit length due to deformation is

$$\begin{aligned}\Delta W&=W''-W'\\&=-\tfrac{1}{8}a^2(\epsilon_2-\epsilon_1)A_1ER\mathrm{I}_0(kR).\end{aligned} \qquad \ldots\ldots(12)$$

The coefficient A_1 is obtained by solving equations (6). It can be shown that

$$A_1=-\frac{k(\epsilon_2-\epsilon_1)E\mathrm{K}_0(kR)}{\epsilon_1\mathrm{I}_1(kR)\mathrm{K}_0(kR)+\epsilon_2\mathrm{K}_1(kR)\mathrm{I}_0(kR)}, \qquad \ldots\ldots(13)$$

and therefore, the change in electrical energy per unit length due to deformation is given by

$$\Delta W=\frac{a^2kR(\epsilon_2-\epsilon_1)^2E^2\mathrm{I}_0(kR)\mathrm{K}_0(kR)}{8[\epsilon_1\mathrm{I}_1(kR)\mathrm{K}_0(kR)+\epsilon_2\mathrm{I}_0(kR)\mathrm{K}_1(kR)]}. \qquad \ldots\ldots(14)$$

We see that ΔW is positive and is of second order in a. Since the change in energy due to deformation is positive the electrical field has a stabilizing effect on the jet.

§ 4. THE CHANGE IN SURFACE TENSION ENERGY PER UNIT LENGTH CAUSED BY THE DEFORMATION

The change in surface tension energy per unit length of the cylinder resulting from the deformation given by equation (2) is given by

$$\Delta\sigma=\frac{\pi T}{2R}(k^2R^2-1)a^2 \qquad \ldots\ldots(15)$$

where T is the surface tension of the jet.

§ 5. MODES OF INSTABILITY

The total change in potential energy per unit length due to deformation is from equations (14) and (15)

$$\Delta W + \Delta\sigma = \frac{kR(\epsilon_2 - \epsilon_1)^2 E^2 \mathrm{I}_0(kR)\mathrm{K}_0(kR)a^2}{8[\epsilon_1 \mathrm{I}_1(kR)\mathrm{K}_0(kR) + \epsilon_2 \mathrm{I}_0(kR)\mathrm{K}_1(kR)]} + \frac{\pi T}{2R}(k^2R^2 - 1)a^2. \qquad \ldots\ldots(16)$$

The above equation leads to the following conclusions. (i) A jet is always dynamically stable for $kR \gg 1$. (ii) For $kR \ll 1$ a jet is stable when

$$E^2 > \frac{4\pi T[\epsilon_1 \mathrm{I}_1(kR)\mathrm{K}_0(kR) + \epsilon_2 \mathrm{I}_0(kR)\mathrm{K}_1(kR)]}{(\epsilon_2 - \epsilon_1)^2 kR^2 \mathrm{I}_0(kR)\mathrm{K}_0(kR)}. \qquad \ldots\ldots(17)$$

Following the procedure of Chandrasekhar and Fermi (1953), it can be shown that the equation

$$\frac{\pi T}{2R}(x^2 - 1)a^2 + \frac{k(\epsilon_2 - \epsilon_1)^2 E^2 \mathrm{I}_0(x)\mathrm{K}_0(x)a^2}{8[\epsilon_1 \mathrm{I}_1(x)\mathrm{K}_0(x) + \epsilon_2 \mathrm{I}_0(x)\mathrm{K}_1(x)]} = 0 \qquad \ldots\ldots(18)$$

where $kR = x$ allows a single positive root. Let $x = x_c$ denote this root. Then

$$\Delta W + \Delta\sigma > 0 \quad \text{for} \quad x > x_c \qquad \ldots\ldots(19)$$

and

$$\Delta W + \Delta\sigma < 0 \quad \text{for} \quad x < x_c. \qquad \ldots\ldots(20)$$

Hence all modes with $x < x_c$ are unstable. In the table we have listed x_c for a jet of water for a few values of E. This table exhibits the strong stabilizing effect of the electric field.

x_c	E_c (v cm^{-1})	x_m	$1/p_m$ (sec)
0·01	3720·0	0·0070	96·6
0·02	2013·9	0·0140	48·4
0·03	1416·0	0·0209	32·7
0·04	1110·0	0·0277	24·6
0·05	916·5	0·0347	19·7

The critical modes x_c, maximum unstable modes x_m and the growth constant $1/p_m$ of the maximum unstable mode of a water jet for various values of longitudinal electric field. The radius of the jet is 2 cm, $T = 74$ dyn cm^{-1}, $\epsilon_1 = 81$, and $\epsilon_2 = 1$ (air).

§ 6. THE MODE OF MAXIMUM INSTABILITY

In the preceding section we have seen that for a given electric field a dielectric liquid jet is unstable for all modes of deformation with wavelengths exceeding a certain critical value. We shall now show that there exists a wavelength for which the instability is maximum. For this purpose we shall assume that the amplitude a of the deformation is a function of time and seek an equation of motion for it.

We have shown that the potential energy of deformation per unit length of the cylinder is given by equation (16). The kinetic energy per unit length associated with the time dependent deformation is given by (Chandrasekhar and Fermi 1953)

$$K = \frac{\pi\rho R^2 \mathrm{I}_0(x)}{2x\mathrm{I}_1(x)}\left(\frac{da}{dt}\right)^2, \qquad \ldots\ldots(21)$$

where ρ is the density of the fluid. Using equations (16) and (21) we can write the Lagrangian equation of motion for the deformation as

$$\frac{\pi\rho R^2 \mathrm{I}_0(x)}{x\mathrm{I}_1(x)}\left(\frac{d^2a}{dt^2}\right) + \frac{\pi T(x^2-1)a}{R} + \frac{(\epsilon_2-\epsilon_1)^2 x E^2 \mathrm{I}_0(x)\mathrm{K}_0(x)a}{4[\epsilon_1\mathrm{I}_1(x)\mathrm{K}_0(x)+\epsilon_2\mathrm{I}_0(x)\mathrm{K}_1(x)]} = 0 \qquad \ldots\ldots(22)$$

or alternatively,

$$\frac{d^2a}{dt^2} = \frac{x\mathrm{I}_1(x)}{\pi\rho R^2\mathrm{I}_0(x)}\left[\frac{\pi T(1-x^2)}{R} - \frac{(\epsilon_2-\epsilon_1)^2E^2x\mathrm{I}_0(x)\mathrm{K}_0(x)}{4\{\epsilon_1\mathrm{I}_1(x)\mathrm{K}_0(x)+\epsilon_2\mathrm{I}_0(x)\mathrm{K}_1(x)\}}\right]. \qquad \ldots\ldots(23)$$

If we write

$$a = \text{const.}\ \mathrm{e}^{\pm pt} \qquad \ldots\ldots(24)$$

we have from equation (23)

$$p^2 = \frac{x\mathrm{I}_1(x)}{\pi\rho R^2\mathrm{I}_0(x)}\left[\frac{\pi T(1-x^2)}{R} - \frac{(\epsilon_2-\epsilon_1)^2E^2x\mathrm{I}_0(x)\mathrm{K}_0(x)}{4\{\epsilon_1\mathrm{I}_1(x)\mathrm{K}_0(x)+\epsilon_2\mathrm{I}_0(x)\mathrm{K}_1(x)\}}\right]. \qquad \ldots\ldots(25)$$

Equation (25) shows that $p=0$ both for $x=0$ and $x=x_{\mathrm{c}}$. There is, therefore, an intermediate value of x, say x_{m}, for which p is maximum, say p_{m}. The wave number x_{m} clearly represents the mode of maximum instability; for it is the mode for which the amplitude of the deformation increases most rapidly. For $x \ll 1$ we may replace the Bessel functions which occur in equation (25) by their dominant terms for $x \to 0$. The expression on the right-hand side of equation (25) attains its maximum when

$$x_{\mathrm{m}}^2[-\gamma - \log x_{\mathrm{m}}/2 - \tfrac{1}{4}] = \frac{2\pi\epsilon_2 T}{(\epsilon_2-\epsilon_1)^2E^2k}, \qquad \ldots\ldots(26)$$

where γ is Euler's constant 0·5772..... Also the critical mode x_{c} is given by (for $x \ll 1$)

$$x_{\mathrm{c}}^2[-\gamma - \log x_{\mathrm{c}}/2] = \frac{4\pi\epsilon_2 T}{(\epsilon_2-\epsilon_1)^2E^2k}. \qquad \ldots\ldots(27)$$

For various values of x_{c} the values of E and x_{m} for the water jet are computed from equations (26) and (27) by numerical solution. Also the value of $1/p_{\mathrm{m}}$ where p_{m} is the value of p given by equation (25) when $x = x_{\mathrm{m}}$ is calculated. $1/p_{\mathrm{m}}$ gives the scale of time interval in which the amplitude of the disturbance grows by a factor of e.

ACKNOWLEDGMENTS

We are greatly indebted to Professor D. S. Kothari and Professor F. C. Auluck for suggesting the problem and for helpful discussions.

REFERENCES

CHANDRASEKHAR, S., and FERMI, E., 1953, *Astrophys. J.*, **118**, 113.
GLONTI, G. A., 1958, *J. Exp. Theor. Phys.*, **34**, 917.
STRATTON, J. A., 1941, *Electromagnetic Theory* (New York, London: McGraw-Hill), Chap. II.

Low Energy Stopping Power of Atomic Hydrogen

BY A. DALGARNO

Department of Applied Mathematics, The Queen's University of Belfast

Communicated by D. R. Bates; *MS. received* 30*th October* 1959

Abstract. The stopping powers of atomic hydrogen towards beams of protons, neutral hydrogen atoms and negative hydrogen ions are computed for beam energies up to 100 ev.

---

§ 1. INTRODUCTION

THE energy losses of low-energy beams of particles travelling in unlike gases arise almost entirely from the transfer of momentum in elastic collisions and some representative data have been provided by Massey and Sida (1955) and by Sida (1957). Their calculations do not apply to particles travelling in the parent gas for, quite apart from the losses which may occur through resonance charge transfer processes, the symmetry properties of the collisions must be taken into account. The case of low-energy beams of protons, neutral hydrogen atoms and negative hydrogen ions in atomic hydrogen is of particular interest and may be treated with high accuracy.

§ 2. THEORY

It may be shown by elementary considerations that the contribution to the stopping power arising from the transfer of momentum in an elastic collision of a particle of kinetic energy E with a stationary particle of equal mass is given by

$$\Delta_{\mathrm{m}} = \tfrac{1}{2} E Q_{\mathrm{d}} \qquad \ldots\ldots (1)$$

where Q_{d} is the momentum loss or diffusion cross section defined according to

$$Q_{\mathrm{d}} = 2\pi \int_{-1}^{+1} I(\theta)\,(1-\cos\theta)\,d(\cos\theta), \qquad \ldots\ldots (2)$$

$I(\theta)$ being the differential cross section for elastic scattering through an angle θ. For particles moving in unlike gases it suffices to use the classical formula

$$Q_{\mathrm{d}} = 4\pi \int_{0}^{\infty} p \cos^2\alpha(p)\,dp \qquad \ldots\ldots (3)$$

where p is the impact parameter and α is given by

$$\alpha = \int_{R_0}^{\infty} \frac{dR}{R\phi(R)} \qquad \ldots\ldots (4)$$

with

$$\phi(R) = \left\{ \frac{p^2}{R^2} - 1 - \frac{2R^2 V(R)}{E} \right\}^{1/2}, \qquad \ldots\ldots (5)$$

$V(R)$ being the interaction potential at the separation R and R_0 being the outermost zero of $\phi(R)$ (cf. Massey and Burhop 1952). For particles moving in their parent gas it is necessary to use the quantal formula

$$Q_{\rm d}=\frac{4\pi}{k^2}\sum_{l=0}^{\infty}(l+1)\sin^2(\delta_l-\delta_{l+1}) \qquad \ldots\ldots(6)$$

where k is the wave number of the relative motion and δ_l is the elastic scattering phase shift of order l (cf. Mott and Massey 1949).

For the unlike case, it may be shown that the classical and quantal formulae become identical when Jeffreys approximation is used for the phase shifts and the summation over l in (6) is replaced by an integration over $p=\{l(l+1)\}^{1/2}/k$ (de Boer and Bird 1954). This equivalence does not exist in the like case for which there are two possible modes of interaction, one, $V^+(R)$, symmetric with respect to interchange of the nuclei and the other, $V^-(R)$, antisymmetric, and if δ_l is associated with $V^\pm(R)$, δ_{l+1} is associated with $V^\mp(R)$. However we may write down as a classical approximation to (6) in the like case

$$Q_{\rm d}=2\pi\int_0^\infty p\{\sin^2\zeta^+(p)+\sin^2\zeta^-(p)\}dp \qquad \ldots\ldots(7)$$

where

$$\zeta^\pm(p)=\delta_l{}^\pm-\delta_{l+1}{}^\mp \qquad \ldots\ldots(8)$$

in an obvious notation (Dalgarno 1958). If Jeffreys approximation to the phase shifts is used, the accuracy of (7) is comparable with that of (3).

The integral (7) is usually evaluated by splitting the range of integration into two parts according to

$$Q_{\rm d}=\pi(p^*)^2+2\pi\int_{p^*}^\infty p\{\sin^2\zeta^+(p)+\sin^2\zeta^-(p)\}dp \qquad \ldots\ldots(9)$$

where p^* is such that $\sin^2\zeta^\pm(p)$ are rapidly oscillating functions of p when $p<p^*$. Regarded as a function of p^*, $Q_{\rm d}$ oscillates with small amplitude about a mean value which can be taken as the correct value of (7) (Boyd and Dalgarno 1958). Provided p^* is not too small, it suffices to use the Massey–Mohr approximation (Massey and Mohr 1934) to the phase shifts in which case

$$\zeta^\pm(p)=\pm\Gamma(p)+\beta^\pm(p) \qquad \ldots\ldots(10)$$

where

$$\Gamma(p)=\frac{k}{E}\int_p^\infty\frac{V^+(R)-V^-(R)}{\{1-p^2/R^2\}^{1/2}}dR \qquad \ldots\ldots(11)$$

$$\beta^\pm=-\frac{1}{E}\frac{\partial}{\partial p}\int_p^\infty\frac{V^\pm(R)}{\{1-p^2/R^2\}^{1/2}}dR, \qquad \ldots\ldots(12)$$

distance being measured in units of a_0 and energy in rydbergs (Dalgarno, McDowell and Williams 1958). If p^* is large enough, $\beta^+\sim\beta^-$ and (9) may be written

$$Q_{\rm d}=\pi(p^*)^2+4\pi\int_{p^*}^\infty p\{\sin^2\Gamma+\sin^2\beta-2\sin^2\Gamma\sin^2\beta\}\,dp. \qquad \ldots\ldots(13)$$

The contribution to the stopping power arising from resonance charge transfer processes is given by

$$\Delta_{\rm c}=\frac{m}{M}EQ_{\rm c} \qquad \ldots\ldots(14)$$

(Dalgarno and Griffing 1955) where m is the electron mass, M is the mass of the parent atom and Q_c is the cross section for the process. Provided E is not so large that the transfer of electron momentum affects Q_c significantly (cf. Bates and Dalgarno 1952, Dalgarno and Yadav 1953), Q_c may be written (Bates, Massey and Stewart 1953)

$$Q_c = 2\pi \int_0^\infty p \sin^2 \Gamma(p)\, dp. \qquad \ldots\ldots(15)$$

§ 3. CALCULATIONS

For the cases H$^+$ in H and H$^-$ in H the momentum-loss cross section Q_d is equal to twice the capture cross section Q_c for all energies of interest and Q_c has previously been calculated for H$^+$ in H by Dalgarno and Yadav (1953) and for H$^-$ in H by Dalgarno and McDowell (1956), their results being in harmony with recent experimental data (Fite, Brackmann and Snow 1958, Branscomb, Fite, Hummer and Stebbings 1959, private communication). For the case H in H, the energies of interaction $V^{\pm}(R)$ calculated by Dalgarno and Lynn (1956) were fitted by combinations of exponential and polynomial functions and (11) and (12) could then be evaluated analytically (Dalgarno and McDowell 1956, Boyd and Dalgarno 1958).

§ 4. RESULTS AND DISCUSSION

The momentum-loss cross sections Q_d for the collision of a proton, a neutral hydrogen atom and a negative hydrogen ion respectively with a neutral hydrogen atom are given in the table for various impact energies. The cross sections are greatest for negative hydrogen ion collisions and least for neutral atom collisions. The effect of the symmetry requirements is considerable and the cross sections are one or two orders of magnitude greater than for the collision of two unlike particles (Massey and Sida 1955, Sida 1957).

Momentum-loss Cross Sections in units of πa_0^2

Impact energy (ev)	H$^-$–H	H–H	H$^+$–H
0·1	735	47	141
1	494	37	114
10	312	29	85
100	176	22	57

The energy loss associated with momentum transfer in elastic collisions is M/m times that associated with resonance charge transfer processes. Charge transfer is important, however, for it causes a progressive neutralization of the charged constituents of an incident beam. It should be noted that because the large energy losses are associated with scattering at large angles, an incident beam will not appear to be slowed but merely attenuated, most of the slowed particles being scattered out of the beam.

ACKNOWLEDGMENTS

The author is grateful to Mrs. N. Scott for computational assistance. The work reported has been supported in part by the United Kingdom Atomic Energy Research Establishment.

References

Bates, D. R., and Dalgarno, A., 1952, *Proc. Phys. Soc.* A, **65,** 919.

Bates, D. R., Massey, H. S. W., and Stewart, A. L., 1953, *Proc. Roy. Soc.* A, **216,** 437.

de Boer, J., and Bird, R. B., 1954, *Physica*, **20,** 185.

Boyd, T. J. M., and Dalgarno, A., 1958, *Proc. Phys. Soc.*, **72,** 694.

Dalgarno, A., 1958, *Phil. Trans. Roy. Soc.* A, **250,** 426.

Dalgarno, A., and Griffing, G. W., 1955, *Proc. Roy. Soc.* A, **232,** 423.

Dalgarno, A., and Lynn, N., 1956, *Proc. Phys. Soc.* A, **69,** 821.

Dalgarno, A., and McDowell, M. R. C., 1956, *Proc. Phys. Soc.* A, **69,** 615.

Dalgarno, A., McDowell, M. R. C., and Williams, A., 1958, *Phil. Trans. Roy. Soc.* A, **250,** 411.

Dalgarno, A., and Yadav, H. N., 1953, *Proc. Phys. Soc.* A, **66,** 173.

Fite, W. L., Brackmann, R. T., and Snow, W. R., 1958, *Phys. Rev.*, **112,** 1161.

Massey, H. S. W., and Burhop, E. H. S., 1952, *Electronic and Ionic Impact Phenomena* (Oxford: Clarendon Press).

Massey, H. S. W., and Mohr, C. B. O., 1934, *Proc. Roy. Soc.* A, **144,** 188.

Massey, H. S. W., and Sida, D. W., 1955, *Phil. Mag.*, [7], **46,** 190.

Mott, N. F., and Massey, H. S. W., 1949, *The Theory of Atomic Collisions* (Oxford: Clarendon Press).

Sida, D. W., 1957, *Phil. Mag.*, [8], **2,** 761.

High Pressure Neon Flash Tubes

By H. COXELL and A. W. WOLFENDALE
Department of Physics, Durham Colleges in the University of Durham

Communicated by G. D. Rochester; MS. received 27th July 1959, *in revised form 26th October* 1959

Abstract. The properties of high pressure neon flash-tubes suitable for the detection of cosmic rays are described. The tubes have high efficiency for flashing after traversal by ionizing particles, short sensitive time and low rate of spurious flashing A search for an ageing effect has been made by subjecting each of a batch of tubes to 10^6 flashes; no important deterioration in performance has been found.

§ 1. Introduction

The neon flash-tube was first introduced by Conversi and Gozzini (1955) and consists of a glass tube filled with neon and mounted between parallel electrodes. When an ionizing particle passes through the tube and a suitable high voltage pulse is applied across the plates the tube has a high probability of flashing with such intensity that a photographic record can easily be made.

The original tubes of Conversi and co-workers were filled with spectroscopically pure neon at low pressure and had quite high efficiency for pulses applied within 2 μsec of the passage of the ionizing particle. Gardener *et al.* (1957) subsequently showed that comparatively impure gas could be used ('commercial' neon) and that the region of high efficiency could be extended further by increasing the pressure to nearly one atmosphere.

The work of Gardener *et al.* has been extended in order to improve the characteristics of the tubes and in particular to obtain sufficient data to design tubes for particular applications.

This paper is devoted mainly to the experimental aspect of the operation of the tubes; the theoretical treatment of a restricted aspect is considered in an accompanying paper by Lloyd (1960).

§ 2. The Characteristics under Investigation and the Experimental Arrangement

The characteristics to be investigated have been chosen bearing in mind the usual requirements of cosmic ray experiments, namely: *a*, high efficiency for flashing after traversal by ionizing particles, *b*, short sensitive time, *c*, low rate of spurious flashing, *d*, high spatial resolution, *e*, stability of operation, *f*, long lifetime.

The apparatus used for testing the tubes was similar to that used by Gardener *et al.* The stack contained 81 tubes in 9 layers with electrodes every third layer. Alternate plates were earthed and a positive pulse, of variable size, shape and delay was applied to the remaining plates when a fourfold coincidence of a Geiger telescope indicated that a particle had passed through the stack. The arrangement is given in figure 1 where the characteristic parameters of the pulse are also shown. The resulting flashes were recorded on Ilford HPS (red sensitive) film using a camera having an f/3·5 lens. Unless otherwise stated the measurements refer to tubes filled with commercial neon.

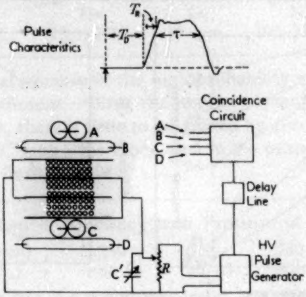

Figure 1. The experimental arrangement and the pulse characteristics. The rise-time T_R and pulse width τ are measured at a field of 2/3 of the maximum value, $E_{\max}$. A, B, C and D are the Geiger counter trays comprising the counter telescope.

As in previous work, two efficiencies can be defined: (i) the layer efficiency η_L the ratio of the number of single flashes observed in a layer to the number of particles having passed through that layer, (ii) the internal efficiency η derived from η_L by multiplying by the ratio R of the separation of the tube centres to the internal diameter of the tubes. This definition involves the reasonable assumption that only those particles traversing the gas of a tube can cause a flash in that tube.

The statistical uncertainty in η_L is derived from the experimental data using the following relation:

$$\sigma_L = \eta_L(1-\eta_L)^{1/2}/n^{1/2}$$

where n is the observed number of flashes. For the value of n used in most of the experiments (of the order of one hundred) the relation is accurate for layer efficiencies to within a few per cent of the maximum possible value. The internal efficiency is thus

$$\eta = R\left\{\eta_L \pm \frac{\eta_L(1-\eta_L)^{1/2}}{n^{1/2}}\right\}.$$

Of the two efficiencies the internal efficiency η is the more fundamental quantity and this will be used in the analysis.

§ 3. THE EXPERIMENTAL RESULTS

3.1. *The Characteristics of Tubes having High Efficiency for Flashing*

3.1.1. *Variation of efficiency with pressure of neon.*

The dependence of plateau efficiency on time delay in the pressure range 0·8–3·0 atmospheres is shown in figure 2. It will be seen that there is considerable advantage in increasing the pressure of the gas to at least 2 atmospheres if, as is usual, time delays in the region of 5 μsec are to be encountered.

3.1.2. *Variation of efficiency with parameters of the pulse.*

Since it is found that a pressure of 2·3 atmospheres is best suited to many applications detailed measurements have been made on tubes filled at this pressure. The variation of efficiency with field is shown in figure 3 (curve a).

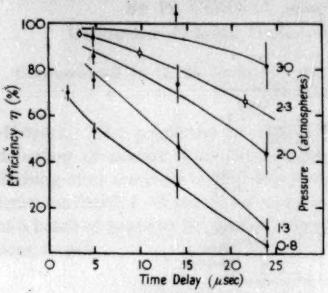

Figure 2.

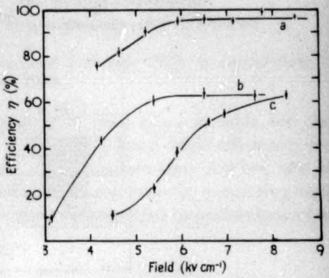

Figure 3.

Figure 2. The efficiency, time delay characteristics of flash tubes with gas pressure as parameter. $E_{\max}=6·3$ kv cm^{-1}, $T_R=0·5$ μsec and $\tau=3·0$ μsec.

Figure 3. The dependence of efficiency on field for tubes filled at 2·3 atmospheres.

a, $T_R=0·5$ μsec, $\tau=3·5$ μsec, $T_D=3·4$ μsec;
b, $T_R=0·5$ μsec, $\tau=3·5$ μsec, $T_D=26$ μsec;
c, $T_R=2·0$ μsec, $\tau=3·5$ μsec, $T_D=4·0$ μsec.

Apart from the peak height of the pulse its main parameters are delay time T_D and rise time T_R. Of these T_D is often fixed by external factors (see later). The variation of plateau efficiency with rise time is shown in figure 4 and the dependence of efficiency on field for extreme values of rise time is shown in figure 3. It is usually possible to reduce the rise time to 0·5 μsec (for example 400 tubes can be fed from one pulsing unit with this value of T_R).

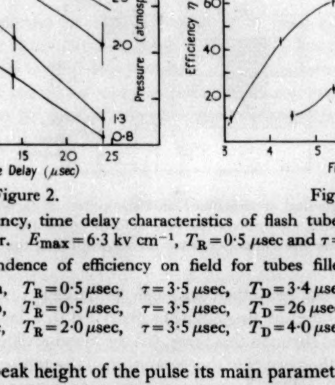

Figure 4. The variation of plateau efficiency with rise time. Neon pressure, 2·3 atmospheres; $E_{\max}=7·0$ kv cm^{-1}, $T_D=4·0$ μsec and $\tau=3·5$ μsec.

3.1.3. *Purity of the gas.*

A typical sample of commercial neon has the constituents shown in table 1. The constituent showing by far the largest variation in quantity from one cylinder to another is nitrogen. Tests have therefore been made on tubes containing spectroscopic neon and various concentrations of nitrogen (all at 0·8 atmosphere pressure). The results, given in table 2, show no apparent reduction in efficiency even at the highest concentration of nitrogen.

Table 1. Constituents of Commercial Neon (vpm = volumes per million)

Gas	Ne	He	O_2	N_2	A
Concentration	98% ± 0·2%	2% ± 0·2%	10 vpm	100–200 vpm	~ 0·5 vpm

Oxygen is detrimental because of the high probability of negative ions being formed by electron attachment. Since the oxygen content of commercial neon can be as high as 0·001% there is little to be gained by evacuating the tubes to a pressure below about 10^{-3} mm; the tubes used in the present investigation were in fact evacuated to this limit.

Table 2. The Variation of Efficiency with Pressure of Nitrogen Impurity

Nitrogen content (vpm)	250	500	750	1000
Internal efficiency (%)	85–90	80–85	80–85	94–100

The neon in the tubes was of spectroscopic quality at a pressure of 0·8 atmosphere. The pulse characteristics were $E_{\max} = 6{\cdot}5$ kv cm^{-1}, $T_R = 0{\cdot}6$ μsec, $T_D = 4{\cdot}0$ μsec and $\tau = 3{\cdot}5$ μsec.

3.2. *The Sensitive Time of the Flash-Tubes*

It has already been stated that a higher gas pressure enables higher efficiencies to be achieved at longer time delays: the consequence of this is a correspondingly longer sensitive time. Thus, in a stack of tubes, flashes will appear due not only to the triggering particle but also to earlier particles. Obviously the number of such flashes must be kept to a minimum and a compromise pressure must be adopted for which the layer efficiency is high and the rate of unwanted flashes low. When

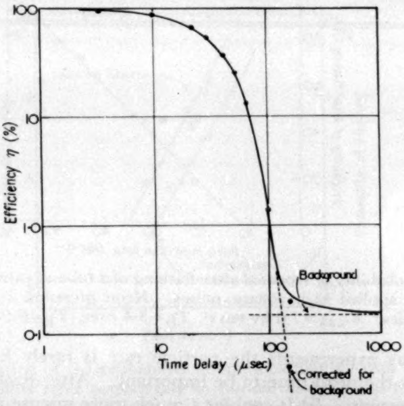

Figure 5. The variation of plateau efficiency with time delay for the tubes containing neon at 2·3 atmospheres pressure. The variation is also shown after correction for background. $E_{\max} = 8{\cdot}5$ kv cm^{-1}, $T_R = 0{\cdot}5$ μsec and $\tau = 3{\cdot}5$ μsec.

time delays in the region of 5–10 μsec are expected this optimum pressure is about 2·3 atmospheres for tubes of internal diameter 5·5 mm.

The variation of efficiency with time delay is shown in figure 5. At long time delays the curve flattens off to the background rate (see § 3.4). After subtracting the background the sensitive time is found by

$$T_s = \int_{-\tau}^{\infty} \eta(t)\,dt = 39\,\mu\text{sec}.$$

The lower limit $-\tau$ allows for flashes produced by particles traversing a tube during the time τ for which the pulse is applied. This value of T_s is sufficiently short for most cosmic ray experiments but in certain experiments with particularly high particle rates this sensitive time could be excessive. Theoretically it should be possible to reduce it by applying a static clearing field which would sweep unwanted electrons to the walls of the tube. The measured values of electron mobility suggest that a field of about 100 v cm^{-1} should reduce the sensitive time to some 5 μsec. Experimentally, fields as high as 2 kv cm^{-1} failed to produce a significant variation in sensitive time. The reason is unknown.

3.3. *The Dead-Time of the Flash-Tubes*

In most particle detectors a certain dead-time follows each detected particle during which subsequent particles will not be recorded. After a neon tube has flashed there is a probability of the same tube flashing again (so-called 'after-flashing') when a subsequent pulse is applied, due to the presence of electrons remaining in the tube from the previous avalanche. The probability falls rapidly from unity after a characteristic 'dead-time'.

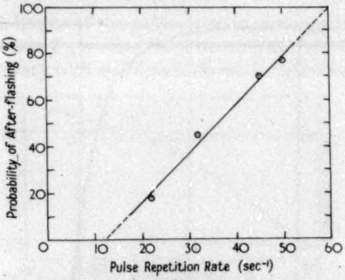

Figure 6. The probability of repeated after-flashing of a tube as a function of the repetition rate of the applied high voltage pulses. Neon pressure, 2·3 atmospheres; pulse characteristics: $E_{\max} = 7{\cdot}0$ kv cm^{-1}, $T_D = 3{\cdot}4$ μsec, $T_R = 0{\cdot}5$ μsec and $\tau = 3{\cdot}5$ μsec.

In cosmic ray experiments the particle rate is rarely high enough for the limitation set by the dead time to be important. After-flashing can, in fact, be useful for two reasons. (i) It enables a much more intense photographic record to be made when a rapid succession of high voltage pulses follows the flash-initiating pulse. This is useful since at high pressures the intensities of the flashes can be rather low. (ii) Repeated flashes give the system a memory so that, for example, some selection of events can be made on the basis of the number, or geometry, of the initial flashes and the camera shutter only opened for the selected events.

An experimental study has been made of the pulse repetition rate required to give repeated flashing. Pulses were applied at a repetition rate varying from about 20 to 50 per sec for 2 seconds and the probability of after-flashing determined visually. The criterion of after-flashing was a minimum of 4 consecutive flashes. Actually in most cases the after-flashing continued for the full period of 2 seconds. The result is shown in figure 6. It is seen that a repetition rate of about 60 pulses per second is required to give fully efficient after-flashing.

The repetition rate for a 50% probability of after-flashing is 36 per second corresponding to a repetition period of 28 msec. The probability of a flash being followed by another will thus fall to 50% for a time interval rather greater than 28 msec and the 'dead time' of the detector is thus of this order of magnitude.

3.4. *The Rate of Spurious Flashes*

In order to find the probability of a tube flashing under a random pulse—that is a pulse not directly associated with an incident particle—the tubes were subjected to about 70 pulses per minute. With $E_{\max}=8{\cdot}5$ kv cm^{-1}, $T_R=0{\cdot}5\ \mu$sec, and $\tau=3{\cdot}5\ \mu$sec, the flashing probability p is found to be $1{\cdot}12\times10^{-4}$ per pulse per tube. The background rate plotted in figure 5 is accordingly pn/R where n is the number of tubes in a layer and R the geometrical factor defined in § 2.

The flashing probability due solely to cosmic rays at times before the instant of application of the pulse is given by $p_e=NT_s$, where N is the rate of cosmic rays through a single tube. On substituting the appropriate values and applying corrections for the effect of showers and knock-on electrons we find $p_e=2{\cdot}64\times10^{-5}$. The ratio of observed to expected is thus 4·2 : 1.

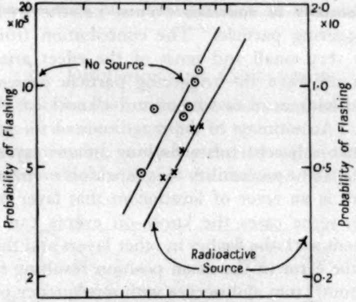

Figure 7. The variation of the probability of spurious flashing with applied field. The two sets of points refer respectively to normal flashing and to flashing under the influence of a radioactive source. The lines drawn through the experimental points have slope 2. The tubes and pulse characteristics are as for figure 3 (a).

The most likely source of the extra flashes is radioactive contamination of the glass and the surroundings. Most of the flashes due to radioactivity arise from photoelectrons, liberated by γ-rays, which give rise to widely differing degrees of ionization of the gas. Consequently an appreciable variation of 'spurious' flashing with field is expected since at higher fields smaller numbers of electrons are required to initiate a discharge. This effect has been studied by varying the size of the applied pulse. The results are shown in figure 7 and show that the probability of spurious flashing varies approximately as the square of the field. Also shown in figure 7 is the result of a similar experiment in which the rate of spurious flashing was greatly increased by the proximity of a radioactive source. The form of the variation is very similar to that observed with no source and seems to confirm that most of the spurious flashes are of radioactive origin. Further evidence in favour of this hypothesis is the fact that the ratio of genuine to total flashes (1 : 4) is of the same order as the ratio of cosmic ray to total counts in a typical copper-in-glass Geiger counter where radioactive impurities are responsible for the non-cosmic-ray counts.

For most applications spurious flashes present no serious disadvantage.

3.5. *The Accuracy of Spatial Resolution*

High spatial resolution is best attained by using several layers of tubes staggered so as to give roughly constant resolution over the angle of acceptance of incident particles. The situation for tubes of rather low internal efficiency (~72%) has been described by Ashton, Kisdnasamy and Wolfendale (1958), where it is shown that the standard deviation of the positional uncertainty from a stack consisting of five layers of tubes, of identical diameter to those used in the present study, is 0·6 mm. For the high pressure tubes described here the uncertainty should be appreciably lower and a geometrical analysis indicates a value of 0·46 mm for five layers of tubes staggered in the optimum manner. The distribution in deviations between the known and predicted track position, found by geometrical analysis, is roughly Gaussian. In practice a longer 'tail' is expected due essentially to spurious events, i.e. the flashing of tubes not traversed by the triggering particle. The contribution from the phenomena described in § 3.4 is very small and most of the effect arises from knock-on electrons. These occur when the triggering particle passes through the gap between the sensitive volumes of two tubes and a knock-on electron produces a flash in one of them. An estimate of the magnitude of this effect can be made. The probability of two adjacent tubes flashing in one layer is found experimentally to be 3·75%. The probability of a knock-on event will be of the order of 5%, and the result is an error of location in that layer of almost one tube radius. However, in some cases the knock-on events can be recognized on account of misalignment with the flashes in other layers and the effect is reduced. It is concluded that the error in the mean position resulting from unrecognized knock-on events is about 1 mm and occurs with a frequency of about 3% which is comparable with that expected on the Gaussian distribution; the effect is thus barely significant.

3.6. *Stability of Operation*

The stability of operation depends on ambient temperature and humidity. Since the electron agitation energy is related to the ambient temperature a change in temperature might change the plateau efficiency. However detailed measurements have shown no significant change over the temperature range 14 – 40°c.

Difficulties of operation are not encountered unless the humidity is abnormally high (R.H. $\gtrsim$ 80%).

3.7. *Lifetime*

An important property of any detector is its expectation of life. If the flash-tube contained only a pure gas an infinite life might be expected. However impurities are present in the original gas filling and others are introduced from the glass walls by ionic impact. Since the characteristics of a discharge are affected by very small quantities of impurities it cannot be stated *a priori* that the lifetime will be long and an experimental check must be made.

A set of tubes of previously measured efficiency was subjected to pulses at a rate of about 1 per second for 13 days. A nearby radioactive source produced a flash in each tube for nearly every pulse and the total number of flashes was over 10^6 for each tube. The efficiencies were measured again at the end of the experiment with the result given in table 3. There is no significant difference in η for short time delays but for a long delay there appears to have been an appreciable reduction. This may be due to a change in surface conditions after the repeated ionic bombardment. It is likely that for comparatively new tubes more of the electrons produced by a pre-triggering particle either do not stick to the wall on collision or if they do stick are easily detached by the high voltage pulse. The change in characteristics is obviously unimportant in practice.

Table 3. Lifetime Test

	$T_D = 4$ μsec	$T_D = 40$ μsec
Efficiency at start (%)	$97{\cdot}5 \pm 3{\cdot}4$	$47{\cdot}0 \pm 2{\cdot}8$
Efficiency after 10^6 flashes (%)	$94{\cdot}5 \pm 3{\cdot}4$	$35{\cdot}5 \pm 2{\cdot}9$

Pulse characteristics: $E_{\max} = 10$ kv cm^{-1}, $T_R = 0{\cdot}6$ μsec, $\tau = 3{\cdot}5$ μsec.
The tubes contained commercial neon at a pressure of 2·3 atmospheres.

§ 4. Discussion and Conclusions

Our work shows that the flash-tubes are characterized by low frequency of spurious flashes, long lifetime and stability of operation. The design of a flash-tube for a particular application is usually carried out in two stages. Firstly, a tube diameter is chosen which will give the required spatial resolution without

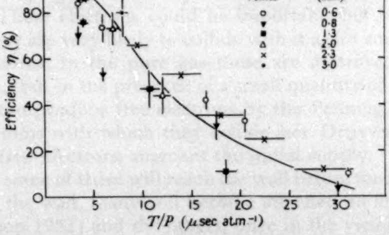

Figure 8. The variation of efficiency with the ratio of time delay to pressure. The curve is an approximate best-fit to the experimental points.

requiring an excessive number of layers. Secondly, the gas pressure is chosen so that the plateau efficiency is high enough for the prescribed time delay, and the rate of spurious flashes sufficiently low.

To facilitate the choice of optimum pressure the possibility of establishing a universal relation between the efficiency and some function of time delay and pressure has been examined. The single parameter T_D/P is found to be suitable. The variation of η with T_D/P is shown in figure 8. In addition to the measurements made in the present work those of Gardener *et al.* for a pressure of 46·1 cm Hg are also included. It is apparent that the simple relation $\eta=f(T_D/P)$ holds to a fair approximation over a wide range of pressures. The efficiency for a given time delay can now be determined for pressures between 0·6 and 3 atmospheres and the frequency of spurious flashes can then be found from the area under the (η, T_D) curve, the known cosmic ray rate, and the contribution from radioactive particles. The significance of the universal curve of figure 8 is discussed by Lloyd (1960).

Acknowledgments

The authors wish to thank Professor G. D. Rochester for his support and interest in the work. We are greatly indebted to Mr. S. Kisdnasamy, for his assistance in filling the majority of the flash-tubes, and Mr. J. L. Lloyd for many stimulating discussions. We should also like to thank the Department of Scientific and Industrial Research for supporting this work and for the award of a maintenance grant to one of us (H.C.). We are grateful, to Mr. J. Pennington of the Rare Gas Department of British Oxygen Co. Ltd., for his co-operation in analysing various samples of gas.

References

Ashton, F., Kisdnasamy, S., and Wolfendale, A. W., 1958, *Nuovo Cim.*, **8,** 615.
Conversi, M., and Gozzini, A., 1955, *Nuovo Cim.*, **2,** 189.
Gardener, M., Kisdnasamy, S., Rössle, E., and Wolfendale, A. W., 1957, *Proc. Phys. Soc.* A, **70,** 687.
Lloyd, J. L., 1960, *Proc. Phys. Soc.*, **75,** 387.

On the Efficiency of the Neon Flash Tube

By J. L. LLOYD[†]

Department of Physics, The Durham Colleges in the University of Durham

Communicated by G. D. Rochester; MS. received 27th July 1959, *in revised form 28th September* 1959

Abstract. **Using simple assumptions, the expected efficiency of neon flash-tubes (Conversi counters) is calculated as a function of time delay and numerical results are given, subject to one adjustable parameter. Satisfactory agreement with experiment is obtained, and the diffusion coefficient for thermal electrons in neon at 1 atmosphere and 20°c is found to be $1800 \pm 100\,\mathrm{cm}^2\,\mathrm{sec}^{-1}$.**

§ 1. INTRODUCTION

Neon flash-tubes (Coxell and Wolfendale 1960) have been considerably developed, but the mechanism is still in some doubt. The experimental feature most amenable to theoretical treatment is the efficiency for flashing as a function of the delay between the passage of the ionizing particle and the application of the electric field. This feature will be investigated using simple assumptions, and the predicted variation will be compared with experimental results.

When an ionizing particle passes through the gas in the tube it leaves a trail of positive ions, electrons and excited neon atoms; and these, with photons, must include the agents which initiate the discharge when the electric field is applied. Now the positive ions can play no part: they scarcely move before or during the flash, recombination is negligible (Gardener *et al.* 1957), and they are too few to distort the applied field significantly. The excited atoms may radiate resonance or non-resonance photons, or may be metastable. Resonance photons progress very slowly through gas: they are continually absorbed and re-emitted and may take 10^{-2} sec to cross the tube, whereas the field is applied and removed within 10^{-5} sec of the passage of the primary particle. Such photons, then, are 'locked up' in the gas during the critical period and cannot help to initiate the discharge. Non-resonance photons go immediately to the wall and perhaps produce photoelectrons there. These electrons could be important, but because they are so close to the wall they are very likely to collide with it again and stick. As for the metastable neon atoms, in the pure gas these are destroyed with emission of resonance photons; but in the presence of a small quantity of argon impurity the metastable atoms can produce free electrons by the Penning effect, that is, they can ionize argon atoms with which they collide (see Druyvesteyn and Penning 1940), and these free electrons augment the initial supply. The free electrons diffuse rapidly and some of them will reach the wall before the field is applied. Of those which reach the wall, many will become attached on first colliding with it (Massey and Burhop 1952) and the others, once in the vicinity of the wall, will repeatedly collide with it until they too stick. Electrons which have stuck to the wall probably skate over the surface when the field is applied, without re-entering the gas†; and it seems reasonable to suppose that the free electrons present in the gas at the start of the pulse, or produced during the pulse, are solely responsible for the initiation of the discharge.

[†] Now at Physics Department, Brighton Technical College.

The probability that the tube will flash must then depend upon the number of free electrons which have remained in the gas, and the evaluation of this number forms the central problem of this paper. Earlier attempts have been made by Conversi *et al.* (1955 a, b) and Gardener *et al.* (1957), but have been based upon invalid approximations; the present work is more exact. The result is then used to predict, in a manner that does not demand a knowledge of the discharge process, the efficiency as a function of the time that elapses between the passage of the primary particle and the application of the electric field; this prediction is based upon the postulate that each free electron has a chance f, of starting a discharge, and that f depends on the tube operating conditions in an unspecified way, but not on the time.

§ 2. THEORY

The formal theory will cover the general case of neon with a little argon; it will then be applied to the case of pure neon.

2.1. *Electron Diffusion*

Consider an electron freed at time $t=0$ in a tube whose internal surfaces are given by the cylindrical coordinates $r=a$, $z=0$ and l. The electron wanders from its starting point, and we may determine the probability that it will later be found in some other part of the tube by making use of the solution of the analogous problem in thermal conduction (Carslaw and Jaeger 1947); explicitly, the probability that an electron, freed at (r', θ', z') will be found within the volume element $rd\theta drdz$ at time t is

$$\rho(r', \theta', z'; t) = \frac{2}{\pi a^2 l} \sum_{m=1}^{\infty} \exp\left(-Dm^2\pi^2 \frac{t}{l^2}\right) \sin\frac{m\pi z}{l} \cdot \sin\frac{m\pi z'}{l}$$
$$\times \sum_{n=-\infty}^{\infty} \cos n(\theta-\theta') \sum_{\alpha} \exp(-D\alpha^2 t) \frac{J_n(\alpha r) J_n(\alpha r')}{[J_n'(\alpha a)]^2} \, r d\theta \, dr \, dz.$$

Here D is the diffusion coefficient for thermal electrons and αa are the positive roots of $J_n(\alpha a)=0$.

We shall consider events which are far removed from the ends of the tube; then after summing over z and noting that only $n=0$ yields a non-zero average over θ we find the probability that the electron remains in the gas is

$$\rho(r'; t) = 2 \sum_{\beta} \exp(-\beta^2 Dt/a^2) \, J_0(\beta r'/a)/\beta J_1(\beta)$$

where $\beta=\alpha a$ and takes the values 2·4048, 5·5201, 8·6537 . . . etc. (Jahnke and Emde 1945).

2.2. *Electron Liberation*

In addition to the cylindrical coordinates, we use cartesian coordinates x and y, whose axes are perpendicular to the tube axis and whose origin is at the tube centre.

---

† If the wall is assumed to exert a short-range attractive force upon an electron, consideration of the resultant force shows that the electron will move tangentially provided that the field does not rise too rapidly. Also, if the electrons were able to re-enter the gas, the sensitive time of the tubes would be very much longer than is observed.

The primary particle passes along the line $x = \text{constant}$. If the probability that it produces a free electron in dy is $Q_1\,dy$, then the number of free electrons surviving to time t follows a Poisson distribution with mean

$$\bar{n}_1 = \int Q_1 \rho(r'\,;\,t)\,dy = 2Q_1 \sum_\beta \frac{\exp(-\beta^2 Dt/a^2)}{\beta J_1(\beta)} \int J_0(\beta r'/a)\,dy.$$

Meanwhile metastable atoms produced by the primary particle with mean number Q_2 per unit length have been reduced in number by destructive collisions. At time t there remain $\int Q_2 \exp[-(\mu_1+\mu_2)t]\,dy$ metastable atoms and with them n_2 electrons:

$$\bar{n}_2 = \sum_\beta \int_0^t 2\left\{\exp[-(\mu_1+\mu_2)t']\,\frac{\mu_1 Q_2}{\beta J_1(\beta)} \exp\left[-\frac{\beta^2 D}{a^2}(t-t')\right] \int J_0(\beta r'/a)\,dy\right\} dt'$$

$$= 2Q_2 \sum_\beta \frac{\mu_1}{\mu_1+\mu_2-\beta^2 D/a^2} \{\exp[-\beta^2 Dt/a^2] - \exp[-(\mu_1+\mu_2)t]\} \frac{\int J_0(\beta r'/a)\,dy}{\beta J_1(\beta)}$$

where μ_1 and μ_2 are the rates of destruction of the metastable atoms respectively with and without production of a free electron†.

The functions

$$2\int J_0(\beta r'/a)\,dy/\beta a\, J_1(\beta)$$

are shown in figure 1 for the first four values of β.

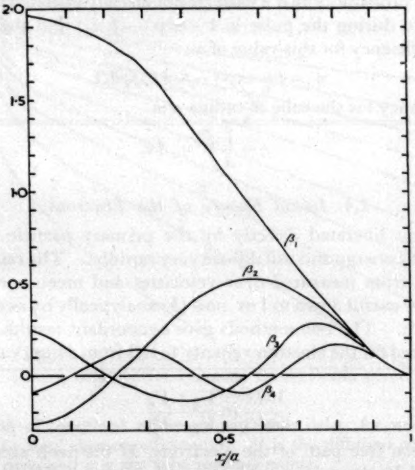

Figure 1. The first four functions $2\int J_0(\beta r'/a)dy/a\beta J_1(\beta)$, which are defined and used in § 2.2.

---

†Destruction of a metastable atom without production of a free electron can occur by a collision with another neon atom, in which the metastable atom is raised to a radiating state with a lifetime of some 10^{-8} sec. If the radiation is ' imprisoned ' in the gas, there will almost always be an atom in the radiative state, and it might be thought that reversion to metastability could occur. The experiment of Jesse and Sadauskis (1955) is best explained, however, by not entertaining this possibility, as is the variation of ionization coefficient with argon content.

During the pulse, which lasts from t to $t+\Delta t$, the number of electrons liberated by metastable atoms formed by the primary particle has mean value

$$\bar{n}_3 = \frac{\mu_1}{\mu_1+\mu_2} \exp\left[-(\mu_1+\mu_2)t\right]\left(1-\exp\left[-(\mu_1+\mu_2)\,\Delta t\right]\right)\int Q_2\,dy.$$

2.3. *Efficiency*

The tube has been traversed by a particle along some particular value of x, and at the start of the pulse there are n free electrons in the gas, such that $\bar{n} = \bar{n}_1 + \bar{n}_2$. Let the probability that an avalanche be caused when $n=1$ be f_1, considered independent of the place of production of this free electron; this assumption is reasonable because the shape of the electron density function soon becomes independent of place of production—the electrons (if they survive) have a short memory. (However, for small values of Dt/a^2 the electrons are still distributed along the path of the primary particle, and the results given in figure 2 are approximations only.)

Then the probability that a flash will be caused by those present at the start of the pulse is easily seen to be

$$\exp(-\bar{n}) \sum_{n=0}^{\infty} \left[1-(1-f_1)^n\right]\bar{n}^n/n!$$
$$= 1-\exp(-f_1\bar{n}).$$

Similarly, the probability that a flash (if not already initiated) will be caused by electrons liberated during the pulse is $1-\exp(-f_2\bar{n}_3)$ and the total probability of a flash is the efficiency for this value of x:

$$\eta_x = 1-\exp(-f_1\bar{n}-f_2\bar{n}_3).$$

The overall efficiency for the tube of radius a is

$$\eta = \frac{1}{a}\int_0^a \eta_x\,dx.$$

2.4. *Initial Energy of the Electrons*

Those electrons liberated directly by the primary particle will at first have considerable kinetic energy and will diffuse very rapidly. The rate of loss of energy can be found (*a*) from measured drift velocities and mean energies in fields of various strengths—useful down to 1 ev, and (*b*) analytically by assuming a value for the mean free path. The two methods give concordant results. Using method (*b*) the time required for the electron velocity to fall from a high value to V_2 is found to be

$$\frac{3M\lambda}{8mV_0}\ln\frac{V_2+V_0}{V_2-V_0}$$

where λ is the mean free path of the electrons, M the neon atomic mass, m the electron mass and V_0 the velocity of a thermal electron. We do not distinguish between the various averages of velocity. The slowing down is essentially complete within a microsecond.

Where Dt has occurred in the equations, we should instead write $\int D'\,dt$, where D' is the diffusion coefficient of the energetic electrons. We find that

$$\int_0^t D'\,dt = D\,(t+\delta t), \quad \text{with} \quad \delta t = \frac{3M\lambda}{4mV_0}\ln\frac{V_1}{2V_0}$$

where V_1 is the initial velocity of the electrons. For reasonable values of the constants the correction at one atmosphere pressure is $\delta t = 0{\cdot}5\,\mu$sec, which is negligible.

2.5. *Knock-on Electrons from the Wall*

If a fraction g of the primary particles produce in the glass a knock-on electron which traverses the gas we should replace η_x by

$$\eta_x\,[1+g\,(1-\eta_x)].$$

We shall ignore this complication, since g is unlikely to exceed 0·03 (Seren 1942).

§ 3. Results from the Theory

From the work of Jesse and Sadauskis (1955) we may assume that $Q_2 = 0{\cdot}46 Q_1$; we also find, from formulae given by these authors, that $1/\mu_2 = 7{\cdot}5\,\mu$sec at one atmosphere pressure and that for an argon concentration of 10 atoms per million of neon, $1/\mu_1 = 180\,\mu$sec, at the same pressure. Accordingly in most of the work of Wolfendale and his associates the initial metastable atoms are unimportant. Conversi and his co-workers have used neon–argon mixtures in which μ_1 exceeded μ_2, but have not published results suitable for testing the theory.

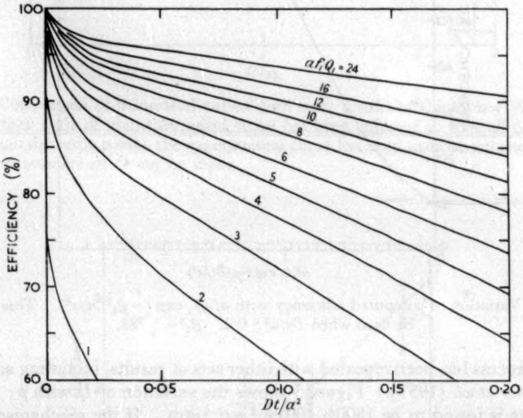

Figure 2. Variation of computed efficiency with time delay, for small time delay, as a function of f_1, the ' electron efficiency '. D is the diffusion coefficient of thermal electrons in neon and a is the tube internal radius.

Computations have been made only for the case in which the metastable neon atoms are never converted (or are immediately converted). Figure 2 shows the computed efficiencies against Dt/a^2, with af_1Q_1 as parameter. For time delays so long that Dt/a^2 exceeds 0·2 the first term of the β-series may be used alone; then the efficiency depends only on $af_1Q_1 \exp\,(-\beta_1{}^2\,Dt/a^2)$, in the manner shown in figure 3; this is the theoretical foundation for the empirical rule found by Coxell and Wolfendale, for if a is constant and f_1Q_1 almost so, the efficiency depends only on Dt, i.e. on t/p.

§ 4. DISCUSSION

Figure 4 shows a family of theoretical curves with the separate time scales so adjusted that all curves pass through the same point at an efficiency of 5%. A specially precise set of experimental results determined by Coxell and Wolfendale (1960) has been treated similarly. It will be seen that the curve marked $af_1Q_1 = 6$ gives reasonable agreement with experiment. D is obtained from the equation $D \simeq (a^2/\beta_1^2 t_{5\%}) \ln(20af_1Q_1)$ and the value of Dp so found (where p is the pressure of the neon) is $1900 \pm 130\ \mathrm{cm^2\,sec^{-1}\,atm}$.

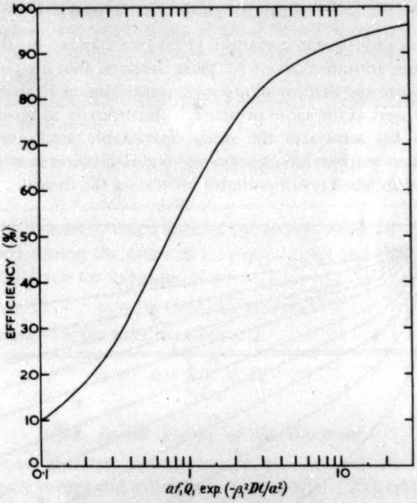

Figure 3. Variation of computed efficiency with $af_1Q_1 \exp(-\beta_1^2Dt/a^2)$. This curve may be used when $Dt/a^2 > 0{\cdot}2$. $\beta_1^2 = 5{\cdot}783$.

This process has been repeated with other sets of results, including some given by Gardener *et al.* (1957). Figure 5 shows the variation of D with p; the mean value of Dp is found to be $1800 \pm 100\ \mathrm{cm^2\,sec^{-1}\,atm}$. If the mechanism investigated here is the dominant one, then this seems to be the first experimental evaluation of Dp for thermal electrons. However, it had been surmised that this quantity lay in the range 600–2200 $\mathrm{cm^2\,sec^{-1}}$ atm for neon, in agreement with the present value (private communication from Dr. A. von Engel).

In practice, from a comparison of theory and experiment, it is found that $f_1 \simeq 1$, being typically 0·4 for $p = 2{\cdot}3$ atm and near unity for $p = 0{\cdot}6$ atm for tubes of radius 0·3 cm in normal operation. It remains to show that these values are reasonable. Consider a tube filled at a pressure of one atmosphere with neon containing 1 part in 2 million of argon (typical of the tubes used by Coxell and Wolfendale 1960). An electric field is applied, rising initially at the rate of

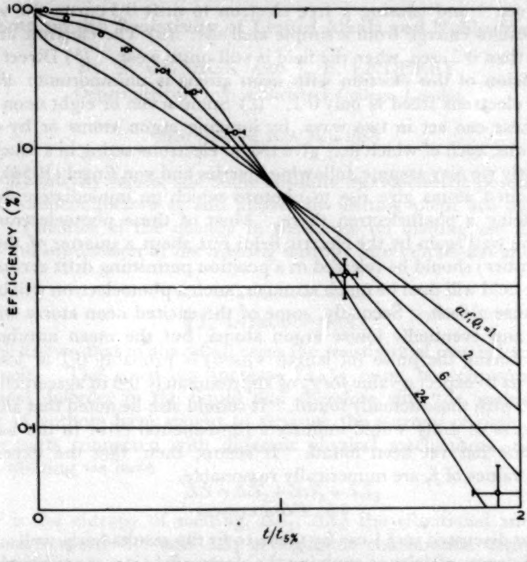

Figure 4. Comparison of theoretical curves with some results of Coxell and Wolfendale. The time scale of each theoretical curve has been adjusted so that all curves pass through the same point; the experimental curve has been likewise adjusted. From this an estimate of D can be made.

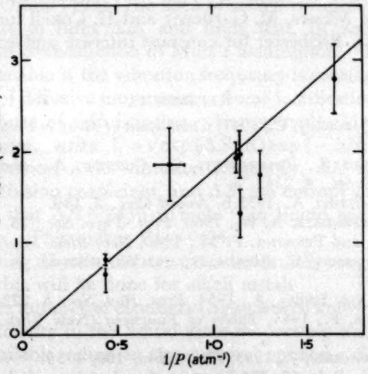

Figure 5. Values of D, the diffusion coefficient of thermal electrons, estimated as in figure 4, for various pressures p.

10^{10} v cm^{-1} sec^{-1} and causing a free electron to drift 0·3 cm to the wall. The following results emerge from a simple analysis: (*a*) The electron drifts to the wall in less than 0·2 μsec, when the field is still quite weak. (*b*) Direct ionization by the collision of this electron with neon atoms is unimportant: the average number of electrons freed is only 0·1. (*c*) Some seven or eight neon atoms are excited; these can act in two ways, by ionizing argon atoms or by producing photoelectrons, each of which may give rise to electrons acting in a much stronger field. Firstly we may assume, following Harries and von Engel (1954), that 30% of these excited atoms give rise to photons which go immediately to the wall, each producing a photoelectron there. Most of these photoelectrons will be driven to the wall again by the electric field, but about a quarter of them (0·6 in average number) should be released in a position permitting drift across the tube. Because the field will then be much stronger, such a photoelectron will be unlikely to fail to cause a flash. Secondly, some of the excited neon atoms will become metastable and eventually ionize argon atoms, but the mean number of such ionizations during the pulse (of length 4 μsec) is probably 0·1 or less. These results lead us to expect a value for f_1 of approximately 0·6 in agreement, perhaps fortuitously, with those actually found. It should also be noted that an empirical value in excess of unity would indicate a fundamental error in the basic ideas; no such value has yet been found. It seems, then, that the experimentally determined values of f_1 are numerically reasonable.

§ 5. CONCLUSION

The ideas discussed in § 1 can be made to fit the results fairly well: the effect, upon the efficiency, of delay in applying the electric field is compatible with the loss of electrons by diffusion to the walls. Support for the theory lies in the fact that the diffusion coefficient found falls in the expected range. One electron may be sufficient to initiate a flash, and this is not unexpected.

ACKNOWLEDGMENTS

The author wishes to thank Drs. A. W. Wolfendale, W. A. Prowse and S. Kisdnasamy and Messrs. M. Gardener and H. Coxell for valuable discussion and Professor G. D. Rochester for constant interest and encouragement in the work.

REFERENCES

CARSLAW, H. S., and JAEGER, J. C., 1947, *Conduction of Heat in Solids* (Oxford: University Press), p. 313.

CONVERSI, M., FOCARDI, S., FRANZINETTI, C., GOZZINI, A., and MURTAS, P., 1955 a, *Nuovo Cim., Suppl.*, **4**, 234.

CONVERSI, M., and GOZZINI, A., 1955 b, *Nuovo Cim.*, **2**, 189.

COXELL, H., and WOLFENDALE, A. W., 1960, *Proc. Phys. Soc.*, **75**, 378.

DRUYVESTEYN, M. J., and PENNING, F. M., 1940, *Rev. Mod. Phys.*, **12**, 87.

GARDENER, M., KISDNASAMY, S., RÖSSLE, E., and WOLFENDALE, A. W., 1957, *Proc. Phys. Soc.* A, **70**, 687.

HARRIES, W. L., and VON ENGEL, A., 1954, *Proc. Roy. Soc.* A, **222**, 490.

JAHNKE, E., and EMDE, F., 1945, *Tables of Functions* (New York: Dover Publications), p. 166.

JESSE, W. P., and SADAUSKIS, J., 1955, *Phys. Rev.*, **100**, 1755.

SEREN, L., 1942, *Phys. Rev.*, **62**, 204.

MASSEY, H. S. W., and BURHOP, E. H. S., 1952, *Electronic and Ionic Impact Phenomena* (Oxford: University Press), p. 321.

A Note on the Resistivity of Liquid Alkali and Noble Metals

By N. CUSACK and J. E. ENDERBY
Department of Physics, Birkbeck College, London

MS. received 15*th July* 1959

Abstract. Resistivity values, and some absolute thermoelectric powers, for pure metals and semiconductors at and above the melting point are collected and tabulated. Theories of the change in resistance on melting are discussed in relation to the subdivision of the melting entropy into vibrational and structural parts.

---

§ 1. INTRODUCTION

It is well known that in almost all cases the resistivity of metals increases when they melt. The resistivity increase $(\Delta\rho)_{\mathrm{m}}$ must be connected with the additional disorder in the liquid and therefore with the melting entropy. A number of authors have sought to separate the entropy of both liquids and solids into parts connected with different physical mechanisms and if this is applied to melting we have

$$\Delta S=\Delta S_1+\Delta S_2+\Delta S_3 \qquad \ldots\ldots(1)$$

where ΔS is the entropy of melting, ΔS_1, ΔS_2, the vibrational and structural contributions respectively, and ΔS_3 a negligible contribution connected, in a metal, with the conduction electrons.

There have been various suggestions for apportioning ΔS_1 and ΔS_2. For face-centred cubic metals Borelius (1958) has based his analysis of thermal data on the assumption $\Delta S_1=0$. In his original explanation of $(\Delta\rho)_{\mathrm{m}}$ Mott (1934) assumed $\Delta S_2=0$. No doubt, in so far as equation (1) represents a valid subdivision, neither ΔS_1 nor ΔS_2 is really zero, and the question is one of estimating their relative sizes. Oriani (1951) has used observed compressibility and thermal expansion coefficients to infer ΔS_1 and finds that, in sodium for example, $\Delta S_1 \sim 12\%$ of ΔS, in contradiction to Mott's assumption. The separation into ΔS_1 and ΔS_2 is reasonable if the vibration frequency is considerably greater than the jump frequency of diffusive movement. Some justification for assuming this is found in observations of self-diffusion. For example, Meyer and Nachtrieb (1955), quoting Zener, write $\Gamma=\nu\exp(\Delta S'/R)\exp(-\Delta H/RT)$, where Γ is the mean jump frequency, ν the vibration frequency, ΔH the exponent in the expression for the diffusion coefficient, and $\Delta S'$ the entropy of activation. They find by experiment that $\Delta H=2430\,\mathrm{cal\,mole}^{-1}$ in liquid sodium and that $\Delta S'$ is small, pehaps zero. This makes $\Gamma/\nu \sim 0{\cdot}04$.

It is possible, using Mott's theory, to estimate ΔS_1 roughly from electrical resistivity data and this will be done for alkali metals.

For a considerable number of elements $(\Delta\rho)_{\mathrm{m}}$ is well known, and the temperature variation of resistivity in the liquid state moderately well known. Table 1 presents the best available values in the authors' opinion. Since no recent and complete collection of these data has been made, it was thought useful to include all conducting elements for which information could be traced although only some cubic metals are discussed in the present paper.

Table 1

Element	T_m (°K)	ρ_S ($\mu\Omega$ cm)	ρ_L ($\mu\Omega$ cm)	$(\rho_L/\rho_S)_{T_m}$	Ref. no.	α $\left(\frac{\mu\Omega \text{ cm}}{\text{deg}^{-1}}\right)$	β ($\mu\Omega$ cm)	Temp. range T_m to:	Ref. no.
Li	452			Insufficient data					
Na	370·9	6·598	9·573	1·451	1	0·038	−4·5	573	2
K	336·8	8·32	12·97	1·56	3	0·064	−8·5	573	4
Rb	312·1	13·7	22·0	1·60	3	0·086	−4·8	373	5
Cs	301·6	21·7	36·0	1·66	3	Insufficient data			
Cu	1356	10·3(5)	21·1	2·04	6	0·0089	9·1	1473	6
		9·4(5)	20·0	2·1	22	0·0102	6·2	1873	22
Ag	1233·6	8·2(5)	17·2(5)	2·09	6	0·0090	6·2	1473	6
Au	1336	13·68	31·2(5)	2·28	6	0·014	12·5	1473	6
Be	1557	No data							
Mg	924	15·4	27·4	1·78	6	0·0050	22·9	1173	6
Ca	1123	No data							
Sr	1043	No data							
Ba	983	~82	~134	1·62	7	Insufficient data			
Zn	692·6	16·7	37·4	2·24	6	Not linear			6
Cd	594	17·1	33·7	1·97	8	Not linear			6
Hg	234·2	18·4 (par.)	90·96	4·94 (par.)	9 sol.	Not linear			
		24·3 (perp.)		3·74 (perp.)	10 liq.				
Al	933·3	10·9	24·2	2·20	6	0·0145	10·7	1473	6
Ga	303	~56 *c* axis	25·8	0·45 *c*	11	0·0195	19·9	670	12
		~18 *a*		1·46 *a*					
		~8 *b*		3·12 *b*					
In	427	15·2	33·1	2·18	6	0·0255	22·2	1273	6
Tl	576	35·5	73·1	2·06	6	0·0292	56·3	1073	6
Si	1713	~2400	~81	0·034	13	0·113	−113	1820	13
Ge	1232	900	60	0·067	14	Insufficient data			
		1200	63	0·053	15				
		1100	85	0·077	16				
Sn	505	22·8	48·0	2·10	6	0·0249	35·4	1473	6
Pb	600·5	49·0	95·0	1·94	6	0·0479	66·6	1273	6
Sb	903·6	183	113·5	0·61	6	0·0270	87·9	1273	6
Bi	544	290·8	130·2	0·45	6	0·0570	99·2	1273	6
Se	493·6	$\sim 10^{3\cdot5}$	$\sim 10^7$	~1000	17	Not linear			18
Te	703·1	~5500 (par.)	~500	0·091 (par.)	19	Not linear			19
		11000 (perp.)		0·048 (perp.)					
Mn	1516	66	40	0·61	20	Insufficient data			
Fe	1808	127·5	138·6	1·05	21				
		122	110	0·9	22	0·033	50	1973	22
Ni	1726	65·4	85·0	1·3	22	0·0127	63	1973	22
Co	1768	97	102	1·05	22	0·0612	−6	1973	22

ρ_L(in $\mu\Omega$ cm) is given by $\alpha T + \beta$ from the melting point to the temperature in column 9.

References for table

1. Bradshaw, F. J., and Pearson, S., 1956, *Proc. Phys. Soc.* B, **69,** 441.
2. *Liquid Metals Handbook Sodium* (NaK) Suppl. 1955.
3. Bridgman, P., 1921, *Proc. Amer. Acad. Arts Sci.*, **56,** 104; 1925, *Ibid.*, **60,** 385.
4. Bornemann, Rauschenplatt, 1912, *Metallurgy*, **9,** 473, 505.
5. Kurnakov, N. S., and Nikitinski, A. I., 1914, *Z. anorg. Chem.*, **88,** 151.
6. Roll, A., and Motz, H., 1957, *Z. Metallk.*, **48,** 272.
7. Grube, G., and Dietrich, 1938, *Z. Elektrochem.*, **46,** 755.
8. Northrup, E., and Suydam, V., 1913, *J. Franklin Inst.*, **175,** 153.
9. Sckell, O., 1930. *Ann. Phys.*, **6,** 932.
10. Jaeger, and Steinwehr, 1914, *Ann. Phys.*, **45,** 1089.
11. Powell, R. W., 1951, *Proc. Roy. Soc.*, A, **209,** 525.
12. Cusack, N., and Kendall, P., 1960, *Proc. Phys. Soc.*, **75,** 309.
13. Mokrovski, H. P., and Regel, A. R., 1956, *Zh. Tekh. Fiz.* **23,** 779.,
14. Keyes, R., 1951, *Phys. Rev.*, **84,** 367.
15. Domenicali, C., 1957, *J. Appl. Phys.*, **28,** 749.
16. Blum, Mokrovski, H. P., and Regel, A. R., 1952, *Izvestia Akad. Nauk SSSR* (*Ser. Fiz.*) **16,** 139.
17. Borelius, G., 1944, *Ark. Mat. Astr. Fys.*, **30A,** No. 14.
18. Lizell, J., 1952, *J. Chem. Phys.*, **20,** 672.
19. Epstein, A. S., Fritzsche, H., and Lark-Horowitz, K., 1957, *Phys. Rev.*, **107,** 412.
20. Grube, G., and Spiedel, H., 1940, *Z. Elektrochem.*, **46,** 233.
21. Powell, R. W., 1953, *Phil. Mag.*, **44,** 772.
22. Regel, A. R., and Mokrovski, H. P., 1953, *Zh. Tekh. Fiz.*, **23,** 2121.

The assumptions of Mott's original treatment of $(\Delta\rho)_m$ are: (i) the type of structural disorder that exists in a liquid does not appreciably increase the resistance; (ii) the resistivity is given in both liquid and solid states by the formula

$$\rho = \frac{N_1 N_2 T}{\Theta^2} \qquad \ldots\ldots(2)$$

where N_1 is a numerical constant, N_2 depends on the atomic weight and electronic states, and Θ is the Einstein temperature; (iii) the atomic vibrations in the liquid are about irregularly distributed equilibrium positions and the increase in resistivity is due solely to a decrease in vibration frequency ν. The term N_2 is assumed the same in both states; (iv) the change in ν may be calculated from the entropy of melting.

§ 2. ALKALI METALS

According to equation (2), the intercept in the resistivity axis at absolute zero is zero, but table 1 shows that all metals, except Na, K, and Rb, show a positive 'residual resistance'. There is enough additional information to show that the negative residual resistances of Na and K are not really anomalous and vanish if the variation of ρ with volume is taken into account. The compressibility of liquid sodium has been measured by Pochapsky (1951). Bridgman (1952) has measured that of solid sodium, and also the variation of resistivity with pressure for both liquid and solid sodium. A combination of these results shows that $\rho \propto T$, at constant volume, for both liquid and solid sodium within, say, 150° from the melting point, in agreement with equation (2). This is also true of potassium but not of most other liquid metals. For Cs, Rb and Li, the data are insufficient to decide.

According to Mott's theory,

$$\frac{\rho_L}{\rho_S} \simeq \frac{\Theta_S^2}{\Theta_L^2} = \frac{\nu_S^2}{\nu_L^2}. \qquad \ldots\ldots(3)$$

It is reasonable to suppose that this equation applies to sodium in particular, for the following reasons: (i) the assumptions underlying equation (1) are realistic for this metal (Jones 1956); (ii) the proportionality of ρ to T has been established by experiment, and this argues that only thermal vibrations are important to sodium resistivity near the melting point; (iii) it is, *a priori*, plausible that the number of free electrons does not change when sodium melts and this is supported by the fact that the thermoelectric power is unchanged (Heiber 1935) and by preliminary observations on the constancy of the Hall coefficient at melting (Kendall, private communication); (iv) the theory of Gubanov can be invoked to provide additional evidence that structural disorder is unimportant to resistivity in liquid sodium (see below).

However, equation (3) does not give a good result for Na if Θ_S/Θ_L is calculated from the latent heat of fusion L, assuming $\Delta S_2 = 0$. The relevant equation, using the Einstein model is,

$$\frac{L}{3RT_m} = \frac{\Delta S}{3R} = \log\frac{1-\exp(-\Theta_S/T_m)}{1-\exp(-\Theta_L/T_m)} + F\left(\frac{\Theta_L}{T_m}\right) - F\left(\frac{\Theta_S}{T_m}\right) \qquad \ldots\ldots(4a)$$

where

$$F\left(\frac{\Theta}{T}\right) = \frac{\Theta/T}{e^{\Theta/T}-1}.$$

At high temperatures, equation (4 *a*) reduces to the most widely used equation of Mott's theory:

$$\rho_L/\rho_S = \exp(80L/T_m) \qquad \ldots\ldots (4b)$$

where L is in kilojoules mole^{-1}.

In principle the Einstein temperature must be known for Na in order to use (4 *a*). In so far as characteristic temperatures derived from specific heats and from resistivity differ, the one from resistivity should presumably be used. In the literature, Debye temperatures are normally given and there is a wide range of recent values for sodium (Blackman 1951, Bradshaw and Pearson 1956). In practice, however, if the observed latent heat is substituted in either (4 *a*) or (4 *b*), they give the same value of ρ_L/ρ_S for any reasonable Θ_S; this value is 1·77 which is too high.

If equation (4) is regarded as an equation for ΔS_1, with $(\Theta_S/\Theta_L)^2$ chosen to equal ρ_L/ρ_S, ΔS_1 comes to 0·00455 kilojoule mole^{-1} deg^{-1} or 65% of ΔS†. The Debye model gives the same result.

Table 2

	Li	Na	K	Rb	Cs
ρ_L/ρ_S obs.	?	1·45	1·56	1·60	1·66
ρ_L/ρ_S calc., $\Delta S_2 = 0$	1·74	1·77	1·76	1·76	1·75
$\Delta S_1/\Delta S$	?	0·65	0·78	0·84	0·92
$\Delta S_2/\Delta S$	?	0·35	0·22	0·16	0·08
$\Delta V/r^3$	1·00	0·70	0·50	0·42	0·38

Table 2 shows the results of similar calculation for all the alkali metals assuming that Rb and Cs can be treated like Na and K. It appears that the structural entropy of melting steadily decreases from approximately 35% for Na to approximately 10% for Rb and Cs.

As previously mentioned, Oriani found a much smaller fraction of vibrational entropy of melting. This may be due to the fact the his method of calculating ΔS_1 allows only for the effect of expansion on the vibrations and not for structural change. But in alkali metals the expansion on melting is unusually small, presumably because of the structural change to closer packing. It has been argued, for example, by Mackenzie and Hillig (1958), that the ion should be regarded as the unit of relative movement in liquid metals. If so, large values of ΔS_2 should be the more favoured, the larger the value of $\Delta V/r^3$, where ΔV is the volume increase per mole on melting and r is the ionic radius. Table 2 shows $\Delta V/r^3$ in arbitrary units and its trend is qualitatively the same as that of ΔS_2.

§ 3. Noble Metals

For the noble face-centred cubic metals, Borelius (1958) gives arguments which fit well with the assumption that their melting entropy is *all* structural. The arguments do not hold so well for the alkali metals, in qualitative agreement with the conclusion above. According to Oriani, approximately 0·7 of the entropy of melting of copper is structural. If, however, the vibrational entropy does not increase discontinuously at the melting point, some other explanation than equation (3) must be found for $(\Delta\rho)_m$ in the noble metals.

---

† *Note added in proof.* L. S. Kothari *et al.* have proceeded similarly in connection with neutron scattering (Kothari, L. S., *et al.*, 1956, *Phil. Mag.*, **1**, 560).

In this connection two ideal cases can be envisaged: (i) a liquid metal satisfying Mott's original theory, with $\rho \propto T$ (at constant volume) and $(\Delta\rho)_m$ due to a change in atomic vibrations; (ii) a metal in which $(\Delta\rho)_m$ is entirely due to an injection of ' residual resistance ', arising from some structural disorder at T_m, while for $T > T_m$, ρ varies linearly with T because of the steady increase of vibrational energy. If P denotes the quantity $\beta/(\Delta\rho)_m$ (see table 1), P will be zero in the first case and 1·0 in the second. P is indeed very small for Na and K if the volume correction is applied. For the noble metals, the information is not available for applying the volume correction, but without it, $P \sim 0{\cdot}7$, and a volume correction would increase this value. There is thus a difference of behaviour between alkali and noble metals. Therefore, despite the good agreement of Mott's original theory with the observations for noble metals, it is reasonable to ask whether in fact some structural feature is not really responsible for $(\Delta\rho)_m$ in these cases.

Scala and Robertson (1953) have demonstrated that small concentrations of impurities in liquid copper, result in the same increase in resistivity as in the solid, and they infer that the disorder in the liquid state relative to the solid "cannot be large because the effect of one foreign atom in one hundred would be lost in comparison with the extensive disorder". But this does not altogether preclude the existence of localized departures from order corresponding to what in the solid would be point defects. If these exist, then Scala and Robertson's results suggest that their resistive effective effects would be similar in liquid and solid.

According to a suggestion of Borelius (1958), the entropy of melting of Cu is connected with the introduction into the structure of vacancies and interstitials in approximately equal numbers. If this is so, the results of van Bueren (1957) can be used to estimate how many such defects would account for the observed $(\Delta\rho)_m$. Since one atomic per cent of vacancies plus the same number of interstitials in solid copper gives an added resistivity of about 6 $\mu\Omega$cm, the observed $(\Delta\rho)_m$ would require 2 atomic per cent. The energy required to form a vacancy and an interstitial is about 6 ev, and 2 atomic per cent therefore require about 11 kilojoules per mole which is about the same as the latent head of fusion. While no significance can be attached to the numerical agreement of such rough estimates, it may be concluded that the assumption $\Delta S_1 = 0$ in the noble metals is not necessarily inconsistent with the resistivity observations. It seems possible, therefore, that $(\Delta\rho)_m$ is associated in the alkali metals chiefly with vibrational change and in the noble metals with structural change. So far as interstitials are concerned, it is believed that much of their resistive effect in the close-packed metals is due to the induced local strains, which are considerable, and not to the extra charge (van Bueren 1957). This effect, and therefore the corresponding resistance, is likely to be considerably less in the body-centred alkalis. It should also be mentioned that the resistance ' anomaly ' in solid sodium just below the melting point has been attributed to $\frac{1}{4}$% of vacancies which add resistivity to the extent of 1·5$\mu\Omega$cm per atomic per cent (Machlup 1956). However, the careful measurements of Bradshaw and Pearson (1956) make it unlikely that the anomaly is really there, so that either the vacancies are absent also, or they have much less than their theoretically estimated resistivity. The latter alternative is somewhat favoured by the fact that there is other evidence to suggest that about $\frac{1}{2}$% of vacancies are indeed present (Machlup 1956). So far as they go, these considerations are in line with the view that structural factors are much less important to the resistance than vibrations near the melting point of sodium, and less important to sodium than to copper.

§ 4. ELECTRON STATES

All the preceding remarks are based on the assumption that the conduction electrons are not much altered by melting. While this is *a priori* probable for alkali metals, there is not much actual evidence. According to Fakidov (1948) the Hall Coefficient of Rb is constant across the melting point to within an experimental error of 10%. The same is true of Na according to recent work by Kendall (private communication). More is known of the absolute thermoelectric power S for which the values are given in table 3.

Table 3. S at Melting Point in μv deg^{-1}

Element	Li	Na	K	Rb	Cs	Cu	Ag	Au
S_S	15·5	−9·9	−17·8	−10·9	0·6	7·2	10·4	3·7
S_L	21·5	−9·9	−15·5	−7·1	6·4	16·7	10·4	3·7
$S_L - S_S$	6·0	0·0	2·3	3·8	5·8	9·5	0·0	0·0

The values are from Heiber (1935) and Lander (1948) and were obtained by subtracting from the observed thermoelectric power the S of the other member of the couple. On this account S may be of the order of 1μv in error but $S_L - S_S$ is directly given by the experiments.

It is interesting to note that where S changes on melting it always increases, and the biggest increases, in both the alkali and noble groups, are in the metals in which the Fermi surface in the solid is believed on other grounds to be closest to, if not actually touching, the zone boundary (Cohen and Heine 1958). A recent paper by Ziman (1959) on residual resistance in copper may give a clue to the behaviour of S at the melting point of noble metals. This paper suggests that (i) impurities in solid copper break the contact between the zone faces and the Fermi surface and make the latter more spherical; (ii) this affects electron transport properties and, in particular, gives a large positive increment to S. The latter effect is not observed in solid Cu. If the Fermi surface remains in contact with the zone face up to high temperatures in pure solid Cu, then the disordering effect of melting may well have the same influence on its shape as the introduction of impurities in the solid. The positive increment of 9μv deg^{-1} would then arise by a mechanism similar to that described by Ziman. It does not occur in Ag and Au, perhaps because the Fermi surface does not touch the zone face, as suggested by Cohen and Heine (1958).

It should be mentioned that formal account of all types of electron scattering in liquid metals is taken by Gubanov's recent theory (1957). However, since this theory is only developed in the free electron approximation it is only reasonable to apply the expression for S to sodium. From Gubanov's formulae it follows that

$$S_L - S_S = \frac{\pi^2 \boldsymbol{k}^2 T}{3|e|\,\epsilon'} \left[\frac{2A_1 k_F^4 + 3B_1 k_F^6}{A_1 k_F^4 + B_1 k_F^6 + D_1} \right] \qquad \ldots\ldots(5)$$

where k_F is the electron wavenumber at the Fermi level; the A_1 and B_1 terms arise from scattering of electrons by both sharply localized and smoothly varying departures from long-range order in the liquid; D_1 comes from electron–phonon scattering. The observation that $S_L - S_S$ is zero or very small, then indicates that the A_1 and B_1 terms are negligible compared with D_1. Since A_1, B_1 also express the structural contribution to $(\Delta\rho)_m$, the thermoelectric observations confirm that structural disorder is unimportant to liquid sodium resistance near T_m.

We conclude that when, as in liquid sodium, there is reason to believe that the electron free path is chiefly determined by thermal vibrations, the resistivity can be used as an alternative source of information about the structural contribution to the melting entropy. In other cases, there still remains considerable doubt as to how the mechanism of the resistivity increase on melting is best described.

REFERENCES

BLACKMAN, M., 1951, *Proc. Phys. Soc.* A, **64,** 681.

BORELIUS, G., 1958, *Solid State Physics*, **7,** 65 (New York: Academic Press).

BRADSHAW, F. J., and PEARSON, S., 1956, *Proc. Phys. Soc.* B., **69,** 441.

BRIDGMAN, P., 1952, *The Physics of High Pressure* (London: Bell).

VAN BUEREN, H. G., 1957, *Philips Res. Rep.*, **12,** 1, 190.

COHEN, M. H., and HEINE, V., 1958, *Phil. Mag. Suppl.*, **7,** 395.

FAKIDOV, I. G., 1948, *Dokl. Akad. Nauk, S.S.S.R.*, **63,** 123.

GUBANOV, A. I., 1957, *Soviet Phys. (Tech. Phys.)*, **2,** 1.

HEIBER, E., 1935, *Ann. Phys., Lpz.*, (Ser. 5), **3,** 111.

JONES, M., 1956, *Handb. d. Phys.*, **19,** 227 (Berlin: Springer).

LANDER, J. J., 1948, *Phys. Rev.*, **74,** 479.

MACHLUP, S., 1956, *J. Chem. Phys.*, **24,** 169.

MACKENZIE, J. D., and HILLIG, W. B., 1958, *J. Chem. Phys.*, **28,** 1259.

MEYER, R. E., and NACHTRIEB, N. H., 1955, *J. Chem. Phys.*, **23,** 1851.

MOTT, N., 1934, *Proc. Roy. Soc.* A, **146,** 465.

ORIANI, R. A., 1951, *J. Chem. Phys.*, **19,** 93.

POCHAPSKY, T. E., 1951, *Phys. Rev.*, **84,** 553.

SCALA, E., and ROBERTSON, W. D., 1953, *J. Metals, N.Y.*, **5,** 1141.

ZIMAN, J. M., 1959, *Proc. Roy. Soc.* A, **252,** 63.

'Atoms in Molecules': A Simple Approach

By E. THEAL STEWART
Chemistry Department, Queen's College, Dundee, Scotland
(University of St. Andrews)

MS. received 9th September 1959

Abstract. The principles underlying Moffitt's method of atoms in molecules and Hurley's intra-atomic correlation correction are examined with the minimum of mathematical analysis, initially by reference to a wave function not involving configuration interaction (the simplest wave function for the lowest $^1\Sigma_u^+$ state of the hydrogen molecule). Because of variational difficulties in more complex systems, and difficulties of interpretation in all systems, it is suggested that the evidence which Hurley has presented in support of asymptotic *energy* adjustments, convincing though it seems, should not be taken to justify the use of the intra-atomic correlation correction as a means of improving molecular wave functions.

§ 1. Introduction

It is customary in the simplest non-empirical molecular-orbital or valence-bond calculations to use the same value of the exponential scale parameter Z for the various states of excitation of a molecular system, and to equate this value to that appropriate to the composite neutral atoms. This leads to errors of the same high order as those obtained in calculations of atomic ionization energies in which the same value of Z is used for the initial and the final states.

Endeavouring to produce a means of eliminating these errors, together with a miscellany of others conventionally attributed to the lack of provision for electron 'correlation' in simple wave functions, Moffitt (1951) developed what is now commonly known as the method of atoms in molecules. He showed that it is possible to formulate a valence-bond calculation (or, equivalently, a molecular-orbital calculation) in such a way as to isolate terms corresponding to the valence-state energies of the dissociation products† of the molecule concerned; and he suggested that the calculated values of these 'asymptotic' energy terms might with advantage be replaced by spectroscopic values. He applied his technique, with considerable success in two cases (Moffitt 1953, Moffitt and Scanlan 1953 a), to a number of π-electron systems, for which calculations on a strict wave-mechanical basis are still overwhelmingly difficult.

Pauncz (1954) and Hurley (1955) independently applied the method of atoms in molecules to the investigation of 'covalent-ionic resonance' in the ground state of the hydrogen molecule. They obtained surprisingly good results with a rather poor wave function (having $Z=1$), but uncovered a number of difficulties on studying improved wave functions. Hurley (1956 a) subsequently demonstrated the need for distinguishing between scaling errors and correlation errors, and introduced his 'intra-atomic correlation correction', in the development of which the method of atoms in molecules has become transformed from a bold device for adjusting energies obtained from crude wave functions to a means of refining calculations of considerable complexity (Hurley 1956 b, c, 1958, 1959). Arai has modified Moffitt's procedure on much the same grounds as Hurley (Arai 1957, Arai and Sakamoto 1958).

---

† The dissociation products must be taken to be those suggested by the form of the approximate wave functions, regardless of spectroscopic evidence.

The main purpose of this paper is to provide a completely unsophisticated account of the application and the effects of asymptotic energy adjustments, by reference to two very straightforward molecular wave functions. In the belief that both the essential simplicity of the method of atoms in molecules and the nature of its assumptions have been seriously obscured by elaborate and highly generalized expositions, we have restricted our analysis throughout to the bare minimum required for the needs of the moment.

Though it avoids the manifest difficulties of the method of atoms in molecules, and has indeed been found to give results in excellent agreement with experimental observations, Hurley's procedure is subject to much the same uncertainties as Moffitt's. One source of trouble is the lack of a demonstrably secure variational basis, and another the fundamental difficulty of correlating changes in molecular wave functions with asymptotic energy changes. In order to examine these separately, we have considered first the simplest valence-bond or molecular-orbital wave function for the lowest ${}^1\Sigma_u^+$ state of hydrogen (a wave function requiring the use of the variation principle only for scaling), and then Weinbaum's (1933) wave function for the ground state.

To facilitate comparison, we have used the same notation as Moffitt and Hurley for *energy* terms in the following discussion, approximation signs (printed as tildes) being used to distinguish symbols for quantities calculated from simple wave functions without empirical adjustment: unembellished, the same symbols represent quantities determined experimentally or calculated very precisely.

§ 2. THE LOWEST ${}^1\Sigma_u^+$ STATE OF HYDROGEN

Four electronic configurations for the hydrogen molecule may be built up from the 1s wave functions of the separate atoms. The following is a convenient set:

$$
\begin{aligned}
({}^1\Sigma_g^+)\quad & \Psi_1=(2+2S^2)^{-1/2}(ab+ba);\\
({}^3\Sigma_u^+)\quad & \Psi_2=(2-2S^2)^{-1/2}(ab-ba);\\
({}^1\Sigma_g^+)\quad & \Psi_3=(2+2S^2)^{-1/2}(aa+bb);\\
({}^1\Sigma_u^+)\quad & \Psi_4=(2-2S^2)^{-1/2}(aa-bb).
\end{aligned}
$$

S is the overlap integral $(a|b)$, and, for example,

$$
\begin{aligned}
aa&=a(1)a(2)=(Z^3/\pi)\exp(-Zr_{a1}-Zr_{a2}),\\
ba&=b(1)a(2)=(Z^3/\pi)\exp(-Zr_{b1}-Zr_{a2}).
\end{aligned}
$$

The triplet wave function Ψ_2 does not admit of any atoms-in-molecules correction; and the 'interaction' of Ψ_1 and Ψ_3 to form an approximate wave function for the ground state has been examined thoroughly by Pauncz (1954) and by Hurley (1955, 1956 a). In this section we shall consider only Ψ_4, where, at the present level of approximation, the problem of configuration interaction does not arise, and the effects of asymptotic energy adjustments are thus immediately apparent. In so far as it is profitable to regard a molecular wave function (in a quantitative sense) as a combination of simple ground-state atomic wave functions, Ψ_4 may be taken to represent the lowest singlet excited state of hydrogen (Herzberg 1950).

In atomic units (which we use throughout) the energy, $\tilde{H}$, corresponding to the function Ψ_4 is

$$\tilde{H}=(1-S^2)^{-1}(2T_0-2ST-2K_0-2K+4SJ+C_0-A)+R^{-1}, \qquad \ldots\ldots(2.1)$$

where

$$T=(a|-\tfrac{1}{2}\nabla^2|b), \quad K=(a|r_b^{-1}|a), \quad J=(a|r_b^{-1}|b),$$

R is the internuclear distance, and C and A are Coulomb and exchange electron-repulsion integrals. Zero subscripts denote one-centre integrals, and these have the values $T_0=\frac{1}{2}Z^2$, $K_0=Z$, $C_0=\frac{5}{8}Z$.

Without necessarily accepting the implication that the hydrogen molecule in its lowest ${}^1\Sigma_u^+$ state dissociates into a proton and a negative hydrogen ion, we may note that the product *aa* appearing in the expansion of Ψ_4 is the simplest wave function which can be formulated for the ion H^-. [Wherever we refer to *a*, *b*, *aa*, *ab*, *ba*, *bb* we mean equally *b*, *a*, *bb*, *ba*, *ab*, *aa*.] The corresponding energy is

$$\tilde{W}=2T_0-2K_0+C_0=Z^2-\frac{11}{8}Z, \qquad \ldots\ldots(2.2)$$

and this has its minimum value ($\tilde{W}'=-0{\cdot}47266$) when $Z=0{\cdot}6875$. The experimental value W of the electronic energy of H^- is uncertain, but accurate calculation (Chandrasekhar 1944) gives $W=-0{\cdot}52756$. From (2.1) it is evident that $\tilde{H}\to\tilde{W}$ as $R\to\infty$.

Now whatever the demerits of the simple product *aa* as a wave function for H^-, it is at least correct in shape, whereas the corresponding molecular combinations $(2\pm 2S^2)^{-1/2}(aa\pm bb)$ are correct only in symmetry. Given optimum values of Z in each case, we may not unreasonably expect the function *aa* to lead to an estimate of the energy of the ion H^- better than that obtained from Ψ_4 for the molecular state ${}^1\Sigma_4^+$ (the more especially if, as spectroscopic evidence indicates, this state does not in fact dissociate into H^++H^-). For no value of R is the calculated energy likely to be in error by less than $0{\cdot}05490$ A.U.; that is

$$\tilde{H}-H>\tilde{W}'-W,$$

where H is the observed electronic energy.

This prediction is readily tested by the substitution of the numerical values of the integrals concerned (Hirschfelder and Linnett 1950) in (2.1). We have calculated $\tilde{H}$ in the range $1\leqslant R\leqslant 5$, treating the scale parameter Z in three different ways. The results are plotted in the figure (curves A) for comparison with the 'observed' results (curve E), which we hope may be represented without significant error by a Morse curve†.

In the present calculations no great difficulty is involved in varying Z so as to provide the best estimate of $\tilde{H}$ for any given internuclear distance (Coulson and Bell 1945), but, bearing in mind the simplifications which are often unavoidable in calculations on more complex systems, we consider also the effects of using arbitrary values of Z independent of R. If we take $Z=1$ (corresponding to the use of unmodified atomic 1s wave functions), we find, as expected, that the calculated energy is much too high over the whole range of R (0·160 A.U. too high at R_e). We next try $Z=0{\cdot}6875$, the optimum value for infinite R: this brings about a slight improvement in $\tilde{H}$ at R_e (reducing the discrepancy between theory and experiment from 0·160 to 0·130 A.U.), and a considerable improvement at larger internuclear distances. Finally we minimize the energy with respect to Z at each value of R, thus effecting a further slight improvement at low values of R, the difference between $\tilde{H}$ and H being now 0·115 A.U. at the equilibrium internuclear distance.

---

† The Morse curve has been constructed from data quoted by Herzberg (1950). In the notation and the units of this paper $R_e=2{\cdot}4429$ and $H_e=-0{\cdot}75666$. We assume, with Mulliken (1932, 1936) and Herzberg (1950), that the asymptotic value of H is $-0{\cdot}625$, corresponding to dissociation into H(1s)+H(2s, 2p), not into $H^++H^-(1s^2)$.

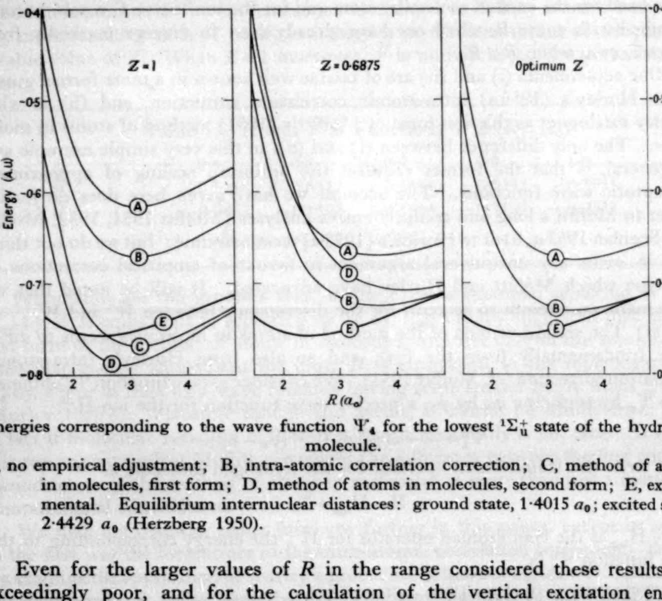

Energies corresponding to the wave function Ψ_4 for the lowest $^1\Sigma_u^+$ state of the hydrogen molecule.

A, no empirical adjustment; B, intra-atomic correlation correction; C, method of atoms in molecules, first form; D, method of atoms in molecules, second form; E, experimental. Equilibrium internuclear distances: ground state, 1·4015 a_0; excited state, 2·4429 a_0 (Herzberg 1950).

Even for the larger values of R in the range considered these results are exceedingly poor, and for the calculation of the vertical excitation energy ($R=1{\cdot}4015$) they are worthless. It is thus of interest to discover whether any improvement can be effected which does not *explicitly* alter the alluringly simple atomic-orbital basis of the calculation. We examine three possibilities, referred to below as (i), (ii) and (iii).

(i) We have already seen that even with optimum scaling of the molecular wave function, $\tilde{H}-H$ for any finite value of R is almost certain to exceed 0·05490 A.U., and we are probably justified in deducting this amount from the calculated values of $\tilde{H}$. The curve showing the effect of this energy correction is labelled B; it is seen to approach the experimental curve quite closely when $R>R_e$ (within the range of the figure), but to diverge badly at lower values of R.

The deduction of 0·05490 A.U. may be made with greater justification, but to lesser effect, in the calculations in which non-optimum values of Z are used.

(ii) If we substitute the quite inappropriate value $Z=1$ in (2.2), we overestimate the energy of the H^- ion by 0·15256 A.U. ($\breve{W}=-0{\cdot}375$). When $\breve{W}$ is calculated with the use of a non-optimum value of Z, there is no reason to suppose that

$$\breve{H}-H>\breve{W}-W,$$

and indeed the inequality may very well be reversed; but if we care to guess that $\breve{H}-H$ and $\breve{W}-W$ are approximately equal, and hence to deduct 0·15256 A.U. from the calculated molecular energy, we obtain, for $R \nless R_e$, a surprisingly good approximation (curve C) to the experimental energy. That this is fortuitous, however, we realize on observing that, if the more suitable value $Z=0{\cdot}6875$ were used for the excited molecular state and for the ion, curve C would become identical with curve B, which we have already seen to diverge markedly from curve E even when $R>R_e$.

Our adjustments (i) and (ii) are of course well known in a more formal guise: (i) is Hurley's (1956 a) intra-atomic correlation correction, and (ii) is what Hurley catalogues as the first form of Moffitt's (1951) method of atoms in molecules. The only difference between (i) and (ii), in this very simple example and in general, is that the former requires the optimum scaling of approximate asymptotic wave functions. The account we have given here does no justice either to Moffitt's long and comprehensive analyses (Moffitt 1951, 1953, Moffitt and Scanlan 1953 a, b) or to Hurley's (1958 a) recent résumé; but we do not think that it omits any unequivocal argument in favour of empirical corrections of the type which Moffitt and Hurley have advocated. It will be noted that we have made no attempt to account for the discrepancy between $\breve{W}'$ and W.

(iii) The second version of the method of atoms in molecules seems to differ quite fundamentally from the first, and so also from Hurley's intra-atomic correlation correction (cf. Moffitt 1951). We consider a wave function Ψ_4^0 obtained from Ψ_4 by replacing *aa* by ϕ_a, a precise wave function for the ion H^-:

$$\Psi_4^0=[2-2(\phi_a|\phi_b)]^{-1/2}(\phi_a-\phi_b).$$

If we write the Hamiltonian operator for the hydrogen molecule as

$$\mathrm{H}=\mathrm{H}_{\text{ion}}+\mathrm{V},$$

where H_{ion} is the Hamiltonian operator for H^-, the energy corresponding to the wave function Ψ_4^0 is

$$\begin{aligned}(\Psi_4^0|\mathrm{H}|\Psi_4^0)&=(\Psi_4^0|\mathrm{H}_{\text{ion}}|\Psi_4^0)+(\Psi_4^0|\mathrm{V}|\Psi_4^0)\\&=[1-(\phi_b|\phi_a)]^{-1}[(\phi_a|\mathrm{H}_{\text{ion}}|\phi_a)-(\phi_b|\mathrm{H}_{\text{ion}}|\phi_a)]+(\Psi_4^0|\mathrm{V}|\Psi_4^0)\\&=[1-(\phi_b|\phi_a)]^{-1}[(\phi_a|\mathrm{H}_{\text{ion}}|\phi_a)-(\phi_b|\phi_a)\,.\,(\phi_a|\mathrm{H}_{\text{ion}}|\phi_a)]\\&\qquad+(\Psi_4^0|\mathrm{V}|\Psi_4^0)\\&=W+(\Psi_4^0|\mathrm{V}|\Psi_4^0).\end{aligned}$$

While there is no reason to suppose that a wave function of any given form is especially accurate when $R\simeq R_e$ merely because its components fulfil their purpose with precision when $R=\infty$, such a wave function may well be better than one known to be unsatisfactory when $R=\infty$. Accordingly, in the second form of the method of atoms in molecules the molecular energy is taken to be $(\Psi_4^0|\mathrm{H}|\Psi_4^0)$ rather than $(\Psi_4|\mathrm{H}|\Psi_4)$. The value of W is known accurately of course, but the interaction term has to be evaluated approximately:

$$(\Psi_4^0|\mathrm{V}|\Psi_4^0) \simeq (\Psi_4|\mathrm{V}|\Psi_4) = (1-S^2)^{-1}(2SJ-2K)+R^{-1} = \tilde{V}. \qquad \ldots\ldots(2.3)$$

Most unfortunately this pleasingly clear-cut procedure offers no advantage over the two already considered (figure, curves D); indeed it is not always the case that $(\Psi_4^0|\mathrm{H}|\Psi_4^0)$, evaluated as in (2.3), is lower than $(\Psi_4|\mathrm{H}|\Psi_4)$. One source of difficulty is readily appreciated: the expansion of the molecular wave function in terms of precise asymptotic wave functions rules out the use of the variation principle for optimum scaling. This might perhaps be unimportant if the interaction term $\tilde{V}$ were insensitive to changes in Z, but, as table 1 shows, it is more sensitive than $\tilde{H}$ itself, and there is no obvious means of selecting a suitable value of Z. When $Z=1$ moreover, $\tilde{V}$ is unduly large for a perturbation term.

Table 1. $\tilde{H}$ and $\tilde{V}$ as Functions of Z ($R=R_e$)

Z	0·6	0·7	0·8	0·9	1·0
$\tilde{H}$	−0·5956	−0·6312	−0·6414	−0·6292	−0·5955
$\tilde{V}$	−0·0453	−0·1107	−0·1664	−0·2139	−0·2533

$[\tilde{V}=(1-S^2)^{-1}(2SJ-2K)+R^{-1}]$

Presumably on the grounds that, in the present example, replacing $\tilde{W}$ (or $\tilde{W}'$) by W is equivalent to replacing *aa* by ϕ_a, it is usually suggested that in the first form of the method of atoms in molecules, and not only in the second, the molecular energy adjustment for finite R is equivalent to the replacement of Ψ_4 by Ψ_4^0, or at least by a wave function having some special merit when $R=\infty$ (Hurley 1958 a). Plausible though this seems, it cannot be wholly true; and in fact if molecular variation of Z is admitted it manifestly is not true. It is for this reason that, unlike Moffitt, we regard the difference between the first and the second forms of the method of atoms in molecules as more than just a matter of computational convenience.

We shall not consider either form any further in this paper, except in so far as the first was the forerunner of the intra-atomic correlation correction. Before we examine the application of Hurley's procedure to more complex wave functions, we should make it quite clear that the arguments outlined in this section have been based on the behaviour as $R\to\infty$ not of the lowest $^1\Sigma_u^+$ state of the hydrogen molecule, but of the simplest approximate wave function that may be used to represent it when $R\simeq R_e$. We have noted that whereas the functions Ψ_4 and Ψ_4^0 suggest H^+ and H^- (1s^2) as the dissociation products, spectroscopic evidence indicates H(1s) and H(2s, 2p). In case this seems to make nonsense of our analysis, we must emphasize that what the procedures (i)–(iii) estimate, correctly or incorrectly, is the difference between $(\Psi_4|\mathrm{H}|\Psi_4)$ and $(\Psi_4^0|\mathrm{H}|\Psi_4^0)$, not the difference between $(\Psi_4|\mathrm{H}|\Psi_4)$ and the true molecular energy. It is not suggested that Ψ_4^0 is a satisfactory wave function for the state we have considered, but merely that it is probably better than Ψ_4.

It follows that asymptotic corrections cannot be used effectively in conjunction with arbitrarily formulated wave functions,† and, in general, this restricts their application to calculations embracing complex sets of atomic configurations.

§ 3. Wave Functions involving Configuration Interaction

The poor results described in §2 are in no way surprising. However satisfactory each may be in its own right, *n* atomic orbitals will not normally provide an adequate quantitative basis for the construction of an *n*-electron molecular wave function; and, furthermore, as we have just seen, a wave function for an excited molecular state cannot well be trusted to give a reliable indication of the nature of the dissociation products if it is compounded solely from ground-state atomic orbitals.‡

There are at least two ways of improving the calculated energies without abandoning an atomic-orbital basis: variation with respect to Z may be carried out in a more flexible way than is customary in calculations based on simple atomic wave functions (Phillipson and Mulliken 1958, Huzinaga 1958), or alternatively interaction between configurations built up on a less restricted basis may be taken into account. It would be of interest to apply the second of these techniques to the $^1\Sigma_u^+$ state of hydrogen, and to study the operation of Hurley's intra-atomic correlation correction on the improved wave function; but, as Hurley's own calculations on Weinbaum's (1933) wave function for the ground state of hydrogen will serve to illustrate all the points involved with little further computation, we shall re-examine them instead.

It is well known that Weinbaum's wave function

$$\Omega = \kappa\Psi_1 + \lambda\Psi_3 = \kappa(2+2S^2)^{-1/2}(ab+ba) + \lambda(2+2S^2)^{-1/2}(aa+bb),$$

with optimum Z and λ/κ, is unique amongst simple molecular wave functions in providing reasonably good values (Kauzmann 1957) not only of the electronic energy (table 2), but also of the equilibrium internuclear distance ($1{\cdot}4135a_0$ instead of $1{\cdot}4015a_0$). It thus serves admirably for an investigation of the effectiveness and the reliability of the intra-atomic correlation correction (in so far as conclusions can be drawn from work on any single wave function).

Adjustments of the straightforward type described in §2 are, of course, not applicable, for the asymptotic behaviour of Weinbaum's wave function is quite unexceptionable ($\kappa \to 1$ and $\lambda \to 0$ as $R \to \infty$). If, however, the assumption is made that the factors which cause the function Ω to overestimate the energy of the hydrogen molecule are (much) the same as those which cause the function *aa* to overestimate the energy of the ion H^- (an assumption we are unable to justify), there are several arbitrary methods which can be used to adjust the calculated energy. Two of these, labelled (*a*) and (*b*), are outlined below; both are *roughly* equivalent to the replacement of Ψ_3 by Ψ_3^0 in Ω.

(*a*) The integrals over atomic orbitals obtained on expanding the molecular integral $(\Omega|H|\Omega)$ include $(aa|H_{\text{ion}}|aa)$, $(ab|H_{\text{ion}}|aa)$, and $(bb|H_{\text{ion}}|aa)$, multiplied by functions of S, κ and λ. With optimum Z, the function *aa* overestimates the energy of the ion H^- by $0{\cdot}05490$ A.U. (§2), and we may feel justified in deducting this amount from the calculated value of $(aa|\mathrm{H}_{\mathrm{ion}}|aa)$, even in the molecular calculation. Less plausibly (but, as it happens, to greater effect), we may also adjust the values of $(ab|\mathrm{H}_{\mathrm{ion}}|aa)$ and $(bb|\mathrm{H}_{\mathrm{ion}}|aa)$ by the deduction of 0·05490 S A.U. and 0·05490 S^2 A.U. respectively, and so obtain one estimate of the decrease in energy which would result if the simple product *aa* in Weinbaum's wave function were replaced by an accurate function for H^- (table 2, adjustment (*a*)).

---

† We should not, for example, expect Hurley's procedure to yield noteworthy results with conventional $2p\pi$-electron wave functions (cf. Hurley 1958 a).

‡ This rather formidable limitation on the applicability of non-empirical methods of calculation to molecular systems is often overlooked.

The justification for modifying the values of $(ab|\mathrm{H}_{\mathrm{ion}}|aa)$ and $(bb|\mathrm{H}_{\mathrm{ion}}|aa)$ in the way just described lies in the assumption that, analogous to the exact relation

$$(\phi_{\mathrm{b}}|\mathrm{H}_{\mathrm{ion}}|\phi_{\mathrm{a}})=(\phi_{\mathrm{b}}|\phi_{\mathrm{a}})W,$$

there exist the approximate relations

$$(ab|\mathrm{H}_{\mathrm{ion}}|aa)\simeq(ab|aa)\bar{W}=S\bar{W},$$
$$(bb|\mathrm{H}_{\mathrm{ion}}|aa)\simeq(bb|aa)\bar{W}=S^2\bar{W},$$

which may perhaps be used fairly safely in the estimation of a small correction term.

Table 2. Ground-state Energy of H_2 (Weinbaum Wave Function). (Bond length $=1{\cdot}4015a_0$)

	Electronic Energy (A.U.)	Dissociation Energy (ev)
No adjustment	−1·148	4·02
Adjustment (*a*)	−1·159	4·33
Adjustment (*b*)	−1·162	4·41
Experimental	−1·174	4·75

Adjustment (*a*): Energy minimized with respect to λ/κ before adjustment of matrix elements.
Adjustment (*b*): Energy minimized after adjustment of matrix elements (intra-atomic correlation correction formula).

(*b*) Hurley's intra-atomic correlation correction, like the method of atoms in molecules on which it was based originally (cf. Hurley 1958 a), goes further than our adjustment (*a*): not only are the values of the integrals arising from the expansion of $(\Psi_3|\mathrm{H}|\Psi_3)$ and $(\Psi_1|\mathrm{H}|\Psi_3)$ modified as above, but λ/κ and even Z are then varied to produce a new energy minimum (table 2, adjustment (*b*)).

Though in this case their effects are very similar, there is an important difference between the two adjustments in that the intra-atomic correlation correction is intended, unlike (*a*), to improve not only the energy but also the molecular wave function (by altering the balance between 'covalent' and 'ionic' components).

Either of the adjustments (*a*) and (*b*) roughly halves the discrepancy between the energy corresponding to Weinbaum's wave function and the observed molecular energy. It would perhaps be rash to attach too much meaning to this seemingly satisfactory result considered in isolation, for any small adjustment which cannot but reduce the calculated energy is bound to appear to be an improvement. But the results which Hurley has obtained in a variety of other systems, under very much more searching conditions, give no cause for scepticism.

Using carefully chosen atomic-orbital bases, Hurley (1956, 1958, 1959) has carried out calculations on the ground states ($R=R_{\mathrm{e}}$ only) of the diatomic molecules N_2, LiH, BH, CH, NH, OH and FH, and also on the lower excited states of the series BH to FH, improving both binding energies and excitation energies most strikingly by applying the intra-atomic correlation correction (i.e. our adjustment (*b*), suitably organized and extended).

§ 4. DISCUSSION AND CONCLUSIONS

Like all computational procedures in which energies are minimized after matrix elements representing non-observable quantities have been adjusted by reference to empirical data, Hurley's intra-atomic correlation correction seems to do some violence to the variation principle, though whether to an important extent, as in the method of atoms in molecules (Pauncz 1954, Hurley 1955), we cannot decide. It is most unfortunate in this respect that there is as yet no means of assessing the significance of the apparent improvements in wave functions (as evinced by changes in calculated dipole moments and transition probabilities) brought about by the application of Hurley's procedure. This is partly because the intra-atomic correlation correction has been applied, except in the case of hydrogen (Hurley 1956 a), only to calculations based on non-optimum molecular scale parameters, partly because of the interpretative difficulty mentioned in the next paragraph, but mainly because of the paucity of experimental data.

If a molecular wave function is formulated as an antisymmetrized linear combination (with optimum interaction coefficients) of the approximate wave functions of the corresponding dissociation products, it is by no means obvious that the electron-density distribution represented by the molecular wave function is necessarily improved by an adjustment of the coefficients not strictly controlled by the variation principle. Indeed it is not clear what meaning can be assigned to the adjusted coefficients: even in principle the intra-atomic correlation correction is only roughly equivalent to a calculation in which approximate asymptotic wave functions are replaced by their more precise counterparts (§ 2); in practice (in the calculation of dipole moments and transition probabilities) the approximate asymptotic wave functions remain unchanged, and so also the corresponding electron-density distributions. While Hurley's procedure probably provides a reasonably safe method of allowing for intra-atomic errors in molecular energy calculations, perhaps by some implicit form of guided extrapolation, as a means of improving molecular wave functions it seems insecure and difficult to interpret.

The removal of the uncertainty caused by the use of non-optimum scale parameters in calculations of the type Hurley has carried out would require extensive computations. It is perhaps not unreasonable to hope that almost equally good non-empirical results might now be obtained, with comparatively little additional effort, from calculations embodying a very flexible treatment of atomic-orbital scale parameters (see, e.g., Phillipson and Mulliken 1958); such calculations would have an unassailable variational basis, and would provide wave functions free from the unavoidable ambiguities associated with the application of intra-atomic correlation corrections.

ACKNOWLEDGMENTS

The author is very much indebted to Professor C. A. Coulson and to Dr V. W. Maslen for comments on an early draft of this paper. The work described was carried out during the tenure of Deeds and Carnegie Research Fellowships.

REFERENCES

ARAI, T., 1957, *J. Chem. Phys.*, **26**, 435, 451.
ARAI, T., and SAKAMOTO, M., 1958, *J. Chem. Phys.*, **28**, 32.
CHANDRASEKHAR, S., 1944, *Rev. Mod. Phys.*, **16**, 301.
COULSON, C. A., and BELL, R. P., 1945, *Trans. Faraday Soc.*, **41**, 141.
HERZBERG, G., 1950, *Spectra of Diatomic Molecules* (New York: Van Nostrand).
HIRSCHFELDER, J. O., and LINNETT, J. W., 1950, *J. Chem. Phys.*, **18**, 130.
HURLEY, A. C., 1955, *Proc. Phys. Soc.* A, **68**, 149.
—— 1956 a, *Ibid.*, **69**, 49.
—— 1956 b, *Ibid.*, **69**, 301.
—— 1956 c, *Ibid.*, **69**, 868.
—— 1958 a, *J. Chem. Phys.*, **28**, 532.
—— 1958 b, *Proc. Roy. Soc.*, A, **248**, 119.
—— 1959, *Ibid.*, **249**, 402.
HUZINAGA, S., 1958, *Progr. Theor. Phys. Japan*, **20**, 15.
KAUZMANN, W., 1957, *Quantum Chemistry* (New York: Academic Press Inc.).
MOFFITT, W., 1951, *Proc. Roy. Soc.*, A, **210**, 224, 245.
—— 1953, *Ibid.*, **218**, 486.
MOFFITT, W., and SCANLAN, J., 1953 a, *Proc. Roy. Soc.*, A, **218**, 464.
—— 1953 b, *Ibid.*, **220**, 530.
MULLIKEN, R. S., 1932, *Rev. Mod. Phys.*, **4**, 78.
—— 1936, *Phys. Rev.*, **50**, 1017, 1028.
PAUNCZ, R., 1954, *Acta Physica, Hung.*, **4**, 237.
PHILLIPSON, P. E., and MULLIKEN, R. S., 1958, *J. Chem. Phys.*, **28**, 1248.
WEINBAUM, S., 1933, *J. Chem. Phys.*, **1**, 593.

Shock Waves and Controlled Thermonuclear Fusion

By J. K. WRIGHT

Atomic Weapons Research Establishment, Foulness, Southend on Sea, Essex

MS. received 13*th March* 1959, *in final form* 13*th October* 1959

Abstract. An assessment is given of the various types of thermonuclear device based on shock heating. The classical shock heating process in which the mean free path in the shocked gas is much smaller than the dimensions of the apparatus is analysed and it is shown that shock heating alone is unlikely to yield temperatures in excess of the order of 3×10^6 deg K with present day techniques. The temperature may be increased in principle to a value required for power production by isentropic compression after the shock heating phase. The so-called Z pinch types of apparatus are limited by the growth of instabilities whereas the θ pinch devices are limited by the difficulty of recovering energy without undue ohmic losses.

---

§ 1. INTRODUCTION

ONE of the requirements of a successful power producing controlled thermonuclear reactor is that the temperature of a suitable gas such as deuterium should be raised to many times 10^7 deg K. One method that has been suggested of achieving such temperatures is to shock heat the gas and various experiments have been described (Artsimovich *et al.* 1956, Anderson *et al.* 1957, Bodin and Reynolds 1957, Kolb 1957, Hagerman and Mather 1958, Elmore, Little and Quinn 1958 are typical) in which temperatures of the order of 10^6 deg K have been attained when deuterium was shock heated by waves generated electromagnetically. This paper describes a theoretical assessment of the potentialities and limitations of shock heating in relation to controlled thermonuclear reactors. The theory is based on the assumption that the mean free path in the gas is always much smaller than the dimensions of the apparatus so that the results of classical shock wave theory are valid. In order to obtain numerical results it has been necessary to postulate reasonable values of circuit parameters and the actual numerical results are therefore only approximate although the general conclusions are valid.

§ 2. GENERAL DESCRIPTION OF THE APPARATUS AND PHYSICAL PHENOMENA

Figure 1 shows some of the experimental arrangements that may be used to generate strong shock waves. Arrangement A is known as a fast linear pinch apparatus on which there has been much experimental work (Artsimovich *et al.* 1956, Anderson *et al.* 1957, Bodin and Reynolds 1957, Hagerman and Mather 1958). An axial discharge current starts in a cylindrical sheet near the walls of the discharge tube where the resulting circuit inductance is a minimum and the resulting circumferential magnetic field drives the current-carrying gas particles towards the axis with such violence that, providing the initial assumption that the mean free path in the gas is much smaller than the dimensions of the apparatus is valid, an intense shock wave is produced. This shock wave is reflected at the axis and the gas is once again shocked. The subsequent motion of the gas is very complex, but in it the pressure differences across any shocks are small compared with the ambient pressure and the gas condition can be calculated to a high degree of approximation by assuming the changes to be isentropic as the plasma is compressed by the rising magnetic field.

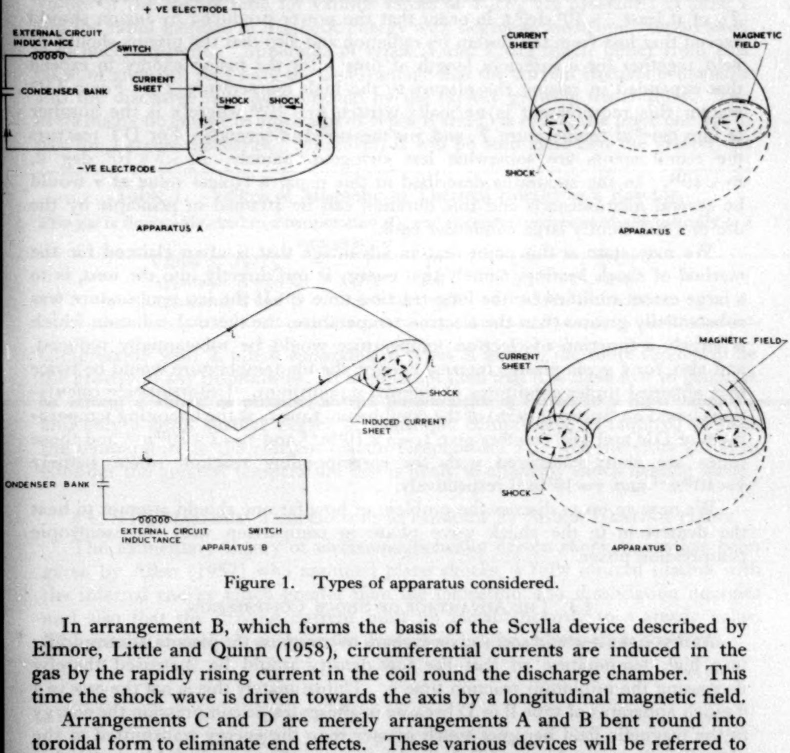
+ VE ELECTRODE
EXTERNAL CIRCUIT INDUCTANCE
SWITCH
CONDENSER BANK
CURRENT SHEET
SHOCK
SHOCK
-VE ELECTRODE
APPARATUS A
CURRENT SHEET
MAGNETIC FIELD
SHOCK
APPARATUS C
SHOCK
INDUCED CURRENT SHEET
ONDENSER BANK
EXTERNAL CIRCUIT INDUCTANCE
SWITCH
APPARATUS B
MAGNETIC FIELD
CURRENT SHEET
SHOCK
APPARATUS D

Figure 1. Types of apparatus considered.

In arrangement B, which forms the basis of the Scylla device described by Elmore, Little and Quinn (1958), circumferential currents are induced in the gas by the rapidly rising current in the coil round the discharge chamber. This time the shock wave is driven towards the axis by a longitudinal magnetic field.

Arrangements C and D are merely arrangements A and B bent round into toroidal form to eliminate end effects. These various devices will be referred to as A, B, C and D respectively in the following discussion. A and C are often called Z pinches because the current flows along the axis of the discharge whereas apparatus of type B and D are called θ pinches because the current is in the azimuthal direction.

The hot ionized deuterium behaves as a monatomic gaseous mixture of deuterons and electrons, since detailed calculations show that the ionization energy of the deuterium can be neglected in approximate calculations at temperatures above 10^6 deg K. W assume, initially, that the electrons and deuterons are in thermodynamic equilibrium. According to standard strong shock wave theory the density of a singly shocked gas then rises to four times the ambient density and the density of the doubly shocked gas is ten times ambient density. Throughout the subsequent isentropic compression the plasma density rises rapidly with pressure and temperature in the usual form $\rho \propto p^{3/5}$ and $\rho \propto T^{3/2}$. Thus whereas the shock heated gas is at a high temperature but relatively low density, the temperature rise in the subsequent isentropic compression is accompanied by a large density increase. It is well known (see, for example, Lawson 1957) that the requirements for a successful DD reactor are that the ions should be raised to a temperature T_F of at least 2×10^8 deg K in order that the power produced by fusion should exceed that lost from the system by radiation and also that the plasma should be held together for a sufficient length of time τ for the fusion energy to exceed that expended in raising the plasma to the high temperature T_F. For a DD reactor this requirement is normally written $n\tau > 10^{16}$ where n is the number of ions cm^{-3} at temperature T, and τ is measured in seconds. For DT reactors the requirements are somewhat less stringent, namely, $T_F > 3 \times 10^7$ deg K, $n\tau > 10^{14}$. In the apparatus described in this paper a typical value of τ would be several microseconds and this duration can be attained in principle by the use of a sufficiently large condenser bank.

We may state at this point that an advantage that is often claimed for the method of shock heating, namely that energy is put directly into the ions, is to a large extent nullified by the long reaction time τ. If the ion temperature was substantially greater than the electron temperature, the thermal radiation which is largely a function of electron temperature would be substantially reduced, and also, for a given plasma internal energy, the ion temperature would be twice that obtained under conditions of thermal equilibrium. Unfortunately calculations based on Spitzer (1956) of the equilibrium time t_e at the operating temperatures of DD and DT reactors give $t_e = 3 \times 10^{14} n^{-1}$ and $t_e = 2 \times 10^{13} n^{-1}$ and these times are short compared with the corresponding reaction times, namely $\tau = 10^{16} n^{-1}$ and $\tau = 10^{14} n^{-1}$ respectively.

We now go on to discuss the problem of how far one should attempt to heat the deuterium in the shock wave phase in comparison with the isentropic compression phase.

§ 3. THE ADVANTAGE OF SHOCK COMPRESSION

At first sight it would seem advantageous to compress the plasma isentropically to a high temperature so that the ion density would be increased thereby decreasing the minimum reaction time τ. Unfortunately this is not the case in a θ pinch apparatus of type B or D because in an isentropic compression the energy in the magnetic field becomes much greater than the energy transmitted to the plasma and copper losses will limit the amount of magnetic field energy that can be converted directly back into electrical energy. As a consequence the value τ must be increased above the figures quoted above, which do not take copper losses into account. The detailed theory shows that, for a given ambient density, the value τ is approximately independent of the degree of isentropic compression when we consider ohmic losses in the circuit. Suppose the plasma is double shocked to a temperature T_R and then compressed isentropically to a temperature T_F, it can be shown, by equating magnetic and hydrodynamic pressure, that for apparatus of type A and C the ratio of magnetic to thermal energies on the system is given by

$$\frac{E_{\mathrm{M}}}{E_{\mathrm{T}}}=\ln\left(\frac{T_{\mathrm{F}}}{T_{\mathrm{R}}}\right)+\tfrac{2}{3}\ln 10, \qquad \ldots\ldots(1)$$

whereas for types B and D, the ratio is

$$\frac{E_{\mathrm{M}}}{E_{\mathrm{T}}}=\frac{2}{3}\left\{10\left(\frac{T_{\mathrm{F}}}{T_{\mathrm{R}}}\right)^{3/2}-1\right\}. \qquad \ldots\ldots(2)$$

Values of the energy ratio for various values of $T_{\mathrm{F}}/T_{\mathrm{R}}$ are presented in table 1 and the rapid increase in magnetic energy with degree of isentropic compression is at once apparent. Apparatus of types A and C are much better from this point of view but they have the disadvantage that the current channel is unstable and the discharge may be quenched by the rapidly growing instabilities. The extra magnetic energy in apparatus of types B and D is in fact the price one has to pay for a stable discharge. Moreover, it will be seen later that the greater the compression with Z pinch apparatus of types A and C, the more rapid will be the growth of any instabilities. It is apparent then that it is desirable to generate as strong a shock as possible so the temperature is raised to a high value T_{R} and only a small further degree of isentropic compression is required to raise the temperature to the efficient reactor temperature T_{F}. We therefore go on to consider the greatest temperature one is likely to attain by shock heating alone.

Table 1. Values of Magnetic to Thermal Energy in a Reactor

The gas is doubly shocked to a temperature T_{R} and thereafter compressed adiabatically to a temperature T_{F}

Values of $T_{\mathrm{F}}/T_{\mathrm{R}}$	1	10	100	1000
Apparatus A and C	1·5	3·8	6·1	8·4
Apparatus B and D	6·0	$2{\cdot}1\times10^{2}$	$6{\cdot}7\times10^{3}$	$2{\cdot}1\times10^{5}$

§ 4. The Maximum Temperature attainable by Shock Heating alone

The elementary theory of electromagnetically driven shock waves has been given by Allen (1957) who assumed plane shocks, a fully ionized plasma with the internal energy much greater than the ionization and dissociation energies and also that the driving current built up instantaneously to a steady value. The results of such an analysis for deuterium can be expressed in the form

$$T_{\mathrm{S}}=3{\cdot}6\times10^{10}V_0 b^{-1}n_0^{-1/2} \qquad \ldots\ldots(3)$$

$$n_{\mathrm{S}}=4n_0 \qquad \ldots\ldots(4)$$

$$w^2=6\boldsymbol{k}T_{\mathrm{S}}/M \qquad \ldots\ldots(5)$$

$$T_{\mathrm{R}}=2{\cdot}4T_{\mathrm{S}}=8{\cdot}6\times10^{10}V_0 b^{-1}n_0^{-1/2} \qquad \ldots\ldots(6)$$

$$n_{\mathrm{R}}=10n_0 \qquad \ldots\ldots(7)$$

where T_{S} is the temperature of the imploding shocked plasma (°K), V_0 is the potential applied across the discharge (volts), b is the length of the discharge path (cm), n_0 is the number of deuterons cm^{-3} in the unshocked gas, n_{S} is the number of deuterons cm^{-3} in the singly shocked gas, w is the particle speed behind the imploding shock (cm sec^{-1}), M is the mass of a deuteron (g), $\boldsymbol{k}$ is Boltzmann's constant ($1{\cdot}38\times10^{-16}$ erg g^{-1}), T_{R} is the temperature in the doubly shocked gas (°K), n_R is the number of deuterons cm^{-3} in the doubly shocked gas. These formulae do not take cylindrical convergence effects into account. The main consequence of these is that the shock strength is increased as it approaches the centre and that the imploding shocked gas is compressed isentropically as it converges. This isentropic compression can be treated as part of the general isentropic compression that takes place in the rising magnetic field subsequent to the shock heating stage, after the shock process has been completed. The actual increase in shock strength results in a higher temperature in the shock front but the mass of gas that is raised to a temperature appreciably higher than average is only a small fraction of the whole so that no very great error is introduced by neglecting the effects of convergence.

Returning to equation (6), there is at first sight no limit to the temperature that may be obtained if one increases the quantity $V_0 b^{-1} n_0^{-1/2}$. However this quantity is in fact limited by two considerations, namely that, in order to get the full potential V_0 across the discharge, the impedance of the discharge circuit must be considerably greater than the internal impedance of the current source, and, secondly, the gas density must be sufficiently high for the thickness of the shock transition to be small compared with the size of the apparatus. The problem of build up of voltage across the discharge has been studied by Wright and Black (1959) who integrated the equations of motion of the shocked gas using the method of characteristics. The main conclusion is that the voltage has built up sufficiently for the shock to be travelling at 90% of its final speed by the time the inductance of the whole circuit has built up to three times the initial inductance. If we postulate that this speed should be attained by the time the current sheet has travelled a fraction 0·2 of the distance towards the axis we may estimate a value of V_0/b for the various forms of apparatus by also postulating an initial circuit inductance of $10^{-13} V_0$ henrys. This represents the lower limit of practicable values with present day commercially available dielectrics. The values V_0/b are presented in table 2 together with corresponding values of the radius of the cylinder. The values are only approximate because of the assumptions it was necessary to make. However the optimum apparatus parameters are not very sensitive to the approximations and in any case the comparison between the various types of apparatus is valid. In apparatus types A and B it was assumed that the length of the cylinder must be at least twice the radius in order to avoid cooling of the plasma by the walls of the apparatus.

Table 2. Optimum Parameters of the various types of Apparatus

Apparatus	V_0/b	r	T_R	n_0
A	2×10^3	$2{\cdot}5 \times 10^{-4} V_0$	$1{\cdot}6 \times 10^5 V_0^{1/4}$	$10^{18} V_0^{-1/2}$
B	6×10^3	$0{\cdot}25 \times 10^{-4} V_0$	$1{\cdot}6 \times 10^5 V_0^{1/4}$	$10 \times 10^{18} V_0^{-1/2}$
C	2×10^3	$0{\cdot}8\phi \times 10^{-4} V_0$	$1{\cdot}2\phi^{1/4} \times 10^5 V_0^{1/4}$	$2\phi^{-1/2} \times 10^{18} V_0^{-1/2}$
D	$2 \times 10^3\phi$	$0{\cdot}8/\phi \times 10^{-4} V_0$	$1{\cdot}2\phi^{1/4} \times 10^5 V_0^{1/4}$	$2\phi^{3/2} \times 10^{18} V_0^{-1/2}$

ϕ is the ratio of minor to major radii of the torus. A maximum value would be about 0·3.

We must now estimate the minimum gas density for the thickness of the shock transition to be small compared with the size of the apparatus. This condition is necessary because, if it were not observed, there would be no collision between particles and hence none of the entropy change that is associated with shock heating. Detailed calculations show that the thickness of the reflected shock front is large compared with that of the incident shock and we only consider the former case here. The reflected shock front is a region where a stream of particles with velocity centred around a value w impinges on a hot gas at temperature T_R. After a time t_E the energy exchange time (and hence a distance $\delta = wt_E$) the particles have collided with particles of the hot gas and the directed energy has become converted into random (i.e. thermal) energy. The length $\delta = wt_E$ is therefore a measure of the thickness of the shock transition. According to Spitzer (1956) this may be written

$$\delta = wt_E = \frac{w^4}{4A_D G(l_1 w)} \qquad \ldots\ldots(8)$$

where, in our notation,

$$A_D = \frac{8\pi e^4 n_R \ln \Lambda}{M^2}$$

and

$$l_1^2 = \frac{M}{2\boldsymbol{k} T_R}.$$

Here e is the electronic charge (e.s.u.), $\ln \Lambda$ is a slowly varying function of temperature and density and is of the order of 10; and $G(l_1 w)$ is a function of $l_1 w$ tabulated by Spitzer. Using equations (5), (6) and (7) we get

$$\delta \sim 1000 T_R^2 n_0^{-1}. \qquad \ldots\ldots(9)$$

Since the doubly shocked gas is compressed by a factor 10, we will have a reflected shock provided $\delta < 10^{-1/2} r$. We therefore choose our requirement as $\delta = 0{\cdot}1r$ and we have a minimum deuteron density given by

$$n_0 = 10^4 T_R^2 / r. \qquad \ldots\ldots(10)$$

Substituting in equation (6) we get

$$T_R^2 = 8{\cdot}6 \times 10^8 \, V_0 r^{1/2} / b. \qquad \ldots\ldots(11)$$

Obtaining values of V_0/b and r from table 2 we may now estimate reflected temperatures and, using (10), optimum deuteron densities. These are presented in table 2. The optimum reactor parameters for 100 kv and 10 kv working voltage are presented in table 3. It will be noticed that the apparatus dimensions calculated here are somewhat smaller than those used in practice to date. It will be appreciated that the above calculations refer to a pure deuterium gas

Table 3

Apparatus	Radius (cm)	T_R (°K)	n_0
Reactor working at 100 kv			
A	25	$2{\cdot}8 \times 10^6$	$3{\cdot}5 \times 10^{15}$
B	2·5	$2{\cdot}8 \times 10^6$	$3{\cdot}2 \times 10^{16}$
C	2·0	$1{\cdot}5 \times 10^6$	$1{\cdot}3 \times 10^{16}$
D	32	$1{\cdot}5 \times 10^6$	$7{\cdot}9 \times 10^{14}$
Reactor working at 10 kv			
A	2·5	$1{\cdot}6 \times 10^6$	10^{16}
B	0·25	$1{\cdot}6 \times 10^6$	10^{17}
C	0·2	$0{\cdot}84 \times 10^6$	4×10^{16}
D	3·2	$0{\cdot}84 \times 10^6$	$2{\cdot}5 \times 10^{15}$

ϕ is taken to be 0·25.

and that, with a DT mixture, the theoretically attainable temperatures would be somewhat greater. Even so they fall short of the minimum operating temperature of a reactor by a factor of 10 or so and a considerable degree of isentropic compression would be required, after the shock heating stage.

Finally we examine the effect of a deviation from the optimum apparatus dimensions. Suppose all the dimensions were increased by a factor α, the voltage V_0 being kept constant. In equation (11) both r and b are increased by a factor α and hence the temperature T_R is increased by $\alpha^{-1/4}$. It follows that doubling the apparatus dimensions leads to a maximum temperature which is only a factor 1·2 lower than optimum.

§ 5. COMPARISON OF THE VARIOUS TYPES OF APPARATUS

We must now consider each of the types of apparatus in the light of our calculations. We restrict our discussion to the least stringent of the operating conditions, i.e. the DT reactor. The most attractive schemes from the point of view of instabilities are the θ pinch apparatus. Type B is theoretically neutrally stable whilst the discharge column in type D tends to expand to the outer walls of the torus but is otherwise stable. With apparatus type B working at 100 kv it would be necessary to raise the temperature of the doubly shocked gas by a factor 10 by isentropic compression to achieve 3×10^7 deg K. According to table 1, this implies that the magnetic energy is 200 times the thermal energy in the apparatus. Reasonable circuit parameters are a circuit resistance, storage capacity and pinched inductance of 2×10^{-3} ohm, 16 μF and 50 mμH respectively giving copper losses of the order of 10% of the magnetic energy per cycle; consequently the value $n\tau$ of the efficiency criterion must be increased from 10^{14} to 2×10^{15}. The amount of fuel burnt per cycle increases from the order of 1% to the order of 20%. It is clear from these general considerations that it might just be possible to build a DT reactor of the type B with a positive energy yield.

The same considerations apply to reactor type D but here the magnetic energy is some 600 times the thermal energy at the operating temperature and it is unlikely that a successful toroidal θ pinch apparatus will ever be built.

In order to overcome this difficulty with θ pinches it might be possible to build a reactor in which the gas is first shock heated and partially compressed in an apparatus of type B and size quoted in table 3 and is then transported laterally to a second small chamber where it is compressed to its final stage by a strong magnetic field acting over a small volume (see figure 2). The magnetic energy is reduced in such a device but the practical difficulties attendant on such a scheme may well be prohibitive.

The alternative Z pinch method of apparatus A and C is limited by the rate of growth of instabilities. In fact it is generally accepted that the neutrons that have been observed from linear pinch devices are probably due to local intense fields associated with instabilities and are not a measure of the ion temperature. But the important question from the point of view of reactor design is not so much whether instabilities exist but whether they grow at such a rapid rate that the plasma reaches the walls or the current channel becomes broken up. The problem of the plasma reaching the walls is not likely to be of great importance since at the high working densities reaction times τ are in the microsecond order of magnitude and the conducting walls exert a stabilizing influence on the discharge. The problem of sausage shape instabilities is more difficult. They may be eliminated by means of a d.c. magnetic field of sufficient strength but this must be compressed by the plasma and one is back to the problem of excess magnetic to thermal energy as the price of stability. We may define two times that are of importance. The first of these, t_H, is the time to build up the current to compress the plasma isentropically after the initial shock heating period. The current for this compression is given by the well-known relation first derived by Bennet (1934):

$$i^2 = 400\pi r^2 n_0 \boldsymbol{k} T_F \qquad \ldots\ldots(12)$$

where i is in amps.

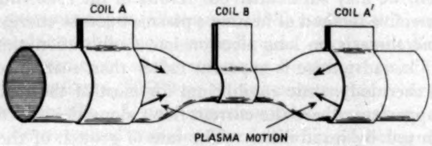

Figure 2. Possible two stage compression device. The plasma is generated at coils A and A′ and transported laterally to coil B where it is further compressed.

The inductance of the system in the pinched state is $2b \ln (r/r_F) \times 10^{-9}$ henrys or $b \ln (n/n_0) \times 10^{-9}$ henrys. Hence the time for current build up is of the order

$$\begin{aligned} t_H &= b \ln (n/n_0) \times 10^{-9} i/V_0 \\ &= 3{\cdot}6 \times 10^{-8} \frac{b}{V_0} r n_0^{1/2} (\boldsymbol{k} T_F)^{1/2} \ln \left(\frac{n}{n_0}\right). \qquad \ldots\ldots(13) \end{aligned}$$

The second of these times is the time of growth of sausage type instabilities denoted by t_I. This is a difficult quantity to estimate but a dimensional analysis shows it to be equal to the time for a wave travelling at the local sound speed to traverse a certain number of radii of the pinched discharge. We may therefore express

$$t_I = 10^{-12} \lambda r \left(\frac{n_0}{n_F}\right)^{1/2} \frac{1}{(\boldsymbol{k} T_F)^{1/2}} \qquad \ldots\ldots(14)$$

where λ is the number of radii. Intuition suggests λ should be of the order 10. If instabilities are not to upset the working of the reactor, the ratio t_I/t_H should be as large as possible and at least unity.

We have, using equation (6) and the fact that density is proportional to the three halves power of the temperature in an adiabatic compression,

$$\frac{t_H}{t_I} \sim \frac{1}{\lambda} \left(\frac{T_F}{T_R}\right)^{7/4} \ln \left(\frac{n}{n_0}\right). \qquad \ldots\ldots(15)$$

$\ln (n/n_0)$ is a slowly varying function of n/n_0 and can be considered as constant and of the order 7. Hence, in order for the current to build up in a time small compared with the growth of instabilities the temperature of the doubly shocked gas should be as high as possible in comparison with the fusion temperature. This means that it is advantageous to use a DT fuel and to use the working conditions of tables 2 and 3 to obtain as strong a shock as possible. Even so, the minimum value of T_F/T_R is likely to be of order 10 and, hence if instabilities are not to grow to serious proportions, the value λ would need to be of the order 500. One feels intuitively that such a value is not likely to be achieved in practice although there is surprisingly little experimental evidence on this point. It is also important that the time for instability growth should be more than the reaction time τ, which for the DT reactor is $10^{14}n^{-1}$. If we compare τ with the current build up time for the various devices in table 3 we find that the two times are of the same order of magnitude although the actual ratio between them varies with the type of apparatus and working voltage. Hence the same criterion $\lambda \sim 500$ applies to this time to a good approximation and the best set of reactor parameters is close to those presented in table 3.

§ 6. CONCLUSIONS

In conclusion, we may summarize our results in the following way. Shock heating is an attractive method of heating a plasma because energy is put directly into the ions and there is no long electron ion equilibration time to be taken into account. This advantage is apparent rather than real since the electrons and ions are in thermodynamic equilibrium for most of the reaction time. In those types of apparatus where the current flows along the axis the discharge is eventually destroyed by instabilities. The rate of growth of these is relatively least when the gas is shocked to as high a temperature as possible. The value of those types of apparatus where the current flow is circumferential is limited by the fact that the currents flowing are so great that copper losses outweigh the energy generated by fusion. This effect is again least when the gas is initially shocked to as high a temperature as possible and the effect may possibly be overcome by a modification of the apparatus geometry. There is an upper limit to the temperature to which it is possible to raise a plasma by shock heating alone and the optimum design of apparatus to achieve this temperature is presented in tables 2 and 3.

Although it seems just possible to build a small pulsed DT reactor using shock heating it is very unlikely that the more stringent conditions required for a successful DD reactor will ever be attained by this method.

ACKNOWLEDGMENTS

I am indebted to my colleagues at Foulness and in particular Mr. W. T. Eeles for helpful discussion of the ideas and manuscript of this paper. I am also indebted to the Director of the Atomic Weapons Research Establishment for permission to publish the paper.

REFERENCES

ALLEN, J. E., 1957, *Proc. Phys. Soc.* B, **70,** 24.
ANDERSON, D. A., BAKER, W. R., COLGATE, S., GILBERT, F. C., ISE, J., PYLE, R. V., and WHITE, R. S., 1957, *Conference on Plasma Physics Venice* (*June* 1957).
ARTSIMOVICH, L., ANDRIANOV, A. N., BAZILEVSHAYA, O. A., PROKHOVOV, YU. G., and FILIPPOV, N, V., 1956, *Atomnaya Energiya*, **3,** 76.
BENNET, W. H., 1934, *Phys. Rev.*, **45,** 890.
BODIN, H. A. B., and REYNOLDS, J. A., 1957, *Engineering*, **184,** 538.
ELMORE, W. C., LITTLE, E. M., and QUINN, W. E., 1958, *Phys. Rev. Letters*, **1,** 32.
HAGERMAN, D. C., and MATHER, J. W., 1958, *Nature, Lond.*, **181,** 226.
KOLB, A. C., 1957, *Phys. Rev.*, **107,** 345.
LAWSON, J. D., 1957, *Proc. Phys. Soc.* B, **70,** 6.
SPITZER, L., 1956, *Physics of Fully Ionised Gases* (New York: Interscience Publications), Chap. 5.
WRIGHT, J. K., and BLACK, M. C., 1959, *J. Fluid Mech.*, **6,** 289.

The Measurement of Flow Anisotropy in Pure Liquids†

By J. V. CHAMPION
Sir John Cass College, Jewry Street, London, E.C.3

Communicated by R. H. Humphry; MS. received 3rd *June* 1959, *in revised form* 4*th September* 1959

Abstract. In a previous paper (Champion 1958) a calculation was made of the optical anisotropy due to shearing a simple liquid. A coaxial cylinder apparatus suitable for the measurement of the streaming birefringence of pure liquids at very high velocity gradients (50 000 sec^{-1}) was constructed in order to test this calculation experimentally. A new experimental technique to enable a weak birefringence to be measured was developed, the liquid being sheared for the shortest possible time ($\sim$10 sec), so that the heating effects within the liquid were negligibly small. Measurements on ethyl cinnamate, chloroform and carbon tetrachloride are described and for the tetrahedral molecule (CCl_4) there is a favourable agreement between experiment and theory. This agreement shows that the assumptions made and the conclusions drawn in the previous paper are reasonable.

§ 1. Introduction

In a previous paper (Champion 1958, referred to as I) a magnitude for the optical anisotropy produced in a flowing liquid due to distortion of the radial distribution function was calculated. This calculation was based on the theory of Eisenschitz (1949) which described the steady non-uniform state of a liquid. A value of $\Delta n = 7 \times 10^{-8}$ was obtained for the birefringence produced in chloroform when subjected to a velocity gradient of 50 000 sec^{-1}. This value arises from the distortion of the radial distribution function and does not include any effect produced by orientation of the molecule in flow.

As indicated in I, anisotropy of flow in a pure liquid has normally been associated with an orientation or distortion of the molecule itself, producing a considerably larger effect than that due to distortion of the radial distribution function. The magnitude calculated for chloroform will not differ greatly from that arising from the same cause in a related molecule, viz. carbon tetrachloride which, being tetrahedral, would show no orientation anisotropy. The streaming birefringence of both carbon tetrachloride and chloroform was measured, there being an additional effect due to orientation in the case of chloroform. The reliability of the apparatus was tested by measurements of the birefringence of *trans*-ethyl cinnamate, the range of velocity gradient being extended well beyond that used by other observers. As a result a new technique was developed for use when the high velocity gradients necessary for liquids exhibiting very weak birefringence were involved.

The coaxial cylinder arrangement is the most suitable type of apparatus for the detection and measurement of the flow anisotropy of the above liquids.

---

† Part (abridged) of a thesis approved for the Ph.D. degree of the University of London.

§ 2. THE COAXIAL CYLINDER APPARATUS

The liquid is placed between two coaxial cylinders, one of which is rotated. The double refraction in the liquid is measured by passing a beam of light through it in the direction of the common axes of the cylinders. The apparatus is designed (*a*) to produce a velocity gradient over the range 0–50 000 $\sec^{-1}$ with laminar flow in the liquid, (*b*) to enable a birefringence of the order $\Delta n = 10^{-8}$ to be measured.

2.1. *Dimensions of the Cylinders*

As an extremely high velocity gradient is required, it is essential that the outer cylinder be rotated and the inner cylinder kept stationary (Taylor 1936). Apparatus in this form has been described previously by Edsall *et al.* (1952) and Jerrard (1955) but the maximum velocity gradients producible in the liquid, while retaining laminar flow, were only of the order of 12 000 $\sec^{-1}$. In order to obtain considerably higher values, the optimum dimensions of the apparatus (the radius R of the rotor, and the gap t between the two cylinders) were obtained from data given by Taylor (1936).

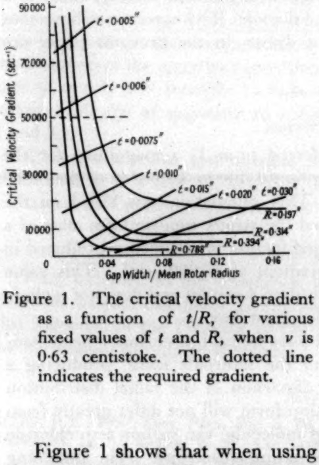

Figure 1. The critical velocity gradient as a function of t/R, for various fixed values of t and R, when ν is 0·63 centistoke. The dotted line indicates the required gradient.

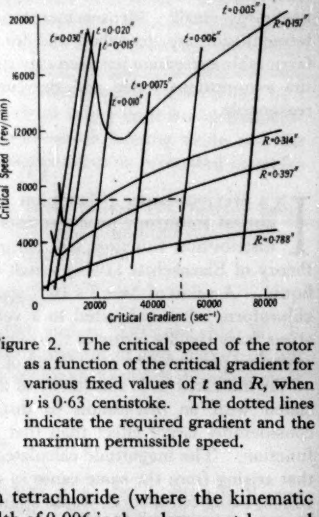

Figure 2. The critical speed of the rotor as a function of the critical gradient for various fixed values of t and R, when ν is 0·63 centistoke. The dotted lines indicate the required gradient and the maximum permissible speed.

Figure 1 shows that when using carbon tetrachloride (where the kinematic viscosity at 18°c is 0·63 centistoke), a gap width of 0·006 inch or less must be used to obtain uniform velocity gradients up to 50 000 $\sec^{-1}$, irrespective of the radius of the rotor. It can also be seen that there is a considerable advantage in having R small, as the critical velocity gradient increases with decreasing R. However, for small R the rotor has to be driven at a proportionally higher speed than one of greater radius, in order to provide a similar velocity gradient between the cylinders. If the rotor speed exceeds about 7000 rev/min, the mechanical difficulties of alignment and stability become overwhelming.

Figure 2 shows the critical speed plotted against the critical velocity gradient for various values of R and t for carbon tetrachloride in the apparatus. The required critical gradient (50 000 sec^{-1}) and the maximum suitable speed (7000 rev/min) are shown as dotted lines on the graph. In order to utilize the full range of available speeds, the critical gradient must occur at a speed only slightly greater than 7000 rev/min. Hence the curve for a given radius must lie just outside these limits to ensure that turbulence does not occur. It follows that the most favourable range for the radius of the rotating cylinder is 0·3 to 0·4 inch. For liquids in which the kinematic viscosity is greater than 0·64 centistoke the critical velocity gradient is proportionally higher, and laminar flow is ensured.

The above criteria for the onset of turbulence in a coaxial cylinder arrangement only hold for Newtonian liquids when the outer cylinder is rotating. Figures 1 and 2 were constructed from the curve given by Taylor (1936), and the theory of dynamical similarity was used to enable different values of t and R to be considered. Any vibration or extraneous force acting on the liquid will tend to change the conditions and turbulence will occur before the above critical values are reached.

2.2. *Practical Considerations*

(*a*) For a high intensity of the beam of light passing through the annular gap, parallel to the common axes of the cylinders, the gap width has to be reasonably large. Also a uniform gap is required, and the cylinders must be accurately coaxial at all speeds. If a gap width of 0·005 inch is to be used, the machining and alignment errors of the cylinders and the eccentricity of the rotor must be as small as possible, and in practice cannot be reduced below ± 0·0001 inch. For a given tolerance of machining and alignment, the relative uniformity will increase with the gap width.

(*b*) A constant speed of rotation is necessary and, to avoid undesirable rises in temperature in the sheared liquid, the high speed must be attainable in a short time. It was found that the apparatus did not reach a temperature equilibrium in the time suggested by Bjornstahl (1942).

(*c*) All vibration must be eliminated from the rotating cylinder assembly so that turbulence does not occur prematurely.

(*d*) The path length L through the liquid has to be large so that the phase difference δ between the two components of the electric vector parallel to the two principal axes of the liquid in the plane of the streamlines can be measured with reasonable accuracy to give the birefringence Δn, since

$$\delta = \frac{2\pi}{\lambda} L \, \Delta n. \qquad \ldots\ldots (1)$$

2.3. *Description of the Apparatus*

The coaxial cylinder assembly is shown diagrammatically in figure 3. The stator was turned between centres on a lathe and the bore of the rotor ground so that they were circular and parallel along their lengths to within ± 0·0001 inch. The two bearings were a selected pair, the inner race having an eccentricity of less than 0·0001 inch when the outer races were preloaded. The stator and rotor were aligned with the centring device, the annular gap between the cylinders being made uniform by distorting the brass ring and lead washers shown in figure 3. The final adjustments were made with the apparatus on an optical bench, and the diffraction patterns (of the gap at each end of the cylinders) were made as uniform as possible (Janeschitz-Kriegel 1957).

When the outer cylinder was rotated at high speeds (> 3500 rev/min) the liquid in the annular gap tended to be thrown out, and to prevent this the filling hole was made vacuum tight and a vertical brass tube attached to the inner edge of the glass annulus. Any small amounts of liquid thrown over this tube were caught in a tray above the bearings of the rotor. The outer cylinder was rotated by a continuous belt drive from a variable speed motor, and the speed of the rotor determined with a continuously recording electromagnetic system.

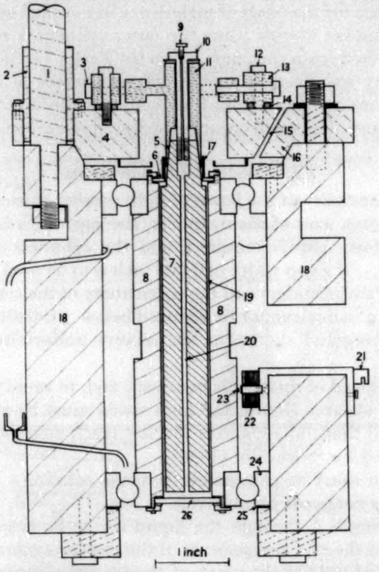

Figure 3. The coaxial cylinder assembly. 1, vertical pillar; 2, brass collar sliding over 1; 3, bolt for adjusting lateral position of the stator; 4, the top plate located by the cone fitting 16; 5, cone fitting of the central plug; 6, upper glass annulus; 7, stator; 8, rotor; 9, small bolt and rubber washer sealing the filling tube; 10, retaining bolt holding the stator in its cone fitting; 11, central plug of centring device; 12, bolt for adjusting stator tilt; 13, brass ring; 14, lead washer; 15, hole for oiling bearings; 16, cone fitting of the top plate; 17, brass collar cemented to the upper glass annulus with Araldite; 18, main housing; 19, annular gap between cylinders; 20, filling tube; 21, socket for leads from search coil; 22, search coil; 23, Alnico magnet fixed to the rotor; 24, ball races; 25, brass foil for preloading outer races of the bearings; 26, lower glass annulus.

The optical system, shown in figure 4, consisted of two optical benches, one horizontal and one vertical. The source was a high pressure mercury arc 1 mm in diameter and 3 mm long (type ME/D as manufactured by the British Thomson-Houston Co. Ltd.), and was sufficiently stable after an initial heating up period. The beam of light was accurately collimated, and the mercury green line isolated with a Wratten 77A filter, transmitting 79% of the light of this wavelength.

Surface aluminized mirrors were used to rotate the beam through a right angle where necessary, the final beam being viewed with the aid of a telescope.

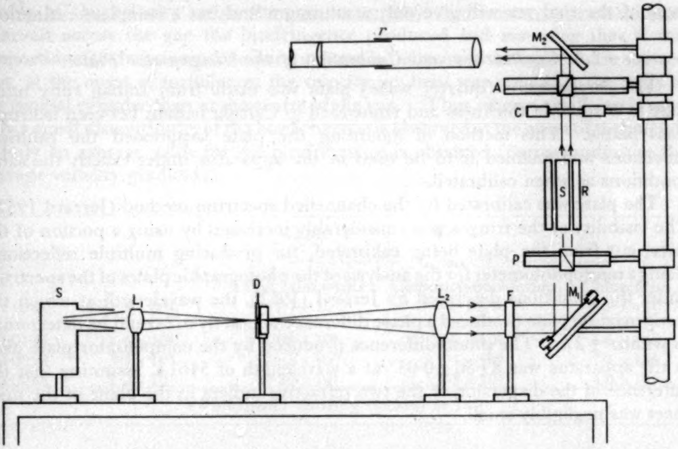

Figure 4. Schematic optical system. S, mercury arc source; L_1, achromatic condensing lens; L_2, long focal length achromatic collimating lens; D, small adjustable iris diaphragm; F, filter; M_1, M_2, surface silvered mirrors; P, polarizer; R, rotor: S, stator; C, compensator plate; A, analyser; T, telescope.

The Sénarmont compensator (quarter wave plate) is the most suitable arrangement for determining the double refraction produced in the liquid (Jerrard 1952). The beam of light passes through a ½-inch square aperture Glan–Thompson polarizing prism, mounted in a circle, before entering the liquid. The emergent light passes through the compensating plate, which is a suitably orientated quarter wave mica plate, and extinction is obtained with an analyser (similar to the polarizer) mounted in a 6-inch circle. When using a quarter wave plate as a compensator in the usual way, it can be readily shown that

$$\pm\delta = 2\alpha \pm 2n\pi \qquad \ldots\ldots(2)$$

where δ is the phase difference between two vibrations at right angles produced by the anisotropic medium and α is the rotation of the analyser from the original crossed position to the position of extinction. This method of measuring the phase difference, and hence the birefringence, reduces to a measurement of a rotation of a plane of polarization thus allowing rapid determinations. Equation (2) is only correct when ϕ, the angle between the original linear vibration and the fast axis of the birefringent medium, is $\pi/4$ and the phase difference produced by the quarter wave plate is exactly $\pi/2$.

The errors in the compensator have been discussed by Jerrard (1954), and it can easily be seen that, for an error of less than 1% in the value of δ determined, the axes of the compensator must be correctly orientated to less than 0·3°, and the compensator made to have a phase difference as near to 90° as possible for the wavelength used. Also, if the axes are not correctly orientated at $\pi/4$ with the original plane of vibration, and the phase difference produced by the compensator is not 90°, the light leaving the compensator is not linearly polarized, and adjustment of the analyser will give only a minimum and not a complete extinction.

2.4. *Construction and Calibration of the Compensator Plate*

The compensator (quarter wave) plate was made from Indian ruby mica, split to a suitable thickness and embedded in Canada balsam between isotropic glass plates. This method of mounting the plate suppressed the multiple reflections and enabled it to be used in the apparatus under exactly the same conditions as when calibrated.

The plate was calibrated by the channelled spectrum method (Jerrard 1952). The visibility of the fringes was considerably increased by using a portion of the mica, cut from the plate being calibrated, for producing multiple reflections. Using a microphotometer for the analysis of the photographic plates of the spectrum under the conditions described by Jerrard (1952), the wavelength at which the compensating plate produced a phase difference of exactly $\pi/2$ could be determined to within ± 2 Å. The phase difference produced by the compensator plate used in the apparatus was $89{\cdot}80 \pm 0{\cdot}03^\circ$ at a wavelength of 5461 Å, assuming that the difference of the dispersion of the two refractive indices in the plane of the mica sheet was negligibly small.

§ 3. EXPERIMENTAL CRITERIA AND TECHNIQUES

3.1. *The Velocity Gradient*

It may be shown (Jerrard 1950) that, in a liquid held between two vertical coaxial cylinders, the velocity gradient G produced at a point distance r from the common axis, when the outer cylinder is rotating and the inner cylinder is held stationary, is given by

$$G(r) = \frac{\omega_2 R_2^2}{R_2^2 - R_1^2}\left\{1 + \frac{R_1^2}{r^2}\right\}$$

where ω_2 is the angular velocity of the outer cylinder, R_1 and R_2 being the radii of the inner and outer cylinders respectively.

When the largest gap width (0·019 in.) is used in the apparatus the variation of $G(r)$ across the gap is only 3%, and decreases to less than 1% in the case of the smallest gap (0·0048 in.). The birefringence produced is directly proportional to the velocity gradient, and will thus vary across the gap. However, as the gap widths are small, it is virtually impossible to determine the small variation of birefringence and only an average value is obtained, which corresponds to the average velocity gradient. Hence $G(r)$ may be considered to be constant and given by $G = 2\pi NR/t$ where $R_1 \simeq R_2$; $\frac{1}{2}(R_1 + R_2) = R$; $R_2 - R_1 = t$ and N is the number of revolutions per second.

3.2. *Turbulence*

The critical velocity gradients G_c for the various gap widths and liquids used are given in table 1.

The effect of turbulent flow on the birefringence was first investigated by Sadron (1936), Signer and Gross (1933) and Cerf (1951) with results that appear contradictory, since Signer and Gross found a decrease, Cerf an increase in the birefringence above G_c, whilst Sadron could obtain neither. Jerrard (1950) qualitatively indicated the effects to be expected, and the more recent work of Wayland (1955) has confirmed them by measurement. Wayland obtained a profile of the velocity across the gap, using ethyl cinnamate, by measuring at intervals across the gap the birefringence produced and assuming that it was proportional to the principal shearing stresses in that part of the liquid. He showed that, at the onset of turbulence, the velocity gradient was greater at the walls of the coaxial cylinder than in the centre of the gap. Thus when a small gap is used only a small discontinuity of the birefringence is observed at the onset of turbulence as only an average value for the birefringence is obtained (corresponding to the average velocity gradient).

Table 1

		$G_c(\text{sec}^{-1})$		
t (in.)	$G_c\nu^{-1}$ (cm^{-2})	Ethyl cinnamate $\nu = 7{\cdot}7 \times 10^{-2}$	Carbon tetrachloride $\nu = 6{\cdot}3 \times 10^{-3}$	Chloroform $\nu = 3{\cdot}3 \times 10^{-3}$
0·0190	$1{\cdot}4 \times 10^{6}$	$1{\cdot}08 \times 10^{5}$	$8{\cdot}8 \times 10^{3}$	$4{\cdot}6 \times 10^{3}$
0·0098	$3{\cdot}4 \times 10^{6}$	$2{\cdot}62 \times 10^{5}$	$2{\cdot}1 \times 10^{4}$	$1{\cdot}1 \times 10^{4}$
0·0048	$1{\cdot}2 \times 10^{7}$	$9{\cdot}30 \times 10^{5}$	$7{\cdot}5 \times 10^{4}$	$4{\cdot}0 \times 10^{4}$

ν = kinematic viscosity (stokes) at 18°c

Wayland (1955) also showed that G_c, exhibited by this small discontinuity, corresponded, within experimental error, to the value obtained by calculation from the curves given by Taylor (1936) for the transition from laminar to turbulent flow. We may conclude from this that (i) if the values of G_c given in table 1 for the various liquids are not exceeded, the flow will be laminar, (ii) when a small gap is being used, and the birefringence is weak, it will be difficult to detect the point of transition due to the small discontinuity in the average value of the birefringence.

3.3. *Heating of the Liquid*

The work performed on the liquid while it is being sheared will cause a temperature rise in the liquid and a temperature gradient across the gap, with possible deviation of the beam of light, which may then be further polarized by reflection at the walls of the metal cylinders. Considerable error in the measured birefringence may thus be introduced.

The effect of heating has been considered by Bjornstahl (1942), who obtained an approximate expression for the difference in temperature existing between the central and outer layers of the sheared liquid when thermal equilibrium is attained.

Preliminary experiments were carried out on the apparatus described above in which a small thermocouple was placed in the centre of the gap at the top of the coaxial cylinders and the temperature rise of the central layers of liquid was measured. Using a gap of 0·019 in., and maintaining a velocity gradient of 10 000 sec^{-1} in ethyl cinnamate, the temperature rise was 0·8 deg c whilst a rise of only 0·12 deg c is predicted at equilibrium using the theory of Bjornstahl. Due to the relatively large masses of metal in the rotor and stator the rise in temperature of these was immeasurably small, and it appeared that equilibrium would only be attained after a considerable time.

Preliminary experiments using ethyl cinnamate (figure 5) showed that the birefringence was apparently decreased and the scatter of the values was greater, as the total time of shearing the liquid and the temperature gradient across the gap increase. However, this effect may be made negligibly small by shearing the liquid for only a very short time (less than 10 seconds). When this was done, a linear relation was obtained between the velocity gradient and the birefringence produced in the liquid, as shown in figure 6.

3.4. *Experimental Procedure*

The speed of the rotor was calibrated directly against a recording millivoltmeter. Before assembly, the apparatus must be thoroughly cleaned, removing all traces of grease and dust from the cylinder surfaces and the glass windows. The collimation of the beam of light and the uniformity of the annular gap were tested by examining the diffraction pattern produced. Before filling the apparatus, the rotor was spun at its maximum speed to detect any residual or strain birefringence produced in the glass windows. None could be detected provided the retaining screws had been uniformly tightened during assembly.

The apparatus was filled from the bottom with the aid of a long hypodermic needle and syringe. Air bubbles formed in the annular gap were easily detected by observing a discontinuity in the beam of light passed through the gap. When filling the smallest annulus (0·0048 inch), several attempts were generally necessary (the assembly being dismantled, cleaned and the glass windows retested as above) due to air bubbles being trapped between the walls of the cylinders by particles of dust. By slowly rotating the outer cylinder whilst filling, a large number of the bubbles were brought to the top of the gap and trapped beneath the upper glass annulus. These were removed with a piece of bent fine wire (48 s.w.g.), by guiding them to the free surface of the liquid. The liquid was then left at rest between the metal cylinders for several minutes to ensure a temperature equilibrium, the thermoelectromotive force being continuously recorded. The motor drive was then brought up to the required speed, taking approximately four seconds, and the millivoltmeter switched over from recording temperature to speed. The Glan–Thompson prisms were arranged such that two adjacent arms of the cross of isocline could be viewed. The analyser was then rotated until the two arms of the cross of isocline collapsed, the motor shut off, and the recorder switched from speed to temperature measurement. The complete determination took approximately ten seconds and the liquid was allowed to regain its temperature equilibrium before a further determination was made.

§ 4. RESULTS

The bore of the outer cylinder was 0·6277 ± 0·0001 in., and circular along its length to within the same limits. The diameters of the various stators used are given in table 2, two measurements at right angles being made at equal intervals along the stator with a high precision vernier micrometer.

The rotor and stator can be aligned to within ± 0·0001 in., thus when stator C is used the possible non-uniformity of the gap can be of the order of ± 5%. Hence the calculated velocity gradient can vary by this amount, the error being proportionally less for larger gaps.

Table 2

Dimension	Stator A (in.)		Stator B (in.)		Stator C (in.)	
Diameter	0·5897	0·5897	0·6082	0·6083	0·6182	0·6182
	0·5897	0·5897	0·6083	0·6082	0·6182	0·6183
	0·5896	0·5896	0·6082	0·6082	0·6183	0·6182
	0·5897	0·5896	0·6082	0·6082	0·6182	0·6182
	0·5897	0·5897	0·6082	0·6082	0·6182	0·6182
Mean diameter	0·5897		0·6082		0·6182	
Length	4·421		4·391		4·416	
Gap width	0·0190		0·0098		0·0048	

The continuously recording millivoltmeter was calibrated to give the velocity gradient produced in the liquid when a particular stator was used. The speed of the rotor was measured with a stroboscope, which according to the manufacturers' calibration, had a maximum error of 1%.

Before any observations were made, the analysing and polarizing prisms must be crossed. By taking a large number of readings of the crossed position it would be found that the standard deviation of a single setting was 1·0 minute of arc. The compensator plate was then inserted and rotated until its axes corresponded to the transmission planes of the crossed prisms, a complete extinction being obtained. The standard deviation of a single setting was found to be 0·9 minute of arc.

Thus the total deviation of setting up the optical system produces in Δn an error which is small compared with that which exists in the determination of the velocity gradient.

4.2. *Results for Pure Liquids*

(a) Ethyl cinnamate.

The liquid used in these experiments was tested for purity by freezing point and boiling point determinations, and was found to be *trans*-ethyl cinnamate containing less than 0·1% impurity. The initial results (figure 5) show that at a given velocity gradient, the birefringence decreases as the time to take the observation and the temperature rise in the liquid increase. It is well known that the ratio $\Delta n/G$ decreases with increase of temperature. Tsvetkov and Kibardina (1948) show that for a number of organic liquids the ratio $\Delta n/G$ decreases by 2% to 3% per centigrade degree rise, but as a fall of approximately 15% per centigrade degree was obtained in the present work, it appears that another effect is producing this change. This could be due to the increasing temperature gradient across the gap increasing the number of reflections of the beam of light from the walls of the cylinders as suggested by Bjornstahl (1942).

Further experiments showed that by shearing the liquid for the shortest possible time necessary to make an observation (~ 10 sec) both the effects above are eliminated. The results in figure 6 show a linear relation between the birefringence and the velocity gradient, the line passing through the origin. The ratio $\Delta n/G$ from the slope of the curve is $M = \Delta n/G = 5{\cdot}74 \times 10^{-11}$ sec and is compared with the results of other workers in table 3. The values are obtained from the average values of $\Delta n/\eta G$ given by the authors, and by using $\eta = 7{\cdot}74 \times 10^{-2}$ poise at 25° and $\eta = 7{\cdot}15 \times 10^{-2}$ poise at 18°C for the viscosity of *trans*-ethyl cinnamate (as determined with an Ostwald viscometer).

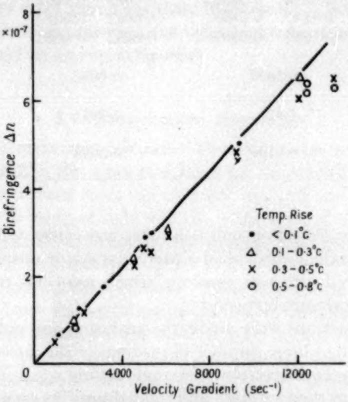

Figure 5. Birefringence of *trans*-ethyl cinnamate. The temperature rise during the determination is indicated by the series of points as shown.

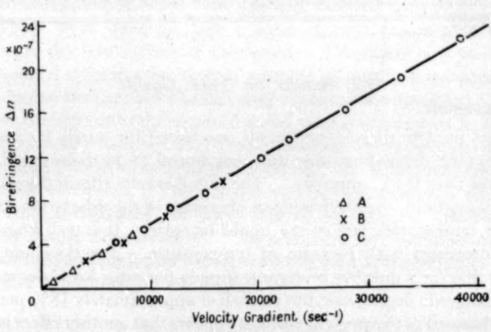

Figure 6. Birefringence of *trans*-ethyl cinnamate, with a temperature rise of less than 0·1°C, the points indicate measurements taken with rotors, A, B and C as shown.

Table 3. Values of M for Ethyl Cinnamate (sec)

Edsall *et al.* (1952)	$6{\cdot}45 \times 10^{-11}$
Leray (1955)	$5{\cdot}72 \times 10^{-11}$
Wayland (1955)	$5{\cdot}04 \times 10^{-11}$
Value from figure 6	$5{\cdot}74 \pm 0{\cdot}07 \times 10^{-11}$

Leray (1955) suggested that the discrepancy between his value and those obtained by other workers was most probably due to impurities in the liquid. The present result obtained for the pure liquid is in good agreement with Leray's.

(*b*) *Carbon tetrachloride and chloroform.*

Several samples of carbon tetrachloride and chloroform were used, all being 'Analar' reagents, containing an impurity of less than 0·1%. The results are shown in figures 7 and 8 respectively giving

$$\text{for } CCl_4 \qquad M = 1{\cdot}21 \times 10^{-12}\,\text{sec},$$

$$\text{for } CHCl_3 \qquad M = 2{\cdot}39 \times 10^{-12}\,\text{sec}.$$

In all the measurements the technique of making a single complete observation in a minimum time was used.

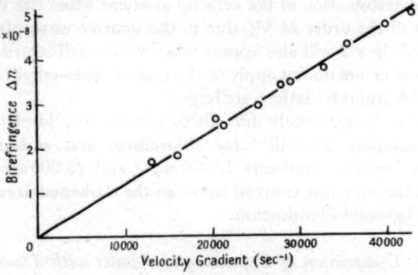

Figure 7. Birefringence of carbon tetrachloride.

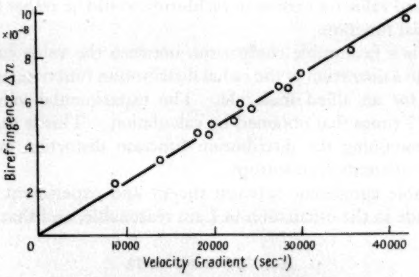

Figure 8. Birefringence of chloroform.

§ 5. Discussion

5.1. *The Determination of M*

It has been shown that by using the technique of only shearing the liquid for the shortest possible time, a straight line graph passing through the origin is obtained for the birefringence as a function of velocity gradient. This shows that the birefringence measured is that produced in the liquid by the velocity gradient and that any spurious birefringence has been made negligibly small. The value of M obtained for *trans*-ethyl cinnamate confirms the work of Leray (1955) over an extended range of velocity gradients, Leray using 0 to 8000 sec^{-1}, whilst 0 to 40 000 sec^{-1} was used in the present investigation.

The value of M for chloroform has not been measured previously, as a sufficiently high velocity gradient could not be attained without turbulence appearing in the liquid. A value for CCl_4 was obtained by Buchheim *et al.* (1939) giving $M < 0{\cdot}09 \times 10^{-12}$. The discrepancy between this value and that given in this paper is most probably due to the heating effects discussed above, and to an insufficiently high velocity gradient being used to produce a measurable value. As the graphs of the birefringence as a function of velocity gradient for $CHCl_3$ and CCl_4 are straight lines, passing through the origin, as in the case of *trans*-ethyl cinnamate, it can be concluded that the results for these liquids are trustworthy. The values of M given above may be subject to an error of $\pm 5\%$ due to the large inaccuracy incurred in the determination of the velocity gradient when the very small gap is used. An error of the order of 5% due to the quarter wave plate not having a retardation of exactly $\pi/2$ will also appear when very small retardations are being measured. These errors do not apply in the case of *trans*-ethyl cinnamate where both the gap width and retardations are large.

It was found to be extremely difficult to observe any birefringence below a value of approximately $2{\cdot}0 \times 10^{-8}$ for chloroform and carbon tetrachloride, corresponding to velocity gradients 10 000 sec^{-1} and 15 000 sec^{-1} respectively. This was due to the very low contrast between the darkened areas of the field of view and the background illumination.

5.2. *Comparison of Experimental Results with Theory*

The constant obtained in the theoretical calculation was $M = 1{\cdot}46 \times 10^{-12}$ sec. As the polarizability of carbon tetrachloride is slightly larger than that of chloroform, the expected value for carbon tetrachloride would be rather larger, assuming a similar potential function.

Thus there is a favourable comparison between the value calculated for the anisotropy due to a distortion of the radial distribution function, and that obtained experimentally for an allied molecule. The experimental value obtained for chloroform is 1·7 times that obtained by calculation. This is due to the experimental value containing the distribution function distortion anisotropy and a small amount of orientation anisotropy.

The favourable agreement between theory and experiment shows that the assumptions made in the calculation in I are reasonable, and that the conclusions there are valid.

ACKNOWLEDGMENTS

The work described was performed at Sir John Cass College, London. The author wishes to thank Mr. R. H. Humphry, Head of the Physics Department, for his interest and encouragement, and the Central Research Fund of the University of London for providing the stroboscope and high intensity mercury light source.

REFERENCES

BJORNSTAHL, Y., 1942, *Z. Phys.*, **119,** 245.
BUCHHEIM, W., STUART, H. A., and MENZ, H., 1939, *Z. Phys.*, **112,** 407.
CERF, R., 1951, *J. Chim. Phys.*, **48,** 85.
CHAMPION, J. V., 1958, *Proc. Phys. Soc.*, **72,** 711.

Edsall, J. T., Rich, A., and Goldstein, M., 1952, *Rev. Sci. Instrum.*, **23**, 695.
Eisenschitz, R., 1949, *Proc. Phys. Soc.* A, **62**, 41.
Janeschitz-Kriegel, H., 1957, *J. Polym. Sci.*, **23**, 181.
Jerrard, H. G., 1950, *J. Appl. Phys.*, **21**, 1007.
—— 1952, *J. Opt. Soc. Amer.*, **42**, 159.
—— 1954, *Ibid.*, **44**, 289.
—— 1955, *Rev. Sci. Instrum.*, **26**, 1007.
Leray, J., 1955, *J. Chim. Phys.*, **52**, 755.
Sadron, C., 1936, *J. Phys. Radium*, **7**, 263.
Signer, R., and Gross, H., 1933, *Z. phys. Chem.* A, **165**, 161.
Tsvetkov, V., and Kibardina, B., 1948, *Dokl. Akad. Nauk, S.S.S.R.*, **62**, 223.
Taylor, G. I., 1936, *Proc. Roy. Soc.* A, **157**, 546.
Wayland, H., 1955, *J. Appl. Phys.*, **26**, 1197.

A Simple Interferometric Arrangement for the Measurement of Optical Frequency Response Characteristics

By P. HARIHARAN and D. SEN
National Physical Laboratory of India, New Delhi, India

MS. received 30*th September* 1959

Abstract. In the instrument described, collimated light from the lens which is being tested is directed into a triangular path interferometer in which the two beams are sheared by tilting a single, parallel plate, while the path difference between them is varied linearly with time, over a range of one wavelength, by means of a polarizing system. The modulus and argument of the frequency response of the lens are obtained directly from the amplitude and phase of the resultant sinusoidal variation of the total flux in the interference pattern.

§ 1. INTRODUCTION

THE use of a shearing interferometer for the measurement of the optical frequency response characteristics of a lens system was first suggested by Hopkins (1955 a) who pointed out the advantages of such a technique over more conventional direct scanning methods. Subsequently, an interferometer of this type was constructed by Baker (1955), while, more recently, Kelsall (1959) has shown how such an arrangement can be modified to make automatic recordings of frequency response curves. Both these instruments are basically Michelson interferometers in which the end mirrors have been replaced by corner-cube prisms (Peck 1948), permitting the introduction of a lateral shear between the two wave fronts. However, such instruments, while satisfactory in other respects, are relatively complicated and expensive. The present paper describes a simplified arrangement for measurements of frequency response characteristics which utilizes a triangular path interferometer.

§ 2. THEORY

The theory of the interferometric method for measurements of the frequency response of a lens has already been discussed in some detail (Hopkins 1955 a, Kelsall 1959) and hence will only be briefly outlined here. The basic feature of the method is that an illuminated slit placed at the focus of the lens under test produces a collimated beam of light which is directed into the interferometer, where it is divided into two beams which are laterally sheared with respect to one another, interference taking place in the region of overlap. For two circular pupils of unit radius, the relative shear s is numerically equal to the spatial frequency parameter. If we make the simplifying assumption that the amplitudes of the two beams are equal and uniform over the whole area of the two pupils, we can show that $D(s)$, the normalized frequency response in the plane of shear (which being a complex quantity can be written in the form $D(s)=T(s)\exp i\theta(s)$), is related to $F(\delta)$ the total flux in the interference pattern by the equation

$$F(\delta)=F_0\{1+V_{21}\,T(s)\cos[(2\pi/\lambda)\delta-\theta(s)]\} \qquad \ldots\ldots(1)$$

where F_0 is the total flux through the pupils, V_{21} is the coherence factor for the two beams, and δ is the path difference introduced between the two beams. The value of the coherence factor V_{21} may be taken equal to unity, provided the width of the slit placed at the focus of the lens and the spectral line width of the source do not exceed certain critical limits (Hopkins 1957). It then follows, from equation (1), that if the path difference is made to vary linearly with time, the total light flux in the interference pattern will undergo a sinusoidal variation whose amplitude and phase give respectively the modulus $T(s)$ and argument $\theta(s)$ of the frequency response.

§ 3. OPTICAL SYSTEM

The optical system of the instrument is shown schematically in figure 1. A narrow slit S illuminated with monochromatic light from the mercury arc lamp A is placed at the focus of the lens L_1 which is being studied. The collimated beam from this lens, which is incident on the semi-reflecting mirror M_0, is divided into two beams which traverse the closed triangular path $M_0 M_1 M_2 M_0$ in opposite directions, before emerging approximately at right angles to the original, incident beam. These two beams are brought to a focus by the lens L_2 on a diffuser D placed in front of the photocathode of a photomultiplier tube PM. The anode current of this tube is then a measure of the total flux in the interference pattern.

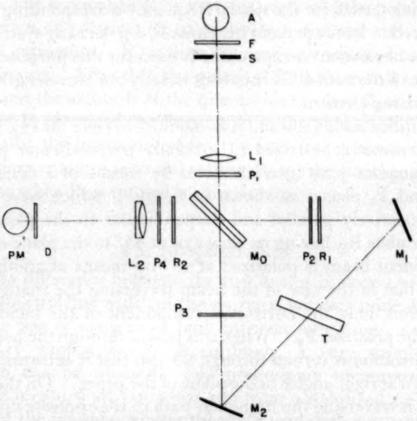

Figure 1. Schematic diagram of the optical system. A, mercury arc; F, monochromatic filter; S, slit; L_1, lens under test; M_0, beam divider; M_1, M_2, end mirrors; T, shear plate; P_1, P_2, P_3, P_4, polarizers; R_1, half-wave plate; R_2, quarter-wave plate; L_2, lens; D, diffuser; PM, photomultiplier tube.

3.1. *Shearing Mechanism*

In a triangular interferometer of this type, any two rays traversing the triangular path in opposite directions which are formed by the division of a single ray incident on M_0 will always emerge parallel to one another, though, in general, there will be a finite lateral shear between them. In addition, it can also be shown that when the interferometer is adjusted so that these rays run parallel to one another over the whole triangular path, the path difference between these two beams will be equal to zero. Once this adjustment has been made, it is possible to shear the rays without introducing a path difference between them, merely by moving the mirrors M_1 and M_2 as a unit. However, a more convenient and sensitive method is to use a tilted, plane-parallel plate (Hariharan and Singh 1959) of thickness t, introduced in the path of the two beams at T. This shears the two beams by an equal amount d, in opposite directions, given by the relation

$$d = t \sin\alpha \, [1 - (\mu^2 - \sin^2\alpha)^{-1/2} \cos\alpha] \qquad \ldots\ldots (2)$$

where μ is the refractive index of the material of the plate and α is the angle of incidence. This method has the advantages that for small values of α the shear is very nearly proportional to α, and the sensitivity of the shear control can be easily modified by choosing a plate of suitable thickness.

3.2. *Path Changing System*

As has been pointed out earlier, it has been shown that if the path difference between the two beams is made to vary as a linear function of time, this results in a sinusoidal variation in the total light flux in the interferogram whose amplitude and phase directly give the modulus and argument of the frequency response of the lens which is being tested, for the spatial frequency corresponding to the particular value of shear used. In the present instrument, a polarizing system similar to that employed in the Senarmont compensator is used for this purpose. This permits a linear variation of the path difference over exactly one wavelength, by the rotation of a single polarizing element.

In order to utilize such a system, it is essential to have the two beams emerging from the interferometer polarized in mutually perpendicular planes. This is done in the triangular path interferometer by means of a combination of two polarizers P_2 and P_3 placed as shown in figure 1, which have their planes of polarization respectively parallel and perpendicular to the plane of the paper, with a half-wave plate R_1, having its slow axis at 45° to the plane of the paper. If the original incident beam is polarized at 45° by means of another polarizer P_1, it is easily seen that in the case of the beam traversing the triangular path in the clockwise direction, only the horizontal component of the incident vibration is transmitted by the polarizer P_2. When this passes through the half-wave plate R_1, its plane of polarization is turned through 90°, so that it is transmitted by P_3 and emerges polarized at right angles to the plane of the paper. On the other hand, for the beam which is traversing the triangular path in the opposite direction, only the vertical component is passed by P_3. This also has its plane of polarization turned through 90° by the half-wave plate R_1, after which it is transmitted by P_2 and emerges polarized in the plane of the paper.

The Senarmont compensator consists of a quarter-wave plate R_2 with its slow axis at 45° to the plane of the paper, followed by a rotatable analyser P_4. The function of the quarter-wave plate is to convert the two beams which are polarized at right angles into two circularly polarized beams, one right-handed and the other left-handed. These normally combine to produce linearly polarized light whose azimuth is determined by the phase difference between the two beams. If, then, the azimuth of the analyser makes an angle ϕ with this plane, it is seen that this is equivalent to advancing the phase of one circularly polarized wave by ϕ and retarding the other by an equal amount, so that a further phase difference 2ϕ is introduced between the two beams. By rotating the analyser at a steady rate, the phase difference between the two beams can be made to vary linearly by an amount ranging from $+\pi$ to $-\pi$.

§ 4. Adjustment

The interferometer has to be set initially so that the shear is equal to zero over the whole path, when the shear plate is normal to the beams. For this, the rays are first made parallel to each other over the whole path by adjusting the angles of the beam divider M_0 and one end mirror, after which any residual shear is eliminated by translating one of the end mirrors. The progress of this adjustment can be followed with a fair degree of accuracy by introducing a pair of cross-wires at various points in the path, and checked by observing the shear fringes seen with an eyepiece at D when the slit S is opened up. When the shear plate is normal to the beams, the zero-order fringe should cover the whole field. There should also be no displacement of the zero-order fringe when the shear plate is rotated by equal angles to either side of this position. Finally, the slit S is narrowed and set so that it coincides with the centre of the zero-order fringe.

The adjustment of the polarizing system is also relatively easy and is carried out as follows. The half-wave plate R_1 is first removed, and the polarizers P_2, P_3 are set with their planes of polarization respectively horizontal and vertical, so that there is complete extinction. R_1 is then replaced and adjusted so that the transmission is a maximum. After this, the polarizer P_1 is set so that one of the beams is extinguished, and the azimuth of the quarter-wave plate R_2 is adjusted, so that when the analyser P_4 is rotated the fluctuation in the photomultiplier current is a minimum. Finally, the intensities of the two interfering beams are made equal, by making the shear equal to zero and setting P_1 so that the change in the photomultiplier current when P_4 is rotated is a maximum.

§ 5. Measurements

Since the path difference between the two beams is always very small in this instrument, the spectral line width of the source is not very critical (Kelsall 1959). This permits the use of sources of high intrinsic brightness, such as the high pressure, mercury vapour lamp. Accordingly, a very simple photoelectric detecting system can be utilized. For preliminary measurements with this arrangement, the mercury arc lamp was run from a stabilized a.c. line, while the output current of the photomultiplier tube was read with a mirror galvanometer. For each setting of the shear plate, the maximum and minimum values of the output current as well as the azimuth angles of the polarizer P_4 corresponding to these values were noted. From these readings, the corresponding values of the contrast transmission factor and its spatial phase shift could be easily obtained. A typical experimental curve secured with this set up for a defocused telescope objective is presented in figure 2. This curve was obtained with a defect of focus $w_{20} = 2{\cdot}5\lambda$, and agrees reasonably well with the theoretical curve for this value (Hopkins 1955 b). The phase jump of π on passing through the first zero of the response curve is clearly shown.

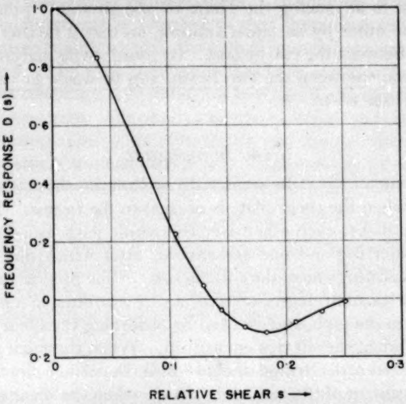

Figure 2. **Response curve obtained with the instrument for a defocused telescope objective.** Defect of focus, $w_{20}=2\cdot5\lambda$.

In a more recent version of this instrument, the analyser P_4 is rotated at 150 rev/min by a small motor, and the a.c. output from the photomultiplier tube is fed to an oscilloscope with a long persistence screen, whose time base is synchronized with the rotation of P_4. The values of the modulus and the argument of the frequency response can then be read directly from the amplitude and phase shift of the a.c. wave displayed on the oscilloscope screen.

§ 6. CONCLUSIONS

The interferometric system described is comparatively simple and inexpensive and permits rapid determinations of the frequency response characteristics of lenses. All the three basic units, namely the interferometer, the path changing mechanism, and the arrangement for shearing the beams, are extremely stable and easy to adjust. In addition, a very simple photoelectric detecting system can be used with this instrument, since it is possible to use sources of high intrinsic brightness with it.

ACKNOWLEDGMENT

The authors wish to thank the Director, National Physical Laboratory of India, for permission to publish this paper.

REFERENCES

BAKER, L. R., 1955, *Proc. Phys. Soc.* B, **68**, 871.
HARIHARAN, P., and SINGH, R. G., 1959, *J. Opt. Soc. Amer.*, **49**, 732.
HOPKINS, H. H., 1955 a, *Optica Acta*, **2**, 23.
—— 1955 b, *Proc. Roy. Soc.* A, **231**, 91.
—— 1957, *J. Opt. Soc. Amer.*, **47**, 508.
KELSALL, D., 1959, *Proc. Phys. Soc.*, **73**, 465.
PECK, E. R., 1948, *J. Opt. Soc. Amer.*, **38**, 66, 1015.

RESEARCH NOTES

The Correlation Energies of the Helium Sequence

By A. DALGARNO

Department of Applied Mathematics, The Queen's University of Belfast

Communicated by D. R. Bates; MS. received 7th December 1959

§ 1. Introduction

In discussing the correlation energy of an atomic system, defined as the difference between the exact non-relativistic energy and the Hartree–Fock energy, it is instructive to develop it as a series in inverse powers of the nuclear charge Z. Recently Fröman (1958) and Löwdin (1959) have obtained the first non-vanishing term for the helium sequence (the two leading terms are zero) by fitting a power series expansion to the available Hartree–Fock energies. It is possible to formulate a theory such that all terms of the series expansion of the Hartree–Fock energies can be calculated exactly, and in this note the theory is briefly described and the leading term of the correlation energy is evaluated.

§ 2. Theory

Writing the wave function $\psi(\mathbf{r}_1, \mathbf{r}_2)$ of any member of the helium sequence in the product form $\psi(\mathbf{r}_1, \mathbf{r}_2) = u(r_1)u(r_2)$, $\mathbf{r}_1$ and $\mathbf{r}_2$ being the position vectors of the two electrons referred to the nucleus, the orbital $u(r)$ satisfies in the Hartree–Fock approximation the equation

$$\left(-\tfrac{1}{2}\nabla^2 - \frac{Z}{r} - \int \frac{|u(r')|^2}{|\mathbf{r}-\mathbf{r}'|}\,d\mathbf{r}' - \epsilon\right)u(r) = 0, \qquad \ldots\ldots (1)$$

atomic units being used throughout. We expand $u(r)$ and ϵ according to

$$u(r) = \sum_{n=0}^{\infty} u_n(r), \quad \epsilon = \sum_{n=0}^{\infty} \epsilon_n \qquad \ldots\ldots (2)$$

where $u_0(r)$ and ϵ_0 satisfy the unperturbed equation

$$\left(-\tfrac{1}{2}\nabla^2 - \frac{Z}{r} - \epsilon_0\right)u_0(r) = 0. \qquad \ldots\ldots (3)$$

Thus

$$u_0(r) = \left(\frac{Z^3}{\pi}\right)^{1/2} \exp(-Zr), \quad \epsilon_0 = -\tfrac{1}{2}Z^2. \qquad \ldots\ldots (4)$$

Corresponding to (3) and (1) we define a perturbing potential

$$v(r) = -\int \frac{|u(r')|^2}{|\mathbf{r}-\mathbf{r}'|}\,d\mathbf{r}' \qquad \ldots\ldots (5)$$

and it also may be expanded according to

$$v(r) = \sum_{n=1}^{\infty} v_n(r) \qquad \ldots\ldots (6)$$

where

$$v_1(r) = -\int \frac{|u_0(r')|^2}{|\mathbf{r}-\mathbf{r}'|}\,d\mathbf{r}' \qquad \ldots\ldots (7)$$

$$v_2(r) = -2\int \frac{|u_0(r')u_1(r')|}{|\mathbf{r}-\mathbf{r}'|}\,d\mathbf{r}' \qquad \ldots\ldots(8)$$

$$v_2(r) = -\int \frac{2|u_0(r')u_2(r')| + |u_1(r')|^2}{|\mathbf{r}-\mathbf{r}'|}\,d\mathbf{r}'. \qquad \ldots\ldots(9)$$

Then substitution in (1) yields the set of equations in increasing order in the perturbation:

$$\left(-\tfrac{1}{2}\nabla^2 - \frac{Z}{r} - \epsilon_0\right)u_0 = 0 \qquad \ldots\ldots(10)$$

$$\left(-\tfrac{1}{2}\nabla^2 - \frac{Z}{r} - \epsilon_0\right)u_1 + (v_1 - \epsilon_1)u_0 = 0 \qquad \ldots\ldots(11)$$

$$\left(-\tfrac{1}{2}\nabla^2 - \frac{Z}{r} - \epsilon_0\right)u_2 + (v_1 - \epsilon_1)u_1 + (v_2 - \epsilon_2)u_0 = 0 \qquad \ldots\ldots(12)$$

which yield the formulae

$$\epsilon_1 = (u_0, v_1u_0), \quad \epsilon_2 = (u_0, [v_1 - \epsilon_1]u_1) + (u_0, v_2u_0). \qquad \ldots\ldots(13)$$

It is convenient to require that $(u_0, u_1) = 0$. It follows almost immediately that

$$\epsilon_2 = 3(u_0, v_1u_1). \qquad \ldots\ldots(14)$$

The Hartree–Fock energy is given by

$$E = 2\epsilon - \int v(r)|u(r)|^2 d\mathbf{r} \qquad \ldots\ldots(15)$$

so that writing

$$E = \sum_{n=0}^{\infty} E_n$$

there results

$$E_0 = 2\epsilon_0 = -Z^2 \qquad \ldots\ldots(16)$$

$$E_1 = \epsilon_1 = \frac{5Z}{8} \qquad \ldots\ldots(17)$$

$$E_2 = 2(u_0, v_1u_1). \qquad \ldots\ldots(18)$$

The function $u_1(r)$ may be determined by numerical integration of (11) or by minimizing the functional

$$J = \left(u_1, \left[-\tfrac{1}{2}\nabla^2 - \frac{Z}{r} - \epsilon_0\right]u_1\right) + 2(u_1, [v_1 - \epsilon_1]u_0). \qquad \ldots\ldots(19)$$

I have employed the latter alternative since it yields an analytical expression for $u_1(r)$. The result is that

$$E_2 = -0{\cdot}111003, \qquad \ldots\ldots(20)$$

correct to the number of figures given.

The non-relativistic energy expansion is (Hylleraas and Midtdal 1956)

$$E_{nr} = -Z^2 + \frac{5Z}{8} - \frac{0{\cdot}315311}{2} \qquad \ldots\ldots(21)$$

so that the leading term of the expansion of the correlation energy is independent of Z and has magnitude

$$E_{\text{corr}} = -0{\cdot}046652_5 \qquad \ldots\ldots(22)$$

which may be compared with the value of $-0{\cdot}047$ derived by Löwdin (1959).

References

Fröman, A., 1958, *Phys. Rev.*, **112**, 870.
Hylleraas, E., and Midtdal, J., 1956, *Phys. Rev.*, **103**, 829.
Löwdin, P. O., 1959, *J. Molec. Spectr.*, **3**, 46.

The Relativistic and Radiative Corrections to the Eigenvalues of the Helium Sequence

By A. DALGARNO† and A. L. STEWART‡

Department of Applied Mathematics† and Department of Physics,‡
The Queen's University of Belfast

Communicated by D. R. Bates; MS. received 5th November 1959

§ 1. Relativistic Corrections

If Z is the nuclear charge and $\mathbf{r}_1$ and $\mathbf{r}_2$ denote the position vectors of the two electrons with respect to the nucleus, the relativistic corrections to $O(\alpha^2)$, α being the fine structure constant, for the ground states of the helium iso-electronic sequence are given by (Bethe and Salpeter 1957)

$$\Delta E_{\mathrm{R}}=(E_1'+E_1''-E_1'''+E_3')\alpha^2 \text{ ryd}$$

where

$$E_1'=-\tfrac{1}{2}(\phi,\ \nabla_1^4\phi),$$
$$E_1''=2\pi Z(\phi,\ \delta(\mathbf{r}_1)\phi),$$
$$E_1'''=-2\pi(\phi,\ \delta(\mathbf{r}_{12})\phi),$$
$$E_3'=\left[\phi,\frac{1}{r_{12}}\{\nabla_1\,.\,\nabla_2+\mathbf{n}\,.\,(\mathbf{n}\,.\,\nabla_1)\nabla_2\}\phi\right],$$

ϕ being the eigenfunction, $\delta(\mathbf{r})$ the three-dimensional Dirac δ-function and $\mathbf{n}$ a unit vector parallel to $\mathbf{r}_{12}=\mathbf{r}_1-\mathbf{r}^2$.

Writing $\phi=\phi_0+\phi_1$ where $\phi_0=(Z^3/\pi)\exp\{-Z(r_1+r_2)\}$ and ϕ_1 is the solution of

$$\left(-\nabla_1^2-\nabla_2^2-\frac{2Z}{r_1}-\frac{2Z}{r_2}+2Z^2\right)\phi_1+\left(\frac{2}{r_{12}}-\frac{5Z}{4}\right)\phi_0=0 \qquad \ldots\ldots(1)$$

it follows immediately that to $O(Z^4\alpha^2)$, $\Delta E_{\mathrm{R}}=-0{\cdot}5Z^4$ and that to $O(Z^3\alpha^2)$, $E_1'''=-0{\cdot}25Z^3$, $E_3'=0$. These results have been given previously. The purpose of this note is to give the *exact* values of E_1' and E_1'' to $O(Z^3)$ and consequently the exact expression for ΔE_{R} to $O(Z^3\alpha^2)$.

To $O(Z^3)$,

$$E_1'=-\{\phi_1,\ [\nabla_1^4-5Z^4]\phi_0\}, \qquad \ldots\ldots(2)$$
$$E_1''=4\pi Z\{\phi_1,\ [\delta(\mathbf{r}_1)-Z^3/\pi]\phi_0\}. \qquad \ldots\ldots(3)$$

It is not possible to solve equation (1) exactly but by using the methods of Dalgarno and Stewart (1957, 1958), equations (2) and (3) can be written in the form

$$E_1'=-2\left\{\phi_1',\left(\frac{2}{r_{12}}-\frac{5Z}{4}\right)\phi_0\right\},$$
$$E_1''=-2\left\{\phi_1'',\left(\frac{2}{r_{12}}-\frac{5Z}{4}\right)\phi_0\right\}$$

where ϕ_1' and ϕ_1'' are solutions of, respectively,

$$\left(-\nabla_1^2-\nabla_2^2-\frac{2Z}{r_1}-\frac{2Z}{r_2}+2Z^2\right)\phi_1'-\tfrac{1}{2}(\nabla_1^4-5Z^4)\phi_0=0$$

and

$$\left(-\nabla_1^2-\nabla_2^2-\frac{2Z}{r_1}-\frac{2Z}{r_2}+2Z^2\right)\phi_1''+2\pi Z\left(\delta(\mathbf{r}_1)-\frac{Z^3}{\pi}\right)\phi_0=0.$$

Using the fact that $\nabla^2(r^{-1})=-4\pi\delta(\mathbf{r})$, we find that

$$\phi_1'=Z\left\{\frac{1}{r_1}-2Z\ln r_1-Z^2r_1\right\}\phi_0$$

and that

$$\phi_1''=\tfrac{1}{2}Z\left\{-\frac{1}{r_1}+2Z\ln r_1+2Z^2r_1\right\}\phi_0.$$

Hence by elementary integration

$$E_1'=-2{\cdot}5Z^4+(-24\ln 2+33)Z^3/8$$

and

$$E_1''=2Z^4+(12\ln 2-19)Z^3/8.$$

The relativistic shift in the ionization potential is then

$$\Delta I_{\mathrm{R}}=\tfrac{1}{4}\alpha^2Z^2[Z^2-Z(7-6\ln 2)]=\tfrac{1}{4}\alpha^2Z^2(Z^2-3{\cdot}84\ 1117\ Z)$$

which may be compared with the leading terms of the expression given by Bethe and Salpeter (1957)

$$\Delta I_{\mathrm{R}}=\tfrac{1}{4}\alpha^2Z^2(Z^2-4{\cdot}25Z)$$

and of the expression given by Dalgarno and Stewart (1958)

$$\Delta I_{\mathrm{R}}=\tfrac{1}{4}\alpha^2Z^2(Z^2-3{\cdot}80Z).$$

§ 2. RADIATIVE CORRECTIONS

The radiative corrections of $O(\alpha^3)$ have been derived by Araki (1957) but not in a form suitable for computation. His results for the shift in the ionization potential may be written more conveniently as

$$\Delta I_{\mathrm{L}}=(E_{\mathrm{L},1}-E_{\mathrm{L},2}-E'_{\mathrm{L},2}-E''_{\mathrm{L},2})\alpha^3\ \mathrm{ryd}$$

where $E_{\mathrm{L},1}$ is the Lamb shift for the one-electron ion

$$E_{\mathrm{L},1}=\frac{8}{3}\pi Z^4\left(-2\ln-\ln K_0+\frac{19}{30}\right),$$

K_0 being an average excitation energy (Bethe 1947, Harriman 1956),

$$E_{\mathrm{L},2}=\frac{8}{3\pi}E_1''\left(-2\ln\alpha-\ln k_0+\frac{19}{30}\right),$$

k_0 being the appropriate excitation energy for the two-electron system,

$$E_{\mathrm{L},2}'=-\frac{14}{3\pi}E_1'''\ln\alpha$$

and

$$E''_{\mathrm{L},2}=-\frac{7}{3\pi}\lim_{a\to 0}\left\{\int\!\!\int\frac{|\phi(\mathbf{r}_1,\mathbf{r}_2)|^2}{r_{12}{}^3(a)}\,d\boldsymbol{r}_1\,d\boldsymbol{r}_2-2(\gamma+\ln a)E_1'''\right\}-\frac{164}{15}\pi E_1'''$$

where $\phi(\mathbf{r}_1, \mathbf{r}_2)$ is the non-relativistic atomic wave function, γ is Euler's constant and

$$\frac{1}{r_{12}{}^3(a)} = \frac{1}{r_{12}{}^3} \quad r_{12} > a,$$

$$= 0 \quad r_{12} < a,$$

r_{12} being the inter-electronic distance. Apart from $E_{L,2}''$ which they do not consider, the terms have been given previously in this form by Kabir and Salpeter (1957) who show also that to a close approximation

$$k_0 \sim K_0 = 19{\cdot}77Z^2. \qquad \ldots\ldots(4)$$

Using our earlier results, it follows that to $O(Z^3\alpha^3)$,

$$\Delta I_L = \frac{8Z^4\alpha^3}{3\pi}\left\{(-7{\cdot}490 + 2\ln Z) + \frac{1}{Z}(11{\cdot}41 - 3{\cdot}11 \ln Z)\right\} \text{ ryd}$$

which may be compared with the leading terms of the expression given by Bethe and Salpeter (1957)

$$\Delta I_L = \frac{8Z^4\alpha^3}{3\pi}\left\{(-7{\cdot}490 + 2\ln Z) + \frac{1}{Z}(11{\cdot}93 - 2{\cdot}61 \ln Z)\right\} \text{ ryd}$$

and of the expression given by Dalgarno and Stewart (1958)

$$\Delta I_L = \frac{8Z^4\alpha^3}{3\pi}\left\{(-7{\cdot}490 + 2\ln Z) + \frac{1}{Z}(12{\cdot}11 - 2{\cdot}66 \ln Z)\right\} \text{ ryd}$$

from which the $E''_{L,2}$ term was omitted.

$E''_{L,2}$ for helium.

If the atomic wave function is written in the form adopted by Hylleraas (1929)

$$\phi(\mathbf{r}_1, \mathbf{r}_2) = \sum c_{lmn} s^l u^m t^n \exp(-\tfrac{1}{2}s)$$

where

$$s = 2Zk(r_1 + r_2), \qquad u = 2Zkr_{12}, \qquad t = 2Zk(r_2 - r_1).$$

It may be shown after some manipulation that

$$E''_{L,2} = -\frac{E_1'''}{\pi}\left(\ln 2Zk + \frac{527}{45}\right) - \frac{56}{3\pi} Z^3k^3 \frac{F}{G}$$

where

$$F = \sum_{\mu+\nu\neq 0} c_{lmn}c_{l'm'n'}S_{\lambda,\mu-3,\nu} + 2\sum c_{l00}c_{l'00}(\lambda+2)!\sum_{p=1}^{\lambda+2} p^{-1}$$

and

$$G = \sum c_{lmn}c_{l'm'n'}S_{\lambda,\mu,\nu}$$

with

$$\lambda = l + l', \qquad \mu = m + m', \qquad \nu = n + n',$$

and

$$S_{\lambda,\mu,\nu} = \{1 + (-1)^\nu\}(\lambda+\mu+\nu+5)!\left\{\frac{1}{(\nu+1)(\mu+\nu+3)} - \frac{1}{(\nu+3)(\mu+\nu+5)}\right\},$$

a result which agrees with Sucher (1958) apart from the factor of $(\lambda+2)!$ in the expression for F. Using the value of E_1''' given by Pekeris (1958) and the wave function of Hylleraas (1929) to evaluate k^3F/G, we obtain for helium $E''_{L,2} = -0{\cdot}0685 \text{ cm}^{-1}$ compared with Sucher's value of $-0{\cdot}072 \text{ cm}^{-1}$.

REFERENCES

ARAKI, H., 1957, *Progr. Theor. Phys.*, **17,** 619.
BETHE, H. A., 1947, *Phys. Rev.*, **72,** 339.
BETHE, H. A., and SALPETER, E. E., 1957, *Encyclopaedia of Physics,* **35** (Berlin: Springer).
DALGARNO, A., and STEWART, A. L., 1957, *Proc. Roy. Soc.* A, **240,** 274.
—— 1958, *Ibid.*, **247,** 245.
HARRIMAN, J. M., 1956, *Phys. Rev.*, **101,** 594.
HYLLERAAS, E. A., 1929, *Z. Phys.*, **54,** 347.
KABIR, P. K., and SALPETER, E. E., 1957, *Phys. Rev.*, **108,** 1256.
PEKERIS, C. L., 1958, *Phys. Rev.*, **112,** 1649.
SUCHER, J., 1958, *Phys. Rev.*, **109,** 1010.

An Investigation of the ^{28}Si(^{3}He, d)^{29}P and ^{28}Si(^{3}He, α)^{27}Si Reactions at a Bombarding Energy of 9·16 MeV

BY S. HINDS AND R. MIDDLETON

Atomic Weapons Research Establishment, Aldermaston, Berks.

Communicated by K. W. Allen; *MS. received 28th October* 1959

§ 1. INTRODUCTION

DURING a recent study of the ^{3}He reactions with ^{16}O (Hinds and Middleton 1959 b) using the Aldermaston 6 MeV Van de Graaff accelerator and broad-range magnetic spectrograph, several deuteron and α-particle groups were observed arising from the ^{28}Si component of the silica target. Alpha particle energy spectra have previously been measured at an incident energy of 5·8 MeV and the positions of several levels in ^{27}Si have been determined (Hinds and Middleton 1959 a). In the present communication deuteron and α-particle angular distributions measured at an incident energy of 9·16 MeV are presented. An attempt has been made to fit these with theoretical curves calculated on the basis of a direct reaction process.

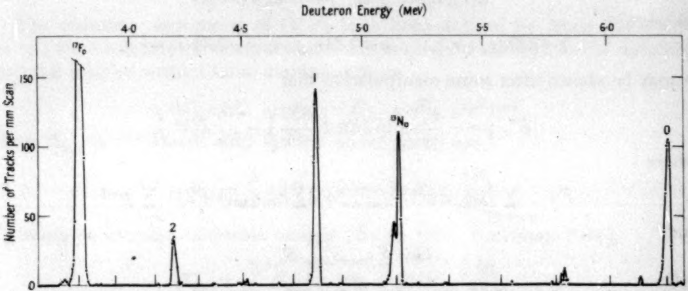

Figure 1. Energy spectrum of the deuterons from the ^{28}Si(^{3}He, d)^{29}P reaction measured at an incident energy of 9·16 MeV and an angle of 20°.

§ 2. THE ^{28}Si (^{3}He, d)^{29}P REACTION

In figure 1 is shown a deuteron energy spectrum measured at an angle of observation of 20°. Following our usual procedure, groups corresponding to states in ^{29}P are labelled numerically and those arising from target impurities by the symbol for the final nucleus. The group labelled $^{13}N_0$ is due to carbon and appears as a doublet due to carbon deposits forming on both sides of the target. The weak unlabelled groups at radii of 45, 51 and 52·5 cm are due to unidentified target impurities.

The energy of the incident ^{3}He beam was determined to be $9{\cdot}156 \pm 0{\cdot}010$ MEV from measurements made on the elastically scattered groups from oxygen, silicon and gold. From this value the Q-value for the ^{28}Si(^{3}He, d)^{29}P reaction was calculated to be $-2{\cdot}731 \pm 0{\cdot}012$ MEV and the mass of ^{29}P to be $28{\cdot}990978 \pm 16$ a.m.u. The latter was obtained using the masses of the d, ^{3}He and ^{28}Si reported respectively by Quisenberry, Giese and Benson (1957), Friedman and Smith (1958) and Endt and Braams (1957). This mass value differs by about four times the experimental error from the previous value of $28{\cdot}991035 \pm 12$ a.m.u. measured by Giese and Benson (1958) from the ^{29}P β^+ decay end point. No reason is known for this discrepancy.

The excitation energies of the first and second excited states of ^{29}P were determined to be 1·386 and 1·960 MEV respectively within an experimental error of ± 10 kev. These levels have previously been observed by Calvert, Jaffe and Maslin (1957) from a study of the ^{28}Si (d, n)^{29}P reaction. The corresponding states in the mirror nucleus ^{29}Si occur at 1·278 and 2·027 MEV (Van Patter and Buechner 1952).

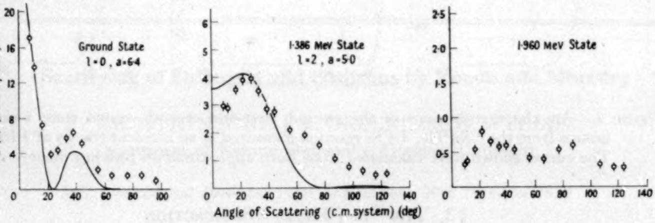

Figure 2. Angular distributions of the deuteron groups from the ^{28}Si(^{3}He, d)^{29}P reaction measured at an incident energy of 9·16 MEV corresponding to the ground, first and second excited states. The curves were calculated from Born approximation stripping theory.

In figure 2 are shown the angular distributions of the deuteron groups leading to the ground, first and second excited states of ^{29}P. The ground and first excited state distributions have been fitted with Born approximation stripping curves calculated from the theory of Newns (1952). The *l*-value assignments of 0 and 2 respectively agree with those obtained from the ^{28}Si(d, n)^{29}P reaction by Calvert *et al.* (1957). It may be noted that the radius of interaction required for the ground state distribution is equal to the Gamow radius + 1 fermi. The authors have found that this radius provides satisfactory agreement for a number of other (^{3}He, d) reactions and is equivalent to using the Gamow radius in Butler stripping theory. However, this value was unsatisfactory for the first excited state distribution and better agreement was obtained with a radius less than the Gamow value by 0·4 fermi.

The second excited state angular distribution does not exhibit a good stripping pattern, although there is an ill defined peak at about 20° which might indicate an $l=2$ transition. Also the maximum differential cross section is only one fifth of that of the first excited state. This contrasts with the results of Calvert *et al.* for the ^{28}Si(d, n)^{29}P reaction who report that the second excited state angular distribution is of similar shape and intensity as that of the first excited state. The corresponding transition in the mirror reaction ^{28}Si(d, p)^{29}Si has also been studied by Holt and Marsham (1953). They also observed a good stripping pattern with a peak differential cross section between $\frac{1}{2}$ and $\frac{1}{3}$ of that of the first excited state. The reason for this discrepancy is at present unknown. A possible explanation is that Coulomb effects are responsible since they would be expected to be larger for a (^{3}He, d) reaction than for a deuteron stripping reaction. It may be noted that the Coulomb barrier for ^{3}He particles incident on ^{29}Si is 9·2 MeV which is slightly in excess of our beam energy. However, it is surprising that the first excited state angular distribution has not been similarly affected.

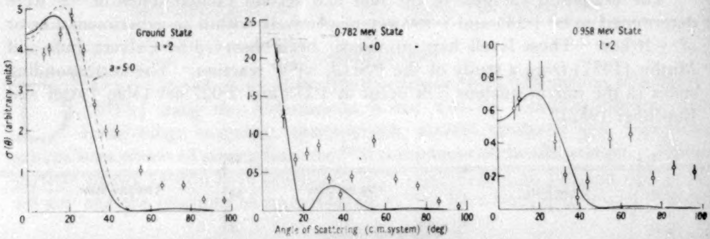

Figure 3. Angular distributions of the ground, first and second excited state α-particle groups from the ^{27}Si(^{3}He, α)^{27}Si reaction measured at an incident energy of 9·16 MeV. The curves shown were calculated from Born approximation pick-up theory.

§ 3. THE ^{28}Si (^{3}He, α) ^{27}Si REACTION

In figure 3 are shown the angular distributions of the ground, first and second excited state α-particle groups measured at an incident energy of 9·16 MeV. The arbitrary unit of cross section is the same as that used for the deuteron angular distributions in figure 2. Although several groups were observed corresponding to higher excited states, angular distributions were not measured because most of these were weak and partially obscured by a background of α-particles and spuriously scattered ^{3}He particles.

The curves shown in figure 3 were calculated from Born approximation pick-up theory (Newns 1952 and private communication) using a radius of interaction of 5·4 fermi, i.e. Gamow radius. In the case of the ground state group, slightly better agreement was obtained with a radius of 5·0 fermi, as is shown by the broken curve.

The measure of agreement between the theoretical curves and the experimental points is quite satisfactory, particularly since Coulomb effects are neglected in the theory. Also the *l*-value assignments of 2, 0 and 2 respectively for the ground, first and second excited states of ^{27}Si are in agreement with the known spins and parities of the mirror states of ^{27}Al, i.e. $\frac{5}{2}^+$, $\frac{1}{2}^+$ and $\frac{3}{2}^+$ (Endt and Braams 1957). Thus, these results provide further evidence that the pick-up process plays a major part in (^{3}He, α) reactions at intermediate energies and confirms the conclusions of previous investigations of the ^{12}C(^{3}He, α)^{11}C and ^{16}O(^{3}He, α)^{15}O reactions (Hinds and Middleton 1959 c, 1960).

ACKNOWLEDGMENTS

We would like to thank Dr. K. W. Allen for his encouragement and advice and Dr. H. C. Newns for much useful discussion.

REFERENCES

CALVERT, J. M., JAFFE, A. A., and MASLIN, E. E., 1957, *Proc. Phys. Soc.*, **70**, 78.
ENDT, P. M., and BRAAMS, C. M., 1957, *Rev. Mod. Phys.*, **29**, 683.
FRIEDMAN, L., and SMITH, L. G., 1958, *Phys. Rev.*, **109**, 2214.
GIESE, C. F., and BENSON, J. L., 1958, *Phys. Rev.*, **110**, 712.
HINDS, S., and MIDDLETON, R., 1959 a, *Proc. Phys. Soc.*, **73**, 727.
—— 1959 b, *Ibid.*, **74**, 762.
—— 1959 c, *Ibid.*, **74**, 775.
—— 1960, *Ibid.*, **75**, in the press.
HOLT, J. R., and MARSHAM, T. N., 1953, *Proc. Phys. Soc.* A, **66**, 467.
NEWNS, H. C., 1952, *Proc. Phys. Soc.* A, **65**, 916.
QUISENBERRY, K. S., GIESE, C. F., and BENSON, J. L., 1957, *Phys. Rev.*, **107**, 1664.
VAN PATTER, D. M., and BUECHNER, W. W., 1952, *Phys. Rev.*, **87**, 51.

Scattering of Electrons and Positrons by Xenon and Mercury

BY J. R. ATKINSON†, J. R. GREER‡ AND G. WYLLIE
Department of Natural Philosophy, Glasgow University

MS. received 2nd December 1959, *in final form 29th December* 1959

THE scattering of electrons and positrons of moderate energy by atomic nuclei is described in first approximation by the 'relativistic Rutherford' cross section introduced by Neher (1931)

$$\sigma=\left(\frac{Ze^2}{2mv^2}\right)^2(1-\beta)^2\operatorname{cosec}^4\tfrac{1}{2}\theta$$

where σ is the cross section for scattering per unit solid angle round scattering angle θ, Z the atomic number of the scatterer, m the rest mass and v the velocity of the scattered particle, and $\beta=v/\mathbf{c}$. Even in classical mechanics the relativistic mass change, as the speed varies in the scattering, produces a precession of the orbit in opposite senses for electron and positron. An extension of Sommerfeld's analysis of the hydrogen fine structure to open orbits shows that the main part of the cross section is given by the same (relativistic Rutherford) expression with $\operatorname{cosec}^4 \frac{1}{2}\theta$ replaced by

---

† Now at Dounreay Experimental Establishment, Atomic Energy Authority.
‡ Now at Department of Physiology, Glasgow University.

$$[\cos\phi \cos^3(\gamma\phi)]^{-1} \frac{d}{d\phi}(\gamma\phi)$$

where

$$[1-\gamma^2(1-\beta^2)]\cos^2(\gamma\phi) = 1-\gamma^2$$

and $\theta = \pi - 2\phi$ for positrons, $2\phi - \pi$ for electrons.

At small speeds and scattering angles this modification is equivalent to multiplying the relativistic Rutherford cross section by $1 \pm (\pi\beta^2/4) \sin \frac{1}{2}\theta$, the positive sign for electrons and the negative for positrons. However, since the angular momenta in Sommerfeld's fine-structure analysis are known to be wrongly assigned, only the signs in this result can be taken seriously. A calculation based on the Dirac equation of motion gives a correction factor

$$1 - \beta^2 \sin^2 \tfrac{1}{2}\theta \pm \pi\alpha\beta \sin \tfrac{1}{2}\theta\,(1 - \sin \tfrac{1}{2}\theta)$$

where $\alpha = Ze^2/\hbar c \simeq Z/137$ (McKinley and Feshbach 1948).

The difference between the behaviour of positrons and electrons will be most readily measured for scatterers of large Z and at scattering angles near $\pi/2$, and the cross sections must then be computed numerically (Massey 1942). Few materials of large Z are available as vapours at room temperature, but foil targets introduce serious complications. Champion and Barber (1938), using a cloud chamber containing mercury dimethyl vapour, obtained results in serious disagreement with the theory. Experiments have been carried out at Glasgow using cloud chambers either with xenon, or with mercury dimethyl vapour as scattering material. The experimental technique and the method of analysing the results are described by Greer (1955). An attempt to run a chamber using mercury dimethyl as sole condensable vapour was unsuccessful, and the results on mercury scattering were obtained with a chamber containing the dimethyl, water, and either argon or nitrogen.

In xenon 260 m of track of electrons of mean energy 0·83 MeV, and 111 m of track of positrons of mean energy 0·7 MeV were analysed. In a preliminary experiment on mercury dimethyl with argon, 64 m of electron track at mean energy 0·61 MeV and 12 m of positron track at mean energy 0·48 MeV were analysed. Within the large statistical errors both sets of results were in agreement with the theoretical predictions of Massey (1942).

A carefully replanned experiment at lower energies, using mercury dimethyl with nitrogen in a chamber of piston, rather than the previous diaphragm, type, led to the analysis of 35 m of electron track at mean energy 0·195 MeV and 26 m of positron track at mean energy 0·185 MeV. The absolute cross section, angular distribution, and electron–positron ratio of cross sections, all agreed with those to be expected for nitrogen alone.

This contradiction between our successive experiments with mercury dimethyl led us to reconsider the anomalous results obtained by Champion and Barber (1938), who reported scattering by mercury of one-sixth the expected amount. If the actual vapour pressure of mercury dimethyl in Champion's experiment, and in our second experiment, were much lower than the saturation vapour pressure of about 3 cm Hg, the anomalies would be explained. For such a situation to exist in a steady state there must be a mechanism removing the vapour from the chamber, and perhaps also one depressing its rate of replacement from the liquid phase, which was always present.

The density, and equilibrium vapour pressure between 0°c and 20°c, of the mercury dimethyl were measured and found to agree with published data. To find whether the dimethyl was being destroyed by a reaction in the gas phase, mixtures of dimethyl vapour, over the free liquid, and argon or nitrogen, were exposed to ionizing radiation or high-frequency discharge in vessels connected to manometers. The main decomposition product of the dimethyl, ethane, would have shown its presence in a steady pressure rise. No decomposition was observed in the presence of either argon or nitrogen with treatment far more severe than the irradiation of an expansion chamber in normal use.

Mercury dimethyl is very rapidly absorbed by rubber : a rubber sealing cap in contact with the liquid absorbed a third of its weight of the liquid in four hours. However, the expansion chamber used with argon, with rubber working parts, showed a rise in pressure of 3·3 cm Hg when the mercury dimethyl was introduced, and tracks in it showed scattering ascribable to this concentration of vapour, which is the probable saturated vapour concentration at the (not recorded) chamber temperature.

Thus it was necessary to suppose that in the experiments with mercury dimethyl in nitrogen by both sets of workers, not only was vapour absorbed by the rubber components of the chamber, but the rate of supply of vapour was restricted. In fact, in each of these experiments the liquid mercury dimethyl was present as a single pool of restricted surface area, which could readily become covered by a water film as a result of slight local cooling. Since mercury dimethyl is little soluble in water, such a film would be a serious barrier to evaporation. In the argon experiments the liquid dimethyl was dispersed in fine droplets over a thin gelatine layer covering the velvet background of the chamber, and its surface is unlikely to have been largely occluded by liquid water. The velvet was absent in our second chamber.

The main outcome of the present experiments is the explanation we now offer for the otherwise puzzling results of Champion and Barber. In the experiments not complicated by loss of scattering material, the confirmation of the existing theory of electron and positron scattering by xenon and mercury nuclei is no better than has been obtained for other materials in the form of foils.

ACKNOWLEDGMENTS

We are greatly indebted to Messrs. Lunevale Products Ltd. for the supply of a sample of the very toxic mercury dimethyl, and to Mr. J. T. Lloyd of the Glasgow Department of Natural Philosophy, who carried out almost all of the manipulations in which this material was exposed. The photographs of scattering in xenon were taken by J. R. Atkinson and A. F. Howatson.

REFERENCES

CHAMPION, F. C., and BARBER, A., 1938, *Proc. Roy. Soc.* A, **168**, 159.
GREER, J. R., 1955, *Ph.D. Thesis*, Glasgow University.
MCKINLEY, W. A., and FESHBACH, H., 1948, *Phys. Rev.*, **74**, 1759.
MASSEY, H. S. W., 1942, *Proc. Roy. Soc.* A, **181**, 4.
NEHER, H. V., 1931, *Phys. Rev.*, **38**, 1321.

Direct Measurement of Long Spin–Lattice Relaxation Times

By L. O. BOWEN

Carroll Magnet Laboratory, School of Applied Physics, University of New South Wales

MS. received 31*st August* 1959, *in revised form* 23*rd October* 1959

§ 1. Introduction

Existing methods for the measurement of the spin–lattice nuclear relaxation time T_1 are well described in the literature (see for instance Andrew 1956). The c.w. methods used for long times suffer from inaccuracy and/or inconveniently long observation times. Pulse techniques (Hahn 1949, Carr and Purcell 1954) are preferable but require sophisticated equipment.

Adiabatic reversal of the nuclear magnetization was first used to estimate the order of long spin–lattice relaxation times by Bloch (Bloch, Hansen and Packard 1946) using a sudden change in the value of the static field H_0. However, unless the conditions as described below are maintained, observation of the decay of the resulting transient requires a measurement of signal amplitudes, and/or a correction, in terms of the times spent above and below resonance per modulation cycle.

The adiabatic fast-passage technique used for relaxation times of the same order as the sweep period (Drain 1949) was extended for long T_1 by using long modulation periods (Chiarotti *et al.* 1954). However the latter method requires either a measurement of four quantities ($H_0 \neq H^*$) or the obtaining of two records ($H_0 = H^*$) to evaluate T_1 with an observation time much greater than T_1. Here H_0 is the static magnetic field and H^* the nuclear resonant field.

§ 2. Method

A direct c.w. method for the measurement of $T_1 \gg \tau_S$, the sweep period of the magnetic field, has been developed from Bloch's method and used (Bowen 1954, unpublished thesis) for some time in this laboratory. The method retains a reasonable degree of accuracy and measures T_1 directly in an observation time of the same order with a required measurement of only one parameter. Where changes in T_1 are occurring (e.g. due to temperature changes) observation times much greater than T_1 may well cause erroneous values of T_1 to be obtained.

To use the adiabatic nuclear induction technique for the measurement of T_1 one requires, besides the adiabatic condition (Bloch 1946),

$$\frac{dH_z(t)}{dt} \ll |\gamma| H_1^2 \qquad \ldots\ldots(1)$$

the conditions

$$\tau_R \ll \tau_S; \qquad T_2 \gg \tau_R \qquad \ldots\ldots(2)$$

in order to exclude transverse relaxation. Here τ_R = resonance time $\simeq \tau_S H_1/2\pi H_S$, τ_S = sweep period, T_2 = spin–spin relaxation time†, $H_z(t) = H_0 + H_S \sin \omega_S t$, H_S = modulation field, H_1 = radio-frequency field perpendicular to $H_z(t)$, γ = gyromagnetic ratio.

---

† This includes the effect of inhomogeneity in H_0.

If the static field H_0 is adjusted so that the resonant field H^* is reached just before the modulation field reaches its peak value then

$$\tau_1 \gg \tau_2 \qquad \ldots\ldots (3)$$

where τ_1 is the time spent below resonance in one modulation cycle, and τ_2 the time spent above resonance.

The observed nuclear resonance dispersion signal at dynamic equilibrium is then due to the time variation of a nuclear magnetization, approximately equal to M_0 the static magnetization, since the time τ_2 during which the magnetization is reversed (and when T_1 decay can occur) is much less than $\tau_1 \simeq \tau_S$.

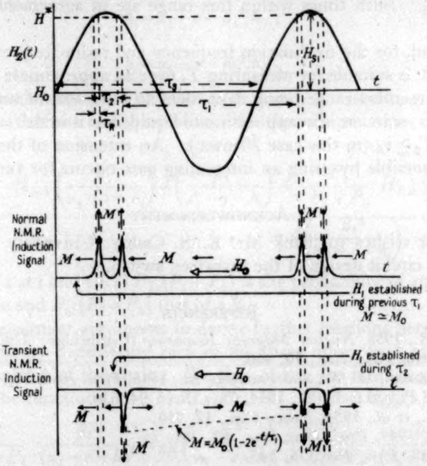

H^*
$H_z(t)$
H_0
τ_S
τ_2
τ_R
τ_1
H_S
t
Normal N.M.R. Induction Signal
M
M
H_0
M
t
H_1 established during previous τ_1
$M \simeq M_0$
Transient N.M.R. Induction Signal
H_1 established during τ_2
H_0
t
M
M
M
$M=M_0(1-2e^{-t/\tau_1})$
M

However, if the nuclear sample is initially subjected to only the field $H_z(t) = H_0 + H_S \sin \omega_S t$ and subsequently H_1 is switched on during the time τ_2, the nuclear magnetization will be in the same direction as H_0, instead of reversed as it would be for dynamic equilibrium. Thus a transient negative signal initially proportional to M_0 will be obtained which decays to a positive signal proportional to M_0 through zero in a time $\tau_{\text{null}} = T_1 \ln 2$ the T_1 decay now occurring in the time τ_1. (See figure). The method is analogous to the Carr–Purcell (Carr and Purcell 1954) pulse method in which τ_{null} is obtained by adjustment of the time interval between a π and $\pi/2$ pulse. In this latter case it is necessary to adjust this time interval to measure different values of T_1.

§ 3. EXPERIMENTAL DETAILS

It is important for accuracy that the experimental values be adjusted so that the inequalities (1), (2) and (3) are maintained. Typical values and times used are: $H_1 = 3$ oersted, $\tau_S = 20$ msec, $\tau_2 = 0{\cdot}6$ msec, $H_S = 50$ oersted, $\tau_R = 0{\cdot}2$ msec, $\tau_1 = 19{\cdot}0$ msec.

Accurate observation of τ_{null} requires a good signal to noise ratio and consequently radio-frequency amplification of the signal may be required before

detection. The nuclear induction apparatus used is conventional but incorporates a fast relay actuated from a modulation voltage-controlled thyratron to actuate the radio-frequency oscillator. It is necessary to adjust the phase of the incoming trigger since the modulation field has a phase difference with respect to the modulation current. This arrangement allows H_1 to be established during time τ_2. A cine camera was used to measure τ_{null} at leisure from a cathode-ray oscilloscope display, a continuous record of T_1 being obtained simply by starting and stopping H_1. It is intended to replace this method of recording with a phase sensitive detector and electronic counter. Spin–lattice relaxation times for various proton-containing substances have been measured with an estimated error of $\pm 5\%$. Such times within this range are in agreement with accepted values.

The method, for the modulation frequency and radio-frequency field amplitude as quoted, is suitable for measuring T_1 over an approximate range of 0·5 sec to a few minutes, this range being dependent to some extent on the method of recording. Its main use is in application to liquids but it is also suitable for some solids where $T_2 \gtrsim \tau_s$ (in this case 20 msec). An extension of the upper limit of T_1 would be possible by using an integrating gate circuit for very weak signals.

ACKNOWLEDGMENT

The author wishes to thank Mr. R. S. Caddy, University of New South Wales, for the circuit design of the thyratron switch.

REFERENCES

ANDREW, E. R., 1956, *Nuclear Magnetic Resonance* (Cambridge: University Press).
BLOCH, F., 1946, *Phys. Rev*, **70,** 460.
BLOCH, F., HANSEN, W. W., AND PACKARD, M., 1946, *Phys. Rev.*, **70,** 474.
CARR, H., and PURCELL, E. M., 1954, *Phys. Rev.*, **94,** 630.
CHIAROTTI, G., *et al.*, 1954, *Nuovo Cim.*, **12,** 519.
DRAIN, L. E., 1949, *Proc. Phys. Soc.*, **62,** 301.
HAHN, E., 1949, *Phys. Rev.*, **76,** 145.

Functional Equations for the Vibrational Spectra of Diatomic Chains

BY P. DEAN AND J. L. MARTIN
Mathematics Division, National Physical Laboratory, Teddington, Middlesex

MS. received 29th September 1959

§ 1. INTRODUCTION

THE functional equation of Dean (1959, hereafter referred to as I) for the vibrational spectrum of a disordered chain of atoms applies only to cases in which no correlation exists between successive matrix elements. Thus, while it is successful in dealing with a number of simplified models—such as the type 1 chain of Dyson (1953) and (after modification) the alloy of Schmidt (1957)—it cannot be used, as was at first thought, for more complex systems.

In this note we use a probability argument which takes into account correlation between matrix elements to derive a system of equations for the spectrum of the general binary lattice (subject to nearest neighbour harmonic forces). The method is based upon Sturm's theorem, as in I.

§ 2. DERIVATION OF THE FUNCTIONAL EQUATIONS

We use the notation of I and, in particular, refer to the table of § 4 of that paper. The suffixes of α, β and P, in the following, correspond to row numbers of the table.

Let $H_{\mathrm{XY}}(h_i)$ be the probability distribution of h_i when an X atom occurs at the ith site and a Y at the $(i+1)$th site. We consider first the case when both X and Y are A atoms. The relation between h_i and h_{i-1} can then have either of the forms

$$h_i = \alpha_1 - \nu - \beta_1{}^2/h_{i-1}$$

or

$$h_i = \alpha_5 - \nu - \beta_5{}^2/h_{i-1}$$

according to whether the $(i-1)$th atom is an A or a B. Equating the probability of values of h_i with those of h_{i-1} we obtain, for the infinite lattice,

$$H_{\mathrm{AA}}(h_i)\,dh_i = \frac{P_1}{P_1+P_5}\,H_{\mathrm{AA}}\left(\frac{\beta_1{}^2}{\alpha_1-\nu-h_i}\right)d\left(\frac{\beta_1{}^2}{\alpha_1-\nu-h_i}\right)+\frac{P_5}{P_1+P_5}\,H_{\mathrm{BA}}\left(\frac{\beta_5{}^2}{\alpha_5-\nu-h_i}\right)\times d\left(\frac{\beta_5{}^2}{\alpha_5-\nu-h_i}\right), \quad \ldots\ldots(1)$$

where (with A's at i and $i+1$) $P_1/(P_1+P_5)$ is the probability of an A occurring at the $(i-1)$th site and $P_5/(P_1+P_5)$ that of a B.

We may use similar arguments to derive further relations between the distribution functions by considering each of the three other ways of occupying the i and $(i+1)$th places of the chain. We thus obtain the following system of four equations for the functions $H_{\mathrm{AA}}(h)$, $H_{\mathrm{AB}}(h)$, $H_{\mathrm{BA}}(h)$ and $H_{\mathrm{BB}}(h)$:

$$\begin{aligned}
H_{\mathrm{AA}}(h) &= \frac{P_1}{P_1+P_5}\,\frac{\beta_1{}^2}{(\alpha_1-\nu-h)^2}\,H_{\mathrm{AA}}\left(\frac{\beta_1{}^2}{\alpha_1-\nu-h}\right)+\frac{P_5}{P_1+P_5}\,\frac{\beta_5{}^2}{(\alpha_5-\nu-h)^2}\times H_{\mathrm{BA}}\left(\frac{\beta_5{}^2}{\alpha_5-\nu-h}\right),\\
H_{\mathrm{AB}}(h) &= \frac{P_2}{P_2+P_6}\,\frac{\beta_2{}^2}{(\alpha_2-\nu-h)^2}\,H_{\mathrm{AA}}\left(\frac{\beta_2{}^2}{\alpha_2-\nu-h}\right)+\frac{P_6}{P_2+P_6}\,\frac{\beta_6{}^2}{(\alpha_6-\nu-h)^2}\times H_{\mathrm{BA}}\left(\frac{\beta_6{}^2}{\alpha_6-\nu-h}\right),\\
H_{\mathrm{BA}}(h) &= \frac{P_3}{P_3+P_7}\,\frac{\beta_3{}^2}{(\alpha_3-\nu-h)^2}\,H_{\mathrm{AB}}\left(\frac{\beta_3{}^2}{\alpha_3-\nu-h}\right)+\frac{P_7}{P_3+P_7}\,\frac{\beta_7{}^2}{(\alpha_7-\nu-h)^2}\times H_{\mathrm{BB}}\left(\frac{\beta_7{}^2}{\alpha_7-\nu-h}\right),\\
H_{\mathrm{BB}}(h) &= \frac{P_4}{P_4+P_8}\,\frac{\beta_4{}^2}{(\alpha_4-\nu-h)^2}\,H_{\mathrm{AB}}\left(\frac{\beta_4{}^2}{\alpha_4-\nu-h}\right)+\frac{P_8}{P_4+P_8}\,\frac{\beta_8{}^2}{(\alpha_8-\nu-h)^2}\times H_{\mathrm{BB}}\left(\frac{\beta_8{}^2}{\alpha_8-\nu-h}\right),
\end{aligned} \quad \ldots\ldots(2)$$

(cf. the equations (A 15) of Schmidt (1957), derived in a different context).

According to the theory of I, the integral distribution function for the normal mode frequencies is

$$M(\nu)=\int_{-\infty}^{0} H(h)dh \Big/ \int_{-\infty}^{\infty} H(h)dh, \qquad \ldots\ldots(3)$$

where $H(h)$ is the weighted sum:

$$H(h)=(P_1+P_5)H_{\mathrm{AA}}(h)+(P_2+P_6)H_{\mathrm{AB}}(h)+(P_3+P_7)H_{\mathrm{BA}}(h)$$
$$+(P_4+P_8)H_{\mathrm{BB}}(h). \qquad \ldots\ldots(4)$$

It should be noted that the P's are not all independent and may be determined very simply in terms of the imposed order parameters of the chain, as in I.

§ 3. PERIODIC LATTICES

When the lattice under consideration is *periodic*, the functional equations reduce to very simple forms. For the monatomic lattice of A atoms, $P_1=1$ and all other $P_i=0$. In this case the system (2) reduces to

$$H_{\mathrm{AA}}(h)=H_{\mathrm{AA}}\left(\frac{\beta_1^2}{\alpha_1-\nu-h}\right)\frac{\beta_1^2}{(\alpha_1-\nu-h)^2}, \qquad \ldots\ldots(5)$$

the other H_{AB}, H_{BA} and H_{BB} becoming indeterminate; relation (4) becomes $H(h)=H_{\mathrm{AA}}(h)$.

Equation (5) has the straightforward solution

$$H_{\mathrm{AA}}(h)=\begin{cases}[h^2-(\alpha_1-\nu)h+\beta_1^2]^{-1} & (\text{when } |\alpha_1-\nu|<2\beta_1),\\ \delta(h-h_0) & (\text{when } |\alpha_1-\nu|>2\beta_1),\end{cases}$$

where h_0 satisfies $h_0^2-(\alpha_1-\nu)h_0+\beta_1^2=0$; other considerations show that h_0 must be the root of smallest absolute value. The relation (3) now leads to the familiar frequency spectrum of a monoatomic lattice (cf. Brillouin 1946).

The regular diatomic lattice ... ABABA ... is only slightly more complicated. In this case, $P_3=P_6=\frac{1}{2}$, and the functional equations are

$$H_{\mathrm{AB}}(h)=\frac{\beta_6^2}{(\alpha_6-\nu-h)^2}H_{\mathrm{BA}}\left(\frac{\beta_6^2}{\alpha_6-\nu-h}\right),$$
$$H_{\mathrm{BA}}(h)=\frac{\beta_3^2}{(\alpha_3-\nu-h)^2}H_{\mathrm{AB}}\left(\frac{\beta_3^2}{(\alpha_3-\nu-h)}\right),$$

and $H(h)=\frac{1}{2}H_{\mathrm{AB}}(h)+\frac{1}{2}H_{\mathrm{BA}}(h)$. When

$$[\beta_3^2+\beta_6^2-(\alpha_3-\nu)(\alpha_6-\nu)]^2<4\beta_3^2\beta_6^2,$$

that is, when ν lies inside the acoustic or optical bands, the solution is

$$H_{\mathrm{AB}}(h)=\{(\alpha_3-\nu)h^2-[\beta_3^2-\beta_6^2+(\alpha_3-\nu)(\alpha_6-\nu)]h+\beta_3^2(\alpha_6-\nu)\}^{-1},$$
$$H_{\mathrm{BA}}(h)=\{(\alpha_6-\nu)h^2-[\beta_6^2-\beta_3^2+(\alpha_6-\nu)(\alpha_3-\nu)]h+\beta_6^2(\alpha_3-\nu)\}^{-1}.$$

For other values of ν, H_{AB} and H_{BA} are simple δ-functions.

No such solutions are known in the disordered cases. The alternative is to attempt to solve the equations (2) numerically but the method given in I is much more direct and accurate (cf. Dean 1960).

ACKNOWLEDGMENT

The work described above has been carried out as part of the research programme of the National Physical Laboratory and this paper is published by permission of the Director of the Laboratory.

REFERENCES

Brillouin, L., 1946, *Wave Propagation in Periodic Structures* (New York: McGraw Hill).
Dean, P., 1959, *Proc. Phys. Soc.*, **73**, 413.
—— 1960, *Proc. Roy. Soc.* A, **254**, 507.
Dyson, F. J., 1953, *Phys. Rev.*, **92**, 1331.
Schmidt, H., 1957, *Phys. Rev.*, **105**, 425.

Ageing Process in Triglycine Sulphate

By J. STANKOWSKA and J. STANKOWSKI
Institute of Experimental Physics, A. Mickiewicz University, Poznań, Poland
Polish Academy of Sciences, Institute of Physics, Dielectric Laboratory, Poznań, Poland

Communicated by A. Piekara; MS. received 15th July 1959,
in revised form 25th September 1959

In the ageing of a ferroelectric, changes of its dielectric properties (ϵ, $\tan\delta$, P_s, E_c, etc.) occur with time. In the present case, the same samples were investigated when old and when young. A sample that has not been subjected to heat treatment or an a.c. electric field for a considerable period of time (the time depends on the kind of ferroelectric material dealt with) is termed old. An old sample can exhibit a double hysteresis loop. A sample heated to a temperature above that of the Curie point is termed young. A young sample always exhibits a normal hysteresis loop. The process converting an old sample into a young one is termed rejuvenation. The inverse process is that of ferroelectric ageing (figure 1). An a.c. electric field can also act as a rejuvenating agent.

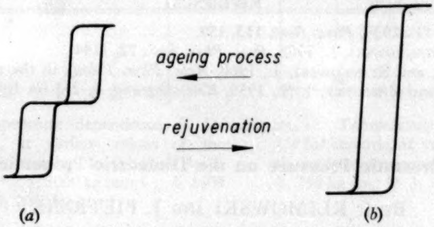

Figure 1. Schematic representation of the shape of the hysteresis loop in (*a*) an old and (*b*) a young sample.

The rejuvenating action of an a.c. field upon pure triglycine sulphate salt is shown in figure 2 (Plate). Picture (*a*) is that of the old sample; subsequently, a much stronger a.c. field is applied for 5 minutes for rejuvenation (*b*). Picture (*c*) shows hysteresis loops of the sample rejuvenated by the action of the former a.c. field. In pure triglycine sulphate salt the shape of the loop changes very rapidly, so that at high intensities of the electric field the effect can be overlooked. The process of rejuvenation by applying a field is much more conveniently observed in triglycine sulphate that has been doped with $CuSO_4$. The admixture increases the activation energy for domain reorientation; in such material, the double hysteresis loop can be observed at leisure on the oscillograph screen.

Figure 3 (*a*) (Plate) shows the hysteresis loop obtained with an old sample of triglycine sulphate doped with $CuSO_4$; figure 3 (*b*) is that of the same sample subsequent to heating to a temperature exceeding that of the Curie point. The asymmetry of the loop shown in figures 2 (*a*) and 3 (*a*) is related to the region from which the sample was cut.

Higher concentration of admixtures was found to produce a decrease in ϵ and P_s and a rise in the coercive field E_c. Temperature hysteresis connected with the process of rejuvenation was also observed.

From investigations on ageing carried out jointly with Pajak (Pajak and Stankowski 1958) and from results of Chynoweth (1959) and Yureen and Zheludev (1959), ageing may be considered to consist of two processes occurring simultaneously: (i) reorientation of the domains, finally yielding antiparallel domain configuration, and (ii) diffusion of the admixtures towards the walls separating the domains, tending to fix the state of a domain as antiferroelectric. In various ferroelectric materials the two component processes participate to a various degree. In $BaTiO_3$, it is the first that plays a considerable part, while in Rochelle salt and triglycine sulphate, where domain configuration is antiparallel by nature, it is diffusion of the defects towards the walls between the domains that is the more important of the two.

Hence it may be concluded that for practical purposes it is most convenient to use pure ferroelectric materials, wherein ϵ, P_s and E_c change but little in the course of time. Results are to be published in detail (Stankowska and Stankowski 1960).

The authors wish to thank Professor Dr. A. Piekara for directing the present investigation and for his numerous valuable discussions.

REFERENCES

CHYNOWETH, A. G., 1959, *Phys. Rev.*, **113,** 159.
PAJAK, Z., and STANKOWSKI, J., 1958, *Proc. Phys. Soc.*, **72,** 1144.
STANKOWSKA, J., and STANKOWSKI, J., 1960, *Acta. Phys. Polon.*, in the press.
YUREEN, V. A., and ZHELUDEV, I. S., 1959, *Kristallografia*, **4,** 253 (in Russian).

Effect of Hydrostatic Pressure on the Dielectric Properties of $BaTiO_3$†

BY J. KLIMOWSKI AND J. PIETRZAK
Institute of Experimental Physics, A. Mickiewicz University, Poznań, Poland

Communicated by A. Piekara; MS. received 15*th July* 1959
and in revised form 25*th September* 1959

A CONSIDERABLE number of papers dealing with the effect of hydrostatic pressure upon ferroelectric properties has been published. Vul and Vereshtchagin (1945) found that hydrostatic pressure raises the capacity of a polycrystalline $BaTiO_3$ plate, the relative change in capacity per unit pressure amounting to $1{\cdot}2 \times 10^{-5}\,cm^2\,kg^{-1}$. Merz (1950) detected a linear depression of the Curie point in a monocrystal subjected to hydrostatic pressure, amounting to $-5{\cdot}8 \times 10^{-3}$ deg atm^{-1}. Shirane and Sato (1951) investigated (Ba–Sr)TiO_3 solid solutions and found a depression of the Curie point of $-6{\cdot}0 \times 10^{-3}$ deg atm^{-1}.

---

† The present investigation has been supported in part by the Institute of Physics of the Polish Academy of Sciences.

The present authors investigated the effect of hydrostatic pressure on the dielectric permittivity of both monocrystalline and ceramic $BaTiO_3$ above and below the Curie point. Crystals grown by Remeika's method had the shape of thin 0·2–0·3 mm plates of an area of 4–10 mm². Silver electrodes were made on the surface by evaporation. Monocrystals (*c*-plates) exhibiting a hysteresis loop of 94% 'squareness' and a dielectric permittivity of 300 at 2 kc/s and room temperature were used for measurements. Ceramic samples were obtained from polycrystalline $BaTiO_3$ of grain size not exceeding 100 μ by well-known methods (see Trzebiatowski and co-workers 1952). Hydrostatic pressure was produced within the piezostat by a pressure intensifier filled with paraffin oil. The pressure was measured to an accuracy of ± 1%. The temperature was measured with a thermocouple. The dielectric permittivity of $BaTiO_3$ single crystals and ceramics was measured with a Schering type bridge. The accuracy in measuring the capacity attained ± 0·2 pF. The measuring field did not exceed 10 v cm^{-1}; the frequency of the measuring signal was 2 kc/s. In each measurement of the temperature dependence of the capacity at constant pressure, the sample was cooled from a temperature of 180°c. The rate of cooling was 30 deg per hour and was kept constant. The temperature- and pressure-induced variations of the stray capacity did not exceed ± 0·1% and could be neglected.

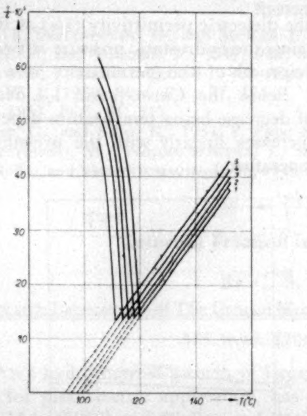

Figure 1. Temperature dependence of $1/\epsilon$ for crystal, at various values of the hydrostatic pressure: 1, 0 kg cm^{-2}; 2, 500 kg cm^{-2}; 3, 1000 kg cm^{-2}; 4, 1500 kg cm^{-2}; 5, 2000 kg cm^{-2}.

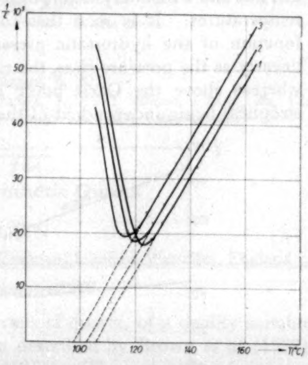

Figure 2. Temperature dependence of $1/\epsilon$ for ceramic, at various values of the hydrostatic pressure: 1, 0 kg cm^{-2}; 2, 740 kg cm^{-2}; 3, 1600 kg cm^{-2}.

Figure 1 shows the reciprocal value of the dielectric permittivity of a monocrystal as plotted against the temperature, at various values of the hydrostatic pressure. As the pressure increases, the Curie point (corresponding to the maximum value of ϵ) undergoes a linear shift towards lower temperatures, amounting to $-4{\cdot}1 \times 10^{-3}$ deg cm² kg^{-1}, and the maximum value of the permittivity rises monotonically. Hydrostatic pressure is seen to produce no change in the sign of the tangent to the $\epsilon(T)$ curve below the Curie point, and, hence, the

$BaTiO_3$ monocrystal may be assumed to retain its original *c*-domain structure. The Curie–Weiss temperature (for which $1/\epsilon = 0$) decreases as the hydrostatic pressure rises; this decrease is, however, less than that of the Curie point and amounts to $-3{\cdot}6 \times 10^{-3}$ deg cm² kg⁻¹, the Curie constant undergoing no change and equalling $1{\cdot}1 \times 10^4$ °c. Thus, as the hydrostatic pressure rises, the difference between the Curie point and the Curie–Weiss temperature diminishes.

Measurements of the dielectric permittivity of $BaTiO_3$ ceramics (figure 2) against the temperature and the hydrostatic pressure revealed a linear fall in the Curie point and Curie–Weiss temperature resulting from a rise in pressure and amounting to $-4{\cdot}5 \times 10^{-3}$ deg cm² kg⁻¹. The latter value is larger than that for a crystal and is in agreement with the experimental results of Jaffe and co-workers (1957). The Curie–Weiss constant is independent of the hydrostatic pressure and amounts to $0{\cdot}9 \times 10^4$ °c.

In figure 3, the reciprocal value of the dielectric permittivity ($1/\epsilon$) of $BaTiO_3$ ceramic and a monocrystal is plotted against the hydrostatic pressure at two fixed temperatures. It is seen that the reciprocal of the permittivity is a linear function of the hydrostatic pressure. Below the Curie point, $1/\epsilon$ decreases linearly as the pressure rises, the rate of decrease being temperature dependent, whereas above the Curie point $1/\epsilon$ increases linearly with the pressure, the steepness being independent of the temperature.

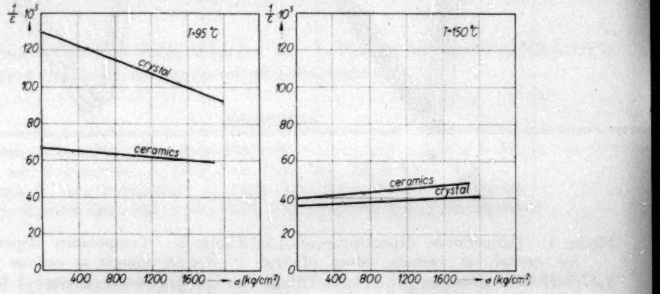

Figure 3. Dependence of $1/\epsilon$ on the hydrostatic pressure.

The results obtained for a monocrystal within the region above the Curie point can be compared with Devonshire's theory. For this, the free energy is expressed as a function of the hydrostatic pressure and the polarization (Klimowski and Pietrzak 1959)

$$A(\sigma, P) = -\tfrac{1}{2}\kappa\sigma^2 + \eta\sigma P^2 + A(0, P) \qquad \ldots\ldots (1)$$

wherein σ denotes the hydrostatic pressure, $\kappa = 3/(c_{11} + 2c_{12})$ the coefficient of compressibility, $\eta = -(g_{11} + 2g_{12})/(c_{11} + 2c_{12})$ the coefficient of volume electrostriction, and $A(0, P)$ is the free energy given as a function of the polarization at zero values of the stresses. From equation (1), the dielectric permittivity is computed as follows:

$$\frac{1}{\epsilon_\sigma} = \frac{\eta}{2\pi}\sigma + \frac{1}{\epsilon} \qquad \ldots\ldots (2)$$

with ϵ_σ denoting the permittivity under hydrostatic pressure, and ϵ that in the absence of stress. By equation (2), above the Curie point $1/\epsilon_\sigma$ is a linear function of the hydrostatic pressure. The foregoing result is in agreement with experiment (figure 3). The coefficient η can now be computed assuming $1/\epsilon_{\sigma} - 1/\epsilon = 5{\cdot}3 \times 10^{-5}$ for $\sigma = 2{\cdot}000$ kg cm^{-2}, yielding a value of $\eta = 1{\cdot}7 \times 10^{-13}$ cm^2 dyn^{-1}. On the other hand, η can be computed from the relative change of volume and the spontaneous polarization at the Curie point. Differentiating equation (1) with respect to the hydrostatic pressure and assuming $\sigma = 0$ yields $\Delta V/V = \eta P^2$, whence, putting $\Delta V/V = 4{\cdot}9 \times 10^{-4}$ (Kay and Vousden 1949) and $P = P_s = 18\,\mu$c cm^{-2} (Merz 1953), we have $\eta = 1{\cdot}7 \times 10^{-13}$ cm^2 dyn^{-1}, a result in good agreement with the value of η computed from measurements by the present authors.

The authors wish to thank Professor Dr. A. Piekara for directing the present investigation and for his valuable advice throughout the measurements.

REFERENCES

JAFFE, H., BERLINCOURT, D., and MCKEE, J. M., 1957, *Phys. Rev.*, **105**, 37.
KAY, H. F., and VOUSDEN, P., 1949, *Phil. Mag.*, **40**, 1019.
KLIMOWSKI, J., and PIETRZAK, J., 1959, *Acta Phys. Polon.*, in the press.
MERZ, W. J., 1950, *Phys. Rev.*, **77**, 52.
—— 1953, *Ibid.*, **91**, 513.
SHIRANE, G., and SATO, K., 1951, *J. Phys. Soc. Japan*, **6**, 20.
TRZEBIATOWSKI, W., WOJCIECHOWSKA, J., and DAMM, J., 1952, *Roczn. Chem.*, **26**, 12.
VUL, B. M., and VERESHTCHAGIN, L. F., 1945, *Dokl. Akad. Nauk S.S.S.R.*, **48**, 662.

Internal Friction in Synthetic Quartz

BY C. S. BROWN
Research Laboratories of The General Electric Company Limited, Wembley, England

MS. received 10*th November* 1959

THE hydrothermal growth of large crystals of quartz, of a quality suitable for piezoelectric application, has been described by Brown *et al.* (1952), Hale (1952) and Walker and Buehler (1954). The properties of conventional oscillator crystal units cut from synthetic quartz have been measured (Brown and Thomas 1957, Bechmann 1955), and found to be closely similar to those made from natural quartz in all respects, including *Q*-factor.

However, conventional quartz crystal units are insensitive to changes in the intrinsic damping in the material, the changes largely being masked by the extraneous losses imposed by the mounting system. It is now possible, using a special design of crystal unit described by Warner (1952), to reduce extraneous losses to a very low level and so obtain a measure of the internal friction in the quartz.

A study of synthetic quartz using this type of unit was first made by King (1957, 1959) and he showed that at 20°c the internal friction of natural quartz is considerably less than that of any synthetic quartz then available. More recently, similar studies have been carried out in these laboratories which have confirmed these results. In fact, quartz grown on a seed plate cut perpendicular to the optic axis at a rate of 0·5 mm per day on each side of the seed was shown to have a *Q*-factor of the order of 3×10^5 at 5 Mc/s compared with a figure of $2{\cdot}5$ to $3{\cdot}0 \times 10^6$ for natural quartz. It must be stressed that even this change of one order hardly affects the activity of conventional oscillator units which have a *Q*-factor of 10^5 or less.

An examination of a number of samples of synthetic quartz grown on different seed orientations by slightly varying processes has suggested that the losses are relatively independent of the growth process for a given growth rate. A number of crystals has been grown at rates varying from 0·10 to 0·55 mm per day in order to determine the effect of growth rate under carefully controlled conditions. Measurements of internal friction have been made using 13·5 mm diameter AT-cut contoured vibrators operating at 5 Mc/s on their fifth overtone. The values of Q^{-1} at 20°C are plotted as a function of growth rate in the figure, from which it will be seen that the internal friction is a rapidly varying function of growth rate, closely approaching the value for natural quartz at rates below 0·15 mm per day.

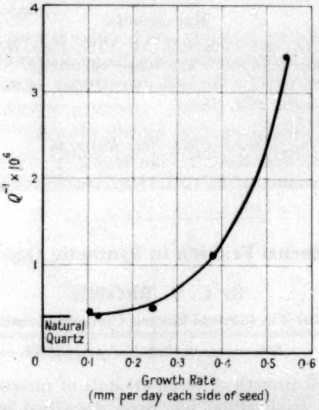

Internal friction in synthetic quartz as a function of growth rate.

Although for conventional piezoelectric applications it would still be more economic to employ a higher growth rate, for special applications, such as frequency standards, where the highest possible Q is required, crystals grown at the reduced rates would be essential.

Studies are being carried out to determine the internal friction of synthetic quartz grown at different rates of growth as a function of temperature in the range 4–400°K, together with the effects of X-irradiation. These results will be published at a later date.

REFERENCES

BECHMANN, R., 1955, *I.R.E. Convention Record*, **3**, A.9, 56.

BROWN, C. S., KELL, R. C., THOMAS, L. A., WOOSTER, N., and WOOSTER, W. A., 1952, *Mineralogical Magazine*, **29**, 858.

BROWN, C. S., and THOMAS, L. A., 1957, *Proc. Instn Elect. Engrs*, **104C**, 174.

HALE, D. R., 1952, *Brush Strokes*, December (Brush Development Corporation).

KING, J. C., 1957, *Proceedings of the 11th Annual Symposium on Frequency Control*, U.S. Army Signal Engineering Laboratories, p. 62.

—— 1959, *Bell Syst. Tech. J.*, **38**, 573.

WALKER, A. C., and BUEHLER, E., 1954, *Industrial and Engineering Chemistry*, **46**, 1670.

WARNER, A. W., 1952, *Proc. Inst. Radio Engrs, N.Y.*, **40**, 1030.

LETTERS TO THE EDITOR

The Absorption Spectrum of Neon

The absorption of neon has been measured in the region 600 Å to 220 Å by methods previously reported (Ditchburn and Heddle 1953, Ditchburn 1955). The absorption cross section is shown in figure 1 in comparison with the curve obtained by Po Lee and Weissler (1953). The results are in good agreement except in the regions near the L_3L_2 series limit (575 Å) and near the L_1 series limit (256 Å). The new curve is very probably correct in the region near 575 Å because it agrees not only with the present measurements but also with some measured points of Weissler which he ignored in smoothing his curve. In the region near the L_1 edge, the position is more uncertain since the emission lines used for making the measurements are photographically very weak, both in the present experiment and in Weissler's. Some points lie considerably above the curve. The deviations may be due to experimental error or to weak auto-ionization lines.

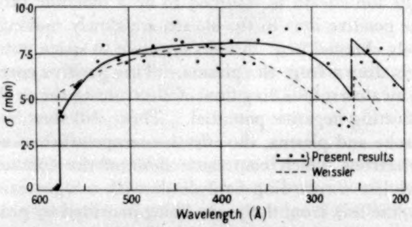

Figure 1. Absorption cross section for neon (1 mbn = 10^{-18} cm²) as a function of wavelength.

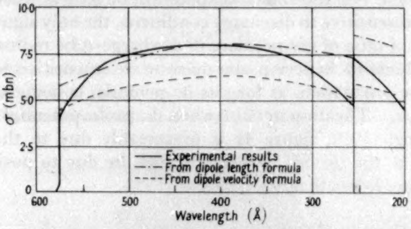

Figure 2. Absorption cross section for neon.

In figure 2 what is believed to be the best experimental curve, taking account both of the present results and of those obtained by Weissler, is compared with theoretical curves calculated by Seaton (1954) using a dipole length and a dipole velocity approximation respectively. It may be seen that the dipole length formula gives the better fit, except in the regions near to the series limits.

This agreement indicates that strong auto-ionization effects similar to those found in thallium (Marr 1954) are not present.

I wish to thank Mr. J. F. James and Mr. G. Wood for help in this work.

Physics Research Laboratory,
University of Reading.
9th December 1959.

R. W. Ditchburn.

Ditchburn, R. W., 1955, *Proc. Roy. Soc.* A, **229**, 44.
Ditchburn, R. W., and Heddle, D. O., 1953, *Proc. Roy. Soc.* A, **220**, 61.
Po Lee and Weissler, G. L., 1953, *Proc. Roy. Soc.* A, **219**, 71.
Marr, G. V., 1954, *Proc. Roy. Soc.* A, **224**, 83.
Seaton, M. J., 1954, *Proc. Phys. Soc.* A, **67**, 927.

Noise Spectra of a Probe in a Hot-Cathode Discharge

The noise potentials at a floating probe (Singh 1959) can be explained qualitatively if the ion sheath is assumed to be a dynamic rather than a static structure, i.e. the positive ions in the sheath are slowly moving in to the probe which is negatively charged (e.g. 15 volts negative to space potential) and being replaced by others drawn from the plasma. This positive current to the probe will be balanced by a corresponding flow of electrons to the probe, just sufficient to maintain the floating negative potential. There will then be a finite conductance between probe and plasma, the effective temperature of which is governed mainly by the electrons which contribute most of the conductivity; and the probe will behave like a retarding-field diode with a high-resistance leak from anode to cathode, the leak from the probe being provided by positive ions. It is also known both theoretically and experimentally (Druyvesteyn 1933, Knol 1951) that the effective temperature T_e of the negative electrons in a plasma approximates to $eV/\boldsymbol{k}$ where V is the ionization potential of the gas and $\boldsymbol{k}$ is Boltzmann's constant. T_e is insensitive to discharge conditions, the only significant correction being a function of ratio of gas pressure to discharge-tube radius.

One would therefore expect probe noise to be insensitive to discharge conditions and probe orientation, as long as its potential is being controlled by the arrival of electrons. The drop in noise when the probe potential is taken to minus 30–40 volts (Singh 1959, figure 4) is presumably due to the elimination of electron current to the probe. Noise will then be due to positive ions, which have a temperature lower than T_e.

Electrical Engineering Dept.,
The University,
Birmingham, 15.
14th January 1960.

D. A. Bell.

Druyvesteyn, M. J., 1933, *Z. Phys.*, **81**, 571.
Knol, K. S., 1951, *Philips Res. Rep.*, **6**, 288.
Singh, C., 1959, *Proc. Phys. Soc.*, **74**, 42.

On the Thermomagnetic Effects of Monovalent Metals

In his article, Blatt (1957) mentions that "The observation of positive values of these (Nernst and Ettingshausen) coefficients in copper and other metals poses a problem more serious even than the positive absolute thermoelectric powers of lithium and noble metals". Jones (1955, 1957) has resolved the question of positive thermoelectric power of noble metals by considering the Fermi surface to be lying very close to the Brillouin zone boundaries in these metals. But theoretical studies of the Fermi surface in these metals are deficient as is pointed out by Callaway (1958), in order to verify Jones' assumption. A consideration similar to that of Jones appears to explain the positive Nernst and Ettingshausen coefficients.

The expressions for two of the thermomagnetic coefficients (for these are the ones that are of interest) namely Nernst and Ettingshausen coefficients for a model of a single band of standard form, in the limit of small magnetic field and the lowest order in k_0T/η (Jones uses results to this order) are respectively

$$A_{\mathrm{N}_i} = -\frac{\pi^2 k_0{}^2 T}{3m^*c}\left(\frac{\partial\tau}{\partial\epsilon}\right)_{\epsilon=\eta} \qquad \ldots\ldots(1)$$

$$A_{\mathrm{E}} = -\frac{T}{nc}\left(\frac{\partial\log\tau}{\partial\epsilon}\right)_{\epsilon=\eta}. \qquad \ldots\ldots(2)$$

The notations are as in Blatt's article. One may notice a change of sign in these coefficients from those given by Sondheimer (1948) and also Wilson (1954). The latter authors denote A_{N_i} by $B_{\mathrm{EN}}{}^i$. A misprint in the formula for A_{E}, which occurs in the article of Blatt, is here corrected.

Both these coefficients should be negative if τ is a monotonically increasing function of ϵ and this is true of scattering by lattice vibrations, while they would be positive if τ is a decreasing function of ϵ near the edge of the Brillouin zone (Wilson 1954).

According to Jones (1955), when the Fermi surface is a slightly distorted sphere and lies very close to the Brillouin zone boundaries

$$\tau = \beta\epsilon^2/N(\epsilon) \qquad \ldots\ldots(3)$$

where β is a positive constant involving some universal constants like $\hbar$, π and q_0, the radius of the Debye sphere in the space of the wave vector of the lattice vibrations. Substitution of this in (1) and (2) gives

$$A_{\mathrm{N}_i} = -\beta\frac{\pi^2 k_0{}^2 T\eta}{3m^*c\,N(\eta)}\left[2-\left(\frac{\epsilon}{N(\epsilon)}\frac{\partial N}{\partial\epsilon}\right)_{\epsilon=\eta}\right] \qquad \ldots\ldots(4)$$

$$A_{\mathrm{E}} = -\frac{T}{nc\eta}\left[2-\left(\frac{\epsilon}{N(\epsilon)}\frac{\partial N}{\partial\epsilon}\right)_{\epsilon=\eta}\right]. \qquad \ldots\ldots(5)$$

The second term in the square brackets in (4) and (5) is $\frac{1}{2}$ for free electrons. But for monovalent metals in which the Fermi surface is very close to the Brillouin zone boundaries, this term may be much larger. From the same arguments as Jones' (1955), if this is the case, this factor may very well exceed 2 and hence lead to positive values of A_{N_i} and A_{E}.

Thus, we see that the arguments of Jones for an explanation of an anomalous sign in the thermoelectric power of some monovalent metals predict similar anomalies in the signs of Nernst and Ettingshausen coefficients in the same metals and not vice versa (since for positive thermoelectric power $[(\epsilon/N(\epsilon))\,\partial N/\partial\epsilon]_{\epsilon=\eta}$ should be greater than 7/2). Also, such an explanation leads to an extra additional term in the electronic specific heat at very low temperatures, also linear in temperature (Jones 1957).

Wilson (1954) very correctly anticipated "No model which has this property (τ, a decreasing function of ϵ) at high temperatures has so far been proposed, in addition to giving negative values for $B_{EN}{}^{i}$ and A_E, it would presumably explain the positive thermoelectric powers of Cu, Ag and Au".

It is a great pleasure to thank Prof. R. S. Krishnan for his keen interest and kind encouragement. I am indebted to Dr. R. Srinivasan for reading the manuscript and for his comments.

Department of Physics, A. K. Rajagopal.
Indian Institute of Science,
Bangalore-12, S. India.
24th November 1959.

Blatt, F. J., 1957, Article in Seitz–Turnbull: *Solid State Physics*, **4**, 235, 236.
Callaway, J., 1958, Article in Seitz–Turnbull : *Solid State Physics*, **7**, 198.
Jones, H., 1955, *Proc. Phys. Soc.* A, **68**, 1191.
—— 1957, *Proc. Roy. Soc.* A, **240**, 321.
Sondheimer, E. H., 1948, *Proc. Roy. Soc.* A, **193**, 484.
Wilson, A. H., 1954, *The Theory of Metals* (Second Edition), (Cambridge : University Press), pp. 221, 222.

REVIEWS OF BOOKS

Metal Fatigue, edited by J. A. POPE. Pp. xiii + 381. (London: Chapman and Hall, 1959.) 70*s*.

This volume is the published version of a course on the fatigue of metals held in the Engineering Department of Nottingham University in September, 1955. Each of the twenty chapters in the book is a self-contained entity representing one lecture, and each is written by an expert in the particular field dealt with so that a wide field of knowledge is covered in an authoritative manner. The book is intended primarily for design and development engineers who have to deal in practice with fatigue problems and as a result the emphasis throughout is almost entirely on the macroscopic aspects of the problem rather than the microscopic. One cannot help feeling, however, that one or two chapters on the present state of knowledge regarding the initiation and growth of fatigue cracks, from the point of view of the basic physics and metallurgy of the processes, would have provided valuable background material for a number of the present chapters, and perhaps given the engineer some idea of whether better alloys to resist fatigue might be produced in the future.

Nevertheless, the book can be welcomed very warmly indeed, and it certainly fulfils a real need in gathering together so many aspects of fatigue which are of importance to designers.

The first eight chapters are devoted to fundamentals of fatigue and cover the general background theory for simple and complex stresses, stress concentration effects, residual stresses, cumulative damage, statistical analysis, corrosion fatigue, fretting corrosion, and crack propagation and temperature effects in steels.

Then follow eight chapters dealing with the fatigue of engineering materials and components, such as high temperature alloys, aluminium alloys, cast irons, copper alloys, bearing metals, welds, joints, aircraft and aircraft structures. In view of the great engineering importance of steels it might be felt an omission that no chapter is devoted specifically to their fatigue properties. Steels are of course referred to many times throughout the book as a whole, but one short chapter bringing together the most important facts about their fatigue behaviour would have been worthwhile. The overlap caused by this would not have been serious since by the very nature of the book, involving as it does a large number of authors, there is some overlapping at present.

The final four chapters are devoted to various aspects of fatigue testing such as the reproducibility of test results, fatigue testing of bearings, of welded structures and of aircraft structures.

Throughout the book as a whole the quality of the writing is high and the numerous excellent diagrams, tables and illustrations make for easy reading. References are provided at the end of each chapter, but a deliberate effort has been made to include in the text the salient points of any work referred to, since an engineering designer may not have available such a comprehensive library as a research worker. In this connection the value of the book would be still further increased by a larger index. The present five-page index, which includes authors, is definitely rather meagre for a book of 375 pages; containing as it does such a mass of valuable detailed information. G. C. SMITH.

A New Method in the Theory of Superconductivity, by N. N. BOGOLIUBOV, V. V. TOLMACHEV and D. V. SHIRKOV. Pp. iii + 121. (New York : Consultants Bureau ; London : Chapman and Hall, 1959.) 50*s*.

This monograph has previously been published in Russian and in a shortened English translation in the *Fortschritte der Physik*. It gives a full and connected account of Bogoliubov's 'quasi-particle' transformation for fermions, and its application to the theory of superconductivity. In physical content the theory of Bogoliubov *et al.* is similar to that of Bardeen, Cooper and Schrieffer, but the mathematical scheme is more rigorous and elegant, and lends itself better to detailed calculations.

The quasi-particle transformation is applied to the BCS Hamiltonian, to the Bloch–Fröhlich electron–phonon Hamiltonian, and to a more complicated model Hamiltonian in which Coulomb interactions are explicitly included. The latter model yields a criterion for superconductivity, to which that of BCS is a first approximation. The collective modes are discussed, in Fröhlich's model. In Chapter III (not included in the abridged *Fortschritte* version), boson and fermion quasi-particle transformations are applied together, to obtain a 'superconducting' ground state for the electrons, together with Fröhlich's renormalization of the phonon frequencies and the coupling constant.

The authors claim to present a *complete* solution to the problem of superconductivity. The reviewer cannot agree, since no demonstration is given of the Meissner effect, nor of the anomalous Knight shift. Nevertheless, this book will be very welcome to theoreticians with any interest at all in the theory of superconductivity, especially as the material is so clearly written and presented.

C. G. K.

Fluctuation Phenomena in Semiconductors, by A. VAN DER ZIEL. Pp. viii + 168. (London : Butterworths Scientific Publications, 1959.) 35*s*.

The subject of fluctuations in semiconductors is of considerable theoretical interest and has recently become of great practical importance. This book starts with a brief introduction to methods of noise measurement and the mathematics of fluctuations. Subsequent chapters deal with the major sources of noise in semiconductors: generation–recombination noise, flicker noise and noise in diodes. The results are applied to obtain expressions for the noise figure of photoconductors, rectifiers, diode mixers and amplifiers and transistors. Those who are not already familiar with the subject will probably find this book very difficult to read, one is often overwhelmed with algebra and unable to see clearly in which direction one is going or what is the ultimate goal. In some places the treatment is very condensed and, in others, there is an excess of unimportant detail. No real attempt has been made to present the essential features of the subject in the simplest possible form or to indicate which of the results are of major importance. The chapters on semiconductor devices would be of more use and greater interest if more practical results had been included. It would, for example, be useful to have some actual values for the noise figure of transistors so that the reader could easily make a comparison between the performance of transistors and vacuum tubes. Although the book contains over three hundred equations and several hundred symbols are used, there is no list of symbols, so that much time is wasted by the reader in hunting through the text to find their definition. One of the most useful features is the extensive and up-to-date bibliography containing nearly three hundred references which will certainly be of great value to research workers in this field. B. V. ROLLIN.

Elements of Solid State Theory, by G. H. WANNIER. Pp. vii + 270. (Cambridge: University Press, 1959.) 35*s*.

The phrase which is used as the title of this book is not altogether without ambiguity. Interpreted literally it would imply a vast range of physical sciences, for example, crystallography, metallurgy, large parts of chemistry, and even geology. In fact the phrase ' solid state physics ' became popular in the decade following the second world war and was used primarily to denote the topics associated with the electron theory and the lattice dynamics of metals and semiconductors. The author of this book has taken a rather wider view. The book opens with a chapter on crystallography and ends with one on cohesion and chemical bonding. There is much of interest between—and including—these chapters. For example, there are chapters dealing with lattice dynamics, cooperative phenomena, electron theory of solids and friction in electron dynamics. Many topics which the reader might reasonably expect to find under such a title are absent and, indeed, the author himself states in the preface " some topics of current interest are missing altogether and others will be found only in skeletonized form ". In fact, it is probably fair to say that from the topics omitted or only touched upon, another book could be written which would qualify for the same title.

In a book which attempts to cover such a wide field it is inevitable that no particular topic can be treated in great detail, but if in some cases detail is absent, there can be no question about the depth of the treatment. The principles underlying the various topics dealt with are in all cases most carefully elucidated. Many readers who have made solid state physics their speciality will still find much in this volume that is stimulating and enlightening. It is doubtful whether this book is really suitable for the beginner. Only those who are familiar with the mathematics and notation of modern theoretical physics will be able to appreciate many of the formulae which appear. To the well-equipped graduate student who wants to survey the principles on which solid state theory is based, the book can be thoroughly recommended. H. JONES.

Handbuch der Physik, Vol. XLIV. *Nuclear Instrumentation* I, edited by S. FLÜGGE (co-editor E. CREUTZ). Pp. vii + 473. (Berlin : Springer, 1959.) DM. 125.

The science of nuclear accelerator design has developed with spectacular success since 1930 and the implementation of its conclusions now commands an important fraction of the total scientific budget in many countries. It is timely that a volume containing authoritative accounts of the main instruments, as seen at the end of 1957, should now appear, since development and experiment have usually outstripped publication and details of many machines have been available so far only in laboratory reports. The authors of the articles in this volume have covered the available material exhaustively as far as their respective machines are concerned; the reader may perhaps only regret that no general survey article relating the different accelerators and comparing their performance has been included.

The arrangement of the material in the book follows a historical sequence. The chapter (in German) on cascade generators, by E. Baldinger, reminds the reader that transformers, rectifiers and condensers are standard components to the electrical engineer, and that multiplying networks can be treated in considerable detail by circuit theory. The auxiliary apparatus of a cascade accelerator, such as ion source and accelerating tube, is not discussed. The following article on Van de Graaff generators, by R. G. Herb, necessarily treats the installation as a whole and gives a thorough account of the development of this most precise and controllable member of the accelerator family, with particular reference to the important contributions of the University of Wisconsin.

The next five articles deal with accelerators which employ time-varying fields. The necessary theories of orbit stability are developed in several places and typical examples are generously discussed. B. L. Cohen writes on the classical cyclotron and the removal of its relativistic limitation, following the enunciation of the principle of phase stability, by the development of the synchrocyclotron. He also shows how the later proposal of azimuthally-varying-field machines offers both high energy and high intensity. Electron synchrotrons (including the strong focusing type) are discussed by R. R. Wilson, and betatrons by D. W. Kerst, in stimulating articles which clearly exhibit the electrodynamic principles of these machines. No article deals with the microtron, which seems to merit treatment at this point. G. K. Green and E. D. Courant have written an account of the proton synchrotron which provides a detailed comparison of the design and operating problems of four large machines of this type, and leads on to a discussion of the alternating gradient principle and the AG machines under construction. This thorough and informative article is likely to be the standard reference on its subject for many years. L. Smith concludes the descriptions of machines with a comprehensive account of linear accelerators for electrons, protons and heavy ions.

The Editors have rightly decided that the production of neutrons is as useful in nuclear physics as the acceleration of charged particles and D. J. Hughes gives a survey of the more important reactor techniques. This article concludes a well-produced volume whose contents form a remarkable tribute to the courage and ingenuity of physicists and engineers over three decades.

W. E. BURCHAM.

Vector Space—and its application in crystal-structure investigation, by MARTIN J. BUERGER. Pp. xiv + 347. (New York: John Wiley; London: Chapman and Hall, 1959.) 96*s*.

The power of certain techniques has frequently been recognised before scientific workers had the tools to make full use of new ideas. For instance, the theory of space groups had been worked out and was ready for use once von Laue had shown that crystals can diffract x-rays. The simultaneous growth in the understanding of Patterson vector maps, due to a great extent to the work of Buerger, and the development of electronic digital computers is perhaps a similar happy coincidence. Thus the publication of Martin Buerger's most recent book *Vector Space* is most opportune.

Patterson showed that it is possible to construct a Fourier synthesis which represents the vector relationship between the scattering matter in a crystal, when all vectors are transposed to the origin. The advantage of the Patterson synthesis is that it requires only experimental data, while the construction of an electron density map requires both the experimentally measurable structure factors, and their relative phases, which cannot be measured, but must be derived. The great problem in crystallography is either to find, using indirect means, the phase of each structure factor or to reconstruct the crystal from vector relationships found in the Patterson map. This is the problem which forms the main subject of this book.

The Patterson function is introduced in Chapter 2, and some of its properties are investigated in Chapters 3 to 6. Chapters 1 to 5 might well be omitted by those who are already familiar with the basic properties of vector space. Buerger then enlarges on the consequences of symmetry on Patterson maps and considers the possibility of solving a structure by the use of so-called Harker sections and implication diagrams alone (Chapter 7). However, more complicated organic structures (Buerger quotes tartaric acid and DL-methionine) have strong non-Harker background on Harker sections. Hence the most vital part of this book lies in Chapters 8 and 10 to 13 where the theory of image seeking functions is developed and different superposition functions are compared.

The scragginess of the contours of the examples chosen show that graphical methods must suffer a good deal of approximation, although the final answers show a remarkable resemblance to the final electron density maps. The reader is left to speculate on how close an approximation to electron density could be achieved by repeated superposition with the Buerger minimum function and the accuracy made possible by the use of an electronic computer. Further, if the time taken for an attempted superposition is not prohibitive it becomes less important if a multiple vector has accidentally been chosen as a point of superposition, for another attempt at solution can then be made.

The practising crystallographer will want to know whether the better method of solution to his particular problem lies in, say, the use of the heavy atom technique, or in the superposition of the Patterson maps; or perhaps in the use of difference Pattersons as compared with usual isomorphous replacement techniques. In general, what is the exact equivalence between vector space and reciprocal space solutions ? Until these questions receive an answer the full power of vector methods cannot be correctly assessed, but the many problems which have already been solved by the use of vector methods make it clear that those who are interested in the analysis of complex crystal structures should have a copy of *Vector Space* in their own library. MICHAEL G. ROSSMANN.

Mécanique Quantique, Vol. 1, by A. MESSIAH. Pp. xv + 430. (Paris : Dunod, 1959.) 3.900 fr.

The time has surely come when the appearance of yet another textbook of quantum mechanics should be received with reserve if not with suspicion. At all events I must confess to such sentiments when I opened this first volume of Dr. Messiah's work. Very soon, however, I had to admit that here was something new which tried to present the subject in a manner quite different from what one is accustomed to. Until the second volume has appeared I think one must suspend any final judgment upon this presentation; but it is already clear that, whatever the student will make of it, the teacher will find it invaluable. After a fairly lengthy exposition of the origins of the quantum theory the bulk of this first volume is concerned with setting up the formalism of quantum mechanics in a modern framework, particular attention being paid to mathematical niceties. It assumes a level of mathematical sophistication which may be appropriate to the average French student but which is considerably above what one can expect of the British undergraduate. Halfway through the book, for example, one finds a lengthy exposition of the properties of projection operators and these are used extensively thereafter. Although one warmly welcomes the use of such powerful concepts in principle, one wonders to what use they can be put and to what extent they can be understood by a student who, at this stage, has been shown very little in the way of practical applications. It is not until the last third of the volume that there is a study of the standard problems of angular momentum, scattering, the hydrogen atom, and the harmonic oscillator, for which much that has gone before is unnecessary. Characteristically, the third page of the treatment of the harmonic oscillator introduces creation and annihilation operators. However, all of the formalism of this volume is valuable, if not entirely necessary, when one comes to the study of perturbation theory and relativistic quantum mechanics. These topics are promised in the second volume, and one therefore awaits its appearance with considerable interest. Personally, I am not inclined to recommend this book to students; but I shall certainly use it myself, and shall encourage other teachers of quantum mechanics to do likewise. B. H. FLOWERS.

Atlas of γ-ray Spectra from Radiative Capture of Thermal Neutrons, by L. V. GROSHEV, A. M. DEMIDOV, V. N. LUTSENKO and V. L. PELEKHOV; translated from the Russian by J. B. SYKES. Pp. iv + 198. (London, New York, Paris, Los Angeles: Pergamon Press, 1959.) 140*s*.

Detailed study of the energy and intensity of the cascades of gamma radiation following slow neutron capture is of great interest to the nuclear spectroscopist. The power and value of such studies was first fully revealed by the experiments of Kinsey and his collaborators at Chalk River but this work did not adequately survey the many low energy transitions owing to the limitations of the magnetic pair spectrometer. These limitations are largely (though not entirely) removed by the use of a Compton spectrometer and experiments with such an instrument by the authors of this book and others, at the Atomic Energy Institute of the Academy of Sciences of the U.S.S.R., confirm and extend the Chalk River results.

The introduction to this volume briefly surveys and compares the different techniques of measurement, and is followed by a useful table of thermal neutron capture cross sections and neutron binding energies. The body of the book presents, nucleus by nucleus, a table of all measured energies and intensities in the gamma-ray spectra, experimental curves obtained with the Compton spectrometer, corrected curves from which instrumental effects have been removed, and finally a scheme of bound levels showing observed transitions and spins and parities where known. Appendices deal with internal conversion electrons and gamma rays associated with beta decay.

The atlas gives a valuable picture of the low-lying levels of nuclei and should be useful to both experimentalist and theoretician. There are some small imperfections in the diagrams and tables, due probably to photographic reproduction, but these do not affect the general clarity and utility of the presentation.

W. E. BURCHAM.

Seventh Symposium (International) on Combustion, published for the Combustion Institute. Pp. xlvi + 959. (London: Butterworths Scientific Publications, 1959.) £11 4*s*. 0*d*.

The seventh international symposium on combustion (the first to be held outside the United States) was held in London and Oxford in 1958. This account of it, which runs to nearly a thousand pages, has been printed with exemplary speed and clarity. It contains one hundred and twenty-four papers on eleven topics which include the mechanism of combustion reactions, the structure and propagation of flames, combustion in practical flowing systems, detonation and its initiation, and related subjects ranging as far as spectroscopy and instrumentation. There is a just balance of theory and application, and the volume is an admirable cross section of recent work in these developing fields.

J. BRONOWSKI.

Physics and Heat Technology of Reactors, by various authors. Pp. v + 174. (New York: Consultants Bureau, Inc., 1958.) Price £8 8*s*. 0*d*.

This collection of eighteen papers originally appeared as Supplement No. 1, 1958, to the *Soviet Journal of Atomic Energy*. Articles in this journal of interest to English readers, are usually translated and published in the *Journal of Nuclear Energy* (Pergamon Press), but this procedure has not been applied to the supplements. Consultants Bureau have therefore performed a useful service in issuing this volume, which covers a wide range of problems in reactor theory, reactor physics and reactor engineering.

The first paper derives multigroup diffusion equations from the basic and adjoint diffusion–age equations, which remain valid for strong absorption during slowing-down; in the second paper the diffusion equations for one- and two-dimensional regions are replaced by finite difference equations. Next we have a discussion on the relation between critical mass and critical volume in homogeneous reactors. Two papers outline a synthetic kernel method for neutron diffusion in hydrogeneous and non-hydrogeneous materials; the elastic collision function is replaced by a synthetic function of the form

$$ae^{-\beta u}\delta(\mu-1)+b\delta(u)+c\delta(\mu-1)\delta(u)$$

making it possible to derive an integral equation for the flux.

A report on the pulse method of investigating neutron slowing down in graphite, shows that after the elastic slowing-down stage, the neutrons interact with the lattice as if they were a hot Maxwellian gas subject to Newton's law of cooling. A set of three papers on fission products, deals with the overall rate of decay, the yield in the mass number range 139–153 for ^{233}U, and a determination of σ_c for ^{135}Xe. A report is given of the experimental determination of the spectrum of scattered γ-rays emerging from a lead shield. The use of ^{235}U as a coating on thermocouples for measuring neutron flux, is then discussed. An account is given of the experimental determination of the maximum permissible thermal-neutron flux, using a paraffin dummy.

The papers of engineering interest start with the determination of the power–weight ratio for various designs of fuel elements. This is followed by an analysis of the optimum thermodynamic cycle for atomic power stations, obtained by minimizing the total cost. The use of saturated steam in atomic power stations is discussed. A paper on boiling water reactors deals with the efficiency and the loading factor, i.e. the fraction of heat transferred to water. The use of freon as a working fluid in single and dual supercritical thermal cycles is discussed. The final paper deals with radioactive contamination in the steam circuits of atomic power plants.

Reactor physicists and engineers should find much to interest them in this volume; the translations run smoothly. A minor criticism is the inadequacy of the references and particularly those of original British and American books and articles. J. WOODROW.

Introduction to the Theory of Compressible Flow, by SHIH-I PAI. Pp. xiii + 385. (Princeton, N.J.; Toronto; London; New York: van Nostrand, 1959.) 73*s*.

Over the last decade, the increasing interest in high speed flow has been reflected in an increasing number of textbooks and treatises on compressible fluid theory, some designed for the student with no prior knowledge of the field and others written with the research worker or specialist in mind. Professor Pai's book seems to fall into the first category; the specialist will find little that he is not already familiar with, and the treatment rarely goes far enough for it to be useful as a reference book. However, as an introductory text it suffers, at least in the reviewer's opinion, from various defects.

The treatment is often too brief or condensed to make for easy reading by the student. This appears to be due, in part at least, to the fact that the coverage of the field is almost complete, including accounts of comparatively recent developments like hypersonic boundary layers and magnetogasdynamics, so that of necessity much of the material has to be condensed to get it into 377 pages. The reviewer feels that many portions of the book may not be clear to the student fresh to compressible fluid theory. Moreover, the author tends to manipulate equations formally, rather than give a clear description of the fundamental concepts and a satisfactory development of the subject. For example, the student is unlikely to appreciate the significance and usefulness of the exact solution for supersonic flow round a sharp corner (the Prandtl–Meyer expansion) when it is introduced as a ' lost solution ' of the hodograph equations.

The problems at the end of each chapter appear to be badly chosen; in few cases do they serve to illustrate the text. Moreover, the author adopts the practice of referring to reports with limited circulation. This is to be deplored in a textbook for students, since in the majority of cases a student would have great difficulty in obtaining such reports. Furthermore, it usually requires a person of some experience to abstract the relevant information or results from them. P. G. SAFFMAN.

Semiconductor Abstracts, edited by E. PASKELL. Pp. ix + 456. (New York: John Wiley; London: Chapman and Hall, 1959.)

PARIS: PUBLICATIONS SCIENTIFIQUES ET TECHNIQUES DU MINISTÈRE DE L'AIR:

Résolution par analogie électrique d'équations aux derivées partielles du quatrième ordre intervenant dans divers problèmes d'élasticité, par J. BOSCHER. Pp. xxi + 130. No. 348, 1958. 2250 *fr*.

Contribution à l'étude des ultrasons aériens: production et applications, par R. BOUCHER. Pp. xiv + 138. No. N.T. 79, 1958. 2548 *fr*.

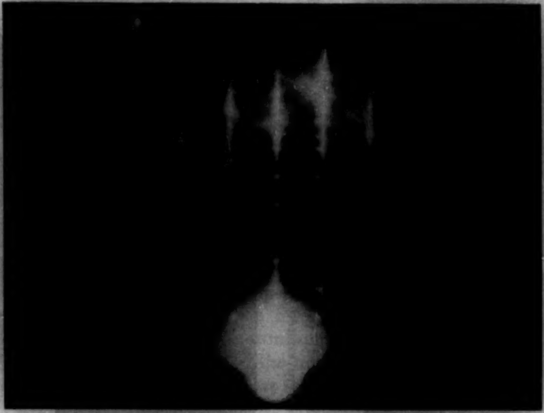

Figure 1 (*a*). Oriented layers formed on the (00.1) face of a haematite single crystal heated in air at 550°c for 1½ hrs. Beam directed along [10.0] direction.

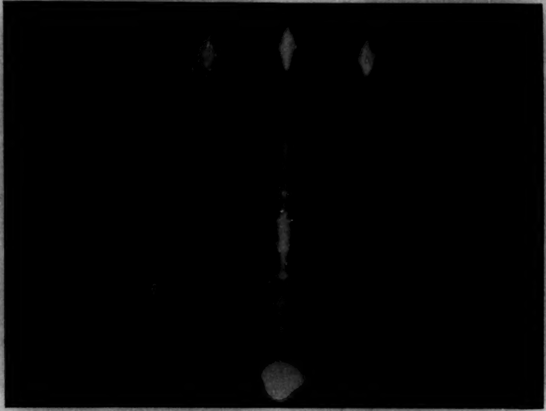

Figure 1 (*b*). Same as figure 1 (*a*) except that the beam is directed along the [1$\bar{1}$.0] direction.

(*a*) (*b*) (*c*)

Figure 2. Oscillograms showing rejuvenation by applying an a.c. field: (*a*) old sample, $E=600$ v cm^{-1}, (*b*) after 5 minutes of applying a field of $E=1600$ v cm^{-1}, (*c*) sample rejuvenated with a.c. field of $E=600$ v cm^{-1}.

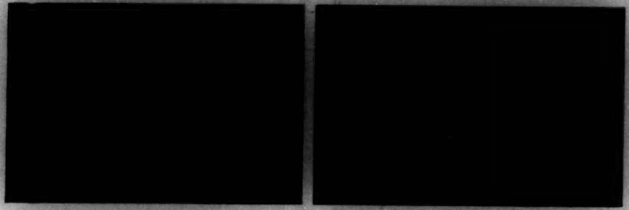

(*a*) (*b*)

Figure 3. Oscillograms showing typical loops for triglycine sulphate doped with $CuSO_4$: (*a*) old sample, (*b*) young sample (after heating to 80°c). The field intensity amounted to about 2000 v cm^{-1}.

Study of Quartz Imperfections by Light Scattering

By LUCIENNE TAUREL† AND S. P. F. HUMPHREYS-OWEN‡

† Laboratoire des Recherches Physiques, 1, Rue Victor Cousin, Paris

‡ Department of Physics, Birkbeck College, University of London

MS. received 1st *July* 1959, *in revised form* 4*th November* 1959

Abstract. Light scattered by natural crystalline quartz is studied as a function of temperature and wavelength, and of time after change of temperature. Anomalous scattered flux is found to be divisible into two distinct fractions. The first fraction is highly anisotropic and orientation-sensitive and is consistent with the existence of 'needles' lying parallel to the *c* axis. This fraction reacts at a different rate to change of temperature, depending on whether the temperature is raised or lowered. A semi-quantitative interpretation is given in terms of substituted impurity atoms which form atmospheres near edge dislocation lines lying parallel to the axis. On lowering the temperature there is a drift to the atmospheres, and on raising the temperature there is a (faster) diffusion away from them. A single diffusion coefficient of the order $10^{-20}\,\mathrm{cm}^2\,\mathrm{sec}^{-1}$ is derived for both processes. The equilibrium temperature dependence allows an estimate of the mean binding energy of an impurity atom to the dislocation line to be made which agrees with prediction from the theory of Cottrell and Bilby. The second fraction is not readily explained in terms, directly, of defects, and it is tentatively suggested that defects are indirectly responsible through perturbation of the spectrum of lattice vibrations, leading to a modification of thermal scattering.

---

§ 1. Introduction

The luminous flux scattered by a perfect crystal is caused by thermal vibrations of the lattice. The acoustical branch produces Rayleigh scattering and the optical branch Raman scattering. The intensity of Raman scattering in quartz is less than 10% of Rayleigh scattering at visible wavelengths and is almost independent of temperature below 200°c (Landsberg and Mandelstam 1928, Landsberg and Leontowitsch 1929). Raman scattering will be ignored for the purpose of this paper. The theory of Rayleigh scattering predicts an intensity which is proportional to the absolute temperature and inversely proportional to the fourth power of the wavelength (λ^{-4} law). In view of some ambiguity in the use of the term 'Rayleigh' we shall refer to this scattering as 'thermal'.

Real crystals scatter additional light because of imperfections. The presence of this 'real structure' contribution is recognized when the scattering power differs between crystals of the same kind, and is suspected when the magnitude and characteristics of the scattering power differ from the predictions of the thermal theory. Strictly the latter observations are not conclusive evidence for the existence and characteristics of a real structure contribution because the very probability of imperfections being present has so far prevented the confirmation of the thermal theory. Nevertheless it has been customary to assume that the thermal theory is sufficiently well founded for its correctness to be assumed, and that information about real structure scattering can be obtained by subtracting the theoretical thermal flux from the observed flux.

This paper describes experimental results obtained by one of us with the original intention of confirming a theory of thermal scattering in quartz (Barriol, Chapelle and Taurel 1954). It turns out that subjection of quartz to cycles of temperature between room temperature and a high upper temperature can bring it temporarily into a state in which the temperature and wavelength dependence of the scattered flux appears to be in accordance with the thermal theory. But the magnitude and certain depolarization properties are not, and moreover the magnitude is not the same for all crystals. Therefore a real structure residue remains and the theory cannot be confirmed.

Before, and long after, the cyclic treatment the scattered flux is quite at variance with the predictions of the thermal theory and another real structure contribution appears to be manifest. We have adopted the procedure of assuming the correctness of the thermal theory and of ascribing excess scattering to a real structure contribution. The available measurements have been used in a discussion of the two distinct real structures which appear in general to be present in quartz.

§ 2. NOTATION AND EXPERIMENTAL MATTERS

Experimental details have already been published (Chapelle and Taurel 1955). The source of light was a high pressure mercury vapour arc type Osram HBO.500. The lines 4358 Å, 5461 Å and 5780 Å could be isolated by interference filters. Reception was by photomultiplier and galvanometer without further amplification. The characteristics of source multiplier and glass lenses produced a detected light confined effectively within the above wavelength range with most of the intensity in the 4358 Å line. Incident and scattered beams, of small aperture of the order 1/20 radian, could be separately polarized by polaroids. The angle between incident and scattered beams was always 90°.

The received scattered flux ϕ will have in general two suffixes. The first relates to the polarization of the incident beam, the second to that of the scattered beam. A suffix will be I when the electric vector is normal to the plane of scattering (vertical polarization), and will be i when it is in the plane of scattering (horizontal polarization). The sum of the four possibilities will receive the suffix Q, thus

$$\phi_{\mathrm{Q}} = \phi_{\mathrm{II}} + \phi_{\mathrm{iI}} + \phi_{\mathrm{Ii}} + \phi_{\mathrm{ii}}.$$

When the incident beam is unpolarized, only one suffix, that relating to the scattered beam, will be shown. Then

$$\phi_{\mathrm{Q}} = \phi_{\mathrm{I}} + \phi_{\mathrm{i}}.$$

Depolarization factors ρ are defined as follows:
incident beam unpolarized:

$$\rho_{\mathrm{u}} = (\phi_{\mathrm{Ii}} + \phi_{\mathrm{ii}})/(\phi_{\mathrm{II}} + \phi_{\mathrm{iI}}),$$

incident beam vertically polarized:

$$\rho_{\mathrm{v}} = \phi_{\mathrm{II}}/\phi_{\mathrm{II}},$$

incident beam horizontally polarized:

$$\rho_{\mathrm{h}} = \phi_{\mathrm{iI}}/\phi_{\mathrm{ii}}.$$

Two orientations of crystals with respect to the beams have been used, selected so as to preserve the simple condition that directions of polarization remain parallel to the principal axes of the ellipsoid of the refractive indices. Orientation S: plane of scattering normal to *c* axis, incident beam parallel to a binary axis; orientation P: plane of scattering containing the *c* axis, incident beam parallel to the *c* axis, scattered beam parallel to a binary axis; in this orientation, in order to avoid the complications of rotatory power, only ϕ_{I} and ϕ_{i} are measured.

Five colourless crystals, A, B, C, D, E, have been studied. In A and B, from Madagascar, a few small white flakes can be seen in the beam of light. But a volume free from these could always be selected. C, D, E, from Brazil, are entirely free from visible imperfections. E was turned in the form of a right cylinder with generator parallel to the *c* axis. A, B, C, D, are rectangular blocks with one pair of faces normal to the *c* axis and one other face normal to a binary axis.

§ 3. FORMULA FOR COMPARISONS WITH THERMAL THEORY

In accordance with usual practice the flux scattered by a crystal is compared with that scattered by an identical volume of the standard liquid benzene, prepared in the same laboratory as that of Chollot and Morlot referred to below. The following values for R_{B}, the experimental Rayleigh ratio of benzene at 20°C, have been used (Chollot and Morlot 1958)

$$(47 \pm 5) \times 10^{-6} \text{ at } 4358\,\text{Å}$$

$$(14{\cdot}9 \pm 1{\cdot}5) \times 10^{-6} \text{ at } 5461\,\text{Å}$$

$$(11{\cdot}8 \pm 1{\cdot}2) \times 10^{-6} \text{ at } 5780\,\text{Å}.$$

Having regard to the similar values of Carr and Zimm (1950), and to the values derived from known molecular weights of macromolecules, the accuracy is probably higher than the above estimate of 10%, being perhaps nearer 6%.

For the orientations which have been used the ratio of the flux scattered by quartz to that scattered by benzene is theoretically

$$F_{\mathrm{Q}} = \frac{\phi_{\mathrm{Q}}}{\phi_{\mathrm{B}}} = \sum_{j,k} \frac{n_j{}^4 n_k{}^4}{(n_j+1)^2(n_k+1)^2} \frac{(n_{\mathrm{g}}+1)^4}{n_{\mathrm{g}}{}^2} \; n_{\mathrm{B}}{}^2 \; \frac{\pi^2 \boldsymbol{k} T}{2R_{\mathrm{B}}\lambda^4} \sum \frac{\beta^2{}_{k,j}}{sV^2} \quad \ldots\ldots (1)$$

n_j, n_k are indices of quartz relating respectively to the directions of polarization of incident and scattered beams. With polarization normal to the *c* axis one has n_{o} of the ordinary ray, and with polarization parallel to the *c* axis one has n_{e} of the extraordinary ray. n_{g} is the index of the glass of the cell containing benzene, n_{B} the index of benzene, λ the vacuum wavelength, $\boldsymbol{k}$ Boltzmann's constant, T the absolute temperature, $\beta_{k,j}$ a function of the photoelastic constants, s the density of quartz and V the velocity of an active acoustic wave. The second summation is over the three active acoustic waves and the terms in it are calculated for orientation S by Chapelle and Taurel (1955).

Table 1 gives the values of the indices employed in calculating from equation (1).

Table 1. Values of Indices employed in calculating from equation (1)

Wavelength (Å)	n_{o}	n_{e}	n_{g}	n_{B}
4358	1·558	1·563	1·470	1·530
5461	1·546	1·555	1·461	1·503
5780	1·544	1·553	1·460	1·500

§ 4. EXPERIMENTAL RESULTS AS FUNCTION OF TEMPERATURE

4.1. *Above Room Temperature*

Crystals were subjected to cycles of temperature between 18°C and various selected upper temperatures. Before any measurement of scattered flux was made the crystal was maintained at the particular temperature for 14 hours. In between measurements, changes of temperature were carried out at a rate of 10° per hour. Figure 1 shows a typical behaviour for orientation S. In the figure the separate points are numbered in sequence of time. For the first part of the experiment an upper temperature of 120°C was reached. Then, after two cycles, the upper temperature was raised to 200°C. The following are the salient characteristics of the behaviour: (*a*) The flux falls during initial heating stages. (*b*) During *all* cooling stages the flux is a linear function of the temperature and produces a set of *parallel* straight lines. (*c*) The distinction between the heating and the cooling stages vanishes after a sufficient number of cycles and the two stages merge into a single straight line; in the figure this state has not quite been reached with the 120°C upper temperature, but has been reached with the 200°C upper temperature. (*d*) The single straight line, when extrapolated, has in general an intercept on the ordinate axis at 0°K; the higher the upper temperature of the cycles the lower is this intercept; the crystal D had a nearly zero intercept for an upper temperature of 150°C. (*e*) The common slope of the cooling lines, which is also that of the final single line, is greater than the slope predicted by the theory for thermal scattering, in the figure the slope is 0·0033 arbitrary units, and to the same scale the theoretical slope should be 0·0017 units. (*f*) The state represented by the single straight line is not permanent: after crystals are left at room temperature for several weeks the scattered flux reverts to the values obtained before the cyclic treatment. (*g*) The speed

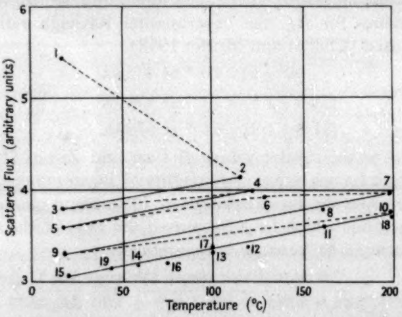

Figure 1. Scattered flux from a typical crystal during cycles of temperature above 18°C. Full lines are for decreasing temperature, broken lines for increasing temperature. The former are all parallel. After a number of cycles the cooling and warming stages coalesce. This has not quite happened with the upper temperature 120°C (points 4 to 5 and 5 to 6), but has with the upper temperature 200°C (points 10 to 19). The final single line extrapolates to an ordinate 2·3 units at 0°K. Its slope, 0·0033 units, is more than the theoretical slope, 0·0017 units on the same scale, for thermal scattering.

with which the single straight line is obtained, as indicated by the number of cycles necessary, is increased when the upper temperature is raised. (*h*)The crystal E, which had been mechanically turned into cylindrical form, was not affected by the cycles. Throughout such experiments its flux, temperature curve was a single straight line extrapolating to the 0°K origin. The slope of this line was, as with the other crystals, in excess of theory.

We interpret these results as follows. There are two distinct contributions to the scattered flux. The first contribution, F_a say, is an inverse function of temperature but with a long reaction time to raised temperature and an even longer reaction time to lowered temperature. The second contribution F_b is proportional to the absolute temperature over the range of experiment and is effectively reversible.

During an early heating stage F_a falls but does not have time to reach the equilibrium value appropriate to the upper temperature. Its fall is greater than the rise of F_b and there is a net fall of flux. During the ensuing cooling stage (and all cooling stages) the reaction of F_a is so slow that its value is effectively stationary and only the fall of F_b is seen. Thus a cooling stage is a straight line with a slope which gives the constant of proportionality of F_b, and with an intercept at 0°K which gives the temporarily stationary value of F_a.

Later heating stages bring F_a nearer to equilibrium, as illustrated by the successively lowered intercepts of the cooling lines. After a number of cycles F_a attains the equilibrium value appropriate to the upper temperature and is therefore stationary both during heating and cooling. In this state there is no longer a distinction between heating and cooling stages and they merge to a single straight line with an intercept at 0°K which is the equilibrium value of F_a for the upper temperature of the cycles, and with a slope which is the constant of proportionality of F_b.

The reaction of F_a to lowered temperature cannot be detectable during a cooling stage, for otherwise the final single line of crystal D would have shown a rise of flux during cooling and hence an intercept. This slowness of reaction to lowered temperature is also exemplified by the long time, measured in weeks, taken for recovery from the cycles.

It might be that pure thermal scattering is responsible for F_b, but in §5.2 below we produce evidence that F_b is not the same for all crystals. Also the depolarization factors are not quite consistent with thermal theory and the magnitude of F_b is in excess of theory. At one time it was thought (Chapelle and Taurel 1955) that the magnitude of F_b agreed with thermal theory. But this conclusion was based on an old value for R_B (Cabannes and Rocard 1929), namely 27×10^{-6} at 18°C for 4358 Å, which is now considered to be incorrect. Also different crystals had not been investigated at that time.

For these reasons we conclude that there is a real structure residue in F_b. F_b does not show the slowness of response to change of temperature which is shown by F_a, but the experimental procedure did not permit a conclusion that the response is effectively instantaneous. We shall distinguish the two real structures responsible for F_a and part of F_b respectively by referring to them hereafter as the *slow structure* and the *fast structure*.

The slow structure flux is investigated as a function of temperature above room temperature by the cyclic experiments. Its value at a particular temperature is the intercept of the final single line when that particular temperature has been the upper temperature of the cycles. Its value at room temperature is obtained by subtracting the room temperature value of F_b (fast structure plus thermal flux) either from the total flux at room temperature as measured before the cyclic experiment or from the total flux long after the cyclic experiment.

Furthermore, since F_b reacts relatively rapidly, it will have its room temperature value as soon as the crystal is at room temperature, and before the slow structure has attained equilibrium. Therefore, once F_b has been evaluated for room temperature, the evolution with time at room temperature of the slow structure as it recovers from a past state at a different temperature can be studied by subtracting F_b from the total flux.

In § 4.2 we report an investigation of the evolution of the slow structure at room temperature as it recovers from an immediate past history at −80°c.

4.2. *Recovery from a Low Temperature State*

The crystal D was maintained for 15 days in a cold bath of solid CO_2 suspended in acetone. It was not practicable to measure the scattered flux while the crystal was in the bath so it is not certain whether the slow structure had time to reach the −80°c equilibrium, but we assume that it was not far from equilibrium. After the 15 days the crystal was withdrawn from the bath and left at room temperature for 2 hours. Measurement of scattered flux was then started and was continued at intervals for a further 80 hours. Figure 2 shows the results. The value of the flux after the 80 hours was found to be the same as before immersion in the cold bath. This supports the conclusion that the slow structure flux is a definite function of temperature but with a long reaction time. One notes also the shorter time required to attain the state of raised temperature (−80°c to 18°c) compared with the weeks required to attain the state of lowered temperature (150°c to 18°c) during recovery from the cyclic treatment.

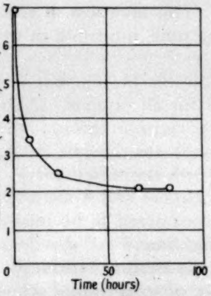

Figure 2.

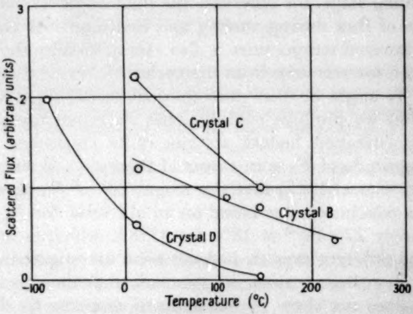

Figure 3.

Figure 2. Slow structure scattered flux at 18°c from crystal D plotted as a function of time starting from 2 hours after withdrawal from a bath at −80°c. The flux has returned to the value it had before the crystal was immersed in the bath after a lapse of time of about 80 hours.

Figure 3. Slow structure scattered flux as an equilibrium function of temperature. In all cases the flux falls with increased temperature. In crystal D it is nearly zero at 150°c.

It must be admitted that the flux will have fallen somewhat from the −80°c value during the 2 hours which elapsed before the measurements were started. Therefore the initial point in figure 2 does not correspond exactly to scattering in the −80°c state.

However, we have neglected this error and we have included this point in figure 3, which shows the equilibrium slow structure flux as a function of temperature in general. The fall with rise of temperature is seen, and it may be correct to postulate that the flux tends to zero with rise of temperature. The cylinder E, which had no slow structure flux during the cycles, also showed no enhancement of flux as a result of cooling.

It should be emphasized that figure 2 shows the evolution with time *at* room temperature, not the evolution with time as the temperature rises.

§ 5. EXPERIMENTAL RESULTS AS FUNCTION OF POLARIZATION

5.1. *The Slow Structure*

The slow structure flux was not detectable when orientation P was used. This fact will be commented on below. The depolarization factors were found not to be sensitive to change of temperature. Table 2 gives some fluxes and depolarization factors for the slow structure in orientation S at 18°c. The uncertainty in the depolarization factors is about 20%.

Table 2. Slow Structure Fluxes and Depolarization Factors in Orientation S

	F_{II}	F_{I}	F_{iI}	F_{Ii}	F_{i}	F_{ii}	ρ_u	ρ_v	ρ_h
Crystal A	1·4		0·30	0·24		0·45	0·4	0·2	0·5
Crystal B	1·2		0·57	0·40		0·70	0·6	0·3	0·8
Crystal C		3·0			1·6		0·5		
Crystal D		1·0			0·6		0·6		
Crystal E	All components nil								
Thermal theory	3·0		0·21	0·26		1·15	0·13	0·09	1·40

The depolarization factors are quite different from theory and indicate high anisotropy. Absence of flux in orientation P, meaning that scattering elements are not randomly orientated, prevents representation of the scattering by a tensor of polarizabilities, and hence inference from the depolarization factors. But this absence is consistent with the existence of 'needles' parallel to the *c* axis, for with the incident beam parallel to *c* there can be destructive interference (Van der Hulst 1957).

5.2. *The Fast Structure*

Table 3 gives some flux ratios and depolarization factors for the fast structure at 18°c in the two orientations. Depolarization factors were not sensitive to temperature change. Measurements were more difficult than for the slow structure and depolarization factors have an uncertainty of about 50%.

There is no significant effect when the orientation of the crystal is changed. This indicates that the scattering elements are randomly orientated. The fluxes are significantly different for crystal C, which makes it necessary to suppose the presence of a real structure. The structure appears to be common to all the

Table 3. Flux Ratios $\times 10^3$ and Depolarization Factors for the Fast Structure at 18°c

	Orientation S									Orientation P		
Crystal	F_{II}	F_{I}	F_{II}	F_{II}	F_{i}	F_{ii}	ρ_u	ρ_v	ρ_h	F_{I}	F_{i}	ρ_u
A & B	2·8 ±0·3		0·19 ±0·05	0·16 ±0·04		0·26 ±0·06	0·14 ±0·07	0·06 ±0·03	0·73 ±0·36			
C	1·7 ±0·2		0·11 ±0·03	0·06 ±0·01		0·17 ±0·04	0·13 ±0·06	0·04 ±0·02	0·65 ±0·32			
		1·8 ±0·2			0·23 ±0·06		0·13 ±0·06			2·0 ±0·2	0·4 ±0·1	0·2 ±0·1
D		2·8 ±0·3			0·35 ±0·09		0·13 ±0·06			$F_Q = 2{\cdot}8 \pm 0{\cdot}3$		
E		3·0 ±0·3			0·45 ±0·11		0·15 ±0·06					
Thermal theory	3·0		0·21	0·26		0·15	0·13	0·09	1·40	2·4	0·3	0·13

crystals since the depolarization factors do not differ significantly amongst the crystals. The anisotropy of the scattering is not quite the same as that in the thermal theory. The scattering is such that it can be associated with a tensor of polarizabilities with nearly equal non-diagonal elements small (about $\frac{1}{10}$) compared with the diagonal elements. This suggests that the scattering elements are nearly isotropic. Quantitatively, the anisotropy δ given by

$$\delta^2 = 5\rho_V/(3-4\rho_V)$$

for randomly orientated elements, has the fairly low value $\pm 0{\cdot}3$.

The general features are those produced by fairly small (see §6.2 below) nearly isotropic scattering centres orientated at random.

In tables 2 and 3 the theoretical values were calculated from equation (1) for a wavelength of 4358 Å. On the other hand some of the experimental values were obtained using total light. This does not affect significantly the comparison of theory with experiment. The theoretical F_{jk} changes by 20% between 4358 Å and 5780 Å. In the apparatus used its experimental value for total light is in this range and near the value for 4358 Å. We estimate a consistent error of 10%, which will not invalidate the two main conclusions, that the scattering power of crystal C is different from the others, and that the anisotropy of the fast structure flux is not quite the same as that in thermal theory.

§ 6. Experimental Results as Function of Wavelength

6.1. *The Slow Structure*

Measurements at only three wavelengths will not provide a very sensitive indication of wavelength variations but will be sufficient for a test of departure

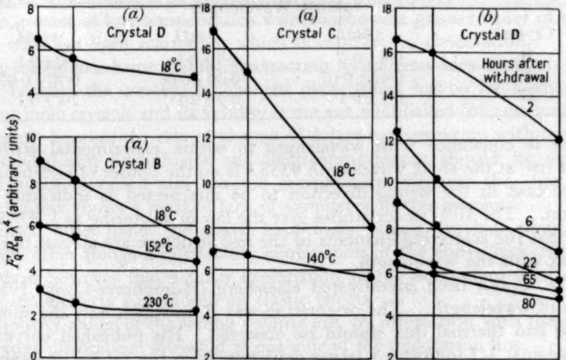

Figure 4. (*a*) The quantity $F_Q R_1 \lambda^4$ for the slow structure scattered flux plotted against wavelength at different equilibrium temperatures. The quantity would be constant if λ^{-4} law were obeyed. Rise with increasing wavelength indicates an exponent less than 4, and the presence of a dimension in the scattering elements comparable with the wavelength. Deviation from λ^{-4} law appears to be lessened at the higher temperatures.

(*b*) The same plot for crystal D during recovery from immersion in the cold bath. The conclusions are similar.

from λ^{-4} law. In equation (1), if the quartz obeys this law, the quantity $F_{jk}R_B\lambda^4$ will be a function of wavelength only to the extent that the refractive indices vary with wavelength. This effect over the wavelength range employed is smaller than our experimental error and can be neglected. Therefore if the quartz obeys the λ^{-4} law, the experimental $F_{jk}R_B\lambda^4$ should be independent of wavelength.

Measurements were made with unpolarized light because the insertion of a wavelength filter and two polaroids cut down the light too much. Figure 4 (*a*) shows the wavelength variation of $F_Q R_B\lambda^4$ for the slow structure at different equilibrium temperatures. Figure 4 (*b*) shows the wavelength variation of this quantity in the case of crystal D at 18°c as it recovered from immersion in the cold bath. It is seen that $F_Q R_B\lambda^4$ increases with increasing wavelength. This shows that the slow structure flux obeys a law $\lambda^{-(4-\epsilon)}$, where ϵ is positive. For then $F_Q R_B\lambda^4$ is proportional to λ^{ϵ}.

This kind of result indicates the presence of a linear dimension in the scattering elements which is comparable with the wavelength. It is also to be noted in figure 4 that the rise of $F_Q R_B\lambda^4$ with increasing wavelength becomes less at higher temperatures, as though the large linear dimension is reduced when the temperature is raised.

6.2. *The Fast Structure*

Table 4 shows $F_I R_B\lambda^4$ for the sum of fast structure and thermal flux tabulated against wavelength for three crystals at 18°c in orientation S.

Table 4. $F_I R_B\lambda^4 \times 10^{24}$ for the Sum of Fast Structure and Thermal Flux tabulated against Wavelength

Crystal	5780Å	5461Å	4358Å
B	$0{\cdot}8 \pm 0{\cdot}1$	$0{\cdot}9 \pm 0{\cdot}1$	$1{\cdot}0 \pm 0{\cdot}1$
C	$0{\cdot}62 \pm 0{\cdot}07$	$0{\cdot}60 \pm 0{\cdot}06$	$0{\cdot}70 \pm 0{\cdot}07$
D	$0{\cdot}9 \pm 0{\cdot}1$	$0{\cdot}9 \pm 0{\cdot}1$	$1{\cdot}1 \pm 0{\cdot}1$

There is constancy with wavelength to within experimental error. The apparent rise at the short wavelength 4358 Å is on the border of significance, but is in any case in the wrong direction to be interpreted as indicating a large dimension. The 10% uncertainties give the law of scattering as $\lambda^{-(4\pm 0{\cdot}3)}$. One can say that the scattering elements of the fast structure are at least fairly small compared with the wavelength.

Crystal C has been investigated elsewhere (Humphreys-Owen 1956) as a function of wavelength. The orientation was P, in which only the sum of fast structure and thermal flux should be observed. His published curve of flux plotted against λ^{-4} indicates a larger departure from the λ^{-4} law than shown by the present results. But in the light of more recent experience it is likely that the curve is partly erroneous. In order to avoid having to immerse the crystal in a liquid, inconvenient for work in the ultra-violet, end pieces were fixed to the crystal with the purpose of removing entrance and exit reflections of the incident beam from the scattered beam. Later experience has shown that this expedient is not entirely successful. Secondly, the interpretation of the curve, that scattering elements behaved like spheres, was based on Cabannes' old value of R_B and so is not valid.

§ 7. DISCUSSION

7.1. *The Slow Structure*

There is evidence from other experimental fields that crystalline quartz has anomalous properties in the direction of the c axis. From anelasticity Bommel, Mason and Warner (1956) suppose the existence of stationary dislocation lines lying at a small angle to the axis and made up of straight sections of length $1{\cdot}8\times10^{-3}$ cm linked by impurities or dislocation nodes. Their estimate of dislocation density is $10^3\,\mathrm{cm}^{-2}$. On the other hand Despujols (1957), from broadening of Debye–Scherrer rings, estimates $10^6\,\mathrm{cm}^{-2}$. The electrical conductivity is also anomalous, having values up to 1000 times greater in directions parallel to the axis than in directions perpendicular.

The slow structure scattered flux indicates the presence of long imperfections lying parallel to the axis. One can suppose, after Bommel *et al.*, that these are dislocation lines, in which case there are the following possibilities to explain the anomalous light scattering: (*a*) An electrostatic hypothesis, under which charged defects are attracted to oppositely charged dislocations. (*b*) An elastic hypothesis, under which impurity atoms, not necessarily charged, relieve the strain caused by their presence by migrating to dislocations and forming the so-called Cottrell atmospheres. In (*a*) and (*b*) the extra light scattering can be caused by the extra polarizability of the defect concentrations near the dislocations. There is also a third possibility: (*c*) A strain hypothesis, under which the defects do not introduce extra polarizability in themselves, but only by virtue of the distortion of the lattice.

We consider that (*c*) can be ruled out for the reason that the concentration of defects, which tends to be dissipated at high temperatures because of diffusion, will be greater at low temperatures with consequent greater relief of strain and hence with less light scattering, which is contrary to observation.

We intend to assume that the electrostatic hypothesis does not apply to quartz, partly because the concept of charged dislocations has so far been developed only for ionic crystals and its validity is not yet established for non-ionic crystals, but mainly because the rate of change of defect concentration with temperature, if controlled only by diffusion and electrostatic forces, should be symmetrical with respect to raised and lowered temperature, whereas the slow structure scattered flux shows a marked lack of symmetry in this respect.

On the other hand, the elastic hypothesis, which we shall adopt, provides amongst other things a satisfactory explanation of the above lack of symmetry. We admit however that a fuller explanation might necessitate the inclusion of electrostatic effects superposed on elastic effects.

Impurity atoms of the wrong volume are, by interaction with the stress field of an edge dislocation, attracted to one side of the dislocation line. At the same time they have a random motion at non-zero temperatures tending to disperse them. The result is an equilibrium distribution near the line which is a function of temperature. The simplest expression for this distribution is (Cottrell 1948)

$$c(r,\theta)=c_0\exp\{U(r,\theta)/\boldsymbol{k}T\} \qquad \ldots\ldots(2)$$

where c is the concentration of impurity atoms at a point (r,θ) in the plane containing the slip direction and the normal to the slip plane ($\theta=0$ in the slip plane), c_0 is the concentration far from dislocation lines, and $U(r,\theta)$ is the binding energy of the impurity atom to the line. This energy (Bilby 1950) is given by

$$U(r, \theta) = (4\mu b \epsilon a^3 \sin\theta)/r = (A \sin\theta)/r \text{ say.}$$

μ is a modulus of rigidity, b is the magnitude of the Burgers vector of the dislocation, and $\epsilon = \delta a/a$ where δa is the difference of radius between the correct atom of radius a and the impurity atom.

For a given sign of δa there is attraction to one side (positive $\sin\theta$) and repulsion from the other side (negative $\sin\theta$). To interpret the light scattering results we consider attraction only. There will be attraction to both sides if 'large' and 'small' impurity atoms are present (both signs of δa). Now impurity atoms can be in substitutional and interstitial sites. The only substitutional atom commonly found in natural quartz is Al, which substitutes for Si, and for which ϵ is $+0{\cdot}2$. On the other hand there is a choice of interstitial atoms. It will be slightly simpler to consider the substituted Al only, meaning attraction to one side of the line only. Neglect of possible interstitial migration will not affect our estimates in order of magnitude. But apart from the simplicity gained, it is not unplausible to assume that because of the rather voluminous open spaces in the quartz lattice interstitial atoms will not cause appreciable strain, and will therefore not migrate to dislocations under the Cottrell mechanism. We have support in this opinion from Klemens (1951) who also assumes that interstitial atoms in quartz cause no distortion of the lattice.

Thus, considering Al only, with $\mu = 4 \times 10^{11}\,\text{dyn cm}^{-2}$, $b = 3 \times 10^{-8}\,\text{cm}$, $a^3 = 1{\cdot}6 \times 10^{-24}\,\text{cm}^3$, one calculates $A = 1{\cdot}5 \times 10^{-20}\,\text{dyn cm}^2$. Then at $T = 293^\circ\text{K}$, equation (2) gives the distribution $c/c_0 = \exp(3{\cdot}75 \times 10^{-7} \sin\theta/r)$. A polar diagram of this distribution looks like a set of circles with a common tangent $\sin\theta = 0$. c/c_0 is less than 1·2 outside the circle of radius 10^{-6} cm approximately. If the value 1·2 is taken as a lower limit for effectiveness in light scattering, one sees that the 'needle-like' anisotropy of the scattered flux is explained. An increase of temperature by 200° does not greatly affect this conclusion.

c/c_0 begins to rise steeply with decreasing r within the circle of radius 2×10^{-7} cm. We should not follow it much below this value of r because atomic dimensions are being approached and equation (2), based on macroscopic theory, becomes invalid. In fact it is probable that in reality c/c_0 ceases to rise and tends to a limit for values of r not much less than this. We shall arbitrarily replace the distribution by a circle (cylinder in three dimensions) of radius $\bar{r} = 1 \times 10^{-7}$ cm, in which there is a uniform concentration $\bar{c} = c_0 \exp(\bar{U}/\boldsymbol{k}T)$ with a uniform binding energy $\bar{U} = A/\bar{r} = 15 \times 10^{-14}$ erg, (0·09 ev). The scattered flux will be proportional to $\bar{c} - c_0$, and, introducing a factor of proportionality F_0,

$$F = F_0[\exp(\bar{U}/\boldsymbol{k}T) - 1]. \qquad \ldots\ldots(3)$$

Equation (3) represents the scattered flux as an equilibrium function of temperature and it may be compared with figure 3. We plotted the ordinates of figure 3 against $\exp(\bar{U}/\boldsymbol{k}T) - 1$, with different trial values of $\bar{U}$. The plots were quite sensitive to $\bar{U}$, and only for the value $\bar{U} = 8 \times 10^{-14}$ erg, (0·05 ev) could straight lines through the origin be fitted to the points. The high temperature (150°c) point of crystal D was an exception. Even with adjustment of the slightly suspect point corresponding to -80°c no value of $\bar{U}$ produced agreement with equation (3). If the high temperature point is accepted as bad, and not explained, the curves of figure 3 become consistent with equation (3). The slopes of the straight lines gave the F_0's as $(F_0)_B = 0{\cdot}22$, $(F_0)_C = 0{\cdot}34$, $(F_0)_D = 0{\cdot}10$. All the points in figure 3 are contained in figure 5, which is a plot of F/F_0, where F is an ordinate in figure 3, against $\exp(8 \times 10^{-14}/\boldsymbol{k}T) - 1$, using the above values of F_0.

Apart from the one unexplained bad point the agreement with the theory is quite good considering the simplifications made.

Two complications in particular have been ignored. From § 6.1 and figure 4 there is apparently a shortening of the atmospheres with rise of temperature, indicating that a two-dimensional treatment is insufficient. Secondly, the cylinder E may have, as a result of the mechanical treatment, an exceptional number of dislocations. There is no slow structure flux from this crystal, and we suggest that there are so many dislocations that, with a given density of impurity atoms, there are not enough of them to bring up the concentration per atmosphere to detectable level.

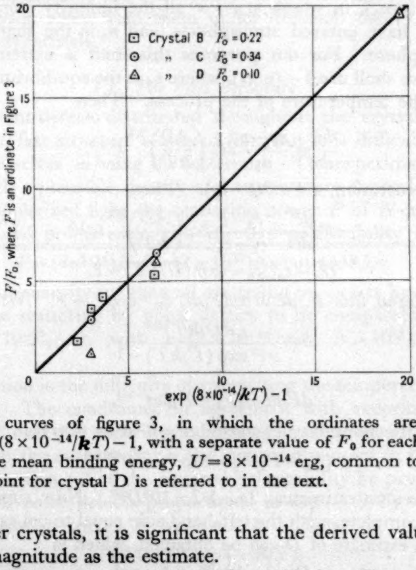

Figure 5. The curves of figure 3, in which the ordinates are F, are fitted to $F/F_0 = \exp(8 \times 10^{-14}/\boldsymbol{k}T) - 1$, with a separate value of F_0 for each crystal, but with a value of the mean binding energy, $U = 8 \times 10^{-14}$ erg, common to the three crystals. The bad point for crystal D is referred to in the text.

For the other crystals, it is significant that the derived value of $\bar{U}$ is of the same order of magnitude as the estimate.

The non-equilibrium processes are of two kinds. First there is the drift towards atmospheres resulting from a lowering of temperature. Secondly there is the diffusion away from atmospheres resulting from a rise of temperature. For the first process we do not have detailed results but only the observations that it takes about a month for the atmospheres to return to the room temperature state after having been in a high temperature state, and that the process is too slow to be detected during the period of a cooling stage in figure 1. For the second process we have figure 2, and also the observation, from the cyclic experiments, that it is more rapid than the first process.

Some guidance to the first process can be obtained from the theory of strain ageing. In this theory there are initially no atmospheres, but, when the crystal is overstrained, impurity atoms migrate towards free dislocations and anchor them by forming atmospheres. Under our hypothesis we regard the dislocations as initially present and anchored, and assume that an initial state of zero excess concentration in atmospheres can exist as a result of a past history at high temperature. The law of flow into the atmospheres will be the same in both situations.

Let n be the excess number of impurity atoms per unit length of atmosphere, n being assumed uniform in cylinders of radius $\bar{r}$ and zero outside. According to Cottrell and Bilby (1949) the rate of rise of n is

$$dn/dt = 2c_0(AD/\boldsymbol{k}T)^{2/3}t^{-1/3},$$

where D is the diffusion coefficient. The equation ignores the fact that n must tend to a limit as $t \to \infty$.

Harper (1951) introduced a limit by multiplying the right-hand side of the equation by $1-(n/n_0)$, in which at $t \to \infty$ all the impurity atoms in the crystal are supposed to have entered atmospheres, and n_0 is the share taken by unit length of atmosphere. For our purposes this limit is extreme. In place of Harper's factor we shall use $1-(n/n_2)$, where n_2 is the equilibrium value to which n is tending at the temperature of the process. Then

$$\frac{dn}{dt} = \frac{n_2-n}{n_2} 2c_0 \left(\frac{AD}{\boldsymbol{k}T}\right)^{2/3} t^{-1/3}.$$

In terms of concentration, $n = \pi\bar{r}^2(\bar{c}-c_0)$. Then

$$\pi\bar{r}^2 \frac{d\bar{c}}{dt} = \frac{\bar{c}_2-\bar{c}}{\bar{c}_2-c_0} 2c_0 \left(\frac{AD}{\boldsymbol{k}T}\right)^{2/3} t^{-1/3}$$

where $$(\bar{c}_2-c_0)/c_0 = \exp(\bar{U}/\boldsymbol{k}T)-1.$$

In terms of scattered flux F, $d\bar{c}/dt \propto dF/dt$, $\bar{c}_2-\bar{c} \propto F_2-F$. Write

$$\sigma = \frac{(AD/\boldsymbol{k}T)^{2/3}}{\pi\bar{r}^2 \exp(\bar{U}/\boldsymbol{k}T)-1}.$$

Then

$$dF/dt = (F_2-F)2\sigma t^{-1/3}.$$

Integration with the boundary condition $F=0$ at $t=0$ gives

$$(F_2-F)/F_2 = \exp(-3\sigma t^{2/3}),$$

where, using previous estimates, $3\sigma = 1{\cdot}2 \times 10^8 D^{2/3}$. Now supposing that the process is nearly complete, with the left-hand side equal to 0·8 say, in one month ($2{\cdot}6 \times 10^6$ sec), an estimate of D can be obtained, which is

$$D = 3 \times 10^{-20}\,\mathrm{cm^2\,sec^{-1}}.$$

The other process, diffusion away from atmospheres, is not physically the reverse. It is ordinary diffusion down concentration gradients, whereas the drift in the theory of Cottrell and Bilby is akin to hydrodynamic flow. But the controlling coefficient of diffusion should be the same. The diffusion away from atmospheres is opposed by the low intensity field with potential U. This makes the problem too difficult to be worth a rigorous attack in the present context. Instead, the field will be neglected and a textbook solution with pure cylindrical symmetry will be used.

At time $t=0$ let the concentration, c_1, be uniform in a long cylinder of radius $\bar{r}$ and zero elsewhere. When at later times the matter diffuses away into infinite space, $c(r,t)$ is known and Crank (1956) gives curves of $c(r)/c_1$ plotted against $r/\bar{r}$ for $(Dt/\bar{r}^2)^{1/2}=\frac{1}{4}, \frac{1}{2}, 1$. We put $\bar{r}=10^{-7}$ cm and make $c(r=\bar{r})/c_1$ correspond to the difference between an ordinate and the final ordinate in figure 2, divided by the initial ordinate. The fall with time of $c(r=\bar{r})/c_1$ in Crank's curve superposes quite well on the experimental curve with $D=10^{-19}\,\mathrm{cm^2\,sec^{-1}}$.
When $(Dt/\bar{r}^2)^{1/2}=0{\cdot}25,\ 0{\cdot}5,\ 1{\cdot}0$, and $\bar{r}=10^{-7}$ cm,
$Dt\times 10^{16}=6{\cdot}25,\ 25,\ 100$. Hence with $D=10^{-19}\,\mathrm{cm^2\,sec^{-1}}$
$t\times 10^4=0{\cdot}62,\ 2{\cdot}5,\ 10$. At these times, from Crank,
$c/c_1=0{\cdot}34,\ 0{\cdot}22,\ 0{\cdot}06$. But from figure 2 at the same times
$c/c_1=0{\cdot}45,\ 0{\cdot}15,\ 0{\cdot}06$.

The agreement in order of magnitude between the diffusion coefficients as estimated in the two processes does indicate that our experimental results are consistent with flow towards the atmospheres under the theory of Cottrell and Harper, and diffusion away from them under diffusion theory, in agreement with our general hypothesis.

7.2. *The Fast Structure*

Presumably point defects distributed throughout the crystal are somehow responsible for the fast structure scattered flux, but it is difficult to regard the point defects themselves as being the scatterers. The experimental results are not consistent with a plausible density and temperature dependence. For 90° scattering and unpolarized light the scattering power P of N per unit volume randomly distributed points each with effective polarizability α is

$$P=(8\pi^2/\lambda^4)N\alpha^2=(2\times 10^{20})N\alpha^2 \text{ at } 4358\,\text{Å}.$$

The corresponding quantity for thermal scattering by quartz has the magnitude 2×10^{-7}. For the scattering by point defects to be comparable with thermal scattering $N\alpha^2>10^{-27}$, or, with $\alpha=3\times 10^{-24}\,\mathrm{cm^3}$, $N>10^{21}\,\mathrm{cm^{-3}}$. This is excessive.

Another objection is the difficulty of reconciling the temperature dependence with experiment. The conditions for agreement with experiment (scattering proportional to T over the experimental range) are that the curvature of $P(T)$ should be low over the range and that the tangent at a point in the range should pass through the origin. Let the squared polarizability be proportional to T^n, and the density of point defects proportional to $\exp(-B/T)$ where B will be related to an activation energy H by $B=H/\boldsymbol{k}$. Then

$$P(T)\propto T^n \exp(-B/T).$$

The condition for the tangent at $T=T_1$ to pass through the origin is

$$B=T_1(1-n).$$

B is essentially positive, therefore only values of n negative, zero, or unity are to be considered. One might say that the density of defects is scarcely a function of temperature over the experimental range, and put $B=0$. Then $n=1$, and $P\propto T$. But one cannot imagine polarizability increasing with temperature. On the other hand one might make the polarizability constant with $n=0$, $B=T_1$. Choosing $T_1=400$°K say, in the middle of our range, this means that

H has to be $5{\cdot}5\times10^{-14}$ erg (0·035 ev) which is surely unacceptably low for the creation of a point defect. A reasonable value for H, say 0·9 ev, requires the absurd $n=-24$. Also the requirement that $P(T)$ should have small curvature is disobeyed with high negative values of n.

These considerations make it unlikely that the point defects are the direct cause of the fast structure scattered flux. But it is conceivable that they are the indirect cause through their perturbation of the spectrum of lattice vibrations. This would amount to a modification of thermal scattering and the proportionality with T would be retained. But the suggestion is tentative because it may be difficult to show that the modification could be comparable with the original scattering by fluctuations in the perfect lattice.

ACKNOWLEDGMENT

We are grateful to Dr. R. Fürth who has read the manuscript and made helpful comments and suggestions.

REFERENCES

BARRIOL, J., CHAPELLE, J., and TAUREL, L., 1954, *J. Chim. Phys.*, **51**, 334.
BILBY, B. A., 1950, *Proc. Phys. Soc.* A, **63**, 191.
BOMMEL, H. E., MASON, W. P., and WARNER, A. W., 1956, *Phys. Rev.*, **102**, 64.
CABANNES, J., and ROCARD, Y., 1929, *La diffusion moléculaire de la lumière* (Paris: Les Presses Universitaires).
CARR, C. I., and ZIMM, B. H., 1950, *J. Chem. Phys.*, **18**, 1616.
CHAPELLE, J., and TAUREL, L., 1955, *J. Chim. Phys.*, **52**, 307.
CHOLLOT, B., and MORLOT, G., 1958, *J. Chim. Phys.*, **55**, 515.
COTTRELL, A. H., 1948, *Report on the Strength of Solids* (London: Physical Society), 30.
COTTRELL, A. H., and BILBY, B. A., 1949, *Proc. Phys. Soc.* A, **62**, 49.
CRANK, J., 1956, *The mathematics of diffusion* (Oxford: Clarendon Press), 29.
DESPUJOLS, J., 1957, *Bull. Soc. Franc. Minér.*, **80**, 450.
HARPER, S., 1951, *Phys. Rev.*, **83**, 709.
HUMPHREYS-OWEN, S. P. F., 1956, *Proc. Phys. Soc.* B, **69**, 350.
KLEMENS, P. G., 1951, *Proc. Roy. Soc.* A, **208**, 108.
LANDSBERG, G., and LEONTOWITSCH, M., 1929, *Z. Phys.*, **53**, 439.
LANDSBERG, G., and MANDELSTAM, L., 1928, *Z. Phys.*, **50**, 769.
VAN DER HULST, H. C., 1957, *Light Scattering by Small Particles* (New York: John Wiley & Sons), 317.

The Theory of Light Scattering and X-ray Low Angle Scattering by Semi-stiff Chain Molecules

By A. R. STOKES
Wheatstone Physics Laboratory, King's College, London

Communicated by C. Domb; *MS. received* 23*rd October* 1959, *in final form* 11*th December* 1959

Abstract. Numerical values of the normalized intensity of scattering by semi-stiff chain molecules are calculated. The method depends on the calculation of the inverse Laplace transform of an expression first obtained by Daniels, which is also derived in this paper by an alternative method. The values obtained from this calculation are compared with those given by Peterlin's formula. The normalized intensity is also calculated for a polydisperse system of chains of constant stiffness parameter.

§ 1. Introduction

The problem of finding theoretically the angular distribution of light or x-rays scattered by semi-stiff chain molecules in suspension is one which has not been completely solved. For a Gaussian chain, in which there is complete freedom of both rotation and bending between any two links, the problem is comparatively simple; but when stiffness is introduced between links it becomes difficult and has only been solved, in an incomplete manner, by Kratky and Porod (1949), Hermans and Ullman (1952), Benoit and Doty (1953), and Peterlin (1953 a, b).

It is apparently impossible to obtain any closed mathematical expression for the distribution of scattered light in this case. One can only obtain functions which are approximations to the required function. The procedure here adopted is to use one of these approximate functions to compile tables of the scattering function, and, by comparison with another function that is known to be a better approximation to estimate the limits of error of the tabulated function.

Experimental studies of the scattering of light and x-rays by chain molecules have been made by a number of workers, including Kratky and Porod (1949) (polyvinyl bromide) and Hermans (1959) (desoxyribose nucleic acid). Peterlin (1953 a, b) also quotes measurements on thymonucleic acids.

Definitions and assumptions.

By a *semi-stiff* chain we mean a chain consisting of many identical links, such that, if the angle between the nth link and the $(n+1)$th link is ϕ_n, (i) every ϕ_n has the same probability distribution; (ii) every ϕ_n is statistically independent of every other $\phi_{n'}$; (iii) there is complete freedom of rotation about the long axis of each link, i.e. the plane containing the $(n-1)$th and the nth links is equally likely to make any angle with the plane containing the nth and the $(n+1)$th links.

A special case is a chain in which every link makes a fixed angle with the next link; the statistical distribution of ϕ_n then only allows of one fixed value.

We shall assume in addition that the length of a link is much smaller than the wavelength of light; or much smaller than $\lambda/\vartheta_{\max}$ in the case of X-ray scattering up to angles $\vartheta_{\max}$: so that the structure of individual links does not enter into the problem. We also assume that there is a negligible probability of any part of the chain colliding with any other part.

The degree of stiffness is defined by a parameter a called the *stiffness parameter* (or *persistence length*). If ψ is the angle between the directions of two links that are separated by n joints, it follows from the statistical independence of the ϕ's and the free rotation about the axis of any link that

$$\overline{\cos\psi} = (\overline{\cos\phi})^n$$

where the bar denotes an average value. If s is the length of chain making up these n links, and b is the length of a link, then $s = nb$, and if we define a so that $\overline{\cos\phi} = \exp(-b/a)$, it follows that

$$\overline{\cos\psi} = \exp(-s/a) \qquad \ldots\ldots(1)$$

and the stiffness parameter is therefore equal to the length of chain which has $\overline{\cos\psi} = 1/\mathrm{e}$. For a short section of chain, for which $s \ll a$, equation (1) becomes

$$\tfrac{1}{2}\overline{\psi^2} = s/a. \qquad \ldots\ldots(1\,a)$$

This definition is equivalent to that used by Kratky and Porod (1949) and others.

§ 2. The Distribution Function of Link-to-link Distances

The scattering function is related to the distribution function of link-to-link distances for a given length of chain. The normalized intensity of scattering is given by

$$I(\vartheta)/I(0) = \tfrac{1}{2}(1+\cos^2\theta)P(\omega)$$

where

$$P(\omega) = \frac{1}{t^2}\int_0^t\int_0^t \frac{\sin\omega r_{12}}{\omega r_{12}}\,ds_1\,ds_2 \qquad \ldots\ldots(2)$$

(see, for instance, Guinier and Fournet 1955) in which r_{12} is the distance between any two elements of the chain of lengths ds_1 and ds_2 and t is the total chain length; r_{12} is statistically distributed in some way to be determined, and $\omega = (4\pi/\lambda)\sin(\vartheta/2)$; ϑ is the angle of scattering and λ is the wavelength in the liquid in which the chain molecules are suspended.

Let $D(s;\,r)4\pi r^2\delta r$ be the probability that r_{12} lies between r and $r+\delta r$ when ds_1 and ds_2 are separated by a length s of chain; this probability function is independent of the behaviour of the rest of the chain. Then

$$P(\omega) = \frac{1}{t^2}\int_{-t}^{t}\int_0^\infty |t-s|\,D(s;\,r)\,\frac{\sin\omega r}{\omega r}\,4\pi r^2\,dr\,ds. \qquad \ldots\ldots(3)$$

If $F_0(s;\,\omega)$ is the three-dimensional Fourier transform of $D(s;\,r)$, then

$$P(\omega) = \frac{2}{t^2}\int_0^t (t-s)F_0(s;\,\omega)\,ds. \qquad \ldots\ldots(4)$$

It is only for a Gaussian chain that we can obtain the function $D(s;\,r)$ in a simple form; it is then a Gaussian error function of r (cf. Debye 1947). It is possible to determine the moments of the distribution for a semi-stiff chain; thus

$$\overline{r^2}=2a^2\{\exp(-s/a)-1+s/a\} \qquad \ldots\ldots(5)$$

and $\bar{r}_4$ and higher moments can be obtained (Porod 1953), but the expressions for these rapidly become very complicated.

The Laplace transform of the function F_0 has been obtained explicitly by Daniels (1952), but an alternative derivation is given here in the belief that it is simpler and that the method may have other applications.

We consider a length s of chain with one end held at the origin O with its tangent vertical, and let $D(s;\,r,\theta)\,dv$ be the probability that the other end will lie inside a volume dv around a point whose polar coordinates with respect to O are (r,θ,ϕ); this probability is symmetrical about the axis of the coordinates and is therefore independent of ϕ. Let $F(s;\,\omega,\theta)$ be the three-dimensional Fourier transform of D, expressed in terms of polar coordinates (ω,θ,ϕ), and let

$$F(s;\,\omega,\theta)=\sum_{n=0}^{\infty}F_n(s;\,\omega)\mathrm{P}_n(\cos\theta) \qquad \ldots\ldots(6)$$

where $\mathrm{P}_n(\cos\theta)$ is the nth Legendre polynomial.

We now add a short element of length δs to the length of the chain at the origin end, and consider the effect on the density distribution $D(s;\,r,\theta)$; namely (i) to shift it upwards through a distance δs, and (ii) to 'smear' it, by oscillating it around the vertical axis through small angles whose mean square value is $2\delta s/a$ as in equation (1*a*). The corresponding effects on the function $\mathrm{P}_0(s;\,\omega,\theta)$ are (*a*) to multiply it by $\exp(i\omega\cos\theta\delta s)$, and (*b*) to 'smear' it as described above. The effect of this smearing on a single spherical harmonic function $\mathrm{P}_n(\cos\theta)$ is to multiply it by a constant factor $(1-\frac{1}{4}n(n+1)\overline{\psi^2})$, provided that $\overline{\psi^4}$ and higher moments are negligibly small. We have, therefore, to the first order in δs,

$$\sum_n F_n(s+\delta s;\,\omega)\mathrm{P}_n(\cos\theta)=\sum_n F_n(s;\,\omega)\mathrm{P}_n(\cos\theta)\{1+i\omega\cos\theta\delta s-\tfrac{1}{2}n(n+1)\delta s/a\}.$$

If we subtract $\sum_n F_n\mathrm{P}_n$ from each side and equate the coefficients of $\mathrm{P}_n(\cos\theta)$, we obtain

$$\frac{d}{ds}F_n(s;\,\omega)=i\omega\left(\frac{n+1}{2n+3}F_{n+1}+\frac{n}{2n-1}F_{n-1}\right)-\frac{1}{2a}n(n+1)F_n. \qquad \ldots\ldots(7)$$

If we denote by $B_n(p;\,\omega)$ the Laplace transform

$$\int_0^{\infty}F_n\exp(-ps)\,ds$$

of $F_n(s;\,\omega)$, then equation (7) becomes

$$pB_n-F_n(0;\,\omega)=i\omega\left(\frac{n+1}{2n+3}B_{n+1}+\frac{n}{2n-1}B_{n-1}\right)-\frac{1}{2a}n(n+1)B_n. \qquad \ldots\ldots(8)$$

Now $\sum_n F_n(0;\,\omega)\mathrm{P}_n(\cos\theta)$ is the Fourier transform of the distribution function for a zero-length chain and is therefore equal to 1 everywhere; hence

$$F_0(0;\,\omega)=1;\quad F_n(0;\,\omega)=0 \quad \text{for} \quad n\geqslant 1,$$

and equation (8) becomes

$$-1+pB_0=\tfrac{1}{3}i\omega B_1$$

$$pB_n=i\omega\left(\frac{n+1}{2n+3}B_{n+1}+\frac{n}{2n-1}B_{n-1}\right)-\frac{1}{2a}n(n+1)B_n, \qquad \ldots\ldots(9)$$

and hence

$$B_0=\frac{1}{p-\frac{1}{3}i\omega(B_1/B_0)}$$

$$i\omega\frac{B_0}{B_1}=p+\frac{1}{a}-\frac{2}{5}i\omega\frac{B_2}{B_1}$$

$$\frac{2}{3}i\omega\frac{B_1}{B_2}=p+\frac{3}{a}-\frac{3}{7}i\omega\frac{B_3}{B_2} \quad \text{etc.},$$

which, on elimination of the ratios B_{n+1}/B_n, gives B_0 in the form of a continued fraction†

$$B_0=\frac{1}{p+}\,\frac{(1/3)\omega^2}{p+1/a+}\,\frac{(2/3)(2/5)\omega^2}{p+3/a+}\,\frac{(3/5)(3/7)\omega^2}{p+6/a+}\cdots \qquad \ldots\ldots(10)$$

§ 3. DERIVATION OF THE LIGHT-SCATTERING FUNCTION FROM THE DISTRIBUTION FUNCTION

Since $F_0(s;\,\omega)$ is the average of $F(s;\,\omega,\theta)$ over all directions, and $D(s;\,r)$ is the average of $D(s;\,r,\theta)$, it follows that $F_0(s;\,\omega)$ is the Fourier transform of $D(s;\,r)$, as already defined for the purposes of equation (4). In order to evaluate $P(\omega)$ we must therefore apply an inverse Laplace transformation to B_0 so as to obtain F_0, and then substitute in equation (4). Equivalently, we can obtain $F(\omega)$ by finding the inverse Laplace transform of $p^{-2}B_0$, and multiplying by $2/t^2$.

We shall therefore consider practical methods of obtaining the inverse Laplace transform of B_0. We shall put $a=1$, for convenience, since our unit of length is arbitrary: this is equivalent to putting p for pa, ω for ωa, and B_0 for B_0/a.

§ 4. METHODS OF OBTAINING THE INVERSE LAPLACE TRANSFORM OF B_0

(*a*) *Series expansion in powers of* p^{-1}.

We expand B_0 as a power series in p^{-1}, and take the inverse Laplace transform term by term. Thus

$$B_0=\frac{1}{p}-\frac{1}{3}\omega^2\frac{1}{p^3}+\frac{1}{3}\omega^2\frac{1}{p^4}+\left(\frac{1}{5}\omega^4-\frac{1}{3}\omega^2\right)\frac{1}{p^5}-\frac{2\omega^4}{3p^6}+\ldots \qquad \ldots\ldots(11a)$$

$$F_0=1-\frac{1}{6}\omega^2s^2+\frac{1}{18}\omega^2s^3+\left(\frac{1}{5}\omega^4-\frac{1}{3}\omega^2\right)\frac{1}{24}s^4-\frac{1}{180}\omega^4s^5+\ldots$$

and ......(11*b*)

$$P(\omega)=1-\frac{1}{36}\omega^2t^2+\frac{1}{180}\omega^2t^3+\left(\frac{1}{5}\omega^4-\frac{1}{3}\omega^2\right)\frac{t^4}{360}-\frac{\omega^4t^5}{3780}+\ldots. \qquad \ldots\ldots(11c)$$

---

† This is the same as Daniels' equation (1952, p. 305), if allowance is made for slight differences of notation and for the fact that Daniels uses the 'p-multiplied' Laplace transform.

Clearly this is only of practical use when t and ω are small enough to give a rapidly converging series.

(*b*) *Expansion in powers of* ω^{-1} *and functions of* ω/p.

Equation (11*a*) suggests an expansion, which can be obtained rigorously from equation (9):

$$B_0 = \frac{1}{\omega}\tan^{-1}\frac{\omega}{p} + \frac{1}{3\omega^2}\frac{\omega^4}{(\omega^2+p^2)^2} + \ldots \qquad \ldots\ldots(12a)$$

which gives

$$F_0 = \frac{\sin \omega t}{\omega t} + \frac{\sin \omega t - \omega t \cos \omega t}{6}\frac{1}{\omega} + \ldots \qquad \ldots\ldots(12b)$$

from which $P(\omega)$ may be obtained.The first term leads to the scattering formula for straight rods. This expansion can only be of use if ω is large and ωt is not large.

(*c*) *Approximate function-fitting method.*

The inverse Laplace transform of $1/(p+p_1)$ is $\exp(-p_1 t)$, therefore if we can express B_0 sufficiently accurately as a sum of functions of this sort, e.g.

$$B_0 \simeq \frac{A_1}{p+p_1} + \frac{A_2}{p+p_2} + \frac{A_3}{p+p_3}, \qquad \ldots\ldots(13)$$

we can then find the corresponding functions F_0 and $P(\omega)$.

The difficulty here is to know what constitutes 'sufficient' accuracy, since there is no simple method of assessing the maximum error in an inverse Laplace transform from the errors in the given function B_0. We therefore express B_0 in terms of a series of the type (13) with only two terms, and then as a series with three terms, and compare the resulting numerical values of $P(\omega)$. Since the three-term approximation must be better than the two-term aproximation (since it has two more disposable parameters) we may safely assume that the errors in the two-term approximation are only of the same order as the differences between the two approximations.

In the two-term approximation there are four disposable parameters; A_1, A_2, p_1, p_2. These are made to satisfy the following four conditions:

(i) and (ii): The coefficients of p^{-1} and p^{-2} must be 1 and 0 respectively, as in equation (11*a*); hence

$$A_1 + A_2 = 1; \quad A_1 p_1 + A_2 p_2 = 0$$

or

$$A_1 = p_2/(p_2 - p_1); \quad A_2 = -p_1/(p_2 - p_1). \qquad \ldots\ldots(14a)$$

(iii) and (iv): The approximate expression must tend to the right value and have the right slope as $p \to 0$, i.e.

(iii) $$B_0(0) = \frac{1}{p_1} + \frac{1}{p_2}. \qquad \ldots\ldots(14b)$$

(iv) $$-B_0'(0) = \frac{1}{p_1^2} + \frac{1}{p_1 p_2} + \frac{1}{p_2^2}. \qquad \ldots\ldots(14c)$$

$B_0(0)$ and $B_0'(0)$ were obtained numerically from (10) for each of a series of values of ω, and p_1 and p_2 were calculated. Since the sum, $p_1 + p_2$, and the product, $p_1 p_2$, are nearly linear functions of w^2, these are tabulated in table 1.

Knowing p_1 and p_2 for given values of ω^2 we can calculate

$$F_0(s;\,\omega)=\frac{p_2}{p_2-p_1}\exp(-p_1 s)-\frac{p_1}{p_2-p_1}\exp(-p_2 s) \qquad \ldots\ldots(15)$$

and

$$P(\omega)=\frac{2}{(p_2-p_1)t^2}\left[\frac{p_2}{p_1^2}\{p_1 t-1+\exp(-p_1 t)\}-\frac{p_1}{p_2^2}\{p_2 t-1+\exp(-p_2 t)\}\right]. \qquad \ldots\ldots(16)$$

Table 1. Sum and Product of p_1 and p_2

ω^2	p_1+p_2	$p_1 p_2$
1	1·120	0·3432
2	1·242	0·7057
3	1·365	1·0871
4	1·491	1·4870
5	1·618	1·9048
6	1·746	2·3400
7	1·875	2·7921
8	2·005	3·2604
9	2·136	3·7443
10	2·268	4·2431

Table 2. $P^{-1}(\omega)$ for Chains of Uniform Length, (with $a=1$), calculated from equation (17)

$\omega^2 \rightarrow$ t	1	2	3	4	5	6	7	8	9	10
0·0	1·000	1·000	1·000	1·000	1·000	1·000	1·000	1·000	1·000	1·000
0·5	1·006	1·014	1·018	1·029	1·034	1·043	1·050	1·058	1·065	1·075
1·0	1·024	1·048	1·073	1·100	1·121	1·155	1·182	1·210	1·239	1·269
1·5	1·049	1·100	1·153	1·209	1·265	1·325	1·384	1·445	1·506	1·568
2·0	1·079	1·168	1·256	1·351	1·447	1·548	1·648	1·751	1·853	1·955
3	1·161	1·335	1·522	1·718	1·918	2·123	2·319	2·513	2·700	2·879
4	1·256	1·543	1·848	2·169	2·482	2·785	3·075	3·344	3·596	3·833
5	1·362	1·779	2·217	2·660	3·079	3·472	3·830	4·162	4·475	4·767
6	1·479	2·037	2·611	3·165	3·674	4·141	4·572	4·975	5·350	5·701
7	1·605	2·304	3·012	3·663	4·262	4·810	5·316	5·787	6·226	6·637
8	1·733	2·577	3·401	4·163	4·850	5·454	6·061	6·600	7·103	7·572
9	1·869	2·857	3·804	4·661	5·438	6·121	6·805	7·413	7·979	8·507
10	2·008	3·145	4·201	5·159	6·027	6·820	7·549	8·226	8·856	9·443

For values of ω^2 greater than about 0·9 the roots p_1 and p_2 are complex, so it is convenient to denote them by

$$p_1=p_0\exp(i\epsilon);\quad p_2=p_0\exp(-i\epsilon),$$

and substitution in equation (16) then gives

$$P(\omega)=\frac{2}{p_0^2 t^2\sin\epsilon}\left[\exp(-p_0 t\cos\epsilon)\sin(p_0 t\sin\epsilon+3\epsilon)-\sin 3\epsilon+p_0 t\sin 2\epsilon\right]. \qquad \ldots\ldots(17)$$

The reciprocal of the light-scattering function, as calculated from these formulae, is given in table 2. The reciprocal is used because its dependence upon ω^2 is much more nearly linear than that of $P(\omega)$, and it is therefore convenient for comparison with experimental results, and for interpolation.

In order to assess the effects of error in this approximation, the three-term approximation to B_0 was also obtained, by a similar procedure, and the corresponding light-scattering functions calculated for $\omega^2=10$. The two-term and three-term approximations are compared in table 3 and it is seen that the differences between them are too small to be of consequence in almost any comparisons with measurements of light scattering. We may therefore assume that the two-term approximation is sufficiently good for values of ω^2 up to 10. But if ω^2 is increased to larger values it would eventually become necessary to use three or more terms in the approximation, and the calculations would become correspondingly more tedious.

Table 3. Comparison of Results of Two-term and Three-term Approximations

t	$P(\sqrt{10})$, 2-term	$P(\sqrt{10})$, 3-term	Difference
0·5	0·930	0·939	0·009
1·0	0·788	0·804	0·016
1·5	0·637	0·650	0·013
2·0	0·512	0·517	0·005
3	0·347	0·347	0·000
4	0·261	0·260	−0·001
5	0·210	0·210	0·000

Asymptotic form of $P(\omega)$ for large values of t

When t is large enough for the exponential terms in equations (16) or (17) to be neglected, the expression for $P(\omega)$ reduces to

$$P(\omega)\sim 2B_0(0)t^{-1}+2B_0'(0)t^{-2}. \qquad \ldots\ldots(18)$$

Moreover, the same asymptotic expression is obtained whatever number of terms are used in the approximation (13).

Table 4. Difference between P_P (Peterlin) and P_S (Stokes)

t	P_P-P_S $\omega^2=3$	P_P-P_S $\omega^2=6$	P_P-P_S $\omega^2=9$
1	0·006	0·014	0·024
2	0·020	0·042	0·068
3	0·040	0·074	0·088
4	0·052	0·093	0·088
5	0·065	0·084	0·080
6	0·070	0·078	0·074

Comparison with Peterlin's formula

Peterlin (1953a, b) assumed that the function $D(s;r)$† could be replaced, to a good approximation, by a three-dimensional Gaussian distribution having the same value of the second moment, as given by equation (5). It is then possible to integrate equation (3) with respect to r, and to integrate the result with respect to s so as to give an infinite series whose sum, under favourable conditions, converges rapidly. Hermans and Hermans (1958) have suggested a variant on this method.

It is clear that this assumption will lead to erroneous results when the chains are very short and stiff, but it is very difficult to make an estimate of the error to be expected. The difference between values of $P(\omega)$ obtained from equation (17) and values obtained from Peterlin's formula are given in table 4.

---

† Peterlin's assumption was in fact that the function $F_0(s;\ \omega)$ was nearly Gaussian, but this implies the above assumption.

§ 5. Scattering by Polydisperse Systems

A particle-size distribution which is sometimes taken as a basis for comparison with experimental results is that in which the fraction of particles having masses lying in the range m to $m+\delta m$ is given by $\alpha \exp(-\alpha m)\delta m$, where α is constant. In the case of chain molecules this means that the fraction having their lengths between t and $t+\delta t$ is $\alpha \exp(-\alpha t)\delta t$, where the average length is $1/\alpha$.

Since the intensity of scattering from one particle is proportional to t^2 times the normalized intensity I/I_0 for that particle, it follows that the intensity for a polydisperse system is given by

$$\bar{P}(\omega)=\frac{\displaystyle\int_0^\infty t^2P(t\,;\,\omega)\alpha\exp(-\alpha t)\,dt}{\displaystyle\int_0^\infty t^2\alpha\exp(-\alpha t)dt}=\tfrac{1}{2}\alpha^3\int_0^\infty t^2P(t\,;\,\omega)\exp(-\alpha t)\,dt. \qquad \ldots\ldots(19)$$

But from equation (4) we have

$$\int_0^\infty t^2P(t\,;\,\omega)\exp(-pt)\,dt=2\int_0^\infty\int_0^t(t-s)F_0(s\,;\,\omega)\exp(-pt)\,ds\,dt$$
$$=\frac{2}{p^2}B_0(p\,;\,w)$$

hence

$$\bar{P}(\omega)=\alpha B_0(\alpha\,;\,w). \qquad \ldots\ldots(20)$$

Thus $\bar{P}$ is much simpler to calculate than P. The function is given, in terms of the average length $1/\alpha$, in table 5.

Table 5. $[\bar{P}(\omega)]^{-1}$ for Polydisperse Chains (see text) ($a=1$) obtained from equation (20)

$\omega^2\rightarrow$ $1/\alpha$	1	2	3	4	5	6	7	8	9	10
0·5	1·055	1·109	1·162	1·213	1·263	1·312	1·360	1·407	1·453	1·497
1·0	1·162	1·315	1·459	1·597	1·728	1·852	1·971	2·085	2·194	2·298
1·5	1·288	1·555	1·802	2·034	2·251	2·455	2·648	2·830	3·004	3·169
2·0	1·424	1·811	2·165	2·494	2·800	3·084	3·351	3·603	3·840	4·066
2·5	1·564	2·075	2·539	2·966	3·360	3·726	4·068	4·388	4·690	4·976
3·0	1·709	2·344	2·920	3·446	3·929	4·376	4·793	5·182	5·548	5·893
3·5	1·855	2·617	3·304	3·930	4·503	5·031	5·522	5·980	6·410	6·815
4·0	2·000	2·892	3·692	4·417	5·080	5·690	6·255	6·782	7·276	7·740
4·5	2·151	3·169	4·081	4·906	5·659	6·350	6·990	7·586	8·143	8·667
5·0	2·300	3·448	4·472	5·397	6·239	7·013	7·727	8·392	9·013	9·596

From this result it is a simple matter to derive the light-scattering functions for certain other distributions: an example is that one for which the fraction of chains with lengths lying between t and $t+\delta t$ is

$$\frac{\alpha\beta}{\beta-\alpha}[\exp(-\alpha t)-\exp(-\beta t)]\delta t$$

where α and β are constants. A special case of this is obtained if we let $\alpha\rightarrow\beta$, to give a distribution having the function $\alpha^2t\exp(-\alpha t)$, for which

$$\bar{P}(\omega)=\alpha^2\left[-\frac{d}{d\alpha}B_0(\alpha\,;\,\omega)\right]. \qquad \ldots\ldots(21)$$

This is a simple case of a distribution function with a maximum; the maximum lies at $t=1/\alpha$ and the mean length is $2/\alpha$.

REFERENCES

Benoit, H., and **Doty, P.**, 1953, *J. Phys. Chem.*, **57**, 958.

Daniels, H. E., 1952, *Proc. Roy. Soc. Edinburgh*, **63**, 290.

Debye, P., 1947, *J. Phys. Chem.*, **51**, 18.

Guinier, A., and **Fournet, G.**, 1955, *Small-angle Scattering of X-rays* (New York: Wiley; London: Chapman and Hall).

Hermans, J., 1959, *J. Phys. Chem.*, **63**, 175.

Hermans, J., and **Hermans, J. J.**, 1958, *J. Phys. Chem.*, **62**, 1543.

Hermans, J., and **Ullman, R.**, 1952, *Physica*, **18**, 951.

Kratky, O., and **Porod, G.**, 1949, *Proc. International Colloq. on Macromolecules* (Amsterdam: D. B. Centen), p. 251–266.

Peterlin, A., 1953 a, *J. Polym. Sci.*, **10**, 425.

—— 1953 b, *Nature, Lond.*, **171**, 259.

Porod, G., 1953, *J. Polym. Sci.*, **10**, 157.

The Cross Section of ^{20}Ne(p, γ) ^{21}Na

By G. C. THOMAS and N. W. TANNER
Clarendon Laboratory, Oxford

MS. received 3rd November 1959, *in final form* 23rd *November* 1959

Abstract. The integrated cross section of the 1170 kev resonance of ^{20}Ne(p, γ)^{21}Na has been measured by counting the ^{21}Na positron activity following the proton bombardment of a neon gas target. Assuming $\Gamma_p \gg \Gamma_\gamma$ we find $\omega\Gamma_\gamma = 1{\cdot}13 \pm 0{\cdot}07$ ev for the resonance. Using this result as a calibration for previous work on the non-resonance capture process in ^{20}Ne(p, γ)^{21}Na we obtain a value for the cross section parameter S (used for describing nuclear reactions in stars) of 40 kev barns.

§ 1. Introduction

A previous investigation (Tanner 1959) of the reaction ^{20}Ne(p, γ)^{21}Na produced evidence for the existence of a non-resonant process which was described as direct radiative capture. This process is particularly interesting in ^{20}Ne(p, γ)^{21}Na as it is believed to provide the major contribution to the cross section at the thermal energies effective in stars ($E_p \sim 25$ kev for this reaction). ^{20}Ne(p, γ)^{21}Na is important as a source of ^{21}Ne which can undergo the reaction ^{21}Ne(α, n)^{24}Mg thereby providing neutrons for heavy element synthesis (Burbridge *et al.* 1957).

The absolute cross section for direct radiative capture (Tanner 1959) was based on the cross section obtained by Broström *et al.* (1947) for the 1170 kev resonance of ^{20}Ne(p, γ)^{21}Na using absorbed gas targets. However, because of the nature of these targets, the resonance cross section was uncertain by, perhaps, a factor of two. It was clear that a simple gas target measurement could provide a more accurate value for the resonance cross section.

§ 2. Experimental Method

The reaction was observed by detecting the ^{21}Na positron activity remaining after proton bombardment of a neon gas target. Spectroscopically pure neon of natural isotopic abundance was used as the target gas.

Figure 1 shows the target assembly. The proton beam entered the chamber through a nickel foil 0·00004 in. thick (150 kev for 1 Mev protons), which had been soldered to the end of a tube of 0·16 in. internal diameter. The beam had been reduced to 0·10 in. diameter by a stop. It was possible to replace the gas chamber and foil by a quartz plate, and so visually check that the apparatus was aligned and the beam would go through the foil.

The beam current, about 1 μA, was measured on a 'leaky integrator', viz. a 0·5 μF T.C.C. 'plastapack' condenser shunted by a resistance so that the half-life of the combination was equal to the 22·8 second half-life of ^{21}Na. This automatically compensated for the decay of the ^{21}Na during bombardment, the delay before counting and fluctuations in beam current. The voltage on the condenser was measured with a valve voltmeter of high impedance.

The positrons from ^{21}Na stopped in the walls of the gas chamber and were there annihilated. The two 0·511 Mev annihilation quanta were detected by two 4 in. × 4 in. NaI crystals mounted on opposite sides of the target and about 1½ in. from the centre of the target. The counters were biased just below the 0·511 photopeak, and used in coincidence.

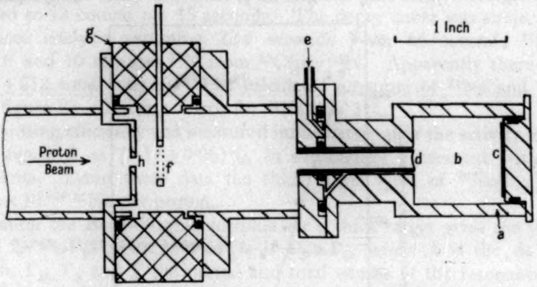

Figure 1. Gas target assembly in cross section. a, Cylindrical brass gas chamber; b, gas volume; c, tantalum disc; d, nickel foil 0·00004 in. thick; e, gas inlet; f, guard ring; g, Perspex insulator; h, beam defining stop.

The counting efficiency was measured with a ^{22}Na source of about 1 μc deposited on a 0·001 in. thick Al foil of about 0·25 in. diameter. This foil was supported by a wire frame at the centre of an identical gas chamber which could be substituted for the original. The 1·28 MEV photons coincident with the ^{22}Na positrons were detected in a 2 in. NaI crystal, and the efficiency of counting positrons given by the ratio of the triple coincidence counting rate to the singles counting rate in the 2 in. crystal, due allowance being made for the 11% electron capture. The counting geometry for the ^{22}Na activity (approximately a point source) was not identical with the geometry for the distributed ^{21}Na activity. (The activity was distributed over the walls of the gas chamber rather than through the volume of the gas. This was shown by pumping out the gas immediately after bombardment with a loss of only 20% of the ^{21}Na activity.) However, in both cases the positrons must be annihilated in the walls of the chamber as this was the only available material sufficiently thick to stop the positrons. Another possible source of error lies in the different ranges of the ^{21}Na positrons (end point 2·50 MEV) and ^{22}Na positrons (end point 0·54 MEV). In fact, the error was less than 1% mainly because the counters were much larger than the target chamber.

The ^{21}Na activity measurements were made by bombarding the target for 30 seconds and, after a delay of 5 seconds, counting the positron activity in 15 second intervals for several minutes. As the count was started, the resistor of the 'leaky integrator' was disconnected leaving the condenser with a memory of the *effective* proton bombardment. Figure 2 shows the sum of two decay curves obtained from such bombardments.

As the 1170 kev resonance of ^{20}Ne(p, γ)^{21}Na is known to be quite narrow compared with the target thicknesses used in the present experiment (Tanner 1959) the resonance curve should be flat topped with a maximum independent of target thickness, i.e. gas pressure. However, straggling and multiple scattering in the nickel foil and in the gas spread the energy and the path length in the gas. The result of such processes is demonstrated in figure 3 which shows excitation curves for various target gas pressures. The curves for pressures of 28 and 41 cm Hg both have flat tops and agree in maximum yield, indicating that for quite a range of bombarding energies all protons that enter the gas pass through the resonance energy while in the gas. The widths of the curves in figure 3 are about 10% smaller than the widths calculated from the stopping power of neon (Whaling 1959). This seems quite good agreement in view of the apparent straggling and scattering.

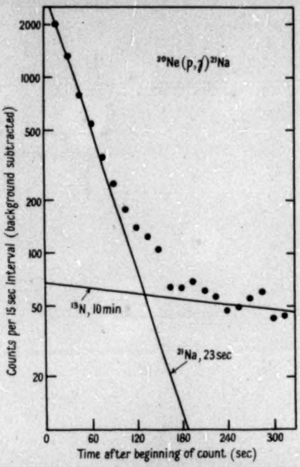

Figure 2. The sum of two decay curves of the positron activity following the bombardment with 1·37 MeV protons of neon gas at a pressure of 41 cm Hg. The 23 second and 10 minute lines were fitted by a least squares analysis.

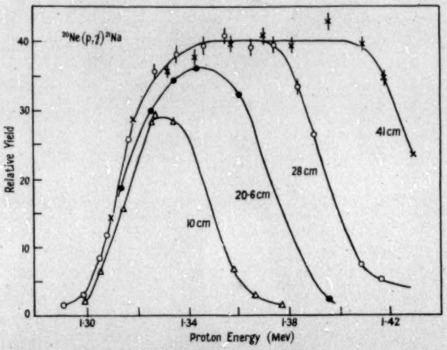

Figure 3. Excitation curve of ^{20}Ne(p, γ)^{21}Na using a neon gas target at various pressures. The pressures, in cm Hg, are indicated on the curves.

§ 3. RESULTS

Figure 2 contains the data used in calculating the cross section. The decay curve is the sum of two runs taken with a gas pressure of 41 cm Hg and proton bombarding energy of 1·37 MEV. Room background has been subtracted; it amounted to 18 counts per 15 seconds. The decay curve was subjected to a least squares analysis assuming 22·8 seconds ^{21}Na, 66 seconds ^{17}F from ^{16}O(p, γ)^{17}F and 10 minutes ^{13}N from ^{12}C(p, γ)^{13}N. Apparently there was no ^{17}F (-34 ± 212 total counts). The calculated amounts of ^{21}Na and ^{13}N are shown in figure 2; the r.m.s. error for ^{21}Na was 3%.

The counting efficiency was measured immediately after the activity measurements of figure 2 as $(2{\cdot}17 \pm 0{\cdot}06)\%$, in satisfactory agreement with earlier measurements. From these data the thick target yield of ^{20}Ne(p, γ)^{21}Na is $(6{\cdot}5 \pm 0{\cdot}3) \times 10^{-10}$ ^{21}Na per proton.

Integrating the Breit–Wigner formula for a thick target gives the yield per proton as $2\pi^2\lambda\!\!\!^{-2}\omega\Gamma_p\Gamma_\gamma/\Gamma\epsilon \simeq 2\pi^2\lambda\!\!\!^{-2}\omega\Gamma_\gamma/\epsilon$ if $\Gamma_p \gg \Gamma_\gamma$, where $\lambda\!\!\!^{-}$ is the de Broglie wavelength, Γ_p, Γ_γ and Γ the partial and total widths of the resonance, ω the statistical factor and ϵ the stopping power. Using $\epsilon = (5{\cdot}55 \pm 0{\cdot}2) \times 10^{-18}$ kev cm^2 (Whaling 1959) we find $\omega\Gamma_\gamma = 1{\cdot}13 \pm 0{\cdot}07$ ev; Broström *et al.* (1947) found $\omega\Gamma_\gamma \sim 2$ ev. Using the new value for $\omega\Gamma_\gamma$ the cross section for direct radiative capture becomes $0{\cdot}74 \pm 0{\cdot}15$ μbn at a bombarding energy of 1050 kev.

Some measurements were also made at a bombarding energy of 1·13 MEV and a gas pressure of 52 cm Hg. The proton energy inside the foil was then about 1 MEV. The ^{21}Na activity, which was comparable with the ^{13}N background, amounted to $(1{\cdot}25 \pm 0{\cdot}4) \times 10^{-11}$ ^{21}Na per proton. The cross section was obtained from this yield by assuming an energy dependence

$$\sigma = SE^{-1} \exp\left(-2\pi Z_1 Z_2 e^2/\hbar v\right)$$

where E is the centre of mass energy, v the relative velocity, Z_1 and Z_2 the charge numbers of the proton and target nucleus and S is a constant (the cross section parameter). For $E = 1$ MEV, $\sigma = 1{\cdot}0 \pm 0{\cdot}3$ μbn which agrees with the measurement quoted above of $0{\cdot}74 \pm 0{\cdot}15$ μbn. The weighted mean of these two measurements is $0{\cdot}80 \pm 0{\cdot}13$ μbn, which gives $S = 10{\cdot}4 \pm 1{\cdot}7$ kev barns. This is in rather better agreement with the value calculated by R. F. Christy and I. M. Duck (quoted by Tanner 1959) of $S = 4{\cdot}9$ kev barns.

Using the experimental value of $S = 10{\cdot}4$ kev barns at 1050 kev and the energy dependence of S given by Christy and Duck, then at thermal energies effective in stars ($E_p \sim 25$ kev), $S = 40$ kev barns.

ACKNOWLEDGMENTS

We are grateful to Dr. K. W. Allen, Atomic Weapons Research Establishment, Aldermaston, for the use of the 3 MEV Van de Graaff generator, and to Mr. D. Akers and the operating staff for their assistance.

REFERENCES

BROSTRÖM, K. J., HUUS T., and KOCH, J., 1947, *Nature, Lond.*, **160**, 498.

BURBRIDGE, E. M., BURBRIDGE, G. R., FOWLER, W. A., and HOYLE, F., 1957, *Rev. Mod. Phys.*, **29**, 547.

TANNER, N. W., 1959, *Phys. Rev.*, **114**, 1060.

WHALING, W., 1959, *Hand. d. Phys.*, vol. XXXIV (Berlin: Springer).

Proton Elastic Scattering Polarization as a Test of the Low Energy Optical Model

By A. STRZAŁKOWSKI, M. S. BOKHARI, M. A. AL-JEBOORI
AND B. HIRD
Nuclear Physics Research Laboratory, University of Liverpool

Communicated by H. W. B. Skinner; *MS. received* 29*th July* 1959,
in final form 5*th November* 1959

Abstract. The polarization produced in the elastic scattering of protons from carbon has been measured at several scattering angles using a bombarding energy of 9·4 MeV. This was compared with an optical model calculation of Bjorklund and Fernbach. At 40° scattering angle, the energy dependence of the polarization was measured. It was found to vary smoothly with energy down to 7·5 MeV. The polarization from proton scattering by copper at 35°, 45° and 55°, at an average scattering energy of 6·8 MeV was also measured.

§ 1. Introduction

The elastic scattering of protons by nuclei in the medium energy region has been analysed with considerable success by representing the nucleus as a potential well (Glassgold, Cheston, Stein, Schuldt and Erickson 1957, Gibson, Prouse and Rotblat 1958, Melkanoff, Nodvik, Saxon and Woods 1957). The maxima and minima of the diffraction pattern, which result from this shape scattering, are well reproduced in the experimental differential cross section results. The success of these theoretical fits is rather surprising in the case of light nuclei in the medium energy region, since compound elastic scattering can then be important, and the levels through which this type of scattering proceeds are not dense enough to give a good statistical average with the energy resolution usually used in the measurements. Indications of compound elastic scattering have been found in differential cross sections which, though still retaining the general shapes associated with optical model predictions, show rapid fluctuations with energy. (Gibson, Prowse and Rotblat 1958, Greenlees, Kuo and Petravić 1958.)

Measurement of the polarization of the scattered protons provides independent data for comparison with the optical model predictions. It is expected that this polarization will be particularly sensitive to the presence of compound elastic scattering, so that it may be possible to determine the contribution which this makes to the elastic scattering.

The optical model in its low energy formulation is a theoretical description of energy averaged results, where all the rapid variations over the different compound levels have been smoothed out. For this energy averaging to give the equivalent of potential scattering by a suitable optical potential, it is necessary to assume that there is no interference between the different types of scattering which are, in fact, present. Thus the assumption must be made that the interference terms between shape elastic scattering and the compound elastic scattering, and also between the different compound levels, do not occur. The first type of interference is usually eliminated by assuming that all compound states, excited in the scattering process, have lifetimes which are long compared to the passage of the shape scattered wave. The compound elastic wave and the shape scattered wave are therefore separated in time and hence are incoherent (Friedman and Weisskopf 1955); this requires the widths of the levels to be small compared with the energy resolution of the measurements. The second type of interference comes from the overlap of different energy levels, and is eliminated by making the assumption that the level widths are much smaller than the level spacing. If this is not true, the interference may still be eliminated by the statistical assumption that, when an average over many levels is taken, these terms cancel each other out. When these assumptions have been made, the scattering is reduced to the sum of the potential scattering and the compound elastic scattering separately. Moreover without interference between levels, the compound elastic part cannot produce polarization and the effect of its presence is merely to dilute the polarization from the potential part of the scattering. At high energies of course none of these matter since compound elastic scattering makes a negligible contribution to the elastic scattering cross section.

There exists an energy range for proton scattering by light nuclei which is high enough for some, or all, of the above assumption to be unjustified, but low enough for compound elastic scattering still to be significant. The polarization, itself an interference effect, may then be very different from that which is predicted by the spin–orbit part of the optical potential even when broad energy resolution is used.

In a previous paper (Al-Jeboori *et al.* 1959) measurements of the polarization produced by proton elastic scattering from oxygen at an energy of 8·7 Mev were described. Evidence for rapid energy variation of the polarization was obtained when a change in the beam energy spread was made. In spite of this, the general shape of the polarization angular distribution was consistent with optical model scattering. At higher energies where the compound elastic scattering should be less important, Brockman (1958) found little variation in the polarization of protons scattered from carbon over the energy range 15·9 Mev to 18·1 Mev.

This paper describes further measurements of the polarization of protons scattered from carbon. Since both the angular and energy variations are of interest, measurements were made at a single scattering angle, 40°, over a range of proton energies from 8·7 Mev to 7·45 Mev, and also at several scattering angles for a fixed incident energy of 9·4 Mev. A few measurements were also made using a copper target. For this nucleus the compound elastic scattering should be negligible so that the optical model predictions are expected.

§ 2. EXPERIMENTAL DETAILS

The polarization was deduced from measurements of the left–right scattering asymmetry when protons of known polarization were scattered from the target. Two counter telescopes, each consisting of a proportional counter and a CsI scintillator, measured simultaneously the left-scattering and right-scattering events. The whole scattering and counting system was placed in an inverted position during half the running time, by rotating it through an angle of 180°

about the incident proton direction. It was possible to deduce the true scattering asymmetry, independent of the counter efficiencies and many of the geometrical errors, by using in the calculation the product of the two left–right counting ratios as measured in the two positions.

The polarized proton beam, used in these measurements, was produced by the deuteron stripping reaction. A graphite target was subjected to bombardment by the circulating beam of the 37 in. cyclotron. The cyclotron fringe field and a wedge magnet focused the protons, corresponding to the ground-state group of the stripping reaction, on to the second target placed four metres from the cyclotron, where the scattering asymmetry was measured. The experimental arrangement was similar to that used for the oxygen scattering measurements previously described (Al-Jeboori *et al.* 1959).

Nuclear emulsion, exposed directly to the proton beam, was used to find its energy spectrum. The polarization of the proton beam was determined by filling the scattering chamber with helium and measuring the scattering asymmetry in the usual way. It was necessary to repeat both these calibrations whenever the internal target was changed, since slightly different focusing conditions were needed for each target. Fortunately they lasted long enough for us to be able to complete each group of measurements without making a target change.

Considerable deuteron contamination was present in the proton beam. Since all the focusing was with magnetic fields, deuterons of half the proton beam energy follow the same trajectories, and it was possible for deuterons scattered inelastically by the internal target to reach the second target. Fortunately the Q-values for deuteron stripping in carbon were low enough for any protons, produced by this reaction in the second target, to be rejected by the energy selection of the counter telescopes. In the measurements with copper, even though the stripping cross section is comparatively small, it was decided to eliminate the deuterons completely from the beam by passing it through 32 mg cm^{-2} of aluminium.

The self-supporting carbon targets were made by abrading pieces of pile graphite down to a thickness of 25 mg cm^{-2} for the angular distribution measurements, and to a thickness of 12·5 mg cm^{-2} for the measurement of the energy variation of the polarization. The copper target consisted of a foil rolled to a thickness of 21·2 mg cm^{-2}.

A typical pulse height spectrum from one of the counter telescopes is shown in figure 1. This was obtained at a scattering angle of 40° using the 12·5 mg cm^{-2} graphite target. The width of the elastic scattering peak is consistent with this target thickness and the energy spread in the beam. The background count from neutrons and γ-rays was determined by running without the target. It was in all cases confined to the lowest channels so that, except at the lowest energies used, it was clear of the elastic scattering peak. No detectable difference in the position or width of the peak was found for the two positions of each counter telescope.

A possible source of error which is not eliminated by inverting the counting system and target chamber comes from the uncertainty in the direction of the incident protons. This uncertainty was mainly due to the convergence of the proton beam from the wedge magnet. If the mean direction of the beam did not coincide with the axis of rotation of the counting system, a false asymmetry would be produced. This source of error is most serious at angles where the differential cross section varies rapidly. The angular spread in the beam striking the target was 0·7°, and this corresponds to a possible systematic error of 4% in the carbon polarizations at the 40° scattering angle; at larger angles where the differential cross section changes more slowly the error is smaller. Another systematic error which does not cancel out when the system is inverted may be produced by non-uniformity of the beam over the area of the target. The widest beams used were in the carbon angular distribution measurements. Before these were made, the spatial distribution of the beam at the position of the target was determined and found to be uniform enough for this type of error to be negligible.

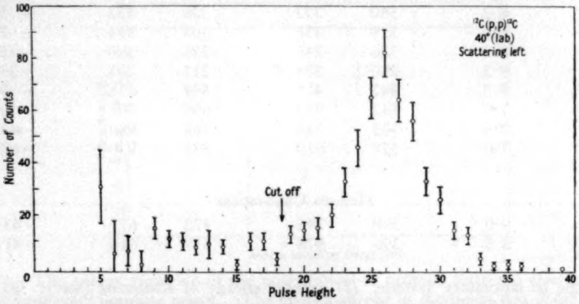

Figure 1. A pulse height distribution from one of the counter telescopes, showing the protons scattered to the left at 40° from a proton beam of energy 8·5 ± 0·3 Mev by a graphite target 12·5 mg cm^{-2} thick.

§ 3. Results

The angular and energy variations of the carbon scattering polarization are shown in table 1, and graphically in figures 2 and 3.

The copper scattering polarization results are shown in table 2.

The angular distribution part of the carbon measurements was made using a proton beam energy of $9{\cdot}4^{+0\cdot3}_{-1\cdot0}$ Mev and polarization −43 ± 7%. Allowing for the variations in thickness of the 25 mg cm^{-2} target, the mean energy at which the scattering occurred was calculated to be about 8·2 Mev. The internal target in the cyclotron had to be changed for the 40° energy variation measurements, and at the optimum focusing condition the beam energy then became 8·7 ± 0·5 Mev, with a polarization −41 ± 8%. In this part of the measurements the target was 12·5 mg cm^{-2} thick, which had the effect of reducing the average scattering energy by about 0·4 Mev. The energy variations were produced by inserting appropriate thicknesses of aluminium foils in the beam just before it entered the scattering chamber. In the case of the copper scattering measurements, another change in the internal graphite target and the 32 mg cm^{-2} of aluminium which was inserted in the beam, produced a proton beam whose average energy of scattering in the 21·2 mg cm^{-2} target was 6·8 Mev.

In view of the smallness of the asymmetries found in the copper measurements, it did not seem worth while to make a separate helium calibration, and, in calculating the results, the polarization of the proton beam was taken as −43 ± 7%.

Table 1

(1)	(2)	(3) L	(3) R	(4) L	(4) R	(5)
		Carbon Scattering				
34° ± 2°	8·2	1268	965	963	1437	− 7·4 ± 3·7
40° ± 2°	8·2	663	678	511	700	−19·6 ± 5·6
50° ± 2°	8·2	561	447	491	509	+11·1 ± 5·6
60° ± 2°	8·2	411	309	456	306	+39·5 ± 9·0
70° ± 2°	8·2	359	118	200	116	+91·4 ± 16·7
80° ± 2°	8·2	524	214	360	268	+67·4 ± 12·5
90° ± 2°	8·2	363	174	338	369	+37·4 ± 9·0
100° ± 2°	8·2	743	304	396	660	+22·2 ± 6·5
110° ± 2°	8·2	580	322	326	533	+ 5·6 ± 5·9
120° ± 2°	8·2	529	358	308	514	− 7·1 ± 6·6
130° ± 2°	8·2	326	245	236	390	−12·6 ± 7·6
140° ± 2°	8·2	250	334	211	293	−35·7 ± 10·5
40° ± 2°	8·3	487	471	594	616	− 0·2 ± 5·4
40° ± 2°	7·9	542	652	606	705	−20·5 ± 6·4
40° ± 2°	7·5	503	740	568	880	−49·3 ± 10·1
40° ± 2°	7·0	377	613	535	930	−62·1 ± 13·0
		Helium Calibration				
40° ± 5°	9·0	598	744	472	677	−43·0 ± 7·0
40° ± 5°	8·5	396	578	515	616	−41·0 ± 8·0

(1) Angle in laboratory system; (2) average energy of scattering (Mev); (3) number of counts left and right with frame upright; (4) number of counts left and right with frame inverted; (5) polarization (%), in the case of the helium measurements this refers to the incoming protons assuming that the analysing power of the helium scattering is −33·5%.

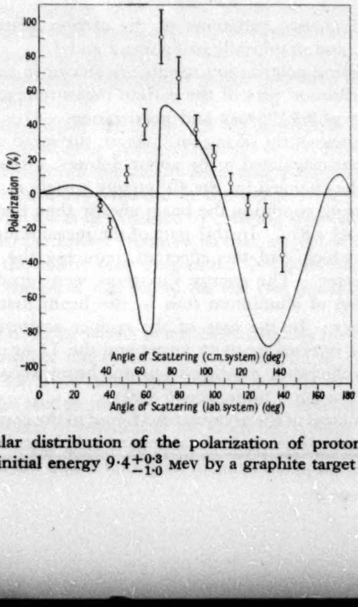

Figure 2. The angular distribution of the polarization of protons scattered elastically from a beam of initial energy $9\cdot4^{+0\cdot3}_{-1\cdot0}$ Mev by a graphite target 25 mg cm^{-2} thick.

The errors shown in the results represent the combined statistical error of each measurement and its corresponding helium calibration run, but they exclude the effects of any error in the assumed analysing power of the helium scattering. This analysing power was calculated from phase shifts which originally had been obtained by analysing differential cross section measurements. It was difficult to ascribe meaningful errors to the results of such a calculation, and it seemed better to exclude them altogether from the quoted errors and to give explicitly the value of the analysing power which was used for calculating the beam polarization from the calibrated runs, so that if more accurate phase shifts became available the present results may be adjusted.

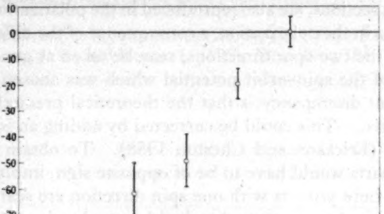

Figure 3. The energy variation of the polarization of protons scattered elastically from a 12·5 mg cm^{-2} graphite target. The energy spread in the beam was ±0·5 MeV.

Table 2. The Polarization in Proton Scattering by Copper at an Average Energy of 6·8 MeV

Angle (laboratory) (deg)	35	45	55
Polarization (%)	$-2{\cdot}5 \pm 4{\cdot}8$	$-3{\cdot}8 \pm 5{\cdot}0$	$-5{\cdot}0 \pm 6{\cdot}1$

Putnam, Brolley and Rosen (1956) give phase shifts up to and including the D waves for helium scattering at 9·48 MeV. Those predict an analysing power of −33·5% for 40° scattering, the angle used in the calibrations. In view of the expected slow change with energy at this scattering angle, Brockman (1958), this value was used for both the 9·4 MeV and the 8·7 MeV proton beams.

The apparent inconsistency of the 40° carbon scattering result as obtained in the angular variation and in the energy variation measurements, is probably due to the greater target thickness and considerable low energy tail in the proton beam which were involved in the angular variation measurements. In comparing the two results the effective energy of the latter should therefore be reduced perhaps to a value below that of the energy variation measurements, so that the negative polarization obtained seems reasonable.

To illustrate the polarization predicted by the optical model part of the scattering we have included a polarization calculation by Bjorklund and Fernbach (private communication). The optical model they use has a Saxon type central real potential, a surface Gaussian central imaginary potential, and a Thomas type real spin–orbit potential. The magnitudes of the parameters used in this calculation, which was made for a proton energy of 10 MeV, were $r_0 = 1{\cdot}25 \times 10^{-13}$ cm, $a = 0{\cdot}65 \times 10^{-13}$ cm, $b = 1{\cdot}2 \times 10^{-13}$ cm, $V_{CR} = 45{\cdot}6$ MeV, $V_{CI} = 11{\cdot}0$ MeV, and $V_{SR} = 9{\cdot}36$ MeV.

§ 4. DISCUSSION

The smallness of the polarization obtained in the copper measurements suggests that there is too much Coulomb scattering at this energy to give much information about the other scattering processes.

In the carbon elastic scattering, there is a general similarity between the angular variation of the polarization as measured experimentally, and as calculated from the optical model. The diffraction effects, which are a strong feature in the differential cross sections, are also reproduced in the polarization. The magnitude of the oscillations in the polarization, a consequence of the difference in the diffraction patterns of the two spin directions, may be taken as general confirmation of the magnitude of the spin–orbit potential which was chosen for the calculation. The most evident discrepancy is that the theoretical prediction is almost everywhere too negative. This could be corrected by adding an imaginary part to the spin–orbit term (Erickson and Cheston 1958). To obtain agreement the real and imaginary parts would have to be of opposite sign, implying that, in regions of the nucleus where protons with one spin direction are scattered most, protons with this same spin direction are absorbed least. In view of the limited validity of the optical model in this energy region, such detailed fitting of the optical model parameters may be unprofitable.

The smooth energy variation in the polarization, shown in figure 3, seems at first sight, to be a characteristic of the optical model, rather than of a compound nucleus process, which would in general produce a random variation with energy. However the particular distribution and widths of the ^{13}N energy levels involved may account for the results.

The level structure of ^{13}N at this excitation has not been measured, but the mirror nucleus ^{13}C is known to have a single broad level of width 1·1 MeV at an excitation of 8·4 MeV; other neighbouring levels being all much narrower (McGruer, Warburton and Bender 1955). This broad level also shows the largest cross section for the reaction ^{12}C(d, p)^{13}C so it is likely to have a large single particle width. If this level is also present in ^{13}N, it should be strongly excited in proton scattering. All the other neighbouring levels should be narrow enough to fulfil the assumptions required by the optical model, and they should contribute little or nothing to the polarization. The compound elastic contribution to the polarization may then be reasonably attributed entirely to this one broad level. In ^{12}C(p, p)^{12}C it should correspond to a bombarding energy of about 6·5 MeV. Our results may then just represent the consequence of the smooth variation of the phase and magnitude of the compound elastic amplitude on the high energy side of this resonance. It is also of course, possible that the optical model part of the polarization makes a significant contribution to the observed energy variation.

ACKNOWLEDGMENTS

The authors wish to thank Professor Cheston and Professor Fernbach for communicating unpublished work. One of us (A.S.) thanks the Polish Academy of Sciences for a grant. M.A.A. wishes to acknowledge the receipt of a scholarship from the Iraq Government.

REFERENCES

AL-JEBOORI, M. A., BOKHARI, M. S., HIRD, B., and STRZAŁKOWSKI, A., 1959, *Proc. Phys. Soc.*, **74,** 705.

BROCKMAN JR., K. W., 1958, *Phys. Rev.*, **110,** 163.

ERICKSON, G. W., and CHESTON, W. B., 1958, *Phys. Rev.*, **111,** 891.

FRIEDMAN, F. L., and WEISSKOPF, V. F., 1955, *Niels Bohr and the Development of Physics* (London: Pergamon Press), p. 134.

GIBSON, W. M., PROWSE, D. J., and ROTBLAT, J., 1958, *Proc. Roy. Soc.*, **243,** 237.

GLASSGOLD, A. E., CHESTON, W. B., STEIN, M. L., SHULDT, S. B., and ERICKSON, G. W., 1957, *Phys. Rev.*, **106,** 1207.

GREENLEES, G. W., KUO, L. G., and PETRAVIĆ, M., 1958, *Proc. Roy. Soc.*, **243,** 206.

MELKANOFF, M. A., NODVIK, J. S., SAXON, D. S., and WOODS, R. D., 1957, *Phys. Rev.*, **106,** 793.

MCGRUER, J. N., WARBURTON, E. K., and BENDER, R. S., 1955, *Phys. Rev.*, **100,** 235.

PUTNAM, T. M., BROLLEY, J. E., and ROSEN, L., 1956, *Phys. Rev.*, **104,** 1303.

Bounds for Elastic and Inelastic Scattering

By A. WEINMANN

Mathematics Department, University of Leicester

MS. received 10*th November* 1959, *in final form* 10*th December* 1959

Abstract. Two methods are given for obtaining bounds for functions satisfying certain systems of coupled integral equations. Application to the integral equations for potential scattering (elastic or inelastic, three dimensional or in partial wave expansion) results in bounds for the wave functions, and hence for the scattering amplitudes and cross sections. The method gives sufficient conditions for the convergence of the Born iteration series, and estimates for the truncation errors for a wide variety of problems. A simple example illustrates the methods. It is also indicated how they can be employed in more complicated situations than those considered here.

§ 1. INTRODUCTION

It is well known that the unitarity of the S-matrix gives rise to upper bounds for the partial cross sections for elastic or inelastic scattering. This has proved useful in actual applications, in providing a definite upper limit, without any approximation (see e.g. Erskine and Massey 1952, Seaton 1955).

It seems reasonable to expect that when the scattering potential is small (or the energy or angular momentum high), then the cross sections will also be small; and it should be possible to obtain a bound which uses the smallness of the potential. Kohn (1954) has studied the radial wave equation for elastic scattering by a spherically symmetric potential. His expressions for the truncation errors of the nth Born approximation provide such bounds for this case.

Both upper and lower bounds for the lth order phase shifts, based on a variational method, have been studied by Spruch and Kelly (1958), and by Spruch (1958). So far their methods do not seem to have been extended to the case of coupled equations. Khuri (1957), following the methods of Jost and Pais (1951), has studied the analytic behaviour of the scattering amplitude (as a function of k) for three-dimensional scattering by a spherically symmetric potential. Although the Fredholm formulae used by Khuri give valuable information, they do not appear to be suitable for obtaining explicit bounds.

It is the purpose of this note to show how exact bounds can be obtained in many cases involving only a finite number of 'internal states', when a certain quantity is sufficiently small. Such bounds should be useful in providing a definite upper limit against which to compare approximate calculations of unknown accuracy. Kohn (1954) has stressed the fact that several of the usual rules of thumb, used for estimating the validity of Born expansions, are quite unreliable. The basis of the present method is to obtain an upper bound for the wave functions, or suitable associated functions. This bound follows by applying simple inequalities to the scattering integral equations. In fact, the use of a suitably generalized modulus, well known in the theory of differential equations, makes the treatment of coupled equations little more difficult than that of a single equation. The method also gives sufficient conditions for the convergence of the Born (iteration) series, and expressions for truncation errors.

§ 2. BOUNDS FOR FUNCTIONS SATISFYING INTEGRAL EQUATIONS

2.1. *First Method*

The integral equation for scattering, involving only n 'internal states', has the form

$$F(q)=A(q)+\int K(q,q')dq'F(q'), \qquad \ldots\ldots(1)$$

where q denotes the appropriate set of coordinates; $F(q)$ the unknown wave function, an $n\times 1$ matrix; $A(q)$ the incident wave, also an $n\times 1$ matrix; and $K(q,q')$ the scattering kernel, an $n\times n$ square matrix. Examples are given in § 3. For brevity, it will be assumed that $A(q)$, $K(q,q')$ and the solution of (1) are sufficiently well behaved for the following manipulations to be valid. This excludes, for instance, the direct use of an energy or momentum representation.

For any matrix M (square or rectangular) with elements $M_{\lambda\mu}$, let the *modulus* $||M||$ be defined by

$$||M||=\sum_{\lambda,\mu}|M_{\lambda\mu}|; \qquad \ldots\ldots(2)$$

this is a non-negative real number. This special modulus satisfies many of the same rules as the ordinary modulus of a complex number (see e.g. Bellman 1953). In particular

$$||A+B||\leqslant||A||+||B||,\quad ||CD||\leqslant||C||.||D||,\quad ||\int E(q)dq||\leqslant\int||E(q)dq,|| \ldots\ldots(3)$$

as easily verified from the definition (2).

Any definition of the modulus, which satisfies the above rules, could be used instead of the definition (2). We could for example define the modulus of a square matrix M and of a column vector ϕ as the usual *norms*

$$||M||=\max_{\psi}[(M\psi,\ M\psi)/(\psi,\ \psi)]^{1/2},\quad ||\phi||=(\phi,\ \phi)^{1/2}, \qquad \ldots\ldots(4)$$

where $\max_{\psi}$ denotes the least upper bound for all non-zero ψ, and (ψ,ψ) etc. are scalar products in the n-dimensional vector space. This is not so convenient, however, in most applications.

Taking the modulus of (1), and using the rules (3),

$$\begin{aligned}\max_q||F(q)||&\leqslant\max_q[||A(q)||+||\int K(q,q')dq'F(q')||]\\&\leqslant\max_q[||A(q)||+\int||K(q,q')||dq'||F(q')||]\\&\leqslant\max_q||A(q)||+[\max_q||F(q)||][\max_q\int||K(q,q')||dq'], \qquad \ldots\ldots(5)\end{aligned}$$

where $\max_q$ denotes the least upper bound as q varies. This can be rearranged to give a bound for $||F(q)||$, thus

$$\left.\begin{aligned}&\max_q||F(q)||\leqslant\max_q||A(q)||[1-\max_q\int||K(q,q')||dq']^{-1},\\ \text{provided}\quad&[1-\max_q\int||K(q,q')||dq']>0.\end{aligned}\right\} \qquad \ldots\ldots(6)$$

It is easily verified that the condition given in (6), together with some further restrictions requiring $A(q)$ and $K(q, q')$ to be sufficiently well behaved, are sufficient to ensure the uniform convergence of the Born iteration series for equation (1) to an actual solution of (1). In fact, iteration of equation (1) gives the Born series

$$\sum_{s=0}^{\infty} F^{(s)}(q), \qquad \ldots\ldots(7)$$

where

$$F^{(0)}(q) = A(q); \quad F^{(s+1)}(q) = \int K(q, q')dq' F^{(s)}(q'), \quad s \geqslant 0. \qquad \ldots\ldots(8)$$

From this it follows, by reasoning similar to that used in the case of a single equation, that

$$\begin{aligned} \|F^{(s)}(q)\| &\leqslant [\max_q \|A(q)\|] \max_q \int \|K(q, q_1)K(q_1, q_2) \ldots K(q_{s-1}, q_s)\| dq_1 dq_2 \ldots dq_s \\ &\leqslant [\max_q \|A(q)\|] \max_q \int \|K(q, q_1)\| dq_1 \|K(q_1, q_2)\| dq_2 \ldots \|K(q_{s-1}, q_s)\| dq_s \\ &\leqslant [\max_q \|A(q)\|][\max_q \int \|K(q, q')\| dq']^s, \quad s \geqslant 1. \qquad \ldots\ldots(9) \end{aligned}$$

When the condition given in (6) is satisfied, it follows that the series $\sum \|F^{(s)}(q)\|$ converges uniformly, and therefore so also does the series (7). From this it is easily deduced that the sum (7) satisfies equation (1).

A bound for the truncation error involved in taking the first N terms of (7) is easily obtained by the use of (9). Thus, if $N \geqslant 1$,

$$\|F(q) - \sum_{s=0}^{N-1} F^{(s)}(q)\| \leqslant \frac{[\max_q \|A(q)\|][\max_q \int \|K(q, q')\| dq']^N}{[1 - \max_q \int \|K(q, q')\| dq'}. \qquad \ldots\ldots(10)$$

A better, but more complex, estimate is given by replacing the factor $[\ ]^N$ in (10) by

$$\max_q \int \|K(q, q_1)K(q_1, q_2) \ldots K(q_{N-1}, q_N)\| dq_1 dq_2 \ldots dq_N, \qquad \ldots\ldots(11)$$

or by

$$\max_q \int \|K(q, q_1)\| dq_1 \|K(q_1, q_2)\| dq_2 \ldots \|K(q_{N-1}, q_N)\| dq_N. \qquad \ldots\ldots(12)$$

The expression (12) is fairly easy to evaluate for the special types of kernel occuring in scattering theory (see §3.2 and §4). It is also possible to obtain bounds for the individual components of the expression on the left-hand side of (10).

2.2. *Alternative Method*

Instead of considering the whole set of equations to which (1) is equivalent together, we may take the ordinary modulus of each component separately. Reasoning as in the derivation of (5) results in n inequalities

$$F_\lambda \leqslant A_\lambda + \sum_\mu K_{\lambda\mu} F_\mu, \qquad \ldots\ldots(13)$$

where

$$\begin{aligned} F_\lambda = \max_q |F_\lambda(q)|, \quad A_\lambda = \max_q |A_\lambda(q)|, \\ K_{\lambda\mu} = \max_q \int |K_{\lambda\mu}(q, q')| dq'. \end{aligned} \qquad \ldots\ldots(14)$$

Let K be the $n \times n$ square matrix with elements $K_{\lambda\mu}$, and I the $n \times n$ unit matrix. If $[(I-K)^{-1}]_{\lambda\mu} \geqslant 0$ for all λ, μ, then the λth inequality of the system (13) can be multiplied by $[(I-K)^{-1}]_{\nu\lambda}$ and summed over λ, with the result

$$\left.\begin{aligned} F_\lambda \leqslant \sum_\mu [(I-K)^{-1}]_{\lambda\mu} A_\mu, \\ \text{provided} \qquad [(I-K)^{-1}]_{\lambda\mu} \geqslant 0, \text{ for all } \lambda, \mu. \end{aligned}\right\} \qquad \ldots\ldots(15)$$

This can sometimes give better bounds than given by (6) (see §4).

It is also possible to obtain a bound for the difference between $F(q)$ and the sum of the first N terms of the Born iteration series. This is obtained by iterating equation (1) $N-1$ times, and estimating the last term by use of (15), assuming the condition given in (15) to be satisfied. This gives, for instance, if $N \geqslant 1$

$$\|F(q) - \sum_{s=0}^{N-1} F^{(s)}(q)\| \leqslant \|(I-K)^{-1}A\|[\max_q \int \|K(q,q')\| dq']^N, \qquad \ldots\ldots(16)$$

where A is the $n \times 1$ matrix with elements A_λ.

It appears from simple examples that the conditions $[(I-K)^{-1}]_{\lambda\mu} \geqslant 0$ should be sufficient for the convergence of the Born series, but we have not yet obtained a proof of this.

§ 3. APPLICATION TO CERTAIN SCATTERING PROBLEMS

3.1. *Three-dimensional Equations*

Neglecting exchange terms, the usual equations for scattering of two atomic systems having only n internal states take the form (1), with $q = \mathbf{r}$, and (Mott and Massey 1949)

$$A_\lambda(\mathbf{r}) = \exp(ik_{\mathrm{a}}z)\delta_{\lambda\mathrm{a}}, \quad K_{\lambda\mu}(\mathbf{r},\mathbf{r}') = -\frac{\exp\{ik_\lambda|\mathbf{r}-\mathbf{r}'|\}}{4\pi|\mathbf{r}-\mathbf{r}'|} U_{\lambda\mu}(\mathbf{r}'), \qquad \ldots\ldots(17)$$

where $U_{\lambda\mu}(\mathbf{r}) = 2MV_{\lambda\mu}(\mathbf{r})$, $V_{\lambda\mu}(\mathbf{r})$ being the matrix elements of the scattering potential between the internal states, and M the reduced mass. Also $(2M)^{-1}k_{\mathrm{a}}^2 + E_{\mathrm{a}} = (2M)^{-1}k_\lambda^2 + E_\lambda$, where E_λ are the internal energies and $(2M)^{-1}k_{\mathrm{a}}^2$ is the initial kinetic energy of relative motion. Atomic units are used, and the initial state is labelled a . Considering the case of uncharged systems, the asymptotic forms of the wave functions are

$$F_\lambda(\mathbf{r}) \sim \exp(ik_{\mathrm{a}}z)\delta_{\lambda\mathrm{a}} + r^{-1}\exp(ik_\lambda r) f_{\lambda\mathrm{a}}(\theta,\phi), \quad \text{as } r \to \infty. \qquad \ldots\ldots(18)$$

The differential cross section for scattering with the internal state changing from a to b is

$$d\sigma_{\mathrm{ba}} = (k_{\mathrm{b}}/k_{\mathrm{a}})|f_{\mathrm{ba}}(\theta,\phi)|^2 d\Omega, \qquad \ldots\ldots(19)$$

where $d\Omega$ is an element of solid angle about the scattering direction (θ,ϕ). From (17), (18) and (1) one finds the usual relation

$$f_{\mathrm{ba}}(\theta,\phi) = -\frac{1}{4\pi}\int \exp(-i\mathbf{k}_{\mathrm{b}}\cdot\mathbf{r}) \sum_\lambda U_{\mathrm{b}\lambda}(\mathbf{r})F_\lambda(\mathbf{r})d^3r, \qquad \ldots\ldots(20)$$

where $\mathbf{k}_{\mathrm{b}}$ is taken in the direction (θ,ϕ).

Equation (20) gives a bound for $f_{\mathrm{ba}}(\theta,\phi)$, when a bound for the wave functions $F_\lambda(\mathbf{r})$ is given. Such a bound follows, for instance, from (6). Using the fact that $|F_\lambda(\mathbf{r})| \leqslant \|F(\mathbf{r})\|$, this gives the estimate

$$\left.\begin{array}{l} |f_{\mathrm{ba}}(\theta,\phi)| \leqslant \dfrac{1}{4\pi D}\displaystyle\int \sum_\lambda |U_{\mathrm{b}\lambda}(\mathbf{r})|d^3r, \\ \text{provided} \qquad D \equiv 1 - \dfrac{1}{4\pi}\max_{\mathbf{r}} \displaystyle\int \frac{1}{|\mathbf{r}-\mathbf{r}'|}\sum_{\lambda,\mu}|U_{\lambda\mu}(\mathbf{r}')|d^3r' > 0. \end{array}\right\} \qquad \ldots\ldots(21)$$

A bound for the integral occurring in the expression for D can be obtained, for instance, by the methods of Weinmann (1955).

The condition $D > 0$ is satisfied if all the potentials $U_{\lambda\mu}(\mathbf{r})$ are sufficiently small. From (19) and (21) it is clear that when the potentials are small, then the cross sections are small too. Unfortunately the potentials occurring in typical realistic problems (e.g. (e, H) or (n, p) elastic scattering) are too large to satisfy the condition $D > 0$, so that the method will not work for the three-dimensional equations in the above form.

It follows from the discussion in § 2 that sufficient conditions for the convergence of the Born iteration series are, for instance, that: (i) there is an α, $0 \leqslant \alpha < 2$, for which all the quantities $r^{\alpha} U_{\lambda\mu}(\mathbf{r})$ are continuous and bounded, (ii) all the integrals $\int |U_{\lambda\mu}(\mathbf{r})| d^3 r$ converge, (iii) D, defined by (21), is positive. As far as we are aware, this is the first time that such conditions have been given (see Jost and Pais 1951, footnote 8).

3.2. *Partial Wave Expansion*

The rather stringent requirement that $D > 0$, which limits the usefulness of the preceding bounds, can be overcome by employing a partial wave expansion. For simplicity the present discussion is restricted to the case where the $U_{\lambda\mu}(\mathbf{r})$ are spherically symmetric. It will appear from what follows that bounds can always be obtained if the angular momentum or the energy is sufficiently high, and certain integrals involving the potentials converge.

Let the wave functions be expanded as

$$F_{\lambda}(\mathbf{r}) = \sum_{l=0}^{\infty} (2l+1) i^{l} \mathrm{P}_l(\cos\theta) r^{\beta-1} F_{\lambda l}(r), \qquad \ldots\ldots(22)$$

where the factor r^{β} is inserted for later convenience. The spherical harmonic expansions of the incident wave and the kernels are well known to be (Watson 1944)

$$\left.\begin{aligned} \exp(ik_{\mathrm{a}} z) &= \sum_{l=0}^{\infty} (2l+1) i^{l} \mathrm{P}_l(\cos\theta) \mathrm{j}_l(k_{\mathrm{a}} r), \\ \frac{\exp\{ik_{\lambda}|\mathbf{r}-\mathbf{r}'|\}}{|\mathbf{r}-\mathbf{r}'|} &= \sum_{l=0}^{\infty} (2l+1) \mathrm{P}_l(\cos\Theta) Z_l(k_{\lambda};\, r, r'), \end{aligned}\right\} \qquad \ldots\ldots(23)$$

where Θ is the angle between $\mathbf{r}$ and $\mathbf{r}'$, and the factor $Z_l(k_{\lambda};\, r, r')$ is given by

$$Z_l(k;\, r, r') = \begin{cases} ik\mathrm{h}_l^{(1)}(kr)\mathrm{j}_l(kr'), & r \geqslant r', \\ ik\mathrm{h}_l^{(1)}(kr')\mathrm{j}_l(kr), & r \leqslant r', \end{cases} \qquad \ldots\ldots(24)$$

and where the spherical Bessel function $\mathrm{j}_l(x) = [\pi/(2x)]^{1/2} \mathrm{J}_{l+1/2}(x)$, and

$$i\mathrm{h}_l^{(1)}(x) \equiv (-)^l \mathrm{j}_{-(l+1)}(x) + i\mathrm{j}_l(x).$$

These equations result in the following integral equations for the radial functions:

$$F_{\lambda l}(r) = r^{1-\beta} \mathrm{j}_l(k_{\mathrm{a}} r) \delta_{\lambda\mathrm{a}} - \int_0^{\infty} \sum_{\mu} [r^{1-\beta} Z_l(k_{\lambda};\, r, r') r'][U_{\lambda\mu}(r') \mathbf{r}'^{\beta}] dr' F_{\mu l}(r'). \qquad \ldots\ldots(25)$$

Further, let the functions $f_{\lambda\mathrm{a}}(\theta, \phi)$, defined by (18), be expanded as

$$f_{\lambda\mathrm{a}}(\theta, \phi) = \sum_{l=0}^{\infty} (2l+1) \mathrm{P}_l(\cos\theta) f_{\lambda\mathrm{a}}(l). \qquad \ldots\ldots(26)$$

Equation (19) combined with (26) gives for the total a→b cross section

$$\sigma_{\mathrm{ba}} = \sum_{l=0}^{\infty} \sigma_{\mathrm{ba}}(l), \quad \sigma_{\mathrm{ba}}(l) = 4\pi (k_{\mathrm{b}}/k_{\mathrm{a}})(2l+1) |f_{\mathrm{ba}}(l)|^2. \qquad \ldots\ldots(27)$$

Also, equation (20) gives the usual relation

$$f_{\mathrm{ba}}(l) = -\int_0^\infty \mathrm{j}_l(k_{\mathrm{b}}r)r\sum_\lambda U_{\mathrm{b}\lambda}(r)r^\beta dr F_{\lambda l}(r). \qquad \ldots\ldots(28)$$

These equations can be treated in the same way as were the corresponding equations in §3.1 in deriving the bound given by (21), and the result is that

$$\left.\begin{aligned} &|f_{\mathrm{ba}}(l)| \leqslant D_l^{-1}\{\max_r|r^{1-\beta}\mathrm{j}_l(k_{\mathrm{a}}r)|\}\int_0^\infty \sum_\lambda |\mathrm{j}_l(k_{\mathrm{b}}r)rU_{\mathrm{b}\lambda}(r)r^\beta|dr,\\ \text{provided}\quad &D_l \equiv 1-\max_r\int_0^\infty \sum_{\lambda,\mu}|[r^{1-\beta}Z_l(k_\lambda;\, r,\, r')r']U_{\lambda\mu}(r')r'^\beta|dr' > 0. \end{aligned}\right\} \qquad \ldots\ldots(29)$$

The factor $|r^{1-\beta}\mathrm{j}_l(k_{\mathrm{a}}r)|$ is certainly bounded if $0 \leqslant \beta \leqslant 1$, and β can be chosen in this range to make D_l as large as possible. More generally, it may be advantageous to insert a factor $g_{\lambda l}(r)$ into the expansion (22), thus multiplying the kernel in (25) by $[g_{\lambda l}(r)]^{-1}g_{\mu l}(r')$: the functions $g_{\lambda l}(r)$ can then be chosen to make the corresponding D_l as large possible.

For comparison, the unitarity of the S-matrix gives the bounds

$$\left.\begin{aligned} &|f_{\mathrm{ba}}(l)|^2 \leqslant (4k_{\mathrm{a}}k_{\mathrm{b}})^{-1}, \quad \mathrm{b} \neq \mathrm{a}; \quad |f_{\mathrm{aa}}(l)|^2 \leqslant k_{\mathrm{a}}^{-2};\\ \text{and}\quad &\sum_{\mathrm{b}} k_{\mathrm{b}}|f_{\mathrm{ba}}(l)|^2 \leqslant k_{\mathrm{a}}^{-1}. \end{aligned}\right\} \qquad \ldots\ldots(30)$$

If the $U_{\lambda\mu}(r)$ are sufficiently well behaved, and $D_l > 0$, then it can be shown that the Born iteration series for the equations (25) will converge to a solution of these equations.

3.3. *Behaviour of D_l at High Energies*

In order to prove the statement made at the beginning of §3.2 it must be shown that $D_l > 0$, if all the k_λ are sufficiently large. First choose β with $0 \leqslant \beta < 1$, so that

$$\int_0^\infty |U_{\lambda\mu}(r)r^\beta|dr \quad \text{converges for all } \lambda,\, \mu; \qquad \ldots\ldots(31)$$

this is a restriction on the type of potentials to which the result applies. From equation (24) it follows that

$$|r^{1-\beta}Z_l(k;\, r,\, r')r'| \leqslant k^{-(1-\beta)}M_l(\beta), \qquad \ldots\ldots(32)$$

where

$$M_l(\beta) = \max_{x,\,y}\begin{cases} x^{1-\beta}y|\mathrm{h}_l^{(1)}(x)\mathrm{j}_l(y)|, & x \geqslant y,\\ x^{1-\beta}y|\mathrm{h}_l^{(1)}(y)\mathrm{j}_l(x)|, & x \leqslant y. \end{cases} \qquad \ldots\ldots(33)$$

The fact that a finite bound $M_l(\beta)$ exists when $0 \leqslant \beta \leqslant 1$ follows from well-known properties of Bessel functions (Watson 1944). Using the bound (32) to estimate the integrals in (29), it follows that

$$D_l \geqslant 1 - \sum_{\lambda,\mu}(k_\lambda)^{-(1-\beta)}M_l(\beta)\int_0^\infty |U_{\lambda\mu}(r)r^\beta|dr. \qquad \ldots\ldots(34)$$

If k_{a}, and therefore also all other k_λ, is sufficiently large, then the right-hand side of (34) will be positive, as $1-\beta > 0$. It follows that the condition $D_l > 0$ will certainly be satisfied at sufficiently high energies, so that the bound given by (29) will then be applicable.

Kohn (1954) has made use of bounds of the form (32). There can be considerable advantage, however, in retaining the more complex Z_l factors, particularly when the potentials are large and D_l is only just positive (see § 4). Also the above use of the factor r^β makes it unnecessary to consider separately potentials which behave like r^{-1} near the origin (Kohn 1954, § 5).

3.4. *Behaviour of D_l for large l*

To show that $D_l > 0$ at a given energy, if l is sufficiently large, we proceed as follows. First choose $\beta = 1$, and suppose that all the integrals

$$\int_0^\infty |U_{\lambda\mu}(r) r^2| dr, \quad \int_0^\infty |U_{\lambda\mu}(r) r| dr, \qquad \ldots\ldots (35)$$

converge. It is shown in the Appendix that

$$|Z_l(k; r, r')| r' \leqslant (2l+1)^{-1/2}[kr' + (2l+1)^{-1/2}], \qquad \ldots\ldots (36)$$

this being a very crude estimate which suffices for the present purpose. Using (36) to estimate the expression for D_l given in (29) with $\beta = 1$, it follows that $D_l > 0$ if l is sufficiently large, because of the common factor $(2l+1)^{-1/2}$ which appears outside all the integrals. This demonstrates the desired property of D_l.

§ 4. AN EXAMPLE

As a concrete example, we have considered the excitation of the 2s state of hydrogen by electron impact, neglecting both exchange and all but the 1s and 2s states. This problem is not of great physical interest, but is a convenient source of potentials.

Using atomic units, and labelling the 1s, 2s states by suffixes 0, 1 respectively, the potentials for this problem are (with $U_{\lambda\mu} = 2V_{\lambda\mu}$)

$$\left.\begin{aligned} U_{00} &= -2r^{-1}\{1+r\} \exp(-2r), \\ U_{01} = U_{10} &= (2^{5/2}/27)\{2+3r\} \exp(-3r/2), \\ U_{11} &= -(4r)^{-1}\{8+6r+2r^2+r^3\} \exp(-r). \end{aligned}\right\} \qquad \ldots\ldots (37)$$

Also $k_1{}^2 = k_0{}^2 - \frac{3}{4}$. Calculations were only made with $\beta = 1$. The potentials, particularly U_{11}, are so large that the partial wave expansion of § 3.2 will not give bounds for $l = 0$, near the threshold of the reaction. The conditions are first satisfied for $l = 2$. The method of § 2.2 applied to the partial wave equations (25), gives better bounds for the present case. The table gives values of $K_{\lambda\mu}$ evaluated by numerical integration from the formula

$$\begin{aligned} K_{\lambda\mu} &= \max_r \int_0^\infty |Z_l(k_\lambda; r, r') U_{\lambda\mu}(r') r'^2| dr' \\ &= \max_r \left[k_\lambda |\mathrm{h}_l^{(1)}(k_\lambda r)| \int_0^r |\mathrm{j}_l(k_\lambda r') U_{\lambda\mu}(r') r'^2| dr' \right. \\ &\qquad \left. + k_\lambda |\mathrm{j}_l(k_\lambda r)| \int_r^\infty |\mathrm{h}_l^{(1)}(k_\lambda r') U_{\lambda\mu}(r') r'^2| dr' \right]. \end{aligned} \qquad \ldots\ldots (38)$$

The special form of the Z_l kernels makes numerical integration an efficient method for obtaining the $K_{\lambda\mu}$. The conditions $[(I-K)^{-1}]_{\lambda\mu} \geqslant 0$, given in (15), are here

$$1 \geqslant K_{00}, \quad 1 \geqslant K_{11}, \quad (1-K_{00})(1-K_{11}) \geqslant K_{01}K_{10}. \qquad \ldots\ldots (39)$$

These are satisfied for $l = 2$. Further (see equation (25))

$$A_0 = \max_r |\mathrm{j}_2(k_0 r)| = 0{\cdot}32, \quad A_1 = 0, \qquad \ldots\ldots (40)$$

for all k_0. With these values, (15) leads to the following bounds for the wave functions, defined as in (14):

$$\left.\begin{array}{l} F_0 \leqslant 0{\cdot}36 \\ F_1 \leqslant 0{\cdot}05 \end{array}\right\} \text{ at } k_0 = 1,\ l=2; \qquad \left.\begin{array}{l} F_0 \leqslant 0{\cdot}36 \\ F_1 \leqslant 0{\cdot}03 \end{array}\right\} \text{ at } k_0 = 0{\cdot}87,\ l=2. \qquad \ldots\ldots (41)$$

(The values of K_{00}, K_{01} required at $k_0 = 0{\cdot}87$, $k_1 = 0$ were estimated from the table, by using less favourable values at $k_0 = 0{\cdot}5$ or $k_0 = 1$.)

Table. Values of $K_{\lambda\mu}$, defined by (38), as functions of k_λ and l, for the Potentials (37) ($\beta = 1$). K_{10} is exactly the same function of k_1 as K_{01} is of k_0

	K_{00} $l=1$	K_{01} $l=1$	K_{11} $l=1$	K_{00} $l=2$	K_{01} $l=2$	K_{11} $l=2$
$k_\lambda = 0$	0·21	0·10	0·88	0·09	0·05	0·36
$k_\lambda = 0{\cdot}5$	—	—	1·43	0·09	0·06	0·56
$k_\lambda = 1{\cdot}0$	—	—	—	0·10	0·09	—

Using these bounds in (28), one obtains bounds for $f_{00}(l)$ and $f_{10}(l)$ at $l=2$. The contribution from the terms $l=2$ to the total cross sections follows from (27). We find that for values of k_0 near the threshold, and at $k_0 = 1$,

$$\left.\begin{array}{ll} |f_{10}(2)| \leqslant 0{\cdot}8k_1^2, \quad \sigma_{10}(2) \leqslant 46k_1^5, & \text{if} \quad k_1 \ll 1; \\ |f_{10}(2)| \leqslant 0{\cdot}15, \quad \sigma_{10}(2) \leqslant 0{\cdot}71, & \text{at} \quad k_0 = 1. \end{array}\right\} \qquad \ldots\ldots (42)$$

Also

$$|f_{00}(2)| \leqslant 0{\cdot}045, \quad \sigma_{00}(2) \leqslant 0{\cdot}13, \quad \text{at} \quad k_0 = 1. \qquad \ldots\ldots (43)$$

The accuracy of these bounds is limited only by the errors in the numerical calculations, estimated as of order 20%.

These bounds can be compared with the bounds (given in (30)) derived from the unitarity of the S-matrix, which are not exceeded by the above values. They can also be compared with more exact calculations of the *S* wave scattering (Erskine and Massey 1952, Massey and Moiseiwitsch 1951), which is expected to give the main contribution to the total cross sections at these low energies. The contribution of the *D* wave scattering to the elastic cross section, estimated in (43) at $k_0 = 1$, is negligible compared with the contribution of order 10 from the *S* wave. However, the bound for the *D* wave inelastic cross section, estimated in (42) at $k_0 = 1$, just exceeds the value, of order 0·6, for the *S* wave. To study this further, the scattering amplitudes $f_{10}(l)$ have been calculated in 1st and 2nd Born approximation, for the *P* and *D* waves at $k_0 = 1$, with the result

$$\left.\begin{array}{ll} f_{10}(1)^{\mathrm{B1}} = -0{\cdot}087, & f_{10}(1)^{\mathrm{B2}} \simeq -0{\cdot}18 - 0{\cdot}07i; \\ f_{10}(2)^{\mathrm{B1}} = -0{\cdot}021, & f_{10}(2)^{\mathrm{B2}} \simeq -0{\cdot}033 - 0{\cdot}005i, \end{array}\right\} (k_0 = 1). \qquad \ldots\ldots (44)$$

For $l=2$, $D_l > 0$, so that the Born series must converge (see the last paragraph of §3.2); equations (44) show that this convergence is actually not very rapid, but the estimate given in (42) at $k_0 = 1$ is apparently a considerable overestimate. For $l=1$, (44) shows very poor convergence of the Born series (if it converges at all); the usual criterion for convergence, that the value of $f_{10}(l)^{\mathrm{B1}}$ is much less than the maximum allowed by the conditions for the unitarity of the S-matrix is clearly a very unreliable guide for this case.

§ 5. Discussion

The methods described for obtaining bounds can be varied in many ways. Much depends on the nature of the potentials $U_{\lambda\mu}$, which may vary from the short range potentials of nuclear theory to the long range potentials occurring in the theory of slow collisions between atoms. Each type requires a separate discussion of details, and different methods may give better bounds for different problems.

It should be possible to treat Coulomb potentials by forming the integral equations with modified kernels consisting of the appropriate Coulomb wave functions: the methods of § 2 can then be applied. Even if the potentials $U_{\lambda\mu}(\mathbf{r})$ are not spherically symmetric, the total angular momentum operators for the complete system usually commute with the total Hamiltonian. An appropriate expansion of the total wave function in terms of eigenfunctions of the total angular momentum operator then gives sets of coupled equations of the type already considered, and there is no coupling between the sets of equations for different eigenvalues of the total angular momentum. Hence the methods of § 2 can again be applied.

It is also possible to obtain bounds for some types of integro-differential equations which occur when exchange effects are allowed for; this follows because the integro-differential equations can be turned into integral equations by using the appropriate Green's function. Thus, for instance, the integro-differential equations of Erskine and Massey (1952) for the excitation of the 2s state of hydrogen by electron impact give rise to integral equations whose kernels are of the form

$$K(\mathbf{r},\mathbf{r}') = -\frac{1}{4\pi}\left[\frac{\exp\{ik|\mathbf{r}-\mathbf{r}'|\}}{|\mathbf{r}-\mathbf{r}'|}U(\mathbf{r}') \pm \int d^3r''\,\frac{\exp\{ik|\mathbf{r}-\mathbf{r}''|\}}{|\mathbf{r}-\mathbf{r}''|}\right.$$

$$\left.\times\,\psi(\mathbf{x}'')\{(2E_0-k^2)\psi(\mathbf{r}')^* + 2\psi(\mathbf{r}')^*|\mathbf{r}''-\mathbf{r}'|^{-1}\}\right], \qquad \ldots\ldots(45)$$

where $\psi(\mathbf{r})$ are bound state hydrogen atom wave functions. The extra terms do not give any difficulties in principle, so that one can proceed to discuss the equations similarly to § 3. In a partial wave analysis the conclusions of § 3.3 (except for S wave scattering, where the factor $2E_0-k^2$ in (45) causes difficulties) and of § 3.4 can be shown to be valid.

The methods do not give any information when there is an infinite number of coupled equations, such as are necessary to describe the real physical situation in which there is an infinite number of internal states. (The methods of § 2 can still be applied, but do not appear to be useful.) Thus the bounds for the cross sections do not have the same generality as those obtained from the unitarity of the S-matrix.

It would be very desirable to have bounds (other than those resulting from the unitarity of the S-matrix), in the cases where the present methods fail (at fixed energy and angular momentum) when the necessary conditions of (6) and (15) are not satisfied.

In view of the widespread use of the Born approximation, it is of considerable interest that the present methods can be used to obtain sufficient conditions for the convergence of the Born series for a wide variety of problems.

APPENDIX

To establish the inequality (36), we start from the well-known integral representation of the Z_l functions

$$2Z_l(k\,;\,r,\,r')=\int_{-1}^{+1}\mathrm{P}_l(\mu)\sigma^{-1}\mathrm{e}^{ik\sigma}d\mu,\quad \sigma^2=r^2+r'^2-2rr'\mu,\quad (r\neq r')\qquad\ldots\ldots(\mathrm{A1})$$

(Watson 1944; this follows also from equation (23)). Writing $\mathrm{e}^{ik\sigma}=(\mathrm{e}^{ik\sigma}-1)+1$, and taking the modulus of (A1), we obtain

$$|2Z_l|\leqslant\left|\int_{-1}^{+1}\mathrm{P}_l(\mu)\sigma^{-1}d\mu\right|+\left|\int_{-1}^{+1}\mathrm{P}_l(\mu)\sigma^{-1}(\mathrm{e}^{ik\sigma}-1)d\mu\right|.\qquad\ldots\ldots(\mathrm{A2})$$

Now

$$\int_{-1}^{+1}\mathrm{P}_l(\mu)\sigma^{-1}d\mu=\begin{cases}\dfrac{2}{(2l+1)}\dfrac{r^l}{r'^{(l+1)}}, & r<r',\\[2ex] \dfrac{2}{(2l+1)}\dfrac{r'^l}{r^{l+1}} & r>r',\end{cases}\qquad\ldots\ldots(\mathrm{A3})$$

and r' times the right-hand side of (A3) is less than $2/(2l+1)$. Further, by Schwartz's inequality, and as $|(\mathrm{e}^{ik\sigma}-1)/\sigma|\leqslant k$, we have

$$\begin{aligned}\left|\int_{-1}^{+1}\mathrm{P}_l(\mu)\sigma^{-1}(\mathrm{e}^{ik\sigma}-1)d\mu\right| &\leqslant k\int_{-1}^{+1}|\mathrm{P}_l(\mu)|d\mu\\ &\leqslant k\left[\int_{-1}^{+1}\{\mathrm{P}_l(\mu)\}^2d\mu\,.\int_{-1}^{+1}d\mu\right]^{1/2}\\ &=2k/(2l+1)^{1/2}.\end{aligned}\qquad\ldots\ldots(\mathrm{A4})$$

Combining these results we obtain the inequality (36).

The inequality can be improved, by using the bound (Bateman Manuscript Project 1953)

$$(\sin\theta)^{1/2}|\mathrm{P}_l(\cos\theta)|\leqslant(\pi l/2)^{-1},\quad 0\leqslant\theta\leqslant\pi,\qquad\ldots\ldots(\mathrm{A5})$$

which gives

$$k\int_{-1}^{+1}|\mathrm{P}_l(\mu)|d\mu\leqslant\frac{2^{7/2}\pi^{1/2}k}{[\Gamma(\frac{1}{4})]^2 l},\qquad\ldots\ldots(\mathrm{A6})$$

so that $|Z_l|$ has a l^{-1} dependence for large l.

REFERENCES

BATEMAN MANUSCRIPT PROJECT, 1953, *Higher Transcendental Functions*, Vol. 2 (New York: McGraw-Hill), p. 206.

BELLMAN, R., 1953, *Stability Theory of Differential Equations* (New York: McGraw-Hill).

ERSKINE, G. A., and MASSEY, H. S. W., 1952, *Proc. Roy. Soc.* A, **212**, 521.

JOST, R., and PAIS, A., 1951, *Phys. Rev.*, **82**, 840.

KHURI, N. N., 1957, *Phys. Rev.*, **107**, 1148.

KOHN, W., 1954, *Rev. Mod. Phys.*, **26**, 292.

MASSEY, H. S. W., and MOISEIWITSCH, B. L., 1951, *Proc. Roy. Soc.* A, **205**, 483.

MOTT, N. F., and MASSEY, H. S. W., 1949, *The Theory of Atomic Collisions*, 2nd edn (Oxford: Clarendon Press), p. 116, and Ch. VIII.

SEATON, M. J., 1955, *Proc. Phys. Soc.* A, **68**, 457.

SPRUCH, L., 1958, *Phys. Rev.*, **109**, 2149.

SPRUCH, L., and KELLY, M., 1958, *Phys. Rev.*, **109**, 2144.

WATSON, G. N., 1944, *A Treatise on the Theory of Bessel Functions*, 2nd edn (Cambridge: University Press), Ch. XI, and § 3.1, and § 3.4.

WEINMANN, A., 1955, *Proc. Phys. Soc.* A, **68**, 1197.

Note added in proof.—A different method of obtaining bounds has been studied by I. C. PERCIVAL (1960, *Phys. Rev.*, in the press) to whom my thanks are due for a preprint.

Ionization Times of Impurities in Hydrogen Plasmas

By R. W. P. McWHIRTER
Atomic Energy Research Establishment, Harwell, Berks.

MS. received 24th July 1959, in final form 5th November 1959

Abstract. The problem discussed is the calculation of the time it takes for impurity atoms and ions to become ionized in the hydrogen plasma produced in pulsed thermonuclear machines. Classical ionization cross sections are used to calculate ionization rates and the effect of radiative recombination is included. The importance of taking into account the time dependence of the state of ionization is illustrated by an example where the energy radiated by an impurity of carbon is estimated. The time for impurity ions to reach the steady state is compared with the duration of the discharge for a number of operating thermonuclear machines and it is found that the latter times are too short for the steady state to be established. The assumption of the steady state is shown to be acceptable for a power producing D–D reactor.

§ 1. Introduction

The importance of quite small percentages of impurities in calculating the radiation emitted by the high temperature hydrogen plasmas generated in laboratory thermonuclear devices has already been pointed out by Knorr (1958). It has been predicted that a steady state is reached when the rate of ionization by electron collision is balanced by the rate of radiative recombination of ions with electrons as in the solar corona (Elwert 1952). However most laboratory thermonuclear devices are pulsed so that it is important in calculating the radiation in these cases to consider the time dependence of the ionization process.

In this paper classical ionization cross sections are used to calculate the rates of ionization of impurity ions which, it is supposed, are suddenly introduced into a hydrogen plasma having a constant electron density $n_e(\mathrm{cm}^{-3})$ and constant electron temperature $T_e(\mathrm{ev})$. Radiative recombination is also taken into account in estimating the ionic concentrations. The intensities of the main spectral lines and of the recombination continuum emitted by these ions is then estimated. As a specific example the radiation emitted by carbon in a plasma such as that which may be produced in ZETA is calculated.

The time for the impurity ions to reach the steady state is estimated for the general case, and this time is compared with the duration of the discharge in a number of operating laboratory devices and with the energy containment time which will be necessary for a power-producing reactor.

§ 2. The Ionization Equation

Following Elwert (1952) a quantity $S(T_e)$ is introduced such that $n_e S(T_e)$ is the probability per unit time of ionizing an impurity atom or ion by electron collision. $S(T_e)$ has been calculated by averaging what are essentially classical ionization cross sections over Maxwellian velocity distributions. In fact mean values of cross sections for atoms from a review by Bates *et al.* (1950) were used as suggested by Allen (1955). The values of S are plotted as functions of T_e in figure 1 for a range of ionization potentials χ.

Radiative recombination coefficients $\alpha(T_e)$ have been evaluated for recombination to all states of hydrogen-like ions using a formula due to Seaton (1959). These are plotted in figure 1 for ions having a charge Z from unity to 80. The approximation will be made in this paper that the radiative recombination coefficient for any ion is the same as that for the hydrogen-like ion having the same charge Z'.

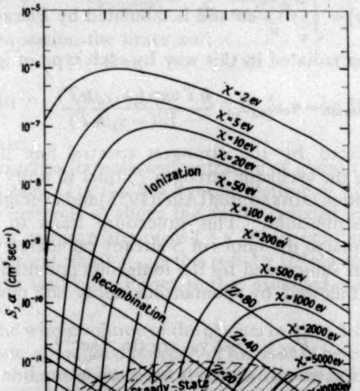

Figure 1. Ionization and recombination rate coefficients.

The rate of ionization of any impurity may now be calculated to the accuracy of the coefficients S and α by solving a set of equations

$$\frac{dn_i}{dt} = -S_i n_i n_e + \alpha_{i+1} n_{i+1} n_e + S_{i-1} n_{i-1} n_e - \alpha_i n_i n_e \qquad \ldots\ldots (1)$$

where n_i is the density (cm^{-3}) of atoms ($i=0$) or ions ($i=1$ to Z). The initial density of impurity atoms is

$$N_0 = \sum_{i=0}^{Z} n_i \text{ and at } t=0,\ n_0 = N_0.$$

§ 3. THE RADIATION FROM IMPURITY IONS

Three classes of radiation arise from the interaction of electrons with the ions of a plasma, viz. (*a*) bremsstrahlung (free–free transitions), (*b*) recombination continuum (free–bound transitions), (*c*) line radiation (bound–bound transitions). Except where there are no atoms or ions having bound electrons bremsstrahlung is negligible in comparison with the other two.

Each radiative recombination process results in the emission of a photon having average energy

$$\frac{\boldsymbol{k}T\exp(-\chi_i/\boldsymbol{k}T)}{-\mathrm{Ei}(-\chi_i/\boldsymbol{k}T)}$$

where χ_i is the appropriate ionization potential.

$$\left(-\mathrm{Ei}(-x)=\int_x^\infty \frac{e^{-u}}{u}\,du \text{ and is tabulated by Placzek 1954.}\right)$$

Thus the total power radiated in this way by each type of ion is

$$P_{\mathrm{recomb}}=n_e n_{i+1}\alpha_{i+1}\frac{\boldsymbol{k}T\exp(-\chi_i/\boldsymbol{k}T)}{-\mathrm{Ei}(-\chi_i/\boldsymbol{k}T)}. \qquad \ldots\ldots(2)$$

The power radiated by the strongest spectral line of each ion may be estimated by putting the oscillator strength f equal to unity in the approximate formula for the excitation cross section (Allen 1955) and averaging over Maxwellian electron velocity distributions. This procedure leads to excitation rate coefficients X almost equal to the values of S already calculated where the excitation potential χ_{ex} has been substituted for the ionization potential χ. Assuming that excitation is always followed by spontaneous decay the power radiated as line radiation is

$$P_{\mathrm{ex}}=n_e n_i X\chi_{\mathrm{ex}}\,\mathrm{erg\,cm^{-3}\,sec^{-1}}. \qquad \ldots\ldots(3)$$

The strongest transition usually accounts for most of the line radiation of a given atom or ion.

§ 4. A CALCULATION FOR CARBON IMPURITY IN A HYDROGEN PLASMA

It is instructive to carry out a calculation of the energy radiated in a specific case. The conditions chosen are those which may exist in the plasma produced in ZETA, viz. $n_e=10^{14}\,\mathrm{cm^{-3}}$, $T_e=50\,\mathrm{ev}$, $N_0=10^{12}$ carbon atoms $\mathrm{cm^{-3}}$ (1% impurity).

When radiative recombination balances ionization to establish the steady state among the carbon ions their concentrations are related as follows:

$$\left.\begin{array}{ccccccc} n_i & : & n_{i+1}=\alpha_{i+1} & : & S_i \\ \mathrm{C\,IV} & : & \mathrm{C\,V} & : & \mathrm{C\,VI} & : & \mathrm{C\,VII} \\ 5\times10^{-4} & : & 0{\cdot}96 & : & 0{\cdot}04 & : & 2\times10^{-4}. \end{array}\right\} \qquad \ldots\ldots(4)$$

The values of α_{i+1} and S_i have been taken from figure 1.

The radiation from these ions may be calculated by the methods of § 3. The results of such a calculation are tabulated below.

(1)	(2)	(3)	(4)	(5)	(6)
C IV	64·5	$5{\cdot}83\times10^3$	2s–2p	8	9×10^4
C V	392	$2{\cdot}07\times10^3$	$1s^2$–1s2p	304	$1{\cdot}2\times10^4$
C VI	490	$3{\cdot}13\times10$	1s–2p	367	5×10

(1) Ion; (2) χ_{ion} (ev); (3) P_{recomb} (erg $\mathrm{cm^{-3}\,sec^{-1}}$); (4) strongest transition; (5) χ_{ex} (ev); (6) P_{ex} (erg $\mathrm{cm^{-3}\,sec^{-1}}$).

For comparison the power radiated by the hydrogen ions is noted:

$$P_{\text{bremsstrahlung}} = 1 \times 10^4\,\text{erg cm}^{-3}\,\text{sec}^{-1}, \quad P_{\text{recomb}} = 8{\cdot}75 \times 10^3\,\text{erg cm}^{-3}\,\text{sec}^{-1}.$$

Despite its small concentration *C* IV accounts for the majority of the power radiated. It does so because it has a low-lying first excited state. During the transient phase of the ionization process all the carbon ions must pass through the C IV state and at that time a relatively large amount of energy will be radiated.

The time to reach the steady state is approximately the sum of the reciprocals of the ionization rates thus

$$\tau_{\text{transient}} = \sum_{i=0}^{Z'_{\max}} \frac{1}{n_e S_i(T_e)}. \qquad \ldots\ldots(5)$$

For the ions in question the times are:

Ion	C I	C II	C III	C IV	C V
$\frac{1}{n_e S_i(T_e)}$	$1{\cdot}2 \times 10^{-7}$	$6{\cdot}5 \times 10^{-7}$	3×10^{-6}	7×10^{-6}	2×10^{-1} sec

and $\tau_{\text{transient}} = 0{\cdot}2$ sec.

In particular C IV reaches its peak concentration at about $t = 5\,\mu$sec by the ionization of C III and each C IV ion has a mean lifetime of 7 μsec.

Using the same methods as above the power radiated in the strongest line of C IV for the 7 μsec of its mean lifetime is $1{\cdot}8 \times 10^8$ erg cm^{-3} sec^{-1}. Averaged over the whole of the transient phase τ_{trans} this is $6{\cdot}3 \times 10^3$ erg cm^{-3} sec^{-1}. However, the discharge in ZETA lasts only 3 msec so that averaged over this period it gives $4{\cdot}2 \times 10^5$ erg cm^{-3} sec^{-1}.

Summed over the whole volume of the plasma in ZETA $1{\cdot}8 \times 10^8$ erg cm^{-3} sec^{-1} is equivalent to 50 MW of radiated power. This should be compared with a mean available power of about 100 MW from the electrical circuit.

§ 5. THE TIME TO REACH THE STEADY STATE IN THE GENERAL CASE

The steady state is characterized by the equality of $n_i S_i$ and $n_{i+1}\alpha_{i+1}$. Because the ionization coefficients S vary sharply with temperature T_e then, for a given plasma in the steady state, there are never more than about two or three different ionic species (of a given element) present. These species will be characteristic of the plasma in question and they may be predicted by equating S_i and α_{i+1} for that ion. Thus points on figure 1 where $S_i = \alpha_{i+1}$ represent the steady state. By plotting all such points for all species of all ions a band is obtained as shown on figure 1. Over this band, to an order of magnitude $S = \alpha = 10^{-12}$ cm^3 sec^{-1} for all temperatures T_e between 1 ev and 100 kev.

The physical reason for the limited spread of the points is that for a given charge an ion has an ionization potential from a restricted range of values. In particular for hydrogen-like ions $\chi = Z^2\chi_H$ ($\chi_H = 13{\cdot}6$ ev).

The charge $Z'_{\max}$ on the ions which are characteristic of the plasma in the steady state may be determined and these are plotted in figure 2.

The time to reach the steady state is the sum of the reciprocals of the ionization rates, equation (5), and, of the sum, the most important term is the ionization time of the most highly charged ion to be produced ($Z'_{\max}$) i.e. $1/n_e S_{Z'_{\max}}$ (cf. the case of the C V ions discussed above). In the discussion that follows $\tau_{\text{transient}}$ will be equated to the ionization time for the last ion,

$$\text{i.e. } \tau_{\text{trans}} \simeq \frac{1}{n_e S_{Z'_{\max}}} \simeq \frac{10^{12}}{n_e}\ \text{sec} \qquad \ldots\ldots(6)$$

and this will be a lower limit. The actual time to reach the steady state will be greater than this by a factor less than five or six,

$$\text{i.e. } 10^{11} < n_e \, \tau_{\text{trans}} < 2 \times 10^{13}. \qquad \ldots\ldots(7)$$

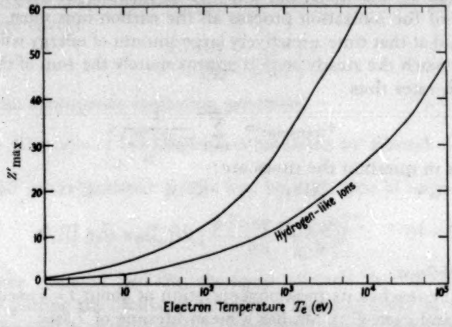

Figure 2. The curves represent the upper and lower limits of the charge that an ion (having at least one bound electron) may have in a plasma in the steady state (as defined in the text).

§ 6. IONIZATION TIMES IN DEVICES AT PRESENT IN OPERATION

Taking $T_e = 50$ ev as typical of the electron temperature found in devices working today the corresponding value for $S_{Z'_{\max}}$ is from figure 1 between 10^{-11} and 10^{-12} cm^3 sec^{-1}. In the following table τ_{trans} as calculated using this value is compared with the pulse duration times of various devices.

Device	Pulse duration (sec)	n_e (cm^{-3})	Range of τ_{trans} (sec)
ZETA (Butt *et al.* 1958)	3×10^{-3}	10^{14}	$1\text{–}60 \times 10^{-3}$
Fast pinch devices			
Kurchatov (1957)	$1\text{–}10 \times 10^{-6}$	10^{16}	$10\text{–}600 \times 10^{-6}$
Bodin *et al.* (1959)			
Hagerman and Mather (1958)			
Stellarator (B − 1) (Coor *et al.* 1958)	1×10^{-3}	10^{13}	$10\text{–}600 \times 10^{-3}$

If the 100 μsec energy containment time calculated by Pease (Butt *et al.* 1958) for ZETA also represents the ion containment time then this value should be compared with τ_{trans} instead of the pulse duration.

It is therefore not realistic to assume the steady state in calculating the radiation from any of these devices.

§ 7. IONIZATION TIMES IN POWER-PRODUCING REACTORS

Finally the duration of the transient phase will be compared with Lawson's criteria (Lawson 1957) for an economic pulsed power-producing reactor. It is assumed that the concentration of impurities is so low that it does not seriously modify the criteria. For $T_e > 10$ kev, $n_e \tau_{\text{trans}} = 10^{11}$ to 5×10^{12} cm^{-3} sec Lawson's criteria are: for a D–D reactor $nt > 10^{16}$ cm^{-3} sec, for a D–T reactor $nt > 10^{14}$ cm^{-3} sec, where n = density of hydrogen ions ($= n_e$) and t = energy containment time.

Thus in calculating the radiation from a D–D power-producing reactor it is a good approximation to neglect the transient phase and assume the steady state. For a D–T reactor it may be necessary to take account of the transient phase.

§ 8. CONCLUSIONS

The radiation from an impurity of 1% of carbon in a ZETA type plasma has been calculated. For this case it was found that the power radiated as line radiation by C IV ions is about 1000 times greater for a short period during the transient phase that the total power radiated assuming the steady state.

It was shown that the transient phase is longer than the pulse duration for a number of thermonuclear devices in operation. For future D–D power-producing reactors it is a good approximation to assume the steady state in calculating the radiation.

ACKNOWLEDGMENTS

The work described here has benefited from discussions with members of Dr. M. J. Seaton's group at University College, London, with Dr. R. F. Post and with colleagues at Harwell. I am grateful to Mr. R. S. Pease, Mr. G. N. Harding and Mr. T. F. Johns for their criticism of the manuscript and I wish to thank the Director of the United Kingdom Atomic Energy Authority Research Group for permission to publish it.

REFERENCES

ALLEN, C. W., 1955, *Astrophysical Quantities* (London : University of London).

BATES, D. R., FUNDAMINSKY, A., LEECH, J. W., and MASSEY, H. S. W., 1950, *Phil. Trans.* A, **243**, 93.

BODIN, H. A. B., PEACOCK, N. J., and REYNOLDS, J. A., 1959, *Fourth International Conference on Ionization Phenomena (Uppsala)*, Paper IV a. 9.E.

BUTT, E. P., *et al.*, 1958, *Atomic Energy Conference (Geneva)*, Paper A/Conf 15/P/1519.

COOR, T., *et al.*, 1958, *Atomic Energy Conference (Geneva)*, Paper A/Conf 15/P/362.

ELWERT, G., 1952, *Z. Naturf.*, **7a**, 432.

HAGERMAN, D. C., and MATHER, J. W., 1958, *Nature, Lond.*, **181**, 226.

KNORR, G., 1958, *Z. Naturf.*, **13a**, 941.

KURCHATOV, I. V., 1957, *J. Nucl. Energy*, **4**, 193, in English.

LAWSON, J. D., 1957, *Proc. Phys. Soc.* **B**, **70**, 6.

PLACZEK, G., 1954, *U.S. Nat. Bur. Stand., Appl. Maths. Series*, 37.

SEATON, M. J., 1959, *Mon. Not. R. Astr. Soc.*, **119**, 81.

Experiments involving the Emission of Particles from Compound Nuclei

By R. S. STOREY, W. JACK and A. WARD

Department of Natural Philosophy, The University, Glasgow

MS. received 29th June 1959, in revised form 28th September 1959

Abstract. A scintillation counter technique is described which allows rapid measurements of energy spectra and cross sections in (n, p) reactions, integrated over essentially 4π geometry. At a neutron energy of 14·1 Mev, measurements were made on ^{27}Al, ^{54}Fe, ^{56}Fe, ^{58}Ni, ^{59}Co, ^{60}Ni, ^{63}Cu, ^{64}Zn and ^{65}Cu, and at 13·0 and 15·7 Mev on ^{54}Fe, ^{58}Ni and ^{64}Zn.

When corrected for barrier transmission the measured energy spectra have a Maxwellian form $\exp(-E/T_{\mathrm{m}})$ and excluding ^{27}Al and ^{65}Cu the average value of $E_{\mathrm{c}}^*/AT_{\mathrm{m}}^2$ is constant within the experimental error of 3% in T_{m}, and equals $0{\cdot}158 \pm 0{\cdot}003$ Mev^{-1}. (E_{c}^* is the excitation energy and A is the atomic mass number of the compound nucleus.)

The values of the integrated cross sections $\sigma(\mathrm{n, p})$ are in reasonable agreement with the relation $\sigma(\mathrm{n, p}) \propto \exp[-(E_{\mathrm{b}}+P)/T_{\mathrm{m}}]$ where E_{b} is the binding energy and P is related to the pairing energy in the compound nucleus.

Measured values of T_{m} and $\sigma(\mathrm{n, p})$ are tabulated. Some results of others are used to obtain values of T_{m} and integrated cross sections, and these are not inconsistent with the results of the experiments described here.

§ 1. Introduction

Many measurements of (n, p) spectra have been made using nuclear emulsion techniques (Allan 1957, Brown *et al.* 1957, March and Morton 1958 a, b) but the time required to analyse tracks in plates inhibits the use of this technique in a general investigation on many elements. Fairly recently Colli *et al.* (1958) have shown that scintillation counters can be used successfully in measurements on fast protons from targets bombarded by 14 Mev neutrons. This technique requires rather large areas of separated isotopes, and the full use of available intensities of neutron fluxes is apparently prevented by a relatively large random rate of coincidences. A technique similar to that of Colli has been described by Jack and Ward (1960) which avoids these difficulties, but both techniques have really been developed to estimate the contribution of 'direct' effects in reactions by measuring proton energy spectra at small forward angles. The technique which is described here has been developed to measure directly the energy spectra and cross sections averaged over almost a 4π geometry. Small forward angles are avoided, and it is therefore hoped that the measured energy spectra correspond closely to the emission of particles from compound nuclei formed by capture of the incident neutron.

§ 2. Experimental Method

Figure 1 is a diagram of the apparatus used for measurements of cross sections and energy spectra of protons in (n, p) reactions at incident neutron energies of 13·0 and 15·7 Mev. Measurements were also made at 14·1 Mev and in this case the brass screening plate was 7·5 in. long, that is twice as long as that shown in figure 1. It will be seen that the purpose of the apparatus is to attenuate the neutron flux reaching the CsI(Tl) crystal used to detect protons from (n, p) reactions in the completely exposed separated isotope target, without introducing too large a gap between the two. To achieve the required sharp separation between screened and unscreened regions, the tritium–titanium target which formed the neutron source, when bombarded by deuterons in a Cockcroft–Walton accelerator, was carefully soldered flat down to the cooling block and the brass plate accurately machined. To avoid slow changes in relative positions, the apparatus was made very rigid, but the apparatus can rotate with respect to the deuteron beam in order to give a range of neutron energies, and the position of the complete crystal-target assembly (shown enlarged in the inset of figure 1) can be varied in a direction perpendicular to the parallel planes containing the CsI(Tl) crystal, separated isotope target, brass plate and tritium target. The crystal-target assembly had fine screw threads on the rim which fitted into corresponding threads in the brass plate; by rotating the assembly the crystal and the separated isotope target were moved at a fixed distance from each other an accurately known distance into the brass plate.

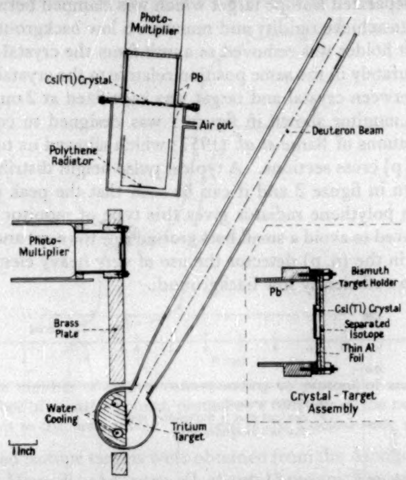
Photo-
Multiplier
CsI(Tl) Crystal
Pb
Air out
Deuteron Beam
Polythene
Radiator
Photo-
Multiplier
Bismuth
Target Holder
Pb
CsI(Tl) Crystal
Separated
Isotope
Thin Al
Foil
Brass
Plate
Crystal - Target
Assembly
Water
Cooling
Tritium
Target
1 Inch

Figure 1. Apparatus used for measurements of proton energy spectra from (n, p) reactions. Inset—crystal target assembly, twice scale.

The CsI(Tl) crystals were obtained from the Harshaw Chemical Co. The thickness of the crystals used were chosen as a compromise between edge effects for the highest proton energies and the achievement of a low background rate. At 14·1 Mev the crystal was 0·035 in. thick and at 13·0 and 15·7 Mev the crystal was 0·045 in. thick. In the experiments, the crystal was mounted quite rigidly with 0·005 in. platinum wire at a distance of 1·6 in. from the glass top of the Du Mont 6292 photomultiplier, primarily to avoid background due to (n, p) reactions in the glass, but we have also found that this improves the energy resolution (probably because of non-uniform response across the photomultiplier cathode). Also to reduce background, the brass outer casing around the crystal was lined with thin lead. A very thin layer of aluminium was evaporated on to the surface of the lead and a very thin aluminium foil was placed immediately behind the crystal, to act as light reflectors. Platinum was used as the backing material for the separated isotope target which was clamped between a ring and a disc of bismuth to achieve rigidity and maintain a low background. To change targets, the target holder was removed as a unit from the crystal-target assembly and replaced accurately in the same position relative to the crystal. In the experiments the gap between crystal and target was kept fixed at 2 mm.

The neutron monitor shown in figure 1 was designed to correspond to the accurate computations of Bame *et al.* (1957) which allowed us to obtain absolute values for the (n, p) cross sections. A typical pulse height distribution for 14 MeV neutrons is shown in figure 2 and it can be seen that the peak due to knock-on protons from the polythene radiator gives this type of monitor a high stability. The air was removed to avoid a small background due to (n, p) and (n, d) reactions in nitrogen. As in the (n, p) detector the use of very heavy elements is required in order to give a sufficiently low background.

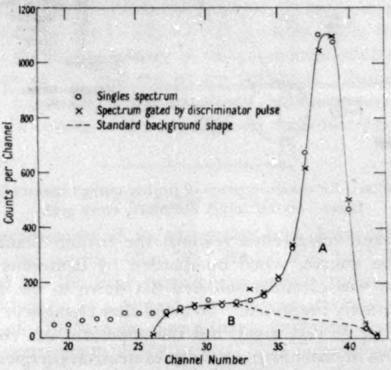

Figure 2. Pulse height distributions in monitor.

Before measurements of (n, p) spectra were carried out, the apparatus was checked and the best position of the crystal-target assembly obtained, relative to the brass plate, by observing the number of counts in the CsI(Tl) crystal for a fixed neutron monitor count as the crystal-target assembly was rotated. A typical result is shown in figure 3, the zero of the abscissa scale is not significant. Curve B was obtained for no target, and curve A for a 15 mg cm^{-2} target of ^{58}Ni. The bias on the scaler recording counts was set at approximately 8 MeV. No appreciable change was found in the positions of the edges when these runs were repeated, and a position about halfway along the lower plateau in curve A

($D \sim 4$ mm) was chosen for the experiments. Figure 3 was obtained for the longer brass plate. If the attenuation is defined as the ratio of the ordinates at $D = 1$ mm and $D = 8$ mm in curve B, the attenuation of the plate 7·5 in. long was 20 : 1 and of the plate 3·75 in. long about 3 : 1. The flat plateaux observed in figure 3 show that there is little evidence of appreciable scattering by the brass plate increasing the neutron flux above that measured on the monitor. The rounding off of the edges is attributed to residual misalignment of the planes containing the crystal, brass plate and tritium target. Much of the width in the edge of curve B is due to the finite thickness of the CsI(Tl) crystal.

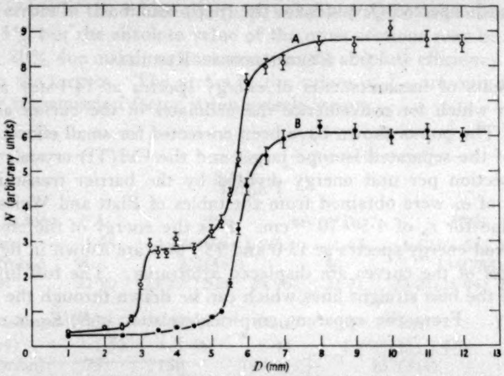

Figure 3. N, the number of counts corresponding to protons of energy ~ 8 Mev, for a fixed number of monitor counts, plotted as a function of the position of the crystal with respect to the brass plate. The zero of the abscissa scale is not significant.

The separated isotope targets were obtained from the Atomic Energy Research Establishment, Harwell, and were all about 15 mg cm^{-2} mounted on a 0·0005 inch platinum backing. Preliminary runs using platinum foils were made to ensure that the background remained unchanged when the platinum foil was inserted into the target holder. Three runs were made at each neutron energy for the targets ^{54}Fe, ^{58}Ni, ^{64}Zn, and three runs were made at 14·1 Mev for ^{27}Al, ^{54}Fe, ^{56}Fe, ^{58}Ni, ^{59}Co, ^{60}Ni, ^{63}Cu, ^{64}Zn and ^{65}Cu. Each run required about half an hour and between runs the gain of the photomultiplier was checked using a ^{137}Cs source of gamma rays. The position of the peak in the neutron monitor was frequently checked. The results of each run were first plotted separately to check for consistency, then averaged. The background was measured six times at intervals between measurements for the same neutron flux as in each of the target runs, and each background was plotted separately before they were all averaged. The pulses from the photomultipliers were clipped to 2 μsec and amplified and the pulse height distributions measured on a 100-channel pulse-height analyser. Pulses from the monitor were fed to a ratemeter so that the neutron flux could be maintained constant. The neutron energies 13·0 and 15·7 Mev were obtained by making measurements at forward and backward angles to the incident deuteron beam at 600 kev. The neutron energy of 14·1 Mev was obtained by making measurements at 90° to the incident deuteron beam at 160 kev. The thickness of the tritium targets used was about 70 kev at both energies; the corresponding spread in neutron energy was about 0·1 Mev. Beam currents were of the order of 100 μA on the tritium target which was 1 in. in diameter. All the runs at 14·1 Mev were made using the same tritium target and the neutron yield remained at about 5×10^9 neutrons per second into 4π. The end points of the (n, p) spectra were not used to calibrate the crystal; instead, an independent calibration was made using proton groups from the reactions ^{3}He(d, p)^{4}He, ^{10}B(d, p)^{11}B, and ^{2}H(d, p)^{3}H. It was found that the response of the crystal was linear over the range of proton energies measured in the (n, p) spectra and the calibration was used to check for consistency by comparing the measured and expected Q values for the (n, p) reactions.

§ 3. Experimental Results

The results of measurements of energy spectra at 14·1 Mev are shown in figure 4, in which for convenience the ordinates of the curves are arbitrarily displaced. The points shown have been corrected for small effects due to finite thickness of the separated isotope target and the CsI(Tl) crystal. $\sigma(E)/E\sigma_c$ is the cross section per unit energy divided by the barrier transmission factor. The values of σ_c were obtained from the tables of Blatt and Weisskopf (1952), using a value for r_0 of $1·5 \times 10^{-13}$ cm. E is the energy of the emitted proton. The measured energy spectra at 13·0 and 15·7 Mev are shown in figure 5; again the ordinates of the curves are displaced arbitrarily. The full lines in figures 4 and 5 are the best straight lines which can be drawn through the points above about 6 Mev. From the apparent empirical relation $\sigma(E)/E\sigma_c \propto \exp(-E/T_m)$

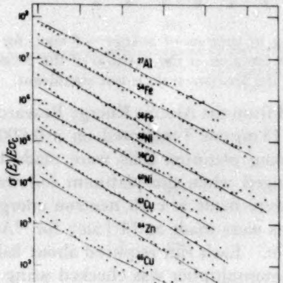

Figure 4. Curves giving $\sigma(E)/E\sigma_c$ obtained from measurements of the energy spectra of the protons from the (n, p) reaction in ^{27}Al, ^{54}Fe, ^{58}Ni, ^{59}Co, ^{60}Ni, ^{63}Cu, ^{64}Zn and ^{65}Cu plotted as a function of the emitted proton energy E. The neutron bombarding energy was 14·1 Mev. The curves are displaced arbitrarily with respect to the ordinate scale for convenience.

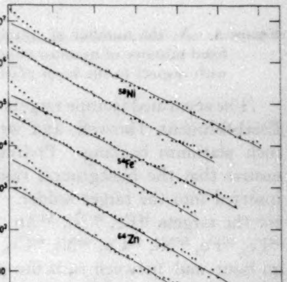

Figure 5. Curves giving $\sigma(E)/E\sigma_c$ obtained from measurements of the energy spectra of the protons from the (n, p) reaction in ^{58}Ni, ^{54}Fe and ^{64}Zn plotted as a function of E the energy of the emitted proton. The neutron bombarding energies were 15·7 and 12·9 Mev, the upper curve in each case corresponding to the higher bombarding energy. The curves are displaced arbitrarily with respect to the ordinate scale for convenience.

the values of $T_{\rm m}$ of the compound nuclei shown in table 1 were obtained from the slopes of these lines. The values of $T_{\rm m}$ shown in brackets in table 1 are the values at 13·0 and 15·7 MEV, the value at the lower neutron energy being given first. The values of the integrated cross sections $\sigma({\rm n, p})$ in table 1 were obtained by extrapolating the straight lines in figures 4 and 5 back to zero proton energy, and assuming that the angular distribution of the protons in the (n, p) reactions is isotropic. The rise in the experimental points above the straight line below 6 MEV proton energy is attributed at least partly to the reaction (n, np). The values of σ (n, p) in brackets in table 1 correspond to a neutron energy of 15·7 MEV. The relative errors in the values of σ (n, p) in table 1 at the same neutron energy are about ± 5% but the absolute value of the cross sections may be in error by as much as ± 20% due mainly to uncertainty in the absolute efficiency of counting protons from the targets. The errors in the values of $T_{\rm m}$ are only about ± 3% if the barrier transmission factor is not grossly wrong.

Table 1

Target isotope	^{27}Al	^{54}Fe	^{56}Fe	^{58}Ni
$T_{\rm m}$(MEV)	1·75	1·65(1·58; 1·76)	1·45	1·575(1·54; 1·74)
σ(n, p)(mbn)	90	333(561)	90	534(754)
$E_{\rm c}^*$ (MEV)	21·80	23·37(22·24; 24·96)	21·71	23·07(21·94; 24·66)

Target isotope	^{59}Co	^{60}Ni	^{63}Cu	^{64}Zn	^{65}Cu
$T_{\rm m}$ (MEV)	1·59	1·48	1·44	1·45(1·42; 1·54)	1·76
σ(n, p)(mbn)	75	158	149	257(344)	30
$E_{\rm c}^*$ (MEV)	21·56	22·60	21·98	22·00(20·87; 23·59)	21·07

The errors in the values of $T_{\rm m}$ are all about ± 3%. The errors in the absolute and relative values of σ(n, p) are about ± 20% and ± 5% respectively. σ(n, p) is essentially the cross section for emission of a proton from the compound nucleus (see text, § 3).

§ 4. EMPIRICAL RELATIONS

Table 1 summarizes our experimental results.

If we exclude ^{27}Al and ^{65}Cu the value of $E_{\rm c}^*/AT_{\rm m}^2$ is constant within the experimental errors in $T_{\rm m}$ over the narrow range of $E_{\rm c}^*$ and A (the atomic mass number of the compound nucleus) involved in these experiments. The average value excluding ^{27}Al and ^{65}Cu is:

$$E_{\rm c}^*/AT_{\rm m}^2 = 0{\cdot}158 \pm 0{\cdot}003\ {\rm MEV}^{-1} \qquad \ldots\ldots (1)$$

and the results are plotted as solid circles in figure 6.

It is not so obvious that there is a simple relation between the values of $\sigma({\rm n, p})$, but in figure 7(a) we have plotted $\log\,[\sigma({\rm n, p})/\{\sigma_{\rm r} - \sigma({\rm n, p})\}]$ against a quantity Δ. The values of $\sigma_{\rm r}$ were obtained from the results of Flerov and Tolyzin (1957). $\Delta = B_{\rm p} - B_{\rm n}$ for odd (proton)–odd (neutron) compound nuclei (open circles) and $\Delta = B_{\rm p} + P - B_{\rm n}$ for even–odd compound nuclei (full circles).

$$P = \tfrac{1}{2}B_{\rm p}(A+{\rm p}) + \tfrac{1}{2}B_{\rm p}(A-{\rm p}) - B_{\rm p}(A)$$

where $B_{\rm p}(A+{\rm p})$, $B_{\rm p}(A-{\rm p})$, $B_{\rm p}(A)$ are the binding energies of protons in the corresponding nuclei and A is the atomic mass number of the compound nucleus.

It can be seen from figure 7(a) that the empirical relation between the values of $\sigma(\mathrm{n, p})$ in table 1 can be expressed as:

$$\log\left[\frac{\sigma(\mathrm{n, p})}{\sigma_\mathrm{r}-\sigma(\mathrm{n, p})}\right]=\text{constant}-\frac{\Delta}{K} \qquad \ldots\ldots(2)$$

where K is roughly constant. The full line in figure 7(a) corresponds to a value for $K=1{\cdot}55$ which is the average value of T_m in table 1.

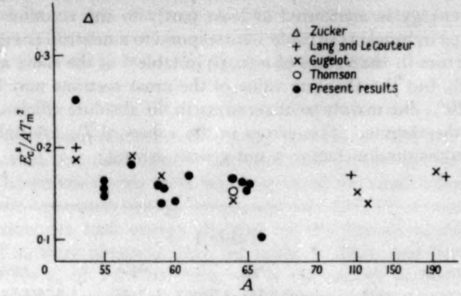

Figure 6.

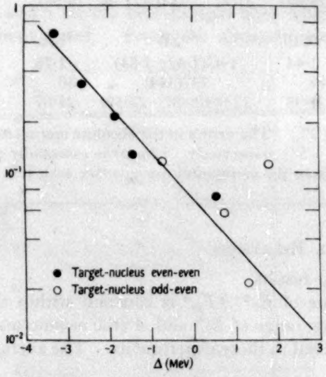

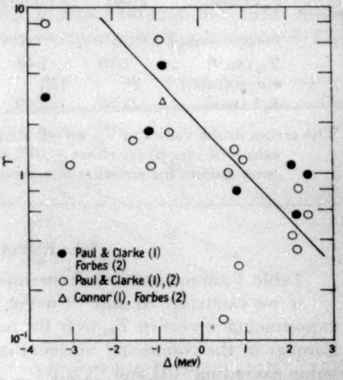

Figure 7(a). Υ the ratio $\sigma(\mathrm{n, p})/\sigma(\mathrm{n, n'})$ plotted as a function of $\Delta=B_\mathrm{p}-B_\mathrm{n}+P_\mathrm{p}$ where B_p and B_n are the binding energies of a proton and a neutron respectively in the compound nucleus and P_p is related to the pairing energy (see text).

Figure 7(b). Υ the ratio $\{\sigma_1(\mathrm{n}, \alpha)/\sigma_1(\mathrm{n,n})\}$ $\{\sigma_2(\mathrm{n, n'})/\sigma_2(\mathrm{n}, \alpha)\}$ plotted as a function of $\Delta=(B_{\alpha_1}-B_{\mathrm{n}1})-(B_{\alpha_2}-B_{\mathrm{n}2})$. B_n and B_α are the binding energies of a neutron and an alpha particle in the compound nucleus; the (1) and (2) refer to two neighbouring nuclei.

§ 5. EXPERIMENTAL RESULTS OF OTHERS

Before discussing our experimental results, we assemble here some of the experimental results of others in reactions involving the decay of compound nuclei. Without changing the published values we have rearranged the material to suit our purpose. (Energies and temperatures are in Mev, and A is the atomic mass number of the compound nucleus.)

In figure 8 we have redrawn Gugelot's (1954) measurements of proton spectra at 150° in (p, p′) experiments at an incident proton energy of 18·2 Mev. The direct effects at the higher proton energies are well known and have been studied by Cohen (1957). The values of T_m shown in table 2 below are taken from these spectra by drawing straight lines through the parts least likely to be affected by direct effects and multiple particle emission. For Sn, Pt and Al the errors in T_m are quite large but are probably only about ±5% in the others.

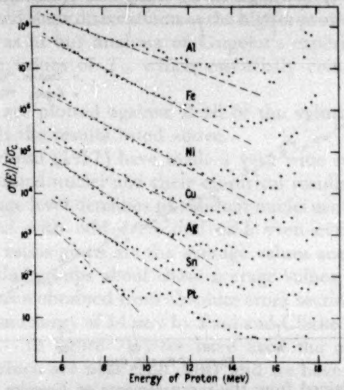

Figure 8. $\sigma(E)/E\sigma_c$ obtained from Gugelot's measurements of the energy spectra of the protons inelastically scattered from Al, Fe, Ni, Cu, Ag, Sn and Pt plotted as a function of E the energy of the emitted proton. The curves are arbitrarily displaced with respect to the ordinate scale.

Table 2

A	28	57	59	64	109	120	196
T_m	2·28	1·65	1·64	1·68	1·26	1·25	0·88
E_c*	27	29·5	26·6	26·1	26·5	26·3	26·5

The errors in T_m for $A=28$, 120, 196 are quite large but are probably only about ±5% in the others.

In figure 9 we have redrawn the results of Gugelot (1954) and Thomson (1957) for Cu(p, p′) and Cu(p, n) at incident proton energies of 18·2 Mev and 18·1 Mev respectively. From Thomson's measurements we find

$$A=64, \quad T_m=1{\cdot}73\pm0{\cdot}05, \quad E_c{}^*=28{\cdot}4.$$

Zucker (1958) has measured the energy spectra of protons and alpha particles from ^{41}Ca at an excitation energy of 39·3 Mev, formed by bombarding ^{27}Al by ^{14}N ions. We have plotted his results against emitted particle energy in figure 10. From the proton spectra we find $A=41$, $T_m=1{\cdot}68\pm0{\cdot}05$, $E_c{}^*=39{\cdot}3$.

Lang and Le Couteur (1954) have analysed the results of some experiments involving the decay of compound nuclei using the Weisskopf formulation. From their analysis they propose an expression for the nuclear equation of state, and use the parameters U and t. t is essentially our T_m and U is approximately $E_c^* - 8$ MeV. The values of E_c^*/AT_m^2 shown below were obtained by making these changes and using the results given by Lang and Le Couteur in their figure 3.

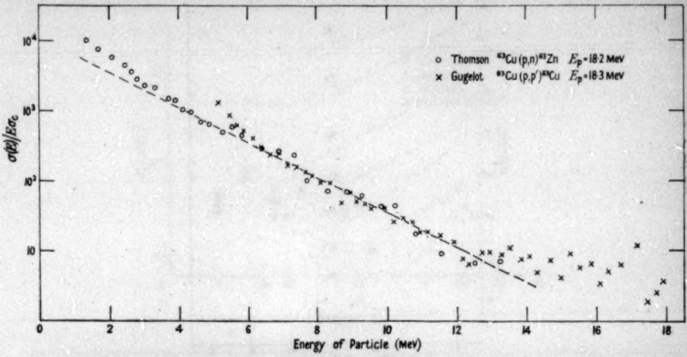

Figure 9. $\sigma(E)/E\sigma_c$ obtained from the measurements of Gugelot and Thomson plotted as a function of the energy of the emitted particle. The curves are displaced arbitrarily with respect to the ordinate scale.

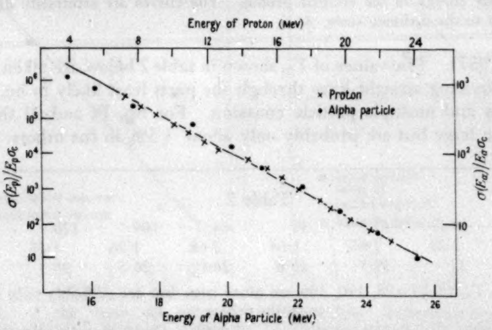

Figure 10. $\sigma(E)/E\sigma_c$ obtained from Zucker's measurements of the energy spectra of the protons and alpha particles emitted following the formation of the compound nucleus ^{41}Ca by ^{27}Al + ^{14}N plotted as a function of the energy of the emitted particle. The curves are displaced arbitrarily with respect to the ordinate scale.

(We have used the values of t obtained by them in their analysis of the experimental results.) The values of t obtained by Lang and Le Couteur have quite large experimental errors and to try to overcome this we have taken the average of the values of E_c^*/AT_m^2 obtained for the three values of A used by Lang and Le Couteur. For each value of A the scatter in the values of E_c^*/AT_m^2 corresponds roughly to the errors assigned by Lang and Le Couteur. The errors we have attached to the values of E_c^*/AT_m^2 are calculated on the basis that the scatter in individual values for the same A is due to random errors. They are:

A	28	104	201
E_c^*/AT_m^2	$0{\cdot}20 \pm 0{\cdot}05$	$0{\cdot}17 \pm 0{\cdot}03$	$0{\cdot}17 \pm 0{\cdot}05$

Jack and Ward (1960) have measured the energy spectra of protons emitted from separated isotope targets in the forward direction for 14 MEV neutrons. The spectra as expected show direct effects at the higher proton energies. Adopting the same procedure as in our analysis of Gugelot's experiments, the results of Jack and Ward give values of T_m which essentially coincide with the values given in table 1.

In figure 6 we have plotted against A all of the values of E_c^*/AT_m^2 which can be obtained from the results listed above.

Brown and Muirhead (1957) have made a very wide survey of the apparent level densities in residual nuclei and their empirical results can be expressed by stating that the average level densities of residual nuclei are in the ratio 1 : 5 : 5 : 12 for compound nuclei with odd–even : odd–odd : even–even : even–odd, protons and neutrons. The ratios given are the average values and there are quite large fluctuations in the four groups about these average values.

Figure 7(*b*) has been obtained from absolute cross sections for (n, α) reactions at an incident neutron energy of 14 MEV by Paul and Clarke (1953), Forbes (1952) and Conner (1953). In figure 7(*b*) we have used the cross sections in pairs choosing elements which are near each other and we have plotted

$$\log\left[\frac{\sigma_1(\mathrm{n},\alpha)}{\sigma_1(\mathrm{n},\mathrm{n}')}\frac{\sigma_2(\mathrm{n},\mathrm{n}')}{\sigma_2(\mathrm{n},\alpha)}\right] \quad \text{against} \quad \Delta$$

where $\Delta=(B_{\alpha 1}-B_{n1})-(B_{\alpha 2}-B_{n2})$ and $B_{n1(2)}$ and $B_{\alpha 1(2)}$ are the experimental binding energies of neutrons and alpha particles in compound nucleus 1 (2). We have neglected pairing energy effects and for some of the points in figure 7(*b*), $\sigma(\mathrm{n},\mathrm{n}')$ is equated to σ_r as we were unable to find a value for $\sigma(\mathrm{n},\mathrm{p})$. The results themselves are in such disagreement that it is doubtful whether it is worth being more precise at this time.

§ 6. DISCUSSION

The usual way of interpreting the results of experiments involving the emission of particles from excited Bohr type compound nuclei is the well-known theory attibuted to Weisskopf (1937). In this, a strictly valid general expression is first obtained for cross sections per unit energy in terms of the level density of the corresponding residual nuclei at the corresponding excitation energy. A second stage in the Weisskopf approach is not so strictly valid although it is generally thought to involve only rather weak assumptions concerning the capture cross section for the inverse reaction. In the second state, expressions for the level density are obtained using particular nuclear models and are inserted into the strictly valid general solution, the resulting expressions are then compared with experimental results. The most natural variable in following the Weisskopf procedure, both in the general expressions for level densities and in the analysis of experimental results, is the excitation energy E_R^* of the residual nucleus. Several authors (Colli *et al.* 1957, Thomson 1957, Gugelot 1954) have however pointed out that there appears to be more correspondence between the results of different experiments when the energy spectra of emitted particles are plotted against emitted particle energy E rather than the excitation energy E_R^* of the corresponding residual nucleus. It will be noticed that we also have preferred to carry out our analysis in terms of E rather than E_R^*. One reason for this is that we have found in practice that this is the most convenient and simple way of analysing and correlating the results. This does not mean that our results are in conflict with the strictly valid Weisskopf general solution, and our results can if wished be used as empirical data for the level density term in the general solution.

The interpretation of the results given here involves nuclear thermodynamics and will be given in a further theoretical paper. In this paper we shall limit ourselves simply to a discussion of the range of empirical validity of the expressions used in the analysis.

The results have been analysed by (i) fitting the spectra, after correction in the usual manner for surface barrier effects, with the form $\exp(-E/T_m)$ to extract values of T_m, (ii) fitting the values of T_m thus found with the relation $E_c^* \propto A T_m^2$ which has the form of the familiar Fermi gas law, (iii) the fitting of cross sections for neighbouring isotopes at similar excitation energies using expressions of the form $\exp[-(E_b+P)/T_m]$ where E_b is the experimental binding energy of the emitted particle in the compound nucleus and P is a pairing energy term added to smooth out variations in E_b due to pairing energy effects.

(The Maxwellian form, Fermi gas expressions and the use of pairing energy terms are of course not original, they have been used by previous authors.) We shall consider the three parts of our analysis in turn.

(i) Our own results are relatively independent of small variations in the choice of parameters in calculating σ_c and do not appear to be distorted by the types of direct effects which result in sharp structure. The proton energy region below about 6 MeV was not readily accessible due to target thickness and the onset of (n, np) reactions, and it would be interesting if further experiments were carried out at lower neutron energies to see whether the same analysis yields the expected values of T_m. While our own results and to some extent our analysis of the results of others are consistent with a Maxwellian, or near Maxwellian form, we feel that further experiments over a much wider range of E_c^* and A are required to examine whether the Maxwellian form is quite general. In such experiments it will be very important to avoid direct effects. As stated above, measurements by Jack and Ward of protons emitted at small forward angles from the same targets bombarded by 14 MeV neutrons show pronounced sharp structure and superficially are much more like the results of Gugelot for (p, p′) than our own results for (n, p) reactions. There appears to be a much greater contribution from direct effects in (p, p′) as compared with (n, p) reactions and it may be that this is generally true of reactions in which the incident particle is the same as the emitted particle. For this reason, and also because separated isotopes can be used and the barrier for emission is small we think that a study of (p, n) reactions will be profitable. The technical difficulties in (p, n) reactions are of course greater than in (n, p), but the trouble involved in developing suitable techniques may be justified by the scope and usefulness of the results.

The one example of an alpha particle spectrum (Zucker's) we consider appears to show a deviation from the Maxwellian form, and there appears to be a shortage of available results for alpha spectra. This may be due to the increased technical difficulties and we would like to draw attention to the recent discovery that the scintillation decay time of crystals of CsI(Tl) varies with density of ionization (Storey *et al.* 1958) and can be used to obtain mass selection in experiments

(Robertson and Ward 1958). We think this development may be of use in evolving efficient and accurate techniques for measurements of alpha spectra in the presence of other types of particles.

(ii) In the narrow region $A = 55$–70 where the values of T_m are known accurately the ratio E_c^*/AT_m^2 is probably constant. The high value of T_m for ^{65}Cu may be in error as the yield for this reaction in our experiments is low and the results are more susceptible to error due to background subtraction. The range of E_c^* and A involved is however small and again further experiments over a much wider range are required. For $A > 70$ the values of T_m may be significantly in error as the contribution from the direct effects appears to increase in heavier elements. For $A < 55$ the value of T_m obtained from our analysis of Zucker's experiment is very much smaller than the general trend of results for the other reactions which involve the capture of a single nucleon rather than the fusion of two nuclei. Perhaps this corresponds to the stimulation in the latter of more degrees of freedom, and further experiments of the latter type may show that this is generally true. We are not sure why our value of T_m for the light element Al is small and the apparent agreement between the other two points in figure 6 (for $A < 55$) and the general trend of results may be illusory, as the errors in these points are large.

Our analysis of Zucker's experiment suggests that if values of T_m for alpha spectra can be obtained they may be close to the expected value for neutrons and protons from the same compound nucleus.

(iii) Our measured values of integrated (n, p) cross sections shown in figure 7(*a*) are clearly well correlated using the form $\exp[-(E_b + P)/T_m]$ and we feel confident this will be found quite generally. We think that it may be possible to improve the correlation even more by calculating the pairing energy term more precisely. Our analysis of integrated (n, α) cross sections in figure 7 (*b*) is disappointing. This is partly due to our neglect of the pairing energy terms but is also due to the large discrepancies in measured values. A further point is that lack of data made it necessary to take the ratio between cross sections for nuclei which were further apart in the atomic mass scale than we would have preferred. It would be very interesting to repeat this analysis with greater care using more suitable and more accurate data. The correlation is figure 7 is very rough, but bearing in mind the factors stated above, is to some extent encouraging.

The empirical relation found by Brown and Muirhead can be fitted into the pattern of the present results by inserting average values for the pairing energy terms P. To illustrate this, if we let $T_m = 1{\cdot}55$ and $P_n = 0$ or 2, $P_p = 0$ or 2 as average values, the ratio of the terms $\exp[-(P_p - P_n)/T_m]$ is $1:3{\cdot}6:3{\cdot}6:13$ for odd–even; odd–odd; even–even; and even–odd compound nuclei.

§ 7. CONCLUSIONS

We have considered many experimental results and it appears to be possible to correlate them using relatively simple expressions. Within the very narrow range covered by our own experiments the results can be conveniently and fairly accurately summed up by stating that, almost without exception, they are consistent with the expression

$$\sigma(E)/\sigma_r \propto E\sigma_c \exp[-(E + E_b + P)/T_m]$$

where $E_c^*/AT_m^2 = 0{\cdot}158 \pm 0{\cdot}003$ Mev^{-1}. There may, however, be other factors in a general expression for $\sigma(E)$ which depend essentially on A and E_c^*, as we have limited our experiments and analysis largely to a comparison of neighbouring isotopes. The results of others are not inconsistent with our own results but many further experiments must be carried out over a much wider range of E_c^*, A, and type of emitted particle before this simple expression could be generally adopted on empirical grounds.

There is also an indication in the results of Zucker that the general trend of values of T_m may be found to be different for fusion reactions than for reactions involving capture of single nucleons.

The dependence of the cross sections on the pairing energy and the association of the correction with the binding energy may mean that in general the binding energies should be corrected to smooth out any sudden variations whatever the cause.

The purpose of experiments designed to avoid direct effects and study the emission of particles from compound nuclei is partly to establish general and accurate expressions which will allow the approach to be reversed and permit a more precise examination of direct effects. The operation of this procedure is illustrated on a small scale by comparing this present paper with that of Jack and Ward.

The results of experiments of the type described here are also, of course, of value in developing the theory of nuclear thermodynamics and this aspect of the results as stated above will be discussed in a further paper.

ACKNOWLEDGMENTS

One of us (R.S.S.) would like to acknowledge the receipt of an I.C.I. Fellowship, and another (W.J.) wishes to acknowledge the assistance of the Sir James Caird Travelling Scholarship Trust.

REFERENCES

ALLAN, D. L., 1957, *Proc. Phys. Soc.* A, **70**, 195.
BAME, S. J., JR., HADDAD, E., PERRY, J. E., JR., and SMITH, R. K., 1957, *Rev. Sci. Instrum.*, **28**, 997.
BLATT, J. M., and WEISSKOPF, V. F., 1952, *Theoretical Nuclear Physics* (New York: Wylie).
BROWN, G., MORRISON, G. C., MUIRHEAD, H., and MORTON, W. T., 1957, *Phil. Mag.*, **2**, 785.
BROWN, G., and MUIRHEAD, H., 1957, *Phil. Mag.*, **2**, 473.
COHEN, B. L., 1957, *Phys. Rev.*, **105**, 1549.
COLLI, L., FACCHINI, U., IORI, I., MARCAZZAN, A., and SONA, A., 1958, *Nuovo Cim.*, **7**, 400.
COLLI, L., FACCHINI, U., and MICHELETTI, S., 1957, *Nuovo Cim.*, **5**, 502.
CONNER, J. P., 1953, *Phys. Rev.*, **89**, 712.
FLEROV, N. N., and TALYZIN, V. M., 1957, *J. Nucl. Energy*, **4**, 529.
FORBES, S. G., 1952, *Phys. Rev.*, **88**, 1309.
GUGELOT, P. C., 1954, *Phys. Rev.*, **93**, 425.
JACK, W., and WARD, A., 1960, *Proc. Phys. Soc.*, **75**, in the press.
LANG, J. M. B., and LE COUTEUR, K. J., 1954, *Proc. Phys. Soc.* A, **63**, 259.
MARCH, P. V., and MORTON, W. T., 1958 a, *Phil. Mag.*, **3**, 143.
—— 1958 b, *Ibid.*, **3**, 577.
PAUL, E. B., and CLARKE, R. L., 1953, *Canad. J. Phys.*, **31**, 267.
ROBERTSON, J. C., and WARD, A., 1958, *Proc. Phys. Soc.*, **73**, 523.
STOREY, R. S., JACK, W., and WARD, A., 1958, *Proc. Phys. Soc.*, **72**, 1.
THOMSON, D. M., 1957, *Proc. Phys. Soc.* A, **69**, 447.
WEISSKOPF, V. F., 1937, *Phys. Rev.*, **52**, 295.
ZUCKER, A., 1958, *Nucl. Phys.*, **6**, 420.

The Influence of Temperature on the Eddy Current Anomaly Factor

By L. ALBERTS and B. J. SHEPSTONE
Physics Department, University of the Orange Free State, Bloemfontein, S. Africa

MS. received 22nd October 1959

Abstract. The difference between the classically calculated and measured value for the eddy current loss in magnetic sheet materials has been ascribed to the existence of a discrete domain structure in the material. In this investigation the theory has been tested by altering the domain structure in an iron specimen through raising the temperature up to the Curie point. The results indicate that in principle the domain hypothesis is correct. The influence of the applied frequency on the eddy current anomaly factor has also been measured and agrees with the qualitative deductions based on the domain model.

§ 1. INTRODUCTION

THE well-known classical expression for the eddy current loss in magnetic materials is based on a calculation for a magnetically isotopic material, i.e. uniformly magnetizable throughout the specimen (see, for instance, Bozorth 1952). The loss resistance in a coil with a core consisting of laminated rings, is given by

$$\Delta R = \frac{128\pi^3 N^2 A d^2 \mu_0^2 f^2 \times 10^{-9}}{\rho D(24 + 16\pi^4 d^4 \mu_0^2 f^2/\rho^2)} \text{ ohms},$$

where N is the number of turns, A the cross-sectional area of the core, μ_0 the initial permeability, f the frequency of the applied field, ρ the resistivity of the core material, D the mean diameter of the core and d the lamination thickness. The second term in the denominator is usually left out in textbooks. It is however of importance if the permeability is high, as is the case near the Curie temperature.

The discrepancy between the measured and the classically calculated value is known as the eddy current anomaly and the ratio of the two as the eddy current anomaly factor. Several authors have presented a calculation based on a domain model to account for the anomaly. Pry and Bean (1958) have deduced the following formula for the anomaly factor in magnetic sheet material:

$$\frac{\Delta R}{\Delta R_c} = \frac{96}{\pi^3}\frac{L}{d}\sum_{\substack{1 \\ n \text{ odd}}}^{\infty}\frac{1}{n^3}\coth\left(\frac{n\pi L}{d}\right)$$

where $2L$ is the observed domain width in a slab of thickness d.

Neurath (1959) and Hu and Wiener (1959) reported quantitative discrepancies between actual measurements and calculations based on the Pry–Bean formula. Carr (1959) and Neurath (1959) suggested that the number of domain walls moving at a given instant depends on the applied frequency, i.e. as the frequency of the applied magnetic field is raised more walls participate at a given instant. Such an effect would account for the Pry–Bean formula giving values for the eddy current anomaly factor that are too low.

In this investigation both the effect of domain wall spacing and the effect of applied frequency were tested in the following way. By heating the specimen under investigation the domain structure was altered and loss measurements were taken for varying frequencies and temperatures.

§ 2. Experimental Procedure

The material employed was in the form of rings cut from very high purity iron sheet prepared by Messrs. Johnson Matthey. Primary and secondary windings of wire, insulated with ceramic material, covered the iron rings, the latter being insulated from one another by thin mica sheets. Prior to the winding of the coils the rings were annealed for several days in an atmosphere of first wet and then dry hydrogen. This ensured the absence of surface oxidation layers, carbon impurities, etc. Moreover, as a result of the long period of annealing, no more grain growth took place during measurements at the higher temperatures. The final grain size was of the order of a millimetre.

For the purpose of measurement the specimen was raised to the required temperatures in an accurately temperature-controlled tubular oven through which a stream of purified hydrogen passed all the time. The loss resistance was determined by means of a sensitive a.c. bridge apparatus. The magnitude of the applied alternating magnetic field was kept well within the reversible region of the magnetization curve so that hysteresis losses could not occur. Values of the initial permeability, resistivity and resistance of coil windings were determined at each temperature without disturbing the specimen.

§ 3. Theoretical Considerations and Results

The variation of domain wall spacing with temperature, in a single crystal, can be calculated in principle if the corresponding temperature variations of the factors involved are known. The relevant assumption made in this investigation is that the variation of domain size with temperature in the polycrystalline specimen employed is the same as the corresponding variation in a single crystal specimen. According to the results of Bloor and Martin (1959) the calculations of domain size for single crystals apply reasonably well to polycrystalline specimens and thus favour the assumptions made.

The ratio of domain wall spacing to slab thickness in a single cubic crystal is given by (Kittel and Galt 1956)

$$\frac{2L}{d} = \frac{1}{d}\left(\frac{4\sigma_W h}{c_{11}\lambda_{100}{}^2}\right)^{1/2}$$

where (i) $\sigma_W = 2(KA)^{1/2}$ is the Bloch wall energy per unit area; with K the anisotropy constant and $A = 2Js^2/a$; where J is the exchange energy integral; $2s$ the number of unpaired electron spins in the atom and a the lattice constant, (ii) h is the length of the crystal along the axis of the easy magnetization, (iii) c_{11} is an elastic constant, (iv) λ_{100} the magnetostriction in the 100 direction, and (v) d the sheet thickness.

In calculating the variation of the ratio $2L/d$ with temperature the appropriate values for K and λ_{100} were taken from publications (Kittel 1949, Takaki 1937). The expressions for evaluating J (Kittel and Galt 1956) do not include temperature dependent factors and hence it is assumed to be temperature independent.

The sheet thickness does not vary appreciably in the temperature range under consideration and the rate of variation of c_{11} with temperature is taken to be the same as that of the ordinary elastic modulus for polycrystalline iron, the latter being obtainable from tables. A value of 1 mm, roughly that of the grain size, was taken for h. Since we are interested here in correlating the temperature variation of calculated and measured values rather than comparing the actual values themselves, this somewhat arbitrary choice for h is not important. It may be accepted that it did remain constant during the experiment since any effect that the elevated temperatures may have had on the growth of the crystallites was completed in the long period of annealing beforehand.

Other constants for the toroidal winding were as follows: $N = 85$; $A = 0{\cdot}2356\ \text{cm}^2$; $D = 3{\cdot}93$ cm; $d = 0{\cdot}1365$ mm.

Table of Eddy Current Loss Resistance as measured and calculated for a frequency of 1000 c/s

(1)	(2)	(3)	(4)	(5)	(6)	(7)	(8)	(9)	(10)
0	466250	19·5	2·42	8·59	923	10·28	1·291	7·96	3·481
200	300000	26	2·29	22·6	1040	3·76	0·6356	5·92	2·435
400	128750	31	2·08	43·1	1440	2·23	0·6412	3·45	1·836
600	17500	29	1·87	69·8	2550	2·58	1·243	2·08	1·432
620	6250	28	1·84	72·5	2740	2·71	1·381	1·96	1·297
700	→0	21·5	1·74	84·5	3900	3·82	2·391	1·60	→1·0
770	→0	—	1·65	95·1	12580	28·15	21·32	1·32	→1·0

(1) temperature (°c); (2) K (erg cm^{-3}); (3) $\lambda_{100} \times 10^6$; (4) $c_{11} \times 10^{-12}$ (erg cm^{-3}); (5) ρ (μ ohm cm); (6) μ_0 (gauss oersted^{-1}); (7) ΔR (experimental) (ohms); (8) ΔR_c (classical) (ohms); (9) $\Delta R/\Delta R_c$ (experimental); (10) $\Delta R/\Delta R_c$ (theoretical).

In figure 1 and the last two columns of the table the experimental and theoretical values for the eddy current anomaly factor are depicted. The calculated values tend to be lower than the experimental ones which is consistent with the findings

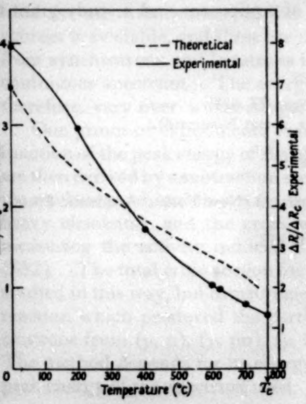

Figure 1. Variation of the anomaly factor with temperature for 1000 c/s.

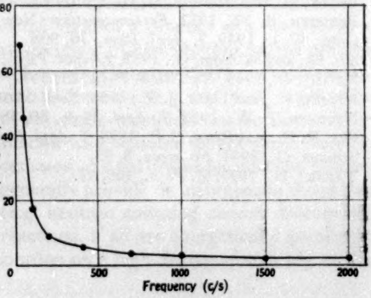

Figure 2. Variation of the anomaly factor with frequency at room temperature.

of previous investigators (Neurath 1959, Hu and Wiener 1959). The variation with temperature exhibits a fair correlation indicating that as the domain size decreases with rise in temperature the anomaly factor approaches unity. One would not necessarily expect it to actually reach unity in practice since, even if the domain widths become vanishingly small near the Curie point, there are bound to be slight inhomogeneities in the material that would cause an anomaly factor greater than unity (Sorger 1954). The above curves are typical for other frequencies. In figure 2 the influence of the frequency on the anomaly factor is depicted. According to Carr (1959) the number of domain walls simultaneously in motion depends strongly on applied frequency, being small as the frequency approaches zero and as it becomes high all the walls participate simultaneously in the magnetization process. Thus at low frequencies, the effective wall spacing is larger, and this would give a greater value for the anomaly factor (see the Pry–Bean formula). Carr's work is at present not in a form where it lends itself to a quantitative test but the curve in figure 2 does add weight to his arguments.

§ 4. SUMMARY AND CONCLUSIONS

These investigations indicate that the existence of a discrete domain structure in magnetic materials accounts in principle for the eddy current anomaly or part thereof. The influence of temperature on the eddy current anomaly factor, as calculated for a corresponding temperature variation in domain size, does show a fair correlation with the measured values. The frequency of the applied magnetic field has an influence on the loss factor. The domain model also lends itself to an explanation of this phenomenon. The main requirement at this stage is the necessity of bringing the theory into quantitative alignment with the experimentally determined values.

ACKNOWLEDGMENTS

It is a pleasure to thank the South African Council for Scientific and Industrial Research for financial support in procuring of equipment and a study grant to one of us (B.J.S.).

REFERENCES

BLOOR, D., and MARTIN, D. H., 1959, *Proc. Phys. Soc.*, **73**, 694.
BOZORTH, R. M., 1952, *Ferromagnetism* (New York : van Nostrand).
CARR, W. J., 1959, *J. Appl. Phys.*, **30**, 90S.
HU, H., and WIENER, G., 1959, *J. Appl. Phys.*, **30**, 86S.
KITTEL, C., 1949, *Rev. Mod. Phys.*, **21**, 541.
KITTEL, C., and GALT, J. R., 1956, *Solid State Physics*, **3** (New York : Academic Press).
NEURATH, P. W., 1959, *J. Appl. Phys.*, **30**, 88S.
PRY, R. H., and BEAN, C. P., 1958, *J. Appl. Phys.*, **29**, 532.
SORGER, G., 1954, *Frequenz*, **8**, 83.
TAKAKI, H., 1937, *Z. Phys.*, **105**, 92.

The Photodisintegration of Nitrogen

By D. BALFOUR† and D. C. MENZIES‡
Department of Natural Philosophy, University of Glasgow

MS. received 14th August 1959, in final form 15th October 1959

Abstract. The (γ, p), (γ, n), (γ, pn) reactions in nitrogen are studied. A cloud chamber, operating at a pressure of about 40 cm of mercury, was exposed to a bremsstrahlung beam from the 340 MeV Glasgow synchrotron, and the energy and angular distributions of the recoil nuclei from the reactions $^{14}N(\gamma, p)^{13}C$, $^{14}N(\gamma, n)^{13}N$, and $^{14}N(\gamma, pn)^{12}C$ were measured. The results are compared with the distributions to be expected from several nuclear models, and it is concluded that Wilkinson's model describes the (γ, p) and (γ, n) reactions satisfactorily, while the (γ, pn) reaction appears to proceed either by a statistical or a knock-on process. No evidence is found to suggest that many of the observed (γ, pn) events could be explained by Levinger's quasi-deuteron model.

§ 1. Introduction

Several models have been proposed (e.g. Wilkinson 1956, Courant 1951, Levinger 1951, Goldhaber and Teller 1948) to describe the photodisintegration process, but none has been completely successful. Since the validity of each model depends on the energy of the photon involved, a critical test of a model must include a measurement of this quantity. A homogeneous source, such as the γ-rays from a nuclear reaction (e.g. $^7Li(p, \gamma)^8Be$) would be ideal for an investigation of this type, but only a limited number of suitable sources is available, and these are normally weak. The bremsstrahlung radiation from synchrotrons and betatrons is much more intense, but is in the form of a continuous spectrum. The energy of the photon causing a particular event can, therefore, vary over a wide range, and must be measured by some other means.

One group of experiments examines the yield of a product of a reaction as a function of the peak energy of the photon spectrum. Cross sections for the process are then derived by a subtraction method (Katz and Cameron 1951). For example, the nucleus produced in certain reactions is radioactive (e.g. the (γ, n) reaction in heavy elements), and the cross section for these reactions can be derived by measuring the activity induced by radiation in a suitable target (e.g. Horsley 1952). The total cross section for the emission of a particular particle can also be studied in this way, but measurements generally provide no information about the reaction which produced the particle (e.g. neutron counting cannot distinguish neutrons from (γ, n), (γ, pn), $(\gamma, 2n)$ reactions, if all are energetically possible). The method depends for its energy resolution on a high degree of stability in the peak energy of the spectrum used.

---

† Now at A.E.I. Research Laboratories, Aldermaston Court, Aldermaston, Berks.
‡ Now at Atomic Energy Research Establishment, Dounreay, Caithness.

A second group of experiments has been devoted to the study of the energy and angular distributions of the particles emitted by a target irradiated by a continuous bremsstrahlung spectrum. In some cases it is possible to infer the energy of the photons responsible for a group of particles (e.g. Wright *et al.* 1956), and to identify the reaction, but this is not always so, since all the fragments from a disintegration are seldom detected. It is usually necessary to use a detector external to the target, and the energy resolution is therefore degraded by the passage of the emitted fragments through the target, and other matter before the detector is reached. Nevertheless, much useful information has been gathered in this way, using nuclear emulsions and counter systems as detectors.

These drawbacks are largely overcome by the use of a visual detector, such as a cloud chamber. Since the track of a charged particle can be recorded from its origin, there is no degradation of the energy. All charged particles are detected, and can be identified fairly easily, thus dispelling most of the doubt as to which reaction is occurring. Unfortunately, because of the low stopping power of the gas filling, energetic particles will generally leave the sensitive volume of the chamber, making a study of their energy by range measurements impossible. On the other hand, many nuclear reactions result in the formation of heavy fragments (e.g. recoil nuclei) which have a short but measurable range, and will remain within the confines of the chamber. Much information can be obtained by a study of the energy and angular distribution of these recoils.

This paper reports the results of a study of the recoil nuclei from the (γ, p), (γ, n), and (γ, pn) reactions in nitrogen, using a cloud chamber. The chamber was filled to a pressure of $\frac{1}{2}$ atmosphere with cylinder nitrogen of commercial purity and was irradiated with photons from the 340 MEV Glasgow synchrotron in a bremsstrahlung spectrum with a maximum energy of 200 MEV. This peak energy was chosen since the short range of the recoil nuclei made it possible to study them over a very wide energy range, and the low operating pressure further reduced the stopping power of the chamber gas, so that the recoil tracks were sufficiently long for accurate measurement. In addition, the yield of reactions resulting from a 200 MEV peak bremsstrahlung was sufficient to produce reactions at each expansion.

§ 2. APPARATUS AND METHOD

An expansion chamber of conventional design, was used in this experiment. The cloud chamber was expanded and the collimated beam from the synchrotron was passed through a 0·0005 in. mylar window into the sensitive volume. Some 80 msec later the resulting events were photographed by firing two Mullard LSD16 flash tubes. The collimator, cloud chamber, and electronic equipment are all described elsewhere (Atkinson *et al.* 1957).

Three cameras were used, mounted so that their image planes all coincided, and were parallel to, and 70 cm above, the chamber base. They were fixed at the vertices of an equilateral triangle, of side 20 cm, and the axis of each lens was displaced from the centre of the film so that the image it formed filled the whole width of the 60 mm film used.

The conventional method of analysis by reprojection is unrivalled in its speed of interpretation and accuracy, provided that the tracks to be measured are longer than 2–3 cm. Since few of the tracks in this experiment were as long as this, a more accurate method was adopted which made use of a microscope. It is possible to calculate from microscope measurements alone the range and spatial angles of any track, but this process is time consuming and liable to large errors. The microscope was therefore used only to measure the length and direction of each film image of every track, and the orientation in a reprojection system of an 'artificial track' was used to relate these quantities to the real dimensions of the track in space. The accuracy of the ranges determined in this way, ± 0·05 cm for any length, is limited only by the dimensions of the film image of the track. Since a reprojection system was used, long tracks could be measured independently by that method and excellent agreement was obtained with the results obtained from microscope measurements.

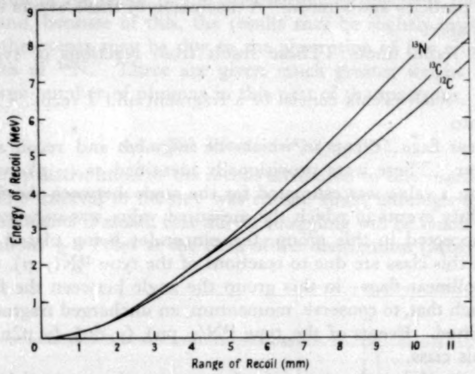

Figure 1. The range–energy relations for ^{13}N, ^{13}C and ^{12}C recoils used in this experiment.

The (γ, p), (γ, n), and (γ, pn) reactions in nitrogen result in the formation of ^{13}C, ^{13}N and ^{12}C recoil nuclei and range–energy relations for these particles were therefore required. Few data have been published on this subject (Blackett and Lees 1933, Lillie 1952 Feather 1935, Wrenshall 1940). Since Lillie's results cover the range of energies observed in this experiment, they were employed to synthesize the curves used (figure 1). Lillie quotes relations for ^{13}C and ^{11}B, and the following assumptions were made to provide relations for ^{12}C and ^{13}N:

(i) The formula

$$R_m(E) = \frac{m}{m_0}\left(\frac{Z}{Z_0}\right)^2 R_{m_0}\left(\frac{m}{m_0}E\right),$$

where m, E, Z are the mass, energy, and charge of a particle, m_0, Z_0 refer to a second particle, and $R_m(E)$ is the range of a particle of mass m and energy E, holds for recoil nuclei of this type.

(ii) The charges on ^{13}C and ^{12}C recoils of the same velocity are equal.

(iii) The ratio of the charges on nitrogen and carbon recoils is equal to the corresponding ratio for carbon and boron, if all are travelling at the same speed.

The first two assumptions are easily acceptable, but the third may require some justification. It would perhaps be more correct to include a factor in the form of the ratio of the squares of the atomic numbers concerned, but since this quantity is almost equal for the cases considered ($7^2:6^2=1\cdot 37$ and $6^2:5^2=1\cdot 44$) it was decided to ignore it.

The curves obtained in this way (figure 1) agree satisfactorily with the published low energy data and with some high energy data (Lalovic and Reid 1958, private communication).

§ 3. CLASSIFICATION OF THE OBSERVED EVENTS

Each photograph was examined with a low power microscope and all events were recorded. They were then measured, and classified as follows:

(i) Stars: This class included all events involving the emission of two or more charged particles and a recoil. A discussion of these events is beyond the scope of this paper.

(ii) Single recoil tracks: These result from reactions of type $^{14}N(\gamma, n)$, $(\gamma, 2n)$, etc.

(iii) Flags: Such events consist of a fragment and a recoil. The group is sub-divided into

(*a*) Collinear flags: events in which the fragment and recoil appear to be almost collinear. These were provisionally identified as (γ, p) events, and on this assumption a value was estimated for the angle between the fragment and the recoil. Only events in which the measured value was consistent with this were finally accepted in this group, the remainder being placed in class (*b*). The events in this class are due to reactions of the type $^{14}N(\gamma, p)$, (γ, d).

(*b*) Non-collinear flags: in this group the angle between the fragment and the recoil is such that, to conserve momentum, an uncharged fragment must also have been emitted. Events of the type $^{14}N(\gamma, pn)$, (γ, dn), $(\gamma, p2n)$ etc. will be included in this class.

(*c*) Events involving the emission of an α-particle. α-particle tracks were distinguished from those of protons by their density. The group includes events from the (γ, α) and $(\gamma, \alpha n)$ reactions: some of these could be positively identified with the reaction $^{14}N(\gamma, \alpha)$ since both fragments stopped within the sensitive volume of the chamber, and it was therefore possible to compute a momentum balance.

§ 4. RESULTS

In this paper three reactions have been studied particularly, namely $^{14}N(\gamma, p)^{13}C$, $^{14}N(\gamma, n)^{13}N$, and $^{14}N(\gamma, pn)^{12}C$. It is assumed that group (ii) above consists mainly of (γ, n) events and very few $(\gamma, 2n)$ events. Measurements have shown that the cross section for the second reaction is small (Panofsky and Reagan 1952) and the assumption therefore appears to be reasonable.

Group (iii) (*a*) was assumed to contain a preponderance of (γ, p) events since it was found quite impossible to distinguish between protons and deuterons which did not terminate in the sensitive volume of the chamber. The assumption is justifiable since the number of deuterons is expected to be small from consideration of isotopic spin (Burcham 1955), and this has been observed (Wright *et al.* 1956) using a peak photon energy of 23 MEV.

Any effect due to deuterons in group (iii) (*b*) was also neglected, and these events were all identified with the (γ, pn) reaction.

With these assumptions it was possible to assess the relative integrated cross sections for these reactions:

Group	Reaction	Number	Relative number
(ii)	$^{14}N(\gamma, n)^{13}N$	627	1·18
(iii) (*a*)	$^{14}N(\gamma, p)^{13}C$	528	1·00
(iii) (*b*)	$^{14}N(\gamma, pn)^{12}C$	786	1·49
(iii) (*c*)	$^{14}N(\gamma, \alpha)^{10}B$ $(\gamma, \alpha n)$ etc.	28	0·05

No account of the shape of the bremsstrahlung spectrum has been taken at this stage, and, because of this, the results may be slightly misleading, since a number of the events may be due to the absorption of low energy X-rays into excited states of ^{14}N. These are given much greater weight because of the relatively large number of photons in this part of the spectrum.

4.1. *The Reaction* $^{14}N(\gamma, p)^{13}C$

The energy distribution of the recoils attributed to this reaction is shown in figure 2. The interval of 0·2 MeV was chosen since, although the error due to range measurements is small, that due to straggling will be much larger, and will amount to about ± 0·1 MeV at the peak of the distribution (Morrison 1958).

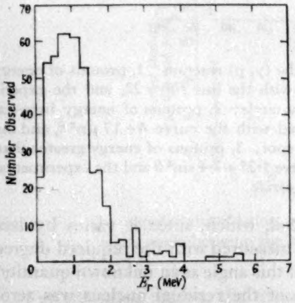

Figure 2. The energy distribution of the recoil nuclei from the reaction $^{14}N(\gamma, p)^{13}C$.

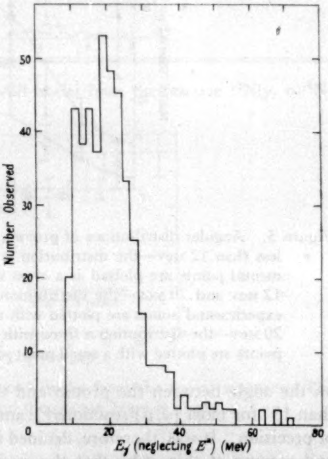

Figure 3. The distribution of the energy of the photons absorbed, in the reaction $^{14}N(\gamma, p)^{13}C$, assuming that the residual nucleus is formed in its ground state.

The energy of the emitted proton was calculated from the energy and direction of the recoil. The kinematics of the system are such that three independent equations can be derived to relate the energy and momentum of all the particles involved. Since only three parameters are unknown (proton energy, photon energy, and the state of excitation of the residual nucleus) it would appear that the problem can be solved exactly. Unfortunately, the solution depends critically on the angle between the proton and the recoil, which, since it varies by less than 15° for most (γ, p) reactions†, cannot be measured with the required degree of precision. It was, therefore, decided to treat this angle as an unknown quantity, and assume at this stage that the excitation of the residual nucleus was zero. On this basis, the energy of the photon responsible for each reaction was calculated: the resultant histogram is shown in figure 3.

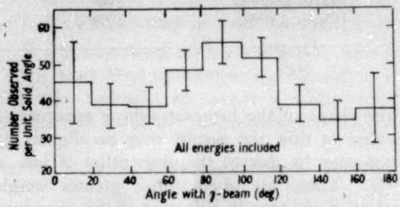

Figure 4. The angular distribution of all protons from the (γ, p) reaction, with respect to the photon beam direction.

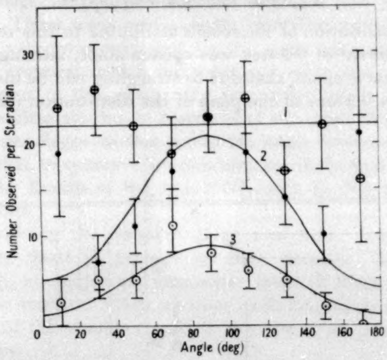

Figure 5. Angular distributions of protons from the (γ, p) reaction: 1, protons of energy less than 12 MeV—the distribution is fitted with the line $f(\theta) = 22$, and the experimental points are plotted as a cross within a circle; 2, protons of energy between 12 MeV and 20 MeV—the distribution is fitted with the curve $4 + 17 \sin^2 \theta$, and the experimental points are plotted with a large spot; 3, protons of energy greater than 20 MeV—the distribution is fitted with the curve $1{\cdot}25 + 7{\cdot}4 \sin^2 \theta$ and the experimental points are plotted with a small point within a circle.

---

† i.e. for photon energies between 15 and 200 MeV; larger variations are possible if absorption energies just above the threshold are included, but in such cases the recoil ranges are too short for accurate measurement.

The angular distributions of the protons from the (γ, p) reactions are shown in figures 4 and 5. Figure 4 shows all the observed protons, figure 5 shows the distributions for protons of different energy. All the distributions show the number of protons emitted per steradian.

4.2. *The Reaction* $^{14}N(\gamma, n)^{13}N$

The energy distribution of the recoils from this reaction is shown in figure 6, the energy resolution being the same as in the (γ, p) case. Further interpretation of these results is difficult, since the emitted neutron was not detected, and it was therefore seldom obvious which end of the recoil track corresponded to the origin of each event. Thus it was impossible to calculate accurately the energy of the emitted neutron, or of the photon responsible for the reaction.

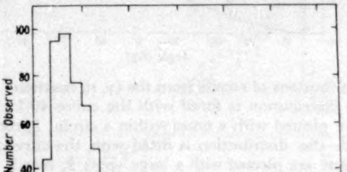

Figure 6. The energy distribution of the recoil nuclei from the reaction $^{14}N(\gamma, n)^{13}N$.

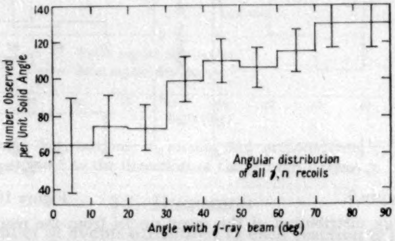

Figure 7. The angular distribution of all recoil nuclei from the (γ, n) reaction. The acute angle between the recoil and the photon beam is plotted.

For the same reason, the measured angular distributions were ambiguous: it was assumed that, as for the (γ, p) reaction, the angular distributions would be symmetric about 90°. The acute angle between the recoil and the x-ray beam was plotted, and the resulting distributions are shown in figures 7 and 8. Figure 7 includes all events, and figure 8 shows the angular distributions for recoils in certain energy ranges.

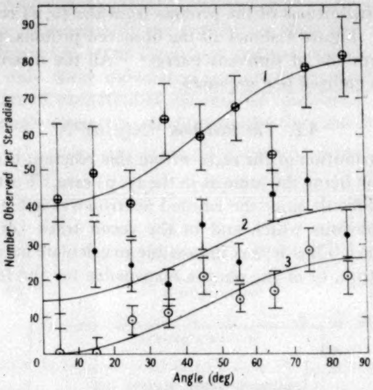

Figure 8. Angular distributions of recoils from the (γ, n) reaction: 1, recoils of energy less than 1 MeV—the distribution is fitted with the curve $40(1+\sin^2\theta)$ and the experimental points are plotted with a cross within a circle; 2, recoils of energy between 1 MeV and 2 MeV—the distribution is fitted with the curve $15+25\sin^2\theta$, and the experimental points are plotted with a large spot; 3, recoils of energy greater than 2 MeV—the distribution is fitted with the curve $26\sin^2\theta$, and the experimental points are plotted with a spot within a circle.

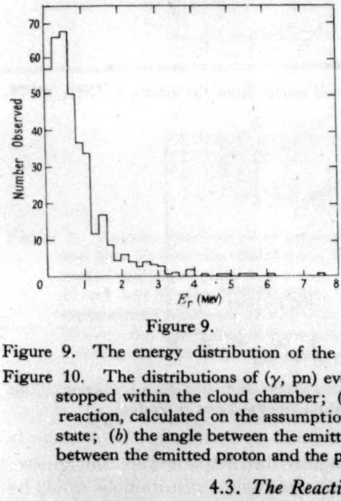

Figure 9.

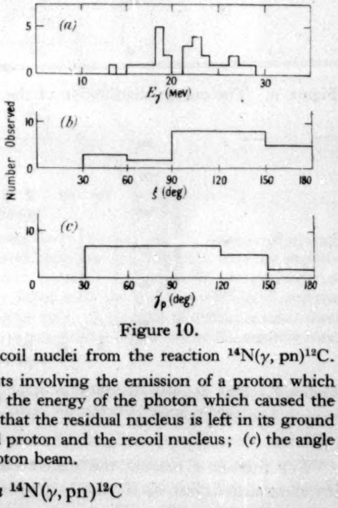

Figure 10.

Figure 9. The energy distribution of the recoil nuclei from the reaction $^{14}N(\gamma, pn)^{12}C$.

Figure 10. The distributions of (γ, pn) events involving the emission of a proton which stopped within the cloud chamber; (*a*) the energy of the photon which caused the reaction, calculated on the assumption that the residual nucleus is left in its ground state; (*b*) the angle between the emitted proton and the recoil nucleus; (*c*) the angle between the emitted proton and the photon beam.

4.3. *The Reaction* $^{14}N(\gamma, pn)^{12}C$

The (γ, pn) events can be divided into two groups: (i) events involving the emission of a slow proton which stopped inside the sensitive part of the chamber, (ii) events from which the proton left the cloud chamber. In the first group, it is possible to solve the kinematical equations exactly, and, assuming that the residual nucleus is left in its ground state, to calculate the energy of the photon responsible. Unfortunately, only 30 events fall into this class: the energy and angular distributions relating to these events are shown in figure 10.

The recoil energy distribution for all the (γ, pn) events is shown in figure 9. The form is similar to those (γ, p) and (γ, n) reactions, but the peak occurs at a much lower energy.

Various angular distributions were compiled for this reaction; figure 11 shows the angle between the proton and the recoil tracks (the observed number per 10° interval has been plotted in this case). Figure 12 shows the angular distributions of the protons and recoils with respect to the photon beam.

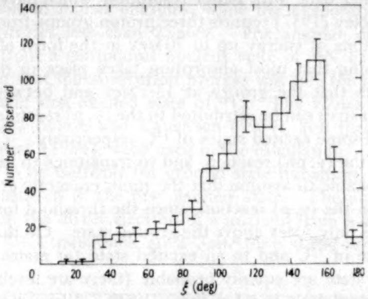

Figure 11 The angular distribution of protons from (γ, pn) events, with respect to the direction of the recoil nucleus.

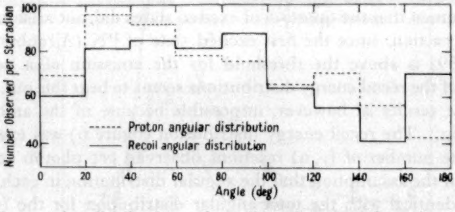

Figure 12. The angular distributions of recoils and protons from (γ, pn) events, with respect to the direction of the photon beam.

§ 5. DISCUSSION

The relative number of events attributed to each reaction is in general agreement with the consideration that the Coulomb barrier in a light nucleus, such as nitrogen, is small, and proton emission therefore is not strongly suppressed in favour of neutron emission. The emission of α-particles is expected to be forbidden at low energies (< 25 MEV) by isotopic spin selection rules (Burcham 1955) and this is borne out in the table.

5.1. *The Reactions* $^{14}N(\gamma, p)^{13}C$ *and* $^{14}N(\gamma, n)^{13}N$

These reactions are discussed together since both involve the absorption of a photon followed by the emission of a single nucleon by a nucleus consisting of equal numbers of protons and neutrons. The charge independence of nuclear forces suggests that the general characteristics of these reactions should be similar, and this is observed.

The variation of the cross sections of these reactions with energy is of some importance, and is not easy to measure accurately over a wide range. Its exact calculation from the above results is not possible, but by using certain simplifying assumptions, curves showing this variation were obtained.

It has already been observed that the total energy involved in a (γ, p) reaction cannot be computed with certainty since the energy state of the residual nucleus is unknown. A correction, for the effect of the excited states of ^{13}C can be made from a study of other data, with better resolution, which have been published on this reaction. Livesey (1957) reports three proton groups from the irradiation of nitrogen with photons of energy up to 70 MeV in the form of a bremsstrahlung spectrum. Assuming that most absorption takes place in the giant resonance region, he suggests that the groups at 13·7 MeV and between 9·5 and 11 MeV (which are equal in size) can be attributed to the (γ, p) reaction, being transitions to the ground, and some excited states of ^{13}C respectively. The third group, he suggests, is due to the (γ, pn) reaction, and to transitions to higher energy states of ^{13}C. It is reasonable to assume that the more energetic groups include most of the protons from the (γ, p) reaction, since the threshold for the emission of a neutron from ^{13}C is only 5 MeV above the ground state. On this basis, transitions to the ground state of ^{13}C and to an excited state (or states) at about 3·5 MeV above the ground state are equally probable (there are levels at 3·09, 3·68 and 3·86 MeV, Ajzenberg-Selove and Lauritsen 1959). Using this fact, the relative number of (γ, p) reactions observed per photon energy interval was calculated from the distribution shown in figure 3.

It was assumed that the question of excited states did not arise in the analysis of the (γ, n) reaction, since the first excited state of ^{13}N (Ajzenberg-Selove and Lauritsen 1959) is above the threshold for the emission of a neutron. The simple shape of the recoil energy distributions seems to bear this out. The precise analysis of the results is, however, impossible because of the ambiguity in the recoil direction. The recoil energy distribution (figure 6) was examined statistically, and the number of (γ, n) reactions observed per photon energy interval was derived on the assumption that the angular distribution in each recoil energy interval was identical with the total angular distribution for the (γ, n) reaction (figure 7). The kinematical methods which were used in the study of the (γ, p) reaction were again applied here.

Thus the relative number of events observed per photon energy interval for these reactions was obtained. The number of photons $N(E)$ of energy E in each energy interval dE was assumed to be given by

$$N(E)\,dE = k\,dE/E$$

and the variation with energy of the cross sections of ^{14}N for the $^{14}N(\gamma, p)^{13}C$ and $^{14}N(\gamma, n)^{13}N$ reactions was calculated. Figure 13 shows this variation, normalized to the peak value of the (γ, n) cross section quoted by Horsley, Haslam and Johns (1952).

The angular distributions of the nucleons from the (γ, p) and (γ, n) reactions are shown in figures 4, 5, 7 and 8. The distributions are of the general form $A + B\sin^2\theta$, and it will be seen that the ratio of $B:A$ increases with the energy of the particles considered. This trend can be explained by the following considerations.

The photodisintegration process can be thought of as an interaction between a photon and one nucleon in a definite state in the nucleus (Wilkinson 1956). The nucleon is raised into a higher energy single particle state, and may either escape directly from the nucleus, or interact with it so that the single particle state degenerates into a compound nucleus state. The compound nucleus then de-excites by the statistical evaporation of a nucleon. The relative probability of these channels has been estimated by Wilkinson (1956). His formula suggests that the two processes should be comparable at about 25 Mev, the direct process being more probable at higher energies, while the evaporation process should predominate at energies less than 25 Mev. The angular distributions of the nucleons emitted from a compound nucleus state of ^{14}N have been calculated (on the assumption that the absorption process was E1) for reactions leading to the ground state, and first excited state of ^{13}C. The values of spin and parity quoted by Ajzenberg-Selove and Lauritsen (1959), and the Racah coefficients quoted by Sharp *et al.* (1954), were used in the calculation. The most probable forms were found to be isotropic for ground state transition, and either $1+\cos^2$ for $2+\sin^2$ for transitions to the first excited state. The angular distributions to be expected from the direct ejection of a nucleon from a shell model state in the nucleus for $L-L+1$ transitions, are $2-3\sin^2$ for p–d and $\sin^2$ for s–p transitions (Courant 1951).

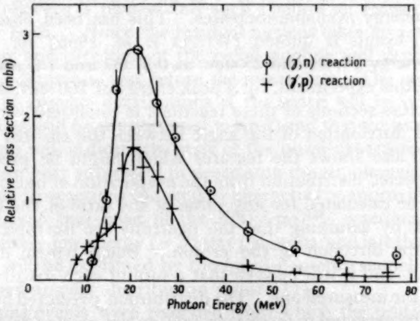

Figure 13. The relative cross sections for the reactions ^{14}N(γ, p)^{13}C and ^{14}N(γ, n)^{13}N.

Thus experimental distributions can be interpreted as follows† :

(*a*) $A+B\sin^2\theta$. A value of $B/A>1/2$ indicates the presence of at least some direct emission.

(*b*) $A+B\cos^2\theta$. This indicates the presence of at least some compound nucleus emission. If $A=B$, there can be no direct emission.

(*c*) Isotropic. Either the emission is purely from a compound nucleus state, or the coefficient of a $\cos^2$ term from such emission is equal to that of the $\sin^2$ term from the direct process.

The magnitude of the ratio $B:A$ can therefore be taken as an indication of the relative amounts of direct and evaporation emission. The experimental value for low energy protons is $0\pm0{\cdot}2$ and rises to about 6 ± 2 for protons of energy greater than 20 MeV. For neutrons, the behaviour is similar: the recoils of energy less than 1 MeV (i.e. energy of neutron < 13 MeV) give $B:A = 1 \pm 0{\cdot}2$, the ratio increases to $1{\cdot}5 \pm 0{\cdot}4$ for all recoils of energy between 1 and 2 MeV, and the value of A is $0 \pm 0{\cdot}4$ for recoils of energy greater than 2 MeV. The distributions therefore indicate that the reactions proceed by a mixture of direct and compound nucleus channels, the latter only being important at low excitation energies (i.e. < 30 MeV), which is consistent with Wilkinson's description of the process.

---

† It is assumed here that the direct and compound nuclear processes are incoherent.

5.2. *The Reaction* ^{14}N(γ, pn)^{12}C

The photoemission of a proton and a neutron by a nucleus can usefully be envisaged in three ways: (i) A quantum interacts with a neutron, which then collides elastically with a proton (or vice versa), both then escaping from the nucleus. (ii) A quantum interacts with a single nucleon, which then suffers several collisions, forming a compound nucleus state. The nucleus then de-excites by the successive emission of a proton and a neutron. (iii) A quantum interacts with a 'quasi-deuteron' sub-unit of the nucleus, giving sufficient energy to both the associated particles for them to escape independently from the nucleus.

In the first two cases, since the mode of absorption is the same as that described for the (γ, p) and (γ, n) reactions, the general shape of all three cross-section curves should be similar. However, since more energy is required for this reaction, the absorption of a low energy photon will tend to result in the emission of a single nucleon, the emission of two particles becoming more and more probable as the energy available increases. This has been observed; the ratio of (γ, p), (γ, pn) events is quoted (Wright *et al.* 1956) for bremsstrahlung spectra of peak energy 19, 21 and 23 MeV, as 0·3, 0·7 and 1·0 respectively. The value obtained in this experiment, for a peak energy of 200 MeV, is 1·5. Thus the variation of the cross sections of these reactions is consistent with these models.

The observed distribution of the angle between the emitted proton and the recoil (figure 11) also shows the features which might be predicted by these models. The expected distribution from the evaporation of one nucleon followed by a second can be calculated for any value of the ratio of the momenta of the emitted nucleons, by assuming that the neutrons are isotropically distributed with respect to the direction of the proton. Some typical distributions are shown in figure 14, and it will be seen that a sum of such distributions will give a result similar to the measured one. The distribution predicted by the 'knock-on process' will also be expected to favour strongly angles greater than 90°. An angle smaller than 90° from this model would require that the secondary nucleon have a momentum greater than that of the primary nucleon, after its interaction with the incident photon, which, since the second nucleon is in a bound state, is improbable.

The recoil energy distribution (figure 9) can be explained qualitatively by the knock-on, or the evaporation model. The distributions should be similar in shape to those from the single nucleon reactions but should peak at a lower energy, since the average energy absorbed from the γ-ray is the same in all cases, but this energy is distributed between three particles in the (γ, pn) reaction. It should perhaps be pointed out that, for the evaporation process, since the decay is purely statistical, the most probable values of the proton, neutron and recoil momenta should be equal. The most probable recoil momentum corresponds to an energy of about 0·4 MeV and the corresponding proton or neutron energy is

5 Mev. Assuming that the sum of these is the most probable value of the energy released in this reaction, the peak in the cross section should lie at about 23 Mev. This agrees with the measured values for the (γ, p) and (γ, n) reactions. Thus both these models can explain in general all the experimental results.

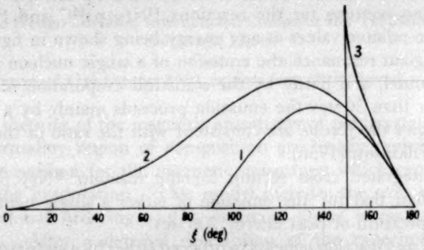

Figure 14. Forms of the angular distribution for the angle between the proton and recoil from the reaction $^{14}N\ (\gamma, pn)^{12}C$ which might be predicted by a statistical model. Curve 1 is calculated for the emission of protons and neutrons of equal momentum, curve 2, for the emission of a fast neutron and a slow proton ($\frac{1}{10}$ of the neutron momentum), and curve 3 for the emission of a fast proton and a slow neutron (the proton having 10 times the momentum of the neutron).

The 'quasi-deuteron' model (Levinger 1951) assumes that a close proton–neutron conjugation can exist inside the nucleus. The (γ, pn) reaction is regarded as an interaction between a photon and such a pair of nucleons resulting in the direct emission of both. Since the residual nucleus takes no active part in the process, the energy and direction of the recoil nucleus will depend only on the state of the 'quasi-deuteron' just before the interaction. The model, therefore, predicts that all the angular distributions of the recoil will be isotropic (i.e. the observed distribution will be proportional to $\sin\theta$) and that the momentum distribution of the recoils will indicate the state of the quasi-deuterons in the nucleus. The model has been very successful in describing the simultaneous emission of a proton and neutron in reactions induced by energetic ($>$ approximately 100 Mev) γ-rays. It is believed that most of the $^{14}N(\gamma, pn)^{12}C$ reactions observed here are caused by relatively low energy (~ 20 Mev) photons, and it is therefore expected that few of them will be explained by the quasi-deuteron model. This is borne out by the observed angular distribution (figure 11).

About 30 (γ, pn) events were recorded from which the proton did not leave the sensitive part of the cloud chamber (figure 10). For these events, the energy of the incident photon was calculated, on the assumption that all transitions led to the ground state of ^{12}C. Although the statistics are poor, it can be seen that the resulting distribution (figure 10(*a*)) exhibits a peak at about 20 Mev, which agrees with the result predicted above, and with the measured value for the (γ, p) and (γ, n) reactions.

The angular distributions for these events are similar in form to the total distributions. The distribution of the angle between the proton and the recoil appears to differ in detail; the most probable angle is about 120°, as compared with 150° for the more general case. The distribution resembles curve 2 (figure 14) which is predicted for the evaporation of a slow proton and a fast neutron. Since the 'knock-on' model has difficulty in accounting for any angle smaller than

90° in this distribution, this result appears to favour the evaporation model of the (γ, pn) reaction.

§ 6. CONCLUSION

From the experimental results, we conclude that:

(i) The cross sections for the reactions $^{14}\mathrm{N}(\gamma, \mathrm{p})^{13}\mathrm{C}$ and $^{14}\mathrm{N}(\gamma, \mathrm{n})^{13}\mathrm{N}$ are comparable, the relative values at any energy being shown in figure 13.

(ii) In the giant resonance, the emission of a single nucleon proceeds partly by a direct channel, and partly by the statistical evaporation of a nucleon. At energies greater than 30 MEV the emission proceeds mainly by a direct channel, and at all energies the results are consistent with the ratio of the two processes predicted by Wilkinson (1956).

(iii) The integrated cross section for the reaction $^{14}\mathrm{N}(\gamma, \mathrm{pn})^{12}\mathrm{C}$ is about 50% greater than that for the emission of either a single neutron or a single proton, for a spectrum of peak energy 200 MEV.

(iv) The (γ, pn) reaction appears to proceed either by a statistical or a knock-on process. The results for protons stopping within the sensitive volume of the chamber favour the statistical model and suggest that most of the observed events result from the absorption of a low energy ($\sim$20 MEV) photon.

(v) No evidence was found to suggest that many of the observed events could be satisfactorily explained by the quasi-deuteron model.

ACKNOWLEDGMENTS

The authors desire to thank Professor P. I. Dee, Mr. J. R. Atkinson and Mr. J. M. Reid for their support and interest in this work and Dr. W. McFarlane and the staff of the synchrotron at Glasgow for their assistance and co-operation in the control of this machine.

We also wish to acknowledge the award of a maintenance grant by the Department of Scientific and Industrial Research to one of us (D.C.M.) and a scholarship granted by the University of St. Andrews to the other (D.B.).

REFERENCES

AJZENBERG-SELOVE, F., and LAURITSEN, T., 1959, *Nucl. Phys.*, **11**, 138.

ATKINSON, J. R., MCFARLANE, W., REID, J. M., and SWINBANK, P., 1957, *Nucl. Instrum.*, **1**, 152.

BLACKETT, P. M. S., and LEES, D. S., 1933, *Proc. Roy. Soc.* A, **134**, 658.

BURCHAM, W. E., 1955, *Progr. Nucl. Phys.*, **4**, 204.

COURANT, E. D., 1951, *Phys. Rev.*, **82**, 43.

FEATHER, N., 1935, *Proc. Roy. Soc.* A, **141**, 194.

GOLDHABER, G., and TELLER, E., 1948, *Phys. Rev.*, **74**, 1046.

HORSLEY, R. J., HASLAM, R. N. H., and JOHNS, H. E., 1952, *Canad. J. Phys.*, **30**, 159.

KATZ, L., and CAMERON, A. G. W., 1951, *Canad. J. Phys.*, **29**, 518.

LEVINGER, J. S., 1951, *Phys. Rev.* **84**, 43.

LILLIE, A. B., 1952, *Phys. Rev.*, **87**, 716.

LIVESEY, D. L., 1957, *Canad. J. Phys.* **35**, 987.

MORRISON, D. R. O., 1958, *Thesis*, Glasgow University.

PANOFSKY, W. K. H., and REAGAN, D., 1952, *Phys. Rev.*, **87**, 543.

SHARP, W. T., KENNEDY, J. M., SEARS, B. J., and Hoyle, M. G., 1954, *Table of Racah Coefficients*, A.E.C.L. 97.

WILKINSON, D. H., 1956, *Physica*, **22**, 1039.

WRENSHALL, G. A., 1940, *Phys. Rev.*, **57**, 1095.

WRIGHT, I. F., MORRISON, D. R. O., REID, J. M., and ATKINSON, J. R., 1956, *Proc. Phys. Soc.*, **69**, 77.

The Induced Magnetic Anisotropy in Evaporated Films of Nickel–Iron Alloys

By M. PRUTTON and E. M. BRADLEY

Research and Design Division, International Computer and Tabulators Limited,
Stevenage, Herts.

MS. received 15*th October* 1959, *in final form* 30*th November* 1959

Abstract. The theories of the magnetic anisotropy of polycrystalline nickel–iron films in the permalloy region of composition are briefly reviewed. A simple model is then described for the magnetic anisotropy which can be induced in such films during evaporation. This model includes the sum of the effects of iron-pair directional ordering and a constant linear stress lying along the annealing field. After a detailed description of the experimental technique used to prepare NiFe films about 1500 Å thick in the region of composition 80–85% nickel, the results of observations of the hysteresis loops measured at 400 c/s are used to derive values of the anisotropy field H_k which are then compared with the values expected should the simple model apply. The experimental observation that increasing the substrate temperature moves the minimum in anisotropy energy to lower nickel content in the film is supported by the simple model. When the complicating effects of fibre growth are included, the major features of the observations are found to agree quite well with the model but the behaviour of the induced anisotropy is shown to be complex and the possibility of contributions due to imperfection ordering are discussed.

§ 1. Some Theoretical Considerations

1.1. *Introduction*

1.1.1. *Historical.*

It has been known for some time that polycrystalline thin films of nickel–iron alloys in the permalloy region of composition exhibit a preferred direction of magnetization along a magnetic field applied during evaporation (Conger 1955, Knorr and Hoffman 1959, Blois 1955, Zaveta 1956, Chikazumi and Oomura 1955, Smith 1959). The nature and magnitude of this anisotropy vary with the temperature of the substrate during evaporation and the composition of the alloy. Previous to the extensive study of magnetic thin films many observers have investigated the anisotropy of bulk nickel–iron alloys and its changes due to magnetic annealing but no satisfactory understanding of this anisotropy due to a magnetic field has yet emerged. This effect is often referred to as 'The Permalloy Problem' and a review article by Bozorth (1956) gives an extensive bibliography of the subject.

Some of the theories which have been proposed as explanations to this problem will be outlined as they help towards some understanding of the physical situation.

1.1.2. *Release of magnetostrictive constraint*.

The first theory put forward to account for the induced anisotropy was by Bozorth *et al.* (Bozorth, Dillinger and Kelsall 1934, Bozorth and Dillinger 1935, Bozorth 1934, 1953). The suggestion was that at the high temperature (~700°K) required for effective magnetic annealing, sufficient plastic flow could occur in the material for magnetostrictive constraints to be released. Both Becker and Döring (1939) and Néel (1954 a) have shown that this effect is much smaller than the observed anisotropy and also that magnetic annealing is effective in single crystals which would not be expected if constraint release were solely responsible for the anisotropy.

1.1.3. *Heterogeneous short-range order.*

In spite of the fact that the materials showing response to magnetic anneal can be random polycrystalline structures, Kaya (1953) has suggested that in the case of the nickel–iron alloys a uniaxial anisotropy might result from the heterogeneous formation of short-range order. The ordered state of the phase Ni_3Fe has a higher saturation magnetization and Curie temperature than the disordered state, so that short-range order should occur in the form of prolate ellipsoids elongated in the direction of the applied field. Such an arrangement could result in a uniaxial anisotropy of the correct order of magnitude (Rathenau 1953) by the shape effect of these ellipsoids as described by Stoner and Wohlfarth (1948).

Such short-range order has not yet been observed and further, the binary nickel–cobalt alloys have been found responsive to magnetic anneal by Masumoto, Inoue and Ukaji (1954) and yet show no known phase change such as the superlattice formation of Ni_3Fe.

1.1.4. *The formation of texture axes.*

Recently published work by Knorr and Hoffman (1959) describes the anisotropy produced during the evaporation of thin films of pure iron. Using the results of Evans and Wilman (1952) and Nelson (1937) they conclude that due to the geometry of the experimental arrangement there can be a contribution to the anisotropy through the formation of [111] iron fibre axes inclined towards the incident vapour beam. Smith (1959) has reached a similar conclusion for thin films of nickel–iron alloys. If a plane substrate is situated symmetrically with respect to a point source of atoms, Smith's results show that the [111] fibre growth causes magnetic easy axes to be distributed with rotational symmetry around the centre of the substrate. Such a geometry cannot account for the nearly uniaxial anisotropy observed in this case although the complications due to the [111] fibre growth may provide the explanation for some of the divergences from simple uniaxial behaviour which are observed. Further, the fibre growth still occurs in the absence of a magnetic annealing field and so cannot be the cause of that part of the anisotropy which can be observed to have been induced by the magnetic field present during the deposition of the film.

1.1.5. *Directional order.*

Both Néel (1954 b, c, 1959) and Taniguchi (1955) independently suggested a mechanism of inducing a uniaxial anisotropy which depends upon the assumption that the coupling coefficients of the spins on different atom pairs are different. At the annealing temperature solute atom pairs can diffuse into an arrangement of minimum energy, i.e. along the annealing field, and on quenching, diffusion is no longer significant so that the anisotropy is retained. The experiments reported by Chikazumi (1950, 1956) and Ferguson (1958) give substantial support for this theory.

It is possible that there could also be a contribution to directional order from the diffusion of non-magnetic inclusions or lattice vacancies because pairs of such imperfections should arrange themselves along the annealing field and then be frozen in upon quenching. The anisotropy due directly to such a process would be much smaller than that expected from directional ordering of ferromagnetic atom pairs because of the small effective diameter of the imperfections. That preferred orientation of imperfections may be responsible for the induced anisotropy was first suggested by Bozorth (1956) and some evidence that oxygen may play a part in the anisotropy of perminvar has been put forward by Burbank and Heidenreich (1959).

1.2. *Directional Order in Nickel–Iron Films*

1.2.1. *Taniguchi's theory.*

The theoretical work by Taniguchi (1955) shows that a B–B atom pair in a substitutional type of cubic solid solution of B atoms in A atoms has a probability $p(\phi)$ of lying at an angle ϕ to the direction of the applied field at temperature T' given by

$$p(\phi)=\frac{1}{Z}\exp\left\{\frac{-CB_1^2(T')(1-3\cos^2\phi)}{\boldsymbol{k}T'}\right\} \qquad \ldots\ldots(1)$$

in this equation Z is the total number of nearest atoms, $B_1(T')$ is the reduced Brillouin function at temperature T' and C is a coupling coefficient given by

$$C=C_{\mathrm{AA}}+C_{\mathrm{BB}}-2C_{\mathrm{AB}} \qquad \ldots\ldots(2)$$

for coupling coefficients C_{AA}, C_{BB} and C_{AB} between A–A, B–B and A–B atom pairs respectively.

Using equation (1) the anisotropy energy F in a plane containing the annealing field can be derived and is given by

$$F=F_0-\Omega_1\cos^2\theta+\Omega_2\cos\theta\sin\theta \qquad \ldots\ldots(3)$$

where F_0 is a constant and θ is the angle between the magnetization vector and the direction of the previously applied annealing field. For a polycrystalline randomly orientated face-centred cubic array the anisotropy Ω_1 and Ω_2 can be shown to be

$$\Omega_1=\frac{9Nn^2C^2B_1^2(T)B_1^2(T')}{\boldsymbol{k}T'}, \qquad \ldots\ldots(4)$$

$$\Omega_2=\frac{27Nn^2C^2B_1^2(T)B_1^2(T')}{8\boldsymbol{k}T'}. \qquad \ldots\ldots(5)$$

In equations (4) and (5): N is the number of atoms per cm^3, n is the concentration of solute atoms which is assumed to be small, C is the effective coupling constant defined in (2), B_1 is the Brillouin function, T' is the annealing temperature, T is the temperature at which observations are made. The values of Ω_1 and Ω_2 can be seen to be proportional thus:

$$\Omega_2=\beta\Omega_1$$

where for random orientations of the crystallites, $\beta = 0{\cdot}375$. If the film should be a single crystal in which the annealing field was applied along the [111], [110] or [001] directions then the anisotropy in the $(1\bar{1}0)$ and (100) planes has $\beta = 0$. If the structure of a film should remain constant then changing processing conditions will bring about corresponding changes in both Ω_1 and Ω_2 together.

With the form of the anisotropy given in (3) it can be seen that the easy direction of magnetization does not lie along the annealing field direction but is twisted away from it by an angle θ_0 given by

$$\tan 2\theta_0 = -\Omega_2/\Omega_1. \qquad \ldots\ldots(6)$$

For a random polycrystalline material $\theta_0 \simeq 10$ degrees.

1.2.2. *The hysteresis loops due to directional ordering.*

Under the appropriate conditions the magnetization reversal process in thin nickel–iron films can be a coherent rotation of the whole magnetization (Bradley and Prutton 1959). If this is the case, the form of the anisotropy in (3) above can be used in Stoner–Wohlfarth type calculations (Stoner and Wohlfarth 1948) of the hysteresis loops. In fact this is a tedious computation which at present is being tackled using a digital computer, but one special case is directly calculable and is of interest. A technique used to measure the anisotropy energy of uniaxial magnetic thin films (discussed in § 2.2 (iv)) is to examine the hysteresis loop at right angles to the preferred direction of magnetization. In the case of a simple uniaxial anisotropy this is the familiar straight line hysteresis loop whose intercepts with the saturation magnetization give a value for the anisotropy field H_K. It is of interest to compare the hard direction loop derived from the anisotropy of equation (3) with this straight line loop.

If a field H is applied at right angles to the preferred direction in the film, the magnetic energy of the system when the magnetization makes an angle θ with the annealing direction is given by

$$F = F_0 - \Omega_1 + \Omega_1 \sin^2\theta + \Omega_2 \sin\theta\cos\theta - MH\sin(\theta - \theta_0). \qquad \ldots\ldots(7)$$

The hysteresis loop can be calculated from this equation by finding the value of $\sin(\theta - \theta_0)$ for various values of H when the system is in equilibrium and $\partial F/\partial\theta = 0$.

$$\sin(\theta - \theta_0) = \frac{M}{2\Omega_1} H\cos 2\theta_0. \qquad \ldots\ldots(8)$$

Equation (7) shows that the hysteresis loop in the hard direction is a straight line but that it does not intercept the saturation magnetization at a field $H_K = 2\Omega_1/M$ as in the case of a simple $\Omega_1 \sin^2\theta$ anisotropy but at a higher value of field H_k given by

$$H_k = H_K(1 + \beta^2)^{1/2}.$$

In the case of a random polycrystalline structure $\beta = 0{\cdot}375$ and so $H_k = 1{\cdot}07 H_K$.

1.2.3. *The quantitative estimation of* Ω_1.

The dependence of Ω_1 upon the concentration of iron n and the substrate temperature T' has been calculated for the permalloy region of composition using equation (4).

The values of the constants used were as follows: $C = 5 \times 10^{-16}$ erg, Van Vleck (1937) gives C between 10^{-15} and 10^{-16} erg; $\boldsymbol{k} = 1{\cdot}37 \times 10^{-16}$ erg deg^{-1};

$B_1^2(T)=1$, valid as observations are made well below the Curie temperature; $N=10^{22}$ atoms cm^{-3}. These values give

$$\Omega_1 = 1{\cdot}8\times10^8\,\frac{n^2B_1^2(T')}{T'}\,\mathrm{erg\,cm^{-3}}$$

which is plotted in figure 1 for three values of n. For substrate temperatures in the region of 700 degrees absolute the value of Ω_1 is between 2 and 7×10^8 erg cm^{-3} which is in fairly good agreement with observation.

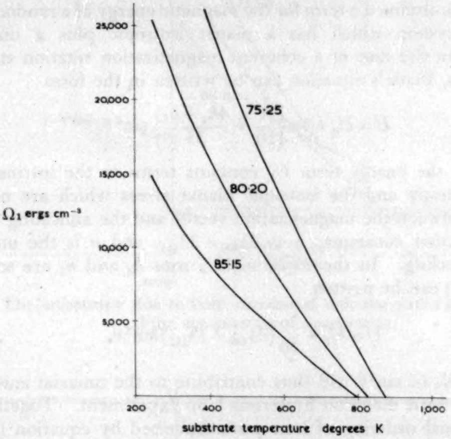

Figure 1. The anisotropy due to the directional ordering of iron pairs.

1.3. *The Contribution from Stresses*

1.3.1. *The effects of stresses.*

The work of MacDonald (1951, 1957) on thin films of nickel prepared by evaporation in the presence of a magnetic field shows that a complex system of stresses can be operative. By means of ferromagnetic resonance and oscillation magnetometer measurements, he established the existence of a large isotropic planar tension and a smaller uniaxial compression along the direction of the annealing field. The physical origin of this stress system is by no means clear but some sources of the planar stress may be:

(i) Differential contraction stress caused by the difference in coefficients of thermal expansion of the substrate and the metal film. In fact, this effect can be made negligibly small by matching the alloy and substrate as for instance can be done with 80/20 nickel–iron and soda-glass which both have coefficients of linear expansion of about $1{\cdot}2\times10^{-5}$ deg^{-1}.

(ii) A stress depending upon the history of the imperfections in the film. This mechanism has been proposed by Hoffman, Anders, Crittenden and Daniels (Hoffman, Anders and Crittenden 1953, Hoffman, Daniels and Crittenden 1954) who suggest that the film in the deposited state contains a large number of lattice vacancies which migrate through the metal at a rate determined by the temperature of the sample. The coalescing of such vacancies into larger aggregates results finally in the formation of dislocation rings (Seitz 1952). This causes a contraction of the crystallites and so a condition of isotropic stress. That part of the uniaxial stress arising because of the annealing field may be associated with the directional ordering of metal atoms or imperfections, with the magnetostriction effects in the alloy or possibly with anisotropic collapse of vacancies to form dislocation rings.

Using the expressions for a stressed monocrystal derived by Baltzer (1957), Blades (1959) has obtained a term for the magnetic energy of a randomly arranged polycrystalline system which has a planar isotropic plus a uniaxial stress configuration. In the case of a coherent magnetization rotation staying in the plane of the film, Blade's equation can be written in the form

$$U = U_0 + 3\sigma\left\{\frac{\Lambda}{10} + \frac{4h_4 + h_5}{35}\right\}\sin^2\theta. \qquad \ldots\ldots(9)$$

In this equation the energy term U_0 contains terms in the intrinsic magnetocrystalline anisotropy and the isotropic planar stress which are not functions of the angle θ between the magnetization vector and the annealing field. h_i are the magnetostriction constants, Λ is $2\lambda_{100} + 3\lambda_{111}$, and σ is the uniaxial stress induced by annealing. In the 80/20 nickel–irons h_4 and h_5 are small so that, to first order, (9) can be written

$$U = U_0 + \frac{3\sigma}{10}(2\lambda_{100} + 3\lambda_{111})\sin^2\theta. \qquad \ldots\ldots(10)$$

The coefficient K_S of $\sin^2\theta$ will thus contribute to the uniaxial anisotropy field measured in the hard direction hysteresis loop experiment. Together with the effect of directional ordering of iron pairs described by equation (7) the term in $\sin^2\theta$ has a coefficient K given by

$$K = \Omega_1 + K_S \qquad \ldots\ldots(11)$$

and the 'observed' anisotropy field H_K becomes

$$H_K = \frac{2(\Omega_1 + K_S)}{M}(1 + \beta^2)^{1/2}$$

for saturation magnetization M.

1.3.2. *The quantitative evaluation of K_S.*

Values of λ_{100} and λ_{111} have been measured by Bozorth and Walker (1953) for monocrystals of different compositions of nickel and iron and Hegg (1910) has measured the magnetic moment of NiFe alloys of different compositions.

In view of the presently unknown origin of the uniaxial stress σ, the value used here will be that quoted by MacDonald (1957) of -4×10^8 dyn cm^{-2} for nickel. Further, for convenience only, it will be assumed that σ is independent of the substrate temperature, and the composition of the alloy.

Figures 2 and 3 show plots of the uniaxial anisotropy energy density K for different alloy compositions and different substrate temperatures for this system of directional ordering plus constant linear stress.

§ 2. EXPERIMENTAL OBSERVATIONS

2.1. *Preparation of the Films*

Many authors (Blois 1955, Conger 1955, Smith 1956, Behrndt and Maddocks 1959) have given descriptions of their experimental arrangements used to produce nearly uniaxial films of nickel–iron alloys. In spite of this there seems to be poor agreement between observers, so it is considered worthwhile to make a fairly detailed statement of the technique used by the present writers.

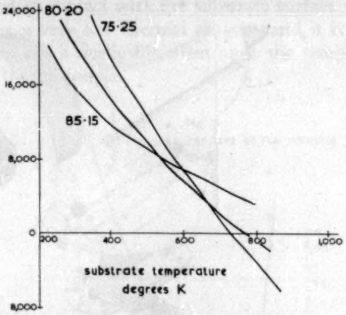

Figure 2. The anisotropy due to both directional ordering and a constant linear stress. Film composition as a parameter.

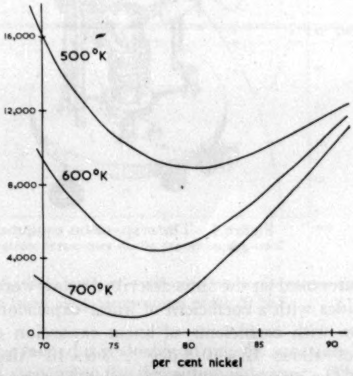

Figure 3. The anisotropy due to both directional ordering and a constant linear stress. Substrate temperature as a parameter.

Figure 4 is a diagrammatic representation of the experimental layout. The alloy is prepared by weighing out the appropriate quantities of powdered nickel and iron to make up a 10 gramme charge into a silica crucible. The powders are produced by Messrs Mond Nickel Co. Ltd., and are known as carbonyl iron grade MCA and nickel grade A. It was considered important to know how much cobalt was present in these two materials as small quantities may contribute considerably to the anisotropy. Analysis revealed no detectable cobalt in the iron and less than 0·1% cobalt in the nickel. The powders are then alloyed by melting in vacuum with radio-frequency induction heating until they are thoroughly outgassed. Once such an ingot has been prepared it is never used for more than ten evaporations to produce 2000 Å thick films because the greater evaporation rate of iron would then result in a significant change in the composition of the ingot.

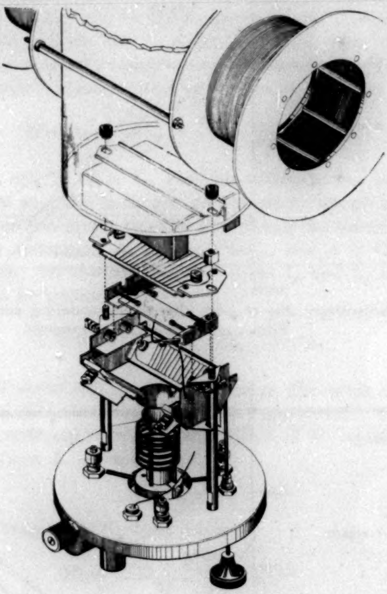

Figure 4. The evaporation equipment.

The substrates used for the films described below were Chance Resistance Glass microscope slides with a coefficient of linear expansion of about 7×10^{-6} deg^{-1}. This compares with coefficients of linear expansion of soda-glass, Pyrex and 80/20 NiFe of about 12×10^{-6} deg^{-1}, $3{\cdot}6 \times 10^{-6}$ deg^{-1} and 12×10^{-6} deg^{-1} respectively. The microscope slides are coated at the ends with silver paste and baked in air to dry the paste. This provides electrical contact to the evaporated film which is used for resistance measurements. The slides are then degreased in *iso*-propyl alcohol at room temperature and clipped into the jig in the vacuum system where they are cleaned by ionic bombardment in air at a pressure of 0·1 to 1·0 mm Hg.

During the evaporation the glass substrate can be maintained at a temperature between 200° and 450°c by the array of radiant heaters arranged around it as shown in figure 4. At a mean temperature of 320°c the temperature drop through the thickness of the slide is 5°c and the variation over the surface of the slide is less than 2°c. The windings on these heaters are arranged so that the magnetic field at the substrate surface due to the heating current is negligibly small. The heater itself is constructed of Brightray wire wound on mica with non-magnetic steel supports. The temperature of the substrate is measured with a chromel–alumel thermocouple with wires about 0·005 inch diameter which are welded together and placed in contact with the substrate surface which is to be coated. This junction has a very low thermal capacity and it is assumed that the heat lost into the wires has a negligible effect upon the temperature in the immediate locality of the thermocouple.

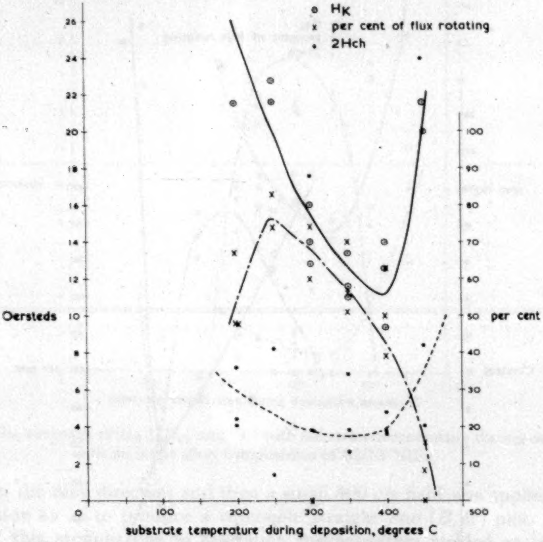

Figure 5. The variation of H_K, $2H_{ch}$ and ' r ' with substrate temperature during deposition with an ingot alloy composition of 80/20 NiFe.

While the ingot is being melted it is shielded from the substrate by a movable mask which can be swung away when the deposition is to start. The film is then deposited at a rate of about 40 Å per second in a magnetic field of 80 oersteds provided by the current through a pair of coils mounted outside the bell jar. The thickness of the film is monitored continuously during the evaporation by measuring the electrical resistance of the film. The deposition is stopped at the required film thickness by masking the source, the heaters are then turned off and the film allowed to cool at a rate of about 25°c min^{-1} until it reaches a temperature of less than 100°c, when air is let into the system. The pressure during the evaporation is generally about 3×10^{-4} mm Hg but it appears that the magnetic properties of the films are independent of pressure between 5×10^{-5} and 10^{-3} mm Hg.

The films discussed below are about 1500 Å thick and in any comparison with the theory it must be borne in mind that because of the greater evaporation rate of iron the films are depleted in nickel with respect to the ingot. The work reported by Smith (1959) suggests that the films are about 2% lower in nickel than the ingot in this region of composition.

2.2. *The Observations*

The hysteresis loops of the films prepared as described above could be measured on the face of an oscilloscope using apparatus described in an earlier publication (Bradley and Prutton 1959). The loops in the easy and hard directions were photographed and the following parameters were measured: (i) The coercivity in the easy direction, H_c. (ii) The coercivity in the hard direction, H_{ch}. For a simple rotational reversal mechanism and an induced anisotropy of the form $K \sin^2 \theta$ this parameter would be zero. (iii) The angle α between the observed anisotropy axis and the direction of the annealing field. (iv) The anisotropy field H_K. This parameter is the most significant in comparisons between theory and observation and so particular care was taken to ensure that, in fact, the whole magnetization of the film being measured was moving by coherent rotation. The

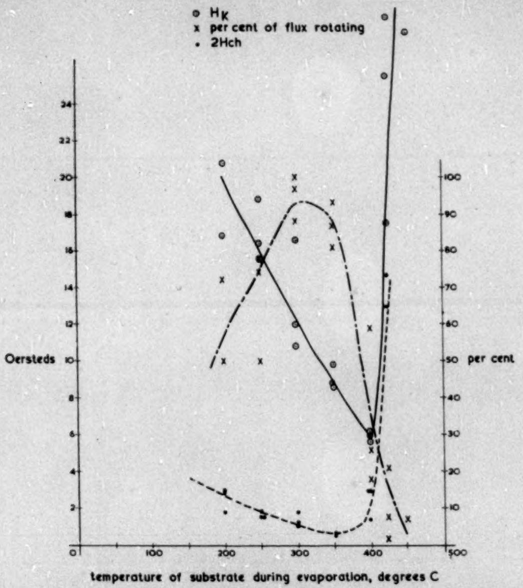

Figure 6. The variation of H_K, $2H_{ch}$ and ' r ' with substrate temperature during deposition with an ingot alloy composition of 81/19 NiFe.

observations using crossed pick-up loops reported by Bradley and Prutton (1959) showed that no net flux rotates when a film is reversed in the hard direction in the 400 c/s loop plotter. However, if a film is saturated along its easy direction and then fields of less than about $0{\cdot}2H_K$ are applied in the hard direction, then with the range of films reported here, the Kerr magneto-optic experiment (Prutton 1959) has shown that whatever the value of H_{ch}, coherent magnetization rotation does occur. Thus, in the loop experiment to measure H_K the film was

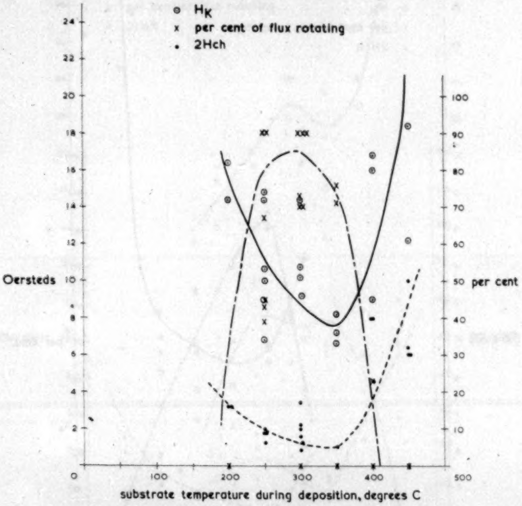

Figure 7. The variation of H_K, $2H_{ch}$ and ' r ' with substrate temperature during deposition with an ingot alloy composition of 82/18 NiFe.

saturated in the easy direction and then a small 400 c/s field was applied in the hard direction so as to produce a reversible straight line (B, H) plot. Extrapolation of this straight line to saturation magnetization yielded an intercept which is interpreted as a measure of the anisotropy field H_K. (v) The percentage of flux rotating, r. Previous work (Bradley and Prutton 1959) has shown that the arrangement in which the hysteresis plotter pick-up loop is orientated so as to detect flux changes at right angles to the reversing field is useful in detecting the amount of flux which is rotating. To measure r the film is arranged so that the easy direction makes an angle of 85 degrees with the reversing field and the flux changes are detected with the crossed pick-up coil. The maximum flux observed is then expressed as a fraction of the total amount of flux reversing in the film.

2.3. *Results*

Ingots with six compositions in the range 80/20 to 85/15 NiFe were used to produce films 1500 Å thick at substrate temperatures at intervals of 50°c between 200° and 450°c.

2.3.1. *The variation of H_c.*

No trend could be discovered in the variation of H_c with processing conditions but it was usually in the range 2–4 oersteds for most of the specimens. This is to be expected as, in the absence of any torque from the reversing field, a rotational switching process is not possible and a nucleation and wall motion mechanism must apply. Observations with the Kerr magneto-optic effect have revealed that this is indeed the case and have shown that the easy direction coercivity is very structure sensitive. The situation in a film where nuclei of reversed magnetization first occur are determined for instance by local variations in thickness, pinhole distributions or microscopic variations in the shape of the edge of the film.

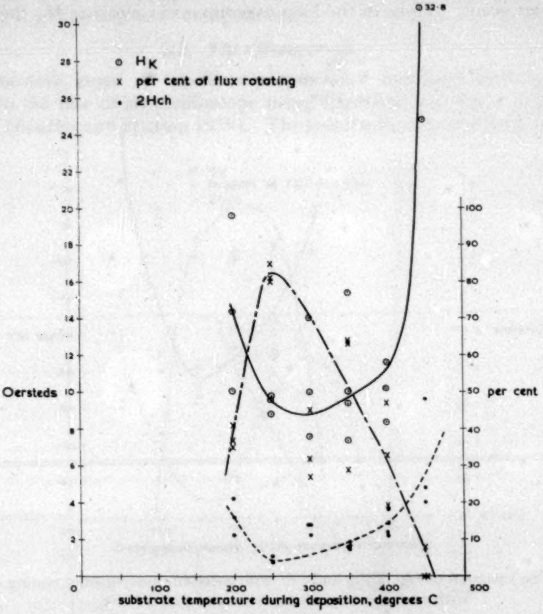

Figure 8. The variation of H_K, $2H_{ch}$ and ‘ r ’ with substrate temperature during deposition with an ingot alloy composition of 83/17 NiFe.

2.3.2. *The variation of H_K, H_{ch} and r.*

These three parameters were found to be critically dependent on substrate temperature and ingot composition and appear to be interrelated. Figures 5 to 10 show the variation of these properties with substrate temperature and figure 11 shows the variation of H_K with ingot composition for various substrate temperatures.

It appears that H_{ch} is of the same form as H_K lying somewhere in the region

$$0{\cdot}1H_K \leqslant H_{ch} \leqslant 0{\cdot}6H_K.$$

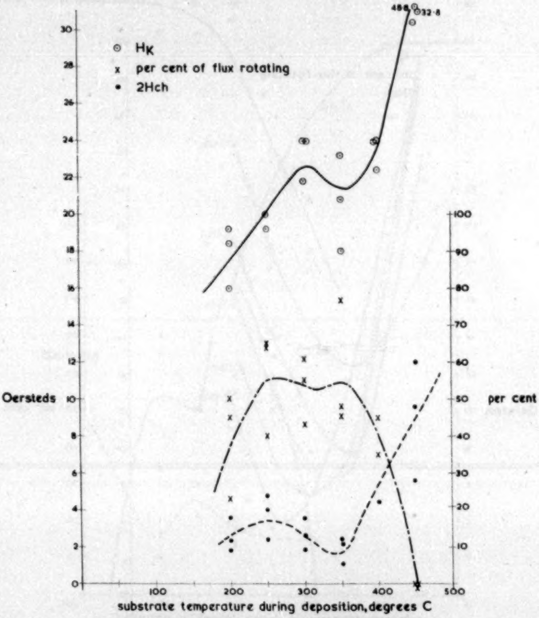

Figure 9. The variation of H_K, $2H_{ch}$ and ' r ' with substrate temperature during deposition with an ingot alloy composition of 84/16 NiFe.

When the substrate temperature is increased above about 400°c the magnetic properties change very rapidly indeed and it would appear that a different physical phenomenon is becoming important. This is shown up particularly well in figure 11 where the curve for a substrate temperature of 450°c can be seen to be quite different from the other five curves for lower substrate temperatures. The films made from ingots containing 84 and 85% nickel at these high substrate temperatures show almost no preferred direction at all.

The percentage of flux rotating appears to be inversely related to H_K in that most flux rotates when H_K is near its minimum values.

2.3.3. *Displacement of the easy axis from the annealing field.*

As the nickel content of the film was increased so did the value of the displacement α.

For the 80/20 and 81/19 ingots α was generally between 0 and 5 degrees, for 82/18 ingots a few films had values of α between 5 and 25 degrees but the majority had values of zero. For the 83, 84 and 85% nickel ingots the average values of α were 38, 24 and 40 degrees respectively.

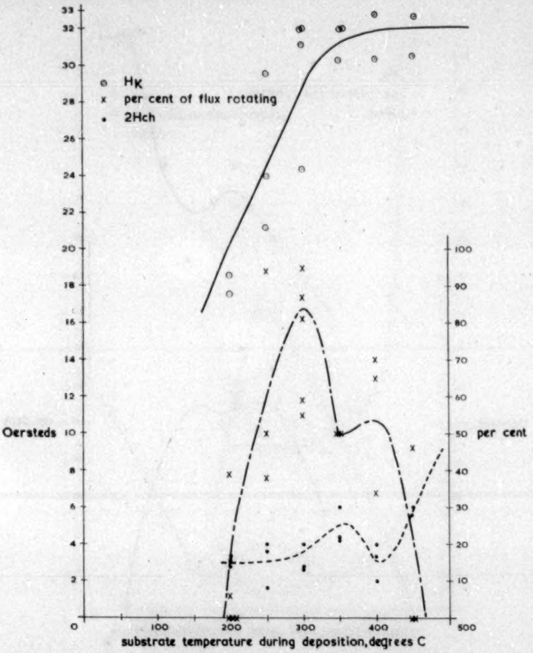

Figure 10. The variation of H_K, $2H_{ch}$ and 'r' with substrate temperature during deposition with an ingot alloy composition of 85/15 NiFe.

§ 3. THE COMPARISON OF EXPERIMENTS WITH THEORY

The theoretical treatment in § 1 which includes effects of directional order and a constant linear stress in a randomly orientated polycrystalline nickel–iron film in the permalloy region of composition suggests that the following magnetic properties should occur in such a system:

(i) The films should exhibit a nearly uniaxial anisotropy with an easy axis tilted through a small angle from the direction of the annealing field. This tilt is determined by the value of the ratio $(\Omega_1 + K_s)/\Omega_2$ and so may be expected to change as the composition of the alloy is changed.

(ii) At constant substrate temperatures there should be a minimum in the anisotropy energy at about 78% nickel in the film.

(iii) For a rotational reversal process the hard direction loop should be a straight line.

(iv) The minimum in anisotropy energy should move to lower percentages of nickel as the substrate temperature is increased.

(v) For constant film composition the anisotropy energy should decrease with increasing temperature.

The observations reported in §2 agree substantially with points (i), (ii) and (iv) but not with (iii) and (v).

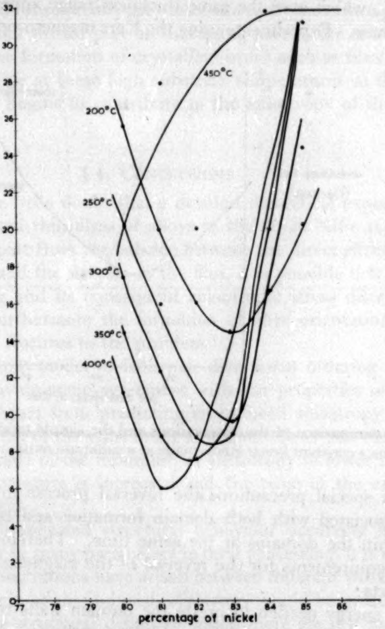

Figure 11. The variation of H_K with percentage of nickel in the starting alloy with substrate temperature as a parameter.

In figure 12 the experimental data for a substrate temperature of 600°K are compared with the theoretical behaviour derived from §1 assuming that the film composition is 2% lower in nickel than the ingot composition and that the measured field H_K can be identified with the uniaxial part of the anisotropy as argued in §2.2 (iv). Although the minimum anisotropy is of the correct magnitude and occurs in the correct region of film composition the observed values of H_K change much more rapidly than do the calculated values as the ingot composition is changed. In spite of this, the agreement is good when it is realized that both (*a*) the effects of any stresses associated with the directional ordering of iron–iron pairs and (*b*) the effects of any directional ordering and related stresses associated with the diffusion of imperfections have been neglected through the assumption of a constant linear stress.

The observations show that the hard direction coercivity is definitely related to the induced anisotropy energy and seems to be similar in form but it does vary between about $0{\cdot}1H_K$ and about $0{\cdot}6H_K$, tending to increase relative to H_K as the substrate temperature is increased. For a rotational reversal process the theory above predicts a value of zero for H_{ch}. Furthermore experiments on a set of films made from the 81/19 ingots showed that H_{ch} is a function of film thickness, increasing with decreasing film thickness below about 2500 Å. This is unlike H_K, which over the same thickness range appears to be independent of film thickness. Experiments using the Kerr magneto-optic effect have revealed that without special precautions the reversal process in the hard direction is definitely associated with both domain formation and coherent magnetization rotation within the domains at the same time. Therefore it is suggested that the energy requirements for the reversal of the magnetization must be thought of in two parts:

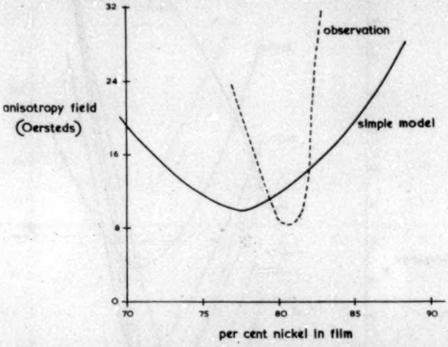

Figure 12. A comparison of the observations and the simple model of directional ordering plus a constant linear stress made at a substrate temperture of 600°K.

(*a*) The energy needed to create the domain walls resulting as the applied field in the hard direction reduces. If these walls are of the Bloch type, then their energy is determined primarily by the exchange energy and the anisotropy arising because of the demagnetizing field acting through the thickness of the film. Thus the contribution of H_{ch} due to the formation of these walls will be dependent upon the film thickness as well as any structure sensitivity of the domain formation but not upon the value of H_K.

(*b*) The existence of a fibre structure in these films means that the orientation of the easy axis with respect to the direction of annealing varies over the surface of a film. Thus some part of the hard direction magnetization reversal will be a non-coherent magnetization rotation. The energy requirements for this process are determined primarily by H_K and not by the film thickness. The total result of the fibre structure and the directional ordering is to give different parts of the film different directions of the anisotropy axis so that there is a distribution of easy axes about the direction of the annealing field. When a reversing field is applied at right angles to the 'average' easy direction some parts of the film are not orientated so as to have a straight line hysteresis loop and so a finite H_{ch} results which must be correlated with H_{K}.

Figures 5 to 10 show that at constant ingot composition the uniaxial anisotropy does not increase with increasing substrate temperature but passes through a minimum between 600° and 700°K. Such behaviour might be expected if lattice vacancies or imperfections are playing an important part in the process of directional ordering. As the substrate temperature is raised the mobility of imperfections rises and consequently they can more easily move into arrangements of minimum energy and should play an increasing part in the anisotropy of the film. Alternatively the formation of crystalline order such as fibre growth may become more favourable at these high substrate temperatures so that magnetocrystalline anisotropy begins to contribute to the anisotropy of the whole film.

§ 4. CONCLUSIONS

There seems to be little doubt that a detailed theoretical explanation of the behaviour of evaporated thin films of alloys in the 80/20 NiFe region must be very complicated. Apart from the balance between the direct effects of iron pair directional ordering, and the stresses in the film, it is possible that the effects of imperfection ordering and its consequent anisotropic stress distributions must also be included. Furthermore the formation of fibre orientation must result in more complicating features to the problem.

However, the simple model of iron pair directional ordering and constant linear stress does provide some agreement with the properties of the films as they are observed. Apart from predicting an induced anisotropy minimum in the region of 78% nickel of the same order of magnitude as that observed it does begin to explain the shift of the minimum in anisotropy to lower nickel content as the substrate temperature is increased and the twist of the easy axis away from the annealing field.

In view of the complicated structural behaviour occurring in these films which is influenced by so many parameters in their processing, it is not surprising that divergences of observations have arisen between different workers. Further elucidation of the origin of the induced anisotropy would be greatly assisted by investigations of these structural details of which there are few published data.

ACKNOWLEDGMENTS

The authors would like to thank the directors of International Computers and Tabulators Ltd. for permission to publish this paper. They would also like to take this opportunity of thanking Messrs. Astwood, Pitman and Wells and Misses Whyman and Farrar who have given their able assistance in the processing of the films and the execution of the experimental studies.

REFERENCES

BALTZER, P. K., 1957, *Phys. Rev.*, **108**, 580.
BECKER, R., and DÖRING, W., 1939, *Ferromagnetismus* (Berlin: Springer) 418.
BEHRNDT, K. H., and MADDOCKS, F. S., 1959, *J. Appl. Phys.*, **30**, 276S.
BLADES, J. D., 1959, *J. Appl. Phys.*, **30**, 260S.
BLOIS, M. S., JR., 1955, *J. Appl. Phys.*, **26**, 975.

Bozorth, R. M., 1934, *Phys. Rev.*, **46**, 742.
—— 1953, *Rev. Mod. Phys.*, **25**, 42.
—— 1956, *Proc. Conf. Magnetism and Magnetic Materials* (Boston : American Institute of Physics), p. 69.
Bozorth, R. M., and Dillinger, J. F., 1935, *Physics*, **6**, 285.
Bozorth, R. M., Dillinger, J. F., and Kelsall, G. A., 1934, *Phys. Rev.*, **45**, 742.
Bozorth, R. M., and Walker, J. G., 1953, *Phys. Rev.*, **89**, 624.
Bradley, E. M., and Prutton, M., 1959, *J. Electron. and Control*, **6**, 81.
Burbank, R. D., and Heidenreich, R. D., 1959, *Phys. Rev. Letters*, **2**, 85.
Chikazumi, S., 1950, *J. Phys. Soc. Japan*, **5**, 333.
—— 1956, *Ibid.*, **11**, 551.
Chikazumi, S., and Oomura, T., 1955, *J. Phys. Soc. Japan*, **10**, 842.
Conger, R. L., 1955, *Phys. Rev.*, **98**, 1752.
Evans, D. M., and Wilman, H., 1952, *Acta Cryst., Camb.*, **5**, 731.
Ferguson, E. T., 1958, *J. Appl. Phys.*, **29**, 252.
Hegg, F., 1910. *Arch. Sci. Phys. Nat.*, **29**, 592; **30**, 15.
Hoffman, R. W., Anders, F. J., and Crittenden, E. C., Jr., 1953, *J. Appl. Phys.*, **24**, 231,
Hoffman, R. W., Daniels, R. D., and Crittenden, E. C., Jr., 1954, *Proc. Phys. Soc.* B, **67**, 497.
Kaya, S., 1953, *Rev. Mod. Phys.*, **25**, 49.
Knorr, T. G., and Hoffman, R. W., 1959, *Phys. Rev.*, **113**, 1039.
MacDonald, J. R., 1951, *Proc. Phys. Soc.* A, **64**, 968.
—— 1957, *Phys, Rev.*, **106**, 890.
Masumoto, H., Inoue, S., and Ukaji, I., 1954, *Sci. Rep. Res. Insts. Tôhoku Univ.* A, **6**, 375.
Néel, L., 1954 a, *J. Phys. Rad.*, **15**, 92S.
—— 1954 b, *Ibid.*, **15**, 225.
—— 1954 c, *C.R. Acad. Sci., Paris*, **238**, 305.
—— 1959 *J. Appl. Phys.*, **30**, 35S.
Nelson, H. R., 1937, *J. Chem. Phys.*, **5**, 252.
Prutton, M., 1959, *Phil. Mag.*, **4**, 1063.
Rathenau, G. W., 1953, *Rev. Mod. Phys.*, **25**, 55.
Seitz, F., 1952, *Advanc. Phys.*, **1**, 43.
Smith, D. O., 1956, *Phys. Rev.*, **104**, 1280.
—— 1959, *J. Appl. Phys.*, **30**, 264S.
Stoner, E. C., and Wohlfarth, E. P., 1948, *Phil. Trans. Roy. Soc.* A, **240**, 599.
Taniguchi, S., 1955, *Sci. Rep. Res. Insts. Tôhuku Univ.* A, **7**, 269.
Van Vleck, J. H., 1937, *Phys. Rev.*, **52**, 1178.
Zaveta, K., 1956, *Czech. J. Phys.*, **6**, 473.

Improved Atomic Wave Functions using a Functional Transformation

By G. G. HALL

Department of Mathematics, Imperial College, London

MS. received 5*th October* 1959, *in final form* 15*th November* 1959

Abstract. The accuracy of an atomic wave function is often increased by an adjustment of the overall scale of the wave function. This method of improving a wave function is here generalized by considering a variable scale factor which can be an arbitrary function of the radius. This type of variation has the valuable property of leaving all the coefficients in the density matrices invariant so that it is much easier to minimize the energy than it is for most parameters. The new integrals which arise are relatively easy to evaluate.

To illustrate the power of the method an application is made to the simplest wave functions for the He isoelectronic sequence. A simple type of variation is found and the results show that a close approximation to the self-consistent-field energies can be obtained from a two-parameter wave function.

---

§ 1. Introduction

Hylleraas (1930) has shown that it is always possible to improve an approximate atomic wave function by introducing an arbitrary scale factor. The optimum scale factor is very readily found once the total kinetic and potential energies are known in any one scale. This variation of scale has even some physical importance since it ensures that the approximate energies satisfy the virial theorem in the same way as the accurate ones do (for further details see Löwdin 1959).

The generalization of this idea of a scale factor which is proposed here is equivalent to the use of a scale which varies with the distance from the nucleus but is independent both of angle and of the particular electron. In practice this variable scale is more difficult to employ than the constant scale factor but is easier than most variations. On the other hand this variation leaves the qualitative form of the wave function unchanged so that there is a limit to the extent of improvement which can be obtained.

§ 2. A Functional Transformation

Atomic wave functions, with very few exceptions, are calculated in terms of some set of orbitals $\psi_s(r, \theta, \phi)$. These functions, in general, have non-vanishing overlap integrals

$$S_{ts}=\iiint \psi_t^*\psi_s r^2\,dr\sin\theta\,d\theta\,d\phi. \qquad \ldots\ldots(2.1)$$

It is often easier to use, instead of ψ_s, the functions

$$\chi_s=r\psi_s \qquad \ldots\ldots(2.2)$$

so that

$$S_{ts}=\iiint \chi_t^*\chi_s\,dr\sin\theta\,d\theta\,d\phi. \qquad \ldots\ldots(2.3)$$

In the usual method of scaling these orbitals are replaced by the scaled functions

$$(k)^{1/2}\chi_s(kr, \theta, \phi), \qquad \ldots\ldots(2.4)$$

where k is the scale factor. To make the orbitals more flexible still they can be replaced by the transformed functions

$$u_s(r, \theta, \phi) = \left(\frac{df}{dr}\right)^{1/2} \chi_s[f(r), \theta, \phi], \qquad \ldots\ldots(2.5)$$

where $f(r)$ is a real function of r which is differentiable and monotonic increasing as r increases.† The overlap integral beween these functions is

$$\begin{aligned}\iiint u_t{}^* u_s\, dr \sin\theta\, d\theta\, d\phi &= \iiint \chi_t{}^*(f, \theta, \phi)\chi_s(f, \theta, \phi)\frac{df}{dr}\, dr \sin\theta\, d\theta\, d\phi \\ &= \iiint \chi_t{}^*(f, \theta, \phi)\chi_s(f, \theta, \phi)\, df \sin\theta\, d\theta\, d\phi \\ &= S_{ts}. \qquad \ldots\ldots(2.6)\end{aligned}$$

Thus the overlap integrals are left invariant for any $f(r)$. This simple result is of very considerable importance since the matrix elements of the density matrices of any order depend entirely on these overlap integrals (Löwdin 1955). This means, in particular, that the coefficients of the various integrals over the orbitals χ_s in the energy expression are exactly equal to the corresponding coefficients for the u_s. The calculation of these coefficients is a major operation in finding an accurate atomic wave function and a variable parameter which leaves them invariant gives a comparatively easy way of improving a wave function.

Although the overlap integrals are left unchanged the other integrals are considerably altered by this transformation. The nuclear attraction integrals are the easiest to calculate. They have the form

$$\iiint \frac{u_t{}^* u_s}{r}\, dr \sin\theta\, d\theta\, d\phi = \iiint \frac{\chi_t{}^* \chi_s}{r(f)}\, df \sin\theta\, d\theta\, d\phi, \qquad \ldots\ldots(2.7)$$

where $r(f)$ is the inverse function to $f(r)$. The conditions imposed on $f(r)$ ensure that this inverse exists. In general it is more important to know $r(f)$ and then invert it to find $f(r)$ if needed. The interelectronic repulsion integrals can be expanded as the usual series in $r_>$ and $r_<$ and calculated by changing the variables to f_1 and f_2 in the same way as in equation (2.6). The angular terms in the kinetic energy can be treated in the same way but the radial terms are more complicated. These have the form

$$-\iiint u_t{}^* \frac{d^2}{dr^2} u_s\, dr \sin\theta\, d\theta\, d\phi = \iiint \frac{du_t{}^*}{dr}\frac{du_s}{dr}\, dr \sin\theta\, d\theta\, d\phi. \qquad \ldots\ldots(2.8)$$

The derivatives can be expressed as

$$\begin{aligned}\frac{du_s}{dr} &= \frac{\partial u_s}{\partial r} + \frac{\partial u_s}{\partial f}\frac{df}{dr} \\ &= \tfrac{1}{2}(f')^{-1/2} f'' \chi_s + (f')^{3/2}\frac{d\chi_s}{df} \qquad \ldots\ldots(2.9)\end{aligned}$$

---

† After this investigation was concluded it was pointed out to the author that a similar idea had been proposed by Löwdin (1954) and that $f(r)$ had been evaluated numerically in Uppsala for all SCF functions then available although without any attempt to describe them analytically.

or as

$$\frac{du_s}{dr} = (r')^{-1}\frac{d}{df}[(r')^{-1/2}\chi_s]$$
$$= \left(r'\frac{d\chi_s}{df} - \tfrac{1}{2}r''\chi_s\right)(r')^{-5/2} \qquad \text{......(2.10)}$$

depending on whether $f(r)$ or $r(f)$ is given. Thus the kinetic energy terms become

$$\iiint (r'\chi_t' - \tfrac{1}{2}r''\chi_t)^*(r'\chi_s' - \tfrac{1}{2}r''\chi_s)(r')^{-4}\,df\sin\theta\,d\theta\,d\phi. \qquad \text{......(2.11)}$$

The evaluation of these integrals may be more difficult but for the simpler forms of $f(r)$ it is usually still possible to integrate in terms of tabulated functions.

In principle it would be possible to find the best $f(r)$, or equivalently $r(f)$, by minimizing the energy. This could be done either by using the calculus of variations to derive the differential equation which the function satisfies or by substituting a sufficiently general expansion for the function and finding the coefficients by minimizing numerically. In practice, however, because of the limitation on the improvement of the energy which can be obtained it is probably not worth while to carry the process of minimization very far.

§ 3. A SIMPLE FUNCTIONAL TRANSFORMATION

There is one example of a function $r(f)$ which is easy enough to handle and yet gives considerable improvements in energy. This is the function

$$r(f) = f(1+\alpha f) \qquad \text{......(3.1)}$$

where α is a parameter. The inverse function is

$$f = [-1 + (1+4\alpha r)^{1/2}]/2\alpha. \qquad \text{......(3.2)}$$

To satisfy the condition on the function, α has to be positive. The limit $\alpha = 0$ corresponds to the identity transformation and often is useful in providing a check on the formulae. A constant scale factor could also be introduced into the transformations (equation (3.1)) but it is more convenient to allow for this afterwards in the usual way. This factor is necessary if the virial theorem is to be satisfied.

The advantage of this particular transformation is that it leads to fairly simple integrals. The nuclear attraction integrals, (equation (2.7)), involve the function

$$1/r = 1/f - \alpha/(1+\alpha f) \qquad \text{......(3.3)}$$

and so split up into

$$\iiint \frac{\chi_t^*\chi_s}{f}\,df\sin\theta\,d\theta\,d\phi - \alpha\iiint \frac{\chi_t^*\chi_s}{1+\alpha f}\,df\sin\theta\,d\theta\,d\phi. \qquad \text{......(3.4)}$$

The first of these integrals is exactly the same as the usual one. The second is more complicated but can usually be evaluated by the change of variable

$$g = 1 + \alpha f. \qquad \text{......(3.5)}$$

The two-electron integrals split up similarly. The kinetic energy terms are more complicated but can be written, using equation (2.10),

$$-\iiint u_t^*\frac{d^2u_s}{dr^2}\,dr\sin\theta\,d\theta\,d\phi$$
$$= \iiint [(1+2\alpha f)\chi_t' - \alpha\chi_t]^*[(1+2\alpha f)\chi_s' - \alpha\chi_s]$$
$$\times (1+2\alpha f)^{-4}\,df\sin\theta\,d\theta\,d\phi. \qquad \text{......(3.6)}$$

These integrals can be evaluated by changing the variable to

$$h = 1 + 2\alpha f. \qquad \ldots\ldots(3.7)$$

If α is very small there is a second method of evaluating the integrals, namely by expanding as power series in α. The nuclear attraction integrals employ the expansion

$$r^{-1} = f^{-1}(1+\alpha f)^{-1} = f^{-1} - \alpha + \alpha^2 f - \ldots \qquad \ldots\ldots(3.8)$$

The first term is again the original one. The second term can be integrated immediately and even the higher terms are not usually difficult. The two-electron integrals can be similarly expanded and the kinetic energy integrals are only a little different. This expansion is only useful when α is very small since it is an asymptotic expansion and breaks down for larger values of α.

§ 4. AN APPLICATION TO THE HELIUM SEQUENCE

The power of this functional transformation method of improving a wave function is most easily shown by taking a simple wave function for the helium isoelectronic sequence as an example. The simplest wave function is

$$\Psi = \psi(1)\psi(2)\sqrt{\tfrac{1}{2}}[\alpha(1)\beta(2) - \alpha(2)\beta(1)] \qquad \ldots\ldots(4.1)$$

where

$$\chi = r\psi = 2r\exp(-r) \qquad \ldots\ldots(4.2)$$

so that

$$\int_0^\infty \chi^2\,dr = 1.$$

When the scale factor alone is varied this wave function does give the major variations along the isoelectronic sequence but it is nevertheless not very accurate.

The calculation of the various integrals that occur when the transformation (equation (3.1)) is applied to this wave function is discussed in the Appendix. The energies can be expressed in closed form in terms of the exponential integral function i.e. equations (A6), (A7), (A8). The values of this integral tabulated by Kotani *et al.* (1955) were used for the larger values of α, but for smaller values of α these tables do not extend sufficiently far and the asymptotic expansions, equations (A1), (A2), (A4) were used instead. The energies were calculated first for some convenient values of α and then minimized for each value of α by interpolation. For the higher ions the interpolation was quadratic in α but for the lower ions α varies more rapidly and the interpolation was taken quadratic in 1/α.

The results of the calculation are shown in table 1. Because of the form of the wave function the energies can never be better than the Hartree–Fock ones.

Table 1. Energies of Two-Electron Ions (Hartrees)

Z	α	This paper	SCF	Saturno and Parr	Exptl
1	0·1559	0·4877	0·4879	0·4788	0·5276
2	0·0452	2·8615	2·8617	2·8542	2·9038
3	0·0277	7·2358	7·2364	7·2293	7·2804
4	0·0214	13·6105	13·6113	13·6043	13·6572
5	0·0154	21·9851	21·9862	21·9794	22·0356
6	0·0122	32·3603	32·3612	32·3544	32·4171

The significant feature of the results is their very close approximation to the Hartree–Fock energies (Green, Mulder, Lewis and Woll 1954) despite the use of only two parameters. In comparison the energies obtained by Saturno and Parr (1958) using an orbital of the form

$$\chi = r^n \exp(-\beta r) \qquad \ldots\ldots(4.3)$$

where both n and β are varied continuously, are seen to be much poorer. The experimental energies are quoted from Green *et al.* (1954).

If the scaling function $f(r)$ were varied freely in this example the lowest energy would occur when the orbital was the Hartree–Fock function. Since the form of these Hartree–Fock functions has been calculated it is then possible to transform them so as to determine the optimum scaling function $f(r)$ for each member of the sequence. The results of this comparison are shown in table 2.† It is convenient, since the functions are almost linear, to use the f/r as the variable.

Table 2. Scaling Functions

H^-									
	r	0·1	0·5	1·0	2·0	3·0	4·0	5·0	—
	f/r	0·776	0·734	0·693	0·630	0·585	0·549	0·540	—
	f_{SCF}/r	0·773	0·745	0·711	0·651	0·606	0·576	0·551	—
He									
	r	0·1	0·2	0·5	1·0	1·5	2·0	2·5	—
	f/r	1·755	1·747	1·724	1·689	1·657	1·627	1·598	—
	f_{SCF}/r	1·761	1·743	1·694	1·632	1·589	1·559	1·539	—
Li^+									
	r	0·05	0·10	0·25	0·50	0·75	1·00	1·25	1·50
	f/r	2·757	2·755	2·742	2·724	2·706	2·688	2·671	2·655
	f_{SCF}/r	2·764	2·750	2·709	2·654	2·613	2·583	2·560	2·542
Be^{2+}									
	r	0·025	0·100	0·2	0·3	0·4	0·6	0·8	1·0
	f/r	3·763	3·757	3·749	3·741	3·734	3·718	3 703	3·688
	f_{SCF}/r	3·768	3·739	3·703	3·672	3·646	3·604	3·573	3·550
B^{3+}									
	r	0·025	0·1	0·2	0·3	0·4	0·5	0·6	0·8
	f/r	4·757	4·752	4·745	4·737	4·730	4·723	4·716	4·702
	f_{SCF}/r	4·768	4·728	4·685	4·650	4·621	4·597	4·578	4·549
C^{4+}									
	r	0·025	0·1	0·2	0·3	0·4	0·5	0·6	—
	f/r	5·755	5·750	5·743	5·736	5·729	5·722	5·715	—
	f_{SCF}/r	5·764	5·719	5·672	5·635	5·607	5·587	5·577	—

It is clear from table 2 that the simple scaling function used here is a good approximation to the optimum one for small r and that it has the correct trend as r increases. Nevertheless there is a growing difference between them as r increases. From table 2 it is seen that for H^- f/r varies more rapidly with r than f_{SCF}/r but for He, Li^+, Be^{2+}, B^{3+} and C^{4+} it varies more slowly. This is due to the much larger value of α for H^- than for the other ions.

The effect of the energy criterion for a wave function is to weight very heavily the space close to the nucleus. It is not surprising, therefore, that the fitting of these functions should be best close to the nucleus. As a different test of the functions it is useful to calculate the diamagnetic susceptibility since this is sensitive to the behaviour of the function at large r. The results are shown in table 3 and compared with the values calculated from the Hartree functons (Stoner 1929) and by a perturbation method (Stewart 1957). The overall scale factor k is also given in table 3.

---

† The author is greatly indebted to Dr. P. O. Löwdin for making available his calculations of $f_{SCF}(r)$, and to F. K. Klauss Appel for preparing the table.

Table 3. Diamagnetic Susceptibility, $-\chi[10^{-6}\,\mathrm{cm}^3\,(\mathrm{g\,ion})^{-1}]$

Z	α	k	$-\chi$	$-\chi_{\mathrm{SCF}}$	$-\chi_{\mathrm{Stewart}}$
1	0·1559	0·7874	15·94	—	8·55
2	0·0452	1·7621	1·900	1·87	1·66
3	0·0277	2·7609	0·714	0·69	0·67
4	0·0214	3·7652	0·372	—	0·36
5	0·0154	4·7591	0·226	—	0·22
6	0·0122	5·7566	0·152	—	0·15

This table shows that the behaviour at large distances is quite satisfactory except for H⁻ whose wave function seems to extend rather too far and so gives an estimate of $\langle r^2\rangle$ which is too large.

ACKNOWLEDGMENTS

This research was begun while the author was visiting the Quantum Chemistry Group, University of Uppsala. The author would like to thank Dr. P. O. Löwdin for his generous hospitality and stimulus; and also the King Gustaf VI Adolf's 70-years Fund for Swedish Culture, Knut and Alice Wallenberg's Foundation, The Swedish Natural Science Research Council and the Aeronautical Research Laboratory, Wright Air Development Centre of the Air Research and Development Command, United States Air Force, whose support made this visit possible.

APPENDIX

The integrals involved in the asymptotic expansion of the energy are most easily evaluated using generating functions. The nuclear attraction for the helium sequence is

$$-2Z\int_0^\infty \chi^2/r\,dr = -2Z\{1-\alpha+1\tfrac{1}{2}\alpha^2-3\alpha^3+7\tfrac{1}{2}\alpha^4-22\tfrac{1}{2}\alpha^5\ldots\}, \qquad \ldots\ldots\text{(A1)}$$

and the kinetic energy is then

$$-\int_0^\infty \chi\chi''\,dr = 1-2\alpha+7\alpha^2-36\alpha^3+240\alpha^4-9120\alpha^5\ldots \qquad \ldots\ldots\text{(A2)}$$

The generating function

$$\int_0^\infty \{\exp(-2f)-\exp(-4f)(1+2f+2f^2)\}\exp(-\gamma f)\,df = (2+\gamma)^{-1}-(4+\gamma)^{-1}-2(4+\gamma)^{-2}-4(4+\gamma)^{-3}, \qquad \ldots\ldots\text{(A3)}$$

enables the repulsion integral to be expanded as

$$\frac{5}{8}-\alpha+\frac{63}{32}\alpha^2-\frac{297}{64}\alpha^3+\frac{3285}{256}\alpha^4-\frac{10\,485}{256}\alpha^5\ldots \qquad \ldots\ldots\text{(A4)}$$

The closed form of the energies is found using the substitutions suggested. If a function $E(x)$ is defined by

$$E(x)=\exp(x)\int_x^\infty \exp(-t)/t\,dt, \qquad \ldots\ldots(\mathrm{A5})$$

then the nuclear attraction is

$$-2Z\{2/\alpha-4/\alpha^2E(2/\alpha)\}. \qquad \ldots\ldots(\mathrm{A6})$$

The kinetic energy similarly is

$$\left[\frac{7}{3}+\frac{5}{6\alpha}+\frac{1}{6\alpha^2}-E(1/\alpha)\left\{\frac{3}{\alpha}+\frac{1}{\alpha^2}+\frac{1}{6\alpha^3}\right\}\right]\Big/2\alpha. \qquad \ldots\ldots(\mathrm{A7})$$

The electronic repulsion gives

$$\frac{5}{8}-\frac{1}{2\alpha}-\frac{5}{\alpha^2}+\frac{4}{\alpha^3}+\frac{8}{\alpha^2}E(2/\alpha)-\frac{8}{\alpha^2}\left(1-\frac{2}{\alpha}+\frac{2}{\alpha^2}\right)E(4/\alpha). \qquad \ldots\ldots(\mathrm{A8})$$

As a check these expressions can be used to find the asymptotic expansions above from the expansion

$$E(x)=x^{-1}(1-x^{-1}+2x^{-2}-6x^{-3}+\ldots). \qquad \ldots\ldots(\mathrm{A9})$$

REFERENCES

Green, L. C., Mudler, M. M., Lewis, M. N., and Woll, J. W., 1954, *Phys. Rev.*, **93**, 757.

Hylleraas, E. A., 1930, *Z. Phys.*, **60**, 624.

Kotani, M., Amemiya, A., Ishiguro, E., and Kimura, I., 1955, *Table of Molecular Integrals* (Tokyo: Maruzen).

Löwdin, P. O., 1954, *Proc. Nikko Symp. Mol. Phys.*, (Tokyo: Maruzen), p. 116.

—— 1955, *Phys. Rev.*, **97**, 1474.

—— 1959, *J. Molec. Spectroscopy*, **3**, 46.

Saturno A. F., and Parr, R. G., 1958, *J. Chem. Phys.*, **29**, 490.

Stewart, A. L., 1957, *Proc. Phys. Soc.*, A, **70**, 756.

Stoner, E. C., 1929, *Proc. Leeds Phil. Litt. Soc.*, **1**, 484.

An Experimental Study of the Nuclear Relaxation Mechanism in Several Crystals

By E. R. ANDREW and K. M. SWANSON†
Physics Department, University College of North Wales, Bangor, Caernarvonshire

MS. received 19*th October* 1959

Abstract. The effective nuclear spin–lattice relaxation mechanism has been determined in a number of crystals by observing the relative saturation behaviour of the lines of their quadrupole-split nuclear magnetic resonance spectra. It is shown that all lines and combinations of lines should have the same saturation behaviour if the mechanism is magnetic, and differing behaviour if the mechanism is quadrupolar. The ^{23}Na relaxation in pure synthetic crystals of sodium nitrate, sodium chlorate and sodium thiosulphate was found in each case to be quadrupolar. The ^{7}Li and ^{27}Al relaxation in natural mineral crystals of spodumene and the ^{27}Al relaxation in a mineral crystal of euclase were found to be magnetic. The ^{11}B relaxation in a pure synthetic crystal of borax was also found to be magnetic. Chemical analysis showed a sufficient concentration of paramagnetic impurity in the mineral specimens to account for the dominance of the magnetic relaxation mechanism, and a sufficiently small concentration of paramagnetic impurity in the three sodium salts to account for the dominance of the quadrupolar mechanism. Despite the purity of the borax crystal, the quadrupole moment of the ^{11}B nuclei is too small to enable the quadrupolar mechanism to compete with the magnetic mechanism.

§ 1. INTRODUCTION

NUCLEAR spin–lattice relaxation in solids is effected through the coupling of the lattice to the magnetic dipole and electric quadrupole moments of the nuclei. For nuclei having spin number $I = \frac{1}{2}$ the quadrupolar interaction is absent, but for $I > \frac{1}{2}$ both interactions contribute to relaxation. The magnetic and electric mechanisms may contribute very unequally to the relaxation process and Pound (1950) devised an experimental method for determining the operative mechanism for single crystals. He applied his method to sodium nitrate and showed that the ^{23}Na nuclei are relaxed by a quadrupolar mechanism. Andrew and Swanson (1957) described another method of making the same distinction which gave the same result for sodium nitrate. This paper reports an extension of the work to the nuclei ^{7}Li, ^{11}B, ^{23}Na and ^{27}Al in crystals of spodumene, borax, sodium chlorate, sodium thiosulphate and euclase.

§ 2. THEORY OF THE EXPERIMENTS

The magnetic resonance spectrum of nuclei situated in a non-cubic environment consists of $2I$ lines (Pound 1950). The relative saturation behaviour of these lines depends upon the relaxation mechanism and thus provides a means of determining which mechanism is effective. The saturation behaviour for each of the two mechanisms is now considered in turn.

---

† Now at the Dounreay Experimental Reactor Establishment, Thurso, Scotland.

2.1. *Magnetic Relaxation*

First we consider the case where the $2I$ lines are resolved. The population N_m of the magnetic energy level m is governed by the equation

$$\begin{aligned}\dot{N}_m = &-N_m(W_{m\to m+1}+W_{m\to m-1}+P_{m\to m+1}+P_{m\to m-1})\\ &+N_{m+1}(W_{m+1\to m}+P_{m+1\to m})+N_{m-1}(W_{m-1\to m}+P_{m-1\to m}).\end{aligned} \qquad \ldots\ldots(1)$$

The W terms are the probabilities per unit time of transitions brought about by the magnetic relaxation process and the P terms are the probabilities of transitions brought about by the radio-frequency field. For magnetic relaxation we may write

$$W_{m\to m-1} = W(I+m)(I-m+1) \qquad \ldots\ldots(2)$$

for a typical upward transition, while the corresponding downward transition probability is related to it by the Boltzmann factor. If the crystal is so oriented that the $2I$ lines are only just resolved, this factor is in all cases given in good approximation by $\exp\Delta$, where $\Delta = \boldsymbol{h}\nu_0/\boldsymbol{k}T \ll 1$, in which ν_0 is the mean frequency of the $2I$ lines. Thus

$$W_{m-1\to m} = W_{m\to m-1}(1+\Delta). \qquad \ldots\ldots(3)$$

If all the P terms are zero, equation (1) describes the spin–lattice relaxation of the system in the absence of radio-frequency power. If at any instant the populations can be described by a spin temperature T_s, with equal differences n_s between the populations of adjacent levels, then equation (1) with equations (2) and (3) reduces to

$$\dot{N}_m = 2W(n_0-n_s)m$$

where $n_0 = N\Delta/(2I+1)$ is the difference between the populations when spin–lattice equilibrium has been achieved, and where $n_0T = n_sT_s$. Thus

$$\dot{N}_m - \dot{N}_{m-1} = 2W(n_0-n_s) \qquad \ldots\ldots(4)$$

which is independent of m. It therefore follows that if at one instant the population differences can be described by a spin temperature, they can be so described at all later times. Integration of equation (4) shows that the spin–lattice relaxation time T_1 is given by $1/2W$.

The P terms in equation (1) can be written (Bloembergen, Purcell and Pound 1948) as

$$P_{m\to m-1} = P_{m-1\to m} = p_{m-1/2}W(I+m)(I-m+1), \qquad \ldots\ldots(5)$$

where for each line $p = \frac{1}{2}\gamma^2H_1{}^2T_1g(\nu)$; γ is the nuclear gyromagnetic ratio, $2H_1$ is the amplitude of the linearly polarized radio-frequency magnetic field and $g(\nu)$ is a normalized line-shape function. At the centre of each line $g(\nu) = 2T_2$ and $p = \gamma^2H_1{}^2T_1T_2$.

Taking the general case in which radio-frequency power is applied to all $2I$ lines, we find from equations (1) to (5) that a steady state is reached when

$$N_m - N_{m-1} = \frac{n_0}{1+p_{m-1/2}}. \qquad \ldots\ldots(6)$$

The measured absorption intensity of any spectral line is proportional to the population difference between the two relevant levels, and from equation (6) this is seen to depend only upon the power applied at the frequency of that line, and is not affected by the simultaneous saturation of other lines. This conclusion is a generalization of the result given for $I=\frac{3}{2}$ by Pound (1950).

So far we have assumed that the $2I$ lines are all resolved and the energy level differences therefore all unequal. Suppose now that some or all of the lines are superposed. Some or all of the energy level differences are now equal and spin–exchange of quanta may occur. Such exchanges take place in times of order T_2 which is much shorter in solids than the time T_1 which governs the spin–lattice relaxation processes. Extra terms must now be added to equation (1) to describe these rapid exchanges. It turns out however that for magnetic relaxation the solution given by equation (6) is unaltered.

Suppose the energy difference between levels m and $m-1$ is identical with that between levels $m'+1$ and m'. Nuclei in levels m and m' can undergo mutual transitions to the levels $m-1$ and $m'+1$ respectively. The probability of this event will be proportional to $N_m N_{m'}$; the reverse process will be proportional to $N_{m-1}N_{m'+1}$. We must therefore add to equation (1) a term which is proportional to

$$(N_m N_{m'} - N_{m-1}N_{m'+1}). \qquad \ldots\ldots(7)$$

However if we substitute from equation (6) and neglect second-order terms we readily find that equation (7) is zero. Thus equation (6) still provides the steady-state solution even when spin–exchange terms are included. The saturation factor for superposed lines is therefore still $(1+p)^{-1}$.

2.2. *Quadrupole Relaxation*

Here the lattice can induce transitions such that $\Delta m = \pm 1$ or ± 2. The equation governing the population of level m is now:

$$\begin{aligned}\dot{N}_m = {} & N_{m+2}W_{m+2\to m} + N_{m+1}(W_{m+1\to m} + P_{m+1\to m}) \\ & - N_m(W_{m\to m+2} + W_{m\to m+1} + W_{m\to m-1} + W_{m\to m-2} + P_{m\to m+1} + P_{m\to m-1}) \\ & + N_{m-1}(W_{m-1\to m} + P_{m-1\to m}) + N_{m-2}W_{m-2\to m}. \qquad \ldots\ldots(8)\end{aligned}$$

We have the relations

$$W_{m-1\to m} = W_{m\to m-1}(1+\Delta), \qquad W_{m-2\to m} = W_{m\to m-2}(1+2\Delta) \qquad \ldots\ldots(9)$$

and from Pound (1950)

$$W_{m\to m-1} = A_1(2m-1)^2(I-m+1)(I+m) \qquad \ldots\ldots(10)$$

$$W_{m\to m-2} = A_2(I+m)(I+m-1)(I-m+1)(I-m+2). \qquad \ldots\ldots(11)$$

The constants A_1 and A_2 are proportional to the appropriate spectral density functions at frequencies ν_0 and $2\nu_0$ respectively. These two constants would be equal if the fluctuations in the electrostatic environment were isotropic and had equal intensity at the two frequencies. In the crystals we are considering these conditions are not fulfilled. The two constants will therefore generally differ, though they can be expected to be of the same order, as is illustrated by the calculations of Van Kranendonk (1954). At the expense of complication, the analysis which follows could be carried through for a general ratio A_2/A_1. However, investigation of some simpler cases shows that the relative saturation behaviour of the spectral lines is not very sensitive to the relative values of A_1

and A_2 provided they are of the same order. In distinguishing between the different saturation behaviour for magnetic and quadrupolar processes we therefore make the approximation $A_1=A_2=A$; the agreement between theory and experiment for those crystals whose relaxation mechanism is quadrupolar is good enough to support the approximation. Pound (1950), who made the same simplification implicitly when calculating the modification of intensity of one spectral line caused by saturation of another, also found reasonable agreement for sodium nitrate at room temperature, while more recently Goldburg (1959), working at 77°K, has found that A_1 and A_2 differ by only 10%. The approximation not only avoids the inclusion in our equations of a parameter whose precise value is generally not known but, as we now show, also enables the spin–lattice relaxation process to be described by a single time T_1, which would otherwise not be the case.

If all the P terms are zero, equation (8) describes the spin–lattice relaxation of the system in the absence of radio-frequency power. If at any instant the populations can be described by a spin temperature T_s, with equal differences n_s between the populations of adjacent levels, then equation (8) with equations (9), (10) and (11) reduces to

$$\dot{N}_m=A(8I^2+8I-6)(n_0-n_s)m. \qquad \ldots\ldots(12)$$

Thus

$$\dot{N}_m-\dot{N}_{m-1}=A(8I^2+8I-6)(n_0-n_s), \qquad \ldots\ldots(13)$$

which is independent of m. It therefore follows, as in the case of magnetic relaxation, that if at one instant the population differences can be described by a spin temperature, they can be so described at all later times. Integration of equation (13) shows that the spin–lattice relaxation time T_1 is given by

$$[A(8I^2+8I-6)]^{-1}.$$

When later we write $1/2W$ for T_1, the value of W for quadrupolar relaxation is given by

$$W=A(4I^2+4I-3). \qquad \ldots\ldots(14)$$

We now proceed to obtain the saturation behaviour of the $2I$ lines. The level populations are now more inter-related and the population difference between two adjacent levels is changed not only by the application of power to the line appropriate to the levels, but also by applying power to other lines. The saturation factors differ from line to line and the general solution is complicated. We therefore treat here only the cases of $I=1$, which is simple, and of $I=\frac{3}{2}$ and $\frac{5}{2}$ which we need later.

$I=1$.

We find from equation (8) with equations (5), (9), (10), (11) and (14) that a steady state is reached when

$$N_1-N_0=\frac{n_0(1+5p_{-1/2})}{(1+3p_{1/2}+3p_{-1/2}+5p_{1/2}p_{-1/2})}, \qquad \ldots\ldots(15)$$

with a similar equation for N_0-N_{-1}. If power is applied to one line only, so that $p_{-1/2}=0$, $p_{1/2}=p$, we have

$$N_1-N_0=\frac{n_0}{1+3p}, \quad \text{and} \quad N_0-N_{-1}=\frac{n_0(1+5p)}{1+3p}. \qquad \ldots\ldots(16)$$

The saturation factor is thus $(1+3p)^{-1}$ for either line. When $p\gg 1$ the population difference of the line to which power is not applied is enhanced by a factor 5/3.

If the crystal is oriented so that the two lines are superposed, we have $p_{1/2}=p_{-1/2}=p$, and we find

$$N_1-N_0=N_0-N_{-1}=\frac{n_0}{1+p}. \qquad \ldots\ldots(17)$$

The saturation factor is thus $(1+p)^{-1}$ for the combined lines. Three times as much power is therefore required to produce the same degree of saturation compared with each line separately. On the other hand if the relaxation process were magnetic no difference in power would be required.

In deriving equation (17) the spin–exchange process has been neglected. A term proportional to $N_1N_{-1}-N_0^2$ should be added to equation (8) when the two lines are superposed to take account of this process. However substitution of equation (17) in this term leads to zero, showing that this symmetrical spin–exchange does not alter the steady-state level population.

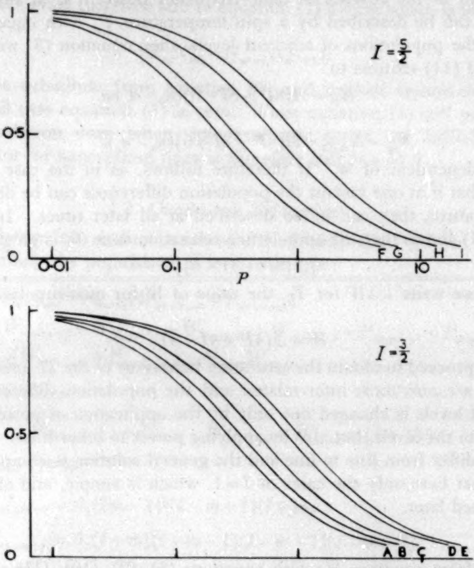

Figure 1. Calculated saturation curves for quadrupolar relaxation. In the upper diagram for $I=\frac{5}{2}$ curve F refers to the centre line, curve G to an inner satellite, curve H to an outer satellite, curve I to all lines superposed. Superposed inner satellites give a curve close to curve F and superposed outer satellites give a curve close to curve H.

In the lower diagram for $I=\frac{3}{2}$ curve A refers to the centre line, curve B to superposed satellites, curve C to a satellite line, curve D to a satellite superposed on the centre line, curve E to all three lines superposed.

For $I=1$ curve B refers to single lines and curve E to the two lines superposed.

Curve B in figure 1 shows the calculated saturation behaviour for each line separately, while curve E shows the behaviour of the superposed lines.

$I=\frac{3}{2}$.

The saturation of the three resolved lines has been treated previously (Andrew and Swanson 1957), and the results are summarized in table 1, together with all others derived here. The saturation factor of a satellite line is $(1+9p/4)^{-1}$ so that its saturation requires 16/9 times the power required to produce the same degree of saturation in the centre line, for which the saturation factor is $(1+4p)^{-1}$. Qualitatively this difference in behaviour arises because, from equation (10), $W_{1/2\to-1/2}$ is zero and there is no direct relaxation between the levels $m=\pm\frac{1}{2}$. Relaxation of the centre line is therefore indirect by sequences of transitions such as $m=\frac{1}{2}$ to $m=-\frac{3}{2}$ followed by $m=-\frac{3}{2}$ to $m=-\frac{1}{2}$. On the other hand $W_{3/2\to1/2}$ and $W_{-3/2\to-1/2}$ are not zero; relaxation is possible by both direct and indirect transitions, and is therefore more rapid.

Table 1. Values of x in the Saturation Factor $(1+xp)^{-1}$

	Magnetic dipole relaxation	Electric quadrupole relaxation
$I=1$, either line	1	3
$I=1$, both lines superposed	1	1
$I=3/2$, centre line	1	4
$I=3/2$, either satellite	1	9/4
$I=3/2$, satellites superposed	1	3
$I=3/2$, centre line and one satellite superposed	1	14/11
$I=3/2$, all lines superposed	1	1
$I=5/2$, either outer satellite	1	837/539
$I=5/2$, either inner satellite	1	1704/539
$I=5/2$, centre line	1	49/11
$I=5/2$, outer satellites superposed	1	18/11
$I=5/2$, inner satellites superposed	1	48/11
$I=5/2$, all lines superposed	1	1

In our earlier paper cases of superposed lines were also considered, but the spin–exchange process, which can occur in these cases, was neglected. Fortunately it turns out that in many cases the inclusion of the spin–exchange process does not affect the solution, while in the others the effect is small.† Three cases must be considered:

(i) When the crystal is so oriented that all three lines are superposed. Putting $p_{-1}=p_0=p_1=p$ in equation (8) we find on reduction that the saturation factor for the combined lines is $(1+p)^{-1}$, exactly as for magnetic relaxation. The spin–exchange terms, when included, do not therefore affect the solution. This case is not commonly encountered in practice since second-order perturbations usually prevent all three lines coalescing at any crystal orientation.

(ii) When the two satellites only are superposed. Putting $p_1=p_{-1}=p$ and $p_0=0$ we obtain a symmetrical set of equations (8), and find a saturation factor of $(1+3p)^{-1}$. Here again the spin–exchange process does not affect the solution, and we can show that this is true generally when a superposed pair of symmetrical satellites is saturated. The population factor, equation (7), which governs this process is

---

† Our attention was drawn to the need to include this process by the work of Abragam and Proctor (1958) on the related problem of ultrasonic relaxation. We are grateful to Dr. Proctor for giving us details of this work before publication.

$$(N_m N_{m'} - N_{m-1} N_{m'+1}) = \left(\frac{N}{2I+1}\right)[(N_m - N_{m-1}) - (N_{m'+1} - N_{m'})]. \qquad \ldots\ldots(18)$$

If we have symmetrical satellites, $m' = -m$, and the symmetry of the equations (8) ensures the equality of the two terms in the square bracket, and makes the population factor zero.

(iii) When the centre line and one satellite are superposed. The spin–exchange terms do affect the solution in this case. Suppose $p_1 = p_0 = p$ and $p_{-1} = 0$. Using equation (18) we must subtract a term $aW(N_{-1/2} - 2N_{1/2} + N_{3/2})$ from equation (8) for $\dot{N}_{-1/2}$ and $\dot{N}_{3/2}$, and add twice this term to the corresponding equation for $\dot{N}_{1/2}$ where the constant a is of order T_1/T_2. Solving the four equations we find that the saturation factor for the combined lines is

$$\left(1 + \frac{11}{4}a + \frac{33}{7}p\right) \Big/ \left(1 + \frac{11}{4}a + \frac{25}{4}p + \frac{7}{2}ap + 6p^2\right). \qquad \ldots\ldots(19)$$

Omission of the spin–exchange process is equivalent to putting $a = 0$ in equation (19), yielding the expression given earlier (Andrew and Swanson 1957). In the crystals examined $T_2 \sim 10^{-4}$ sec and $T_1 \sim 1$ sec so that $a \sim 10^4 \gg 1$, giving in good approximation a saturation factor $(1 + 14p/11)^{-1}$. Actually equation (19) is insensitive to the value of a; as table 2 shows, the saturation factor varies by only 2% as a goes from 0 to ∞.

The calculated saturation curves for the separate and superposed lines are illustrated in figure 1.

Table 2. Values of Expression (13) for:

p	0·01	0·03	0·1	0·3	1	3	10	30
$a = 0$	0·984	0·956	0·873	0·707	0·431	0·206	0·073	0·025
$a = 1$	0·987	0·962	0·882	0·716	0·434	0·206	0·073	0·026
$a = \infty$	0·987	0·963	0·886	0·724	0·440	0·208	0·073	0·026

So far it has been assumed that when resolved, the three resonance lines are sufficiently close to allow all three Boltzmann factors to be given by $h\nu_0/kT$ with sufficient accuracy. The calculation has therefore been extended to the case of wide-splitting using three different Boltzmann factors, and is found to give the same saturation factors as before. The saturation behaviour of a line may nevertheless change with change of orientation of the crystal in the magnetic field since both T_1 and T_2 are in general anisotropic; a different level of radio-frequency power may therefore be needed to maintain the same saturation factor.

$I = \frac{5}{2}$.

The procedure outlined for $I = \frac{3}{2}$ has been repeated for $I = \frac{5}{2}$. The saturation factors are expressible in the form $(1 + xp)^{-1}$, and values of x which range from 1 to 4·45 are given in table 1 for the resolved lines and for various combinations of superposed lines. When all five lines are superposed with all $p_{m-1/2}$ equal, the saturation factor of the combined lines is $(1+p)^{-1}$ as for magnetic relaxation. This is in fact a general result for all I, which may readily be obtained by finding the steady-state solution of the set of equations (8) with all $p_{m-1/2}$ equal. Inclusion of the spin–exchange terms does not affect the solution.

The calculated saturation curves for the separate and superposed lines are illustrated in figure 1.

§ 3. EXPERIMENTAL PROCEDURE

For each crystal the nuclear magnetic resonance spectrum was recorded and the lines were identified by observing their dependence on crystal orientation. The separate lines and certain combinations of lines were then progressively saturated by increasing the applied radio-frequency power. Because of the wide range of power needed to saturate the nuclei in different crystals a bridge method of detection was used followed by phase-sensitive detection. Radio-frequency power was supplied by a signal generator which was equipped with a calibrated attenuator. All experiments were carried out in the field of 6040 oersteds of a permanent magnet. Saturation curves were then obtained in the usual manner and when plotted semi-logarithmically generally gave a family of curves fitting a $(1+xp)^{-1}$ law reasonably well, although in a few cases the family of curves was less steep. Typical curves obtained for ^{23}Na nuclei in sodium nitrate have been shown previously (Andrew and Swanson 1957). After making any necessary correction for differing line width of the resonance lines, relative values of x were obtained and these were compared with ratios of x taken from table 1. If the relaxation mechanism is magnetic, all saturation curves should be identical after adjusting for line-width differences.

Experiments were carried out on the ^{23}Na nuclei in synthetic crystals of sodium nitrate, sodium thiosulphate and sodium chlorate, on the ^{7}Li nuclei in natural crystals of spodumene, on the ^{27}Al nuclei in natural crystals of spodumene and euclase, and on the ^{11}B nuclei in a synthetic crystal of borax.

§ 4. RESULTS

4.1. *Sodium Nitrate, $NaNO_3$*

A crystal rhomb, about 1 cm^3 in volume, was cleaved from a larger synthetic crystal provided by Hilger & Watts Ltd., through the kindness of Mr. J. Skinner. All sodium nuclei are situated on equivalent sites on the trigonal axis of the rhombohedral unit cell. The spectrum consisted of three sharp lines of approximately equal breadth (Eades, Hughes and Andrew 1958). Saturation curves were obtained for the three resonance lines separately and for a satellite superposed on the centre line. Second-order shifts exceeded the line widths and prevented superposition of all three lines. The saturation curves obtained have been published earlier (Andrew and Swanson 1957)† and provide a good illustration of the behaviour expected with quadrupole relaxation. The curves fitted a $(1+xp)^{-1}$ law quite well, and when plotted semi-logarithmically gave three similar curves displaced laterally by an amount which is a measure of the ratio of values of x. The ratio of values of x for the centre line and the satellite was found to be 2·4 dB, for the centre line and the superposed lines it was 5·4 dB, and for the satellite and the superposed lines it was 3·0 dB; the theoretical ratios for quadrupolar relaxation, using table 1, are 2·5, 5·0 and 2·5 dB respectively. The accuracy of the measured ratio is not much better than 1 dB, and the agreement is therefore very satisfactory.

---

† Regrettably the figure in this earlier paper was incorrectly labelled. Curve *a* and the half-filled circles refer to the centre line, while curve *b* and the open circles refer to a satellite line.

4.2. *Sodium Thiosulphate, $Na_2S_2O_3 . 5H_2O$*

Analar material, twice re-crystallized, was used to grow a single crystal, about 2 cm^3 in volume, by slow evaporation from a seeded saturated solution. There are two different molecular orientations in the monoclinic unit cell, each of which has two non-equivalent sodium nuclei. Itoh, Kusaka and Yamagata (1954) therefore found a ^{23}Na resonance spectrum consisting of twelve lines: four centre lines each with two satellites. They found quadrupole coupling constants of 0·83 Mc/s and 2·26 Mc/s for the two ^{23}Na nuclei in each molecule; these nuclei will be referred to as type a and type b respectively.

Saturation curves were obtained for a centre line and its satellites for both types of nuclei at a crystal setting where they were just resolved and for a superposed centre line and satellite of type b. The corrected relative power levels required to produce a saturation factor of 0·5 were:

Line	Relative power for half saturation
Centre, type a	0 dB
Satellite, type a	3·0 dB
Centre, type b	3·8 dB
Satellite, type b	6·5 dB
Superposed centre and satellite, type b	9·2 dB

The relaxation mechanism is therefore quadrupolar for both nuclei. Since the nuclei of type a require a power level approximately 3·7 dB higher to produce the same degree of saturation as nuclei of type b and, since the lines have the same width, it is concluded that the value of T_1 for nuclei of type a is about 2·4 times larger than for nuclei of type b. Since type b nuclei have the larger quadrupole coupling constant, and therefore have a stronger electrostatic interaction with their environment, this result is consistent with a quadrupolar relaxation mechanism.

4.3. *Sodium Chlorate, $NaClO_3$*

Material of commercial grade was purified by nine re-crystallizations and then used to grow a single crystal by slow evaporation from a saturated solution. Each cubic unit cell contains four sodium nuclei disposed tetrahedrally on the body diagonals, with equivalent but differently oriented environments. The crystal was mounted so that the applied magnetic field was normal to a crystal face. In this setting all the body diagonals make an angle $\cos^{-1}(1/\sqrt{3})$ with the field, and the first-order splitting for all sodium nuclei is zero. By turning the crystal through a small angle all the satellite lines could be separated and by turning through a larger angle the centre lines from different nuclei could be separated

Saturation curves were obtained for the centre lines when superposed and when resolved, and as might be expected they did not differ significantly. Nor was any significant difference found among the saturation curves of the various satellites. Saturation curves were also obtained for superposed satellites and for a superposed satellite and centre line.

The satellite lines required 2·9 dB more power to produce the same degree of saturation as the centre lines as illustrated in figure 2. A quadrupolar mechanism is therefore indicated, since as table 1 shows, the ratio predicted is 2·5 dB. The behaviour of the superposed satellites was at first sight anomalous since they required 3·7 dB more power than the centre lines, whereas table 1 predicts only 1·2 dB. However the satellites from nuclei on all four types of site were not all superposed at any orientation of the crystal, and the lines studied originated from nuclei on two of the four sites only; we call these latter nuclei type a and the others, whose lines are not being saturated, we call type b. Although the satellite lines of the two types of nucleus were thus resolved in this crystal orientation, the centre lines from all nuclei were still superimposed. Rapid spin–exchange can therefore take place between states $\pm\frac{1}{2}$ of type a and states $\mp\frac{1}{2}$ of type b, and by this means the relaxation processes of type b nuclei can aid the disposal to the lattice of excess energy possessed by type a nuclei. More power is therefore needed to saturate the superposed satellites of type a than that calculated in §2.2. We omit the details of the calculation of this special case. Four equations of type (8) govern the level populations of type a nuclei and another set of four equations govern the populations for type b nuclei. The two sets of equations are linked through the spin–exchange terms. In the limit of rapid spin–exchange ($T_1 \gg T_2$) the saturation factor for the combined satellites was found to have the form $(1+xp)^{-1}$, where x has the value 9/4. The power required for saturation is now 2·5 dB, which is much closer to the value observed. The anomalous behaviour thus turns out to have the nature of an exception which proves the rule, and also provides a good illustration of the role played by spin–exchange processes.

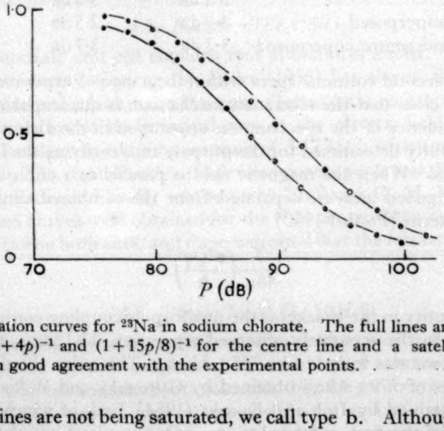

Figure 2. Saturation curves for ^{23}Na in sodium chlorate. The full lines are the theoretical curves $(1+4p)^{-1}$ and $(1+15p/8)^{-1}$ for the centre line and a satellite respectively and are in good agreement with the experimental points.

The saturation behaviour of a single satellite of type a is also modified by spin–exchange when the centre lines of types a and b are superposed. The value of x decreases from 9/4 to 15/8, requiring 0·8 dB more power for saturation.

The superposed satellite and centre line investigated consisted of a satellite from nuclei of type a superposed on a centre line from nuclei of both types. In this case spin–exchange can take place among the three equally spaced levels of type a, and between these levels and the levels $\pm\frac{1}{2}$ of type b. Analysis of this more complicated situation shows that for $T_1 \gg T_2$ the saturation factor is again of the form $(1+xp)^{-1}$, where x has the value 22/13.

The results are summarized below:

	Relative power for half saturation		
Line	Observed	Theory (Quad)	Theory (Mag)
Centre	0 dB	0 dB	0 dB
Satellite	3·1 dB	3·3 dB	0 dB
Satellites superposed	3·7 dB	2·5 dB	0 dB
Satellite and centre superposed	3·3 dB	3·7 dB	0 dB

The first and second columns agree within the range of experimental error, and it is therefore clear that the relaxation mechanism is quadrupolar.

The dependence of the spectrum on orientation in the vicinity of the setting used was carefully determined for the purpose of identifying the lines and superposition angles. When the magnetic field is parallel to a cubic axis all satellite lines are superposed and are separated from the combined centre line by the second-order term (Pound 1950)

$$\frac{7}{48\nu_0}\left(\frac{e^2Qq}{h}\right)^2, \qquad \ldots\ldots(20)$$

where the quantity in the bracket is the quadrupole coupling constant. Equating equation (20) to the accurately observed separation, 13·12 kc/s, the quadrupole coupling constant was found to be 785 ± 8 kc/s. This value should be compared with the values of 779 ± 4 kc/s obtained by Gutowsky and Williams (1957) and 801 ± 8 kc/s obtained by Itoh and Kusaka (1954), both of which were obtained from a study of the first-order splitting. Our result shows that the coupling constant can be accurately determined from the smaller second-order splitting with the relatively small sweep available with a bridge apparatus.

4.4. *Spodumene, $LiAl(SiO_3)_2$*

The ^{7}Li and ^{27}Al resonances were investigated in five natural crystals chosen from a number of mineralogical specimens for their clarity and lack of colouration. One crystal was lent by the Museum d'Histoire Naturelle in Paris, through the kind agency of Dr. N. F. M. Henry.

The four lithium nuclei in the monoclinic unit cell have equivalent environments. Volkoff, Petch and Smellie (1952) investigated the ^{7}Li spectrum and found a quadrupole coupling constant of 75·7 kc/s with an asymmetry parameter of 0·79. The four aluminium nuclei also have equivalent environments. Petch, Cranna and Volkoff (1953) have investigated the ^{27}Al spectrum and found the much larger quadrupole coupling constant of 2·95 Mc/s, with an asymmetry parameter of 0·94.

Saturation curves have been obtained for the ^{7}Li resonance for the centre line, for satellites and for all three lines superposed, and for the ^{27}Al resonance for the centre line and inner satellites. The ^{27} Al lines are broadened more by crystalline imperfections, and no outer satellites were observed. Each family of saturation curves were the same within $\pm 0{\cdot}6$ dB, indicating that the relaxation mechanism is magnetic for both nuclei.

The spin–lattice relaxation times for the ^{7}Li and ^{27}Al nuclei were both shorter in some crystals than in others, as evidenced by the relative power levels necessary for a given degree of saturation after correction for differing line widths. The wide range of values of T_1, covering a ratio of 200, provides further support for a magnetic relaxation process, since the density of magnetic relaxation centres depends upon the purity of the crystal; on the other hand the efficiency of a quadrupolar relaxation process is not expected to differ widely from one crystal to the next.

4.5. *Euclase*, $HBeAlSiO_5$

The monoclinic unit cell contains four aluminium nuclei. An investigation of the ^{27}Al resonance spectrum by Eades (1955) has shown that there are two types of lattice site which have the same electrostatic environment but with a different orientation of the principal axes of the electric-field gradient tensor. He found a quadrupole coupling constant of 5·17 Mc/s with an asymmetry parameter of 0·70. The crystal used in the present experiments was the larger specimen used by Dr. Eades and kindly sent to us by Professor G. M. Volkoff.

Saturation curves were obtained for the ^{27}Al centre lines and inner satellites from the nuclei on both sites, and these indicated that the relaxation was magnetic.

4.6. *Borax*, $Na_2B_4O_7 . 10H_2O$

Analar material, twice re-crystallized, was used to grow a single crystal about 1 cm^3 in volume by slow evaporation from a seeded saturated solution. The monoclinic unit cell contains four molecules, but the structure has not been fully determined. The crystal was mounted with the axis of rotation in its (010) plane. Quadrupole-split spectra for this crystal have not previously been obtained and were not fully explored in the present work. ^{11}B resonance lines were readily found, and saturation curves were obtained for three lines which, from their angular dependence, were identified as a centre line and its two satellites. The corrected saturation curves for the centre line, for a satellite and for a centre line and satellite superposed were the same within $\pm 0{\cdot}3$ dB, indicating that the relaxation mechanism was magnetic. A brief investigation failed to show ^{23}Na lines, and as the bridge spectrometer was not suited to a search this spectrum was not pursued.

§ 5. DISCUSSION

It is not perhaps surprising that the relaxation mechanism was found to be magnetic for all the natural mineral crystals examined since these might be expected to contain considerable paramagnetic impurity. Differing concentrations of impurity would account for the range of 200 in values of T_1 for the specimens of spodumene. The longest values of T_1 for spodumene were approximately

0·1 sec for both ^{7}Li and ^{27}Al. If spin–lattice relaxation is effected by spin–exchange diffusion, as proposed by Bloembergen (1949), the relaxation time should be given, as Khutsishvili (1956) and de Gennes (1958) have shown, by

$$T_1 = (4\pi DcN)^{-1}, \qquad \ldots\ldots (21)$$

where D is the spin-diffusion coefficient, c is a temperature-dependent relaxation length which is a measure of the range of direct nuclear relaxation around each impurity centre, and N is the number of impurities per unit volume. While neither c nor D can be calculated with accuracy, the value of c is probably not far from 2×10^{-7} cm for our crystals at room temperature, while $D \sim 5 \times 10^{-12}$ cm^2 sec^{-1}, thus leading to the order of magnitude relation

$$T_1 \sim 10^{-17} N^{-1}. \qquad \ldots\ldots (22)$$

Using this relation it is seen that an impurity concentration N of order 10^{18} cm^{-3} is required to account for the relaxation time observed for the crystal of spodumene with the largest relaxation times. A spectroscopic analysis of part of this crystal, carried out in the Department of Agricultural Chemistry of the College, revealed 90 parts per million by weight of paramagnetic elements, predominantly manganese; this corresponds to $N \sim 2 \times 10^{18}$ cm^{-3}. This concentration was confirmed in order of magnitude by the integrated intensity of the X-band paramagnetic resonance spectrum, kindly recorded by Professor D. J. E. Ingram. The concentration of impurity is therefore of the right order to account for the relaxation time.

For the pure synthetic crystals of sodium nitrate, sodium thiosulphate and sodium chlorate the relaxation process for the ^{23}Na nuclei was in each case found to be quadrupolar. A spectrophotometric analysis, carried out in the Chemistry Department of the College, showed concentrations of 8, 4 and 3 parts in 10^7 respectively of iron, the principal paramagnetic impurity. If the relaxation process had been magnetic, concentrations of paramagnetic impurity at least ten times greater would have been needed, using equation (21), to account for the observed relaxation times.

Tabulated below are the quadrupole moments and ionic polarization factors γ_∞ given by Bersohn (1958) for the nuclei investigated in this work:

Nucleus	Q (barns)	γ_∞	$Q^2(1-\gamma_\infty)^2$
^{7}Li	0·1	0·256	0·005
^{11}B	0·0355	0·146	0·0009
^{23}Na	0·100	−4·53	0·31
^{27}Al	0·149	−2·59	0·29

The quadrupole moment of the nucleus, together with the surrounding electrons, is $Q(1-\gamma_\infty)$, and the relative strength of the quadrupolar relaxation mechanism in ionic crystals is given in order of magnitude by the square of this quantity, which is shown in the last column. For ^{23}Na and ^{27}Al the values of this quantity are roughly equal and the quadrupolar mechanism should therefore be of comparable strength for each in ionic crystals. In the pure synthetic sodium crystals the magnetic mechanism is some ten times weaker than the quadrupolar mechanism. On the other hand even the purest spodumene crystal contains over a hundred times more paramagnetic impurity than the synthetic crystals; for the ^{27}Al nuclei in the spodumene crystals the magnetic relaxation mechanism therefore dominates. This conclusion applies *a fortiori* to the ^{7}Li nuclei in spodumene since the value of $Q^2(1-\gamma_\infty)^2$ is two orders of magnitude smaller than for ^{27}Al. Further evidence that the relaxation of ^{7}Li nuclei is magnetic in the spodumene crystals is provided by the fact that its relaxation time is of the same order as for the ^{27}Al nuclei; if the effective mechanism were quadrupolar the ^{7}Li relaxation time should be much longer than that for ^{27}Al.

The relaxation of ^{11}B nuclei in borax provided the only example of a pure synthetic crystal for which the relaxation mechanism was found to be magnetic. The magnetic relaxation mechanism is not expected to be appreciably stronger in borax than in the other three synthetic crystals since the amount of iron found was of the same order of magntiude. On the other hand the value of $Q^2(1-\gamma_\infty)^2$ is some three hundred times smaller than for ^{23}Na. Whereas the quadrupolar mechanism is some ten times stronger than the magnetic mechanism for ^{23}Na in the nitrate, chlorate and thiosulphate crystals, it is some ten times weaker than the magnetic mechanism in borax. Using equation (22) we calculate that T_1 for the magnetic relaxation mechanism should be about 5 seconds. The observed value, 1·3 sec, is rather lower, but in view of the very approximate nature of the calculation the discrepancy cannot be regarded as serious.

REFERENCES

ABRAGAM, A., and PROCTOR, W. G., 1958, *Phys. Rev.*, **109**, 1441.
ANDREW, E. R., and SWANSON, K. M., 1957, *Proc. Phys. Soc.* B, **70**, 436.
BERSOHN, R., 1958, *J. Chem. Phys.*, **29**, 326.
BLOEMBERGEN, N., 1949, *Physica*, **15**, 386.
BLOEMBERGEN, N., PURCELL, E. M., and POUND, R. V., 1948, *Phys. Rev.*, **73**, 679.
EADES, R. G., 1955, *Canad. J. Phys.*, **33**, 286.
EADES, R. G., HUGHES, D. G., and ANDREW, E. R., 1958, *Proc. Phys. Soc.*, **71**, 1019.
DE GENNES, P. G., 1958, *J. Phys. Chem. Solids*, **7**, 345.
GOLDBURG, W. I., 1959, *Bull. Amer. Phys. Soc.* II, **4**, 252.
GUTOWSKY, H. S., and WILLIAMS, G. A., 1957, *Phys. Rev.*, **105**, 464.
ITOH, J., and KUSAKA, R., 1954, *J. Phys. Soc. Japan*, **9**, 434.
ITOH, J., KUSAKA, R., and YAMAGATA, Y., 1954, *J. Phys. Soc. Japan*, **9**, 209.
KHUTSISHVILI, G. R., 1956, *J. Exp. Theor. Phys. U.S.S.R.*, **31**, 424.
KRANENDONK, J. VAN, 1954, *Physica*, **20**, 781.
PETCH, H. A., CRANNA, N. G., and VOLKOFF, G.M., 1953, *Canad. J. Phys.*, **31**, 837.
POUND, R. V., 1950, *Phys. Rev.*, **79**, 685.
VOLKOFF, G. M., PETCH, H. E., and SMELLIE, D. W. L., 1952, *Canad. J. Phys.*, **30**, 270.

An Evaluation of the Deuteron Velocity Spectrum in SCEPTRE III

By S. E. HUNT

Research Laboratory, Associated Electrical Industries, Aldermaston, Berkshire

Communicated by D. R. Chick; MS. received 14*th September* 1959, *in final form* 16*th November* 1959

Abstract. The mean energies of protons observed at 45° and 135° to the direction of positive gas current flow in the toroidal pinched discharge apparatus SCEPTRE III and the energy spread of these protons indicate that they originate from fusing deuterons having a range of centre-of-mass velocities in the ϕ direction. The experimental results can be explained in terms of a fast tail of deuterons with velocities between 4×10^7 cm sec^{-1} and 16×10^7 cm sec^{-1} fusing with a much larger number of deuterons travelling at lower velocities. The proton yield indicates that the deuteron population falls off roughly exponentially with increasing velocity, about 1 in 10^3 of the total deuterons present having velocities of between 4 and 16×10^7 cm sec^{-1}. Such a distribution is consistent with a very high proportion of the deuterons present having velocities of less than 10^7 cm sec^{-1} in the ϕ direction, as is indicated by spectroscopic measurements. The proton energy measurements also indicate that the deuterons are moving in the θ sense and the effect of this motion is also considered.

---

§ 1. INTRODUCTION

THE mean energy of protons emitted at 45° to the direction of positive gas current flow in SCEPTRE III (Allen *et al.* 1958) has been found to be significantly higher than that of the protons emitted at 135° (Jones *et al.* 1958, 1960). This energy difference indicates that the centre of mass of the fusing deuterons has a velocity component in the direction of positive gas current flow, i.e. the ϕ direction. Initially a mean value of $4 \pm 1 \times 10^7$ cm sec^{-1} was estimated for this velocity which could be produced either by an accelerated group of deuterons of energy about 8 kev striking deuterons effectively at rest, or by a general motion of the deuteron system in which fusion was produced by a random thermal motion of the deuterons, superimposed on the general mass motion. The second possibility appears to have been eliminated by spectroscopic observations in which the Doppler shifts of impurity lines indicated a general drift velocity of about one order of magnitude less than those required to produce the observed proton energy shifts (Hughes and Kaufman 1959).

Further detailed measurements of the energy spread of the proton groups emitted at 45°, 90° and 135° to the discharge show that this is greater than that which would be produced by an approximately mono-energetic group of incident deuterons.

The purpose of the present paper is to show that the observed proton yield, the difference in the mean energies of protons emitted at 45° and 135° to the direction of positive gas current flow, and the energy spread of these protons can be produced by a continuous distribution of deuteron energies between 2 kev and 30 kev such that the population of deuterons in each energy interval falls rapidly as the energy is increased. Such an energy distribution may well form the high energy tail of a general mass motion of velocity about 5×10^6 cm sec^{-1} for which a mechanism has been proposed by Ware (1959).

Protons are produced by deuterons in the high energy tail fusing with the much larger number of deuterons which have low energy corresponding to the peak in the population of the deutron energy spectrum. The velocity of these deuterons is negligible compared with that of those in the high energy tail so that they add little to the centre-of-mass velocity of the fusing system and, as far as the emitted proton energies are concerned, can be regarded as forming a stationary target. There is also evidence from the nuclear plate measurements of the proton energy that the deuterons have a motion in the θ sense and possibly radially towards and away from the main axis of the discharge. The effect of these motions is also considered.

The statistical accuracy of the observed proton histograms precludes detailed analysis of their shape. They could all be fitted reasonably well to smooth Gaussian curves. The mathematical treatment is approximate since the statistical accuracy of the experimental results did not warrant a very refined treatment, but an effort has been made to estimate the possible limits of error which should be associated with the final estimate of the deuteron energy and velocity spectra.

§ 2. EXPERIMENTAL RESULTS

Details of the experimental methods of measuring the energies of protons emitted from SCEPTRE III are reported elsewhere, as are the experimental proton histograms and the measurements of the instrumental resolution of the proton cameras (Jones *et al.* 1958, 1959, 1960).

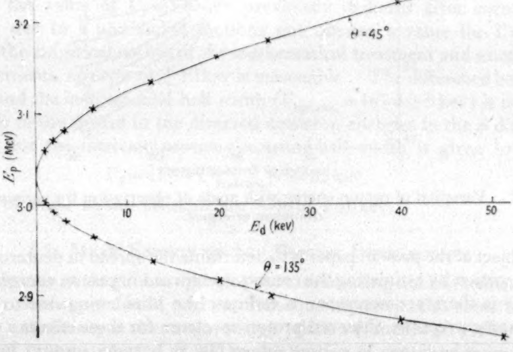

Figure 1. Variation in proton energy observed at 45° and 135° with energy of incident deuteron.

It is only necessary to state briefly here that the experimentally observed half width of four typical proton histograms taken at 45° and 135° to the direction of positive gas current flow were 190 kev, 200 kev, 200 kev and 215 kev, whilst those for monoenergetic protons of energy 3·0 MEV scattered into the proton camera were 165 kev and 170 kev. The uncertainty in half width introduced in fitting a Gaussian curve to the observed histograms was about ± 10 kev in the case of the SCEPTRE III histograms because of the limited statistical accuracy, and ± 5 kev in the case of mono-energetic protons. The mean values for the half widths 201 ± 5 kev and 167·5 ± 3 kev, are significantly different. Since the scanning procedure and processing of the nuclear emulsion plates were identical the increased energy spread in the proton groups observed from SCEPTRE III can be due to three factors : (i) A spread in the velocity spectrum in the ϕ direction of the fusing deuterons. The energy of the protons emitted at 45° to the direction of velocity of the centre of mass as a function of the incident deuteron energy is shown in figure 1. (ii) Motion of the deuterons in the θ sense or radially towards or away from the central axis of the discharge at the time of fusion. (iii) The finite spread in the angle of acceptance about the nominal angles of the 45° and 135° cameras. The proton camera accepts protons of angles between 30° and 60° and 120° and 150° approximately, which leads to an energy spread which can be obtained from figure 2.

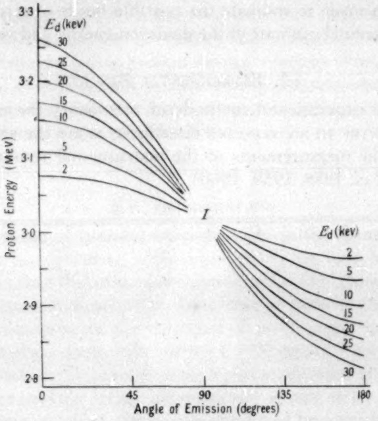

Figure 2. Variation of proton energy with angle of observation for various incident deuteron energies.

The object of the present paper is to determine the spread in deuteron velocities in the ϕ direction by estimating the consequent spread in proton energies observed at 45°. It is therefore necessary to estimate the broadening due to factors (ii) and (iii), and correct the observed proton spectrum for these effects.

§ 3. MOTION IN THE θ SENSE, AND RADIAL MOTION

The geometry of the proton camera was such that if a clockwise θ motion is postulated about an axis in the direction of positive gas current flow the right-hand side of the nuclear emulsion plates records mainly protons produced by deuterons travelling towards the camera in the θ sense and the left-hand side those due to deutrons travelling away from the camera in the θ sense.

The nuclear emulsion plates analysed showed a systematic difference in the mean energies of protons recorded on the left-hand and right-hand sides, the measured values of this difference being 0·08 ± 0·025 MEV ($B_\phi = 500$ gauss), 0·06 ± 0·025 MEV ($B_\phi = 1000$ gauss), 0·076 ± 0·03 MEV and 0·065 ± 0·03 MEV ($B_\phi = 1400$ gauss). The mean difference is 0·07 ± 0·015 MEV, which corresponds to a mean velocity of the fusing deuterons of 4×10^7 cm sec^{-1} in the θ direction, or a mean incident energy of about 2 kev due to this motion. The effect of this increased kinetic energy on the proton yield will be discussed later.

Graphical analysis shows that the addition of two distributions of half width 190 kev with a mean energy separation of 70 kev produces a distribution of half width 200 kev. A value of 190 kev for the half width of the proton spectrum corrected for broadening due to θ motions is therefore reasonable.

The histograms observed at 90° to the discharge have a half width in excess of the instrumental width of the 90° camera, and Jones, Young and Barnard (1960) have interpreted this broadening to be due to radial and θ motions of the fusing deuterons and have established an upper limit of 4×10^7 cm sec^{-1} for the radial plus θ velocity. This is essentially in agreement with the above result.

§ 4. BROADENING DUE TO FINITE ANGLE OF ACCEPTANCE

It will be seen from figure 2 that the variation in energy of the emitted proton with angle in the range 30°–60° and 120°–150° is relatively small for any of the values of deuteron energy of interest.

It is estimated that the finite acceptance angle itself produces a distribution in proton energies of half width $\Gamma_1 = 30$ kev. The corrected half width Γ for the proton spectrum can be obtained approximately by vector subtraction of Γ_1 from the combined half width Γ_2, $\Gamma = (\Gamma_2{}^2 - \Gamma_1{}^2)^{1/2}$, if the distributions are assumed to be of approximately Gaussian shape.

Taking the value of $\Gamma_2 = 190$ kev previously deduced after correction for broadening due to θ and radial motions one obtains a value for $\Gamma = 188$ kev. Because of the empirical nature of the mathematical treatment and uncertainty in the measurements, an error of ± 10 kev is reasonable. The difference between the half width and the instrumental half width ($\Gamma_{\text{instrum}} = 167{\cdot}5 \pm 5$ kev) is interpreted as being due to the spread in the directed deuteron energies in the ϕ direction.

A value for the intrinsic proton spectrum half width is given by

$$\Gamma_{\mathrm{p}} = (\Gamma^2 - \Gamma^2_{\text{instrum}})^{1/2} = 85 \text{ kev}.$$

The limits of error in this estimate are -40 to $+30$ kev.

§ 5. MEAN ENERGY OF THE PROTON DISTRIBUTION

Measurements of the proton energies were made using nuclear emulsion plates protected by thin copper foils, and are consequently subject to some systematic error due to uncertainty in the range–energy relation (Jones *et al.* 1958), but since the energy of protons emitted at 90° to the motion of centre of mass is known (3·03 MEV) and the variation in proton energy as a function of angle (figure 2) is symmetrical about 90°, a good estimate of the true proton energy at 45° can be obtained by adding one half the energy difference between the 135° and 45° observations to the known energy of the protons emitted at 90°.

$$E_{45^\circ\,\text{true}} = 3{\cdot}03 \text{ MEV} + \frac{E_{45\text{rel}} - E_{135\text{rel}}}{2}.$$

The values for $E_{45°\,\mathrm{true}}$ obtained for B_ϕ fields of 500, 1000 and 1400 gauss were 3·12, 3·145 and 3·12 Mev respectively. A mean energy of 3·13 Mev will therefore be taken to correspond to the peak of the intrinsic proton energy spectrum, which is shown in figure 3, where curves of half width 85 kev, 45 kev and 115 kev, corresponding to the calculated value and limits for Γ_p, are drawn.

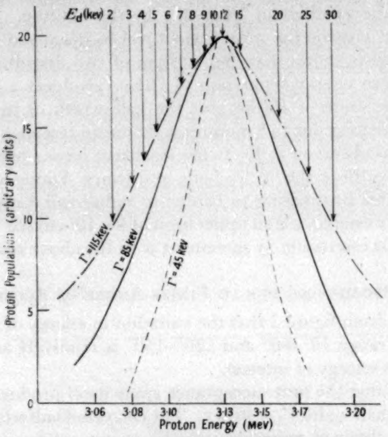

Figure 3. The intrinsic proton spectrum.

§ 6. ESTIMATION OF THE DIRECTED DEUTERON ENERGY SPECTRUM IN THE ϕ DIRECTION

The spread in the proton energies shown in figure 3 is produced by variation in the velocity of the centre of mass of the fusing deuterons in the ϕ direction. Initially the interaction will be considered between energetic deuterons in the fast tail of the energy distribution and slowly moving deuterons.

Since a very high proportion of the total deuterons present will be shown to be moving with low velocity they can be considered as a stationary target of thickness given by $v_d \times t \times d$ where v_d is the velocity of the fast incident particle, t the duration of the discharge (500 μsec) and d the density of target nuclei per cubic centimetre estimated from the known gas pressure and concentration due to the pinch effect ($d = 3 \times 10^{14}$ atoms cm^{-3} (Ware 1959)).

The yield of protons N_p in any given energy interval is thus given by

$$N_p = N_d \times \sigma \times v_d \times t \times d$$

where σ is the (d–d) cross section for the fusion reaction appropriate to the energy of the incident deuteron and N_d is the number of incident deuterons.

The yield of protons corresponding to a given deuteron energy interval can be estimated from figure 3. By measuring the total number of protons recorded and the solid angle of detection of the cameras the yield of protons has been estimated as 3×10^5 protons per discharge, which is in agreement with the estimate of the neutron yield obtained using neutron counters. The total area under each of the curves in figure 3 can therefore be taken to correspond to 3×10^5 protons and the yield in any energy interval estimated graphically.

The cross section for the fusion reaction has been measured for deuteron energies above 13 kev, (Arnold *et al.* 1954, Moffat, Roaf and Sanders 1952) but can be extrapolated to energies as low as a few kev (Brennan 1958). Measured and calculated values for the cross sections are given in table 1.

Table 1. D(d, p)^{3}H Reaction Cross Section

Observed Values

E_d(kev)	σ(d, p) (bn)	Worker
40	256×10^{-5}	Arnold
38	260×10^{-5}	Moffat
36	198×10^{-5}	Arnold
34	180×10^{-5}	Moffat
33	154×10^{-5}	Arnold
30	114×10^{-5}	Arnold
25	63×10^{-5}	Arnold
24	60×10^{-5}	Moffat
22	$39{\cdot}1 \times 10^{-5}$	Arnold
20	$25{\cdot}2 \times 10^{-5}$	Moffat
19	$21{\cdot}3 \times 10^{-5}$	Arnold
17	$14{\cdot}7 \times 10^{-5}$	Moffat
14·5	7×10^{-5}	Moffat
13	$3{\cdot}5 \times 10^{-5}$	Arnold

Calculated Values

E_d(kev)	σ(d, p) (bn)	E_d(kev)	σ(d, p) (bn)
10·0	$8{\cdot}55 \times 10^{-6}$	3·5	$1{\cdot}50 \times 10^{-9}$
9·0	$4{\cdot}44 \times 10^{-6}$	3·0	$2{\cdot}63 \times 10^{-10}$
8·0	$2{\cdot}03 \times 10^{-6}$	2·5	$2{\cdot}71 \times 10^{-11}$
7·0	$7{\cdot}89 \times 10^{-7}$	2·0	$1{\cdot}23 \times 10^{-12}$
6·0	$2{\cdot}38 \times 10^{-7}$	1·75	$3{\cdot}50 \times 10^{-13}$
5·5	$1{\cdot}66 \times 10^{-7}$	1·50	$1{\cdot}29 \times 10^{-14}$
5·0	$5{\cdot}09 \times 10^{-8}$	1·25	$4{\cdot}82 \times 10^{-16}$
4·5	$1{\cdot}92 \times 10^{-8}$	1·00	$5{\cdot}58 \times 10^{-18}$
4·0	$7{\cdot}46 \times 10^{-9}$		

Calculated values using $\sigma = 107/E \exp -44{\cdot}4E^{-1/2}$

In estimating the yield from the fusion reaction, account must be taken of the energy of the fusing system due to θ and possibly radial motions of the incident deuterons.

There must obviously be an energy spread associated with these motions, but in view of the lack of detailed knowledge of this, it is assumed that all incident deuterons have the calculated mean energy of 2 kev as a result of θ and radial motion and the cross section appropriate to the total energy of the fusing system has been used.

The proton energy observed at 45° to the ϕ direction is a function of the centre-of-mass velocity in that direction only, which can be obtained by considering directed energy of the incident deuterons in the ϕ direction. In figure 3 the directed deuteron energies corresponding to the observed proton energies are shown for the three possible intrinsic proton spectra. Only the peak energy and the limits to the possible half widths of these curves have been calculated. The detailed shape is uncertain, particularly near the tails. Any calculation in which portions of the curve outside the limits set by the half width have been used is therefore subject

Table 2. Calculated Deuteron Population for Symmetrical Intrinsic Proton Spectra of half widths 85, 45 and 115 kev

(1)	(2)	(3)	(4)	(5)	(6)			(7)			(8)		
					$\Gamma=85$	$\Gamma=45$	$\Gamma=115$	$\Gamma=85$	$\Gamma=45$	$\Gamma=115$	$\Gamma=85$	$\Gamma=45$	$\Gamma=115$
30–25	2	10^{-3}	15·2	$2\cdot2\times10^{19}$	(1·6)	(0·4)	(1·8)	$(6\cdot4\times10^{11})$	$1\cdot6\times10^{11}$	$7\cdot2\times10^{11}$	$0\cdot5\times10^{-8}$	$0\cdot13\times10^{-8}$	$0\cdot6\times10^{-8}$
25–20	2	6×10^{-4}	13·8	$2\cdot1\times10^{19}$	2·7	(2·0)	2·2	$(2\cdot1\times10^{12})$	$1\cdot6\times10^{12}$	$1\cdot7\times10^{12}$	$1\cdot8\times10^{-8}$	$1\cdot3\times10^{-8}$	$1\cdot5\times10^{-8}$
20–15	2	$2\cdot2\times10^{-4}$	12·1	$1\cdot8\times10^{19}$	3·9	4·7	3·0	$9\cdot6\times10^{12}$	$1\cdot2\times10^{13}$	$7\cdot4\times10^{12}$	$0\cdot8\times10^{-7}$	$1\cdot0\times10^{-7}$	$0\cdot6\times10^{-7}$
15–12	2	8×10^{-5}	10·8	$1\cdot6\times10^{19}$	3·1	5·5	2·2	$2\cdot4\times10^{13}$	$4\cdot2\times10^{13}$	$1\cdot7\times10^{13}$	$2\cdot0\times10^{-7}$	$3\cdot5\times10^{-7}$	$1\cdot5\times10^{-7}$
12–10	2	4×10^{-5}	9·7	$1\cdot5\times10^{19}$	1·9	3·5	1·3	$3\cdot2\times10^{13}$	$5\cdot8\times10^{13}$	$2\cdot2\times10^{13}$	$2\cdot6\times10^{-7}$	$5\cdot0\times10^{-7}$	$1\cdot8\times10^{-7}$
10–9	2	2×10^{-5}	9·0	$1\cdot4\times10^{19}$	1·3	2·2	0·9	$4\cdot8\times10^{13}$	$8\cdot0\times10^{13}$	$3\cdot2\times10^{13}$	$4\cdot0\times10^{-7}$	$6\cdot0\times10^{-7}$	$3\cdot0\times10^{-7}$
9–8	2	$1\cdot2\times10^{-5}$	8·5	$1\cdot3\times10^{19}$	1·8	2·5	1·2	$1\cdot4\times10^{14}$	$2\cdot0\times10^{14}$	$9\cdot6\times10^{13}$	$1\cdot1\times10^{-6}$	$1\cdot6\times10^{-6}$	$0\cdot8\times10^{-6}$
8–7	2	7×10^{-6}	8·0	$1\cdot2\times10^{19}$	1·6	2·3	1·2	$1\cdot9\times10^{14}$	$2\cdot7\times10^{14}$	$1\cdot4\times10^{14}$	$1\cdot5\times10^{-6}$	$2\cdot3\times10^{-6}$	$1\cdot1\times10^{-6}$
7–6	2	$3\cdot3\times10^{-6}$	7·4	$1\cdot1\times10^{19}$	2·0	2·0	1·5	$5\cdot6\times10^{14}$	$5\cdot6\times10^{14}$	$4\cdot0\times10^{14}$	$4\cdot0\times10^{-6}$	$4\cdot0\times10^{-6}$	$3\cdot0\times10^{-6}$
6–5	2	$1\cdot4\times10^{-6}$	6·8	$1\cdot0\times10^{19}$	1·5	1·4	1·3	$10\cdot4\times10^{14}$	$9\cdot2\times10^{14}$	$8\cdot8\times10^{14}$	$8\cdot0\times10^{-6}$	$8\cdot0\times10^{-6}$	$8\cdot0\times10^{-6}$
5–4	2	4×10^{-7}	6·1	$0\cdot9\times10^{19}$	1·3	(0·7)	1·4	$3\cdot7\times10^{15}$	$(1\cdot8\times10^{15})$	$3\cdot9\times10^{15}$	$3\cdot0\times10^{-5}$	$1\cdot5\times10^{-5}$	$3\cdot2\times10^{-5}$
4–3	2	$1\cdot2\times10^{-7}$	5·4	$0\cdot8\times10^{19}$	(1·1)	(0·4)	1·0	$(1\cdot1\times10^{16})$	$(4\cdot0\times10^{15})$	$1\cdot0\times10^{16}$	$1\cdot0\times10^{-4}$	$4\cdot0\times10^{-5}$	$8\cdot0\times10^{-5}$
3–2	2	2×10^{-8}	4·6	$0\cdot7\times10^{19}$	(0·9)	(0·1)	1·2	$(6\cdot4\times10^{16})$	$(8\cdot0\times10^{15})$	$8\cdot4\times10^{16}$	$5\cdot0\times10^{-4}$	$7\cdot0\times10^{-5}$	$7\cdot0\times10^{-4}$

(1) Directed E_d in ϕ direction (kev); (2) E_d due to θ motion; (3) σ (barns); (4) mean $v_d\times10^7$; (5) effective target thickness $v_d\times t\times d$; (6) $N_p\times10^4$; (7) N_d, number of deuterons in given energy interval; (8) N_d/total deuterons present.

to large unknown errors and is given in brackets in table 2, where the population of deuterons in the various energy intervals required to produce the three intrinsic proton spectra are calculated.

It will be observed that the number of deuterons required in each energy interval is not very sensitive to the choice of half width for the intrinsic proton energy spectrum. The maximum discrepancy occurs in the extreme energy groups ($E_d = 2$–3 kev and 25–30 kev). In the final column of table 2 the fraction of the total deuterons present in each of the energy groups is calculated, by dividing by the total number of deuterons present in the system. This has been estimated as $1{\cdot}2 \times 10^{20}$ from pressure and volume measurements on SCEPTRE III. It is seen that the observed proton spectrum could be produced if the fraction of deuterons having energies in the range 2–30 kev is of the order of one per thousand of the total deuterons present.

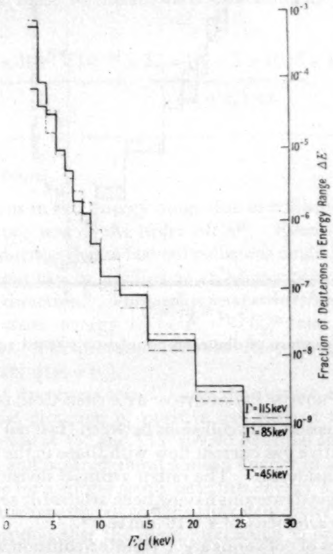

Figure 4. Histogram of deuteron population plotted against energy.

The deuteron energy spectrum is plotted in figure 4, the limits being determined by the values obtained from the three intrinsic proton energy spectra, for which smooth symmetrical curves are assumed.

§ 7. The Deuteron Velocity Spectrum

The histogram of deuteron velocities in the range 4 to 16×10^7 cm sec^{-1} has been plotted in figure 5. The diminution in deuteron population with increasing velocity in this range is very approximately exponential, and extrapolation of the curve towards lower velocities indicates that a high proportion of the deuterons present have velocities between 0 and 10^7 cm sec^{-1}. This is consistent with the mean drift velocity measured spectroscopically.

From the above theory the velocity distribution is unsymmetrical about zero velocity.

A much smaller high velocity tail of deuterons travelling in the opposite direction is not. however, excluded by the experimental evidence, as will be shown later.

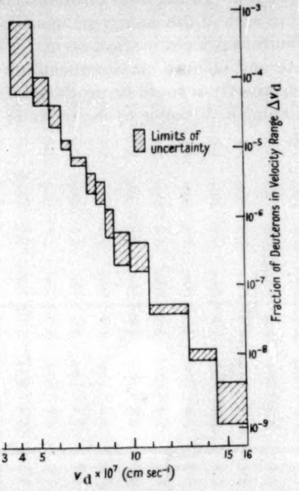

Figure 5. Histogram of deuteron population plotted against velocity.

§ 8. PROTON PRODUCTION BY OTHER COLLISIONS

In the present discussion only collisions between 'fast tail' deuterons travelling in the direction of positive gas current flow with those in the lower velocity part of the distribution are considered. The rather artificial division between 'fast tail' deuterons and slow target deuterons having been arbitrarily set at an energy of about 2 kev corresponding to a velocity of 4×10^7 cm sec^{-1}.

Other possible types of collisions are : (i) inter-collision with deuterons having energies less than 2 kev; (ii) collision of 'fast tail' deuterons with a smaller number of 'fast tail' deuterons travelling in the opposite direction; (iii) collision of 'fast tail' deuterons travelling in the opposite direction with the slow deuterons; (iv) collision of 'fast tail' deuterons travelling in the same direction between themselves.

Inter-collision of deuterons of energy less than 2 kev has a very low yield since the (d–d) cross section is falling rapidly in this region. This is confirmed by the experimental evidence, since for these collisions the centre-of-mass velocity is low and the protons produced, observed either at 45° or 135°, would have energies near 3·03 MEV, so that peaks of this energy would be superimposed on the observed histograms. By graphical subtraction of the 45° and 135° histograms it can be shown that any protons in this energy range make up less than 10% of the total proton yield.

The number of deuterons available for collisions between fast tails is low, but the cross section is high. Consider two groups of energy, E_1 and E_2, and mean velocities v_1 and v_2. The energy in the centre-of-mass system is $(\sqrt{E_1}+\sqrt{E_2})^2$ and the velocity of centre-of-mass is $\frac{1}{2}(v_1-v_2)$.

Collisions between a fast group in the energy range 20–25 kev with the deuterons in the energy range 4–10 kev travelling in the opposite direction produce a system of centre-of-mass velocities between 10^7 cm sec^{-1} and 4×10^7 cm sec^{-1} (corresponding to protons of energy 3·05 to 3·10 MEV observed at 45°).

The cross section of this reaction appropriate to a centre-of-mass energy of 40 kev is 260×10^{-5} barns.

If the number of deuterons in the energy tail in the reverse direction is assumed to be a fraction K of those in the forward direction, the proton yield for this reaction is given by

$$N_{\mathrm{p}} = \underbrace{K2\times10^{12}}_{\substack{N_{\mathrm{d}}\\(20\text{–}25\,\mathrm{kev})}} \times \underbrace{260\times10^{-5}\times10^{-24}}_{\sigma} \times \underbrace{22\times10^{7}-5\times10^{-4}}_{(v_1+v_2)\times t} \times \underbrace{4{\cdot}5\times10^{4}\times3\times10^{14}}_{\substack{\mathrm{d\ for\ 4\text{–}10\ kev}\\ \mathrm{deuterons}\\(\Gamma=85\,\mathrm{kev})}}$$

$$=8\times K \text{ protons.}$$

The yield of protons in this energy range due to collision of fast tail deuterons with the slow deuterons was of the order of 10^5. Even if K were to approach unity, the proton production due to fast tail collisions could be neglected.

The same argument can be applied to collisions between fast tail deuterons travelling in the same direction. This case is less favourable for proton production, since the centre-of-mass energy is $(\sqrt{E_1}-\sqrt{E_2})^2$ and the cross section is consequently smaller. The protons produced have energies appropriate to the centre-of-mass velocity $\frac{1}{2}(v_1+v_2)$.

If the numbers of deuterons travelling in the reverse direction were equal to those travelling in the direction of positive gas current flow ($K=1$) the mean proton energies observed at 45° and 135° would be equal and the spectra would be appreciably broader, and centred about a mean energy of about 3·03 MEV. Since there was no evidence for a strong group near this energy K must be small and any interaction between the reverse tail and the slow deuterons correspondingly small.

The initial assumption that the main interaction is between the high energy forward tail and the low energy part of the distribution therefore appears to be justified, and the proposed deuteron spectrum appears to account for all the features observed in the proton energy measurements, and not to conflict with the spectroscopic evidence. It cannot claim to be exclusive since some of these features can be explained using other models (Herdan and Hughes, to be published) for the deuteron interactions, but can claim the merit of simplicity.

§ 9. LIMITS OF ERROR

The limits of uncertainty shown in figures 4 and 5 refer to the range of values of deuteron population obtained using symmetrical intrinsic proton spectra of half widths between the limits of 45 and 115 kev. Deuteron population histograms have also been calculated for intrinsic proton spectra of half widths 85 kev and the same mean energy, but heavily skewed towards higher and lower energies. The estimated deuteron populations from these limiting cases varied by a factor of five in the low energy range and two in the high energy range.

Evidence of the existence of θ and radial motion is strong, but the arbitrary assignment of 2 kev energy to all the incident deuterons due to this motion is an obvious over simplification. If this is reduced to 1 kev the population of deuterons in the 2–3 kev region is increased by an order of magnitude, whilst the population of the higher energy deuterons is only slightly increased. It can be argued that since acceleration in the ϕ and θ directions is time dependent, the assumption that the θ velocity in proportion to the ϕ velocity is reasonable. If this is done the deuteron population in the lower energy and velocity groups is increased by rather more than an order of magnitude and that in the higher groups reduced slightly.

The effect of slight errors in the determination of the mean energy of the intrinsic proton spectrum on the shape of the deuteron energy and velocity spectrum is negligible.

The absolute values calculated for the deuteron populations are all inversely proportional to the assumed density of the target nuclei. The value $d = 3 \times 10^{14}$ atoms/sec has been estimated from magnetic probe measurements.

The final calculated spectra can therefore only be claimed to be accurate to about an order of magnitude, although relative values in the mid-energy and velocity region are probably correct to a higher accuracy.

ACKNOWLEDGMENTS

Many of the basic ideas in the present work originated from discussions between Dr. D. R. Chick and the author, who would also lik eto acknowledge helpful discussions with Dr. W. M. Jones, Dr. A. A. Ware, Messrs. R. Herdan and T. P. Hughes, and the assistance of Mr. K. M. Young and Miss A. M. Germontani in the detailed calculations.

Thanks are also due to Dr. T. E. Allibone, Director of the Laboratory, for permission to publish this paper.

REFERENCES

ALLEN, N. L., *et al.*, 1958, *Nature, Lond.*, **181**, 222.
ARNOLD, W. R., PHILLIPS, J. A., STOVALL, E. J., and TUCK, J. L., 1954, *Phys. Rev.*, **93**, 483.
BRENNAN, J. G., 1958, *Phys. Rev.*, **111**, 1592.
HUGHES, T. P., and KAUFMAN, S., 1959, *Nature, Lond.*, **183**, 7.
JONES, W. M., BARNARD, A. C. L., HUNT, S. E., and CHICK, D. R., 1958, *Nature, Lond.*, **182**, 216.
JONES, W. M., YOUNG, K. M., and BARNARD, A. C. L., 1960, to be published.
JONES, W. M., *et al.*, 1959, *Nucl. Instrum. Methods*, **5**, 327.
MOFFAT, J., ROAF, D., and SANDERS, J. H., 1952, *Proc. Roy. Soc.* A, **212**, 220.
WARE, A. A., 1959, *Nature, Lond.*, **183**, 8.

Dislocations and Twinning in Graphite

By A. J. KENNEDY

The College of Aeronautics, Cranfield, Bletchley, Bucks.

MS. received 29*th October* 1959, *in revised form* 19*th November* 1959

Abstract. The twin composition plane in graphite is a 20° tilt boundary between lattices which are rotated, relatively, about an axis in the basal plane. Previous work has led to the proposition that some special type of structure must necessarily exist in the neighbourhood of the boundary which violates the normal hexagon arrangement of the carbon atoms. It is demonstrated that a tilt boundary of the required form can be explained as an array of partial dislocations, such a boundary being possible in either the hexagonal or the rhombohedral form. A boundary of this type is mobile, and can, by its movement, introduce or eliminate stacking faults and thus change the volume of rhombohedral graphite present in the normal hexagonal lattice. Such effects have been reported previously. The true twinning plane in this model is not the composition plane, which is the plane $\{1\bar{1}01\}$ referred to the structural (not the morphological) axes, but the plane $\{11\bar{2}1\}$.

THE graphite structure consists of parallel layers of aromatic carbon rings, the C–C spacing in the rings being 1·42 Å, the hexagon width *a* 2·456 Å and the layer spacing *c* 3·348 Å.

The standard work on the twinning features in graphite is that of Palache (1941), which identifies the twin composition plane as $\{11\bar{2}1\}$ with respect to the morphological axes. We shall throughout this note use the hexagonal structural axes (see figure 1) in which system the indices of the composition plane become $\{1\bar{1}01\}$. The angle of tilt between the twins was determined by Palache as 20° 36′, which is very close to $\tan^{-1} a/2c$, (20° 9′ using the above values) and equivalent to the insertion of one hexagon width in every other basal plane. We shall use the value 20° 9′ throughout in the following discussion. The true twinning plane (as distinct from this twin composition plane) is not established: this may, or may not, be $\{1\bar{1}01\}$. The theory advanced by Platt (1957) for the structure of the twin boundary results in the twinning plane and the composition plane being the same. To produce this result, quite special structures must be created in every other atomic plane of the type illustrated in figure 2, which Platt refers to as 8–4–8 structures. It is, in fact, unnecessary to adopt such a special arrangement to explain the observed structure as this may be interpreted more satisfactorily in dislocation terms.

Graphite may exist in either the hexagonal, ABABAB... stacking sequence, or in the rhombohedral ABCABC... stacking sequence. Consider first the hexagons drawn in figure 3(*a*) which shows the relative positions of the A, B and C planes. The C position may be achieved from the B position by a translation along, say, XY. A partial dislocation with a Burgers vector XY, that is $\sqrt{3}a/2$ [1000], can therefore constitute a boundary between hexagon sheets in the B and C positions. Such a dislocation can, of course, be either positive or negative: the hexagons in the region of the partial dislocation may be either compressed or extended, the overall lateral strain being $a/2$, which is the shift involved in the translation illustrated in figure 3. In figure 3(*b*) a line of hexagon nets is shown in the transition region between the B and C stacking positions, from which it will be evident that, in this case, an extension of $a/2$ has been

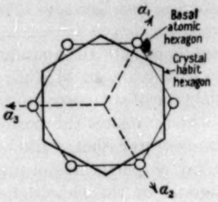

Figure 1. The relation between the structural and the morphological hexagons. The twin composition plane is $\{1\bar{1}01\}$ with respect to the $a_1a_2a_3$ and c axes.

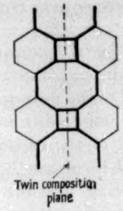

Figure 2. The boundary structure proposed by Platt.

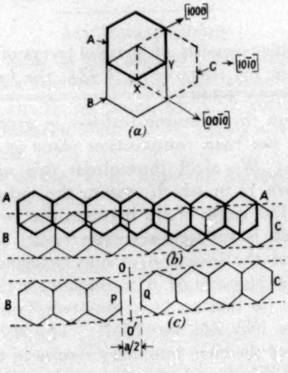

Figure 3. (*a*) The relative positions of hexagons in the A, B and C planes. (*b*) The distortion introduced into a row of hexagons in the neighbourhood of a partial dislocation, taking the A layer as a rigid reference network. (In fact, both layers are sheared similarly, of course.) (*c*) The B–C row of hexagons showing the gap, of width $a/2$, closed by the lattice rotation of 20° 9′.

introduced (as well as a shear, of course). For simplicity the distortion is shown relative to an undistorted A layer; in fact the strain is distributed symmetrically over both layers, but the *relative* strain is the same as that shown. Let us suppose the B–C line of hexagons to be cut at OO′, and the strain released. This results in the arrangement of figure 3(*c*). Suppose now that the hexagons of both layers are rotated about OO′, so that the gap PQ, of width $a/2$, is closed by the rotation. The angle of tilt required to achieve this is $\tan^{-1} a/2c$, or 20° 9′. Thus a boundary is formed which is equivalent to the insertion (or removal) of an extra half-hexagon on each successive plane (or a full hexagon width a on every alternate plane). The operation of the dislocations, $\sqrt{3}a/2$ [1000] and $\sqrt{3}a/2$ [00$\bar{1}$0], in sequence on successive planes is obviously equivalent to the perfect dislocation a [10$\bar{1}$0] on alternate planes in the hexagonal stacking.

The structure which will satisfy the observed tilt angle is drawn in detail in figure 4, for the case of both hexagonal graphite (above the dotted line) and rhombohedral graphite (below the dotted line), and again the A plane has been taken, for convenience, as an undistorted reference plane. In each case a partial dislocation of the type discussed is introduced into the intermediate layer of hexagons (wavy lines), as evidenced by the difference in position between extreme left and right, but with the strain removed by an operation of the type illustrated in figure 3(*b*) and (*c*), the gap created being shown in black. For both the hexagonal and rhombohedral cases, the tilt required to close such gaps in the planes is the same, namely 20° 9′. In each case the original type of structure can be preserved: hexagonal ABABAB... twins to hexagonal ACACAC... and rhombohedral ABCABC.... can twin to rhombohedral BACBAC... In figure 4 the rhombohedral transformation illustrated shows ABC.... twinning to ACB.... and the exact sequence obviously depends on the direction of the Burgers vector, as any plane (say A) may be transformed to either of the other two possibilities (B or C) by a similar vector of different direction. Stacking faults can therefore exist. If, then, the lattice is rotated as described above, the structure will now fit along the cut planes when the angle of rotation is 20° 9′. This is illustrated diagrammatically by the diagram at the foot of figure 4. Thus a sequence of partial dislocations can give a tilt boundary of the observed angle. The twin boundary in such a structure is thus an array

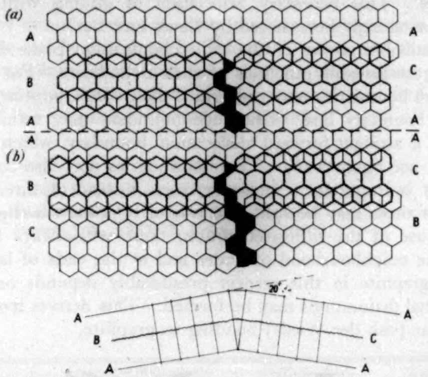

Figure 4. Successive layer planes in graphite showing the twin boundary dislocation structure for (*a*) hexagonal and (*b*) rhombohedral graphite. The lower diagram demonstrates (for the hexagonal case) how a rotation of about 20° closes up the lattice in the required way. For the arrangement shown this angle has a value 20° 9′.

of partial dislocations, forming a tilt boundary, and is evidently mobile, which is consistent with experimental observations (Laves and Baskin 1956).

Once this possibility is recognized, a number of characteristics of the graphite structure become resolvable. It follows that twinning in the hexagonal structure does not necessarily involve any transformation to the rhombohedral form (as was deduced by Laves and Baskin from x-ray measurements), although rhombohedral stacking faults could be perpetuated through the twinned structure, or even created. Apart from the twinning question, such partial dislocations can obviously constitute the boundaries of stacking faults, and thus the gliding of these dislocations under stress can increase (or diminish) the amount of rhombohedral graphite. This necessary association of gliding with rhombohedral development has already been noted by Laves and Baskin.

The dislocation structure of the twin composition plane imposes certain restrictions on the possible junctions of such boundaries. For example, as in figure 5 (*a*), two boundaries may conform if their common vector lies along the third possible boundary line. One such boundary may terminate either on another or at a straight-forward dislocation boundary which is not of the twinning type; see figure 5 (*b*). Three boundaries may also conform, but the sign of the tilt is important. In some cases, instead of three twin lamellae meeting, one of these may be split into two of opposite tilt (figure 5 (*c*)). In any case, because of the tilting condition, there will always be very special restraints in the neighbourhood of nodes and at the ends of lamellae and the adaptation of graphite in this respect presumably depends on the readiness with which partial dislocations may be formed. This derives from the relatively weak interplanar (van der Waals) bonding in graphite.

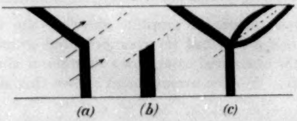

Figure 5. Possible twinning forms : (*a*) two lamellae with common boundary vectors, (*b*) a single lamella terminating at a dislocation boundary, and (*c*) the possible split into two lamellae of opposite tilt.

It is not at once evident why the composition plane observed is $\{11\bar{2}1\}$ rather than $\{1\bar{1}01\}$, as the creation of the latter requires the same type of transformation: in this case the insertion of a hexagon length into every other plane (see figure 4) leading to a tilt angle across the $\{1\bar{1}01\}$ plane of $\tan^{-1} 2a/3c$, or $22^\circ 57'$. One of the differences between these two possible planes is that, for a tilt of a given sign, there is only one possible partial for each layer plane in the $\{1\bar{1}01\}$ case, whereas in the case of $\{11\bar{2}1\}$ there may be two possibilities. Thus suppose the positions of a given plane in the original structure and the twinned structure to be symbolized by B–C: this is the case, for example, in the second plane drawn in figure 4. Rhombohedral stacking sequences of the following type are possible across $\{11\bar{2}1\}$: B–C, C–A, A–B,.... or B–C, C–B, A–C... Using similar notation for the (theoretical) case of the $\{1\bar{1}01\}$ composition plane, these alternatives do not arise. The sequence must be

B–C, C–A, A–B. In the simple hexagonal twinned lattice, A–A, B–C, A–A, ... there is no distinction, as one possibility only exists for both cases. For A–B, B–C, A–B, however, which is also pure hexagonal stacking in each twin, another possibility arises in the $\{11\bar{2}1\}$ case, namely A–B, B–A, A–B. This is again a structure which could not conform with a $\{1\bar{1}01\}$ tilt boundary. Particularly where stacking faults exist, then, the $\{11\bar{2}1\}$ boundary is much less restrictive in the necessary conditions it imposes, and would appear to be much more likely to form in lattices containing a distribution of stacking faults. No cases of the observation of a $\{1\bar{1}01\}$ composition plane appear to have been reported, although it may be possible to produce such twins in thin flakes of very perfect graphite.

The point of this discussion is, then, that the principal twinning characteristics of graphite can be explained in dislocation terms, and that, on this basis, the true twinning plane (as distinct from the twin composition plane) is $\{11\bar{2}1\}$ in the *structural* (not the morphological) system of axes. An experimental confirmation of this proposition would be valuable.

REFERENCES

LAVES, F., and BASKIN, Y., 1956, *Z. Kristallogr.*, **107**, 22.
PALACHE, C., 1941, *Amer. Min.*, **26**, 709.
PLATT, J. R., 1957, *Z. Kristallogr.*, **109**, 3.

Hypersonic Velocity in Viscous Liquids as revealed from Brillouin Spectra

By S. N. SEN

Department of Physics, Jadavpur University, Calcutta-32, India

MS. received 28th September 1959

Abstract. Taking into consideration Lamb's theory for the propagation of high frequency acoustical waves in viscous liquids, and the idea of Maxwell regarding complex viscosity, a theoretical expression has been deduced for the velocity of high frequency acoustical waves through viscous liquids. It is observed that if Frenkel's expression for the rigidity modulus of a liquid be introduced into the formula for wave propagation then the theoretical formula explains the dispersion of sound velocity in viscous liquids as was observed by Venketeswaran from Brillouin spectra and the theoretical value is in good agreement with the experimental result. Further, the introduction of complex viscosity partly explains the propagation of these high frequency waves through viscous liquids.

§ 1. INTRODUCTION

The Brillouin scattering of light in liquids provides a method of determining the velocity of hypersonic vibrations which are supposed to be the cause of the appearance of hyperfine structure in the case of Rayleigh scattering. The shift in frequency is given by the expression

$$d\nu = \pm 2\nu \frac{v}{\mathbf{c}/\mu} \sin \tfrac{1}{2}\theta \qquad \ldots\ldots(1)$$

where ν is the original frequency of light, v is the velocity of sound waves in liquid, μ the refractive index of the liquid for light of frequency ν, $\mathbf{c}$ the velocity of light and θ the angle between the incident light and the direction of observation. Thus it is clear that the velocity of sound waves causing the Brillouin spectra can be obtained if the frequency shift $d\nu$ can be measured. The wavelength, and consequently the frequency, of these acoustical waves can be obtained from the relation

$$\lambda_0 = 2\lambda_s \mu \sin \tfrac{1}{2}\theta \qquad \ldots\ldots(2)$$

where λ_0 is the wavelength of incident light and λ_s the wavelength of the sound wave.

From equation (2) it can be shown that for almost all the liquids studied, the frequency of these acoustical waves lies within the range 10^9 to 10^{10} c/s, whereas the maximum frequency of ultrasonic waves at which the experimental observations have been carried out is of the order of 10^6 c/s. Thus Brillouin scattering of light provides us with a method of ascertaining whether any dispersion of sound velocity actually occurs as we pass from the ultrasonic (10^6 c/s) to the hypersonic range (10^9 c/s or higher). The first systematic observations in this range were made by Venketeswaran 1942 a, b) and Sunanda Bai (1942) and later by Rank *et al.* (1948, 1949). They have confirmed that in the case of liquids which are mobile at ordinary temperatures no dispersion occurs as we pass from the ultrasonic to the hypersonic range; but in the case of viscous liquids, such as glycerine and castor oil, Venketeswaran (1942 a) found that there actually occurs a dispersion and the same was noted by Rank *et al.* (1949) in the case of acetone at a temperature of −78°c. The results obtained by Venketeswaran for glycerine and castor oil, which are highly viscous at ordinary temperatures, are shown in table 1.

Table 1. Hypersonic Velocity as measured from Brillouin Spectra

Liquid	Glycerine	Castor oil
Temperature of observation (°c)	26	28
Velocity from Brillouin spectra (m/sec)	2500	1626
Ultrasonic velocity (m/sec)	1957	1508

Venketeswaran has tried to explain this dispersion on the assumption that for these high frequency waves the viscous liquids possess the properties of solids and the velocity of wave propagation is given by $v=\{(K+4n/3)/\rho\}^{1/2}$ instead of ultrasonic velocity $v=(K/\rho)^{1/2}$, where K is the adiabatic bulk modulus, n is the supposed modulus of rigidity of the liquid and ρ is the density of the liquid. He further maintains that whereas in the case of crystals the central component is weak and the modified components are strong, in the case of these viscous liquids the reverse is true and the intensity falls with the increase of viscosity, so these liquids are more akin to amorphous solids like glass than to crystals; but in the same paper he has noted that no trace of displaced component can be observed in the case of glass and glucose solution.

Another point which has been raised is that according to classical thermodynamics, plane sound waves propagated through a liquid of high viscosity suffer a diminution in its amplitude in the ratio e^{-1} in traversing a number of wavelengths of sound given by $3v\lambda_s/8\pi^2\eta$, where v is the velocity of the sound wave, λ_s the wavelength of the sound wave and η the coefficient of viscosity of the liquid. If $\lambda=4722$ Å then for glycerine and castor oil these waves would not have any significance at all and so the corresponding components would not have been observed because for these two liquids this factor comes out to be a small fraction of unity. Venketeswaran thus maintains that the appearance of these components signifies that thermal sound waves are propagated as if the kinematic viscosity has little or no influence on them at all. Bearing these facts in mind, the theory of propagation of sound of high frequency through a viscous liquid has been re-examined and the present paper deals with the case of propagation of sound waves through glycerine and castor oil which have been studied by Venketeswaran.

§ 2. THEORETICAL CALCULATION

The object of this paper is to show that the observed dispersion can be explained if the theory of Lamb regarding the propagation of sound through viscous liquids is extended further with the idea of Maxwell regarding the occurrence of complex viscosity in the case of viscous liquids. Lamb (*Hydrodynamics* 1953) has given the expression for the amplitude of a plane sound wave in a viscous liquid

$$u=u_0 \exp i\omega\,(t+mx/i\omega) \qquad \ldots\ldots(3)$$

where

$$m=\pm\frac{i\omega}{\sqrt{\dfrac{K}{\rho}\left(1+\dfrac{4i\omega\eta}{3K}\right)^{1/2}}} \qquad \ldots\ldots(4)$$

where x is the direction of propagation, ω the angular frequency of the sound wave, η the coefficient of viscosity, K the adiabatic bulk modulus and ρ the density of the liquid.

From equation (3) the velocity of wave propagation is given by

$$v = -\frac{i\omega}{m} = \sqrt{\frac{K}{\rho}}\left(1 + \frac{4i\omega\eta}{3K}\right)^{1/2}. \qquad \ldots\ldots(5)$$

In the case of an ordinary sound wave the quantity $\omega\eta/3K$ is very small compared with unity and so for all practical purposes the velocity of the sound wave can be taken as $v = (K/\rho)^{1/2}$, but when we are dealing with hypersonic vibrations of frequency 10^{10} c/s and a liquid of high viscosity we cannot neglect this term. Further, according to Maxwell (1868) the behaviour of a liquid under a shearing strain is given by

$$\frac{ds}{dt} = \frac{1}{n} \cdot \frac{dF}{dt} + \frac{F}{\eta}$$

where s is the shearing strain, F the corresponding stress, t the time, n the modulus of rigidity and η the coefficient of viscosity. If the deformation is constant, $ds/dt = 0$, so the solution of the above equation is

$$F = F_0 \exp(-t/\tau)$$

where

$$\tau = \eta/n. \qquad \ldots\ldots(6)$$

τ has been defined by Maxwell as the time of relaxation. Mason *et al.* (1948) have measured the mechanical properties of long chain molecular liquids of polyisobutylene type by means of shear and longitudinal waves in the ultrasonic frequency range. The shear waves show that these liquids behave as Maxwell relaxing liquids at high frequencies. They consider that the effect of a shear can be represented as the action of a compliance in parallel with a viscous resistance. At low frequencies the liquids behave in flow as viscous liquids, but at sufficiently high frequencies a movement of one part of it is transmitted as a shear wave. Hence, if it is assumed that the fluid possesses an acoustical reactance in the Maxwellian sense and a complex viscosity as has been assumed by Schallamach (1949) such that

$$\eta = \frac{\eta_0[1 - i\omega\tau]}{1 + \omega^2\tau^2}, \qquad \ldots\ldots(7)$$

then we get from equation (5)

$$\begin{aligned} v &= v_0\left[1 + \frac{4i\omega}{3K}\frac{\eta_0(1 - i\omega\tau)}{1 + \omega^2\tau^2}\right]^{1/2} \\ &= v_0\left[\left\{1 + \frac{4\omega^2\tau\eta_0}{3K(1 + \omega^2\tau^2)}\right\}^2 + \frac{16\omega^2{\eta_0}^2}{9K^2(1 + \omega^2\tau^2)^2}\right]^{1/4} \qquad \ldots\ldots(8) \end{aligned}$$

where $v_0 = (K/\rho)^{1/2}$.

It is clear that in order to calculate τ the time of relaxation of the liquid it is necessary to know n the rigidity modulus of the liquid. Frenkel (1946) from his kinetic theory of liquids has given an expression for n which is

$$n = \frac{6kT}{d^3} \qquad \ldots\ldots(9)$$

where d is the distance between the two molecules, $\boldsymbol{k}$ is Boltzmann's constant and T the absolute temperature; if it is assumed that $d=a$, the radius of the molecule, then

$$n=\frac{6\times 4\pi \boldsymbol{k}T\boldsymbol{N}\rho}{M}=\frac{24\pi \boldsymbol{k}T\boldsymbol{N}\rho}{M} \qquad \ldots\ldots(10)$$

where M is the molecular weight of the liquid, $\boldsymbol{N}$ is Avogadro's number and ρ is the density of the liquid.

If calculations are carried out for glycerine and castor oil then table 2 gives the values of n for these liquids. The third row gives the values of τ and the fourth row gives the value of τ obtained by Venketeswaran (1942 a).

Table 2. Calculation of Rigidity Modulus and Time of Relaxation of Liquids

Liquid	Glycerine	Castor oil
Value of n dynes cm^{-2}	$2{\cdot}545\times 10^{10}$	$0{\cdot}168\times 10^{10}$
Time of relaxation τ (sec)	$3{\cdot}748\times 10^{-10}$	36×10^{-10}
τ obtained by Venketeswaran (sec)	$4{\cdot}2\times 10^{-10}$	33×10^{-10}

As castor oil is a mixed glyceride, an approximate estimate of its molecular weight has been made assuming it contains 87·5% of receonilic acid, and the molecular weight has been taken as 927·3. Inserting the values of the time of relaxation of these liquids in equation (8) the velocity of hypersonic vibrations in these liquids has been calculated and entered in table 3.

Table 3. Hypersonic Velocity as calculated from Equation (8)

Liquid	(1)	(2)	(3)	(4)	(5)	(6)	(7)
Glycerine	$9{\cdot}79\times 10^{10}$	9·54	$3{\cdot}748\times 10^{-10}$	$4{\cdot}83\times 10^{10}$	2548·3	2500	1957 at 28°c[a]
Castor oil	$6{\cdot}28\times 10^{10}$	6·04	36×10^{-10}	$2{\cdot}18\times 10^{10}$	1601·2	1626	1508 at 18°c[b]
Acetone	$4{\cdot}784\times 10^{9}$	3×10^{-3}	$1{\cdot}180\times 10^{-13}$	$1{\cdot}053\times 10^{10}$	1153·3	1139	1153·3 at 28°c[c]

(1) ω as calculated from eqn (2) (radians); (2) η (poise); (3) relaxation time τ (sec); (4) bulk modulus (dyn cm^{-2}); (5) calculated velocity (m/sec); (6) measured velocity (Venketswaran 1942 b); (7) ultrasonic velocity (m/sec); [a] Bhagavantam and Rao 1939, [b] Zachoval 1939 a, [c] Zachoval 1939 b.

§ 3. DISCUSSION

From the above calculation we see that if the theory of Lamb regarding the propagation of high frequency sound waves through viscous liquids is extended further with the idea of Maxwell that these viscous liquids possess a complex viscosity, then the theoretical value of the velocity of sound waves agrees well with the experimental observation of Venketeswaran (1942 b). As ordinary mobile liquids have a very low value of viscosity it is clear from equation (8) that their velocities will not be much affected; that this is the case has been shown by the experimental results of Rank *et al.* (1949) and Venketeswaran (1942 b) for all mobile liquids. The theoretical value of velocity for acetone has been calculated and entered in table 3. This equation is thus seen to be a general one and holds for all liquids whether mobile or viscous. Though Frenkel in his kinetic theory of liquids has observed that his expression for n the rigidity modulus is only approximate, the value obtained by his expression and those obtained by Venketeswaran by assuming the liquid as a solid for these high frequency vibrations show agreement not only in order of magnitude but also in actual value.

This formula shows that the region of dispersion of sound for almost all the common liquids will lie beyond the range of 10^{10} c/s and so, up to the present time, no direct experimental proof has been furnished regarding the positive dispersion of sound velocity in these liquids.

With the introduction of the idea of complex viscosity the propagation of high frequency waves in viscous liquids can be accounted for. In that case the number of wavelengths after which the amplitude will fall to 1/e of its original value will be given by

$$\frac{3v\lambda}{8\pi^2\eta_0}\,\frac{1+\omega^2\tau^2}{1-i\omega\tau} \simeq \frac{3v\lambda}{8\pi^2\eta_0}(1+\omega^2\tau^2)^{1/2}\exp i\omega\tau$$

which becomes a number many times greater than unity. It is therefore concluded that if the assumption regarding the complex viscosity is accepted then the dispersion of sound velocity as well as its propagation in viscous liquids can be accounted for.

REFERENCES

BHAGAVANTAM, S., and RAO, J., 1939, *Proc. Indian Acad. Sci.* A, **9**, 312.
FRENKEL, J., 1946, *Kinetic Theory of Liquids* (Oxford: Clarendon Press), p. 199.
LAMB, H., 1953, *Hydrodynamics* (Cambridge: University Press), p. 647.
MASON, W. P., BAKER, W. O., MCSKIMIN, H. J., and HEISS, J. H., 1948, *Phys. Rev.*, **73**, 1074.
MAXWELL, J. C., 1868, *Phil. Mag.*, **35**, 133.
RANK, D. H., MCCARTNEY, J. S., and SZASZ, G. J., 1948, *J. Opt. Soc. Amer.*, **38**, 287.
RANK, D. H., SHULL, E. R., and AXFORD, D. W., 1949, *Nature, Lond.*, **164**, 67.
SCHALLAMACH, A., 1949, *Proc. Phys. Soc.* B, **62**, 70.
SUNANDA BAI, K. S., 1942, *Proc. Indian Acad. Sci.* A, **15**, 349.
VENKETESWARAN, C. S., 1942 a, *Proc. Indian Acad. Sci.* A, **15**, 362.
—— 1942 b, *Ibid.*, **15**, 371.
ZACHOVAL, M. L., 1939 a, *C.R. Acad. Sci., Paris*, **208**, 265.
—— 1939 b, *J. Physique*, **10**, 350.

RESEARCH NOTES

Molecular Motion in Liquid n-Octyl Bromide by Proton Magnetic Resonance

By J. G. POWLES and A. HARTLAND

Physics Department, Queen Mary College, University of London

MS. received 4*th November* 1959

We have measured the proton spin–lattice relaxation time T_1 in liquid *n*-octyl bromide at 21·5 Mc/s in the temperature range -77 °c to 127 °c. The melting point is -55 °c and it was possible to supercool only to -77 °c. The boiling point is 202 °c. T_1 was measured by a transient technique using a 180°, 90° pulse sequence (Hahn 1950, Carr and Purcell 1954) and the apparatus has been described elsewhere (Luszczynski and Powles 1959 a). The decay of longitudinal magnetization was found to be exponential in all cases and so we give only the decay constant T_1 in the figure as a function of temperature on an Arrhenius plot. Care was taken to remove dissolved oxygen which, being paramagnetic, could reduce T_1 and usually would have an important effect if T_1 is longer than about one second.

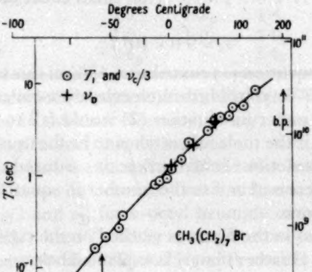

Measured values of the proton spin–lattice relaxation time T_1 in seconds as a function of temperature (left-hand scale). The right-hand scale gives the values of $\nu_c/3$ deduced from T_1. Also shown are values of ν_D (Hennelly *et al.* 1948) (right-hand scale); b.p. and m.p. indicate the boiling and melting points respectively.

From the measured values of T_1 one can deduce a correlation frequency ν_c for nuclear motion (or a correlation time $\tau_c = 1/2\pi\nu_c$) which from the theories of nuclear resonance relaxation are related as in equation (1) if $\nu_c \gg \nu_r$ where ν_r is the resonance frequency. We expect this to be so in the present instance since we are evidently well removed from the minimum of T_1.

$$\nu_c/T_1 = A(\gamma^4\hbar^2/2\pi)[d^{-6} + B\pi(N/V)a^{-3}]. \qquad \ldots\ldots(1)$$

Where γ is the proton gyromagnetic ratio, d is the fixed separation of a proton pair, N/V is the number of protons per cm^3 and a is the effective radius of the diffusing 'molecule' containing the proton pair.

In the theory of Bloembergen, Purcell and Pound (1948) $A = 9/10$ and $B = 3/2$; in the theory of Kubo and Tomita (1954) $A = 3/2$ and B is not obtained; in the theory of Skrotskii and Kokin (1959) $A = 3/2$ and $B = 6/5$. These results require modification for other than a pair of nuclei. For three nuclei arranged in an equilateral triangle of side b, Hubbard (1958) finds $A = 9(19 + \sqrt{61})/80 = 3{\cdot}01\ldots$ and B is not obtained. Actually the theoretical decay is slightly non-exponential but this would be difficult to detect experimentally. (A value $A = 3$, as compared with $A = 3/2$ for a pair of nuclei, would be expected from a calculation of the nuclear interaction using second moments (Van Vleck 1948).)

None of these results is directly applicable to *n*-octyl bromide but possibly that of Skrotskii and Kokin is a suitable approximation for the methylene protons. For the methyl protons we shall use Hubbard's result together with $B = 6/5$. Since we observe exponential decay we do not distinguish the signals from the methyl and methylene protons although it must be admitted that their T_1 values would have to differ by a factor two or greater for us to distinguish them clearly. We shall therefore use an appropriately weighted value of A namely,

$$A = 3 \times 3/17 + 3/2 \times 14/17 = 30/17.$$

We also use in equation (1), $B = 6/5$, $\gamma = 2{\cdot}68 \times 10^4$, $d = 1{\cdot}78$ Å (the H–H distance in $-\mathrm{CH_2}$ or $-\mathrm{CH_3}$), $a = 2{\cdot}1$ Å (an approximation for the radius of a methyl or methylene group), and $N/V = 5{\cdot}9 \times 10^{22}$ (the small effect of thermal expansion is neglected), hence

$$\nu_c = 9{\cdot}0 \times 10^9\, T_1. \qquad \ldots\ldots(2)$$

The second term in equation (1) contributes 45% of this total. If we took for a the radius of the whole *n*-octyl bromide molecule, even coiled up, this term would be negligible and the number in equation (2) would fall to about one half of the value given. However if the molecule is taken to be the unit in this way, although the intermolecular interaction contribution is reduced, the intra-molecular contribution must be increased and so the number in equation (2) would be raised and is still a reasonable one.

The scale of ordinates in the figure is marked on the right to give $\nu_c/3$ directly from T_1 (the choice of $\nu_c/3$ rather than ν_c is explained below).

It is of interest to compare our values of ν_c with the dielectric correlation frequency ν_D. ν_D is the frequency at which a maximum of dielectric loss occurs as a function of frequency at constant temperature. We note that ν_D refers to the motion of the C–Br bond. Also, for the same motion, $\nu_c/3 = \nu_D$ because of the different angle functions involved (Bloembergen *et al.* 1948).

Values of ν_D are available at the temperatures 1°, 25° and 55°C from microwave measurements (Hennelly *et al.* 1948) and are plotted in the figure on the same scale of ordinates as $\nu_c/3$. We see that the numerical values of ν_D are almost identical with those of $\nu_c/3$. We are therefore encouraged to predict that the values of $\nu_D(T)$ in the temperature range −77° to 127°C will be as given by the curve of the figure using the right-hand scale of ordinates. Since the values of $\nu_c/3$ and ν_D agree both in their variation with temperature and in actual magnitude it seems probable that the motion of the dipolar part of the molecule is rather similar to that of the rest of the molecule.

However the dielectric measurements indicate a slight distribution of correlation frequencies characterized by a Cole–Cole (1941), $\alpha \simeq 0{\cdot}23$. The effect on T_1 well above its minimum of a distribution of correlation frequencies, if it exists, is to reduce T_1 below the value it would otherwise have. If for simplicity we assume a 'rectangular' distribution on a logarithmic scale such as

$$\begin{aligned} I(\ln \nu_c) &= 1/(2 \ln b) \qquad && \nu_g/b < \nu_c < b\nu_g \\ &= 0 && \nu_c > b\nu_g \quad \text{and} \quad \nu_c < \nu_g/b \qquad \ldots\ldots(3) \end{aligned}$$

then ν_g is the geometric mean value of ν_c. Use of a more realistic distribution function will not affect the conclusions significantly. Well above its minimum, T_1 is reduced by the factor $2 \ln b/(b - 1/b)$ (Luszczynski and Powles 1959 b). From the dielectric results (Hennelly *et al.* 1948) if we assumed here also a rectangular distribution we would have $b = 6$. Hence if the nuclear motion is subject to the same distribution, the correction factor to equation (2) might be 1·65 and we would have

$$\nu_g = 15 \times 10^9\, T_1. \qquad \ldots\ldots(2\,a)$$

The difference between $\nu_g/3$ and ν_D is now greater than the combined experimental error but still within the limits of uncertainty expected for the theory. If the theory for ν_c is assumed to be accurate the present results suggest that the distribution of correlation frequencies for the interproton vectors is smaller than for the dipolar vector.

Temperature (°c)	1	20	25	40	55
η (cP)	$2{\cdot}3$	$1{\cdot}6_5$	$1{\cdot}4_9$	$1{\cdot}2_1$	$0{\cdot}9_8$
$\eta T_1/T \times 10^4$	$1{\cdot}0_6$	$1{\cdot}0_8$	$1{\cdot}0_9$	$1{\cdot}0_5$	$1{\cdot}0_6$
$\eta \nu_D/T \times 10^{-5}$	$3{\cdot}6_9$	–	$3{\cdot}6_5$	–	$3{\cdot}4_7$

We note that, as expected (Luszczynski and Powles 1959 b) the distribution of correlation frequencies in nuclear resonance, if any, does not lead to non-exponential decay of the longitudinal magnetization.

The plot of $\ln \nu_c$ against the reciprocal of the absolute temperature is clearly not a straight line and so we do not obtain activation energies.

The equality of $\nu_c/3$ and ν_D for *n*-octyl bromide contrasts with the result for *n*-octyl alcohol which has $T_1 = 0{\cdot}8_5$ sec (Powles and Cutler 1959) and $\nu_D = 9 \times 10^7$ c/s (Dalbert *et al.* 1949) at 25°c. A similar calculation to the one given here yields the result $\nu_c/3\nu_D = 28$ so that in this case the motion of the dipole (–OH) is markedly slower than that of the remainder of the molecule and is no doubt due to the restrictive effect of intermolecular hydrogen bonding. However there is a higher frequency weak dielectric absorption process in *n*-octyl alcohol having $\nu_D = 3 \times 10^9$ c/s at 25°c (Dalbert *et al.* 1949) and for this $\nu_c/3\nu_D = 0{\cdot}8$ so that the motion of the protons may be connected with this. In other words the motion of the chain of the molecule is faster than that of the dipole but nevertheless an attenuated part of this motion is transmitted to the dipole. In *n*-octyl alcohol the distribution of dielectric correlation frequencies is small and so no correction need be considered.

A comparison of T_1 with macroscopic viscosity may also be made although viscosity values are only available over the range 1° to 55°c (Hennelly *et al.* 1948). If we assume that the viscosity is related to a molecular jump frequency ν_v, of translation and/or rotation, then we may consider the constancy of $\eta T_1/T$ as in the table.

Within the accuracy of the measurement $\eta T_1/T$ is constant in the temperature range 1° to 55 °C suggesting a close relation between ν_V and ν_C just as there is between ν_V and ν_D. The temperature range is too small to allow any very significant conclusions but it is worth mentioning that for water $\eta T_1/T$ falls in the same temperature range by 7% (Simpson and Carr 1958).

ACKNOWLEDGMENTS

Part of the equipment was provided by the Central Research Fund of the University of London. One of us (A.H.) was supported by a grant from the Department of Scientific and Industrial Research.

REFERENCES

BLOEMBERGEN, N., PURCELL, E. M., and POUND, R. V., 1948, *Phys. Rev.*, **73**, 7.
CARR, H. Y., and PURCELL, E. M., 1954, *Phys. Rev.*, **94**, 630.
COLE, S. K., and COLE, R. H., 1941, *J. Chem. Phys.*, **9**, 341.
DALBERT, R., MAGAT, M., and SURDUT, A., 1949, *Bull. Soc. Chim. France*, D 345.
HAHN, E. L., 1950, *Phys. Rev.*, **80**, 580.
HENNELLY, E. J., HESTON, W. M., and SMYTH, C. P., 1948, *J. Amer. Chem. Soc.*, **70**, 4102.
HUBBARD, P. S., 1958, *Phys. Rev.*, **109**, 1153.
KUBO, R., and TOMITA, K., 1954, *J. Phys. Soc., Japan*, **9**, 888.
LUSZCZYNSKI, K., and POWLES, J. G., 1959, *J. Sci. Instrum.*, **36**, 57.
—— 1959 b, *Proc. Phys. Soc.*, **74**, 408.
POWLES, J. G., and CUTLER, D., 1959, *Arch. des Sci.*, **12**, 136 (8th Colloque AMPERE).
SIMPSON, J. H., and CARR, H. Y., 1958, *Phys. Rev.*, **111**, 1201.
SKROTSKII, G. V., and KOKIN, A. A., 1959, *J. Expt. Theor. Phys.* (English translation), **36**, 481.
VAN VLECK, H. J., 1948, *Phys. Rev.*, **74**, 1168.

LETTERS TO THE EDITOR

Electron Spin Resonance Intensity in Anisotropic Substances

When magnetic resonance is observed in a polycrystalline sample of a substance with an anisotropic g-factor, the line shape (neglecting broadening due to spin–lattice and spin–spin interactions) depends on the probability of a crystallite lying at a given orientation to the external magnetic field. On this basis, Bleaney (1950) and Sands (1955) have given expressions for the line shape in a substance whose g-factor is axially symmetric; Searl, Smith and Wyard (1959) have extended these by including the effect of a finite line width with Lorentzian shape. When there is considerable anisotropy, however, allowance must also be made for the change in transition probability with orientation of the oscillatory magnetic field which induces the transitions. This is evaluated below for a powder where the g-factor has axial symmetry, and fine or hyperfine structure splittings are absent.

If the static magnetic field H is applied in the plane $y=0$ at an angle θ to the axis of symmetry (z axis) the static spin Hamiltonain is

$$\mathscr{H}=\beta H(g_x S_x \sin\theta + g_z S_z \cos\theta) \qquad \ldots\ldots(1)$$

and this is diagonalized by changing to a new set of axes (x', y', z') derived from the original axes by a rotation about the y axis through an angle ϕ such that $\tan\phi=(g_x/g_z)\tan\theta$ (cf. Bleaney 1951). The static spin Hamiltonian then reduces to

$$\mathscr{H}=g\beta H S_z' \qquad \ldots\ldots(2)$$

where

$$g^2=g_x{}^2\sin^2\theta+g_z{}^2\cos^2\theta. \qquad \ldots\ldots(3)$$

If the oscillatory field $H_1\cos\omega t$ is linearly polarized along a direction making an angle η with the y axis, and whose projection on the xz plane makes an angle θ' with the z axis, the oscillatory Hamiltonian is

$$\mathscr{H}_1=\beta H_1\cos\omega t\{g_x S_x \sin\eta\sin\theta' + g_y S_y\cos\eta + g_z S_z \sin\eta\cos\theta'\}. \qquad \ldots\ldots(4)$$

On transferring this to the (x', y', z') system, and writing $S_{\pm}'$ for $S_x'\pm iS_y'$, we obtain

$$\mathscr{H}_1=\beta H_1\cos\omega t\{\tfrac{1}{2}g_1 S_+' + \tfrac{1}{2}g_1{}^* S_-' + g_z' S_z'\} \qquad \ldots\ldots(5)$$

where

$$\left.\begin{aligned} g_1&=(g_x g_z/g)\sin\eta\sin(\theta-\theta')-ig_y\cos\eta \\ g_z'g&=\{g_x{}^2\sin\theta\sin\theta'+g_z{}^2\cos\theta\cos\theta'\}\sin\eta \end{aligned}\right\} \qquad \ldots\ldots(6)$$

and $g_1{}^*$ is the complex conjugate of g_1. The intensity of transitions in which the magnetic quantum number changes by one unit is proportional to the square of the coefficients of $S_{\pm}'$; that is, to

$$g_1{}^2=(g_x g_z/g)^2\sin^2\eta\sin^2(\theta-\theta')+g_y{}^2\cos^2\eta. \qquad \ldots\ldots(7)$$

It is clear from (7) that, whatever the value of η, the greatest intensity is obtained when $\theta-\theta'=\pi/2$; i.e. when the oscillatory field is normal to the static field. This result is not surprising, but is not obvious when anisotropy is present. It can readily be seen in another way: if there is a component of H_1 parallel to H, then when the static Hamiltonian is diagonalized by an appropriate change of axes, this component of H_1 will give rise only to a corresponding term in S_z' in the transformed oscillatory Hamiltonian, which will be inoperative as far as transitions of the normal kind are concerned.

If the oscillatory field is normal to H_1, then for a single crystal a value of η can be chosen to make g_1^2 a maximum. It is obvious that this value is 0 or $\pi/2$, according to whether g_y is greater or smaller than $(g_x g_z/g)$; since we have assumed axial symmetry, $g_x = g_y = g_\perp$, so that this criterion reduces to whether $g_\perp$ is greater or smaller than $g_z = g_\parallel$. For a powder, all values of η are equally probable, so that on averaging we get

$$g_1^2 = \tfrac{1}{2}\{(g_x g_z/g)^2 + g_y^2\} = \tfrac{1}{2} g_\perp^2 \{(g_\parallel/g)^2 + 1\}. \qquad \ldots\ldots (8)$$

This analysis can readily be extended to the case of a circularly polarized oscillatory field of amplitude H_1, which we shall assume to be in the plane normal to H. The oscillatory Hamiltonian is then

$$\mathscr{H}_1 = \beta H_1 \{(g_x S_x \cos\theta - g_z S_z \sin\theta)\cos\omega t + g_y S_y \sin\omega t\} \qquad \ldots\ldots (9)$$

for a field rotating in the right-handed sense about H_1; a field in the opposite sense is obtained by reversing the sign of ω. On transforming to the (x', y', z') system this becomes

$$\begin{aligned}\mathscr{H}_1 = \tfrac{1}{4}\beta H_1 \Bigg[& \left(\frac{g_x g_z}{g} - g_y\right)(S_+' \mathrm{e}^{+i\omega t} + S_-' \mathrm{e}^{-i\omega t}) \\ & + \left(\frac{g_x g_z}{g} + g_y\right)(S_+' \mathrm{e}^{-i\omega t} + S_-' \mathrm{e}^{+i\omega t}) \\ & + \left(\frac{g_x^2 - g_z^2}{g}\right) S_z' \sin 2\theta (\mathrm{e}^{+i\omega t} + \mathrm{e}^{-i\omega t}) \Bigg]. \qquad \ldots\ldots (10)\end{aligned}$$

We now assume that the sign of g is always positive, thereby removing the sign ambiguity in (3) (if g_x, g_z are not both positive, the angle ϕ lies in a different quadrant from θ). Then the level $S_z' = M$ lies higher in energy than $M-1$, and the transition between these two levels has intensity proportional to $\{(g_x g_z/g) + g_y\}^2$ for the right-handed sense, and $\{(g_x g_z/g) - g_y\}^2$ for the left-handed sense. Hence experimental observation of which sense gives the higher intensity yields the relative signs of $g_x g_z$ and g_y; i.e. it determines the sign of $(g_x g_y g_z)$, or of g_z if $g_x = g_y$ (axial symmetry), as pointed out by Pryce (1959) (see also Bleaney and O'Brien 1956). It will be noted that the intensity is not zero for a powder for radiation polarized in the wrong sense unless g is isotropic; for a single crystal it would be zero for $\theta = 0$, if there is axial symmetry, since then $g = g_z$ and $g_x = g_y$.

It will be seen from equations (5), (6) and (10) that even if H_1 is normal to H there is in general a component of H_1 parallel to the z' axis in the coordinate system which diagonalizes the static Hamiltonian. This means that transitions of the type $\Delta S_z' = 0$, which may occur when a crystal field splitting or hyperfine structure is present (cf. Bleaney 1951), will still be visible if H_1 is normal to H, provided that θ is not 0 or $\pi/2$. Similarly the effect of a low frequency modulating field will not fall to zero under these circumstances even if its direction happens to be perpendicular to *H*.

Clarendon Laboratory,
Oxford. B. Bleaney.

20th February 1960.

Bleaney, B., 1950, *Proc. Phys. Soc.* A, **63**, 407.
—— 1951, *Phil. Mag.*, **42**, 441.
Bleaney, B., and O'Brien, M. C. M., 1956, *Proc. Phys. Soc.* B, **69**, 1216.
Pryce, M. H. L., 1959, *Phys. Rev. Letters*, **3**, 375.
Sands, R. H., 1955, *Phys. Rev.*, **99**, 1222.
Searl, J. W., Smith, R. C., and Wyard, S. J., 1959, *Proc. Phys. Soc.*, **74**, 491.

The Dependence of Solvent–Solute Energy Transfer in Liquid Organic Solutions on Excitation Wavelength†

In a recent publication Birks and Cameron (1958) claim to have demonstrated a marked dependence of the efficiency of solvent–solute energy transfer on the wavelength of the exciting radiation in liquid or organic solutions, and from this draw the conclusion that the second excited electronic singlet state of toluene transfers energy efficiently to the solute (*p*-terphenyl) despite the expected short-lived nature of this state. Their paper includes a discussion and some criticism of an article published by the present authors (Cohen and Weinreb 1956) in which we concluded that the transfer efficiency shows no marked dependence on the excitation wavelength for solutions of *para*-terphenyl in toluene.

Since our article did not present the results of this particular experiment in detail, and since Birks and Cameron reached contradictory conclusions, it seems worth while to display here the experimental results (figure). It is true that the results would not be inconsistent with the transfer efficiency becoming slightly dependent on wavelength at the higher concentrations, although the variation from the mean value for a given concentration is not more than about 5%.

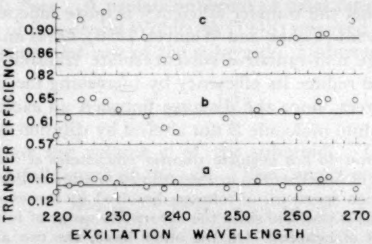

Energy transfer efficiency plotted against excitation wavelength for solutions of *p*-terphenyl in toluene. *a*, 0·1 g l⁻¹; *b*, 1 g l⁻¹; *c*, 5 g l⁻¹.

---

† Work performed under the auspices of the United States Atomic Energy Commission.

However, the trend differs from that observed by Birks and Cameron in that the transfer efficiency shows a decrease followed by an increase as the wavelength is increased. The values at 2700 Å† (within the excitation region of the first excited state) and 2250 Å (second excited state) are moreover in good agreement. However, it is rather difficult to make a precise estimate of the errors involved, in view of the various corrections which have to be applied. Hence, we think it is probable that the apparent small departures from uniformity are within the experimental error and therefore conclude that the transfer efficiency is independent of excitation wavelength for the investigated region.

A major difference also seems to exist between the absolute values of transfer efficiencies given in the paper of Birks and Cameron and those obtained by us. In their paper they suggest that one of the reasons for this discrepancy might be the correction for excitation depth used in their work. This correction seems to us to be applied in the wrong direction. If all the exciting light is absorbed, and since the fluorescence was measured by transmission, a more penetrating exciting radiation should give rise to a higher measured intensity, rather than to a lower one, contrary to their article. Since the fluorescence is created in a region which is nearer to the detector, a better geometry is obtained and self-absorption is reduced. The assumption that practically all the incident exciting radiation is absorbed by the solution holds up to at least 3130 Å for the two higher concentrations presented in the figure, and up to at least 3050 Å for the lowest concentration. Thus, no reason is seen for applying the proposed correction to the computed transfer efficiencies. This is true also for all the solutions presented in figure 3‡ of the paper of Birks and Cameron. The proposed correction was apparently suggested by the fact, shown in this figure, that a slow decrease in fluorescent intensity with increasing wavelength was observed even at the highest concentrations, although up to at least 3130 Å all the exciting light was completely absorbed by the solute. However, this decrease cannot be explained by a mere decrease in the absorbance of the solution, and the application of the derived correction by extrapolation of the values given in figure 5 of their paper has thus to be justified.

From the fact that the transfer efficiency is quite independent of dilution of the transferring solvent (Cohen and Weinreb 1956), Birks and Cameron conclude that any short-range non-radiative solvent–solute transfer process is excluded, since dilution would reduce its efficiency by increasing the diffusion time. This conclusion is incorrect, since the distance between an excited solvent molecule and an accepting solute molecule is not altered by dilution of the solvent as long

† Birks and Cameron do not evaluate transfer efficiencies at wavelengths greater than about 2650 Å because of uncertainties in the absorption edge of the solvent, toluene. We measured the absorption spectrum of toluene dissolved in benzene in the vicinity of the absorption edge. This is possible since the absorption range of toluene extends to longer wavelengths than that of benzene. On the other hand, the two are spectroscopically so similar that one is likely to assume that the energy levels of the toluene molecules in benzene will be the same as for pure toluene. The results show that the molar absorption coefficient of toluene at 2700 Å is still about 260 $cm^2\ mmol^{-1}$. The evaluation of transfer efficiencies for excitation wavelengths up to 2700 Å is thus justified.

‡ In a private communication Dr. Birks kindly pointed out that the scale of fluorescence intensity is different for each of the individual curves in figures 3 and 4, and that the actually observed intensities for all the solutions in the region of complete solute absorption were similar.

as the solute concentration relative to the bulk solution is kept constant, as was done in our experiments.

In conclusion it may be mentioned that Brown, Furst and Kallmann (1959) have recently rechecked the question of dependence of transfer efficiency on excitation wavelength and their results show that it remains constant. The numerical values of the transfer efficiencies they obtain approach unity as do the transfer efficiencies we obtain for *p*-terphenyl in toluene, in apparent contradiction with the theory developed in the article of Birks and Cameron.

Radiation Laboratory,
University of California,
Berkeley.
S. G. Cohen.†

Argonne National Laboratory,
Lemont,
Illinois.
A. Weinreb.†

4th December 1959.

† On leave of absence from the Hebrew University, Jerusalem, Israel.

Birks, J. B., and Cameron, A. J. W., 1958, *Proc. Phys. Soc.*, **72,** 53.
Brown, F. H., Furst, M., and Kallmann, H., 1959, paper presented at the " Conference on Energy Transfer with Special Reference to Biological Systems ", Nottingham, April 1959.
Cohen, S.G. and Weinreb, A., 1956, *Proc. Phys. Soc.*, **69,** 593.

Correction to a Single Domain Calculation

Dr. F. D. Stacey (1959 b) has recently calculated the relaxation time for a single domain particle of iron, and suggested it was so short that the remanence of an array of such particles, of maximum volume consistent with retaining a single domain form, should decay spontaneously, due to thermal agitation, in a time of order 5×10^{-8} sec. A prolate spheroid of axial ratio 1·1 was considered and equation (6.12) of Stoner and Wohlfarth (1948) was used to find the maximum value of b, the shortest *semi-axis* of the spheroid. Unfortunately, however, the formula

$$v=\frac{\pi}{6}ab^2=\frac{1\cdot1\pi}{6}b^3$$

was used to calculate the volume v of the spheroid. This formula is only applicable if b is the *full* length of the axis. The correct volume is given by

$$v=\frac{4\pi}{3}ab^2=\frac{4\cdot4\pi}{3}b^3\sim2\cdot4\times10^{-18}\,\text{cm}^3.$$

Thus at room temperature E_0/kT for a single domain particle of maximum volume is 100. Using this value in equation (1) of Stacey (1959 b), and assuming the value of C calculated by Stacey (1959 a), the probability of a single domain inclusion undergoing a spontaneous reversal of magnetization in time dt is given by

$$dP=C\exp\left(-\frac{E_0}{kT}\right)dt\sim2\cdot2\times10^{-31}\,dt.$$

Thus the remanence of an array of such particles would decay in a time of order 5×10^{30} sec rather than the 5×10^{-8} sec derived previously. The single domain hypothesis to account for the magnetic properties of heterogeneous alloys cannot, therefore, be criticized on the grounds that the remanence of an array of such particles would decay spontaneously, due to thermal agitation, in a very short time.

The author thanks Dr. Stacey for helpful correspondence in which he has expressed his agreement with this revised estimate of the relaxation time.

Department of Physics, P. GAUNT.
University of Sheffield.

9th February 1960.

STACEY, F. D., 1959 a, *Proc. Phys. Soc.*, **73**, 136.
—— 1959 b, *Ibid.*, **73**, 517.
STONER, E. C., and WOHLFARTH, E. P., 1948, *Phil. Trans. Roy. Soc.*, **240**, 599.

REVIEWS OF BOOKS

Handbuch der Physik, Vol. XLI/1, *Nuclear Reactions II: Theory*, edited by S. Flügge. Pp. vii + 580. (Berlin: Springer, 1959.) 145 DM.

This volume of the *Handbuch* consists of one major article by Professor G. Breit on the resonance theory of nuclear reactions followed by three shorter, but still substantial, articles written in collaboration with Professor Breit and concerned with Coulomb wave functions, Coulomb excitation, and the polarization of nucleons scattered by nuclei. As one would expect, the result is a work of great and lasting value, although not entirely suitable (in the writer's opinion) as a first introduction to the subject. One does wonder, however, whether the addition of an introductory article, written in a more homely manner, might not have increased the appeal of the whole. The essentials of reaction theory are simple enough: it is the 'ifs and buts' which make it appear so difficult, and they have not been spared here. It is a pity, too, that the first article treats rather briefly the theoretical foundations of the optical model and of direct interactions. Perhaps it was written a little too early to include the very recent work on this subject which has contributed so much to our understanding of reaction theory. Many will welcome the article on Coulomb wave functions which summarizes so many years of work by the Yale group gathered together here for the first time. The publishers and printers have maintained their usual standards of excellence in the face of a very difficult task. B. H. FLOWERS.

Properties of Matter, by F. C. Champion and N. Davy. Third edition. Pp. xvi + 334. (London, Glasgow: Blackie and Son, 1959.) 40*s*.

'Champion and Davy' is now so firmly established as a standard text on Properties of Matter that any detailed account of its contents is quite unnecessary. In the third edition a very few items which appeared in its predecessors have been omitted (e.g. Sentis's method for the measurement of surface tension), there is a new section on paper chromatography, an account of recent (1955) recalculations of the atomic constants and several additional paragraphs mostly relating to physical interpretations of phenomena dealt with in the book. Among them are paragraphs dealing with 'pictorial' models of gravitational phenomena, the elastic behaviour of single cubic crystals, the structure of the earth, diffusion in solids, and the viscosity of liquids. D. O. W.

Electron Physics and Technology, by J. Thompson and E. B. Callick. Pp. xiv + 527. (London: English Universities Press, 1959.) 50*s*.

This book will be of interest to the student and professional worker requiring a general introduction to Electron Physics. It deals with conduction *in vacua*, in gases and in solids. Like many other books in this field the emphasis on the various branches of the subject is far from uniform and reflects to a marked extent the special interests of the authors.

The first seven chapters deal with basic principles, covering such topics as atomic and molecular structure, electron emission, gaseous conduction and semiconductors. The following 18 chapters of the book are largely concerned with application to various electronic devices and the final six chapters are devoted to the technology of materials and fabrication. The only slight weakness in this book is in the section dealing with basic principles, particularly in the discussion of atomic energy states in chapter 1 and in the account of gaseous conduction in chapter 5. In the first chapter the discussion of the various quantum numbers of atomic theory would have been much improved by an explanation of the physical significance of these numbers which are very often mysterious to the engineering student. In chapter 5 it is said that in a gas-filled diode the effect of a small electric field is to increase the temperature of the gas; whereas a much more significant effect, which is not mentioned, is the very much larger increase in the temperature of the drifting electrons.

Passing from the first hundred pages to the main sections of the book which deal with electronic devices and the principles of their operation, no reader can fail to be impressed by the thorough and comprehensive survey to be found in these pages. Conventional valves are dealt with in detail, starting with the diode and triode and including multi-electrode valves. Similarly, the principles of operation and use of transistors are fully discussed. Separate chapters are devoted to magnetrons and klystrons followed by an account of associated radar devices such as crystal mixers, duplexer tubes and pulse modulator switches. Special mention must be made of an excellent chapter on travelling wave tubes which includes a description of backward-wave amplifiers and oscillators. Further chapters deal with various forms of cathode-ray tubes, camera tubes, image intensifiers and storage tubes.

A fairly comprehensive final section dealing with the technology of materials and fabrication is a somewhat unusual but very welcome addition to a book of this kind.

Having reached the end pages most readers will be impressed by the wealth of material which the authors have been able to include in a volume of moderate size and price. It will have a special appeal to advanced students of engineering and physics and at the same time constitute a helpful reference work for the professional research workers. J. SAYERS.

Applications of Finite Groups, by J. S. LOMONT. Pp. ix + 346. (New York, London: Academic Press, 1959.) $11.00.

Many physicists, while admitting that group theory is of value to those who have mastered it, seem to have a mental barrier when it comes to learning it. It is therefore with considerable interest that one turns to a book which deals with the application of group theory to quantum-mechanical problems. Unfortunately, the author seems to have done nothing towards removing the difficulties and, in fact, his treatment will probably confirm many readers in their erroneous belief that group theory is difficult.

At the same time one cannot help but have an admiration for the book, for the text is mathematically very compact and carefully prepared. Practically all the topics in theoretical physics to which group theory is applied are considered, except that the value of the Wigner–Eckart theorem is not emphasized. But perhaps this is because it is usually used to prove that two operators have the same matrix elements, so that further group theory can then be avoided.

My objection is simply that the treatment is far too difficult to be readily assimilated by the average physicist, but to one, such as myself, who has learnt group theory from more elementary texts it is extremely interesting to see what a mathematician can do when he really tries! K. W. H. STEVENS.

Matrix Calculus, by E. Bodewig, 2nd Edition. Pp. xi + 464. (Amsterdam: North Holland Publishing Co., 1959.) 65*s*.

The first edition of Dr. Bodewig's book appeared in 1956 and was deservedly praised for the freshness of its approach and for its comprehensive coverage of the field of matrix calculation—linear equations, inversion of matrices and the determination of eigenvalues and vectors. The present edition has been completely revised and is over 100 pages longer than the first. New material has been included in all chapters, the most notable additions being sections on orthogonal matrices and their geometrical properties, on Rutishauser's *LR*-algorithm and on Lanczos' *pq*-algorithm for the computation of eigenvalues. The author rightly preserves his frank critiques of the many different computing schemes found in the literature, which were a valuable and stimulating feature of the first edition. Only occasionally as, for example, in his comments on the solution of Schrödinger's equation with the aid of the theory of 'geodetic matrices', does he seem to let his enthusiasm get the better of him.

A major criticism of the first edition was the 'Dutchness of the English' and it is to be greatly regretted that for this new edition the author or his publisher did not obtain the services of an English speaking mathematician in order to revise the language throughout the book. As it is, the book is rather difficult to read (and at times definitely confusing) and misprints are quite frequent. This is a pity since it restricts the scope of the book to that of a work of reference, albeit an encyclopaedic and authoritative work. MICHAEL E. FISHER.

Statistical Theory of Irreversible Processes, by R. Eisenschitz. Pp. viii + 84. Oxford Library of the Physical Sciences. (Oxford: University Press, 1958.) 8*s*. 6*d*.

The author, who is a recognized authority in the field of the theory of transport phenomena, endeavours in this little book to give a concise account of the fundamentals of the statistical mechanics of non-equilibrium systems with applications to some important irreversible processes. Whereas on the one hand the statistical mechanics of systems in equilibrium, or of reversible processes in the strict thermodynamic sense and, on the other hand, the kinetic theory of gases in non-equilibrium are well established and presented in many excellent textbooks, the general statistical mechanics of irreversible processes is still in its development stages, and the subject is only known to a relatively small number of experts. The present book is therefore a very welcome addition to the literature in this field.

Owing to the restrictions imposed on the size of the book the author was only able to give the explicit derivations of the basic formulae and could in most cases only quote the results of their applications to specific problems. This makes it difficult to appreciate what kind of special assumptions and simplifications were used in the derivation of these results. The notation is occasionally ambiguous, and many readers who are not familiar with the tensor notation would have greatly benefited by the addition of one page of definitions and explanations of the symbols; at present there is only one two-line footnote which is quite insufficient. There is also a considerable number of more or less obvious errors in the formulae which ought to be thoroughly checked for a further edition.

The book is very well written and contains many critical and illuminating remarks as well as indications where further research is needed. The mathematical presentation is clear and elegant. R. FÜRTH.

Electronic Apparatus for Biological Research, by P. E. K. DONALDSON. Pp. xii +718. (London: Butterworths Scientific Publications, 1958.) 120*s*.

Workers of several different disciplines are engaged in the many fields of biological research today and, as he states in the preface, the author of this volume was presented with the problem of where to start and what to include. He has chosen to assume no prior knowledge of electricity. Starting with Ohm's law the text progresses through circuit theory and practice to a section on transducers and related devices, and concludes with a selection of complete electronic circuits.

Much of the material of Part 1 (Theory) and Part 2 (Practice), which together cover the first 330 pages, is common to several existing textbooks of electronics. The present text however is written with the non-specialist in mind, and with emphasis on careful explanation of electrical terminology which may be unfamiliar to the reader. The subject receives adequate mathematical treatment, however, including a small amount of elementary calculus.

It is in Part 3 (Transducers, Electrodes and Indicators) and in Part 4 (Complete Apparatus) that most of the material suggested by the title of this volume is to be found. The biological material itself is introduced in Part 3, in which a number of specialists describe some types of physical measurement commonly employed. This section comprises chapters by Mr. F. W. Campbell (Light Sources and Detectors), Dr. J. W. L. Beament (Temperature and Humidity), Dr. R. D. Keynes (Assay of Radioactivity), Mr. P. E. K. Donaldson (Visual Indicators), Dr. K. E. Machin (Transducers and Relays), Dr. D. W. Kennard (Glass Electrodes) and Dr. I. A. Silver (Other Electrodes).

The examples of complete apparatus described in Part 4 are mainly of physiological application, but the section contains valuable chapters on layout and fault tracing, wherein the principles described can be extended to other branches of research.

Combining as it does the functions of textbook and work of reference, this volume is well produced and well proportioned, and will doubtless find a place in the more progressive biological laboratories. E. M. D.

Grundlagen und Anwendung der Röntgen-Feinstruktur-Analyse, by HANS NEFF. Pp. 447. (München: Oldenbourg, 1959.) 73 DM.

Although this book is written in a language in which the reviewer is not greatly proficient, he nevertheless feels no compunction in reviewing it. It is clearly written, and so well illustrated with photographs and diagrams that its scope is quite readily assessable. It deals with the practice and theory of x-ray diffraction and covers the ground it sets itself fairly thoroughly, although it omits single-crystal work almost completely. It deals, at a fairly elementary level, with x-ray apparatus and the methods used to examine powders and polycrystalline materials, and it concludes with a chapter on simple crystal structures and the light they throw on crystal chemistry.

Although it is obviously competently written and well produced, the book would appear to have no particular value to the English student; there are now several works in English that cover almost exactly the same ground, and would obviously serve the student much better. H. LIPSON.

The Transuranium Elements, by G. T. Seaborg. Pp. xx + 328. (Reading, Mass.: Addison-Wesley Publishing Co., 1958.) 53*s.*

This volume has been developed from the Silliman lectures given by the author at Yale University in 1957. The development has evidently been extensive; although addressed to the non-specialist the work is a mine of authoritative information about these elements, and especially plutonium. At the same time Professor Seaborg has retained the informality and simplicity of style not so much of the lecture theatre as of the seminar room.

The first chapter begins with the discovery of plutonium and ends by listing the books which have been already published on the element. In between the reader will find a fascinating blend of personal and scientific history. The magnitude of the technical achievements which are described is impressive; almost equally remarkable is the flexibility of organization of manpower and facilities which made them possible in so short a time.

The chemical properties of the actinide elements are summarized in the second chapter, largely in terms of the regularities exhibited in the existence of different oxidation states, the values of oxidation-reduction potentials and ionic radii, optical properties, and ion-exchange behaviour. This is followed by a chapter on their nuclear properties, such as the excitation functions governing their production, the systematics of their energy levels and decay schemes, and their induced and spontaneous fission. In both these chapters there is a nice balance between over-simplification and crowded detail.

Finally Professor Seaborg allows himself a few minutes gazing into what is evidently a rather cloudy crystal ball, as he predicts the preparation and properties of elements beyond mendelevium (element 101, the last element to be recognized without question at the time of writing). The book concludes with a table of nuclear properties of the heavy elements, a short bibliography and indices. In keeping with the general style there are no references to the original literature, although the names of some 800 investigators are mentioned in the text. The printing and production are very good.

In a work of such uniform excellence one would not care to single out any section for special praise. Its merit is rather that readers with very different scientific backgrounds are sure to find in it much material of immediate appeal, while those already familiar with the field will enjoy its balance and breadth of outlook. K. F. CHACKETT.

Groupes Finis de Symétrie et Recherche de Solutions de L'Equation de Schrödinger, by L. Mariot. Pp. viii + 106. (Paris: Dunod, 1959.) 960 *fr.*

This little book on the use of group theory in crystal physics is an excellent one for those who like to learn a subject rapidly. The first two chapters are concerned with the essentials of the formal theory of groups and their matrix representation, expressed in such a way that the results are in just the form required for later use and a short outline of space groups makes the third chapter. The Ritz variation principle and origin and properties of the secular equation completes the formal theory, but it is a pity that it is not made clear that most of this applies equally to many-electron wave functions and to one-electron functions, and to every kind of eigenvalue problem in a crystal.

The method of orthogonalized plane waves is selected for a detailed study of one-electron functions, and the crystal group chosen is that of diamond O_k^7.

The factorization of the secular determinant by selection of symmetrical combinations of plane waves is clearly demonstrated. Though the subject matter is limited, the treatment is clear and concise, and will be adequate for most interested physicists to follow. A most welcome little book. The short bibliography unfortunately covers only the same limited ground as the book itself. W. M. LOMER.

The Classical Theory of Fields, by L. D. LANDAU and E. M. LIFSHITZ. Translated by M. HAMERMESH from the Russian 2nd Edition. (*Course of Theoretical Physics*, Vol. 2.) Pp. ix + 354. (London : Pergamon Press, 1959.) 70*s*.

This book is not a revised edition, but simply a reprint of that published by Addison-Wesley in 1951, now being published uniformly with the other parts of the nine-volume Course of Theoretical Physics by Landau and Lifshitz. The title does not reveal the wide range of topics covered. The first two chapters cover the special theory of relativity and relativistic mechanics. The main section of the book deals with the electromagnetic field *in vacuo*, including geometrical optics, diffraction and radiation. Finally there are two chapters on the gravitational field and general relativity, with the necessary tensor analysis. The clarity of style, the conciseness of treatment, and the originality and variety of illustrative problems make this a book which can be highly recommended. Its appeal will be mainly to the advanced student and research worker; for while the deductive development, based on the variational principle, which the authors use, produces a delightful elegance and simplicity of presentation, it is foreign to most undergraduate courses in this country. A. NISBET.

Methods of Experimental Physics, Vol. 6, *Solid State Physics*, Part B, *Electrical, Magnetic and Optical Properties*, by K. LARK-HOROVITZ and VIVIAN A. JOHNSON. Pp. xiv + 416. (New York, London : Academic Press, 1959.) $ 11.00.

This volume deals with a wide range of electrical properties of solids, including dielectric properties, superconductivity, thermoelectric effects, thermionic emission and surface states; with galvanomagnetic and thermomagnetic effects, susceptibility, ferro- and ferri-magnetism and neutron and electron spin resonance; with optical properties, including double refraction and rotation, thin films and x-ray spectroscopy; with luminescence, including electroluminescence and colour centres; and with photoelectric phenomena, including photoconductivity, photovoltaic effects and photoelectric emission.

The approach in each case is to present briefly the theory underlying the experiment and the basic principles of the method, and to outline the equipment and procedure, and some of the sources of error and special problems arising. Clearly, with such a large number of topics, the equipment and procedure cannot be described in any great detail. The reader concerned for the first time with one of these experiments will often need further details. The bibliography is good however, and such readers will be able to look up the relevant original papers. D. A. WRIGHT.

The Theory of Critical Opalescence in Binary Mixtures

By F. J. PEARSON†
Department of Physics, College of Advanced Technology, Birmingham

MS. received 14*th August* 1959, *in final form* 17*th December* 1959

Abstract. The present theory of X-ray scattering by simple fluids and binary mixtures is applied to the phenomenon of critical opalescence in binary mixtures. Firstly, the condition for phase separation is expressed in terms of the three radial distribution functions for a binary mixture, and then it is shown that, at phase separation, these functions are all of the same form, although they differ in scale. The form of these functions can then, in principle, be determined from experimental observations of visible opalescence, although the normalization requires further discussion.

The theory is then applied to the work of Fürth and Williams, and of Quantie, who suggested analytic representations of two types of radial distribution function. Only one of these is found to be acceptable.

§ 1. Introduction

It is well known (see, for example, de Boer 1949) that at distance R from the scatterer, the intensity $I(s)$ of electromagnetic radiation of wavelength λ scattered through angle θ from the direction of a primary beam of intensity I_0 by a simple fluid of N systems, each of scattering power $f(s)$, occupying volume V, is given by

$$I(s)=I_0Nf^2(s)\left(\frac{e^2}{mc^2}\right)^2\frac{1+\cos^2\theta}{2R^2}\left\{1+4\pi\rho\int_0^\infty r^2(g(r)-1)\frac{\sin rs}{rs}\,dr\right\}, \quad \ldots\ldots(1)$$

where $s=4\pi\lambda^{-1}\sin\frac{1}{2}\theta$, $\rho=N/V$, e^2/mc^2 is the classical radius r_0 of the electron and $g(r)$ is the radial distribution function. Pearson and Rushbrooke (1957) have shown that the corresponding formula for a binary mixture, of N_A A-systems and N_B B-systems of scattering powers $f_A(s)$ and $f_B(s)$, can be written

$$\begin{aligned}I(s)=I_0Nr_0^2\frac{1+\cos^2\theta}{2R^2}\Big\{&(x_Af_A+x_Bf_B)^2\left[1+\rho\int_0^\infty\{x_A^2(g_{AA}-1)\right.\\&\left.+x_B^2(g_{BB}-1)+2x_Ax_B(g_{AB}-1)\}\frac{\sin rs}{rs}\,dr\right]\\&+2(f_A-f_B)(x_Af_A+x_Bf_B)\left[\rho x_Ax_B\int_0^\infty\{x_A(g_{AA}-1)-x_B(g_{BB}-1)\right.\\&\left.+(x_B-x_A)(g_{AB}-1)\}\frac{\sin rs}{rs}\,dr\right]\\&+(f_A-f_B)^2x_Ax_B\left[1+\rho x_Ax_B\int_0^\infty\{g_{AA}+g_{BB}-2g_{AB}\}\frac{\sin rs}{rs}\,dr\right]\Big\},\end{aligned}$$
$$\ldots\ldots(2)$$

---

†Now at: Department of Applied Physics, Lanchester College of Technology, Coventry.

where $x_A, x_B = N_A/V,\ N_B/V$ and $g_{AA}(r)$, $g_{BB}(r)$ and $g_{AB}(r)$ are the appropriate radial distribution functions. In (2), the three terms in square brackets differ from the following equations for certain mean square fluctuations

$$\frac{\langle(\Delta N)^2\rangle}{\langle N\rangle} = 1+\rho\int_0^\infty \{x_A{}^2(g_{AA}(r)-1)+x_B{}^2(g_{BB}(r)-1) \\ +2x_Ax_B(g_{AB}(r)-1)\}d\mathbf{r}, \qquad \ldots\ldots(3)$$

$$\langle\Delta N\Delta x\rangle = \rho x_Ax_B\int_0^\infty \{x_A(g_{AA}(r)-1)-x_B(g_{BB}(r)-1) \\ +(x_B-x_A)(g_{AB}(r)-1)\}d\mathbf{r}, \qquad \ldots\ldots(4)$$

$$\langle(\Delta x)^2\rangle = \frac{x_Ax_B}{\langle N\rangle}\left[1+\rho x_Ax_B\int_0^\infty \{g_{AA}(r)-2g_{AB}(r)+g_{BB}(r)\}d\mathbf{r}\right], \qquad \ldots\ldots(5)$$

only by the presence in the integrands of the Fourier factor $(\sin rs)/rs$. The bracket $\langle\,\rangle$ denotes a mean value, and $x \equiv x_A$.

Now, it is also well known that, from (1), $g(r)$ can be determined by a suitable Fourier inversion of experimental observations. Unfortunately, this cannot be done directly from (2) in the case of a binary mixture, because there are now two scattering powers dependent upon s, and three radial distribution functions.

As they stand, (1) and (2) apply to the scattering of all wavelengths. The integrations involved represent the limits of summations over elementary volume cells. In the case of X-ray scattering, these cells must accommodate only one molecule, because the wavelength is comparable with the intermolecular separation. X-ray observations are therefore capable of elucidating the form of the radial distribution function for small r. Indeed, away from the critical point, it becomes unity when r is of the order of a few molecular diameters. In the case of critical opalescence under visible irradiation, however, the wavelength is so long that the volume cells can be large enough to possess thermodynamic functions. At the same time, the range of intermolecular correlation becomes of the same order as the linear dimensions of the container (for example, when a binary mixture undergoes phase separation). Consequently, the radial distribution functions now display this long range correlation in that they do not become unity until r is comparatively large (from the molecular point of view). Observations of critical opalescence are therefore capable of elucidating these long range effects inherent in what we shall call the *critical* distribution functions. However, visible radiation is incapable of determining these functions for small r—only X-ray scattering can achieve this. Therefore, their limiting behaviour as r tends to zero will not come out of the experimental observations, i.e. appropriate *normalization* is required.

§ 2. The Theory of Critical Opalescence

In considering a binary mixture near phase separation, we shall distinguish the critical distribution functions by means of a prime. At the same time, our volume cells are now large enough to possess thermodynamic functions. We then have, explicitly, for the mean values of the products of the fluctuations $\Delta\rho_j$ and Δx_k, in number density and concentration, in the cells j and k a distance r_{jk} apart, the following equations, analogous to (3), (4) and (5),

$$\langle\Delta\rho_j\Delta\rho_k\rangle = \rho^2[x_A{}^2(g_{AA}'(r_{jk})-1)+x_B{}^2(g_{BB}'(r_{jk})-1)+2x_Ax_B(g_{AB}'(r_{jk})-1)], \qquad \ldots\ldots(6)$$

$$\langle \Delta\rho_j \Delta x_k \rangle = x_A x_B \rho [x_A(g_{AA}'(r_{jk})-1) - x_B(g_{BB}'(r_{jk})-1) + (x_B - x_A)(g_{AB}'(r_{jk})-1)], \quad \ldots\ldots(7)$$

$$\langle \Delta x_j \Delta x_k \rangle = x_A^2 x_B^2 [(g_{AA}'(r_{jk})-1) + (g_{BB}'(r_{jk})-1) - 2(g_{AB}'(r_{jk})-1)]. \quad \ldots\ldots(8)$$

Furthermore, Pearson and Rushbrooke (1957) have shown that for fluctuations in a cell of volume V containing N systems

$$V^2 \langle (\Delta\rho)^2 \rangle = N\boldsymbol{k}T\left(\frac{\partial\rho}{\partial p}\right)_{xT} + V^2\left(\frac{\partial\rho}{\partial x}\right)^2_{pT} \langle (\Delta x)^2 \rangle, \quad \ldots\ldots(9)$$

$$\langle \Delta\rho \Delta x \rangle = \left(\frac{\partial\rho}{\partial x}\right)_{pT} \langle (\Delta x)^2 \rangle. \quad \ldots\ldots(10)$$

However, at phase separation, $\langle (\Delta x)^2 \rangle$ is so large that it overwhelms the contribution to $\langle (\Delta\rho)^2 \rangle$ of the term $N\boldsymbol{k}T(\partial\rho/\partial p)_{xT}$ in (9). We therefore obtain, strictly,

$$\langle (\Delta\rho_j)^2 \rangle = \left(\frac{\partial\rho}{\partial x}\right)^2_{pT} \langle (\Delta x_j)^2 \rangle \quad \text{and} \quad \langle \Delta\rho_j \Delta x_j \rangle = \left(\frac{\partial\rho}{\partial x}\right)_{pT} \langle (\Delta x_j)^2 \rangle.$$

These results suggest that, when dealing with mean values, the relation

$$\Delta\rho_j = \left(\frac{\partial\rho}{\partial x}\right)_{pT} \Delta x_j \quad \ldots\ldots(11)$$

can be used. But if the volume cells are large enough to possess thermodynamic functions, then equation (11) can be written down straight away, since the fluctuations are occurring at constant pressure and temperature in the present context. Indeed, it is clearly possible to adopt the reverse procedure and begin by writing down (11) first and showing that this assumption that the volume cells in which these fluctuations are taking place are large enough to possess thermodynamic functions can only hold if $(\partial\rho/\partial p)_{xT}$ in (9) is negligibly small. This in turn implies that $\langle (\Delta x)^2 \rangle$ is large, i.e. that phase separation is occurring. However, this latter approach leads naturally to the question as to why phase separation is involved, rather than condensation or boiling. The answer requires a discussion of the behaviour of $(\partial\rho/\partial p)_{xT}$ and $(\partial\rho/\partial x)_{pT}$ during the boiling of a binary mixture (see, for example, Prigogine and Defay 1954) and is hardly relevant to our main theme.

It then follows from (6), (7), (8) and (11) that

$$(g_{AA}'(r_{jk})-1)(g_{BB}'(r_{jk})-1) = (g_{AB}'(r_{jk})-1)^2. \quad \ldots\ldots(12)$$

This is, in effect, the condition for phase separation expressed in terms of the critical distribution functions, and it holds for all values of r_{jk} which are large enough to satisfy the initial assumption that the volume cells j and k are themselves large enough to possess thermodynamic functions (see also equations (19) *et seq.*). Furthermore, if we express (12) in terms of the theory of Born and Green (1946–1948) as extended to binary mixtures by Fournet (1951), or in terms of the appropriate extension to binary mixtures of the asymptotic solution for the simple fluid radial distribution function developed by Rosenfeld (1951), then this condition is essentially the same as the corresponding Born–Green condition discussed by Rushbrooke (1952).

Again, using (6), (7), (8) and (11), it is possible to express (2) in terms of integrals resembling (3), (4) and (5). In this context $I(s)$ becomes the intensity,

$I_{\rm crit}(s)$ say, of critical opalescence under visible irradiation. Explicitly, therefore, one possibility is the equation

$$I_{\rm crit}(s) = I_0 r_0^2 \frac{1+\cos^2\theta}{2R^2}\frac{NF^2(s)}{\rho^2}\left[x_A x_B\left(1+\rho x_A x_B\int_0^\infty \{g_{AA}'(r)+g_{BB}'(r) - 2g_{AB}'(r)\}\frac{\sin rs}{rs}\,dr\right)\right] \qquad \ldots\ldots(13)$$

where

$$F(s) = (x_A f_A(s) + x_B f_B(s))\left(\frac{\partial\rho}{\partial x}\right)_{pT} + \rho(f_A(s) - f_B(s)). \qquad \ldots\ldots(14)$$

Now James (1948) has shown that, for visible radiation of wavelength λ,

$$r_0 f_\alpha(s) = \left(\frac{2\pi}{\lambda}\right)^2 \epsilon_\alpha, \qquad \ldots\ldots(15)$$

where $\alpha = A$ or B and ϵ is the corresponding polarizability. This is related to the macroscopic refractive index n of the fluid by the appropriate extension of the Clausius–Mosotti equation thus

$$\frac{n^2-1}{n^2+2} = \frac{4\pi\rho}{3}(x_A\epsilon_A + x_B\epsilon_B). \qquad \ldots\ldots(16)$$

So from (14), (15) and (16) we find that

$$F(s) = \frac{18\pi n}{\lambda^2 r_0 (n^2+2)^2}\left(\frac{\partial n}{\partial x}\right)_{pT}. \qquad \ldots\ldots(17)$$

In other words, $F(s)$ is a function, $F(\lambda)$ say, only of λ (and not of θ) in the present context, i.e. it is a constant for monochromatic light. And so, of course, from (15), are f_A and f_B.

The Fourier inversion of (13) is therefore

$$(g_{AA}'-1)+(g_{BB}'-1)-2(g_{AB}'-1) = \frac{1}{2\pi^2\rho x_A x_B} \times \int_0^\infty s^2\left\{\frac{2R^2\rho^2 I_{\rm crit}(s)}{I_0 r_0^2(1+\cos^2\theta)N x_A x_B F^2(\lambda)} - 1\right\}\frac{\sin rs}{rs}\,ds = f_{AB}(r) \text{ say.} \qquad \ldots\ldots(18)$$

Clearly, two further similar equations can be obtained, involving essentially the right-hand sides of (6) and (7). However, using (11) as well we find that

$$g_{AA}'(r) - 1 = x_B^2\left[\frac{x_A}{\rho}\left(\frac{\partial\rho}{\partial x}\right)_{pT} + 1\right]^2 f_{AB}(r)$$

$$g_{AB}'(r) - 1 = x_A x_B\left[\frac{x_B}{\rho}\left(\frac{\partial\rho}{\partial x}\right)_{pT} - 1\right]\left[\frac{x_A}{\rho}\left(\frac{\partial\rho}{\partial x}\right)_{pT} + 1\right] f_{AB}(r)$$

$$g_{BB}'(r) - 1 = x_A^2\left[\frac{x_B}{\rho}\left(\frac{\partial\rho}{\partial x}\right)_{pT} - 1\right]^2 f_{AB}(r) \qquad \ldots\ldots(19)$$

satisfying (12). In other words, the critical distribution functions are all of the same *form* $f_{AB}(r)$, although they differ in *scale*.

Also, equations (19) hold only in that region of large r (from the molecular point of view) which is being studied experimentally by means of visible opalescence. They break down for small r, when their left-hand sides all tend to the same limit -1, i.e. the normalization requires further discussion. Furthermore, it is not possible experimentally to extend s to infinity in (18), and large s, implying mainly small λ, corresponds physically to small r again. Consequently, some loss of generality is inevitable in the experimental determination of these distribution functions purely from observations of visible opalescence, although, in principle they are determinable from a knowledge of $I_{\text{crit}}(s)$, $F(\lambda)$ and $(\partial\rho/\partial x)_{pT}$.

But (2) applies to all wavelengths, and therefore, *inter alia*, to monochromatic visible radiation, when the scattering powers are functions only of λ. In this context, (2) yields the correct normalization

$$\int_0^\infty s^2\left[\frac{2R^2 I(s)}{I_0 N r_0^2(1+\cos^2\theta)} - (x_A f_A^2 + x_B f_B^2)\right] ds = -2\pi^2\rho(x_A f_A + x_B f_B)^2. \qquad \ldots\ldots(20)$$

So if we define the reduced intensity

$$J(s) = 2R^2 I(s)/I_0(1+\cos^2\theta), \qquad \ldots\ldots(21)$$

and

$$J' = N r_0^2\,(x_A f_A^2 + x_B f_B^2), \qquad \ldots\ldots(22)$$

then we can write

$$A\int_0^\infty s^2\,(J(s) - J')\,ds = -1 \qquad \ldots\ldots(23)$$

as a suitable normalization equation, where A is a positive constant. In (22) and (23), J' is the reduced scattered intensity due to internal scattering alone, when correlation effects can be ignored. Also, it is conventional practice in discussing simple fluids to investigate the function $J(0)$ or $I(0)$ by replacing $(\sin rs)/rs$ in (1) by the limit unity as s tends to zero, obtaining

$$I(0) = I_0 N f^2 r_0^2 \frac{1+\cos^2\theta}{2R^2}\left\{1 + 4\pi\rho\int_0^\infty r^2(g(r)-1)\,dr\right\},$$

$$= I_0 N f^2 r_0^2 \frac{1+\cos^2\theta}{2R^2}\,\boldsymbol{k}T\left(\frac{\partial\rho}{\partial p}\right)_T.$$

This equation is usually interpreted in two ways. Firstly, it is applied to the scattering of long wave radiation (i.e. Rayleigh scattering) and secondly, Fournet and Guiner (1949) suggest that it is empirically useful in plotting results, since the limit $\theta = 0$ is incapable of precise experimental determination, although it can be approached. In the case of a binary mixture, $J(0)$ is clearly related to (5), but neither J' nor $J(0)$ seem to have been considered experimentally.

However using (23), equations (19) can now be summarized in the form

$$f_{AB}(r) \text{ or } (g_{\alpha\beta}'(r) - 1) \sim \text{const.}\int_0^\infty s^2(J(s) - J')\frac{\sin rs}{rs}\,ds, \qquad \ldots\ldots(24)$$

where α, $\beta = A$, B, for brevity. Equation (24) has, in fact, the correct normalization, and with (23) gives finally

$$f_{AB}(r) \text{ or } (g_{\alpha\beta}'(r) - 1) \sim -\int_0^\infty s^2(J(s) - J') \times \frac{\sin rs}{rs}\,ds \Bigg/ \int_0^\infty s^2(J(s) - J')\,ds, \qquad \ldots\ldots(25)$$

Here, we notice a loss of generality in that (25) gives only the *form* of the radial distribution functions, their *scale* being determined by the thermodynamic functions in (18) and (19) (which fail in the limit $r \to 0$).

§ 3. Treatment of Experimental Observations

Fürth and Williams (1954), in considering the experimental observations of Quantie (1954), defined a correlation function $g_c(r)$ thus

$$I_{\text{crit}}(s) \propto \int_0^\infty r^2 g_c(r) \frac{\sin rs}{rs}\, dr, \qquad \ldots\ldots(26)$$

from which it follows that

$$g_c(r) = \int_0^\infty s^2 J(s) \frac{\sin rs}{rs}\, ds \Big/ \int_0^\infty s^2 J(s)\, ds. \qquad \ldots\ldots(27)$$

Equation (27) differs from (25) mainly in its neglect of J'. This implies that, if the integrals in (27) could in practice be extended over their full range, then they well might be divergent. However, if the upper limit of the observations is $s = s_1$ say, then Fürth and Williams extrapolated $J(s)$ by drawing a tangent at s_1 which cut the s axis at s_2. This process ensured the convergence of the integrals in (27), although their integrands in the range from 0 to s_1 were, of course, $J(s)$ rather than the $J(s) - J'$ of (25). Nevertheless, bearing in mind the limitations of the method, their computation of the integrals in (27) can be taken as a first approximation to those in (25). Indeed, it is perhaps also worth noting that they found that their $g_c(r)$ was slightly dependent upon λ. While they attributed this to the effect of multiple scattering, it may also be due to just this difference between the integrands of (25) and (27). However, if we accept that

$$g_{\alpha\beta}'(r) \simeq 1 - g_c(r) \qquad \ldots\ldots(28)$$

then clearly their results for $g_c(r)$ can immediately be reinterpreted in terms of the more familiar (critical) radial distribution functions of the conventional theory of fluids.

Now, their most important conclusion was that critical mixtures could be divided into two classes. The first class exhibited a peak in the experimental curve of $J(s)$ against s while the computed $g_c(r)$ exhibited a region of 'negative correlation'. These effects were alleged to be absent in the case of class II mixtures, although peaks did in fact appear in the class II $J(s)$ curves at shorter wavelengths.

Furthermore, they calculated a given $g_c(r)$ from a $J(s)$ curve for only one particular wavelength, thus restricting the range of values of the parameter s. It is therefore perhaps worth noting that from equations (13), (14) and (15) we have

$$I_{\text{crit}}(s) \propto \frac{1+\cos^2\theta}{\lambda^4}\left[1 + \rho x_A x_B \int_0^\infty \{g_{AA}'(r) + g_{BB}'(r) - 2g_{AB}'(r)\} \frac{\sin rs}{rs}\, dr\right].$$

Hence, scattering curves for different wavelengths can be plotted together as functions of s by appropriate weighting with the factor $\lambda^4/(1+\cos^2\theta)$ above, in order to extend the range of values of s.

However, they suggested analytic representations of the $g_c(r)$ from which, using (19) and (28), it follows that

class I mixtures: $f_{AB}(r) = -(1 - b^2r^2)\exp(-a^2r^2)$ ......(29)
class II mixtures: $f_{AB}(r) = -\exp(-a^2r^2)$ ......(30)

where a and b are adjustable constants. Consequently, using (3), (4), (5), (19) and (29) or (30), it is possible to calculate various fluctuations. For example, using (5),

$$\text{class I:} \quad \langle(\Delta x)^2\rangle = \frac{x_A x_B}{N}\left[1 + \frac{x_A x_B \rho \pi^{3/2}}{a^3}\left(\frac{3b^2}{2a^2} - 1\right)\right], \qquad \ldots\ldots(31)$$

$$\text{class II:} \quad \langle(\Delta x)^2\rangle = \frac{x_A x_B}{N}\left[1 - \frac{x_A x_B \rho \pi^{3/2}}{a^3}\right]. \qquad \ldots\ldots(32)$$

However, in developing the theory, we assumed that $\langle(\Delta x)^2\rangle$ was 'large' at phase separation, i.e. more precisely, we must have $\langle(\Delta x)^2\rangle$ positive and very much greater than the perfect gas mixture value $x_A x_B/N$.

Clearly, (32) does not satisfy these conditions, while from (31) we must have

$$3b^2 > 2a^2. \qquad \ldots\ldots(33)$$

So the proposed distribution functions for class II mixtures do not appear to be correct. This would seem to be largely due to the fact that they were calculated from comparatively long wave $J(s)$ curves which did not exhibit any peaks. On the other hand, (29) is admissible, provided (33) is also satisfied.

Fürth and Williams provide graphs of class I $g_c(r)$ for aniline *cyclo*hexane mixtures at various temperatures differing by ΔT from that of critical mixing. For $\Delta T = 0{\cdot}04^\circ$ the choice of $a^2 \simeq 1/0{\cdot}12\lambda^2$ and $b^2 \simeq 1/0{\cdot}13\lambda^2$ in (29) produces a theoretical curve which is practically coincident with their computed one, hence (33) is, in fact, satisfied. Furthermore, as ΔT increases, then ultimately (33) is not satisfied, i.e. far enough away from phase separation, fluctuations cease to be 'large', which is physically reasonable. This suggests that (33) is a useful criterion, that (29) might be a suitable asymptotic form for all mixtures at phase separation, and that (30) arose from a neglect of the shorter wavelength $J(s)$ curves.

REFERENCES

DE BOER, J., 1949, *Rep. Progr. Phys.*, **12,** 305 (London: Physical Society).

BORN, M., and GREEN, H. S., 1946–1948, see, for example, GREEN, H. S., 1952, *The Molecular Theory of Fluids* (Amsterdam: North-Holland).

FOURNET, G., 1951, *J. Phys. Rad.*, **12,** 292.

FOURNET, G., and GUINIER, A., 1949, *C. R. Acad. Sci. Paris,* **228,** 66.

FÜRTH, R., and WILLIAMS, C. L., 1954, *Proc. Roy. Soc.* A, **224,** 104.

JAMES, R. W., 1948, *Optical Principles of Diffraction of X-rays* (London: Bell and Sons).

PEARSON, F. J., and RUSHBROOKE, G. S., 1957, *Proc. Roy. Soc. Edinb.* A, **64,** 305.

PRIGOGINE, I., and DEFAY, R., 1954, *Chemical Thermodynamics* (London: Longmans Green).

QUANTIE, C., 1954, *Proc. Roy. Soc.* A, **224,** 90.

ROSENFELD, L., 1951, *Theory of Electrons* (Amsterdam: North-Holland).

RUSHBROOKE, G. S., 1952, *Phil. Mag.*, **43,** 1276.

Collision-free Hydromagnetic Disturbances of Large Amplitude in a Plasma

By J. H. ADLAM and J. E. ALLEN†
A.E.R.E., Harwell, Didcot, Berks.

MS. received 24*th July* 1959, *in revised form* 4*th November* 1959

Abstract. Calculations are given of certain collision-free hydromagnetic disturbances produced by the rapid compression of a plasma containing a magnetic field.

§ 1. INTRODUCTION

In this paper calculations are given referring to the hydromagnetic disturbances which are launched into a plasma, when the latter is rapidly compressed. The calculations refer to the case where collisions between particles are unimportant and where the interactions are effected only by macroscopic electric and magnetic fields. It is assumed that the plasma is compressed by a magnetic field which is parallel to the internal magnetic field; figure 1 is a schematic diagram illustrating a laboratory experiment with this configuration. The calculations refer to plane disturbances, an approximation that suffices for the early stages of the compression.

In an earlier paper (Adlam and Allen 1958 a) an analysis was made of the structure of strong hydromagnetic waves which were propagated through a plasma, across a magnetic field, under conditions where collisions could be neglected. The treatment referred to a plane wave which propagated into an undisturbed plasma and the thermal motion of the particles was ignored. One interesting result of the previous work was the emergence of a characteristic distance $(mc^2/4\pi ne^2)^{1/2}$ which was independent of the magnetic field strength. It was assumed, however, that the wave profile remained constant; the present paper describes more realistic situations where this assumption is no longer made. Some of the results have already been reported at the Second Geneva Conference (Adlam and Allen 1958 b).

Another generalization of the situation described in the first paper can be made by considering waves (of constant profile) which travel into a plasma which is not initially undisturbed. This case has been discussed recently by Davis, Lüst and Schlüter (1958).

§ 2. FUNDAMENTAL EQUATIONS

The equations are the same as those used in the previous work on collision-free hydromagnetic waves (Adlam and Allen 1958 a). The coordinate system is chosen so that the magnetic field is in the z direction and the plasma initially occupies the space represented by positive values of x. There are no variations in the y or z directions. The equations of motion for the electrons and ions can be written as follows, where u and v are the velocity components in the x and y directions and suffixes 1 and 2 refer to the electron and ion respectively,

---

† Now at the C.N.R.N. Laboratorio Gas Ionizzati, Istituto Fisico dell Università, Roma.

$$\frac{\partial u_1}{\partial t}+u_1\frac{\partial u_1}{\partial x}=\frac{e_1}{m_1}\left[E_x+\frac{v_1B_z}{c}\right] \qquad \ldots\ldots(1)$$

$$\frac{\partial v_1}{\partial t}+u_1\frac{\partial v_1}{\partial x}=\frac{e_1}{m_1}\left[E_y-\frac{u_1B_z}{c}\right] \qquad \ldots\ldots(2)$$

$$\frac{\partial u_2}{\partial t}+u_2\frac{\partial u_2}{\partial x}=\frac{e_2}{m_2}\left[E_x+\frac{v_2B_z}{c}\right] \qquad \ldots\ldots(3)$$

$$\frac{\partial v_2}{\partial t}+u_2\frac{\partial v_2}{\partial x}=\frac{e_2}{m_2}\left[E_y-\frac{u_2B_z}{c}\right]. \qquad \ldots\ldots(4)$$

The original thermal velocities are ignored; in practice they can be small compared with the directed velocities which the particles acquire.

The equations of continuity are

$$\left.\begin{aligned}\frac{\partial n_1}{\partial t}&=-\frac{\partial}{\partial x}(n_1u_1)\\ \frac{\partial n_2}{\partial t}&=-\frac{\partial}{\partial x}(n_2u_2)\end{aligned}\right\} \qquad \ldots\ldots(5)$$

where n is the particle density, and the field equations, neglecting the displacement current, are

$$\frac{\partial H_z}{\partial x}=-\frac{4\pi}{c}[n_1e_1v_1+n_2e_2v_2] \qquad \ldots\ldots(6)$$

$$\frac{\partial E_y}{\partial x}=-\frac{1}{c}\frac{\partial B_z}{\partial t} \qquad \ldots\ldots(7)$$

and

$$\frac{\partial E_x}{\partial x}=\frac{4\pi}{k}[n_1e_1+n_2e_2]. \qquad \ldots\ldots(8)$$

Gaussian units are used in this paper so that the numerical values of μ and k (the permeability and dielectric constant of a vacuum) are both unity. These quantities, however, will not be dropped from the equations. The latter will be simplified, as in the previous work, (Adlam and Allen 1958 a) by using the fundamental property of a plasma, namely $|n_1-n_2|\ll n$. The difference between n_1 and n_2 is ignored, except in Poisson's equation (equation (8)); this small difference produces the electrostatic field E_x which dominates the motion of the massive positive ions. It has been assumed that the latter are singly charged, so that $e_1+e_2=0$.

The current must flow in the y direction, since the magnetic field is in the z direction and varies only with x. Thus $u_1=u_2=u$ (say), since $n_1=n_2$, and the relative velocity between the electrons and ions may be written $v=v_1-v_2$. Dropping the subscript from B_z and eliminating E_x from equations (1) and (3) gives

$$\frac{\partial u}{\partial t}+u\frac{\partial u}{\partial x}=-\frac{e_2vB}{(m_1+m_2)c} \qquad \ldots\ldots(9)$$

and equations (2) and (4) yield

$$\frac{\partial v}{\partial t}+u\frac{\partial v}{\partial x}=-\frac{e_2(m_1+m_2)}{m_1m_2}\left[E_y-\frac{uB}{c}\right]. \qquad \ldots\ldots(10)$$

Equations (5) degenerate to form one equation:

$$\frac{\partial n}{\partial t} = -\frac{\partial}{\partial x}(nu) \tag{11}$$

and the field equations become

$$\frac{\partial H}{\partial x} = \frac{4\pi n e_2 v}{c} \tag{12}$$

and

$$\frac{\partial E_y}{\partial x} = -\frac{1}{c}\frac{\partial B}{\partial t}. \tag{13}$$

Equations (9)–(13) form a set of five simultaneous differential equations relating the five unknowns, u, v, B, E_y and n.

§ 3. CHANGE TO A LAGRANGIAN COORDINATE SYSTEM

A Lagrangian coordinate h will now be introduced. This coordinate is a constant for any particular particle and is equal to the x coordinate of that particle at $t=0$. Then

$$\left(\frac{\partial}{\partial t}\right)_h = \left(\frac{\partial}{\partial t}\right)_x + \left(\frac{\partial x}{\partial t}\right)_h \left(\frac{\partial}{\partial x}\right)_t$$

and

$$\left(\frac{\partial}{\partial x}\right)_t = \left(\frac{\partial h}{\partial x}\right)_t \left(\frac{\partial}{\partial h}\right)_t$$

but $(\partial x/\partial t)_h$ is equal to u, the velocity of the particle in the x direction, and $(\partial h/\partial x)_t = (n/n_0)$ so that

$$\left(\frac{\partial}{\partial t}\right)_h = \left(\frac{\partial}{\partial t}\right)_x + u\left(\frac{\partial}{\partial x}\right)_t$$

and

$$\left(\frac{\partial}{\partial x}\right)_t = \left(\frac{n}{n_0}\right)\left(\frac{\partial}{\partial h}\right)_t.$$

The differential equations (9)–(13), when expressed in terms of the independent variables, h and t, become

$$\frac{\partial u}{\partial t} = -\frac{e_2 v B}{(m_1+m_2)c} \tag{9 a}$$

$$\frac{\partial v}{\partial t} = -\frac{e_2(m_1+m_2)}{m_1 m_2}\left[E_y - \frac{uB}{c}\right] \tag{10 a}$$

$$\frac{\partial}{\partial t}\left(\frac{n_0}{n}\right) = \frac{\partial u}{\partial h} \tag{11 a}$$

$$\frac{\partial H}{\partial h} = \frac{4\pi n_0 e_2 v}{c} \tag{12 a}$$

and

$$\frac{\partial E_y}{\partial h} = \frac{1}{c}\left[u\frac{\partial B}{\partial h} - \frac{n_0}{n}\frac{\partial B}{\partial t}\right]. \tag{13 a}$$

§ 4. INTRODUCTION OF DIMENSIONLESS QUANTITIES

The following dimensionless quantities will now be introduced:

$h_{\rm n} = h/d$, $t_{\rm n} = t/\tau$, $u_{\rm n} = u/v_{\rm A}$, $v_{\rm n} = v/v_*$, $B_{\rm n} = B/B_0$, $E_{\rm n} = E_y/E_0$ and $n' = n_0/n$,

where

$$d = \left[\frac{m_1 m_2 c^2}{4\pi n_0 \mu e_2{}^2(m_1+m_2)}\right]^{1/2}, \qquad \tau = \frac{(m_1 m_2)^{1/2} c}{e_2 B_0}$$

$$v_{\rm A} = \left[\frac{B_0{}^2}{4\pi n_0 \mu (m_1+m_2)}\right]^{1/2}, \qquad v_* = \left[\frac{B_0{}^2(m_1+m_2)}{4\pi n_0 \mu m_1 m_2}\right]^{1/2}$$

and $E_0 = v_A B_0/c$. Equations (9 *a*)–(13 *a*) can now be written as follows

$$\frac{\partial u_n}{\partial t_n} = -v_n B_n \qquad \ldots\ldots(9\,b)$$

$$\frac{\partial v_n}{\partial t_n} = -E_n + u_n B_n \qquad \ldots\ldots(10\,b)$$

$$\frac{\partial n'}{\partial t_n} = \frac{\partial u_n}{\partial h_n} \qquad \ldots\ldots(11\,b)$$

$$\frac{\partial B_n}{\partial h_n} = v_n \qquad \ldots\ldots(12\,b)$$

and

$$\frac{\partial E_n}{\partial h_n} = u_n \frac{\partial B_n}{\partial h_n} - n' \frac{\partial B_n}{\partial t_n}. \qquad \ldots\ldots(13\,b)$$

On eliminating u_n, v_n and E_n from these equations, the following pair of simultaneous equations is obtained for B_n and n':

$$\frac{\partial^2 n'}{\partial t_n^2} = -\frac{\partial}{\partial h_n}\left(B_n \frac{\partial B_n}{\partial h_n}\right) \qquad \ldots\ldots(14)$$

and

$$\frac{\partial^3 B_n}{\partial h_n^2 \partial t_n} = \frac{\partial}{\partial t_n}(n' B_n). \qquad \ldots\ldots(15)$$

§ 5. BOUNDARY CONDITIONS

Initially the plasma is assumed to be in a uniform and steady state so that

$$B_n = 1 \quad \text{when} \quad t_n = 0 \qquad \ldots\ldots(a)$$

$$n' = 1 \quad \text{when} \quad t_n = 0 \qquad \ldots\ldots(b)$$

and

$$\frac{\partial n'}{\partial t} = 0 \quad \text{when} \quad t_n = 0. \qquad \ldots\ldots(c)$$

The last condition can be obtained from equation (11 *b*) by putting $u_n = 0$ when $t_n = 0$.

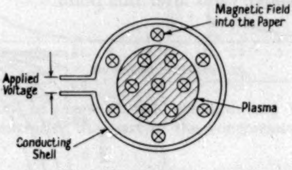

Figure 1. Schematic diagram of an experiment for the compression of a plasma by a magnetic field which is parallel to the internal magnetic field.

At sufficiently large distances within the plasma the magnetic field remains undisturbed, i.e.

$$B_n \to 1 \quad \text{as} \quad h_n \to \infty. \qquad \ldots\ldots(d)$$

The magnetic field strength at the plasma boundary increases with time; in the experiment shown in figure 1, for example, it depends on the waveform of the current which is passed through the conducting shell. Two different cases are considered here, namely

$$\left.\begin{aligned} &B_n = 1 + \alpha t_n \quad \text{at} \quad h_n = 0 \\ \text{and} \quad &B_n = 1 + C[1 - \exp(-\alpha t_n)] \quad \text{at} \quad h_n = 0 \end{aligned}\right\} \qquad \ldots\ldots(e)$$

where α and C are constants.

Using conditions (*a*) and (*b*), equation (15) can be directly integrated to yield

$$\frac{\partial^2 B_{\mathrm{n}}}{\partial h_{\mathrm{n}}^2} = n' B_{\mathrm{n}} - 1. \qquad \ldots\ldots(16)$$

§ 6. NUMERICAL RESULTS

In obtaining a numerical solution of equations (14) and (16) the equations are solved alternately in the following manner.

(1) Equation (16) is solved for time t_1 to give B_{n} as a function of h_{n}, n' being known.

(2) Equation (14) is solved to give n' and $\partial n'/\partial t_{\mathrm{n}}$ at time $t_1 + \Delta t$ for a range of values of h when n', $\partial n'/\partial t_{\mathrm{n}}$ and B_{n} are known at time t_1.

In the solution of type (1) the boundary conditions (*d*) and (*e*) are used, and in the solution of type (2) the boundary conditions (*b*) and (*c*) are used when $t_{\mathrm{n}} = 0$. The boundary condition (*d*) was replaced by the condition $B_{\mathrm{n}} = 1$ when $h_{\mathrm{n}} = H$ and H was made as large as was practicable.

Case I. Linear variation of the magnetic field strength at the plasma boundary.

Calculations have been made referring to the linear variation of magnetic field strength at the plasma boundary given by $B_{\mathrm{n}} = 1 + \alpha t_{\mathrm{n}}$, for the particular case where $\alpha = 1$. Figure 2 shows the computed distributions of B_{n} and n' (as functions of h_{n}) for different values of t_{n}. Figure 3 shows the spatial variations of magnetic field strength and ion density at different times; these curves have been obtained from those of figure 2, using the relation $(dx_{\mathrm{n}}/dh_{\mathrm{n}}) = n'$. Figure 4 shows the position of the plasma boundary as a function of time.

Shortly after $t_{\mathrm{n}} = 1{\cdot}6$, $n' \to 0$ at $h_{\mathrm{n}} = 0$, i.e. $n \to \infty$ at the plasma boundary. Physically this means that the outermost ions are overtaking their neighbours. The equations are no longer valid after this point.

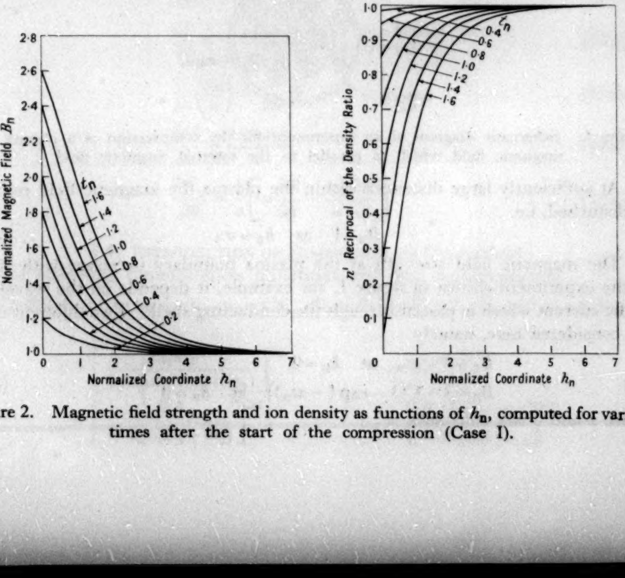

Figure 2. Magnetic field strength and ion density as functions of h_{n}, computed for various times after the start of the compression (Case I).

Case II. Exponential variation of the magnetic field strength at the plasma boundary.

Numerical results have been obtained for the case of exponential variation of the magnetic field strength at the plasma boundary. The calculations refer to the particular case where $\alpha = 1$ and $C = 1$. Figure 5 shows the results, plotted against the independent variable h_n. Plots against the spatial coordinate x_n, however, would roughly resemble the curves shown, and it is clear that a train of hydromagnetic waves is launched into the plasma. As the waves propagate into the plasma they also grow in amplitude.

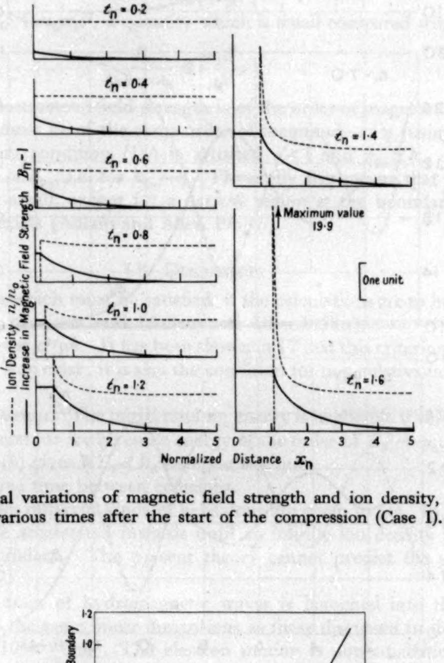

Figure 3. Spatial variations of magnetic field strength and ion density, computed for various times after the start of the compression (Case I).

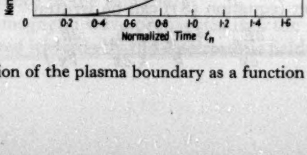

Figure 4. Position of the plasma boundary as a function of time (Case I).

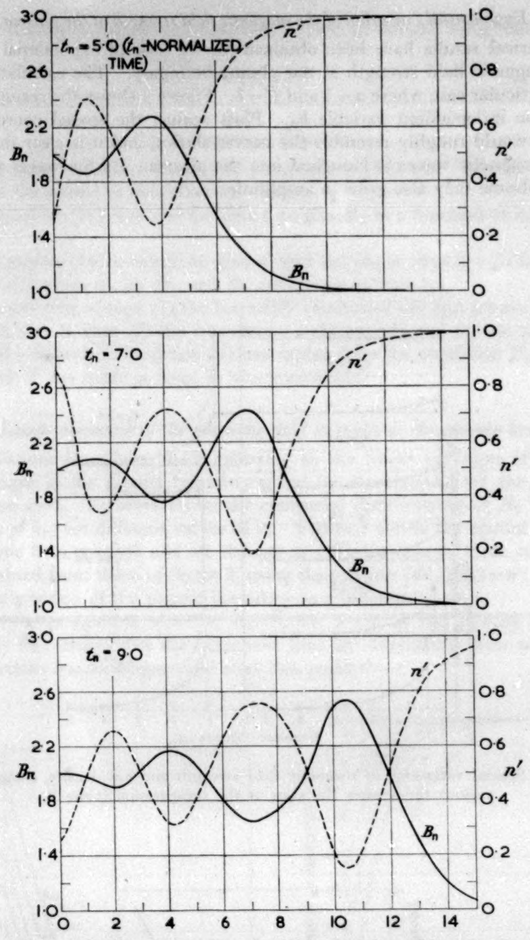

Figure 5. Magnetic field strength and ion density, as functions of h_n, computed for various times after the start of the compression (Case II).

§ 7. EXAMINATION OF THE PLASMA PROPERTY $|n_1 - n_2| \ll n_1$

If instead of introducing the variable h as in § 3 two such quantities are introduced, namely h_1 and h_2, referring to the electrons and positive ions respectively, then Poissons' equation (equation (8)) can be written

$$\frac{\partial E_x}{\partial x} = \frac{4\pi n_0 e_2}{k}\left(\frac{\partial h_2}{\partial x} - \frac{\partial h_1}{\partial x}\right)$$

which can be integrated to give

$$E_x = \frac{4\pi n_0 e_2}{k}(h_2 - h_1).$$

This equation can be normalized and written as

$$\eta E_x = h_{2n} - h_{1n} \qquad \ldots\ldots(17)$$

where the unit of electrostatic field strength is

$$\left(\frac{m_2 - m_1}{m_2 + m_1}\right)\frac{v_* B_0}{c}$$

and

$$\eta = \frac{k B_0{}^2 (m_2 - m_1)}{4\pi n_0 m_1 m_2 c^2}.$$

In practice $\eta \simeq kB_0{}^2/4\pi n_0 m_1 c^2$, a quantity which is small compared with unity if

$$\frac{B_0{}^2}{4\pi\mu n_0} \ll \frac{m_1 c^2}{\mu k}. \qquad \ldots\ldots(18)$$

The normalized electrostatic field strength is of the order of magnitude of unity, so that $(h_{2n} - h_{1n})$ must be of the same order of magnitude as η (using equation (17)). Thus when condition (18) is satisfied $\eta \ll 1$ and $h_{2n} \simeq h_{1n}$ except for very small values of h_{2n}, i.e. for $h_{2n} \sim \eta$. Physically this means that the charge separation is very small, except for a narrow region at the boundary where a 'surface charge' exists (Adlam and Allen 1958 b).

§ 8. DISCUSSION

The conditions which must be satisfied, if the calculations are to be valid, are the same as in the previous work (Adlam and Allen 1958 a).

(*a*) $B_0{}^2/4\pi n_0\mu \ll m_1 c^2/\mu k$. It has been shown in § 7 that this criterion must hold if quasi-neutrality is to exist; it is also the condition for non-relativistic equations to be valid.

(*b*) $\boldsymbol{k}T_1 \ll B_0{}^2/4\pi n_0\mu$. The initial random energy is negligible if this condition holds, since the electrons are given an energy of the order of $B_0{}^2/4\pi n_0\mu$. Combination of (*a*) and (*b*) gives $\boldsymbol{k}T_1 \ll B_0{}^2/4\pi n_0\mu \ll m_1 c^2/\mu k$.

(*c*) $\tau \ll$ mean free time between collisions.

Examples of two different kinds of behaviour are given in § 6. In Case I the outermost ions are accelerated inwards until an infinite ion density is built up at the plasma boundary. The present theory cannot predict the subsequent behaviour.

In Case II a train of hydromagnetic waves is launched into the plasma. These waves have the same linear dimensions as those discussed in the previous work, i.e. $d \simeq 5 \times 10^5 n^{-1/2}$ cm. The electron motion is non-adiabatic, i.e. B/n_1 is not constant, and the term on the left-hand side of equation (16) is a direct measure of the non-adiabaticity. When this term is small compared with unity $n'B_n = 1$, i.e. $n/n_0 = B/B_0$ and the electrons can be visualized as being 'tied' to the magnetic lines of force. In the rapid compressions considered here, however, the electrons are not 'tied' to the magnetic lines of force but 'slip' relative to them by a distance of the order of *d*.

When a strong hydromagnetic wave propagates into the plasma the massive positive ions are accelerated inwards by the electrostatic field while the electrons attain high velocities in a transverse direction (the direction of current flow). The high electron velocities result from the ' slipping ' of the electrons relative to the magnetic lines of force. Both the electrons and the positive ions receive an energy comparable with the original magnetic energy per particle.

ACKNOWLEDGMENTS

The authors are indebted to Dr. J. Howlett for assistance with the computations. They also wish to thank Dr. P. C. Thonemann for encouraging this work.

REFERENCES

ADLAM, J. H., and ALLEN, J. E., 1958 a, *Phil. Mag.*, **3**, 448.
—— 1958 b, *Proc. Second U.N. International Conf. on the Peaceful Uses of Atomic Energy*, **31**, 221.
DAVIS, L., LÜST, R., and SCHLÜTER, A., 1958, *Z. Naturf.*, **13a**, 916.

Coagulation, Optical Absorption and Photoconductivity of Colloid Centres in Alkali Halides

By W. T. DOYLE†

Department of Electronics, University of Southampton

MS. received 28th August 1959, *in revised form 16th November* 1959

Abstract. The effects of optical illumination and impurities on colloid formation are studied in additively coloured KCl and in NaBr coloured by ultra-violet light. It is shown that at elevated temperatures additively coloured KCl behaves as an auto-sensitized photographic system. A theory of the colloid band is presented which takes account of ion core polarization and harmonic mean effective mass for arbitrary ellipsoidal particles. The colloid band is identified as a bounded plasma resonance, shifted into the visible region by the boundary conditions. Plasma frequencies computed from the positions of the colloid bands are in good agreement with other estimates. The spectral dependence of photoconductivity associated with the colloid band is related to the band structure of the host medium.

§ 1. INTRODUCTION

THE F-band in alkali halides may, under suitable conditions, be transformed into a narrow band at longer wavelengths which by its position, shape, and temperature independence is attributed to colloidal particles of reduced metal (Scott, Smith and Thompson 1953). Confirmation of this assignment has been obtained from measurements of photoconductivity (Gyulai 1925), electron diffraction (McLennan 1951), x-ray scattering (Smallman and Willis 1957), nuclear magnetic resonance (Ring, O'Keefe and Bray 1958), and electron spin resonance (Doyle, Ingram and Smith 1959). The presence of colloidal metal is thus well established. There are, however, several aspects of the coagulation process, optical absorption, and photoconductivity of the colloidal particles which deserve further study. In the present paper observations bearing on these topics will be presented. The discussion will stress in turn the role of optical illumination and impurities in the coagulation process, the colloid band as a collective oscillation of the alkali metal valence electrons, and differences between the selective photoelectric effect and spectral dependence of photoconductivity accompanying the colloid band.

§ 2. OPTICAL COAGULATION IN ADDITIVELY COLOURED KCl

The F-band in additively coloured alkali halides is known to be unstable with respect to optical and thermal treatment. Early experiments (Glaser 1937) showed that coagulation can be achieved by illumination with strong arc light. More recently, Scott and Bupp (1950) showed that the amount and kinds of coagulation products obtained by arc illumination depend upon whether or not the crystal is allowed to warm up. When the crystal is held at room temperature only limited R-, M-, and N-bands are formed; if the crystal is allowed to warm up, coagulation goes to completion with the formation of a broad band, R′. This experiment established the need for elevated temperatures for complete coagulation, but left open the question of the effect of light. Later, Scott, Smith and Thompson (1953) found that the colloid band can be developed by annealing in the dark and that an heterogeneous equilibrium exists between the F-centres and the colloid particles. The equilibrium concentration of F-centres does not depend upon the amount of excess alkali metal, provided there is sufficient metal present to saturate the sample with F-centres at the annealing temperature. Thus illumination is not essential for the coagulation process. However, Theissen and Scott (1952) found that thermal coagulation is greatly accelerated by illumination. They offered two possible explanations: either the photo-electrons ejected from the F-centres are captured by the colloidal particles already thermally forming to hasten the particle growth, or, the ejected electrons are trapped to form R-centres which then assist the coagulation, possibly by serving as nuclei.

---

† National Science Foundation Postdoctoral Fellow. On leave from Dartmouth College, Hanover, New Hampshire, U.S.A.

It is difficult to assess the relative importance of the two proposed mechanisms in Theissen and Scott's experiment since both optically induced and thermal coagulation occur simultaneously. One can, however, separate the two effects by illuminating samples containing less than the equilibrium concentration of F-centres at temperatures high enough to permit ionic motion. Thermal coagulation is then absent. In this section the results of such experiments on KCl will be reported. Since these measurements were carried out it has been found that similar results had been obtained earlier by Shatalov (1956, 1957), and interpreted differently. For this reason our results will be presented in abbreviated form accentuating differences in emphasis and interpretation.

Additively coloured samples of Harshaw KCl were prepared by electrolysis as previously described (Doyle 1958 a). The optical absorption spectra were measured at room temperature with a Beckman DU spectrophotometer. The samples were subjected to a variety of optical and thermal treatments, after each of which the optical absorption was measured.

In figure 1 the results obtained on a typical KCl are plotted. The broken line shows the initial F-band at 560 mμ. Since this absorption spectrum was unchanged by prolonged heating in the dark at 250°c the sample contained less than the equilibrium concentration of F-centres at that temperature. The specimen was then placed in a furnace, brought to thermal equilibrium, exposed *in situ* to a three second burst of light (Spindler and Hoyer 5 ampere arc, concentrated to a spot one inch in diameter with the standard iris-lens attachment), and quickly brought to room temperature. The optical absorption spectrum shown by the solid line in figure 1 was then observed. The F-band has been replaced by a new symmetrical band at 730 mμ. This photolytic process was subjected to further experiments which established the following points:

(*a*) Strong illumination at an elevated temperature can cause considerable coagulation of F-centres, even under conditions where the F-band is thermally stable.

(*b*) The new band, identified here with R′, is thermally unstable in lightly coloured crystals. It reverts to the F-band if kept in the dark at the same temperature at which it was produced.

(*c*) The band may be retained indefinitely at elevated temperatures by continuous illumination.

(*d*) The rate of thermal re-conversion at a given temperature depends strongly upon the temperature at which the photolysis was originally carried out. The band decays rapidly at 250°c if it was produced at 200°c, while it is much more stable at 250°c if it was produced at that, or a higher temperature.

(*e*) The integrated absorption is unchanged during the transformation to within an uncertainty of about 5%. This was checked by re-cycling the same sample a number of times.

(*f*) The position of the new band does not depend upon the temperature at which the photolysis is carried out, but formation at lower temperatures leads to a broader band.

(*g*) The band position is not dependent upon the temperature of measurement.

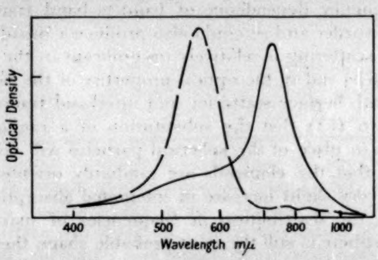

Figure 1. Optical coagulation in additively coloured KCl. The broken line shows the initial F-band at 560 mμ. The solid line shows the colloid band at 730 mμ formed by momentary exposure to intense arc light at an elevated temperature.

These observations tend, in the main, to confirm Shatalov's results, but not, it is thought, his conclusions regarding the exact nature of the centres involved. Shatalov concluded that the R′-band (X in his notation) is due to the F_2-centre. It is difficult to see how the properties listed under (*d*), (*f*) and (*g*) can be associated with this type of centre, since a specific type of centre, such as F_2, should always give rise to a unique absorption band, independent of the temperature of formation. On the other hand, all of the properties of the R′-band are consistent with a colloidal origin, as originally proposed by Glaser (1937).

Since the term 'colloidal', as used here, does not imply a definite particle size, the name metallic centres might be more appropriate. The essential assumption is that the optical properties of the centres may be adequately described by starting from an expression for the optical constants of the metal, and this degree of similarity could exist even in quite primitive centres. What is required is a similarity in electronic structure. The optical properties of the colloid band will be considered in greater detail in § 4. In the present section we shall merely indicate how the observed properties may be reconciled with the colloid model. It will be seen that the model is very flexible, and so, not surprisingly, is able to account for the observed features of the R′-band. It is felt that the agreement is sufficiently good to warrant the assignment. Moreover, the flexibility of the model finds a counterpart in the somewhat irregular behaviour of the band itself which has led to its being labelled 'composite' (Seitz 1954).

The free electron theory of the colloid band (Doyle 1958 b) predicts that the integrated absorption should be constant in the transformation from F-centres to colloid (*e*), and that the maximum absorption should occur at 720 mμ in KCl (*g*). The half width depends upon the particle size, being larger for smaller particles, due to mean free path limitations. Any reduction in the mean free path of the dispersion electrons (or the mean lifetime of the excitation) leads to a broadening of the band without change in peak position (*f*). This is in accord with the observation that formation at lower temperature leads to a broader room temperature spectrum, since it is to be expected that at lower temperatures smaller particles will be stable. Shatalov's high temperature absorption spectra (Shatalov 1956) show increased broadening with increasing temperature of measurement, possibly indicating an increase in electron lattice interaction due to increasing disorder in the molten metal particles. An increase in either the probability or frequency dependence of band-to-band transitions could also arise from lattice disorder and so could also produce a broadening. It may be noted that thermal scattering is relatively insignificant in the room temperature spectra (Doyle 1958 b) and in the optical properties of the bulk metal (Butcher 1951), compared with surface scattering and interband transitions.

It will be shown (§ 3) that the substitution of a random distribution of ellipsodial particles in place of the spherical particles will not affect these conclusions, provided that the ellipsoids are randomly oriented. The principle differences are: a very slight increase in integrated absorption and a spurious broadening due to the distribution in frequencies of maximum absorption. Provided that the sphere is still the most probable shape there will be no shift in the observed maximum.

The initial photochemical act in these samples is undoubtedly the ionization of the F-centre. No colloid particles are present initially so that the first products of photolysis must be other colour centres which then serve as nuclei for colloid formation. The experiments of Petroff (1950) at room temperature show that the nuclei are probably R-centres. Whatever the nature of the colloid nuclei may be, they are probably followed very rapidly by the formation of larger particles of reduced metal which will be much less susceptible to photo-ionization and thermal dissociation than the simpler centres (see § 5 for a quantitative estimate). Thus, even though the negative ion vacancies may have a much larger electron capture cross section (Neilson and Scott 1954), the colloid particles will become negatively charged under strong illumination. The charge will assist the further growth of the particles by attracting negative ion vacancies and by promoting an electrode reaction at the surface of the particle. Both mechanisms proposed by Theissen and Scott (1952) seem to be involved in the optical coagulation of lightly coloured crystals.

It is concluded that additively coloured KCl behaves at elevated temperatures as an extremely simple form of autosensitized photographic system that conforms rather closely to the theory of the photographic process (Mitchell 1951). The system lends itself well to demonstration experiments and rather striking 'contact prints' may be prepared. The grain size is limited only by the dislocation pattern (Hedges and Mitchell 1953, Amelinckx 1956), and the pictures may be erased without destroying the photographic sensitivity of the crystal. As a model photographic system it deserves further study.

§ 3. THERMAL COAGULATION IN PHOTOCHEMICALLY COLOURED NaBr

Earlier reports that photochemically coloured alkali halides can exhibit a colloid band (Przibram 1956) have recently been confirmed in crystals that have been irradiated with electrons (McLennan 1951), γ-rays (Compton 1957), and neutrons (Ring, O'Keefe and Bray 1958). The common feature of these observations is the high doses required to develop the colloid band. Intense irradiation, however, is not sufficient to produce colloidal aggregates. The presence of small amounts of impurities seems to play a very important part in the coagulation process. Compton (1957) has shown that the colloid band appears in irradiated samples only in the presence of hydroxyl ions. In contrast, divalent cation impurities greatly inhibit coagulation in additively coloured crystals (Watson and Scott 1959). In the experiment to be described the colloid band has been observed in photochemically coloured NaBr. The experiment differs from the others just cited in that only lightly coloured crystals were used and ultra-violet light was employed instead of ionizing radiation. Nevertheless, F-centre concentrations effectively much greater than the equilibrium value were attained. The results will be interpreted in terms of the action of impurities.

Because it is rather hygroscopic, sodium bromide is not a convenient crystal to study, and no previous observations using additively coloured NaBr have been made. With the original intention of establishing the position of the aggregate bands in this material, single crystals, obtained from Taylor, Taylor and Hobson, Ltd., were coloured electrolytically in air. During the heating of the crystals hydrolysis at the surface was observed. After colouration all attempts to obtain a pure F-band failed; no matter how quickly the crystals were quenched coagulation was virtually complete before the sample reached room temperature. In view of Compton's observations on photochemically coloured crystals this extreme behaviour was attributed to the presence of hydrolysis products, OH^- and H^+, diffusing in from the surface.

In further experiments it was found that the colour could be bleached by holding the crystals at high temperature after coloration. After this treatment the crystals were completely transparent to visible light. The rapid bleaching was thought to be due to the conversion of F-centres into U- and OH-centres and this interpretation received support from the subsequent observation that those portions of the crystals which had been electrolytically coloured and bleached were much more sensitive to x-irradiation. Such portions of x-irradiated crystals resisted bleaching by visible light, just as do crystals that have been photochemically sensitized by hydride (Martienssen and Pick 1953).

When crystals which had been prepared in the manner described were exposed to a strong mercury vapour lamp (2537Å) the previously coloured portions developed a strong F-band at 540 mμ, while the other part of the crystal remained clear. In this way pure F-bands, as shown by the broken line in figure 2, were obtained. The position and half width agree with the values reported by Ottmer (1928). After the F-band had been fully developed by ultra-violet irradiation the crystals were heated for a few seconds to a temperature of about 300°C, whereupon the F-band was immediately converted into the strong narrow band at 590 mμ shown as a solid line in figure 2. From the position, shape, half width and apparent insensitivity to temperature the long wavelength band is attributed to colloidal particles.

The great reduction in integrated absorption apparent in the transformation depicted in figure 2 was puzzling at first, since experience with optically coagulated KCl (§ 2), as well as with thermally coagulated NaCl (Doyle 1958 b), shows that such transformations take place with constant integrated absorption. However, further experiments showed that continued heating at the same temperature led to the slow disappearance of all visible bands. Renewed exposure to ultra-violet light resulted in the reappearance of the F-band and the whole process could be repeated. Thus, heating after exposure to ultra-violet light causes two reactions: a very rapid coagulation of the F-centres, accompanied by a slow reconstitution of centres (probably U-centres) which possess no visible bands. For this reason no significance can be attached to the loss of integrated absorption in figure 2. Preliminary observations indicate absorption in the ultra-violet region, but further work will be needed to establish the positions of the U- and OH- bands in NaBr.

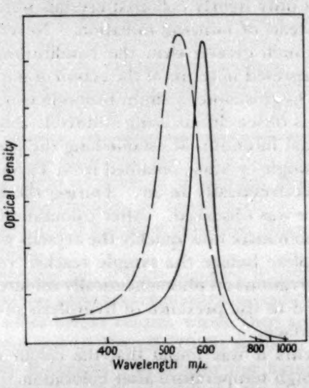

Figure 2. Thermal coagulation in sensitized NaBr (see § 3) coloured by ultra-violet light. The broken line shows the intitial F-band at 540 mμ. The solid line shows the colloid band at 590 mμ produced by heating.

Considering the manner of preparation of the sample there is some ambiguity in whether the sample should be considered as an additively or a photochemically coloured crystal, although it is usual to speak of such crystals as photochemically sensitized. On the other hand, there is certainly an excess of alkali metal present, and in a form which does not give rise to a visible coloration. There seems little doubt that this is the explanation of the colour centre 'precursors' observed by Hacskaylo and his co-workers (Hacskaylo and Groetzinger 1952, Hacskaylo and Otterson 1953, and Hacskaylo, Otterson and Schwed 1953). Whether one chooses to emphasize the non-stoichiometric ratio of alkali to halogen, or the photochemical nature of the coloration, the effect of the hydroxyl ions is even more pronounced than in the experiments of Compton (1957). The mechanism by which this effect is produced is not known. It seems quite possible that at least part of the action of the hydroxyl ions is due to reactions with residual divalent cation impurities, which by themselves would tend to inhibit coagulation. There is optical evidence that such an interaction occurs, for the addition of divalent cations removes the characteristic hydroxide absorption band (Etzel and Patterson 1958).

§ 4. Optical Absorption

The position of the colloid band may be computed using Mie's theory (Mie 1908) for the absorption of light by metal spheres (Savostianova 1930, Scott, Smith and Thompson 1953), which relates the colloid band directly to the macroscopic optical constants of the alkali metal and the index of refraction of the host medium. Further insight into the nature of the colloid band is obtained by combining the free electron theory of metals and the Mie theory (Doyle 1958 b). It may then be shown that the wavelength for maximum absorption in the colloid band, $\lambda_0 = 2\pi c/\omega_0$, occurs when $\lambda_0 = (1 + 2n_0^2)^{1/2}\lambda_c$, where n_0 is the index of refraction of the host medium and λ_c is the Wood–Zener wavelength for the onset of ultra-violet transparency of the metal (Wood 1933, Zener 1933). This relation holds for spherical particles which are small compared with the wavelength λ_0.

There are two ways of viewing the pronounced resonance in absorption which gives rise to the colloid band. The position of the resonance is largely determined by the wavelength dependence of the real part of the complex dielectric constant of the metal, so the frequency for maximum absorption coincides with that for which the internal field is a maximum. Thus the colloid band may be regarded as a frequency dependent local field phenomenon. Alternatively, the colloid band may be considered as a localized elementary excitation of the system consisting of the particle plus surrounding medium, i.e. a collective dipole oscillation of the conduction electrons in the particles. Thus the colloid band is a bounded 'plasma resonance' (Pines 1956) which has been shifted into the visible region by the special boundary conditions obtaining at the surface of the spherical particles.† The intimate connection with plasma theory is apparent in the expression for maximum absorption, when it is recalled that the Wood–Zener wavelength occurs at a zero of the complex dielectric constant of the metal. (Hubbard 1955, Fröhlich and Pelzer 1955).

In this section we shall first consider the modifications introduced into the free electron theory of the colloid band by including the effect of core polarization and allowing for departures from spherical shape. New experimental values of the position of the colloid band will then be presented and used to compute the plasma frequencies of the alkali metals.

The theory of the colloid band has been given for spherical particles neglecting core polarization. Both restrictions are easily removed. Indeed, because the various refinements may be made independently, the colloid band affords an unusual opportunity for the introduction of more realistic and detailed treatments of the internal electronic structure of the centre, while taking account of the interaction with the surrounding medium in a correct and unambiguous way. The results obtained are not without an heuristic value in the treatment of the more complex 'simpler' centres.

In the present treatment the effect of core polarization is included in the starting expression for the complex index of refraction of the metal $\mathbf{n}$. Thus (Mott and Jones 1936)

$$\mathbf{n}^2 = 1 + 4\pi N\alpha + 4\pi(i\omega/\sigma_0 - \omega^2 m/N_0 e^2)^{-1} \qquad \ldots\ldots (1)$$

---

† Bounded plasma resonances were considered by Tonks (1931), who called them simply 'plasma resonances' while reserving the name 'plasma-electron resonance' for the infinite plasma. We conform to current usage here.

where α is the ion core polarizability, N is the number of ion cores per unit volume of the metal, ω is the angular frequency of the light, m and e are the mass and charge of the conduction electrons, σ_0 is the conductivity, and N_0 is the effective number of dispersion electrons per unit volume of the metal. For convenience one may put $N_0 = N$ and retain generality by replacing m with an harmonic mean optical effective mass m^*. While equation (1) is not the most general expression for the optical constants of a metal, it will suffice for the present discussion. Moreover, it is known to give an accurate description of the optical properties of the alkali metals (Cohen 1958).

To take account of departures from spherical shape we use the expressions for the absorption of light by ellipsoidal particles. For the general ellipsoid there will be three bands of absorption corresponding to the oscillations induced by components of the electric vector of the light wave along the three major axes. For light polarized along a single axis there will be a single peak and the absorption constant k for this band is given by (Gans 1912)

$$k = -2\pi N'V/\lambda' \mathcal{I}\left[\frac{\mathbf{n}^2 - n_0^2}{n_0^2 + (\mathbf{n}^2 - n_0^2)\,P/4\pi}\right] \qquad \ldots\ldots(2)$$

where N' is the number of metal particles per unit volume of the crystal, $\mathbf{n}$ is the complex index of refraction of the metal, n_0 is the real index of refraction of the host material, V is the volume of the individual ellipsoids, and $P/4\pi$ is the depolarization factor for the axis of polarization.

Inserting the index of refraction $\mathbf{n}$ given by equation (1) into equation (2) one finds

$$k = \frac{N'Vn_0^3\omega_0^4}{(P/4\pi)^2 4\pi c\sigma_0}\left[\frac{\omega^2}{(\omega_0^2 - \omega^2)^2 + (\Delta\omega_{1/2})^2\omega^2}\right] \qquad \ldots\ldots(3)$$

where

$$\omega_0^2 = \omega_c^2/[1 + 4\pi N\alpha + n_0^2(4\pi/P - 1)], \qquad \ldots\ldots(4)$$

$$\omega_c^2 = 4\pi N_0 e^2/m \qquad \ldots\ldots(5)$$

and

$$\Delta\omega_{1/2} = N_0 e^2/m\sigma_0. \qquad \ldots\ldots(6)$$

Thus the band is Lorentzian regardless of the particle shape, but the maximum may occur at any frequency between zero and the plasma frequency, depending upon the depolarization factor $P/4\pi$ (and thus on the shape) of the ellipsoid. The integrated absorption $\frac{1}{2}\pi k_{\max}\Delta\omega_{1/2}$ is given by

$$\int k(\nu)\,d\nu = \mathbf{N}\frac{\pi e^2}{m^* c}\frac{n_0^3}{[n_0^2 + (1 + 4\pi N\alpha - n_0^2)P/4\pi]^2}, \qquad \ldots\ldots(7)$$

where $\mathbf{N}$ is the total number of excess electrons per unit volume of the crystal. These expressions all reduce to those obtained for spherical particles by putting $P/4\pi = \frac{1}{3}$ and $4\pi N\alpha = 0$. Comparing the general results with the spherical case it may be noted that the three major features: band position, width, and integrated absorption are all shape dependent. Thus the peak occurs at shorter wavelengths the shorter the particle along the electric vector of the light wave. The integrated absorption is greater for shorter particles if the index of refraction of the host medium n_0 differs from unity. This departure from the sum rule appears in the guise of a local electric field. On an atomic scale, however, the effect arises directly from the interaction between the dispersion electrons and the surrounding high-frequency oscillators of the medium, and is actually compensated by an accompanying change in the integrated absorption of the medium at higher frequencies. This is not apparent here because the host medium is represented only through the constant n_0. When $n_0 = 0$ the sum rule is obeyed independently of shape, as it must be, since there are then no high-frequency oscillators present. The width of the absorption lines may also differ for particles of different shape if surface scattering is not negligible, as the mean free path for surface scattering is also shape dependent. These remarks apply only to the special case where the light is polarized with the electric vector parallel to a single axis of a uniformly oriented distribution of identical ellipsoids. This is an unusual situation, but it may be realized experimentally (Rohloff 1952).

For the more usual case of a random distribution of shapes and orientations the departures from the behaviour of spherical particles is not so marked. For such a distribution it is necessary to average the expressions for the absorption constant, equation (3), over all the axes of all of the ellipsoids of each shape and orientation, weighting each term by the square of the cosine of the angle between the electric vector of the wave and the axis in question (Gans 1912). Consider first a randomly orientated distribution of identically shaped ellipsoids. Such a distribution can give rise to three peaks, if the separation of the resonant frequencies is greater than the half widths of the three bands. Otherwise there will be merely a distortion of the band shape from the simple Lorentzian shape. In any case, the integrated absorption over all the bands will depart only very slightly from the spherical value. In fact, of all randomly oriented distributions of ellipsoids, a collection of spheres gives rise to the minimum integrated absorption. However, the departures from the minimum value are very small for a wide range of depolarization values and particle shapes, as may be seen in figure 3, where the integrated absorption of a randomly oriented distribution of identical spheroids is plotted against $P/4\pi$ (solid lines). The corresponding axial ratio of the ellipsoids is also indicated. The typical cases shown are for free electron metal particles of arbitrary orientation in free space (curve A), and randomly oriented particles of sodium metal in sodium chloride (curve B). Wide departures from spherical shape cause only small changes in the integrated absorption. The corresponding behaviour for particles aligned along the electric vector is more drastic as curve C shows. It should be quite possible to observe the shape dependence of integrated absorption in experiments similar to Rohloff's. The integrated absorption could then be used as well as the peak position to determine the shape of the particles.

For a random distribution of shapes departing more or less from spheres the effect on the integrated absorption is, of course, still smaller, since only the mean value averaged over the distribution of the quantity shown in figure 3 (curve B) will be measured. This fact probably explains why the integrated absorption is conserved even for colloids prepared at low temperature where a variety of shapes may be expected to be stable. For a random distribution of shapes only a single peak will be observed. It will appear spuriously broadened if the distribution of resonant frequencies is greater than the width of the individual plasma resonance 'packets'. In such cases a wide variety of band shapes can occur. However, the distribution is not completely arbitrary since the depolarization factors of an ellipsoid must satisfy the requirement $\Sigma P/4\pi = 1$, and this leads to a corresponding restriction on the resonant frequencies of the three absorption bands for the ellipsoid. If the sphere is the most probable shape the position of the band will still correspond to that of the sphere. A narrow symmetrical band may be taken as an indication that the distribution approximates quite closely to the behaviour of spherical particles, both with regard to peak position and integrated absorption. Equations (3) to (6) may be applied immediately to spherical, or nearly spherical, particles by putting $P/4\pi = \frac{1}{3}$, since the summation over the three axes is just cancelled by the factor $\frac{1}{3}$ introduced by the averaging over the square of the direction cosines.

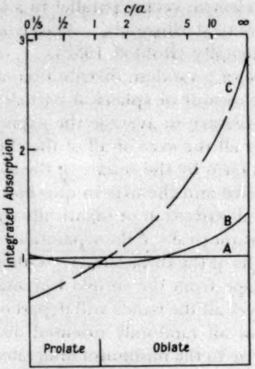

Figure 3. Integrated absorption cross section for spheroidal particles in units of $\pi e^2/mc$ plotted against the depolarization factor of the symmetry axis, $P/4\pi$, and the axial ratio c/a. The solid lines are for randomly oriented distributions of identically shaped ellipsoids. The broken line is for particles aligned with the symmetry axis parallel to the electric vector of polarized light. Curve A applies to particles containing free electrons in a vacuum ($n_0 = 1$). Curves B and C apply to sodium metal particles in sodium chloride ($n_0 = 1{\cdot}55$).

The colloid band has been observed in additively coloured NaCl, NaBr, KCl, and KBr, using thermal and optical coagulation. The peak positions are tabulated in table 1. The small half widths, which are also shown, indicate spherical particles. The calculated positions were computed using the empirical values of $4\pi N\alpha$ and the harmonic mean effective mass m^* obtained by Cohen

Table 1. Colloid Bands

	$\hbar\Delta\omega_{1/2}$ (ev)	λ_0(obs)(mμ)	λ_0(calc)(mμ)
NaCl	0·32	555	510
NaBr	0·28	590	540
KCl	0·38	730	720
KBr	0·35	770	750

Wavelength for maximum absorption in the colloid band, compared with values calculated using Ives and Briggs (1936, 1937) empirical optical constants (Cohen 1958). The narrow half widths, $\hbar\Delta\omega_{1/2}$, indicate spherical particles.

(1958) from a re-analysis of Ives and Briggs optical constants of sodium and potassium metal. The agreement is quite good though the observed wavelengths are somewhat longer than those calculated using the empirical optical constants. This is consistent with Scott's suggestion that coagulation does not involve a compression of the metal (Scott 1954), since compression would tend to increase N_0 and make the observed bands fall at shorter wavelengths.

The plasma frequencies of the alkali metals, $\omega_p^2 = \omega_c^2/(1+4\pi N\alpha)$, computed from the observed positions of the colloid band in their respective salts are shown in table 2. For sodium and potassium the values shown are averages for the two salts listed in table 1, while for lithium the colloid band in LiF at 270 mμ (Pringsheim 1954) has been used. No measurements are available for the rubidium and caesium salts. However, the selective photoelectric effect may be treated as a frequency dependent local field phenomenon taking place in a surface distribution of colloidal particles of metal, and the maximum emission for disc-shaped particles on a reflecting backing occurs at the plasma frequency (Doyle 1959). Ives and Briggs (1938) have measured the spectral distribution of photoemission under these conditions finding maxima at 345, 380, and 400 mμ for potassium, rubidium, and caesium respectively. The corresponding frequencies are displayed in the second column of table 2.

Table 2. Plasma Frequencies

Metal	(1)	(2)	(3)	(4)	(5)	(6)
Li	10·2	—	—	8·0	9·5	7·90
Na	5·08	—	5·62	5·9	5·4	5·60
K	3·60	3·6	3·67	3·9	3·8	3·87
Rb	—	3·3	3·01	3·6	—	3·40
Cs	—	3·1	2·91	3·3	—	2·94

Plasma frequencies computed from: (1) positions of the colloid band listed in table 1; (2) selective photoelectric effect (Ives and Briggs 1938, Doyle 1959); (3) optical constants (Ives and Briggs 1936, 1937, Cohen 1958); (4) ultra-violet transparency (Wood and Lukens 1938); (5) characteristic energy loss spectra (Marton and Leder 1954); (6) lattice constants (Pearson 1958) and ion core polarizabilities (Tessman, Kahn and Shockley 1953).

Independent experimental estimates of the plasma frequency based upon optical constants (Ives and Briggs 1936, 1937), ultra-violet transparency (Wood and Lukens 1938), characteristic electron energy losses (Marton and Leder 1954), as well as the values calculated from the density of the metal (Pearson 1958) and ion core polarizabilities, are also tabulated for comparison. The last three columns of the table are similar to the table given by Pines (1956), except that the iron core polarizabilities of Tessman, Kahn and Shockley (1953) have been used in obtaining columns (1) and (6); the remaining columns are taken directly from experiment. The colloidal values of the plasma frequency are in satisfactory agreement with the other estimates. Considering the extreme simplicity and ease of the absorption measurements the colloid values may well be the most trustworthy.

Band-to-band transitions have not been taken into account. These will have two principal effects: broadening of the colloid band due to limitation of the lifetime of the collective oscillations, and a shift in the maxima due to their influence on the harmonic mean effective mass. Electron lattice collisions, on the other hand, will lead to a broadening of the band without shift in peak position, in contrast with the behaviour of the Wood–Zener wavelength in bulk metal

(Cohen 1958). In principle it would be possible to separate and study these effects in colloids but this has not yet been done.

Bounded plasmas can sustain oscillations at the plasma frequency itself if the displacement of the charge is normal to the surface (Tonks 1931). This is the case for the disc shaped spheroids, mentioned above, and for radial oscillations in the cylinder and the sphere as well. Radial oscillations cannot be induced by a plane electromagnetic wave so they are of no importance in the study of the colloid band. However, it is possible to observe both radial and transverse 'Coulomb excitation' of small particles by the methods employed in the study of characteristic energy losses in thin films. Indeed, such films often consist of a surface distribution of colloids (Sennett and Scott 1950). For thicker films a colloidal dispersion could easily develop if surface oxidation occurred. This may be an explanation for some of the low-frequency loss peaks occasionally observed in energy loss spectra (Marton, Leder and Mendlowitz 1955).

§ 5. PHOTOCONDUCTIVITY

The optical properties of the colloid band seem tolerably well understood. In contrast with this the spectral dependence of photoconductivity, although often studied (Gyulai 1925, Glaser 1937, Neilson and Scott 1954), still presents difficulties. Indeed, even the threshold frequency and the wavelength for maximum photoconductivity require clarification.

Additively coloured specimens were prepared and coagulated by optical and thermal methods as described above. The samples were cleaved to a size of about 1 mm × 3 mm × 3 mm and were mounted on edge on insulated supports in a dry, closed, and opaque box. Photocurrents were measured with a General Radio electrometer. The monochromator of the Beckman DU was used as the light source. The intensity of the light was measured with a calibrated thermopile, light chopper and 10 c/s amplifier. All photocurrents were reduced to unit incident intensity.

A large number of samples of additively coloured coagulated Harshaw NaCl crystals were examined for colloidal photoconductivity. In figure 4 the spectral response of a typical sample is shown as a solid line. Although this sample had a particularly well-developed colloid band, the photoconductivity appears to arise entirely from residual F-centres. The latter are in evidence, if at all, only as a slight asymmetry in the colloid band. Assuming that the asymmetry is entirely due to a residual F-band (ignoring band-to-band transitions) and that not more than 10% of the photoconductivity is due to colloidal particles, the relative probability for ionization of a colloidal particle is less than 1/100 that of the F-centre. This difference alone could account for the coagulative properties of light at high temperature (§ 1).

Because the behaviour of the Harshaw NaCl was at variance with that observed by Gyulai, samples of natural blue rocksalt (Stassfurt halite), obtained from Wards Scientific Establishment, were also examined. Figure 5 shows the optical absorption (broken line) and photoconductivity (solid line) of this material. The similarity to the curves obtained by Gyulai on samples 'of unknown origin' is very close and may indicate a common sample origin. The difference between natural blue rocksalt and the additively coloured NaCl is quite marked, probably because the natural samples have F-centre concentrations corresponding to much lower temperatures than can be used in the laboratory.

The complexity of the absorption spectrum of the natural material is often ascribed to a distribution of particle sizes. This explanation cannot account for the appearance of a short wavelength peak since the limiting wavelength for particles of zero diameter is 555 mμ. Moreover, differences in amounts of scattered light observed for the natural and synthetic is not consistent with a size effect. It is possible, however, to account for both the strange absorption spectrum and the lack of scattered light by assuming a distribution of particle shapes.

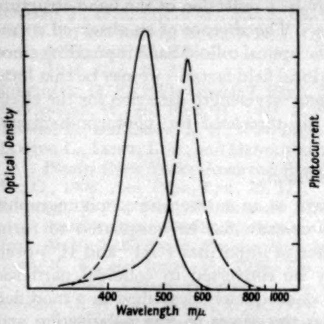

Figure 4. Spectral dependence of photoconductivity (solid line) and optical absorption (broken line) of additively coloured NaCl.

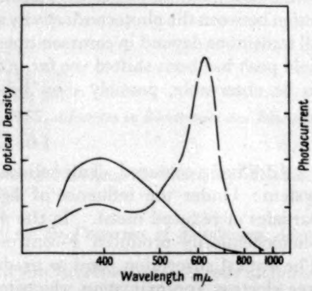

Figure 5. Spectral dependence of photoconductivity (solid line) and optical absorption (broken line) of natural blue Stassfurt halite.

The threshold for photoconductivity obtained by Gyulai is corroborated here for Stassfurt halite. It occurs at 650 mμ, or 0·5 ev less than the corresponding threshold for the photoelectric effect on the alkali metal. The difference in the apparent work function in the two cases is due, according to Mott (1938), to the electron affinity χ of the host crystal NaCl. On this interpretation the bottom of the conduction band in NaCl lies 0·5 ev below the vacuum potential outside the crystal surface. Recent attempts to observe photoemission directly from a metal into the conduction band of NaCl using surface electrodes have yielded conflicting results. Gilleo (1953) observed electron emission from silver into NaCl and found $\chi = 0{\cdot}4$ ev in good agreement with Mott's estimate, and with the results reported here. However, Turner (1956) has repeated the experiment and has been unable to find any emission at all. The discrepancy remains unexplained.

It has often been noted that the spectral response for photoconductivity bears a strong resemblance to the spectral selective photoelectric effect in sodium metal. There is, however, an important difference between the two phenomena, since the maximum photoconductivity does not coincide with a maximum optical absorption. Of the various frequency dependent factors entering the expression for the probability of ionization of a colloidal particle, and thus determining the wavelength dependence of photoconductivity, for example, local field, transition probability, barrier penetration, available initial states, and accessible final states, only the first and last named will be significantly different for particles imbedded in a crystalline lattice instead of free space. It is the strong maximum in the frequency dependent local field which gives rise to the colloid absorption band (§4) and to the strong spectral selective photoelectric effect in the alkali metals

(Doyle 1959). The peak in colloidal photoconductivity, however, does not coincide with the colloid band and so, if it is due to the same group of particles, it must arise from the other factor. For particles in a vacuum the density of accessible final states is a monotonic increasing function of frequency and no maximum corresponding to this factor is observed in the selective photoelectric effect. For particles imbedded in a crystalline field, however, the density of final states is zero for transitions leading to the forbidden bands. Thus, the observed maxima in photoconductivity may be a reflection of the band structure of the host medium just as the threshold is. The absence of an observed correlation between the photoconductivity and the optical colloid band is puzzling since all transitions depend in common upon the local field factor. It may be that local field peak has been shifted too far in the long wavelength direction for the effect to be observable, possibly even beyond the threshold for photoconductivity.

§ 6. CONCLUSION

Additively coloured alkali halides behave as an autosensitized photographic system: Under the influence of light, F-centres may be coagulated to form particles of reduced metal. In the presence of impurities (OH^- and H^+) even photochemically produced F-centres may be converted to colloidal particles. The optical absorption band so produced is adequately described in a modified free electron approximation which includes the effects of core polarization and optical effective mass. Departures from spherical shape lead to negligible changes in integrated absorption for random distributions of particles. Provided that spherical shape is most probable, the band position is unchanged, though spurious broadening may occur. The colloid band is closely related to plasma oscillations in the infinite metal: plasma frequencies deduced from the position of the colloid band are in good agreement with independent estimates. In spite of the apparent similarity, the photoconductivity associated with the colloid band differs from the spectral selective photoelectric effect of alkali metals in an important respect: the optical absorption and photoconductivity maxima do not coincide. The occurrence of a maximum in the photoconductivity and the displacement of the threshold wavelength are both due to the band structure of the host crystal.

ACKNOWLEDGMENTS

Much of this work was carried out while the author was a guest of the Microwave Physics Group in the Department of Electronics at the University of Southampton. The author wishes to thank Professor E. E. Zepler and Dr. D. J. E. Ingram for their kind hospitality.

REFERENCES

AMELINCKX, S., 1956, *Phil. Mag.*, **1**, 269.
BUTCHER, P. N., 1951, *Proc. Phys. Soc.* A, **64**, 765.
COHEN, M. H., 1958, *Phil. Mag.*, **3**, 762.
COMPTON, W. D., 1957, *Phys. Rev.*, **107**, 1271.
DOYLE, W. T., 1958 a, *Phys. Rev.*, **111**, 1072.
—— 1958 b, *Ibid.*, **111**, 1067.
—— 1959, *Proc. Phys. Soc.*, **74**, 27.
DOYLE, W. T., INGRAM, D. J. E., and SMITH, M. J. A., 1959, *Phys. Rev. Letters*, **2**, 497.
ETZEL, H. W., and PATTERSON, D. A., 1958, *Phys. Rev.*, **112**, 1112.

Fröhlich, H., and Pelzer, H., 1955, *Proc. Phys, Soc.* A, **68**, 525.
Gans, R., 1912, *Ann. Phys. Lpz.*, **37**, 881.
Gilleo, M. A., 1953, *Phys. Rev.*, **91**, 534.
Glaser, G., 1937, *Nachr. Ges. Wiss. Göttingen*, **3**, 31.
Gyulai, Z., 1925, *Z. Phys.*, **35**, 411.
Hacskaylo, M., and Groetzinger, G., 1952, *Phys. Rev.*, **87**, 790.
Hacskaylo, M., and Otterson, D., 1953, *J. Chem. Phys.*, **21**, 552.
Hacskaylo, M., Otterson, D., and Schwed, P., 1953, *J. Chem. Phys.*, **21**, 1453.
Hedges, J. N., and Mitchell, J. W., 1953, *Phil. Mag.*, **44**, 223.
Hubbard, J., 1955, *Proc. Phys. Soc.* A, **68**, 441, 976.
Ives, H. E., and Briggs, H. B., 1936, *J. Opt. Soc. Amer.*, **26**, 181, 395.
—— 1937, *Ibid.*, **27**, 238.
—— 1938, *Ibid.*, **28**, 330.
McLennan, D. E., 1951, *Canad. J. Phys.*, **29**, 122.
Martienssen, W., and Pick, H., 1953, *Z. Phys.*, **134**, 309.
Marton, L., and Leder, L. B., 1954, *Phys. Rev.*, **94**, 203.
Marton, L., Leder, L. B., and Mendlowitz, H., 1955, *Advances in Electronics and Electron Physics* (New York: Academic Press).
Mie, G., 1908, *Ann. Phys., Lpz.*, **25**, 377.
Mitchell, J. W., 1951, *Fundamental Mechanisms of Photographic Sensitivity* (London: Butterworths Scientific Publications), p. 242.
Mott, N. F., 1938, *Trans. Faraday Soc.*, **34**, 500.
Mott, N. F., and Jones, H., 1936, *The Theory of the Properties of Metals and Alloys* (Oxford: University Press).
Neilson, G. W., and Scott, A. B., 1954, *Defects in Crystalline Solids—Report of Bristol Conference* (London: Physical Society), p. 297.
Ottmer, R., 1928, *Z. Phys.*, **46**, 798.
Pearson, W. B., 1958, *A Handbook of Lattice Spacings and Structures of Metals and Alloys* (London: Pergamon Press).
Petroff, S., 1950, *Z. Phys.*, **127**, 443.
Pines, D., 1956, *Rev. Mod. Phys.*, **28**, 184.
Pringsheim, P., 1954, *Z. Phys.*, **136**, 573.
Przibram, K., 1956, *Irradiation Colors and Luminescence* (London: Pergamon Press).
Ring, P. J., O'Keefe, J. G., and Bray, P. J., 1958, *Phys. Rev. Letters*, **1**, 453.
Rohloff, E., 1952, *Z. Phys.*, **132**, 643.
Savostianova, M., 1930, *Z. Phys.*, **64**, 262.
Scott, A. B., 1954, *Phil. Mag.*, [7], **54**, 610.
Scott, A. B., and Bupp, L. P., 1950, *Phys. Rev.*, **79**, 341.
Scott, A. B., Smith, W. A., and Thompson, M. A., 1953, *J. Phys. Chem.*, **57**, 757.
Seitz, F., 1954, *Rev. Mod. Phys.*, **26**, 7.
Sennett, R. S., and Scott, G. D., 1950, *J. Opt. Soc. Amer.*, **40**, 203.
Shatalov, A. A., 1956, *Soviet Physics, J.E.T.P.*, **2**, 725.
—— 1957, *Optika i Spektrosk.*, **3**, 610.
Smallman, R. E., and Willis, B. T. M., 1957, *Phil. Mag.* [8], **2**, 1018.
Tessman, J. R., Kahn, A. H., and Shockley, W., 1953, *Phys. Rev.*, **92**, 890.
Theisen, F., and Scott, A. B., 1952, *J. Chem. Phys.*, **20**, 529.
Tonks, L., 1931, *Phys. Rev.*, **38**, 1219.
Turner, W. J., 1956, *Phys. Rev.*, **101**, 1653.
Watson, L. R., and Scott, A. B., 1959, *J. Chem. Phys.*, **30**, 342.
Wood, R. W., 1933, *Phys. Rev.*, **44**, 353.
Wood, R. W., and Lukens, C., 1938, *Phys. Rev.*, **54**, 332.
Zener, C., 1933, *Nature, Lond.*, **132**, 968.

Optical Constants of Aluminium†

By H. MENDLOWITZ
National Bureau of Standards, Washington, D.C.

Communicated by L. Marton; MS. received 1*st June* 1959, *in final form* 11*th December* 1959

Abstract. The optical constants of aluminium from the near ultra-violet (2500 Å) to the near infra-red ($5\,\mu$) can be described, at least qualitatively, in terms of the Drude formula by the two parameters N and τ, the density of free electrons and the relaxation time, respectively. The value for N is taken to correspond to 2·4 free electrons per atom and the value for τ is taken to be $1{\cdot}2\times10^{-15}$ second.

§ 1. Introduction

In the course of our investigations on the characteristic electron energy losses in solids (Marton, Leder and Mendlowitz 1955, Marton 1956), it became clear that a knowledge of the optical constants of the solids would be very desirable, because the loss spectrum is determined by the behaviour of the complex dielectric constant $\epsilon(\omega)$ as a function of the frequency ω. The optical absorption process, which is the interaction of the transverse components of the electromagnetic field with matter, can be characterized by

$$I_{\mathrm{em}}(\omega)\sim\mathscr{I}\epsilon(\omega), \qquad \ldots\ldots(1a)$$

$$\omega=2\pi\mathbf{c}/\lambda, \qquad \ldots\ldots(1b)$$

where $\mathbf{c}$ is the velocity of light, λ the wavelength, $I_{\mathrm{em}}(\omega)$ is the probability of the elementary electromagnetic absorption process at the frequency ω, and $\mathscr{I}\epsilon(\omega)$ is the imaginary part of the dielectric constant. On the other hand, the characteristic electron energy absorption process within a solid, which is the interaction of the longitudinal components of the electromagnetic field with the matter, is characterized by (Marton, Leder and Mendlowitz 1955, Fröhlich and Pelzer 1955, Hubbard 1955)

$$I_{\mathrm{el}}(\omega)\sim\mathscr{I}\frac{1}{\epsilon^*}=\frac{\mathscr{I}\epsilon(\omega)}{|\epsilon(\omega)|^2}, \qquad \ldots\ldots(2)$$

where $I_{\mathrm{el}}(\omega)$ is the probability of the elementary electron energy absorption process in the solid at the frequency ω. Thus, to study the electron loss spectrum one must know the behaviour of the real part of the dielectric constant as a function of frequency in addition to the behaviour of the imaginary part. In principle, if we knew the frequency dependence of either the real or the imaginary part of the dielectric constant for all frequencies, it would be possible to obtain the other through the Kramers–Kronig dispersion relations (Kronig 1926, Kramers 1927). This was not a very feasible method, before the advent of the high-speed computers, except when the frequency dependence could be expressed in terms of simple analytic functions. Also, more often than not, the complete frequency dependence of the real or imaginary part of ϵ was not known. This was not a major problem because both n and k, the index of refraction and extinction

---

† Supported in part by the U.S. Atomic Energy Commission.

coefficient, respectively, were usually measured in the frequency range of interest. These are directly related to the complex dielectric constant $\epsilon(\omega)$ by

$$\epsilon(\omega)=(n+ik)^2, \qquad \ldots\ldots(3\,a)$$

$$\mathscr{I}\epsilon(\omega)=+2nk, \qquad \ldots\ldots(3\,b)$$

$$\mathscr{R}\epsilon(\omega)=n^2-k^2. \qquad \ldots\ldots(3\,c)$$

(One may find in the literature that $\epsilon(\omega)=(n-ik)^2$ instead of as in equation (3 *a*). The difference between the two forms depends upon whether the time dependence of the electromagnetic field is written as $e^{i\omega t}$ or $e^{-i\omega t}$.)

Although the frequency range of major interest for the electron energy loss spectra is in the far ultra-violet, it is necessary to know the frequency dependence of ϵ in the other frequency regions in order to check the information on the oscillator strengths. Since the electron energy absorption spectrum in aluminium is the most thoroughly studied (Marton, Leder and Mendlowitz 1955, Marton 1956) it was decided to compare the information on the distribution of oscillator strengths gained from electron absorption in that metal with that obtained from electromagnetic spectra. In what follows, we shall assume that the total oscillator strength for the possible electromagnetic absorptions from zero frequency to the far ultra-violet ($\hbar\omega \sim 20$ ev) is accounted for by the three valence electrons in aluminium. In this paper our attention will be directed mainly to the region between 2500 Å and 5 μ.

§ 2. MEASUREMENTS OF OPTICAL CONSTANTS IN ALUMINIUM

The optical constants in aluminium in the visible and ultra-violet have been studied for a long time because of the practical application of utilizing aluminium as a mirror far into the ultra-violet. It has been shown (Hass, Hunter and Tousey 1956) that the optical properties of aluminium films depend on the processing methods as well as on the age of the film. Therefore, in this discussion, we will limit ourselves to some of the more recent measurements of the optical constants (Hass 1960, Schulz 1954, Schulz and Tangherlini 1954, Beattie 1955, Beattie and Conn 1955, 1956, Hodgson 1955) where it is assumed that adequate care has been taken in the preparation to ensure uniform, reproducible results.

§ 3. DRUDE THEORY

On the basis of the Drude free electron gas theory we can express the real and imaginary parts of the dielectric constant as

$$\mathscr{R}\epsilon(\omega)=1-\frac{\omega_{\mathrm{p}}{}^2\tau^2}{1+\omega^2\tau^2}\,, \qquad \ldots\ldots(4\,a)$$

$$\mathscr{I}\epsilon(\omega)=\frac{\omega_{\mathrm{p}}{}^2\tau}{\omega(1+\omega^2\tau^2)}\,, \qquad \ldots\ldots(4\,b)$$

where τ is the relaxation time which corresponds to the interaction of the electrons with their surroundings and among themselves, and

$$\omega_{\mathrm{p}}{}^2=4\pi N\boldsymbol{e}^2/\boldsymbol{m}, \qquad \ldots\ldots(5)$$

where N is the density of the free electrons, $\boldsymbol{e}$ the electronic charge, and $\boldsymbol{m}$ the electronic mass. In the limit of extremely large $\omega\tau$ (but ω is still small enough so that we do not excite interband transitions), we have the condition of a free electron gas without any interaction and the real and imaginary parts of the dielectric constant are then

$$\mathscr{R}\epsilon(\omega)=1-\frac{\omega_p^2}{\omega^2}=1-\omega_p^2(2\pi\mathbf{c})^{-2}\lambda^2 \qquad \ldots\ldots(6a)$$

$$\mathscr{I}\epsilon(\omega)=\frac{\omega_p^2}{\omega^3\tau}. \qquad \ldots\ldots(6b)$$

§ 4. PARAMETERS FOR DRUDE FORMULAE

If we plot $1-\mathscr{R}\epsilon(\omega)=k^2-n^2+1$ in the limit of large $\omega\tau$ as a function of the inverse frequency squared (or as a function of λ^2) we should obtain a straight line whose slope is $\omega_p^2(2\pi\mathbf{c})^{-2}$ (eqn (6 *a*)). Figure 1 is a plot of the data obtained from Hass (1960). The slope of this curve gives ω_p^2. After substitution into equation (5) we obtain a density of free electrons in aluminium which corresponds to 2·4 free electrons per atom in aluminium. A similar plot of the Schulz and Tangherlini data is given in figure 2 for comparison. (Deviations from the straight line approximation in the long wavelength region are to be expected because equation (6 *a*) has to be replaced by equation (4 *a*). Furthermore, there may be a weak interband transition in the 0·7 μ to 1 μ region.) Thus we have one of the required parameters to substitute into the Drude formulae

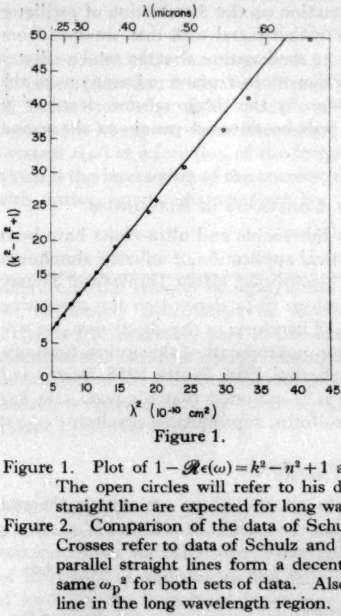

Figure 1.

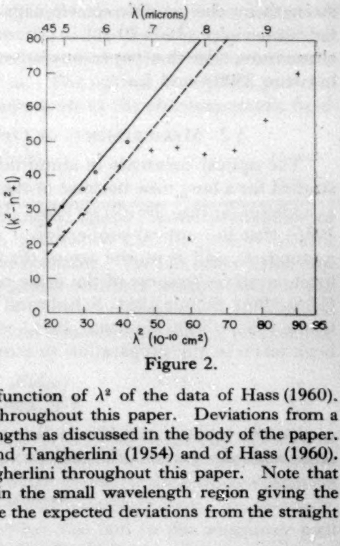

Figure 2.

Figure 1. Plot of $1-\mathscr{R}\epsilon(\omega)=k^2-n^2+1$ as a function of λ^2 of the data of Hass (1960). The open circles will refer to his data throughout this paper. Deviations from a straight line are expected for long wavelengths as discussed in the body of the paper.

Figure 2. Comparison of the data of Schulz and Tangherlini (1954) and of Hass (1960). Crosses refer to data of Schulz and Tangherlini throughout this paper. Note that parallel straight lines form a decent fit in the small wavelength region giving the same ω_p^2 for both sets of data. Also note the expected deviations from the straight line in the long wavelength region.

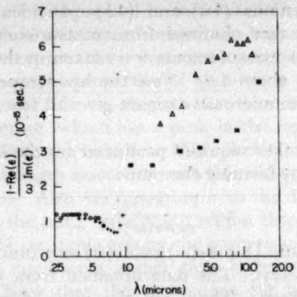

Figure 3. $(1-\mathscr{R}\epsilon(\omega)/(\omega\mathscr{I}\epsilon(\omega))$ is plotted for all wavelengths for which there are data. Throughout the paper the triangles refer to data of Beattie and Conn and the rectangles to those of Hodgson. For the Drude model the ordinate gives τ, the relaxation time. Observe the consistent value of the ordinate in the small wavelength region and the increase in the long wavelength region.

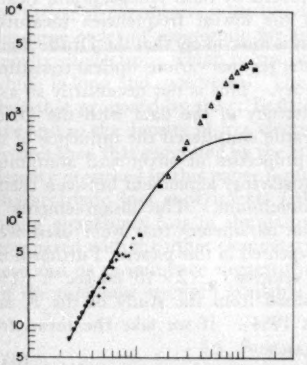

Figure 4.

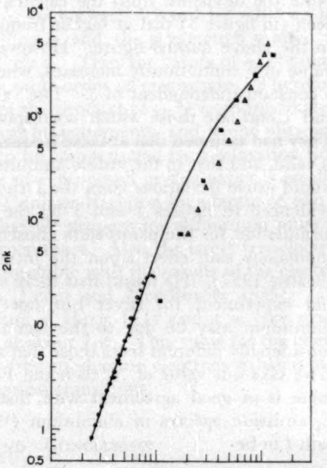

Figure 5.

Figure 4. $1-\mathscr{R}\epsilon(\omega)=k^2-n^2+1$ is plotted as a function of wavelength. Solid curve is calculated from equation (4 (*a*)) with τ taken as $1{\cdot}2\times10^{-15}$ sec and N as 2·4 free electrons per atom. Notice that the curve gives a good qualitative fit of the data up until about 5 μ.

Figure 5. $\mathscr{I}\epsilon(\omega)=2nk$ is plotted as a function of wavelength. Solid curve is that calculated from equation (4 (*b*)) with the parameters listed in figure 4. This curve gives a rather good fit throughout most of the wavelength region shown.

which are given in equations (4*a*) and (4*b*). Incidentally, this density is considerably larger than that obtained from measurements by Hodgson and Beattie and Conn. Their measurements were taken in the infra-red region for wavelengths greater than about 1 μ. Note the low temperature measurements by Chambers (1952) in the microwave region give 2·2 free electrons per atom in aluminium.

We can obtain τ, the other required parameter for the Drude formulae, from equations (4*a*) and (4*b*) by forming the ratio

$$\tau = \frac{1-\mathscr{R}\epsilon(\omega)}{\omega\mathscr{I}\epsilon(\omega)}. \qquad \ldots\ldots(7)$$

In figure 3, we plot the ratio $[1-\mathscr{R}\epsilon(\omega)]/\omega\mathscr{I}\epsilon(\omega)$ as a function of λ. This ratio gives τ in the Drude theory. The data obtained from Hass give a value of approximately $1{\cdot}2\times10^{-15}$ sec. There are also given the values of the above ratio obtained for larger values of λ. In figure 4 are plotted the experimental values of $1-\mathscr{R}\epsilon=k^2-n^2+1$ as a function of wavelength; the solid curve is calculated from equation (4*a*) ($N=2{\cdot}4$/atom and $\tau=1{\cdot}2\times10^{-15}$ sec). Note that the solid curve gives the qualitative behaviour of $\mathscr{R}\epsilon$ over this region. In figure 5 is displayed $\mathscr{I}\epsilon=2nk$ as a function of wavelength. The solid curve is calculated from equation (4*b*). This gives a rather good fit to the experimental information. Note the deviation from the calculated values in the region near 0·9 μ. It is seen (in figure 3) that at higher frequencies (smaller λ) the value of τ stabilizes to the above quoted figure. However, at the lower frequencies (larger λ) the value of τ continuously increases, whereas on the basis of the Drude theory τ is a constant independent of λ. The values quoted by both Hodgson and Beattie and Conn are those which correspond to the lowest frequencies measured. They had assumed that at these frequencies it is most likely that the Drude theory is valid, and that in the visible and ultra-violet regions various optical transitions would cause deviations from the Drude theory. This is not necessarily so as is evidenced in figures 1 and 3 by the consistency of the data with the Drude formulation for the parameters chosen. Beattie considered the influence of the anomalous skin effect upon the infra-red properties of silver and aluminium (Beattie 1957). He found that there was satisfactory agreement between theory and experiment for silver but not for aluminium. The disagreements in aluminium may be due to the fact that the parameters that were used were considerably different from those that are presented in this paper. Furthermore, if we take our value of N, then the Fermi velocity $v_{\mathrm{F}}\simeq2\times10^8$ cm sec^{-1}. This value is in good agreement with that obtained from the study of the K and L_3 emission spectra in aluminium (Wilson 1954). If we take the mean free path l to be

$$l\simeq v_{\mathrm{F}}\tau, \qquad \ldots\ldots(8)$$

then $l\simeq2{\cdot}5\times10^{-7}$ cm, about five lattice spacings. The skin depth δ is given by

$$\delta=\mathbf{c}/(2\pi\omega\sigma_0\mu')^{1/2}, \qquad \ldots\ldots(9)$$

where σ_0 is the d.c. conductivity and is given by

$$\sigma_0=\lim_{\omega\to0}\frac{\omega}{4\pi}\mathscr{I}\epsilon(\omega), \qquad \ldots\ldots(10)$$

and μ' is the magnetic permeability which can be taken as unity in this frequency range (Dingle 1953). Therefore

$$\delta=1{\cdot}3\times10^{-6}\lambda^{1/2}\ \mathrm{cm}, \qquad \ldots\ldots(11)$$

where the wavelength λ is expressed in microns. Thus in the region from $1\,\mu$ to $10\,\mu$, the skin depth is an order of magnitude larger than the mean free path and so one might not expect that it is necessary to consider the anomalous skin effect in treating the optical properties of aluminium in this region. We must not, however, completely rule out the fact that there may be a weak absorption, due to the band structure, which has a peak in the region of $0{\cdot}9\,\mu$ (cf. figures 4 and 5). There is good reason to believe (Mendlowitz, to be published)† that the maximum oscillator strength associated with this absorption corresponds to about 0·3 electrons per atom. Also, we may note from the data presented in figures 3, 4 and 5 that even in the same wavelength region there is a marked discrepancy for the quoted optical constants among the various authors. Thus, one may at best hope to give a qualitative, rather than a quantitative description of the optical constants. Now that the techniques for preparing films and their behaviour is better understood, it is very desirable to have additional measurements made over the complete wavelength region (from far infra-red to ultra-violet) in order to check the previous measurements and the model proposed in this paper.

The measurements of the d.c. conductivity in bulk material give a value of $3{\cdot}2 \times 10^{17}$ e.s.u. in aluminium. The electrical measurements on evaporated films give a value of about $1{\cdot}5 \times 10^{17}$ e.s.u. (Beattie and Conn 1955, 1956). From their optical measurements, the values of σ_0 are between 1·1 and $1{\cdot}2 \times 10^{17}$ e.s.u., Hodgson's measurements give $0{\cdot}73 \times 10^{17}$ e.s.u. and the parameters quoted in this paper give a value of about $0{\cdot}45 \times 10^{17}$ e.s.u. Thus the values of σ_0 obtained from the optical measurements are of the same order of magnitude. Therefore the fitting of parameters must be such that the product of $\omega_p{}^2\tau$ is approximately the same order of magnitude for all optical measurements, and if one obtains a density of electrons which is low, it has to be compensated by a relaxation time which is long and vice versa. The value of τ proposed in this paper is smaller than that proposed by either Beattie and Conn or Hodgson by a factor of two to five and so the density of free electrons that we propose for aluminium must be greater than that suggested by the other two authors. Also, the larger free electron density proposed in this paper is more compatible with the results of the electron characteristic loss experiments (Marton, Leder and Mendlowitz 1955). The major elementary loss in aluminium occurs at about 15 ev and it is very strong compared with the other elementary loss at about 7 ev. This value for the energy loss and its prominence suggest that the free conduction electrons exhaust most of the oscillator strength available for optical transitions.

§ 5. SUMMARY AND CONCLUSION

Although the density of free electrons in aluminium ($N = 2{\cdot}4$/atom) suggested in this paper is considerably higher than those for many of the good conductors, the comparatively poorer conducting qualities of aluminium are due to the small relaxation time ($\tau = 1{\cdot}2 \times 10^{-15}$ sec) which is at least an order of magnitude smaller than, for example, that of copper. Note that we have not endeavoured to discuss the frequency dependent conductivity in terms of the band structure of aluminium because we have found that the simple Drude approach seems to give an adequate qualitative description. One may try to study the temperature dependence of τ in aluminium in a relatively straightforward manner by measuring the optical constants in the visible and near ultra-violet as a function of temperature and applying the analysis that gave the data for figure 3. This may be a rather direct method to obtain information on the electron–phonon interaction, although at low temperatures one may have to consider the anomalous skin effect in interpreting the data.

---

† This information is obtained from an estimate of the oscillator strength of the transition in the 1000 Å region.

ACKNOWLEDGMENTS

The author is indebted to Dr. L. Marton, Chief, Electron Physics Section, National Bureau of Standards, for constant encouragement and advice, to Dr. Georg Hass, Chief of the Physics Research Laboratories, Ft. Belvoir, for permission to use his unpublished data, to Drs. J. A. Simpson and L. B. Leder for asking thought-provoking questions, and to M. D. Wagner for aid in preparing the figures.

REFERENCES

BEATTIE, J. R., 1955, *Phil. Mag.*, **46**, 235.
—— 1957, *Physica*, **23**, 898.
BEATTIE, J. R., and CONN, G. K. T., 1955, *Phil. Mag.*, **46**, 222.
—— 1956, *Proc. Inst. Radio Engrs, N.Y.*, **44**, 78. (They report on measurements in the infra-red.)
CHAMBERS, R. G., 1952, *Proc. Roy. Soc.* A, **215**, 481.
DINGLE, R. B., 1953, *Physica*, **19**, 348. This author has a series of four papers in this volume on the anomalous skin effect in metals.
FRÖHLICH, H., and PELZER, H., 1955, *Proc. Phys. Soc.* A, **68**, 525.
HASS, G., 1960, *J. Opt. Soc. Amer.*, in the press (visible and ultra-violet).
HASS, G., HUNTER, W. R., and TOUSEY, R., 1956, *J. Opt. Soc. Amer.*, **46**, 1009.
HODGSON, J. N., 1955, *Proc. Phys. Soc.* B, **68**, 593. (The measurements in this paper overlap those of Beattie and Conn.)
HUBBARD, J., 1955, *Proc. Phys. Soc.* A, **68**, 441.
KRAMERS, H. A., 1927, *Atti Congr. del Fisici, Como*, 545.
KRONIG, R., 1926, *J. Opt. Soc. Amer.*, **12**, 547.
MARTON, L., 1956, *Rev. Mod. Phys.*, **28**, 172.
MARTON, L., LEDER, L. B., and MENDLOWITZ, H., 1955, *Adv. in Electronics and Electron Physics* (New York: Academic Press), **7**, 83. These papers give a fairly complete list of references on characteristic electron energy losses to date of their publication.
SCHULZ, L. G., 1954, *J. Opt. Soc. Amer.*, **44**, 357.
—— 1957, *Advanc. Phys.* (*Phil. Mag. Suppl.*), **6**, 102.
SCHULZ, L. G., and TANGHERLINI, F. R., 1954, *J. Opt. Soc. Amer.*, **44**, 362 (visible and near infra-red).
WILSON, A. H., 1954, *The Theory of Metals*, 2nd Edn (Cambridge : University Press).

Liquid Partition Function and the Free Energy

By G. H. A. COLE
Physics Division, Clarke, Chapman and Co., Gateshead, Co. Durham

Communicated by H. S. W. Massey; MS. received 19*th October* 1959, *in final form* 2*nd December* 1959

Abstract. A procedure is proposed, involving a coupling parameter, for the determination of the partition function and free energy of a classical condensed system of particles in terms of the structure of the system (that is, short range order) represented by the pair distribution. The present paper forms a sequence with two previous papers by the author, published in 1959 and 1960, concerned with the accurate calculation of the pair distribution. The present paper, when taken together with these previous papers, gives a theory for the determination of the thermodynamic properties of a classical fluid in terms of the partition function, and using the principles of particle dynamics. Errors due to the use of the superposition approximation in the calculation of the structure can be controlled. The theory may be applied equally to spherical or non-spherical constituent particles.

§ 1. INTRODUCTION

ACCORDING to the well-established principles of classical statistical mechanics (see for example Tolman 1938) the equilibrium macro- and micro-physics of all matter are linked according to the expression

$$F = -kT \log Z. \qquad \dots\dots (1)$$

Here, F is the macroscopic Helmholtz free energy, k is the Boltzmann constant, T is the absolute temperature, and Z is the partition function defined by $Z = \lambda^N Z_r$, where

$$h^3\lambda = (2\pi mkT)^{3/2} \qquad \dots\dots (2a)$$

and

$$N!\,Z_r = \int \dots \int \exp\{-\mathrm{X}(\mathbf{r}_1, \mathbf{r}_2, \mathbf{r}_3, \dots \mathbf{r}_N)\}\, d\mathbf{r}_1\, d\mathbf{r}_2\, d\mathbf{r}_3 \dots d\mathbf{r}_N. \qquad \dots\dots (2b)$$

In (2), $\mathbf{r}_i$ is the configuration vector for the particle i (representative of all the N identical particles of mass m contained in a fixed volume V, which forms the model to replace the actual system in the theory); $\mathrm{X}(\mathbf{r}_1, \mathbf{r}_2, \mathbf{r}_3, \dots \mathbf{r}_N)$ is the reduced total particle interaction potential related to the total actual interparticle potential $\Psi(\mathbf{r}_1, \mathbf{r}_2, \mathbf{r}_3, \dots \mathbf{r}_N)$ through the formula $kT\mathrm{X} = \Psi$. To very good approximation, Ψ is independent of the temperature.

For simple systems composed of mutually interacting particles with no internal degrees of freedom (such as will concern us throughout this paper), Ψ is the sum of the mutual pair interactions between constituent doublets. If $\psi(\mathbf{r}_i, \mathbf{r}_j)$ is the actual pair interaction potential between particles i and j, then a reduced pair potential, $\chi(\mathbf{r}_i, \mathbf{r}_j)$ is introduced such that $kT\chi=\psi$, and we may write:

$$\mathrm{X}(\mathbf{r}_1, \mathbf{r}_2, \mathbf{r}_3, \ldots \mathbf{r}_N)= \sum_{i=1}^{N}\sum_{j>i}^{N} \chi(\mathbf{r}_i, \mathbf{r}_j). \qquad \ldots\ldots(3)$$

The macroscopic thermodynamic functions are obtained theoretically by the appropriate differentiation or F, or $\log Z$, with respect, for example, to the temperature or the volume. For example, the entropy S and the pressure p are given by

$$S=-\left.\frac{\partial F}{\partial T}\right|_{V,N} \quad \text{and} \quad p=-\left.\frac{\partial F}{\partial V}\right|_{T,N}. \qquad \ldots\ldots(4a)$$

The internal energy U then follows from the relation

$$F=U-TS \qquad \ldots\ldots(4b)$$

and is explicitly

$$U=kT^2\frac{\partial}{\partial T}\log Z. \qquad \ldots\ldots(4c)$$

The calculation of the thermodynamic functions of a classical condensed system of particles using the formulae (1) to (4) without any modification is totally impracticable because of the impossibility of evaluating the expression (2) for the partition function directly in this case. Two methods for circumventing this situation, that have proved valuable in the past, are relevant here. The first attributes a cell structure to the fluid (Lennard-Jones and Devonshire 1937, de Boer 1952, Kirkwood 1950, Green 1956), each particle moving in a mean potential force field due to neighbours. Z_r is then inferred by a process of essentially empirical correction against known experimental data, possibly involving the structure of the corresponding crystalline solid.

The second method (Kirkwood and Boggs 1942, Born and Green 1949, Cole 1958, for a full discussion see Cole 1959 b) accounts explicitly for particle movement under definite laws of motion. It avoids any direct appeal to equations (2) and (1) for Z_r and F respectively, but instead accounts explicitly for the liquid short range order through the pair distribution. Simple expressions are obtained for the fluid internal energy and pressure in terms of the pair distribution; these can be expected also to include the interphase condensation region. Unfortunately numerical tests (Kirkwood, Lewinson and Alder 1952) show them to be very sensitive to the exact details of the pair distribution; in addition the inclusion of non-spherical particles into the theory presents rather more than just formal difficulty.

In the present paper we are concerned with the formal problem of deriving the liquid thermodynamic functions using all the equations (1) to (4), with the partition function determined using the arguments of particle dynamics. For this purpose Z_r is derived from (2) by invoking explicitly the details of the short range spatial order of the condensed system calculated independently, using a procedure of variable interparticle coupling for all particles simultaneously. Non-spherical particles can also be included into the theory. The present paper forms a natural sequence with two earlier papers (Cole 1959 a, 1960, hereafter referred to as I and II respectively).

§ 2. Basic Equations

It will be assumed that the short range spatial ordering of the condensed system is adequately represented by a pair distribution function describing the probability for the occurrence of any specified relative pair configuration of particles. For two particles, labelled 1 and 2, the dimensionless pair distribution $n^{(2)}(\mathbf{r}_1, \mathbf{r}_2)$ is defined by

$$(N-2)!\, Z_r n^2 n^{(2)}(\mathbf{r}_1, \mathbf{r}_2) = \int \dots \int \exp\{-\mathrm{X}\}\, d\mathbf{r}_3\, d\mathbf{r}_4 \dots d\mathbf{r}_N \quad \dots\dots(5)$$

where $nV = N$. Higher order distributions, such as the triplet can be defined (cf. for example paper I) by analogous expressions which need not be written down here.

A hypothetical variation of the actual coupling between all the particles simultaneously can be achieved theoretically by introducing a coupling parameter γ continuous in the range 0 to 1. Thus, $\gamma = 0$ refers to completely uncoupled particles, whereas $\gamma = 1$ refers to the coupling of the actual system. Hypothetical changes in the interparticle coupling can be simulated alternatively by actual changes of temperature, a correspondence existing between γ and $1/T$. For this reason the range of the coupling parameter $0 \leqslant \gamma \leqslant 1$ has an associated actual temperature range $\infty \geqslant T \geqslant T_{\mathrm{R}}$, where T_{R} is the actual temperature of the system. In particular we can link γ and T through the equivalence $\gamma(\partial/\partial\gamma) \sim -T(\partial/\partial T)$ for conditions of constant volume.

Variable coupling will be introduced into the theory through the potential expressions

$$\mathrm{X} = \gamma \mathrm{X}_{\mathrm{R}} \quad \text{and} \quad \chi = \gamma \chi_{\mathrm{R}} \quad \dots\dots(6)$$

where X_{R} and χ_{R} are respectively the total and pair potentials appropriate to the coupling of the actual system (i.e. for which $\gamma = 1$). The pair distribution and partition function corresponding to any coupling will be written $n^{(2)}(\mathbf{r}_1, \mathbf{r}_2 : \gamma)$ and $Z_r(\gamma)$ respectively.

The dependence of Z_r on the parameter γ is obtained immediately from (2), using (3) and (6), by differentiation with respect to γ:

$$N!\, \frac{\partial Z_r(\gamma)}{\partial \gamma} = -\frac{N(N-1)}{2} \gamma \iint \chi_{\mathrm{R}}(\mathbf{r}_1, \mathbf{r}_2) \exp\{-\gamma \mathrm{X}_{\mathrm{R}}\}\, d\mathbf{r}_1\, d\mathbf{r}_2\, d\mathbf{r}_3 \dots d\mathbf{r}_N.$$

By virtue of (5) and using (3) this expression can be reduced to the form

$$\frac{\partial Z_r(\gamma)}{\partial \gamma} = -\frac{\gamma n^2 Z_r(\gamma)}{2} \iint \chi_{\mathrm{R}}(\mathbf{r}_1, \mathbf{r}_2) n^{(2)}(\mathbf{r}_1, \mathbf{r}_2 : \gamma)\, d\mathbf{r}_1\, d\mathbf{r}_2 \quad \dots\dots(7)$$

which takes explicit account of the liquid structure.

§ 3. DETERMINATION OF PARTITION FUNCTION

If the pair distribution is known for any particular value of γ ($=\gamma_1$ say), then $\partial Z_r/\partial\gamma$ can be derived from (7) if $Z_r(\gamma_1)$ is also already known. This being so, $Z_r(\gamma_1 + \Delta\gamma)$ is also readily derivable if $\Delta\gamma$ is some small increment of γ. A full knowledge of $n^{(2)}$ as function of γ allows this simple procedure to be repeated continuously to give ultimately the value of Z_r for the case $\gamma = 1$, i.e. for coupling appropriate to that of the actual system. We now consider this procedure in more detail.

3.1. *Pair Distribution and the Superposition Approximation*

The function $n^{(2)}(\gamma)$ can be determined in the range $0 \leqslant \gamma \leqslant 1$ according to the arguments previously developed in I and II. In these arguments the partition function does not explicitly appear, i.e. the equation (5) is used independently of equation (2), in conformity with the approach of other authors. As usual the equations are closed by invoking the superposition approximation according to which the correlation between the many particles of a group is expressed in terms of lower order correlations between the particles of composing sub-groups. Because the total interaction potential is assumed in (3) to be expressible as the sum of pair interactions, the superposition approximation allows the triplet and higher order distributions to be expressed ultimately in terms of the pair distributions. As explained in I, however, the triplet distribution can be freed from this approximation, and in principle higher order distributions can be similarly freed. Alternatively, the form of the approximation as conventionally employed (which is characterized by the neglect of interparticle forces) can be improved to account, at least in part, for the action of these forces (Cole, to be published).

3.2. *Weak Coupling*

If γ is sufficiently small (alternatively if the temperature is sufficiently high) the equation (2) for the partition function can be evaluated to form a starting point for the application of equation (7). The procedure must account for the exact details of the pair potential and in particular for its indefinitely large value at small separation distances (particle impenetrability).

For simple non-polar molecules, of which argon is typical, the reduced potential is well represented over the full physical range of r by the expression

$$\chi(r) = A\left[\left(\frac{\sigma}{r}\right)^{s} - \left(\frac{\sigma}{r}\right)^{6}\right] \qquad \ldots\ldots (8)$$

where σ is the classical particle radius, A is a dimensionless constant, and s has a value between 9 and 15, often taken to be 12. The insertion of (8) and (3) into (2*b*) does not lead to an infinite value of the integrand of this last equation at the origin, however, because the exponential function vanishes in the limit of vanishing separation distance for any particle pair. Consequently Z_r has a finite value for any χ of physical interest, and this must be reflected in $Z_r(\gamma)$ for all γ. To ensure this behaviour for weak coupling ($\gamma \ll 1$), and at the same time to obtain a form which is simple, it is convenient to divide the full range of relative particle pair separation into two regions, viz. the region $r > r_0$ for which $\gamma\chi_{\mathrm{R}} \gg (\gamma\chi_{\mathrm{R}})^2$, and the region $r \leqslant r_0$ for which this is not so. In this way the strong repulsion of the interparticle force in the region of the origin is distinguished from the remaining region which is part repulsive, but which contains the attractive features. This separation into regions is controlled by the value of γ; the smaller γ, the smaller r_0 may be set.

For the region of configuration for which $r > r_0$ for each particle, the exponential factor appearing in (2) can be expanded as far as the linear term to give for large N

$$Z_r = \frac{V^N}{N!} z(\gamma) \qquad \ldots\ldots (9a)$$

where

$$z(\gamma) = 1 - \frac{\gamma n^2}{2} \iint \chi_{\mathrm{R}}(\mathbf{r}_1, \mathbf{r}_2)\, d\mathbf{r}_1\, d\mathbf{r}_2. \qquad \ldots\ldots (9b)$$

In (9) it is understood that the lower limit of each integration is r_0. In (9) no distinction is made between V and $(V - 4\pi r_0^3/3)$.

The purely repulsive region ($r \leqslant r_0$) is to be treated by modifying an artifice previously employed by Kirkwood, Lewinson and Alder (1952) in another connection. According to this method, χ is assumed to have the form of a hard spherical core, i.e. $\chi(r) = \infty$ for $r \leqslant r_0$. Consequently, the expression (8) is to apply for $r > r_0$ only, although the value of r_0 itself depends upon the value chosen for γ. For $r \leqslant r_0$, $\exp\{-\gamma X_R\} = 0$, and the contribution to $Z_r(\gamma)$ due to the core region is zero. Although the repulsion of the core is artificially strengthened in this way, the effect can be reduced by decreasing the value of γ which allows for a corresponding reduction in the value of r_0 and so also a reduction in the error due to the use of the hard core assumption. As r_0 is reduced (with more of the repulsive region included in the expressions (9)), a value will be reached below which the difference between the 'hard core' expression for χ and that given by (8) will be negligibly small for a classical system of finite energy in which particles are ultimately impenetrable and with a non-zero radius. For this value of r_0 the core makes no contribution to z and $Z_r(\gamma)$ is given by (9) for small γ. Judging from the numerical calculations reported by Kirkwood, Lewinson and Alder (1952) it is reasonable to expect that a value of r_0 not smaller than $\sigma/10$, and possibly somewhat larger, will be sufficient, though this can only be properly ascertained in the light of detailed calculation.

If the largest value of γ consistent with the above arguments is γ_c (say), then Z_r $(\gamma = \gamma_c)$ is determined from (9) by putting $\gamma = \gamma_c$.

3.3. *Strong Coupling*

For values of $\gamma > \gamma_c$ appeal is made to the data relating $n^{(2)}$ to γ, derived from the arguments of I and II and here assumed known. The procedure, starting from the value $Z_r(\gamma = \gamma_c)$ derived from equation (9), is the continual use of equation (7) for successive small increments of particle coupling $\Delta\gamma$ which is terminated when the value of Z_r is reached for which γ is unity. This last value is the partition function appropriate to the coupling conditions of the actual system. Although requiring much repetitive work in its application, the procedure is within the range of electronic computational techniques.

§ 4. FREE ENERGY AND THERMODYNAMIC DATA

With Z_r determined according to the arguments of the last section, F follows immediately from (1). If, further, F is known as a function of the volume and the temperature for a given N in the immediate neighbourhood of the points $\gamma = 1$ and $T = T_R$, then the corresponding thermodynamic functions follow from equations such as (4).

The temperature dependence of Z_r, and so also of F, at constant volume can be inferred in the region $\gamma \simeq 1$ from the steps involved in the theory, due to the equivalence between γ and $1/T$, and between $\partial/\partial\gamma$ and $(-1/T^2)\partial/\partial T$. Using equations (7) and (1), and the notation $kTF^*(T) = F(T)$, the free energy at temperature $T - \Delta T$ is related to that at temperature T according to:

$$F^*(T-\Delta T) = F^*(T) + \Delta T\left[\frac{3}{2T} + \frac{n^2}{2T}\int\int \chi_R(\mathbf{r}_1, \mathbf{r}_2) n^{(2)}(\mathbf{r}_1, \mathbf{r}_2 : T)\, d\mathbf{r}_1 d\mathbf{r}_2\right]$$

where ΔT is the small temperature increment corresponding to $\Delta\gamma$. Because the temperature dependence of the pair distribution has not yet been derived in adequate analytic form (see Green 1952 in this connection), the temperature dependence of F cannot itself be given in analytic form.

The dependence of Z_r, and F, on the total volume at constant temperature must also be presented numerically for similar reasons. For a macroscopic system the magnitude of $V^{1/3}$ is indefinitely large in comparison with the effective range of χ so that the effect of volume change on the expressions of I and II, as in the present paper, appears essentially through the number density n $(=N/V$: N constant) only. By repeating the calculations for small variations of n about the value appropriate to the actual system (or by more elegant methods that will not be discussed here) the dependence of Z_r, and so also of F, on V can be numerically inferred.

§ 5. CONCLUSIONS

By a procedure of (hypothetical) variation of the interparticle potential using a coupling parameter, a method of determining directly the partition function for a system of particles at liquid densities has been proposed. The treatment is made possible by invoking a knowledge of the pair distribution, derived according to arguments set down in two previous papers (Cole 1959 a, 1960). In as far as the equivalence between the coupling parameter and the inverse of temperature noted in § 2 has an exact physical counterpart throughout the full range of these parameters, the equations of the present paper can be expected also to give at least qualitative information concerning the interphase region between the gas and the condensed fluid.

The theory should fall within the range of modern electronic computational techniques in its application to specific systems, and can be expected to lead to numerical equation of state data for the fluid in the complete range from gas to condensed system, using the unmodified equations of statistical mechanics. In addition the theory can be applied, with roughly equal difficulty, to cases of spherical or non-spherical particles. It is intended to consider these matters further later, in the light of the results of detailed numerical calculations.

REFERENCES

DE BOER, J., 1952, *Proc. Roy. Soc.* A, **215**, 4.
BORN, M., and GREEN, H. S., 1949, *A General Kinetic Theory of Liquids* (Cambridge : University Press).
COLE, G. H. A., 1958, *J. Chem. Phys.*, **28**, 912.
—— 1959 a, *Proc. Phys. Soc.*, **73**, 713.
—— 1959 b, *Advanc. Phys.*, (*Phil. Mag.* Suppl.), **8**, 225.
—— 1960 *Proc. Phys. Soc.*, **75**, 77.
GREEN, H. S., 1952, *The Molecular Theory of Fluids* (Amsterdam: North-Holland).
—— 1956, *J. Chem. Phys.*, **24**, 732.
KIRKWOOD, J. G., 1950, *J. Chem. Phys.*, **18**, 380.
KIRKWOOD, J. G., and BOGGS, E. M., 1942, *J. Chem. Phys.*, **10**, 394.
KIRKWOOD, J. G., LEWINSON, V. A., and ALDER, B. J., 1952, *J. Chem. Phys.*, **20**, 929.
LENNARD-JONES, J., and DEVONSHIRE, A., 1937, *Proc. Roy. Soc.* A, **163**, 63.
TOLMAN, R. C., 1938, *Principles of Statistical Mechanics* (Oxford : University Press).

The Influence of Coma on the Response Function of an Optical System[†]

By A. M. GOODBODY[‡]
Department of Physics, Imperial College, London

Communicated by H. H. Hopkins; MS. received 26th October 1959, *in final form 11th December* 1959

Abstract. The treatment used in a previous paper dealing with the effect of spherical aberration on optical response functions has been extended to cases of coma, an aberration which is not an even function in the pupil coordinates x and y, and consequently gives rise to lateral shifting in the image.

Different positions of the focal plane, the state of correction for higher order aberration, and different azimuths of the line structure in the object are considered. Detailed results are given first for primary circular coma, when the wave-front aberration coefficient has the values $w_{31} = +0\cdot63$, $+1\cdot26$ and $+1\cdot89$ wavelengths: three focal planes and the azimuths $\psi = 0$ (radial lines) and $\psi = \pi/2$ (tangential lines) are treated. Results are also given for secondary coma for the values $w_{51} = -2\cdot6$, $-3\cdot9$, $-5\cdot85$ and $-7\cdot8$ wavelengths, with three different states of correction and again in three focal planes and two azimuths.

It is found with negative values of w_{51} that the relative phase shifting of frequency components within the image has no appreciable effect on the image quality in the cases considered when this negative secondary coma is compensated with a suitable numerically larger positive primary coma ($w_{31} + w_{51} > 0$), if focal planes situated a long way from the paraxial focal plane are excepted.

§ 1. Introduction

In a previous paper (Goodbody 1958) an account was given of the evaluation of the integral expressing the frequency response of an optical system for a large number of cases of primary and secondary spherical aberration in various states of correction and in different focal planes. The numerical calculations were carried out on a DEUCE computer programmed for the numerical integration of the double integrals involved by a method described by Hopkins (1957a). The present communication describes a similar investigation for optical systems suffering from coma.

The frequency response of an optical system is in general a complex number; the modulus is the ratio of the contrast in the image of a cosinusoidal intensity distribution to the contrast in the object itself, while the argument represents a phase shift which is associated with a lateral shift in the image. The analytical expression for the complex frequency response in monochromatic light may be written in the form

---

[†] The contents of this paper form part of the subject matter of a thesis which has been approved by the University of London for the award of the Ph.D. degree.

[‡] Now at The English Electric Co. Ltd., London, W.C.2.

$$D(s,\psi)=\frac{1}{A}\iint_S \exp\left\{\frac{2\pi i}{\lambda}\,sV(x,y;s)\right\}dxdy \qquad \ldots\ldots(1)$$

where

$$sV(x,y;s)=W(x+\tfrac{1}{2}s,y)-W(x-\tfrac{1}{2}s,y). \qquad \ldots\ldots(2)$$

A is the area of the pupil, $W(x,y)$ is the aberration function of the system referred to coordinate axes (x,y) in the pupil, the y axis being parallel to the 'lines' of the sinusoidal grating of reduced spatial frequency s, and S is the area common to two pupil areas centred on the points $(\pm\tfrac{1}{2}s, 0)$; ψ is the angle of the line structure to the meridian plane of the optical system. If R' is the number of 'lines' per unit length in the image, the variable

$$s=\frac{\lambda}{n'\sin\alpha'}\,R' \qquad \ldots\ldots(3)$$

is used to define the reduced spatial frequency, λ is the wavelength of light and $n'\sin\alpha'$ the numerical aperture of the image forming cone.

The method of computation has been described in detail in the above mentioned paper (Goodbody 1958) and the numerical method is described in a paper by Hopkins (1957 a). Unlike the spherical aberration case, however, the aberration function is not an even function in both x and y. Consequently the integration has, in general, to be extended over all four quadrants of the pupil area although in special cases either one or two quadrants may be sufficient. Furthermore, the asymmetrical nature of the aberration function gives rise to an imaginary part in the response function. If the response function is written in terms of its real and imaginary parts,

$$D(s,\psi)=\mathscr{R}(s,\psi)+i\mathscr{I}(s,\psi) \qquad \ldots\ldots(4)$$

and the method of integration employed leads to the formulae

$$\left.\begin{aligned}\mathscr{R}(s,\psi)&=\frac{1}{N_A}\sum_p\sum_q \cos Z\,\frac{\sin X}{X}\,\frac{\sin Y}{Y}\\ \mathscr{I}(s,\psi)&=\frac{1}{N_A}\sum_p\sum_q \sin Z\,\frac{\sin X}{X}\,\frac{\sin Y}{Y}.\end{aligned}\right\} \qquad \ldots\ldots(5)$$

The quantities Z, X and Y used here are defined by the relations

$$\left.\begin{aligned}Z&=V(x_p,y_q;s)\\ X&=\epsilon_x V_x'(x_p,y_q;s)\\ Y&=\epsilon_y V_y'(x_p,y_q;s).\end{aligned}\right\} \qquad \ldots\ldots(6)$$

N_A is the number of rectangles whose centres lie in the pupil area A and (x_p,y_q) are the coordinates of the centre of a typical rectangle which lies within the region of integration S, each rectangle leaving sides of length $2\epsilon_x$, $2\epsilon_y$.

The response may also be written in terms of its modulus and argument, namely

$$D(s,\psi)=T(s,\psi)\exp\{i\theta(s,\psi)\}. \qquad \ldots\ldots(7)$$

The modulus $T(s,\psi)$ is known as the contrast transfer function and $\theta(s,\psi)$ is the phase shift. It is often convenient to consider the relative response defined by

$$M(s,\psi)\exp\{i\theta(s,\psi)\}=D(s,\psi)/D_0(s,\psi), \qquad \ldots\ldots(8)$$

so that

$$M(s,\psi)=T(s,\psi)/T_0(s,\psi). \qquad \ldots\ldots(9)$$

$D_0(s, \psi)$ and $T_0(s, \psi)$ represent $D(s, \psi)$ and $T(s, \psi)$ respectively in the absence of aberrations. $M(s, \psi)$ is thus the ratio of contrast reduction in the presence of aberration to that obtained with the same system in the absence of aberration. The quantities

$$\left.\begin{aligned} T(s,\psi) &= \frac{1}{N_A}\left[\{\mathscr{I}(s,\psi)\}^2 + \{\mathscr{R}(s,\psi)\}^2\right]^{1/2} \\ M(s,\psi) &= \frac{1}{N_S}\left[\{\mathscr{I}(s,\psi)\}^2 + \{\mathscr{R}(s,\psi)\}^2\right]^{1/2} \\ \text{and} \qquad \theta(s,\psi) &= \arg\{\mathscr{R}(s,\psi) - i\mathscr{I}(s,\psi)\} \\ & \qquad\qquad -\pi \leqslant \theta(s) \leqslant \pi \end{aligned}\right\} \qquad \ldots\ldots(10)$$

are computed bythe machine and punched out at the completion of the calculation.

§ 2. CHOICE OF ABERRATION VALUES

The wave-front aberration for primary and secondary circular coma together with a defocusing term has the form

$$\begin{aligned} W(x,y) = w_{20}(x^2+y^2) + w_{31}(x^2+y^2)(y\cos\psi + x\sin\psi) \\ + w_{51}(x^2+y^2)^2(y\cos\psi + x\sin\psi) \end{aligned} \qquad \ldots\ldots(11)$$

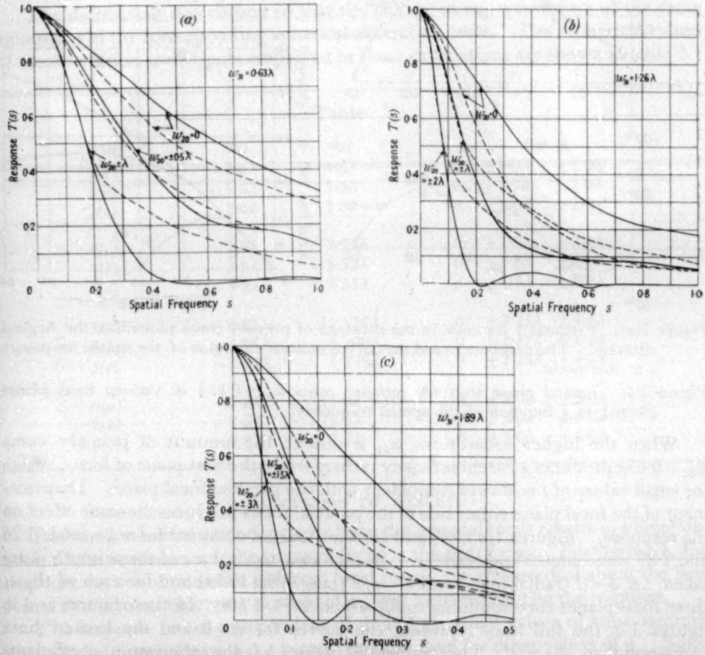

Figure 1. Frequency response in the presence of primary coma in various focal planes. The full lines correspond to $\psi=0$ and the broken lines to $\psi=\pi/2$.

where w_{20}, w_{31} and w_{51} measure defect of focus from the paraxial image plane, primary and secondary coma respectively. It will frequently be convenient to express the aberration coefficients in equations (11) by means of the ratios

$$\beta_{23}=w_{20}/w_{31}, \qquad \beta_{25}=w_{20}/w_{51}, \qquad \beta_{35}=w_{31}/w_{51}. \qquad \ldots\ldots(12)$$

The value of β_{35} corresponding to the best form of correction for low frequencies according to the tolerance criterion of Hopkins (1957 b) will be denoted by β_{35}'.

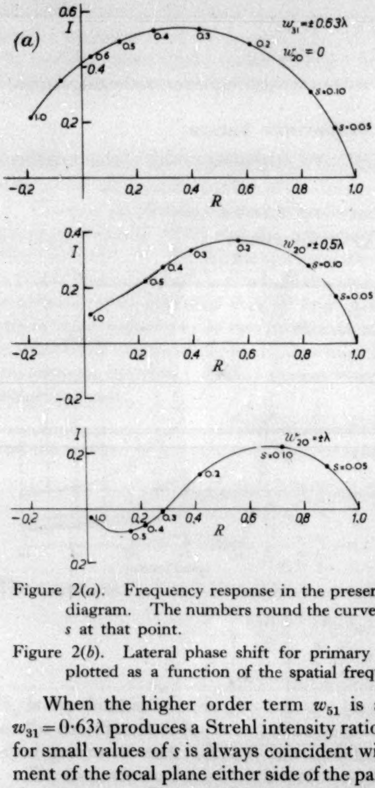

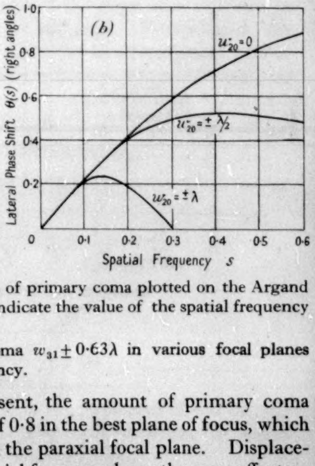

Figure 2(*a*). Frequency response in the presence of primary coma plotted on the Argand diagram. The numbers round the curves indicate the value of the spatial frequency s at that point.

Figure 2(*b*). Lateral phase shift for primary coma $w_{31}\pm 0{\cdot}63\lambda$ in various focal planes plotted as a function of the spatial frequency.

When the higher order term w_{51} is absent, the amount of primary coma $w_{31}=0{\cdot}63\lambda$ produces a Strehl intensity ratio of 0·8 in the best plane of focus, which for small values of s is always coincident with the paraxial focal plane. Displacement of the focal plane either side of the paraxial focus produces the same effect on the response. Figures 1(*a*), (*b*) and (*c*) show curves obtained for $w_{31}=0{\cdot}63$, 1·26 and 1·89 wavelengths respectively. In each case two values of the azimuth ψ are taken, i.e. $\psi=0$ (radial lines) and $\psi=\pi/2$ (tangential lines) and for each of these, three focal planes corresponding to $\beta_{23}=0{\cdot}00$, 0·79, 1·59. In these figures and in figures 3–6 the full lines represent the curves for $\psi=0$ and the broken lines correspond to $\psi=\pi/2$. The numerical values of the aberration coefficients employed in the calculations are shown in table 1.

Figures 3–6 show the results obtained for secondary coma. Those labelled (*b*) in each case represent the optimum low frequency correction for higher order coma, in the sense of Hopkins (1957 b). The initial value of w_{51} was chosen according to the Strehl intensity criterion, giving $w_{51} = -2{\cdot}6\lambda$; the other values $-3{\cdot}9$, $-5{\cdot}85$ and $-7{\cdot}8$ wavelengths being the same multiples of the initial values as those used in the case of spherical aberration (Goodbody 1958). It will be clear that the calculated optimum values of β_{35} will depend on the azimuth ψ. The difference between the optimum values of β_{35} calculated for $\psi = 0$ and $\psi = \pi/2$ is, however, only slight. Accordingly, the formula corresponding to $\psi = \pi/2$ was always used so that a direct comparison could be made between the cases $\psi = 0$ and $\psi = \pi/2$.

Table 1

Figure	w_{31}	w_{20}		
1(*a*)	$0{\cdot}63\lambda$	$0{\cdot}0$	$\pm 0{\cdot}5\lambda$	$\pm 1{\cdot}0\lambda$
1(*b*)	$1{\cdot}26\lambda$	$0{\cdot}0$	$\pm 1{\cdot}0\lambda$	$\pm 2{\cdot}0\lambda$
1(*c*)	$1{\cdot}89\lambda$	$0{\cdot}0$	$\pm 1{\cdot}5\lambda$	$\pm 3{\cdot}0\lambda$

The defocusing was chosen so that the change in w_{20} was always of the same amount as in the corresponding spherical aberration cases. The numerical values of the aberration coefficients employed in these calculations are shown in table 2.

Table 2

Figure	w_{51}	w_{31}	w_{20}		
3(*a*)	$-2{\cdot}6\lambda$	$4{\cdot}6\lambda$	0	$\pm 1{\cdot}0\lambda$	$\pm 2{\cdot}0\lambda$
3(*b*)	$-2{\cdot}6\lambda$	$3{\cdot}3\lambda$	0	$\pm 1{\cdot}0\lambda$	$\pm 2{\cdot}0\lambda$
3(*c*)	$-2{\cdot}6\lambda$	$2{\cdot}0\lambda$	0	$\pm 1{\cdot}0\lambda$	$\pm 2{\cdot}0\lambda$
4(*a*)	$-3{\cdot}9\lambda$	$7{\cdot}25\lambda$	0	$\pm 1{\cdot}5\lambda$	$\pm 3{\cdot}0\lambda$
4(*b*)	$-3{\cdot}9\lambda$	$5{\cdot}30\lambda$	0	$\pm 1{\cdot}5\lambda$	$\pm 3{\cdot}0\lambda$
4(*c*)	$-3{\cdot}9\lambda$	$3{\cdot}35\lambda$	0	$\pm 1{\cdot}5\lambda$	$\pm 3{\cdot}0\lambda$
5(*a*)	$-5{\cdot}85\lambda$	$11{\cdot}125\lambda$	0	$\pm 2{\cdot}25\lambda$	$\pm 4{\cdot}5\lambda$
5(*b*)	$-5{\cdot}85\lambda$	$8{\cdot}200\lambda$	0	$\pm 2{\cdot}25\lambda$	$\pm 4{\cdot}5\lambda$
5(*c*)	$-5{\cdot}85\lambda$	$5{\cdot}275\lambda$	0	$\pm 2{\cdot}25\lambda$	$\pm 4{\cdot}5\lambda$
6(*a*)	$-7{\cdot}8\lambda$	$15{\cdot}0\lambda$	0	$\pm 3{\cdot}0\lambda$	$\pm 6{\cdot}0\lambda$
6(*b*)	$-7{\cdot}8\lambda$	$11{\cdot}1\lambda$	0	$\pm 3{\cdot}0\lambda$	$\pm 6{\cdot}0\lambda$
6(*c*)	$-7{\cdot}8\lambda$	$7{\cdot}2\lambda$	0	$\pm 3{\cdot}0\lambda$	$\pm 6{\cdot}0\lambda$

§ 3. DISCUSSION OF RESULTS

For small values of *s* any departure from the paraxial focus results in a deterioration of the response, i.e. the paraxial focus is the best focus. Furthermore, the response curves obtained in different focal planes are symmetrical about the best focus, that is to say changing the sign of w_{20} will have no effect on the response.

The response is not independent of ψ, and for small values of *s* the azimuth $\psi = 0$ (radial lines) always has a better response than for other values of ψ. Since for coma the frequency response is in general complex, it is instructive to plot the complex numbers representing the response for different frequencies on the

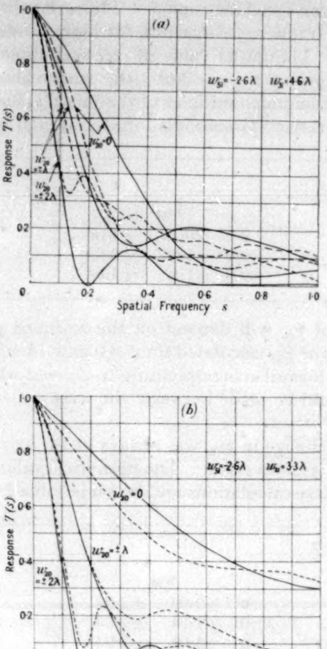

Figure 3.

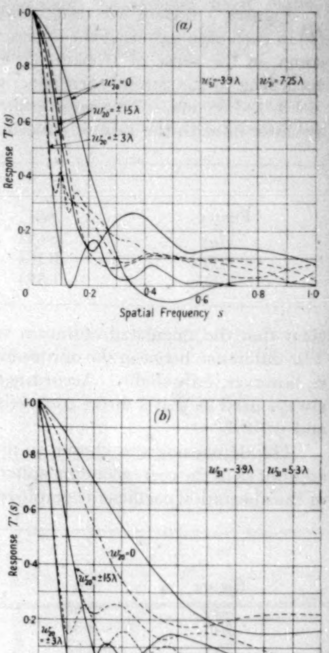

Figure 4.

Figures 3 and 4. Frequency response in the presence of primary and secondary coma in various focal plans. The full lines correspond to $\psi = 0$ and the broken lines to $\psi = \pi/2$.

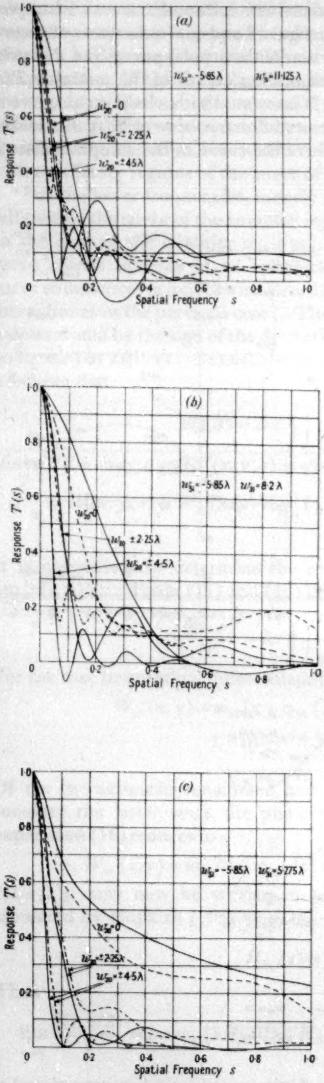

Figure 5.

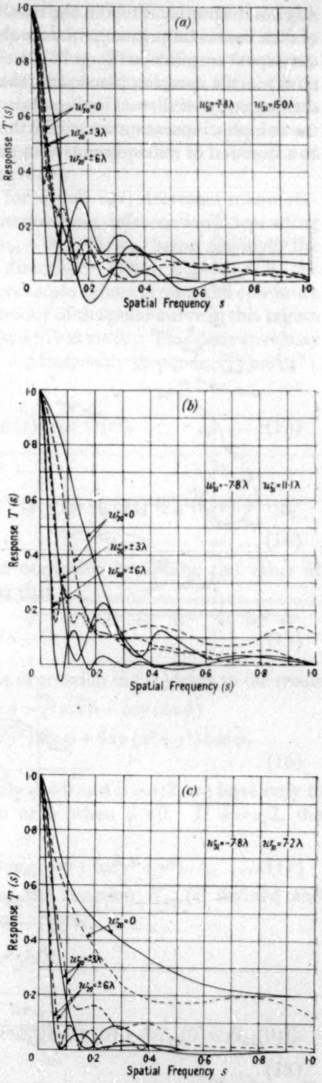

Figure 6.

Figures 5 and 6. Frequency response in the presence of primary and secondary coma in various focal planes. The full lines correspond to $\psi=0$ and the broken lines to $\psi=\pi/2$.

Argand diagram and to join the resulting points with a smooth curve. Examples of such curves for primarycoma are shown in figure 2 and curves for cases of secondary coma are given in figure 7. A comparison of these polar curves (i.e. Nyquist plots) in the complex plane with the corresponding curves of the modulus $T(s)$ shows that an oscillation in the value of $T(s)$ is associated with a loop in the curve of the complex representation. Furthermore, a stationary value of $T(s)$ considered as a function of s corresponds to a point where the curve in the complex plane is

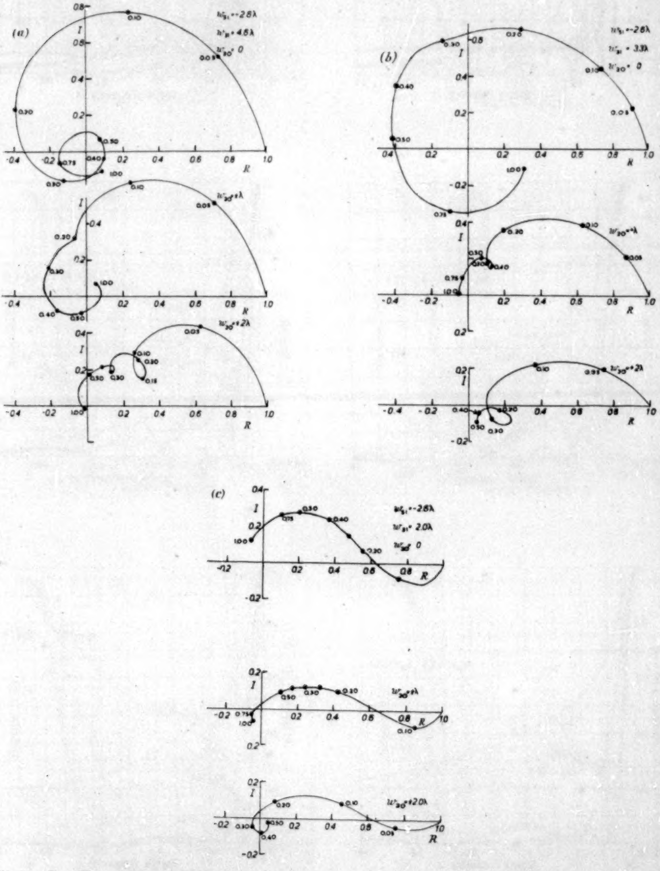

Figure 7. Frequency response in the presence of primary and secondary coma plotted on the Argand diagram. The numbers round the curves indicate the value of the spatial frequency s at that point.

perpendicular to the radius vector from the origin. If the argument of the frequency response is proportional to the spatial frequency, the image suffers merely a bodily displacement without relative shifting of the different frequency components. When the polar curve in the complex plane has a loop, there will be not only an oscillation in the value of $T(s)$, but also an oscillation in the phase, which will result in relative phase shift between the different components in the image. Qualitatively, therefore, one would not expect good image quality to be associated with oscillatory regions of the curve of $T(s)$ against s.

For the lower frequencies, namely those for which $T(s)$ decreases monotonically with s, the curve of the complex representation has a different form depending on the sign of the quantity $w_{31}+w_{51}$. If $w_{31}+w_{51}>0$, w_{51} being negative, the curve spirals inwards in an anticlockwise direction. When $w_{31}+w_{51}<0$, the curve commences in a clockwise direction but reverses almost at once and continues thereafter as in the previous case. The behaviour of the polar curve in this region is determined by the sign of the derivative $\partial\theta(s,\psi)/\partial s$ at $s=0$. This derivative may be formed as follows: from the expressions for frequency response, (1) and (7), it follows that

$$\theta(s,\psi)=2\pi s\iint_S V(x,y;s)\,dS+\mathrm{O}(s^3), \qquad \ldots\ldots(13)$$

where $dS=dxdy/s$ and $V(x,y;s)$ is given by

$$V(x,y;s)=W_x{}'(x,y)+\frac{1}{3!}(\tfrac{1}{2}s)^2W_x{}'''(x,y)+\frac{1}{5!}(\tfrac{1}{2}s)^4W_x{}^{\mathrm{v}}(x,y). \qquad \ldots\ldots(14)$$

It is convenient to determine the required derivative by finding the value of $\lim_{s\to 0}\{\theta(s,\psi)/s\}$. From (13) and (14) it is clear that

$$\frac{\theta(s,\psi)}{s}=2\pi\iint_S W_x{}'dS+\mathrm{O}(s^2). \qquad \ldots\ldots(15)$$

For the case in question, differentiation of the expression in (11) leads to the result

$$\begin{aligned}W_x{}'(x,y)=w_{20}2x+w_{31}\,(3x^2\sin\psi+y^2\sin\psi+2xy\cos\psi)\\ +w_{51}\{(5x^4+y^4+6x^2y^2)\sin\psi+4xy\,(x^2+y^2)\cos\psi\}.\end{aligned} \qquad \ldots\ldots(16)$$

Of the two azimuths considered here, namely $\psi=0$ and $\psi=\pi/2$, we have only to consider the latter since the phase is zero or π when $\psi=0$. If $\psi=\pi/2$, the expression (16) reduces to

$$W_x{}'(x,y)=w_{20}2x+w_{31}(3x^2+y^2)+w_{51}(5x^4+6x^2y^2+y^4). \qquad \ldots\ldots(17)$$

$\theta(s,\pi/2)/s$ may now be written in terms of the function $H_{k,l}(s)$ defined and tabulated by Hopkins (1957 b) to be

$$H_{k,l}(s)=\iint_S x^ky^ldS.$$

Thus

$$\lim_{s\to 0}\frac{\theta(s,\pi/2)}{s}=2\pi\{w_{31}[3H_{20}(0)+H_{02}(0)]+w_{51}[5H_{40}(0)+6H_{22}(0)+H_{04}(0)]\}. \qquad \ldots\ldots(18)$$

The quantities in square brackets in (18) both reduce to unity when $s\to 0$ so that

$$\theta(s,\pi/2)=2\pi s(w_{31}+w_{51})+\mathrm{O}(s^3) \qquad \ldots\ldots(19)$$

and

$$\left[\frac{\partial\theta(s,\pi/2)}{\partial s}\right]_{s=0} = 2\pi(w_{31}+w_{51}). \qquad \ldots\ldots(20)$$

The derivative of $\theta(s,\pi/2)$ at the origin is thus the same for all focal planes, and depends only on the sum of the primary and secondary coma coefficients.

The lateral shift of the component of spatial frequency s is given by the formula

$$\delta u' = \frac{-\theta(s,\pi/2)}{2\pi s}$$

so that in the presence of coma, components of limitingly small frequency are shifted by an amount

$$[\delta u']_{s=0} = -(w_{31}+w_{51}).$$

If this lateral shift remains constant for finite values of s up to the value for which the response has fallen to say 0·2, all significant frequency components in the image will suffer the same lateral displacement. No deterioration of image quality will then result from phase shift since the image will merely be displaced as a whole, apart from those components having only very low contrast. Results of investigations carried out indicate that the above condition is fulfilled within very small limits with the low-frequency optimum correction and best focal plane.

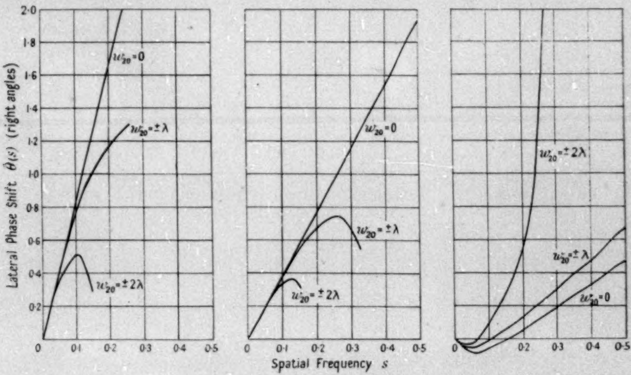

$w_{31}=4{\cdot}6\lambda$ $w_{31}=3{\cdot}3\lambda$ $w_{31}=2{\cdot}0\lambda$

Figure 8. Lateral phase shift for primary and secondary coma $w_{51}=-2{\cdot}6\lambda$ in various focal planes plotted as a function of the spatial frequency.

By plotting $\theta(s,\pi/2)$ against s on a suitably large scale, useful information may be obtained regarding the extent to which the curve departs from a straight line through the origin, and therefore on the influence of relative phase shifting on the image quality. This was done for all the results obtained and the best fitting straight line drawn through the origin (see figures 2*b* and 8). Hopkins (private communication) has proposed a way of specifying a tolerance on phase shift and has shown that a departure of 0·2 radians from linear variation of $\theta(s,\psi)$ with s represents a maximum change in intensity at any point of about 20%. By noting the value of s at which the curve of $\theta(s, \pi/2)$ first differed from a straight line through the origin by this amount, and also the value of $D(s, \pi/2)$ when this occurred it was possible to draw the following conclusions:

(i) In the best plane of focus for low frequencies, i.e. the paraxial focal plane, and when, for negative values of w_{51} the marginal part of the wave front in the azimuth $\phi=0$ (meridian plane) is behind the reference sphere $(w_{31}+w_{51}>0)$ the curve of $\theta(s, \pi/2)$ lies within the above tolerance for all frequencies for which $D(s, \pi/2)$ exceeds 0·2. Frequency components for which the response is less than 0·2 would not be expected to make a significant contribution to the image. The phase shift may thus usually be ignored in these cases. Examples illustrating this rule will be found in the curves for the best plane of focus in the diagrams labelled (*a*) and (*b*) of figures (3)–(6).

(ii) Again in the paraxial plane of focus, but when the marginal wave front is in front of the reference sphere $(w_{31}+w_{51}<0)$, relative phase shifting begins to be significant at the point where the response has dropped to about 0·4. This would frequently be expected to affect the image quality, since frequency components having a response of 0·4 can easily be significant in the image. Examples of such cases will be found in the diagrams labelled (*c*) in figures 3–6.

(iii) The relative phase shifting becomes significant when the gradient of the graph of $T(s)$ plotted as a function of s suffers a sharp change. This is so in the examples referred to in (ii) above and also when the marginal wave front is considerably behind the reference sphere as may be seen in the diagrams labelled (*a*) for the cases when the focal plane is at a considerable distance from the best focus. In such cases a flattening of the response curve takes place. For this reason one might reasonably expect good resolution from a Cobb chart for relatively high frequencies, whereas the phase shifting could seriously affect the general performance of the lens. Caution should therefore be exercised when using Cobb charts to test lenses suffering from asymmetrical aberrations. The results on which these conclusions are based are shown in table 3; s' is the greatest value of s for which the relative phase shift lies within the tolerance.

Table 3

		$w_{20}=0$		2nd focal plane		3rd focal plane	
w_{51}	w_{31}	s'	$D(s')$	s'	$D(s')$	s'	$D(s')$
−2·6	4·6	0·40	0·10	0·20	0·32	0·10	0·41
−2·6	3·3	2·00	0·00	0·25	0·28	0·15	0·13
−2·6	2·0	0·50	0·39	0·45	0·10	0·20	0·13
−3·9	7·25	0·20	0·13	0·10	0·42	0·10	0·38
−3·9	5·30	0·75	0·22	0·15	0·31	0·10	0·15
−3·9	3·35	0·30	0·45	0·25	0·16	0·15	0·04
−5·85	11·125	0·14	0·11	0·08	0·32	0·04	0·44
−5·85	8·200	0·80	0·19	0·10	0·31	0·06	0·19
−5·85	5·275	0·25	0·40	0·15	0·20	0·10	0·02
−7·8	15·0	0·08	0·22	0·06	0·31	0·03	0·43
−7·8	11·1	0·95	0·14	0·08	0·28	0·04	0·27
−7·8	7·2	0·35	0·21	0·16	0·15	0·14	0·01

ACKNOWLEDGMENT

My thanks are due to Dr. H. H. Hopkins for suggesting this problem and for many useful discussions relating to it.

REFERENCES

DE, M., and NATH, B. K., 1958, *Optik*, **15**, 739.
GOODBODY, A. M., 1958, *Proc. Phys. Soc.*, **72**, 441.
HOPKINS, H. H., 1957 a, *Proc. Phys. Soc.* B, **70**, 1002.
—— 1957 b, *Ibid.*, **70**, 449.

Note.—Since the preparation of this paper, De and Nath (1958) have published an account of the calculation of response functions for systems suffering from primary coma. These authors have employed an analytical method which leads to a double series of Bessel functions.

Neutron-Proton Pairing Interaction in Transuranic Elements

By N. C. GHOSH and D. SEN†
Department of Physics, University of Calcutta

MS. received 22nd September 1959, *in final form* 1st *December* 1959

Abstract. An attempt has been made to analyse the data on the last nucleon binding energies of transuranic elements. Some interesting results are obtained regarding the behaviour of the λ term introduced by Ghoshal. Some confirmatory evidence is also obtained regarding the sub-shell at $N=152$.

---

§ 1. INTRODUCTION

STUDIES have been made on the pairing interaction between neutrons and protons in the unfilled shells (Feather 1953, Green 1953, Edmonds 1953, Ghoshal and Saxena 1956). Discontinuities have been found to occur in the binding energy of the last nucleon in the 'magic number' zones. These and other discontinuities have been more or less explained on the basis of the *jj*-coupling shell model of Mayer. Here an attempt has been made to analyse, from this point of view, the data on last nucleon binding energies of 'transuranic elements' compiled by Hyde and Seaborg (1957). We have followed the method of analysis of Ghoshal and Saxena (1956) and have used it for transuranic elements. The results obtained, however, differ in certain aspects from Ghoshal's findings. He introduced a new term λ to account for the interaction between the last odd proton and the last odd neutron. This λ is seen to have an interesting behaviour.

§ 2. ESTIMATION OF λ

According to Ghoshal, the mass formula for a nucleus having $Z+1$ protons and $N+1$ neutrons, may be written as

$$M(Z+1,N+1)=f(Z+1,N+1)-2\sum_{j}^{Z/2}\pi_j-2\sum_{k}^{N/2}\nu_k-\lambda(Z+1,N+1)$$

where $f(Z,N)$, Z and N being even, expresses the functional dependence of nuclear mass on Z and N; π_j and ν_k are the pairing energies per nucleon of protons and neutrons respectively. The λ term is introduced to account for the pairing interaction between the last odd neutron and the last odd proton. Here we have assumed that the pairing energy of neutron pairs or proton pairs has no effect on the last nucleon binding energy, i.e. we have assumed that the addition of an extra nucleon does not disturb the original shell-configuration. We hope to find out later on if there is any such perturbation effect, with the help of a method followed by Pryce (1952).

---

† Now at the Physics Department, Jadavpur University.

Following the above mass formula, we have, for a series of isotones containing an even number of neutrons,

$$B_n^{ee}(Z,N)=\Delta f_n(Z,N)+2\nu_{N/2} \qquad \ldots\ldots(1a)$$

$$B_n^{oe}(Z+1,N)=\Delta f_n(Z+1,N)+2\nu_{N/2}-\lambda(Z+1,N-1) \qquad \ldots\ldots(1b)$$

$$B_n^{ee}(Z+2,N)=\Delta f_n(Z+2,N)+2\nu_{N/2}. \qquad \ldots\ldots(1c)$$

For the case of odd neutron isotones,

$$B_n^{eo}(Z,N-1)=\Delta f_n(Z,N-1) \qquad \ldots\ldots(2a)$$

$$B_n^{oo}(Z+1,N-1)=\Delta f_n(Z+1,N-1)+\lambda(Z+1,N-1) \qquad \ldots\ldots(2b)$$

$$B_n^{eo}(Z+2,N-1)=\Delta f_n(Z+2,N-1). \qquad \ldots\ldots(2c)$$

Δf_n here gives the variation in bulk binding energy in the mass equation between the nuclei (Z,N) and $(Z,N-1)$ together with the neutron mass. Further, there is enough evidence to take Δf_n as varying linearly with A.

For the binding energy of the last proton, we have, for a series of isotopes containing an even number of protons,

$$B_p^{ee}(Z+2,N-2)=\Delta f_p(Z+2,N-2)+2\pi_{(Z+2)/2} \qquad \ldots\ldots(3a)$$

$$B_p^{eo}(Z+2,N-1)=\Delta f_p(Z+2,N-1)+2\pi_{(Z+2)/2}-\lambda(Z+1,N-1) \qquad \ldots\ldots(3b)$$

$$B_p^{ee}(Z+2,N)=\Delta f_p(Z+2,N)+2\pi_{(Z+2)/2}. \qquad \ldots\ldots(3c)$$

For the case of odd proton isotopes,

$$B_p^{oe}(Z+1,N-2)=\Delta f_p(Z+1,N-2) \qquad \ldots\ldots(4a)$$

$$B_p^{oo}(Z+1,N-1)=\Delta f_p(Z+1,N-1)+\lambda(Z+1,N-1) \qquad \ldots\ldots(4b)$$

$$B_p^{oe}(Z+1,N)=\Delta f_p(Z+1,N). \qquad \ldots\ldots(4c)$$

Behaviour of Δf_p is analogous to that of Δf_n. A study of the above equations shows that the introduction of λ causes a zigzag curve for plots (B_p, N) or (B_n, Z), which would have otherwise been approximately linear.

Values of λ have been estimated by taking the average of the independent evaluations of λ given by the four following equations (Ghoshal and Saxena 1956):

$$\lambda(Z+1,N-1)=\tfrac{1}{2}[B_n^{ee}(Z,N)+B_n^{ee}(Z+2,N)-2B_n^{oe}(Z+1,N)] \qquad \ldots\ldots(5a)$$

$$\lambda(Z+1,N-1)=-\tfrac{1}{2}[B_n^{eo}(Z,N-1)+B_n^{eo}(Z+2,N-1)-2B_n^{oo}(Z+1,N-1)] \qquad \ldots\ldots(5b)$$

$$\lambda(Z+1,N-1)=\tfrac{1}{2}[B_p^{ee}(Z+2,N-2)+B_p^{ee}(Z+2,N)-2B_p^{eo}(Z+2,N-1)] \qquad \ldots\ldots(5c)$$

$$\lambda(Z+1,N-1)=-\tfrac{1}{2}[B_p^{oe}(Z+1,N-2)+B_p^{oe}(Z+1,N)-2B_p^{oo}(Z+1,N-1)]. \qquad \ldots\ldots(5d)$$

To check whether it is possible to take an average value for λ, curves for independent λ values are plotted against N for constant Z value and it is found that they do not depart much from each other.

§ 3. BEHAVIOUR OF THE CURVES

3.1. (B_n, Z) *Plot*

Figures 1 and 2 give B_n plotted against Z (at constant N) for $Z > 92$ and B_p plotted against N (at constant Z) for $N > 134$ (transuranic zone). The binding energy values have been taken from the compilations of Hyde and Seaborg (1957).

Following Ghoshal we also grouped the B_n curve for an odd N with the B_n curve for the next higher even N, and likewise for the B_p curves.

From figure 1 it is seen that there is more or less regularity in neutron binding energy. The e–o points (for odd N) and e–e points (for even N) increase linearly with Z up to $N=146$, though there are some irregularities in between. This linearity is still maintained up to $N=150$ with more irregularities. This may be due to errors in binding energies that have been considered.

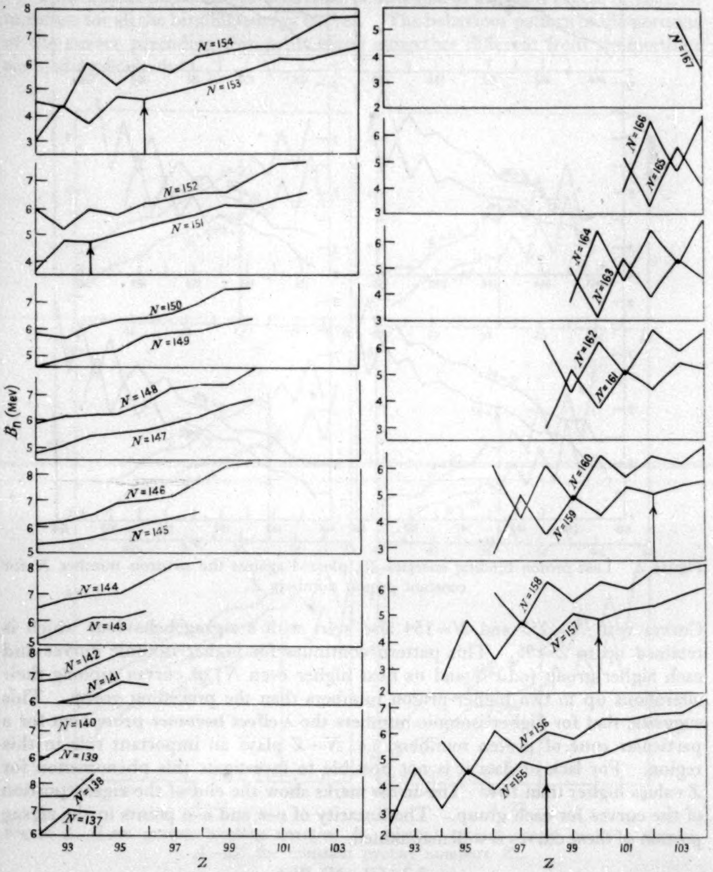

Figure 1. Last neutron binding energies B_n plotted against the proton number Z for constant neutron numbers N.

A peculiarity is observed for the curves with $N=151$ and $N=152$. The curves begin with prominent alterations from $Z=92$, which die off at $Z=94$ and then they show the same characteristics as have been found in the former curves.

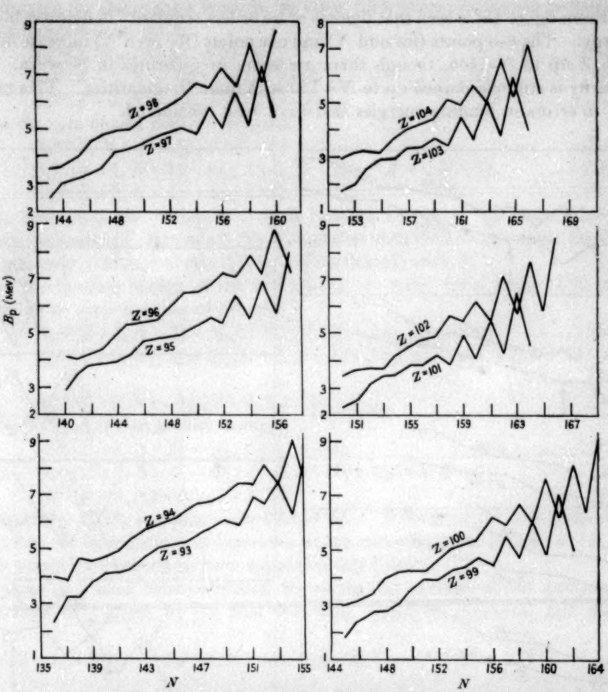

Figure 2. Last proton binding energies B_p plotted against the neutron number N for constant proton numbers Z.

Curves with $N = 153$ and $N = 154$ also start with a zigzag behaviour which is retained up to $Z = 96$. This pattern continues for higher isotonic curves and each higher group (odd N and its next higher even N) of curves prolong their alterations up to two higher proton numbers than the preceding group. This suggests, that for higher isotonic numbers the λ effect becomes prominent for a particular zone of proton numbers, i.e. $N - Z$ plays an important role in this region. For lack of data it is not possible to investigate this phenomenon for Z values higher than 104. The arrow marks show the end of the zigzag portion of the curves for each group. The linearity of e–e and e–o points in the zigzag portion of these curves is well maintained.

3.2. (B_p, N) *Plot*

Figure 2 gives the plot of B_p against N for different isotopic numbers. These are also grouped as in the case of B_n against Z. These also show regularity in proton binding energies as expected from the equations. As in the case of (B_n, Z) plots, remarkable λ effect is observed for isotopic series $Z = 93$ and $Z = 94$ from $N = 150$. This is observed in all the isotopic series considered here and these pronounced alterations start for the next group just after an excess of two neutrons from the preceding group. This has been studied for isotopic series starting from $Z=93$ to $Z=104$. The portions of the curves showing violent zigzag nature give the maximum linearity; o–e (for odd Z) and e–e (for even Z) points when joined show linear increase with N.

Thus a clear departure in behaviour is obtained at a certain excess in neutron numbers for all the binding energy curves. The behaviour pattern of the portions of the curves preceding this point being altogether different from the portions succeeding this point.

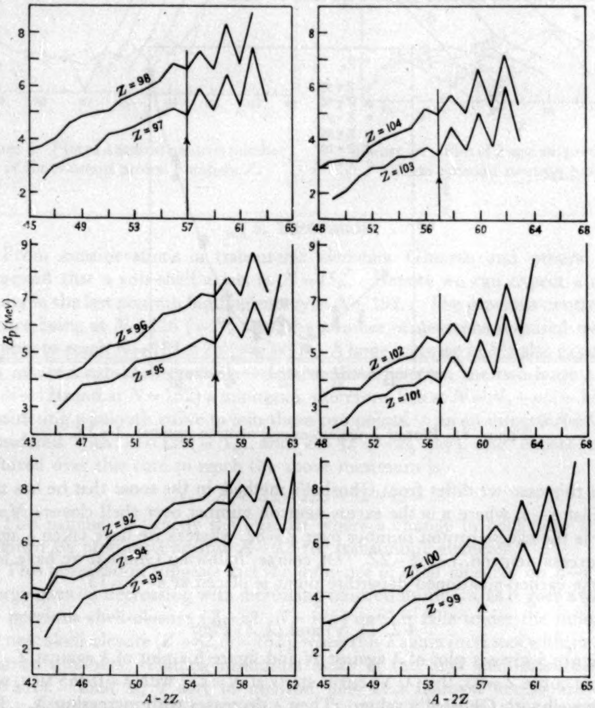

Figure 3. **Last proton binding energies** B plotted against excess neutron number $A-2Z$ for constant proton numbers Z.

3.3. ($B_p, A-2Z$) *Plot*

Prompted by the above suggestion, we have plotted B_p against $A-2Z$ in figure 3. A study of these gives an interesting result in that they show the above-mentioned departure point to be placed at an excess neutron number 57 for all the curves.

§ 4. BEHAVIOUR OF λ

4.1. (λ, $A-2Z$) *Plot*

Figure 4 gives a plot of λ (average) against $A-2Z$ which gives a minimum near $A-2Z=51$. The λ value for $Z=93$, $A-2Z=44$ has been checked with Ghoshal's data and was found to agree well with his observation. This curve starts with $\lambda=0{\cdot}455$ Mev at $A-2Z=44$, with a decrease in λ value with increase in $A-2Z$, until it becomes negative at $A-2Z=50$. After this the λ value increases with increase in $A-2Z$ with a steep inclination starting from $A-2Z=56$. This has been investigated up to $A-2Z=62$, where λ is still on increasing trend. This could not be studied further for lack of data.

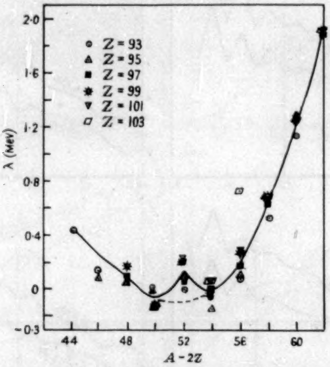

Figure 4. Plot of λ against excess neutron number $A-2Z$.

In this case we differ from Ghoshal's method in the sense that he has taken λ against $n-z$, where n is the excess neutron number over shell closure $N=126$ and z is the excess proton number over $Z=82$, whereas we have taken λ against total excess neutron, i.e. $A-2Z$. Of course, following Ghoshal we have found that the earlier-mentioned departure point is placed at $n-z=13$.

4.2. (λ, N) and (λ, Z) *Plots*

Figure 5 gives a plot of λ against N and figure 6 a plot of λ against Z. For isotopic curve $Z=93$, the (λ, N) curve starts at $N=137$ with $\lambda=0{\cdot}455$ Mev, which agrees well with Ghoshal's value. Then λ decreases with increasing N. From $N=147$, λ increases linearly with increasing N. Between $N=143$ to 147 the curve reaches a minimum, this zone of the curve being more or less horizontal. Other isotopic curves $Z=95$, 97, etc. start from minimum zones and then increase linearly with increasing N from $N=149$, 151, etc. respectively. This characteristic is maintained for all the isotopic curves.

The isotonic curves given in figure 6 show λ to decrease with increasing Z. Our plots of (λ, N) and (λ, Z) show exactly opposite trends in their behaviour to that obtained by Ghoshal. This, however, seems to be explicable.

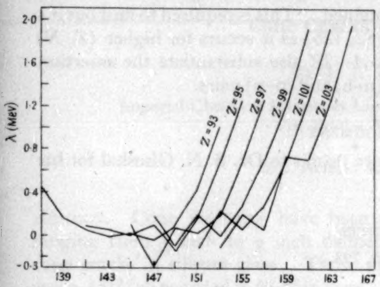

Figure 5. Plot of λ against neutron number N for constant proton numbers Z.

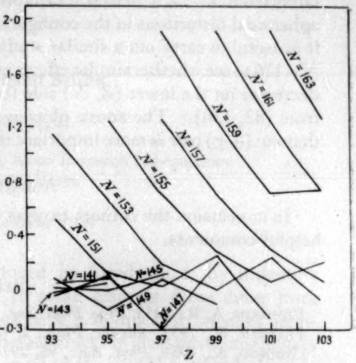

Figure 6. Plot of λ against proton number Z for constant neutron numbers N.

§ 5. Discussion

From considerations in transuranic elements Ghiorso and others (1954) suggested that a sub-shell exists at $N=152$. Hence, we can expect a discontinuity in the last neutron binding energy at $N=152$. The previous neutron shell closure being at $N=126$ ($=N_0$ say), the number of neutrons required over this number to reach $N=152$ is 26 ($=n$ say). A large increase in λ is also expected at this neutron sub-shell crossing. Intermediate between the two large λ values (at $N=126$ and at $N=152$) a minimum, therefore, lies at $N=N_0+n/2=126+13$, considering a smooth curve to join these two points. As an unperturbed core is considered with $N=126(=N_0)$ and $Z=82$ ($=Z_0$ say), the excess neutron required over this core to reach the above minimum is

$$N_0-Z_0+n/2=126-82+13=57.$$

This number is exactly the number where a change in behaviour starts, as obtained by plotting λ against $A-2Z$ for transuranic elements.

This observation suggests that the influence of shell closures on n–p pairing energy goes on decreasing with increasing neutron numbers, as it goes away from the previous shell-closure ($Z=82$, $N=126$) until it falls under the influence of the next shell-closure ($Z=82, N=152$), when this λ again increases with increasing neutron numbers, reaching maximum again at the next shell-closure ($Z=82$, $N=152$). That is, a sort of neutron hole and neutron excess are formed symmetrically on the two sides of the shell-closure as the $(\lambda, A-2Z)$ curve approaches and crosses this point respectively.

This also explains why the trends in the curves obtained by Ghoshal are exactly opposite to those given here. They worked in the region of decline of the $(\lambda, A-2Z)$ curve preceding the point $A-2Z=57$ whereas our work is confined mainly to the region of the curve under the influence of the next higher neutron sub-shell assignment at $N=152$, after crossing $A-2Z=57$. As our plotting has been started just from the point where Ghoshal ended we have also worked in the trough region of the $(\lambda, A-2Z)$ curve which yielded the minimum region of the curve from $A-2Z=50$ to $A-2Z=56$. This shift in value from 57 may be due to spheroidal distortions in the configurations in the heavy nuclide zone. We think it is useful to carry out a similar study over the large (Z, N) region below $Z=82$, $N=126$ to see whether similar effects are obtained. This is required to find out if λ decreases on the lower (Z, N) side from (82, 126) as it occurs for higher (Z, N) from (82, 126). The above plots against $A-2Z$ also substantiate the assertion that the (n–p) pair is more important than (n–n) and (p–p) pairs.

ACKNOWLEDGMENT

In conclusion the authors express sincere thanks to Dr. S. N. Ghoshal for his helpful comments.

REFERENCES

EDMONDS, A. R., 1953, *Proc. Phys. Soc.* A, **66,** 793.
FEATHER, N., 1953, *Advanc. Phys.*, **2,** 141.
GHIORSO, A., 1954, *Phys. Rev.*, **95,** 293.
GHOSHAL, S. N., and SAXENA, A. N., 1956, *Proc. Phys. Soc.* A, **69,** 293.
GREEN, A. E. S., and EDWARDS, D. F., 1953, *Phys. Rev.*, **91,** 46.
HYDE, E. K., and SEABORG, G. T., 1957, *Hand. d. Phys.*, **42,** 294 (Berlin: Springer).
PRYCE, M. H. L., 1952, *Proc. Phys. Soc.* A, **65,** 776.

Cone Cracks in Fused Silica

By J. J. BENBOW†

Imperial Chemical Industries Limited, Akers Research Laboratories,
The Frythe, Welwyn, Herts.

MS. received 4th November 1959

Abstract. Cone fractures have been produced in fused silica, by indenters ranging from $\frac{1}{64}$ inch to $\frac{1}{4}$ inch diameter. In some respects these differ from cone cracks in silicate glass. Those in silica have a significantly smaller semi-angle, 65·5° as opposed to 68·5° in glass. Whereas cracks in glass grow indefinitely under a constant load, and remain visibly open when the load is removed, those in quartz cease to grow about ten minutes after each increment of the load, and cannot be seen when the specimen is unloaded.

§ 1. Introduction

Experiments on stable fractures which involved the production of cone cracks in blocks of glass have been described by Roesler (1956, to be referred to as I). Stable fractures can also be produced in sheets of plastic and measurements on these can be used to determine the specific fracture energy of high polymers (Benbow and Roesler 1957, to be referred to as II, see also Svensson 1958).

Several questions arise out of the work described in I. For example, the fracture energy found for glass is surprisingly large in comparison with that found by Griffith (1924), although small compared with values found in II for high polymers. Cone cracks in glass continue to grow under a constant indenter force; their growth has been measured over a period of many hours (see figure 2 of I). When the force is removed the cracks in glass do not quite close up, which suggests that plastic deformation has occurred.

It is of interest to study these effects in other typically brittle substances. Fused silica is ideal for this purpose since many of its properties are appreciably different from those of composite glasses; it has a much higher softening point, very small internal friction and an exceptionally low Poisson's ratio.

§ 2. Experimental Method

The apparatus used with indenters having diameters greater than $\frac{1}{16}$ inch was that described in I. Essentially, this is a hydraulic press capable of producing forces up to about 5×10^8 dynes. To produce a cone crack the indenter was put on one face of the specimen (in the form of a block 2 in. × 2 in. × $1\frac{1}{2}$ in.) and both were placed into the press. The load was slowly increased until the initial ring crack appeared, and then held constant for ten minutes. A preliminary experiment had shown that in silica the crack did not increase appreciably in diameter after the load, or increments to the load, had been applied for ten minutes. Thus after ten minutes had elaspsed the diameter of the base of the cone was measured with a cathetometer with an accuracy to ± 0·02 mm. The load was then increased by at least 10% and the diameter again measured after a lapse of ten minutes. At each increment of the load the force on the piston was measured. Since the forces to be measured varied over a wide range two gauges were used to obtain the maximum accuracy, one for the small indenters the other for the large.

---

† Present address: I.C.I. Ltd., Plastics Division, Welwyn Garden City, Herts.

For indenters of less than $\frac{1}{16}$ inch diameter a spring loaded press was used. Six tension springs in parallel could be extended by a screw, and the resulting force was used to press the indenter against the silica block. A proving ring mounted in series with the springs and the indenter holder was used to measure the force. As a check on the apparatus a few measurements were made on this press with an indenter of $\frac{1}{16}$ inch diameter. These agree with those obtained with the hydraulic press.

The small indenters were easily damaged. At first they were produced by turning down silver–steel rods and then hardening the tips (the process was also used for the large indenters). A better method was developed in which the small indenters were made from ball bearings. To do this $\frac{1}{64}$ inch and $\frac{1}{32}$ inch diameter ball bearings were carefully ground by hand until they were hemispherical. The grinding was done sufficiently slowly to prevent excessive heating. The flat surface was then used as the indenter. These indenters could be easily replaced when necessary.

Using both forms of apparatus the indenters diameters could be varied from $\frac{1}{64}$ inch to $\frac{1}{4}$ inch. An eye-piece mounted in a vernier protractor and fitted with a cross-wire was used to measure the angle of the cones. The accuracy to which the angle could be measured (± 5 min) was ample in view of the variation of the angle between experiments. The average value of the semi-angle was 65·5 ± 1°. Figure 1 (Plate) shows a typical crack.

§ 3. DISCUSSION OF RESULTS

A convenient way of summarizing the results is by plotting the logarithm of the cone diameter as a function of the logarithm of the force, as in figure 2. By introducing the small indenters already referred to it has been possible to produce cracks under forces from 10^7 to 240×10^7 dynes. The scatter of the results for silica is greater than for the glass experiments in I because only a limited number of silica blocks was available. This necessitated every crack being measured. Glass blocks were plentiful so that Roesler discarded poorly formed cones. The increased scatter of the present experiments at low forces may further be due to imperfections in the hand-ground indenters which may not have been absolutely flat.

The theory of the dependence of the cone diameter on the indenter force is discussed in I. Equation (5) of I states that if the Griffith hypothesis is valid (i.e. if the balance of fracture energy and mechanical energy controls the fracture process) then for an idealized cone fracture the relation

$$S/P^{2/3} = n \qquad \ldots\ldots(1)$$

should be true, where n is a constant of the material, S is the diameter at the base of the cone and P the force on the indenter.

Thus a logarithmic plot of S against P should be linear and have a slope of 2/3. Such a line has been drawn in figure 2 of the present paper and the experimental points for fused silica fit it well over the entire range. The average value of P for $S = 2$ cm was $1{\cdot}26 \times 10^9$ dynes.

It is clear then that the Griffith hypothesis is true for fused silica, just as it was found to be true for glass in I, and for plastics in II. The determination of the numerical value of the fracture energy would require knowledge of the constant ω, as defined in I, for the empirical crack angle and the Poisson's ratio characteristic of silica. Work on this question and on the improvement of the accuracy of the computations for glass is being carried out by Dr. F. C. Roesler at I.C.I. Ltd., Billingham Division, but it may be some time before his results will be available.

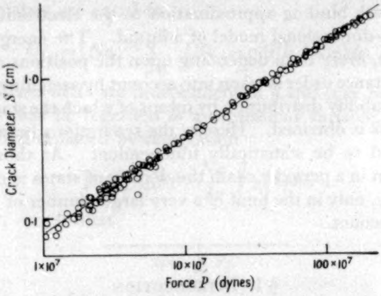

Figure 2. Variation of the crack diameter with indenter force.

REFERENCES

Benbow, J. J., and **Roesler, F. C.**, 1957, *Proc. Phys. Soc.* B, **70**, 201.
Griffith, A. A., 1924, *Proc. Inst. Congr. Appl. Mech.* (*Delft*), 55.
Roesler, F. C., 1956, *Proc. Phys. Soc.* B, **69**, 981.
Svensson, N. L., 1958, *Proc. Phys. Soc.* B, **71**, 136.

Electrons in Weak Interaction with a Chain of Atoms

By PRIYAMVADA SAH† and R. EISENSCHITZ
Department of Physics, Queen Mary College, University of London

MS. received 7th December 1959

Abstract. The weak binding approximation to the electronic energy spectrum is applied to a one-dimensional model of a liquid. The energy is expanded in a perturbation series, every term depending upon the positions of all atoms. The absence of long distance order is taken into account by assigning to the coordinates of the atoms a probability distribution by means of which the statistical expectation of the energy levels is obtained. Hereby the separations between neighbouring atoms are assumed to be statistically independent. At those energies which would be forbidden in a periodic chain the density of states is reduced but would vanish, presumably, only in the limit of a very large number of terms in the series being taken into account.

§ 1. INTRODUCTION

THE electronic energy spectrum of a one-dimensional array of atoms was investigated by Eisenschitz and Dean (1957) using the tight binding approximation. A band structure was found but it is not known whether this result is perhaps due to the method of approximation which tends to overrate discontinuities. As a check the same problem is considered in the present paper by a weak binding theory which is somewhat biased against discontinuities. This approach has the additional merit that it could provide wave functions and be applicable to liquids in three dimensions.

From the outset is may be taken for granted that a weak binding theory cannot give any account of a band structure in the conventional low approximations. This follows from the corresondence of the theory with the theory of x-ray diffraction (cf. Krishnan and Bhatia 1945) and the fact that the diffraction pattern of liquids shows haloes but no sharp rings. It remains to investigate the contributions to the energy of virtual multiple transitions. In this paper expressions are obtained for these contributions and their significance is discussed.

§ 2. ASSUMPTIONS AND NOTATION

Single conduction electrons are assumed to be subject to forces of interaction with all atoms in a linear chain. The forces are independent of the time and are to take account of the mean mutual interaction of the conduction electrons and of their interaction with the ions. It is assumed that the interaction of the electron with any atom is independent of the presence of other atoms. This is taken into account by letting the potential energy U have the form

$$U(x) = \sum_{l=1}^{N} u(x - x_l) \qquad \ldots\ldots(2.1)$$

---

† Now at New G2 Quarters, B.H.U., Varanasi, India.

where x and x_l are the coordinates of the electron and the atoms and u is the contribution of any single atom.

In weak binding theories the unperturbed wave functions are

$$\psi_k(x) = (Na)^{-1/2} \exp(ikx) \qquad \ldots\ldots (2.2)$$

$$k = 2\pi\nu/Na \qquad \nu = 0, \pm 1, \pm 2 \ldots \qquad \ldots\ldots (2.3)$$

and where a is the mean distance between neighbouring atoms. The unperturbed energy levels are the eigenvalues of the kinetic energy and equal to $\hbar^2 k^2/2m$ where m is the electronic mass; every level is twofold degenerate. Elements of the perturbation matrix are equal to

$$U_{kp} = (Na)^{-1} \int_0^{Na} U(x) \exp[i(k-p)x]dx. \qquad \ldots\ldots (2.4)$$

The diagonal elements of U are independent of k and may be set equal to zero.

If N is large k may be regarded as a continuous variable. Summation of a function $\chi(k)$ is then replaced by integration

$$\lim_{N\to\infty} \sum_k \chi(k) = \frac{Na}{2\pi} \int \chi(k) dk. \qquad \ldots\ldots (2.5)$$

Let $r_l = x_l - x_{l-1}$, $r_1 = x_1$ so that

$$x_l = \sum_{j=1}^{l} r_j. \qquad \ldots\ldots (2.6)$$

Denote the Fourier transform of u by

$$\left.\begin{aligned} v(q) &= \int \exp(iqy) u(y) dy \\ v(0) &= 0 \end{aligned}\right\} \qquad \ldots\ldots (2.7)$$

and the 'sum over phases' by

$$\rho(q) = \sum_{l=1}^{N} \exp(iqx_l) = \sum_{l=1}^{N} \exp\left(iq \sum_{j=1}^{l} r_j\right). \qquad \ldots\ldots (2.8)$$

Then the perturbation matrix is written in the form

$$U_{kp} = (Na)^{-1} v(k-p) \rho(k-p). \qquad \ldots\ldots (2.9)$$

The energy levels of an electron are determined by products of these matrix elements. They are, by the way of ρ, explicitly dependent upon the coordinates of the atoms.

In order to obtain the energy spectrum of a chain with short range order the atomic coordinates are considered to be random variables to which a probability distribution $[F(x_1, x_2, \ldots\ldots x_N)]$ is assigned. The expectation of $\rho(q)$ for $q \neq 0$ will then be finite. In contrast $\rho(q)$ in a periodic chain would either vanish or be infinite $O(N)$. Hereby it is assumed that the distances between neighbouring atoms are statistically independent, so that

$$F = \prod_{l=1}^{N} f(r_l) \qquad \ldots\ldots (2.10)$$

where f is a probability distribution for a single variable.

$$f \geqslant 0 \quad \text{and} \quad \int_0^\infty f(r_l) dr_l = 1 \qquad \int_0^\infty r_l f(r_l) dr_l = a.$$

The function f is not specified in detail but it is assumed that $f(0) = 0$.

The Fourier transform of the probability distribution is denoted by

$$s(q)=\int f(r_l)\exp(iqr_l)\,dr_l \qquad \ldots\ldots(2.11)$$

and $|s(q)|<1$ if $q\neq 0$.

The statistical expectation of the energy levels depends upon the statistical expectation of the sum over phases and of products of these sums. The deduction of these statistical averages is the main problem in the weak binding theories and can be solved correctly for our one-dimensional system. This deduction is performed in §§ 3–6, and applied in §§ 7–10 to the perturbation expansion of the energy. Results are discussed in § 11.

§ 3. PRODUCT OF SUMS OVER PHASES

The quantity

$$\Xi(n,N)=\prod_{j=1}^{n}\rho(q_j) \qquad (n<N) \qquad \ldots\ldots(3.1)$$

depends upon the atomic coordinates by the way of $r_1 \ldots r_N$. It depends also upon n real numbers $q_1 \ldots q_n$ which are supposed to differ from 0. Further, these quantities are to comply with the conditions that every sum of 2, 3, ... n of these quantities differs from zero. The statistical expectation, $\langle\Xi\rangle$, as derived by means of the distribution function (2.10), depends upon the q_j and, indirectly, upon N, but no longer on the coordinates. It will now be shown how $\langle\Xi\rangle$ is expressed in terms of s as defined by equation (2.11).

On account of (3.1) and (2.6) Ξ has the form

$$\Xi=\sum_{Q(1)}\ldots\sum_{Q(N)}\exp\left(i\sum_{l=1}^{N}Q_l r_l\right) \qquad \ldots\ldots(3.2)$$

where every $Q_l=Q(l)$ is the sum of a sub-set out of the set $q_1 \ldots q_n$, including the full and the empty set. The exponential function in (3.2) is summed with respect to $Q_1, Q_2 \ldots\ldots Q_N$ over all admissible values of these quantities.

In the exponents of (3.2) some r_l will, in general, be absent since their coefficient may vanish. On account of the definition (2.6) r_l is present only if r_{l-1} is present in the same exponent; r_1, however, is present in every term. The factor of r_l obtains contributions from those q_j only which contribute to the factor of r_{l-1}. In every exponent of (3.2) the quantities Q_l are mutually dependent in such a way that the set of q_j which add up to Q_l must be a sub-set of the set of those q_j which add up to Q_{l-1}. The term sub-set includes hereby the empty set ($Q_l=0$) and the full set ($Q_l=Q_{l-1}$). Also

$$Q_1=\sum_{j=1}^{n}q_j \qquad \ldots\ldots(3.3)$$

is a fixed number so that the first summation sign in (3.2) is to be omitted.

In consequence an alternative notation is now employed so that those Q_l which have equal values are given the same symbols and that non-vanishing quantities only are recorded. Let accordingly $\kappa_0=Q_1$, and $\kappa_1, \kappa_2 \ldots \kappa_j$ be the values of the Q_l in ascending order of l subject to the conditions that $\kappa_i\neq\kappa_0$, $\kappa_i\neq\kappa_h$ and $\kappa_i\neq 0$. The exponent of (3.2) is then written in the form

$$i\sum_{l=1}^{N}Q_l r(l)=i\{\kappa_0[r(1)+\ldots+r(\lambda)]+\kappa_1[r(\lambda+1)+\ldots+r(\lambda_2)]$$
$$+\ldots+\kappa_{j-1}[r(\lambda_{j-1}+1)+\ldots+r(\lambda_j)]\} \qquad \ldots\ldots(3.4)$$

where $r(l)$ is written for r_l and $\lambda=\lambda_1, \lambda_2 \ldots \lambda_j$ are natural numbers less than or equal to N.

Ξ is now expanded into a series of sub-sums (denoted by ξ) which are obtained by summations with respect to $\lambda_2, \lambda_3 \ldots \lambda_j$ whereas λ, j and $\kappa_0 \ldots \kappa_{j-i}$ are held constant. Thus

$$\Xi = \sum_{j=0}^{n} \sum_{\kappa(1)} \cdots \sum_{\kappa(j-1)} \sum_{\lambda=1}^{N+1-j} \xi(n, N, \lambda, j; \kappa_0 \ldots \kappa_{j-1}). \quad \ldots\ldots (3.5)$$

ξ still depends upon the coordinates but its expectation depends only upon the *number* of variables r_l which are multiplied in (3.4) into every κ_i but not upon the values l of these variables.

At first auxiliary relations involving the sub-sums are deduced.

§ 4. AUXILIARY RELATIONS

Consider two mean partial sums as defined by (3.5)

$$\left.\begin{aligned} A &= \sum_{\lambda=1}^{N-\mu-j+1} \langle \xi(n, N-\mu, j, \lambda;\ \kappa_0 \ldots \kappa_{j-1}) \rangle \\ B &= \langle \xi(n, N, j+1, \mu;\ \kappa_0 \ldots \kappa_j) \rangle \end{aligned}\right\} \quad \ldots\ldots (4.1)$$

where μ is a number, $1 \leqslant \mu \leqslant N-j$ and equal to the value of λ in the second sum. A relation between the sums A and B is now established.

Either partial sum consists of terms carrying exponents of the form (3.4), every κ_i being multiplied by a sum of variables r_l. The exponents are shown in table 1 where the subscripts of those r_l are entered into the same row which are multiplied by one and the same κ_i, which is entered at the beginning of the row. These exponential functions are summed with respect to λ whereas μ is held constant.

Table 1

	A	B
κ_0	$1 \ldots\ldots \lambda$	$1 \ldots\ldots \mu$
κ_1	$(\lambda+1) \ldots\ldots \lambda_2$	$(\mu+1) \ldots\ldots (\mu+\lambda)$
κ_2	$(\lambda_2+1) \ldots\ldots \lambda_3$	$(\mu+\lambda+1) \ldots\ldots (\mu+\lambda_2)$
κ_{j-1}	$(\lambda_{j-1}+1) \ldots\ldots \lambda_j$	$(\mu+\lambda_{j-2}+1) \ldots\ldots (\mu+\lambda_{j-1})$
κ_j	no entry	$(\mu+\lambda_{j-1}+1) \ldots\ldots (\mu+\lambda_j)$
O	$(\lambda_j+1) \ldots\ldots (N-\mu)$	$(\mu+\lambda_j+1) \ldots\ldots N$

Every term in A gives rise to a term in B in such a way that some of the r_l are shifted into the next following row. Every term in B originates in a term in A. This is shown by inspecting the entries in the column B. There are μ variables r_l in the row κ_0. The remaining number of variables is $N-\mu$ and thus equal to the number of variables in A. They are located so that the number of variables in the row κ_i of B is equal to the number of variables in the row κ_{i-1} of A. The variables absent in the exponent are entered in the row 'O'. Their number is equal in A and B.

It follows that B is the product of two factors. One factor originates in the variables in the row κ_0 and is equal to $[s(\kappa_0)]^\mu$. The other factor differs from A

by substituting κ_i for κ_{i-1}. Hence

$$\langle \xi(n, N, j+1, \mu;\ \kappa_0 \ldots \kappa_j)\rangle = [s(\kappa_0)]^{\mu} \sum_{\lambda=1}^{N-\mu-j+1} \langle \xi(n, N-\mu, j, \lambda;\ \kappa_1 \ldots \kappa_j)\rangle \qquad \ldots\ldots(4.2)$$

the subscripts of the κ_i on the right-hand side being increased by 1 as compared with the definition of A. The expectation of a partial sum is, by (4.2), expressed in terms of the expectation of a simpler partial sum.

§ 5. AUXILIARY RELATIONS CONTINUED

The following equation is now to be proved:

$$\sum_{\lambda=1}^{N+1-j} \langle \xi(n, N, j, \lambda;\ \kappa_0 \ldots \kappa_{j-1})\rangle = \prod_{h=0}^{j-1} s(\kappa_h)[1-s(\kappa_h)]^{-1} + \sum_{h=0}^{j-1} c(h, j)[s(\kappa_h)]^N. \qquad \ldots\ldots(5.1)$$

Here the coefficients c depend upon $\kappa_0 \ldots \kappa_{j-1}$ and, thus, indirectly upon n but are independent of N; they are not specified otherwise.

Equation (5.1) is readily verified for $j=1$. In this case $h=0$ only. By definition

$$\sum_{\lambda=1}^{N} \xi(n, N, 1, \lambda;\ \kappa_0) = \sum_{\lambda=1}^{N} \exp\left(i\kappa_0 \sum_{l=1}^{\lambda} r_l\right).$$

By taking the average it follows that

$$\sum_{\lambda=1}^{N} \langle \xi(n, N, 1, \lambda;\ \kappa_0)\rangle = s(\kappa_0)[1-s(\kappa_0)]^{-1}\{1-[s(\kappa_0)]^N\}. \qquad \ldots\ldots(5.2)$$

This is identical with (5.1) if $j=1$ and

$$c(0, 1) = -s(\kappa_0)[1-s(\kappa_0)]^{-1}.$$

Assuming that equation (5.1) is valid for any particular value of j it will now be proved that it remains valid if this value is increased by unity. Entering with (5.1) into the right-hand side of (4.2) it follows that

$$\langle \xi(n, N, j+1, \mu;\ \kappa_0 \ldots \kappa_j)\rangle = [s(\kappa_0)]^{\mu} \left\{ \prod_{h=1}^{j} s(\kappa_h)[1-s(\kappa_h)]^{-1} + \sum_{h=1}^{j} c(h, j)[s(\kappa_h)]^{N-\mu} \right\}. \qquad \ldots\ldots(5.3)$$

Summation with respect to μ and rearrangement results in

$$\begin{aligned}\sum_{u=1}^{N-j} \langle \xi(n, N, j+1, \mu;\ \kappa_0 \ldots \kappa_j)\rangle &= \prod_{h=0}^{j} \frac{s(\kappa_h)}{1-s(\kappa_h)} \\ &\quad - [s(\kappa_0)]^{N-j} \left\{ \prod_{h=0}^{j} \frac{s(\kappa_h)}{1-s(\kappa_h)} + \sum_{h=1}^{j} c(h, j) \frac{s(\kappa_0)}{s(\kappa_h)} \left[1 - \frac{s(\kappa_0)}{s(\kappa_h)}\right]^{-1} [s(\kappa_0)]^j \right\} \\ &\quad + \sum_{h=1}^{j} [s(\kappa_h)]^N c(h, j) \frac{s(\kappa_0)/s(\kappa_h)}{1-[s(\kappa_0)/s(\kappa_h)]}. \end{aligned} \qquad \ldots\ldots(5.4)$$

The first term on the right-hand side of (5.4) is identical with the corresponding term in (5.1) if $j+1$ is substituted for j. The same is true for the other terms on the right-hand side of (5.4) since the factors of $[s(\kappa_h)]^N$ are independent of N and can, accordingly, be identified with the coefficients $c(h, j+1)$.

By this induction in conjunction with equation (5.2) the validity of (5.1) is established.

As every $\kappa_h \neq 0$ the coefficients $c(h, j)$ are finite; also $|s(\kappa_h)| < 1$. In the limit $N \to \infty$, n being finite, most terms in (5.1) vanish and

$$\left.\begin{aligned} \lim \sum_{\lambda=1}^{N} \langle \xi(n, N, j+1, \lambda;\ \kappa_0 \ldots \kappa_j) \rangle &= \prod_{h=0}^{j} g(h) \\ g(h) = s(\kappa_h)[1 - s(\kappa_h)]^{-1}. & \end{aligned}\right\} \qquad \ldots\ldots (5.5)$$

§ 6. EXPECTATION OF THE PRODUCT OF SUMS OVER PHASES

The above relations are now used for obtaining the statistical expectation of Ξ. By entering with (5.5) into (3.5) and writing $\Xi(n)$ for the limit of $\Xi(n, N)$, we have

$$\langle \Xi(n) \rangle = g(0)\left[1 + \sum_{j=1}^{n-1} \sum_{\kappa_j} \cdots \sum_{\kappa_1} \prod_{h=1}^{j} g(h)\right]. \qquad \ldots\ldots (6.1)$$

In the products of $g(h)$ not all admissible values of κ_1 are present but only those which are sums of j out of the n quantities q_i. Denoting these values of κ_1 by $\kappa(1, j)$ and putting

$$g(1, j) = s[\kappa(1, j)]\{1 - s[\kappa(1, j)]\}^{-1}$$

the right-hand side of (6.1) can be simplified

$$\langle \Xi(n) \rangle = g(0)\left[1 + \sum_{\kappa(1,1)} g(1, 1) + \sum_{j=2}^{n-1} \sum_{\kappa_j} \cdots \sum_{\kappa_2} \sum_{\kappa(1,j)} g(1, j) \prod_{h=2}^{j} g(h)\right]. \qquad \ldots\ldots (6.2)$$

In equation (6.1) the quantities $\kappa_1 \ldots \kappa_{n-1}$ are derived from a given set of quantities $q_1 \ldots q_n$. If j out of these n quantities are selected, equation (6.1) can be used for defining expressions of the form $\langle \Xi(j) \rangle$ in many [i.e. $n!/j!(n-j)!$] different ways. Denoting these expressions by $P(j, n)\langle \Xi(j) \rangle$ and their sum by $\sum_P$, the terms in (6.2) can be expressed in terms of the $\langle \Xi(j) \rangle$:

$$\langle \Xi(n) \rangle = g(0)\left[1 + \sum_{j=1}^{n-1} \sum_{P} P(j, n)\langle \Xi(j) \rangle\right]. \qquad \ldots\ldots (6.3)$$

This is a recurrence formula expressing $\langle \Xi(n) \rangle$ in terms of $\langle \Xi(1) \rangle \ldots \langle \Xi(n-1) \rangle$. Since (6.1) is readily evaluated for $n = 1$ the expectation of any higher product is conveniently derived by repeated application of (6.3).

Repeating the premisses as laid down in § 3 we point out that the sum of every non-empty sub-set out of the set $q_1 \ldots q_n$ must differ from zero. This is a necessary condition for the validity of equation (6.3).

These premisses are now modified. It is assumed that

$$\sum_{j=1}^{n} q_j = \kappa_0 = Q_1 = 0$$

whereas the other sub-sets are to comply with the above conditions. The product of the sums over phases will, when derived from the modified set of q_i, be denoted by Ξ'.

In re-writing equation (3.2) all terms $Q_l r_l$ in the exponent are omitted for which $l < \lambda$, λ being defined by (3.4). Also, for every value of λ, $Q_{\lambda+1}$ may correspond to the empty set so that the corresponding exponent vanishes; the exponent vanishes further if $\lambda = N$. Summing the terms with vanishing exponent it follows that

$$\Xi'(n, N) = N - 1 + \sum_{\lambda=1}^{N-1} \sum_{Q(\lambda+1)} \dots \sum_{Q(N)} \exp\left(i \sum_{l=\lambda+1}^{N} Q_l r_l\right). \quad \dots\dots(6.4)$$

In the remaining summations all exponents differ from zero if any r_l differs from zero. Summations can, accordingly, be performed in accordance with equations (6.1) or (6.3).

As the probability distribution (2.10) does not distinguish between the different values of l in r_l and as the values of $Q_{\lambda+1}$ are independent of λ, the expectation of (6.4) can be written in a form in which the values of l are changed according to convenience:

$$\langle \Xi'(n) \rangle = N + \lim_{N \to \infty} \sum_{\mu=2}^{N-1} \sum_{Q(\mu)} \dots \sum_{Q(2)} \exp\left(i \sum_{l=1}^{\mu} Q_l r_l\right). \quad \dots\dots(6.5)$$

Summation with respect to μ is performed in two stages, from 2 to M and from M to $N-1$ where $1 \ll M \ll N$ and where M remains fixed when the limit of infinite N is taken. The second sum consists of $N - M \simeq N$ terms. Summation with respect to $Q_2 \dots Q_M$ may, without any appreciable error, be replaced by a summation with respect to $Q_2 \dots Q_{N-1}$. This results in $\Sigma\Sigma P(j,n) \langle \Xi(j) \rangle$ and the summation with respect to μ multiplies this expression by N. For the sum $\mu = 2$ to M an upper limit is obtained by setting the exponents equal to zero; this limit is not larger than $n!\, M^2$ and for $N \to \infty$ negligible in comparison with the first sum. We have finally

$$\langle \Xi'(n) \rangle = N[1 + \sum_{j=1}^{n-1} \sum_{P} P(j,n) \langle \Xi(j) \rangle + O(N^{-1})]. \quad \dots\dots(6.6)$$

Equations (6.3) and (6.6) are the main results of the last three sections. They are directly applicable to the deduction of the energy spectrum and its expressions in the form of a perturbation series.†

§ 7. Equation Determining Energy Levels

Deduction of the energy spectrum of a particle in interaction with a large number of centres of force is made by a method which follows the theory of a large number of interacting particles (Hugenholtz 1957, 1959). The degeneracy of the unperturbed energy levels is ignored, a justification is given in § 10.

The energy is determined by the operator equation

$$(H - zI)b = 0 \quad \dots\dots(7.1)$$

where H and I are the energy and unit operators, b is the state symbol and z is a numerical parameter. An equation of similar form

$$(H - zI)b = I \quad \dots\dots(7.2)$$

is solved by

$$b = (H - zI)^{-1} = R(z) \quad \dots\dots(7.3)$$

---

† As an alternative approach the formulae obtained in this section can be applied to the deduction of the moments of the energy distribution over the wave numbers. This would provide an insight in the structure of the energy spectrum and is presumably better to handle than the expressions in the perturbation expansion. This approach was not followed up because it would be necessary to cut out the high energy values and the justification of this procedure requires a preliminary investigation; (cf. Domb and Montroll 1959, Ford 1959).

R is said to be the resolvent operator of (7.2). Those values of z for which R does not exist are the required eigenvalues of H.

In the present problem $H = H_0 + U$ where H_0 is the kinetic energy and U, the potential energy, is regarded as a weak perturbation. With the notation

$$(H_0 - zI)^{-1} = T(z) \qquad \ldots\ldots(7.4)$$

the identities

$$R = T[I - UR] = [I - RU]T \qquad \ldots\ldots(7.5)$$

are derived from (7.3). From (7.4) the iteration series

$$R = T - TUT + TUTUT - \quad + \ldots.. \qquad \ldots\ldots(7.6)$$

is obtained and used in the following deductions.

In the plane wave representation T is diagonal and the terms in the series (7.6) have the form

$$(TUT \ldots\ldots UT)_{kp} = T_k \, U_{kl} \, T_l \ldots.. U_{mp} \, T_p \qquad \ldots\ldots(7.7)$$

where $n+1$ eigenvalues of T are multiplied into n matrix elements of U. The latter are, by (2.4), proportional to N^{-1} and depend upon the atomic coordinates by a factor ρ. Expressions of the form (7.7) represent contributions to the R-matrix by virtual n-fold transitions. For the purpose of evaluating equation (7.5) it is necessary to distinguish between different kinds of processes. This is done in the following two sections.

§ 8. IRREDUCIBLE DIAGRAMS

Processes specified in equation (7.7) are conveniently represented by diagrams, so that for an n-fold product $n+1$ segments specify particle states and n 'vertices' specify transitions. As an example the diagram corresponding to a fourfold product is shown in figure 1; virtual processes are supposed to progress from the left to the right.

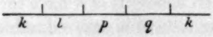

Figure 1.

Diagrams in which the initial and final state are identical are said to be diagonal. Diagrams in which the intermediate states differ from each other and from the initial and final state are said to be irreducible. The set of differences of wave numbers between successive states comply in irreducible non-diagonal diagrams with the same conditions as the numbers q_j in deriving equation (6.3), the differences in an irreducible diagonal diagram comply with the same conditions as the numbers q_j in deriving equation (6.6).

By (2.9) every matrix element (7.7) carries a product of sums over phases. Considering at first only irreducible diagrams and deriving the statistical expectation of the products of matrix elements it follows from (6.3) and (6.6) that the diagonal elements of R are of a higher order of magnitude in powers of N than the non-diagonal elements.

The integrations with respect to the wave numbers in (7.7) depend upon the particular choice of the potential energy. It is plausible to assume that the integrals are neither divergent nor zero. Then the order of magnitude of the matrix elements is readily assessed. n matrix elements of U carry (by 2.4) a factor N^{-n}. There are $n-1$ wave numbers of intermediate states carrying (by 2·5) the factor N^{n-1}. The expectation of Ξ' and of Ξ carries the factor N or 1 respectively. Thus, independently of n, the diagonal elements of (7.7) are of order unity, the non-diagonal elements are of order N^{-1}.

The R-matrix has accordingly a ' delta singularity '

$$R_{kp}=\delta_{kp}F(k,\ z) \qquad \ldots\ldots(8.1)$$

where δ is the Kronecker symbol; it has to be replaced by Dirac's $\delta(k-p)$ if k and p are regarded as continuous variables. F is, apart from singular points in the complex z-plane, a continuous function of k.

The validity of equation (8.1) is, so far, established for irreducible diagrams only; it is necessary to consider now diagrams of a less simple type.

§ 9. GENERAL DIAGRAMS

In figure 2 an irreducible diagram (a) is inserted into another irreducible diagram (b) in which a segment is cut; the result is another diagram (c) which is not irreducible.

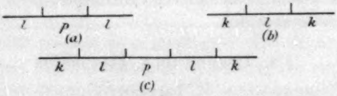

Figure 2.

A similar procedure can be applied to two or more segments in one and the same diagram or in the resulting diagrams. Diagrams which originate from simpler diagrams by this procedure are said to be ' reducible '.

Contributions to the matrix elements of R have the same order of magnitude in powers of N whether they are reducible or irreducible. If a segment is cut and a diagonal irreducible diagram is inserted it contributes a factor of order unity. Summation with respect to the segment that had been cut makes the same contribution as before cutting. It follows that the estimate of orders of magnitude as made in the preceding section remains valid if contributions of reducible and irreducible diagrams are taken into account. In particular it may be said quite generally that the R-matrix has a delta singularity.

In these arguments no account was taken of diagrams in which a pair of equal states is separated by another pair of equal states, such as shown in figure 3. Here

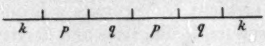

Figure 3.

a diagonal sub-diagram (pqp) makes a contribution of order unity. The equality of a segment inside and outside the sub-diagram has the consequence that there is one integration less than in a reducible diagram with the same number of vertices and that, accordingly, the order of magnitude is reduced by a factor N^{-1}. Contributions of diagrams of this kind are, accordingly, ignored.

As R has now been shown to be a diagonal matrix it is seen that the terms in the expansion (7.6) arise from diagonal diagrams only. Every term is obtained by summing the contributions of reducible and irreducible diagrams with equal numbers of vertices. Every diagram represents a sum (integral) of products of matrix elements.

If an intermediate segment or the final segment of a diagram is cut, diagonal diagrams are inserted and a summation is performed, this is expressed by replacing in (7.7) a factor T_k by R_k. In evaluating any term in (7.6) all possible diagrams are to be taken into account but every diagram is to be taken into account only once. This is automatically achieved by starting with irreducible diagrams and inserting irreducible diagrams; at first they are inserted into irreducible diagrams, then, successively, in the resulting reducible diagrams. Insertions into the initial segment would result in diagrams that had been obtained by inserting into the final segments and is therefore ruled out. This apparently involved procedure of constructing the members of the expansion (7.6) is greatly simplified by the argument at the beginning of this paragraph. It is merely necessary to replace the original intermediate and final factors T by factors R and to restrict the matrix elements to contributions by irreducible diagrams

$$R = T - R[U - URU + URURU - \quad + \dots]_{\text{irr}}\, T \qquad \dots\dots (9.1)$$

(whereby the subscript irr means restriction to irreversible diagrams). The expansion (7.6) is now replaced by an operator equation, in practice, integral equation; this complication is, however, made good by the relative simplicity of the expansion terms. Equation (9.1) lends itself readily to solution by successive approximation.

§ 10. Expansion of the Energy

Equation (9.1) is re-written in the form

$$R = [H_0 - zI + U - URU + URURU - \quad + \dots]_{\text{irr}}^{-1}. \qquad \dots\dots (10.1)$$

The points in the complex z-plane where R has poles are idential with the points where the bracket expression vanishes. For these a zero approximation is obtained by neglecting the potential energy altogether:

$$z(k) = (H_0)_k. \qquad \dots\dots (10.2)$$

This corresponds to

$$R = R_0 = T(H_0) = T_0$$

which is, by (10.2), the difference between two eigenvalues of H_0. As only irreducible diagrams are considered and degeneracy is ignored this difference does not vanish. By inserting the approximate expression for R into the right-hand side of (10·1) the series is obtained

$$z = H_0 + [U - UT_0U + UT_0UT_0U - \quad + \dots]_{\text{irr}}. \qquad \dots\dots (10.3)$$

This series has a form similar to the series of the simplest terms in Schrödinger's perturbation expansion. It differs from it by the subscript irr. In the present theory this series is regarded as a first approximation. Higher approximations are obtained by inserting the value (10.3) of z into (10.1) for the purpose of deriving a better approximation to R. Every term in the expansion (10.1) gives rise to terms in the higher approximations which involve a higher product of elements of the U-matrix. In this way orders of approximation are defined without any ambiguity although every term in the expansion is an infinite series involving all powers of U. In the present paper only the first approximation is taken into consideration.

The energy is thus given by

$$E_k = \frac{\hbar^2 k^2}{2m} + \langle U_{kk} \rangle - \left(\frac{2m}{\hbar^2}\right) \sum_p \frac{\langle U_{kp} U_{pk} \rangle}{p^2 - k^2} + \left(\frac{2m}{\hbar^2}\right)^2 \sum_p \sum_q \frac{\langle U_{kp} U_{pq} U_{qk} \rangle}{(p^2 - k^2)(q^2 - k^2)} - + \dots \qquad \dots\dots (10.4)$$

In the summations the wave numbers p, q, ... must differ from each other and from k. As the degeneracy of the unperturbed system is to be ignored it is necessary to omit also those values of the wave numbers which are equal to $-k$. In the present problem $\langle U_{kk} \rangle = 0$.

The feature specific for the absence of long distance order is the appearance of the statistical averages of the matrix elements in (10.4). Every term carries a factor $\langle \Xi'(n) \rangle$ as determined by equation (6.6).

In evaluating the terms of the series, summations are replaced by integrations in accordance with (2.5). In order to exclude the vanishing denominators principal values of the integrals are to be taken.

In justifying the omission of those terms which involve vanishing denominators on account of degeneracy, an estimate is made of the separation which would result from a degenerate level by removing the degeneracy. This is of the order of magnitude of $\langle U_{k,-k} \rangle$ and is found to be $O(N^{-1/2})$. It is accordingly negligible in comparison with the terms in (10.4) which are of the order unity.

The problem of finding the electronic energy spectrum of a chain in absence of long distance order has accordingly been solved, at least formally. A full evaluation of the result obtained would require extensive numerical work. It is shown in the following section that even at the present stage some insight is gained into the structure of the spectrum.

§ 11. DISCUSSION

The present theory could, in principle, be applied to a liquid in three dimensions. The perturbation theory would merely have to be re-worded by substituting vectors for k, x and x_l and replacing products kx by scalar products. The wave functions (2.2) would be multiplied by $(Na)^{-1}$ but this change in the order of magnitude is compensated by a factor $(Na/2\pi)^2$ in the volume element of (2.5). However, the statistical assumptions expressed in terms of the distribution function (2.10), are not valid in three dimensions. It would be necessary to employ the doublet, triplet, . . n-tuplet distributions of statistical mechanics both for evaluating the terms of (10.4) and for establishing the delta singularity of the R-matrix. At present the doublet distribution is broadly known but the higher distributions are virtually unknown. An evaluation of the formulae in three dimensins is for this reason impracticable.

There is, accordingly, some interest in the one-dimensional model. We evaluated the third term in (10·4) and obtained numerical data connected with the fourth term. It was assumed that the potential energy (2.1) is derived from the expression

$$u(y) = \begin{cases} -(\tfrac{1}{4}) + (y^2/8) - (y^4/64) & |y| \leqslant 2 \\ 0 & |y| > 2 \end{cases} \qquad \dots\dots (11.1)$$

where y is the distance of the electron from an atom. The probability distribution (2.10) is derived from

$$f(r) = \begin{cases} -48\,a^{-3}\,[(r-a)^2-(a^2/16)] & |r-a| \leqslant \tfrac{1}{4}a \\ 0 & |r-a| > \tfrac{1}{4}a \end{cases} \qquad \ldots\ldots(11.2)$$

In (11.1) and (11.2) the lengths and energies are expressed in atomic units and a is equal to four units of length.

The third term in (10.4) is obtained by means of

$$E_k - H_0(k) = (2m/a^2\hbar^2)\,\mathscr{P}\int_{-\infty}^{\infty} (k^2-q^2)^{-1}\,|v(k-q)|^2\{1+s(q-k)[1-s(q-k)]^{-1} + s(k-q)[1-s(k-q)]^{-1}\}dq \qquad \ldots\ldots(11.3)$$

where $\mathscr{P}$ means the principal value. Results of numerical integration are shown in table 2.

Table 2

ka	1·50	2·00	2·50	2·80	3·00	3·10	3·15	3·20	3·50	4·00	4·50	5·00
$100[E_k-(H_0)_k]$	−0·98	−1·23	−2·17	−4·09	−3·79	−1·21	0·37	1·93	3·75	1·43	0·86	0·56

It is seen that the energy is lowered when $|k| < \pi/a$ and elevated when $|k| > \pi/a$. In a periodic structure a similar shift of the energy would occur but it would be accompanied by a discontinuity at $|k| = \pi/a$. The calculated displacement of the energy is comparable with the displacement in a periodic structure but it progresses gradually over a wide range of k.

Multiplying the integrand of (11·3) by (k^2-q^2) and plotting the product against $k-q$, results in a graph with a marked maximum to which a Gaussian curve can be fitted. Analytical integration shows that in the neighbourhood of $|k| = \pi/a$

$$E_k - (H_0)_k = \text{const. } (\pi - ak) \qquad \ldots\ldots(11.4)$$

in accordance with numerical results. The last expression depends on the coincidence of two maxima in the integrand, at $q^2 = k^2$ and at $k-q = 2\pi a$ if $k = \pi/a$.

It was further found that $\langle \Xi'(2) \rangle$ as a function of k has a leading maximum and two subsidiary maxima, thus resembling the corresponding function in three dimensions which determines the intensity of diffracted x-rays.

Value of $\langle \Xi'(3) \rangle$ were computed as a function of two independent variables ($k-q$ and $k-p$). It would be found that this function has similar maxima as $\langle \Xi'(2) \rangle$.

It is likely that the higher terms in (10.4) make contributions to the energy in the neighbourhood of $|k| = (\pi/a)$ which are of a similar form as (11.4). This would imply that the energy spectrum approaches asymptotically a discontinuity at $|k| = \pi/a$ if a sufficient number of higher terms is taken into account. Presumably the accuracy of the series is poor near this energy range but better at some distance. It is in any case important to note that the weak binding approximation tends towards a band structure, even if only asymptotically.

ACKNOWLEDGMENTS

We wish to thank the University of London, Central Research Fund for the loan of a ‘Facit’ calculator. One of us (P.S.) is indebted to the Banaras Hindu University for leave of absence granted.

REFERENCES

DOMB, C., and MONTROLL, E., 1959, *Phys. Rev.*, **115**, 18, 24.
EISENSCHITZ, R., and DEAN, P., 1957, *Proc. Phys. Soc.*, **70**, 713.
FORD, J., 1959, *J. Chem. Phys.*, **30**, 1546.
HUGENHOLTZ, N. M., 1957, *Physica*, **23**, 481.
—— 1959 *The Many-body Problem*, ed. Université de Grenoble (New York : John Wiley and Son), p. 1.
KRISHNAN, K. S., and BHATIA, A. B., 1945, *Nature, Lond.*, **156**, 713.

The Influence of Aberration and Detector Response on Optical Images

By F. A. DIXON
Technical Optics Section, Imperial College, London

Communicated by H. H. Hopkins; *MS. received* 18*th September* 1959

Abstract. The optical-frequency response function is used to obtain the intensity distribution in the image of a step function of intensity, and from this the image intensity distributions for strips and Cobb test units are obtained. Detectors having a Gaussian type response function of different equivalent bandwidths s_0 are assumed. The treatment is applied to systems having secondary spherical aberration of amounts $w_{60} = -6\lambda, -9\lambda, -12\lambda$, with different amounts of primary spherical aberration and several planes of focus in each case, and for a range of values of s_0, the equivalent bandwidth of the detector. From these calculations the edge gradient in the image of a step function of intensity, the limit of detection and the limit of resolution, using a criterion of 0·2 for the necessary image contrast, are found; these different methods for the assessment of optical systems are then intercompared. It is shown for example that if two systems are assessed by two different test methods the order of the figure of merit for the two systems can be significantly different, and furthermore the order of merit in which the two systems are placed depends strongly on the response function of the detector employed. The differences are large enough to be of real significance in practice.

It is generally known from qualitative considerations of optical image formation that when the detector employed has a narrow bandwidth the shape of the frequency response function is of greater importance for low values of the spatial frequency s, the response function for higher spatial frequencies having little influence on the image quality, while for a system employing a detector of wide bandwidth the shape of the frequency response function for the higher frequencies is important, as these frequencies can now contribute to the formation of the image. An attempt has been made to study quantitatively the effect of detector bandwidth on the formation of the images of some standard test objects.

§ 1. Introduction

Frequency response methods for optical image evaluation are now widely accepted. The response function can be calculated and measured and detailed experimental verification of theoretical results has recently been obtained (Kelsall 1959, Birch 1959). The frequency response function specifies image quality directly for extended periodic objects, and gives a general analytical description of image quality. Typical test objects and detail occurring in practice often have relatively complex Fourier spectra: as examples the following may be cited: (*a*) a narrow strip and (*b*) a unit of a Cobb resolution chart. For these cases numerical integration of a function involving the product of the frequency response and the Fourier spectrum of the distribution of intensity in the object is a lengthy and cumbrous procedure. It has been found more convenient to evaluate first the response to a step function and treat such intensity objects as (*a*) and (*b*) above as being made up by the addition or subtraction of suitably located step functions (Hopkins 1958).

A step function of intensity $H(u)$ such that

$$\begin{aligned} H(u) &= 1 \qquad u>0 \\ &= 0 \qquad u<0 \end{aligned}$$

has an aerial image with the intensity distribution given by

$$H'(u') = \tfrac{1}{2} + \frac{1}{2\pi i}\int_{-\infty}^{+\infty} \frac{D(s,\psi)}{s} \exp\,(i2\pi u's)\,ds, \qquad \ldots\ldots(1)$$

where $D(s,\psi)$ is the complex frequency response of the optical system for the given azimuth ψ. In terms of the contrast transfer function $T(s,\psi)$ and the phase $\theta(s,\psi)$, the complex response is $D(s,\psi) = T(s,\psi)\exp i\theta(s,\psi)$ and

$$H'(u') = \tfrac{1}{2} + \frac{1}{\pi}\int_{0}^{\infty} \frac{T(s,\psi)}{s} \sin\{2\pi u's + \theta(s,\psi)\}. \qquad \ldots\ldots(2)$$

In most practical cases it is necessary to include as an additional factor with $D(s,\psi)$ the response function of the detector, the response function for the combination of optical system and detector being simply the product of the two separate response functions. Thus if $D_{\mathrm{d}}(s)$ is the frequency response function for the detector, the intensity distribution in the image of a step function of intensity is given by

$$H'(u') = \tfrac{1}{2} + \frac{1}{2\pi i}\int_{-s_{\mathrm{m}}}^{+s_{\mathrm{m}}} D_{\mathrm{d}}(s)\,\frac{D(s,\psi)}{s} \exp\,(i2\pi u's)\,ds \qquad \ldots\ldots(3)$$

where s_{m} is the value of the spatial frequency s beyond which the response of the detector can be assumed to be zero.

In initial calculations a detector having a response such that

$$\begin{aligned} D_{\mathrm{d}}(s) &= 1 \qquad |s| < s_0 \\ &= 0 \qquad |s| > s_0 \end{aligned} \qquad \ldots\ldots(4)$$

was considered. This led to there being negative values of intensity at parts of the edge image when the detector bandwidth was much less than that of the optical system. For an aberration-free system the frequency response according to geometrical optics is equal to unity for all values of s, so that the image obtained with a square shaped detector response (4) will be given, from equation (1), by

$$\begin{aligned} H'(u') &= \tfrac{1}{2} + \frac{1}{2\pi i}\int_{-s_0}^{+s_0} \frac{1}{s} \exp\,(i2\pi u's)\,ds \\ &= \tfrac{1}{2} + \frac{1}{\pi}\,\mathrm{Si}(2\pi u's_0) \end{aligned}$$

where $\mathrm{Si}(x)$ is the sine integral defined by

$$\mathrm{Si}(x) = \int_0^x \frac{\sin t}{t}\,dt. \qquad \ldots\ldots(5)$$

The values of $H'(u')$ when $u' = \pm 0{\cdot}5/s_0$ are equal to approximately $1{\cdot}09$ and $-0{\cdot}09$ respectively and each represents an impossible result. Similar results are obtained from the use of diffraction theory. These results show that a detector of the type considered, having a sharp cut-off, could not occur in practice. It would in any case require the detector to have an impulse response of infinite extent and taking on negative values.

For the above reasons a detector having a Gaussian response curve

$$D_d(s) = \exp(-s^2/2\sigma^2) \qquad \ldots\ldots(6)$$

was assumed for all subsequent calculations; σ is the standard deviation of the distribution. The response is unity when $s=0$ and is practically zero at and beyond $s=3\sigma$. The area under the curve described by equation (6) between the limits $0 \leqslant s \leqslant \infty$ is equal to $\sigma\sqrt{(\frac{1}{2}\pi)}$, and as $D_d(s)=1{\cdot}0$ when $s=0$ this area, denoted by s_0, is also the area of a rectangle of unit height and width s_0; s_0 is defined here to be the equivalent bandwidth of the detector, and is related to σ the standard deviation by the relation

$$\sigma = s_0\sqrt{(2/\pi)} \simeq 0{\cdot}8s_0.$$

When $s=s_0$ the response of the detector is approximately equal to 0·5; s_0 is then also the half-value bandwidth.

§ 2. Formulae for Numerical Calculation

2.1. *Image of an Edge, with Gaussian Detector Response*

The response to a step function is now given by

$$H'(u') = \tfrac{1}{2} + \frac{1}{2\pi i}\int_{-\infty}^{+\infty} \frac{D(s,\psi)}{s} \exp\left(\frac{-s^2}{2\sigma^2}\right) \exp(i2\pi u's)\, ds$$

and if only symmetrical aberrations are present, and the bandwidth is limited to $|s| \leqslant 3\sigma$,

$$H'(u') = \tfrac{1}{2} + \frac{1}{\pi}\int_{0}^{3\sigma} \frac{D(s,\psi)}{s} \exp\left(\frac{-s^2}{2\sigma^2}\right) \sin(2\pi u's)\, ds,$$

this limit being assumed since when $|s| > 3\sigma$ the product of the two response functions will be negligibly small. The response to a step function may now be written

$$H'(u') = \tfrac{1}{2} + S(u') \qquad \ldots\ldots(7)$$

where

$$S(u') = \frac{1}{\pi}\int_{0}^{1} \frac{D(3\sigma r, \psi)}{r} \exp(-4{\cdot}5r^2) \sin(2\pi u' 3\sigma r)\, dr. \qquad \ldots\ldots(8)$$

In this latter formula r has been written for $s/3\sigma$ and $S(u')$ for the variable part of $H'(u')$. Clearly $S(-u') = -S(u')$ and so this need only be computed for positive values of u'.

If the expression (3) is differentiated with respect to u', and u' is put equal to zero, the gradient at the image of an edge is found to be given by

$$S'(0) = \left|\frac{\partial}{\partial u'} H'(u')\right|_{u'=0} = \int_{-\infty}^{+\infty} D(s,\psi) D_d(s)\, ds \qquad \ldots\ldots(9)$$

which, by (8), is given by the formula

$$S'(0) = 6\sigma \int_{0}^{1} \mathscr{R}\{D(3\sigma r, \psi)\} \exp(-4{\cdot}5r^2)\, dr \qquad \ldots\ldots(10)$$

where $\mathscr{R}\{\,\}$ denotes the real part of the frequency response. The edge gradient $S'(0)$ can also be obtained numerically with good approximation from the numerical variation of $H'(u')$ with u' for small values of u'.

2.2. *The Image of a Strip: Limit of Detection*

The distribution of intensity in the object may be written $B(u)=1-\gamma B_1(u)$ where γ is a constant depending upon the object contrast and

$$B_1(u)=1 \qquad |u|<\tfrac{1}{2}a$$
$$B_1(u)=0 \qquad |u|>\tfrac{1}{2}a.$$

The intensity in the image is then given by $B'(u')=1-\gamma B_1'(u')$, and in terms of the response to a step function

$$B'(u')=1-\gamma\{H'(u'+\tfrac{1}{2}a)-H'(u'-\tfrac{1}{2}a)\}, \qquad \ldots\ldots(11)$$

where $H'(u')$ defined by the expression (3) is the response to a step function of intensity situated at $u'=0$. Should the width of the strip be steadily reduced the contrast between the centre of the strip and the bright surround will decrease until at some width $a=a_0$ the contrast will have fallen to a value V_0 below which it will not be possible to detect the presence of the strip in the image. This serves to define the limit of detection. From (11) the contrast in the image is found to be

$$V_0=\frac{\gamma\{H'(\tfrac{1}{2}a_0)-H'(-\tfrac{1}{2}a_0)\}}{2-\gamma\{H'(\tfrac{1}{2}a_0)-H'(-\tfrac{1}{2}a_0)\}} \qquad \ldots\ldots(12)$$

which, substituting from (7), gives

$$V_0=\frac{\gamma S(\tfrac{1}{2}a_0)}{1-\gamma S(\tfrac{1}{2}a_0)}. \qquad \ldots\ldots(13)$$

The contrast in the object plane is given by

$$V=\gamma/(2-\gamma) \qquad \ldots\ldots(14)$$

and is never attained in the image since $S(\tfrac{1}{2}a_0)<\tfrac{1}{2}$.

2.3. *Image of Cobb Unit: Limit of Resolution*

The distribution of intensity in a Cobb object of line separation a is given by $B(u)=1-\gamma B_1(u)$ where

$$B_1(u)=1 \qquad \tfrac{1}{4}a<|u|<\tfrac{3}{4}a$$
$$B_1(u)=0 \qquad |u|<\tfrac{1}{4}a; \quad |u|>\tfrac{3}{4}a.$$

The intensity in the image is then $B'(u')=1-\gamma B_1'(u')$ which, in terms of the response to step function, gives

$$B'(u')=1-\gamma\{H'(u'+\tfrac{3}{4}a)-H'(u'+\tfrac{1}{4}a)+H'(u'-\tfrac{1}{4}a)-H'(u'-\tfrac{3}{4}a)\}. \quad \ldots\ldots(15)$$

Again, as the line spacing a is reduced, the contrast between the opaque lines and the bright space between them will decrease, and for some value a_0 of a the contrast will have fallen to V_0 where it will not be possible to resolve the two lines. The limit of resolution so defined is given by

$$V_0=\frac{\gamma\{H'(\tfrac{5}{4}a_0)+H'(-\tfrac{3}{4}a_0)-2H'(\tfrac{3}{4}a_0)+2H'(\tfrac{1}{4}a_0)-2H'(-\tfrac{1}{4}a_0)\}}{2-\gamma\{H'(\tfrac{5}{4}a_0)-H'(-\tfrac{3}{4}a_0)\}}$$

or using (8),

$$V_0=\frac{\gamma\{S(\tfrac{5}{4}a_0)-3S(\tfrac{3}{4}a_0)+4S(\tfrac{1}{4}a_0)\}}{2-\gamma\{S(\tfrac{5}{4}a_0)+S(\tfrac{3}{4}a_0)\}}\ ;$$

the object contrast being given by $V=\gamma/(2-\gamma)$.

§ 3. METHOD OF COMPUTATION

The formula for the response to a step function (8) is well suited to evaluation by Simpson's rule, using values of $D(s,\psi)$ obtained independently. The calculation was programmed for the electronic computer DEUCE, using a tabulative interpretive scheme, it being so arranged that the edge intensity function, the intensity distribution across the image of a strip, and the intensity distribution across the image of a Cobb unit, were calculated in one cycle of operations. The frequency response function $D(s,\psi)$ for the optical system under consideration was read into the computer in numerical tabular form and stored. When required, the values of the response over any range of spatial frequency s covered by the table are found automatically by interpolation, and used to calculate the edge intensity function by Simpson's rule. Then, by the simple addition or subtraction of suitably spaced coordinates on the edge intensity curve, the distributions of intensity across the strip or Cobb unit images are calculated by means of expressions (11) and (15) respectively.

If a Cobb unit of line separation a is considered and an initial value allocated to the product as_0, values of the edge intensity function are calculated for a set of values, such as those defined by

$$u's_0 = \tfrac{1}{4}as_0, \quad \tfrac{1}{2}as_0, \quad \tfrac{3}{4}as_0, \quad as_0, \quad \tfrac{5}{4}as_0, \quad \tfrac{3}{2}as_0.$$

From these results the intensity distributions for the strip and Cobb unit can be calculated for a chosen value of s_0, and printed out together with the points calculated for the edge intensity function. An increment can then be added to as_0 and the process repeated until the required range of as_0 has been covered. The value of s_0 can then be modified automatically by the computer and the whole procedure repeated. This method gives a greater density of points on the edge intensity curve for small u' values, which is, of course, desirable. In some cases the same point is calculated twice, and this serves as a useful check on the calculation. It is important that the incremental value of the argument of the sine function in (8) is restricted sufficiently to give an accurate result from the use of Simpson's rule.

§ 4. RESULTS

The present study was restricted to the study of image formation in the presence of primary and secondary spherical aberration with defect of focus. The optical system is assumed to have a circular aperture. Frequency response curves from the diffraction treatment for a number of systems having various states of correction were available (Goodbody 1958) and corresponding curves for the geometrical optical approximations were calculated independently. The wave-front aberration of the system as a function of radius of aperture is defined by

$$W(r) = w_{20}r^2 + w_{40}r^4 + w_{60}r^6$$

the coefficients w_{20}, w_{40}, w_{60} specifying respectively defect of focus, primary and secondary spherical aberration. The states of correction between primary and secondary spherical aberration considered for the case of $w_{60} = -6\lambda$, using diffraction theory, and the geometrical optical approximation, were $\beta_{46} = \beta_{46}' - 0{\cdot}5$, β_{46}', $\beta_{46}' + 0{\cdot}5$, where β_{46}' is the value of w_{40}/w_{60} which optimizes the frequency

Table 1. Limit of Detection a_0. Tables of $a_0 s_0$

(*a*) Diffraction treatment

	$w_{60} = -6\lambda$									$w_{60} = -9\lambda$		$w_{60} = -12\lambda$	
β_{46}	$-2·13$			$-1·63$			$-1·13$			$-1·69$	$-1·19$	$-1·72$	$-1·22$
β_{26}	1·11	1·36	1·61	0·51	0·76	1·01	$-0·10$	0·15	0·40	0·80	0·43	0·83	0·44
$s_0 w_{60}$													
$\to 0$	0·18	0·18	0·18	0·18	0·18	0·18	0·18	0·18	0·18	0·18	0·18	0·18	0·18
0·5	0·23	0·21	0·24	0·21	0·19	0·22	0·24	0·21	0·22	0·19	0·22	0·19	0·21
1·0	0·36	0·27	0·35	0·29	0·22	0·32	0·36	0·27	0·26	0·23	0·25	0·23	0·24
1·5	0·49	0·34	0·48	0·38	0·25	0·45	0·49	0·33	0·29	0·27	0·28	0·28	0·27
2·0	0·62	0·40	0·62	0·45	0·29	0·59	0·62	0·40	0·32	0·32	0·30	0·33	0·29

(*b*) Geometrical optical treatment

β_{46}	$-2·30$			$-1·80$			$-1·30$		
β_{26}	1·32	1·57	1·82	0·65	0·90	1·15	$-0·02$	0·23	0·48
$s_0 w_{60}$									
$\to 0$	0·18	0·18	0·18	0·18	0·18	0·18	0·18	0·18	0·18
0·5	0·25	0·21	0·24	0·22	0·19	0·22	0·25	0·21	0·21
1·0	0·40	0·30	0·34	0·31	0·24	0·30	0·39	0·28	0·24
1·5	0·56	0·39	0·44	0·40	0·29	0·39	0·52	0·35	0·26
2·0	0·72	0·49	0·54	0·49	0·36	0·48	0·64	0·42	0·29

Gaussian detector: equivalent bandwidth s_0. Above values for 0·2 contrast.

Table 2. Cobb Limit of Resolution a_0

(*a*) Diffraction treatment

	$w_{60}=-6\lambda$									$w_{60}=-9\lambda$		$w_{60}=-12\lambda$	
β_{46}		$-2·13$			$-1·63$			$-1·13$		$-1·69$	$-1·19$	$-1·72$	$-1·22$
β_{26}	1·11	1·36	1·61	0·51	0·76	1·01	$-0·10$	0·15	0·40	0·80	0·43	0·83	0·44
$s_0 w_{60}$													
$\to 0$	0·65	0·65	0·65	0·65	0·65	0·65	0·65	0·65	0·65	0·65	0·65	0·65	0·65
0·5	0·88	0·78	0·90	0·80	0·73	0·83	0·90	0·77	0·79	0·72	0·78	0·72	0·77
1·0	1·37	1·02	1·35	1·11	0·81	1·17	1·38	0·95	0·83	0·83	0·83	0·85	0·83
1·5	1·88	1·32	1·88	1·48	0·92	1·59	1·97	1·16	0·93	0·99	0·89	1·03	0·89
2·0	2·45	1·60	2·44	1·90	1·04	2·06	2·58	1·40	1·00	1·17	0·95	1·23	0·95

(*b*) Geometrical optical treatment

β_{46}		$-2·30$			$-1·80$			$-1·30$	
β_{26}	1·32	1·57	1·82	0·65	0·90	1·15	$-0·02$	0·23	0·48
$s_0 w_{60}$									
$\to 0$	0·65	0·65	0·65	0·65	0·65	0·65	0·65	0·65	0·65
0·5	0·94	0·82	0·91	0·84	0·72	0·82	0·95	0·79	0·76
1·0	1·54	1·15	1·34	1·21	0·89	1·11	1·54	1·03	0·81
1·5	2·23	1·52	1·74	1·63	1.09	1·47	2·22	1·34	0·87
2·0	2·93	1·92	2·30	2·07	1·36	1·87	2·95	1·65	0·97

Gaussian detector: equivalent bandwidth s_0. Above values for 0·2 contrast.

Table 3. Edge Gradient Functions $S(0)$

(*a*) Diffraction Treatment

	$w_{60} = -6\lambda$									$w_{60} = -9\lambda$		$w_{60} = -12\lambda$	
β_{46}	−2·13			−1·63			−1·13			−1·69	−1·19	−1·72	−1·22
β_{26}	1·11	1·36	1·61	0·51	0·76	1·01	−0·10	0·15	0·40	0·80	0·43	0·83	0·44
$s_0 w_{60}$													
→ 0	1·00	1·00	1·00	1·00	1·00	1·00	1·00	1·00	1·00	1·00	1·00	1·00	1·00
0·5	0·72	0·83	0·73	0·80	0·89	0·77	0·72	0·81	0·78	0·89	0·80	0·89	0·81
1·0	0·49	0·64	0·49	0·59	0·78	0·54	0·48	0·65	0·68	0·76	0·70	0·76	0·72
1·5	0·36	0·52	0·36	0·47	0·68	0·37	0·36	0·53	0·61	0·64	0·64	0·63	0·65
2·0	0·29	0·45	0·29	0·40	0·67	0·29	0·29	0·43	0·56	0·54	0·60	0·52	0·60

(*b*) Geometrical optical treatment

β_{46}	−2·30			−1·80			−1·30		
β_{26}	1·32	1·57	1·82	0·65	0·90	1·15	−0·02	0·23	0·48
$s_0 w_{60}$									
→ 0	1·00	1·00	1·00	1·00	1·00	1·00	1·00	1·00	1·00
0·5	0·70	0·80	0·72	0·78	0·90	0·80	0·69	0·82	0·83
1.0	0·44	0·58	0·52	0·56	0·74	0·58	0·46	0·63	0·73
1·5	0.32	0·44	0·41	0·44	0·59	0·45	0·35	0·50	0·66
2·0	0·26	0·36	0·33	0·37	0·49	0·36	0·29	0·43	0·60

Gaussian detector: equivalent bandwidth s_0. Above values $D(s_0) = \frac{1}{2}s_0$ (edge gradient), response $D(s, \psi)$ for low values of spatial frequency (Hopkins 1957, Goodbody 1958). For each system three planes of focus were considered given by $\beta_{26} = \beta_{26}' - 0.25$, β_{26}', $\beta_{26}' + 0.25$, β_{26}' being the value of w_{20}/w_{60} giving the optimum focal plane for the particular value of β_{46}. For the secondary aberration values $w_{60} = -9\lambda$ and $w_{60} = -12\lambda$, only the two more interesting cases suggested by Goodbody's results for spherical aberration, namely $\beta_{46} = \beta_{46}'$, $\beta_{26} = \beta_{26}'$; $\beta_{46} = \beta_{46}' + 0.5$, $\beta_{26} = \beta_{26}' + 0.25$ were considered. These two systems are in future referred to as the optimum and over-corrected systems respectively.

Key to figures. The following schedule refers to all figures.

Object contrast $= 1$: $\gamma = 1$

Gaussian type detector: equivalent bandwidth s_0

——————— Optimum corrected system

$\beta_{46} = \beta_{46}'$; $\beta_{26} = \beta_{26}'$

– – – – – – – Over-corrected system

$\beta_{46} = \beta_{46}' + 0.5$; $\beta_{26} = \beta_{26}' + 0.25$

	Optimum corrected system		Over-corrected system	
β_{46} / w_{60}	β_{46}'	β_{26}'	$\beta_{46}' + 0.5$	$\beta_{26}' + 0.25$
-6λ	-1.63	0.76	-1.13	0.40
-9λ	-1.69	0.80	-1.19	0.43
-12λ	-1.72	0.83	-1.22	0.44
Geometrical optics	-1.80	0.90	-1.30	0.48

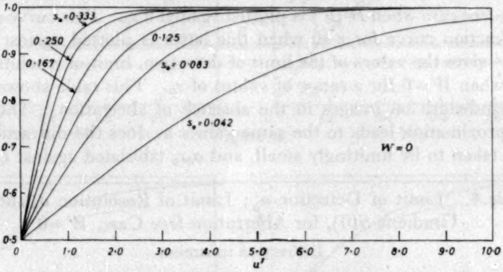

Figure 1. The effect of detector bandwidth on the response to a step function ($W = 0$).

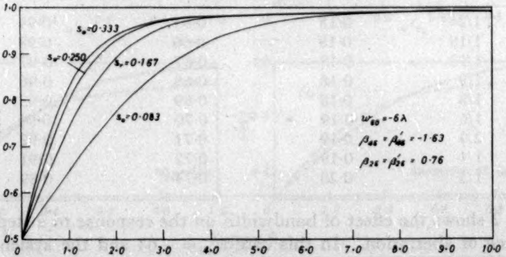

Figure 2. The effect of detector bandwidth on the response to a step function ($w_{60} = -6\lambda$).

Four values of the equivalent bandwidth were considered for each case in the diffraction treatment, and four values of the product $s_0 w_{60}$ for the geometrical optical approximation. For completeness the case of no aberration $W = 0$, was treated by both the diffraction theory and the geometrical approximation for all values of s_0 used.

The object contrast was taken to be unity ($\gamma = 1$), and the limit of detection and resolution were each taken to be defined by $V_0 = 0{\cdot}2$. The contrast

$$V = \frac{I_{\max} - I_{\min}}{I_{\max} + I_{\min}}$$

was calculated for strips and Cobb units of various widths and the value of a_0, where $V = V_0 = 0{\cdot}2$, found by interpolation. Values of the limit of detection, limit of resolution, and edge gradients are given for the systems considered in tables 1, 2 and 3. In the geometrical optical approximation, $a_0 s_0$ is usefully plotted as a function of $s_0 w_{60}$, since in this case, if the aberration is, say, doubled and the equivalent bandwidth is halved, the limit of detection and the limit of resolution are correspondingly increased by a factor two. To allow more direct comparison between the results according to geometrical optics and diffraction, tables of $a_0 s_0$ against $s_0 w_{60}$ are given in all cases. The tables give the edge gradient $S'(0)$ in the scale normalized form $S'(0)/2s_0$ for the same reason.

In figure 1 the edge intensity function $H'(u')$ is plotted against u' for six values of s_0 for the aberration-free case $W = 0$. If $H'(u')$ is plotted against $u's_0$ there is no appreciable spread over a range of s_0 ($s_0 < 0{\cdot}33$) which includes most practical detectors. The geometrical approximation gives only one curve for the aberration-free case when $H'(u')$ is plotted against $u's_0$. This curve approximates to the diffraction curve for $s \to 0$ when this latter is plotted against $u's_0$.

Table 4 gives the values of the limit of detection, limit of resolution, and edge gradients when $W = 0$ for a range of values of s_0. This table shows the effect of detector bandwidth on images in the absence of aberration. The geometrical optical approximation leads to the same values as does the diffraction treatment when s_0 is taken to be limitingly small, and $a_0 s_0$ tabulated against s_0.

Table 4. Limit of Detection a_0; Limit of Resolution a_0 and Edge Gradient $S(0)$, for Aberration-free Case, $W = 0$

Diffraction treatment

s_0	$a_0 s_0$	$a_0 s_0$	$\frac{1}{2}s_0 S(0)$
1/24	0·18	0·65	0·99
1/18	0·18	0·66	0·98
1/12	0·18	0·67	0·97
1/9	0·18	0·68	0·96
1/8	0·18	0·69	0·95
1/6	0·19	0·70	0·94
2/9	0·19	0·71	0·92
1/4	0·19	0·72	0·91
1/3	0·20	0·74	0·89

Figure 2 shows the effect of bandwidth on the response to a step function in the presence of aberration. In this case $w_{60} = -6\lambda$ and the system considered has optimum correction, that is $\beta_{46} = \beta_{46}'$ and $\beta_{26} = \beta_{26}'$. Figure 3 gives similar

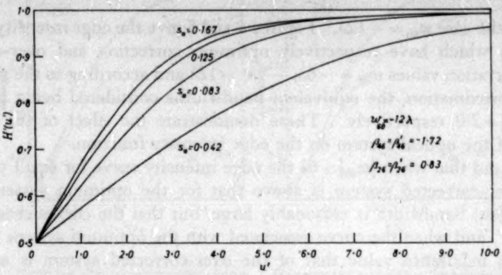

Figure 3. The effect of detector bandwidth on the response to a step function ($w_{60} = -12\lambda$).

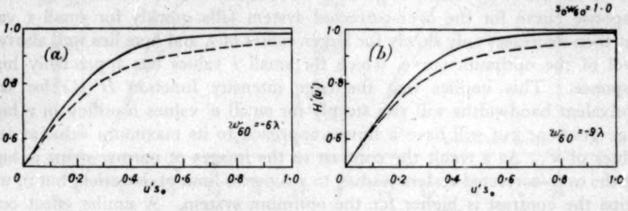

Figure 4.

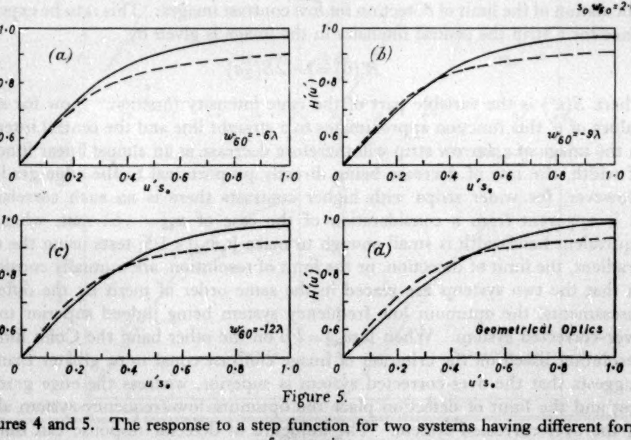

Figure 5.

Figures 4 and 5. The response to a step function for two systems having different forms of correction.

curves for the case $w_{60} = -12\lambda$. Figures 4 and 5 give the edge intensity functions of systems which have respectively optimum correction and over-correction, for the aberration values $w_{60} = -6\lambda$, -9λ, -12λ and according to the geometrical optical approximation, the equivalent bandwidths considered being $|s_0 w_{60}| = 1{\cdot}0$ and $|s_0 w_{60}| = 2{\cdot}0$ respectively. These demonstrate the effect of the frequency response of the optical system on the edge intensity function.

It is found that when $|w_{60}| > 6\lambda$ the edge intensity curve for small values of u' for the over-corrected system is above that for the optimum system when s_0 the equivalent bandwidth is reasonably large, but that the curves cross at larger values of u', and when the curve associated with the optimum system has almost reached its maximum value that of the over-corrected system is appreciably below it. This effect can be understood by reference to the frequency response curves for the two systems as given by Goodbody (1958). When $|w_{60}| > 6\lambda$ the response curve for the over-corrected system falls quickly for small s values but then decreases only slowly for larger values of s, and here lies well above the level of the optimum curve, which for small s values has appreciably higher response. This implies that the edge intensity function $H'(u')$ for larger equivalent bandwidths will rise steeply for small u' values resulting in a higher edge gradient but will have a slower approach to its maximum value at larger values of u'. As a result the contrast in the images of narrow strips is higher for the over-corrected system leading to a superior limit of detection, but in wider strips the contrast is higher for the optimum system. A similar effect occurs in the case of Cobb resolution units imaged by the two systems. The contrast in the image of a strip is by equation (13) clearly superior for the system having the greater value for the edge intensity function at a value of u' equal to half the width of the strip. The point of intersection of the two intensity curves gives the value of where the contrast for the two systems is the same and beyond this point there is a reversal of the order of merit for the two systems.

It is found for all values of s_0 and w_{60} that the order of merit placed on any system by calculation of the edge gradient is consistent with that given by calculation of the limit of detection for low contrast images. This is to be expected since for a strip the central intensity in the image is given by

$$B'(0) = 1 - 2S(\tfrac{1}{2}a)$$

where $S(u')$ is the variable part of the edge intensity function. Now for small values of u' this function approximates to a straight line and the central intensity in the image of a narrow strip will therefore decrease as an almost linear function of width, the rate of decrease being directly proportional to the edge gradient. However, for wider strips with higher contrasts there is no such correlation. It is apparent from a consideration of the case of $w_{60} = -6\lambda$ that, when the equivalent bandwidth is small enough to make $|s_0 w_{60}| < 1{\cdot}5$, tests using the edge gradient, the limit of detection, or the limit of resolution, are mutually consistent in that the two systems are placed in the same order of merit by the different assessments, the optimum low frequency system being judged superior to the over-corrected system. When $|s_0 w_{60}| = 2{\cdot}0$ on the other hand the Cobb limit of resolution based on the criterion of image contrast equal to or greater than 0·2 suggests that the over-corrected system is superior, whereas the edge gradient test and the limit of detection place the optimum low frequency system ahead of the over-corrected system. The influence of detector response can thus be

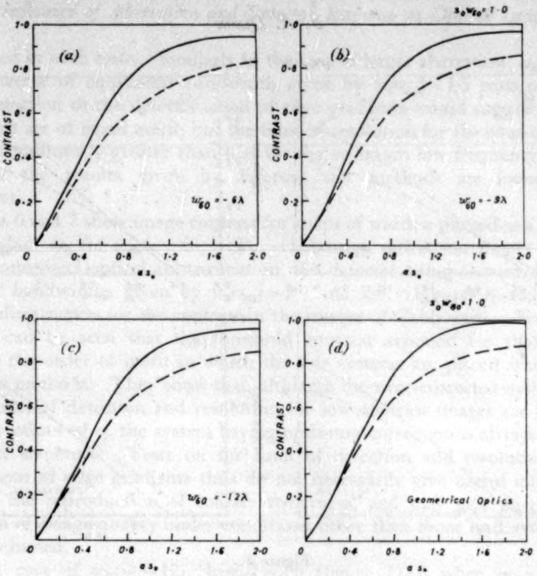

Figure 6.

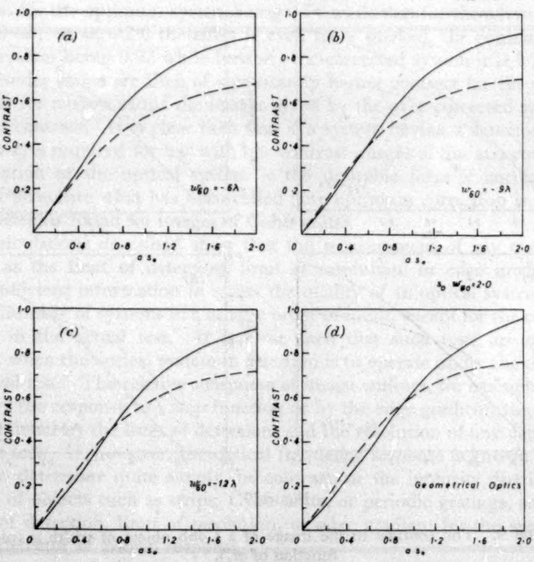

Figure 7.

Figures 6 and 7. The contrast in the image of a strip of width a (plotted as a function of as_0).

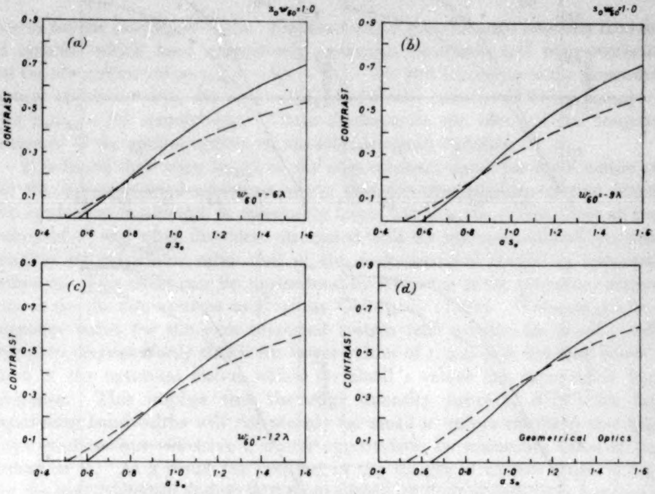

Figure 8.

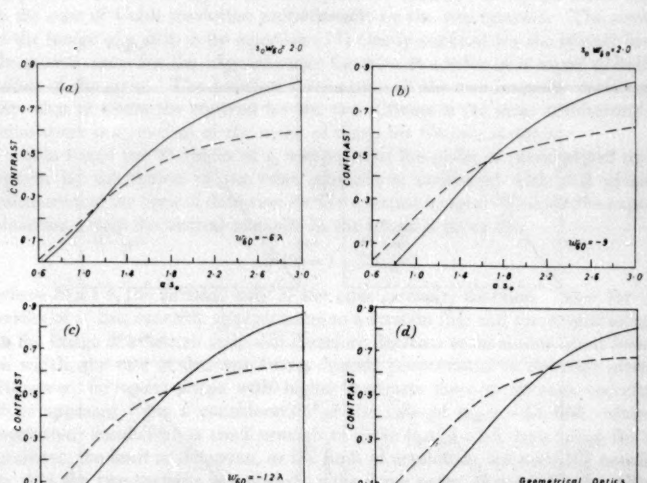

Figure 9.

Figures 8 and 9. The contrast in the image of a Cobb object of width a (plotted as a function of as_0).

very marked in such tests. Similarly in the case of larger aberration, $w_{60} = -9\lambda$, with a detector of equivalent bandwidth given by $|s_0 w_{60}| = 1{\cdot}5$ tests using the limit of detection or the determination of edge gradients would suggest that the two systems are of equal merit, but the limit of resolution for the over-corrected system is significantly greater than that for the optimum low frequency system, and again the results given by different test methods are found to be inconsistent.

Figures 6 and 7 show image contrast for strips of width a plotted as a function of the product as_0 for $w_{60} = -6\lambda$, -9λ, -12λ using diffraction theory and also for the geometrical optical approximation, the detector being asssumed to have equivalent bandwidths given by $|s_0 w_{60}| = 1{\cdot}0$ and $2{\cdot}0$. Figures 8 and 9 show corresponding curves for the contrast in the images of Cobb units. From these curves it can be seen that the threshold contrast assumed for the detector influences the order of merit in which the two systems are placed when tested by the two methods. They show that, although the over-corrected system gives a better limit of detection and resolution for low contrast images for $|w_{60}| > 6\lambda$ and larger values of s_0, the system having optimum correction is always superior for coarser structure. Tests on the limit of detection and resolution or the measurement of edge gradients thus do not necessarily give useful information regarding the reproduction of coarser structures, and may give an erroneous impression of image quality under conditions other than those under which the test is conducted.

In the case of $w_{60} = -12\lambda$, $|s_0 w_{60}| = 2{\cdot}0$ (figure 7 (*c*)) when $as_0 = 0{\cdot}33$ the contrast in the image of a strip is 0·20 for the system with optimum correction and 0·23 for the over-corrected system: when $as_0 = 0{\cdot}7$ the order is reversed, the contrast for the optimum system being 0·74 while that for the over-corrected system is 0·62; at $as_0 = 2{\cdot}0$ the effect is even more marked, the contrast for the optimum system being 0·92 while for the over-corrected system it is 0·72. The images of wider strips are then of significantly higher contrast for the optimum system, but for narrow strips the images given by the over-corrected system are of superior contrast. It is clear then that if a system having a detector of large bandwidth s_0 is required for use with low contrast images of fine structures, then over-correction of the optical system is the desirable form of correction, but for coarser structure what has been called here optimum correction is required. A similar effect is found for images of Cobb units.

The calculations described show that the measurement of any one of such functions as the limit of detection, limit of resolution, or edge gradient does not give sufficient information to assess the quality of an optical system or even to place a number of systems in a unique order of merit, except for the conditions employed in the actual test. It is clear then that such tests are only fully significant when the optical system in question is to operate under the conditions of the actual test. The relative sharpness of image outlines, for example, may be assessed by the response to a step function or by the edge gradient, the detection of isolated detail by the limit of detection, and the resolution of fine detail by the Cobb unit test. If, however, the optical frequency response is known it is then possible to determine quite simply the contrast, or the intensity distribution in the image of objects such as strips, Cobb units, or periodic gratings, and to find the limit of detection, limit of resolution, or edge gradient for the system used with any detector of known response.

ACKNOWLEDGMENTS

I am grateful to Dr. H. H. Hopkins for suggesting the subject of this paper and for many helpful discussions. My thanks are due to Dr. A. M. Goodbody who provided the detailed Frequency Response tables used in many of the calculations. I am indebted to the Chief Scientist, Department of Supply, Australia, for the opportunity of studying in England.

REFERENCES

BIRCH, K. G., 1959, *Ph.D. Thesis*, London University.
GOODBODY, A. M., 1958, *Proc. Phys. Soc.*, **72**, 411.
HOPKINS, H. H., 1957, *Proc. Phys. Soc.* B, **70**, 449.
—— 1958, *Image Assessment Using Frequency Response Techniques*, Proceedings of Summer School, Imperial College, London, p. 54.
KELSALL, D., 1959, *Proc. Phys. Soc.*, **73**, 465.

Pre-breakdown Phenomena in Uniform Fields

By D. T. A. BLAIR, F. M. BRUCE, J. E. MATTHEWS and D. J. TEDFORD

The Royal College of Science and Technology, Glasgow

MS. received 11*th November* 1958, *in revised form* 15*th October* 1959; *paper read before the Society at Swansea Conference, September* 1958

Abstract. Observations were made of pre-breakdown phenomena in uniform field gaps under ambient atmospheric conditions and measured irradiation intensities, in which current and light pulses were recorded. From measurements of the current pulse duration a value for the mobility of positive ions of $2\cdot6\,\mathrm{cm}^2\,\mathrm{sec}^{-1}\,\mathrm{v}^{-1}$ was obtained at field strengths approaching the breakdown value.

During the study of static voltage breakdown in air between radium irradiated uniform field electrodes (Bruce 1947), a pre-breakdown discharge when the voltage was within a few per cent of the sparkover value was identified by noise and a faint glow at the anode. Both effects increased in intensity as the voltage was raised or the intensity of irradiation increased.

The first measurements of pre-breakdown current on approach to sparkover were made with a galvanometer circuit, and recorded an increasing current flow of about 1μA as the applied voltage approached sparkover in the case of an irradiated gap, but no measurable pre-breakdown current for non-irradiated gaps. An oscillographic technique having a much lower time constant was then developed to give a record, on moving film, of gap current whilst the applied voltage was steadily increased to breakdown. This revealed the pre-breakdown current as consisting of a number of discrete pulses, figure 1 (*a*) (Plate). The general level of pulse amplitude and recurrence rate increased as the voltage approached breakdown. For a non-irradiated gap there were only occasional pulses due to background ionization, but the recurrence rate was greatly increased by irradiation. The height of the pulses was not affected by the intensity of irradiation or increase in gap spacing.

The next phase of the investigation was to reduce further the time constant of the measuring circuits in order to resolve the pulse shape, coupled with simultaneous recordings of light emission by a photomultiplier technique, on a double-beam oscillograph. The oscillograph time-base was tripped at random while the gap voltage was within 2% of the breakdown value. A current pulse rise-time of less than 1μsec was accompanied simultaneously by a light pulse of short duration; the current pulse then fell from the initial peak value to a value up to 20μA, and current continued to flow for a time dependent upon gap length, and constant for a given gap length (figure 1 (*b*)).

The current pulse characteristics can be explained on the assumption that each is associated with a single electron avalanche (see also Raether 1956). The fast rise is produced by the travel of the avalanche itself across the gap, producing considerable ionization and excitation, especially in the vicinity of the anode, and resulting in the appearance of an anode glow. Residual positive ions move more slowly towards the cathode, maintaining current flow until the process is complete. On this basis, and neglecting electron transit time, the duration of a single pulse would be determined by the transit time of positive ions to move from anode to cathode, regardless of the point in the uniform field at which the electron avalanche was initiated. Pulse duration would then be constant for a given electrode spacing and field strength.

Figure 2 gives measured pulse duration for gap lengths of 1·0 to 4·0 cm, and values of E/p in the range 40 to 34 v cm^{-1} (mm Hg)$^{-1}$. The pulse duration was taken as the time between the occurrence of the avalanche and the instant when the current had fallen to 50% of the 'plateau' value (Schmidt 1954). If we assume this duration to be a measure of positive ion drift velocity, the experimental data are seen to agree well with a curve calculated for a constant ionic mobility of 2·6 cm^2 sec^{-1} v^{-1}. This mobility was determined by neglecting the effect on the pulse duration of the circuit parameters and electron attachment. The latter process may be important in the presence of water vapour and unknown impurities but a consideration of the theory of Schmidt (1954) and of the pulse shapes obtained suggests that the error in pulse duration due to these two factors is not likely to exceed 10%.

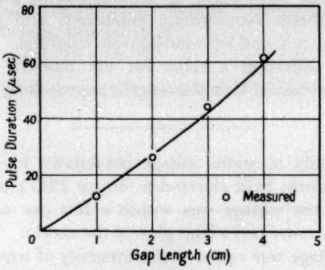

Figure 2. Variation of pulse duration with gap length. Comparison of measured pulse lengths with a curve obtained by taking a constant ionic mobility of 2·6 cm^2 sec^{-1} v^{-1}.

The value of this method of determining ionic mobility is that measurements are made at voltages near to the sparking potential and under ambient atmospheric conditions.

Figure 3 summarizes the fundamental pulse shapes for gap spacings of 1·0 to 5·0 cm between uniform field electrodes for which the limiting spacing for sparkover in the uniform field region occurred at 3·8 cm. The pulse recurrence rate was of the order of 10^4/sec, so that many cases of superposition of the fundamental shapes were recorded.

It will be seen that, as the region of maximum electrode surface gradient moves out to the curved edges of the electrodes at the higher spacings, a subsidiary peak appears on the tail of the pulses with increasing frequency, and was present on all pulses for the 5·0 cm gap (figure 1 (*c*)). This latter characteristic is also found on pulses recorded in the divergent field between spherical electrodes. It is believed that this second maximum is due to ion movement in the diverging field between the edges of the uniform field electrodes, the velocity of such ions being reduced as they pass through the relatively weaker field strength in the mid-gap plane.

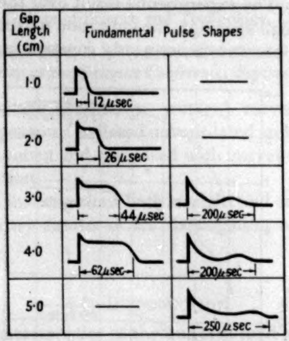

Figure 3. Fundamental current pulse shapes for different gap lengths.

To investigate these pre-breakdown discharges further, it was necessary to specify the irradiation conditions in terms of the initial ionization current I_0 produced in the gap. The onset of the pre-breakdown pulses occurs within 2% of the breakdown voltage and is thus strongly dependent on voltage, whereas the initial ionization current I_0 is independent of the applied voltage over a wide range. Therefore the pre-breakdown pulses are formed in the strongest part of the field, that is between the plane surfaces, while the initial ionization current I_0 is distributed over the entire electrode surface including the curved portions. Measurements of the ionization current I_0 should only detect that part of the current associated with the region in which the pre-breakdown pulses occur. For this purpose one electrode was modified so that the curved edge area formed a guard ring insulated from the central plane area. With this as the earthed electrode of the gap, and an applied field strength of 120 v cm^{-1}, I_0 could be measured as the total current between the two electrodes, or as the component currents to the flat and curved areas respectively. A null method of measurement was used when determining the component currents, arranged so that both parts of the guard ring electrode were at earth potential throughout.

Radium irradiation was obtained by locating a capsule of radium bromide on the axis of the high voltage electrode (anode), at a depth of 1 mm below the sparking surface. Radiations which do not produce secondary effects at the electrode surfaces disperse from the inter-electrode gap and have no effect on the breakdown processes, and the proportion of the total so lost will increase with gap spacing. As the spacing is increased, the intensity of irradiation on the guard-ring cathode is decreased, and in addition there is a marked reduction in the proportion of total radiation incident upon the central area of this electrode. As a result, the percentage of total current in the uniform field region falls from 25% to 19% as the spacing is increased from 1 cm to 4 cm.

Absorption of gamma rays by the electrodes releases beta particles into the gap, the total being a constant quantity from the radium-bearing electrode, and a quantity dependent on gap length from the other electrode. As the gap length is increased, the total radiation available for ionization decreases, but the consequent reduction in ionization is offset by the fact that a larger number of gas molecules is available. The experimental result over the range of spacings here considered is that, at small spacings, the ionization current first increases rapidly with spacing, and then becomes more nearly constant, as illustrated in figure 4.

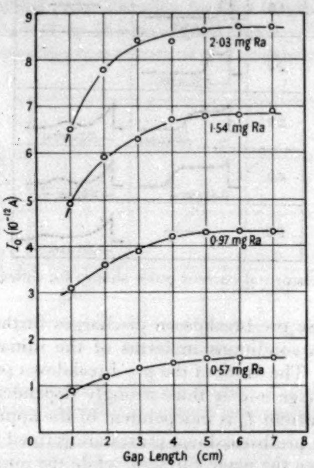

Figure 4. Variation of ionization current to inner electrode with gap length. Voltage gradient 120 v cm^{-1}; area of inner electrode 10·8 cm^2.

If the ionization current I_0 is plotted against the weight of radium for any given spacing, it will be seen that the ionization current is proportional to the weight of radium salt, indicating that background ionization is relatively insignificant.

ACKNOWLEDGMENTS

The authors are indebted to the Sir James Caird Scholarship Trust and the Research Council of the Central Electricity Authority for Scholarships and Grants in aid of these investigations.

REFERENCES

BRUCE, F. M., 1947, *J. Instn Elect. Engrs*, Pt. II, **94**, 138
RAETHER, H., 1956, *Appl. Sci. Res.* B, **5**, 23.
SCHMIDT, K. J., 1954, *Z. Phys.*, **139**, 251.

Some Sparkover Phenomena with Enclosed Gaps

By A. AKED, F. M. BRUCE and C. GORDON
The Royal College of Science and Technology, Glasgow, C.1

MS. received 11*th November* 1958, *in revised form* 15*th October* 1959; *paper read before the Society at the Swansea Conference, September* 1958

Abstract. The (percentage breakdown, voltage) curves obtained by applying 1/50 μsec impulse voltages to an enclosed unventilated and non-irradiated uniform field gap have been examined and compared with curves obtained under a variety of conditions of ventilation.

In the course of the investigations both straight and stepped spark paths were observed, and preliminary results of an investigation of this phenomenon are described.

---

§ 1. INTRODUCTION

The breakdown characteristics of the uniform field spark gap are dependent upon the pressure, temperature and humidity of the atmosphere in which the gap is located. Work is proceeding in a controlled atmosphere tank in which these characteristics will be investigated. The volume of gas contained in this tank will be subjected to repeated electrical stressing and discharges, and physical and chemical changes may occur having significant effect upon the breakdown characteristics of the gap.

Repeated application of an impulse voltage across a spark gap produces an increasing percentage of breakdowns as the peak value of the voltage is raised. ΔV, the width of the (percentage breakdown, voltage) curve, is the increase in peak voltage required to produce the transition from 0% to 100% breakdown. A width of less than 1% can occur when standard 1/50 μsec impulses are applied to a uniform field gap irradiated by radium or ultra-violet light. If the level of irradiation is reduced to that occurring naturally, ΔV is found to increase and becomes sensitive to changes occurring in the availability of initiatory electrons in the gap.

The widths of the (percentage breakdown, voltage) curves obtained for an enclosed, non-irradiated and unventilated uniform field gap had a large spread. Experiments were carried out, under varying conditions of gap ventilation, to find a simple method of reducing this spread. The results obtained also indicated possible causes of this improved performance of the gap.

In the course of the investigations, both straight and stepped spark paths were observed and preliminary results of an investigation of this phenomenon are described.

§ 2. PROCEDURE

Standard 1/50 μsec positive impulse voltages, generated by a multistage impulse generator, were applied to a 1 cm gap between 100 kv Stephenson profile (Bruce 1947) electrodes. The spark gap was centrally situated in a $3\frac{3}{4}$ ft × $3\frac{3}{4}$ ft × $2\frac{3}{4}$ ft hard-board box, the sides of which were covered with aluminium, and was not subjected to imposed irradiation. The generator output voltage was proportional to the charging voltage, which was measured by a high voltage d.c. potentiometer and controlled to within ±0·05%. After cleaning the electrodes and setting the gap, twenty impulses were applied at each of several increasing voltages over the range from 0% to 100% breakdown. The time between the application of successive impulses was 30 sec. Temperature, pressure and relative humidity were measured, and the voltages all reduced to N.T.P. Voltage oscillograms were recorded, and at the completion of each experiment the electrodes were photographed to record the distribution of the spark roots over the surface.

For ease of comparison of the (percentage breakdown, voltage) curves obtained, all voltages were expressed as a percentage of a fixed voltage taken close to the d.c. breakdown voltage.

§ 3. PERCENTAGE BREAKDOWN, VOLTAGE CURVES

3.1. *Enclosed Gap without Air Circulation*

Large variations were observed in the shape and width of the (percentage breakdown, voltage) curves obtained under this condition, although all curves originated from a common value on the voltage axis. Widths ranging from 15% to 35% were measured, and in several instances considerable scatter of the points occurred, particularly at the higher voltages, making curve estimation difficult. In general the results indicated a (percentage breakdown, voltage) characteristic which was linear at the lower voltages but of decreasing gradient as the frequency of breakdown rose above 50%. The envelope diagram containing six curves is shown as A in figure 1.

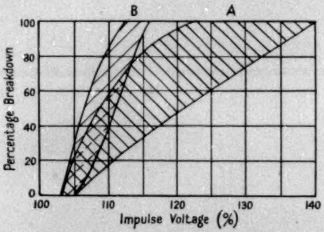

Figure 1. (Percentage breakdown, voltage) curves. A, no air circulation; B, continuous air circulation.

Observations of the distribution of the spark roots over the electrode surfaces showed a tendency towards grouping at the edge of the electrode flats.

3.2. *Enclosed Gap with Air Circulation*

A series of (percentage breakdown, voltage) curves was obtained with air circulation in the enclosing chamber. The three systems used for the air circulation are shown in figure 2.

Nine (percentage breakdown, voltage) curves were measured with the chamber ventilated for about 20 sec between each impulse. These curves displayed a common breakdown threshold voltage similar to that found when there was no air circulation in the chamber. Values of ΔV were, however, significantly lower than previously recorded, ranging from 6% to 14%, and all the curves were approximately linear in shape. The greatest consistency between curves was obtained with intermittent ventilation using system (*c*) (figure 2) when the values of ΔV ranged from 6% to 9%.

The envelope diagram B in figure 1 contains four curves obtained with air circulated continuously by the ventilation system (*c*). The curves are similar to those obtained with intermittent ventilation but the values of ΔV ranged from 6% to 12%.

A uniform distribution of spark roots over the electrode flats was observed.

3.3. *Non-irradiated Gap in Open Laboratory*

(Percentage breakdown, voltage) curves were measured for the 1 cm gap situated in the open laboratory. During the investigations the impulse generator was enclosed to prevent ultra-violet irradiation of the spark gap. Values of ΔV recorded ranged from 6% to 20%, the narrower curves being linear in shape and the wider curves having the drooping characteristic. An apparently uniform spark root distribution was observed.

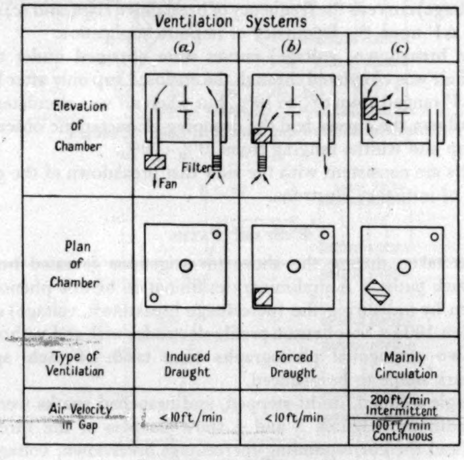

Ventilation Systems
(a)
(b)
(c)
Elevation of Chamber
Filter
Fan
Plan of Chamber
Type of Ventilation
Induced Draught
Forced Draught
Mainly Circulation
Air Velocity in Gap
< 10 ft/min
< 10 ft/min
200 ft/min Intermittent
100 ft/min Continuous

Figure 2. Ventilation systems.

3.4. *Discussion of Results*

The results show the improvements in the impulse breakdown characteristics of an enclosed, non-irradiated, uniform field gap which may be obtained by circulation of the air in the enclosing chamber.

The most consistent results were achieved using ventilation system (*c*) which produced mainly circulation and mixing of the air. Under this condition the width of the (percentage breakdown, voltage) curve was reduced in range from 15%–35% to 6%–12%. Although the first two systems produced an airflow of considerably less than 10 ft min^{-1}, the widths of the (percentage breakdown, voltage) curves were significantly reduced. The results obtained by continuous ventilation of the gap are of interest in the case of a controlled atmosphere tank in which air must be continuously circulated to achieve atmospheric control. The velocity of circulation in this is, however, only of the order of 2 ft min^{-1} and additional air circulation, ensuring adequate air velocity in the gap, should therefore be used. The improvements obtained by ventilation will permit the use of the non-irradiated, uniform field gap in the controlled atmosphere tank for investigations into breakdown characteristics.

(Percentage breakdown, voltage) curves obtained with a non-irradiated gap in the open laboratory have values of ΔV ranging from 6% to 20% and thus lie between those for the enclosed gap with and without air circulation. Air circulation is therefore recommended under this condition.

The strongly irradiated uniform field gap has a very narrow (percentage breakdown, voltage) curve (about 0·7% (Bruce 1954)) and therefore no significant effects caused by ventilation have yet been encountered.

The results obtained for an enclosed gap with no air circulation possess the following interesting characteristics: (*a*) a breakdown threshold voltage similar to that with air circulation applied, (*b*) a drooping of the (percentage breakdown, voltage) curve as the frequency of breakdown rises, and (*c*) an apparent dependence of ΔV upon the frequency of impulse application.

(Percentage breakdown, voltage) curves were obtained under two further conditions. If air was circulated through the enclosed gap only after breakdown, the values of ΔV ranged from 6% to 10%, but when air was circulated only after each non-breakdown the curves had the drooping characteristic observed for the unventilated gap and widths ranging from 10% – 20%.

These results are consistent with the view that breakdown of the gap reduces the availability of initiatory electrons.

§ 4. SPARK PATHS

Photographs taken during the above investigations revealed both straight and stepped spark paths. A preliminary examination of this phenomenon has been undertaken by measuring the (percentage breakdown, voltage) curves for a 1 cm gap between 100 kv Stephenson profile electrodes with and without imposed irradiation. Two orthogonal photographs were taken of each spark, thus allowing the spark shape to be deduced.

Straight, single stepped, multi-stepped, and branched sparks were observed under each condition. Figures 3 and 4 show samples of the three types of stepped sparks and the corresponding (percentage breakdown, voltage) curves.

4.1. *Non-irradiated Gap in Open Laboratory*

In figure 3 the envelope containing seven (percentage breakdown, voltage) curves obtained for positive and negative impulses is shown. In addition to samples of stepped sparks, a record showing two straight sparks which occurred for a single impulse is also shown. This was one of only two double sparks observed during these investigations. An analysis of the percentage of stepped sparks occurring at various voltage levels shows a significant decrease in the proportion of stepped sparks as the impulse voltage is raised above the threshold value.

4.2. *Radium-irradiated Gap in Open Laboratory*

The gap was irradiated by two $\frac{1}{2}$ mg radium capsules diametrically placed in the plane of the gap, 33 cm from the axis. The initial ionization current was 4×10^{-12} amp.

A (percentage breakdown, voltage) curve of width 1·2% is shown in figure 4 together with samples of the stepped sparks observed, which include a second sample of a double spark. The proportion of sparks which were stepped is shown beside each experimental point on the (percentage breakdown, voltage) curve. Over the 0% to 100% breakdown transition range this value is consistently high.

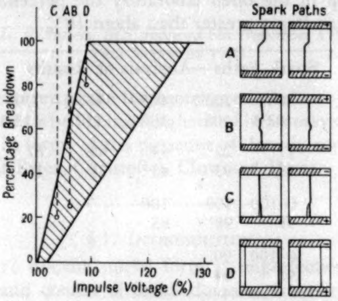

Figure 3. Non-irradiated gap in open laboratory.

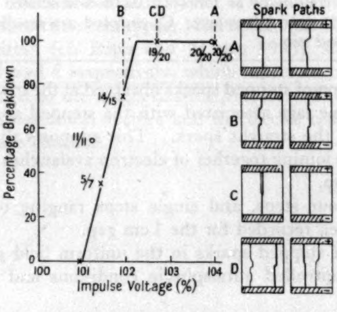

Figure 4. Radium-irradiated gap in open laboratory.

4.3. *Irradiated Enclosed Gap*

The 1 cm uniform field gap was enclosed in the chamber and the air was not circulated. The gap was irradiated either by ultra-violet light from the impulse generator stage gaps passing through a slit in the side of the enclosing chamber or by a ½ mg capsule of radium located on the axis of the anode, 1 mm behind the sparking surface. Under both conditions, (percentage breakdown, voltage) curves of width 0·6% were obtained for positive impulses. The proportion of the sparks which were stepped was high in each case. Further investigations are required before conclusions may be drawn about the relation between the voltage and the proportion of sparks which are stepped, over the limited transition range.

4.4. *Discussion of Results*

A complete analysis showing the percentage of stepped sparks occurring at different impulse voltage levels is given in the table. This percentage is very high, ranging from 85% to 93%, for the lowest voltage range. For the non-irradiated gap in the open laboratory the percentage of stepped sparks decreases considerably over the 0% to 100% breakdown range of voltages. With the radium irradiated gap in the open laboratory the percentage is only reduced significantly with overvoltages greater than about 10%.

Spark Paths—Analysis of Results

	Impulse Voltage Range (%)	100–102·5	102·5–105	105–107·5	107·5–110	110–112·5	112·5–115	115–117·5	117·5–120
A	Breakdown (%)	17	22	44	69	87		95	
	Stepped sparks (%)	85	93	43	31	16		26	
B	Breakdown (%)	0–100	100	100			100		100
	Stepped sparks (%)	91	98	85			40		5
C	Breakdown (%)	0–100	90						
	Stepped sparks (%)	91	94						
D	Breakdown (%)	0–100							
	Stepped sparks (%)	87							

A, B, C, D: irradiation conditions as follows: A, non-irradiated gap in open laboratory; B, radium irradiated gap in open laboratory; C, enclosed gap irradiated by ultra-violet light; D, radium irradiated enclosed gap.

The high proportion of stepped sparks observed at the lower voltages indicates that the formative time lags associated with the stepped spark are shorter than those associated with the straight spark. This supports the view that stepped sparks result from the joining together of electron avalanches initiated at different points in the spark gap.

A maximum of four steps, and single steps ranging up to 1·5 mm radial displacement have been recorded for the 1 cm gap.

The occurrence of stepped sparks in the uniform field gap is being further investigated under controlled atmospheric conditions and at longer sparking distances.

ACKNOWLEDGMENT

The authors are indebted to the Research Council of the Central Electricity Authority for grants in aid of these investigations.

REFERENCES

BRUCE, F. M., 1947, *J. Instn Elect. Engrs*, Pt. II, **94**, 138.
—— 1954, *Endeavour*, **13**, 61.

Thermomagnetic Behaviour of Ferromagnetic Domain Nuclei

By P. F. DAVIS†
University of Nottingham

Communicated by L. F. Bates; MS. received 6th November 1958, *in revised form* 19*th November* 1959

Abstract. Certain features of the thermomagnetic behaviour of a single crystal specimen of silicon–iron when being magnetized in an easy direction of magnetization are explained in terms of the presence of domain nuclei in the specimen, following the work of Bates, Christoffel, Clow and Davis.

---

§ 1. INTRODUCTION

FERROMAGNETIC domain nuclei form at imperfections in a crystal, such as inclusions, and consist of small domains from which larger domains can be formed, when suitable changes in field strength occur, by growth and interaction with other domains. The nucleation and growth of domains has been studied by Bates and Martin (1953, 1956). The nuclei occurring in iron may be divided into two main types, Néel spikes (cf. Néel 1944), and nuclei of reverse magnetization (cf. Bates and Martin 1956), and illustrated by the diagrams in figures 1 and 2 respectively, which represent cross sections of the nuclei in planes parallel to the magnetization vectors. The arrows indicate the directions of the magnetization vectors and the circles represent the inclusions to which the nuclei are attached.

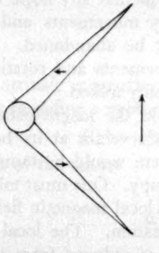

Figure 1. Néel spikes.

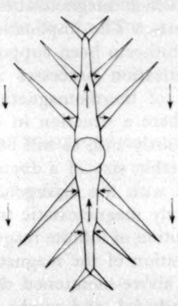

Figure 2. Nuclei of reversed magnetization.

In the investigations of Bates *et al.* (1957) a correlation was found between the presence of domain nuclei in a single crystal specimen of silicon–iron magnetized in a [001] direction and the thermomagnetic behaviour of the specimen.

---

† Now at English Electric Co., Whetstone.

Above the knee of the magnetization curve the only domains present in a crystal magnetized in an easy direction of magnetization are domain nuclei, and it was found that in this region of the magnetization curve the reversible thermal change Q_{R}' accompanying a magnetic field change from -600 Oe to H could be represented by

$$Q_{\mathrm{R}}' = a\int_{-600}^{H} d(HI) + c''\int_{-155}^{H} (H-H_{\mathrm{c}})\,dI_{\mathrm{R}} \qquad \ldots\ldots(1.1)$$

where I is the magnetization, and dI_{R} an infinitesimal reversible change in magnetization. H_{c} is the coercive field, $a = -(T/I_{\mathrm{s}})(dI_{\mathrm{s}}/dT)$, T is the absolute temperature and I_{s} is the intrinsic magnetization; c'' is a constant which was found to have the value $-0{\cdot}43$. In the region of the coercive field the reversible thermal equation were represented by

$$Q_{\mathrm{R}}' = a\int_{-600}^{H} d(HI) + c''\int_{-155}^{H} (H-H_{\mathrm{c}})\,dI_{\mathrm{R}} + d''\int_{-5}^{H} (H-H_{\mathrm{c}})\,dI_{\mathrm{R}}, \qquad \ldots\ldots(1.2)$$

where the constant $d'' = -1{\cdot}05$.

The first term on the right-hand side of equation (1.1) represents the magnetocaloric effect, and therefore the second term represents the thermomagnetic behaviour of the domain nuclei in fields greater than 5 Oe in magnitude.

Now, the value of c'' obtained by experiment is not significantly different from $(T/K)dK/dT$, where K is the first anisotropy constant, so that in fields $H \gg H_{\mathrm{c}}$ equation (1.1) approximates to

$$Q_{\mathrm{R}}' = \frac{-T}{I_{\mathrm{s}}}\frac{dI_{\mathrm{s}}}{dT}\int_{-600}^{H} d(HI) + \frac{T}{K}\frac{dK}{dT}\int_{-155}^{H} H\,dI_{\mathrm{R}}. \qquad \ldots\ldots(1.3)$$

Equation (1.3) is identical, for the stated limits of integration, with that obtained by Stoner and Rhodes (1949) for a specimen in which the only magnetization process of significance is that of domain vector rotations, whereas in the present case movements of the domain boundary of nuclei predominate as the mode in which magnetization takes place, as was confirmed by Bitter figure observations. The implication is that equation (1.1) is of greater generality than has hitherto been supposed, and it might seem that any hope of analysis of magnetization processes into domain boundary movements and rotations by means of thermomagnetic measurements must be abandoned. However, we have here a situation in which boundary movements and rotations occur simultaneously and, as will be shown, are energetically linked.

The stable size of a domain nucleus depends on the magnetostatic energy associated with the divergence of the magnetization vector at its boundaries, but a purely magnetostatic treatment of the problem would be tantamount to an assumption of infinite magnetocrystalline anisotropy. One must take account of the rotation of the magnetization vector by the local magnetic fields arising from the above-mentioned divergence in magnetization. The local fields are thereby reduced, and so the magnetostatic energy is reduced from that which would be obtained for a case of infinite magnetocrystalline anisotropy, by an amount dependent on the magnitude of the anisotropy constant. Consequently, the size and thermomagnetic behaviour of the domains are dependent on the anisotropy constant.

When the magnetic field applied to the specimen is changed two processes occur; one is a change in the size of the domain nuclei involving a change in their magnetostatic energy and, therefore, in magnetocrystalline anisotropy energy, while the other is the rotation of the magnetization vectors in the nuclei due to the change in the applied field. Each process gives rise to a change in the magnetization of the specimen and to thermomagnetic effects dependent on the magnetocrystalline anisotropy constants.

The following derivation of the thermomagnetic behaviour of domain nuclei is considered to be valid when the field strength is sufficiently small for the following μ^* approximation to be used, but large enough for the pressures exerted by the boundaries of the nuclei, due to a tendency to reduce the total Bloch wall energy, to be neglected in comparison with other pressures acting. In these circumstances magnetoelastic energy can also be neglected. An adverse applied field tends to cause the nuclei to shorten, whereas the forces of interaction between the effective poles on the boundary of a domain nucleus tend to cause the nucleus to lengthen in order to reduce its demagnetization energy. The resultant magnetic field in the neighbourhood of a domain nucleus, in general, rotates the magnetization vectors away from the easy directions of magnetization against the action of magnetocrystalline anisotropy. Because of the relative values of the intrinsic magnetization and anisotropy constants of iron, the equation (1.3) for Q' is obtained, since the demagnetization energies of the nuclei are approximately proportional to the first anisotropy constant.

§ 2. THE μ^* APPROXIMATION

We begin with a brief account of the μ^* approximation, first used by Landau and Lifshitz in 1935. In calculating the magnetic field near a domain nucleus we have now to take account of the rotation of the domain magnetization vectors by the field. The calculation may be very much simplified, for materials with uniaxial or iron-like cubic anisotropy in low field regions, by the use of the μ^* approximation. When a magnetic field is applied to domains magnetized in the z direction, for example, the direction of magnetization in the domains will in general be rotated, and if the rotation is small the relations between the components of the field H and the induction B inside the domains are given by

$$B_x=\mu^* H_x, \quad B_y=\mu^* H_y, \quad B_z=H_z+4\pi I_s, \qquad \ldots\ldots (2.1)$$

where

$$\mu^*=1+2\pi I_s^2/K \qquad \ldots\ldots (2.2)$$

I_s is the intrinsic magnetization and K is the first anisotropy constant. It is convenient to define a vector $\mathbf{B}^*$ such that

$$B_x^*=\mu^* H_x, \quad B_y^*=\mu^* H_y, \quad B_z^*=H_z, \qquad \ldots\ldots (2.3)$$

or in terms of the tensor

$$\boldsymbol{\mu}^*=\begin{Bmatrix} \mu^* & 0 & 0 \\ 0 & \mu^* & 0 \\ 0 & 0 & 1 \end{Bmatrix} \qquad \ldots\ldots (2.4)$$

giving

$$\mathbf{B}^*=\boldsymbol{\mu}^*\mathbf{H}. \qquad \ldots\ldots (2.5)$$

If a vector $\mathbf{I}^*$ is defined such that for a domain magnetized in the z direction,

$$I_x^*=0, \quad I_y^*=0, \quad I_z^*=I_s \qquad \ldots\ldots (2.6)$$

then

$$\mathbf{B}=\mathbf{B}^*+4\pi\mathbf{I}^*. \qquad \ldots\ldots (2.7)$$

and

$$\operatorname{div}\mathbf{B}^*=-4\pi \operatorname{div}\mathbf{I}^*. \qquad \ldots\ldots (2.8)$$

§ 3. ENERGY BALANCE IN THE SPECIMEN

3.1. *General Statement*

In field strengths greater than about 5 Oe the magnetoelastic and Bloch wall energies of the domain nuclei may be neglected in comparison with their magnetostatic and magnetocrystalline anisotropy energies, so that the energy E per unit volume of the specimen may be written

$$E=-\int_0^{v=1}(\tfrac{1}{2}\mathbf{H}_{\mathrm{D}}.\mathbf{I}+\mathbf{H}_{\mathrm{a}}.\mathbf{I})\,dv+K\int_0^{v=1}(\alpha_1{}^2\alpha_2{}^2+\alpha_2{}^2\alpha_3{}^2+\alpha_3{}^2\alpha_1{}^2)\,dv \qquad \ldots\ldots(3.1.1)$$

where H_{a} is the applied field and H_{D} is the local value of the demagnetizing field in the element dv of the volume of the specimen; α_1, α_2, α_3 are the direction cosines of the magnetization vector $\mathbf{I}$ in the element of volume dv. The first term on the right-hand side of equation (3.1.1) represents the magnetic energy, and the second represents the anisotropy energy.

The stable magnetic state of the specimen corresponds to a minimum of the energy E, so that

$$0=dE=-\int_0^{v=1}(\mathbf{H}_{\mathrm{D}}+\mathbf{H}_{\mathrm{a}}).\,d\mathbf{I}\,dv+K\int_0^{v=1}d(\alpha_2{}^2\alpha_1{}^2+\alpha_2{}^2\alpha_3{}^2+\alpha_3{}^2\alpha_1{}^2)\,dv. \qquad \ldots\ldots(3.1.2)$$

The factor $\frac{1}{2}$ disappears on differentiation of the term $\frac{1}{2}\mathbf{H}_{\mathrm{D}}.\mathbf{I}$ as H_{D} is produced by the divergences in the magnetization.

If the specimen has a macroscopic demagnetization factor N the field will not necessarily be uniform on a microscopic scale as there are local divergences in magnetization associated with the domain nuclei.

Let

$$\mathbf{h}=\mathbf{H}_{\mathrm{D}}+N\mathbf{I} \qquad \ldots\ldots(3.1.3)$$

where N is the demagnetization factor of the whole specimen, so that $\mathbf{h}$ represents the demagnetizing effects of poles on the sides of the spikes, etc. Substituting for $\mathbf{H}_{\mathrm{D}}$ in equation (3.1.2) gives

$$0=-(H_{\mathrm{a}}-NI)dI-\int_0^{v=1}\mathbf{h}.\,d\mathbf{I}\,dv+K\int_0^{v=1}d(\alpha_1{}^2\alpha_2{}^2+\alpha_2{}^2\alpha_3{}^2+\alpha_3{}^2\alpha_1{}^2)\,dv. \qquad \ldots\ldots(3.1.4)$$

3.2. *Examination of an Energy Term*

Let us consider the term

$$\int_0^{v=1}\mathbf{h}.\,d\mathbf{I}\,dv$$

on the right-hand side of equation (3.1.4). From equation (2.8) we have

$$-4\pi\,\mathrm{div}\,\mathbf{I}^*=\mathrm{div}\,\mathbf{B}^*=\mathrm{div}\,\boldsymbol{\mu}^*\mathbf{H}=\mathrm{div}\,\mu^*\mathbf{h} \qquad \ldots\ldots(3.2.1)$$

since the macroscopic magnetizing field $\mathbf{H}_{\mathrm{a}}-N\mathbf{I}$, is uniform inside the specimen; $\boldsymbol{\mu}^*$ is the tensor, defined in equation (2.4), for a domain magnetized in the z direction, and $\boldsymbol{\mu}^*\mathbf{h}$ has the magnitude

$$[(\mu^*h_x)^2+(\mu^*h_y)^2+h_z{}^2]^{1/2}. \qquad \ldots\ldots(3.2.2)$$

At a domain boundary the normal component of magnetization is either continuous or there is only a small divergence in the magnetization; consequently, the boundaries of domain nuclei in iron approximate to 90° and 180° boundaries. For an approximate 180° boundary nearly parallel to the magnetization vector in the z direction, the local field $\mathbf{h}$ produced by the divergence in magnetization at the boundary will be such that

$$h_z \simeq 0 \quad \text{and} \quad h \simeq (h_x^2 + h_y^2)^{1/2}.$$

For a Néel spike inside a region magnetized in the z direction, h_z and h_x or h_y will be of the same order of magnitude inside and outside the spike, but since $\mu^* \gg 1$ for iron, the expression (3.2.2) reduces approximately to

$$\mu^*(h_x^2 + h_y^2)^{1/2} \qquad \ldots\ldots (3.2.3)$$

for the region outside the spike. Inside the spike the magnitude of the vector $\boldsymbol{\mu}^*\mathbf{h}$ is given by

$$\mu^*(h_y^2 + h_z^2)^{1/2} \quad \text{or by} \quad \mu^*(h_x^2 + h_z^2)^{1/2} \qquad \ldots\ldots (3.2.4)$$

depending on whether the spike is magnetized in the x or the y direction, respectively.

Now, from equations (3.2.1) to (3.2.4)

$$\operatorname{div} \mathbf{h} = \frac{-4\pi}{\mu^*} \operatorname{div} \mathbf{I}^*. \qquad \ldots\ldots (3.2.5)$$

But I^* is proportional to the saturation magnetization I_S; therefore,

$$h \propto I_S/\mu^*. \qquad \ldots\ldots (3.2.6)$$

Further, the energy of the specimen depends on its degree of magnetization, so that one may write

$$\int_0^{v=1} \mathbf{h} \, . \, d\mathbf{I} \, dv = \frac{I_S}{\mu^*} F_1\left(\frac{I}{I_S}\right) dI \qquad \ldots\ldots (3.2.7)$$

where $F_1(I/I_S)$ is a function of the reduced magnetization I/I_S. Now, in the case of iron μ^* is large and approximates closely to $2\pi I_S^2/K$. Therefore,

$$\int_0^{v=1} \mathbf{h} \, . \, d\mathbf{I} \, dv = \frac{KF_1}{2\pi} \frac{I}{I_S} d\left(\frac{I}{I_S}\right). \qquad \ldots\ldots (3.2.8)$$

Similarly, the term

$$K \int_0^{v=1} d(\alpha_1^2\alpha_2^2 + \alpha_2^2\alpha_3^2 + \alpha_3^2\alpha_1^2) \, dv$$

in equation (3.1.4.) can be expressed in the form

$$KF_2(I/I_S) d(I/I_S) \qquad \ldots\ldots (3.2.9.)$$

where $F_2(I/I_S)$ is another function of the reduced magnetization.

§ 4. DERIVATION OF THE THERMOMAGNETIC RELATIONS

From equations (3.1.4.), (3.2.8) and (3.2.9) it follows that

$$H_a - NI = \frac{KG(I/I_S)}{I_S} \qquad \ldots\ldots (4.1)$$

where $G(I/I_S)$ is a function of the reduced magnetization I/I_S, and, by substituting

$$H_a - NI = H, \qquad \ldots\ldots (4.2)$$

equation (1.3) may be derived, following the method of Teale and Rowlands (1957).

§ 5. CONCLUSIONS

It has been shown that although the magnetization process in the case under investigation is predominantly one of the movement of the domain walls of nuclei, the fact that the thermomagnetic experiments of Bates and others seem to indicate domain vector rotation processes, in accordance with the equation

$$Q' = \frac{-T}{I_s}\frac{dI_s}{dT}\int d(HI) + \frac{T}{K}\frac{dK}{dT}\int H\,dI,$$

derived by Stoner and Rhodes (1949), can be explained in terms of the conditions governing the equilibrium positions of the domain walls of nuclei when the field strength exceeds about 5 Oe.

ACKNOWLEDGMENTS

The Author wishes to thank Professor L. F. Bates for his encouragement and interest in this work, and the Electrical and Allied Industries Research Association for financial support which enabled him to carry out this study during the course of experimental work at Nottingham.

REFERENCES

BATES, L. F., CHRISTOFFEL, D. A., CLOW, H., and DAVIS, P. F., 1957, *Proc. Roy. Soc.* A, **243**, 160.
BATES, L. F., and MARTIN, D. H., 1953, *Proc. Phys. Soc.* A, **66**, 162.
—— 1956, *Proc. Phys. Soc.* B, **69**, 145.
LANDAU, L., and LIFSHITZ, E., 1935, *Phys. Z. Sowjet*, **8**, 153.
NÉEL, L., 1944, *Cah. Phys.*, No. 25, 21.
STONER, E. C., and RHODES, P., 1949, *Phil. Mag.*, **40**, 481.
TEALE, R. W., and ROWLANDS, G., 1957, *Proc. Phys. Soc.*, **70**, 1123.

An Investigation of the (^{3}He, p), (^{3}He, d) and (^{3}He, α) Reactions with ^{12}C at Bombarding Energies between 6 and 10 MeV

BY S. HINDS AND R. MIDDLETON
Atomic Weapons Research Establishment, Aldermaston, Berks.

Communicated by K. W. Allen; MS. received 29th October 1959

Abstract. Angular distributions have been measured of some proton, deuteron and α-particle groups arising from the bombardment of ^{12}C with 5·98, 8·83, 9·37 and 10·14 MeV ^{3}He particles. Excitation functions have also been measured at a laboratory angle of 10° in the energy interval 5·7 to 10·23 MeV. The results indicate that at most energies the (^{3}He, d) and the (^{3}He, α) reactions proceed predominantly by a direct process, but this is not true for the (^{3}He, p) reaction.

§ 1. INTRODUCTION

THE ^{12}C(^{3}He, p)^{14}N reaction has previously been studied by Bromley *et al.* (1957) in the energy range 1·0 to 2·8 MeV and by Johnston *et al.* (1958) in the range 2·0 to 5·0 MeV. Both authors observed pronounced resonances in the excitation curves and angular distributions which are not directly explicable from either a compound nucleus or a direct interaction process. Since the direct reaction mechanism is expected to predominate at higher energies it was considered worth while extending these measurements to incident energies of about 10 MeV.

Bromley *et al.* have also studied the ^{12}C(^{3}He, n)^{14}O and the ^{12}C(^{3}He, α)^{11}C reactions. They found that the total cross section of the ground state (^{3}He, α) reaction is approximately an order of magnitude greater than that of the (^{3}He, n) reaction which strongly suggests that the former, even below 3 MeV, is proceeding largely via a direct process. It was therefore expected that in the energy range 6 to 10 MeV the α-particle angular distributions would be strongly characteristic of a direct process and from them it might be possible to make certain spin and parity deductions. Although no previous work has been reported on the ^{12}C(^{3}He, d)^{13}N reaction, the angular distributions were expected to be of a stripping type from previous studies on other (^{3}He, d) reactions (Hinds and Middleton 1959 a, b).

The angular distributions of the ground and first six excited state proton groups from the ^{12}C(^{3}He, p)^{14}N reaction have been measured at incident energies of 5·98, 8·83, 9·37 and 10·14 MeV. At the same energies, the ground and first excited state α-particle groups from the ^{12}C(^{3}He, α)^{11}C reaction and the ground state deuteron group from the ^{12}C(^{3}He, d)^{13}N reaction have also been measured. Excitation curves have been measured for all groups at a laboratory angle of 10° and between energy limits of 5·7 and 10·2 MeV.

All measurements were made with the Aldermaston 6 MeV Van de Graaff accelerator and broad-range spectrograph. Apart from the 5·98 MeV data, which were obtained with the usual singly charged ^{3}He beam, all the other data were obtained using doubly charged ^{3}He particles. The intensity of the latter beam had previously been considerably enhanced by the insertion of a gas stripper tube a short way down the accelerating tube. A detailed account of this modification is intended for publication at a later date elsewhere. The rest of the experimental procedure followed closely that described in a previous communication (Hinds and Middleton 1959 a).

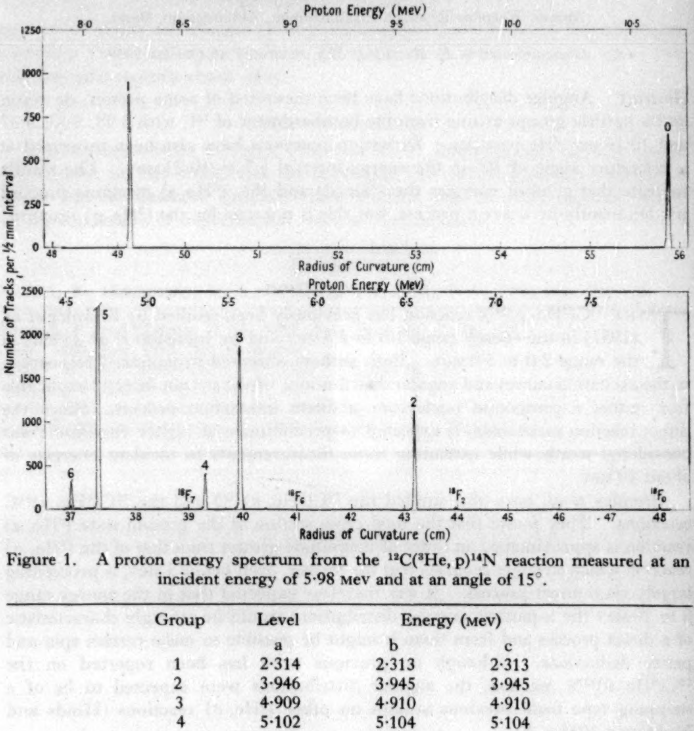

Figure 1. A proton energy spectrum from the ^{12}C(^{3}He, p)^{14}N reaction measured at an incident energy of 5·98 MeV and at an angle of 15°.

Group	Level	Energy (MeV)	
	a	b	c
1	2·314	2·313	2·313
2	3·946	3·945	3·945
3	4·909	4·910	4·910
4	5·102	5·104	5·104
5	5·686	5·686	
6	5·830	5·829	

a, present investigation: experimental error for all levels ±10 kev; b, Woodbury, Tollestrup and Day (1953) and Clegg and Wilkinson (1953) from the ^{13}C(p, γ)^{14}N reaction; c, Bockelman, Browne, Buechner and Sperduto (1953) from the ^{14}N(p, p$'$)^{14}N reaction.

§ 2. Results

A proton energy spectrum from the ^{12}C(^{3}He, p)^{14}N reaction measured at an incident energy of 5·98 MeV and at an angle of 15° is shown in figure 1. Following the notation used in previous communications, groups corresponding to states in ^{14}N are labelled numerically and impurity groups by the symbol for the final nucleus. The energy of the incident beam was determined to be 5·980 ± 0·012 Mev from observations, at several angles, of the elastically scattered ^{3}He particles from carbon and also the thin gold backing. From this the *Q*-value of the reaction was calculated to be 4·780 ± 0·015 Mev, which is in good agreement with the value of 4·772 Mev expected from the mass defects (Ajzenberg-Selove and Lauritsen 1959). In the table are listed the excitation energies of the first six excited states of ^{14}N together with the previously determined values.

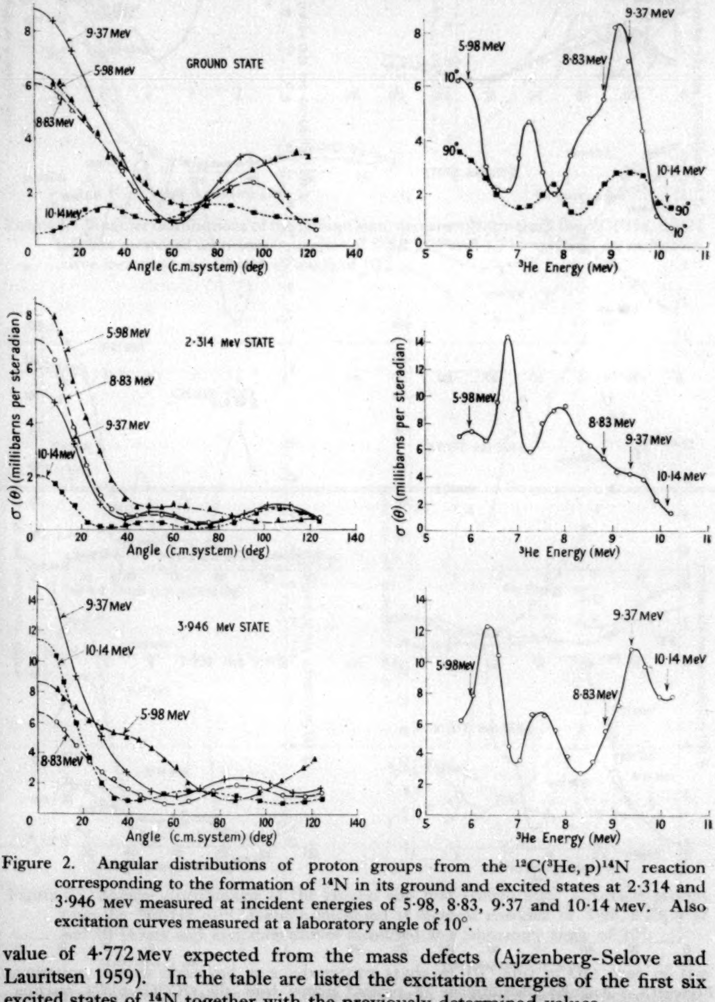

Figure 2. Angular distributions of proton groups from the ^{12}C(^{3}He, p)^{14}N reaction corresponding to the formation of ^{14}N in its ground and excited states at 2·314 and 3·946 Mev measured at incident energies of 5·98, 8·83, 9·37 and 10·14 Mev. Also excitation curves measured at a laboratory angle of 10°.

The angular distributions of seven proton groups measured at energies of 5·98, 8·83, 9·37 and 10·14 Mev are shown in figures 2 and 3. Also shown are the

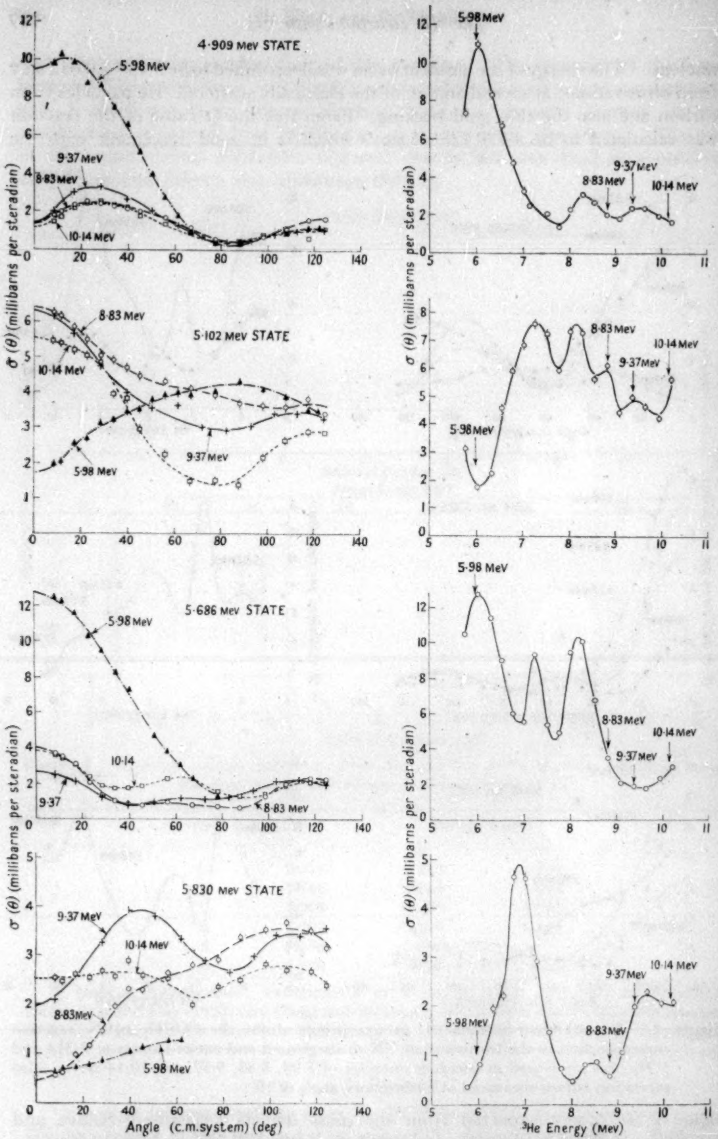

Figure 3. Angular distributions of proton groups from the $^{12}C(^{3}He, p)^{14}N$ reaction corresponding to excited states in ^{14}N at 4·909, 5·102, 5·686 and 5·830 Mev measured at incident energies of 5·98, 8·83, 9·37 and 10·14 Mev. Also excitation curves measured at a laboratory angle of 10°.

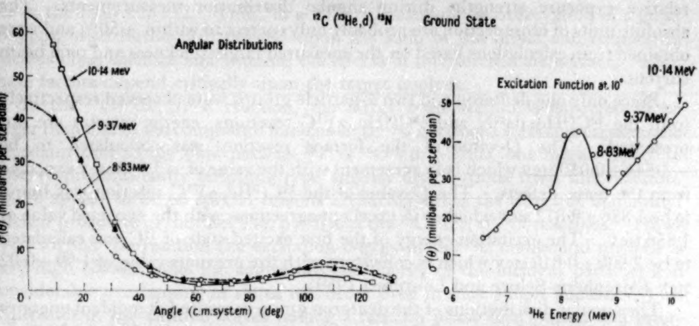

Figure 4. Angular distributions of the ground state deuteron group from the $^{12}C(^{3}He, d)^{13}N$ reaction measured at incident energies of 8·83, 9·37 and 10·14 Mev and an excitation curve measured at a laboratory angle of 10°.

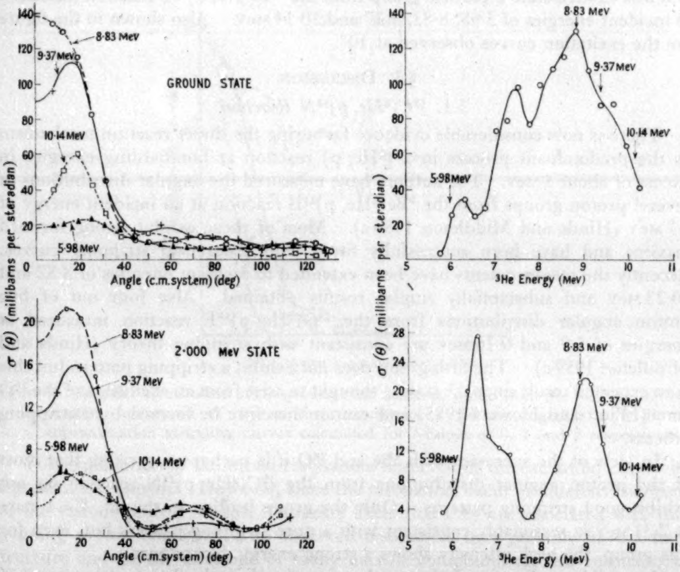

Figure 5. Angular distributions of the ground and first excited state α-particle groups from the $^{12}C(^{3}He, \alpha)^{11}C$ reaction measured at incident energies of 5·98, 8·83, 9·37 and 10·14 Mev and excitation curves measured at a laboratory angle of 10°.

excitation curves observed at a laboratory angle of 10° and in the case of the ground state group also at 90°. The latter was measured with a scintillation counter which is normally used in addition to a current integrator to monitor relative exposure strengths during angular distribution measurements. The absolute units of cross section are probably only correct to within ± 50% and were obtained from calculations based on the measured target thickness and total beam current.

Since only one deuteron and two α-particle groups were observed respectively from the $^{12}C(^{3}He, d)^{13}N$ and $^{12}C(^{3}He, \alpha)^{11}C$ reactions, energy spectra are not presented. The Q-value of the former reaction was calculated to be $-3{\cdot}544 \pm 0{\cdot}010$ Mev which is in agreement with the value of $-3{\cdot}553$ Mev expected from the mass defects. The Q-value of the $^{12}C(^{3}He, \alpha)^{11}C$ reaction was found to be $1{\cdot}856 \pm 0{\cdot}012$ Mev which is in excellent agreement with the expected value of 1·856 Mev. The excitation energy of the first excited state of ^{11}C was calculated to be $2{\cdot}000 \pm 0{\cdot}010$ Mev which is consistent with the previous value of $1{\cdot}99 \pm 0{\cdot}02$ Mev (Ajzenberg-Selove and Lauritsen 1959).

The angular distributions of the deuteron group measured at incident energies of 8·83, 9·37 and 10·14 Mev and the excitation curves measured at 10° are shown in figure 4. No measurements were made at 5·98 Mev since the spectrograph field, which was primarily chosen for the protons, was too high to record this group simultaneously. In figure 5 are shown the angular distributions of the ground and first excited state α-particle group from the $^{12}C(^{3}He, \alpha)^{11}C$ reaction measured at incident energies of 5·98, 8·83, 9·37 and 10·14 Mev. Also shown in the figure are the excitation curves observed at 10°.

§ 3. DISCUSSION

3.1. $^{12}C(^{3}He, p)^{14}N$ *Reaction*

There is now considerable evidence favouring the direct reaction mechanism as the predominant process in a (^{3}He, p) reaction at bombarding energies in excess of about 5 Mev. The authors have measured the angular distributions of several proton groups from the $^{9}Be(^{3}He, p)^{11}B$ reaction at an incident energy of 5·7 Mev (Hinds and Middleton 1959 a). Most of these exhibit strong forward maxima and have been successfully fitted with theoretical stripping curves. Recently the measurements have been extended to incident energies of 8·82 and 10·23 Mev and substantially similar results obtained. Also four out of five proton angular distributions from the $^{16}O(^{3}He, p)^{18}F$ reaction measured at energies of 5·9 and 9·16 Mev are consistent with stripping theory (Hinds and Middleton 1959 c). The fifth group does not exhibit a stripping pattern but this is an expected result since the state is thought to arise from an excitation of the ^{16}O core (Elliott and Flowers 1955) and cannot therefore be formed by a stripping process.

In view of the successes with ^{9}Be and ^{16}O it is perhaps surprising that most of the proton angular distributions from the $^{12}C(^{3}He, p)^{14}N$ reaction do not exhibit good stripping patterns. Only the group leading to the 0^{+}, $T=1$ state at 2·31 Mev is reasonably consistent with a pure stripping process but, even for this group, the peak intensity shows a strong energy dependence.

A possible explanation is that in the case of carbon the direct and compound nucleus cross sections are of similar magnitude and interference occurs. In general the direct part of a (^{3}He, p) reaction cross section is expected to be less than that of a (^{3}He, d) or a (^{3}He, α) reaction since two particles are involved in the transfer as compared with a single particle in the latter reactions. This is generally confirmed experimentally and for carbon at 9·37 Mev the ground state peak differential cross sections of the (^{3}He, p), (^{3}He, d) and (^{3}He, α) reactions are in the ratio 1 : 5 : 12. Thus, in a (^{3}He, p) reaction the observation of a good stripping distribution will depend upon the ratio of the direct and compound nucleus cross sections and whether the effects of interference are serious. Both these factors depend critically upon the target nucleus.

In the ^{16}O(^{3}He, p)^{18}F reaction, the direct cross section is expected to be larger than that of the compound nucleus since ^{16}O is a closed shell and a reasonable approximation to the final nucleus ^{18}F is ^{16}O + d. Thus, one might expect to observe predominantly stripping type angular distributions from this reaction. There appear to be no special reasons favouring either the direct or compound nuclear processes in the ^{9}Be(^{3}He, p)^{11}B and the ^{12}C(^{3}He, p)^{14}N reactions. However, for the ^{9}Be reaction the excitation energy of the ^{12}C compound nucleus is very high (26 Mev plus the centre-of-mass energy of the incident particle) and considerable overlapping of states will occur even in such a light nucleus. This will result in the emitted waves having a random phase distribution and interference will be minimized. Carbon differs from beryllium in this respect, the excitation of the compound nucleus, ^{15}O, being only 12 Mev, and complete overlapping of states will not occur. Thus the effects of interference will be more evident.

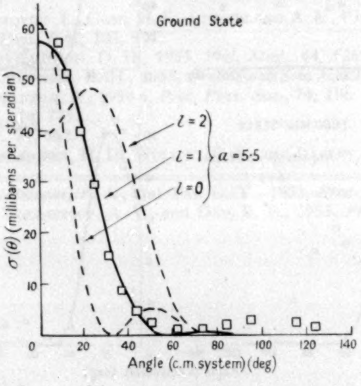

Figure 6. Angular distribution of the ground state deuteron group from the ^{12}C(^{3}He, d)^{13}N reaction measured at an incident energy of 10·14 Mev together with Born approximation stripping curves calculated for *l*-values of 0, 1 and 2 respectively.

The explanation of the broad resonances observed in the excitation curves is at present not known. However, since the resonances occur at different energies for the various proton groups, it appears likely that they are associated with the outgoing proton channel. The observed resonances may possibly have a fine structure and be the envelope of many narrow compound nuclear resonances. These, as a result of a statistical fluctuation, may have non-random properties and therefore cause a collective enhancement. Alternatively the resonances may arise from some optical model effect.

3.2. ^{12}C(^{3}He, d)^{13}N *Reaction*

Most of the (^{3}He, d) angular distributions measured by the authors at energies greater than about 5·5 Mev have been found to be consistent with stripping theory.

The ground state deuteron group from carbon is no exception, certainly at the investigated energies of 8·83, 9·37 and 10·14 MeV. However, the excitation function measured at 10° (figure 4) does exhibit a small resonance at about 8·1 MeV, but, unfortunately no angular distributions were measured close to this energy.

In figure 6 the 10·14 MeV experimental data are shown together with Born approximation stripping theory curves calculated for a radius of 5·5 fermi and *l*-values of 1, 0 and 2. The $l=1$ curve agrees closely with the experimental points. The same *l*-value was required by Middleton, El-Bedewi and Tai (1953) for the corresponding transition in the ^{12}C(d, n)^{13}N reaction.

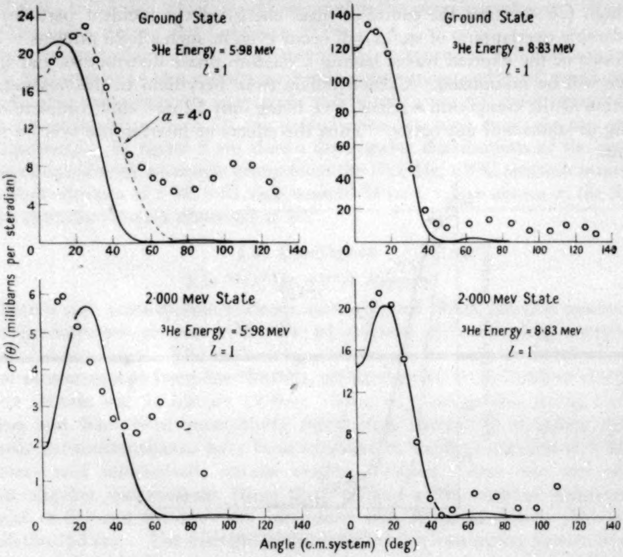

Figure 7. Angular distributions of the ground and first excited state α-particle group from the ^{12}C(^{3}He, α)^{11}C reaction measured at incident energies of 5·98 and 8·83 MeV together with curves calculated from Born approximation pick-up theory.

3.3. ^{12}C(^{3}He, α)^{11}C *Reaction*

The 10° excitation function of the α-particle groups proceeding to the ground and first excited states of ^{11}C both exhibit a marked resonance behaviour. The shapes of the angular distributions at small angles however are not appreciably affected and are consistent with the reaction proceeding via a pick-up process. This is illustrated in figure 7 where the 5·98 and 8·83 MeV angular distributions are shown fitted with Born approximation pick-up curves. These distributions were chosen since they have respectively the weakest and strongest peaks observed. The theoretical curves were calculated for $l=1$ and a radius of interaction equal to the Gamow radius plus one fermi (5·5 fermi) unless otherwise indicated. It may be noted that better agreement was achieved with the ground state α-particle group at 5·98 MeV using a slightly smaller radius (broken curve, figure 7), and probably better agreement could have been attained for the first excited state at the same energy using a larger radius.

It is of interest to note that the peak differential cross section of the ground state α-particle groups in the energy range 8 to 10 MeV is about twice that of the deuteron group and about ten times that of any of the proton groups.

ACKNOWLEDGMENTS

It is with pleasure that we acknowledge Dr. K. W. Allen for his continued interest in this work and Dr. H. C. Newns for much helpful discussion. We would also like to thank Mr. D. A. Proctor and Mr. H. Marchant for assisting with the exposures, Mr. A. H. F. Muggleton for preparing the carbon targets, and Mrs. N. E. Neville and her group of microscopists for scanning the nuclear plates.

REFERENCES

AJZENBERG-SELOVE, F., and LAURITSEN, T., 1959, *Nucl. Phys.*, **11**, 1.

BOCKELMAN, C. K., BROWNE, C. P., BUECHNER, W. W., and SPERDUTO, A., 1953, *Phys. Rev.*, **92**, 665.

BROMLEY, D. A., ALMQVIST, E., GOVE, H. E., LITHERLAND, A. E., PAUL, E. B., and FERGUSON, A. J., 1957, *Phys. Rev.*, **105**, 957.

CLEGG, A. B., and WILKINSON, D. H., 1953, *Phil. Mag.*, **44**, 1269.

ELLIOTT, J. P., and FLOWERS, B. H., 1955, *Proc. Roy. Soc.* A, **229**, 536.

HINDS, S., and MIDDLETON, R., 1959 a, *Proc. Phys. Soc.*, **74**, 196.

—— 1959 b, *Ibid.*, **74**, 775.

—— 1959 c, *Ibid.*, **74**, 762.

JOHNSTON, R. L., HOLMGREN, H. D., WOLICKI, E. A., and ILLSLEY, E. G., 1958, *Phys. Rev.*, **109**, 884.

MIDDLETON, R., EL-BEDEWI, F. A., and TAI, C. T., 1953, *Proc. Phys. Soc.* A, **66**, 95.

WOODBURY, H. H., TOLLESTRUP, A. V., and DAY, R. B., 1953, *Phys. Rev.*, **92**, 1199.

A Study of the ^{9}Be(^{3}He, p)^{11}B and the ^{9}Be(^{3}He, d)^{10}B Reactions in the Energy Range 5·7 to 10·2 Mev

By S. HINDS AND R. MIDDLETON
Atomic Weapons Research Establishment, Aldermaston, Berks.

Communicated by K. W. Allen; MS. received 7th December 1959, in final form 15th January 1960

Abstract. Angular distributions and excitation functions have been measured of ten proton and five deuteron groups arising from the bombardment of ^{9}Be with 5·7 to 10·2 Mev ^{3}He particles. The proton excitation functions, measured at 10°, are essentially smooth and most of the angular distributions exhibit strong forward peaks which appear to be consistent with a predominantly direct process. All of the deuteron angular distribution and excitation functions are consistent with stripping theory.

---

§ 1. INTRODUCTION

In a previous communication (Hinds and Middleton 1959, hereafter referred to as I) the results of some proton and deuteron angular distribution measurements from the bombardment of ^{9}Be with 5·7 Mev ^{3}He particles were reported. The majority of the angular distributions had strong forward maxima and appeared to be consistent with a predominantly direct reaction mechanism. This result was surprising, particularly for the protons, since similar measurements made on the protons from a number of neighbouring elements at incident energies up to 4·7 Mev provided little evidence in favour of the direct process. Recently, when higher energy ^{3}He beams became available, it was considered worth while extending the earlier measurements to 10·2 Mev and also measuring some excitation curves.

Proton and deuteron angular distributions have been measured at 8·82 and 10·23 Mev and excitation curves between 5·6 and 10·2 Mev using the same experimental procedure as described in I. The higher energies were obtained from our 6 Mev Van de Graaff generator by accelerating doubly charged ^{3}He particles. Normally the yield of these is limited to about one part in 500, from a conventional r.f. ion source and it is difficult to obtain analysed beams greater than about 0·02 μA. Apart from the low intensity, stabilizing is also difficult because of the presence of other molecular beams of comparable intensity and similar charge to mass ratio. By using a gas stripper placed about 500 kev below the ion source both these difficulties have been overcome. Analysed beams of between $\frac{1}{2}$ and 1 μA have been obtained and since removal of the second charge occurs after a pre-acceleration, these particles are unique in energy and can readily be distinguished from other spurious molecular beams. It is intended to publish a more detailed account of this modification at a later date elsewhere.

At 8·82 and 10·23 Mev the angular distributions of the ground and first excited state proton groups and the fourth excited state deuteron group have been measured, in addition to the groups previously measured at 5·7 Mev and reported in I. It was possible to measure more groups at the higher bombarding energies since the stronger spectrograph fields required resulted in a larger range of energies being recorded on the 30 in. nuclear plate.

§ 2. Results and Discussion

2.1. *The $^9Be(^3He, p)^{11}B$ Reaction*

The angular distributions of the groups corresponding to the ground and first nine excited states of ^{11}B have been measured at energies of 8·82 and 10·23 Mev and these are shown in figure 1. Also shown in the figure, plotted in the same arbitrary units, are the angular distributions measured at 5·7 Mev and previously presented in I. Alongside each distribution is the excitation function measured at a laboratory angle of 10°, and for the ground and first excited states also at 90°. The latter were measured using a scintillation counter which is normally used as an exposure monitor during angular distribution measurements.

It is significant that the majority of the angular distributions are essentially energy independent. This applies particularly to those which exhibit strong forward peaks and may be described as being of the stripping type. The only systematic tendencies are for peak differential cross sections to decrease with increasing energy and for peaks to move towards smaller angles. It is also significant that the 10° excitation curves show no pronounced resonances and are essentially smooth. This contrasts sharply with our results for the ^{12}C(^{3}He, p)^{14}N reaction (Hinds and Middleton 1960) where angular distributions were observed to be strongly energy dependent and the excitation curves exhibited pronounced resonances. This difference is probably attributable to the large difference in binding energies of the ^{3}He particle in the respective compound nuclei ^{12}C and ^{15}O, viz. 26 Mev compared with 12 Mev. In the beryllium case, the decay of the compound nucleus is expected to be completely statistical and interference between this contribution and the stripping part will be minimized. Thus, one would expect to observe the stripping component superimposed on a compound nucleus background which is symmetrical about 90°.

Seven of the ten angular distributions measured appear to be consistent with a predominantly stripping process, the exceptions being the groups corresponding to the states at 6·76, 7·30 and 7·99 Mev. The former, measured at an incident energy of 8·82 Mev, are shown in figure 2 fitted with theoretical curves calculated from an expression derived by Newns (to be published, see also I) for a double stripping process. The angular dependence for such a process is given by

$$\sigma(\theta) \propto \exp\left(-\frac{K^2}{4\gamma^2}\right)\sum_L |A(L)J_L(ka)|^2$$

which is a similar expression to that used in I except for the addition of the exponential factor. This factor arises from the internal motion of the ^{3}He particle and has the effect of shifting the peak to smaller angles. Thus, using the above expression one gets similar results to those in I with a slightly smaller radius of interaction. The curves shown in figure 2 were all calculated for a radius equal to 6·0 fermi. It is evident, however, that better agreement could have been obtained particularly for the 4·46 and the 8·92 Mev angular distributions if a slightly smaller radius had been used. The 10·23 Mev angular distribution can also be fitted with theoretical curves using the same radius of interaction and with the same degree of success as the 8·82 Mev data.

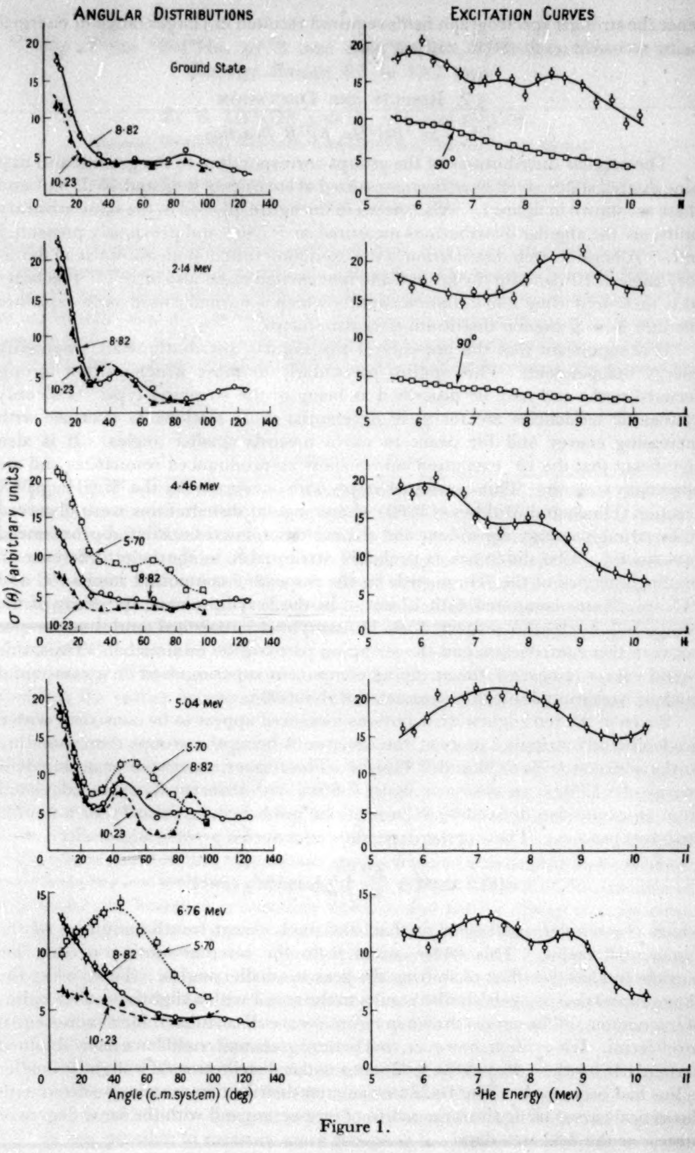
ANGULAR DISTRIBUTIONS
EXCITATION CURVES
Ground State
8·82
10·23
90°
2·14 Mev
4·46 Mev
5·70
5·04 Mev
6·76 Mev
σ (θ) (arbitrary units)
0 20 40 60 80 100 120 140
5 6 7 8 9 10 11
0 5 10 15 20
Angle (c.m.system) (deg)
³He Energy (Mev)

Figure 1.

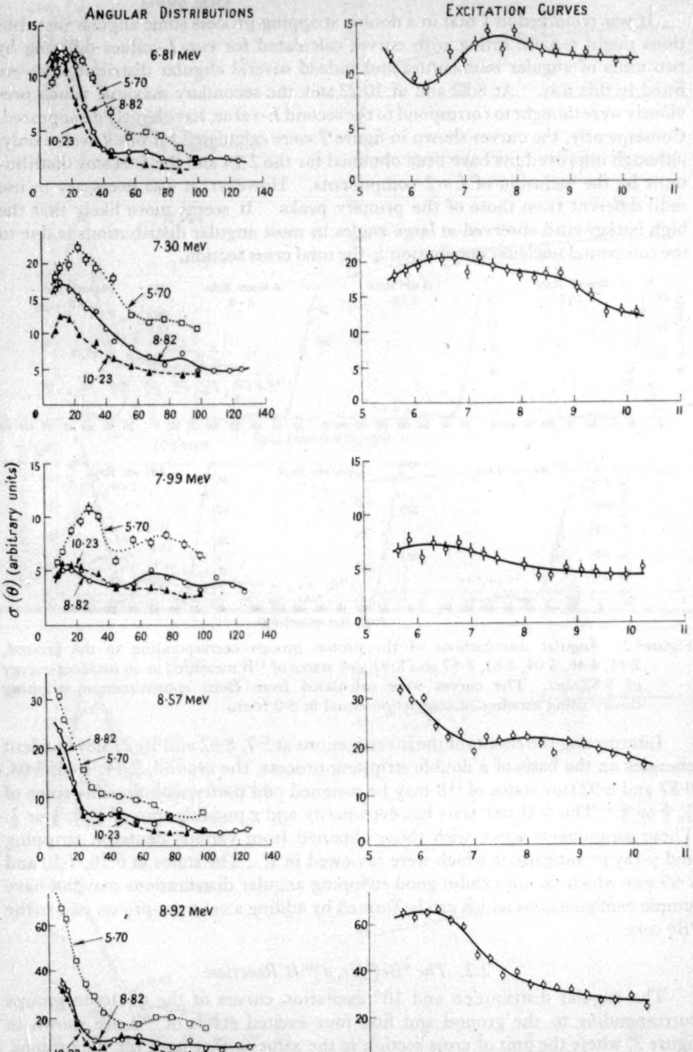

Figure 1. Angular distributions of the ground and first nine excited state proton groups from the reaction $^9Be(^3He, p)^{11}B$ measured at incident energies of 5·7, 8·82 and 10·23 MeV. Also shown are excitation curves measured at a laboratory angle of 10° and in the cases of the ground and first excited states also at 90°.

It was remarked in I that in a double stripping process some angular distributions might require fitting with curves calculated for two L-values differing by two units of angular momentum and indeed several angular distributions were fitted in this way. At 8·82 and at 10·23 Mev the secondary maxima, which previously were thought to correspond to the second L-value, have largely disappeared. Consequently, the curves shown in figure 2 were calculated for one L-value only, although improved fits have been obtained for the 2·14 and the 5·04 Mev distributions by the inclusion of $L=2$ components. However, it was necessary to use radii different from those of the primary peaks. It seems more likely that the high background observed at large angles in most angular distributions is due to the compound nucleus contribution to the total cross section.

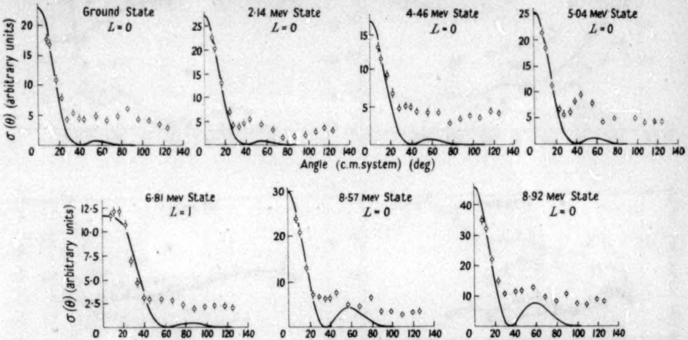

Figure 2. Angular distributions of the proton groups corresponding to the ground, 2·14, 4·46, 5·04, 6·81, 8·57 and 8·92 Mev states of ^{11}B measured at an incident energy of 8·82 Mev. The curves were calculated from Born approximation stripping theory using a radius of interaction equal to 6·0 fermi.

Interpreting the results of the investigations at 5·7, 8·82 and 10·23 Mev incident energies on the basis of a double stripping process, the ground, 2·14, 4·46, 5·04, 8·57 and 8·92 Mev states of ^{11}B may be assigned odd parity with possible spins of $\frac{1}{2}$, $\frac{3}{2}$ or $\frac{5}{2}$. The 6·81 Mev state has even parity and a possible spin of $\frac{1}{2}$, $\frac{3}{2}$, $\frac{5}{2}$ or $\frac{7}{2}$. These assignments agree with those obtained from various deuteron stripping and γ-ray investigations which were reviewed in I. The states at 6·76, 7·30 and 7·99 Mev which do not exhibit good stripping angular distributions may not have simple configurations which can be formed by adding a neutron–proton pair to the ^{9}Be core.

2.2. *The* $^{9}Be(^{3}He, d)^{10}B$ *Reaction*

The angular distribution and 10° excitation curves of the deuteron groups corresponding to the ground and first four excited states of ^{10}B are shown in figure 3, where the unit of cross section is the same as that used for the protons. It should be noted that an error was made in paper I in the deuteron cross section units. The cross section scales (figure 4, paper I) should be multiplied by 2·4 for comparison purposes with the proton angular distributions presented in the same communication.

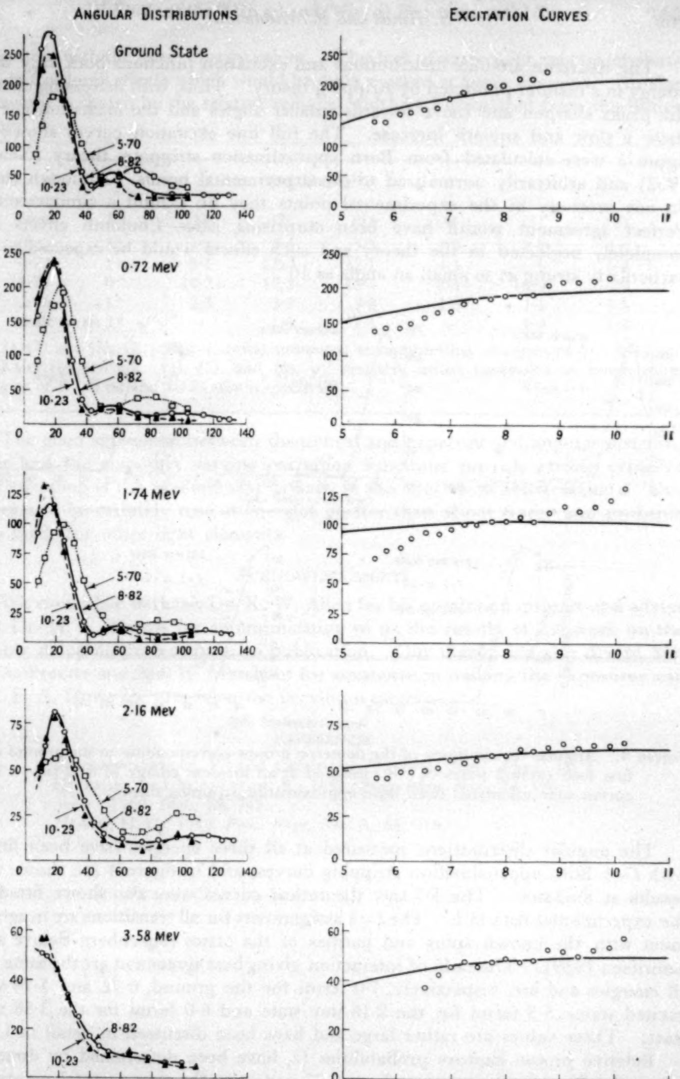

Figure 3. Angular distributions of the ground and first four excited state deuteron groups from the reaction ^{9}Be(^{3}He, d)^{10}B measured at incident energies of 5·7, 8·82 and 10·23 MEV. On the right-hand side are shown excitation curves measured at a laboratory angle of 10°; the full curves were calculated from Born approximation stripping theory and have been arbitrarily normalized.

The deuteron angular distributions and excitation functions both vary with energy in a manner predicted by stripping theory. Thus, with increasing energy the peaks sharpen and move towards smaller angles and the excitation curves show a slow and smooth increase. The full line excitation curves shown in figure 3 were calculated from Born approximation stripping theory (Newns 1952) and arbitrarily normalized to the experimental points. Although these do not precisely fit the experimental points they do exhibit a similar trend. Perfect agreement would have been surprising since Coulomb effects are completely neglected in the theory and such effects would be expected to be particularly strong at so small an angle as 10°.

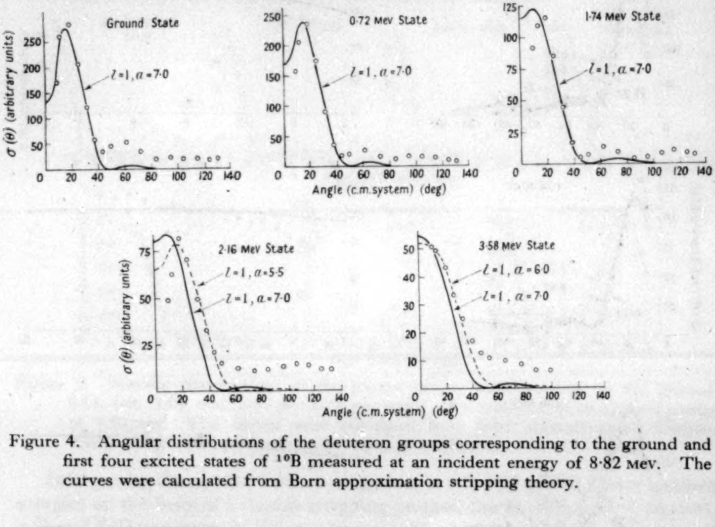

Figure 4. Angular distributions of the deuteron groups corresponding to the ground and first four excited states of ^{10}B measured at an incident energy of 8·82 Mev. The curves were calculated from Born approximation stripping theory.

The angular distributions measured at all three energies have been fitted with $l=1$ Born approximation stripping curves, and in figure 4 are shown the results at 8·82 Mev. The 5·7 Mev theoretical curves were also shown fitted to the experimental data in I. The $l=1$ assignments for all transitions are in agreement with the known spins and parities of the states (Ajzenberg-Selove and Lauritsen 1959). The radii of interaction giving best agreement are the same for all energies and are, respectively, 7·0 fermi for the ground, 0·72 and 1·74 Mev excited states, 5·5 fermi for the 2·16 Mev state and 6·0 fermi for the 3·58 Mev state. These values are rather large and have been discussed in detail in I.

Relative proton capture probabilities Ω_1 have been determined by directly fitting the Born approximation theoretical curves to the experimental points in the angular range 20° to 40°. In a similar way, relative reduced widths γ_1^2 have been obtained using Butler stripping theory. These values, obtained at the three bombarding energies, are shown in the table. It will be noticed that the values of Ω_1 at the two higher energies agree well, but these are not in such good agreement with the lower energy values. This lack of agreement may be attributable to Coulomb effects which would be more marked at lower energies. Similar behaviour is shown by the relative reduced widths γ_1^2 calculated from the Butler theory.

Level energy (Mev)	J^π	$^9Be(^3He, d)^{10}B$ (1)	(2)	(3)	(4)	(5)	(6)
0	3^+	3·8	5·6	5·5	1·9	2·7	2·6
0·72	1^+	8·1	12·7	12·2	4·3	6·5	6·4
1·74	0^+	14·7	19·2	17·4	8·4	10·9	9·9
2·16	1^+	3·3	3·9	3·8	2·6	3·1	3·1
3·58	2^+	–	1·4	1·5	–	1·3	1·3

(1), (2) and (3), Ω_1 (relative units) measured at bombarding energies of 5·7, 8·82 and 10·23 Mev respectively; (4), (5), and (6), γ_1^2 (relative units) measured at bombarding energies of 5·7, 8·82 and 10·23 Mev respectively.

The good agreement between theoretical and experimental angular distributions and the smoothly varying excitation functions provide strong evidence that stripping is the predominant process in the $^9Be(^3He, d)^{10}B$ reaction. This appears to be certainly true at energies greater than about 6 Mev and probably also holds for other light elements.

ACKNOWLEDGMENTS

We would like to thank Dr. K. W. Allen for his continued interest and advice and Dr. H. C. Newns for communicating to us the results of his work on the double stripping process prior to publication. Our thanks are also due to Mr. D. A. Procter and Mr. H. Marchant for assistance in making the exposures and Mr. F. A. Howe for preparing the beryllium targets.

REFERENCES

Ajzenberg-Selove, F., and Lauritsen, T., 1959, *Nucl. Phys.*, **11**, 1.
Hinds, S., and Middleton, R., 1959, *Proc. Phys. Soc.*, **74**, 196.
—— 1960, *Ibid.*, **75**, 745.
Newns, H. C., 1952, *Proc. Phys. Soc.* A, **65**, 916.

Experimental Determination of the Individual Secondary Ionization Coefficients in Hydrogen and their Dependence on Cathode Work Function

BY F. LLEWELLYN JONES AND EIFIONYDD JONES
Department of Physics, University College of Swansea

MS. received 30th September 1959, in final form 9th December 1959

Abstract. This paper describes measurements of the formative time lag to breakdown in hydrogen in uniform electric field for a range of E/p from 50 to 250 v cm^{-1} (mm Hg)$^{-1}$. The preliminary work showed that the time lag was critically dependent upon the state and nature of the cathode surface. The formative time lags were therefore measured with different cathode surfaces, and the state of each surface was specified by measuring its work function. Previous work in this laboratory has shown that measurements of formative time lags can be analysed in terms of Davidson's current growth equation to yield determinations of the individual secondary ionization coefficients. A similar analysis has been carried out of the results of the present experimental data, and it was found that if the cathode work function was decreased by 0·25 ev, the magnitudes of the secondary coffiecients were increased by a factor of two.

---

§ 1. INTRODUCTION

SOME of the problems involved in an investigation of the temporal growth of ionization have in recent years been studied both experimentally and theoretically in some detail in this laboratory (Dutton, Haydon and Llewellyn Jones with Davidson 1953; Davidson 1955, 1956, 1957; Morgan 1956). Application of the mathematical theory to experimental data on temporal growth provides a method of determining the separate magnitudes of the individual secondary cathode ionization coefficients (γ due to positive ions and δ/α due to photons, α being the Townsend primary coefficient) which contribute to the growth of ionization currents in gases. By applying the theory to experimental measurements of the formative time lag from voltage application to voltage collapse in the gap, it has been shown that satisfactory accuracy in the determination of the secondary ionization coefficients is possible. The full mathematical expressions for the current at a given time depend upon a number of parameters. The solution has been given in two convenient forms (Davidson, see Dutton *et al.* 1953): an exact solution and an approximate solution. Earlier treatments of the problem had been given by Steenbeck (1930) and Schade (1937) who considered a gas with only a single secondary cathode process, and by Bartholomeyczyk (1940) and von Gugelburg (1947) who considered the case in which both photon and positive ion secondary cathode processes are present. But these earlier formulae, though satisfying the continuity equations, did not satisfy the correct initial and boundary conditions. Davidson's solutions take account of both secondary processes; his approximate formula satisfies the continuity equations and the correct boundary conditions, while his exact solution satisfies also the correct initial conditions. For studying current growth during the first few electron transit times the approximate solution is definitely inadequate. However, in the cases with which we are concerned in this work with hydrogen, the growth time was of the order of a few ion transit times, and since the amplification attained at those times was very large, it was evident from the known values of $\gamma+\delta/\alpha$ that the process did not approximate to a pure γ effect; δ/α must have been more than a small fraction of γ. In such cases Davidson's approximate formula is adequate for calculating the time to a given amplification. In many such cases, because the δ effect amplification is so much more rapid than the γ effect amplification, the time taken to attain a given amplification would not have been very different if the γ process had been absent. For the case in which from time zero onwards an external illumination generates a current I_0 at the cathode, the essential equations of Davidson's approximate solutions are

$$\frac{1}{W_-}\frac{\partial I_-}{\partial t} = -\frac{\partial I_-}{\partial x} + \alpha I_- \qquad \ldots\ldots(1\,a)$$

$$\frac{1}{W_+}\frac{\partial I_+}{\partial t} = \frac{\partial I_+}{\partial x} + \alpha I_- \qquad \ldots\ldots(1\,b)$$

where

$$I_-(0, t) = I_0/P + C\exp\lambda t \qquad \ldots\ldots(2)$$

$$P = 1-(\omega/\alpha)(\exp\alpha d - 1) \qquad \ldots\ldots(3)$$

$$1 = \frac{\gamma\alpha}{\alpha-\lambda/W}\left\{\exp\left[\left(\alpha-\frac{\lambda}{W}\right)d\right]-1\right\} + \frac{\delta}{\alpha-\lambda/W_-}\left\{\exp\left[\left(\alpha-\frac{\lambda}{W_-}\right)d\right]-1\right\}$$

where $\ldots\ldots(4)$

$$\frac{1}{W} = \frac{1}{W_-} + \frac{1}{W_+}, \qquad \ldots\ldots(5)$$

and

$$\omega/\alpha = \gamma + \delta/\alpha \qquad \ldots\ldots(6)$$

W_- and W_+ being the electron and ion drift velocities.

Equations $(1\,a)$ and $(1\,b)$ are the continuity equations and the solution of these is in the form of an expression which gives the current I as a function of the distance x from the cathode at time t. In particular, equation (2) is the electron current at the cathode $(x=0)$ at time t.

The constant C in expression (2) may be given a value which gives agreement with the initial conditions, for example, if the initial value of $I_-(0, t)$ is c, the solution can be made to have that initial value by taking $C=c-I_0/P$. In the present experimental investigation this C would not differ greatly from $-I_0/P$, and the expression would then be

$$I_-(0, t) = I_0(1-\exp\lambda t)/P. \qquad \ldots\ldots(7)$$

Davidson's exact solution, which shows in detail the rather complex shape of the current growth curve, differs from his approximate solution by assigning a definite value to the constant C and specifying the correction terms (which are oscillatory in time) which must be added to make the expression exact.† As might be expected, the best value to use for C in the approximate solution is the value which it has in the exact solution; this gives the simple approximate curve of current growth the best general agreement of which it is capable with the complex exact curve. In our case, the value $C = -I_0/P$ used in (7) is an adequate approximation to this C, and was used in the calculations.

---

† Davidson (1955, 1957) has also given his exact solution in other mathematical forms, suitable for particular purposes. Some workers (P. L. Auer, *Phys. Rev.*, 1955, **98**, 320; H. W. Bandel, *Phys. Rev.*, 1954, **95**, 1117; Y. Myoshi, *Phys. Rve.*, 1956, **103**, 1609) have considered Davidson's exact solutions as too complicated for application in practice. This is not correct; they have been applied to numerous data on current growth in air and hydrogen. The complexity of form for certain experimental conditions is merely arithmetical and is not a serious difficulty.

§ 2. General Principle of the Investigation

If a potential V, in excess of the static sparking potential V_s, is applied to a parallel plate gap, an initial current I_0 will be amplified at an ever increasing rate because the replacement condition for electrons $(\omega/\alpha)(e^{\alpha d}-1)$ is greater than unity, so that for every electron disappearing into the anode more than one new electron appears at the cathode, and the current increases accordingly. In practice, the current eventually attains a value large enough to discharge the condenser formed by the gap and the potential difference between the electrodes then collapses. This collapse once started is rapid, and for this reason one can define a formative time lag t_f as the time which elapses between the application of the potential difference V and the beginning of this rapid collapse.

The object of the present experimental investigation was to obtain values of the individual secondary (γ and δ/α) coefficients comprising the total secondary ionization coefficient ω/α, and their dependence upon the work function of the particular cathode surfaces used. The values are obtained by applying the theoretical growth equations to measurements of the formative time lag of voltage collapse (breakdown) in hydrogen at low pressures and in uniform electric fields.

The method used for analysing the experimental measurements of t_f has been explained in detail previously by Dutton *et al.* (1953) and by Morgan (1956). Only a brief outline of this method is given here along with a summary of the stringent precautions which must be taken when obtaining the experimental data.

In order to evaluate γ and δ/α, the individual secondary coefficients for ions and photons, from the growth equation at any given value of E/p, it is necessary to know the primary coefficient α, the total secondary coefficient $\omega/\alpha (=\gamma+\delta/\alpha)$, W_- and W_+, and t_f; ω/α can be found from measured values of α and the static breakdown potential V_s for the particular value of E/p using the Townsend criterion $1-(\omega/\alpha)(\exp \alpha d_s - 1) = 0$. This procedure required measurement of α and V_s to an appropriately high order of accuracy, and it is clearly advisable to obtain all these quantities under the same conditions for the particular gas sample used. This was done for all these quantities except the ion and electron mobilities because independent measurement of these quantities would involve considerable complication at this stage. The published values of these quantities W_- and W_+ which are available, though not recent, nevertheless appear to be generally accepted. In the analysis of the experimental data the values of W_+ (mobility $\mu = 8{\cdot}2$) in hydrogen published by Bradbury (1932) for low values of E/p ($< 50\,\text{v cm}^{-1}(\text{mm Hg})^{-1}$) were used; in this range of low E/p the values of W_- measured by Townsend and Bailey (1921) were 100 times larger than Bradbury's measured value of W_+. Because of the lack of recent experimental data at larger values of E/p it was also assumed in this work that W_- was still equal to $100W_+$ at these higher values of E/p and also that Bradbury's value of the mobility still held good. At this stage, therefore, the absolute values γ and δ/α obtained in the present work depend upon the accuracy of the published values of W_- and W_+. For example, at $E/p = 250\,\text{v cm}^{-1}(\text{mm Hg})^{-1}$ at 20°c and for a cathode surface of mean work function 4·3 ev, the value of γ obtained by using Bradbury's values of W_+, as outlined above, is equal to 0·011 electron per ion. However, if the actual values of W_+ used in the calculation is increased, say, six times, then the value of γ is also increased and becomes 0·05 electron per ion; the value of δ/α would be correspondingly decreased because $\omega/\alpha = \gamma + \delta/\alpha$ and ω/α remains of course unchanged at its measured value.

The position is somewhat different with regard to published values of α, and it was considered necessary for the present work to make a separate determination of α (Jones and Llewellyn Jones 1958), and the values obtained are lower than others previously published for values of $E/p > 130$ v cm^{-1} (mm Hg)$^{-1}$.

The accuracy of the final evaluation of γ and δ/α clearly depends on the accuracy of the quantities α, ω/α, t_f, W_+ and W_- used in the equations. The time t_f must have a stable constant reproducible value (i.e. no large statistical variations), while V_s, in particular, must be determined to a high order of accuracy.

It must be strongly emphasized that quite apart from sensitivity, accuracy and stability of the measuring apparatus itself, the measured values of these quantities at any given value of E/p depend upon the consistency and stability not only of the gas samples but also of the electrode surfaces. (Llewellyn Jones 1957, Dutton and Jones 1959). Physically significant experimental data, i.e. data to which the theory based on constant coefficients can be applied, can be obtained only when the necessary conditions of stability and consistency are fulfilled, which is unlikely to be the case with untreated electrode surfaces or in the presence of gases which are decomposed into chemically active constituents during the passage of an ionization current. Morgan (1956) has shown experimentally in this laboratory that consistent functional dependence of t_f on E/p with purified hydrogen was only obtained by extensive treatment of the electrode surfaces until the necessary high degree of stability is obtained.

Consequently, in the present investigation special attention has been paid to the question of surface stability and its influence on observed t_f. Clearly a mean value of t_f can be properly substituted in the growth equation only if a constant reproducible value is obtained experimentally for the given value of E/p. The necessity for surface stability is regarded as fundamental in this experimental investigation, as the necessity also applies to the determination of the total coefficient ω/α from experimental measurement of V_s. This quantity V_s is of considerable significance in this investigation, as not only is an accurate value required in order that an accurate value of ω/α be found, but it is also essential that the experimental conditions be such that a stable reproducible value of V_s is obtainable in order that the impulse percentage overvoltage ($= [(V - V_s)/V_s] \times 100\%$) can be specified to the experimental order of accuracy. It is for this reason that great attention was paid in this investigation to the whole question of surface stability and its specification. In this context the physically significant quantity is the work function of the actual surface of the cathode under the conditions of the investigation, and when the precise state of the surface is unknown (e.g. because of the presence of a thin tarnish film) the surface may still be specified by measuring the effective work functions. It will be shown below that when the precautions outlined above are taken, this procedure of using experimental time lag data with theoretical growth equations can yield suitably accurate determinations of γ and δ/α.

The main results of this investigation were briefly reported at the Physical Society Conference on Gas Discharges, held at Swansea during September 1958.

§ 3. APPARATUS

Three discharge tubes were used in the present work. They formed part of the same vacuum system so that the same gas sample was present in all three during the experiments. The first tube was used to obtain accurate determinations of the primary ionization coefficient α, and has been described elsewhere (Jones and Llewellyn Jones 1958). Thus for each sample of gas used in the experiments, the value of α was known accurately. The second tube simply contained a parallel plate gap consisting of two copper electrodes, set at 1·5 cm apart, and was used for the preliminary work on formative time lags in order to obtain orders of magnitude and to explore the general cathode effects.

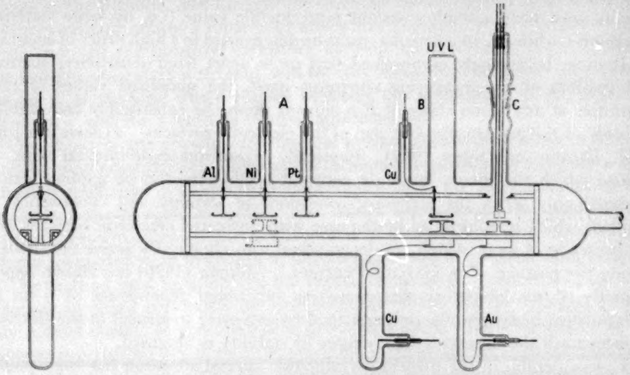

Figure 1. Tube used for measurement of work functions.

The third tube was one in which not only t_f was accurately measured but also the work functions of a number of different cathode surfaces. The design of this tube is shown by the detailed diagram of figure 1. The different surfaces were obtained by sputtering a moveable copper cathode at A; the sputtered metals were aluminium, platinum and nickel. The work functions of these surfaces were measured at C, and the formative time lags were measured for each surface at B. The cathode was mounted on two rails and moved into the different positions by an external magnet.

The h.t. source, impulse generator and time bases used in this work were the same as those used by Morgan (1956) who has described them in detail elsewhere. It is sufficient to state here that in all this work the voltages were maintained with an accuracy to better than 0·01%. The usual vacuum techniques were employed using numerous liquid air traps in conjunction with oil diffusion pumps. It may perhaps be noted that considerable time was involved with the preliminary work of conditioning and preparation of the electrodes and measurement of α and V_s before the final work on the time lags proper was carried out. Thus, after the initial evacuation to a pressure of less than 10^{-6} mm Hg, and outgassing, the leak-free tubes and gas system were washed out numerous times, while in operation over a period of many months, with samples of hydrogen which had been carefully prepared from uranium hydride.

§ 4. RESULTS AND CONCLUSIONS

The essential data required for applying the growth equations, i.e. the primary ionization coefficient α, the static breakdown potential V_s (from which ω/α is determined), the formative time lag t_f and the precise voltage V applied to the gap, were measured over a range of values of E/p for each gas sample. For reasons explained above, the values of the mobilities of electrons and ions were obtained from the published data of Townsend and Bailey and of Bradbury.

A stable reproducible value of t_f was obtained only after careful treatment of the cathode surface by positive ion bombardment in hydrogen and subsequent heating. This fact is illustrated by figure 2, in which 2 (*a*) gives the scatter of some 200 measurements of the formative time lag t_f using a cathode which had not been treated in this way. It is seen that 60 measurements gave a value of t_f of 42μsec, another 80 measurements gave a value of 45μsec while about ten of them were nearly 65μsec in length. Therefore, with the cathode in this 'unstable' condition, the scatter in the results was too great to permit specification of any particular value of t_f to be used in the growth equations. After making these observations the cathode was subjected to prolonged treatment and 200 consecutive measurements of t_f were again made with the same conditions of E/p, p, d, and gas purity as those obtaining in the first measurements. These measurements of t_f are shown in figure 2 (*b*) and it is seen that, within the experimental error, all of them are equal to 40μsec. In this way, using controlled conditions, a specific value of t_f was obtained.

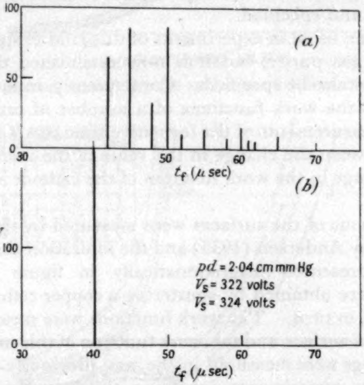

Figure 2. Effect of cathode surface on t_f where N is the number of time lags of duration t_f in the interval Δt_f ($\sim$5% t_f): (*a*) cathode untreated, (*b*) cathode extensively treated.

In all these experiments it was necessary to eliminate statistical variation in the photoelectric emission of initiatory electrons. Thus, during the establishment of the electric field E (greater than the breakdown field E_S) at $t = 0$, it was necessary to produce a large number of electrons (about 50) at the cathode; this number corresponds to a continuous emission of 10^9 electrons/sec or to a value of I_0 of 10^{-10} A. Preliminary work on the measurement of the formative time lags showed that an initial current I_0 of this magnitude was large enough to eliminate any statistical scatter from this source and yet not large enough to produce a space charge in the gap at $t=0$, and this value of I_0 was therefore adopted in the work.

Under these conditions, therefore, the scatter due to the inherent statistical nature of the discharge parameters, which a very small value ($\sim 10^{-16}$ A) of I_0 would have emphasized, was smoothed by using a larger value of 10^{-10}A for the externally generated current I_0.

When all the conditions governing the cathode stability and choice of I_0 were taken into consideration, it was possible to obtain one value of the formative time lag t_f corresponding to a given set of conditions provided that the voltage, the current I_0, the gas purity, and especially the state of the cathode surface, were all controlled and specified.

It has always been usual in experiments of this kind to specify applied voltage, the current I_0 and gas purity, but it is now established that the state of the cathode surface must also be specified. Consequently, in the present work it was decided to examine the work functions of a number of cathode surfaces at the same time as the measurements of the formative time lags were being carried out. Any correlation between the change in the value of the individual secondary coefficients with a change in the work function of the cathode surface could then be investigated.

The work functions of the surfaces were measured by the retarding potential method developed by Anderson (1935) and the ionization chamber used for these experiments is represented diagrammatically in figure 1. Different work function surfaces were obtained by sputtering a copper cathode with aluminium, platinum and nickel, in turn. The work functions were measured by comparison with a standard gold surface and the work function of this surface was taken to be 4·5 ev. The time lags were measured in the way previously described.

The preliminary experiments involving the measurements of the work functions of sputtered surfaces showed that there was a variation of the order of 0·2 ev over the total area of the electrode surface. Therefore the work functions at eight different regions on the cathode surface were measured, and the values quoted in the results are the mean values obtained. Throughout the experiments the work functions of the small regions on the gold surfaces remained constant to within the experimental error of measurement of $\pm 0{\cdot}03$ ev.

From measurements of time lags with a given cathode surface, it has been shown that it is possible to compute values of the individual coefficients γ and δ/α for that surface. Thus by measuring t_f for different cathode surfaces it is possible to obtain the dependence of γ and δ/α on the work function of the surface.

The results of these experiments are given in figures 3 and 4 and in the table. Figure 3 shows values of ω/α for surfaces of different work function over a range of E/p from 50 to 250 v cm^{-1} (mm Hg)$^{-1}$, and figure 4 gives values of both γ and δ/α for the same range of work function and of E/p.

The table gives values of γ and δ/α taken from the curves at $E/p=60$ v cm^{-1} (mm Hg)$^{-1}$ at 20 °c, so that their dependence on the work function may be examined more closely. It can be seen from examination of this table that the magnitudes of the coefficients were nearly doubled when the work function of the cathode surface was decreased by only 0·23 ev. This demonstrates the great influence of small changes in the state of the cathode surface on the cathode secondary coefficients and on the growth of ionization. The table also shows

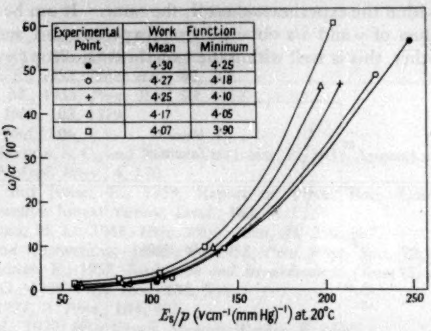

Figure 3. ω/α plotted against E/p for cathodes of different work function.

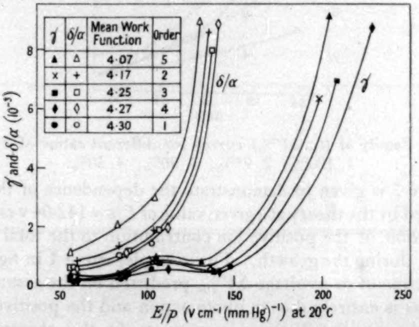

Figure 4. γ and δ/α plotted against E/p for cathodes of different work function.

(1)	(2)	(3)	(4)	(5)	(6)
60	1·1	6·0	4·30	4·25	1
	1·20	5·9	4·27	4·18	4
	2·0	7·0	4·25	4·10	3
	2·2	8·0	4·17	4·05	2
	3·8	11·0	4·07	3·90	5

(1) E/p (v cm^{-1} (mm Hg)$^{-1}$); (2) $\gamma \times 10^{-4}$; (3) $\delta/\alpha \times 10^{-4}$; (4) mean work function (ev); (5) minimum work function (ev); (6) order of experiment.

that the time lag method of determining γ and δ/α is capable of giving consistent and reproducible results. The last column in the table indicates the order in which the experiments were carried out. The first experiment was carried out when the work function of the surface was 4·3 ev, and afterwards the cathode state was changed (by sputtering) to different values for experiments 2 and 3 and eventually to experiment 4 for which the mean work function was 4·27 ev. Thus, to within the experimental error of determining the work function, the cathode surface used in experiment 4 was in the same condition as that obtaining in experiment 1; consequently, the values of γ and δ/α for experiments 1 and 4 should also be, within the experimental error, the same. It can be seen from the table that the values of γ and δ/α obtained from experiments 1 and 4 are within $\pm 10\%$ of each other, this is well within the experimental error ($\pm 20\%$) of their determination.

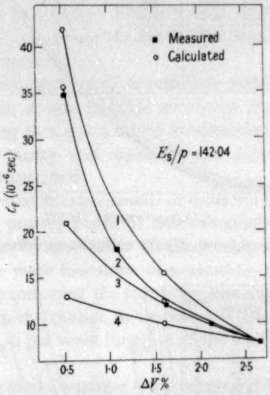

Figure 5. Family of (t_f, $\Delta V\%$) curves for different ratios of δ/α to ω/α. 1, 100%; 2, 95%; 3, 90%; 4, 50%.

Finally, figure 5 is given to demonstrate the dependence of the values of the time lags predicted by the theory at a given value of $E/p = 142{\cdot}04$ v cm^{-1} (mm Hg)$^{-1}$ upon the proportion of the positive ion contribution to the total secondary ionization operating during the growth. For example, curve 1 in figure 5 gives the times t_f as a function of overvoltage $\Delta V\%$, predicted on the assumption that the secondary process is entirely due to photo action and the positive ion process is negligible. If the predicted time is made to fit the observed time when $\Delta V\% = 2{\cdot}7\%$ then the predicted times (assuming $\delta/\alpha = \omega/\alpha$) are considerably higher (by 30%) than the observed times. Similarly if it is assumed that $\gamma = \delta/\alpha$ (i.e. each coefficient is 50% of ω/α) then the predicted times are about half the magnitudes of those observed. These differences are far greater than the experimental error in determining the times. The kind of agreement that is possible between predicted and observed times is illustrated in curve 2 in which the full line represents the predicted variation of t with $\Delta V\%$, on the assumption that the constituents of the total secondary coefficient ω/α were $\gamma = 5\%\ \omega/\alpha$ and $\delta/\alpha = 95\%\ \omega/\alpha$, and the black circles represent the measured formative time lags. The agreement is satisfactory and, consequently, these are the proportions of γ and δ/α which are taken to be operating at this value of E/p. The same result would also be obtained if the curves had been drawn by fitting the predicted times to the observed times at the other end of the scale, i.e. at an overvoltage equal to 0·5%.

ACKNOWLEDGMENTS

We wish to thank the Electricity Supply Research Council for a maintenance grant for one of us and for a grant for apparatus during the period 1957/1959. We also thank Dr. C. G. Morgan for discussion in the earlier stages of this investigation during the design of the apparatus and ionization chamber.

REFERENCES

ANDERSON, P. A., 1935, *Phys. Rev.*, **47**, 958.
BARTHOLOMEYCZYK, W., 1940, *Z. Phys.*, **116**, 235.
BRADBURY, N. E., 1932, *Phys. Rev.*, **40**, 508.
DAVIDSON, P. M., 1955, *Phys. Rev.*, **99**, 1072.
—— 1956, *Ibid.*, **103**, 1879.
—— 1957, *Ibid.*, **106**, 1.
DUTTON, J., HAYDON, S. C., and LLEWELLYN JONES, F., 1953, Appendix by Davidson, P. M., *Brit. J. Appl. Phys.*, **4**, 170.
DUTTON, J., and JONES, E., 1959, Report of Phys. Soc. Conference (Paper by F. Llewellyn Jones) *Nature, Lond.*, **183**, 91.
VON GUGELBURG, H. L., 1947, *Helv. Phys. Acta*, **20**, 250, 307.
JONES, E., and LLEWELLYN JONES, F., 1958, *Proc. Phys. Soc.*, **72**, 363.
LLEWELLYN JONES, F., 1957, *Ionization and Breakdown in Gases* (London: Methuen).
MORGAN, C. G., 1956, *Phys. Rev.*, **104**, 566.
SCHADE, R., 1937, *Z. Phys.*, **104**, 487.
STEENBECK, M., 1930, *Wiss Veroff. Siemens-Werken*, **9**, 43.
TOWNSEND, J. S., and BAILEY, V. A., 1921, *Phil. Mag.*, **42**, 873.

An Investigation of Some (^{3}He, α) Reactions on Light Nuclei at 5·2 MeV

By I. J. TAYLOR, F. de S. BARROS†, P. D. FORSYTH,
A. A. JAFFE and S. RAMAVATARAM
The Physical Laboratories, University of Manchester

MS. received 14*th January* 1960

Abstract. The reactions ^{11}B(^{3}He, α)^{10}B, ^{10}B(^{3}He, α)^{9}B, ^{14}N(^{3}He, α)^{13}N, ^{16}O(^{3}He, α)^{15}O and ^{27}Al(^{3}He, α)^{26}Al, have been investigated at an incident energy of 5·2 MeV, using a broad range magnetic spectrograph. Angular distributions and absolute cross sections for alpha particles leading to the ground states and several excited states of the final nuclei have been measured. The angular distributions of many of the alpha-particle groups suggest the predominance of a direct interaction mechanism for these reactions, and in several cases features which are indicative of a pick-up process are mentioned.

---

§ 1. Introduction

There is little available evidence at present concerning the mechanism of the (^{3}He, α) reaction on light nuclei at bombarding energies in the neighbourhood of 5·0 MeV and above.

The ^{16}O(^{3}He, α)^{15}O reaction, which has been investigated at bombarding energies in the region of 2·6 MeV (Bromley, Kuehner and Almqvist 1959), has suggested that at higher energies the reaction might proceed predominantly by means of a direct interaction process, rather than through the formation and decay of a compound nucleus.

The ^{13}C(^{3}He, α)^{12}C reaction has been investigated at a bombarding energy of 4·5 MeV (Holmgren *et al.* 1957), and has been interpreted at forward angles in terms of a pick-up process (Owen, Madansky and Edwards 1959). However, the ^{13}C(^{3}He, α)^{12}C reaction would seem to be a favourable case for which pick-up of a neutron by the ^{3}He particle might occur, and the possibility that the (^{3}He, α) reaction might invariably proceed, at least in part, by a pick-up process at sufficiently high bombarding energy has not been established; (see, however, Bromley and Almqvist 1959).

If this were so, (^{3}He, α) reactions, which have favourable Q values, could be used to investigate the properties of nuclear states in place of the corresponding (p, d) reactions, for which a pick-up mechanism is usual. However, the Q values of the (p, d) reactions are generally so highly negative that they prohibit investigation with electrostatic generators.

The reactions ^{11}B(^{3}He, α)^{10}B, ^{10}B(^{3}He, α)^{9}B, ^{14}N(^{3}He, α)^{13}N, and ^{27}Al(^{3}He, α) ^{26}Al, have therefore been investigated at 5·2 MeV bombarding energy, using the Manchester University Van de Graaff generator and a broad range magnetic spectrograph.

---

† On leave of absence from the Brazilian Centre for Physical Research.

Angular distributions and absolute differential cross sections have been obtained for the reactions leading to several levels of the final nuclei ^{9}B, ^{10}B, ^{13}N and ^{26}Al, and also the angular distribution has been obtained for the ^{16}O(^{3}He, α)^{15}O ground state reaction.

§ 2. Experimental Details

Targets of natural boron and of adenine were evaporated on to aluminium foil backings, and bombarded with beams of singly ionized ^{3}He particles, using exposures of up to 900 microcoulombs. The experimental arrangement has been described in a previous publication (Barros *et al.* 1959). An investigation of the (^{3}He, d) reactions, which were recorded simultaneously with the (^{3}He, α) reactions, has also been described previously (Forsyth *et al.* 1960). Target thicknesses were measured using an alpha particle thickness gauge, and are considered accurate to ± 20%. The boron target had a thickness of $30\,\mu\mathrm{g\,cm^{-2}}$, the adenine target contained nitrogen equivalent to $25\,\mu\mathrm{g\,cm^{-2}}$, and the aluminium foil backing was $170\,\mu\mathrm{g\,cm^{-2}}$ thick.

§ 3. Results

A spectrum of alpha particles obtained from the boron target is shown in figure 1.

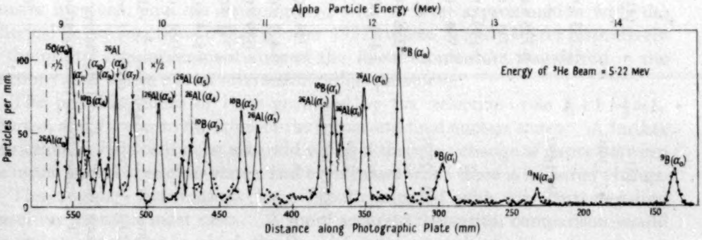

Figure 1. The spectrum of alpha particles from the boron target at 35°.

Reactions leading to the ground state of ^{9}B and to an excited state at 2·33 Mev were identified, there being no indication of a ^{9}B level to correspond to the 1·75 Mev level of the mirror nucleus ^{9}Be. This is in agreement with the result obtained from an investigation of the ^{10}B(^{3}He, α)^{9}B reaction at the lower bombarding energy of 2 Mev (Ajzenberg-Selove and Lauritsen 1959). An upper limit of 0·02 mbn sterad^{-1} can be placed upon the cross section for the transition to such a level, from the spectrum at 35° (figure 1).

Alpha-particle groups were observed leading to the ground state and first four excited states of ^{10}B, from the ^{11}B(^{3}He, α)^{10}B reaction, and the energies are in agreement with the known energy levels of ^{10}B.

From the adenine target, the ground state and first excited states of ^{13}N were obtained, together with the unresolved groups to the second and third excited states.

(1)	(2)	(3)	(4)	(5)	(6)	(7)	(8)
$^{10}B(^3He, \alpha_0)^9B$	12·110 ± 0·020	12·139$^{(a)}$	–	–	1	5·4	0·44
$^{10}B(^3He, \alpha_1)^9B$	–	–	2·333 ± 0·010	2·37 ± 0·020	–	–	0·52
$^{11}B(^3He, \alpha_0)^{10}B$	9·101 ± 0·020	9·114$^{(a)}$	–	–	1	4·5	0·69
$^{11}B(^3He, \alpha_1)^{10}B$	–	–	0·725 ± 0·010	0·717 ± 0·010$^{(c)}$	1	3·8	0·38
$^{11}B(^3He, \alpha_2)^{10}B$	–	–	1·741 ± 0·010	1·744 ± 0·010$^{(c)}$	1	4·5	0·29
$^{11}B(^3He, \alpha_3)^{10}B$	–	–	2·149 ± 0·010	2·156 ± 0·010$^{(c)}$	1	4·5	0·34
$^{11}B(^3He, \alpha_4)^{10}B$	–	–	3·594 ± 0·015	3·583 ± 0·005$^{(a)}$	1	5·0	0·26
$^{14}N(^3He, \alpha_0)^{13}N$	10·029 ± 0·016	10·027$^{(a)}$	–	–	1	6·6	1·07
$^{14}N(^3He, \alpha_1)^{13}N$	–	–	2·358 ± 0·010	2·365 ± 0·003$^{(a)}$	–	–	0·12
$^{14}N(^3He, \alpha_2 + \alpha_3)^{13}N$	–	–	3·471 ± 0·015	3·507 ± 0·007$^{(a)}$	(1)	(7·3)	0·86
$^{16}O(^3He, \alpha_0)^{15}O$	4·920 ± 0·030	4·923$^{(a)}$	–	–	1	5·5	–
$^{27}Al(^3He, \alpha_0)^{26}Al$	7·519 ± 0·015	7·523 ± 0·015$^{(b)}$	–	–	2	4·5	0·14
$^{27}Al(^3He, \alpha_1)^{26}Al$	–	–	0·234 ± 0·010	0·228 ± 0·010$^{(b)}$	2	4·0	0·03
$^{27}Al(^3He, \alpha_2)^{26}Al$	–	–	0·422 ± 0·010	0·416 ± 0·010$^{(b)}$	–	–	0·08
$^{27}Al(^3He, \alpha_3)^{26}Al$	–	–	1·059 ± 0·010	1·050 ± 0·010$^{(b)}$	2	4·5	0·07
$^{27}Al(^3He, \alpha_4)^{26}Al$	–	–	1·741 ± 0·010	1·755 ± 0·010$^{(b)}$	2	4·5	0·08
$^{27}Al(^3He, \alpha_5)^{26}Al$	–	–	1·844 ± 0·010	1·846 ± 0·010$^{(b)}$	–	–	0·03
$^{27}Al(^3He, \alpha_6)^{26}Al$	–	–	2·064 ± 0·010	2·065 ± 0·010$^{(b)}$	2	5·2	0·32

(1) Reaction; (2) measured *Q* value (MEV); (3) previous *Q* value (MEV); (4) measured excitation (MEV); (5) previous excitation (MEV); (6) *l* value$^{(d)}$; (7) radius (10^{-13}cm); (8) observed peak differential cross section (mbn sterad^{-1}).

(a) From mass excesses and excitations listed by Ajzenberg-Selove and Lauritsen (1959); (b) Hinds and Middleton (1959 a); (c) Hinds and Middleton (1959 b); (d) The values found by comparison with $j_l^2(kr)$.

Many of the alpha-particle groups in these spectra originate from the $^{27}Al(^3He, \alpha)^{26}Al$ reaction. Good agreement was obtained with the recently published energy level scheme of ^{26}Al, derived by magnetic analysis of the same reaction (Hinds and Middleton 1959 a) and with the levels observed by magnetic analysis of the $^{28}Si(d, \alpha)^{26}Al$ reaction (Browne 1959).

The observed ground state Q values and excitation energies for the levels investigated, are presented in the table and compared with previously published values.

Angular distributions for the reactions $^{27}Al(^3He, \alpha)^{26}Al$, leading to the ground state and first six excited states of ^{26}Al have been obtained. The boron exposures provided angular distributions for transitions leading to the ground state and first four excited states of ^{10}B, and to the ground state and 2·33 MEV excited state of ^{9}B. From the nitrogen exposures, angular distributions for transitions to the ground state, first excited state and the unresolved second and third excited states of ^{13}N were obtained. In addition, the angular distribution for the ground state group of the reaction $^{16}O(^3He, \alpha)^{15}O$ was obtained from both the boron and nitrogen exposures, the oxygen being present in each case as a target impurity.

§ 4. DISCUSSION

4.1. *Angular Distributions*

For a surface interaction mechanism, by either a pick-up or an exchange process, the angular distributions are characterized by the angular momentum transfer involved, and can be compared with a first approximation with the spherical Bessel functions $j_l^2(kr)$ (Butler 1957) where $l\hbar$ and $k\hbar$ refer respectively to the orbital angular momentum and the linear momentum transferred in the reaction; and where r is an interaction radius parameter.

The possible values of l are governed by the selection rule $\mathbf{J}_\mathrm{i}+\mathbf{l}+\frac{1}{2}=\mathbf{J}_\mathrm{f}$, where J_i and J_f refer to the spins of the initial and final nuclear states. A further restriction on l is that it must take odd values if there is a change of parity between the initial and final nuclear states, and even values when there is no parity change.

The angular distributions have been compared with the corresponding Bessel functions in most cases. A more accurate theoretical comparison would demand an expression in which the Bessel function is multiplied by a form factor, which would depend on the reaction mechanism (Butler 1957). The variation of such a factor would be relatively small over the angular range of the main peak, and its predominant effect would be to move the position of the theoretical maximum of the angular distribution to smaller angles, so that a somewhat smaller value of the radius parameter, than that used here, would be required to give the best fit.

The angular distributions corresponding to the $^{11}B(^3He, \alpha)^{10}B$ reaction are shown in figure 2, and comparison has been made with the functions $j^2(kr)$ using $l=1$ and a radius of $4{\cdot}5 \times 10^{-13}$ cm for all but the α_1 and α_4 groups, for which radii of $3{\cdot}8 \times 10^{-13}$ cm and $5{\cdot}0 \times 10^{-13}$ cm are used respectively. The angular distributions corresponding to the $^{10}B(He, \alpha)^{9}B$ reaction, leading to the ground state and 2·33 MEV state of ^{9}B, are shown in figure 3, and comparison has been made with the curve for $l=1$, $r=5{\cdot}6 \times 10^{-13}$ cm for the ground state group. An intense elastically scattered $^3He^+$ group coincided with the ^{9}B ground state group at laboratory angles between 10° and 25°, and conseqeuntly the form of the angular distribution is somewhat uncertain at small angles.

The angular distributions corresponding to the $^{14}N(^3He, \alpha)^{13}N$ reaction are shown in figure 4. The ^{13}N ground state is expected to have spin ½ and negative parity, and therefore the angular distribution for the ground state group to be characterized by $l = 1$, the only allowed value. The observed angular distribution has been compared with the curve for $l = 1$, and using $r = 6{\cdot}6 \times 10^{-13}$ cm to obtain agreement with the position of the first maximum. The first excited state group is weak, and extraction from aluminium groups, with which it overlapped at several angles, is responsible for the large errors on several of the experimental points. The target was insufficiently thin and uniform to resolve the second and third

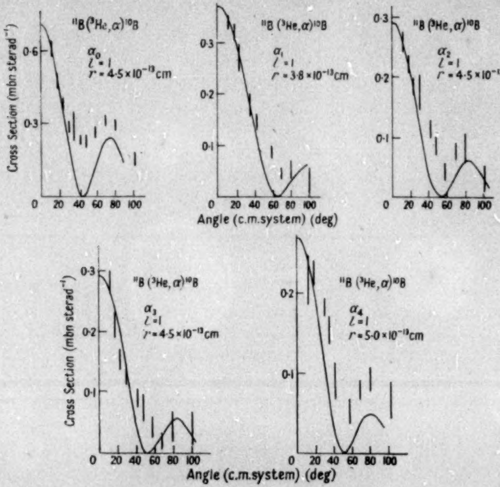

Figure 2. Angular distributions of the alpha particle groups from the $^{11}B(^3He, \alpha)^{10}B$ reaction.

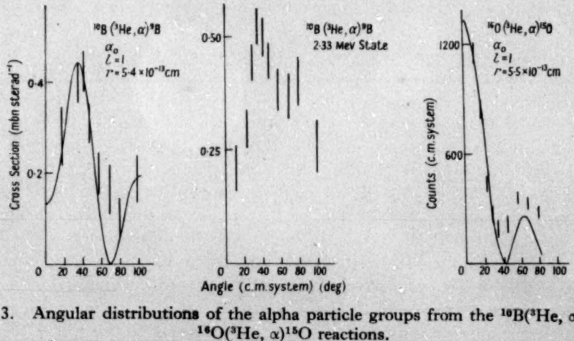

Figure 3. Angular distributions of the alpha particle groups from the $^{10}B(^3He, \alpha)^9B$ and $^{16}O(^3He, \alpha)^{15}O$ reactions.

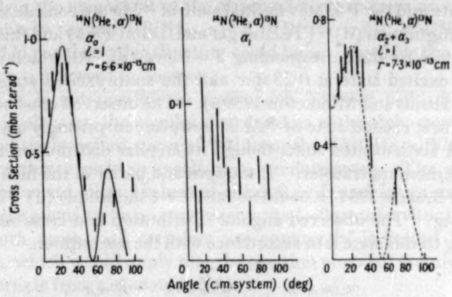

Figure 4. Angular distributions of the alpha particle groups from the $^{14}N(^3He, \alpha)^{13}N$ reaction.

excited states of ^{13}N, separated in energy by approximately 50 kev, and overlap with groups from the $^{27}Al(^3He, \alpha)^{26}Al$ reaction at several angles has prevented a complete angular distribution for the combined groups from being obtained. A tentative comparison has however been made with the curve for $l = 1$, $r = 7\cdot3 \times 10^{-13}$ cm. The $^{14}N(d, t)^{13}N$ reaction, at an incident deuteron energy of 14·8 Mev, has been investigated by Warburton and McGruer (1957). They point out that on the basis of the shell model, this reaction would not be likely to lead to the first and third excited states of ^{13}N by the simple pick-up of a neutron. The same considerations apply for the $^{14}N(p, d)^{13}N$ reaction leading to these states, observed at 18 Mev by Standing (1956). The observed ratio of the peak differential cross sections of the ground state and first excited state groups for the $^{14}N(p, d)^{13}N$ reaction is 12·5 : 1 and for the $^{14}N(d, t)^{13}N$ reaction it is 200 : 1. In our results, the intensity of the first excited state group from the $^{14}N(^3He, \alpha)^{13}N$ reaction is also low, the observed ratio of the peak differential cross sections of the ground state and first excited state groups being 11·0 : 1.

The angular distribution for the $^{16}O(^3He, \alpha)^{15}O$ reaction, leading to the ground state of ^{15}O, is shown in figure 3, and compared with the curve for $l = 1$, $r = 5\cdot5 \times 10^{-13}$ cm. The oxygen occurred as an impurity on the targets and the absolute differential cross section, though evidently large, could not be determined. Good agreement was obtained between the observed angular distributions from both the boron and adenine targets, indicating that the proportion of oxygen present remained essentially constant throughout the exposures.

The angular distributions obtained for the $^{27}Al(^3He, \alpha)^{26}Al$ reaction are shown in figure 5. The fifth excited state group, not shown, has a low intensity with an average cross section of 0·03 mbn sterad^{-1}, and the angular distribution appeared to be isotropic to within 20%. The intensity of the sixth excited state group is contrastingly high, and the angular distribution compares reasonably well with the calculated curve for $l = 2$, $r = 5\cdot2 \times 10^{-13}$ cm. On the basis of a pick-up process, preferred transitions are expected from the ^{27}Al ground state, for which it may be assumed that the simple shell model configuration $(d)^{-1}$ predominates, to levels of ^{26}Al having the $(d)^{-2}$ configuration. Transitions to states of ^{26}Al in which the $(d)^{-2}$ configuration is mixed with the $(d)^{-3}$ s configuration, would be expected to be inhibited to an extent depending upon the admixture involved.

The ground state and the 1·83 MeV excited state of ^{26}Mg are considered to have the shell model configuration $(d)^{-2}$ (Theiberger and Talmi 1956) and this suggests the same configuration for the corresponding $T=1$ levels of ^{26}Al, which would appear to be the first excited state at 0·23 MeV and the sixth excited state at 2·07 MeV (Browne 1959, Hinds and Middleton 1959 a). The observed cross section for the reaction to the first excited state of ^{26}Al is, however, surprisingly small compared with that to the sixth excited state, though its angular distribution may be fitted with an $l=2$ momentum transfer. If the spin and parity of the fifth excited state is 2^+ (Endt and Braams 1957) it could not also have the simple $(d)^{-2}$ configuration with *j–j* coupling. The observed angular distribution and cross section for the reaction leading to this state is in accordance with the assumption.

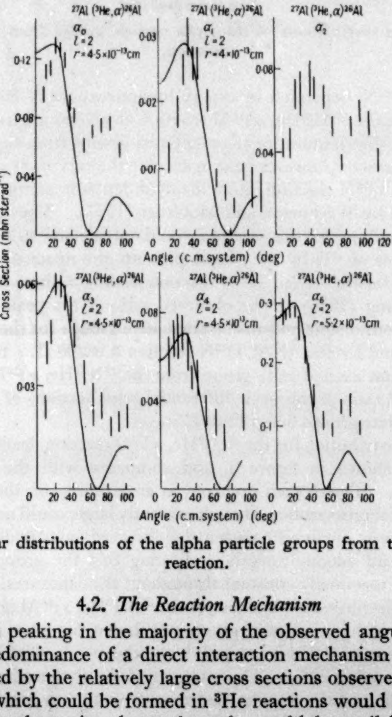

Figure 5. Angular distributions of the alpha particle groups from the ^{27}Al(^{3}He, α)^{26}Al reaction.

4.2. *The Reaction Mechanism*

The forward peaking in the majority of the observed angular distributions suggests the predominance of a direct interaction mechanism in the reactions. This is supported by the relatively large cross sections observed, since the compound nucleus which could be formed in ^{3}He reactions would have high excitations, and many alternative decay channels would be available (e.g. neutron emission). The reactions may be interpreted in terms of neutron pick-up and exchange processes, both of which will give essentially the same form of angular distributions. The theoretical expression for the cross section of the exchange process involves the product of the alpha particle and the ^{3}He particle reduced widths for the initial and final nuclei respectively, and this has to be quite large if one is to explain the magnitude of the observed cross sections on this basis alone. Although unlikely for the ^{11}B(^{3}He, α)^{10}B, ^{10}B(^{3}He, α)^{9}B, ^{14}N(^{3}He, α)^{13}N, and ^{27}Al(^{3}He, α)^{26}Al reactions, this situation could be envisaged for the ^{16}O(^{3}He, α)^{15}O reaction which is observed to be strong.

Although it is not possible to distinguish between pick-up and exchange mechanisms in all cases, the angular distributions of the alpha particles leading to the fourth and sixth excited states of ^{26}Al from the ^{27}Al(^{3}He, α)^{26}Al reaction, provide evidence that a pick-up mechanism predominates. The spin and parity selection rules would allow l values of either 0 or 2, and for an exchange process therefore, there seems to be no reason why the $l=0$ transfer should not predominate. In both cases $l=2$ transfers are apparently indicated by the angular distributions, which would imply that the reaction proceeds mainly by the pick-up of a single particle from a d state in ^{27}Al.

However, in the ^{27}Al(^{3}He, α)^{26}Al reaction, at the incident energies used here, Coulomb and nuclear interactions are likely to be important. The angular distributions of the alpha particle groups leading to the ground state and the first and third excited states of ^{26}Al fall well below the Bessel function curves at angles lower than that of the first maximum. This may be due to the above factors, particularly the Coulomb effect (Holmgren, Wolicki and Johnston 1959). The angular distributions for the fourth and sixth excited state groups fit the $l=2$ theoretical curves quite closely at small angles, and it may be that there is some $l=0$ contribution, arising from the exchange mechanism in these cases, which would tend to cancel the above effect.

In the reactions investigated here, the spins and parities of the initial and final nuclear states were known. The l values which have been fitted were uniquely determined by the spin and parity selection rules in the case of the ^{11}B(^{3}He, α)^{10}B (second excited state), ^{14}N(^{3}He, α)^{13}N (ground state), ^{16}O(^{3}He, α)^{15}O (ground state) and ^{27}Al(^{3}He, α)^{26}Al (ground state) reactions, and in these, as in all the other cases, they are consistent with the values expected from simple shell models for the pick-up of a single particle.

The radii which have been used to fit the angular distributions remain relatively constant for a particular reaction, and are generally within $1{\cdot}0\times10^{-13}$ cm of the Gamow–Critchfield value $(1{\cdot}22A+1{\cdot}7)\times10^{-13}$ cm, except for the ^{14}N(^{3}He, α)^{13}N reaction, where a radius of $6{\cdot}6\times10^{-13}$ cm has been used for the angular distributions of the ground state group. In the corresponding (p, d) reaction between the same states however, an anomalously large radius is similarly required to fit the angular distribution (Standing 1956).

REFERENCES

AJZENBERG-SELOVE, F., and LAURITSEN, T., 1959, *Nucl. Phys.*, **11**, 1.

BARROS, F. DE. S., FORSYTH, P. D., JAFFE, A. A., and TAYLOR, I. J., 1959, *Proc. Phys. Soc.*, **73**, 793.

BROMLEY, D. A., and ALMQVIST, E., 1959, *Atomic Energy of Canada Ltd., Chalk River.* Report " Nuclear Reactions with ^{3}He Ions " (to be published in shorter form in *Rep. Progr. Phys.*, **23**).

BROMLEY, D. A., KUEHNER, J. A., and ALMQVIST, E., 1959, *Atomic Energy of Canada Ltd., Chalk River*, Report No. P-D 309.

BROWNE, C. P., 1959, *Phys. Rev.*, **114**, 807.

BUTLER, S. T., 1957, *Phys. Rev.*, **106**, 272.

ENDT, P. M., and BRAAMS, C. M., 1957, *Rev. Mod. Phys.*, **29**, 683.

Forsyth, P. D., Barros, F. de S., Jaffe, A. A., Taylor, I. J., and Ramavataram, S., 1960, *Proc. Phys. Soc.*, **75**, 291.
Hinds, S., and Middleton, R., 1959 a, *Proc. Phys. Soc.*, **73**, 501.
—— 1959 b, *Ibid.*, **74**, 202.
Holmgren, H. D., Geer, E. H., Johnston, R. L., and Wolicki, E. A., 1957, *Phys. Rev.*, **106**, 102.
Holmgren, H. D., Wolicki, E. A., and Johnston, R. L., 1959, *Phys. Rev.*, **114**, 1281.
Owen, G. E., Madansky, L., and Edwards, S., 1959, *Phys. Rev.*, **113**, 1575.
Standing, K. G., 1956, *Phys. Rev.*, **101**, 152.
Theiberger, R., and Talmi, I., 1956, *Phys. Rev.*, **102**, 923.
Warburton, E. K., and McGruer, J. N., 1957, *Phys. Rev.*, **105**, 639.

The Temperature Dependence of Magnetostriction in Polycrystalline Gadolinium

By W. D. CORNER and F. HUTCHINSON†
Department of Physics, Durham Colleges in the University of Durham

Communicated by G. D. Rochester; *MS. received* 12*th November* 1959, *in final form* 11*th January* 1960

Abstract. The magnetostriction and magnetization of an ellipsoid of polycrystalline gadolinium have been measured in the temperature range 78°K to 365°K. The results show that gadolinium has a large volume magnetostriction which is proportional to the square of the paramagnetic magnetization above the Curie point. The saturation magnetostriction shows an anomaly at 150°K, and becomes zero at 233°K. The contribution of the volume magnetostriction to the thermal expansion of gadolinium is shown to be too small to account for the thermal expansion anomaly.

§ 1. INTRODUCTION

GADOLINIUM is a simple type of ferromagnetic substance compared with the more common elements in that the spontaneous magnetization at 0°K is very nearly equivalent to the parallel alignment of seven electron spins per atom. Since there are seven electrons in the incomplete 4f band, it seems probable that these are the carriers of the magnetic moment. This expected simplicity is not borne out by experiment, however, as the reduced (magnetization, temperature) curve (Elliot *et al.* 1953) shows a greater divergence from the theoretical curve for seven electron spins than do similar curves for the other ferromagnetics, with the appropriate number of electron spins. Since magnetization and magnetostriction are intimately connected, measurements on the temperature variation of the magnetostriction may throw further light on this matter. In addition there is an anomaly in the temperature coefficient of expansion near the Curie point which is most probably connected with the disappearance of spontaneous magnetization at that temperature. Measurements have therefore been made of the temperature variation of the magnetostriction and magnetization in the range 78°K to 365°K.

§ 2. METHOD

A polycrystalline specimen was prepared from a sample of gadolinium supplied by Messrs. Johnson, Matthey and Co. containing the following impurities: Pr, 0·1%; Nd, 1·5%; Sm, 0·2%; Fe, 0·005%.

The final shaping to the form of a prolate ellipsoid was made in a lathe using a very fine file and fine grade emery paper, the profile of the specimen being projected on to an outline of the correct shape. The distortion produced in the surface layer during the shaping of the specimen was removed by etching in a very dilute solution of sulphuric acid and ferric chloride. The profile of the ellipsoid was carefully measured with a travelling microscope and showed good agreement between the calculated and actual shapes. In its final form the ellipsoid was 1·746 cm long with a maximum diameter of 0·274 cm, giving a demagnetizing factor of 0·498. This value compared well with that calculated from the initial slope of the magnetization curves.

---

†Now at Regional Physics Department, Eastern Regional Hospital Board, Dundee.

Magnetostriction measurements were made, using a capacitance bridge method (Corner and Hutchinson 1958), in the temperature range 78°K to 365°K. Only one slight modification in the original apparatus was needed. The aluminium temperature compensator was not used as the temperature coefficient of expansion of gadolinium between 120°K and 290°K, the Curie temperature, is very small, $-2 \times 10^{-6}\,\mathrm{deg}^{-1}$ (Bannister *et al.* 1954).

Intensity of magnetization (I) measurements were made on the specimen in the same applied field H_a and temperature range as used for the magnetostriction ($\Delta L/L$) measurements. The usual search coil and Grassot fluxmeter method was used, with a mutual inductance to compensate for the effect of the solenoid field on the flux coil. As the primary of this inductance was required to take the full solenoid current of 250 amp, it was constructed of 5/16 in. o.d. copper tubing, and cooled by passing water through the tubing.

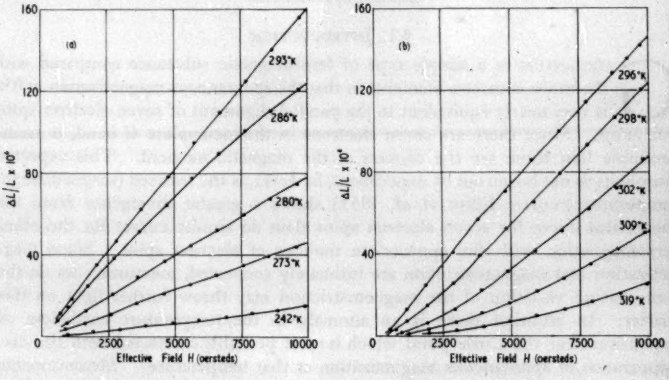

Figure 1. Variation of magnetostrictive strain with effective field for temperatures in the range (*a*) 242°K to 293°K, and (*b*) 296°K to 319°K.

§ 3. RESULTS

It was fairly easy to obtain measurements of the intensity of magnetization I at any desired temperature so they were noted at the same temperature as the $\Delta L/L$ measurements. Graphs of ($\Delta L/L$, H_a) and (I, H_a) were drawn and from these, values of I, $\Delta L/L$ and H obtained, where H denotes the internal field strength. There was very little scatter in the experimental points, measurements being repeatable to within 1%. The overall accuracy of the $\Delta L/L$ measurements was to about 5%, and that of the I measurements to about 2%. The results for temperatures below 242°K are shown in the table and those for higher temperatures in figure 1 (*a*) and 1 (*b*). Magnetization curves for the higher range of temperatures are shown in figure 2. In each case only representative experimental points are given and for greater detail see Hutchinson (1959).

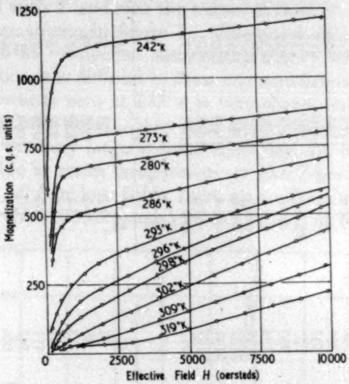

Figure 2. Initial magnetization curves for temperatures between 242°K and 319°K.

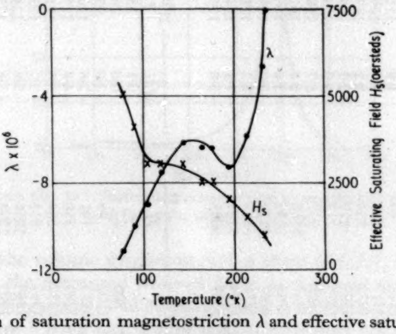

Figure 3. Variation of saturation magnetostriction λ and effective saturating field H_S with temperature.

§ 4. DISCUSSION

At low temperatures the variation of magnetostrictive strain with field is similar to that observed in iron. There is at first a small increase in length in fields up to about 150 oersteds, followed by a decrease in length. This decrease reaches a limiting value and then expansion again begins. The limiting value of $\Delta L/L$ is taken to be the saturation magnetostriction λ, and any change in dimensions which occurs after that state has been reached must be due to an effect dependent on an increase in the spontaneous magnetization. This is thought to be a volume magnetostrictive effect and will be referred to as such though no measurements have been made of the change in volume.

Dependence of Magnetostriction and Intensity of Magnetization on Magnetic Field at Temperatures below 242°K

	78°K			104°K			143°K		
H_{app}	$\Delta L/L$	I	H	$\Delta L/L$	I	H	$\Delta L/L$	I	H
200	0·2	—	—	0·1	—	—	0·1	—	—
400	0·8	788	1	0·8	744	28	0·9	788	6
600	1·6	1103	49	1·9	1110	45	1·9	1124	38
800	1·4	1317	141	1·7	1299	150	1·4	1260	170
1000	0·4	1432	284	0·2	1432	284	−1·0	1345	327
1250	−2·0	1523	477	−2·3	1496	502	−3·2	1410	515
1500	−4·5	1575	712	−4·0	1546	727	−4·1	1446	777
1750	−6·2	1625	937	−5·7	1589	955	−4·6	1478	1011
2000	−7·6	1661	1168	−6·8	1613	1194	−5·1	1500	1250
3000	−10·1	1733	2134	−8·6	1661	2169	−5·9	1539	2230
4000	−11·0	1747	3126	−9·0	1695	3152	−6·0	1564	3218
6000	−11·2	1776	5112	−8·2	1718	5141	−5·4	1589	5205
8000	−10·9	1799	7101	−7·1	1747	7127	−4·5	1618	7191
10000	−10·2	1829	9085	−5·8	1774	9113	−3·3	1647	9177

	175°K			213°K			242°K		
H_{app}	$\Delta L/L$	I	H	$\Delta L/L$	I	H	$\Delta L/L$	I	H
200	—	—	—	0·1	358	21	0·1	333	34
400	0·15	800	—	0·0	702	49	0·2	605	98
600	0·25	1102	49	−2·0	974	113	0·4	852	174
800	−1·4	1217	191	−3·6	1106	247	0·6	952	324
1000	−3·5	1289	356	−4·8	1179	411	0·7	1024	488
1250	−4·5	1332	584	−5·5	1214	543	1·0	1069	717
1500	−5·3	1367	811	−5·7	1231	884	1·2	1090	965
1750	−5·7	1389	1056	−5·8	1244	1128	1·5	1104	1198
2000	−6·0	1403	1298	−5·8	1251	1374	1·8	1110	1445
3000	−6·4	1430	2285	−5·5	1271	2365	3·1	1131	2434
4000	−6·4	1446	3277	−4·9	1287	3357	4·5	1144	3428
6000	−5·8	1473	5263	−3·5	1316	5342	7·4	1170	5415
8000	−5·0	1493	7254	−1·9	1339	7331	10·4	1192	7404
10000	−3·9	1514	9243	0·0	1367	9316	13·5	1213	9393

Values of field in oersteds, intensity in c.g.s units. Effective field H calculated from applied field H_{app} and the demagnetizing factor 0·498, for the ellipsoidal specimen. All values of $\Delta L/L$ multiplied by 10^6.

The value of T for which λ equals zero is $233^\circ \pm 1^\circ$K. The initial increase in length, for temperatures below 233°K, is reduced as the temperature increases from 78°K, but is present up to 233°K. Above 233°K, $\Delta L/L$ increases with increasing field strength at all temperatures for which measurements were made.

The variation of λ with T and also the values of field H_s required to produce technical saturation are shown in figure 3. The graph of λ against T shows an anomaly at about 150°K. Since no satisfactory theory has been advanced to explain a (λ, T) variation it is difficult to draw any conclusion from this anomaly. The approach of λ towards zero at 233°K is very sharp and does not show any tailing off towards the Curie point. Any such effect would, of course, be masked by a combination of the very large volume effect and the form effect, $(\Delta L/L)_f$. The latter gives a value at room temperature of $(\Delta L/L)_f \sim 10^{-12} I^2$. The comparatively high value of I in low fields right up to the Curie point (at 286°K, $I = 500$ c.g.s. units for $H = 1000$ oersteds) gives $(\Delta L/L)_f$ of the order of 10^{-7}.

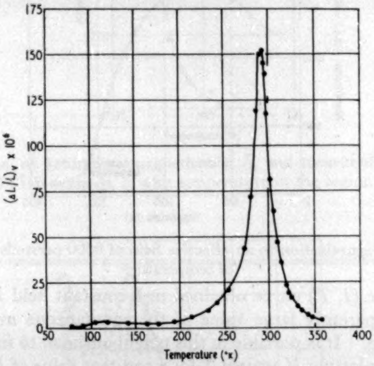

Figure 4. Linear strain due to volume magnetostriction in an effective field of 9500 oersteds as a function of temperature.

Assuming that the volume magnetostriction effect $(\Delta L/L)_v$ in a field H is the difference between the measured value of $\Delta L/L$ in that field and λ, then figure 4 shows a plot of $(\Delta L/L)_v$ against T in a constant field H of 9500 oersteds. Changing the ordinate in figure 3 from $(\Delta L/L)_v$ to $\partial(\Delta L/L)/\partial H$ does not alter the shape of the curve. It is impossible to separate the linear and the volume effects by extrapolating the $(\Delta L/L, H)$ curves back to $H = 0$, since the volume effect is only linear with respect to field once the specimen has been saturated.

The maximum value of $(\Delta L/L)_v$, 164×10^{-6}, is obtained at 293°K. Rough measurements were made of the magneto-caloric effect in the region of the Curie point in order to estimate the strain produced by thermal expansion associated with this effect. The maximum temperature rise found in a field H of 9500 oersteds, was 0·4°K at 292°K. Above the Curie point the temperature coefficient of expansion is 10×10^{-6} deg^{-1}, below, -2×10^{-6} deg^{-1}, corresponding to strains due to the magneto-caloric effect of $+4 \times 10^{-6}$ and -8×10^{-7} respectively. This is small compared with the observed values of $(\Delta L/L)_v$ of the order of 150×10^{-6}, and for the present calculation has been neglected.

No saturation values of I are quoted in the results, as the number of experimental points available for extrapolation was too small. The results showed that I is proportional to $1/H$ only for fields above about 7500 oersteds. This agrees more with the results of Trombe (1937) than with those of Elliot *et al.* (1953). The former found $I \propto 1/H$ in fields above 9500 oersteds, whereas the latter found this to be true in fields above 4000 oersteds. In the equation $I_{H,T}=I_{\infty,T}(1-a/H)$ the constant a gives an estimate of the magnetic hardness. From the above results a figure of 700 is obtained, compared with Trombe's value of 1250, and Elliot's of 170. The difference is more probably due to a domain size effect than a difference in the purity of the specimens.

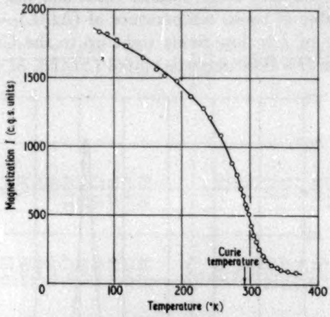

Figure 5. Magnetization in an effective field of 9500 oersteds as a function of temperature.

Figure 5 is the (I, T) curve obtained in a constant field H of 9500 oersteds, and shows an apparently large value of the spontaneous magnetization at the Curie temperature. It is possible in this neighbourhood to find the spontaneous magnetization by plotting H against T for a constant value of I, and extrapolating back to $H=0$. This gives the temperature at which the chosen value of I is equal to the spontaneous magnetization. Unfortunately, this method cannot be used to find I_s at temperatures well below the Curie point, as the maximum field obtainable from the solenoid, 10 500 oersteds, was not large enough to produce an increase in I_s at a constant temperature. The Curie point, determined from a plot of I_s^2 against T, is 292°K.

Figure 6 shows I_s and measured I values for $H=9500$ oersteds. The difference between the two, I_v, must be due to an increase in I_s produced by the application of a large magnetic field. At 300°K I_s is only about 30 c.g.s. units and is rapidly decreasing in value, so that above this temperature it is reasonable to use the measured value of I as being equal to I_v. I_v and $(\Delta L/L)_v$ have their maximum values at different temperatures, I_v at 296°K. $(\Delta L/L)_v$ at 292°K. Figure 7 shows values of $((\Delta L/L)_v^{1/2}, T)$ and (I_v, T), both reduced to the same value at 296°K. It shows that in this region, i.e. the paramagnetic region, the relation between $(\Delta L/L)_v$ and I_v is given by $(\Delta L/L)_v=KI_v^2$ where K is a constant.

The number of experimental points was not sufficient to test this relationship in the ferromagnetic region by normalizing the curves below 292°K. Even so the fact that it is possible to produce volume magnetostriction at low temperatures may indicate that a corresponding increase in the spontaneous magnetization has been produced. This would invalidate any (I_s, T) curve obtained by plotting $(I, 1/H)_T$ and extrapolating back to infinite field. The only correct points in the curve would be in the immediate neighbourhood of 0°K. If the volume magnetostriction were associated with rotations this would not apply.

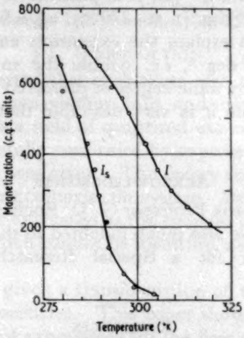

Figure 6. Variation of saturation magnetization I_s and measured magnetization in an effective field of 9500 oersteds, I, with temperature in the region of the Curie point.

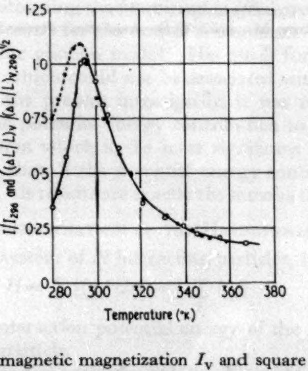

Figure 7. Variation of paramagnetic magnetization I_V and square root of linear strain due to volume magnetostriction, $(\Delta L/L)_V^{1/2}$, with temperature. Both quantities are reduced to unity at 296°K. The full circles refer to $(\Delta L/L)_V^{1/2}$ and the open circles refer to I_V.

There is an anomaly in the thermal expansion curve of gadolinium at the Curie point, and also at approximately 120°K (Trombe and Foex 1952). Bannister *et al.* (1954) have shown this to be due to the hexagonal axis expanding as the temperature decreases in this interval, and suggested that it is due to a magnetostrictive effect.

As the temperature is increased towards the Curie point, the additional volume change caused by the destruction of the spontaneous magnetization gives rise to a linear expansion coefficient α_{m}, where

$$\alpha_{\mathrm{m}} = \frac{1}{3}\frac{\partial \omega}{\partial T} = \frac{1}{3}\left(\frac{\partial \omega}{\partial H}\right)_T \left(\frac{\partial H}{\partial T}\right)_I .$$

If we assume that $(\Delta L/L)_{\mathrm{v}} = \frac{1}{3}\omega$, it is possible to obtain an estimate of α_{m}. At 290°K, $\alpha_{\mathrm{m}} = 7{\cdot}2 \times 10^{-6}\,\mathrm{deg}^{-1}$, at 279°K, $\alpha_{\mathrm{m}} = 5{\cdot}1 \times 10^{-6}\,\mathrm{deg}^{-1}$, at 273°K, $\alpha_{\mathrm{m}} = 4{\cdot}9 \times 10^{-6}\,\mathrm{deg}^{-1}$. To explain the expansion anomaly in this temperature region requires $\alpha_{\mathrm{m}} = 10^{-5}\,\mathrm{deg}^{-1}$, i.e. double the measured value. This discrepancy could be caused by some degree of preferred crystal orientation in either specimen. To resolve this it is very desirable that measurements should be made on single crystals.

ACKNOWLEDGMENTS

The authors wish to thank Professor G. D. Rochester for the facilities placed at their disposal. They are also much indebted to the Department of Scientific and Industrial Research for a Special Research Grant and a Research Assistantship for F.H.

REFERENCES

BANNISTER, J. R., LEGVOLD, S., and SPEDDING, F. H., 1954, *Phys. Rev.*, **94**, 1140.
CORNER, W. D., and HUTCHINSON, F., 1958, *Proc. Phys. Soc.*, **72**, 1049.
ELLIOT, J. F., LEGVOLD, S., and SPEDDING, F. H., 1953, *Phys. Rev.*, **91**, 28.
HUTCHINSON, F., 1959, *Thesis*, University of Durham.
TROMBE, F., 1937, *Ann. Phys., Lpz.*, **7**, 385.
TROMBE, F., and FOEX, M., 1952, *C.R. Acad. Sci., Paris*, **235**, 42.

RESEARCH NOTES

Transport of Energy and Momentum by Phonons in Fluids

By A. CROWE†
Queen Mary College, University of London

MS. received 14*th October* 1959, *in revised form* 23*rd December* 1959

§ 1. INTRODUCTION

LANDAU (1941) has asserted that at absolute zero temperature liquid helium behaves as a perfect non-viscous fluid, and that at finite temperatures it should be regarded as a field of quantized excitations that are propagated in it. This idea was successfully confirmed by experiment, but it was some time before a microscopic theory was given. The theory consists of a transformation of the dynamical variables that comprise the system. By means of this transformation the Hamiltonian can be expressed as the energies of a perfect Bose–Einstein system of quasi-particles which cannot be identified with the individual particles of the system.

Bogolyubov (1947) has given a transformation of the Hamiltonian which is valid for low energy quasi-particles. This paper shows how his transformation can be applied to the classical expressions for the flow of energy and momentum that have been derived by Eisenschitz (1955) who has demonstrated that these results are also valid in quantum mechanics.

This problem has already been attempted by Eisenschitz (1956) by using a different method of transforming the Hamiltonian (Zubarev 1953, Bogolyubov and Zubarev 1955). His result for the flow of momentum was satisfactory and fully in accordance with the phonon model. His result for the flow of energy contained an energy term which could not be associated with a phonon energy.

During the course of the present investigation it was revealed that he did not correctly deal with the potential energy contribution to the flow of energy. He omitted this contribution which is the most significant term in the flow of energy. It can be shown that, if the potential energy contribution is included in Eisenschitz's deduction, his results are exactly the same as those presented here.

§ 2. TRANSFORMATION OF THE HAMILTONIAN

The Hamiltonian of a system of N interacting particles, in its usual form, is

$$H = \sum_j \left[(p_j^2/2m) + \tfrac{1}{2} \sum_i U_{ji} \right]$$

where U_{ji} is the mutual interaction potential energy of the pair (j, i) and $\mathbf{p}_j$ is the momentum of the jth particle.

In the formalism of second quantization this is presented in the following way:

$$H = -\frac{\hbar^2}{2m} \int \Psi^+(\mathbf{r}) \nabla^2 \Psi(\mathbf{r})\, d\mathbf{r} + \tfrac{1}{2} \int U(|r-r'|) \Psi^+(\mathbf{r}) \Psi(\mathbf{r}) \Psi^+(\mathbf{r}') \Psi(\mathbf{r}')\, d\mathbf{r}\, d\mathbf{r}'$$

where

$$\left.\begin{aligned} \Psi &= \left(\frac{1}{V}\right)^{1/2} \sum_{\mathbf{k}} a_{\mathbf{k}} \exp\left[i(\mathbf{k}\,.\,\mathbf{r})/\hbar\right] \\ \Psi^+ &= \left(\frac{1}{V}\right)^{1/2} \sum_{\mathbf{k}} a_{\mathbf{k}}^+ \exp\left[-i(\mathbf{k}\,.\,\mathbf{r})/\hbar\right]. \end{aligned}\right\} \qquad \ldots\ldots (1)$$

---

† Now at St. Peter's Hall, University of Oxford.

The $a_{\mathbf{k}}$'s and the $a_{\mathbf{k}}{}^{+}$'s are particle annihilation and creation operators which obey the following commutation laws:

$$a_{\mathbf{k}}a_{\mathbf{k}'}-a_{\mathbf{k}'}a_{\mathbf{k}}=0 \quad a_{\mathbf{k}}a_{\mathbf{k}'}{}^{+}-a_{\mathbf{k}'}{}^{+}a_{\mathbf{k}}=\delta_{\mathbf{k}\mathbf{k}'}.$$

The operator $N_{\mathbf{k}}=a_{\mathbf{k}}{}^{+}a_{\mathbf{k}}$ represents the number of particles with momentum $\mathbf{k}$. For a finite volume V the vector $\mathbf{k}$ is quantized.

Bogolyubov (1947) showed that the Hamiltonian may be transformed to

$$H=H_0+\sum_{\mathbf{k}} E(k)n_{\mathbf{k}}$$

where H_0 is the ground state energy and

$$E(k)=\left[2T(k)\frac{N_0u(k)}{V}+T(k)^2\right]^{1/2}$$

$$u(k)=\int U(|R|)\exp\left[-i(\mathbf{k}\,.\,\mathbf{R})/\hbar\right]d\mathbf{R}$$

$$T(k)=k^2/2m.$$

The $E(k)$ terms are energies of single quasi-particles which cannot be identified with the individual particles of the system. For small $\mathbf{k}$ the $E(k)$ terms may be identified with phonon energies. The $n_{\mathbf{k}}$ are the occupation numbers of the single quasi-particle states.

Bogolyubov also obtains a relationship between the annihilation and creation operators $a_{\mathbf{k}}$ and $a_{\mathbf{k}}{}^{+}$ for the individual particles of the system and the annihilation and creation operators $b_{\mathbf{k}}$ and $b_{\mathbf{k}}{}^{+}$ for the quasi-particles:

$$a_{\mathbf{k}}=\frac{b_{\mathbf{k}}+L_k b_{-\mathbf{k}}{}^{+}}{[1-|L_k|^2]^{1/2}}\exp\left(E_0t/i\hbar\right)$$

$$a_{\mathbf{k}}{}^{+}=\frac{b_{\mathbf{k}}{}^{+}+L_k{}^{+}b_{-\mathbf{k}}}{[1-|L_k|^2]^{1/2}}\exp\left(iE_0t/\hbar\right) \qquad \ldots\ldots(2)$$

where

$$L_k=[E(k)-T(k)-(N_0/V)u(k)][V/N_0u(k)].$$

The $b_{\mathbf{k}}$ and $b_{\mathbf{k}}{}^{+}$ operators obey the same commutation laws as the $a_{\mathbf{k}}$ and $a_{\mathbf{k}}{}^{+}$, and $b_{\mathbf{k}}{}^{+}b_{\mathbf{k}}=n_{\mathbf{k}}$.

This transformation will next be applied to the expressions for the flow of momentum and energy.

§ 3. EXPRESSIONS FOR THE FLUXES

The expressions for the fluxes derived by Eisenschitz (1955) are

$$P=\frac{1}{mV}\sum_j\left\langle(\mathbf{p}_j\mathbf{p}_j)-\tfrac{1}{2}m\sum_i(\mathbf{r}_j-\mathbf{r}_i)\partial U_{ji}/\partial(\mathbf{r}_j-\mathbf{r}_i)\right\rangle \qquad \ldots\ldots(3)$$

$$\mathbf{Q}=\frac{1}{2m^2V}\sum_j\left\langle p_j{}^2\mathbf{p}_j+\tfrac{1}{2}m\sum_i\left[U_{ji}-(\mathbf{r}_j-\mathbf{r}_i)\,.\,\partial U_{ji}/\partial(\mathbf{r}_j-\mathbf{r}_i)\right](\mathbf{p}_j-\mathbf{p}_i)\right\rangle. \qquad \ldots\ldots(4)$$

The average as indicated by $\langle\ldots\rangle$ is taken over an ensemble. In order to apply Bogolyubov's transformation it is convenient to write the tensors $\mathbf{r}\partial U/\partial\mathbf{r}$ and the scalars $\mathbf{r}\,.\,\partial U/\partial\mathbf{r}$ in the form of Fourier series:

$$\mathbf{r}\frac{\partial U}{\partial\mathbf{r}}=\frac{1}{V}\sum_{\mathbf{k}}\nu(\mathbf{k})\exp\left[\frac{i(\mathbf{k}\,.\,\mathbf{r})}{\hbar}\right]. \qquad \ldots\ldots(5)$$

The $\nu(\mathbf{k})$ is a tensor which has the form

$$\nu(\mathbf{k})=\int\mathbf{r}\frac{\partial U}{\partial\mathbf{r}}\exp\left[\frac{-i\mathbf{k}\,.\,\mathbf{r}}{\hbar}\right]dr$$

$$=\int\left[\frac{\partial(\mathbf{r}U)}{\partial\mathbf{r}}-\mathbf{1}\,U+i\mathbf{r}\mathbf{k}U\right]\exp\left[\frac{-i\mathbf{k}\,.\,\mathbf{r}}{\hbar}\right]\mathbf{dr}.$$

In the above integral the first part is zero by Gauss' theorem, the second part is $-\mathbf{1}u(k)$ where $\mathbf{1}$ is the unit tensor, and the third part makes contributions to (5) which, for small $\mathbf{k}$, give zero on summation. Thus for small $\mathbf{k}$ we have

$$\mathbf{r}\frac{\partial U}{\partial \mathbf{r}} = -\mathbf{1}\frac{1}{V}\sum_{\mathbf{k}} u(k)\exp\left[\frac{i\mathbf{k}.\mathbf{r}}{\hbar}\right]. \qquad \ldots\ldots (6)$$

It may similarly be shown that

$$\mathbf{r}.\frac{\partial U}{\partial \mathbf{r}} = -\frac{3}{V}\sum_{\mathbf{k}} u(k)\exp\left[\frac{i\mathbf{k}.\mathbf{r}}{\hbar}\right]. \qquad \ldots\ldots (7)$$

§ 4. THE FLOW OF MOMENTUM

The potential energy part of expression (3) is transformed according to expression (6) and, since this involves only the unit tensor, we can omit this contribution because it is isotropic and has no significance in viscous flow. The remainder of expression (3) is written in the formalism of second quantization:

$$P = \frac{1}{mV}\left\langle \int \Psi^{+}(\mathbf{r})\mathbf{p}(\mathbf{r})\mathbf{p}(\mathbf{r})\Psi(\mathbf{r})\,d\mathbf{r}\right\rangle.$$

After the insertion of equations (1) for the Ψ^{+} and the Ψ this becomes:

$$P = \frac{1}{mV}\langle \sum_{\mathbf{k}} \mathbf{k}\mathbf{k}a_{\mathbf{k}}{}^{+}a_{\mathbf{k}}\rangle.$$

The $a_{\mathbf{k}}$ operators are now replaced by the $b_{\mathbf{k}}$ operators according to expressions (2). For the case of small $\mathbf{k}$ we can make certain approximations:

$$E(k) \simeq [k^2 N_0 u(0)/mV]^{1/2} \qquad \ldots\ldots (8)$$

$$L_k \simeq -1 \qquad \ldots\ldots (9)$$

$$1-|L_k|^2 \simeq 2[2T(k)mV/N_0 u(0)]^{1/2}. \qquad \ldots\ldots (10)$$

In view of these approximations the expression for P finally reduces to:

$$P = \frac{1}{V}\left\langle \sum_{\mathbf{k}}\left(\frac{\mathbf{k}\mathbf{k}}{k^2}\right)E(k)n_{\mathbf{k}}\right\rangle + \frac{1}{2V}\left\langle \sum_{\mathbf{k}}\left(\frac{\mathbf{k}\mathbf{k}}{k^2}\right)E(k)\right\rangle.$$

This is the result obtained by Eisenschitz. The second term is finite.

§ 5. THE FLOW OF ENERGY

In the formalism of second quantization expression (4) is

$$\mathbf{Q} = \frac{1}{2m^2V}\left\langle \int \Psi^{+}(\mathbf{r})p(\mathbf{r})^2\mathbf{p}(\mathbf{r})\Psi(\mathbf{r})\,d\mathbf{r} + \tfrac{1}{2}m\int \Psi^{+}(\mathbf{r}')\Psi^{+}(\mathbf{r})\left[U-(\mathbf{r}-\mathbf{r}')\frac{\partial u}{\partial(\mathbf{r}-\mathbf{r}')}\right][\mathbf{p}(\mathbf{r})+\mathbf{p}(\mathbf{r}')]\Psi(\mathbf{r}')\Psi(\mathbf{r})\,d\mathbf{r}\,d\mathbf{r}'\right\rangle. \qquad \ldots\ldots (11)$$

With the help of expression (7) the potential part in the above expression is written in the form of a Fourier series. Expressions (1) for the Ψ's are inserted and, after the integration has been performed, the above expression in terms of the $a_{\mathbf{k}}$ operators is

$$\mathbf{Q} = \frac{1}{mV}\left\langle \sum_{\mathbf{k}} \mathbf{k}T(k)a_{\mathbf{k}}{}^{+}a_{\mathbf{k}}\right\rangle + \frac{2N_0}{mV^2}\left\langle \sum_{\mathbf{k}} \mathbf{k}[u(0)+u(k)]a_{\mathbf{k}}{}^{+}a_{\mathbf{k}}\right\rangle. \qquad \ldots\ldots (12)$$

The first term on the right-hand side of this expression is the contribution from the kinetic part of expression (11). This expression is now put in terms of the

$b_{\mathbf{k}}$ operators according to expressions (2). After using the approximations given in expressions (8), (9) and (10), we obtain:

$$\mathbf{Q}=\frac{4}{mV}\left\langle\sum_{\mathbf{k}}\mathbf{k}\left[\frac{N_0u(0)}{V}\right]n_{\mathbf{k}}\right\rangle.$$

The kinetic energy part of expression (12) does not contribute to the above expression because, for small $\mathbf{k}$, $T(k)$ is neglected as being very much smaller than $N_0u(0)/V$.

Knowing that $E(k)=C|k|$, where C is the velocity of sound at absolute zero, and, by using expression (8), we obtain finally:

$$\mathbf{Q}=\frac{4}{V}\left\langle\sum_{\mathbf{k}}\left(\frac{\mathbf{k}}{k}\right)E(k)Cn_{\mathbf{k}}\right\rangle.$$

§ 6. CONCLUSIONS

The expression for the flow of momentum is the same as that obtained by Eisenschitz. It is fully in accordance with the phonon model consisting of an angular term multiplied by the energy density. The expression for the energy flow is also in accordance with the phonon model. The potential interaction part of the expression for the flow of energy contributes the dominant term when the transformation is made. It can be shown that Eisenschitz would obtain the same result if the potential interaction part is included in his deduction. Thus, in contrast to what was originally supposed, the particle momentum parts of the expressions, after they have been transformed, contribute leading terms only to the flow of momentum.

The fact that by using a different method of transforming the Hamiltonian, we can obtain the same as the amended results of Eisenschitz, indicates that the theory has some validity.

ACKNOWLEDGMENT

The author is very much indebted to Professor R. K. Eisenschitz who, in addition to suggesting this problem, has made himself available for much helpful discussion.

REFERENCES

BOGOLYUBOV, N. N., 1947, *J. Phys.*, **1**, 23.
BOGOLYUBOV, N. N., and ZUBAREV, D. N., 1955, *J. Exper. Theor. Phys., U.S.S.R.*, **28**, 129.
EISENSCHITZ, R. K., 1955, *Phys. Rev.*, **99**, 1059.
—— 1956, *Proceedings of the International Symposium on Transport Processes in Statistical Mechanics* (New York, London: Interscience Publishers), p. 266.
LANDAU, L D., 1941, *J. Phys., Moscow*, **5**, 71.
ZUBAREV, D. N., 1953, *J. Exper. Theor. Phys., U.S.S.R.*, **25**, 548.

The Thermal Expansion of a Silicon Single Crystal

BY R. R. BIRSS AND R. J. HORNE
Department of Electrical Engineering, Imperial College, London

MS. received 22*nd October* 1959, *in final form* 16*th November* 1959

SINCE the normal thermal expansion of a solid is due to anharmonicity of the interatomic forces it may be calculated, in principle, from the observed elastic anharmonicity (Sheard 1958). In practice, however, calculations of thermal expansion often rely upon a single phenomenological parameter as an average measure of the anharmonicity. This parameter is the Grüneisen (1926) constant γ which may, to this approximation, be expressed in terms of the coefficient of linear thermal expansion β by means of the equation

$$\gamma = \frac{3V\beta}{\chi C_V},$$

where χ is the isothermal compressibility and C_V the heat capacity at constant volume V. In judging to what extent the same factor γ may be associated with the different frequencies of the lattice vibrations, substances which exhibit negative values of β, and hence apparently of γ, are of considerable interest. It has been suggested that such behaviour occurs with atoms having fourfold coordination in loosely packed structures with strong interatomic covalent bonding since it is to be expected that the restoring force for the transverse modes of the bonds may be weak in these cases. The present investigation is concerned with the thermal expansion of a single crystal of silicon in a ⟨111⟩ direction. The thermal expansion has been measured from − 195° to 100°c and the results are compared with data obtained by Gibbons (1958).

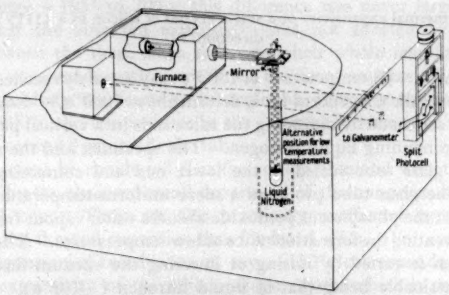

Figure 1. Schematic diagram of the apparatus.

The apparatus was designed to facilitate measurements of the thermal expansion, within the range − 195° to 1000°c, of small single crystals in the form of rods about 1 cm × 4 mm. The principle of its construction and operation may be seen from figure 1. The specimen, which is in the form of a rod with opposite ends ground flat and perpendicular to the axis of the rod, is located between a circular quartz base-plate and the centre rod of three fused silica rods. The outer two rods are fused to the quartz base-plate, and brass clamp fittings on the ends of all three rods permit a force to be applied to the centre rod to keep the specimen in position. Pivot steel rollers of small diameter are placed between the silica rods in two places and also between the brass blocks. One of the rollers between the brass blocks carries a small concave mirror, and a beam of light, after reflection from the mirror, is arranged to illuminate equally two halves of a split photocell connected in series opposition through a sensitive galvanometer. Any change in length of the specimen is communicated by the centre silica rod to the corresponding brass block causing a rotation of the concave mirror. A new null position may then be found in which the photocell output is zero and the corresponding displacement of the photocell may be measured on a micrometer head to 1×10^{-4} cm. In practice the sensitivity is governed by the accuracy with which the null position may be located and when the mirror is illuminated by a 40 w lamp, the optical path length being 2×70 cm, a displacement of 10^{-4} cm can be measured to better than 1%. All thermal expansion measurements must be corrected for the expansion of fused silica and allowance is made for this using the data of Cook (1956). For high temperature operation the specimen is mounted horizontally in a furnace, wound with 20 s.w.g. Kanthol A.1 wire and energized from a variable voltage a.c. source. (A temperature of 1300°c may be safely reached but the silica rods, which are of the translucent type, deform above 1000°c.) Low temperature measurements are made by mounting the silica rods in a vertical position above a vacuum flask containing liquid nitrogen. The specimen and the silica rods are enclosed in a glass tube sealed at the lower end and containing phosphorus pentoxide. The glass tube produces a more uniform temperature around the specimen whilst the phosphorus pentoxide absorbs water vapour from the atmosphere thus preventing the formation of ice at low temperatures. The temperature of the specimen is varied by raising or lowering the vacuum flask, the lowest temperature attainable being that of liquid nitrogen (−195°c). Temperature measurements are made with a thermocouple, potentiometer and standard cell, a platinum : 13% rhodium–platinum thermocouple being used above room temperature and a copper : Eureka thermocouple below. The whole apparatus is compact and is fitted into a Dexion framework which is light-proofed with hardboard and fire-resisting sheet (Syndano). The photocell is illuminated by a 40 w lamp the brightness of which may be controlled to facilitate rapid location of the null position. In addition, the photocell is screened from light from the lamp supplying the reflecting galvanometer. The temperature measuring equipment

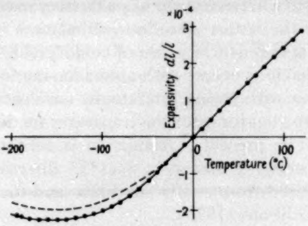

Figure 2. The thermal expansivity of a single crystal of silicon in a ⟨111⟩ crystallographic direction.

and the controls for the furnace and lamps are located directly below the photocell assembly unit.

The specimen used for the present investigation was a single crystal of pure silicon in the form of a rod 2·3 cm long with its long axis parallel to a ⟨111⟩ crystallographic direction. Figure 2 depicts a typical set of measurements of the variation with temperature of the thermal expansivity, that is the fractional change in length of the specimen referred to 0°c. The broken curve is taken from the data of Gibbons (1958) which confirm the existence of a region below −150°c in which the coefficient of thermal expansion, and hence the Grüneisen factor, is negative. Such a region would not appear, however, to extend to quite such high values of temperature as is indicated by the data of Gibbons. In view of the discrepancy between the two curves at low temperatures it was considered to be of some interest to determine whether this could be due to an error in the absolute calibration of the apparatus. Since the effect of such an error on the observed expansivity would be proportional to temperature, the thermal expansion of a rod of high purity cobalt was measured at temperatures up to 1000°c. A comparison with the data of Bozorth (1951) indicated that the discrepancy shown in figure 2 cannot be attributed to a calibration error—a conclusion which was confirmed by thermal expansion measurements on a number of other materials including high purity iron and nickel.

Although it is obvious from the form of the curves shown in figure 2 that the disagreement with Gibbons' data is unlikely to arise from any error in temperature measurement, it was considered desirable to investigate the distribution of temperature around the specimen and the silica rods. This was achieved by performing two auxiliary experiments. To confirm that the temperature of the specimen was the same as that of the adjacent segments of the silica rods, two thermocouples, in contact respectively with the specimen and one rod, were used to measure the temperature difference between these members. Within the temperature range −195° to 200°c this difference was never larger than 1½°c. To confirm that the observed expansivity was not affected by temperature differences between the three silica rods over their whole lengths, expansivity measurements were made with a specimen cut from another silica rod. The differential expansivity was found to be negligible except at temperatures above 1000°c. At 1000°c the temperature in the (empty) furnace tube is constant to ±2°c over the central 4 cm inside the tube.

It may therefore be concluded that the results obtained with this apparatus are unaffected by the observed small departures of the temperature distribution from the ideal one. They are also practically unaffected by any supposed uncertainty in the thermal expansion data for fused silica. For example, a 10% error in the expansion of fused silica at, say, −150°c corresponds to an error in the observed expansivity of the silicon single crystal which is only 1% of the discrepancy, shown in figure 2, between the experimental results and the data of Gibbons.

References

Bozorth, R. M., 1951, *Ferromagnetism* (New York: Van Nostrand), p. 262.

Cook, A. H., 1956, *Brit. J. Appl. Phys.*, **7**, 285.

Gibbons, D. F., 1958, *Phys. Rev.*, **112**, 136.

Grüneisen, E., 1926, *Geiger–Scheel Handb. d. Phys.*, **10**, 1.

Sheard, F. W., 1958, *Phil. Mag.*, **3**, 1381.

Photo-Ionization of Helium

By A. L. STEWART and W. J. WILKINSON
Department of Physics, The Queen's University of Belfast

Communicated by K. G. Emeleus; *MS. received* 18*th December* 1959

§ 1. Introduction

Recent theoretical work (Kabir and Salpeter 1957, Dalgarno and Lynn 1957) has indicated the need for more precise values of the helium oscillator strengths and, in particular, of the oscillator strengths for photo-ionization of helium in its ground state near the spectral head. Calculations have been made by a number of workers (Wheeler 1933, Vinti 1933, Körwien 1934, Huang 1948) each of whom assumed that the hydrogenic approximation to the continuum wave function adequately represented the ionized state. An assessment of the accuracy of this assumption is desirable.

§ 2. Theory

Expressing energy in rydbergs and all other dynamical variables in atomic units the quantal dipole length and dipole velocity formulae for the photo-ionization oscillator strengths of helium are respectively

$$\left(\frac{df}{d\epsilon}\right)_{\mathrm{L}} = (I+\epsilon)\left|\int \Psi_1{}^*(\mathbf{r}_1+\mathbf{r}_2)\Psi_f(\epsilon)d\mathbf{r}_1\,d\mathbf{r}_2\right|^2 \qquad \ldots\ldots(1)$$

$$\left(\frac{df}{d\epsilon}\right)_{\mathrm{V}} = (I+\epsilon)\left|\frac{2}{I+\epsilon}\int \Psi_1{}^*(\nabla_1+\nabla_2)\Psi_f(\epsilon)d\mathbf{r}_1 d\mathbf{r}_2\right|^2, \qquad \ldots\ldots(2)$$

where $\mathbf{r}_j=(r_j,\theta_j,\phi_j)$ is the position vector of the jth electron with respect to the nucleus, I is the first ionization potential of the normal atom and ϵ is the energy of the electron in the continuum, Ψ_1 is the normalized wave function of the atom in its ground state and $\Psi_f(\epsilon)$ is the wave function for the ionized system in the $(1s)(\epsilon p)^1P$ state with zero angular momentum about the polar axis, normalized according to

$$\int \Psi_f{}^*(\epsilon')\Psi_f(\epsilon)d\mathbf{r}_1 d\mathbf{r}_2=\delta(\epsilon-\epsilon'). \qquad \ldots\ldots(3)$$

The formulae (1) and (2) give identical results (Chandrasekhar 1945) if Ψ_1 and Ψ_f are exact solutions of the Schrödinger equation

$$\left\{-\nabla_1{}^2-\nabla_2{}^2-\frac{4}{r_1}-\frac{4}{r_2}+\frac{2}{r_{12}}-E\right\}\Psi=0, \qquad \ldots\ldots(4)$$

where

$$r_{12}=|\mathbf{r}_1-\mathbf{r}_2|.$$

With Huang we take

$$\begin{aligned}\Psi_1=\exp\{-\alpha(r_1+r_2)\}[c_0+c_1\alpha r_{12}+c_2\alpha^2(r_2-r_1)^2\\ +c_3\alpha(r_1+r_2)+c_4\alpha^2(r_1+r_2)^2+c_5\alpha^2r_{12}{}^2],\end{aligned} \qquad \ldots\ldots(5)$$

where the parameters c_1, c_2, c_3, c_4, c_5 and α have been determined by Hylleraas (1929) using the variation method. For the continuum wave function we write

$$\Psi_f(\epsilon)=\frac{(3)^{1/2}}{\pi}[\exp(-2r_1)r_2{}^{-1}f(r_2)\cos\theta_2+\exp(-2r_2)r_1{}^{-1}f(r_1)\cos\theta_1], \qquad \ldots\ldots(6)$$

which is in accord with the normalization condition (3) if

$$f(r) \sim \frac{1}{(\pi^2\epsilon)^{1/4}} \sin\left\{\epsilon^{1/2}r + \frac{1}{\epsilon^{1/2}}\log(2\epsilon^{1/2}r) - \frac{\pi}{2} + \arg\Gamma\left(2 - \frac{i}{\epsilon^{1/2}}\right) + \eta\right\}. \qquad \ldots\ldots(7)$$

The phase shift η is zero when the continuum wave function represents an electron moving in a Coulomb field of charge $Z=1$. Substituting (6) into (4), multiplying the resulting equation by $\exp(-2r_2)$ and integrating over the space of $\mathbf{r}_2$ yields

$$\frac{d^2f(r_1)}{dr_1^2} + \left\{\frac{2}{r_1} + \exp(-4r_1)\left(4 + \frac{2}{r_1}\right) - \frac{2}{r_1^2} + \epsilon\right\}f(r_1)$$
$$= \frac{64}{3}\exp(-2r_1)\left\{\frac{1}{r_1}\int_0^{r_1} f(r_2)\exp(-2r_2)r_2^2 dr_2 + r_1^2\int_{r_1}^{\infty} f(r_2)\exp(-2r_2)\frac{1}{r_2}dr_2\right\}, \qquad \ldots\ldots(8)$$

an equation analogous to the Hartree–Fock equation for the radial function representing a bound electron moving in the field of an undisturbed atomic core (cf. Seaton 1953). If we omit the exchange term on the right of equation (8) we derive the equation analogous to the Hartree equation for a bound electron

$$\frac{d^2f(r)}{dr^2} + \left\{\frac{2}{r} + \exp(-4r)\left(4 + \frac{2}{r}\right) - \frac{2}{r^2} + \epsilon\right\}f(r) = 0, \qquad \ldots\ldots(9)$$

which may be further simplified by omitting the exponential term in the potential to give the Coulomb equation

$$\frac{d^2f_{\mathrm{C}}(r)}{dr^2} + \left\{\frac{2}{r} - \frac{2}{r^2} + \epsilon\right\}f_{\mathrm{C}}(r) = 0. \qquad \ldots\ldots(10)$$

The phase shift η, which gives a measure of the departure of the field of the helium nucleus and the bound electron from the Coulomb field with charge $Z=1$, can be determined directly from the solutions of (8) and (10) at very large radial distances or by means of the integral equation

$$\eta = \sin^{-1}\left[\pi\int_0^{\infty} f_{\mathrm{C}}\{fS - G\}\,dr\right], \qquad \ldots\ldots(11)$$

where $S = (4 + 2/r)\exp(-4r)$ and G is the exchange term on the right of equation (8) (cf. Mott and Massey 1949).

§ 3. CALCULATIONS

Substituting (5) and (6) into (1) and (2) and integrating over the coordinates of the bound electron yields

$$\left(\frac{df}{d\epsilon}\right)_{\mathrm{L,\,V}} = (I+\epsilon)\left|\int_0^{\infty} W_{\mathrm{L,\,V}}(r)f(r)dr\right|^2, \qquad \ldots\ldots(12$$

where W_{L} and W_{V} are the functions of the radial distance which result when the length and velocity matrix elements respectively are integrated over the space of the bound electron. Thus the problem reduces to numerical integration once f has been determined and the functions W_{L} and W_{V} have been tabulated.

The solutions of (8), (9) and (10) have been determined by the numerical technique of Fox and Goodwin (1949). The solution of (8) is a lengthy computation, which requires the exchange term to be initially evaluated using the solution of (9) and successively improved by iteration.

§ 4. RESULTS AND DISCUSSIONS

The phase shifts derived from (11) using the numerical solutions of (8), (9) and (10) are presented in table 1 where they are compared with the values given by the quantum defect method (cf. Seaton 1957). The quantum defects for the $(1s)(np)^1P$ series of terms in helium have been computed from the spectroscopic term values given by Moore (1949). It is apparent that at the spectral head the Hartree–Fock wave function is superior to both the Coulomb and the Hartree solutions. Indeed the Hartree solution gives the wrong sign for the phase. Since extrapolation of the quantum defects to energies as large as $\epsilon = 0·5$ is of doubtful validity the superiority of the Hartree–Fock wave function to the Coulomb wave function is not certain except at the spectral head. Although the integrand in (11) is weighted closer to the origin than either of the integrands in (12) it might nevertheless be concluded that, since the Hartree wave function is gravely in error in predicting the phase shifts, it will be unreliable in calculating oscillator strengths.

Table 1. Values of the Phase η due to Departures from the Coulomb Field

ϵ	(1)	(2)	(3)	(4)
0	0	0·036	−0·064	−0·038
0·5	0	0·048	−0·081	—
1·0	0	0·058	−0·079	—

(1) Coulomb field; (2) Hartree field; (3) Hartree–Fock field; (4) Quantum defect method.

Table 2. Values of the Oscillator Strength $df/d\epsilon$

ϵ	(1)	(2)	(3)	(4)	(5)	(6)	(7)	(8)
0	0·930	0·970	0·955	1·041	0·898	0·890	0·914	0·91
0·5	0·624	0·629	0·627	0·670	0·638	0·607	0·624	0·62
1·0	0·421	0·421	0·413	0·445	0·449	0·422	0·421	0·41

(1) Coulomb, dipole length; (2) Coulomb, dipole velocity; (3) Hartree, dipole length; (4) Hartree, dipole velocity; (5) Hartree–Fock, dipole length; (6) Hartree–Fock, dipole velocity; (7) recommended values; (8) experiments of Lassettre.

This conclusion is supported by the results in table 2, where the oscillator strengths derived from the dipole length and dipole velocity matrix elements using the numerical solutions of (8), (9) and (10) are displayed, which show that the values derived using the Hartree wave function are the most sensitive to the formulation used at all the energies investigated. The spread of the values at the spectral head is noticeably less in the dipole length formulation than in the dipole velocity, a result which is in accord with calculations of the oscillator strengths for discrete transitions in helium (Low and Stewart, unpublished). The opposite is true at $\epsilon = 1$. This is to be expected since the velocity formulation gives very closely the correct asymptotic form as the energy tends to infinity (Kabir and Salpeter 1957, Dalgarno and Stewart 1960). The alternative formulations are almost equally sensitive to the choice of continuum wave function at $\epsilon = 0·5$ and so we cannot prefer the results of one formulation to the other in this case.

The recommended values based on these considerations are given in column (7) of table 2. The value at $\epsilon = 0$ is the arithmetic mean of the Coulomb and

Hartree–Fock values using the dipole length formula, the value at $\epsilon=0{\cdot}5$ is the mean of the Coulomb and Hartree–Fock values using both formulations and the value at $\epsilon=1{\cdot}0$ is the mean of the Coulomb and Hartree–Fock values using the velocity formula. In column (8) of table 2 are the experimental values of Lassettre†; these are seen to be in satisfactory agreement with the recommended values.

ACKNOWLEDGMENT

We express our thanks to Dr A. Dalgarno for drawing our attention to this problem.

REFERENCES

CHANDRASEKHAR, S., 1945, *Astrophys. J.*, **102,** 223.
DALGARNO, A., and LYNN, N., 1957, *Proc. Phys. Soc.* A, **70,** 802.
DALGARNO, A., and STEWART, A. L., 1960, *Proc. Phys. Soc.*, in the press.
FOX, L., and GOODWIN, E. T., 1949, *Proc. Camb. Phil. Soc.*, **45,** 373.
HUANG, S., 1948, *Astrophys. J.*, **108,** 354.
HYLLERAAS, E. A., 1929, *Z. Phys.*, **54,** 347.
KABIR, P. K., and SALPETER, E. E., 1957, *Phys. Rev.*, **108,** 1256.
KÖRWIEN, H., 1934, *Z. Phys.*, **91,** 1.
MOORE, C. E., 1949, *Atomic Energy Levels* (Washington: Nat. Bur. Stand.)
MOTT, N. F., and MASSEY, H. S. W., 1949, *The Theory of Atomic Collisions* (Oxford: Clarendon Press).
SEATON, M. J., 1953, *Phil. Trans. Roy. Soc.* A, **245,** 469.
—— 1957, *Proc. Phys. Soc.* A, **70,** 620.
VINTI, J. P., 1933, *Phys. Rev.*, **44,** 524.
WHEELER, J. A., 1933, *Phys. Rev.*, **43,** 258.

Flow Anisotropy and the Boundary Conditions in the Molecular Theory of Liquids

BY J. V. CHAMPION AND A. SUDDABY
Department of Physics, Sir John Cass College, London

MS. received 3rd November 1959

In the molecular theory of the steady non-uniform state of a liquid (Eisenschitz 1949, Kirkwood, Buff and Green 1949), a differential equation (the Smoluchowski equation) is solved for the distortion of the relative pair distribution. After separation of the angular dependent part of the solution, which shows that the distortion renders the pair distribution anisotropic, the radial equation is

$$\frac{d^2u}{dr^2}+\left\{\frac{2}{r}-\frac{1}{\boldsymbol{k}T}\frac{d\phi}{dr}\right\}\frac{du}{dr}-\frac{6u}{r^2}=-\frac{\alpha\beta m}{(\boldsymbol{k}T)^2}r\frac{d\phi}{dr}$$

where the notation is that used by Champion (1958).

The boundary conditions may be applied in such a way that the solution is made to vanish at the origin, or alternatively to cause the solution to tend to zero at large distances such that $r^3 u \to 0$ as $r \to \infty$. Eisenschitz has referred to the first case as the 'weak condition' and the second, which necessarily admits a solution which is infinite at the origin, as the 'strong condition'. Kirkwood, Buff and Green have used the weak condition in the calculation of the viscosity of liquid argon. On the other hand, the use of the strong condition by Eisenschitz (1949), Cole (1952) and Champion (1958) leads respectively to reasonable results for the temperature dependence of viscosity, the electro-viscous effect, and flow anisotropy of liquids.

---

† Privately communicated to Dr. A. Dalgarno to whom we are indebted for the information.

In justifying the strong condition Eisenschitz (1949) argued that a monatomic liquid (or one with spherically symmetric molecules) showed no anisotropy of flow and pointed out that to exclude this the distortion $u(r)$ must vanish at a rate greater than r^{-3}. He dealt with the difficulty of an infinite solution at the origin by assuming a pole of the first order at the origin of the pair potential curve.

Subsequently it has been shown (Eisenschitz and Suddaby 1953, Suddaby 1954) that the difficulty at the origin can be explained and the strong condition justified on mathematical grounds. The Smoluchowski equation is a first approximation (in an expansion in powers of $1/\beta^2$) to the Kramers–Chandrasekhar equation which determines the pair distribution in phase space. The expansion procedure diverges at small values of r and the solutions of the two equations are not comparable at the origin. Boundary conditions cannot then be applied at the origin but conditions must be applied to ensure that the solutions correspond at large distances. This may be done by requiring the distortion to vanish when the intermolecular force $d\phi/dr$ vanishes, so that the solution for $d\phi/dr=0$ corresponds to that of a flowing gas. This procedure selects the solution which conforms to the strong condition.

That part of the flow anisotropy of chloroform which is due to the distortion of the molecular distribution function has been estimated (Champion 1958) from the $u(r)$ calculated by Cole (1952). This cannot be confirmed directly by experiment since it is masked by an orientation effect, but the value shows good agreement with that measured experimentally for carbon tetrachloride (Champion 1960), a similar molecule for which the orientation effect cannot occur. The existence of optical anisotropy and its prediction by use of the strong condition appears to invalidate Eisenschitz's appeal to the isotropy of flow of simple liquids. It is therefore of interest to calculate a magnitude for the anisotropy predicted by the weak condition.

Using the method of calculation described by Champion (1958) the anisotropy in terms of a double refraction Δn, namely, the optical anisotropy, can be calculated for a distortion $u(r)$ determined by the application of the weak condition The anisotropy is given by

$$\Delta n = \frac{2\pi}{n} N_0 \alpha \frac{\Delta E}{E} \frac{3}{(3-4\pi N_0 \alpha)}$$

where ΔE is the variation of the applied field E (the electric vector) due to the anisotropic distribution of the surrounding induced molecular dipoles, and is calculated from the distortion by means of the expression

$$\frac{\Delta E}{E} = \frac{32\pi^2}{5} \sin\psi \cos\psi \frac{N}{V} \alpha \int_r^R \exp\left\{-\frac{\phi}{\boldsymbol{k}T}\right\} \frac{u(r)}{r}\, dr.$$

The function $\{u(r)\}/r$ is shown in figure 1 and the integrand in figure 2. The contributions to the integral are $6{\cdot}2\alpha$ in the range 4 Å to 8·2 Å and $-2{\cdot}9\alpha$ in the range 8·2 Å to ∞. From this the value of the anisotropy can be obtained, and it is found that $\Delta n = 2{\cdot}8 \times 10^{-9}$, using the same potential curve and constants as before.

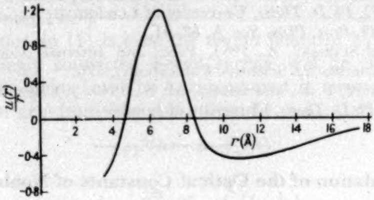

Figure 1.

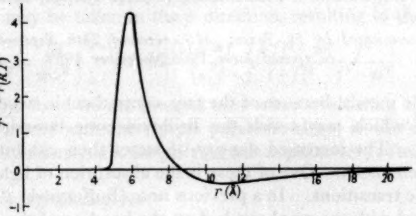

Figure 2.

It can be seen that the main contribution to the anisotropy arises from the range 4 Å to 8 Å as in the case of the strong condition. The calculated value for chloroform using the strong condition is $\Delta n = 7{\cdot}1 \times 10^{-8}$ when subjected to a rate of shear of 50 000 sec^{-1}, compared with $\Delta n = 0{\cdot}28 \times 10^{-8}$ at the same rate of shear for the weak condition.

The optical anisotropy calculated for the weak condition is thus seen to be about 1/25 of that given by the strong condition, the latter agreeing very well with the value obtained experimentally (Champion 1960).

Thus, although the results show that the experimental measurement of the optical anisotropy does indeed support the strong condition of Eisenschitz against the weak condition used by Kirkwood, this support does not take the form anticipated by Eisenschitz when he first drew attention to the possibility of optical anisotropy arising from a distorted distribution function.

The appeal made by Eisenschitz to the optical isotropy of simple liquids was based on the assumption that appreciable anisotropy would arise from a divergent contribution at large distances which could only arise in the case of the weak condition. In fact neither condition gives a divergent contribution, and the anisotropy in both cases arises from the range 4 Å to 8 Å. The value of the anisotropy is not related to the precise way in which $u(r)$ decreases at large distances.

This situation does not throw doubt on the validity of the strong condition but, on the contrary, supports it. The strong condition has the independent theoretical justification already referred to (Suddaby 1954), and, as opposed to the weak condition, is provided with additional experimental support by the observations on anisotropy.

REFERENCES

CHAMPION, J. V., 1958, *Proc. Phys. Soc.*, **72**, 711.
—— 1960, *Ibid.*, **75**, 421.
COLE, G. H. A., 1952, *Ph.D. Thesis*, University of London.
EISENSCHITZ, R., 1949, *Proc. Phys. Soc.* A, **62**, 41.
EISENSCHITZ, R., and SUDDABY, A., 1953, Proc. 2nd Internat. Congress on Rheology (London: Butterworths Scientific Publcations), 320.
KIRKWOOD, J. G., BUFF, F. P., and GREEN, M. S., 1949, *J. Chem. Phys.*, **17**, 988.
SUDDABY, A., 1954, *Ph.D. Thesis*, University of London.

A Calculation of the Optical Constants of Noble Metals

BY M. SUFFCZYNSKI AND S. MICHAELSON
Department of Mathematics, Imperial College, London

Communicated by H. Jones; *MS. received 24th September* 1959,
in revised form 19*th November* 1959

THE noble metals, because of the face-centred cubic structure, have a Fermi surface which may touch the Brillouin zone boundary or approach it closely. The increased density of states then exhibits itself in several observable phenomena. One of these is the absorption of light due to the interband electronic transitions. In a previous note (Suffczynski 1959) a band model was investigated with the emphasis laid on the bending of the energy bands near the zone boundary. In that particular model it was possible to evaluate all the formulae for the optical constants in a closed analytical form. More general models can be investigated with the help of numerical integration. The interband contribution to the complex dielectric constant can be written in the form

$$\epsilon_{\mathrm{p}}+i\epsilon_{\mathrm{p}}'=\frac{e^2}{\pi m^2 h}\frac{2}{(2\pi)^3}\frac{2}{3}\sum_{\mathrm{s}'}\sum_{\mathrm{s}}\int|\mathbf{P}_{\mathrm{s}'\mathrm{s}}|^2\left[\frac{\mathscr{P}}{\nu_{\mathrm{s}'\mathrm{s}}(\nu_{\mathrm{s}'\mathrm{s}}{}^2-\nu^2)}+\frac{i\pi}{2\nu^2}\delta(\nu_{\mathrm{s}'\mathrm{s}}-\nu)\right]d^3k. \quad \ldots\ldots(1)$$

Here $\nu=c/\lambda$ is the frequency of the incident light, $h\nu_{\mathrm{s}'\mathrm{s}}=E_{\mathrm{s}'}-E_{\mathrm{s}}$ is the energy difference between the unoccupied state s′ and the occupied state s and $\mathbf{P}_{\mathrm{s}'\mathrm{s}}$ is the dipole matrix element between the corresponding one-electron states. We will take $|\mathbf{P}_{\mathrm{s}'\mathrm{s}}|$ as an adjustable constant.

We consider one band of energy $E_-(\mathbf{k})$, occupied by electrons up to the energy E_{F}, and another empty band above it $E_+(\mathbf{k})$. We chose the k_z axis along the ΓL line in the Brillouin zone of the face-centred cubic lattice. The dependence of the energy on the wave vector in the two bands will be assumed in the axially symmetric form

$$E_-(\mathbf{k})=\frac{\hbar^2 k_{\mathrm{L}}{}^2}{2m}\left[\frac{m}{m_{\mathrm{T}-}}\rho^2+\frac{m}{m_-}f_-(k)\right]$$

$$E_+(\mathbf{k})=\frac{\hbar^2 k_{\mathrm{L}}{}^2}{2m}\left[\frac{m}{m_{\mathrm{T}+}}\rho^2+\frac{m}{m_+}f_+(k)\right] \quad \ldots\ldots(2)$$

where k_{L} is the length ΓL, and

$$k=k_z/k_{\mathrm{L}} \quad \rho=(k_x{}^2+k_y{}^2)^{1/2}/k_{\mathrm{L}}. \quad \ldots\ldots(3)$$

The ordinary electron mass is m, the m's with subscripts correspond to the different effective masses. We will require that both functions $f_{\mp}(k)$ have zero slope at $k=0$ and $k=1$. This requirement, at $k=0$, was not fulfilled in the model of reference (Suffczynski 1959).

The $\mathbf{k}$-integration in (1) is over the region bounded by the Fermi surface $E_-(\mathbf{k})=E_F$. A singly connected Fermi surface will be characterized by its distance k_1 from the point L. The k_1 is measured in terms of k_L as unit. We have to integrate over ρ from 0 to $\rho_F(k)$ given by

$$\rho_F^2(k)=\phi-f_-(k) \qquad \ldots\ldots(4)$$

where

$$\phi=\frac{2m}{\hbar^2 k_L^2}E_F=f_-(1-k_1).$$

We have taken for simplicity $m_{T-}=m_-=m$. In the evaluation of ϵ_p the principal value integration may be taken in the ρ-direction, resulting in the integral

$$\epsilon_p=\frac{M}{\alpha w^2}\int_0^{1-k_1} dk\ln\left|\frac{[\alpha(\phi-f_-)+f]^2-w^2}{[\alpha(\phi-f_-)+f]^2}\frac{f^2}{f^2-w^2}\right|. \qquad \ldots\ldots(5)$$

This is the general form of the integral met when evaluating ϵ_p in any axially symmetric band model with the simple parabolic shape in the transverse ρ coordinate. Axial symmetry is a simplifying assumption very often made (Ziman 1958).

For ϵ_p' the ρ-integration gives

$$\epsilon_p'=\frac{\pi M}{\alpha w^2}\int_{k_b(w)}^{k_c(w)} dk. \qquad \ldots\ldots(6)$$

Here

$$M=\frac{e^2 m}{3\pi\hbar^2 k_L\gamma^2}\left|\frac{\mathbf{P}_{+-}}{\hbar k_L}\right|^2, \qquad w=\frac{2\pi\nu m}{\hbar k_L^2\gamma}$$

$$\alpha=\frac{1}{2\gamma}\left(\frac{m}{m_{T+}}-\frac{m}{m_{T-}}\right), \qquad \gamma=\frac{1}{2}\left(\frac{m}{m_+}+\frac{m}{m_-}\right)$$

$$f=\frac{m}{2\gamma}\left[\frac{f_+(k)}{m_+}-\frac{f_-(k)}{m_-}\right]. \qquad \ldots\ldots(7)$$

The $k_b(w)$ and $k_c(w)$ are the k ordinates of the points of intersection of the curve $\alpha\rho^2+f(k)-w=0$ with the boundaries of the ρ, k region of integration.

The integrals (5), (6) can be evaluated numerically. A programme for evaluating them has been written for the Ferranti Mercury computer, see Appendix.

To obtain numerical results the $f_{\mp}$ functions have been taken in the form suggested by Leigh (1951) and Jones (1952):

$$f_-(k)=k^2-k^{2r}/r, \quad f_+(k)=f_0-k^2+k^{2r}/r \qquad \ldots\ldots(8)$$

where f_0 is a constant determined by the energy gap at the point L. This form of k-dependence has the advantage of allowing the band curvature near the zone boundary to be changed by taking different values of r. For large r the function $f_-(k)$ is nearly parabolic except in the immediate vicinity of the zone boundary. This is the shape usually found for the valence band in the theoretical band calculations. Since this shape f_- (k) has been used with success in the calculation of the elastic constants of the face-centred cubic metals it seemed reasonable to apply it in the calculation of the optical constants for which the negative band curvature near the energy gap is probably important. The r values were taken usually greater than 3, often 8 or 10.

The numerical computations have been carried out for copper. The interband contributions, $\epsilon_p + i\epsilon_p'$ have been added to the intraband ones, $\epsilon_D + i\epsilon_D'$, calculated from the simple Drude formulae without any special wavelengths of relaxation as used by Roberts (1955, 1959). The two Drude parameters, the static conductivity σ_0 and the ratio N/m^* of the number of free electrons to their effective mass, have been taken from the paper of Schulz (1957). The extinction coefficient $k(\lambda)$ and the refractive index $n(\lambda)$ have been calculated for wavelengths λ from 0·05 to 3 microns. Several dozen curves have been computed, for different values of k_1, α and γ. One example of the curves is given in the figure. As is seen from the figure the rise of the refractive index n at the threshold for the interband absorption is reproduced here qualitatively but not quantitatively. The present band model being slightly more satisfactory than the previous one (Suffczynski 1959) strengthened the feeling that the dip in the k/λ curve can be explained by the Fermi surface running close to the Brillouin zone boundary, that is $k_1 \leqslant 10^{-2}$. Calculations with the surface having a contact with the zone face led again to the impression that it is more difficult to reproduce the experimental dispersion curve with a Fermi surface having a large area of contact, though a very small contact might not be excluded.

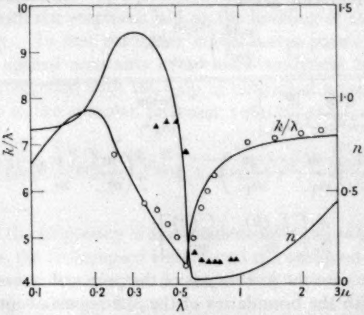

The calculated values of the extinction coefficient divided by the wavelength k/λ and of the refractive index n, plotted against ln λ for copper. The energy gap at the point L was assumed 2·2 ev. The effective masses were taken $m_{T-} = m_- = m$, $m_+ = m/3$, $\alpha = 0{\cdot}25$ and $r = 8$, the distance $k_1 = 10^{-4}$ and $M = 0{\cdot}61$. The circles denote the experimental values of k/λ and the triangles those of n obtained by Schulz (1957).

The main uncertainty in the optical calculations based on an assumed band model lies in the unknown effective masses. Only certain combinations, essentially differences of the inverse effective masses, enter into the formulae, see (7). These masses are not known and, since the empty higher band is involved, they cannot be expected to be known in the near future. Thus the calculations rest necessarily on some values of α and γ, arbitrarily assumed. The computations for different values of m_+ in the range $1/3 \leqslant m_+/m \leqslant 1$, that is for different spreads of the energy bands involved, confirmed the simple observation that the dip in the κ/λ curve becomes narrower as the spread of the bands diminishes. For singly connected Fermi surfaces the values of α may be taken from 0 to 0·25 without difficulty in fitting the k/λ dispersion curve. It should be borne in mind that the square of the dipole matrix element is always taken as an adjustable parameter. Its value must be chosen smaller the smaller the values of k_1 and of α. The calculations with a matrix element which is not a constant but varies over the Brillouin zone would not give rise to any complication in the present approach but it seems unwarranted because of the lack of knowledge of the actual electronic wave functions.

ACKNOWLEDGMENT

We should like to express our thanks to the London University Computer Unit for the allocation of the computer time and to Professsor Jones for his advice and encouragement.

REFERENCES

JONES, H., 1952, *Phil. Mag.*, **43**, 105.
LEIGH, R. S., 1951, *Phil. Mag.*, **42**, 139.
ROBERTS, S., 1955, *Phys. Rev.*, **100**, 1667.
—— 1959, *Ibid.*, **114**, 104.
SCHULZ, L., 1957, *Phil. Mag. Suppl.*, **6**, 102.
SUFFCZYNSKI, M., 1959, *Proc. Phys. Soc.*, **73**, 671.
ZIMAN, J. M., 1958, *Phil. Mag.*, **3**, 1117.

APPENDIX

Before the evaluation of the improper integral ϵ_{p} it was necessary to locate the singularities of the integrand, that is to evaluate $k_{\mathrm{b}}(w)$ and $k_{\mathrm{c}}(w)$, which also yielded ϵ_{p}'. The singularities had to be located with a greater accuracy than that required in ϵ_{p}, and this was done using a Weierstrass bisection technique. Having found $k_{\mathrm{b}}(w)$ and $k_{\mathrm{c}}(w)$ the range of integration, 0 to $1-k_1$, was split into sub-ranges at the points k_{b}, $\frac{1}{2}(k_{\mathrm{b}}+k_{\mathrm{c}})$, k_{c}, the programme being applied to each sub-range and the results combined.

Now, if

$$\int_{a_0}^{k} g(k)dk$$

exists for k between a_0 and a, but $g(k)$ is singular at $k=a$, it is possible to define the improper integral of g from a_0 to a as

$$I=\int_{a_0}^{a} g(k)dk=\lim_{\eta\to 0}\int_{a_0}^{a-\eta} g(k)dk,$$

provided the limit exists. The value of I is then the limit of the sequence of integrals

$$I_s=\int_{a_0}^{a-\eta_s} g(k)dk$$

where $\eta_s=2^{-s}(a-a_0)$.

The convergence of the sequence to I may be accelerated by making an allowance for the integral over the end of the range.

For a logarithmic singularity, a suitable amount to add to I_s is $\eta_s g(a-\eta_s)$, and a further improvement in the rate of convergence was obtained by forming the sequence G_s of linear extrapolates to $\eta=0$, defined by

$$G_s=2[I_s+\eta_s g(a-\eta_s)]-[I_{s-1}+\eta_{s-1}g(a-\eta_{s-1})].$$

The integrals I_s were obtained in sequence, since

$$I_s=I_{s-1}+\int_{a-\eta_{s-1}}^{a-\eta_s} g(k)dk.$$

The successive incremental integrals were evaluated by Simpson's rule, the step h being repeatedly halved until consecutive estimates, $J(2h)$ and $J(h)$, satisfied the condition

$$|J(2h)-J(h)|\leqslant 7\cdot 5t[|J(h)|+2^{-s-1}],$$

t being the tolerance on the estimate of I. This condition ensured that the error in I_s was less than the larger of t and $t|I_s|$. A similar criterion was used to test the adequacy of G_s as an estimate of I, namely

$$|G_s-G_{s-1}|\leqslant 0\cdot 5t[|G_s|+1].$$

LETTERS TO THE EDITOR

On Resonant Charge Transfer for Positive Ions

For the calculation of a simple transfer cross section of an electron between parent atom and its ion we shall apply the following simplified mechanism: the transition of an electron from the ground state of an atom to the corresponding state of an ion is equivalent to the quantum problem of a single electron on two identical ionic centres, a and b. We shall use therefore the hydrogen-like approximation, taking as trial function

$$\psi(r_a) = \frac{\alpha^{3/2}}{\sqrt{\pi}} \left(\frac{Z^*}{n^* a_0}\right)^{3/2} \exp\left(-\alpha \frac{Z^*}{n^* a_0} r_a\right) \qquad \ldots\ldots (1)$$

where starred Z and n represent the usual effective quantities, related to the first ionization energy I by

$$I = \frac{1}{2} \frac{mc^2}{137^2} \left(\frac{Z^*}{n^*}\right)^2 \qquad \ldots\ldots (2)$$

and r_a is the position coordinate of the electron with respect to nucleus a taken as origin. The parameter α (which for non-S states also allows for the average for angular distribution) is obtained from the best fit with experimental data.

Let us put for the transfer cross section Q (Massey and Smith 1933)

$$Q = \frac{\pi}{k^2} \sum_{l=0}^{\infty} (2l+1) \sin^2 (\eta_l^+ - \eta_l^-) \qquad \ldots\ldots (3)$$

where phase differences will be obtained by semi-classical approximation (Dalgarno 1958)

$$\zeta_l \equiv \eta_l^+ - \eta_l^- = \frac{1}{\hbar v} \int_{\frac{l+\frac{1}{2}}{k}}^{\infty} \frac{E(r_{ab})^+ - E(r_{ab})^-}{[1 - \{(l+\frac{1}{2})/kr_{ab}\}^2]^{1/2}} \, dr_{ab}, \qquad \ldots\ldots (4)$$

r_{ab} being the distance between the nuclei.

For the difference of energy from symmetrical to anti-symmetrical state, the asymptotic form, calculated with the help of wave function (1), is used:

$$E^+ - E^- = -\frac{4}{3} \alpha^3 \frac{mc^2}{137^2} \left(\frac{Z^*}{n^*}\right)^3 \frac{r_{ab}}{a_0} \exp\left(-\alpha \frac{Z^* r_{ab}}{n^* a_0}\right). \qquad \ldots\ldots (5)$$

The computation of the transfer cross section is performed using (3), (4) and (5) and putting instead of the summation (3) a suitable integral over three distinct regions: the oscillating part ($0 \leqslant \zeta_l \leqslant \pi/2$), the intermediary part ($\pi/2 \geqslant \zeta_l \geqslant \pi/4$) and the vanishing part ($\pi/4 \geqslant \zeta_l \geqslant 0$).

The final expression is then (Sena 1948, Firsov 1951, Demkov 1952, Massey and Smith 1933)

$$\sqrt{Q} = A - B \log v \qquad \ldots\ldots (6)$$

where

$$A = \frac{3{\cdot}1}{\alpha\sqrt{I}} 10^{-14} \ln (3{\cdot}86\, e^{31} \alpha \sqrt{I}); \quad B = \frac{7{\cdot}1}{\alpha\sqrt{I}} 10^{-14}. \qquad \ldots\ldots (7)$$

The experimental data generally confirm the relation given by (6) as for instance in the case of argon (see figure). Values of Q obtained by weakening the monokinetic ionic beam are marked in this plot with crosses (Flaks and Soloviev 1958, Fedorenko *et al.* 1956, Gilbody and Hasted 1957, Hasted 1951, Dillon *et al.* 1955, Ziegler 1953), values obtained with the help of usual similarity parameters characterizing an abnormal glow discharge (Badareu *et al.* 1959) by dots and those obtained from mobility data (Kagan and Perel 1955) by circles. The behaviour of other gases is similar to that shown in the figure. Apart from the methods mentioned for obtaining Q, the method of retarding field, positive ions having an energy distribution, was applied in the case of mercury (Badareu and Hagiescu 1959, Popescu 1959 a); Q was also obtained by field measurements at the abnormal glow discharge cathode in the case of helium (Popescu 1959 b).

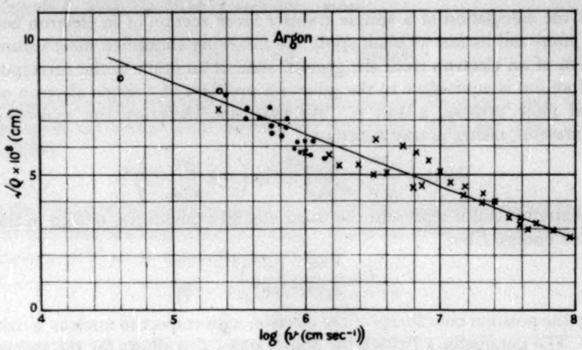

Values A and B for different gases, α_A and α_B respectively, are given in the table.

Atom	$10^8 A$ (cm)	$10^8 B$ (cm)	α_A	α_B	Q reported by	Velocity range (cm sec^{-1})
He	14·4	1·60	0·69	0·71	6, 8, 11, 12, 13, 14, 15	$10^{5\cdot1}$–$10^{8\cdot0}$
Ne	15·7	1·76	0·66	0·69	1, 3, 5, 6, 8	$10^{4\cdot8}$–$10^{7\cdot8}$
A	17·9	1·91	0·68	0·74	1, 2, 3, 4, 5, 6, 7, 8	$10^{4\cdot6}$–$10^{8\cdot0}$
Kr	19·0	2·00	0·68	0·75	1, 5, 6, 8	$10^{4\cdot5}$–$10^{7\cdot4}$
Xe	21·0	2·25	0·66	0·72	1, 5, 6, 8	$10^{4\cdot4}$–$10^{7\cdot4}$
Hg	24·5	2·47	0·60	0·71	9, 10, 16	$10^{5\cdot0}$–$10^{6\cdot5}$
K	41·8	4·16	0·54	0·65	17	$10^{5\cdot7}$–$10^{7\cdot0}$
	44·0	5·00	0·51	0·54	18	

1, Flaks and Soloviev 1958.
2, Fedorenko *et al.* 1956.
3, Gilbody and Hasted 1951.
4, Hasted 1951.
5, Dillon *et al.* 1955.
6, Ziegler 1953.
7, Badareu *et al.* 1959.
8, Kagan and Perel 1955.
9, Badareu and Hagiescu 1959.
10, Popescu 1959 a.
11, Popescu 1959 b.
12, Rostagni 1935.
13, Smith 1934.
14, Wolf 1935, 1937.
15, Rudnick 1931.
16, Paliuh and Sena 1950.
17, Kushnir 1958.
18, Bydin and Buchteev 1959.

The experimental values for α are in the range 0·5–1, as is to be expected theoretically if one starts from a higher approximation suggested by Slater's wave function.

If we apply the experimental values of α to (1), the analogous expressions of the problem of hydrogen-like ionic molecule (Pauling and Wilson 1935) yield to some extent the potential functions $E(r)^{\pm}$ of ion–atom interaction.

The authors are greatly indebted to Acad. Prof. Dr. Eugen Badareu for suggesting the present subject for research and for the encouragement offered.

Gaseous Electronics Laboratory, I. Popescu Iovitzu.
C. I. Parhon University,
Bucharest.

Atomic Physics Institute, N. J. Ionescu Pallas.
Roumanian Academy,
Bucharest.

12th August, 1959.

References

Badareu, E., and Hagiescu, M., 1959, *Stud. Cercet. Fiz.*, in the press.
Badareu, E., Popescu, I., and Iova, I., 1959, *Ann. Phys., Lpz.*, in the press.
Bydin, I. F., and Buchteev, A. M., 1959, *J. Tech. Phys.*, **29**, 12.
Dalgarno, A., 1958, *Phil. Trans. Roy. Soc.* A, **250**, 426.
Demkov, I. N., 1952, *Uci. Zap. Leningrad. G.U.*, **146**, 74.
Dillon, J. A., Sheridan, W. F., Edwards, H. D., and Ghosh, S. N., 1955, *J. Chem. Phys.*, **23**, 776.
Fedorenko, N. V., Afrosimov, V. V., and Kaminker, D. M., 1956, *J. Tech. Phys.*, **26**, 1929.
Firsov, O. B., 1951, *J. Exp. Theor. Phys.*, **21**, 1001.
Flaks, I., and Soloviev, E., 1958, *J. Tech. Phys.*, **28**, 599.
Gilbody, H. B., and Hasted, J. B., 1957, *Proc. Roy. Soc.* A, **238**, 334.
Hasted, J. B., 1951, *Proc. Roy. Soc.* A, **205**, 421.
Kagan, Yu. M., and Perel, V. I., 1955, *J. Exp. Theor. Phys.*, **29**, 884.
Kushnir, R. M., 1958, *Ukrain. Phys. J.*, **3**, 343.
Massey, H. S. W., and Smith, R. A., 1933, *Proc. Roy. Soc.* A, **142**, 142.
Paliuh, B. M., and Sena, L. A., 1950, *J. Exp. Theor. Phys.*, **20**, 481.
Pauling, L., and Wilson, E. B., 1935, *Introduction to Quantum Mechanics*.
Popescu, I., 1959 a, *Rev. Phys. Acad. R.P.R.*, **2**, 199.
—— 1959 b, *Ibid.*, **2**, 211.
Rostagni, A., 1935, *Nuovo Cim.*, **12**, 134.
—— 1935, *Atti Acad. Torino*, **70**, 472.
Rudnick, Ph., 1931, *Phys. Rev.*, **38**, 1342.
Sena, L. A., 1948, *Collisions of Electrons and Ions with Gas Atoms* (Leningrad, Moscow: GTTI).
Smith, R. A., 1934, *Proc. Camb. Phil. Soc.*, **30**, 514.
Wolf, F., 1935, *Ann. Phys., Lpz.*, **23**, 285, 627.
—— 1937, *Ibid.*, **29**, 33; **30**, 313.
Ziegler, B., 1953, *Z. Phys.*, **136**, 108.

Width and Intensity of the Mössbauer Line in Iron-57

The emission and absorption of the 14·4 kev gamma radiation of iron-57 have been studied by Pound and Rebka (1959) and Schiffer and Marshall (1959), who have used cobalt-57 sources incorporated into metallic iron by electrodeposition and diffusion. The width of the line as observed by Pound and Rebka was about twice the intrinsic width as calculated from the mean life of the excited level ($1{\cdot}44 \times 10^{-7}$ sec) (Strominger, Hollander and Seaborg 1958).

We have studied the contour of the line by methods essentially the same as theirs except for the preparation of the source, which in our initial experiments was a fragment of a natural iron (2·2% ^{57}Fe) cyclotron target, beaten and rolled down to a thickness of 20 mg cm^{-2}. Latterly we have used a source prepared by co-precipitation of ^{57}Co and ^{56}Fe hydroxides, followed by reduction to the metal (Chackett, Chackett and Singh 1960) and rolling to 25 mg cm^{-2}. The latter source in particular was therefore thin in relation to the self-absorption of the narrow line.

These sources were mounted on a vibrator driven sinusoidally at 33·3 c/s. The amplitude of vibration was calibrated using a travelling microscope, and was then set at predetermined values by measurement of the applied voltage. The gamma rays were then counted, through a variable thickness of pure natural iron, using a xenon-filled proportional counter†. A single-channel pulse analyser was used to discriminate against the K x-rays of iron, and higher energy gamma radiation from the source; this gamma radiation causes a considerable residual effect in the counting channel which was corrected for by subsidiary measurements. The transmission of a 24·7 mg cm^{-2} absorber, expressed as the ratio of

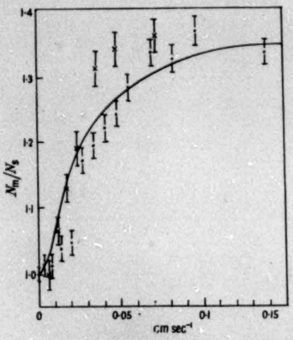

Figure 1.

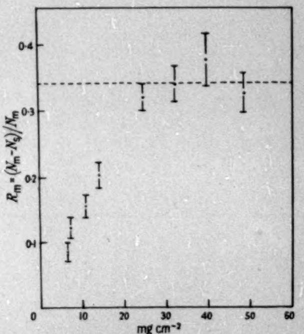

Figure 2.

Figure 1. The velocity spectrum of the narrow line of iron-57. The continuous curve was calculated assuming an emitted line of natural width but broadened by the absorber and the effect of sinusoidal motion.

Figure 2. Experimental data on R_m (see text) as a function of absorber thickness.

---

† 20th Century Electronics, Ltd.

14·4 gamma-ray counting rates with the source moving N_m to those with the source stationary N_s, was found, in two series of measurements, to be as in figure 1.

The observed spectrum is broadened beyond the natural width of the line by virtue of the distribution of velocities associated with sinusoidal motion, and also because the use of an absorber sufficiently thick to produce a large effect necessarily causes broadening by selective absorption of the central part of the line. The continuous line in figure 1 is a theoretical curve which was calculated assuming an emitted line of natural width, but broadened by these two effects. Although the two sets of measurements suggest somewhat different line contours, their half-widths are equal within the accuracy of our velocity calibration (about 15%) and agree with the calculation. We conclude that our sources are emitting lines of ' natural ' width.

With a source speed sufficient to destroy the resonance we varied the thickness of the absorber, obtaining the results shown in figure 2, in which the ordinates are $(N_m - N_s)/N_m = R_m$. It can be proved that the limiting value of R_m, as the absorber becomes 'infinitely thick', is equal to the fraction of the incident radiation which is *emitted* in the narrow line. It is thus expected to be equal to the Debye–Waller factor for the source.

The fraction emitted in the narrow line is observed to be approximately 34%, compared with 20% reported by Pound and Rebka, and an expected value of 72% assuming a Debye temperature of 355°K for iron.

Further, the initial slope of the curve is closely related to the resonant absorption of the narrow line; its photoelectric absorption is already allowed for by plotting the ratio of $N_m - N_s$ to N_m. This slope corresponds to 57 $\mathrm{cm}^2\,\mathrm{g}^{-1}$ (natural Fe), or to a cross section of $2{\cdot}5 \times 10^{-19}\,\mathrm{cm}^2$ for the isotope ^{57}Fe.

If the ground state and the 14 kev level of ^{57}Fe were degenerate in the sense that their splittings in the internal magnetic field were much less than their natural widths, then this cross section should be equal to

$$\frac{\lambda^2}{4\pi}\,\frac{f}{1+\alpha}\,\frac{2I_e+1}{2I_g+1}$$

where f is the fraction of the narrow-line radiation absorbed without recoil, α is the internal conversion coefficient and I_e and I_g are the spins of the first excited and ground states and are believed to be 3/2 and 1/2. Taking $\alpha = 15$ (Lemmer, Segaert and Grace 1955) and $f = 0{\cdot}72$ as calculated from the Debye–Waller factor, we obtain a cross section of $5{\cdot}3 \times 10^{-19}\,\mathrm{cm}^2$ which is about double our experimental value.

Our results are therefore consistent with some degree of splitting of the levels, but evidently not with full splitting of both. Pound and Rebka have observed three subsidiary peaks in their velocity spectrum, as compared with possible numbers up to seven for full splitting of the levels.

We infer that the fraction absorbed in the narrow line is greater than the 34% observed to be emitted therein. Otherwise our absorption coefficient would be inconsistent with any splitting of the levels.

Department of Physics,
University of Birmingham.
19th February 1960.

M. Cordey-Hayes.
N. A. Dyson.
P. B. Moon.

Note added in proof.—Using an isotopically enriched absorber equivalent to 140 mg cm^{-2} of natural iron we have found that R_m rises to 0·48. By fitting a resonance-line absorption curve to the observations we then obtain an emission fraction of 60% and an initial cross section for its resonant absorption of $1{\cdot}4\times10^{-19}$ cm^2, which is more nearly consistent with full splitting of the levels.

CHACKETT, K. F., CHACKETT, G. A., and SINGH, B., 1960, *J. Inorg. Nucl. Chem.*, in the press.
LEMMER, H. R., SEGAERT, O. J. A., and GRACE, M. A., 1955, *Proc. Phys. Soc.* A, **68**, 701.
POUND, R. V., and REBKA, G. A., 1959, *Phys. Rev. Letters*, **3**, 554.
SCHIFFER, J. P., and MARSHALL, W., 1959, *Phys. Rev. Letters*, **3**, 556.
STROMINGER, D., HOLLANDER, J. M., and SEABORG, G. T., 1958, *Rev. Mod. Phys.*, **30**, 585.

CORRIGENDUM

Presidential Address: *Recent Trends in the Theory of the Ionosphere*, by J. A. RATCLIFFE (*Year Book of the Physical Society*, 1959, 1) and *Abstract of Presidential Address* (*Proc. Phys. Soc.*, 1960, **75,** 2).

In the *Year Book* the expression $\beta=10^{-4}\exp[(h_0-h)/50]\ \text{sec}^{-1}$ appearing on pages 10 and 11 and in the caption to figure 8, and the expression $\beta=10^{-4}\exp[(h-h_0)/50]\ \text{sec}^{-1}$ in the caption to figure 9 *should read*

$$\beta=10^{-4}\exp[(300-h_{\text{km}})/50]\ \text{sec}^{-1}.$$

In the *Abstract* the expression $\beta=10^{-4}\exp[(170-h_{\text{km}})/50]\ \text{sec}^{-1}$ *should read*

$$\beta=10^{-4}\exp[(300-h_{\text{km}})/50]\ \text{sec}^{-1}.$$

REVIEWS OF BOOKS

Astronomy, by THEODORE G. MEHLIN. Pp. viii + 392. (New York: John Wiley; London: Chapman and Hall, 1959). 64*s*.

Progress in astronomy has left high and dry the usual notions of the non-astronomer as to what the subject is now all about. It is in no way to decry the beauty and achievement of classical astronomy, based primarily on the so-called laws of gravitation and on Euclidian geometry, to say that the subject today properly consists in a vigorous, broadly based, and systematic application of all the available physical laws to objects outside our own tiny Earth. In this process, the laws of gravitation and dynamics are today equal partners among the other physical laws.

The average popular or text book unfortunately gives little inkling of this revolution. The first third is commonly devoted to coordinate systems, spherical trigonometry and the definition of a set of archaic terms which the working astronomer would have to look up if he needed them. There follow descriptive chapters on the Moon and Sun; and on the separate planets and collective debris of the solar system. Then the distances and motions of the stars are considered, and after a brief account of their spectra and luminosities the final chapter has some such title as " Star clusters, nebulae and galaxies ". There is little here to disabuse those who may believe that astronomers indulge either in Victorian star-gazing or in the laborious compilation of data hardly to be distinguished in intellectual value from the cataloguing of pebbles on a beach.

Dr. Mehlin's book is important because it breaks away from this historical layout and aims at attaining a new balance. He takes stars and their energy sources as fundamental to astronomy, so that his treatment of their structure and evolution is placed immediately after an up-to-date introductory chapter on " Tools of the Trade ". The discussion of stellar distances and motions follows logically from this, and the Sun is treated as a special case of a star. The significance of variable and peculiar stars is well brought out without plunging the reader too deeply into the natural history and ideopathology of the subject. The grouping of stars into galaxies is given space comformable with its importance, and our own Milky Way has a chapter to itself as a special example. Only at this stage of the book is there a description of the solar system, including its natural and artificial satellites. The treatment of the relations between comets, asteroids, meteors and meteorites is especially clear. A final chapter discusses theories of the origin of the solar system. Coordinate systems are placed for reference in an appendix. This is not a mere re-arrangement of material, but a radical and much needed re-alignment of emphasis and method in a text full of up-to-date information.

The limitations of the book arise mainly from its design for use by first year college students. It is presumably this circumstance that has limited the density of equations, with the result that the discipline of the subject loses some of its incisiveness and one sometimes feels in the realm of the planetarium rather than that of the observatory. Nevertheless, the arguments show welcome signs of having been polished in class use, and the density of quantitative information is high. The illustrations are good and a number of familiar bad diagrams are notably absent.

Of course it is easy to criticise details, and there are a few places where the reviewer would say that the text gives a misleading impression. For example, the catastrophic theories of the origin of the solar system are given a prominence which leaves the reader unaware that the dynamical objections are now usually regarded as conclusive; and nothing is said of the chemical evidence (such as the N/Ze ratio of the Earth's atmosphere) which, whatever view eventually prevails, must always condition theories of the formation of the planets.

The book can be recommended as an excellent introduction to real astronomy. It is suitable for school libraries for sixth form reading, for the informed amateur or non-specialist, and for the student beginning to study astronomy professionally. Even at the research level it provides a better source of general information than was available to the reviewer when he entered the subject. P. F.

A Supplement to 'Helium', by E. M. LIFSHITS and E. L. ANDRONIKASHVILI. Pp. v + 167. (New York: Consultants Bureau; London: Chapman and Hall, 1959.) 60*s*.

In 1949 a Russian translation was published of W. H. Keesom's classical monograph '*Helium*' (the author was then still alive, contrary to the statement on the dust cover). The translation contained two additional chapters on superfluidity. The first one by E. M. Lifshits was a reprint of a survey article in the *Uspekhi* (Progress in Physics) which deals with the theories of superfluidity, particular the Russian work in this field.

The second chapter by Andronikashvili deals with experiments on the superfluid properties of liquid helium, discussing such topics as heat transport in helium II, viscosity, the thermo-mechanical effect, critical velocities, second sound, films, and the role of impurities. Both Russian and non-Russian work is discussed in detail.

As Keesom's monograph was published in 1942, this volume supplies us with a very welcome supplement dealing with work done between 1942 and 1949, a period during which our understanding both through theoretical work and through extensive experimental investigations was greatly extended. The fact that these chapters are now available in English will be welcomed by the many low-temperature physicists who are unable to read Russian. The price seems exorbitant for a book produced by a photolitho process and is one more case of the kind of blackmail practised these days by far too many publishers.

D. TER HAAR.

Molecular Science and Molecular Engineering, edited by ARTHUR R. VON HIPPEL. Pp. xv + 446. (New York : John Wiley; London : Chapman and Hall, 1959.) 148*s*.

This book is the third in a trilogy edited by Professor von Hippel on modern materials research. It is aimed both at the engineer, particularly the electronics engineer, and the physicist, pure and applied, who are using the modern molecular and crystalline materials with special properties, and it will be undoubtedly of great value to them.

Owing to the very nature of the field covered it is evidently impossible to provide a book which exactly meets the needs of all such users; and what Professor von Hippel has done with marked success, is to build up a series of chapters which can be read as separate articles and should provide between them everything that will be needed either by the pure physicist in looking for the uses of special materials, or by the engineer in striving to understand the physics underlying the equipment which he is developing.

Unlike most books of this character it is remarkably well integrated and the personality of the editor appears in the seven out of 25 chapters which he has written himself. Some of these, on general theory of atoms and molecules, and thermodynamics, ensure the book will be valuable for teaching purposes, and indeed it should be an admirable textbook in all schools of applied physics and modern electrical engineering.

It is impossible in a short review to cover a book of this kind, the reviewer's own interests are directed to a solid and liquid rather than the ionized gases and plasmas, which take up the first seven chapters. Here we have an admirable review of crystal growth by Dr. Smakula and on the plasticity of growth materials by Dr. Orowan. Much of the latter part of the book, in fact up to the last ten chapters, is taken up with the modern development von Hippel calls in a general way Dipoles and Coupled Dipole systems, which include ferroelectrics and ferromagnetics and their multitudinous applications in electronics, in rectifiers and transistors, mazers and memories. Here the book touches the most rapidly advancing parts of applied physics which is dangerous ground because probably before it was printed many of these devices have become relatively obsolete. But they are explained so simply and with such a wealth of admirable illustrations that they will still serve the student even though they may be of less value to the development engineer. J. D. BERNAL.

Principles of Radiation Dosimetry, by G. N. WHYTE. Pp. vii + 124. (New York: John Wiley & Sons; London : Chapman and Hall, 1959.) 56*s*.

Principles of Radiation Dosimetry has clearly been written for workers using radiation as a tool, rather than for those with a prime interest in dosimetry, who will prefer the larger volume *Radiation Dosimetry* edited by G. J. Hine and G. L. Brownell (1956).

The emphasis throughout is on the physical basis of the subject; for the benefit of the non-specialist, a considerable fraction of the book is devoted to the interaction of radiation with matter. The measurement of dose from electromagnetic radiations is obviously treated in greatest detail, followed by short chapters on the dosimetry of charged particles, and neutron dosimetry. The advantages and limitations of ' secondary instruments ', i.e. those having a response which varies with the amount of radiation, without yielding absolute measurements, are discussed in the final chapter, but, in the main, practical details are lacking. Liberal provision throughout of graphs and orders of magnitude should, however, give the reader a ' feel ' for the subject and there is a good list of references at the end of each chapter. H. D. EVANS.

Étude des Textures Piezoélectriques, by A. V. SHUBNIKOV, I. S. ZHLUDEV, V. P. KONSTANTINOVA and I. M. SILVESTROVA. Translated from the Russian by A. DAKNOFF. Pp. xi + 207. (Paris: Dunod, 1958.) 2750 fr.

This is a full account of a class of piezoelectric material not commonly used. Textures, as defined by the authors, are homogeneous bodies formed from small particles and in which, although there is no lattice structure to the material as a whole, the individual particles are arranged in some specific manner. The important piezoelectric textures are seignette salt bodies in which needle-like microcrystals are aligned, polarized ceramics of the barium titanate class, and bodies containing these same mixed oxides as fine, polarized powders bonded by polystyrene, by a lacquer, or by a rubber.

In their theoretical development of the subject, the authors give a good, concise account of the dielectric and piezoelectric properties of the basic ferroelectric materials which are used, and this is followed by an orthodox treatment of the properties of mixtures as applied to these textures. There is also a particularly clear and straightforward account of the basic theory of piezoelectricity.

The method of building up the oxide textures by either cold or hot pressing of powders is described in detail and the problems which arise from powder flow during pressing are well discussed. Chapters are devoted to the preparation and the properties of thin films of the seignette salt or oxide textures which perform as either single or bimorph vibrating plates according to their mode of formation and can be bonded to metal. Their investigation by means of Chladni figures makes fascinating reading.

To summarize, though perhaps too much of this book is devoted to very detailed data on the performance of particular preparations, it is a book which can be recommended for the more general information which it contains. It can be read with advantage as an introduction to both a general study of piezoelectric materials, and to the techniques of electrical ceramic preparation. C. F. O.

Tabellen zur Röntgen-Emissione- und Absorptions-Analyse, by VON K. SAGEL. Pp. vii + 135. (Berlin, Göttingen, Heidelberg: Springer, 1959.)

The Cathode-Ray Tube and its Applications, by G. PARR and O. H. DAVIE. Pp. xii + 433. (London: Chapman and Hall, 1959.) 50*s*.

Beiträge zur Physik und Chemie des 20. Jahrhunderts. Pp. xiv + 285. (Braunschweig: Friedr. Vieweg und Sohn, 1959.)

Astronomischer Jahresbericht. Band 57. *Die Literatur des Jahres* 1957. Pp. xxxviii + 525. (Berlin: Walter de Gruyter, 1959.)

Elements of Wave Mechanics, by N. F. MOTT. Pp. ix + 156. (Cambridge: University Press, 1958.) 15*s*.
A cheap edition of this book is very welcome.

La Mesure Précise du Temps en fonction des exigences nouvelles de la Science, by B. DECAUX. Pp. vi + 127. (Paris: Masson, 1959.) 1300 *fr*.

Tables of the Incomplete Elliptic Integrals of the First and Third Kind, prepared by F. A. PAXTON and J. E. ROLLIN. Pp. 436. (Quehanna, Pennsylvania: Curtiss-Wright Corporation Research Division, 1959.)

PARIS: PUBLICATIONS SCIENTIFIQUES ET TECHNIQUES DU MINISTÈRE DE L'AIR.

Étude d'une méthode de mesure des températures utilisant la sensibilité thermique des couleurs de fluorescence, par P. THUREAU. Pp. xxiii + 131. No. 349, 1959. 3240 *fr*.

Viscosimètre balistique, by F. CHARRON. Pp. xviii + 15. No. 350, 1959. 430 *fr*.

Lieu des Racines d'une Equation algébraique dépendant d'un Paramètre: Application a la Stabilité et au Guidage des Fusées, by F. SALLES. Pp. x + 69. No. 351, 1959. 1810 *fr*.

Recherches Expérimentales sur les Ondes de Choc produites par les Décharges condensées dans les Gaz rares, by M. CLOUPEAU. Pp. xx + 62. No. 352, 1959. 1180 *fr*.

Actes du Colloque de Calcul numérique, Perigueux 1957. Pp. xii + 87. No. N.T. 80, 1959. 1800 *fr*.

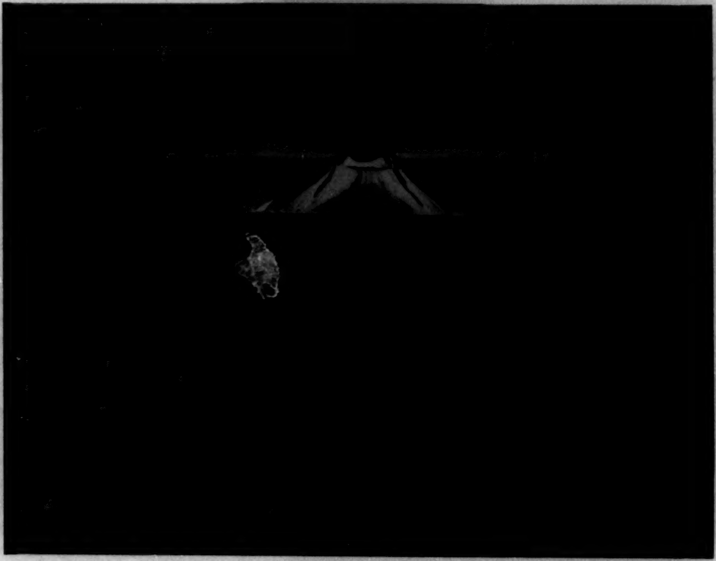

Figure 1.

(*a*) Moving film records

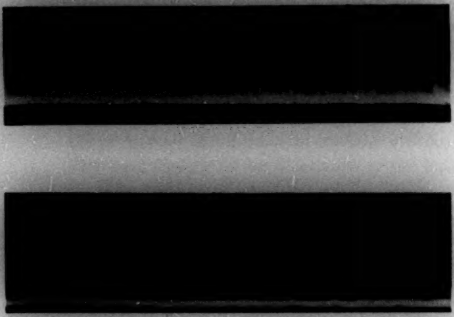

(*b*) 1 cm gap (uniform field region)

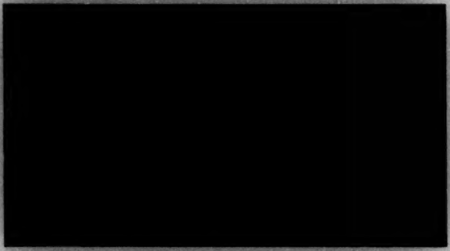

(*c*) 5 cm gap (non-uniform field region)

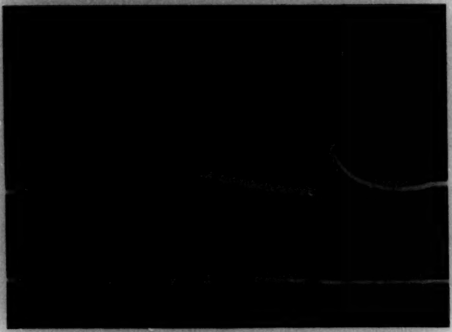

Figure 1. Oscillograms of pre-breakdown pulses of current and light in a uniform field gap.

Intensity Measurements on the CO⁺ Comet Tail, and the BO α and β Molecular Band Systems

By D. ROBINSON† and R. W. NICHOLLS‡
Department of Physics, University of Western Ontario, London, Canada

MS. received 29*th December* 1959

Abstract. Relative band intensities of the comet tail system ($A^2\Pi$–$X^2\Sigma$) of CO⁺ and of the $\alpha(A^2\Pi$–$X^2\Sigma)$ and $\beta(B^2\Sigma$–$X^2\Sigma)$ systems of BO have been measured photoelectrically. They have been interpreted with the aid of Franck–Condon factors $q_{v'v''}$ and r-centroids $\bar{r}_{v'v''}$ to show the variation of electronic transition moment $R_e(r)$ with internuclear separation r and thereby to give 'smoothed' arrays of relative vibrational transition probabilities $p_{v'v''}$ and intensities at infinite temperature I_∞. The isotope effect on the Franck–Condon factors and intensities in the case of ^{10}BO and ^{11}BO band systems has been examined.

---

§ 1. Introduction

The measurements discussed below are part of a programme for the establishment of intensity and transition probability data for molecular band systems, particularly those of astrophysical, aeronomical, and combustion interest. Measurements have previously been made on the N_2 First Positive system (Turner and Nicholls 1954 a, b) and N_2 Second Positive and N_2^+ First Negative systems (Wallace and Nicholls 1955), the CN red system (Dixon and Nicholls 1958) and the O_2^+ Second Negative, CO Ångström and Third Positive and NO β and γ band systems (Robinson and Nicholls 1958 a).

Such intensity measurements have been interpreted by a method proposed by Fraser (1954 a) which involves the r-centroid $\bar{r}_{v'v''}$ and Franck–Condon factor $q_{v'v''}$ concepts, to provide information (i) upon the variation of the electronic transition moment $R_e(r)$ with internuclear separation r, (ii) upon arrays of 'smoothed' relative vibrational transition probabilities $p_{v'v''}$ for the band systems and (iii) upon the relative populations $N_{v'}$ in the upper vibrational levels v' involved.

The bases of the method have been fully discussed in the above papers and also reviewed by Nicholls (1958). It will therefore be sufficient to recall that the measured intensity $I_{v'v''}$ of the v', v'' band of a system may be written as

$$I_{v'v''}=DN_{v'}E^4{}_{v'v''}p_{v'v''} \qquad \ldots\ldots(1)$$

where

$$p_{v'v''}=R_e{}^2(\bar{r}_{v'v''})q_{v'v''} \qquad \ldots\ldots(2)$$

and thus

$$I_{v'v''}=DN_{v'}E^4{}_{v'v''}R_e{}^2(\bar{r}_{v'v''})q_{v'v''}. \qquad \ldots\ldots(3)$$

---

† Now at the Engineering Center, University of Southern California, Los Angeles 7.

‡ Temporarily on leave of absence at the National Bureau of Standards, Washington, D.C.

Here D is a constant involving units of intensity and the geometry of the optical system, $N_{v'}$ is the population of molecules in the level v' of the upper electronic state of the system, $E_{v'v''}=hc/\lambda_{v'v''}$ is the energy quantum of the v',v'' band of wavelength $\lambda_{v'v''}$, $R_e(r)$ is the electronic transition moment of the electronic transition, $\bar{r}_{v'v''}$ is the r-centroid of the v', v'' band, discussed by Nicholls and Jarmain (1956, 1959), and $q_{v'v''}$ is the Franck–Condon factor (Bates 1952) of the v',v'' band. $p_{v'v''}$ is the relative vibrational transition probability of the v',v'' band. Arrays of Franck–Condon factors calculated by the method of Fraser and Jarmain (Fraser and Jarmain 1953, Jarmain and Fraser 1953, Fraser 1954 b) are available for a number of important band systems. (Jarmain, Fraser and Nicholls 1953, Fraser, Jarmain and Nicholls 1954, Jarmain, Fraser and Nicholls 1955, Nicholls, Fraser and Jarmain 1959, Nicholls, Fraser, Jarmain and McEachran 1960.)

It is readily seen from equation (3) that a plot of $(I_{v'v''}/q_{v'v''}E^4_{v'v''})^{1/2}$ against $\bar{r}_{v'v''}$ is a representation of the variation of $N_{v'}^{1/2}R_e(r)$ with r. For a complete band system such a plot is made up of a number of segments, one for each v'' (v' is constant) progression. The relative separation in ordinate between segments is a measure of the variation of $N_{v'}^{1/2}$ with v'.

The segments may all be objectively placed upon the same ordinate scale by use of multiplicative scaling constants derived from the ratio of the areas under the segments over the regions in which they overlap in r. A smooth curve fitted to the resulting points for the whole system indicates the variation of the electronic transition moment $R_e(r)$ with internuclear separation. Once this is known it is at once possible to compute an array of 'smoothed' values of the relative vibrational transition probabilities $p_{v'v''}$ from equation (2). Such a smoothed array in which intensity measurements for all bands of the system have played a part is clearly superior to one derived, band by band, from equation (1) in which the variable error in measuring intensities of individual bands is proportionally reflected in the respective $p_{v'v''}$ values.

The above procedure has been applied to the CO^+ comet tail and the BO α and β systems. It is the purpose of this paper to discuss the results and their interpretation.

§ 2. EXPERIMENTAL

The CO^+ comet tail system was excited by a 60–100 ev, 400 μA electron beam passing through CO at a pressure of about 5 microns Hg. The electron gun and equipotential box arrangement were a modification of that used by Thomson and Williams (1934). Nickel–chrome accelerating electrodes were used and mounted, together with the tungsten filament assembly, on a double pinch for ease of filament replacement.

The BO α and β systems were excited in the afterglow reaction between active nitrogen and BCl_3 and a trace of oxygen (Mulliken 1925). The active nitrogen was produced in a manner similar to that used by Benson (1951) in an apparatus described by Dixon and Nicholls (1958). Prepurified nitrogen at a pressure of a few mm Hg was flowed in a tube through three condensed sparks spaced a few inches apart. The flow tube was attached perpendicularly to the afterglow tube and window. The sparks were produced by 15 kv transformers, and secondary spark gaps were used in the circuit. The BCl_3 vapour was admitted from a constant temperature reservoir through a side tube and the resulting luminosity of the reaction between active nitrogen and BCl_3 was viewed end-on through the window of the afterglow tube. Spectroscopic surveys of the luminosities in both cases were made with a Hilger f/4 glass and quartz spectrograph, and adjustments were made in source conditions until the band system in question was excited most intensely. Intensities were measured photoelectrically using a Leeds and Northrup Ebert type photoelectric recording spectrometer (Fastie 1952).

The response of the spectrometer was determined using a calibrated Philips standard tungsten lamp and the data of de Vos (1954) and Lowan and Blanch (1940). Band intensities were measured by integration of rectified intensity profiles. In cases of severe overlap between adjacent bands, the methods of fractional band intensities developed by Robinson and Nicholls (1958 b) were used.

§ 3. RESULTS

3.1. CO^+ *Comet Tail System* ($A^2\Pi – X^2\Sigma$)

Photoelectrically measured integrated intensities $I_{v'v''}$ of fourteen bands ($v'=0-5$, $v''=0-3$) are presented in table 1 together with r-centroids $\bar{r}_{v'v''}$

Table 1. Measured Relative Intensities, r-centroids and Wavelengths for the CO^+ Comet Tail System

v''	0	1	2	3
v'				
0	1·4	2·2	—	
	$1{\cdot}17_7$	$1{\cdot}20_2$	$1{\cdot}22_8$	
	4911	5500	—	
1	5·0	5·8	—	
	$1{\cdot}16_0$	$1{\cdot}18_4$	$1{\cdot}20_9$	
	4566	5072	—	
2	10·0	4·7	—	—
	$1{\cdot}14_4$	$1{\cdot}16_7$	$1{\cdot}19_1$	1.21_7
	4272	4711	—	—
3	8·0	1·3	2·2	1·0†
	$1{\cdot}12_9$	$1{\cdot}15_2$	$1{\cdot}17_4$	$1{\cdot}19_8$
	4018	4403	4866	5420
4	5·4	—	2·2	
	$1{\cdot}11_5$	$1{\cdot}13_7$	$1{\cdot}15_9$	
	3796	—	4518	
5	2·8	1·1	—	
	$1{\cdot}01_1$	$1{\cdot}12_2$	$1{\cdot}14_4$	
	3601	3908	—	
6	1·4	1·5	0·5†	
7	0·5	0·8	—	

Order of entry:
$I_{v'v''}$ (arbitrary units)‡
$\bar{r}_{v'v''}$ (Å)
$\lambda_{v'v''}$ (Å)

† Measurements probably significant only to order of magnitude.
‡ $I_{v'v''}$ is normalized to 10·0 for strongest band (2,0). $I_{v'v''}$ only is given for progressions $v''=6$ and 7.

(McEachran, private communication) and wavelength, $\lambda_{v'v''}$ of band heads, used in subsequent calculations. A rescaled plot of $(I_{v'v''}\lambda^4{}_{v'v''}/q_{v'v''})^{1/2}$ against $\bar{r}_{v'v''}$ was made for the bands in the manner discussed in § 1, and it was found that the function

$$R_e(r) = \text{const.} \times (-1 + 1{\cdot}73r - 0{\cdot}74r^2)$$
$$1{\cdot}10\,\text{Å} \leqslant r \leqslant 1{\cdot}21\,\text{Å} \qquad \ldots\ldots(4)$$

could be fitted by a least squares procedure to the points. The Franck–Condon factors $q_{v'v''}$, were calculated with perturbation correction for this system by McEachran (Nicholls, Fraser, Jarmain and McEachran 1960) and are given in table 2 together with appropriate values of smoothed relative vibrational transition probabilities $p_{v'v''}$ calculated from equations (2) and (4). An array of 'intensities at infinite temperature' $I_{\infty v'v''} \propto p_{v'v''}/\lambda^4{}_{v'v''}$ are also given in table 2. As the ratio between $I_{v'v''}$ and $I_{\infty v'v''}$ is proportional to $N_{v'}$, the ratio is useful in the determination of relative vibrational populations in the light source.

Table 2. Smoothed Relative Vibrational Transition Probabilities, Franck–Condon Factors and Intensities at Infinite Temperature for the CO⁺ Comet Tail System

v'' v'	0	1	2	3
0	$0{\cdot}07_1$ $0{\cdot}04_3$ 1·6	$0{\cdot}21_9$ $0{\cdot}15_2$ 3·1	$0{\cdot}25_0$ $0{\cdot}25_0$ 2·2	
1	$0{\cdot}18_8$ $0{\cdot}11_5$ 5·6	$0{\cdot}31_2$ $0{\cdot}19_4$ 6·2	$0{\cdot}10_8$ $0{\cdot}08_1$ 1·3	
2	$0{\cdot}25_5$ $0{\cdot}16_9$ 10·0	$0{\cdot}16_2$ $0{\cdot}09_8$ 4·3	$0{\cdot}00_5$ $0{\cdot}00_3$ —	$0{\cdot}13_1$ $0{\cdot}10_9$ 1·2
3	$0{\cdot}23_8$ $0{\cdot}18_2$ 11·9	$0{\cdot}02_1$ $0{\cdot}01_3$ 0·7	$0{\cdot}12_4$ $0{\cdot}07_5$ 2·9	$0{\cdot}10_3$ $0{\cdot}06_9$ 1·6
4	$0{\cdot}16_9$ $0{\cdot}16_0$ 10·6	$0{\cdot}00_9$ $0{\cdot}00_6$ 0·4	$0{\cdot}16_8$ $0{\cdot}09_7$ 5·3	
5	$0{\cdot}09_5$ $0{\cdot}12_2$ 7·4	$0{\cdot}05_4$ $0{\cdot}04_5$ 3·0	$0{\cdot}07_3$ $0{\cdot}04_8$ 2·9	

Order of entry:
$p_{v'v''}$†
$q_{v'v''}$†
$I_\infty = p_{v'v''}/\lambda^4{}_{v'v''}$‡

† $p_{v'v''}$ and $q_{v'v''}$ are made equal for the (0,2) band.

‡ I_∞ for the strongest band in $v' = 2$ progression is normalized to 10·0.

3.2. *BO α System* ($A^2\Pi$–$X^2\Sigma$)

The spectra of BO are complicated to some extent by noticeable evidence of the isotope effect. The ^{10}B and ^{11}B isotopes have abundance ratio values which have been quoted by a number of authorities (see Strominger, Hollander and Seaborg 1958) to range closely around $^{10}B:19\%$, $^{11}B:81\%$. The reduced masses of the isotopic molecules ($\mu_A(^{11}BO) = 6{\cdot}52305 : \mu_A(^{10}BO) = 6{\cdot}23077$) differ sufficiently for the wavelength separation of similar spectral features to be significant, and the natural abundance ratio is such that ^{10}BO bands are of sufficient intensity that they may be distinguished from the ^{11}BO bands. The isotope effect does not affect the potentials of the two states concerned but it does affect the vibrational and rotational constants of the levels.

Table 3. Franck–Condon Factors, *r*-centroids and Wavelengths for the BO α System

v'' v'	0	1	2	3	4
0	$0{\cdot}03_7$ $0{\cdot}04_1$ $0{\cdot}03_8$ $1{\cdot}27_5$ 4248	$0{\cdot}13_4$ $0{\cdot}14_3$ $0{\cdot}13_6$ $1{\cdot}30_3$ 4613	$0{\cdot}22_7$ $0{\cdot}23_5$ $0{\cdot}22_9$ $1{\cdot}33_0$ 5040	$0{\cdot}24_4$ $0{\cdot}24_4$ $0{\cdot}24_4$ $1{\cdot}35_8$ 5548	$0{\cdot}18_4$ $0{\cdot}17_9$ $0{\cdot}18_3$ $1{\cdot}38_6$ 6160
1	$0{\cdot}10_7$ $0{\cdot}11_4$ $0{\cdot}10_8$ $1{\cdot}25_7$ 4036	$0{\cdot}18_9$ $0{\cdot}19_1$ $0{\cdot}18_9$ $1{\cdot}28_4$ 4363	$0{\cdot}09_6$ $0{\cdot}08_8$ $0{\cdot}09_5$ $1{\cdot}31_1$ 4744	$0{\cdot}00_1$ 0 $0{\cdot}00_1$ $1{\cdot}33_9$ —	$0{\cdot}05_6$ $0{\cdot}06_7$ $0{\cdot}05_8$ $1{\cdot}36_6$ —
2	$0{\cdot}16_5$ $0{\cdot}17_1$ $0{\cdot}16_6$ $1{\cdot}23_8$ 3847	$0{\cdot}10_8$ $0{\cdot}10_1$ $0{\cdot}10_6$ $1{\cdot}26_7$ 4143	0 $0{\cdot}00_1$ 0 $1{\cdot}29_3$ —	$0{\cdot}08_8$ $0{\cdot}09_7$ $0{\cdot}09_0$ $1{\cdot}32_0$ —	$0{\cdot}10_1$ $0{\cdot}09_5$ $0{\cdot}10_0$ $1{\cdot}34_7$ 5351
3	$0{\cdot}18_3$ $0{\cdot}18_5$ $0{\cdot}18_3$ $1{\cdot}22_2$ 3678	$0{\cdot}01_9$ $0{\cdot}01_4$ $0{\cdot}01_8$ $1{\cdot}24_2$ 3950	$0{\cdot}06_1$ $0{\cdot}06_9$ $0{\cdot}06_3$ $1{\cdot}27_6$ —	$0{\cdot}08_2$ $0{\cdot}07_6$ $0{\cdot}08_1$ $1{\cdot}30_3$ —	0 0 0 $1{\cdot}32_9$ —
4	$0{\cdot}16_4$ $0{\cdot}16_3$ $0{\cdot}16_4$ $1{\cdot}20_6$ 3526	$0{\cdot}00_3$ $0{\cdot}00_6$ $0{\cdot}00_4$ $1{\cdot}23_1$ —	$0{\cdot}09_7$ $0{\cdot}09_7$ $0{\cdot}09_7$ $1{\cdot}25_8$ —	$0{\cdot}00_5$ $0{\cdot}00_2$ $0{\cdot}00_5$ $1{\cdot}28_6$ —	$0{\cdot}06_1$ $0{\cdot}06_8$ $0{\cdot}06_2$ $1{\cdot}31_2$ —

Order of entry:
$q_{v'v''}$ ($^{11}B^{16}O$)†
$q_{v'v''}$ ($^{10}B^{16}O$)†
$q_{v'v''}$ (BO)†
$\bar{r}_{v'v''}$ (Å)
$\lambda_{v'v''}$ (Å)

† $q_{v'v''}$ values are made equal for the (0,3) band.

Franck–Condon factor arrays were calculated accordingly for the ^{10}BO and ^{11}BO systems (Fraser, private communication) using the digital computer FERUT at the University of Toronto. These data are presented in table 3 together with a weighted average $q_{v'v''}$(BO) with respect to the abundance ratios. This array may be useful for other workers using spectra in which the isotopic components are not resolved. r-centroids and wavelengths of band heads of ^{11}BO bands are also given in table 3.

Relative photoelectric intensity measurements made on all the strong ^{11}BO α bands accessible to the Leeds and Northrup instrument are presented in table 4. It was found possible to fit a least squares straight line of the form

$$R_e(r) = \text{const.} \times (-1 + 1{\cdot}66r)$$
$$1{\cdot}25\,\text{Å} \leqslant r \leqslant 1{\cdot}36\,\text{Å} \qquad \ldots\ldots(5)$$

to a rescaled plot of $(I_{v'v''}\lambda^4{}_{v'v''}/q_{v'v''})^{1/2}$ for these bands. Thus an array of smoothed relative vibrational transition probabilities $p_{v'v''}$ computed from equations (2) and (5) is also given in table 4 together with an array of intensities at infinite temperature $p_{v'v''}/\lambda^4{}_{v'v''}$.

Table 4. Measured Relative Intensities, Smoothed Relative Vibrational Transition Probabilities and the Relative Intensities at Infinite Temperatures for the BO α System

v' \ v''	0	1	2	3	4
0	4·6 $0{\cdot}05_0$ 2·3	9·2 $0{\cdot}15_6$ 5·1	8·5 $0{\cdot}22_7$ 5·2	6·0 $0{\cdot}20_4$ 3·2	— $0{\cdot}12_8$ 1·3
1	9·5 $0{\cdot}15_9$ 8·9	10·0 $0{\cdot}24_4$ 10·0	3·8 $0{\cdot}10_7$ 3·1	— $0{\cdot}00_1$ —	— $0{\cdot}04_5$ 0·6
2	8·9 $0{\cdot}26_8$ 18·2	4.4 $0{\cdot}15_2$ 7·7	— 0 —	— $0{\cdot}09_3$ 2·4	1·9 $0{\cdot}09_1$ 1·6
3	7·6 0·32 25·9	— $0{\cdot}03_0$ 1·8	— $0{\cdot}08_2$ 3·7	— $0{\cdot}09_6$ 3·1	— 0 —
4	6·8 $0{\cdot}30_8$ 29·5	— $0{\cdot}00_5$ —	— $0{\cdot}14_3$ 7·9	— $0{\cdot}00_6$ —	— $0{\cdot}06_8$ —

Order of entry:
$I_{v'v''}$ (^{11}BO)†
$p_{v'v''}$ (^{11}BO)
$I_\infty = p_{v'v''}/\lambda^4{}_{v'v''}$†

† $I_{v'v''}$ and I_∞ normalized to 10·0 for the (1,1) band.

3.3. *The BO β System* ($B^2\Sigma$–$X^2\Sigma$)

In spite of the isotope effect being clearly observed in this system, the overlap between the bands from the ^{10}BO and ^{11}BO molecules was sufficiently great that it was impossible to separate them. As a result measured band intensities contained contributions from both isotopic components and had to be interpreted as such. The intensity equation in this case is then

$$I^{\mathrm{tot}}_{v'v''} = DN_{v'}{}^{\mathrm{tot}}\bar{E}^4{}_{v'v''}R_e{}^2(\bar{r}_{v'v''})\bar{q}_{v'v''} \qquad \ldots\ldots(6)$$

where $I^{\mathrm{tot}}{}_{v'v''}$ and $N^{\mathrm{tot}}{}_{v'}$ are the respective sums of the contributions from ^{10}BO and ^{11}BO. $\bar{E}^4{}_{v'v''}$ is an average with respect to the two band heads, which are sufficiently close together that the fourth power of the reciprocal of the wavelength of either may be used without significant loss of accuracy. From the well-known monotonic relationship between $\bar{r}_{v'v''}$ and $\lambda_{v'v''}$ (Nicholls and Jarmain 1956) the difference between *r*-centroids for each ^{10}BO and ^{11}BO $v'v''$ band was, as expected so small as to allow the *r*-centroid of the ^{11}BO band to be used for both. $\bar{q}_{v'v''}$ is the weighted average of the Franck–Condon factor with respect to the respective abundances. Relative intensities of all the bands of the β system accessible to the Leeds and Northrup instrument were measured photoelectrically and the measurements are shown in table 5, together with the appropriate wavelengths and *r*-centroids. A rescaled plot of $(I_{v'v''}\lambda^4{}_{v'v''}/q_{v'v''})^{1/2}$ against $\bar{r}_{v'v''}$ leads to a least squares representation of the electronic transition moment as

$$R_e(r) = \text{const.} \times (-1 + 1{\cdot}434r)$$
$$1{\cdot}30\text{Å} \leqslant r \leqslant 1{\cdot}50\text{Å}. \qquad \ldots\ldots(7)$$

Table 5. Measured Relative Intensities, *r*-centroids and Wavelengths for the BO β System

v' \ v''	2	3	4	5	6	7	8	9	10
0	10·0 $1{\cdot}32_8$ 2551	3·5 $1{\cdot}36_4$ 2675	1·9 $1{\cdot}39_9$ 2810	— $1{\cdot}43_4$ 2957	— $1{\cdot}47_1$ —				
1	— $1{\cdot}30_4$ —	6·6 $1{\cdot}33_9$ 2588	8·6 $1{\cdot}37_5$ 2714	4·0 $1{\cdot}40_8$ 2851	2·1 $1{\cdot}44_2$ 3000	— $1{\cdot}48_0$ —			
2	— — —	2·6 1.31_6 2508	1·5 $1{\cdot}35_0$ 2626	9·1 $1{\cdot}38_4$ 2753	8·3 $1{\cdot}41_8$ 2892	4·9 $1{\cdot}45_4$ 3044	2·6 $1{\cdot}49_0$ 3209		
3			5·5 $1{\cdot}32_6$ 2544	— $1{\cdot}36_0$ 2664	1·6 $1{\cdot}39_5$ 2794	4·9 $1{\cdot}42_9$ 2935	4·1 $1{\cdot}46_5$ 3089		
4				2·2 $1{\cdot}33_6$ 2582	1·4 $1{\cdot}37_0$ 2703	— $1{\cdot}40_6$ —	1·2 $1{\cdot}44_0$ 2979	2·2 — 3135	1·9 — 3305

Order of entry:
$I_{v'v''}$ (arbitrary units)†
$\bar{r}_{v'v''}$ (Å)
$\lambda_{v'v''}$ (Å)

†$I_{v'v''}$ normalized to 10·0 for the strongest band (0,2).

Table 6. Smoothed Relative Vibrational Transition Probabilities, Franck–Condon Factors and Intensities at Infinite Temperature of the BO β System

v' \ v''	2	3	4	5	6	7	8
0	$0{\cdot}26_0$ $0{\cdot}26_0$ $10{\cdot}0$	$0{\cdot}15_4$ $0{\cdot}13_8$ $4{\cdot}9$	$0{\cdot}06_7$ $0{\cdot}05_4$ $1{\cdot}8$	$0{\cdot}02_2$ $0{\cdot}01_6$ —	$0{\cdot}00_6$ $0{\cdot}00_6$ —		
1	$0{\cdot}02_3$ $0{\cdot}02_4$ $1{\cdot}0$	$0{\cdot}17_7$ $0{\cdot}17_1$ $6{\cdot}4$	$0{\cdot}24_0$ $0{\cdot}20_8$ $7{\cdot}2$	$0{\cdot}16_9$ $0{\cdot}13_3$ $4{\cdot}2$	$0{\cdot}07_9$ $0{\cdot}05_7$ $1{\cdot}6$	$0{\cdot}02_8$ $0{\cdot}01_8$ —	
2		$0{\cdot}03_4$ $0{\cdot}03_5$ $1{\cdot}4$	$0{\cdot}03_0$ $0{\cdot}02_8$ $1{\cdot}0$	$0{\cdot}18_1$ $0{\cdot}15_3$ $5{\cdot}3$	$0{\cdot}23_2$ $0{\cdot}17_8$ $5{\cdot}4$	$0{\cdot}16_1$ $0{\cdot}11_2$ $3{\cdot}1$	$0{\cdot}07_4$ $0{\cdot}04_7$ $1{\cdot}1$
3			0.11_4 $0{\cdot}11_5$ $4{\cdot}4$	$0{\cdot}00_8$ $0{\cdot}00_7$ —	$0{\cdot}06_6$ $0{\cdot}05_4$ $1{\cdot}6$	$0{\cdot}21_4$ $0{\cdot}15_9$ $4{\cdot}7$	$0{\cdot}22_8$ $0{\cdot}15_4$ $4{\cdot}1$
4				$0{\cdot}10_1$ $0{\cdot}09_8$ $3{\cdot}7$	$0{\cdot}07_4$ $0{\cdot}06_5$ $2{\cdot}3$	$0{\cdot}00_2$ $0{\cdot}00_2$ —	$0{\cdot}22_9$ $0{\cdot}09_3$ $2{\cdot}7$

Order of entry:
$p_{v'v''}$†
$q_{v'v''}$†
$I_\infty = p_{v'v''}/\lambda^4_{v'v''}$‡

† $p_{v'v''}$ and $q_{v'v''}$ are made equal for the (0,2) band.
‡ I_∞ is normalized to 10.0 for (0,2) band.

An array of smoothed relative vibrational transition probabilities $p_{v'v''}$ calculated from equations (2) and (7) is presented in table 6 together with an array of Franck–Condon factors (Nicholls, Fraser and Jarmain 1959) weighted with respect to the abundance ratio. Table 6 also includes an array of intensities at infinite temperature.

§ 4. Discussion

Elliott (1931, 1933) made photographic intensity measurements upon some bands of the BO α and β systems. He compared his measurements on some bands with Franck–Condon factors calculated from Hutchisson's formulae (Hutchisson 1930, 1931) for parabolic and Morse potentials. He also reports unsmoothed relative vibrational transition probabilities ($I_{v'v''}\lambda^4_{v'v''}/q_{v'v''}$) and points out that the intensities do not follow $q_{v'v''}$ exactly over a v'' progression. This is probably due to variation of $R_e(r)$ with r. Where his measurements and ours overlap, agreement is good but it is felt that the smoothed relative vibrational transition probabilities are more meaningful than the unsmoothed values.

The intensity measurements on the CO$^+$ comet tail system may have application to the interpretation of emission spectra of comet tails in which the (1,0), (2,0), (3,0), (4,0), (5,0) ,(6,0), (1,1), (4,1), (6,1) bands frequently appear (Swings and Haser 1956).

ACKNOWLEDGMENTS

We wish to acknowledge many helpful discussions with Dr. P. A. Fraser and also the experimental and computational assistance of Mr. R. P. McEachran.

This work was supported in part by contracts with the Air Force Cambridge Research Center, The Department of Defence Production of Canada and by research grants with the National Research Council of Canada and the Defence Research Board of Canada.

REFERENCES

BATES, D. R., 1952, *Mon. Not. R. Astr. Soc.*, **112**, 614.
BENSON, J. M., 1951, *Nat. Adv. Comm. Aero., T.N.* 2293.
DE VOS, J. C., 1954, *Physica*, **20**, 690.
DIXON, R. N., and NICHOLLS, R. W., 1958, *Canad. J. Phys.*, **36**, 127.
ELLIOTT, A., 1931, *Z. Phys.*, **67**, 75.
—— 1933, *Proc. Phys. Soc.*, **45**, 627.
FASTIE, W. G., 1952, *J. Opt. Soc. Amer.*, **42**, 9.
FRASER, P. A., 1954 a, *Canad. J. Phys.*, **32**, 515.
—— 1954 b, *Proc. Phys. Soc.* A, **67**, 939.
FRASER, P. A., and JARMAIN, W. R., 1953, *Proc. Phys. Soc.* A, **66**, 1145.
FRASER, P. A., JARMAIN, W. R., and NICHOLLS, R. W., 1954, *Astrophys. J.*, **119**, 286.
HUTCHISSON, E., 1930, *Phys. Rev.*, **36**, 410.
—— 1931, *Ibid.*, **37**, 45.
JARMAIN, W. R., and FRASER, P. A., 1953, *Proc. Phys. Soc.* A, **66**, 1153.
JARMAIN, W. R., FRASER, P. A., and NICHOLLS, R. W., 1953, *Astrophys. J.*, **118**, 228.
—— 1955, *Ibid.*, **122**, 55.
LOWAN, A. N., and BLANCH, G., 1940, *J. Opt. Soc. Amer.*, **30**, 70.
MULLIKEN, R. S., 1925, *Phys. Rev.*, **25**, 259.
NICHOLLS, R. W., 1958, *Ann. Geophys.*, **14**, 208.
NICHOLLS, R. W., FRASER, P. A., and JARMAIN, W. R., 1959, *Combustion and Flame*, **3**, 13.
NICHOLLS, R. W., FRASER, P. A., JARMAIN, W. R., and MCEACHRAN, R. P., 1960, *Astrophys. J.*, in the press.
NICHOLLS, R. W., and JARMAIN, W. R., 1956, *Proc. Phys. Soc.* A, **69**, 253.
—— 1959, *Ibid.*, **74**, 133.
ROBINSON, D., and NICHOLLS, R. W., 1958 a, *Proc. Phys. Soc.*, **71**, 957.
—— 1958 b, Scientific Report No. 5, Contract AF19 (604)–1718 University of Western Ontario.
STROMINGER, D., HOLLANDER, J. M., and SEABORG, G. T., 1958, *Rev. Mod. Phys.*, **30**, 585.
SWINGS, P., and HASER, L., 1956, *Atlas of Representative Cometary Spectra* (Liege: Astrophysical Institute).
THOMPSON, N., and WILLIAMS, S. E., 1934, *Proc. Roy. Soc.* A, **147**, 583.
TURNER, R. G., and NICHOLLS, R. W., 1954 a, *Canad. J. Phys.*, **32**, 468.
—— 1954 b, *Ibid.*, **32**, 475.
WALLACE, L. V., and NICHOLLS, R. W., 1955, *J. Atmos. Terr. Phys.*, **7**, 101.

A Note on the Born–Green Linearized Integral Equation

By S. KATSURA† and K. HARUMI‡

† Department of Applied Science,
‡ Department of Physics,
Tôhoku University, Sendai, Japan

MS. received 17*th September* 1959, *in final form* 11*th December* 1959

Abstract. This paper is concerned with the validity of Green's linearized integral equation, or the ring approximation of the virial expansion, in the theory of liquids. It is shown that this approximation is applicable only at high temperatures and low densities, and, by comparing the solution of Green's linearized equation with the exact solution by Gürsey for the one-dimensional square-well potential; that the singularities in Green's equation are attributed to the linear approximation and have nothing to do with the phase transition. The situations are the same in the approximation of Kirkwood (linearized form), of Abe, of Morita, and of Meeron.

---

§ 1. INTRODUCTION

BORN and GREEN (1946), Green (1947) and Rodriguez (1949) regarded the singularity of their linearized integral equation, i.e. the value of the density determined by the zero of the denominator in the integral representation for the molecular distribution function, as the point corresponding to the phase transition. In this paper the authors compare the isotherm given by Green's integral equation with the exact one given by Gürsey (1950) for the one-dimensional square-well potential. It is shown that this approximation is valid only at high temperatures and low densities, and that the singularities of the former are caused by the linear approximation, and they have nothing to do with the phase transition. We also discuss the approximations of Kirkwood, of Abe (1958), of Morita (1958), and of Meeron (1958).

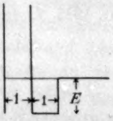

Figure 1. Square-well potential.

§ 2. COMPARISON OF GREEN'S APPROXIMATION WITH THE EXACT ISOTHERM

We consider the molecules in a one-dimensional system which attract with square-well potential as shown in figure 1. For simplicity, we take the diameter of the hard core, the width and the depth of the well as 1, 1 and $E(<0)$.

Takahasi (1942) obtained the equation of state of the one-dimensional substance and showed that it had no phase transition irrespective of its intermolecular force. The equation of state for the one-dimensional square-well potential is given explicitly by Gürsey (1950) in the following form (the special case of the result of Takahasi)

$$\frac{kT}{p}=\frac{1}{\rho}-1+\frac{f}{(1+f)\exp(p/kT)-f}, \qquad \ldots\ldots(1)$$

where p and ρ are the pressure and the density respectively, and

$$f=\exp(-E/kT)-1. \qquad \ldots\ldots(2)$$

Now we consider the Born–Green integral equation. The Born–Green integral equation is derived in the Appendix in a vector form valid for both the one-dimensional case and the three-dimensional case. The equation of state obtained therefrom in the one-dimensional case is

$$\begin{aligned}\frac{p}{\rho kT}&=1-\tfrac{1}{2}\rho\left[(2\pi)^{1/2}\beta(0)-\frac{1}{2}\int_{-\infty}^{\infty}\beta(t)^2dt\right]\\&\quad-\frac{1}{4\pi\rho}\int_{-\infty}^{\infty}\log|1-(2\pi)^{1/2}\rho\beta(t)|dt\\&\quad+\frac{(2\pi)^{1/2}}{4\pi\rho}\int_{-\infty}^{\infty}\frac{\rho\beta(t)dt}{1-(2\pi)^{1/2}\rho\beta(t)} \qquad \ldots\ldots(3)\\&=1-\tfrac{1}{2}(2\pi)^{1/2}\beta(0)\rho\\&\quad-\sum_{\nu=2}^{\infty}\frac{\nu}{\nu+1}\frac{1}{2(2\pi)^{1/2}}[(2\pi)^{1/2}\rho]^{\nu}\int_{-\infty}^{\infty}\beta(t)^{\nu+1}dt, \qquad \ldots\ldots(4)\end{aligned}$$

where

$$\left.\begin{aligned}\beta(t)&=(1+f)\beta_0(t)-2f\beta_0(2t),\\\beta_0(t)&=\left(\frac{2}{\pi}\right)^{1/2}\frac{\sin t}{t}=-\frac{\mathrm{J}_{1/2}(t)}{t^{1/2}}.\end{aligned}\right\} \qquad \ldots\ldots(5)$$

(4) is the expansion of (3) in ρ and is equivalent to the virial expansion in the ring approximation (Montroll and Mayer 1941). The value of $(2\pi)^{1/2}\beta(t)$ is shown in figures 3, 4 and 5 at various temperatures. The series representation (4) has meaning only in its convergence circle. The integral representation (3) is an analytic continuation of (4) up to its first singularity on the positive real axis of ρ. Let the greatest maximum and the least minimum of $(2\pi)^{1/2}\beta(t)$ under constant f (constant temperature), be h_1 and $-h_2$. When ρ is sufficiently small

$$1-(2\pi)^{1/2}\rho\beta(t) \qquad \ldots\ldots(6)$$

has no real zero. When ρ becomes equal to or greater than $1/h_1$, equation (6) has a zero on the real axis of ρ. When $h_1>h_2$ the radius of convergence of (4) is determined by the real positive singularity of (3), $\rho_1=1/h_1$. When $h_1<h_2$ the radius of convergence of (4) is determined by the real negative singularity of (3), $\rho_2=|-1/h_2|$. If it is assumed† that the integral representation (3) is valid beyond the first singularity ρ_1, the isotherm should have an infinite number of singularities at the values of ρ equal to the reciprocal of the second, third, . . . maxima of

† In this case the transformation

$$f(r)=(2\pi)^{-1/2}\int_{-\infty}^{\infty}\frac{(2\pi)^{1/2}\rho\beta(s)^2\cos(rs)ds}{1-(2\pi)^{1/2}\rho\beta(s)} \qquad \ldots\ldots(7)$$

does not belong to L_1 and L_2. Such Fourier transformation is outside its range of validity (Titchmarsh 1948).

$(2\pi)^{1/2}\beta(t)$ (figure 9). In this case the remaining parts of the isotherm are not the analytic continuation of the first branch (4) beyond the singularity. The analytic continuation of the first branch is no longer real beyond the first singularity.

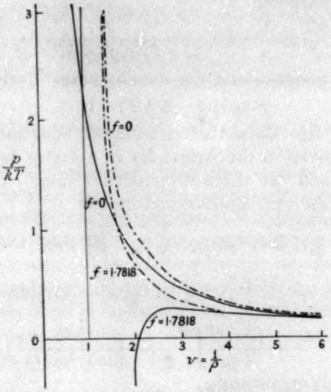

Figure 2. Isotherm of the one-dimensional gas with square-well potential. Full line: solution of Green's linearized integral equation; chain line: exact solution by Gürsey. $\rho=1$ corresponds to the closest packed state.

In figure 2 we show the numerical results of (1) and (3) for $f=0$ ($T=\infty$, or hard core) and $f=1{\cdot}7818$ ($|E|/kT=1$). In this calculation we have used SENAC-1 (Sendai Automatic Computer-1). In the case where $f=0$ (hard core), $h_1\simeq 4/3\pi$, $-h_2\simeq 2$, the radius of convergence is $\rho\simeq 1/2$, the real positive first singularity is $\rho\simeq 3\pi/4$, which is beyond the closest packed state. In the case where $f=1{\cdot}7818$, $-h_2\simeq 3{\cdot}8$, $h_1\simeq 1{\cdot}9$, the radius of convergence is $\rho\simeq 1/3{\cdot}8$, and the real positive singularity is $\rho\simeq 1/1{\cdot}9$. When the temperature is sufficiently low ($f\gtrsim 10$), $h_1\simeq 2(f-1)>h_2$, and the real positive singularity of ρ agrees with the radius of convergence and is given by approximately $1/2(f-1)$. In this case the ring approximation part of the irreducible integrals is always positive.

As stated above, the singularities of Green's equation appear also in the one-dimensional substance, and this fact shows that these singularities are due to the approximations, and are not concerned with the phase transition. This is also evident from the fact that the isotherm expressed in equation (3) has an infinite number of singularities when (3) is considered to be valid in the whole region of positive ρ. Since it is shown that the superposition approximation is valid for one-dimensional nearest-neighbour interacting systems (Salsburg, Zwanzig and Kirkwood 1953), the linear approximation is the cause of the singularities which do not correspond to physical reality.

The integral representation (3) has physical meaning at most up to the first singularity of ρ, and it is only up to a much smaller value of ρ that a good approximation is obtained from (3), that is, the linear approximation is only valid at high temperatures and low densities.

§ 3. Discussion

The above discussion can be applied also to the three-dimensional square-well potential and the three-dimensional Lennard-Jones potential. Figures 6, 7 and 8 show

$$(2\pi)^{3/2}\beta(t)=(2\pi)^{3/2}\{(1+f)\beta_0(t)-8f\beta_0(2t)\}$$
$$(\beta_0(t)=-J_{3/2}(t)t^{-3/2}),$$

which is the Fourier transform of $f(|\mathbf{r}|)=\exp(-\phi(|\mathbf{r}|)/kT)-1$ of the three-dimensional square-well potential.

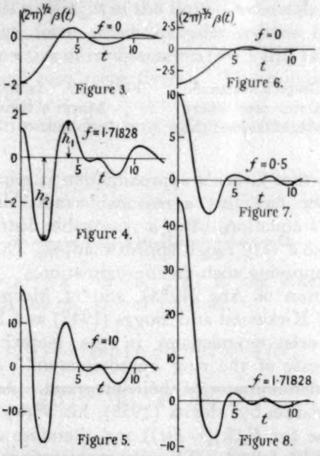

Figures 3, 4, 5. $(2\pi)^{1/2}\beta(t)$ for one-dimensional gas with square-well potential.
Figures 6, 7, 8. $(2\pi)^{3/2}\beta(t)$ for three-dimensional gas with square-well potential.

These features are similar to those in figures 3, 4 and 5. $\beta(t)$ for the Lennard-Jones potential also resembles that of the one-dimensional square-well potential (cf. figure 2 of Rodriguez (1949)). The nature of the exact isotherm of the one-dimensional case is different from that of the three-dimensional, while the solutions of the linearized Green's integral equation show similar behaviour in the two cases.

Born and Green (1946), Green (1947) and Rodriguez (1949) state that the singularity of ρ corresponds to the phase transition, and the Boyle point should be determined by Maxwell's law. When we extend the Rodriguez curve we obtain a curve with many singularities such as figure 9. Therefore we cannot regard the remaining part of the isotherm beyond the first singularity as the liquid phase or the remaining part of the isotherm beyond the second singularity as the solid phase.

From the standpoint of Mayer's condensation theory, Ikeda (1957) concludes that (i) the point of phase transition is not given by the singularity of Green's integral equation, but that (ii) it is given by the maximum point of Green's iostherm. We have confirmed his statement (i) independently of

Mayer's condensation theory. When we would apply Mayer's theory to a system which has irreducible cluster integrals (4), a one-dimensional gas with square-well potential would show the phase transition as shown in figure 10. We will postpone discussion of the problem (ii), i.e. whether the maximum point of Green's isotherm corresponds to the phase transition or not.

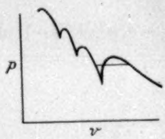

Figure 9. Isotherm by Green's linearized integral equation, in the case where (3) is regarded to be valid beyond the singularity.

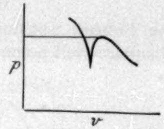

Figure 10. Isotherm in the case where Mayer's theory of condensation is applied.

Scoins (1952) says that Green's approximation is reliable also in the liquid state judging from the fact that a reasonable radial distribution function is obtained from Green's equation. But a reasonable distribution curve may be obtained even if we use a very rough approximation. Our example shows that we must take care in applying such an approximation.

In the approximation of Abe (1958), and of Meeron (1958) and in the linearized equation of Kirkwood and Boggs (1942) and Kirkwood, Maun and Alder (1950), there exist singularities in the isotherm at just the same values of ρ as in the case of the ring approximation. All of them have the same $1-\rho\beta(t)$ in the denominator of their integrand. And also, in the hyper-netted chain approximation by Morita (1958), his $\mathscr{F}(\mathbf{k})$ may be expressed by curves similar to those for $F_0(\mathbf{k})(=\beta(t))$ and therefore an infinite number of singularities may also be found. These approximations are an improvement only in the low density and high temperature region when attractive forces exist. The situations with regard to the point of phase transition are the same as Green's case.

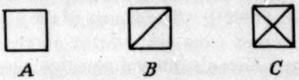

Figure 11. Integrands of the fourth virial coefficients.

Finally, we conclude that the linear approximation in the integral equation is applicable only to the gaseous state at high temperatures and at low densities, and that the singularities appearing in these equations have no relation to the phase transition. Since the linear approximation in the Born–Green integral equations is equivalent to the ring approximation in the virial expansion, this means that the diagrams in which some of the lines cross cannot be neglected even in the transition region, and they contribute dominantly in the low temperature and high density region. One of the authors anticipates these features from the fact that at low temperatures *C* (figure 11) is the dominant one of the components *A*, *B*, *C* of the fourth virial coefficient (Katsura 1959) and that a similar circumstance occurs in the calculation of the cluster sum in the Ising model (Katsura 1958).

ACKNOWLEDGMENTS

The authors express their sincere gratitude to Professor Y. Nomura and Professor J. Oizumi for help in many respects.

APPENDIX

SIMPLIFIED DERIVATION OF THE BORN–GREEN LINEARIZED EQUATION

Here we shall describe the simplified derivation of the Born–Green linearized integral equation. This treatment of the Born–Green equation is much simpler than the original scalar form which includes tedious integration by parts. Further, it is valid irrespective of its dimension ($\nu=3$ and 1 for three-dimensional case and one-dimensional case respectively). The notations are the same as those used by Green (1952).

The molecular distribution function $n_2(\mathbf{r})$ satisfies the integro-differential equation

$$\frac{\partial}{\partial \mathbf{r}}\left\{\log n_2(\mathbf{r})+\frac{\phi(\mathbf{r})}{kT}\right\} + \frac{1}{n^3kT}\int n_2(\mathbf{s})n_2(\mathbf{t})\,\frac{\partial\phi(\mathbf{s})}{\partial \mathbf{s}}\,d\mathbf{s}=0, \qquad \ldots\ldots(\mathrm{A}\,1)$$

where $\mathbf{s}=\mathbf{x}^{(3)}-\mathbf{x}^{(1)}$, $\mathbf{t}=\mathbf{x}^{(2)}-\mathbf{x}^{3)}=\mathbf{r}-\mathbf{s}$, $\phi(\mathbf{r})$ is the intermolecular potential, $\partial/\partial\mathbf{r}$ the gradient and $d\mathbf{s}$ the element of volume.

We substitute

$$n_2(\mathbf{r})=n^2\exp\left(-\phi(\mathbf{r})/kT\right)\{1+f(\mathbf{r})\} \qquad \ldots\ldots(\mathrm{A}\,2)$$

and

$$\alpha(\mathbf{r})=\exp\left(-\phi(\mathbf{r})/kT\right)-1$$

into (A 1), then

$$\frac{\partial}{\partial \mathbf{r}}\log\{1+f(\mathbf{r})\}=n\int\{1+f(\mathbf{t})\}\{1+\alpha(\mathbf{t})\}\{1+f(\mathbf{s})\}\,\frac{\partial\alpha(\mathbf{s})}{\partial \mathbf{s}}\,d\mathbf{s}.$$

Neglecting the second and higher order terms in f and α (this means the substitution of the parameter ϵ equal to unity), we have†

$$\frac{\partial}{\partial \mathbf{r}}\log\{1+f(\mathbf{r})\}=n\int\{f(\mathbf{t})+\alpha(\mathbf{t})\}\,\frac{\partial\alpha(\mathbf{s})}{\partial \mathbf{s}}\,d\mathbf{s}. \qquad \ldots\ldots(\mathrm{A}\,3)$$

Integration by parts gives

$$(\mathrm{A}\,3)=n\int\frac{\partial}{\partial \mathbf{s}}\left[\{f(\mathbf{r}-\mathbf{s})+\alpha(\mathbf{r}-\mathbf{s})\}\alpha(\mathbf{s})\right]d\mathbf{s} \\ -n\int\alpha(\mathbf{s})\,\frac{\partial}{\partial}\{f(\mathbf{r}-\mathbf{s})+\alpha(\mathbf{r}-\mathbf{s})\}\,d\mathbf{s}.$$

The first term on the right-hand side is transformed to the surface integral

$$n\int\{f(\mathbf{r}-\mathbf{s})+\alpha(\mathbf{r}-\mathbf{s})\}\alpha(\mathbf{s})\,\mathbf{ds}. \qquad \ldots\ldots(\mathrm{A}\,4)$$

Here the integration is carried out over the surface of a sufficiently large sphere in $\mathbf{s}$ space ($\mathbf{ds}$ is the vector surface element). (A 4) vanishes since $\alpha(\mathbf{s})=0$ on this boundary.

---

† Linearization means both the neglect of the higher power of f and α of the same argument and the replacement of $\log(1+f)$ by f.

Since $\partial/\partial\mathbf{r} = -\partial/\partial\mathbf{s}$ for the function of $\mathbf{r}-\mathbf{s}$, we have

$$\log\{1+f(\mathbf{r})\} = n\int\{f(\mathbf{r}-\mathbf{s})+\alpha(\mathbf{r}-\mathbf{s})\}\alpha(\mathbf{s})d\mathbf{s}. \qquad \text{......(A 5)}$$

The integration constant is determined by $f(\infty)=0$.

Replacing $\log(1+x)$ by x, we have the linearized integral Born–Green equation written in vector form:

$$f(\mathbf{r}) = n\int\{f(\mathbf{r}-\mathbf{s})+\alpha(\mathbf{r}-\mathbf{s})\}\alpha(\mathbf{s})d\mathbf{s}. \qquad \text{......(A 6)}$$

(A 6) is equivalent to (5.5) of Green (1947) ((6.2) of Green (1952)).

Writing

$$g(\mathbf{u}) = (2\pi)^{-\nu/2}\int f(\mathbf{u})\,e^{i\mathbf{u}\cdot\mathbf{r}}\,d\mathbf{r},$$

and

$$\beta(\mathbf{u}) = (2\pi)^{-\nu/2}\int\alpha(\mathbf{r})\,e^{i\mathbf{u}\cdot\mathbf{r}}d\mathbf{r}, \qquad \text{......(A 7)}$$

we have from (A 6)

$$g(\mathbf{u}) = (2\pi)^{\nu/2}n\{g(\mathbf{u})+\beta(\mathbf{u})\}\beta(\mathbf{u}),$$

so that the solution is

$$f(\mathbf{r}) = \int\frac{n\beta(\mathbf{u})^2\,e^{-i\mathbf{u}\cdot\mathbf{r}}}{1-n(2\pi)^{\nu/2}\beta(\mathbf{u})}d\mathbf{u}. \qquad \text{......(A 8)}$$

From (A 8) the equation of state can be obtained.

REFERENCES

ABE, R., 1958, *J. Phys. Soc., Japan*, **14**, 10.

BORN, M., and GREEN, H. S., 1946, *Proc. Roy. Soc.* A, **188**, 10.

GREEN, H. S., 1947, *Proc. Roy. Soc.* A, **190**, 455.

—— 1952, *The Molecular Theory of Fluids* (Amsterdam: North-Holland).

GÜRSEY, F., 1950, *Proc. Camb. Phil. Soc.*, **46**, 182.

IKEDA, K., 1957, Busseironkenkyu, No. 105.

KATSURA, S., 1958, *Progr. Theor. Phys.*, **20**, 192.

—— 1959, *Phys. Rev.*, **115**, 1419.

KIRKWOOD, J. G., and BOGGS, E. M., 1942, *J. Chem. Phys.*, **10**, 394.

KIRKWOOD, J. G., MAUN, E. K., and ALDER, B. J., 1950, *J. Chem. Phys.*, **18**, 1040.

MEERON, E., 1958, *Phys. Fluids*, **1**, 139.

MONTROLL, E. W., and MAYER, J. E., 1941, *J. Chem. Phys.*, **9**, 626.

MORITA, T., 1958, *Progr. Theor. Phys.*, **20**, 920.

RODRIGUEZ, A. E., 1949, *Proc. Roy. Soc.* A, **196**, 73.

SALSBURG, Z. W., ZWANZIG, R. W., and KIRKWOOD, J. G., 1953, *J. Chem. Phys.*, **21**, 1098.

SCOINS, H. I., 1952, *Phil. Mag.*, **43**, 806.

TAKAHASI, H., 1942, *Proc. Math. Phys. Soc., Japan*, **24**, 60.

TITCHMARSH, E. C., 1948, *Introduction to the Theory of Fourier Integrals* (Oxford: University Press).

A Study of Protons Emitted from Medium Weight Nuclei Bombarded with Neutrons of 14 Mev

By W. JACK and A. WARD†

Department of Natural Philosophy, University of Glasgow

MS. received 23*rd September* 1959, *in revised form* 21*st December* 1959

Abstract. The energy spectra of protons emitted into a small solid angle in the forward direction from separated isotopes ^{19}F, ^{27}Al, ^{54}Fe, ^{56}Fe, ^{59}Co, ^{58}Ni, ^{60}Ni, ^{63}Cu, ^{65}Cu and ^{64}Zn bombarded with 14·1 Mev neutrons are measured with a scintillation counter telescope. The spectra obtained are compared with those measured by Storey *et al.* in 1960, who, using 14·1 Mev neutrons, observed the spectra of protons emitted at 90° into a large solid angle. Peaks due to direct interactions are prominent at the higher proton energies, but little evidence is found for systematic structure similar to that observed in the inelastic scattering of protons of energy 11 to 23 Mev. It is suggested that lower energy peaks found in the present spectra, and in those of other workers, corresponding to excitations of the residual nucleus of 7 Mev are not due to protons, but are in fact deuterons mostly from the ground state n, d pick-up reaction. The 'nuclear temperatures' found from the lower energy protons of the present experiment are in good agreement with those measured by Storey *et al.*

§ 1. Introduction

The energy spectra of the protons emitted from medium weight nuclei bombarded with 14 Mev neutrons have been studied by several groups (Brown *et al.* 1957, Allan 1957, 1958, 1959, March and Morton 1958 a, b, c, Colli *et al.* 1956, 1957 a, b, c, 1958 a, b, Verbinski *et al.* 1957, Eubank *et al.* 1959 and Storey *et al.* 1960) to test the validity of the statistical theory of nuclear reactions (Weisskopf 1937) and to estimate the contribution from non-compound nucleus effects. The spectra obtained are mainly Maxwellian in form with an excess of higher energy protons; the low energy protons have an approximately isotropic angular distribution while the higher energy protons have angular distributions peaked in the forward hemisphere, the anisotropy increasing with proton energy. It is usual to attribute the low energy part of the spectrum to reactions proceeding via a compound nucleus mechanism since the similarity to an evaporation process spectrum is evident (first noted by Frenkel 1936). The anisotropic angular distribution of the higher energy protons suggests their origin in a direct interaction. This might occur either in the surface of the nucleus as postulated by Austern *et al.* (1953) and Elton and Gomes (1957), or throughout the nuclear volume as visualized by Hayakawa *et al.* (1955) and Brown and Muirhead (1957), but in the latter cases a modification to take account of the reflection of outgoing protons at the nuclear surface is necessary (Elton and Gomes 1957).

In the present experiment, the energy spectra of protons emitted into a small solid angle in the forward direction are obtained. These spectra should contain a large contribution from direct effects at the higher proton energies, and may be examined for systematic structure of the type observed by Cohen (1957) in the inelastic scattering of 23 MeV protons. There is also the possibility that the structure attributed to 'giant resonance' effects by Blok and Jonker (1957) and Colli *et al.* (1957 c) may be found. These authors have compared n, p spectra with d, p spectra leading to the same residual nucleus, finding a preferential emission of protons corresponding to several groups of levels in the residual nucleus, i.e. unlike the statistical theory where equal weight is attached to each level, the levels in the aforesaid groups are excited preferentially. These broad energy groups, correlated with neutron single particle states, would be anticipated on the intermediate coupling model.

---

† Now at Department of Natural Philosophy, University of Aberdeen

The region of the present spectra corresponding to higher excitations of the residual nuclei may also be compared with the results of Storey *et al.*, who measured the energy spectra of protons emitted into a large solid angle at 90°. Since markedly anisotropic direct interactions, and reactions of the type n, np do not contribute to this part of the energy spectrum, a comparison with the predictions of the statistical theory can be made.

Important contributions in this field have been made using the nuclear emulsion technique which gives the angular distribution of the protons simultaneously with their energy spectrum, but the difficulty of obtaining sufficiently good statistics limits the applicability of this technique to a series of elements. Colli *et al.* (1956) and Eubank *et al.* (1959) have applied a scintillation counter telescope to the problem and have overcome the difficulty of poor statistics, but in doing so they require rather large areas of target material which limits the use of separated isotope targets. The present technique replaces the proportional counters in the telescopes mentioned by a thin CsI(Tl) crystal. The reduction in random counting rate obtained permits the use of higher neutron fluxes in the experiment, and consequently smaller quantities of target material can be employed. There is an improvement, too, in the energy resolution, energy calibration, and neutron flux monitoring of the present experiment.

§ 2. Experimental Method

The apparatus used is shown in figure 1. The counter telescope consists of two CsI(Tl) crystals mounted in reflecting cavities; protons from the separated isotope target pass through the first crystal producing a pulse proportional to their energy loss, and are stopped in the second crystal giving a pulse proportional to their remaining energy. These pulses are clipped to 2 μsec length and are fed via discriminators to a coincidence unit of resolving time $2\tau = 4\,\mu$sec. The output of the coincidence unit is used to gate pulses from either crystal before they are recorded on a 100 channel pulse height analyser (Hutchinson and Scarrott 1951). Since the decay time of CsI is of the order of 0·5 μsec, the resolving time of the coincidence unit is rather longer than is strictly necessary; however, this leads to very stable and efficient operation. The pulse height response curve of CsI(Tl) for protons of energy up to 15 MeV was obtained in a separate experiment; it is extremely linear.

The unusual method of mounting the crystals was necessary to reduce the background due to n, p events in materials surrounding the crystals. The crystals are each supported by two 0·005 in. platinum wires in cylindrical cavities lined with 0·020 in. lead. A thin layer of aluminium evaporated on to the lead acts as a light reflector. The thick crystal is 1·5 cm in diameter and 0·063 in. thick, while the thin crystal is 1 cm in diameter and 0·0025 in. thick (28 mg cm^{-2}) corresponding to an energy loss of 0·6 MeV for a 10 MeV proton. The reflector mounting of the thick crystal improves the resolution, since the light from any point in the crystal is spread uniformly over the whole photocathode and non-uniformities in the latter are not so important. The counter telescope is evacuated otherwise an undesirable background due to the reactions $^{14}N(n, d)^{13}C$ and $^{14}N(n, p)^{14}C$ is obtained.

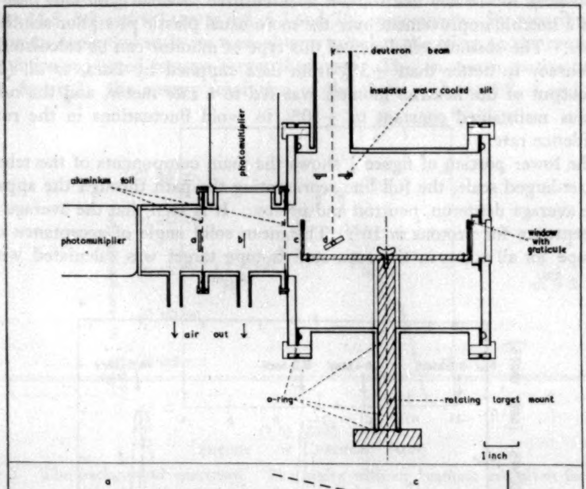
deuteron beam
insulated water cooled slit
photomultiplier
aluminium foil
photomultiplier
a
b
c
d
window with graticule
air out
o-ring
rotating target mount
1 inch
a
b
c
d
16°
thick CsI(Tl) crystal 6·3 thou
thin CsI(Tl) crystal 2·5 thou
separated isotope
tritium target
1 inch

Figure 1. Scintillation counter telescope for measurements of proton energy spectra from n, p reactions.

The separated isotopes were obtained as a deposit 1·5 cm in diameter and of thickness 15 mg cm^{-2} on a 0·0005 in. platinum backing and were mounted in lead holders on the rotating target mount shown. The twelve target holders were spaced equally on the mount, and by bringing the axis of target holder number six, say, on to the graticule, number twelve was accurately on the axis of the telescope. Background runs were obtained using an empty target holder, a preliminary experiment having shown no appreciable contribution from platinum.

The tritium titanium target was water-cooled as was the insulated slit above it. The beam current to the tritium target and to the slit were measured, and enabled us to maintain a diffuse beam over the whole target area (9 mm × 9 mm). A beam current of 6 μamp was sufficient to produce the flux of neutrons required (2×10^8 neutrons sec^{-1} into 4π), and as the experiment progressed the deuteron bombarding energy was raised from 200 to 300 kv to penetrate the thin layer of carbon on the tritium target surface. This did not affect the neutron energy appreciably, since we are observing neutrons emitted at 90°. The neutron monitor, mounted at 90° to the incident deuteron beam, was of the type described by Storey *et al.* This monitor consists of a CsI(Tl) scintillation counter detecting recoil protons from a hydrogeneous radiator. Since it produces a good peak for 14 Mev neutrons, it is insensitive to small gain and bias shifts and is a notable improvement over the more usual plastic phosphor scintillation counter. The absolute efficiency of this type of monitor can be calculated with an accuracy to better than ± 3% from data supplied by Bame *et al.* (1957). The output of the neutron monitor was fed to a rate meter, and the neutron flux was maintained constant to ± 10% to avoid fluctuations in the random coincidence rate.

The lower portion of figure 1 shows the main components of the telescope on an enlarged scale, the full line representing the path through the apparatus of the average deuteron, neutron and proton. It is seen that the average angle of acceptance for protons is 16°. The mean solid angle of acceptance of the telescope for all points in the separated isotope target was calculated with an error ± 5%.

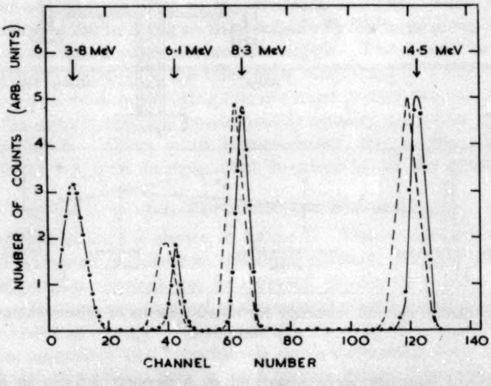

Figure 2. Coincidence spectrum in thick crystal corresponding to proton groups from the reactions ^{3}He(d, p)^{4}He and ^{10}B(d, p)^{11}B.

Due to the finite thickness of the thin crystal, and the variation with energy of energy lost by protons in the thin crystal, the pulse height response of the thick crystal against initial proton energy is not linear. All the spectra obtained were corrected for the slight non-linearity of the energy scale and for the small change in channel width with energy, account being taken of separated isotope target thickness as well as thin crystal thickness. The lower limit of the spectrum was not determined by the background, but by the channel width correction; at this point the correction was 20% of the channel width at 14 Mev. This correction is greatest for the first few channels and is down to 10% at 6·5 Mev. To estimate the average thickness of crystal to use in these corrections, the thin crystal was used as an absorber in front of a CsI(Tl) scintillation counter proton spectrometer. The shift of the ^{10}B(d, p)^{11}B proton groups caused by the introduction of the crystal gave the average thickness of the crystal.

The full line in figure 2 shows the coincidence pulse height spectrum from the thick crystal when the telescope is exposed to the proton groups from the reactions ^{3}He(d, p)^{4}He and ^{10}B(d, p)^{11}B. The energy resolution of the three peaks at 14·5, 8·3 and 6·1 Mev is 4·8, 6·3 and 7% respectively. By recording the peaks on an expanded scale we were able to calculate the effect on the resolution of the finite separated isotope target thickness. This is shown as the broken line in figure 2; the energy resolution of the three peaks is 6·2, 8 and 14%.

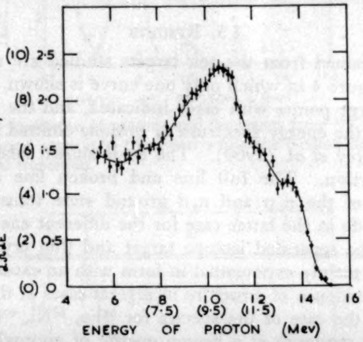

Figure 3. The background spectrum. The scales without brackets are given for comparison with the other spectra. The scales in brackets refer to the energy of protons emitted and cross section of n, p reactions in the thin crystal.

In the experiment proper, the telescope was calibrated and the gain of the thick crystal pulse amplification system was checked using the reaction ^{3}He(d, p)^{4}He, $Q = 18{\cdot}341$ Mev. The thin tritium titanium target contains ^{3}He from the decay of the tritium. One of the empty target holders on the rotating mount had a small hole at its centre covered with 41 mg cm^{-2} of aluminium, and by running the deuteron beam under exactly the same conditions as prevailed in an actual separated isotope irradiation an ample supply of 13·8 Mev protons was obtained to calibrate the energy scale. Having the same flux of neutrons passing through both scintillation counters during irradiation and calibration avoided errors which might have arisen due to the dependence of photomultiplier gain on counting rate. The 13·8 Mev protons were also used to determine the correct setting of the bias level of the thin crystal discriminator so that pulses due to protons were recorded while those due to electrons were rejected. Since the energy loss of the protons in the thin crystal increases as the energy of proton decreases, the telescope will operate at maximum efficiency for all protons. Deuterons and tritons will also be recorded by the telescope, but the thickness of the thin crystal precludes any possibility of alpha particles being accepted.

Each element was irradiated ten or more times, each irradiation lasting approximately 50 minutes, and background runs were interspersed with target runs. The gain of the thick crystal pulse height amplification system was checked with the 13·8 Mev protons at the end of each run; the drift was of the order of 1%. With the neutron flux of 2×10^8 neutrons per second into 4π the random coincidence spectrum was 10% of the background spectrum which is shown in figure 3. Since this spectrum has a broad peak at 11 Mev and a sharp edge at 14 Mev, a bad background subtraction will lead to the introduction of spurious peaks in the final spectrum. To check this subtraction, values of the ratio of counts in each target spectrum to counts in the nearest background spectrum were obtained for each irradiation. The spread in the values of this ratio for most targets was ± 3%. The scales without brackets in figure 3 are given for comparison with the final spectra.

§ 3. RESULTS

The spectra obtained from the ten targets studied are shown in figures 4 to 13. Except in figure 4 in which only one curve is shown, the present results are given by the large points with error indicated, and the smaller points and broken curve show the energy spectrum of protons emitted into approximately 4π obtained by Storey *et al.* (1960). The error shown takes into account the background subtraction. The full line and broken line arrows denote the expected positions of the n, p and n, d ground state transitions respectively, allowance being made in the latter case for the different energy loss of protons and deuterons in the separated isotope target and thin crystal.

The spectra are mainly exponential in form with an excess of higher energy protons and show evidence of structure in several cases at the high energy end of the spectra. In the case of the spectra for ^{54}Fe, ^{58}Ni, ^{65}Cu and ^{64}Zn there is also evidence for structure at a proton energy of approximately 7 to 8 Mev. This latter structure has sometimes been interpreted as being due to giant resonance or anomalous effects, but the present experiment will show that these lower energy groups at about 7·5 Mev may be interpreted as being due to the n, d pick-up reaction.

^{19}F, figure 4. A CF_2 target 10·3 mg cm^{-2} thick was used; there is no contribution to the spectrum from carbon which has large negative *Q*-values for the n, p and n, d reactions. The spectrum is in good agreement with that obtained by Ribe (1957), the peaks at 7·5 and 10 Mev being attributed to the ground state n, d and n, p reactions respectively. Neglecting the correction to the efficiency of the telescope caused by its finite solid angle of acceptance and the anisotropic angular distribution of the reaction products, we find cross sections of 10·8 and 0·7 millibarn per steradian for the two peaks. At the average angle of acceptance of the telescope for isotropic reactions, namely 16°, Ribe finds a cross section of 8 millibarn per steradian for the n, d reaction, which is in agreement with our value when the anisotropy of the reaction is considered. Remembering the fluorine has a single proton outside a closed shell of 8 protons it is understandable that the n, d reaction should be favoured. Ribe does not find the n, p ground state transition at 0°, but finds a cross section of 0·7 millibarn per steradian at 50° for this peak. It is thought that the peak

at 7·5 Mev is due to deuterons entirely, since it is very symmetrical, and its width at half height (1·1 Mev) is fairly close to that calculated (0·9 Mev) for a transition to a single level. The proximity of the deuteron peak to its predicted position on the proton energy scale shows that the luminescent response of CsI(Tl) for deuterons is practically equal to that for protons.

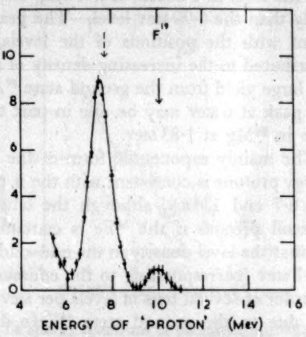

Figure 4. The energy spectrum of protons and deuterons from ^{19}F. The full line arrow denotes the ground state n, p transition while the broken line arrow denotes the ground state n, d transition.

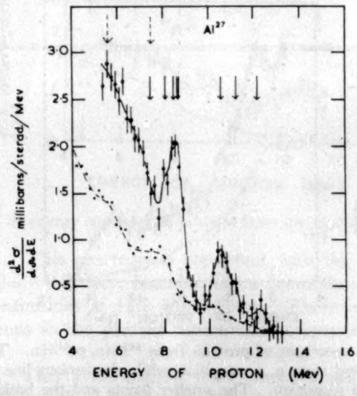

Figure 5. The energy spectrum of protons from ^{27}Al(n, p)^{27}Mg. The full line arrows denote the ground and excited states of ^{27}Mg; the broken line arrows denote the ground and first excited state n, d transitions. The smaller points and broken curve show the spectrum of Storey *et al.* (1960).

^{27}*Al*, ***figure*** 5. The improved statistics and energy resolution of the present experiment are shown to advantage in this spectrum. The full line arrows represent ^{27}Al(n, p)^{27}Mg transitions to the ground, 0·99, 1·66, 3·5, 3·56, 3·76, 4·13 and 4·75 Mev levels in ^{27}Mg as given by Endt *et al.* (1952), Holt and Marsham (1953) and Hinds *et al.* (1958), while the broken line arrows represent ^{27}Al(n, d)^{26}Mg transitions to the ground and 1·83 Mev levels in ^{26}Mg quoted by Endt and Kluyver (1954). It is seen, in agreement with Haling *et al.* (1957), and March and Morton (1958 c), that the ground state n, p transition is only weakly excited if at all, and the level at 1·66 Mev is not only confirmed but seems to be excited more strongly than the 0·99 Mev level. The peak between 8 and 9 Mev is in good agreement with the positions of the levels, and below 8 Mev the spectrum may be attributed to the increasing density of available levels. There is no indication of a large yield from the ground state ^{27}Al(n, d)^{26}Mg transition, but the tendency to peak at 6 Mev may be due in part to the n, d transition to the first excited state in ^{26}Mg at 1·83 Mev.

^{54}*Fe, figure* 6. The mainly exponential form of the ^{54}Fe spectrum with an excess of higher energy protons is consistent with the n, p Q-value ($Q = 0{\cdot}3$ Mev) and shows peaks at 6·7 and 13 Mev, although the latter peak may contain a contribution from recoil protons if the ^{54}Fe is contaminated with hydrogen. When one considers that the level density in the odd–odd residual nucleus ^{54}Mn at an excitation of 7·7 Mev (corresponding to the emission of a 6·7 Mev proton) is likely to be of the order of several tens of levels per Mev, it seems probable that the 6·7 Mev peak is due to the ground state ^{54}Fe(n, d)^{53}Mn, $Q = -6{\cdot}58$ Mev transition shown by the broken line arrow. Correcting for the greater effective thickness of the target in the experiment of Storey *et al.*, the lower curve in figure 6 also seems to show this transition.

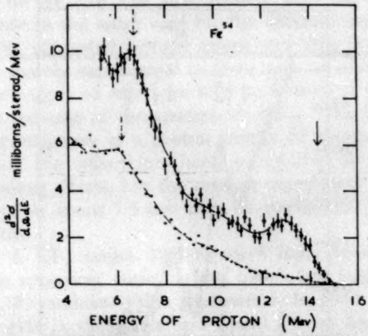

Figure 6. The energy spectrum of protons from ^{54}Fe(n, p)^{54}Mn. The full line arrow denotes the ground state n, p transition while the broken line arrow denotes the ground state n, d transition. The smaller points and the broken curve show the spectrum of Storey *et al.* (1960). This convention is followed throughout.

^{56}*Fe, figure* 7. Broad peaks are superimposed on this spectrum at 13, 10·6 and 8·6 Mev. The peak at 13 Mev which is inconsistent with the n, p Q-value ($Q = -2{\cdot}93$ Mev) will be discussed below. The spectrum obtained by Allan (1957) for this reaction also shows this effect; it is not exponential in form and shows peaks at 11·2, 8·6, 6·3, and 4·4 Mev. March and Morton (1958 a) and Colli *et al.* (1957 a) find an exponential form for the spectrum, and Colli *et al.*

observe discontinuities at 10·3 and 8·3 MeV which seem to agree with those found here. Since the ^{56}Fe(n, d)^{55}Mn, $Q = -7{\cdot}92$ MeV, ground state transition would appear at the lower limit of the spectrum, we cannot say whether it contributes or not; however, the discontinuity in the lower curve at 5·1 MeV is close to the broken line arrow denoting the ground state n, d transition.

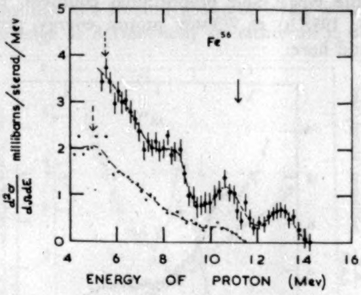

Figure 7. The energy spectrum of protons from ^{56}Fe(n, p)^{56}Mn.

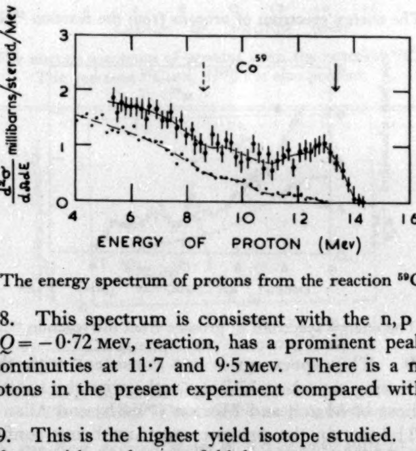

Figure 8. The energy spectrum of protons from the reaction ^{59}Co(n, p)^{59}Fe.

^{59}*Co, figure* 8. This spectrum is consistent with the n, p Q-value for the ^{59}Co(n, p)^{59}Fe, $Q = -0{\cdot}72$ MeV, reaction, has a prominent peak at 13 MeV, and very slight discontinuities at 11·7 and 9·5 MeV. There is a marked excess of high energy protons in the present experiment compared with that of Storey *et al.*

^{58}*Ni, figure* 9. This is the highest yield isotope studied. The spectrum is exponential in form with a plateau of high energy protons, the end point of which is consistent with the n, p Q-value. A very prominent bump at 7·3 MeV in the spectrum does not coincide with the ^{58}Ni(n, d)^{57}Co $Q = -5{\cdot}45$ MeV ground state transition. This is not surprising on consideration of the spins of the ground state target and residual nuclei which are 0^+ and $7/2^-$ respectively, since the large value of l involved in the pick-up reaction will inhibit the ground state pick-up reaction and preclude its observation in the forward direction. The first excited state in ^{57}Co given by Konijn *et al.* (1956) occurs at 1·36 MeV whereas the present result suggests an excited state at 0·9 Mev. Allan (1957) finds no discontinuities between 7 and 10 Mev for ^{58}Ni, but there is a prominent edge in his spectrum at 6 Mev. This confirms the deuteron assignment in the present experiment, since being unable to distinguish between deuterons and protons in the nuclear emulsion, a 7·7 Mev deuteron will look like a 5·8 Mev proton in Allan's experiment. Correcting for the different energy loss of protons and deuterons in the target and proportional counters, the edge found by Colli *et al.* (1957 a, 1958 b) at 7·3 Mev proton energy probably corresponds to the deuteron found here.

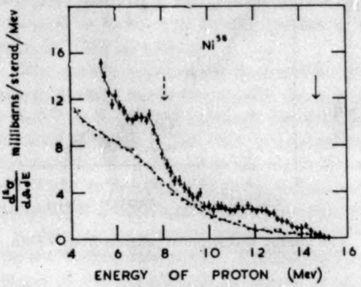

Figure 9. The energy spectrum of protons from the reaction ^{58}Ni(n, p)^{58}Co.

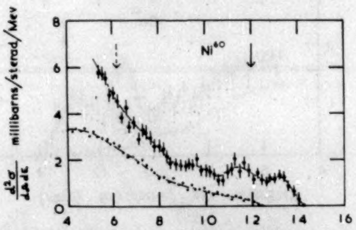

Figure 10. The energy spectrum of protons from the reaction ^{60}Ni(n, p)^{60}Co.

^{60}*Ni, figure* 10. This spectrum is not consistent with the n, p Q-value ($Q = -2{\cdot}03$ Mev) having a peak at 13·2 Mev, otherwise the spectrum is in broad agreement with those of March and Morton (1958 b) and Allan (1957), a slight discontinuity at 11·4 Mev in the present spectrum being confirmed by Allan. Another slight discontinuity at 9·6 Mev is evident, but there is no indication of a large contribution from the n, d ground state transition.

^{63}*Cu, figure* 11. Despite a Q-value of $+0{\cdot}7$ Mev for the ^{63}Cu(n, p)^{63}Ni reaction no yield is observed above 11 Mev in this spectrum. A prominent peak at 9·5 Mev is very near the predicted position of the ^{63}Cu(n, d)^{62}Ni, $Q = -3{\cdot}7$ Mev ground state transition. Allan (1958), quoting peaks at 10·2 and 7·5 Mev for ^{63}Cu, ascribes those to n, p reactions comparable with the anomalous inelastic scattering of 23 Mev protons found by Cohen (1957), but remembering that the emulsion technique cannot distinguish protons from deuterons, it is more probable that the peak found at 7·5 MeV is caused by 10·2 MeV deuterons rather than 7·5 MeV protons. If a correction for the different energy loss of a deuteron in Allan's target foil is made (0·15 MeV) a very good fit is obtained to the *Q*-value of the ground state n, d reaction. In figure 11, then, it would appear that the main peak at 9·5 MeV is due to deuterons, while the slight edge at 10·2 MeV represents an n, p transition to a level or group of levels with excitation energy 4·5 MeV in ^{63}Ni. The edge at 8·5 MeV may be either an n, p transition or the n, d transition to the first excited state at 1·172 MeV, spin 2^+ in ^{62}Ni. Being obtained from a natural copper foil (69% ^{63}Cu, 31% ^{65}Cu), the ^{63}Cu spectrum contains a correction for the effect of ^{65}Cu in the original spectrum. The ^{65}Cu spectrum is of exceptionally low yield except for a peak at 8·3 MeV, but the edge obtained at 8·5 MeV in the ^{63}Cu spectrum is not a consequence of the subtraction of the ^{65}Cu 8·3 MeV peak.

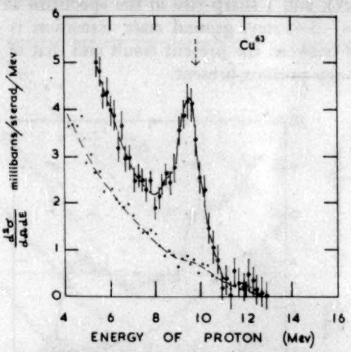

Figure 11. The energy spectrum of protons from the reaction ^{63}Cu(n, p)^{63}Ni. The reaction ^{63}Cu(n, d)^{62}Ni is also present.

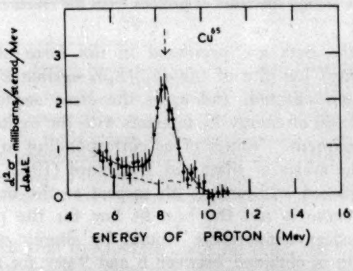

Figure 12. The energy spectrum of protons from the reaction ^{65}Cu(n, p)^{65}Ni. The reaction ^{65}Cu(n, d)^{64}Ni is also present.

^{65}*Cu, figure* 12. This was the lowest yield element studied, no protons being observed beyond 10 MeV although the *Q*-value is −1·02 MeV for the ^{65}Cu(n, p)^{65}Ni reaction. The prominent peak obtained at 8·3 MeV is only

0·1 Mev lower than the predicted position of the n, d ground state transition ^{65}Cu(n, d)^{64}Ni, $Q = -5{\cdot}10$ Mev. Making allowance for a background of n, p reactions, the cross section for this peak is 1·6 millibarns per steradian. Allan (1957) did not observe anything significantly above background for ^{65}Cu. It is not surprising that the n, d pick-up reaction is obtained for the copper isotopes, since the number of protons ($Z = 29$) is one more than the magic number 28, and the residual nuclei both have spin 0^+.

^{64}*Zn, figure* 13. The end point of this spectrum is consistent with the n, p Q-value ($Q = 0{\cdot}2$ Mev), and a sharp rise in the spectrum at the position of the ^{64}Zn(n, d)^{63}Cu, $Q = -5{\cdot}45$ Mev, ground state transition is evident. There is an extreme contrast between the present result and that of Storey *et al.* in the number of high energy protons present.

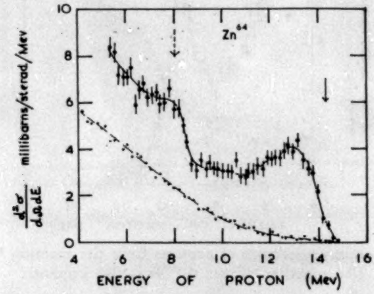

Figure 13. The energy spectrum of protons from the reaction ^{64}Zn(n, p)^{64}Cu.

In figure 14, the data are presented in the form of the conventional 'relative level density' log plot of $(dn/dE_p)/E_p\sigma_c$ against E_p, where E_p is the energy of the proton emitted, and σ_c is the cross section for the inverse reaction where a proton of energy E_p interacts with the excited residual nucleus of the present experiment. Values of σ_c corresponding to $r_0 = 1{\cdot}5 \times 10^{-13}$ cm were taken from the tables of Blatt and Weisskopf (1952). For convenience the curves are displaced arbitrarily with respect to the ordinate scale. The full line on each curve is not the best fit line for the present results but represents the 'nuclear temperature' found by Storey *et al.* for the same reaction. A good fit is obtained between 6 and 9 Mev for all elements except ^{65}Cu and ^{59}Co; above 9 Mev there is an appreciable contribution from direct interaction processes. Aluminium is not included in figure 14, since, being a light element, there are probably insufficient levels in ^{27}Mg between 4 and 7 Mev excitation energy to merit a statistical approach; however, the present result is a good fit to the 'nuclear temperature' of 1·75 Mev found by Storey *et al.* ^{65}Cu is included for completeness, but the poor signal to background ratio for this element means that little significance can be attached to the present result. Nevertheless, it is interesting that the present result indicates a lower 'temperature' ($T = 1{\cdot}5$ Mev) than that measured by Storey *et al.* (1·76 Mev) since the latter 'temperature' is anomalously high when compared with the values obtained for neighbouring nuclei. Having a low yield, it is possible that in the case of ^{59}Co many of the protons originate in direct interactions. Most theories of direct interaction result in a spectrum with a relatively greater number of higher energy protons than the spectrum determined by the level density of the residual nucleus, consequently higher 'nuclear temperatures' are expected for spectra where direct interaction is present. The 'nuclear temperatures' of figure 14 are not in good agreement with those found by March and Morton 1958 a, b, for ^{54}Fe, ^{56}Fe and ^{60}Ni (1·2, 1·2 and 1 MeV respectively) and by Allan (1959) for ^{54}Fe (1·2 MeV).

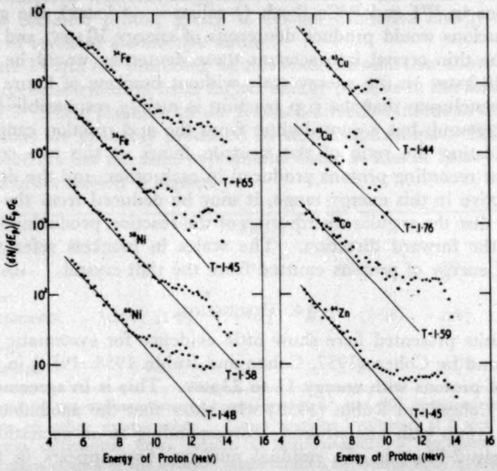

Figure 14. Curves giving $(dn/dE_{\mathrm{p}})/E_{\mathrm{p}}\sigma_{\mathrm{c}}$ against E_{p} obtained from measurements of the energy spectra of protons fron n, p reactions in ^{54}Fe, ^{56}Fe, ^{58}Ni, ^{60}Ni, ^{63}Cu, ^{65}Cu, ^{59}Co and ^{64}Zn. E_{p} is the energy of the proton, and σ_{c} is the cross section for the inverse reaction corresponding to $r_0 = 1{\cdot}5 \times 10^{-13}$ cm. The full line represents the 'nuclear temperature' T (in MeV) measured by Storey *et al.* (1960). The curves are displaced arbitrarily with respect to the ordinate scale for convenience.

It has been noted that the spectra obtained from the ^{56}Fe and ^{60}Ni targets are inconsistent with the n, p Q-value. This is thought to be caused by the absorption of small quantities of hydrogen in the separated isotope targets during their preparation by electrodeposition. From the average angle of acceptance of the telescope, 16°, we would expect a thin hydrogen target to produce a broad peak at 13 MeV, and this is in fact the result obtained. It will be noted, too, that the natural targets of fluorine and aluminium which also have negative n, p Q-values do not show this effect.

Before discussing the results, some remarks concerning the background spectrum can be made. Apart from the 10% of this spectrum due to random coincidences, most of the background must arise from reactions in the crystals themselves. The thick crystal contribution would not be expected to show structure since protons and other particles will be produced at all depths of it, and will lose varying amounts of energy getting out of the crystal to produce a coincidence pulse in the thin crystal. On this basis, the broad peak between 8 and 12 Mev is attributed to n, p, n, d or n, α reactions in the thin crystal. The *Q*-values of the reactions ^{127}I(n, α)^{124}Sb and ^{133}Cs(n, α)^{130}I are 4·4 and 4·0 Mev respectively, but assuming that the n, α reaction will be similar to the p, α reaction studied by Fulmer and Cohen (1958) with 23 Mev protons, and taking into account the fluorescent response of alpha particles relative to protons in CsI(Tl) and the thickness of the thin crystal, an upper limit of 8 Mev is found for the peak of the evaporation spectrum of alpha particles. Considering the n, d reactions in ^{127}I and ^{133}Cs (both Q-values $= -4 \cdot 1$ Mev), the ground state pick-up reactions would produce deuterons of energy 10 Mev, and taking their origin in the thin crystal into account these deuterons would be expected to appear at 10·3 Mev on the energy scale without brackets of figure 3. We are led to the conclusion that the n, p reaction is mainly responsible for the peak in the background, but a contribution from the n, d reaction cannot be ruled out. Calculating the ratio of the neutron fluxes at the two crystals, their efficiency for recording protons produced in each other, and the depth of thick crystal effective in this energy range, it may be deduced from the prominence of the peak that the angular distribution of the reaction producing it is strongly peaked in the forward direction. The scales in brackets refer to the cross section and energy of protons emitted from the thin crystal.

§ 4. Discussion

The results presented here show little evidence for systematic structure of the type found by Cohen (1957, Cohen and Rubin 1958, 1959) in the inelastic scattering of protons with energy 11 to 23 Mev. This is in agreement with the findings of Cohen and Rubin (1958) who show that the anomalous behaviour—a proton group with fine structure corresponding to an excitation energy of approximately 2·5 Mev in the residual nucleus—first appears in the isotopes of Zn. In addition, they find that the cross section for the production of the anomalous proton group increases with bombarding energy, the dependence being most marked in the case of Zn. These authors also find a prominent peak in the elements $Z = 26$ to 30 corresponding to an excitation of the residual nucleus of 1–1·5 Mev. Greenless *et al.* (1958) studying the inelastic scattering of 10 Mev protons find little evidence for the anomalous proton group at 2·5 Mev excitation energy, but the group at 1–1·5 Mev is confirmed. The latter group need not be regarded as due to anomalous behaviour since the level spacing at such low excitation energy is large. The present results for ^{54}Fe and ^{64}Zn seem to show this effect, but the possibility of hydrogen contamination of the targets must be borne in mind.

The spectra for the reactions ^{56}Fe(n, p)^{56}Mn and ^{60}Ni(n, p)^{60}Co shown in figures 7 and 9 do show some similarity, the structure corresponding to excitations of 0·5 and 2·5 Mev in ^{56}Mn and 0·6 and 2·4 Mev in ^{60}Co. Comparing the present ^{56}Fe(n, p)^{56}Mn result with the proton energy spectrum from the reaction ^{55}Mn(d, p)^{56}Mn studied by Green *et al.* (1958), one would be tempted to say that a 'modulation' effect similar to that found by Blok and Jonker (1957) and Colli *et al.* (1957) was present, since a histogram of the number of d, p protons observed per 0·4 Mev energy interval shows unmistakable broad peaks at 0·4 and 2·4 Mev excitation energy of the odd–odd nucleus ^{56}Mn. However, a simple histogram of the number of levels per 0·4 Mev interval shows the same characteristic, so it is probably unnecessary to invoke a special selection rule to account for the structure in the spectra, equal transition probability to all levels being sufficient. In the same way, it may be shown that the peaks in the spectrum for ^{60}Ni(n, p)^{60}Co correspond to the increased number of levels available at excitation energies 0·5 and 2·5 Mev in the odd–odd nucleus ^{60}Co. Foglesong and Foxwell (1954) have determined the levels in ^{60}Co using the reaction ^{59}Co(d, p)^{60}Co. The increased level density at 2·5 Mev found in ^{56}Mn and ^{60}Co may be connected with the suggestion of Cohen and Rubin (1958) that the anomalous inelastic proton group at 2·5 Mev excitation energy is due to the excitation of levels of a collective nature.

In figure 14 and the preceding figures it can be seen that above 9 Mev there is a much larger contribution from higher energy protons in the forward direction than at 90°. Their presence in the forward direction indicates that these additional protons are probably produced by direct interactions. Below 9 Mev, the present spectrum has the same exponential shape as that of Storey *et al.*, but the differential cross section is higher.

Table 1

Target Nucleus	^{54}Fe	^{56}Fe	^{58}Ni	^{60}Ni	^{63}Cu
(*a*) Other Experiments	1·56†; [1·0]	1·67†	1·72*; (1·58)	2·0†	[2·0]; (1·52)
(*b*) Present Experiments	1·73	2·10	1·46	1·78	1·74

(*a*) The ratio of the differential cross sections at 0° and 90° obtained from the angular distributions of other experiments. Cross sections evaluated at 6 Mev proton energy.
(*b*) The ratio differential cross section at approximately 0° (present experiment) to differential cross section at the average angle studied by Storey *et al.* (1960). (Solid angle for acceptance of protons 3·5 steradian centred at 90°.) Cross sections evaluated at 6 Mev proton energy.

Symbols: [ ] Allan (1959); * Colli *et al.* (1958 a); † March and Morton (1958 a, b); ( ) Verbinski *et al.* (1957).

Normally, a comparison of differential cross sections from two different experiments with vastly different geometries would be doubtful. In this case, however, the same neutron monitor and separated isotope targets were used in both experiments. In addition, the ratios of differential cross sections at a specific energy can be compared with angular distributions. Table 1 shows the ratio of differential cross sections at 0° and 90° at 6 Mev proton energy obtained by other workers for comparison with the ratio of the present differential cross section at 6 Mev to that of Storey *et al.* Since the latter experiment observes protons emitted into a large solid angle centred at 90° omitting only the extreme forward and backward angles, we would expect the second ratio to be smaller than the first which is derived from an angular distribution. The small solid angle of acceptance of the telescope of Colli *et al.* (1958 a) is similar to the geometry of the present experiment, and in the case of the high yield isotope ^{58}Ni the agreement is good, the present ratio 1·46 being just less than the 1·72 of Colli *et al.*

Table 2 (*a*) lists the 'nuclear temperatures' T measured by Storey *et al.* (1960) which are a good fit to the present results in the range of proton energy 6 to 9 MeV. In the conventional analysis of evaporation spectra, one expects T to be related to the maximum excitation energy of the residual nucleus by $a = E_m/T^2$ where a is a constant of the form A/k MeV^{-1}, A being the atomic mass number of the residual nucleus. Applying this analysis to the present results, we obtain the values of a shown at (*b*) in table 2. Generally, these values of a are in good agreement with those of Lang and Le Couteur (1954), the latter authors quoting a value of $k = 10{\cdot}5$ MeV.

Table 2

Target Element	^{27}Al	^{54}Fe	^{56}Fe	^{58}Ni	^{60}Ni	^{63}Cu	^{64}Zn
(*a*) T(MeV)	1·75	1·65	1·45	1·57	1·48	1·44	1·45
(*b*) $a = E_m/T^2$(MeV^{-1})	4·0	5·3	5·3	6·0	5·5	7·2	6·8

(*a*) The nuclear temperature measured by Storey *et al.* (1960). (*b*) Values of a derived from $a = E_m/T^2$ where E_m is the maximum energy of excitation possible in the residual nucleus and T is the 'nuclear temperature' of Storey *et al.* (1960).

Returning to table 1, it is seen that there is some evidence that the angular distribution of the lower energy protons is not isotropic as would be predicted by the simple statistical theory (Hauser and Feshbach 1952). If the additional protons in the forward direction are attributed to direct interactions, it is hard to explain why the 'nuclear temperatures' indicated by the present results are so close a fit to those of Storey *et al.*, since most direct effects predict a relatively greater number of higher energy protons corresponding to a higher 'nuclear temperature'. If this anisotropy which has been found in some of the experiments is real, we must conclude that either one of the usual assumptions of the statistical theory is invalid, or the direct interaction mechanism leads to an energy distribution of particles similar to that predicted by the statistical theory.

§ 5. CONCLUSIONS

Evidence is produced that n, d reactions contribute appreciably to the spectra obtained from medium weight nuclei bombarded with 14 MeV neutrons. Little evidence for systematic structure in the proton spectra is obtained, but a direct interaction process is present at the highest proton energies. This direct interaction probably occurs in the surface of the nucleus, since only the low lying levels in the residual nucleus are involved. The energy distributions of the lower energy protons are in fair agreement with the statistical theory, but there is some evidence of an anisotropy incompatible with the usual assumptions of this theory.

ACKNOWLEDGMENTS

The authors wish to express their thanks to Professor P. I. Dee for his interest in the present work. We are also indebted to Dr. M. L. Smith of the Electromagnetic Separation Group, Harwell, who prepared the separated isotope targets, and to Mr. A. Duncan who maintained the high tension generator during the course of the experiment. One of us (W. J.), wishes to acknowledge the receipt of a Sir James Caird Travelling Scholarship.

References

Allan, D. L., 1957, *Proc. Phys. Soc.* A, **70**, 195.
—— 1958, *Nucl. Phys.*, **6**, 464.
—— 1959, *Ibid.*, **10**, 348.
Austern, N., **Butler**, S. T., and **McManus**, H., 1953, *Phys. Rev.*, **92**, 350.
Bame, S. J., Jr., **Haddad**, E., **Perry**, J. E., Jr., and **Smith**, R. K., 1957, *Rev. Sci. Instrum.*, **28**, 997.
Blatt, J. M., and **Weisskopf**, V. F., 1952, *Theoretical Nuclear Physics* (New York: Wiley).
Blok, J., and **Jonker**, C. C., 1957, *Nuovo Cim.*, **6**, 378.
Brown, G., **Morrison**, G. C., **Muirhead**, H., and **Morton**, W. T., 1957, *Phil. Mag.*, **2**, 785.
Brown, G., and **Muirhead**, H., 1957, *Phil. Mag.*, **2**, 473.
Cohen, B. L., 1957, *Phys. Rev.*, **105**, 1549.
Cohen, B. L., and **Rubin**, A. G., 1958, *Phys. Rev.*, **111**, 1568.
—— 1959, *Ibid.*, **113**, 579.
Colli, L., **Facchini**, U., and **Micheletti**, S., 1956, *Nuovo Cim.*, **4**, 671.
Colli, L., and **Facchini**, U., 1957 a, *Nuovo Cim.*, **5**, 309.
Colli, L., **Facchini**, U., and **Micheletti**, S., 1957 b, *Nuovo Cim.*, **5**, 502.
Colli, L., and **Micheletti**, S., 1957 c, *Nuovo Cim.*, **6**, 1001.
Colli, L., **Facchini**, U., **Iori**, I., **Marcazzan**, G., and **Sona**, A., 1958 a, *Nuovo Cim.*, **7**, 400.
Colli, L., **Pignanelli**, M., **Rytz**, A., and **Zurmuhle**, R., 1958 b, *Nuovo Cim.*, **9**, 280.
Elton, L. R. B., and **Gomes**, L. C., 1957, *Phys. Rev.*, **105**, 1027.
Endt, P. M., **Haffner**, J. M., and **Von Patter**, D. M., 1952, *Phys. Rev.*, **86**, 518.
Endt, P. M., and **Kluyver**, J. C., 1954, *Rev. Mod. Phys.*, **26**, 95.
Eubank, H. P., **Peck**, R. A., Jr., and **Zatzick**, M. R., 1959, *Nucl. Phys.*, **10**, 418.
Foglesong, G. M., and **Foxwell**, D. G., 1954, *Phys. Rev.*, **96**, 1001.
Frenkel, I., 1936, *Sov. Phys.*, **9**, 533.
Fulmer, C. B., and **Cohen**, B. L., 1958, *Phys. Rev.*, **112**, 1672.
Green, L. W., **Smith**, A. J., **Buechner**, W. W., and **Mazari**, M., 1958, *Phys. Rev.*, **108**, 841.
Greenlees, G. W., **Lowe**, J., **Robbins**, A. B., and **Rolph**, P. M., 1958, *Proc. Phys. Soc.*, **71**, 904.
Haling, R. K., **Peck**, R. A., and **Eubank**, H. P., 1957, *Phys. Rev.*, **106**, 971.
Hauser, W., and **Feshbach**, H., 1952, *Phys. Rev.*, **87**, 366.
Hayakawa, S., **Kawai**, M., and **Kikuchi**, K., 1955, *Progr. Theor. Phys.* (Japan), **13**, 415.
Hinds, S., **Middleton**, R., and **Parry**, G., 1958, *Proc. Phys. Soc.*, **71**, 49.
Holt, J. R., and **Marsham**, T. N., 1953, *Proc. Phys. Soc.* A, **66**, 258.
Hutchinson, G. W., and **Scarrott**, G. G., 1951, *Phil. Mag.*, **42**, 792.
Konijn, J., **Van Nooijen**, B., **Mostert**, P., and **Endt**., P. M., 1956, *Physica*, **22**, 887.
Lang, J. M. B., and **Le Couteur**, K. J., 1954, *Proc. Phys. Soc.* A, **67**, 586.
March, P. V., and **Morton**, W. T., 1958 a, *Phil. Mag.*, **3**, 143.
—— 1958 b, *Ibid.*, **3**, 557.
—— 1958 c, *Ibid.*, **3**, 1256.
Ribe, F. L., 1957, *Phys. Rev.*, **106**, 767.
Storey, R. S., **Jack**, W., and **Ward**, A., 1960, *Proc. Phys. Soc.*, **75**, 526.
Verbinski, V. V., **Hurlimann**, T., **Stephens**, W. E., and **Winhold**, E. J., 1957, *Phys. Rev.*, **108**, 779.
Weisskopf, V. F., 1937, *Phys. Rev.*, **52**, 295.

The Ionization of Fast Neutral Deuterium Atoms by Hydrogen and by Deuterium

By L. P. CHALKLIN and J. H. FREMLIN
Department of Physics, University of Birmingham

MS. received 30th October 1959

Abstract. Neutral deuterium atoms of energy 8 MeV from the Birmingham cyclotron were passed through hydrogen and deuterium gas at low pressure. Ionized particles were separated by the cyclotron magnetic field from the original beam and the numbers in each beam were found by counting tracks on a nuclear emulsion.

Cross sections for ionizing collisions were found to be $1{\cdot}6 \pm 0{\cdot}25 \times 10^{-18}\,\mathrm{cm}^2$ and $2{\cdot}3 \pm 0{\cdot}25 \times 10^{-18}\,\mathrm{cm}^2$ in hydrogen and in deuterium respectively.

---

§ 1. Introduction

When a cyclotron is adjusted to accelerate deuterons it will also accelerate negative deuterium ions revolving in the opposite sense to the positive deuterons. The negative ions lose electrons readily in collisions with molecules of residual gas (Fremlin and Spiers 1955). The neutral deuterium atoms, resulting from the loss of an electron, are not deflected appreciably by the collisions producing them and hence travel along tangents to the orbits in which they were moving before collision. The cylotron therefore produces close to the median plane of the magnet an azimuthally uniform flux of neutral atoms moving with velocities proportional to the radii of the orbits from which they come. The flux falls rapidly as the energy of the particles increases unless the residual gas pressure in the cyclotron tank is very low, but under good vacuum conditions particles have been observed up to 20 MeV, the maximum energy obtainable for deuterons with the Birmingham machine. Useful numbers of neutral atoms are easily obtained with energies up to 10 MeV and the present paper describes a study of the ionization of these atoms in their passage through hydrogen and deuterium. Similar work on the ionization of fast neutral atoms in an organic foil has already been reported (Chalklin and Fremlin 1956). The velocity of a deuterium atom with 8 MeV energy is some ten times greater than the electron velocity corresponding to the first Bohr orbit in a deuterium atom. It is therefore to be expected that any atomic-interaction cross section will approximately follow a simple $1/v$ law. The precise particle energy chosen for experiments of the type described in the present paper is therefore probably not very important; an energy of 8 MeV was chosen as giving a convenient flux of particles.

§ 2. Experimental Method

We have already described the method for measuring the ionization of fast deuterium atoms from the cylotron by thin Formvar foils. The method used here was similar in principle, a diagram of the camera used being shown in figure 1.

The two fine slits S_1 and S_2, on either side of the gas chamber simultaneously define the direction from which particles come, and hence their energy, and limit the escape of gas. It was necessary of course to make the slits very small and each was approximately 0·1 mm × 1·5 mm. Even so, the residual tank pressure rose appreciably, and sometimes seriously, with the higher gas pressures (1–2 mm) used. The uncertainty in the lengths of effective paths in the gas was only about 0·1 mm on a total of 20 mm which was negligible compared with other errors in the experiment.

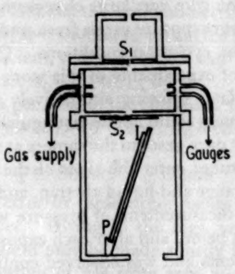

Figure 1.

After passage through the slits the selected beam fell on a small piece of Ilford C2 plate IP, set at an angle of 20° to the beam and with its centre 2·5 cm behind the second slit. Fast neutral atoms falling on this plate were ionized within a small fraction of a micron and left normal deuteron tracks which could be counted individually. Deuterium ions produced by the gas between the slits also struck the plate but, being affected by the field of the cyclotron magnet, were deflected to a different part of the plate. Since ionization might occur anywhere along the path through the camera, the amount of deflection was not constant but the whole of the deflected beam was well resolved from the primary ionized beam, as can be seen in figure 2. Comparison of the numbers of tracks in the deflected and the undeflected beams then gives the probability of ionization in the system and, with knowledge of the gas pressure, the cross section for ionization could be found.

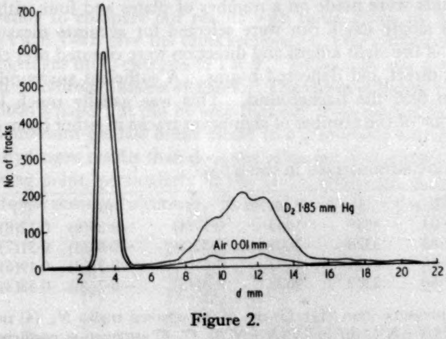

Figure 2.

While the method is simple in principle, to obtain good results takes some time and trouble. Owing to the small size of the slits, the position and orientation of the camera is critical and the optimum position has to be found by trial and error, since the mean plane of the orbits of negative ions in the cyclotron does not coincide with the geometrical median plane of the magnet and is not exactly known. Once found, however, the best orientation seems to remain fairly constant.

The second main problem is to find a suitable exposure to give a good number of easily resolved tracks in each beam. Quite small changes in the residual gas pressure in the cyclotron tank give very large changes in the flux of neutral atoms obtained so that the optimum exposure varies from under a second to ten minutes or more for much the same cyclotron conditions. Consequently much of the time taken by each group of experiments in this work consisted of the exposure and development of test plates showing alternatively no tracks at all and black patches in which separate tracks could not be distinguished.

It is important to supply pure gases to the camera at a suitable known pressure. As shown in figure 1 two tubes enter the sides of the gas chamber; gas passes through one, via a needle gauge and liquid air trap, and the other is connected to the gauges. The absolute measurements of pressure were made by the McLeod gauge, readings being taken before and after each exposure. A Pirani gauge was used for relative measurements and was observed continuously throughout each exposure to ensure that no variations of pressure occurred. The camera was difficult to degas and a ' background ' deflected beam was produced by residual air or other gases, together with scattering from the slit edges. A value for this could easily be found by making an exposure with no gas fed to the camera although this might be somewhat greater than the effective value in working conditions owing to the 'sweeping out ' effect of the mass flow of hydrogen or deuterium. Experiments with gas at different working pressures suggested, however, that this effect was within the limits of experimental error.

Track numbers were compared by direct counting using an M 4000 microscope. Although very laborious, this method practically eliminates background due to seriously scattered particles or to neutron recoil tracks, since the desired tracks are well defined in length and direction.

§ 3. Results

Sample counts were made on a number of plates and four with suitable exposures from a single day's run were selected for accurate measurement. In these, all tracks of the right length and direction were counted over the whole area covered by the direct and deflected beams. A sufficient surrounding area was also counted to find the background. This was usually much less than the standard deviation of the number of significant tracks in either beam and was then neglected.

The results are summarized in the table.

(1)	(2)	(3)	(4)	(5)	(6)	(7)	(8)
Residual	~0·04	4950	1443	0·77(4)	−0·25(6)	0·12(8)	
H_2	1·85	3328	3001	0·52(6)	−0·63(3)	0·31(7)	0·189
D_2	0·45	9994	4782	0·67(6)	−0·39(2)	0·19(6)	0·06(8)
D_2	1·80	8372	9623	0·46(5)	−0·76(6)	0·38(3)	0·25(5)

(1) Gas; (2) pressure (mm Hg), (3) no. of undeflected tracks N; (4) no. of deflected tracks N'; (5) $N/(N+N')$; (6) ln $[N/(N+N')]$; (7, 8) attenuation coefficient; (7) gross, (8) pure gas.

Background < 50 *in toto* for each plate.

The 'attenuation coefficients' given in column (7) still include a contribution due to slit edges, etc., and this contribution will not vary linearly with gas pressure. Uncertainty as to the reduction of residual gas by the hydrogen or deuterium flow is more important than this over the small range of pressure examined. The absorption coefficients for pure hydrogen and for deuterium are therefore obtained simply by subtracting the value 0·12(8) from each of the gross coefficients. The procedure is justified by the fact that the attenuation coefficient for deuterium then varies linearly with pressure, as it should, to within the probable error. The final values for attenuation coefficient, reduced in each case to a pressure of 1 mm Hg, are then $\alpha_H = 0{\cdot}10(2) \pm 0{\cdot}015$, $\alpha_D = 0{\cdot}14(5) \pm 0{\cdot}015$.

These give cross section per *atom* of the two gases, taking the camera temperature as 30°C, as $\sigma_H = (1{\cdot}6 \pm 0{\cdot}25) \times 10^{-18}\,\text{cm}^2$, $\sigma_D = (2{\cdot}3 \pm 0{\cdot}25) \times 10^{-18}\,\text{cm}^2$.

§ 4. SOURCES OF ERROR

The main part of the error in these experiments is due to the presence of residual gas in the chamber. Owing to the high value of cyclotron time the final vacuum connection could only be made shortly before the experiment and a trace of leakage or evolution of gas from taps and rubber connections was difficult to eliminate. The value of residual pressure was measured frequently between successive experiments and showed no rapid variations but it is impossible to be certain that the residual gas did not drop to an abnormally low value during the hydrogen run, so that its effect might be over-compensated. One experiment was performed with 1·55 mm of oxygen in the camera which gave a 'pure gas' attenuation coefficient of 1·8. Then a pressure of 0·04 mm, the normal residual gas pressure, would have given a coefficient of 0·04(8). Assuming the residual gas to behave similarly to oxygen, 0·04(8) of its gross coefficient of 0·12(8) will have been due to gas and 0·08(0) to slit edges, etc. It is not likely that the whole of the residual gas disappeared during the hydrogen run but was restored for both the following deuterium runs. The difference between deuterium and hydrogen may then be real.

§ 5. DISCUSSION OF RESULTS

It is interesting to compare our results with those given by Allison (1958). His tables V-8A and V-8B give the cross sections (σ_{01}) for ionization of hydrogen atoms in hydrogen gas up to energies of 1 MeV. In velocity our deuterium atoms will correspond to hydrogen atoms of 4 MeV. The curve of figure 3 is drawn from the data in Allison's paper; it can be seen that our cross section for ionization of deuterium in deuterium gas lies much closer to a reasonable extrapolation of the lower velocity hydrogen results than does our value for deuterium in hydrogen.

An interesting point, particularly in the D–D_2 collisions, is the question of what happens to the removed electron. Some of the simpler possible interactions are:

(*a*) $D + D_2 \rightarrow D^+ + e^- + D_2$
(*b*) $D + D_2 \rightarrow D + D_2^+ + e^-$
(*c*) $D + D_2 \rightarrow D^+ + D_2^-$
(*d*) $D + D_2 \rightarrow D^- + D_2^+$.

In each case the nearly stationary diatomic molecule or ion may undergo further disintegration but this would not be observable. Our measured cross sections represent a combination of the cross sections for (*a*) and (*c*). Reaction (*b*) we shall not observe except perhaps as a spreading of the neutral peak (figure 2) which would not be easily distinguished from the effect of elastic scattering. Reaction (*d*), however, we might hope to observe and its frequency of occurrence might give a hint as to the likely relative frequency of (*a*) and (*c*).

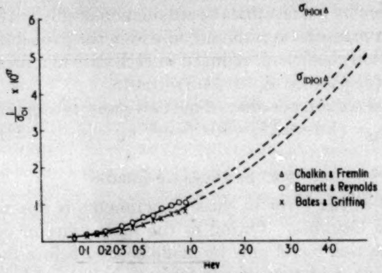

Figure 3.

We have searched for a negative beam on our plates, deflected to the opposite side of the neutral beam. No certain detection of negative particles has been made. With the gas pressures used, however, this does not enable us to set a very low cross section for their production. The cross section for electron loss by D⁻ ions is very high (Fremlin and Spiers 1955). In air at 8 Mev it is $2{\cdot}7 \times 10^{-16}$ cm^2, so that, even in the residual gas alone, most of the negative ions formed in the early part of the camera would be restored to neutrality before emergence. Until further experiments can be performed at lower pressures, we can only say that reaction (*d*) must be only a small fraction of (*a*) + (*c*) and that it is correspondingly likely that the main interaction observed is of type (*a*) with or without break-up of the D_2 molecule.

This is consistent with the results given by Allison, which show a cross section less than a tenth of that for producing positive ions at 30 kev and show also that this ratio is decreasing.

ACKNOWLEDGMENTS

We are grateful to the cyclotron operating staff, especially Messrs Stewart and Lilley, for their assistance with the experiments and for their patience during unsuccessful exposures. We are also grateful to Professor W. E. Burcham for much helpful comment and advice.

REFERENCES

ALLISON, S. K., 1958, *Rev. Mod. Phys.*, **30,** 1137.
BARNETT, C. F., and REYNOLDS, H. K., 1958, *Phys. Rev.*, **109**, 355.
BATES, D. R., and GRIFFING, G., 1953, *Proc. Phys. Soc.* A, **66,** 961.
CHALKLIN, L. P., and FREMLIN, J. H., 1956, *Proc. Phys. Soc.* A, **69,** 352.
FREMLIN, J. H., and SPIERS, V. M., 1955, *Proc. Phys. Soc.* A, **68,** 398.

γ-Radiation from Interaction of 14 Mev Neutrons

By W. M. DEUCHARS and D. DANDY
Atomic Weapons Research Establishment, Aldermaston, Berks.

Communicated by K. W. Allen; *MS. received 6th November* 1959,
in final form 7th December 1959

Abstract. Time-of-flight techniques have been applied to the measurement of γ-ray spectra from the interaction of 14 Mev neutrons with various nuclei. The results for carbon, water, magnesium, aluminium, nickel, copper and lead are presented and are compared with the results from other experiments using lower energy neutrons. Assignments are made for the reaction processes in the light nuclei and isotopic assignments are made for the medium- and heavy-weight nuclei.

---

§ 1. INTRODUCTION

THE application of the time-of-flight principle to fast neutron spectroscopy and in particular to the study of non-elastic scattering (Cranberg 1955, Batchelor and Towle 1959), has yielded valuable information about the low lying states of heavy nuclei and also in some cases light nuclei (Anderson *et al.* 1958).

However, the strength of neutron sources available from particle accelerators, and the limited time resolution obtainable with present day photomultipliers and scintillators, preclude accurate measurements at primary neutron energies greater than a few Mev. Thus the study of de-excitation γ-rays from the higher excited states is still a valuable technique for obtaining information about inelastic scattering processes for neutron energies greater than about 4 Mev.

Previous work in this field has been hampered by the high level of background radiation produced in the γ-ray detector (normally a NaI scintillation spectrometer) by neutrons which have been scattered from the sample. By using time-of-flight techniques we have been able to distinguish between neutrons and γ-rays from the scattering sample and hence have considerably reduced the background level. The application of time-of-flight technique to this type of measurement was first proposed by Cranberg (Day 1955) and used by Day (Freeman 1957).

An excellent review of this type of measurement is given by Day (1955) and many examples of the results obtained appear in the review articles by Ajzenberg-Selove and Lauritsen (1959) and Endt and Braams (1957).

This paper presents the results obtained from the investigation of the spectrum of γ-rays produced in the interaction of 14 Mev neutrons with carbon, water, magnesium, aluminium, nickel, copper and lead.

§ 2. EXPERIMENTAL TECHNIQUE AND APPARATUS

2.1. *General Description*

The neutron source consisted of a solid Ti – T target, obtained from the Atomic Energy Research Establishment, Harwell, bombarded with 500 kev deuterons from the 800 kev Cockcroft–Walton accelerator at the Atomic Weapons Research Establishment. The 14 Mev neutrons were produced in the reaction $T(d, n)^4He$. The neutron flux was measured by detection of the associated α-particle from this reaction. A copper shadow bar, 1½ in. diameter × 30 in. long, shielded the detector from direct source neutrons, and the scatterer, in the form of an annulus, was situated so that its axis coincided with the direction of the deuteron beam incident on the target. The scatterer was placed as close as possible to the target to ensure a maximum neutron flux through it. The normal dimensions of the scattering samples were 7 in. o.d., 3 in. i.d., 2 in. thick. Figure 1 shows a schematic diagram of the experimental apparatus.

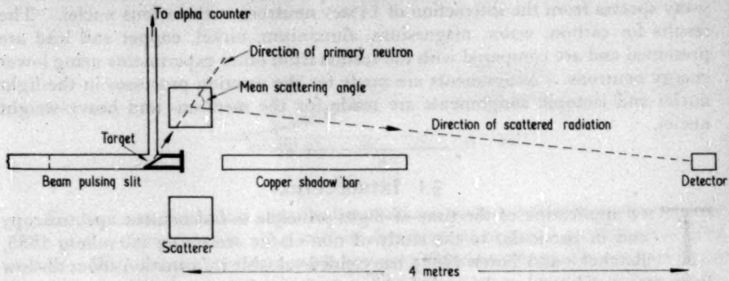

Figure 1. Schematic diagram of experimental apparatus.

The γ-ray detector consisted of a 1¾ in. diameter × 2 in. long sodium iodide crystal mounted on an RCA 6342 photomultiplier. It was shielded from extraneous background by a large water tank and additional lead shielding. The source–detector distance was 4 metres.

2.2. *Time-of-flight Apparatus*

The time-of-flight section of the apparatus was similar in principle to that first described by Cranberg (1955). No detailed account of the apparatus will be given in this paper except in so far as it relates to the application of these techniques to γ-ray spectroscopy.

In the present case stringent requirements on the time resolution of the apparatus were not essential as it was only necessary to distinguish between γ-rays and the secondary neutrons produced by interaction of the primary neutrons with the scattering sample. Thus over a flight path of 4 metres a time resolution of 20 ns(mμsec) was adequate. This enabled the time duration of the primary neutron pulse to be increased and hence increased the neutron flux incident on the scatterer.

2.3. *Electronic Apparatus*

A block diagram of the electronic apparatus is shown in figure 2. The principle of operation was briefly as follows. A fast pulse from the anode of the photomultiplier was amplified by two Harwell-type distributed amplifiers in series and fed into a time-to-pulse height converter (time sorter). When the output of the time sorter was displayed on a kicksorter we obtained a double presentation (figure 3) of the time spectrum due to the fact that we only derived one timing pulse per r.f. cycle but obtained two neutron pulses per cycle due to

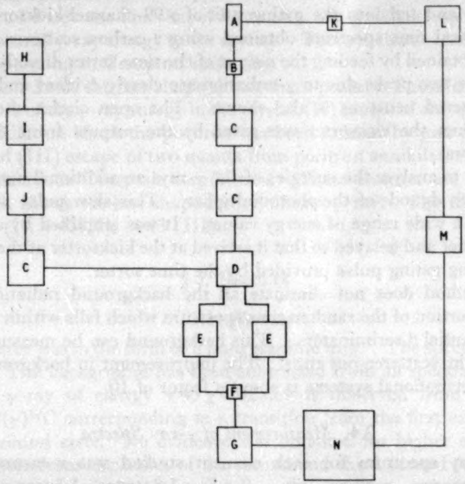

Figure 2. Block diagram of electronic apparatus. A, detector; B, fast head amplifier; C, distributed amplifier; D, time sorter; E, single channel analyser; F, mixer; G, gate of kicksorter; H, r.f. oscillator; I, shaping unit; J, variable delay; K, cathode follower; L, linear amplifier; M, fixed delay; N, kicksorter.

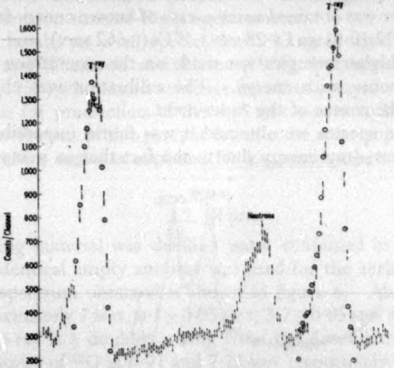

Figure 3. Time spectrum ungated and gated for carbon scatterer.

successive transversal, in opposite directions, of the deuteron beam across the defining slit. By using two differential discriminators set at different bias levels we were able to select only those pulses from the detector which arose from detection of γ-radiation from the scatterer. The outputs of the differential discriminators were mixed and fed into the gating unit of a 99-channel kicksorter. Figure 3 shows a typical time spectrum obtained using a carbon scatterer. The broken curve was obtained by feeding the output of the time sorter directly into the kicksorter. The two peaks due to γ-radiation are clearly evident and a single peak due to scattered neutrons is also shown. The open circles show the results obtained when the kicksorter was gated by the outputs from the differential discriminators.

In order to analyse the energies of the γ-rays an additional output was taken from the fifth dynode of the photomultiplier. This slow pulse was linear with energy over a wide range of energy values. It was amplified by a conventional linear amplifier and delayed so that it arrived at the kicksorter at the middle of the corresponding gating pulse provided by the time sorter.

This method does not eliminate all the background radiation as we still record the portion of the random time spectrum which falls within the bias levels of the differential discriminators. This background can be measured by means of scatterer-in–scatterer-out runs. The improvement in background level over the more conventional systems is about a factor of 10.

2.4. *Measurement of γ-ray Spectra*

The γ-ray spectrum for each element studied was measured over three different energy regions viz. $0 < E_\gamma < 1{\cdot}8$ MeV; $1{\cdot}5$ MeV $< E_\gamma < 4{\cdot}5$ MeV; $4{\cdot}0$ MeV $< E_\gamma \leqslant$ maximum energy.

Each spectrum was obtained by 'scatterer-in–scatterer-out' subtractions and the runs monitored by detection of the associated α-particle from the reaction $T(d, n)^4He$ and also by means of a current integrator. The energy calibration of the spectrometer was obtained using γ-rays of known energy from the following radio-nuclides: ^{22}Na(0·51 and 1·28 MeV), ^{137}Cs(0·662 MeV), and RaTh(2·62 MeV). Extrapolation to higher energies was made on the assumption that the counter had a linear response with energy. The calibration was checked at regular intervals during the course of the experiment.

In most of the spectra we obtained it was found impossible to analyse the results above 4 MeV γ-ray energy due to the fact that so many different energy

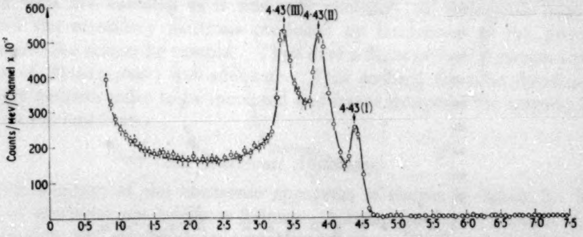

Figure 4. γ-radiation from interaction of 14 MeV neutrons with carbon.

γ-rays were present in the spectrum. However, it was possible to make an analysis of the low-energy regions and in this case we used the line shapes obtained from the calibration γ-rays. The line shape for a particular γ-ray energy was obtained by extrapolation.

When $E_\gamma \lesssim 1{\cdot}5$ MeV the line shape shows only one peak corresponding to the capture of the total γ-ray energy in the crystal. There is also a continuous distribution corresponding to Compton scattering.

When $E_\gamma \gtrsim 1{\cdot}5$ MeV the line shape shows three peaks. These correspond to: (I) total capture of the γ-ray energy in the crystal, (II) escape of one quantum from positron annihilation where the positron has been formed by pair production in the crystal and (III) escape of two quanta from positron annihilation. As before there is a continuous Compton distribution. These features are illustrated in figure 4 which shows the line shape for a 4·43 MeV γ-ray. The three peaks are labelled 4·43 (I), 4·43(II), 4·43 (III).

§ 3. Results

3.1. *Carbon*

The scatterer was in the form of a pure graphite ring. The spectrum is shown in figure 4. The background has been subtracted from all spectra presented.

A single γ-ray of energy $4{\cdot}43 \pm 0{\cdot}02$ MeV is observed from the reaction ^{12}C(n, n′)^{12}C(γ)^{12}C corresponding to a transition from the first excited state of ^{12}C to the ground state. No evidence was obtained for higher energy γ-rays which may arise from excitation of the second and third excited states of ^{12}C at 7·6 and 9·6 MeV respectively.

However the inelastic neutron spectrum from the 14 MeV neutron interaction with carbon shown in figure 5 indicates that the third excited state at 9·6 MeV is excited and hence this level must decay by α-particle emission to ^{8}Be or directly to three α-particles. The neutron spectrum shown in figure 5 was obtained using a conventional neutron time-of-flight spectrometer.

The present results on γ-ray spectra from ^{12}C agree with those of Battat and Graves (1955) and Thomson and Risser (1954), but not with the results of Scherrer *et al.* (1953) who found evidence for other γ-rays. We have estimated the cross section for production of the 4·43 MeV γ-rays to be $0{\cdot}29 \pm 0{\cdot}05$ barn. The angular distribution of this γ-ray is found to be anisotropic but is symmetric about 90° scattering angle as expected for a transition between states of well-defined parity.

3.2. *Water*

The scattering material was distilled water contained in a thin-walled steel annulus. An identical empty annulus was used for the measurement of background. The spectrum obtained is shown in figure 6. Analysis shows γ-rays of energy approximately 7 MeV, $6{\cdot}1 \pm 0{\cdot}05$ MeV, $3{\cdot}7 \pm 0{\cdot}05$ MeV and $2{\cdot}23 \pm 0{\cdot}08$ MeV.

The 7 MeV γ-ray is a doublet arising from the de-excitation of the third and fourth excited states of ^{16}O at 6·91 and 7·12 MeV respectively. The shape of the high-energy portion of figure 6 precludes the assignment of a single γ-ray to this energy and the best fit to the observed shape is obtained by assuming that two γ-rays of energy 7·12 and 6·91 MeV are present in about equal intensity. The 6·1 MeV γ-ray corresponds to a transition from the second excited state of ^{16}O to the ground state. In figure 6 the three peaks corresponding to the 6·1 MEV γ-ray are marked 6·1 (I), 6·1 (II) and 6·1 (III). We were unable to detect any annihilation radiation due to the emission of positron–electron pairs from the first excited state of ^{16}O. This level is known to have spin and parity assignment 0^+ and hence cannot decay by direct γ-transition to the ground state, which is also 0^+.

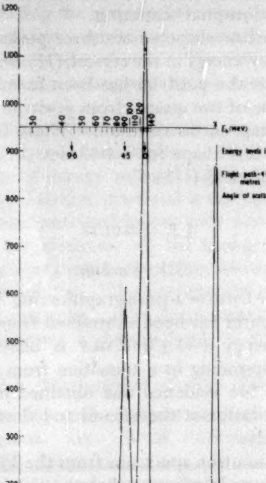

Figure 5. Time spectrum for carbon scatterer.

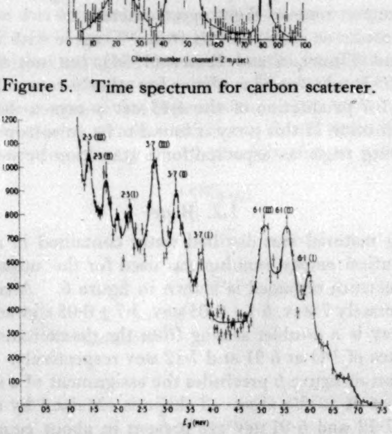

Figure 6. γ-radiation from interaction of 14 MEV neutrons with water.

The 3·7 MeV γ-ray has been assigned to the reaction $^{16}O(n, \alpha)^{13}C^*$ in which the second excited state of ^{13}C at 3·68 MeV is excited. This assignment is in agreement with the results on the observation of α-particles from the (n, α) reaction (Lillie 1952). If this γ-ray is due to a cascade transition in ^{16}O then intensity considerations show that the 6·1 MeV level must be involved in the cascade. Thus the initial state must be at approximately 9·8 MeV. The known 9·84 MeV level in ^{16}O has spin and parity 2^+ and hence can decay by α-emission to ^{12}C in preference to decay by γ-ray emission. This is observed experimentally (Ajzenberg-Selove and Lauritsen 1959). On these considerations we can rule out the assignment of the 3·7 MeV γ-ray to a cascade transition in ^{16}O. The three peaks corresponding to the 3·7 MeV γ-ray are shown in figure 6.

We do not observe any definite evidence for the excitation of the first excited state of ^{13}C at 3·0 MeV as found in the α-particle spectrum, although the small peak at $E_\gamma = 2·0$ MeV may be due to the 'two escape' annihilation peak from a 3·0 MeV γ-ray, the other two peaks at 2·5 and 3·0 MeV being masked by the more intense radiation from the 3·7 MeV γ-ray.

The 2·23 MeV γ-ray can probably be assigned to the reaction $n + p \rightarrow d + \gamma$ (2·23 MeV) as hydrogen is present in the distilled water.

3.3. *Magnesium*

The scattering material was natural magnesium containing 78% ^{24}Mg, 11% ^{25}Mg and 11% ^{26}Mg.

The γ-ray spectra obtained are shown in figures 7 (*a*)–(*d*). The ordinate on the left-hand side refers to both graphs and the energy ordinates lie to the right of each graph. The energy of any peak can be read off from the graph.

We have analysed the results for $E_\gamma < 4·5$ MeV. The region between 4 MeV and the maximum energy detected at about 10 MeV shows signs of definite structure but is so complicated that we have not attempted any detailed analysis. The table lists all the γ-rays found in the energy region $0 < E_\gamma < 4·5$ MeV. Also listed are comparison results from other measurements, the proposed reaction mechanism, the transition between levels of the final nucleus (e.g. $(1) \rightarrow (0)$ implies a transition from the first excited state to the ground state) and the energy of the transition taken from the review article by Endt and Braams (1957).

The high intensity of the 1·37 MeV γ-ray indicates that the majority of cascade transitions from higher excited states in ^{24}Mg proceed through this level. The cross section for production of this γ-ray is estimated to be $0·55 \pm 0·1$ barn.

In general the results obtained are in agreement with those obtained from other reactions.

It will be seen from the table that this experiment has revealed some new γ-rays; in particular no previous evidence had been found for the (nα) or (nd) reactions in ^{24}Mg.

3.4. *Aluminium*

The γ-ray spectrum obtained using an aluminium scatterer is shown in figure 8. The table gives the energy of γ-rays detected for $E_\gamma \leqslant 3.0$ MeV. The spectrum extends up to $E_\gamma \sim 12$ MeV but the high level density of ^{27}Al produces an apparent continuum of γ-rays in the higher energy region. The results in the table have been compared with those of other experiments. The agreement in general is satisfactory. It should be noted that the results of Benveniste *et al.*†

---

†Benveniste, Mitchell, Schrader and Zenger, 1958. Report to the A.E.C. Nuclear Cross Sections Advisory Group (Wash.–1006), p. 34.

using 14 MeV neutrons, were obtained using a similar technique to that described in this paper.

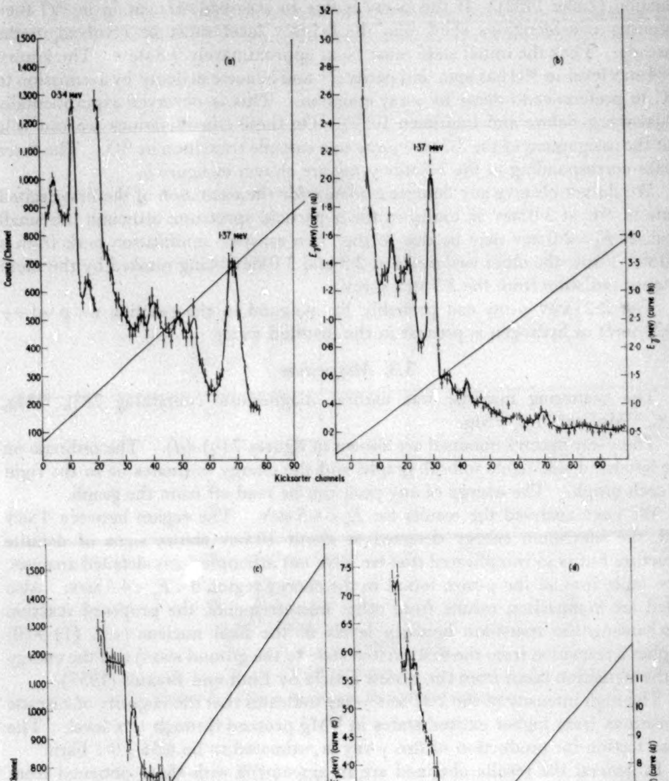

Figure 7. γ-radiation from interaction of 14 MeV neutrons with magnesium.

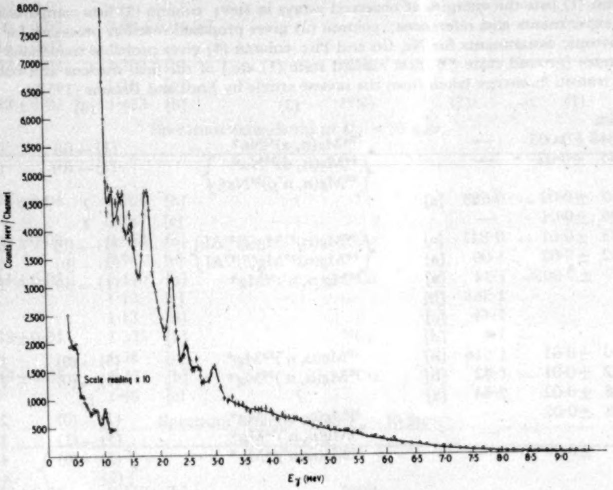

Figure 8. γ-radiation from interaction of 14 MEV neutrons with aluminium.

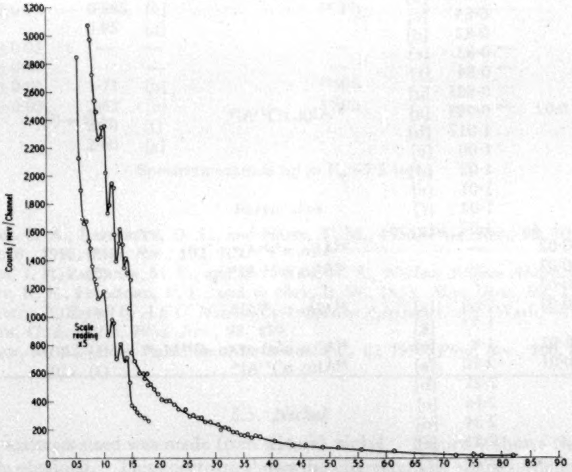

Figure 9. γ-radiation from interaction of 14 MEV neutrons with nickel.

γ-radiation from Interaction of 14 Mev Neutrons

Column (1) lists the energies of observed γ-rays in Mev; column (2) lists comparison results of other experiments and references; column (3) gives proposed reaction processes for Mg and Al and isotopic assignments for Ni, Cu and Pb; column (4) gives probable transitions between excited states [ground state (0), first excited state (1) etc.] of the final nucleus and column (5) gives the transition energy taken from the review article by Endt and Braams (1957).

(1)	(2)		(3)	(4)	(5)
Magnesium					
0·345 ± 0·003	—		^{24}Mg(n, α)^{21}Ne*	(1) → (0)	0·347
0·45 ± 0·02	—		^{24}Mg(n, d)^{23}Na* ^{24}Mg(n, n′p)^{23}Na*	(1) → (0)	0·439
0·67 ± 0·02	0·688	[a]	?	?	?
0·76 ± 0·01	—		?	?	?
0·85 ± 0·01	0·837	[a]	^{26}Mg(n)^{27}Mg(β)^{27}Al	(1) → (0)	0·842
1·02 ± 0·02	1·00	[a]	^{26}Mg(n)^{27}Mg(β)^{27}Al	(2) → (0)	1·013
1·37 ± 0·005	1·34	[a]	^{24}Mg(n, n′)^{24}Mg*	(1) → (0)	1·368
	1·368	[b]			
	1·41	[c]			
	1·4	[d]			
1·60 ± 0·01	1·616	[b]	^{25}Mg(n, n′)^{25}Mg*	(3) → (0)	1·61
1·82 ± 0·01	1·82	[b]	^{26}Mg(n, n′)^{26}Mg*	(1) → (0)	1·83
2·48 ± 0·02	2·44	[a]	?	?	?
2·78 ± 0·02	—		^{24}Mg(n, n′)^{24}Mg*	(2) → (0)	2·754
~3·9	—		^{24}Mg(n, n′)^{24}Mg*	(5) → (1)	3·87
<4·2 ± 0·05	—		^{24}Mg(n, n′)^{24}Mg*	(3) → (0) (2)	4·24 4·12

Spectrum shows unresolvable structure between $E_\gamma \sim 4$ Mev and E_γ(max.) ~ 10 Mev.

Aluminium					
0·84 ± 0·02	0·843	[a]	^{27}Al(n, n′)^{27}Al*	(1) → (0)	0·842
	0·840	[b]			
	0·84	[c]			
	0·82	[d]			
	0·83	[e]			
	0·84	[f]			
	0·835	[g]			
1·01 ± 0·02	0·988	[a]	^{27}Al(n. n′)^{27}Al*	(2) → (0)	1·013
	1·017	[b]			
	1·00	[c]			
	1·02	[d]			
	1·01	[e]			
	1·02	[f]			
	1·02	[g]			
1.18 ± 0·02	—		^{27}Al(n, n′)^{27}Al*	(3) → (2)	1·195
1·33 ± 0·02	—		^{27}Al(n, n′)^{27}Al*	(3) → (1)	1·346
1·51 ± 0·02	?		?	?	?
1·72 ± 0·03	1·69	[a]	^{27}Al(n, n′)^{27}Al*	(4) → (2)	1·716
	1·72	[g]			
1·80 ± 0·03	1·8	[e]	^{27}Al(n, n′p) or (n, d)^{26}Mg*	(1) → (0)	1·85
2·21 ± 0·01	2·10	[a]	^{27}Al(n, n′)^{27}Al*	(3) → (0)	2·208
	2·21	[b]			
	2·16	[c]			
	2·34	[d]			
	2·23	[e]			
	2·27	[f]			
	2·22	[g]			
2·99 ± 0·01	3·0	[e]	^{27}Al(n, n′)^{27}Al*	(6)	2·999
	3·1	[f]		(5) → (0)	2·976

Maximum energy observed is $E_\gamma \sim 12$ Mev.

	(1)	(2)	(3)	(4)	(5)
Nickel					
	0·69 ± 0·03	—		—	—
	1·00 ± 0·02	0·90 ± 0·04 [g]		—	—
	1·16 ± 0·02	—		—	—
	1·32 ± 0·02	1·329 [b]	^{60}Ni	—	—
		1·36 [g]		—	—
	1·43 ± 0·02	1·453 [b]	^{58}Ni	—	—
		Spectrum extends up to E_γ ~10 MEV.			
Copper					
	0·76 ± 0·04	0·764 [b]	?	—	—
		0·78 [c]			
	0·96 ± 0·02	0·958 [b]	^{63}Cu	—	—
		0·96 [c]			
	1·14 ± 0·02	1·110 [b]	^{65}Cu	—	—
		1·12 [c]			
		1·13 [d]			
	1·33 ± 0·03	1·325 [b]	^{63}Cu	—	—
		1·38 [c]			
	1·49 ± 0·05	1·47 [b]	^{65}Cu	—	—
		1·46 [c]			
		Spectrum extends up to E_γ ~ 10 MEV.			
Lead					
	0·53 ± 0·05	0·533 [b]	^{206}Pb	—	—
	0·57 ± 0·05	0·570 [b]	^{207}Pb	—	—
	0·64 ± 0·02	0·661 [b]	^{206}Pb	—	—
	0·80 ± 0·02	0·802 [b]	^{206}Pb	—	—
		0·79 [f]			
	0·88 ± 0·02	0·888 [b]	^{207}Pb		
		0·85 [g]			
	1·01 ± 0·03	— —	—	—	—
	1·07 ± 0·03	— —	—	—	—
	1·70 ± 0·03	1·73 [b]	^{206}Pb	—	—
	2·60 ± 0·03	2·62 [b]	^{208}Pb	—	—
		2·70 [f]			
		2·60 [g]			
		Spectrum extends up to E_γ ~ 7·5 MEV.			

REFERENCES

[a] RAYBURN, L. A., LAFFERETY, D. L., and HAHN, T. M., 1955, *Phys. Rev.*, **98**, 701.
[b] DAY, R. B., 1956, *Phys. Rev.*, **102**, 767.
[c] BARCHUK, I. F., PASCHNIK, M. V., and TSYBULKO, IV. A., *Nuclear Science Abstracts*, 12/8135.
[d] GARRETT, R. E., HEREFORD, F. L., and SLOOPE, B. W., 1953, *Phys. Rev.*, **92**, 1507.
[e] BENVENISTE, J., *Report by A.E.C. Nuclear Cross Section Advisory Group* (Wash.—1006), p. 34.
[f] GRIFFITH, G. L., 1955, *Phys. Rev.*, **98**, 579.
[g] ROTHMAN, M. A., HANS, H. S., and MANDEVILLE, C. E., 1955, *Phys. Rev.*, **100**, 83.

3.5. *Nickel*

The scatterer used was made from natural nickel. Figure 9 shows the γ-ray spectrum obtained. This spectrum shows the characteristic shape obtained from medium- and heavy-weight nuclei, i.e. a continuum of γ-rays extending up to E_γ ~ 10 MEV with discrete low-energy γ-ray lines superimposed on the continuum.

The energy of the discrete lines are given in the table in which we include comparison results from other experiments. The isotopic assignments given in the table were obtained by comparison of the present results with those given by Day (1956).

3.6. *Copper*

The results obtained using a copper scatterer are similar to those obtained for nickel. The energy of discrete γ-rays observed are listed in the table.

3.7. *Lead*

Using a natural lead scatterer we obtained the spectrum shown in figure 10. The closed shell nature of lead nuclei means that the energy levels are more widely spaced than in other heavy nuclei and this is shown by the structured γ-ray spectrum observed.

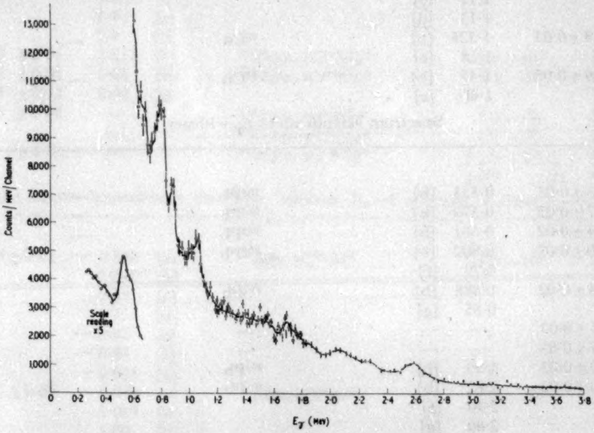

Figure 10. γ-radiation from interaction of 14 MEV neutrons with lead.

The table lists the energy of γ-rays detected and gives comparison results from other experiments.

§ 4. CONCLUSION

The present experiment has demonstrated the applicability of time-of-flight techniques to γ-ray spectroscopy. It should be feasible to apply this technique to experiments of the form (d, nγ) or (^{3}He, nγ) etc. in which it is necessary to discriminate between neutrons and γ-rays.

ACKNOWLEDGMENTS

The authors wish to thank Dr. K. W. Allen for his encouragement and advice. We are indebted to Mr. M. Grant for his assistance in performing the experiments and to the operators of the Cockcroft–Walton accelerator for their efficient running of the machine.

References

Anderson, J. D., Gardner, C. C., McClare, J. W., Nakada, M. P., and Wong, C., 1958, *Phys. Rev.*, **111**, 572.

Ajzenberg-Selove, F., and Lauritsen, T., 1959, *Nucl. Phys.*, **11**, 1.

Batchelor, R., and Towle, J. H., 1959, *Proc. Phys. Soc.*, 73, 193.

Battat, M. E., and Graves, E. R., 1955, *Phys. Rev.*, **97**, 1266.

Cranberg, L., 1955, *Proceedings of the International Conference on the Peaceful Uses of Atomic Energy* (New York: United Nations), Vol. 4, paper 577.

Day, R. B., 1955, *Proceedings of the International Conference on the Peaceful Uses of Atomic Energy* (New York: United Nations), Vol. 2, paper 581.

—— 1956, *Phys. Rev.*, **102**, 767.

Endt, P. M., and Braams, C. M., 1957, *Rev. Mod. Phys.*, **29**, 683.

Freeman, J., 1957, *Proceedings of the International Conference on the Neutron Interactions with the Nucleus* (New York: Columbia University), p. 173.

Lillie, A. B., 1952, *Phys. Rev.*, **87**, 716.

Scherrer, V. E., Theus, R. B., and Faust, W. R., 1953, *Phys. Rev.*, **91**, 1476.

Thomson, L. C., and Risser, J. R., 1954, *Phys. Rev.*, **94**, 941.

Deuteron Stripping with Polarized Deuterons

By B. HIRD and A. STRZAŁKOWSKI
Nuclear Physics Research Laboratory, University of Liverpool

Communicated by the late H. W. B. Skinner; *MS. received* 26*th November* 1959,
in final form 11*th January* 1960

Abstract. The left–right stripping asymmetry of the ground state, and the first excited state proton groups, has been measured at several angles of emission, when a ^{9}Be target was bombarded with 6 Mev deuterons which had been polarized by elastically scattering them from carbon. Measurements have also been made at two angles of the ^{40}Ca (dp) ^{41}Ca ground state group asymmetry.

The results confirm that polarization effects in stripping are caused predominantly by the central part of the deuteron and proton distorting potentials. The opposite sign of the ^{9}Be (dp) ^{10}Be ground state and first excited state asymmetries enables an unambiguous mixing ratio for the j_{n} values possible in stripping to the first excited state, to be assigned.

§ 1. INTRODUCTION

The Butler theory of deuteron stripping has been extended by several authors to include the effects of the various interactions which occur between the incoming deuterons and the target nucleus, and the emitted protons and the final nucleus (Horowitz and Messiah 1953, Tobocman and Kalos 1955, Cheston 1954). One of the most easily observable consequences of these interactions is that the emitted protons are polarized (Newns 1953). Without them the simple stripping theory always gives zero polarization. Measurements of this polarization are therefore a measure of the importance of these interactions.

Considerable simplification occurs in the theory if the spin dependences of the deuteron and proton interactions are neglected. Though these are certainly present, the central forces predominate and the consequences of this approximation should be qualitatively correct. Certain simple rules then emerge, which may be tested by experiment. (*a*) The polarization can never exceed $\frac{1}{3}$. (*b*) The sign of the polarization is opposite for stripping reactions where $j_{\mathrm{n}} = l_{\mathrm{n}} + \frac{1}{2}$ to those where $j_{\mathrm{n}} = l_{\mathrm{n}} - \frac{1}{2}$ (Huby, Refai and Satchler 1958). (*c*) The left–right asymmetry, produced when polarized deuterons are stripped, is simply related to the polarization which the same stripping reaction produces in the emitted protons, when unpolarized deuterons are used. This asymmetry is given by $3P_{\mathrm{d}}P_{\mathrm{p}}$. Here only the vector part of the deuteron polarization is involved and P_{d} is the component of this polarization perpendicular to the reaction plane and parallel to P_{p} (Satchler 1958, Appendix).

Experimentally, the sign of the polarization is found to agree with the rule, being positive when $j_{\mathrm{n}} = l_{\mathrm{n}} + \frac{1}{2}$, and negative when $j_{\mathrm{n}} = l_{\mathrm{n}} - \frac{1}{2}$, except for one reaction, ^{40}Ca (dp) ^{41}Ca (Hird, Cookson and Bokhari 1958). On the other hand polarizations considerably greater than $\frac{1}{3}$ have been found. This is only to be expected away from the stripping peak where processes other than stripping probably are important.

This paper describes measurements to investigate the validity of rule (*c*) by determining the left–right stripping asymmetry at several angles, when targets of beryllium and calcium were bombarded with polarized deuterons. These polarized deuterons had an energy of 6 MeV and were produced by first scattering elastically the deuterons from a carbon target. The polarization properties of these deuterons have been investigated in a separate series of measurements using double deuteron elastic scattering. These will be described in a separate paper. It was originally hoped that only the vector type of polarization would be present in the scattered deuterons, but it appears from the double scattering results that there may be also considerable tensor polarization. If the central force approximation should turn out to be a reasonable assumption in stripping, a measurement of the stripping asymmetry may provide a method of determining the vector part of the polarization in deuteron beams when higher order polarizations are also present.

§ 2. EXPERIMENTAL DETAILS AND RESULTS

The apparatus was similar to that used in the proton elastic scattering measurements previously reported (Al-Jeboori *et al.* 1959). A graphite target was inserted in the last few orbits of the circulating deuteron beam of the 37 in. cyclotron. Particles from this target emerged through a suitably placed hole in the side wall of one of the dees, and were focused on to a second target outside the cyclotron, where the asymmetry produced in some subsequent reaction could be measured with counter telescopes. When this system was originally set up to provide a source of polarized protons, using the polarization properties of the ground state group of the reaction $^{12}C(dp)^{13}C$, it was noticed that there was considerable deuteron contamination present in the beam. In the proton scattering measurements, precautions had to be taken to prevent these deuterons from producing counts in the counter telescopes. By making slight adjustments to the position of the internal target and changing the magnetic focusing to select particles of higher momentum, it proved possible to collect scattered deuterons, with the proton component entirely eliminated. The energy of these deuterons, measured by exposing nuclear emulsion at the point where the second target was normally placed, was found to be 6·0 MeV ± 0·2 MeV. Since the first excited state of ^{12}C is at 4·4 MeV, and the circulating beam, when it struck the internal target, had an energy of about 8 MeV, these deuterons could only be the result of elastic scattering; the loss of energy being due to the thickness of the internal target.

The beryllium target, used in the stripping experiments, consisted of a self-supporting foil 0·003 in. thick of 98% purity beryllium metal. The calcium target was made by rolling flakes of the metal down to a thickness of about 12 mg cm^{-2}. The oxide layer which formed on the latter target was unimportant, because of the much lower stripping *Q*-values of oxygen, so that this element was only capable of producing small pulses in the counter telescopes, and these were not included in the asymmetry calculations.

At the two smallest angles of measurement with the $^{9}Be\ (dp)\ ^{10}Be$ reaction a definite, though not very clear, subsidiary peak was present in the pulse height distribution (figure 1). This was attributed to stripping to the first excited state. The breadth of the subsidiary peak is consistent with the nonlinearity to be expected in the counter telescopes, where a considerable proportion of the energy is lost in windows and in the proportional counter before the protons reach the CsI scintillator.

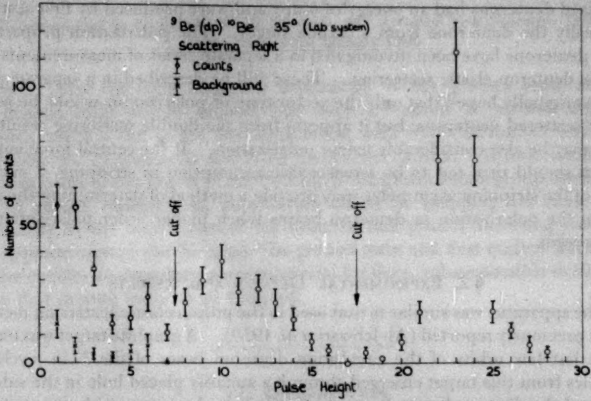

Figure 1. The pulse height distribution produced in one of the counter telescopes by protons stripped from 6 MeV deuterons in the reaction ^{9}Be (dp) ^{10}Be.

The results are shown in the table; figure 2 shows graphically the asymmetries obtained from the ^{9}Be (dp) ^{10}Be measurements. The angular resolution was about ±2°, mainly due to the target and counter widths.

(1)	(2)	(3)		(4)		(5)
^{9}Be (dp) ^{10}Be		L	R	L	R	
ground state	35	341	497	296	341	$+0{\cdot}128 \pm 0{\cdot}026$
	45	232	350	246	424	$+0{\cdot}234 \pm 0{\cdot}028$
	55	159	364	106	232	$+0{\cdot}414 \pm 0{\cdot}039$
	65	125	165	133	141	$+0{\cdot}084 \pm 0{\cdot}042$
	75	127	116	148	121	$-0{\cdot}073 \pm 0{\cdot}053$
^{9}Be (dp) ^{10}Be						
1st excited state	35	399	279	340	246	$-0{\cdot}169 \pm 0{\cdot}031$
	45	167	187	257	142	$-0{\cdot}119 \pm 0{\cdot}064$
^{40}Ca (dp) ^{41}Ca	40	318	295	444	419	$-0{\cdot}033 \pm 0{\cdot}027$
	60	217	138	199	288	$-0{\cdot}021 \pm 0{\cdot}036$

(1) Reaction; (2) angle in laboratory system (deg); (3) number of counts left and right with the frame upright; (4) number of counts left and right with the frame inverted; (5) stripping left–right asymmetry.

The effect of a rapid angular variation of the stripping cross section was considered. This displaces the mean angle of a measurement slightly from the geometrically calculated one. These displacements were calculated to be of the order of 0·1° and were therefore neglected.

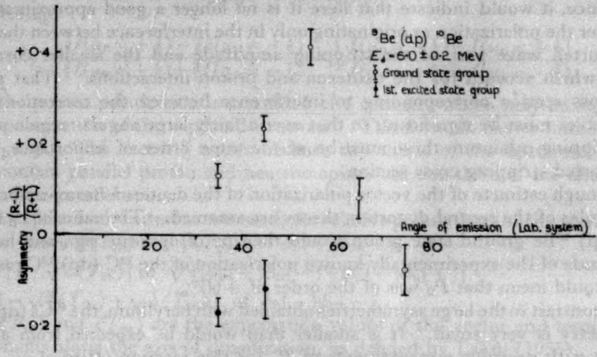

Figure. 2. The angular variation of the left–right asymmetry in the protons emitted from the reaction ^{9}Be (dp) ^{10}Be at 6·0 ± 0·2 MeV.

§ 3. Discussion

The large magnitude of the beryllium asymmetries indicates that considerable vector polarization was present in the deuteron beam. It is unlikely that the tensor part of the deuteron polarization, acting through the relatively small spin dependent part of the distorting potentials, could produce such asymmetries.

The opposite sign for the asymmetry of the two proton groups, together with the angular correlation measurements of Taylor (1959), gives an unambiguous value to the mixing ratio of the two j_n values possible in stripping to the first excited state (Satchler, private communication). From the angular correlation measurements, the ratio of $j_n = l_n + \frac{1}{2}$ to $j_n = l_n - \frac{1}{2}$ is either 2·65 or 0·38. The ground state transition is entirely $j_n = l_n + \frac{1}{2}$, so that the opposite sign of the asymmetry for the first excited state means that the transition must be predominantly $j_n = l_n - \frac{1}{2}$ and therefore the smaller of the two mixing ratios is the correct one.

The sign difference also confirms that the asymmetry is produced more by the central distortions in the stripping than directly through the spin dependence of the distorting potentials, since the latter would give the same asymmetry sign whatever the direction of the neutron spin coupling.

The angular distribution of the ^{9}Be (dp) ^{10}Be asymmetry is very similar in shape to the polarization angular distribution P_p measured for the ^{12}C (dp) ^{13}C reaction at 8·9 MeV. Both show an increase at angles beyond the peak in the differential cross section. and then a rapid fall and a change of sign at an angle near to the first minimum in the differential cross section. There is a slight difference, in that, whereas this sign change was within a degree or so of the stripping minimum as given by the Butler theory in the case of the ^{12}C (dp) ^{13}C polarization, in the ^{9}Be (dp) ^{10}Be asymmetry it occurs at an angle larger by about 12° than the theoretical stripping minimum. This could be due to the wrong choice of stripping radius, $5{\cdot}7 \times 10^{-13}$ cm (Holt and Marsham 1953) which is determined from the position of the maximum in the stripping cross section. However, it seems too large a discrepancy to be accounted for in this way. If this is a genuine difference, it would indicate that here it is no longer a good approximation to consider the polarization as originating only in the interference between the main, undistorted wave part of the stripping amplitude and the smaller correction terms which account for the deuteron and proton interactions. That part of the cross section corresponding to interference between the correction terms themselves must be significant, so that over a fairly large angular region around the stripping minimum these must be of the same order of importance as the undistorted stripping cross section.

A rough estimate of the vector polarization of the deuteron beam can be made if the rules of the central distortion theory are assumed. The value of P_p for the ^{9}Be (dp) ^{10}Be ground state group would then be of opposite sign and half the magnitude of the experimentally known polarization of the ^{12}C (dp) ^{13}C reaction. This would mean that P_d was of the order of $+60\%$.

In contrast to the large asymmetries obtained with beryllium, the ^{40}Ca (dp) ^{41}Ca asymmetry is very small. It is smaller than would be expected from a comparison with previous measurements of P_p for this reaction (Hird *et al.* 1958). This, together with the anomalous sign of P_p seems to indicate that the non-central character of the distortions may be more than usually important in this reaction.

ACKNOWLEDGMENTS

The authors wish to thank Dr. R. Huby for reading the appendix, and Dr. G. R. Satchler for the private communication. They also wish to thank Mr. M. S. Bokhari and Mr. M. A. Al-Jeboori for assistance in taking the readings.

APPENDIX

It is possible to derive all the rules of the central distortion theory without having to work with the scattering amplitudes, and by merely using cross sections. This enables a physical meaning to be given in each step in the derivation.

All spin $\frac{1}{2}$ polarization vectors are perpendicular to the plane of the reaction when parity is conserved, so that by taking this direction as the axis of quantization, nucleon polarization may be expressed in terms of the relative numbers of spins in the positive and negative directions.

If it is assumed that the distorting forces acting on the deuteron and proton are central, then the only spin dependence in the whole stripping process is the neutron capture. It is therefore possible to analyse all the polarization effects in terms of two stripping differential cross sections, one for each neutron spin direction. Denote these by $I(\mu_n = +\frac{1}{2})$ and $I(\mu_n = -\frac{1}{2})$.

The incoming deuterons consist of a mixture of three spin states, the relative amounts of which determine the deuteron polarization. These spin states can be expressed in terms of proton and neutron spin wave functions, $\phi_p(+)\phi_n(+)$, $\sqrt{\frac{1}{2}}/[\phi_p(+)\phi_n(-)+\phi_p(-)\phi_n(+)]$ and $\phi_p(-)\phi_n(-)$. If there is no polarization the populations of all three states are equal, and the stripping cross section is

$$I_0 = \tfrac{1}{3}[|\phi_p(+)\phi_n(+)|^2 I(\mu_n = +\tfrac{1}{2}) + \tfrac{1}{2}|\phi_p(+)\phi_n(-)|^2 I(\mu_n = -\tfrac{1}{2}) \\ + \tfrac{1}{2}|\phi_p(-)\phi_n(+)|^2 I(\mu_n = +\tfrac{1}{2}) + |\phi_p(-)\phi_n(-)|^2 I(\mu_n = -\tfrac{1}{2})].$$

The proton polarization P_{p} is defined as

$$P_{\mathrm{p}}=\frac{I_0(\mu_{\mathrm{p}}=+\tfrac{1}{2})-I_0(\mu_{\mathrm{p}}=-\tfrac{1}{2})}{I_0(\mu_{\mathrm{p}}=+\tfrac{1}{2})+I_0(\mu_{\mathrm{p}}=-\tfrac{1}{2})}.$$

Substituting,

$$P_{\mathrm{p}}=\frac{\tfrac{1}{2}I(\mu_{\mathrm{n}}=+\tfrac{1}{2})-\tfrac{1}{2}I(\mu_{\mathrm{n}}=-\tfrac{1}{2})}{\tfrac{3}{2}I(\mu_{\mathrm{n}}=+\tfrac{1}{2})+\tfrac{3}{2}I(\mu_{\mathrm{n}}=-\tfrac{1}{2})}=\frac{1}{3}\,\frac{I(\mu_{\mathrm{n}}=+\tfrac{1}{2})-I(\mu_{\mathrm{n}}=-\tfrac{1}{2})}{I(\mu_{\mathrm{n}}=+\tfrac{1}{2})+I(\mu_{\mathrm{n}}=-\tfrac{1}{2})}.$$

Thus the proton polarization is one third of a quantity which may be regarded as the polarization of the captured neutrons. This formula shows immediately that $P_{\mathrm{p}}\leqslant\tfrac{1}{3}$. The factor $\tfrac{1}{3}$ enters because two thirds of the deuterons in the beam contain parallel proton and neutron spins, and one third of the deuterons contain anti-parallel spins.

When polarized deuterons are used, the relative populations of the spin states become $[1+\sqrt{\tfrac{3}{2}}\langle T_{10}\rangle+\sqrt{\tfrac{1}{2}}\langle T_{20}\rangle]$ of $\phi_{\mathrm{p}}(+)\phi_{\mathrm{n}}(+)$,

$[1-\sqrt{2}\langle T_{20}\rangle]$ of $\sqrt{\tfrac{1}{2}}[\phi_{\mathrm{p}}(+)\phi_{\mathrm{n}}(-)+\phi_{\mathrm{p}}(-)\phi_{\mathrm{n}}(+)]$

and $[1-\sqrt{\tfrac{3}{2}}\langle T_{10}\rangle+\sqrt{\tfrac{1}{2}}\langle T_{20}\rangle]$ of $\phi_{\mathrm{p}}(-)\phi_{\mathrm{n}}(-)$.

Here $\langle T_{10}\rangle$ and $\langle T_{20}\rangle$ are the expectation values of the vector and tensor spin components along the axis of quantization, as defined by Lakin (1955).

Proceeding as before, the stripping cross section with such a deuteron beam is

$$\begin{aligned}I=\tfrac{1}{3}\{&[1+\sqrt{\tfrac{3}{2}}\langle T_{10}\rangle+\sqrt{\tfrac{1}{2}}\langle T_{20}\rangle]I(\mu_{\mathrm{n}}=+\tfrac{1}{2})+\tfrac{1}{2}[1-\sqrt{2}\langle T_{20}\rangle]\\&\times[I(\mu_{\mathrm{n}}=+\tfrac{1}{2})+I(\mu_{\mathrm{n}}=-\tfrac{1}{2})]+[1-\sqrt{\tfrac{3}{2}}\langle T_{10}\rangle+\sqrt{\tfrac{1}{2}}\langle T_{20}\rangle]I(\mu_{\mathrm{n}}=-\tfrac{1}{2})\}\\=I_0&\left\{1+\sqrt{\tfrac{2}{3}}\langle T_{10}\rangle\frac{I(\mu_{\mathrm{n}}=+\tfrac{1}{2})-I(\mu_{\mathrm{n}}=-\tfrac{1}{2})}{I(\mu_{\mathrm{n}}=+\tfrac{1}{2})+I(\mu_{\mathrm{n}}=-\tfrac{1}{2})}\right\}=I_0\{1+3\sqrt{\tfrac{2}{3}}\langle T_{10}\rangle P_{\mathrm{p}}\}.\end{aligned}$$

The tensor polarization in the deuteron beam therefore does not contribute to the cross section with central forces. The deuteron vector polarization P_{d} is defined as $\langle S_z\rangle=\mathrm{Tr}(\rho S_z)$, which is $\sqrt{\tfrac{2}{3}}\langle T_{10}\rangle$ so that $I=I_0\ (1+3P_{\mathrm{p}}P_{\mathrm{d}})$.

If it is now assumed that the deuterons are polarized along a direction which makes an angle θ with the normal to the stripping plane, then, since $\langle T_{10}\rangle$ transforms as $Y_1^0\ (\theta\phi)$, the component normal to the stripping plane is $P_{\mathrm{d}}\cos\theta$, and the left–right asymmetry for stripping is therefore $3P_{\mathrm{p}}P_{\mathrm{d}}$.

This is the same formula as for a nucleon double scattering apart from the factor 3, which occurs because the proton polarization is one third of the neutron capture polarization. It is the neutron capture polarization which is involved in the stripping cross section and hence in the asymmetry, so that when this is described in terms of P_{p} a factor 3 is needed. The proton and neutron have spins predominantly parallel in the deuteron, so that P_{p} and the neutron capture polarization have the same sign and the asymmetry must therefore have the same sign as in the nucleon double scattering formula.

To relate the neutron capture polarization to its angular momentum, it is necessary to convert the cross sections in terms of the neutron spin directions into cross sections in terms of the neutron angular momentum directions. The relation between the two is

$$I(\mu_{\mathrm{n}})=\sum_m C_{l\frac{1}{2}}^{2}(j,\,m+\mu_{\mathrm{n}};\ m,\,\mu_{\mathrm{n}})I(m)$$

assuming that only one l is involved. Here all the quantum numbers refer to the captured neutron.

The proton polarization P_{p} then becomes

$$\frac{1}{3}\frac{\sum\limits_{m}[C_{l\frac{1}{2}}^{2}(j,m+\tfrac{1}{2};\ m,\tfrac{1}{2})-C_{l\frac{1}{2}}^{2}(j,m-\tfrac{1}{2};\ m,-\tfrac{1}{2})]I(m)}{\sum\limits_{m}[C_{l\frac{1}{2}}^{2}(j,m+\tfrac{1}{2};\ m,\tfrac{1}{2})+C_{l\frac{1}{2}}^{2}(j,m-\tfrac{1}{2};\ m,-\tfrac{1}{2})]I(m)}.$$

Substituting values for the Clebsch–Gordan coefficients,

$$P_{\mathrm{p}}=\frac{\Sigma mI(m)}{3(l+1)\Sigma I(m)}\ \text{when}\ j=l+\tfrac{1}{2},\ \text{and}\ P_{\mathrm{p}}=-\frac{\Sigma mI(m)}{3l\Sigma I(m)}\ \text{when}\ j=l-\tfrac{1}{2}.$$

Thus the proton spin polarization is related, by way of the coupling in the deuteron, to the neutron spin polarization, and this in turn is related by way of the coupling of the neutron spin with its orbital angular momentum, to a term which represents the polarization of the angular momentum $\Sigma mI(m)/\Sigma lI(m)$. This will be approximately the same for stripping reactions where the nuclear radii and distorting potentials are similar. When this is so

$$P_{\mathrm{p}}(j=l+\tfrac{1}{2})=-\frac{l}{l+1}P_{\mathrm{p}}(j=l-\tfrac{1}{2}).$$

REFERENCES

AL-JEBOORI, M. A., BOKHARI, M. S., HIRD, B., and STRZALKOWSKI, A., 1959, *Proc. Phys. Soc.*, **74**, 705.

CHESTON, W. B., 1954, *Phys. Rev.*, **96**, 1590.

HIRD, B., COOKSON, J. A., and BOKHARI, M. S., 1958, *Proc. Phys. Soc.*, **72**, 489.

HOLT, J. R., and MARSHAM, T. N., 1953, *Proc. Phys. Soc.* A, **66**, 1032.

HOROWITZ, J., and MESSIAH, A. M. L., 1953, *J. Phys. Radium*, **14**, 695.

HUBY, R., REFAI, M. Y., and SATCHLER, G. R., 1958, *Nucl. Phys.*, **9**, 94.

LAKIN, W., 1955, *Phys. Rev.*, **98**, 139.

NEWNS, H. C., 1953, *Proc. Phys. Soc.* A, **66**, 477.

SATCHLER, G. R., 1958, *Nucl. Phys.*, **6**, 543.

TAYLOR, R. T., 1959, *Phys. Rev.*, **113**, 1293.

TOBOCMAN, W., and KALOS, M. M., 1955, *Phys. Rev.*, **97**, 132.

Polarization in Deuteron Elastic Scattering from Carbon at 6 Mev

By M. A. AL-JEBOORI, M. S. BOKHARI, A. STRZAŁKOWSKI and B. HIRD
University of Liverpool

Communicated by the late H. W. B. Skinner; MS. received 26*th November* 1959, *in final form* 19*th January* 1960

Abstract. The azimuthal dependence of the cross section at the second of two deuteron elastic scatterings from carbon has been determined at an energy of about 6 Mev. It was found that the left–right part of the asymmetry was small and probably negative, which implies that the vector polarization either changes sign between the two scatterings, or that the tensor polarizations are large. There was no evidence for polarizations of the $\langle T_{22} \rangle$ type.

§ 1. Introduction

The description of the polarization states of particles of spin one is more complicated than that for particles of spin half, where three components of a single vector are all that are required. Lakin (1955) has shown that a complete description of the populations of the various spin states can be given in terms of the expectation values of a set of tensors T_{JM} (Hamilton 1959) of up to the second rank. Of these, the first rank tensors T_{1M} show many of the properties associated with spin-half polarizations; they are axial vectors, and the average values of the spin in the different directions are given in terms of their expectation values. The terms $\langle T_{1M} \rangle$ will be referred to as the vector polarization. In scattering, the only $\langle T_{1M} \rangle$ which are involved are those which represent components of the spin perpendicular to the scattering plane. The T_{2M} contribute five more expectation values which relate the populations of the different spin states, but in such a way that they have no influence on the average spin in any direction. In a cylindrically symmetrical system, quadrupole moments and alignments would be described in terms of them.

Large left–right asymmetries have been found in deuteron stripping when using deuterons which had been polarized by scattering them from carbon (Hird and Strzałkowski 1960). The central force distortion theory of deuteron stripping, which is believed to be reasonably correct where the stripping process predominates, predicts that the T_{2M} do not contribute in any way to the cross section or to the asymmetry (Satchler 1958, Huby, Refai and Satchler 1958). The large asymmetries found in stripping therefore seem to indicate that there was considerable vector polarization present in a direction perpendicular to the stripping plane. The present measurements were made in an attempt to determine independently the vector part of the polarization of these deuterons, by a second elastic scattering from carbon.

Lakin (1955) has shown that the cross section, at the second of the two deuteron elastic scatterings is given by[†]

$$I = I_0 [1 + \langle T_{20}\rangle_1 \langle T_{20}\rangle_2 + 2(i\langle T_{11}\rangle_1 i\langle T_{11}\rangle_2 - \langle T_{21}\rangle_1 \langle T_{21}\rangle_2)\cos\phi + 2\langle T_{22}\rangle_1 \langle T_{22}\rangle_2 \cos 2\phi]$$

where I_0 is the unpolarized cross section, and ϕ is the angle between the two scattering planes. The suffix 1 refers to the polarization state of the beam after the first scattering, and the suffix 2 refers to the polarizing effect of the second scattering. The axis of quantization is here taken along the direction of the beam between the two scatterings, with the x axis in the plane of the first scattering. Parity conservation requires that the expectation values $\langle T_{11}\rangle$ are entirely imaginary, so that in terms of the ordinary definition of vector polarization,

$$P_d = \langle S_y\rangle = (2i/\sqrt{3})\langle T_{11}\rangle.$$

All the other expectation values are real.

We have measured the relative number of deuterons scattered left, right, up and down after the second scattering, in order to determine the coefficients of $\cos\phi$ and $\cos 2\phi$.

§ 2. THE POLARIZED DEUTERON BEAM

The polarized deuteron beam was produced by placing a graphite target inside one of the dees of the 37 in. cyclotron (Al-Jeboori *et al.* 1959). For the first of the measurements at 46° the same internal target as for the stripping measurements was used. This gave a scattered beam of energy $6{\cdot}0 \pm 0{\cdot}2$ MEV. The target had to be renewed for the other measurements, and after the focusing conditions were optimized, the beam energy was found to be 6 ± 1 MEV. The geometry of the first scattering had originally been designed to select particles emitted at about 45° in the centre-of-mass system and for this reason some of the second scattering measurements were done at a similar angle. However, after the experiments were completed, recalculation of the deuteron trajectories in the cyclotron fringe field showed that those deuterons which were collected by the wedge magnet must have been scattered by the internal target at angles near to 40°, so that no measurements were actually made with identical first and second scattering angles.

§ 3. MEASUREMENT OF THE ASYMMETRIES

Measurements were made, with nuclear emulsions, of the deuterons scattered left, right, up and down, at identical angles after the second scattering. The azimuthal variation has the form $I = I_0\,(A + B\cos\phi + C\cos 2\phi)$, and it is possible to obtain the coefficients B/A and C/A from the track densities in the four directions, independently of most of the first-order geometrical errors in the position of the emulsions in the scattering camera. This is done by making two successive exposures. Between the two the camera was rotated through 90° about the incident deuteron direction. If the differential cross section in the four directions is I_L, I_D, I_R, I_U, and if the measured track density on the corresponding emulsions is N_1, N_2, N_3, N_4 in the first exposure, and N_1', N_2', N_3', N_4' in the second, where the suffix refers to the location of the plates in the plateholders, then

---

[†] Note that the sign of the $\langle T_{21}\rangle$ term is incorrect in Lakin's paper.

$$\frac{N_1 N_2'}{N_1' N_2} = \frac{I_L^2}{I_U I_D} \quad \text{and} \quad \frac{N_3 N_4'}{N_3' N_4} = \frac{I_R^2}{I_U I_D}$$

independently of the solid angle subtended by each plate and of the relative magnitudes of the two exposures. From these ratios, the coefficients B/A and C/A are easily calculated.

The scattering camera is shown in the figure. The position of each of the plateholders could be adjusted separately, and then fixed in position. Though the effects of geometrical errors are largely eliminated by the method of calculation, they were kept as small as possible by locating the plateholders accurately with templates, relative to the second target. The track density was particularly sensitive to the angle which the emulsion surface made with the direction of the scattered deuterons, so, after the positions were fixed, an optical lever system was used to determine the variation of this angle from one plate position to another. The mirror for this optical lever consisted of a glass plate inserted successively in each plate holder.

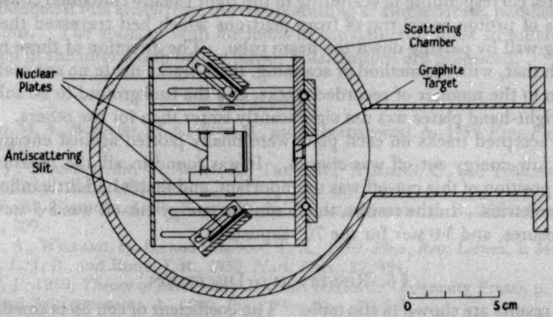

The frame supporting the target and the nuclear plates was located in the scattering chamber by steel balls recessed in the mounting plate, so that when loaded it could be replaced accurately in either of its two positions.

The target was made by abrading pile graphite down to an average thickness of 8 mg cm^{-2}. This represents an energy loss of about 1 MeV to the 6 MeV beam. The target was far from uniform so that a greater energy loss than this would occur in some regions of the target.

As a check on the method of calculation, the two successive exposures were treated as separate measurements, and the asymmetry calculated from each. When these had been corrected for the misalignment there was internal consistency between them and with the other method of calculation.

An error, which did not cancel out, and which would not be revealed by differences in the results of the successive exposures, would be introduced if the mean direction of the incident deuteron was not parallel to the axis of the scattering frame. The largest uncertainty of this direction came from the convergence of the beam from the wedge magnet. Since the distribution of the beam over the aperture of the magnet was not determined, errors of up to ± 1° in the beam direction were possible. The effect of such a misalignment on the asymmetry depends on the rate at which the scattering differential cross section changes with angle. At angles where it changes most rapidly the error in the left–right asymmetry may be of the order of a few per cent. Since the rate of change of the differential cross section was required for a more accurate estimate and it was not available, this type of error was excluded from the errors given in the asymmetry results.

§ 4. Track Analysis

The position, length and direction of all the tracks entering the surface of the nuclear emulsion were recorded. Those corresponding to protons, from deuteron stripping in the target, were easily identified and were ignored. To be acceptable each deuteron track had to have both its dip angle and its azimuthal angle consistent with the deuteron having come from the direction of the target. Deviations of the dip angle and azimuthal angle from the expected direction were calculated, and from graphical plots of these, it was possible to estimate the background of tracks having the correct directions, but not coming from the target. In all the exposures, this background was small and roughly the same on all four plates. The plates corresponding to scattering to the right usually contained considerable numbers of proton recoil tracks from neutrons which had traversed the double shielding wall by passing down the beam tube. The direction of these neutrons was such that, with the method of scanning, these tracks made no noticeable contribution to the number of recorded tracks, and the background to be subtracted for the right-hand plates was not significantly larger than for the others.

The accepted tracks on each plate were finally plotted against energy, and a suitable low-energy cut-off was chosen. It was found in all the measurements that the position of this cut-off was unimportant, and that it had little influence on the asymmetries. In the results, the minimum energy cut-off was 3·5 Mev for the 46° exposures, and 3·0 Mev for the 70° exposures.

§ 5. Results and Discussion

The results are shown in the table. The coefficient of cos 2ϕ is small, so that very little polarization of the type $\langle T_{22} \rangle$ is produced in the scattering.

Angle (c.m. system) (deg)	Energy (Mev)	left	right	up	down	B/A	C/A
$46 \pm 1{\cdot}5$	$6{\cdot}0 \pm 0{\cdot}2$	275	294	269	268	$-0{\cdot}062 \pm 0{\cdot}042$	$+0{\cdot}070 \pm 0{\cdot}020$
		446	397	309	369		
$46 \pm 1{\cdot}5$	6 ± 1	252	209	210	228	$-0{\cdot}097 \pm 0{\cdot}052$	$+0{\cdot}013 \pm 0{\cdot}025$
		204	177	179	205		
70 ± 3	6 ± 1	296	265	284	298	$-0{\cdot}110 \pm 0{\cdot}050$	$+0{\cdot}009 \pm 0{\cdot}025$
		286	210	223	238		

The errors include statistical variations, but exclude the effects of geometrical misalignments.

The negative sign for the coefficient of cos ϕ may be accounted for by predominantly vector polarization only if this changes sign between the two scatterings. Though it is possible that the sign of the polarization changes at some angle between 40° and 46° and then remains the same up to 70°, it is more probable that any change of sign would be due to energy rather than angular variations. The first scattering could have occurred at any energy between 8 Mev and 6 Mev, depending on whether it took place near the front, or near the back of the target. The second scattering reduced the energy by about a further 1 MeV, so that the energy of the two scatterings was significantly different. Deuteron reactions with ^{12}C at these energies show evidence of discrete levels in ^{14}N (Bonner *et al.* 1956), so that rapid energy fluctuations in the polarization are possible. However, in view of the evidence from the stripping asymmetries, of large vector polarization produced in the 40° scattering, it seems unlikely that the second scattering vector polarization would be so small at both 46° and 70°.

Alternatively the small, or negative sign of cos ϕ may be due to tensor polarization of type $\langle T_{21} \rangle$ exceeding the vector polarization. If a resonant process forms the main part of the cross section, then in addition to being responsible for rapid energy fluctuations, it is likely to produce large tensor polarizations because the deuteron as a whole is involved (Goldfarb and Rook 1959, Galonsky, Willard and Welton 1959). On the other hand, direct interactions which involve the two nucleons in the deuterons separately, such as that suggested by Huby and Newns (1951) for inelastic scattering, or the impulse approximation used at higher energies for elastic deuteron scattering (Baldwin *et al.* 1956, Watanabe 1958) are unlikely to produce the required energy variation nor are they likely to produce much tensor polarization. This is because only vector polarization in a spin 1 particle can be produced if this arises from the compounding of two separate, parallel spin $\frac{1}{2}$ polarizations. The spins of both nucleons in the deuteron must simultaneously be involved in the interaction before tensor polarizations are produced.

REFERENCES

AL-JEBOORI, M. A., BOKHARI, M. S., HIRD, B., and STRZAŁKOWSKI, A., 1959, *Proc. Phys. Soc.*, **74**, 705.

BALDWIN, J., CHAMBERLAIN, O., SEGRÈ, E., TRIPP, R., WIEGAND, C., and YPSILANTIS, T., 1956, *Phys. Rev.*, **103**, 1502.

BONNER, T. W., EISINGER, J. T., KRAUS, A. A., JR., and MARION, J. B., 1956, *Phys. Rev.*, **101**, 209.

GALONSKY, A., WILLARD, H. B., and WELTON, T. A., 1959, *Phys. Rev. Letters*, **2**, 349.

GOLDFARB, L. J. B., and ROOK, J. R., 1959, *Nucl. Phys.*, **12**, 494.

HAMILTON, J., 1959, *Theory of Elementary Particles* (Oxford: University Press), p. 391.

HIRD, B., and STRZAŁKOWSKI, A., 1960, *Proc. Phys. Soc.*, **75**, 868.

HUBY, R., and NEWNS, H. C., 1951, *Phil. Mag.*, 1442.

HUBY, R., REFAI, M. Y., and SATCHLER, G. R., 1958, *Nucl. Phys.*, **9**, 94.

LAKIN, W., 1955, *Phys. Rev.*, **98**, 139.

SATCHLER, G. R., 1958, *Nucl. Phys.*, **6**, 543.

WATANABE, S., 1958, *Nucl. Phys.*, **8**, 484.

Domain Tube Structures in Silicon Iron

By L. F. BATES and R. CAREY
Physics Department, University of Nottingham

MS. received 5th January 1960

Abstract. Following a theoretical discussion of Néel spike formation by the extension and subsequent collapse of a domain tube which joins an inclusion to a domain wall, a quantitative study has been made of the phenomena. The results are discussed in terms of a formula given by Brenner, and an attempt is made to assess the importance of the phenomena in the explanation of coercivity.

§ 1. INTRODUCTION

SEVERAL theories of coercivity have been based on a model which postulates impedance to domain wall motion. Kersten (1943) considered the effect of spherical cavities or non-magnetic inclusions on wall movement. He proposed that the increase in coercive force caused by inclusions was due to a simple 'surface tension' effect. However, he made no allowance for the effects of a demagnetizing field at the inclusion and obtained estimates of coercivity which were in excess of experimental values. Néel (1944) rectified this omission and based his calculation of coercivity on surface charge effects, at the surfaces of the inclusions. In passing through an inclusion a domain wall causes a redistribution of magnetic charges, and magnetostatic energy is a minimum when the wall bisects an inclusion. Hence, there is a tendency for a wall to remain anchored to inclusions. Néel further predicted the formation of closure domains at an inclusion which further reduced the magnetostatic energy. The formation of such domains, now known as Néel spikes, is dependent on the size of the inclusion.

Williams and Shockley (1949) observed the motion of a 180° domain wall as it moved past holes and imperfections in a crystal surface. They reported that domain structures around an inclusion united with the wall, forming 'tie domains' or 'tubes', a particular example of which is shown by the drawing in figure 1. As the main wall continued to move, the tube wall became more and more extended and finally broke, suddenly forming a Néel spike structure at the inclusion.

The importance of this process in the theoretical considerations of coercivity was soon realized, and Kondorsky (1949) computed the magnitude of the field required to resist the tension of a tube. Later, Kersten (1955) re-examined the problem and made a new estimation of coercivity incorporating a tube extension mechanism. The absolute value of the coercivity agreed satisfactorily with a value calculated from an approximate formula. In all cases assumptions were made to simplify the mathematical treatment, so that agreement with experiment must be treated with some reserve. Brenner (1955) extended the coercivity formula of Kondorsky by including in his treatment a consideration of the rupture length of a tube. This involved an analysis of the energies involved in the creation of a Néel spike by tube extension and subsequent rupture. He obtained a maximum value of coercivity when the average distance between neighbouring inclusions was of the same order as the rupture length of a tube. Because of the apparent importance of tube rupture in theories relating to coercive force it was decided to examine quantitatively such processes in single crystals of silicon–iron.

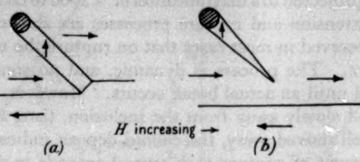

Figure 1. (*a*) ' Tie domain ' or ' tube '; (*b*) Néel spike.

§ 2. The Brenner Theory of Tube Rupture

Brenner assumes that the collapse of a tube to form a spike is possible from the moment that the energy of the tube structure becomes equal to the energy of the spike structure which is stable under the same conditions. From calculations of (*a*) wall energy, (*b*) surface charge energy and (*c*) magnetic energy, he finds that

$$l_t = l_s \frac{6\pi\bar{\gamma}_{90} + 4HI_s d + 2\pi a I_s^2 d^3/l_s^2}{12\bar{\gamma}_{90} + 3HI_s d} \qquad \ldots\ldots (1)$$

where l_t is the rupture length of the tube, l_s is the equilibrium length of the spike replacing it and d is the diameter of the inclusion on which the structure is based; $\bar{\gamma}_{90}$ is the average energy per unit area of a 90° wall, and is assumed to be the same for both the tube and the spike. The factor a is included because of the diminution of the energy of the demagnetizing field, caused by the rotation of the main magnetization vector in the region adjacent to the wall, for finite crystal anisotropy (see Williams, Bozorth and Shockley 1949); a is equal to $2/\mu^*$, where $\mu^* = (1 + 2\pi I_s^2/K)$. There is, however, some doubt about this value of a, and Bates *et al.* (1957) have given calculations which suggest that a is equal to $[2/\mu^*(\mu^*+1)^{1/2}]$. Nevertheless, this does not affect the theoretical limits of equation (1).

From equation (1) it follows that, in general, for very large inclusions, the magnetic term HI_s is dominant, even for small fields. In this case the ratio l_t/l_s tends to the limiting value 4/3. In cases where the wall energy terms swamp other terms, i.e. for inclusions less than 10μ in diameter and for very small fields, the value l_t/l_s tends to $\pi/2$, or approximately 1·57.

§ 3. Experimental Procedure

For the present experiments a single crystal of 2·5% Si–Fe about 0·7 cm square and 0·1 cm thick was available. Its main faces were parallel to within ½° to (100) planes and its edges approximated to [100] directions. It was electropolished in a chromic–acetic acid mixture to obtain a strain-free surface (Bates and Mee 1952).

The specimen was placed between the poles of a small electromagnet with the field parallel to an easy direction of magnetization in the surface. The effective field was measured with a magnetic potentiometer and galvanometer amplifier circuit; the magnetization curve was of standard form, with a coercivity of 0·72 Oe and a technical saturation intensity of magnetization of 1625 G.

Observations of the tube rupture processes were made by the Bitter figure technique. The patterns at the critical tube lengths were photographed, and the negatives were projected to a magnification of × 2000 to facilitate measurement.

Typical tube extension and rupture processes are shown in figures 2 and 3 (Plate). It was observed in most cases that on rupture the wall bounds forward for a short distance. The process is dynamic, and no sign that the tube will rupture is observed until an actual break occurs. However, it was found that if the wall was moved slowly away from the inclusion, then at rupture, although the true domain wall moved away, the colloid deposit indicating the position of the wall at the moment of rupture took several seconds to disperse. A photograph (figure 3(*d*)), taken at such an instant, shows a Néel spike based on an inclusion and a line of colloid particles indicating the position of the 180° wall at rupture. Hence a measure of l_t, l_s, and d could be obtained on one photograph for each process. The diameter of the inclusion d was taken to be the width of the base of the spike, after rupture, measured as close to the inclusion as possible. Direct measurements of d were not always possible because of the almost inevitable agglomeration of colloid particles around the inclusion.

§ 4. Experimental Results

The motion of 180° walls, in the specimen of silicon–iron, was observed during the process of magnetization. Over 100 rupture processes were observed and photographed, and the critical tube length, equilibrium spike length, diameter of the inclusion and effective field at which the rupture occurred were measured in each case.

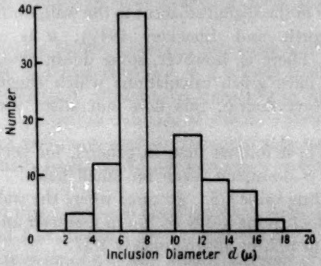

Figure 4. Distribution in the diameters of the inclusions upon which measurements were made.

Figure 4 shows the distributions in the diameters of the inclusions upon which measurements were made. It can be seen that 70% of the spikes observed were based on inclusions which were between 6μ and 12μ in diameter. The inclusions were holes or non-magnetic impurities which were present in the surface; it was not necessary to produce defects in the surface by artificial means. Figure 5(*a*) shows the experimental values of l_t plotted against l_s for all the processes observed. The points conform approximately to a straight line of slope $l_t/l_s = 1{\cdot}35$.

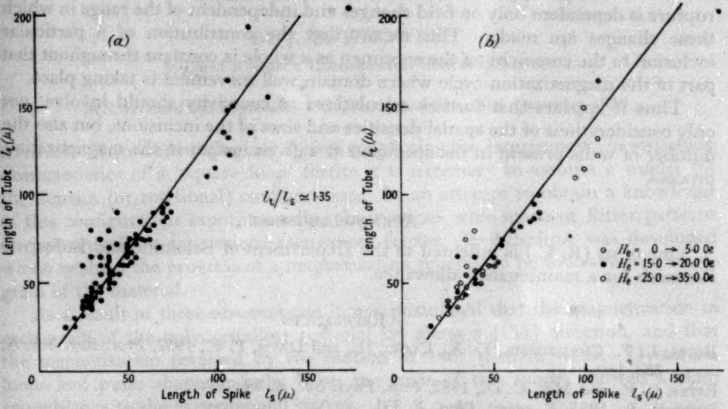

Figure 5. Experimental values of tube length plotted against equilibrium spike-length: (*a*) for all processes observed, (*b*) with points selected from specified field ranges.

Figure 5(*b*) shows the same plot with points selected from measurements made in specified field ranges. It can be seen that the position of these points shows little or no dependence on the field range in which they were measured.

The upper limit to which a tube could be extended appears to be 200μ; however, few processes were observed in which l_t exceeded 100μ. This is due to the inclusion density on the surface of the specimen. A region in which a tube could be extended to a length greater than 100μ before encountering an inclusion was rarely found; the average spacing of the inclusions was about 125μ.

The ratio $l_t/l_s \simeq 1{\cdot}57$, predicted by Brenner to occur when the wall energy terms in equation (1) swamp the other terms, was not reached as the smallest spike-supporting inclusion observed in these experiments was of the order of $3{\cdot}5\mu$. Measurements to bring l_t/l_s in the range 1·57 would have required effective fields of less than 1·0 Oe.

The minimum value of l_t/l_s observed was about 1·14 compared with the value 1·33 predicted by Brenner.

§ 5. Discussion

The measurement of these processes by the above method was difficult because the movement of 180° domain walls was considerably influenced by other obstacles which lay outside the field of view. A 180° wall tends wherever possible to remain fixed to inclusions.

The measurement of the rupture length probably introduced the greatest error; however, errors in the measurements of the spike length and of the inclusion diameter were also present due to the difficulty in ascertaining the exact nature and position of the inclusion. For example, figure 6 (Plate) shows a spike based on a group of large inclusions. In this case measurements of l_t and l_s were made from the base of the spike.

For the range of fields in which rupture lengths were measured, it appears that the ratio l_t/l_s is approximately constant, i.e. the process of tube extension and rupture is dependent only on field changes and independent of the range in which these changes are made. This means that the contribution of a particular inclusion to the coercivity of the specimen as a whole is constant throughout that part of the magnetization cycle where domain wall movement is taking place.

Thus it appears that further calculations of coercivity should involve, not only considerations of the spatial densities and sizes of the inclusions, but also the number of walls present in the specimen at a given instant in the magnetization process.

ACKNOWLEDGMENT

One of us (R. C.) is indebted to the Department of Scientific and Industrial Research for a maintenance allowance.

REFERENCES

BATES, L. F., CHRISTOFFEL, D. A., CLOW, H., and DAVIS, P. F., 1957, *Proc. Roy. Soc.* A, **233**, 160.
BATES, L. F., and MEE, C. D., 1952, *Proc. Phys. Soc.* A, **64**, 129.
BRENNER, R., 1955, *Z. angew. Phys.*, **8**, 391.
KERSTEN, M., 1943, *Grundlagen einer Theorie der ferromagnetischen Hysterese und der Koerzitivkraft* (Leipzig: S. Hirzel).
—— 1955, *Z. angew. Phys.*, **7**, **8**, 397.
KONDORSKY, E., 1949, *Dokl. Akad. Nauk, S.S.S.R.*, **68**, 37.
NÉEL, L., 1944, *Cah. de Phys.*, **25**, 1.
WILLIAMS, H. J., BOZORTH, R. M., and SHOCKLEY, W., 1949, *Phys. Rev.*, **75**, 155.
WILLIAMS, H. J., and SHOCKLEY, W., 1949, *Phys. Rev.*, **75**, 175.

Some Observations of Bitter Patterns on Polycrystalline 'Square Loop' Ferrites, and a Theoretical Explanation of the Loop Shape and Pulse Characteristics of the Material

By J. E. KNOWLES

Mullard Research Laboratories, Salfords, Surrey

MS. received 4*th September* 1959, *in revised form* 30*th December* 1959

Abstract. Before advancing any theory concerning the 'squareness' or switching characteristics of a 'square loop' ferrite it is necessary to assume a model for the domain (or rotational) configuration. In an attempt to obtain a knowledge of this configuration experimentally, observations were made of Bitter patterns on polycrystalline magnesium–manganese ferrite. A technique was developed which enabled the progress of a magnetization reversal to be followed in a single grain of the material.

As a result of these observations it was postulated that the magnetization in each grain of the polycrystalline material lay along a [111] direction, and that the magnetization reversed by the motion of 180° domain walls. Hysteresis loops and pulse shapes calculated on the basis of this model showed a close resemblance to the experimental curves.

---

§ 1. INTRODUCTION

When considering theoretically the behaviour of ferrites having a rectangular hysteresis loop it is customary to postulate some configuration of the magnetization at remanence, and deduce from this model how the configuration will change during a reversal. As is well known, a magnetic material may reverse its magnetization either by a process of domain-wall motion or by a rotation of the magnetization vector. From time to time a number of models based upon one or the other of these mechanisms have been advanced which account for various aspects of the behaviour of 'square loop' ferrite material (see for example Goodenough 1957 and Gyorgi 1957). Unfortunately, there is little experimental evidence available to assist one in evaluating the relative merits of these hypotheses.

It was thought that if Bitter patterns could be observed on the surface of a 'square loop' ferrite and the progress of a magnetization reversal followed, then at least some of these models could be eliminated and perhaps a new model, based on experimental observations, formulated.

§ 2. SOME OBSERVATIONS OF BITTER PATTERNS

Mr. C. E. Fuller of these laboratories kindly supplied some colloid he had prepared to Elmore's recipe (1938). A drop of colloid was placed on the surface of the specimen and a cover glass placed upon it, a drop of immersion oil was then placed on the upper surface of the glass and the 2 mm objective racked down until the image was observed. The specimen was lit by a Wrighton Beck metallurgical illuminator; owing to the turbid nature of the colloid the lens had to be used at a very small aperture to eliminate glare, and also to obtain a good depth of focus. Photographs were taken on Ilford Pan F35 mm film with an exposure time of 45 seconds.

Bitter patterns were viewed on surfaces which had been prepared by four different methods, three of which gave patterns of a rather spurious nature.

Observations were first made on a polished sample of Ferroxcube D1 which is a manganese–magnesium ferrite. Irregular domain walls were seen which were obviously due to stresses induced by the polishing process, so an attempt was made to anneal the sample by heating it to 750°c. This treatment greatly clarified the Bitter patterns which resembled those observed by Bates, Clow, Craik and Griffiths (1958) on the surface of polycrystalline manganese zinc ferrite, that were due to surface stresses. The domains observed here remained immobile when a magnetic field was applied, and it seems that these patterns also must be attributed to residual stresses.

Since polishing the surface introduced difficulties, the unpolished surface of a D1 core was examined to see if domains were visible. Four distinctive types of pattern were found, each pattern being confined to the area of a single grain: (i) no pattern discernible, (ii) an irregular pattern of rather widely spaced domains, (iii) a series of close spaced parallel domain walls and (iv) a maze pattern.

It is probable that this classification refers to grains where the magnetization made increasingly large angles with the surface. The domain walls were highly mobile, but watching the course of a reversal did not yield any useful information: patterns of the type (ii) were so complex that the reversal process could not be followed and patterns type (iii) and (iv) changed their position without altering the spacing of the domain walls.

The grains of the commercial D1 material had a very rough surface which probably gave rise to spurious patterns, and it was apparent from the nature of some of these irregularities that they were due to grinding marks on the surface of the press tool. It was thought that if the punches used to press the prefired powder were given a high polish then perhaps the surface of the grains would be improved. To test this a toroid of D2 Ferroxcube (which is very similar to D1) 1 cm in diameter and 3 mm thick, was pressed and fired for 18 hours in oxygen at 1330°c with the object of forming a very dense material with large grain size: the maximum squareness ratio was found to be about 70%. (The squareness ratio R_s is conventionally defined by the ratio $I_{-H\mathrm{m}/2}/I_{H\mathrm{m}}$ where $I_{H\mathrm{m}}$ is the magnetization corresponding to a field H_m.) Microscopic examination showed that the surfaces of the grains were far smoother than before. The observations to be described would seem to confirm that patterns viewed on these surfaces reflect the domain structure of the interior of the sample, and that patterns observed on surfaces prepared by other methods reflect only the surface conditions. A portion of a typical grain, covered with complex closure domains, is shown in figure 1(*a*) (Plate) ($80\mu \times 50\mu$); probably the bulk magnetization of the grain was making a fairly large angle with the surface. A number of grains however showed a very simple domain structure and a series of photographs, figure 1(*c*) – (*x*) was taken to show the progress of a magnetization reversal in such a grain. The domain walls were almost parallel to the field direction, i.e. the periphery of the toroid, and the figures show an area of about $80\mu \times 55\mu$.

Since the domain structure is very simple it would appear likely that the surface is a (110) plane, and if this is the case it is possible that the domains are separated by 180°, 109° or 71° walls. This question may be resolved by considering the small domain system observed in the bottom left-hand corner of the grain in figure 1*(c)* – *(h)*: the structure is shown on a larger scale in figure 1*(b)*. It would seem that this is a reverse domain and that free poles at its extremity are minimized by the 'ears'. An interpretation of this structure based on the case of 180° walls on a (110) face is shown in figure 2. The shapes of the 'ears' of the observed structure are indicated by the broken lines, the other lines being coincident with those on the photograph. There would seem to be a free pole distribution along the walls indicated by the broken lines but as this domain system is very probably only a surface structure perhaps not too much weight should be attached to this.

The possibility that the exposed surface of the grain was a (112) plane, the walls being in the (110) plane, was also considered but rejected because the shape of the small domain system to be expected on this hypothesis did not agree as well with the observed shape as that given in figure 2. Thus it would appear that the walls in figure 1*(c)* – *(x)* are 180° walls lying in a (112) plane, the exposed face of the grain being in the (110) plane.

The observed thickness of the domain walls was in the region $0{\cdot}2\mu$ to $0{\cdot}6\mu$. The theoretical value based on the approximate relationship $d = 7\sqrt{(A/K)}$ was $0{\cdot}2\mu$ (taking $A = 0{\cdot}14 \times 10^{-6}$ erg cm^{-1} (Dillon and Earl 1959) and $K = 2 \times 10^4$ erg cm^{-3}).

2.1. *Commentary on figure* 1*(c)* – *(x)*

Figure 1*(c)* – *(x)* shows the progress of a magnetization reversal under the influence of a field applied by a magnetizing coil wound on the toroid.

Figure 1	Field (Oe)	
(c)	+4·11	The upper wall crossed the right-hand grain boundary. There was a heavy colloid deposit on the lower wall: presumably the material in this region was under stress.
(d)	+2·06	The upper and lower walls have both advanced slightly, the latter has started to kink over the stressed region.
(e)	0	
(f)	−0·20	The upper wall has advanced and a new domain has been formed in the lower right-hand corner of the grain.
(g)	−0·41	The upper wall has advanced on the left and centre and a small closure domain has formed upon it. The lower wall has remained fixed in the stressed region.
(h)	−0·62	
(i)	−0·86	
(j)	−0·94	
(k)	−1·23	The closure domain on the upper wall has disappeared.
(l)	−1·27	The lower wall has advanced on the left and the colloid deposit on the right has become heavier.
(m)	−1·34	The lower wall has broken free, at first on the left and then on the right.
(n)	−1·40	
(o)	−1·64	
(p)	−2·05	The upper wall which had remained almost immobile since part *(k)* has broken free.
(q)	−3·78	
(r)	−4·11	
(s)	0	Both walls have withdrawn slightly.
(t)	+0·62	
(u)	+1·03	Both walls have withdrawn. The large salient in the lower wall was almost certainly a surface closure structure.
(v)	+2·05	
(w)	+2·18	
(x)	+4·11	Compare with part *(c)*.

It may be seen that the grain was fairly rectangular in plan. If it is assumed that it was rectangular also in cross section so that the domain pattern was essentially the same on the opposite surface, then a measure of the magnetization of the grain will be given by the difference in area of the domains. In determining these areas the various small domains were neglected, as it was believed that they were only surface structures. Figure 3 shows the conventional hysteresis loop of the sample together with the hysteresis loop of the grain: it may be noted that both loops are closed. The field axis is common to both, and the loops have been drawn so that they coincide for $H = +4{\cdot}11$ Oe. The fact that the loop for the grain is displaced in the vertical direction merely indicates that the value taken as the area (i.e. volume) of the whole grain was in error: probably the sides of the grains were not quite perpendicular to the surface of the specimen. Thus it would have been legitimate to draw the loops so that both tips coincided.

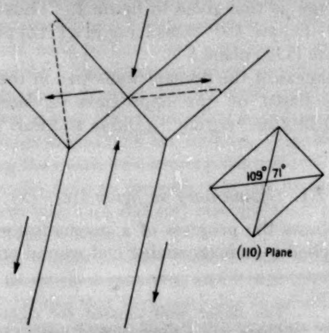

Figure 2. The domain configuration of figure 1(*b*), assuming the surface to be a (110) plane.

It has been remarked that the salient on the right-hand side of the bottom wall in figure 1(*u*) – (*x*) was probably a surface closure structure. The justification for this statement is that if the salient was considered to be in the central domain, then the corresponding points in figure 3 were greatly in error inasmuch as they did not lie on the loop. If, on the other hand, the area of the central domain was taken to be bounded by the faint wall between the salient and the central domain then the points *u* to *x* were obtained, lying approximately on the loop.

From figure 3 it may be seen that the magnetization reversal of the grain took place in four stages:

Stage	Figure 1	
I	(*c*) – (*e*)	Both walls moved slightly.
II	(*f*) – (*k*)	The upper wall moved so that the magnetization altered linearly with the applied field.
III	(*l*) – (*o*)	The lower wall broke free and advanced very rapidly.
IV	(*p*) – (*r*)	The upper wall broke free.

Although the loops of the grain and the toroid are generally similar, the hysteresis loop of the grain does not possess a well-defined 'knee': this portion of the loop is due to the movement of the upper wall, probably in a reversible manner.

One possible interpretation is that the wall was being driven up a stress gradient, another is that the reversible motion of the wall under the influence of an applied field was a result of the rearrangement of the free poles at the ends of the grain. The free pole density I may be estimated, albeit very roughly, by applying the formula derived by Kittel (1949)

$$D = \left[\frac{\text{wall energy} \times L}{1{\cdot}7 \times I^2}\right]^{1/2}.$$

(It must be remembered that this equation is strictly valid only for a semi-infinite medium.) D, the domain wall spacing, was about 20μ, the wall energy was given by $2\sqrt{(AK)}$ where A and K have the values given previously and L, in this case the grain size, was about 60μ.

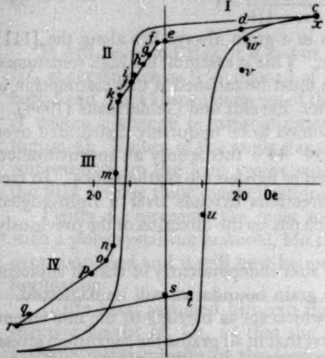

Figure 3. The hysteresis loop of the polycrystalline sample together with that of a grain of it.

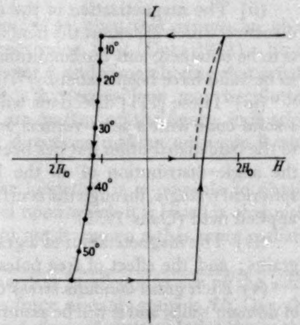

Figure 4. A theoretical hysteresis loop based on irreversible domain wall movements.

Then I was of the order of 9 e.m.u. cm^{-2}, compared with I_s of the order of 220 e.m.u. One grain was observed which was generally similar to that shown here, but with triangular closure domains at the ends of the walls which would of course have diminished the free pole energy on the end faces.

Thus it would appear likely that under the influence of an applied field the walls moved reversibly until they ran into a heavily stressed area, where they were held until the field was sufficiently large to force them past the greatest stress gradient when they moved forward, irreversibly, in a Barkhausen jump to the next stress barrier in their path (see, for example, Stewart 1954). When a wall was in a stressed area it became curved or heavy colloid deposits formed on it showing the presence of free poles. The curvature of the wall has been explained (Craik and Griffiths 1959) as being a result of the wall energy being proportional to the square root of the anisotropy, so that if the effective anisotropy over a small region is changed by stressing the material, or by the presence of excess ferrous iron (to avoid repetition the latter possibility will not be mentioned explicitly again) then it may be energetically favourable for the wall to depart from a plane configuration.

This experiment did not support any of the existing theories of domain wall configuration in polycrystalline 'square loop' ferrites, but on the basis of these observations a new model for the domain configuration will be advanced which yields theoretical expressions which are in quite good accord with experimental results.

§ 3. An Analysis of 'Square Loop' Behaviour based upon a New Model of the Domain Configuration

This model is founded upon the following assumptions:

(i) That the grain just described is in fact typical of all grains in the material, i.e. each grain has one or two 180° domain walls which do not in general cross the grain boundaries but may do so if the orientations of adjacent grains are favourable. The wall area remains essentially constant, and there is no nucleation or annihilation of walls.

(ii) The magnetization of the domains in a grain always lies along the [111] direction which is nearest the field direction. This is essential if a high remanence is to be obtained, and the conditions which must be satisfied if this assumption is to be valid have been stated by Wijn, Gorter, Esveldt and Geldermans (1954).

(iii) These [111] directions will be assumed to be uniformly distributed over a solid cone with a semi-vertical angle of 54° 44′: this is only an approximation to the true distribution but has been adopted to lighten the mathematics. In fact the angle distribution of all the [111] directions extends over a right-angled spherical triangle, through the centre of which passes the direction of the previously applied field (Gans 1932).

(iv) The magnetization of a grain may alter independently of that of adjacent grains; and the effect of free poles on the grain boundaries will be neglected.

(v) Each grain contains stress centres which act as barriers to the movement of domain walls, and it will be assumed at first that in all grains the maximum stress gradient around the stress centres is everywhere the same. Thus while an effective field less than H_0 say, may cause the wall to move reversibly between barriers a field greater than H_0 will cause the wall to move irreversibly across the grain—thus H_0 is the coercive force of the grain.

(vi) It will be assumed at first that the magnetization changes only by irreversible wall movements of the type described in (v) above: thus in effect it will be assumed that the hysteresis loops of the individual grains are perfectly 'square'.

We will now consider how certain properties of 'square loop' ferrite may be explained on the basis of this model.

3.1. *The Hysteresis Loop*

Consider a grain where the [111] direction makes an angle θ with the applied field H. Then the field acting on the domain wall is $H\cos\theta$, and if the grain is to be switched

$$H\cos\theta > H_0$$

or if the grain is to be just switched

$$H = H_0 \sec\theta. \qquad \ldots\ldots(1)$$

Thus if the field is increased in the negative sense slowly from zero, the material being initially in the remanent state (where the position of the domain walls is such that each grain is magnetized almost to saturation), then no change in the magnetization will occur until $H = H_0$ when grains whose [111] directions lie along the applied field will tend to switch. As the field is further increased grains whose magnetization make a rather larger angle with the field will reverse their magnetization, and so on until all the material has been switched.

Consider those grains where the magentization makes an angle less than θ with the field direction. Then it is easily shown that the resolved component of the magnetization along the field direction is given by

$$\frac{I}{I_s} = \int_0^{\theta} \sin\theta\cos\theta\, d\theta \Big/ \int_0^{\theta_m} \sin\theta\, d\theta \qquad \ldots\ldots(2)$$

where $\theta_m = 54°\,44'$,

i.e.
$$I = \frac{I_s}{4(1-\cos 54°\,44')}(1-\cos 2\theta). \qquad \ldots\ldots(3)$$

It will be noted that if θ is put equal to $54°\,44'$ then this expression gives I/I_s at remanence as 0·79 instead of the correct value, 0·87 (Gans 1932). Since both I and H are known in terms of the parameter θ, and remembering that a field H causes a change in magnetization of $2I$, a hysteresis loop may be plotted (figure 4). Values of the angle θ in degrees are marked on the figure, indicating whereabouts on the loop grains with [111] directions making an angle θ with the field reverse their magnetization.

Figure 4 represents the most rectangular loop that it is possible to obtain with a polycrystalline material, but the model upon which it is based is obviously over simplified and it will now be modified to put it upon a rather more realistic foundation.

It has been assumed hitherto that the barriers in all grains are of the same effective height H_0 Oe, so that the coercive force of each grain is H_0 Oe: the extreme rectangularity of the loop of figure 4 does of course derive from this uniformity of the 'barriers'. A more realistic model is that each grain contains a number of stress centres, and that the magnitudes of the maximum stress gradients around the centres are throughout the material distributed in a Gaussian mode about a mean value $\bar{H}_0$ Oe (cf. Néel 1942). The calculation of the loop shape now becomes very difficult, but to simplify matters we shall consider the similar but more artificial hypothesis that each grain has a single coercive force and that the magnitudes of these grain coercive forces are scattered in a Gaussian mode about a mean value $\bar{H}_0$ Oe.

If the applied field is written as $n\bar{H}_0$, then as before the effective field acting on grains whose [111] directions make an angle between θ and $\overline{\theta+\delta\theta}$ with the applied field is $n\bar{H}_0\cos\theta$, and those grains whose coercive forces are less than this will be switched.

Then it is easily shown that the fraction of grains which will be switched is given by

$$F = \frac{1}{2} \pm (2\pi)^{-1/2} \int_0^{\Delta H_0/\sigma} \exp\left\{-\frac{1}{2}\left(\frac{\Delta H_0}{\sigma}\right)^2\right\} d\left(\frac{\Delta H_0}{\sigma}\right)$$

where $\Delta H_0/\sigma = \bar{H}_0\,(n\cos\theta \sim 1)/\sigma$, and σ is the standard deviation of the distribution. (The positive sign above applies when $n\cos\theta > 1$.) Values of the above integral for given values of $\Delta H_0/\sigma$ may be obtained from tables. From (2) the resulting change in the resolved component of the magnetization is

$$\delta I = \frac{2I_sF}{1-\cos 54^\circ 44'} \sin\theta\cos\theta\,\delta\theta. \qquad \ldots\ldots(4)$$

This expression does not readily lend itself to integration and was summed numerically. $\delta\theta$ was taken to be 5°, expressed in radians, and δI was calculated for given values of n for $\theta = 2{\cdot}5^\circ, 7{\cdot}5^\circ, 12{\cdot}5^\circ \ldots 52{\cdot}5^\circ$. σ was at first taken to be equal to $\bar{H}_0/9$, i.e. 0·993 of all grains would have coercive forces lying between $0{\cdot}7\bar{H}_0$ and $1{\cdot}3\bar{H}_0$. A plot of the distribution function together with a family of hysteresis loops is given in figure 5. The squareness ratio R_s of the major loop is 0·75 and that of the minor loops ($H_{\max} = 1{\cdot}4\bar{H}_0$ and $H_{\max} = \bar{H}_0$) is 1·00. In addition, the effect of the reversible component of the magnetization must be considered. In the case of a square loop ferrite this component is approximately proportional to the applied field, i.e. $I = \chi_r H$, and this would shear the loop of figure 5 as if the field axis were rotated in the anticlockwise sense through an angle $\tan^{-1}\chi_r$. Obviously this would result in the squareness of the inner loops being reduced more than that of the outer loops, and so the squareness ratio would pass through a maximum as the field used to switch the core was increased from zero.

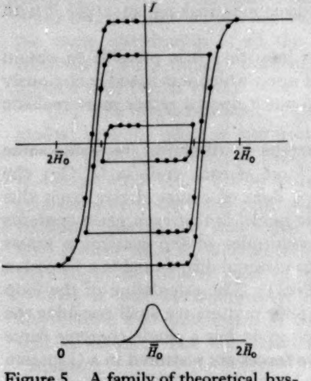

Figure 5. A family of theoretical hysteresis loops, the grains having their coercive forces distributed as indicated.

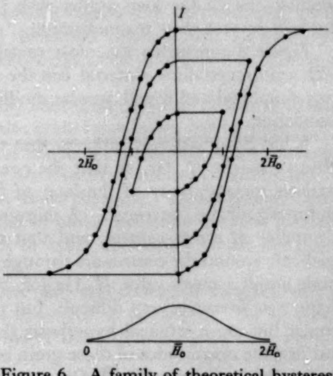

Figure 6. A family of theoretical hysteresis loops, the grains having their coercive forces distributed as indicated.

To investigate the effect of broadening the distribution function a series of loops, figure 6, was plotted for the case $\sigma = \bar{H}_0/2{\cdot}5$, i.e. 0·987 of all grains had coercive forces between 0 and $2\bar{H}_0$. R_s for $H = 2{\cdot}5\bar{H}_0$ is negative; for $H = 1{\cdot}6\bar{H}_0$, $R_s \sim 0{\cdot}50$ and for $H = \bar{H}_0$, $R_s \sim 0{\cdot}55$: the effect of the reversible component of the magnetization would be as before.

Comparing the major loops of figures 4, 5 and 6 it may be seen that the effect of increasing the spread of the grain coercive force around a mean value $\bar{H}_0$ is progressively to shear the loop and to round off the knee, the coercive force of the sample remaining unchanged. From the observed hysteresis loops of 'square loop' material σ would seem generally to lie somewhere between the two rather extreme cases plotted here.

3.2.1. *The pulse output.*

The form of pulse output to be expected from a ferrite with an 'ideal' loop as shown in figure 4 will now be investigated.

The domain wall velocity may be written as a function of the field in the form

$$v=R(H-H_0) \qquad \ldots\ldots(5)$$

where R is an empirical constant. The most recent verification of this expression was by Dillon and Earl (1959) who measured domain wall velocities, at various temperatures, in a single crystal of $Mn_{1.4}Fe_{1.6}O_4$. H_0 in the above expression will be identified with the H_0 of this paper, i.e. the coercive force of a single grain, which is again assumed to have the same value for all grains.

In the case of a polycrystalline material the field acting on a domain wall making an angle θ with it is $H\cos\theta$, and the wall velocity may be written as

$$v=R(H\cos\theta-H_0). \qquad \ldots\ldots(6)$$

The component of the applied field perpendicular to the wall will have a negligible effect on the wall motion for there is present an additional perpendicular component H_e which is much larger than the applied field (Becker 1951, Galt 1954).

From equation (2) the resolved part of the flux along the field direction, at remanence, for grains whose [111] directions make angles $\theta \rightarrow \overline{\theta+\delta\theta}$ with H, the material being in the form of a toroid of cross section A, is given by

$$\delta N=\frac{4\pi I_s A}{(1-\cos 54^\circ 44')}\sin\theta\cos\theta\,\delta\theta. \qquad \ldots\ldots(7)$$

If d, the distance the domain walls move during the switching process, is assumed to be equal for each grain then from equations (6) and (7) the rate of change of flux, measured along the field direction is given by

$$\frac{\delta N}{\delta t}=\frac{2\times 4\pi I_s AR}{(1-\cos 54^\circ 44')\,d}\sin\theta\cos\theta\,(H\cos\theta-H_0)\,\delta\theta. \qquad \ldots\ldots(8)$$

The voltage output from these grains will of course be in the form of a square pulse of duration t_θ, say. The minimum value of t_θ is

$$t_0=d/[R(H-H_0)] \qquad \ldots\ldots(9)$$

which is the time taken for grains to switch whose [111] directions lie along the field direction (i.e. $\theta=0$).

Case 1 : $t<t_0$. All grains with orientations from $\theta=0$ to $\theta=\theta_m$ will contribute to the output which will consequently have its maximum value during this time. θ_m as a function of the applied field is given by equation (1), but in any case $\theta_m \leqslant 54^\circ 44'$. The output in millivolts on a single secondary turn is then given by integrating (8) from $\theta=0$ to $\theta=\theta_m$, i.e. by

$$E_{max}=\frac{8\pi I_s AR\times 10^{-5}}{(1-\cos 54^\circ 44')\,d}\left[\frac{H}{3}(1-\cos^3\theta_m)-\frac{H_0}{2}(1-\cos^2\theta_m)\right]\mathrm{mv}. \qquad \ldots\ldots(10)$$

For values of the drive field greater than $H = H_0 \sec 54° 44'$ so that the core is fully switched $E_{\max}$ will vary linearly with H (as is found experimentally), the slope from equation (10) ($\theta_m = 54° 44'$) being given by

$$\frac{dE_{\max}}{dH} = 15{\cdot}7 I_s A \times 10^{-5} \frac{R}{d} \text{ mv Oe}^{-1}.$$

The magnitude of the intercept H_1 that the extrapolated linear portion of the curve makes with the field axis is $1{\cdot}24 H_0$ which is very nearly equal to the coercive force.

By way of illustration $E_{\max}$ has been calculated, for various values of H, for a 2 mm FX1508 core of Ferroxcube D2 using the following values: $A = 0{\cdot}0023 \text{ cm}^2$; $R = 3000 \text{ cm sec}^{-1} \text{ Oe}^{-1}$: this value has been arrived at by extrapolating to room temperature Dillon's value for $Mn_{1\cdot4}Fe_{1\cdot6}O_4$; $I_s = 220$ e.m.u.; $d = 20 \times 10^{-4}$ cm: this is the domain wall spacing observed experimentally; $H_0 = 1{\cdot}0$ Oe: this is a little less than the coercive force. The resultant curve is plotted in figure 7.

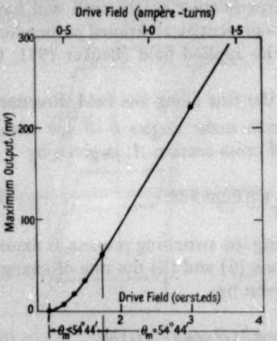

Figure 7. Theoretical plot of peak output against drive field for an idealized FX1508 core.

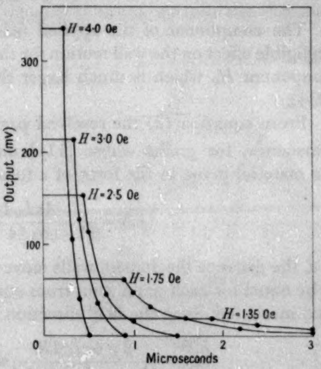

Figure 8. Theoretical output pulses, for various drive fields, of an idealized FX1508 core.

As the hysteresis loop of this material is not, unfortunately, like the 'ideal' loop of figure 4 a good numerical agreement between theoretical and experimental values cannot be expected (the theoretical output for a given drive is too low by a factor of two) but the shape of the curve agrees well with that found experimentally.

Case 2: $t > t_0$. At a time $t > t_0$ all grains whose magnetization makes an angle less than some angle θ' with the field will have finished switching, whilst grains whose magnetization makes a larger angle will be contributing fully to the 'voltage output' of the core. θ' as a function of t may be derived from equation (6), i.e.

$$\theta' = \cos^{-1}\left\{\frac{1}{H}\left(H_0 + \frac{d}{Rt}\right)\right\}. \qquad \ldots\ldots(11)$$

Thus the output from the core at time t will be given by integrating (8) between the limits θ' and θ_{m}, i.e. by

$$E_t = \frac{8\pi I_{\mathrm{s}} AR \times 10^{-5}}{(1-\cos 54°\,44')\,d}\left[\frac{H}{3}(\cos^3\theta' - \cos^3\theta_{\mathrm{m}}) - \frac{H_0}{2}(\cos^2\theta' - \cos^2\theta_{\mathrm{m}})\right] \text{mv.} \qquad \ldots\ldots(12)$$

By giving the parameters the values stated previously and by using appropriate values of θ_{m} and θ', plots may be drawn of the theoretical voltage output of an idealized FX1508 core against time (figure 8). The shape of the low drive curves agrees quite well with that observed experimentally, except that experimental pulses show an initial spike due to reversible wall movements (or possibly rotation of the magnetization). As the drive field is increased it is observed that the pulses take some time to attain their maximum output and this cannot be accounted for by the postulated model. One possible explanation, which is being tested experimentally, is that the domain walls take some time to break free from the stressed areas. This hypothesis is suggested by Dillon and Earl's observations (1959) of domain wall nucleation times in a single crystal of manganese ferrite.

When H is large so that $\theta_{\mathrm{m}} = 54°\,44'$ then the switching process will be completely finished at a time $t = d/[R(H\cos\theta_{\mathrm{m}} - H_0)]$. If H is small and the toroid is not fully switched then from (1), $H = H_0 \sec\theta_{\mathrm{m}}$ where $\theta_{\mathrm{m}} < 54°\,44'$ and theoretically the switching process will never be completed; that is the 'voltage output' from the core will tend to zero asymptotically.

3.2.2. *The calculation of the switching coefficient S_{w}.*

The switch time τ of a core is conventionally defined as the time elapsing between the two occasions at which the output from the core is 10% of its peak value: from figure 8 the first occasion is here at $t = 0$.

The second occasion, which here corresponds to the switch time, may in principle be obtained from the equation

$$nE_t = E_{\mathrm{m}} \text{ (where by convention } n = 10) \qquad \ldots\ldots(13)$$

where E_t and E_{m} are given by (12) and (10) respectively. Remembering that $\cos\theta'$ may be expressed explicitly by (11), on differentiating (13) one finds

$$\left[H - H_0\frac{1+(n-1)\cos^2\theta_{\mathrm{m}}}{1+(n-1)\cos^3\theta_{\mathrm{m}}}\right]\tau = \frac{nd^2\cos\theta'}{R^2\{1+(n-1)\cos^3\theta_{\mathrm{m}}\}}\Big/ S_{\mathrm{w}} \qquad \ldots\ldots(14)$$

where S_{w} is defined by $dH/d(1/t)$.

As θ' is a function of H etc. the relationship between $1/\tau$ and H is not linear, but if $H \gg H_0$ then it may be calculated from (13) that when $n = 10$, $\cos\theta'$ approaches the value 0·6489 (i.e. $\theta' \sim 49°$). Thus for large fields $1/\tau$ is very nearly a linear function of H, and comparing (14) with the conventional expression

$$(H - H_0')\tau = S_{\mathrm{w}}$$

we may write

$$\left[H - H_0\frac{1+(n-1)\cos^2\theta_{\mathrm{m}}}{1+(n-1)\cos^3\theta_{\mathrm{m}}}\right]\tau = S_{\mathrm{w}} = \frac{\mathrm{d}}{R}\left(\frac{n\cos\theta'}{1+(n-1)\cos^3\theta_{\mathrm{m}}}\right)^{1/2}.$$

Putting $n = 10$, $\theta_{\mathrm{m}} = 54°\,44'$ and $\cos\theta' = 0{\cdot}6489$, then

$$[H - 1{\cdot}47H_0]\tau = 1{\cdot}53\, d/R. \qquad \ldots\ldots(15)$$

On figure 9 are plotted points derived from the curves of figure 8 together with a (broken) line plotted from equation (15).

It may be seen that the curve derived from figure 8 approaches (15) asymptotically, and since θ' rapidly approaches its limiting value the curve is substantially linear for fields greater than 2·5 Oe. From (15) we find that for this part of the curve $S_w \sim 1{\cdot}0$ Oe μsec, the experimental value is about 0·8 Oe μsec.

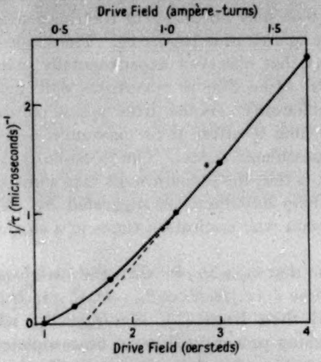

Figure 9. Theoretical plot of 1/(switch time) against drive field for an idealized FX1508 core.

§ 4. CONCLUSIONS

Observations of domain patterns on polycrystalline 'square loop' ferrites suggested a new model for the domain configuration, which accounted for:

(i) The general shape of the hysteresis loop, and the way in which the loop shape alters if the firing conditions are such that there is a large spread in the magnitudes of the maximum stress gradients.

(ii) The shape of the output pulse under various drive conditions resembled that observed experimentally, as did the estimated values of peak output and duration of pulse.

(iii) It was shown that for high drive fields a linear relationship existed between the field and the reciprocal of the conventionally defined switch time. For low drives this curve was concave upwards.

Thus it would seem probable that in materials with a rectangular hysteresis loop the magnetization lies along the [111] direction in each grain ($K < 0$) and that the magnetization generally reverses by the motion of 180° walls: if the drive field is very large the magnetization may reverse by a rotational process (Shevel 1959). The motion is impeded by stress gradients, the maxima of which are of about the same magnitude throughout the material. There is no nucleation of walls, in contrast to the theory of Goodenough (1957).

In brief, the conditions for squareness are:

(i) That if the magnetization is to lie along the [111] direction then the conditions of Wijn *et al.* (1954) must be satisfied, i.e. predominant crystalline anisotropy, a low magnetostriction particularly in the [111] direction and low shape anisotropy. If these conditions are violated so that the magnetization vectors tend to fan out into a cone of large semi-vertical angle θ the remanence I_r will be lowered (see Wijn), and the ratio of the field H_m necessary to reverse all the magnetization to H_0 will increase. From equations (1) and (2) we find, for example,

θ	$54° 44'$	$70°$	$90°$
I_r/I_s	0·79	0·67	0·50
H_m/H_0	1·73	2·92	∞

If the ratio of H_m/H_0 is large one would expect that even the minor loops would have rather a long 'tail' that would preclude coincident current operation, but increasing θ has a negligible effect on the knee of the curve which still closely resembles the knee of figure 4.

(ii) There must be uniformity of the magnitude of the maximum stress gradients through the material. Generally this condition would be facilitated by a material of uniform grain size and low magnetostriction. If there is a large spread in these magnitudes then the 'ideal' loop of figure 4 will be sheared and the knee rounded off.

ACKNOWLEDGMENTS

The author would like to thank the management of Mullard Research Laboratories for permission to publish this paper, and also Dr. F. Berz for some helpful discussions.

REFERENCES

BATES, L. F., CLOW, H., CRAIK, D. J., and GRIFFITHS, P. M., 1958, *Proc. Phys. Soc.*, **72,** 224.
BECKER, R., 1951, *J. Phys. Radium*, **12,** 332.
CRAIK, D. J., and GRIFFITHS, P. M., 1959, *Proc. Phys. Soc.*, **73,** 1.
DILLON, J. Jr., and EARL, H. E. Jr., 1959, *J. Appl. Phys.*, **30,** 202.
ELMORE, W. C., 1938, *Phys. Rev.*, **54,** 309.
GALT, J. K., 1954, *Bell Syst. Tech. J.*, **33,** 1023.
GANS, R., 1932, *Ann. Phys., Lpz.*, **15,** 28.
GOODENOUGH, J. B., 1957, *Proc. Instn Elect. Engrs* B, **104,** Suppl. 5–7, 400.
GYORGI, E. M., 1957, *J. Appl. Phys.*, **28,** 1011.
KITTEL, C., 1949, *Rev. Mod. Phys.*, **21,** 541.
NÉEL, L., 1942, *Cahiers Phys.*, **12,** 1.
SHEVEL, W. LEE, Jr., 1959, *I.B.M. Journal*, **3,** 1.
STEWART, K. H., 1954, *Ferromagnetic Domains* (Cambridge: University Press), Chapter 8.
WIJN, H. P. J., GORTER, E. W., ESVELDT, C. J., and GELDERMANS, P. W., 1954, *Philips Tech. Rev.*, **16,** 49.

The Propagation of Sound in Monatomic Gas Mixtures

By R. HOLMES and W. TEMPEST
Acoustics Laboratory, University of Liverpool

Communicated by H. D. Parbrook; *MS. received 29th January* 1960

Abstract. The velocity and absorption of infinitesimal plane sound waves have been measured in neon–helium, argon–helium and krypton–helium mixtures, with molar fractions of helium from 0 to 1 in each mixture. The measurements were made at 25 °C, at a frequency of 700 kc/s, and at pressures from 0·1 to 2 atm. The observed velocity of sound was correlated with values calculated from simple mixture thermodynamics; the measured absorption coefficients agreed with those calculated from a formula derived by Kohler.

§ 1. INTRODUCTION

In the past thirty years the propagation of sound in gas mixtures has received considerable attention in both experimental and theoretical fields. Almost all the experimental work was concerned with the propagation in mixtures in which one or both components show evidence of a relaxation process involving the vibrational specific heats, and was designed to investigate the transfer of energy into and out of the vibrational modes of molecules. In these circumstances the absorption due to relaxation has usually been of such magnitude as to obscure the much smaller effects due to viscosity, thermal conduction and diffusion.

The earliest theoretical attempt to include the effects of diffusion on sound propagation appears to be that of Rocard (1930, 1935) who derived an approximate expression for the additional absorption in a binary mixture due to mass diffusion. Kohler (1941, 1949) worked out the total absorption due to mass diffusion, thermal diffusion, viscosity and thermal conduction in a binary monatomic mixture and pointed out that, while Rocard's expression gave the correct dependence of the diffusion absorption on density and frequency, it did not give the correct dependence on mixture composition. Meixner (1943) considered the more general case of a mixture with any number of components and included the effects of relaxation of internal energies and also chemical reactions; he noted that for a binary monatomic gas mixture his result can be equated to that of Kohler.

If one investigates the propagation in binary monatomic mixtures there are no complicating relaxation effects and all the transport coefficients (thermal conductivity, viscosity, mass diffusion and thermal diffusion) can be computed with sufficient accuracy.

The only measurements made in such mixtures appear to be those by Petralia (1954) who measured absorption in helium–argon mixtures. He attempted to correlate his results with Kohler's theory but did not obtain agreement.

The purpose of the present experiment was therefore to determine the velocity and absorption in binary mixtures of monatomic gases and to test whether the velocity and absorption could be predicted theoretically.

The mixtures chosen for this work were helium–neon, helium–argon and helium–krypton.

We may remark here that the mixture theory is of particular interest because it is possible (Meixner 1952) to think of a single relaxing gas as a mixture in which the different components are specified by the internal states of the molecules.

§ 2. THEORY

2.1. *Sound Velocity*

If ideal gas behaviour is assumed, the velocity of sound in a mixture of two monatomic gases is given by

$$V^2 = \frac{C_P}{C_V}\frac{\boldsymbol{R}T}{M} \qquad \ldots\ldots(1)$$

where T = absolute temperature (°K), $\boldsymbol{R}$ = gas constant per gramme molecule (erg deg^{-1} mole^{-1}), M = average molecular weight of the mixture = $M_1x_1 + M_2x_2$ where M_1, M_2 = gramme molecular weights of components 1, 2; C_V, C_P = molar heats of the mixture at constant volume, pressure; $C_V = C_{V_1}x_1 + C_{V_2}x_2$, where C_{V_1}, C_{V_2} = molar heats at constant volume of components 1, 2; $C_P = C_V + \boldsymbol{R}$.

2.2. *Sound Absorption*

Kohler (1941, 1949) has used the kinetic theory method to calculate the absorption of sound in a binary mixture in which relaxation of internal energies does not occur. He found the solution for the case of infinitesimal plane waves, using the expressions derived by Chapman (1916, 1917) and Enskog (1917) for the heat flux vector, the pressure tensor, and the mean velocities of the two components. Like the 'Stokes–Kirchhoff' equation for a single gas, the result is only valid so long as the wavelength is much greater than the mean free path.

The total amplitude absorption coefficient (in nepers per cm) may be expressed as the sum of three terms (Kohler 1949)

$$\alpha = \alpha\,(\text{viscosity}) + \alpha\,(\text{thermal conductivity}) + \alpha\,(\text{diffusion})$$

viz.

$$\frac{\alpha p}{f^2} = \frac{8\pi^2\mu}{3V\gamma} + \frac{2\pi^2(\gamma-1)\lambda}{V\gamma c_P} + \frac{2\pi^2\gamma x_1x_2pD_{12}}{V^3}\left\{\frac{M_2-M_1}{M} + \frac{\gamma-1}{\gamma}\frac{k_T}{x_1x_2}\right\}^2 \qquad \ldots\ldots(2)$$

where f = sound frequency (c/s), p = total pressure (dyn cm^{-2}), V = sound velocity in the mixture (cm sec^{-1}), λ = thermal conductivity of the mixture (cal cm^{-2} sec^{-1}), μ = viscosity of the mixture (poise), D_{12} = the mutual diffusion coefficient, k_T = the thermal diffusion ratio, c_P = specific heat per gramme of the mixture (cal g^{-1} deg.^{1}).

It should be noted that the coefficients μ, λ, D_{12}, k_T, c_P, γ in this equation are those for the particular mixture specified by x_1 and x_2 and must be calculated for each pair of values of x_1 and x_2. V is given by equation (1),

and
$$\gamma = \frac{C_P}{C_V} = \frac{\boldsymbol{R} + C_{V_1}x_1 + C_{V_2}x_2}{C_{V_1}x_1 + C_{V_2}x_2}$$

but since for monatomic gases $C_{v_1}=C_{v_2}=3\boldsymbol{R}/2$, then $\gamma=5/3$ for all our mixtures.

The specific heat per gramme for the mixture is given by

$$c_p=\frac{x_1C_{v_1}+x_2C_{v_2}+\boldsymbol{R}}{x_1M_1+x_2M_2}.$$

The transport coefficients μ, λ, D_{12} and k_T can be calculated from kinetic theory. We have calculated them from the equations given by Hirschfelder, Curtiss and Bird (1954), using the Lennard-Jones potential as the molecular model. The force constants for the mixture for this potential were obtained from the force constants for the pure gases using the empirical relations: (e.g. Hirschfelder, Curtiss and Bird 1954)

$$r_{12}=\frac{r_1+r_2}{2} \qquad \text{and} \qquad \frac{\epsilon_{12}}{k}=\left(\frac{\epsilon_1}{k}\frac{\epsilon_2}{k}\right)^{1/2}$$

where r = collision diameter in Å, and ϵ/k = potential parameter in deg K.

The use of these empirically derived force constants in the first approximation expressions for μ, λ and D_{12} gives values within 1 or 2%; these are sufficiently accurate for the present experiment. In the case of k_T, the accuracy of the calculation may not be so high, but is known to be not worse than about 10%; since the contribution of the k_T term to the sound absorption is only about one tenth that of the ordinary diffusion term, this accuracy is also adequate.

Substitution of the appropriate numerical data into equation (2) shows that the diffusion term (the third term) is as large as, or larger than, the viscosity and thermal conduction terms when M_2-M_1 is large and M is small. Helium was therefore chosen as the lighter gas in these experiments.

The ratio $\lambda/\mu c_p$, which has the value 3/2 in a monatomic gas, can have larger values in mixtures; this means that thermal conduction is relatively more important than in pure gases where it contributes less to the absorption than does viscosity.

§ 3. EXPERIMENTAL DETAILS

3.1. *Gas Supplies*

Gases were supplied by British Oxygen Gases Ltd.; details are set out in the table.

Gas	Purity	Principal impurity
Atmospheric helium	99·5% or better	Neon
Helium	‘ Spectrally pure ’	
Neon	‘ Spectrally pure ’	
Argon	99·95%	Nitrogen
Krypton	99% or better	Xenon

Comparison of the sound velocity in the two helium samples showed that the purity of the ‘ atmospheric ’ gas was higher than the figure claimed.

3.2. *Experimental Procedure*

The absorption and velocity were measured using a pulse technique which has been described elsewhere (Parbrook and Tempest 1957, Holmes, Parbrook and Tempest 1960).

The mole fractions of the two components of the gas mixture were found by measuring their partial pressures. The technique used to fill the measuring chamber with the required mixture was as follows: if the required mixture had mole fractions x_1 and x_2 of the components and a total pressure p, then the first component was passed into the evacuated chamber until the pressure reached x_1p. A three-way tap at the entrance to the chamber was then used to connect the chamber to the second gas supply, which was at some pressure considerably above x_1p. The higher pressure of the second supply minimized any back diffusion. The second gas was then admitted until the pressure reached the final value p. After filling it was found necessary to wait for 24 hours before taking measurements to allow the gases to diffuse thoroughly.

In order to reduce the pressure in the chamber without altering the composition of the mixture, the gas filling system was evacuated and the tap on the measuring chamber was opened and then closed when pressure equilibrium had been established. The filling system had a volume of about 1/6 of that of the chamber and this procedure thus reduced the pressure by 1/7. The constancy of composition of the gas at various pressures was established from the velocity measurements.

The assumption that the mole fractions of the gases in the mixture will be in the ratio of the partial pressures is subject to a small error due to the non-ideality of the gases. The correction however is less than the experimental error in the measurements of the mole fractions and was not considered significant.

§ 4. RESULTS

4.1. *Argon–Helium*

Figure 1 shows the measured absorption as a function of inverse pressure; the fact that the points lie near to a straight line passing through the origin verifies that, as predicted by equation (2), αp is constant at constant frequency.

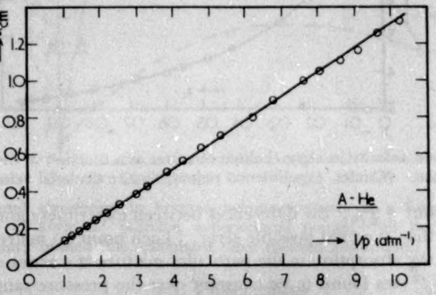

Figure 1. Sound absorption as a function of pressure in a argon–helium mixture containing 20% (molar) helium.

Figure 2 shows the measured values of $\alpha p/f^2$ together with the calculated $\alpha p/f^2$ and the calcuated $\alpha_{\mathrm{vt}}p/f^2$ as a function of the mole fraction of argon. (α_{vt} is the absorption due to viscosity and thermal conduction alone.) The measured $\alpha p/f^2$ fit the calculated curve well and the difference between the total and viscothermal absorptions shows the large effect of diffusion. The accuracy of the measured $\alpha p/f^2$ values is estimated as within ±2% while accuracy of the calculated

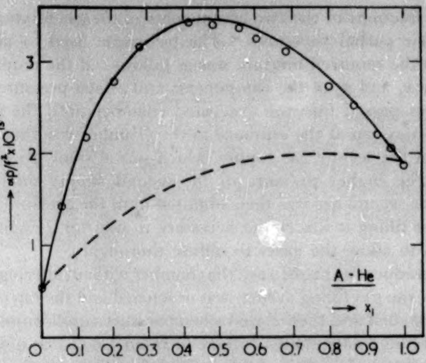

Figure 2. Sound absorption in argon–helium mixtures as a function of the mole fraction of argon. (Circles, experimental points; full line, calculated total absorption; broken line, calculated visco-thermal absorption.)

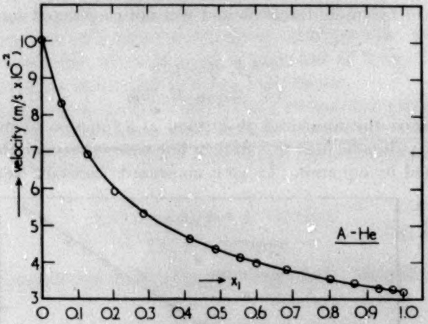

Figure 3. Sound velocity in argon–helium mixtures as a function of the mole fraction of argon. (Circles, experimental points; line, calculated velocity.)

values is to about ± 5%; the differences between experiment and calculation are therefore less than the total possible error. Each point on figure 2 was obtained by measuring the absorption in the particular mixture at a series of pressures and in all cases $\alpha p/f^2$ was found to be constant over the pressure range covered.

Figure 3 shows the measured velocities and the calculated velocity curve as functions of the mole fraction of argon. The points fit the curve within the limits of the accuracy of the measurement of the mole fraction of argon.

4.2. *Neon–Helium*

Figure 4 shows the calculated $\alpha p/f^2$, the calculated $\alpha_{vt}p/f^2$ and the measured points; these agree within the limits of possible error, which are estimated to be about the same as for the argon–helium results.

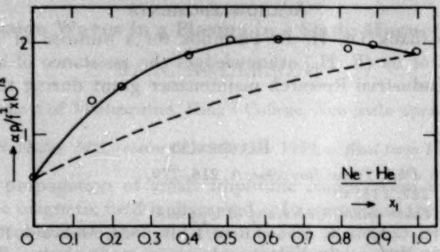

Figure 4. Sound absorption in neon–helium mixtures as a function of the mole fraction of neon. (Circles, experimental points; full line, calculated total absorption; broken line, calculated visco-thermal absorption.)

4.3. *Krypton–Helium*

Figure 5 shows $\alpha p/f^2$ (measured), $\alpha p/f^2$ (calculated), and $\alpha_{vt}p/f^2$ (calculated) as functions of the mole fraction of krypton in a krypton–helium mixture. As in the case of neon–helium, the measured points agree with the calculated curve within the limits of possible error.

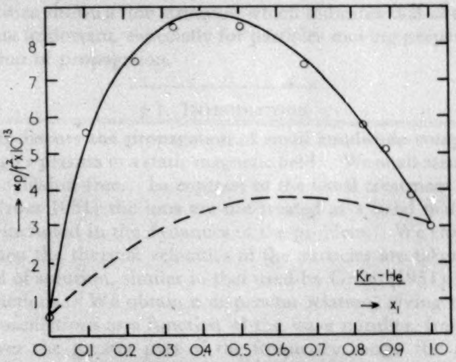

Figure 5. Sound absorption in krypton–helium mixtures as a function of the mole fraction of krypton. (Circles, experimental points; full line, calculated total absorption; broken line, calculated visco-thermal absorption.)

§ 5. CONCLUSIONS

We may conclude from the velocity results that the velocity of sound in a binary mixture of monatomic gases can be predicted from a knowledge of the mole fractions of the components, using the simple theory expressed in equation (1).

The absorption of sound in a binary monatomic gas mixture is accounted for by the Kohler formula (equation (2)) taking into account ordinary and thermal diffusion. This result also provides an interesting confirmation of the validity of the kinetic theory method as applied to the propagation of sound waves in gases.

ACKNOWLEDGMENTS

We wish to thank Dr. H. D. Parbrook for a number of suggestions and criticisms; one of us (R. H.) acknowledges the assistance of a Department of Scientific and Industrial Research maintenance grant during the course of this work.

REFERENCES

CHAPMAN, S., 1916, *Phil. Trans. Roy. Soc.* A, **216,** 279.
—— 1917, *Ibid.*, **217,** 115.
ENSKOG, D., 1917, *Dissertation*, University of Uppsala.
HIRSCHFELDER, J. O., CURTISS, C. F., and BIRD, K. B., 1954, *Molecular Theory of Gases and Liquids* (New York : John Wiley).
HOLMES, R., PARBROOK, H. D., and TEMPEST, W., 1960, *Acustica*, **10,** in the press.
KOHLER, M., 1941, *Ann. Phys., Lpz.*, **39,** 209.
—— 1949, *Z. Phys.*, **127,** 40.
MEIXNER, J., 1943, *Ann. Phys. Lpz.*, **43,** 470.
—— 1952, *Acustica*, **2,** 101.
PARBROOK, H. D., and TEMPEST, W., 1957, *Acustica*, **7,** 354.
PETRALIA, S., 1954, *Nuovo Cim.*, **11,** 570.
ROCARD, Y., 1930, *J. Phys. Radium*, **1,** 426.
—— 1935, *Propagation et Absorption du Son* (Paris : Hermann).

Compression Waves in a Plasma in a Static Magnetic Field

By N. ANDERSON†

Department of Mathematics, King's College, Newcastle upon Tyne

Communicated by R. Hide; *MS. received* 21*st October* 1959, *in final form* 16*th December* 1959

Abstract. The propagation of small amplitude compression waves through a plasma in a static magnetic field is discussed. In contrast to the usual treatment of this type of problem we shall not treat the ions as a fixed neutralizing background but shall include them in the dynamics of the problem. The problem is discussed in the general case in which the thermal velocity distribution is not negligible. The method of solution is to use the linearized Boltzmann equation in conjunction with Maxwell's equations to obtain a distribution function and dispersion relation. To obtain the dispersion relation an approximation method is used and it is shown that over the greater part of the frequency range the oscillations are of a characteristic wave number. We show that the inclusion of the ions in the dynamics is justified by the fact that at integral multiples of the ion gyrofrequency the ions play the dominant role. The results obtained show that the waves are undamped. The graph of the distribution function for particles with large velocities shows a fine structure which indicates that at these velocities collisions become important, especially for particles moving perpendicular to the field and direction of propagation.

§ 1. INTRODUCTION

We shall discuss the propagation of small amplitude compression waves through a plasma in a static magnetic field. We shall assume the motion to be collision-free. In contrast to the usual treatment of this type of problem (see Gross 1951) the ions are not treated as a fixed neutralizing background but are included in the dynamics of the problem. We shall consider the general case when the thermal velocities of the particles are taken into account.

The method of solution, similar to that used by Gross (1951), is by means of distribution functions. We obtain a dispersion relation, giving the frequencies of the possible oscillations as a function of the wave number, from which it can be seen that over the greater part of the frequency range the oscillations are characterized by a constant wave number, and which in the case of low frequencies and zero temperature leads to the well-known result of Alfvén. It also shows the dominant role of the ions when the frequency is near an integral multiple of the ion gyrofrequency. The results obtained indicate that the waves are undamped. In the case of high velocity particles we obtain a simple expression for the distribution function.

§ 2. BASIC EQUATIONS

Consider a plasma, composed of electrons and singly ionized atoms, in a static magnetic field. We shall assume that the plasma is initially in equilibrium and consider the propagation of small amplitude longitudinal waves in a direction perpendicular to the magnetic field.

† Now at Trinity College, Cambridge.

Choose a rectangular coordinate system such that the z axis is in the direction of the magnetic field and suppose that the direction of propagation is that of the positive x axis. If we describe the state of the plasma by a distribution function $f=f(\mathbf{v},\mathbf{r},t)$ where $\mathbf{v}$ is the velocity vector, $\mathbf{r}$ the position vector and t the time, then we can describe the motion of the plasma by the collision free Boltzmann equation

$$\frac{\partial f}{\partial t}+\frac{\partial}{\partial x_i}(fv_i)+\frac{\partial}{\partial v_i}(fF_i)=0 \qquad \ldots\ldots(1)$$

where f is the distribution function of any particle type, v_i are the components of the velocity vector, and F_i are the components of the external force per unit mass, m the mass of the particle. Let e be the charge on the particle, then we have

$$\mathbf{F}=e[\mathbf{E}+(\mathbf{v}\times\mathbf{H})/c]/m \qquad \ldots\ldots(2)$$

where $\mathbf{E}$ is the electric field vector and $\mathbf{H}$ the magnetic field vector, we assume the latter to be constant. Suppose we employ the usual method of linearization and write the distribution function in the form

$$f=f_0+f_1 \qquad \ldots\ldots(3)$$

where f_0 represents an equilibrium distribution and f_1 a small perturbation due to the wave. We assume f_1 is independent of y or z. Throughout the paper we shall use mixed Gaussian units for the electromagnetic field. We shall assume a Maxwellian distribution for f_0 and that the ion and electron temperatures are equal. Hence

$$f_0=A\exp\left[-\lambda(v_x^2+v_y^2+v_z^2)\right]. \qquad \ldots\ldots(4)$$

We also assume that the electric field is small enough so that we can ignore the products of its components with the derivatives of f_1. With these assumptions (1) reduces to

$$\frac{\partial f_1}{\partial t}+v_x\frac{\partial f_1}{\partial x}+\frac{e}{m}\left(E_x\frac{\partial f_0}{\partial v_x}+E_y\frac{\partial f_0}{\partial v_y}\right)+\frac{eH}{mc}\left(v_y\frac{\partial f_1}{\partial v_x}-v_x\frac{\partial f_1}{\partial v_y}\right)=0. \qquad \ldots\ldots(5)$$

Suppose we introduce polar coordinates in velocity space:

$$v_x=\rho\cos\theta \quad v_y=\rho\sin\theta \quad v_z=v_z$$

and if we write $\Omega=eH/mc$ then (5) reduces to

$$\frac{\partial f_1}{\partial t}+v_x\frac{\partial f_1}{\partial x}+\frac{e}{m}\left(E_x\frac{\partial f_0}{\partial v_x}+E_y\frac{\partial f_0}{\partial v_y}\right)-\Omega\frac{\partial f_1}{\partial\theta}=0. \qquad \ldots\ldots(6)$$

We now make the further assumption that f_1, $\mathbf{E}$ and $\mathbf{j}$ are proportional to $\exp[i(\omega t+kx)]$, where $\mathbf{j}$ is the current density. Since f_0 is independent of θ (6) reduces to

$$i(\omega+k\rho\cos\theta)f_1-\Omega\frac{\partial f_1}{\partial\theta}=-\frac{e}{m}(E_x\cos\theta+E_y\sin\theta)\frac{\partial f_0}{\partial\rho}. \qquad \ldots\ldots(7)$$

Hence

$$f_1=\frac{e}{m\Omega}\frac{\partial f_0}{\partial\rho}\exp\left[\frac{i}{\Omega}(\omega\theta+k\rho\sin\theta)\right]\left\{\int_0^\theta(E_x\cos\phi+E_y\sin\phi)\right.$$
$$\left.\times\exp\left[-\frac{i}{\Omega}(\omega\phi+k\rho\sin\phi)\right]d\phi-g(\rho)\right\}$$

where $g(\rho)$ is an arbitrary function of ρ. To comply with physical restrictions on the solution we choose $g(\rho)$ such that f_1 is periodic in θ with period 2π. It is sufficient that for all ρ we have $f_1(\rho, 2\pi)=f_1(\rho, 0)$, which enables us to determine $g(\rho)$.

Introduce the notation $F_1=E_x-iE_y$; $F_2=E_x+iE_y$. Then we wish to consider the integral

$$I(\theta)=\int_0^\theta (E_x\cos\phi+E_y\sin\phi)\exp\left[-i(\omega\phi+k\rho\sin\phi)/\Omega\right]d\phi.$$

Making use of the expression

$$\exp(iz\sin\phi)=\sum_{n=-\infty}^{n=+\infty} \mathrm{J}_n(z)\exp(in\phi)$$

we can evaluate the integral and on substitution into the expression for f_1 we obtain

$$f_1=\frac{ie}{2m}\frac{\partial f_0}{\partial\rho}\sum_{p=-\infty}^{p=+\infty}\sum_{n=-\infty}^{n=+\infty}\mathrm{J}_p\left(\frac{k\rho}{\Omega}\right)\mathrm{J}_n\left(-\frac{k\rho}{\Omega}\right)$$
$$\times\left[\frac{F_1\exp\{i(n+1)\theta\}}{\omega-(n+1)\Omega}+\frac{F_2\exp\{i(n-1)\theta\}}{\omega-(n-1)\Omega}\right]\mathrm{e}^{ip\theta}.$$

Integration of this distribution function over velocity space gives the perturbation in the particle density which is an infinite series of generalized hypergeometric functions.

§ 3. THE DISPERSION EQUATION

We will now consider the relation between the frequency of the oscillation and the wave number. Introduce the notation

$$I_1=\int_0^\infty\int_0^{2\pi}\int_{-\infty}^{\infty} f_1\,\mathrm{e}^{i\theta}\rho^2 d\rho d\theta dv_2\quad I_2=\int_0^\infty\int_0^{2\pi}\int_{-\infty}^{-\infty} f_1\,\mathrm{e}^{-i\theta}\rho^2 d\rho d\theta dv_2.$$

We assume that the undisturbed plasma is electrically neutral which implies from Maxwell's equations that the divergence of the current density is zero, and since we have assumed exponential dependence on x only this is equivalent to a zero x component of current. Hence we have

$$\begin{aligned} e[(I_1)_+-(I_1)_-]&=\ \ icj_y\\ e[(I_2)_+-(I_2)_-]&=-icj_y \end{aligned}\qquad\ldots\ldots(8)$$

where e is now the charge on the ion. If we neglect the displacement current in Maxwell's equations we have

$$\nabla\times\mathbf{H}=4\pi\mathbf{j}\,;\qquad \nabla\times\mathbf{E}=-\frac{1}{c}\frac{\partial\mathbf{H}}{\partial t}$$

which give

$$j_y=ck^2(F_2-F_1)/8\pi\omega.\qquad\ldots\ldots(9)$$

From (8) and (9) we obtain

$$\left.\begin{aligned}(I_1)_+-(I_1)_-&=\gamma(F_2-F_1)\\ (I_2)_+-(I_2)_-&=-\gamma(F_2-F_1)\end{aligned}\right\}\qquad\ldots\ldots(10)$$

where $\gamma=ic^2k^2/8\pi\omega e$.

Write $\quad I_1=\beta^1F_2+\alpha^1F_1;\quad I_2=\beta^2F_2+\alpha^2F_1.$

Then equation (10) becomes

$$\left.\begin{aligned} F_1(\alpha^1_+ - \alpha^1_- + \gamma) + F_2(\beta^1_+ - \beta^1_- - \gamma) = 0 \\ F_1(\alpha^2_+ - \alpha^2_- - \gamma) + F_2(\beta^2_+ - \beta^2_- + \gamma) = 0 \end{aligned}\right\}$$

where subscripts indicate particle type. There exists a non-zero solution, if, and only if, the determinant

$$\begin{vmatrix} \alpha^1_+ - \alpha^1_- + \gamma & \beta^1_+ - \beta^1_- - \gamma \\ \alpha^2_+ - \alpha^2_- - \gamma & \beta^2_+ - \beta^2_- + \gamma \end{vmatrix} = 0. \qquad \ldots\ldots(11)$$

If we write

$$\lambda^1_\pm = \lambda_\pm \Omega^2_\pm / k^2 \quad A_\pm = n_0(\lambda_\pm/\pi)^{3/2} \quad \lambda_\pm = (m_\pm / 2\boldsymbol{k}T)$$

where $\boldsymbol{k}$ is Boltzmann's constant, n_0 the equilibrium particle density and T the absolute temperature, then the coefficients reduce to the form

$$\alpha^1_\pm = \mp \frac{2ien_0(\lambda^1_\pm)^2}{m_\pm} \sum_{n=-\infty}^{n=+\infty} \int_0^\infty \frac{z^3 \exp(-\lambda^1_\pm z^2) \mathrm{J}_n(z) \mathrm{J}_{n+2}(z) dz}{\omega + (n+1)\Omega_\pm} = \beta^2_\pm$$

$$\alpha^2_\pm = \mp \frac{2ien_0(\lambda^1_\pm)^2}{m_\pm} \sum_{n=-\infty}^{n=+\infty} \int_0^\infty \frac{z^3 \exp(-\lambda^1_\pm z^2) \mathrm{J}_n(z) \mathrm{J}_n(z) dz}{\omega + (n-1)\Omega_\pm}$$

$$\beta^1_\pm = \mp \frac{2ien_0(\lambda^1_\pm)^2}{m_\pm} \sum_{n=-\infty}^{n=+\infty} \int_0^\infty \frac{z^3 \exp(-\lambda^1_\pm z^2) \mathrm{J}_n(z) \mathrm{J}_n(z) dz}{\omega + (n+1)\Omega_\pm}.$$

We use this subscript form to avoid unnecessary repetition of results. To check the results so far obtained we will consider the case when the temperature is zero. In the coefficients given we obtain contributions only from those terms which contain products of zero-order Bessel functions. In this case the coefficients reduce to

$$\alpha^1_\pm = \beta^2_\pm = 0 \qquad \alpha^2_\pm = \mp ien_0/[m_\pm(\omega - \Omega_\pm)] \qquad \beta^1_\pm = \mp ien_0/[m(\omega + \Omega_\pm)]$$

and the dispersion relation becomes by substitution in (11)

$$\frac{(m_+ + m_-)\omega^2}{m_+ m_-} = -\frac{c^2 k^2}{4\pi n_0 e^2}\left(\omega^2 - \frac{e^2 H^2}{m_+ m_- c^2}\right). \qquad \ldots\ldots(12)$$

If we assume that the frequency of the oscillations is considerably less than the gyrofrequency of the ions then this reduces to the well-known result of Alfvén

$$k^2 = 4\pi n_0 (m_+ + m_-)\omega^2 / H^2.$$

We shall now return to the general case of non-zero temperature. Following Gross (1951) consider the functions

$$K_p(z) = \sum_{n=-\infty}^{n=+\infty} \left[\frac{\mathrm{J}_{n+p}(z)\mathrm{J}_n(z)}{(n+1) + \omega/\Omega}\right] \qquad L_p(z) = \sum_{n=-\infty}^{n=+\infty} \left[\frac{\mathrm{J}_{n+p}(z)\mathrm{J}_n(z)}{(n-1) + \omega/\Omega}\right].$$

From Janhke and Emde (1954, p. 145) we have

$$\frac{\mathrm{J}_p[\sqrt{2}z(1-\cos\gamma)^{1/2}](1-\mathrm{e}^{-i\gamma})^p}{(\sqrt{2})^p[(1-\cos\gamma)^{1/2}]^p} = \sum_{n=-\infty}^{n=+\infty} \mathrm{J}_{n+p}(z)\mathrm{J}_n(z)\,\mathrm{e}^{in\gamma}.$$

If we multiply both sides by $\exp[i(\omega/\Omega+1)\gamma]$ and integrate from $\gamma=0$ to $\gamma=2\pi$ we obtain $K_p(z)$, similarly using $\exp[i(\omega/\Omega-1)\gamma]$ gives $L_p(z)$. If we substitute these results in the coefficients and reverse the orders of integration we can carry out one of the integrations using the result that

$$\int_0^\infty \mathrm{J}_\nu(at)\exp(-p^2t^2)t^{\mu-1}dt$$
$$=\frac{\Gamma\{\tfrac{1}{2}(\mu+\nu)\}(a/2p)^\nu}{2p^\mu\Gamma(\nu+1)}\exp\left(-\frac{a^2}{4p^2}\right){}_1F_1\left(\frac{\nu-\mu+2}{2};\quad \nu+1;\quad \frac{a^2}{4p^2}\right)$$

and obtain the coefficients in the form of integrals over the range 0 to 2π. We shall now consider the special case when the parameters $\lambda^1_\pm$ are very small; this could correspond to very high temperatures. The integrands in the coefficients are rapidly decreasing and by extending the range of integration to infinity and expanding in terms of the variable γ we can evaluate the integrals in this case. The coefficients become

$$\alpha^2_\pm=-2ien_0c\pi^{1/2}\cot\left(\frac{\pi\omega}{\Omega_\pm}\right)\frac{(\lambda^1_\pm)^{1/2}+(\lambda^1_\pm)^{3/2}[(\omega/\Omega_\pm-1)^2-\frac{1}{4}]}{4H}$$

$$\beta^1_\pm=-2ien_0c\pi^{1/2}\cot\left(\frac{\pi\omega}{\Omega_\pm}\right)\frac{(\lambda^1_\pm)^{1/2}+(\lambda^1_\pm)^{3/2}[(\omega/\Omega_\pm+1)^2-\frac{1}{4}]}{4H}$$

$$\alpha^1_\pm=+2ien_0c\pi^{1/2}\cot\left(\frac{\pi\omega}{\Omega_\pm}\right)\frac{(\lambda^1_\pm)^{1/2}-3(\lambda^1_\pm)^{3/2}[(\omega/\Omega_\pm+1)^2-\frac{1}{4}]}{4H}=\beta^2_\pm.$$

This leads to a dispersion relation

$$\cot(\pi\omega/\Omega_+)=[3\cot(\pi\omega/\Omega_-)(m_+)^{3/2}]/[4\alpha^2(m_-)^{3/2}] \quad \ldots\ldots(13)$$

where we have written $\omega=\alpha\Omega_+$. For values of α such that $\Omega_+\ll\omega\ll|\Omega_-|$ this result implies that $\cot(\pi\omega/\Omega_+)$ has a large negative value, which means that the frequency ω lies close to an integral multiple of the ion gyrofrequency Ω_+. This is analogous to the discovery by Gross of bands of forbidden frequencies at integral multiples of the electron gyrofrequency. Hence if we consider the graph of $(\lambda^1_-)^{-1}$ against ω this curve will have asymptotes near the integral multiples of the ion gyrofrequency.

We have now considered two limiting cases of the problem, when the parameter (λ^1_-) is very large and very small, and we shall now consider an intermediate case. We suppose that ω is not near an integral multiple of the ion gyrofrequency and we shall assume that (λ^1_-) is of order of ten; the results obtained will show the validity of these assumptions. On the basis of these assumptions we see that the ion terms are as in the previous case and are negligible compared with the electron terms. The exclusion of the ion terms enables us to solve the dispersion equation and in this case we obtain the result

$$(\lambda^1_-)^{-1}=\beta \quad \beta=8\pi n\mathbf{k}T/H^2 \qquad \ldots\ldots(14)$$

where the variable β represents the ratio of the gas pressure to the magnetic pressure and in the type of problem considered has a value of the order of 0·1. This result implies that if the frequency of the oscillations is not near an integral multiple of the ion gyrofrequency then the waves have a characteristic wave number given by $k^2=(4e^2\pi n_0/m_-c^2)$. This is the value of the characteristic thickness found by Adlam and Allen (1958) in their study of the structure of strong collision free hydromagnetic waves, although in their case they considered a cold plasma.

All the results obtained for the frequencies and wave numbers are real which indicates that there are no solutions which grow with time, as was shown by Newcomb (Berstein 1958) and the absence of damping in agreement with Stephanov (1958).

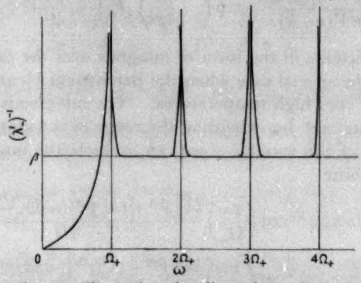

Figure 1. Schematic diagram illustrating the dispersion relation between the parameter $(\lambda 1)^{-1}$ and the frequency ω.

§ 4. THE DISTRIBUTION FUNCTION

We shall now consider the distribution function of the perturbation in more detail. If we write it in the form

$$f_1=\left[\frac{-ie\rho f_0(\rho)}{2\boldsymbol{k}T}\right]\sum_{r=-\infty}^{r=+\infty} a_r(\rho)\exp(ir\theta)$$

then we have for the coefficients

$$a_r(\rho)=(F_1/\Omega)L_{r-1}(z)+(F_2/\Omega)K_{r+1}(z) \quad \text{where } z=k\rho/\Omega.$$

On simplifying the integrands and using the result

$$\mathrm{J}_\mu(z)\mathrm{J}_\nu(z)=\frac{2}{\pi}\int_0^{\pi/2}\mathrm{J}_{\mu+\nu}(2z\cos\theta)\cos[(\mu-\nu)\theta]d\theta \quad \mathscr{R}(\mu+\nu)\geqslant -1$$

we have

$$f_1=\frac{e\pi}{2\boldsymbol{k}T\Omega}\frac{\exp(-2i\pi\omega/\Omega)}{\sin(\pi\omega/\Omega)}\rho f_0(\rho)\left[\sum_{r=0}^{\infty} b_r(z)\exp(ir\theta)+\sum_{r=1}^{\infty} b_r^1(z)\exp(-ir\theta)\right]$$

where

$$\left.\begin{aligned} b_r(z)&=(i)^{2r+3}\,[F_1\mathrm{J}_{\omega/\Omega-1}(z)\mathrm{J}_{r-\omega/\Omega}(z)+F_2\mathrm{J}_{1+\omega/\Omega}(z)\mathrm{J}_{r-\omega/\Omega}(z)]\\ b_r^1(z)&=(i)^{-3}\,[F_1\mathrm{J}_{1-\omega/\Omega}(z)\mathrm{J}_{r+\omega/\Omega}(z)+F_2\mathrm{J}_{r+\omega/\Omega}(z)\mathrm{J}_{-1-\omega/\Omega}(z)]\end{aligned}\right\}.$$

We will now consider the case when the argument z is large and obtain further reduction using the result that for large z we have

$$\mathrm{J}_\nu(z)\sim(2/\pi z)^{1/2}\cos(z-\nu\pi/2-\pi/4).$$

This leads to the coefficients

$$\begin{aligned} b_{2k}(z)&=(-1)^k(i)^3(F_1-F_2)[\cos(2z)+\sin(\pi\omega/\Omega)]\\ b_{2k}^1(z)&=(-1)^k(i)^3(F_1-F_2)[\cos(2z)-\sin(\pi\omega/\Omega)]\\ b_{2k+1}(z)&=(-1)^k(i)^3(F_1-F_2)[\sin(2z)-\cos(\pi\omega/\Omega)]\\ b_{2k+1}^1(z)&=(-1)^k(i)^3(F_1-F_2)[\sin(2z)-\cos(\pi\omega/\Omega)]\end{aligned}$$

and provided $\theta \neq \pm \pi/2$ we can sum the series to give the result

$$f_1 = \frac{2eE_y \exp(-2i\pi\omega/\Omega) f_0(\rho)}{\boldsymbol{k}T \sin(\pi\omega/\Omega)} \Big\{ \sin(\pi\omega/\Omega)[1 + i\tan\theta] - \frac{\cos(2\theta)}{\cos\theta}[\sin(2k\rho/\Omega) - \cos(\pi\omega/\Omega)] \Big\}. \qquad \ldots\ldots(15)$$

To investigate the distribution function in the neighbourhood of the singularity of the above result of $\theta = \pi/2$ we return to equation (7) and put θ approximately equal to $\pi/2$. We put $\theta = \pi/2$ on the right-hand side since there is no singularity there. Then we have

$$i(\omega/\Omega + z\cos\theta) f_1 - \frac{\partial f_1}{\partial \theta} = -\frac{e}{m\Omega} E_y \frac{\partial f_0}{\partial \rho}.$$

Integrating we obtain a solution

$$f_1 = \frac{eE_y}{m\Omega}\frac{\partial f_0}{\partial \rho} \sqrt{(2z)} \exp\left[-\frac{i}{2z}\left(\frac{z\pi}{2} - \frac{\omega}{\Omega}\right)^2\right] \exp\left[i\left(\frac{\omega}{\Omega} + \frac{z(\pi-\theta)}{2}\right)\right] \times [C(\alpha) + iS(\alpha) - g(z)] \qquad \ldots\ldots(16)$$

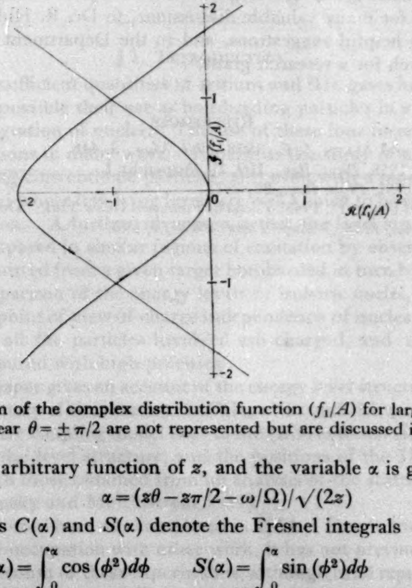

Figure 2. Diagram of the complex distribution function (f_1/A) for large z. The sections of the curve near $\theta = \pm\pi/2$ are not represented but are discussed in the text (§ 4).

where $g(z)$ is an arbitrary function of z, and the variable α is given by

$$\alpha = (z\theta - z\pi/2 - \omega/\Omega)/\sqrt{(2z)}$$

and the functions $C(\alpha)$ and $S(\alpha)$ denote the Fresnel integrals

$$C(\alpha) = \int_0^\alpha \cos(\phi^2)\,d\phi \qquad S(\alpha) = \int_0^\alpha \sin(\phi^2)\,d\phi$$

and the locus of the point $C(\alpha) + iS(\alpha)$ in the complex plane for varying α is a Cornu spiral. Using the results given in Jahnke and Emde (1945) we find that the distance between the spiral centres at this point of irregularity is

$$[z^{3/2} f_0(z) eE_y]/[\pi^{1/2}\Omega \boldsymbol{k}T].$$

Let us consider the physical significance of the spirals on the curve. These indicate bunching of the particles in velocity space into groups such that the mean velocities of adjacent groups differ slightly only in orientation. This leads to a very small relative velocity and hence a large collision cross section and it seems probable that at these values collisions become important and effect a smoothing of the curve.

§ 5. CONCLUSION

We have shown that in the consideration of the longitudinal oscillations of a plasma the ions may be omitted from the dynamics, unless the frequency is near an integral multiple of the ion gyrofrequency when resonance occurs, and that the waves are undamped and characterized by a constant wave number. From the expression obtained for the distribution function we see that collisions become important in the case of particles of large velocity which move perpendicular to both the magnetic field and the direction of propagation.

ACKNOWLEDGMENTS

The author wishes to express his gratitude to Dr. J. W. Dungey for suggesting the problem and for many valuable discussions, to Dr. R. Hide for reading the paper and giving helpful suggestions, and to the Department of Scientific and Industrial Research for a research grant.

REFERENCES

ADLAM, J. H., and ALLEN, J. E., 1958, *Phil. Mag.*, **3**, 448.
BERNSTEIN, I., 1958, *Phys. Rev.*, **109**, 10, Appendix I.
GROSS, E. P., 1951, *Phys. Rev.*, **82**, 232.
JAHNKE, E., and EMDE, F., 1945, *Tables of Functions* (New York: Dover Publications).
STEPANOV, K. L., 1958, *J. Exp. Theor. Phys.*, **7**, 892.

Energy Levels of ^{6}Li and ^{6}He from a Study of the ^{7}Li(^{3}He, α)^{6}Li and ^{7}Li(t, α)^{6}He Reactions

By K. W. ALLEN†, E. ALMQVIST‡ and C. B. BIGHAM‡
Nuclear Physics Research Laboratory, University of Liverpool

Communicated by the late H. W. B. Skinner; *MS. received 27th July* 1959, *in final form 22nd January* 1960

Abstract. An experimental technique is described for accelerating tritium and ^{3}He ions in a 1 Mev h.t. set and recovering the gas used by the ion source. Energy levels in ^{6}He at 1·71 and 3·4 Mev and in ^{6}Li at 2·19, 3·56, 4·3, 5·35, 5·6, 6·63, 7·4, 8·37 and 9·3 Mev were observed in a study of the reactions ^{7}Li(t, α)^{6}He and ^{7}Li(^{3}He, α)^{6}Li at bombarding energies in the range 600 to 900 kev. A classification of the levels has been attempted assuming charge independence of nuclear forces and good agreement is obtained with the intermediate coupling model suggested by Inglis in 1953 for a coupling parameter near the (LS) extreme.

§ 1. Introduction

In recent years sufficient quantities of tritium and ^{3}He gases have become available to make possible their use as bombarding particles in a systematic study of the disintegration of nuclei. The use of these ions increases the scope of nuclear investigations in many ways. It permits the study of nuclei that are not easily formed using conventional particles, and even with a modest accelerator it allows many nuclei whose low-lying levels are well known to be studied in a region of higher excitation. A further advantage is that the level structure of isobaric nuclei can be compared in similar regions of excitation by observing the energies of the particles emitted from a given target bombarded in turn by ^{3}He and tritons. An accurate comparison of the energy levels of isobaric nuclei, which is of great interest from the point of view of charge independence of nuclear forces, becomes possible because all the particles involved are charged, and their energies can therefore be measured with high precision.

The present paper gives an account of the energy level structure of ^{6}Li and ^{6}He obtained from a study of the reaction ^{7}Li(^{3}He, α)^{6}Li and ^{7}Li(t, α)^{6}He. It is found that an intermediate coupling model near to the (LS) extreme (Inglis 1953) gives a good account of the level structure, and the positions of the 3D ($T=0$) levels in ^{6}Li agree well with those obtained from an analysis of the scattering of deuterons by helium (Galonsky and McEllistrem 1955).

The work reported here was completed in 1954. Due to the separation of the authors and their occupation with other work, it has not previously been possible to submit a full account of these experiments, although brief reports have appeared elsewhere (Allen, Almqvist and Bigham 1955). As many recent investigations at Chalk River and the Atomic Weapons Research Establishment represent an extension to higher energies of the work begun at Liverpool, it was thought worth while to give a rather fuller account of the gas recovery system and associated techniques than would otherwise have been warranted at this date.

---

†Now at the Atomic Weapons Research Laboratory, Aldermaston, Berkshire.
‡Now at the Chalk River Laboratory, Atomic Energy of Canada Ltd.

§ 2. GAS HANDLING AND RECOVERY

The gas recovery system fitted to the h.t. set followed in a general way the design developed at Chalk River for a 250 kv accelerator (Allen and Almqvist 1953). That system was developed primarily for handling tritium however, whereas the present system was designed for ^{3}He, although it proved possible to adapt it for tritium when the ^{3}He work had been completed.

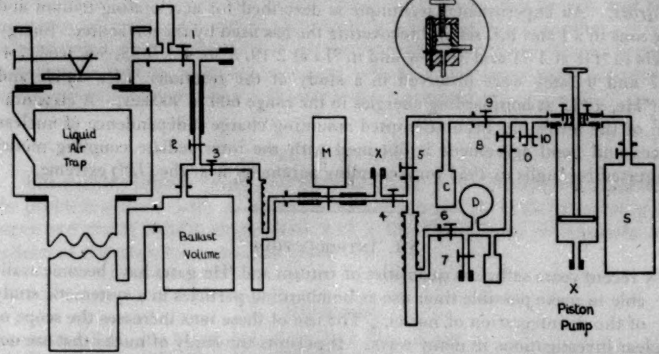

Figure 1. Gas recovery system used with the h.t. set. Letters refer to components described in the text. The points ' X ' are connected so that any gas leaking past the piston is automatically recovered. The type of vacuum valve used is shown in the inset.

The components of the system are shown schematically in figure 1. The main pump, a 6 in. mercury diffusion pump, provided with a liquid air trap and isolating valve, exhausts into $3\frac{1}{2}$ litre ballast volume. The gas is then transferred into the recovery and purification system by the two 1 in. booster pumps capable of operating against a pressure of 8 mm of mercury. A magnetic valve M, operated from a Penning gauge on the high vacuum side, is provided to protect the recovery system from an inrush of air in the event of a leak developing in some part of the target assembly or accelerating tube. Initially, the accelerating tube is evacuated through the by-pass tap 1 with a 10 litre sec^{-1} Kinney pump, which is then used through the tap 2 to back the main diffusion pump. When the high vacuum is of the order of 10^{-5} mm the valve 2 is closed and the main diffusion pump is connected to the recovery system through the tap 3. Helium is then allowed to enter the ion source at a controlled rate of about 6 cm^3 per hour and is subsequently transferred by the diffusion pumps to the recovery system where it accumulates in the O-ring piston pump, the charcoal trap C, and in the various dead spaces of the system. At the end of a run the tap 4 is closed and the gas is transferred into the charcoal trap by means of the piston pump. After allowing the gas to stand in contact with the charcoal for a few minutes the tap 5 is opened and the gas is allowed to circulate until the indication of the 0–20 mm dial gauge D is constant. The residual gas is then pure helium, and it is transferred into a removable evacuated container attached at O ready for the next run. Finally, the residual helium in the dead space beyond tap 10, together with any further traces of gas from the charcoal trap, is transferred to the storage container S. From time to time the contents of S are mixed with the gas recovered after a run to prevent undue accumulation of helium in S. The activated charcoal trap C, which is maintained at liquid nitrogen temperature throughout a run, serves a dual purpose; firstly it acts as an excellent 'backing pump' because it absorbs the gases given off by the accelerating tube electrodes under ion bombardment, traces of air, etc. and secondly it serves to purify the recovered helium *in situ* ready for the next run. The trap operates satisfactorily for very long periods without reactivation. The gauge T is a simple vacuum gauge constructed from a pair of thermistors and provides remote indication of the pressure in the recovery system over the range 50 microns to 5 mm of mercury approximately.

About 14 cm^3 of helium containing 70% ^{3}He were available to us, so that at a gas consumption of 6 cm^3 h^{-1} a single run lasted only about 2·5 hours. Averaged over 200 hours running, the gas loss amounted to 0·6% per run. The greater part of this loss is thought to be in the ion beam itself, which is driven into the target, accelerating tube electrodes, etc. and remains therein. In order to keep this loss to a minimum, and to conserve running time, arrangements were made to cut off the gas supply to the ion source while data were being recorded and plotted. As in the majority of the counting experiments a multichannel pulse height analyser was used, the recording time was comparable with the running time, and the consequent saving of gas was appreciable. It was obviously desirable to be able to interrupt the gas flow without changing the setting of the needle control valve, and this was done by placing a pneumatically operated valve between the needle valve and the ion source. The flow of compressed air to the valve was controlled by solenoid operated pinchcocks at ground potential, operated from the control room.

No systematic study of triton reactions was attempted with the equipment described here. However a few high yield reactions were studied in which the level structure of the residual nuclei was of particular interest in view of the results obtained in the ^{3}He experiments. The technique used was to mix 15 cm^3 of hydrogen containing about 5% of tritum with about 100 ml. of ordinary helium and recover the gas as with ^{3}He. The tritium was recovered from the charcoal trap in which it was absorbed by pumping with the mercury booster pump while maintaining the trap at liquid nitrogen temperature. In this way the tritium was pumped off while most of the impurities were retained in the charcoal trap. The advantage of this technique is twofold; firstly much better ion source utilization of the tritium is obtained than in a tritium–hydrogen mixture (Arnold 1952) and secondly the use of pyrophoric uranium (Allen and Almqvist 1953), a potential fire hazard, is avoided.

§ 3. TARGET ASSEMBLY AND PARTICLE DETECTORS

3.1. *General Description*

The vertical beam from the h.t. set was deflected in a 90° magnet whose field was chosen so that the singly charged ^{3}He$^+$ beam emerged horizontally. The beam was collimated by two $\frac{1}{16}$ in. diameter apertures 6 in. apart and bombarded one of four targets mounted on an insulated water-cooled brass block contained within a brass target chamber (figure 2). The target chamber was cylindrical, 4 in. in diameter, and was equipped with six identical ports. Any one of these could be used either as a beam entry port or as an exit port for the disintegration particles. By choosing the appropriate ports, the angle between the beam and the detector could be varied over a wide range. The Perspex top of the chamber, which carried the target block, could be rotated under vacuum by means of an O-ring seal to bring the target block into position facing any desired exit port. The target block could also be rotated so as to bring any one of the targets into the bombarding position. The target assembly was separated from the main vacuum by a simple isolating valve so that modifications could be made to the target assembly without letting air into the accelerating tube.

Three particle detectors were used with this target assembly. They consisted of a large proportional counter, a NaI crystal spectrometer and a 90° magnetic analyser. The proportional counter and the magnetic analyser will be described here as they were used in the study of the energy levels of ^{6}He and ^{6}Li.

3.2. *The Proportional Counter*

A large proportional counter, similar to that developed at Chalk River (Allen *et al.* 1954), was used to study α-particle energy distributions. It was constructed from a brass cylinder 6 in. in diameter and about 18 in. long with a side window so that the particles crossed the counter diametrically. A stainless steel central wire 0·007 in. in diameter was used. The counter was filled with tank argon mixed with 1% CO_2 to pressures in the range 0·2 to 1·2 atmospheres depending on the energy of α-particles being investigated. The high voltage was applied to the central wire and the value adjusted to give a gas multiplication of about five. Thin mica windows were cemented to brass holders that could be plugged into the counter with an O-ring vacuum seal. The windows were therefore readily changed or replaced.

3.3. *The Magnetic Analyser*

The magnetic analyser is shown diagrammatically in figure 2. Particles emitted from the target were bent through 90° in a homogeneous magnetic field on a mean radius of curvature of 30 cm and focused through a slit placed at the image position on to a KI (Tl) crystal mounted on an E.M.I. 6260 photomultiplier. The geometry was such that the image and object distances were each equal to the radius of curvature. Mounted immediately above the slit was a foil holder that could be set to any one of five positions by means of a rod passing out through a vacuum seal. The foil holder carried a ^{239}Pu α-particle source that was used to calibrate and check the detector, as well as three thin foils used to distinguish between particles of different range. The photomultiplier was mounted in a double walled mild steel housing to shield it from the stray magnetic field and was sealed into the vacuum system by an O-ring which fitted snugly against the glass envelope.

A variable field up to a maximum of about 13000 gauss could be produced in the 1 cm gap between the pole faces. The field was monitored by balancing the e.m.f. from a coil spinning in the fringing field against that from another coil mounted on the same shaft and rotating in a permanent magnetic field.

§4. Experimental Results

4.1. *The $^7Li(^3He, \alpha)^6Li$ Reaction*

The bombardment of ^{7}Li by accelerated ^{3}He particles can lead to the exothermic reactions listed below:

(i) $^7\mathrm{Li} + {}^3\mathrm{He} = {}^6\mathrm{Li} + \alpha + 13{\cdot}321$ Mev
(ii) $= {}^9\mathrm{Be} + \mathrm{p} + 11{\cdot}190$ Mev
(iii) $= {}^9\mathrm{B} + \mathrm{n} + 9{\cdot}338$ Mev
$\downarrow$
$2\alpha + \mathrm{p}$
(iv) $= {}^8\mathrm{Be} + \mathrm{d} + 11{\cdot}748$ Mev
$\downarrow$
2α
(v) $= 2\alpha + \mathrm{n} + \mathrm{p} + 9{\cdot}619$ Mev.

The α-particle energy distribution was studied with the proportional counter at angles of 65°, 90° and 115° to the beam for bombarding energies in the range 600 kev to 900 kev. The distribution was found to consist of several sharp groups from (i) superimposed on a continuum from (v) which also included α-particles from the break up of excited states of ^{9}Be, ^{9}B and ^{8}Be. The proportional counter was useful for studying the high energy α-particles, but those of lower energy were obscured by small pulses from the longer range protons and deuterons which dissipated most of their energy in the far wall of the counter. It proved possible however to extend the range of the α-particle measurements down to 2 Mev, using the magnetic analyser at 90° to a 900 kev beam.

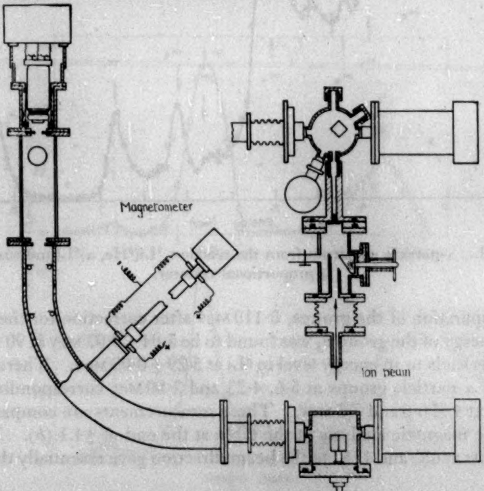

Figure 2. Target chamber and 90° magnetic analyser.

(*a*) *Proportional counter measurements.*

Figure 3 shows the α-particle spectrum measured at 90° to a 750 kev beam. A thick target of isotopic ^{7}Li in the form of $\mathrm{Li_2O}$ was used. The counter was filled to a pressure of 50 cm with an argon with 1% CO_2 mixture, and a mica window 1·0 mg cm^{-2} separated the counter from the target chamber. An energy calibration was established by allowing α-particles from ThC′, ThC, ^{239}Pu, ^{241}Am and ^{238}U to enter the counter through the mica window. In this way approximate energies of the α-particle groups were obtained, and it was determined that the groups α_0, α_1, and α_2 correspond to the ground state and first two excited states of ^{6}Li previously reported at 2·187 and 3·57 MeV respectively (Ajzenberg and Lauritsen 1955). The energy of the strong group α_4 was measured by allowing α-particles from a thin source of ^{239}Pu to enter the counter simultaneously with the disintegration particles from the target (figure 4). The overall counting rate was held reasonably constant at about 20 counts sec^{-1} so that counting rate shifts were negligible. Counting rate shifts can become serious at high average counting rates, and can cause considerable broadening of sharp groups. From the measured separation of the groups, 0·110 MeV after correction for the thick target effect, the energy of the group α_4 was found to be 5·04 ± 0·03 MeV at 90° to a 600 kev beam. This leads to an energy level in ^{6}Li at 5·29 ± 0·05 MeV. There is also some evidence for α-particle groups at 5·6, 4·23 and 3·80 MeV corresponding to energy levels in ^{6}Li at 4·3, 6·6 and 7·3 MeV. These measurements are compared with the results of the magnetic analysis in the table at the end of § 4.1 (*b*). The counter measurements at 65° and 115° to the beam direction gave essentially the same level energies.

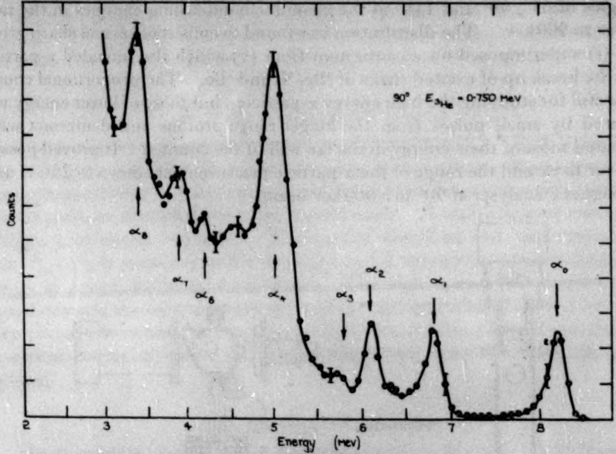

Figure 3. α-particle spectrum from the reaction $^7Li(^3He, \alpha)^6Li$ measured with a proportional counter.

(*b*) *Magnetic analysis.*

In work with the magnetic analyser, output pulses from the photomultiplier were amplified and the pulse height distribution displayed on the 30 channel pulse height analyser. Different particles with the same momentum to

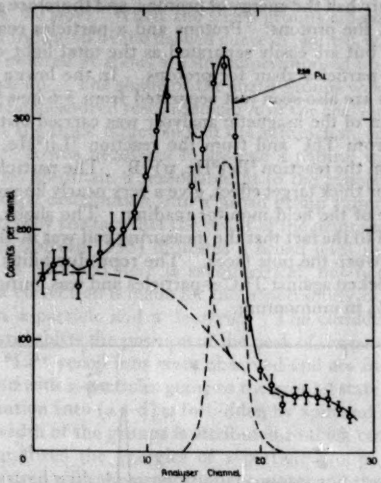

Figure 4. Pulse height distribution when α-particles from the reaction ^{7}Li(^{3}He, α)^{6}Li enter the counter simultaneously with those from ^{239}Pu. Measurements at 90° to a 600 kev beam.

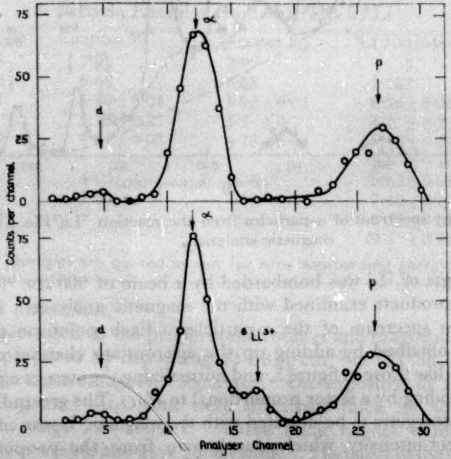

Figure 5. Pulse height spectrum from KI crystal showing separation of different ions with the same momentum to charge ratio.

charge ratio were distinguished by the difference in their pulse heights from the KI crystal. Figure 5 illustrates typical pulse height spectra. For the same $H\rho$, deuterons have only half the energy of protons, and therefore produce pulses about half the height of the protons. Protons and α-particles reach the detector with the same energy, but are easily separated as the total light output of KI(Tl) is rather less for α-particles than for protons. In the lower diagram of figure 5, 5·4 Mev $^6\text{Li}^{3+}$ ions are also seen just separated from 3·6 Mev $^4\text{He}^{2+}$ ions.

The calibration of the magnetic analyser was carried out using α-particles of known energies from ThC and from the reaction $^7\text{Li}(^3\text{He}, \alpha)^6\text{Li}^*$, and known proton groups from the reaction $^9\text{Be}(^3\text{He}, \text{p})^{11}\text{B}$. The particle energies, corrected where necessary for thick target effect, give a very nearly linear curve when plotted against the square of the field monitor reading. The slight departure from linearity is attributed to the fact that the measuring coil was in the fringing field and not in the gap between the pole faces. The reproducibility of the field monitor was frequently checked against ThC α-particles and was found to have a long term stability of ±0·25% in momentum.

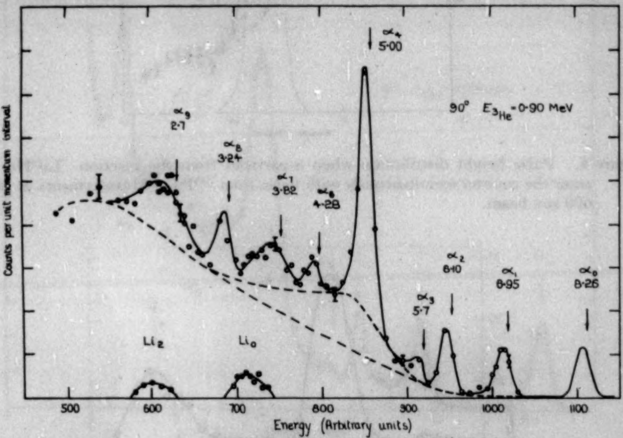

Figure 6. Energy spectrum of α-particles from the reaction $^7\text{Li}(^3\text{He}, \alpha)^6\text{Li}$ measured by magnetic analysis.

A thick target of ^{7}Li was bombarded by a beam of 900 kev ^{3}He ions and the disintegration products examined with the magnetic analyser. Figure 6 shows the momentum spectrum of the α-particles. Each point on the momentum spectrum was obtained by adding up the appropriate channel counts in pulse analyser curves like those in figure 5, and normalizing the sum to equal momentum intervals by dividing by a factor proportional to $H\rho$. The ground state α-particle group was too energetic to be detected with the magnet; it was added to figure 6 with the correct intensity, which was known from the proportional counter measurements, to complete the spectrum.

In addition to the four most energetic α-particle groups studied in the proportional counter, the momentum spectrum shows clear evidence for groups at 4·28, 3·82, 3·24 Mev and a possible group at 2·7 Mev, corresponding to levels in ^{6}Li at

6·63, 7·40, 8·37 and 9·3 Mev. When the sharp groups are subtracted, there remains a distribution indicated by the dashed curve in figure 6, which can be divided into a broad group centred at about 4·8 Mev superimposed on a continuum from the multibody break up. The shape of the sharp groups was fitted as described in (*c*) below, using the measured resolution curve of the analyser and the observed yield function from the thick target so that the subtraction could be carried out with fair certainty. It was necessary to assume a natural width of 0·6 Mev for the group at 3·82 Mev to obtain a reasonable fit to the experimental data. The division of the residual distribution into a broad group superimposed on a continuum was suggested by the fact that the result of the deuteron helium scattering (Galonsky and McEllistrem 1955) indicates a broad level in this region. The shape of the level as obtained here is asymmetrical, but becomes more nearly symmetrical when a correction is made for the penetrability of the barrier against dissociation into an α-particle and a deuteron. The correction varies over the width of the level, and shifts the position of the peak of the group by ~0·2 Mev.

Two groups of ^{6}Li^{3+} recoil ions were observed and are indicated in figure 6. They were associated with α-particles going to the ground state and to the 3·56 Mev level, whose dissociation into (α + d) is forbidden by spin and parity conservation rules. The large width of the groups is attributed to thick target effect.

The table summarizes the energies of α-particle groups from the reaction ^{7}Li(^{3}He, α)^{6}Li measured with the proportional counter and the magnetic analyser. The quantity Γ tabulated is 10/6 of the experimental width of the α-particle group. The excitation of the broad level, 5·6 ± 0·2 Mev, was obtained from the *corrected* experimental curve.

Particle Energies from ^{7}Li(^{3}He, α)^{6}Li

Group	Magnet 90°	Counter 90°	Counter 9_0°	^{6}Li Excitation	Γ (Mev)
0	7·99	7·99	7·99	0	0
1	6·68	6·68	6·68	2·187	<0·1
2	5·83	5·89 ± 0·04	5·92 ± 0·03	3·56 ± 0·06	<0·1
3	5·4	5·55 ± 0·2	5·5 ± 0·1	4·3 ± 0·2	
4	4·73	4·81 ± 0·03	4·78 ± 0·04	5·35 ± 0·07	<0·1
5				5·6 ± 0·2	2·0
6	4·01	4·03		6·63 ± 0·08	0·2
7	3·55	3·69	3·49	7·40 ± 0·10	0·6
8	2·97			8·37 ± 0·08	0·2
9	(2·46)			(9·3 ± 0·2)	0·6

Energies are quoted in Mev for zero bombarding energy.

(*c*) *Thick target corrections.*

The ^{7}Li targets used in the proportional counter and magnetic analyser measurements were prepared by depositing 30–50 μg cm^{-2} of ^{7}Li on heavy backings in the A.E.R.E. electromagnetic separator. On exposure to air, the targets became 70–100 μg cm^{-2} Li$_2$O and were effectively thick for ^{3}He bombarding particles in the range 700–900 kev. These thick targets were used because they were readily available and gave good yields. The effect of the target thickness can be estimated accurately and taken into account as discussed below.

The response curve of the magnetic analyser observing 6·06 Mev α-particles from a thin source of ThC is shown in figure 7. For purposes of computation the experimental points can be fitted by the Gaussian exp $(-y^2/\sigma^2)$ illustrated by the solid line. This has a full width at half maximum of 3·4% in energy corresponding to a value of 123 kev for the parameter σ in this case. The effect of a thick target is to produce an asymmetry in the peak shape which can be calculated if the yield Y as a function of the bombarding energy E is known. This was measured for the ^{7}Li(^{3}He, α)^{6}Li reaction and the experimental results are given in figure 8. These are adequately represented by the curve of the form exp ($8E$). The differential, or thin target yield at any energy is largely determined by the slope of this curve and therefore also shows an approximate exponential energy dependence.

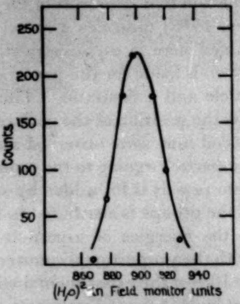

Figure 7. Response of the magnetic analyser to 6·06 Mev α-particles from ThC.

When ^{3}He ions impinge on a thick target, their energy is gradually diminished as they penetrate the target material. The consequent decrease in differential yield with diminution of energy can be obtained from the data in figure 8 and is plotted in figure 9 in arbitrary units. The energy of the ions incident on the target surface is assumed to be 900 kev and this is taken as zero on the energy scale at the top of the figure. For each amount of energy lost by the ^{3}He ions in going into the target, there corresponds a change y in the energy of the emitted particles due to two factors: (i) the decrease in effective bombarding energy, (ii) the energy lost by the emitted particle in coming out through the target material. These energy changes are readily computed and their sum y in kev is given by the scale at the bottom of figure 9 for the 6 Mev α-particles from the ^{7}Li(^{3}He, α)^{6}Li* reaction. The differential yield may be expressed as a function of y and is very closely of the form exp $(-2\lambda y)$ where λ is a parameter determined by the curve in figure 9.

By folding the Gaussian resolution curve of the instrument into the exponential energy distribution from the target, the following result is obtained (Livesey and Wilkinson 1948)

$$F(y)=k\exp(-2\lambda y)\left(1-\frac{2}{\sqrt{\pi}}\int_0^{\lambda\sigma-y/\sigma}\exp(-x^2)\,dx\right) \quad \ldots\ldots (1)$$

λ and σ are parameters determined from the yield curve and the instrumental resolution curve respectively, as indicated above. The expression was evaluated using tables of error functions and the resultant peak shapes obtained.

The solid line in figure 6 was obtained by fitting the function $F(y)$ to the experimental points for each peak when plotted on an energy scale. An underlying continuum shown by the dashed line was assumed. The only adjustable parameters were the peak intensity and the position of the $y=0$ point on the energy scale.

This point corresponds to the energy of particles produced at the surface of the target which in this case is about 50 kev higher than the energy corresponding to the peak of each group. The error, ± 10 kev, in this estimate of the thick target correction is less than the uncertainty in locating the experimental peaks. Consequently with our instrumental resolution, there was little to gain by using thinner targets which would give smaller yields, an important consideration owing to the small quantity of ^{3}He available to us.

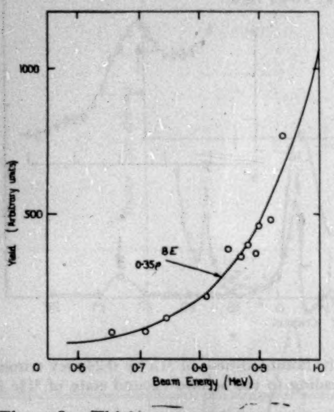

Figure 8. Thick target excitation function for the reaction ^{7}Li(^{3}He, α)^{6}Li.

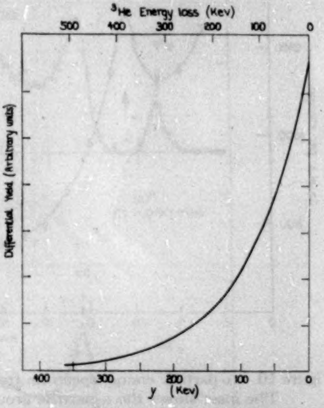

Figure 9. Decrease of differential yield as 900 kev ^{3}He ions penetrate the target material. y is the reduction in energy of the emitted α-particles, which is simply related (see upper scale) to the energy lost by the ^{3}He ions in their passage through the thick target.

The expression (1) was also used to obtain the thick target profile for α-particles detected by the proportional counter. In this case the instrumental resolution parameter was determined by using α-particles from the Pu calibration source. The yield parameter λ was obtained in the same manner as described above.

In the case of broad levels, a value of σ was chosen which gave a good fit to the observed data, and the width of the level was deduced from this value of σ after allowing for the known instrumental resolution.

4.2. *The Reaction $^7Li(t, \alpha)^6He$*

This reaction was first observed at a bombarding energy of 0·240 Mev (Allen *et al.* 1954). The α-particles emitted at 90° to the beam direction were studied with a proportional counter and two sharp groups were observed associated with the ground state of ^{6}He and an excited state at 1·71 Mev. A hitherto unpublished† α-particle spectrum taken with a proportional counter at 131° to a 0·24 Mev triton beam is shown in figure 10. The data were taken with a large proportional counter and a pulse height analyser. In addition to α-particles leading to the ground state and 1·71 Mev state there is a third group leading to an excited state at 3·4 ± 0·2 Mev The identification of this group seems reasonably certain as ^{6}He particles and α-particles from the T + D reaction were unable to penetrate the counter window at the backward angle of 131°. Some additional evidence for this third excited state has been obtained in measurements carried out at Liverpool using bombarding energies in the range 700 to 900 kev. The α-particle spectrum obtained with the proportional counter at 90° to a 705 kev beam is shown in figure 11. The groups α_0, α_1 and α_2 correspond to states in ^{6}He at 0, 1·71 and 3·42 Mev. The group r occurs where the recoil ^{6}He particles are expected and the groups α_4 and p are produced in the reactions ^{12}C(t, α)^{9}Be and ^{12}C(t, p)^{14}C. The proton group goes right through the counter and only spends a fraction of its energy in the counter gas. There is also some evidence for an α-particle group between α_4 and p which is probably due to the reaction D(t, α)n. A very similar spectrum was obtained at 90° and 900 kev. The yield from a thick carbon target is also shown in figure 11. In view of the complex structure of the spectrum below 4 Mev, it is clear that these measurements offer no information about the energy level structure of ^{6}He at an excitation greater than 3·5 Mev.

---

†This measurement was made at Chalk River by one of us (E.A.) in collaboration with T. P. Pepper.

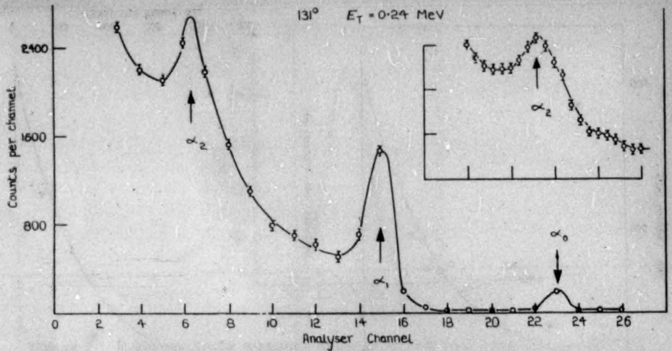

Figure 10. α-particle energy spectrum from the bombardment of ^{7}Li by 0·24 Mev tritons. The inset shows the α-particle group leading to the second excited state of ^{6}He in greater detail.

§ 5. Discussion

The experimental results are summarized in the level diagrams of ^{6}He and ^{6}Li shown in figure 12. The energy values are those observed in this work but the spin and parity assignments are based on comparisons with scattering data as discussed below. The position, spin and parity of the first five excited states of ^{6}Li are well accounted for by the intermediate coupling model reviewed by Inglis (1953) (see figure 13).

If charge independence of nuclear forces is assumed the levels may be divided into two groups; those with isobaric spin $T = 1$ which are common to ^{6}Li and ^{6}He, and those with isobaric spin $T = 0$ which are only possible in ^{6}Li. This convenient

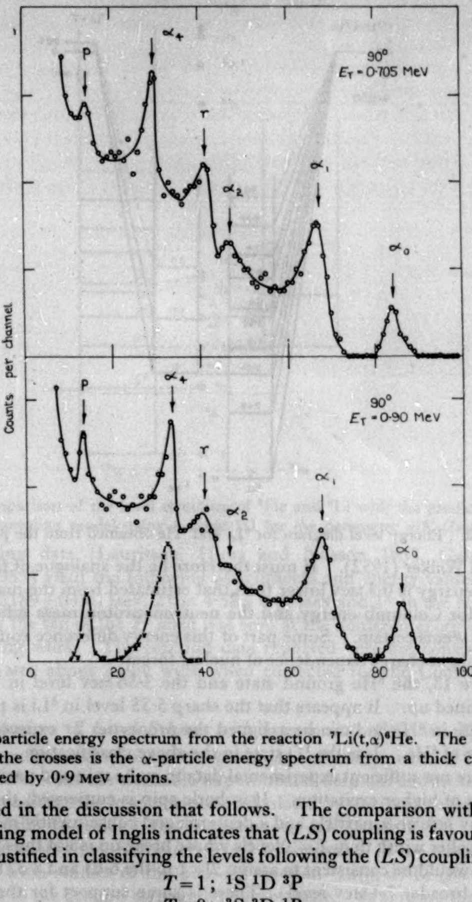

Figure 11. α-particle energy spectrum from the reaction ^{7}Li(t,α)^{6}He. The curve drawn through the crosses is the α-particle energy spectrum from a thick carbon target bombarded by 0·9 MeV tritons.

division is used in the discussion that follows. The comparison with the intermediate coupling model of Inglis indicates that (LS) coupling is favoured and we are therefore justified in classifying the levels following the (LS) coupling scheme:

$$T=1;\ {}^1\mathrm{S}\ {}^1\mathrm{D}\ {}^3\mathrm{P}$$
$$T=0;\ {}^3\mathrm{S}\ {}^3\mathrm{D}\ {}^1\mathrm{P}.$$

The triplet D and P states which are degenerate in (LS) coupling are split into their components by spin–orbit interaction.

5.1. *The* $T=1$ *States*

The lowest $T=1$ state in ^{6}Li is the analogue of the ^{1}S ground state of ^{6}He and consequently is expected to have properties 0^+. Its decay into an α-particle and a deuteron is therefore forbidden by spin and parity considerations as well as by isobaric spin selection rules and it must decay by γ-emission. Our observation of ^{6}Li recoil ions of energy corresponding to the 3·56 MeV level shows that this state does not break up into heavy particles, but is the γ-emitting state identified

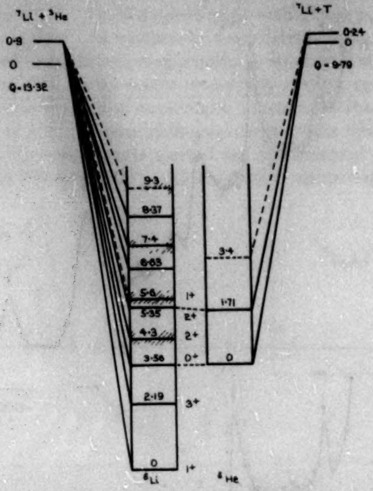

Figure 12. Energy level diagram for ^{6}Li and ^{6}He obtained from the present work.

by Day and Walker (1952). It must therefore be the analogue of the ^{6}He ground state. Its energy is 0·3 Mev lower than that estimated from the mass of ^{6}He after correcting for Coulomb energy and the neutron–proton mass difference, but its assignment seems certain. Some part of this energy difference could conceivably be due to a slight charge dependence of nuclear forces.

In figure 13, the ^{6}He ground state and the 3·56 Mev level in ^{6}Li have been arbitrarily lined up. It appears that the sharp 5·35 level in ^{6}Li is the analogue of the 1·71 state in ^{6}He and can be assigned the properties 2^+ expected for the first excited state of ^{6}He. It is the ^{1}D state in the above classification.

There are not sufficient experimental data to make spin and parity assignments to the levels of higher excitation. If isobaric spin is conserved, then $T=1$ levels cannot decay into an α-particle and a deuteron and consequently may be expected to have a smaller width than $T=0$levels whose break up is not thus inhibited. On this basis it would be consistent to assign $T=1$ to the 6·63 and 8·37 Mev levels, and $T=0$ to the broader 7·4 Mev level. There is some support for the latter assignment in the studies of Sokolov *et al.* (1956) who report observing the break up into α-particles and deuterons of a level near 7·5 Mev in the reaction ^{7}Li(d, t)^{6}Li* (7·5). The $T=1$ levels would be members of the ^{3}P multiplet and one would expect analogue levels in ^{6}He near corresponding energies if nuclear forces are charge independent. Only one level has been observed in ^{6}He in this region at 3·4 Mev and a more thorough investigation of ^{6}He above 3 Mev excitation is desirable to determine the position and separations of the members of the ^{3}P multiplet.

5.2. *The* $T=0$ *Levels*

The levels of ^{6}Li at 2·187, 4·3 and 5·6 Mev can be assigned $T=0$ since they appear in the scattering of deuterons by helium and have no analogues in ^{6}He. Analysis

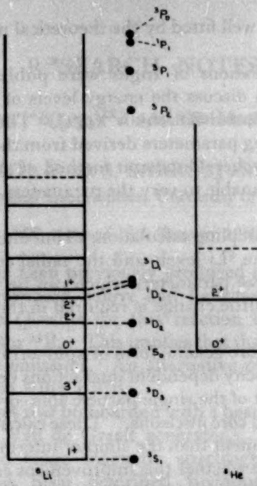

Figure 13. Comparison of the level structure of ^{6}He and ^{6}Li with the predictions of the intermediate coupling model using a value 1·3 for the parameter a/K (Inglis 1953).

of the scattering data (Lauritsen, Huus and Nilsson 1953, Galonsky and McEllistrem 1955) yield the following assignments and energy values for levels in ^{6}Li: 3^+ at $2{\cdot}189 \pm 0{\cdot}001$ Mev, 2^+ at $4{\cdot}52 \pm 0{\cdot}08$ Mev and 1^+ in the region 4·9 to 5·8 Mev. Only the tail of the 1^+ state was seen at the deuteron energies available for the scattering work. The reaction data reported here are consistent with a 1^+ level at 5·6 Mev about 2 Mev wide when corrected for the Coulomb barrier (see § 4.1 (*b*)).

5.3. *Comparison of Level Scheme with Intermediate Coupling Model*

The best experimental values of the positions and assignments of the levels in ^{6}Li and ^{6}He taken from the available experimental data are shown in figure 13. The black dots indicate the level positions calculated by the intermediate coupling model of Inglis using the value 1·3 for the parameter a/K (Inglis 1953). This value of a/K is a little lower than the value 1·4 to 2·1 required to fit the relative reduced widths derived from studies of the pick-up reaction ^{7}Li(p, d)^{6}Li (Reynolds and Standing 1956) to the ground state and 2·19 Mev state. It appears that with a/K near 1·4 the intermediate coupling shell model provides a fair fit to both sets of data. The order and position of the first five levels of ^{6}Li are then reasonably well accounted for.

However, the model predicts an energy gap of 5 Mev before the P levels are reached at about 11 Mev excitation. Experimentally, levels are found at 6·63, 7·4 and 8·37 Mev. If the broad 7·4 Mev level is taken to have isobaric spin $T = 0$ as suggested in § 5.1 then the order of the levels also differs from the predicted order of the P states which is $^3P_2$, $^3P_1$ and $^3P_0$ respectively with increasing energy. Some modification of the theory is therefore required to account for the experimental level structure above 6 Mev. It seems significant however that the lower lying S and D states can all be fairly well fitted by the theoretical model, not only in order but in actual position.

Since the original calculations of Inglis were published, three theoretical papers have appeared which discuss the energy levels of ^{6}Li and ^{7}Li (Meshkov and Uffard 1956, Soper 1957, and Balashkov 1959). These authors all calculate the level structure of ^{7}Li using parameters derived from the ^{6}Li levels. Meshkov and Uffard (1956) use the Bacher–Goudsmit method of atomic spectroscopy and in their calculation they are unable to vary the parameters from one configuration to another.

In Soper's intermediate coupling calculation, all but one of the main parameters are obtained directly from the ^{6}Li levels and the radial integrals and spin–orbit strength are considered as free parameters which can be varied from nucleus to nucleus. In fact, however, little change is required in the derived parameters to fit the levels of ^{7}Li.

In Balashkov's work, a more general form of spin–orbit interaction is used in which account is taken of velocity dependent interactions between pairs of particles in unfilled shells, and not just of the single particle spin–orbit interaction between nucleons in unfilled shells and core nucleons. These calculations are in somewhat better agreement with experiment than the simpler intermediate coupling model, and it will be of interest to see whether this improvement can be extended to more complex nuclei.

ACKNOWLEDGMENTS

We are indebted to the late Professor H. W. B. Skinner for the excellent facilities accorded to us for our experimental programme with ^{3}He and tritium and for much helpful discussion.

We also wish to thank Professor H. T. Richards and Dr. A. Galonsky for communication of their results on deuteron helium scattering in advance of publication.

The ^{3}He gas was prepared by thermal diffusion and purified for us by Dr. R. H. Davies of the Atomic Energy Research Establishment, Harwell, to whom we are most grateful. It was loaned to us through the courtesy of the Director, A.E.R.E. The isotropic ^{7}Li targets were prepared by the E.M. separator group at A.E.R.E., at that time under the direction of Dr. R. H. Dawton and Dr. M. L. Smith.

We also acknowledge financial assistance and leave of absence from Atomic Energy of Canada Ltd. (E.A.) and the award of an Athlone Fellowship (C.B.B.).

REFERENCES

Ajzenberg, F., and Lauritsen, T., 1955, *Rev. Mod. Phys.*, **27**, 77.
Allen, K. W., and Almqvist, E., 1953, *Rev. Sci. Instrum.*, **24**, 70.
Allen, K. W., Almqvist, E., and Bigham, C. B., 1955, *Phys. Rev.*, **99**, 631A.
Allen, K. W., Almqvist, E., Dewan, J. T., and Pepper, T. P., 1954, *Phys. Rev.*, **96**, 684.
Arnold, W. R., 1952, *Rev. Sci. Instrum.*, **23**, 97.
Balashkov, V. V., 1959, *Soviet Physics J.E.T.P.*, **36**, 798.
Day, R. B., and Walker, R. L., 1952, *Phys. Rev.*, **85**, 582.
Galonsky, A., and McEllistrem, M. T., 1955, *Phys. Rev.*, **98**, 590.
Inglis, D. R., 1953, *Rev. Mod. Phys.*, **25**, 390.
Lauritsen, T., Huus, T., and Nilsson, S. G., 1953, *Phys. Rev.*, **92**, 1501.
Livesey, D. L., and Wilkinson, D. H., 1948, *Proc. Roy. Soc.* A, **195**, 123.
Meshkov, S., and Uffard, C. W., 1956, *Phys. Rev.*, **101**, 734.
Reynolds, J. B., and Standing, K. G., 1956, *Phys. Rev.*, **101**, 158.
Sokolov, I. L., Sulkovskaia, M. M., Karpushkina, E. I., and Albitskaia, E. A., 1956, *Soviet Physics J.E.T.P.*, **30**, 740.
Soper, J. M., 1957, *Phil. Mag.*, **2**, 1219.

RESEARCH NOTES

The Reaction $^{11}B(t, p_0)^{13}B$ and the Mass Excess of ^{13}B

By J. MUTO†, F. DE S. BARROS‡ AND A. A. JAFFE
The Physical Laboratories, University of Manchester

MS. received 18*th January* 1960

THE ^{13}B nucleus has been previously produced only by the nuclear reaction $^7Li(^7Li, p)^{13}B$ (Ajzenberg-Selove and Lauritsen 1959). Norbeck (1957) has measured the *Q*-value for this reaction and has established a mass excess 20·39 ± 0·05 MeV for ^{13}B. This implies that the ^{13}B nucleus is stable against decay by heavy particle emission. An alternative method of production of this nucleus is by the reaction $^{11}B(t, p)^{13}B$.

A natural boron target was bombarded with a beam of tritons accelerated to an energy of 5·5 MeV by a Van de Graaff generator. The reaction products were observed using a broad range magnetic spectrograph, with an experimental arrangement which has been described previously (Barros *et al.* 1959). The target consisted of boron evaporated on to a thin carbon film. The target thickness was measured by means of an alpha-particle gauge (Ramavataram and Porat 1959) and the thicknesses of the boron and carbon were found to be 30·5 ± 1·5 μg cm^{-2} and 13·7 ± 1·0 μg cm^{-2} respectively.

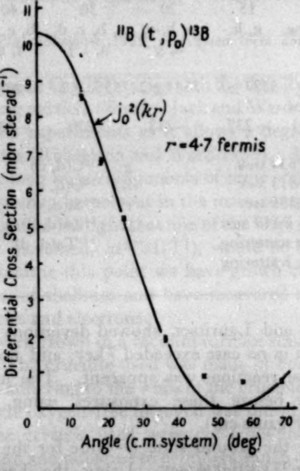

---

† On leave of absence from the Kyoto University of Japan.
‡ On leave of absence from the Brazilian Centre of Physical Researches.

A check on the purity of the target was provided by the elastically scattered tritons observed in exposures with higher spectrograph field settings. The total mass of target impurities was found to be about 12% chiefly consisting of nuclei with masses corresponding to isotopes of Fe, Ni, Cu, Zn and ^{16}O. It is likely that most of this material was deposited during evaporation of the target and before the measurement of the target thickness was made. The differential cross sections shown in the figure have been calculated on this assumption and are believed to be accurate to ± 10%.

An account of several other tritium induced reactions observed from this target will be reported shortly.

The ground state group from the reaction $^{11}B(t, p)^{13}B$ was observed at seven angles in the range 10°–61° and the Q-value and its angular distribution has been determined. This intense group had a full half width of 15 kev and its origin could be identified with certainty by the variation of the proton energy with the angle of observation with respect to the incident beam.

In calculating the Q-value, the energy of the triton beam was determined at six angles from the energies of the ground state groups from the reactions $^{12}C(t, p_0)^{14}C$, $^{12}C(t, d_0)^{13}C$, $^{12}C(t, \alpha_0)^{11}B$ and $^{16}O(t, d_0)^{17}O$, and from elastically scattered deuterons originating from a small beam contamination of HD molecules. The results are shown in the table. It was found that the beam energies calculated from the indicated reactions, using the Q-values taken from Ajzenberg-Selove and Lauritsen showed deviations from the mean values given in the table which in no case exceeded 7 kev, and no inconsistency in the Q-values for any of these reactions was apparent. The magnetic spectrograph was calibrated, shortly before these exposures, using alpha particles from ^{210}Po ($H\rho = 3{\cdot}31644 \times 10^5$ gauss cm).

Angle (deg)	15	20	30	40	50	60
Reactions used to determine beam energy	g, k	a, b, c, d, g	a, b, c, d, h, i, j	b, c, d, f, g	b, d, e, f, g	b, c, d,
Incident triton energy, mean value (kev)	5537 ± 5	5544 ± 2	5553 ± 2	5520 ± 1	5541 ± 2	5516 ± 3
Ground state Q-value for $^{11}B(t, p)^{13}B$ reaction (kev)	− 237	− 233	− 230	− 232	− 238	− 230

a: $^{12}C(t, p_0)^{14}C$ $Q = 4{\cdot}634$ Mev
b: $^{12}C(t, d_0)^{13}C$ $Q = 1{\cdot}313$ Mev
c: $^{12}C(t, a_0)^{11}B$ $Q = 3{\cdot}855$ Mev
d: $^{16}O(t, d_0)^{17}O$ $Q = -2{\cdot}113$ Mev
e: $^{10}B(d, d)$ elastic scattering
f: $^{11}B(d, d)$ elastic scattering
g: $^{12}C(d, d)$ elastic scattering
h: $^{16}O(d, d)$ elastic scattering
i: $^{28}Si(d, d)$ elastic scattering
j: $^{64}Zn(d, d)$ elastic scattering
k: $^{181}Ta(d, d)$ elastic scattering

The mean value for the ground state Q-value for the reaction $^{11}B(t, p)^{13}B$ was found to be $-0{\cdot}233 \pm 0{\cdot}004$ Mev. Using the known mass excess of ^{11}B (11·914 Mev), ^{3}H (15·835 Mev) and ^{1}H (7·585 Mev) the mass excess of the ^{13}B atom was found to be $20{\cdot}397 \pm 0{\cdot}009$ Mev.

The ground state protons from the $^{11}B(t, p)^{13}B$ reaction fall within about 600 kev of the low energy end of the observed spectrum; no further states of ^{13}B were found.

The angular distribution of the proton group was obtained in the range from 12·5° to 68·6° in the centre-of-mass system. The distribution can be fitted by the square of a spherical Bessel function $j_l^2(kr)$, $r = 4{\cdot}7$ fermis, assuming the angular momentum transfer $l = 0$. This angular distribution is understandable on the assumption that a pair of neutrons with anti-parallel spins is stripped off the triton, to fill the two $p_{1/2}$ vacancies in ^{11}B. This would lead to a ground state spin and parity of $\frac{3}{2}^-$ for the ground state of ^{13}B, consistent with a simple shell model assignment.

REFERENCES

AJZENBERG-SELOVE, F., and LAURITSEN, T., 1959, *Nucl. Phys.*, **11**, 1.

BARROS, F. DE S., FORSYTH, P. D., JAFFE, A. A., and TAYLOR, I. J., 1959, *Proc. Phys. Soc.*, **73**, 793.

NORBECK, E., JR., 1957, *Phys. Rev.*, **105**, 204.

RAMAVATARAM, K., and PORAT, D. I., 1959, *Nucl. Instrum.*, **4**, 239.

The Efficiency and Main Decay Time of CsI(Tl) for Electrons and Alpha Particles in Crystals with Different Thallium Concentrations

BY D. A. JONES AND A. WARD

Natural Philosophy Department, University of Aberdeen

MS. received 27*th November* 1959, *in revised form* 25*th January* 1960

THE main decay time in CsI(Tl) varies with the density of ionization produced by the bombarding particle (Storey, Jack and Ward 1958). The effect may be useful in some experiments as it allows a degree of mass selection in measuring energy spectra (Robertson and Ward 1958). A similar effect has been found in the subsidiary long term components of some organic scintillators (Owen 1958) but does not appear to be present in the main components (Kallmann and Brucker 1957). It might be thought that one of the ways in which the magnitude of the effect could be increased, in CsI(Tl), would be by varying the thallium concentration. To examine this point we have grown crystals of CsI(Tl) with different concentrations of thallium and have measured the efficiency and main decay time for α-particles and electrons.

The bulk crystals were grown in a vacuum furnace similar to that described by Stockbarger (1949). The crucible used was made of boron nitride to avoid the difficulty of the crystal adhering to the walls of the crucible after the growth cycle. During the growth cycle oxygen-free nitrogen was introduced to prevent the TlI from boiling off. The crystals used were cut from the interiors of the bulk crystals and were ground and polished to cylinders ¼ inch diameter by ¼ inch long. For comparison a standard Harshaw crystal was ground and polished to the same dimensions. We have not determined the thallium concentrations directly; the maximum percentage molar values (C_m) quoted here refer to the values obtained using the known weight of TlI added to the crucible and the final weight of the crystal taken from the furnace. We believe that the fraction of thallium lost in the growth process is not excessive and is constant.

The crystals were mounted on an EMI6262 photomultiplier and measurements were made separately on α-particles from a polonium source and electrons produced in the crystal by the absorption of gamma rays from a ^{60}Co source. The measuring technique has been described in a previous paper (Storey, Jack and Ward 1958) and consists simply of photographing the traces on an oscilloscope of the integrated current pulses from the photomultiplier. The only essential difference in the experiments described here was that it was found to be impracticable to make use of photographs of single pulses for the oscilloscope used, and each negative contained 100 pulses all nearly the same size. For electrons this was obtained by arranging that only the largest pulses triggered the time base of the oscilloscope.

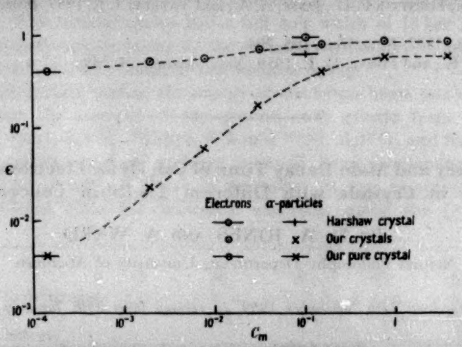

Figure 1. ϵ is the relative height of the integrated current pulse after 4 μsec, for α-particles and electrons, normalized to unity for electrons in the standard Harshaw crystal, and adjusted for equal energy loss.

C_m is the maximum value of the percentage molar concentration of thallous iodide (see text).

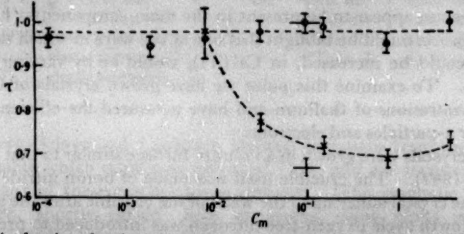

Figure 2. τ is the time for the integrated current pulse to rise from 10% to 90% of the pulse height at 4 μsec, normalized to unity for electrons in the standard Harshaw crystal. The symbols are the same as for figure 1 except that the experimental error is indicated in the usual manner.

The results were analysed in terms of two parameters ϵ and τ; ϵ is the height of the integrated current pulse after 4 μsec per unit energy and τ is the time to rise from 10% to 90% of ϵ. The values of ϵ and τ obtained, corrected for the effect of the bandwidth of the electronics, are shown in figures 1 and 2 normalized to unity for electrons in the standard Harshaw crystal. The results show that from the practical point of view of using the variation of decay time τ with ionization density ρ for mass selection there appears to be no advantage on changing the thallium concentration from the value in the standard Harshaw crystal. Any advantage for particular experiments due to a possible change in the variation of τ with ρ between the two extreme values of ρ used here cannot be deduced from the present results.

ACKNOWLEDGMENTS

We should like to thank Professor R. V. Jones for providing the facilities for this work and for helpful discussions on the problems of crystal growing. We are also grateful to Mr. L. Durno and Mr. A. Gardner of the technical staff for their careful work in connection with the furnaces.

REFERENCES

KALLMANN, H., and BRUCKER, G. J., 1957, *Phys. Rev.*, **108**, 1122.
OWEN, R. B., 1958, *Instn Radio Engrs Trans. Nucl. Sci.*, **NS-5**, No. 3, 198–201.
ROBERTSON, J. C., and WARD, A., 1958, *Proc. Phys. Soc.*, **73**, 523.
STOCKBARGER, D. C., 1949, *J. Opt. Soc. Amer.*, **39**, 731.
STOREY, R. S., JACK, W., and WARD, A., 1958, *Proc. Phys. Soc.*, **72**, 1.

The Heat of Sublimation and Energy of Dissociation of Thallous Chloride

BY R. F. BARROW
Physical Chemistry Laboratory, Oxford University

MS. received 15th February 1960

§ 1. INTRODUCTION

THREE sets of measurements of the vapour pressure of thallous chloride are in reasonable agreement, those of Volmer (1929) and of Barrow, Jeffries and Swinstead (1955) on the solid, and of von Wartenberg and Bosse (1922) on the liquid. Since the discussion (Barrow, Jeffries and Swinstead 1955) of these results, new measurements of the low temperature heat capacity of thallous chloride have been made (Bartky and Giauque 1959), which lead to a reliable value for the standard entropy of the salt. Further, the internuclear distance has been determined from observations of the microwave spectrum (Barrett and Mandel 1958), and rotational analyses of some of the bands of the electronic spectrum have also been made (Barrow 1957). A more reliable value of the heat of sublimation can therefore be derived, by the standard Third Law procedure, than was possible at the time of the earlier discussion. This heat of sublimation may then be linked with that of thallium and the standard heat of formation of thallous chloride, to derive the dissociation energy of the gaseous halide.

§ 2. HEAT OF SUBLIMATION AND THERMOCHEMICAL VALUE OF DISSOCIATION ENERGY

The results of the calculations are given in table 1. These were made using the new value of the entropy, $S^0_{c,298} = 26{\cdot}59$ cal mol^{-1} deg^{-1}, and new spectroscopic constants. The small corrections (Mayer and Mayer 1940) for anharmonicity and centrifugal distortion were also applied. The final value for the heat of sublimation, $\Delta_s H_{298}$, is $32{\cdot}6_4$ kcal mol^{-1}. Combining this with $\Delta_s H_{298}(\mathrm{Tl}) = 43{\cdot}4$ kcal g atom^{-1} (Coleman and Egerton 1935, recalculated Jeffries 1952), $Q_f(\mathrm{TlCl_c}) = -48{\cdot}8$ kcal mol^{-1} (Bartky and Giauque 1959), and $Q_f(\mathrm{Cl_g}) = 19{\cdot}01$ kcal g atom^{-1} (Rossini *et al.* 1952), the dissociation energy of thallous chloride is found to be $D''_{298} = 88{\cdot}5_7$ or $D''_0 = 88{\cdot}0$ kcal mol^{-1}.

Table 1. The Heat of Sublimation of Thallous Chloride

Exptl†	T (deg K)	S°_c, T	S_g, T	$\Delta_s H_{298}$
J	501·2	33·27	96·82	32·65
J	595·1	35·50	88·65	32·84
S.1	507·8	33·44	$95{\cdot}67_5$	32·45
S.1	608·4	35·79	$87{\cdot}46_5$	32·70
S.2	529·3	33·98	93·99	32·70
S.2	543·7	34·34	92·64	32·70
S.3	504·1	33·34	96·48	32·67
S.3	542·1	34·30	92·78	32·70
Volmer	599·2	35·59	87·48	32·32
Volmer	695·2	37·56	82·17	32·65
			mean value	32·64

† For the equilibrium pressures, see table 3 of Barrow, Jeffries and Swinstead (1955).

§ 3. SPECTROSCOPIC VALUES OF THE DISSOCIATION ENERGY

It is of interest to compare the thermochemical value with spectroscopic estimates of the dissociation energy. A transition which, by analogy with other halides of this group, may be written $\mathrm{c}^1\Pi - \mathrm{x}^1\Sigma^+$, leads to fluctuation bands observed in absorption (Neujmin 1934). The position of the dissociation limit, obtained by extrapolating a plot of $(\nu_{v''} + G_{v''})$ against v'', is 38 700 cm^{-1} or $110{\cdot}6_6$ kcal above $v'' = 0$. It is clear that the atomic products here must be $\mathrm{Tl}^*(^2P_{3/2})$, with excitation energy (Moore 1949, 1958) $E_A = 7792{\cdot}7$ cm^{-1} or 22·28 kcal, and either $\mathrm{Cl}(^2P_{3/2})$ or $\mathrm{Cl}^*(^2P_{1/2})$, with $E_A = 0$ or 881 cm^{-1} (2·52 kcal): all other atomic states lie far too high. If in fact $\mathrm{Tl}^*(^2P_{3/2}) + \mathrm{Cl}(^2P_{3/2})$, are the products then $D_0'' = 88{\cdot}3_8$ kcal, in good agreement with the thermochemical value. Correlation with $\mathrm{Tl}^* + \mathrm{Cl}^*$ would lead to the low value $D_0'' = 85{\cdot}8_8$ kcal.

A short extrapolation of the vibrational levels in the first excited state $\mathrm{A}\,0^+$ (Miescher 1941) leads to a dissociation limit at 32 213 cm^{-1} above $v'' = 0$. This state must be correlated with $\mathrm{Tl}(^2P_{1/2}) + \mathrm{Cl}^*(^2P_{1/2})$: this follows since only one 0^+ state arises from the combination $\mathrm{Tl}(^2P_{1/2}) + \mathrm{Cl}(^2P_{3/2})$ and this is presumably the ground state. Thus $D_0'' = 32\,213 - 881 = 31\,332$ or 89·60 kcal. An upper limit comes from the observation of pre-dissociation in $\mathrm{A}\,0^+$, so that bands with $v' = 4$ do not appear in the A–X system in emission. This level lies at 31 750 cm^{-1} above $v'' = 0$, giving $D_0'' \leqslant 90{\cdot}79$ kcal. A lower limit is given by the highest observed level, $v' = 7$, in $\mathrm{A}\,0^+$, which lies at 32 142 above $v'' = 0$.

A third transition, $\mathrm{B}^3\Pi_1 - \mathrm{x}^1\Sigma^+$, also gives rise to fluctuation bands, which may be extrapolated to give $D_0'' \sim 90$ kcal.

The various estimates of the dissociation energy are summarized in table 2. The present value may be given as $89{\cdot}6 \pm 0{\cdot}3$ kcal mol^{-1}, which is close to the estimate first put forward by Butkow (1929). However the conclusions about

Table 2. D_0'' for TlCl (kcal mol^{-1})

		products	
Thermochemical value			88·0
Spectroscopic values :			
$C^1\Pi$	extrapolation	Tl* + Cl	88·4
$B^3\Pi_1$	extrapolation	Tl + Cl	90
$A^3\Pi_0+$	extrapolation	Tl + Cl*	89·60
	highest observed level	Tl + Cl*	> 89·36
	pre-dissociation	Tl + Cl	⩽ 90·8

the states of excitation of the atomic products at the different dissociation limits will be helpful when considering the dissociation energies of other molecules of this group.

REFERENCES

Barrett, A. H., and Mandel, M., 1958, *Phys. Rev.*, **109**, 1572.

Barrow, R. F., 1957, *Proc. Phys. Soc.* A, **70**, 622.

Barrow, R. F., Jeffries, E. A. N. S., and Swinstead, J. M., 1955, *Trans. Faraday Soc.*, **51**, 1650.

Bartky, I. R., and Giauque, W. F., 1959, *J. Amer. Chem. Soc.*, **81**, 4169.

Butkow, K. V., 1929, *Z. Phys.*, **58**, 232.

Coleman, F. F., and Egerton, A., 1935, *Phil. Trans.* A, **234**, 177.

Jeffries, E. A. N. S., 1952, *Thesis*, Oxford University.

Mayer, J. E., and Mayer, M. G., 1940, *Statistical Mechanics* (New York : John Wiley).

Miescher, E., 1941, *Helv. Phys. Acta*, **14**, 148.

Moore, C. E., 1949, 1958, *Atomic Energy Levels*, I, III (Washington: National Bureau of Standards Circular 467).

Neujmin, H., 1934, *Phys. Z. Sowjet.*, **5**, 580.

Rossini, F. D., Wagman, D. D., Evans, W. H., Levine, S., and Jaffe, I., 1952, *Selected Values of Chemical Thermodynamic Properties* (Washington : National Bureau of Standards Circular 500).

Volmer, F., 1929, *Phys. Z.*, **30**, 590.

von Wartenberg, H., and Bosse, O., 1922, *Z. Elektrochem.*, **28**, 384.

Possibility of Molecular Resonance Acoustic Absorption in Solid Cyclohexane

By G. S. VERMA and S. K. JOSHI

Department of Physics, University of Allahabad, Allahabad, India

MS. received 11*th January* 1960

Recently Liebermann (1959) has shown that in molecular crystals resonance phenomena resulting in anomalously high acoustic absorption can occur whenever lattice and internal molecular vibrational frequencies overlap. Resonance absorption has been calculated in the particular case of benzene and was also confirmed experimentally. The absorption arises because of complex nature of specific heat which leads to complex velocity. For a periodic variation of temperature at frequency ω the specific heat is of the form $c = c_0 + c'/[1 + (i\omega/K)]$ where K is the number of transitions per unit time and is given by

$$K = \frac{9A^2(kT)^3N^4}{16h\nu_{01}m_{01}\nu_m{}^7(4\pi^2M)^3}.$$

The coupling parameter A, which is a measure of the strength of the intermolecular binding forces, is a function of Lennard-Jones parameters ϵ, r_0 and the intermolecular spacing d and is given by

$$A = \frac{U^{\mathrm{IV}}}{12} + \frac{U^{\mathrm{II}}}{2d^2}$$

where

$$U(r) = -4\epsilon\left[\left(\frac{r_0}{r}\right)^6 - \left(\frac{r_0}{r}\right)^{12}\right].$$

The internal vibration frequency ν_{01} corresponds to the fundamental vibration and m_{01}, the apparent internal vibrating mass. The parameter ν_m is the Debye maximum lattice frequency and M is the molecular weight. N is Avagadro's number, k is Boltzmann's constant and h is Planck's constant.

As the acoustical frequencies are always much smaller than the transition rate K, the absorption is inversely proportional to the transition rate and a low value for the transition rate leads to large acoustic absorption. In benzene $K = 10^9$ sec^{-1}, which is a low value compared with transition probabilities for other processes.

We have investigated the possibility of resonance absorption in solid cyclohexane. Solidified cyclohexane C_6H_{12} forms cubic crystals which have $a = 8{\cdot}76$ Å at -40°c and 8·41 Å at -70°c. The cubic units contain four molecules in a face-centred array. The frequency ν_{01} in our calculation corresponds to the Raman frequency 382 cm^{-1}, which according to Saxena (1940) belongs to

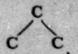

deformation for which the force constant is $0{\cdot}503 \times 10^5$ dynes. The values of the different parameters which we have used in our calculation are given in the table.

Numerical Constants for Cyclohexane

ϵ	(Lennard-Jones parameters†)	$4{\cdot}47 \times 10^{-14}$ ergs
r_0	(Hirschfelder *et al.* 1954)	$6{\cdot}093 \times 10^{-8}$ cm
d	(intermolecular spacing) (Wyckoff 1953)	$6{\cdot}265 \times 10^{-8}$ cm
A	(ϵ, r_0, d) (coupling parameter)	$0{\cdot}206 \times 10^{20}$ erg cm^{-4}
ν_m	(Debye frequency) (Aston *et al.* 1943)	3×10^{12} sec^{-1}
ν_{01}	(internal vibrational frequency) (Rasmussen 1943)	$1{\cdot}146 \times 10^{13}$ sec^{-1}
M	(molecular weight)	84·16 g
m_{01}	(apparent internal vibrating mass) (Saxena 1940)	3·645 g
T	(temperature)	273°K

† In Liebermann's paper the value of Lennard-Jones parameter, ϵ is wrongly quoted. It should be $\epsilon/k = 440$°K or $\epsilon = 6{\cdot}072 \times 10^{-14}$ erg. The coupling parameter A, calculated on the basis of the above parameter, however, does not differ much from that quoted in his paper and hence the rate of transition remains unchanged.

The present calculations show that the transition probability K in solid cyclohexane is $0{\cdot}76 \times 10^8$ sec^{-1}, which is lower than that of benzene. Thus there exists the possibility of obtaining resonance absorption of larger magnitude in solid cyclohexane.

ACKNOWLEDGMENT

The authors are grateful to Professor K. Banerjee for his helpful comments.

References

Aston, J. G., Szasz, G. J., and Fink, H. L., 1943, *J. Amer. Chem. Soc.*, **65**, 1134.
Hirschfelder, J. O., Curtis, C. F., and Bird, R. B., 1954, *Molecular Theory of Gases and Liquids* (New York: John Wiley), p. 1112.
Liebermann, L., 1959, *Phys. Rev.*, **113**, 1052.
Rasmussen, R. S., 1943, *J. Chem. Phys.*, **11**, 249.
Saxena, B. D., 1940, *Proc. Ind. Acad. Sci.*, **12A**, 321.
Wyckoff, R. W. G., 1953, *Crystal Structures*, Vol. III (New York: Interscience Publishers), ch. XV, p. 17.

Anomalous Winter Absorption of Radio Waves

By R. W. MORRISS
Cavendish Laboratory, Cambridge

Communicated by J. A Ratcliffe; *MS. received* 15*th December* 1959

Measurements of the absorption of cosmic radio noise were made on a frequency of 24·3 Mc/s by a method used by Shain and Mitra (1953). This involved comparing the received power from a given part of the galaxy (*a*) at night, and (*b*) at a series of different times in daylight. This meant waiting for the season to change. The absorption was measured only on the days when interference from commercial senders was small (there were between 7 and 15 in a month). The monthly mean values were then found, and the figure shows these plotted against the time of day, together with the standard deviation of the noon values. The period covered was January 1957 to May 1958.

It is immediately noticeable that the average midday absorption in winter (December and January) is about twice as great as that in summer (June and July). It is possible that this difference could be related to the fact that the F layer critical frequency (f_0F) is greater in winter than in summer. Thus an increase in f_0F would decrease the angle of entry of the cosmic radiation through the ionosphere, thereby reducing the power received from outside; it would also add some extra absorption as the wave traversed the denser F region. Simple calculations show however that neither of these causes could account for the observed winter increase in absorption.

Now it is well known (see, for example, Whitehead 1957) that, at the latitude of Cambridge, the absorption of radio waves reflected from the ionosphere at midday in winter is very variable. On a few winter days the absorption is small and can be related to that measured at midday in summer if it is supposed that $\log \rho \propto (\cos \chi)^n$ with $n \simeq 1$. On the majority of days, however, the absorption is considerably greater, and it can even approach that measured in summer, although it seldom exceeds it. This phenomenon has been called the 'winter anomaly' in the absorption of reflected waves.

If an attempt is made to relate the abnormally great absorption of cosmic radio waves in winter to the 'winter anomaly' of reflected waves, two questions arise. First, were there any days of more normal absorption observed in winter: and second, why is the increased absorption of the cosmic radio waves so great in winter that the mean absorption is actually twice that in summer?

In answer to the first question it should be noticed that, among the winter days there were, in fact, two on which the absorption was as small as 0·2 dB, and it is quite possible that these represented days of 'normal' absorption. The ratio of the absorption on these days to that on summer days is about 0·3, which is near the ratio of the corresponding values of cos χ.

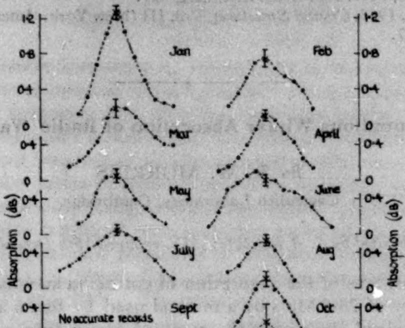

The diurnal variation of the absorption of cosmic radio waves measured on a frequency of 24·3 Mc/s. Each curve represents the average results for between 7 and 15 days in each month.

To answer the second question we note that, with the usual nomenclature, the frequency variation of absorption is given by

$$-\log \rho = A\{(\omega+\omega_L)^2+\nu^2\}^{-1} \qquad \ldots\ldots (1)$$

if, for simplicity, it is supposed that all the absorbing electrons are at a level where the collision frequency is ν. Now routine measurements of $\log \rho$ are made, in several places, for frequencies near 3 Mc/s, and equation (1) is used to deduce the magnitude of the quantity A, the assumption being made that $(\omega+\omega_L)^2 \gg \nu^2$.

The resulting values of A are published by the Ionospheric Research Station at de Bilt, which is near enough to the latitude of Cambridge for us to be able to assume that the absorption should be roughly the same at the two places. If now we take these published values of A for summer midday and use equation (1) to calculate the expected absorption of our cosmic radio waves, making due allowance for the fact that they transverse the absorbing region only once, and that they are incident over a cone of angles, we arrive at values for $\log \rho$ quite close to those observed if it is assumed that $\nu^2 \ll (\omega+\omega_L)^2$. When, however, we take the mean winter midday values of A published from de Bilt, and perform the same calculation, we deduce a value for $\log \rho$ which is about half the measured value.

Suppose, however, a different assumption is made, that in equation (1) ν is not necessarily negligible compared with $\omega_1+\omega_L$, when ω_1 represents the frequencies used in the measurements from which A is determined (e.g. $\omega_1 = 2\pi \times 3 \times 10^6$), but that $\nu \ll \omega_2 + \omega_L$ when $\omega_2 = 2\pi \times 23{\cdot}4 \times 10^6$, the frequency of the cosmic radio noise. Then we should find

$$\frac{\log \rho_2}{\log \rho_1} = \frac{(\omega_1 + \omega_L)^2 + \nu^2}{(\omega_2 + \omega_L)^2}. \qquad \ldots\ldots (2)$$

The suggestion is now made that $\nu^2 \ll (\omega_1 + \omega_L)^2$ in summer and on 'normal' days in winter, but that on 'abnormal' days in winter $\nu \simeq \omega_1 + \omega_L$. The ratio of the absorption measured on 24·3 Mc/s to that measured on frequencies near 3 Mc/s, from which A is deduced, would then be in accordance with equation (1) in summer, but would be twice as great on the abnormal winter days.

This suggestion implies that, on the majority of days in winter, which are of the 'abnormal' type, the absorbing electrons are largely concentrated near the level where $\nu = \omega_1 + \omega_L \simeq 2{\cdot}6 \times 10^7\ \text{sec}^{-1}$. This level is at a height of about 60 km.

ACKNOWLEDGMENTS

This work formed part of the programme of the British National Committee for the International Geophysical Year. The author is indebted to that Committee for a grant, for the equipment, and also to the Department of Scientific and Industrial Research for the award of a maintenance grant.

REFERENCES

SHAIN, A. C., and MITRA, A. P., 1953, *J. Atmos. Terr. Phys.*, **4**, 204.
WHITEHEAD, J. D., 1957, *J. Atmos. Terr. Phys.*, 10, 12.

LETTERS TO THE EDITOR

The First $T=1$ Level in ^{18}F

The low-lying levels of ^{18}F are of considerable theoretical interest (Elliott and Flowers 1955, Redlich 1958), but the spins and parities of the four levels which have been found at excitations of 0·941, 1·044, 1·084 and 1·126 Mev have not yet been uniquely established experimentally. In particular, the position of the first $T=1$ level is in doubt, and its identification would be of value. Spin, parity and isobaric spin of 0^+; 1 have been assigned to the level at 1·085 Mev and 0^-; 0 have been assigned to the level at 1·044 Mev (Ajzenberg-Selove and Lauritsen 1959, Kuehner, Almqvist and Bromley 1958, Macfarlane and French 1959). Recently, however, Hinds and Middleton (1959) have investigated the ^{16}O (^{3}He, p)^{18}F reaction leading to these levels and they suggest that the first $T=1$ level is more probably that at 1·044 Mev.

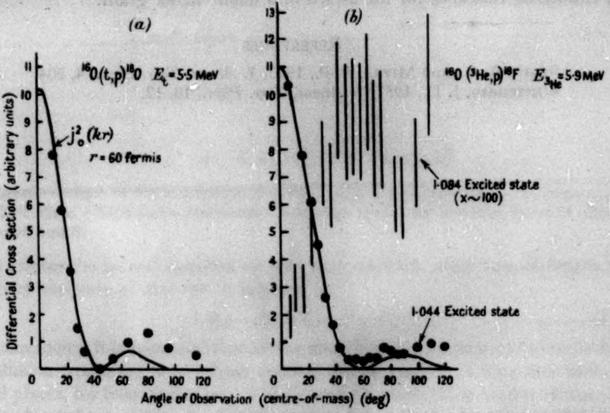

Figure 1 (*a*). The angular distribution of the protons from the reaction ^{16}O(t, p_0)^{18}O.
Figure 1 (*b*). The angular distributions of the protons from the ^{16}O(^{3}He, p)^{18}F reaction leading to the 1·044 and 1·084 Mev levels. These distributions are derived from the results of Hinds and Middleton (1959) and are reproduced for comparison. The full curve is the square of the spherical Bessel function j_0 (*kr*) multiplied by a slowly varying form factor.

We have investigated the ^{16}O(t, p)^{18}O reaction at a bombarding energy of 5·5 Mev and have obtained the angular distribution of the strong proton group leading to the ground state of ^{18}O. The distribution is shown in figure 1 (*a*), and it can be well fitted with the square of the spherical Bessel function j_0 (*kr*), where *k* is the linear momentum transfer in the (t, p) reaction. The angular distributions of Hinds and Middleton for the ^{16}O(^{3}He, p)^{18}F reactions leading to the 1·044 and

1·084 levels are reproduced in figure 1 (*b*). No absolute cross sections are available for the ^{16}O(^{3}He, p) reaction but the proton group leading to the 1·084 level is extremely weak. The similarity of the angular distributions of the ^{16}O(t, p_0)^{18}O group to that of the ^{16}O(^{3}He, p_2)^{18}F reaction leading to the 1·044 level is striking, and it is quite different from that of the ^{16}O(^{3}He, p_3) group. In fact it is also very different from the angular distributions from the (^{3}He, p) reaction leading to any of the four levels of ^{18}F in the region of 1 Mev, though the remaining distributions are not reproduced here.

It is believed that the comparison of this result with those of Hinds and Middleton (1959), assuming a similar double stripping process for both the (^{3}He, p) and (t, p) reactions, removes any doubt that the first $T = 1$ level of ^{18}F is that at 1·044 Mev, which must then have spin and parity 0^+ by comparison with the ground state of ^{18}O. No further positive parity states of spin zero are expected on the basis of the shell model calculations in this region of excitations and the most likely spin, parity and isobaric spin assignments for the level at 1·084 Mev are 0^-; 0.

The Physical Laboratories,
University of Manchester.
11th March 1960.

A. A. Jaffe.
I. J. Taylor.
P. D. Forsyth.

Ajzenberg-Selove, F., and Lauritsen, T., 1959, *Nucl. Phys.*, **11**, 1.
Elliott, J. P., and Flowers, B. H., 1955, *Proc. Roy. Soc.* A, **229**, 536.
Hinds, S., and Middleton, R., 1959, *Proc. Phys. Soc.*, **74**, 762.
Kuehner, J. A., Almqvist, E., and Bromley, D. A., 1958, *Phys. Rev. Letters*, **1**, 260.
Macfarlane, M. H., and French, J. B., 1959, *Stripping Reactions and the Structure of Intermediate Nuclei*, University of Rochester Report NYO—2846.
Redlich, M. G., 1958, *Phys. Rev.*, **110**, 468.

REVIEWS OF BOOKS

Masers—Microwave Amplification and Oscillation by Stimulated Emission, by GORDON TROUP. Pp. x + 168. (London : Methuen & Co., 1959.) 13*s*. 6*d*.

Great advances in microwave techniques were made during the years 1940–1945 mainly due to their application to radar. During the next ten years, however, apart from the extension of these techniques to shorter wavelengths in the millimetric band, no outstanding advances were made and the sensitivity of microwave receivers was only slightly improved. As so often happens in physics, a new burst of research activity in this field has recently been evident, resulting in major advances in technique. This is largely the result of the work of C. H. Townes which showed that stimulated emission could be used to generate and amplify microwave radiation and of N. Bloembergen who showed that the principle could be applied very effectively to crystalline solids cooled to low temperatures.

This small book aims at giving an account of the basic theory underlying the use of stimulated emission in the microwave region of the spectrum and describing recent developments of practical amplifiers and oscillators based on this principle—masers as they are called. The first three chapters deals with the former in an elementary manner. This is mostly standard theory as taught in many honours physics courses, and students may find the book useful in collecting together this material and presenting it in a logical sequence. The rest of the material in the book is rapidly becoming out of date owing to the extremely rapid development of the subject; this is evident at the very beginning since the book starts with " notes added in proof ". This makes one wonder whether a book such as this is timely and whether the material would not have been better presented in the form of a review article.

One has the feeling that the author is not always in touch with current practice although he is clearly familiar with the literature up to 1958. His terminology for discussing receiver performance is slightly confusing and is not in line with what is used in at least some of the leading laboratories in which research is in progress in this field. As an introduction to the subject the book will be found useful, but a second edition is already overdue if the book is not rapidly to become obsolete. R. A. SMITH.

Close Binary Systems, by Z. KOPAL. Pp. xiv + 558. (London: Chapman and Hall, 1959.) 105*s*.

Double stars whose components are too close together to be resolved in telescopes reveal their duplicity by the variations in their combined light and in their velocity displacement of spectral lines as the components revolve around each other. The study of such close binary systems has been of fundamental importance to astronomy, for they alone provide us with individual masses and sizes of stars. Professor Kopal, a leading authority in this field, has now written a substantial book on this subject. A detailed treatment is given of the many intricate problems which arise out of the tidal interaction, the axial rotations and the mutual reflection of a close pair, and which are relevant to the interpretation of observed light curves and velocity curves. There is also a complete exposition of the author's 'iterative methods', among other 'direct methods', of determining the elements of eclipsing binaries. These form the major part of the book and should be of the greatest value to specialists. The remainder (about one fifth), which can be read independently of the bulk, contains a fascinating survey of the whole subject, based on the classification proposed by the author, of these stars into 'detached', 'semi-detached' and 'contact' systems. This last part should appeal to all students of astronomy. The great merit of the book is its comprehensiveness, though the text is marred in places by a tendency towards verbosity. T. KIANG.

Symbolic Logic and Intelligent Machines, by E. C. BERKLEY. Pp. v + 203. (New York: Reinhold; London: Chapman and Hall, 1959.) 52*s*.

The reader is first introduced to the basic ideas of symbolic logic and Boolean algebra, the solution of problems by means of summarized Boolean rules and Venn diagrams, truth tables and the electrical and other interpretations of Boolean expressions. Surprisingly, although the summarized rules include negation, there seems to be no mention of the easily understood de Morgan's theorem, which is a powerful and elegant Boolean tool for the circuit engineer. The author then deals with the concept of machine intelligence and shows that switching circuits can represent simple problems. More complex machines and the basic operations of computers are also considered. The switching elements are confined to mechanical switches and relays, but rectifiers are sometimes included to prevent back-feeds.

Although the book contains useful information, there must, unfortunately, be some adverse criticism. Some parts seem unnecessary. How many readers, for example, will have so poor a scientific background as to need the sentence (page 82) "Now let us think of electric current as a flow of small marbles of electricity (electrons) along hollow tubes drawn as lines (actually wires) in the figure." ? Yet this sentence has been given an index reference under 'Marbles, electricity, 82'. Again, a reader, intrigued by the index entries 'Geniacs, 193' and 'Tyniacs, 193' will be disappointed to find on page 193, the bibliography, that they merely refer to the occurrence of these two words in the title of a publication by the author which, it is stated, is included in a certain constructional kit for making small electric brain machines.

The standard of some of the diagrams is very poor, and the adoption of unusual circuit conventions is irritating and unnecessary. Sometimes explanations and diagrams are not as helpful as they might be and the reader is left to sort things out for himself, not always successfully. An example of this occurs in the problem 'Divorce Mill with Bigamy Alarm' (page 171). After some general discussion, the Boolean circuit equations are finally listed; the text then ends abruptly with "The circuits are shown in Fig. 14–6". Prominently displayed in this diagram are five two-way push-button keys. The two fixed contacts of each key are shown connected *directly* to a current sink (earth, according to the convention on page 82) and the moving contact, *directly* to a current source (small circle according to the convention). The reader, used to normal circuit conventions, must therefore be forgiven for concluding that five distinct short circuits across the supply are an essential feature of the problem. Investigation shows that these key circuits play no part in the problem; it is the *rest* of Fig. 14–6 that matters. Why have they been included to confuse the reader is not explained and hard to understand. One cannot help feeling, therefore, that insufficient care has been taken in the production of the book.

C. E. WYNN-WILLIAMS.

Space Charge Waves and Slow Electromagnetic Waves, by A. H. W. Beck. Pp. viii + 396. (London, New York, Paris, Los Angeles: Pergamon Press, 1958.) 90*s*.

In the early development of radio the existence of electron inertia formed one of the fundamental limitations in extending the range of wavelengths to cover decimetre and centimetre waves. At a somewhat later stage it was realized that these effects could be put to use, the klystron and cavity magnetron being instances where electron inertia is essential to the operation of the device.

During the 1939–45 war the urgent need for centimetre equipment, though valuable in leading to the rapid exploitation of these techniques, encouraged the growth of the subject on an empirical basis. Each device tended to be treated by the best *ad hoc* theory which could be used for intelligent prediction. The advent of travelling wave tubes, magnetron amplifiers, carcinotrons, etc., made it obvious that all consist in one form or another of the interaction between a space-charge wave in the electron beam and a system of cavities or lines in which slow electromagnetic waves can be set up.

The present monograph is written with this in mind and stresses the essential similarity of operation of a wide range of devices. The treatment first applies Maxwell's equations to the circuit in the absence of the beam and deduces the circuit properties in all slow wave structures of importance at the present time. This is followed by Maxwell's equations again, modified by the presence of space charge, and used to describe the electron beam in the absence of the circuit. Space-charge waves play an important part in the description and their existence interprets and clarifies much of the earlier *ad hoc* theory.

With these two sections done separately it is then possible to consider the interaction between circuit and beam in a sufficiently general way to include in the framework all the devices now in use. The result is a comprehensive study of the present-day u.h.f. valves all treated on a unified system which forms a most valuable step towards a general understanding of their operation.

The cavity magnetron is not included, which is perhaps sensible as the beam and circuit geometries here are more difficult and the operation of the valve is less well understood.

The author describes himself in the preface as an engineer and not a mathematician. His knowledge of the mathematical methods required in this work however is extensive and quite rightly in a monograph of this kind he uses the most appropriate mathematical formulation irrespective of difficulty. The serious reader who is doing work in the field either in research, design or teaching, will not object to this and will not find much difficulty in following the mathematics, especially as the steps are quite well explained. The casual reader who wishes to use the book as general education will find that pencil and paper will be necessary and so might be discouraged.

In conclusion the book can be recommended as being essential to those actively engaged in one way or another on microwave devices and undoubtedly forms a basic account of the subject which will be of value for a long time to come.

R. LATHAM.

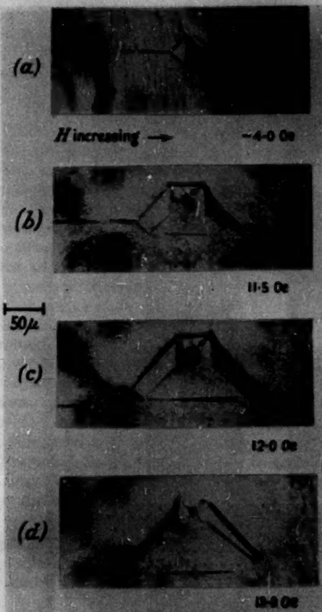
(a)
H increasing →
−4·0 Oe
(b)
11·5 Oe
50μ
(c)
12·0 Oe
(d)

Figure 2.

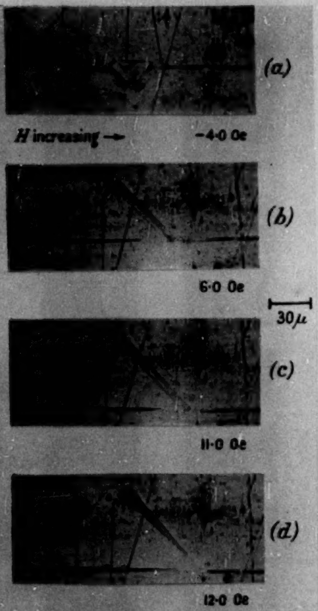
(a)
H increasing →
−4·0 Oe
(b)
6·0 Oe
30μ
(c)
11·0 Oe
(d)
12·0 Oe

Figure 3.

Figure 6.

Figures 2 and 3. Micrographs showing typical tube extension and rupture processes in silicon–iron.

Figure 6. Néel spike based on a group of large inclusions in silicon–iron.

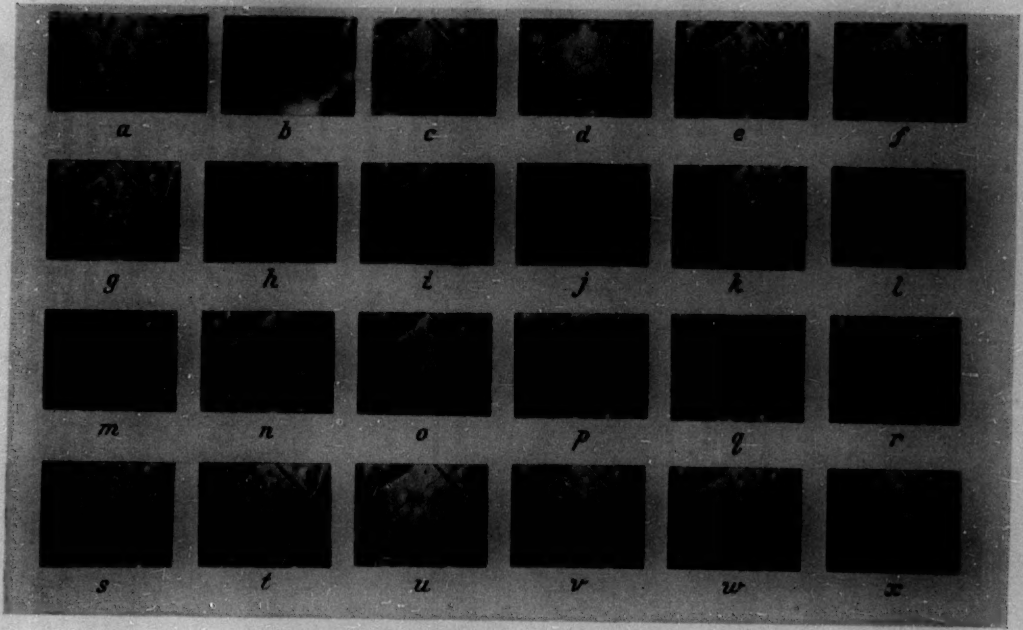
a
b
c
d
e
f
g
h
i
j
k
l
m
n
o
p
q
r
s
t
u
v
w
x

Figure 1. (*a*) Complex closure domains covering a typical grain, (*b*) a portion of figure 1 (*c*) enlarged, (*c*)–(*x*) the reversal process in a grain of square-loop ferrite.

PROCEEDINGS OF THE PHYSICAL SOCIETY

1960—VOL. 75

SUBJECT INDEX

PAGE
Aberration and detector response, influence on optical images 713
Absorption, acoustic, *see* Acoustic absorption
Absorption spectrum of barium vapour 87
Absorption spectrum of calcium vapour in vacuum u.v. (R) . . . 152
Absorption spectrum of neon (L) 461
Acoustic absorption and molecular resonance in solid cyclohexane (R) . . . 936
Acoustical waves, hypersonic, velocity in viscous liquids from Brillouin spectra 612
Ageing process in triglycine sulphate (R) 455
Air showers, *see* Cascade
Alkali halides, colloid centres in, coagulation, optical absorption and photoconductivity in 649
Alkaline earths, arc spectra, u.v. extensions 87
Alloys, nickel–iron, evaporated films, induced magnetic anisotropy in . . 557
Aluminium, optical constants 664
Angular correlation between some coincident γ-rays of ^{192}Pt . . . 61
Atomic polarizabilities 169
Atomic wave function, improved, using functional transformation . . . 575
Atoms, long range forces between (L) 164
Atoms in molecules 402

Band spectra of NiCl and NiBr in visible 275
Band spectrum triplet system, of CO, intensities (L) 162
Band systems, molecular, BO α and β, and intensity measurements on CO$^+$ comet tail 817
Barium titanate, effect of hydrostatic pressure on dielectric properties (R) . . 456
Barium vapour, absorption spectrum 87
Bitter patterns on ferrites 885
Born–Green linearized integral equation 826
Breakdown, *see* Discharges
Brillouin spectra, and hypersonic velocity in viscous liquids . . . 612
Brownian movement, relation between friction constant and force correlation integral 109

Calcium vapour, absorption spectrum in vacuum u.v. (R) 152
Carbon, momentum distribution of protons in 24
Carriers, excess, in semiconductors, effect of electric field on decay (R) . . 157
Cascade theories and Landau approximation 205
Charge dependence of nuclear forces (R) 147
Charge transfer, resonant, for positive ions (L) 807
Cobalt manganese ferrite, static and microwave measurements of magnetocrystalline anisotropy (L) 314
Cobalt, small particles, internal ferromagnetic resonance 33
Colloid centres in alkali halides, various properties 649
Coma, influence on response function of optical system 677
Comet tail, CO$^+$, intensity measurements, and BO α and β molecular band systems 817
Compression waves in plasma in static magnetic field 905
Conduction, *see* Impurity
Conductivity, bombardment, and photoconductivity in rhombic sulphur . . 119
Conductivity of hot electrons in Ge, anisotropy 174

PAGE

Correlation energies of helium sequence (R) 439
Counter technique for measurement of energy spectra and cross sections 526
Cracks, cone, in fused silica 697
Cross section, of ^{20}Ne(p, γ)^{21}Na 498
Crystals, CsI(Tl), effect of Tl concentration on decay time of electrons and α-particles (R) 931
Crystals, nuclear relaxation mechanism, in, experimental study 582
Crystals, single, of α-Fe_2O_3, electron diffraction study of heat treatment 364
Crystals, single, silicon, thermal expansion (R) 793
Crystals, *see also* Polycrystals

Deuterium atoms, neutral, ionization by hydrogen and by deuterium 850
Deuteron polarization, measurement (L) 317
Deuteron stripping with polarized deuterons 868
Deuteron velocity spectrum in SCEPTRE III 596
Deuterons, *see also* Scattering
Diatomic chains, vibrational spectra, functional equations (R) 452
Dielectric constant of germanium at microwave frequencies (R) 306
Dielectric liquid jet, stability in presence of longitudinal electric field 369
Dielectric properties of $BaTiO_3$, effect of hydrostatic pressure (R) 456
Discharges, pre-breakdown phenomena in uniform fields 729
Discharges, sparkover phenomena with enclosed gaps 733
Discharges, *see also* Gas discharge
Dislocations and twinning in graphite 607
Domain, single, relaxation time, correction to calculation (L) 625
Domain tube structures in silicon iron 880

Eddy current anomaly factor, influence of temperature 539
Eddy viscosity in liquid helium II 303
Editorial 1
Elastic scattering, *see under* Scattering
Electric field, longitudinal, effect on stability of dielectric liquid jet 369
Electron capture by protons passing through hydrogen 194
Electron detachment from H$^-$ by electron impact 67
Electron diffraction study of effects of heat treatment on α-Fe_2O_3 single crystals 364
Electron excitation of atomic hydrogen in 2p level 235
Electron spin resonance intensity in anisotropic substances (L) 621
Electron temperature, measurement in high-temperature plasmas 329
Electrons in weak interaction with chain of atoms 700
Emission of particles from compound nuclei 526
Energy levels, first $T=1$ level in ^{18}F (L) 940
Energy levels of ^{28}Al in region of 2 MeV (R) 154
Energy levels of ^{6}Li and ^{6}He from study of ^{7}Li(^{3}He, α)^{6}Li and ^{7}Li(t, α)^{6}He reactions 913
Energy transfer, solvent–solute in liquid organic solutions, dependence on excitation wavelength (L) 623

Ferrites, Bitter patterns, and loop shape in material 885
Ferroelectrics, wall velocity (L) 312
Ferromagnetic domain nuclei, thermomagnetic behaviour 739
Ferromagnetic resonance, internal, in magnetite (R) 149
Ferromagnetic resonance, internal, in small cobalt particles 33
Flash tubes, neon, efficiency 387
Flash tubes, neon high pressure 378
Flow anisotropy, measurement, in pure liquids 421
Fluids, thixotropic, time dependence measurements of viscosity 40
Fluids, transport of energy and momentum by phonons (R) 789
Fluorine 18, first $T=1$ level in (L) 940

PAGE
Frequency response, optical, measurement of characteristics by interferometric method . 434
Friction constant, and force correlation integral in Brownian movement theory . 109
Friction, internal, in synthetic quartz (R) . 459

Gadolinium, polycrystalline, temperature dependence of magnetostriction in 781
Gallium arsenide, magnetoresistance in . 280
Gallium, liquid, viscosity and resistivity (R) . 309
Gamma radiation from interaction of 14 Mev neutrons . 855
Gamma rays from 2^+ states in ^{16}O . 257
Gamma rays of ^{192}Pt, coincident, angular correlation between . 61
Gas, classical hard sphere, lattice model . 262
Gas discharge, collapsing current sheet, ionization by ion impact (L) . 316
Gas discharge, hot-cathode, noise spectra of probe in (L) . 462
Gas mixtures, monatomic, propagation of sound in . 898
Germanium, anisotropy of conductivity of hot electrons in . 174
Germanium, dielectric constant at microwave frequencies (R) . 306
Graphite, dislocations and twinning in . 607

Heat of sublimation and energy of dissociation of thallous chloride (R) . 933
Heat treatment, effects on α-Fe$_2$O$_3$ single crystals, electron diffraction study . 364
Helium II, liquid, eddy viscosity in . 303
Helium, photo-ionization (R) . 796
Helium sequence, correlation energies (R) . 439
Helium sequence, relativistic and radiative corrections to eigenvalues (R) . 441
Hydrogen, atomic, electron excitation in 2p level . 235
Hydrogen, atomic, low energy stopping power . 374
Hydrogen, electron capture by protons passing through . 194
Hydrogen ion, negative, electron detachment by electron impact . 67
Hydromagnetic disturbances, collision-free, in plasma . 640
Hydrostatic pressure, effect on dielectric properties of BaTiO$_3$ (R) . 456
Hyperfine structure of $3\,^2P_{3/2}$ state of sodium and quadrupole moment of ^{23}Na . 51

Impurity conduction, dielectric approach . 185
Integral equation, linearized, Born–Green . 826
Interaction of 14 Mev neutrons, γ-radiation from . 855
Interaction, weak, of electrons with chain of atoms . 700
Ionization by ion impact in collapsing current sheet (L) . 316
Ionization coefficients, secondary, in hydrogen and dependence on cathode work function . 762
Ionization of fast neutral deuterium atoms by hydrogen and by deuterium . 850
Ionization times of impurities in hydrogen plasmas . 520
Ionosphere, theory, recent trends (Presidential Address) . 2, corr. 812
Ionosphere, twisted ray paths in . 357
Iron 57, width and intensity of Mössbauer line (L) . 810
Isomeric reaction from ultrasonic relaxation, thermodynamics (R) . 142

Jet, dielectric liquid, stability in presence of longitudinal electric field . 369

Landau approximation and cascade theories . 205
Lattice model of classical hard sphere gas . 262
Light scattering and X-ray low angle scattering by semi-stiff chain molecules . 489
Light scattering, for study of quartz imperfections . 473
Liquid organic solutions, dependence of solvent–solute energy transfer on excitation wavelength (L) . 623
Liquid partition function and free energy . 671
Liquids, molecular theory, flow anisotropy and boundary conditions (R) . 799
Liquids, non-spherical, simple, pair distribution . 77

PAGE
Liquids, pure, measurement of flow anisotropy in . . . 421
Liquids, pure, ultrasonic vibration potentials in, theory . . . 102
Liquids, viscous, hypersonic velocity in, from Brillouin spectra . . . 612
Long range forces between atoms (L) . . . 164

Magnetic anisotropy, induced, in evaporated films of nickel–iron alloys . . . 557
Magnetic relaxation, proton, and molecular motion in liquid glycerol . . . 243
Magnetic relaxation, *see also* Nuclear magnetic
Magnetite, internal ferromagnetic resonance in (R) . . . 149
Magnetocrystalline anisotropy in cobalt magnanese ferrite, comparison of static and microwave measurements (L) . . . 314
Magnetoresistance in gallium arsenide . . . 280
Magnetostriction in polycrystalline gadolinium, temperature dependence . . . 781
Magnetostriction, saturation, of polycrystals . . . 8
Metals, liquid alkali and noble, resistivity . . . 395
Metals, monovalent, thermomagnetic effects of (L) . . . 463
Methylene chloride, liquid, ultrasonic relaxation in . . . 82
Microwave frequencies, dielectric constant of germanium at (R) . . . 306
Mixtures, binary, critical opalescence in, theory . . . 633
Molecular motion in liquid glycerol by proton magnetic relaxation . . . 243
Molecular motion in liquid *n*-octyl bromide by proton magnetic resonance (R) . . . 617
Molecular-orbital calculations on σ–π systems, scale parameters . . . 220
Molecular resonance, in solid cyclohexane, and acoustic absorption (R) . . . 935
Molecules, semi-stiff chain, X-ray low angle scattering by, and light scattering . . . 489
Momentum distribution of protons in carbon . . . 24
Mössbauer line in iron 57, width and intensity (L) . . . 810

Neon, absorption spectrum (L) . . . 461
Neutrons, *see under* Interaction
Nickel ferrite, thermomagnetic behaviour . . . 17
Nickel halides, band spectra in visible . . . 275
Nitrogen, photodisintegration . . . 543
Noise spectra of probe in hot-cathode discharge (L) . . . 462
Nuclear forces, charge dependence (R) . . . 147
Nuclear magnetic resonance, signal-to-noise ratio in (L) . . . 163
Nuclear relaxation mechanism in crystals, experimental study . . . 582
Nuclei, light, (^{3}He, d) reactions at 5·2 MeV . . . 291
Nucleon magnetic moments, effect of strange particles . . . 217
Nucleons, elastic scattering by tritons and ^{3}He (R) . . . 144

Opalescence, critical, in binary mixtures, theory . . . 633
Optical constants of aluminium . . . 664
Optical constants of noble metals (R) . . . 802
Optical frequency response, measurement of characteristics by interferometric method . . . 434
Optical images, influence of aberration and detector response . . . 713
Optical model for proton elastic scattering polarization . . . 502
Optical system, influence of coma on response function . . . 677
Oxygen 16, 2^+ states, γ-rays from . . . 257

Pair distribution of simple non-spherical liquids . . . 77
Pairing interaction, neutron–proton, in transuranic elements . . . 689
Paramagnetic resonance spectra of impurities in CaF_2 (R) . . . 136
Partition function, liquid, and free energy . . . 671
Phonons, transport of energy and momentum in fluids by (R) . . . 789
Photoconductivity and bombardment conductivity in rhombic sulphur . . . 119
Photodisintegration of nitrogen . . . 543
Photo-ionization of helium (R) . . . 796

PAGE
Photo-spallation, high energy, leading to F 18 4
Pi-electron systems, partial variational calculations on (R) 138
Plasma, collision-free hydromagnetic disturbances in 640
Plasma, in static magnetic field, compression waves in 905
Plasmas, high-temperature, measurement of electron temperature in . . . 329
Plasmas, hydrogen, ionization times of impurities in 520
Polarizabilities, atomic 169
Polarization in neutron–proton scattering at 77 MEV 345
Polarization, *see also* Deuteron
Polycrystals, saturation magnetostriction 8
Presidential Address (abstract): recent trends in theory of ionosphere, 2, corr. 812
Proton magnetic resonance, molecular motion in liquid *n*-octyl bromide by (R) . 617
Protons emitted from medium weight nuclei bombarded with neutrons of 14 MEV . 833
Protons, momentum distribution in carbon 24
Protons, *see also* Electron capture, Scattering, etc.

Quartz imperfections, study by light scattering 473
Quartz, synthetic, internal friction in (R) 459

Radio waves, anomalous winter absorption (R) 937
Reaction ^{11}B(t, p_0) ^{13}B and mass excess of ^{13}B (R) 929
Reaction ^{51}V(d, p)^{52}V 95
Reactions, ^{9}Be(^{3}He, p)^{11}B and ^{9}Be(^{3}He, d)^{10}B in energy range 5·7 to 10·2 MEV . 754
Reactions, (^{3}He, α), on light nuclei at 5·2 MEV 772
Reactions, (^{3}He, d), in light nuclei at 5·2 MEV 291
Reactions, (^{3}He, p), (^{3}He, d) and (^{3}He, α), with ^{12}C at bombarding energies between
  6 and 10 MEV 745
Reactions, ^{7}Li(^{3}He, α)^{6}Li and ^{7}Li(t, α)^{6}He, and energy levels of Li and He . . 913
Reactions, ^{28}Si(^{3}He, d)^{29}P and ^{28}Si(^{3}He, α)^{27}Si, at bombarding energy of 9·16 MEV (R) 444
Relaxation times, long spin–lattice, direct measurement (R) 450
Relaxation, *see also* Magnetic, Ultrasonic
Resistivity of liquid alkali and noble metals 395
Resistivity and viscosity of liquid galium (R) 309
Resonance, *see under* appropriate adjective

Scattering, elastic deuteron, from carbon at 6 MEV, polarization 875
Scattering, elastic and inelastic, bounds for 510
Scattering, elastic and inelastic, of protons by ^{58}Ni 201
Scattering, elastic, of nucleons by tritons and ^{3}He (R) 144
Scattering of electrons and positrons by xenon and mercury (R) 447
Scattering, neutron–proton, at 77 MEV, polarization in 345
Scattering, polarization, proton elastic, as test of low energy optical model . . 502
Scattering, *see also* Light, X-ray
SCEPTRE III, deuteron velocity spectrum in 596
Semiconductors, excess carriers, effect of electric field on decay (R) . . . 157
Semiconductors, *see also* Gallium, Germanium
Shock waves and controlled thermonuclear fusion 412
Silica, fused, cone cracks in 697
Silicon iron, domain tube structures in 880
Sodium, hyperfine structure of 3 $^{2}P_{3/2}$ state, and quadrupole moment 51
Sound, propagation in monatomic gas mixtures 898
Spectra, absorption, *see* Absorption
Spectra, arc, of alkaline earths, u.v. extensions 87
Spectra, vibrational, of diatomic chains, functional equations (R) 452
Spectra, *see also* Paramagnetic resonance
Spectral line shapes, correction for instrumental and other broadening . . . 337
Spectrum, band, *see under* Band spectrum
Stopping power, low energy, of atomic hydrogen 374

PAGE

Strange particles, effect on nucleon magnetic moments 217
Stripping, deuteron, with polarized deuterons 868
Sulphur, rhombic, bombardment conductivity and photoconductivity in . . 119

Thallous chloride, heat of sublimation and energy of dissociation (R) 933
Thermal expansion of silicon single crystal (R) 793
Thermodynamics of isomeric reaction from ultrasonic relaxation (R) 142
Thermomagnetic behaviour of ferromagnetic domain nuclei 739
Thermomagnetic behaviour of pure nickel ferrite 17
Thermomagnetic effects of monovalent metals (L) 463
Thermonuclear fusion, controlled, and shock waves 412
Transuranic elements, neutron–proton pairing interaction 689

Ultrasonic relaxation in liquid methylene chloride 82
Ultrasonic relaxation, thermodynamics of isomeric reaction from (R) . . . 142
Ultrasonic vibration potentials in pure liquids, theory 102

Variational calculations, partial, on π-electron systems (R) 138
Viscosity, eddy, in liquid helium II 303
Viscosity and resistivity of liquid gallium (R) 309
Viscosity of thixotropic fluids, time dependence measurements 40
Visible region, band spectra of nickel halides 275

Wall velocity in ferroelectrics (L) 312
Winds, high altitude, large scale irregularities in 228

X-ray scattering, low angle, by semi-stiff chain molecules and light scattering . 489

INDEX TO AUTHORS (WITH TITLES)

PAGE

Adlam, J. H., and Allen, J. E.: Collision-free hydromagnetic disturbances of large amplitude in plasma . . . 640
Aked, A., Bruce, F. M., and Gordon, C.: Some sparkover phenomena with enclosed gaps . . . 733
Alberts, L., and Shepstone, B. J.: Influence of temperature on eddy current anomaly factor . . . 539
Al-Jeboori, M. A., Bokhari, M. S., Strzałkowski, A., and Hird, B.: Polarization in deuteron elastic scattering from carbon at 6 Mev . . . 875
Al-Jeboori, M. A., with Strzałkowski A., Bokhari, M. S., and Hird, B.: Proton elastic scattering polarization as test of low energy optical mode . . . 502
Allen, J. E., with Adlam, J. H.: Collision-free hydromagnetic disturbances of large amplitude in plasma . . . 640
Allen, K. W., Almqvist, E., and Bigham, C. B.: Energy levels of ^{6}Li and ^{6}He from study of ^{7}Li(^{3}He, α)^{6}Li and ^{7}Li(t, α)^{6}He reactions . . . 913
Almqvist, E., with Allen, K. W., and Bigham, C. B.: Energy levels of ^{6}Li and ^{6}He from study of ^{7}Li(^{3}He, α)^{6}Li and ^{7}Li(t, α)^{6}He reactions . . . 913
Anderson, J. C.: Internal ferromagnetic resonance in small cobalt particles . . . 33
Anderson, J. C., and Donovan, B.: Internal ferromagnetic resonance in magnetite (R) 149
Anderson, N.: Compression waves in plasma in static magnetic field . . . 905
Andreae, J. H., Joyce, P. L., and Oliver, R. J.: Ultrasonic relaxation in liquid methylene chloride . . . 82
Andrew, E. R., and Swanson, K. M.: Experimental study of nuclear relaxation mechanism in several crystals . . . 582
Atkinson, J. R., Greer, J. R., and Wyllie, G.: Scattering of electrons and positrons by xenon and mercury (R) . . . 447

Baart, E. E., Green, L. L., and Willmott, J. C.: Energy levels of ^{28}Al in region of 2 Mev (R) . . . 154
Balfour, D., and Menzies, D. C.: Photodisintegration of nitrogen . . . 543
Barros, F. de S., with Forsyth, P. D., Jaffe, A. A., Taylor, I. J., and Ramavataram, S.: Investigation of some (^{3}He, d) reactions in light nuclei at 5·2 Mev . . . 291
Barros, F. de S., with Muto, J., and Jaffe, A. A.: Reaction ^{11}B(t, p_0)^{13}B and mass excess of ^{13}B (R) . . . 929
Barros, F. de S., with Taylor, I. J., Forsyth, P. D., Jaffe, A. A., and Ramavataram, S.: Investigation of some (^{3}He, α) reactions on light nuclei at 5·2 Mev . . . 772
Barrow, R. F.: Heat of sublimation and energy of dissociation of thallous chloride (R) 933
Bates, L. F., and Carey, R.: Domain tube structures in silicon iron . . . 880
Bates, L. F., and Clow, H.: Thermomagnetic behaviour of pure nickel ferrite . 17
Baynham, A. C., Gibson, A. F., and Granville, J. W.: On dielectric constant of germanium at microwave frequencies (R) . . . 306
Bell, D. A.: Noise spectra of probe in hot-cathode discharge (L) . . . 462
Benbow, J. J.: Cone cracks in fused silica . . . 697
Bhagat, S. M.: Eddy viscosity in liquid helium II . . . 303
Bigham, C. B., with Allen, K. W., and Almqvist, E.: Energy levels of ^{6}Li and ^{6}He from study of ^{7}Li(^{3}He, α)^{6}Li and ^{7}Li(t, α)^{6}He reactions . . . 913
Billington, E. W.: Some measurements of time dependence of viscosity of thixotropic fluids . . . 40
Birss, R. R.: Saturation magnetostriction of polycrystals . . . 8
Birss, R. R., and Horne, R. J.: Thermal expansion of silicon single crystal (R) . 793
Blackman, M., and Kaye, G.: Electron diffraction study of effects of heat treatment on α-Fe_2O_3 (haematite) single crystals . . . 364
Blair, D. T. A., Bruce, F. M., Matthews, J. E., and Tedford, D. J.: Pre-breakdown phenomena in uniform fields . . . 729
Bleaney, B.: Electron spin resonance intensity in anisotropic substances (L) . 621

PAGE

Blin-Stoyle, R. J., and Kearsley, M. J.: Note on charge dependence of nuclear forces (R) 147
Bokhari, M. S., with Al-Jeboori, M. A., Strzałkowski, A., and Hird, B.: Polarization in deuteron elastic scattering from carbon at 6 MEV 875
Bokhari, M. S., with Strzałkowski, A., Al-Jeboori, M. A., and Hird, B.: Proton elastic scattering polarization as test of low energy optical mode 502
Bowen, L. O.: Direct measurement of long spin–lattice relaxation times (R) 450
Bradley, E. M., with Prutton, M.: Induced magnetic anisotropy in evaporated films of nickel–iron alloys 557
Bransden, B. H., Hamilton, R. A. H., and Robertson, H. H.: Elastic scattering of nucleons by tritons and ^{3}He (R) 144
Brown, C. S.: Internal friction in synthetic quartz (R) 459
Bruce, F. M., with Aked, A., and Gordon, C.: Some sparkover phenomena with enclosed gaps 733
Bruce, F. M., with Blair, D. T. A., Matthews, J. E., and Tedford, D. J.: Pre-breakdown phenomena in uniform fields 729
Burfoot, J. C.: Wall velocity in ferroelectrics (L) 312
Burley, D. M.: Lattice model of classical hard sphere gas 262
Butt, D. K.: Angular correlation between some coincident γ-rays of ^{192}Pt 61

Carey, R., with Bates, L. F.: Domain tube structures in silicon iron 880
Chalklin, L. P., and Fremlin, J. H.: Ionization of fast neutral deuterium atoms by hydrogen and deuterium 850
Champion, F. C., with Dean, P. J., and Royce, B. S. H.: Bombardment conductivity and photoconductivity in rhombic sulphur 119
Champion, J. V.: Measurement of flow anisotropy in pure liquids 421
Champion, J. V., and Suddaby, A.: Flow anisotropy and boundary conditions in molecular theory of liquids (R) 799
Chidambaram, R.: Signal-to-noise ratio in nuclear magnetic resonance (L) 163
Clow, H., with Bates, L. F.: Thermomagnetic behaviour of pure nickel ferrite 17
Codling, K., with Garton, W. R. S.: Ultra-violet extensions of arc spectra of alkaline earths: Absorption spectrum of barium vapour 87
Cohen, S. G., and Weinreb, A.: Dependence of solvent–solute energy transfer in liquid organic solutions on excitation wavelength (L) 623
Cole, G. H. A.: Liquid partition function and free energy 671
Cole, G. H. A.: Pair distribution of simple non-spherical liquids 77
Cordey-Hayes, M., Dyson, N. A., and Moon, P. B.: Width and intensity of Mössbauer line in iron 57 (L) 810
Corner, W. D., and Hutchinson, F.: Temperature dependence of magnetostriction in polycrystalline gadolinium 781
Coxell, H., and Wolfendale, A. W.: High pressure neon flash tubes 378
Crowe, A.: Transport of energy and momentum by phonons in fluids (R) 789
Cusack, N., and Enderby, J. E.: Note on resistivity of liquid alkali and noble metals 395
Cusack, N., and Kendall, P.: Note on viscosity and resistivity of liquid gallium (R) 309

Dalgarno, A.: Correlation energies of helium sequence (R) 439
Dalgarno, A.: Low energy stopping power of atomic hydrogen 374
Dalgarno, A., and Stewart, A. L.: Relativistic and radiative corrections to eigenvalues of helium sequence (R) 441
Dalton, A. W., Kirk, A., Parry, G., and Scott, H. D.: ^{51}V(d, p)^{52}V reaction 95
Dandy, D., with Deuchars, W. M.: γ-radiation from interaction of 14 MEV neutrons 855
Davis, P. F.: Thermomagnetic behaviour of ferromagnetic domain nuclei 739
Dean, P., and Martin, J. L.: Functional equations for vibrational spectra of diatomic chains (R) 452
Dean, P. J., Royce, B. S. H., and Champion, F. C.: Bombardment conductivity and photoconductivity in rhombic sulphur 119
Deuchars, W. M., and Dandy, D.: γ-radiation from interaction of 14 MEV neutrons 855

PAGE
Ditchburn, R. W.: Absorption spectrum of neon (L) 461
Dixon, F. A.: Influence of aberration and detector response on optical images . 713
Dodd, J. N., and Kinnear, R. W. N.: Hyperfine structure of $3\,^2P_{3/2}$ state of sodium and quadrupole moment of ^{23}Na 51
Donovan, B., with Anderson, J. C.: Internal ferromagnetic resonance in magnetite (R) 149
Dowell, J. D., Frisken, W. R., Martelli, G., and Musgrave, B.: Momentum distribution of protons in carbon 24
Doyle, W. T.: Coagulation, optical absorption, and photoconductivity of colloid centres in alkali halides 649
Duga, J. J., with Willardson, R. K.: Magnetoresistance in gallium arsenide . . 280
Dvir, M., and Low, W.: Paramagnetic resonance spectra of impurities in calcium fluoride (R) 136
Dyson, N. A., with Cordey-Hayes, M., and Moon, P. B.: Width and intensity of Mössbauer line in iron 57 (L) 810

Eisenschitz, R., with Sah, Priyamvada: Electrons in weak interaction with chain of atoms 700
Enderby, J. E., with Cusack, N.: Note on resistivity of liquid alkali and noble metals 395

Flynn, C. P., and Seymour, E. F. W.: Correction of spectral line shapes for instrumental and other broadening 337
Forsyth, P. D., Barros, F. de S., Jaffe, A. A., Taylor, I. J., and Ramavataram, S.: Investigation of some $(^3\mathrm{He}, d)$ reactions in light nuclei at 5·2 Mev 291
Forsyth, P. D., with Jaffe, A. A., and Taylor, I. J.: First $T=1$ level in ^{18}F (L) . 940
Forsyth, P. D., with Taylor, I. J., Barros, F. de S., Jaffe, A. A., and Ramavataram, S.: Investigation of some $(^3\mathrm{He}, \alpha)$ reactions on light nuclei at 5·2 Mev . . . 772
Fremlin, J. H., with Chalklin, L. P.: Ionization of fast neutral deuterium atoms by hydrogen and deuterium 850
Frisken, W. R., with Dowell, J. D., Martelli, G., and Musgrave, B.: Momentum distribution of protons in carbon 24
Frood, D. G. H.: Dielectric approach to impurity conduction 185

Gardner, J. W.: Cascade theories and Landau approximation 205
Garton, W. R. S., and Codling, K.: Ultra-violet extensions of arc spectra of alkaline earths: Absorption spectrum of barium vapour 87
Gaunt, P.: Correction to single domain calculation (L) 625
Geltman, S.: Electron detachment from negative hydrogen ion by electron impact 67
Ghosh, N. C., and Sen, D.: Neutron–proton pairing interaction in transuranic elements 689
Gibson, A. F., with Baynham, A. C., and Granville, J. W.: On dielectric constant of germanium at microwave frequencies (R) 306
Goodbody, A. M.: Influence of coma on response function of optical system . 677
Gordon, C., with Aked, A., and Bruce, F. M.: Some sparkover phenomena with enclosed gaps 733
Granville, J. W., with Baynham, A. C., and Gibson, A. F.: On dielectric constant of germanium at microwave frequencies (R) 306
Gray, P., with Suddaby, A.: Relations between friction constant and force correlation integral in Brownian movement theory. Comparison of microscopic and macroscopic theories 109
Green, L. L., with Baart, E. E., and Willmott, J. C.: Energy levels of ^{26}Al in region of 2 Mev (R) 154
Greenhow, J. S., and Neufeld, E. L.: Large scale irregularities in high altitude winds 228
Greenlees, G. W., and Rolph, P. M.: Elastic and inelastic scattering of protons by ^{58}Ni 201
Greer, J. R., with Atkinson, J. R., and Wyllie, G.: Scattering of electrons and positrons by xenon and mercury (R) 447

PAGE

Hall, G. G.: Improved atomic wave functions using functional transformation 575

Hamilton, R. A. H., with Bransden, B. H., and Robertson, H. H.: Elastic scattering of nucleons by tritons and ^{3}He (R) 144

Hariharan, P., and Sen, D.: Simple interferometric arrangement for measurement of optical frequency response characteristics 434

Hartland, A., with Powles, J. G.: Molecular motion in liquid *n*-octyl bromide by proton magnetic resonance (R) 617

Harumi, K., with Katsura, S.: Note on Born–Green linearized integral equation 826

Haselgrove, C. B., and Haselgrove, Jenifer: Twisted ray paths in ionosphere 357

Haselgrove, Jenifer, with Haselgrove, C. B.: Twisted ray paths in ionosphere 357

Hinds, S., and Middleton, R.: Investigation of (^{3}He, p), (^{3}He, d) and (^{3}He, α) reactions with ^{12}C at bombarding energies between 6 and 10 MEV 745

Hinds, S., and Middleton, R.: Investigation of ^{28}Si(^{3}He, d)^{29}P and ^{28}Si(^{3}He, α)^{27}Si reactions at bombarding energy of 9·16 MEV (R) 444

Hinds, S., and Middleton, R.: Study of ^{9}Be(^{3}He, p)^{11}B and ^{9}Be(^{3}He, d)^{10}B reactions in energy range 5·7 to 10·2 MEV 754

Hird, B., with Al-Jeboori, M. A., Bokhari, M. S., and Strzałkowski, A.: Polarization in deuteron elastic scattering from carbon at 6 MEV 875

Hird, B., and Strzałkowski, A.: Deuteron stripping with polarized deuterons 868

Hird, B., with Strzałkowski, A., Bokhari, M. S., and Al-Jeboori, M. A.: Proton elastic scattering polarization as test of low energy optical mode 502

Holmes, R., and Tempest, W.: Propagation of sound in monatomic gas mixtures 898

Horne, R. J., with Birss, R. R.: Thermal expansion of silicon single crystal (R) 793

Humphreys-Owen, S. P. F., with Taurel, L.: Study of quartz imperfections by light scattering 473

Hunt, S. E.: Evaluation of deuteron velocity spectrum in SCEPTRE III 596

Hutchinson, F., with Corner, W. D.: Temperature dependence of magnetostriction in polycrystalline gadolinium 781

Ionescu Pallas, N. J., with Popescu Iovitzu, I.: On resonant charge transfer for positive ions (L) 807

Jack, W., with Storey, R. S., and Ward, A.: Experiments involving emission of particles from compound nuclei 526

Jack, W., and Ward, A.: Study of protons emitted from medium weight nuclei bombarded with neutrons of 14 MEV 833

Jaffe, A. A., with Forsyth, P. D., Barros, F. de S., Taylor, I. J., and Ramavataram, S.: Investigation of some (^{3}He, d) reactions in light nuclei at 5·2 MEV 291

Jaffe, A. A., with Muto, J., and Barros, F. de S.: Reaction ^{11}B(t, p_0)^{13}B and mass excess of ^{13}B (R) 929

Jaffe, A. A., with Taylor, I. J., Barros, F. de S., Forsyth, P. D., and Ramavataram, S.: Investigation of some (^{3}He, α) reactions on light nuclei at 5·2 MEV 772

Jaffe, A. A., Taylor, I. J., and Forsyth, P. D.: First $T=1$ level in ^{18}F (L) 940

Jones, D. A., and Ward, A.: Efficiency and main decay time of CsI(Tl) for electrons and alpha particles in crystals with different thallium concentrations (R) 931

Jones, Eifionydd, with Jones, F. Llewellyn: Experimental determination of individual secondary ionization coefficients in hydrogen and their dependence on cathode work function 762

Jones, F. Llewellyn, and Jones, Eifionydd: Experimental determination of individual secondary ionization coefficients in hydrogen and their dependence on cathode work function 762

Joshi, S. K., with Verma, G. S.: Possibility of molecular resonance acoustic absorption in solid cyclohexane (R) 935

Joyce, P. L., with Andreae, J. H., and Oliver, R. J.: Ultrasonic relaxation in liquid methylene chloride 82

Kail, J. A. E., with Luszczynski, K., and Powles, J. G.: Molecular motion in liquid glycerol by proton magnetic relaxation 243

Kaiser, T. R.: Absorption spectrum of calcium vapour in vacuum ultra-violet (R) 152

PAGE
Katsura, S., and Harumi, K.: Note on Born–Green linearized integral equation . 826
Kaufman, A. S., with Williams, R. V.: Measurement of electron temperature in high-temperature plasmas . 329
Kaye, G., with Blackman, M.: Electron diffraction study of effects of heat treatment on α-Fe$_2$O$_3$ (haematite) single crystals . 364
Kearsley, M. J., with Blin-Stoyle, R. J.: Note on charge dependence of nuclear forces (R) . 147
Kendall, P., with Cusack, N.: Note on viscosity and resistivity of liquid gallium (R) 309
Kennedy, A. J.: Dislocations and twinning in graphite . 607
Kinnear, R. W. N., with Dodd, J. N.: Hyperfine structure of $3\,^2P_{3/2}$ state of sodium and quadrupole moment of ^{23}Na . 51
Kirk, A., with Dalton, A. W., Parry, G., and Scott, H. D.: ^{51}V(d, p)^{52}V reaction . 95
Klimowski, J., and Pietrzak, J.: Effect of hydrostatic pressure on dielectric properties of BaTiO$_3$ (R) . 456
Knowles, J. E.: Some observations of Bitter patterns on polycrystalline 'square loop' ferrites, and theoretical explanation of loop shape and pulse characteristics of material . 885
Kundu, S. K.: Effect of strange particles on nucleon magnetic moments . 217
Kyle, H. L., and Merzbacher, E.: Long range forces between atoms (L) . 164

Lloyd, J. L.: On efficiency of neon flash tube . 387
Low, W., with Dvir, M.: Paramagnetic resonance spectra of impurities in calcium fluoride (R) . 136
Luszczynski, K., Kail, J. A. E., and Powles, J. G.: Molecular motion in liquid glycerol by proton magnetic relaxation . 243

McCrea, D., and McKirgan, T. V. M.: Electron excitation of atomic hydrogen in 2p level . 235
McIldowie, J. E. G., with Meads, R. E.: γ-rays from 2^+ states in ^{16}O . 257
McKirgan, T. V. M., with McCrea, D.: Electron excitation of atomic hydrogen in 2p level . 235
McWhirter, R. W. P.: Ionization times of impurities in hydrogen plasmas . 520
Martelli, G., with Dowell, J. D., Frisken, W. R., and Musgrave, B.: Momentum distribution of protons in carbon . 24
Martin, J. L., with Dean, P.: Functional equations for vibrational spectra of diatomic chains (R) . 452
Matthews, J. E., with Blair, D. T. A., Bruce, F. M., and Tedford, D. J.: Pre-breakdown phenomena in uniform fields . 729
Meads, R. E., and McIldowie, J. E. G.: γ-rays from 2^+ states in ^{16}O . 257
Mendlowitz, H.: Optical constants of aluminium . 664
Menzies, D. C., with Balfour, D.: Photodisintegration of nitrogen . 543
Merzbacher, E., with Kyle, H. L.: Long range forces between atoms (L) . 164
Michaelson, S., with Suffczynski, M.: Calculation of optical constants of noble metals (R) . 802
Middleton, R., with Hinds, S.: Investigation of (^{3}He, p), (^{3}He, d) and (^{3}He, α) reactions with ^{12}C at bombarding energies between 6 and 10 Mev . 745
Middleton, R., with Hinds, S.: Investigation of ^{28}Si(^{3}He, d)^{29}P and ^{28}Si(^{3}He, α)^{27}Si reactions at bombarding energy of 9·16 Mev (R) . 444
Middleton, R., with Hinds, S.: Study of ^{9}Be(^{3}He, p)^{11}B and ^{9}Be(^{3}He, d)^{10}B reactions in energy range 5·7 to 10·2 Mev . 754
Moon, P. B., with Cordey-Hayes, M., and Dyson, N. A.: Width and intensity of Mössbauer line in iron-57 (L) . 810
Morriss, R. W.: Anomalous winter absorption of radio waves (R) . 937
Morton, W. T., with Walker, T. G.: High energy photospallation leading to F18 4
Murty, G. S., with Nayyar, N. K.: Stability of dielectric liquid jet in presence of longitudinal electric field . 369

PAGE

Musgrave, B., with Dowell, J. D., Frisken, W. R., and Martelli, G.: Momentum distribution of protons in carbon 24
Muto, J., Barros, F. de S., and Jaffe, A. A. : Reaction ^{11}B(t, p$_0$)^{13}B and mass excess of ^{13}B (R) 929

Nayyar, N. K., and Murty, G. S.: Stability of dielectric liquid jet in presence of longitudinal electric field 369
Neufeld, E. L., with Greenhow, J. S.: Large scale irregularities in high altitude winds 228
Nicholls, R. W., with Robinson, D.: Intensity measurements on CO$^+$ comet tail, and BO α and β molecular band systems 817

Oliver, R. J., with Andreae, J. H., and Joyce, P. L.: Ultrasonic relaxation in liquid methylene chloride 82

Paddi Reddy, S., and Tiruvenganna Rao, P.: Band spectra of NiCl and NiBr in visible 275
Paige, E. G. S.: Anisotropy of conductivity of hot electrons and their temperature in germanium 174
Parkinson, D.: Atomic polarizabilities 169
Parry, G., with Dalton, A. W., Kirk, A., and Scott, H. D.: ^{51}V(d, p)^{52}V reaction 95
Pearson, F. J.: Theory of critical opalescence in binary mixtures 633
Pearson, R. F., and Teale, R. W.: Comparison of static and microwave measurements of magnetocrystalline anisotropy in cobalt manganese ferrite (L) 314
Phillips, N. J.: Ionization by ion impact in collapsing current sheet (L) 316
Phillips, R. J. N.: On measurement of deuteron polarization (L) 317
Pietrzak, J., with Klimowski, J.: Effect of hydrostatic pressure on dielectric properties of BaTiO$_3$ (R) 456
Pillow, M. E., and Rowlatt, A. L.: Intensities in triplet system of CO bands (L) 162
Popescu Iovitzu, I., and Ionescu Pallas, N. J.: On resonant charge transfer for positive ions (L) 807
Powles, J. G., and Hartland, A.: Molecular motion in liquid *n*-octyl bromide by proton magnetic resonance (R) 617
Powles, J. G., with Luszczynski, K., and Kail, J. A. E.: Molecular motion in liquid glycerol by proton magnetic relaxation 243
Prutton, M., and Bradley E. M.: Induced magnetic anisotropy in evaporated films of nickel–iron alloys 557

Rajagopal, A. K.: On thermomagnetic effects of monovalent metals (L) 463
Ramavataram, S., with Forsyth, P. D., Barros, F. de S., Jaffe, A. A., and Taylor, I. J.: Investigation of some (^{3}He, d) reactions in light nuclei at 5·2 Mev 291
Ramavataram, S., with Taylor, I. J., Barros, F. de S., Forsyth, P. D., and Jaffe, A. A.: Investigation of some (^{3}He, α) reactions on light nuclei at 5·2 Mev 772
Ratcliffe, J. A.: Presidential Address (abstract). Recent trends in theory of ionosphere 2, corr. 812
Ridley, B. K.: Effect of electric field on decay of excess carriers in semiconductors (R) 157
Robertson, H. H., with Bransden, B. H., and Hamilton, R. A. H.: Elastic scattering of nucleons by tritons and ^{3}He (R) 144
Robinson, D., and Nicholls, R. W.: Intensity measurements on CO$^+$ comet tail, and BO α and β molecular band systems 817
Rolph, P. M., with Greenlees, G. W.: Elastic and inelastic scattering of protons by ^{58}Ni 201
Rowlatt, A. L., with Pillow, M. E.: Intensities in triplet system of CO bands (L) 162
Royce, B. S. H., with Dean, P. J., and Champion, F. C.: Bombardment conductivity and photoconductivity in rhombic sulphur 119

PAGE
Sah, Priyamvada, and Eisenschitz, R.: Electrons in weak interaction with chain of atoms 700
Scott, H. D., with Dalton, A. W., Kirk, A., and Parry, G.: ^{51}V(d, p)^{52}V reaction 95
Sen, D., with Ghosh, N. C.: Neutron–proton pairing interaction in transuranic elements 689
Sen, D., with Hariharan, P.: Simple interferometric arrangement for measurement of optical frequency response characteristics 434
Sen, S. N.: Hypersonic velocity in viscous liquids as revealed from Brillouin spectra 612
Seymour, E. F. W., with Flynn, C. P.: Correction of spectral line shapes for instrumental and other broadening 337
Shepstone, B. J., with Alberts, L.: Influence of temperature on eddy current anomaly factor 539
Sil, N. C.: Electron capture by protons passing through hydrogen 194
Stafford, G. H., with Whitehead, C., and Tornabene, S.: Polarization in neutron–proton scattering at 77 Mev 345
Stankowska, J., and Stankowski, J.: Ageing process in triglycine sulphate (R) 455
Stankowski, J., with Stankowska, J.: Ageing process in triglycine sulphate (R) 455
Stewart, A. L., with Dalgarno, A.: Relativistic and radiative corrections to eigenvalues of helium sequence (R) 441
Stewart, A. L., and Wilkinson, W. J.: Photo-ionization of helium (R) 796
Stewart, E. Theal: 'Atoms in molecules': a simple approach 402
Stewart, E. Theal: Partial variational calculations on π-electron systems: Atomic analogue (R) 138
Stewart, E. Theal: Scale parameters in non-empirical molecular-orbital calculations on σ–π systems 220
Stokes, A. R.: Theory of light scattering and x-ray low angle scattering by semi-stiff chain molecules 489
Storey, R. S., Jack, W., and Ward, A.: Experiments involving emission of particles from compound nuclei 526
Strzałkowski, A., with Al-Jeboori, M. A., Bokhari, M. S., and Hird, B.: Polarization in deuteron elastic scattering from carbon at 6 Mev 875
Strzałkowski, A., Bokhari, M. S., Al-Jeboori, M. A., and Hird, B.: Proton elastic scattering polarization as test of low energy optical mode 502
Strzałkowski, A., with Hird, B.: Deuteron stripping with polarized deuterons 868
Suddaby, A., with Champion, J. V.: Flow anisotropy and boundary conditions in molecular theory of liquids (R) 799
Suddaby, A., and Gray, P.: Relations between friction constant and force correlation integral in Brownian movement theory. Comparison of microscopic and macroscopic theories 109
Suffczynski, M., and Michaelson, S.: Calculation of optical constants of noble metals (R) 802
Swanson, K. M., with Andrew, E. R.: Experimental study of nuclear relaxation mechanism in several crystals 582

Tanner, N. W., with Thomas, G. C.: Cross section of ^{20}Ne(p, γ)^{21}Na 498
Taurel, L., and Humphreys-Owen, S. P. F.: Study of quartz imperfections by light scattering 473
Taylor, I. J., Barros, F. de S., Forsyth, P. D., Jaffe, A. A., and Ramavataram, S.: Investigation of some (^{3}He, α) reactions on light nuclei at 5·2 Mev 772
Taylor, I. J., with Forsyth, P. D., Barros, F. de S., Jaffe, A. A., and Ramavataram, S.: Investigation of some (^{3}He, d) reactions in light nuclei at 5·2 Mev 291
Taylor, I. J., with Jaffe, A. A., and Forsyth, P. D.: First $T=1$ level in ^{18}F (L) 940
Teale, R. W., with Pearson, R. F.: Comparison of static and microwave measurements of magnetocrystalline anisotropy in cobalt manganese ferrite (L) 314
Tedford, D. J., with Blair, D. T. A., Bruce, F. M., and Matthews, J. E.: Prebreakdown phenomena in uniform fields 729
Tempest, W., with Holmes, R.: Propagation of sound in monatomic gas mixtures 898
Thomas, G. C., and Tanner, N. W.: Cross section of ^{20}Ne(p, γ)^{21}Na 498

PAGE

Tiruvenganna Rao, P., with Paddi Reddy, S.: Band spectra of NiCl and NiBr in visible 275
Tornabene, S., with Whitehead, C., and Stafford, G. H.: Polarization in neutron–proton scattering at 77 MeV 345

Verma, G. S.: Thermodynamics of isomeric reaction from ultrasonic relaxation (R) 142
Verma, G. S., and Joshi, S. K.: Possibility of molecular resonance acoustic absorption in solid cyclohexane (R) 935

Walker, T. G., and Morton, W. T.: High energy photo-spallation leading to F18 4
Ward, A., with Jack, W.: Study of protons emitted from medium weight nuclei bombarded with neutrons of 14 MeV 833
Ward, A., with Jones, D. A.: Efficiency and main decay time of CsI(Tl) for electrons and alpha particles in crystals with different thallium concentrations (R) 931
Ward, A., with Storey, R. S., and Jack, W.: Experiments involving emission of particles from compound nuclei 526
Weinmann, A.: Bounds for elastic and inelastic scattering 510
Weinmann, A.: Theory of ultrasonic vibration potentials in pure liquids 102
Weinreb, A., with Cohen, S. G.: Dependence of solvent–solute energy transfer in liquid organic solutions on excitation wavelength (L) 623
Whitehead, C., Tornabene, S., and Stafford, G. H.: Polarization in neutron–proton scattering at 77 MeV 345
Wilkinson, W. J., with Stewart, A. L.: Photo-ionization of helium (R) 796
Willardson, R. K., and Duga, J. J.: Magnetoresistance in gallium arsenide 280
Williams, R. V., and Kaufman, A. S.: Measurement of electron temperature in high-temperature plasmas 329
Willmott, J. C., with Baart, E. E., and Green, L. L.: Energy levels of ^{26}Al in region of 2 MeV (R) 154
Wolfendale, A. W., with Coxell, H.: High pressure neon flash tubes 378
Wright, J. K.: Shock waves and controlled thermonuclear fusion 412
Wyllie, G., with Atkinson, J. R., and Greer, J. R.: Scattering of electrons and positrons by xenon and mercury (R) 447

INDEX TO REVIEWS OF BOOKS

PAGE
Beck, A. H. W.: *Space charge waves and slow electromagnetic waves* 944
Bendat, J. S.: *Principles and applications of random noise theory* 323
Berkeley, E. C.: *Symbolic logic and intelligent machines* 943
Bodewig, E.: *Matrix calculus* (2nd Edn) 629
Bogoliubov, N. N., Tolmachev, V. V., and Shirkov, D. V.: *A new method in the theory of superconductivity* 466
Buerger, Martin J.: *Vector space—and its application in crystal-structure investigation* 468
Bunge, Mario: *Causality* 325

Champion, F. C., and Davy, N.: *Properties of matter* (3rd Edn) 627
Combustion Institute: *Seventh symposium (international) on combustion*. . . . 471

Donaldson, P. E. K.: *Electronic apparatus for biological research* 630

Eisenschitz, R.: *Statistical theory of irreversible processes* 629

Flügge, S., (Ed.): *Handbuch der Physik.* Vol. 41/1. *Nuclear reactions* II: *Theory* 627
Flügge, S., (Ed.): (Creutz, E., co-ed.): *Handbuch der Physik.* Vol. 44. *Nuclear instrumentation* I 467
Flügge, S., (Ed.): *Handbuch der Physik.* Vol. 52. *Astrophysik* III, *Das Sonnensystem* 326
Flügge, S., (Ed.): *Handbuch der Physik.* Vol. 53. *Astrophysik* IV, *Sternsysteme*. 324

Groshev, L. V., Demidov, A. M., Lutsenko, V. N., and Pelekhov, V. L. (Translated from the Russian by J. B. Sykes): *Atlas of γ-ray spectra from radiative capture of thermal neutrons* 470

Hannay, N. B.: *Semiconductors* 322
von Hippel, Arthur R.: *Molecular science and molecular engineering* 815

Jeans, Sir James: *An introduction to the kinetic theory of gases* 167

Kopal, Z.: *Close binary systems* 942

Landau, L. D., and Lifshitz, E. M. (Translated by M. Hamermesh from the Russian 2nd Edn): *The classical theory of fields—Course of theoretical physics.* Vol. 2 632
Landau, L. D., and Lifshitz, E. M. (Translated by E. Peierls, and R. E. Peierls): *Statistical physics.* Vol. 5. *Course of theoretical physics* 327
Lark-Horovitz, K., and Johnson, Vivian A.: *Methods of experimental physics.* Vol. 6. *Solid state physics*, Part B, *Electrical, magnetic and optical properties* . . 632
Levy, H., and Lessman, F.: *Finite difference equations* 320
Lifshitz, E. M., and Andronikashvili, E. L.: *A supplement to 'Helium'* . . . 814
Lo, A. W., Endres, R. O., Zawels, J., Waldhauer, F. D., and Cheng, C-C.: *Transistor electronics* 166
Lomont, J. S.: *Applications of finite groups* 628

Mariot, L.: *Groupes finis de symétrie et recherche de solutions de l'equation de Schrödinger* 631
Mehlin, Theodore G.: *Astronomy* 813
Messiah, A.: *Mécanique quantique*, Vol. 1 469
Moss, T. S.: *Optical properties of semi-conductors* 321

PAGE
Murray, R. L.: *Nuclear reactor physics* 167
Neff, Hans: *Grundlagen und Anwendung der Röntgen-Feinstruktur-Analyse* 630
New York Consultants Bureau Inc.: *Physics and heat technology of reactors* 471
Newstead, Gordon: *General circuit theory* 166

Pai, Shih-I: *Introduction to the theory of compressible flow* 472
Pope, J. A.: *Metal fatigue* 465

Rowlinson, J. R.: *Liquids and liquid mixtures* 327

Scott, R. B.: *Cryogenic engineering* 168
Seaborg, G. T.: *The transuranium elements* 631
Shubnikov, A. V., Zhludev, I. S., Konstantinova, V. P., and Silvestrova, I. M. (Translated from the Russian by Daknoff, A.): *Étude des textures piezo-électriques* 816

Thompson, J., and Callick, E. B.: *Electron physics and technology* 627
Trillat, Jean-Jacques: *Exploring the structure of matter* 324
Troup, Gordon: *Masers—microwave amplification and oscillation by stimulated emission* 942

Wannier, G. H.: *Elements of solid state theory* 467
Whyte, G. N.: *Principles of radiation dosimetry* 816
Wigner, E. P.: *Group theory and its application to the quantum mechanics of atomic spectra* 325

van der Ziel, A.: *Fluctuation phenomena in semiconductors* 466

Printed in England
Taylor & Francis, Ltd., Red Lion Court, Fleet Street, London, E.C. 4

R